CMBBE2019

ABSTRACT BOOK

16th International Symposium on

Computer Methods in Biomechanics and Biomedical Engineering

and the 4th Conference on

Imaging and Visualization

Columbia University
New York City, The United States
14 - 16 August 2019

www.cmbbe2019.com

[A-01.1]

THE SYNERGISTIC EFFECT OF NIRS-DETECTED LIPID RICH PLAQUE AND WALL SHEAR STRESS METRICS ON HUMAN CORONARY PLAQUE GROWTH

Eline Hartman[1], Ayla Hoogendoorn[1], Anton van der Steen[1], Joost Daemen[1], Jolanda Wentzel[1], ***Frank Gijsen***[1]

1 *Erasmus MC, Rotterdam, Netherlands*

Introduction: Local wall shear stress (WSS) metrics, high local lipid, as well as systemic lipid levels, have been individually associated with atherosclerotic disease progression. However, a possible synergistic effect remains to be elucidated. This study is the first study to combine WSS metrics with near-infrared spectroscopy (NIRS)-detected local lipid content to investigate synergistics effect on plaque progression in human coronary arteries.

Methods: The IMPACT study investigates the relation between atherosclerotic plaque progression and WSS in human coronary arteries. Patients with acute coronary syndrome were included. At baseline and after 1 year follow-up, patients underwent NIRS-IVUS imaging and flow measurements and CT scan. Combining the IVUS derived lumen contours and the CT derived vessel centreline resulted in a 3D reconstruction of the coronary artery including the side branches. The following WSS metrics were computed using CFD: time-average wall shear stress (TAWSS), oscillatory shear index, relative residence time (RRT), cross-flow index and transverse wall shear stress (transWSS).The arteries were divided into 1.5mm/45° sectors. Furthermore, per vessel the shear stress was divided into tertiles (low, intermediate, high). Based on IVUS segmentation of lumen and vessel wall, wall thickness at baseline and follow-up was determined in each sector. Furthermore, each arterial sector was classified for the presence of lipid-rich plaques as NIRS-positive or NIRS-negative. To investigate the synergistic effect of local lipids on shear stress related plaque growth, wall thickness change over time was related to the different shear stress metrics comparing the NIRS-positive with the NIRS-negative sectors.

Results: 15 non-culprit coronary arteries from the first 14 patients were analyzed (age 62±10 years old and 92.9% male). A total of 2219 sectors were studied (5.2%, N=130, NIRS-positive) for wall thickness changes. After studying all five shear stress metrics(fig. A), we found for TAWSS and RRT that presence of lipids, as detected by NIRS, amplified the effect of shear stress on plaque progression. Sectors presenting with lipid-rich plaque, compared to NIRS-negative sectors, showed more progression when they were exposed to low TAWSS (p=0.07) or high RRT (p=0.012) and more regression in sectors exposed to high TAWSS (p=0.10) or low RRT (p=0.06).

Conclusions: We showed that intravascular lipid-rich plaque assessment and local shear stress metric values have a synergistic value to predict plaque progression or regression. This finding suggests that combining local biomechanical assessment with knowledge on local plaque composition could improve patient risk assessment.

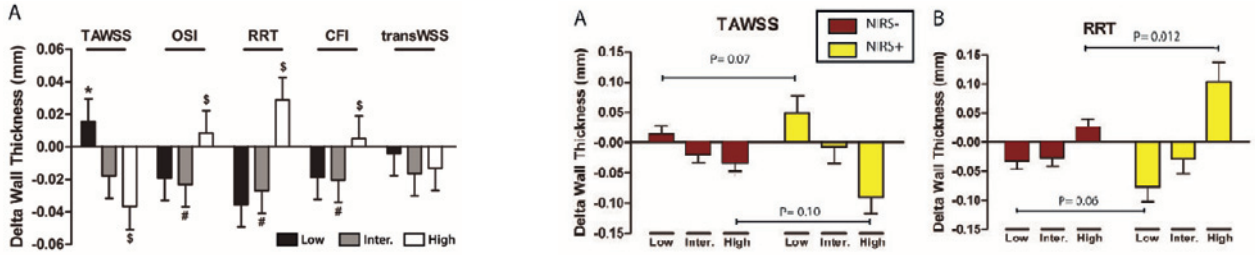

Figure Caption: A: 5 different shear stress metrics change in wall thickness after 1 year for low, intermediate and high shear stress. B/C: Effect of local lipid detection on change in wall thickness after 1 year on TAWSS and RRT. p<0.05: low versus intermediate, # intermediate versus high or $ low versus high*

[A-01.2]

REDUCED ORDER MODELS FOR BLOOD PRESSURE DROP ACROSS ARTERIAL STENOSES

Jeanne Ventre[1], *Francesca Raimondi*[2], *Arthur Ghigo*[3], *José Maria Fullana*[1], *Pierre-Yves Lagrée*[4]

1 *Institut Jean le Rond d'Alembert, Paris, France*
2 *Institut Necker Enfants Malades, Pediatric Cardiology and Radiology, Paris, France*
3 *University of British Columbia, Vancouver, Canada*
4 *Institut Jean le Rond d'Alembert, Paris, France; Cnrs, Paris, France*

Introduction: Stenosis, defined by a partial or full obstruction of arteries is one of the most frequent anomalies in the cardiovascular system. In clinical studies, blood pressure drop across the stenosis gives significant indications regarding the severity of the pathology, and trained medical can find out clinical indications only knowing these specific data. Despite of continuous improvements in the field of medical imaging allowing access to instantaneous velocity field and geometry topology in the vascular network, pressure data cannot be assessed. Modeling has therefore been considered as a relevant option for computing blood flow in stenosed vessels, and to extract pressure data directly or indirectly. In this presentation we propose the evaluation of the blood pressure drop across the stenosis using different models from the 0-D model to more complicated ones.

Models: Inside of the stenosis, blood flow and then blood pressure are highly controlled by the geometric properties and wall rheology. Geometric properties can be reduced to the arterial diameter ratio R0/Rst and stenosis length Lst, and wall rheology is a more complicated parameter to define. Changes in the geometric properties, wall rheology and input flow lead to changes in the flow hemodynamics and therefore in the blood pressure drop across the stenosis. We proposed an exhaustive numerical study involving different models: 2D axi-symetric Navier-Stokes model, steady RNSP model [1] with rigid arterial walls, 2D multi-ring model [2] to study the influence of models parameters. Finally we compared the numerical results against a common 1D model [3] and a classical 0D model frequently used by physicians [4].

Results: One invasive catheter measurement of trans-stenotic pressure shows that 0D model overestimates the pressure drop, 1D model underestimate it and multi-ring model gives a good agreement.

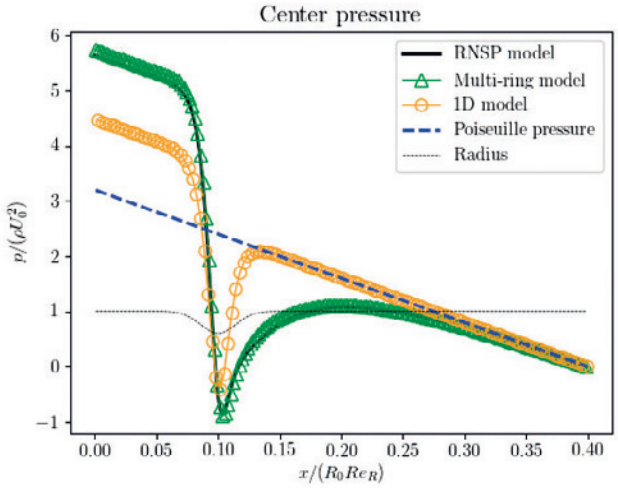

Figure Caption: Center pressure in a rigid stenosed artery using 1D, Multi-ring and RNSP models.

References:

[1] *P.-Y. Lagree and S. Lorthois. The rns/prandtl equations and their link with other asymptotic descriptions: Application to the wall shear stress scaling in a constricted pipe. International Journal of Engineering Science, 2005.*
[2] *A.R. Ghigo, J.-M. Fullana, and P.-Y. Lagrée. A 2d nonlinear multiring model for blood flow in large elastic arteries. Journal of Computational Physics, 2017.*
[3] *N. Stergiopulos, D.F. Young, and T.R. Rogge. Computer simulation of arterial flow with applications to arterial and aortic stenoses. Journal of biomechanics, 1992.*
[4] *B.D. Seeley and D.F. Young. Effect of geometry on pressure losses across models of arterial stenoses. Journal of biomechanics, 1976.*

[A-01.3]

COMPARING APPLES TO ORANGES; MEASURED SKIN VIBRATIONS CORRELATE PHENOTYPICALLY WITH COMPUTED POST-STENOTIC FLOW INSTABILITIES. A PRAGMATIC BUT ROBUST TOOL FOR EARLY DETECTION OF CAROTID STENOSES?

Viviana Mancini[1], *Aslak W. Bergersen*[2], *Kristian Valen-Sendstad*[2], *Patrick Segers*[1]

1 *Ghent University, Ghent, Belgium*
2 *Simula Research Laboratory, Fornebu, Norway*
** Mancini and Bergersen contributed equally to this work.*

Early detection of asymptomatic carotid artery stenosis is crucial for prevention of ischemic stroke. We aim to investigate the ability of Laser Doppler Vibrometry (LDV) to infer asymptomatic stenosis from the intensity of stenosis-induced flow instabilities (IFI), transmitting their energy into mechanical vibrations detectable at the skin. We therefore combined in-silico and in-vitro experiments to understand how the common carotid artery flow rate (Q_{CCA}), internal/external carotid flow split (Q_{ICA}/Q_{CCA}), and degree of stenosis affected IFI. We used the 2nd order fluid-dynamical finite-elements solver Oasis [1] to in-silico simulate three cardiac cycles with stenosis severity of 56, 66, 76, 86, and 96%, in addition to a healthy-subject model. Geometries were obtained from patient-specific computer tomography angiography images [2,3] with an internal carotid artery (ICA) stenosis of 76%. Flow rates (Q_{CCA}: 145-529 ml/min) and flow splits (Q_{ICA}/Q_{CCA}: 11.9 to 70.8%) were varied for a physiologically plausible range, which led to a total of 19 simulations [4,5]. Mesh element and time step sizes were set based on previous spatial and temporal sensitivity studies [6]. We computed IFI from 20Hz high-pass-filtered pressure traces, obtained downstream the stenosis, and found $Re_{stenosis}$ to be the best predictor for the presence of instabilities (Figure 1-A). These results confirmed in-vitro experiments in a compliant replica of the 76% stenosis model where, similarly, $Re_{stenosis}$ was related to an increase in IFI derived from LDV displacement (Figure 1-B) recorded on the skin-mimicking foil surrounding the tissue-mimicking gel in which the model was embedded [7]. The overall correlation between experimental and computational data was $R^2 = 0.9956$. The absence of turbulence in a healthy-subject model allowed us to estimate that $Re_{stenosis}$ can predict moderate and severe stenosis with 77% sensitivity. However, the severe stenosis models did not harbor flow instabilities because of limited Q_{ICA}, and would hence remain undiagnosed using LDV. These findings are in agreement with clinical studies [8] on expertly operated carotid auscultation. We conclude that LDV has the potential to be used as diagnostic tool for asymptomatic carotid stenosis.

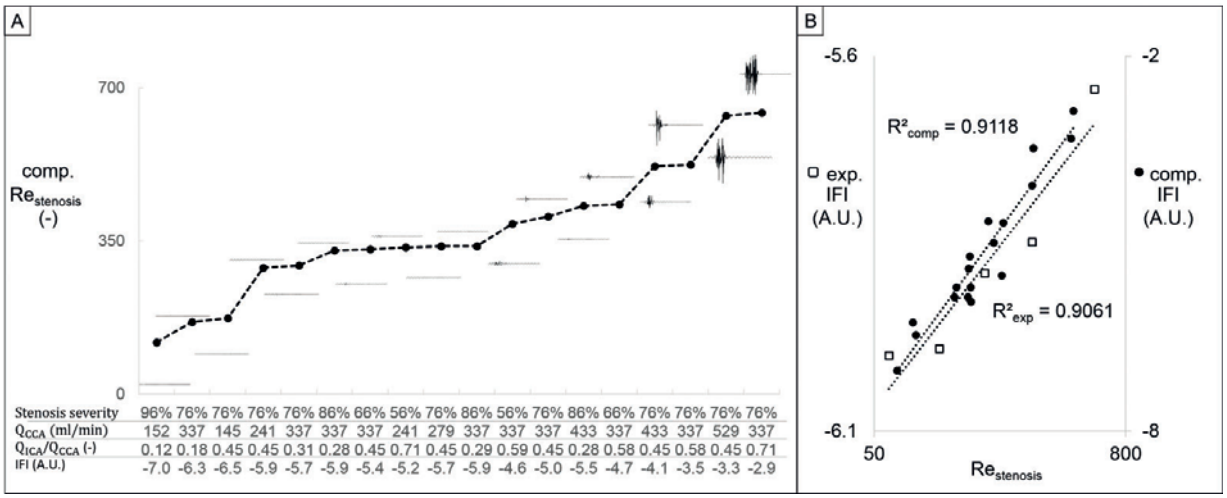

Figure 1: While being largely insensitive to expectedly relevant factors such as stenosis severity, inlet flow rate and flow split (A), the instabilities of high-pass filtered pressure traces from stenosis-induced flow instabilities increased together with Restenosis, both computationally and experimentally (B).

Acknowledgments: H2020 European funded project 644798.

References:

[1] *Mortensen et al., Comput Phys Comm 2015;188:177-188.*
[2] *Bergersen et al., JOSS 2019 – submitted.*
[3] *Iannaccone et al., Int J Artif Organs 2014;37:928-939.*
[4] *Likittanasombut et al., J Neuroimaging 2006;16:34-38.*
[5] *Groen et al., J Biomech 2010,43:2332-8.*
[6] *Mancini et al., Cardiovasc Eng Technol 2019 – submitted.*
[7] *Mancini et al., PlosONE 2019 – submitted.*
[8] *Johansson et al., BMC Neurology 2008;8:1-8.*

[A-01.4]

INTRACARDIAC FLOW DURING EARLY AND LATE LEFT VENTRICULAR FILLING IN ADOLESCENT VOLUNTEER: QUANTITATIVE CHARACTERIZATION USING 4D FLOW MRI

Liwei Hu[1], *Rongzhen Ouyang*[1], *qian Wang*[1], *Zhirong Tong*[2], *Jinlong Liu*[3], *Yumin Zhong*[1]

1 *Department of Radiology, Shanghai Children's Medical Center, Shanghai, China*
2 *Department of Cardiothoracic Surgery, Shanghai Children's Medical Center*
3 *Department of Cardiothoracic Surgery, Shanghai Children's Medical Center, Shanghai Jiao Tong University, Shanghai, China School of Medicine, Shanghai, China; Institute of Pediatric Translational Medicine, Shanghai Children's Medical Center, Shanghai Jiao Tong University, Shanghai, China School of Medicine; Shanghai Engineering Research Center of Virtual Reality of Structural Heart Disease, Shanghai Children's Medical Center, Shanghai Jiao Tong University, Shanghai, China School of Medicine, Shanghai, China*

Purpose: The aim of the study is to assess quantitative method of intracardiac blood flow including flow component, vortex formation time, valve circularity index and index vortex size using 4D flow MRI in adolescent volunteer. Methods: 4D flow CMR data from adolescent volunteer were retrospectively identified from studies performed. The volunteer had normal blood pressure and were free of cardiovascular disease. This case-control study was approved by our institutional review board and research images was performed after signed informed consent. CMR analysis was performed with commercially available software. The EDV, ESV, EF and SV of the LV were determined from short-axis cine images. The mitral valve is defined as the inflow slice and the aorta is defined as the outflow slice by three-chamber cine images, its ability to track mitral valve plane motion. The flow component was calculated by different flow pattern (Figure 1). The trans-mitral valve velocities and time to peak of E-wave and A-wave were determined from the 4D flow CMR data. The orientation of the mitral valve and the ring shape were quantified by the circularity index (CI). We defined the ratio between the valve's short to long as circularity index (Figure 2). The vortex formation time(VFT) was calculated from the following equationVFT=4/π·α^3·EF·EWV/SV=4/π·EWV/D^3 , where, α was defined as: α=(EDV^(1/3))/D with the diameter of the mitral valve(D) calculated as the mean of maximum distance between the leaflet tips during the rapid filling phase, perpendicular to the flow direction, in the three-chamber view, and the distance between the commissures on a short-axis slice through the mitral valve (Figure 2). We use 4D flow images to measure vortex diameter (Figure 3). Results: The results of flow components were highly related with ejection fraction. The value of vortex formation time and E/A ratio were in normal range compared with echocardiography (Figure 5). The CI of peak early filling mitral valve was lower than the peak late filling, it appeared like a circular (1.28 < 1.5). Conclusions: The study provides quantitative characterization by 4D flow MRI which may allow early quantitative evaluation of intracardiac flow in patients with cardiac disease.

Acknowledgments: Research support was provided by an award from China National Key Research and Development Program(No. 2018YFB1107105)"and the fund of The Shanghai Committee of Science and Technology (No.17DZ2253100)"

References:

1 *Pasipoularides A, et al. Journal of Cardiovascular Translational Research, 2015, 8(1):54-58.*
2 *Kamphuis VP, et al. Radiology. 2018 Oct 30:180807.*
3 *Chan B T, et al. Coronary Artery Disease, 2017:1.*
4 *Hirtler D, et al. European Radiology, 2016, 26(10):3598-3607.*

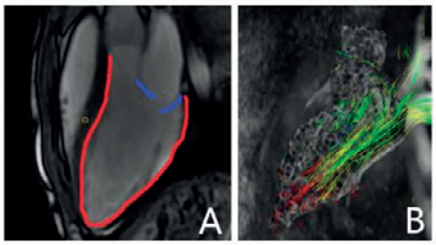

Figure 1. A. We manually delineated the left ventricular endocardium and mitral valve on the 3-chamber view. B. To improve the accuracy of flow component by the automatic track mitral valve motion on the 4D flow image.

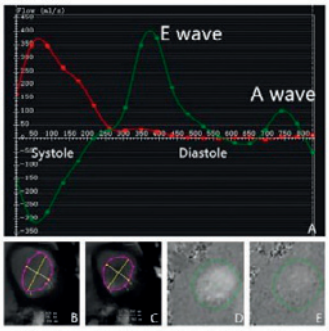

Figure 2. A. The mitral valve was defined as the inflow slice (Green line) and the ascending aorta is defined as the outflow slice (red line). B, D. To assess the valve circularity index and peak velocity of the A wave phase. C, E. To assess the valve circularity index and peak velocity of the E wave phase.

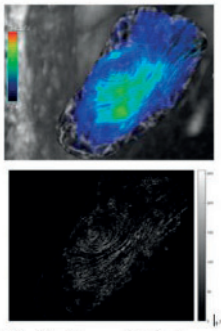

Figure 3. The vortex size was defined the diameter of clockwise vortex in the center of left ventricle at the end of diastole phase. We used 4D flow images to measure vortex diameter by using MATLAB Laplacian filtered.

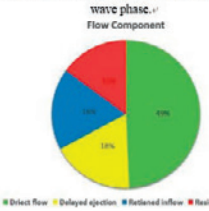

Figure 4. The figure showed the different components of left ventricular (LV) blood flow in Adolescent Volunteer. **Direct Flow:** Blood that enters the LV during diastole and leaves the LV during systole in the analyzed heart beat (green line). **Retained Inflow:** Blood that enters the LV during diastole but does not leave during systole in the analyzed heart beat (yellow line). **Delayed Ejection Flow:** Blood that starts and resides inside the LV during diastole and leaves during systole (blue line). **Residual Volume:** Blood that resides within the LV for at least two cardiac cycles calculations (red line).

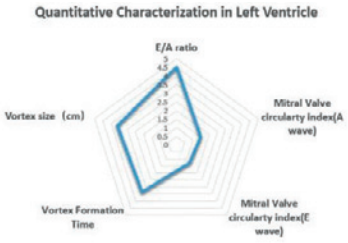

Figure 5. The quantitative criteria of intracardiac blood flow using 4D flow MRI in adolescent volunteer.

[A-01.5]

A META-MODEL OF THE TRANS-VALVULAR PRESSURE-GRADIENT BY COMBINING STATISTICAL SHAPE MODELING AND COMPUTATIONAL FLUID DYNAMICS

Martijn Hoeijmakers[1], *Irina Wächter-Stehle*[2], *Jürgen Weese*[2], *Frans van de Vosse*[3]

1 *Eindhoven University of Technology, Eindhoven, Netherlands, Dept. of Biomedical Engineering; Ansys, Eindhoven, Netherlands*
2 *Philips Research Laboratories, Eindhoven, Netherlands*
3 *Eindhoven University of Technology, Eindhoven, Netherlands, Dept. of Biomedical Engineering*

Advances in medical imaging, segmentation techniques, and high-performance computing have stimulated the use of complex, patient-specific 3D Computational Fluid Dynamics (CFD) simulations. With recent advances in segmentation methods, patient-specific CFD-compatible geometries of the aortic valve are readily obtained from Computed Tomography images [1]. Consequently, these 3D CFD models can be used to obtain patient-specific pressure-flow relationships of the aortic valve. However, 3D CFD models are generally time consuming, require extensive pre- and post-processing of an expert, and are not guaranteed to converge. Hence, it is desirable to reduce these complex 3D CFD simulations to efficient and robust meta-models. The aim of this work is to evaluate the performance of such a meta-model with respect to high-fidelity 3D CFD simulations of the aortic valve.

Computed Tomography images of 74 patients are segmented by a Shape Constrained Deformable Model framework, presented in earlier work [1]. The segmentation framework yields a labeled surface mesh of all cardiac structures with consistent topology. For this study, a sub-mesh (1808 vertices, 4223 triangular faces) of the left ventricular outflow tract, the aortic valve, and the aortic root is extracted. Principal Component Analysis [2] is used to extract the main modes of (shape) variation from the set of 74 segmentation meshes (eigen-decomposition of the covariance matrix). Parameterization is then achieved by approximating the vertex coordinates (x) of any segmentation sub-mesh (x_s) with the main modes of variation (ϕ_m). Effectively, any segmentation sub-mesh is now approximated (x_a) by the mean mesh ($\bar{x}$) and a linear combination of the first four shape modes and their patient-specific coefficients (w_m):

$$\boldsymbol{x_s} \approx \boldsymbol{x_a} = \bar{\boldsymbol{x}} + \sum_{m=1}^{n} w_m \phi_m$$

450 synthetic meshes are created with this statistical shape model, respecting upper- and lower-bounds of w_m. Consequently, 3D steady-state simulations are performed on the synthetic meshes at flow rates between 50 and 600 ml/s to find the corresponding pressure gradient (ΔP) across the aortic valve. The meta-model is trained with the simulation results. It is found that the meta-model approximates the CFD results with reasonable accuracy, (relative) root-mean-square-errors of 3.4 mmHg and 16.8% are found. This study demonstrates that statistical shape modeling can derive a suitable parametric description of the aortic valve. This parametric description can then be used to train meta-models. These meta-models have the potential to replace high-fidelity 3D CFD simulations.

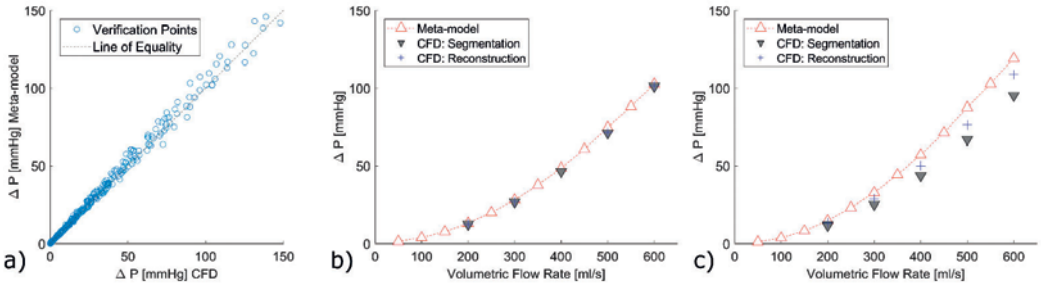

Figure 1. a) CFD results on reconstructed meshes vs. meta-model results. b) and c) typical pressure-low relationship for two cases. Differences between crosses and filled triangles are introduced by the parameterization, differences between upward triangles and blue crosses are introduced by meta-model training.

Acknowledgments: This work was supported in part by the European Research Council Grant (Grant number: 689617) and by the PLGrid Infrastructure.

References:

1. *Weese, J., et al, Med. Phys. 2017.*
2. *Heiman, T., Meinzer, H.P., Med. Image Anal., 2009*

[A-01.6]

A MOCK-FLOW LOOP (MFL) INVESTIGATION OF A SELF-POWERED FONTAN FOR SINGLE - VENTRICLE CONGENITAL HEART DISEASE

Arka Das[1], *Eduardo Divo*[1], *Alain Kassab*[2], *William Decampli*[3]

1 *Embry-Riddle Aeronautical University, Daytona Beach, USA*
2 *University of Central Florida, Orlando, Florida*
3 *Arnold Palmer Hospital, Orlando, Florida*

Around 8% of all newborns with a Congenital Heart Defect (CHD) have only a single functioning ventricle. The Fontan operation has served as a palliation for this anomaly for decades, but the surgery entails multiple complications and survival rate is less than 50% by adulthood [1]. A rapidly testable novel alternative is proposed by creating a bifurcating graft, or Injection Jet Shunt (IJS), used to "entrain" the pulmonary flow and thus provide assistance while reducing the caval pressure. A benchtop Mock Flow Loop (MFL) is configured to validate this hypothesis. Three IJS nozzle of varying diameters 2mm, 3mm and 4mm with two different graft settings i.e. fully open and partially open inlet cannula, are tested to validate the hypothesis and optimize the caval pressure reduction. The MFL is based on a Lumped-Parameter Model (LPM) of the Fontan circulation and is comprised of upper and lower systemic as well as left and right pulmonary compartments. Needle valves are used to accurately replicate vascular resistance (R) while compliance chambers are used to mimic vascular compliance values (C) [2]. The Fontan MFL is driven with cardiac pulsatility provided by a Harvard Apparatus medical pump. Patient-specific models of the centerpiece of the MFL along with the grafts (IJS) are produced via 3D printing. Baseline values are validated against patient-specific waveforms. Hemodynamic parameters such as flowrate and pressure waveforms at specific points in the MFL are acquired via a National Instruments multichannel data acquisition board by using an in-house developed LabView code and then post processed by implementing a customized filtering algorithm involving both Infinite Impulse response (IIR) and Finite Impulse response (FIR) filters developed using Matlab. The best outcome was achieved with the experimental testing of a 3mm IJS by producing an average caval pressure reduction of 5.38 mmHg while maintaining the clinically acceptable ratio of pulmonary (Qp) to systemic flow rate (Qs) of 1.5. Furthermore, homeostasis effects were included in the experimental model of the pulmonary vascular resistance (PVR) by gradually reducing it between 10% and 20% from its baseline value, achieving caval pressure reduction between 6 and 7 mmHg with the 3 mm IJS at the expense of an increase in Qp/Qs ratio from 1.5 to 1.7.

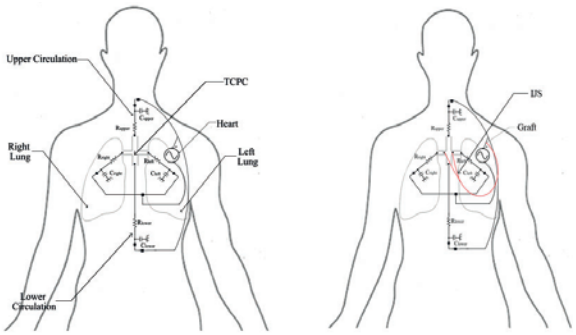

Figure 1: Lumped Parameter of Baseline and IJS model

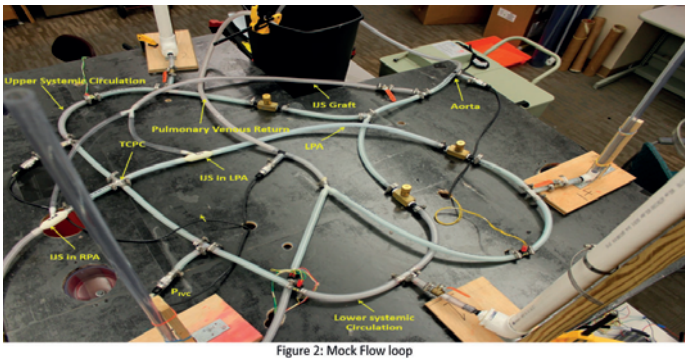

Figure 2: Mock Flow loop

Acknowledgments: This work was supported by American Heart Association (AHA) Grant-in-Aid project 15IRG22470015

References:

[1] *Petrossian, E. D., et al. "Early results of the extracardiac conduit Fontan operation." The Journal of thoracic and cardiovascular surgery 117.4 (1999): 688-696.*
[2] *Vukicevic, Marija, et al. "Mock circulatory system of the Fontan circulation to study respiration effects on venous flow behavior." ASAIO journal (American Society for Artificial Internal Organs: 1992) 59.3 (2013): 253*

[A-02.1]

TOWARD PREDICTIVE PERSONALIZED STENTING TO REDUCE RESTENOSIS AND THROMBOSIS

John LaDisa[1]

1 *Marquette University and the Medical College of Wisconsin, Milwaukee, USA*

The success of stents is limited by two poor clinical outcomes: restenosis and late stent thrombosis (LST)1. For bare metal stents (BMS), wall shear stress (WSS) influences restenosis and endothelialization that protects against LST2. However, for more common drug eluting stents (DES) it is still debated whether optimizing mechanical stimuli beyond WSS3 translates into clinical benefits relative to biological, technical and demographic factors. Our central hypothesis is that patients implanted with DES that optimize favorable mechanical stimuli and drug elution patterns experience the lowest rate of restenosis and LST. Our long-term goal is to eliminate the clinical incidence of restenosis and LST by selecting FDA-approved stents based on patient and lesion characteristics identified during the routine preoperative period. To facilitate this advancement, experimental and modeling tools must progress to the point where they can be used to identify the mechanical and biological stimuli that predict neointimal hyperplasia (NH; the primary component of restenosis) and LST after DES implantation. For example, cluster analysis from our patient-specific computational fluid dynamics results to date revealed indices of WSS that may predict sites of NH and LST. However, a paucity of material property and biological reaction data related to coronary plaques prevents our lab and others from realistically evaluating the contribution of additional DES-induced stimuli to NH and LST. This presentation will discuss progress toward our hypothesis and long-term goal made by quantifying material properties and related terms that are currently missing in the literature for atherosclerotic human coronary arteries. Topics will also include developments to our workflow for multiscale modeling after DES implantation and the use of multivariate, model-based unsupervised learning to identify which mechanical, biological, technical and patient covariates predict risk of restenosis and markers of LST.

Acknowledgments: The authors acknowledge Arash Ghorbanniahassankiadeh, Ali Aleiou, Josh Hughey, Jesse Gerringer, Mehdi Maadooliat PhD, Laura Ellwein PhD, Hiromasa Otake MD, Amirhossein Arzani PhD and David Marks MD for their collaboration and technical guidance with this research.

References:

1 *Garg S, Serruys PW. Coronary stents: Current status. JACC. 2010;56:S1-42*
2 *Hamuro M, Palmaz JC, Sprague EA, Fuss C, Luo J. Influence of stent edge angle on endothelialization in an in vitro model. J Vasc Int Rad. 2001;12:607-611*
3 *Gundert TJ et al. Optimization of cardiovascular stent design using CFD. J Biomech Eng. 2012;134:011002*

[A-02.2]

IMPACTS ON FLOW DIVERTERS ON HEMODYNAMICS OF INTRACRANIAL ANEURYSMS

Trung Le[1]

1 *North Dakota State University, Fargo, USA*

We investigate the hemodynamic impacts of flow diverters in intracranial aneurysms using both in-vitro data and computer simulations. The in-vitro condition is based on the previous work [1] where velocity and pressure measurements were carried out in an in-vitro model of a giant brain aneurysm using the state-of-the-art four dimensional Flow Magenetic Resonance Imaging. This experimental dataset serves as a base-line condition (i.e without the flow diverter implantation). This valuable dataset provides a complete description of the flow conditions in the entire domain of the aneurysmal sac at each instant in the cardiac cycle. The geometry of the aneurysm is reconstructed using the open-source software Slicer3D to create a Computer-Assisted Design model of the aneurysm. In addition, the geometries of the flow diverters is reconstructed in a mesh-like structure. First, using the provided the blood flow condition at the Internal Carotid Artery as the boundary condition, our computer software (Virtual Flow Simulator [2,3]) is applied to simulate the flow dynamics within the aneurysms without flow diverter implantation. The spatial and temporal distribution of wall shear stress (WSS) are computed from the simulation results over the aneurysm dome and are compared with the measurements. At the second step, the virtual implantation of the flow diverter is at the ostium. A second simulation with the implanted flow diverter is carried out to provide hemodynamic conditions after the implantation. We will report the differences of aneurysmal hemodynamics before and after the embolization during our presentation.

Acknowledgments: This project is supported by ND-EPSCOR project #FAR0030612

References:

[1] *Amili, O., Schiavazzi, D., Moen, S., Jagadeesan, B., Van de Moortele, P.F. and Coletti, F., 2018. Hemodynamics in a giant intracranial aneurysm characterized by in vitro 4D flow MRI. PloS one, 13(1), p.e0188323.*

[2] *Le, T.B., Borazjani, I. and Sotiropoulos, F., 2010. Pulsatile flow effects on the hemodynamics of intracranial aneurysms. Journal of biomechanical engineering, 132(11), p.111009.*

[3] *Le, T.B., Troolin, D.R., Amatya, D., Longmire, E.K. and Sotiropoulos, F., 2013. Vortex phenomena in sidewall aneurysm hemodynamics: experiment and numerical simulation. Annals of biomedical engineering, 41(10), pp.2157-2170.*

[A-02.3]

HYPERTROPHIC CARDIOMYOPATHY TREATMENT - A NUMERICAL STUDY

*Asaph Nardi[1], Michael Firer[2], **Idit Avrahami**[3]*

1 *Dep. of Chemical Engineering, Ariel University, Ariel, Israel; Ariel Biomechanics Center, Ariel, Israel*
2 *Dep. of Chemical Engineering and Biotechnology, Ariel University, Ariel, Israel*
3 *Dep. of Mechanical Engineering & Mechatronics; Ariel Biomechanics Center, Ariel, Israel*

Considered the leading cause of sudden cardiac death (SCD) in athletes, Hypertrophic Cardiomyopathy (HCM) is diagnosed in up to one of 200 people of the general population, regardless of prior medical condition. One out of every 500 members of the general population will develop related symptoms. Common treatment for HCM patients is medication, managing the symptoms. However, this treatment impairs the patient's quality of life restricting their daily activities. A common complication of HCM is Hypertrophic Obstructive Cardiomyopathy (HOCM) which develops in up to 70% of these patients. This complication is characterized by the obstructive motion of the anterior mitral leaflet causing mitral regurgitation, compromising systolic left ventricular (LV) reduced ejection fraction, and significant outflow pressure gradients (>30mmHg). Some patients who are unresponsive to medication are prone to highly invasive surgery: myectomy or ablation, exposing them to high mortality and morbidity rates, while research into gene therapy is still in its infancy. Our research is aimed at offering a new approach to the treatment of HOCM patients, utilizing a percutaneous device placed in the LV (a minimally invasive procedure) improving the systolic and diastolic movement of the LV, thus reducing the outflow pressure gradient. Percutaneous devices have been commonly used in vascular procedures such as angioplasty and stenting. Modeling the LV is done by reconstructing the ventricle according to imagery output, using computer aided design (CAD). Using the resulting CAD model we utilize computational fluid dynamics (CFD) software methods to analyze the impact of the suggested procedure on the hemodynamics of the ventricle. Analyzing the fluid structure interaction (FSI) and the structure-structure interaction, this analysis is then compared to an untreated and myectomy treated HOCM cases advising on the improvement of the current treatment and feasibility of the recommended device.

[A-02.4]

NUMERICAL STUDY OF THE CONDUIT HEMODYNAMICS ON THE DIFFERENT TYPES OF SYSTEMIC-TO-PULMONARY ARTERIAL SHUNT

Jinlong Liu[1], Qi Sun[2], Yi Qian[3], Jiwen Xiong[2], Jinfen Liu[2]

1 *Department of Cardiothoracic Surgery, Shanghai Children's Medical Center, Shanghai Jiao Tong University, Shanghai, China School of Medicine, Shanghai, China; Institute of Pediatric Translational Medicine, Shanghai Children's Medical Center, Shanghai Jiao Tong University, Shanghai, China School of Medicine; Shanghai Engineering Research Center of Virtual Reality of Structural Heart Disease, Shanghai Children's Medical Center, Shanghai Jiao Tong University, Shanghai, China School of Medicine*

2 *Department of Cardiothoracic Surgery, Shanghai Children's Medical Center, Shanghai Jiao Tong University, Shanghai, China School of Medicine, Shanghai, China*

3 *Australian School of Advanced Medicine, Macquarie University, Sydney, Australia*

Object: Different types of systemic-to-pulmonary arterial shunts are used as the palliative treatment for the first step procedure of congenital heart disease (CHD). Although the surgical techniques improved over the years, the implantation position of the conduit connected between the systemic circulation and the pulmonary artery is still one of the controversial issues. In the present study, we investigate the hemodynamic features in four types of systemic-to-pulmonary arterial shunts. Methods: A modified central shunt with a conduit of 4 mm in diameter was reconstructed based on the patient-specific medical images and the hemodynamic analysis was done by using the method of computational fluid dynamics (CFD). The technique of computer-aided design (CAD) was employed to perform the virtual procedures according to the initial vascular structures to acquire the geometric models of Modified Blalock-Taussig (mB-T) shunt, Melbourne shunt as well as central shunt with a relatively long U-shaped conduit. Pulsatile simulations were done to capture the physiological information of blood flow. Results: The local hemodynamic features in different models were demonstrated by pressure, streamlines, wall shear stress (WSS), blood flow distribution and energy loss. Relatively higher pressure drops and WSS were generated in the conduits. It may increase the risk of blood cell damage. Conclusion: The pulmonary flow distribution changed as the conduit position varied in all types of the shunts, but was more balanced in the modified B-T shunt and modified central shunt with a short conduit than that in the U-shaped central shunt and Melbourne shunt. The numerical study is a useful approach for the investigation of local hemodynamics and the evaluation of the different types of systemic-to-pulmonary arterial shunts.

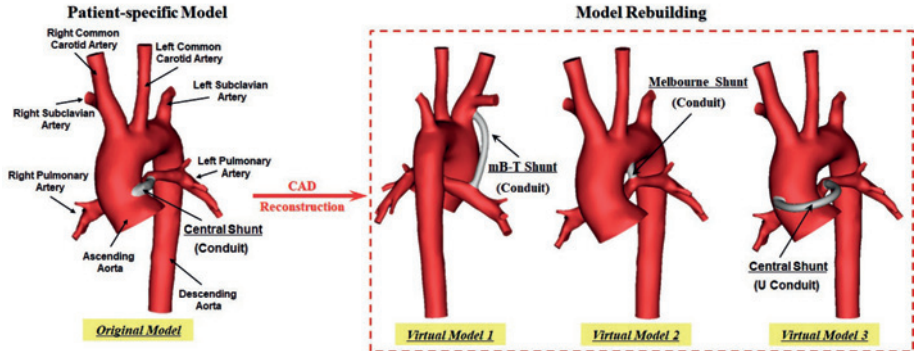

Figure Caption: Figure 1 The 3D patient-specific vascular model of the modified central shunt and its different types of virtual design

Acknowledgments: We have been genuinely appreciative of the support of the National Nature Science Foundation of China (No. 81501558, No. 81870238), the Project of Shanghai International Academic Cooperation and Exchanges (No. 18410721400), and the Fund of The Shanghai Committee of Science and Technology (No. 17DZ2253100).

References:

[1] *Blalock A, Taussig HB. The surgical treatment of malformations of the heart in which there is pulmonary stenosis or pulmonary atresia. JAMA.1945, 128:189-192.*

[2] *Qian Y, Liu JL, Itatani K, et al. Computational Hemodynamic Analysis in Congenital Heart Disease: Simulation of the Norwood Procedure, Annals of Biomedical Engineering. 2010, 38: 2302-2313.*

[3] *Liu JL, Sun Q, Qian Y, et al. Medical Image-Based Hemodynamic Analysis for Modified Blalock-Taussig Shunt, Journal of Mechanics in Medicine and Biology. 2015, 15(3):1550035.*

[4] *Kim H, Sung SC, Choi KH, et al. A central shunt of rehabilitate diminutive pulmonary arteries in patients with pulmonary atresia with ventricular septal defect. Thoracic and Cardiovascular Surgery. 2015, 149(2):515-520.*

[A-02.5]

INFLUENCE OF VENTRICULAR TORSION ON LEFT VENTRICULAR HEMODYNAMICS: A PATIENT-SPECIFIC MODEL USING THE CHIMERA TECHNIQUE

Federico Cane'[1], *gianluca de santis*[2], *alberto redaelli*[3], *patrick segers*[1], *joris degroote*[1]

1 *Ghent University, Ghent, Belgium*
2 *Feops, Ghent, Belgium*
3 *Politecnico DI Milano, Milan, Italy*

Image-based patient specific cardiovascular Computational Fluid Dynamics (CFD) models of the left ventricle (LV) can provide hemodynamics-based biomarkers beyond the capabilities of current imaging modalities, quantifying intraventricular flow and providing clinicians with additional data for early diagnosis, follow-up and treatment planning of patients. A CFD modelling pipeline [1], based on 3D ultrasound and on an Arbitrary Lagrangian Eulerian approach, struggled with numerical convergence issues mainly due to the complex kinematics of both LV endocardium and Mitral Valve (MV) leaflets, leading to mesh-related problems. In this context, we developed a more robust workflow to build patient-specific CFD models of the LV based on the Chimera technique, which is still relatively unemployed within the biofluids community. As an application, we investigated whether torsional motion has an impact on the LV fluid dynamics. We developed a subject-specific LV model from 3D MRI scans and compared three CFD cases where we imposed LV motion (i) without any torsion (no Torsion), (ii) with physiological torsional motion (Torsion X1) and (iii) with torsion multiplied by a factor 2 (Torsion X2). Six cardiac cycles were simulated. Firstly, we observed an important cycle-to-cycle variation in every simulated case (with results shown for the Torsion X1 in Figure 1). Secondly, torsion leads to only minor differences in the spatial distribution and maximum values of velocity and vorticity (Figure 2A, 2B), with the main differences located in the medial plane (SA2). Third, the percentage of the particles staying more than 2 cardiac cycles is 11.4%,17.9%,15.6% in the no Torsion, Torsion X1, Torsion X2 cases, respectively. We conclude that the chimera technique proved robust in setting up a subject-specific CFD model of the LV. Torsion does not seem to have a major impact on wall shear stress or on vorticity. The impact of torsion on RT is somewhat larger and unexpected, but caution is warranted given the physical absence of the mitral valve (MV), the papillary muscles and the trabeculae. The effects of the MV will be evaluated within a FSI simulation framework as further development of the current model.

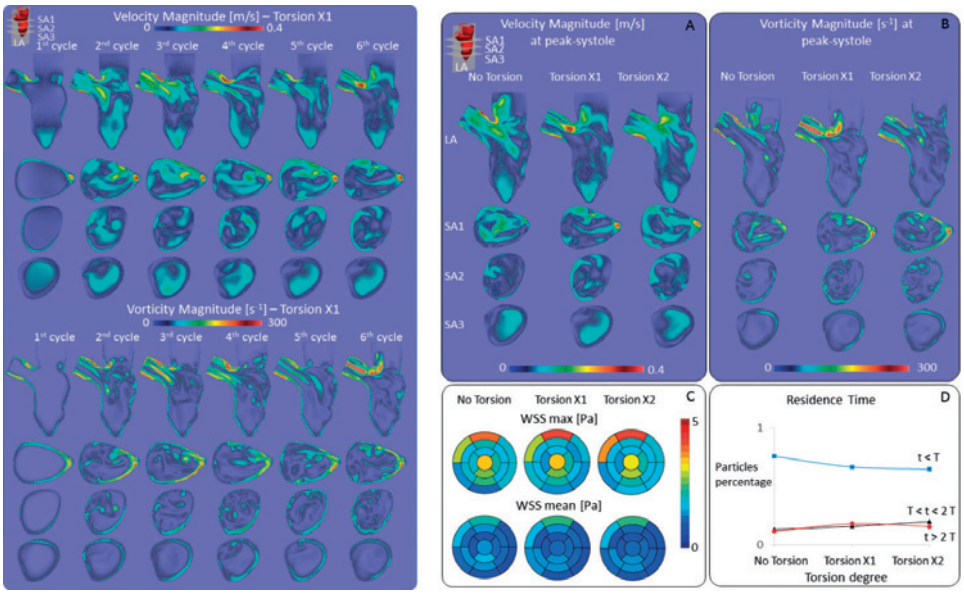

Figure Caption: (1) Cycle-to-cycle variation of velocity and vorticity magnitude during end systole in the Torsion X1 case; (2) Investigated variables to evaluate the impact of torsion in the 3 simulated cases.SA: short axis; LA: long axis.

Acknowledgments: H2020 European Commission MSCA-ITN-ETN Training Networks (project 642458).

References:

[1] *Bavo, A et al., J Biomech, 50:144-150, 2017.*

[A-02.6]

NUMERICAL SIMULATIONS OF BLOOD FLOW PATTERNS IN THE PATIENT-SPECIFIC LEFT VENTRICLE MODEL WITH DYNAMIC MITRAL AND AORTIC VALVES

Fei Xu[1], *Sasa Kenjeres*[1]

1 *Delft University of Technology, Delft, Netherlands*

Keywords: Computational fluid dynamics (CFD), left ventricle, vortex structure, Direct Numerical Simulation (DNS), Large Eddy Simulation (LES), Detached Eddy Simulation (DES)

The left ventricle is one of the chambers in the human heart. It is connected with the aorta by the aortic valve and the left atrium by the mitral valve. The left ventricle is responsible for pumping the blood through the aortic valve into aorta and then to the whole body. Hence it is the most important heart chamber. Besides, in the left ventricle the blood flow has the most complex pattern and pressure variation during cardiac cycles.

The current work aims at providing a credible and cost-effective image (CT and/or MRI) based numerical simulations of the flow patterns and pressure within a patient-specific human left ventricle with bioprosthetic mitral and aortic valves. An image based simulation technique has been developed for the blood flow simulation in realistic patient-specific ventricles.

The series of images and basic geometry data are received from collaborative Magnetic Resonance Imaging (MRI) and Particle Imaging Velocimetry (PIV) measurements. The processed data from the mesurements provides the main input for defining motion of the left ventricle and the valves during a cardiac cycle. Based on the dynamics of the ventricle and valves the RBF (radial basis functions) method is implemented to morph the computational mesh according to the motion of the left ventricle as well as the valves.

The numerically calculated velocity components and the vortex structure have been compared with available PIV as well as MRI measurements at characteristic time instants during a cardiac cycle. Obtained results are in a good agreement with experimental data, confirming validity of the most fundamental direct numerical simulation (DNS) approach. Furthermore, the vorticity as well as the velocity components have been compared between DNS different simulation approaches based on a numerical resolving of the most energetic flow modes only (i.e. Large Eddy and Detached Eddy Simulation, LES and DES, respectively) at specific locations. Additionally, the energy spectra of the velocity time series at characteristic monitoring locations within the left ventricle have been analyzed to identify the turbulent/laminar regions in the flow field.

In conclusion, the obtained results provided detailed insights into energetics of the instantaneous flow features of the left ventricle model. The presented method can be applied for future analysis of the practical clinical conditions for the patient-specific geometries.

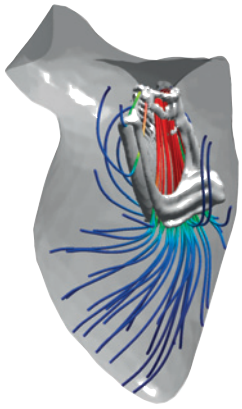

Figure Caption: The vortex structure and the streamlines in a left ventricle model during diastole.

[A-03.1]
MULTISCALE MODELING OF THROMBUS FORMATION

George Karniadakis[1]

1 *Brown University, Providence, USA*

Multiscale modeling of thrombus formation: I will present methods for atomistc-continuum coupling

That enable multi-fidelity modeling of the multiscale processes taking place in thrombus formation and in the early stages. Specifically, we use dissipative particle dynamics, force coupling methods and phase field methods to bridge different time and spatial scales involved in the thrombus formation process.

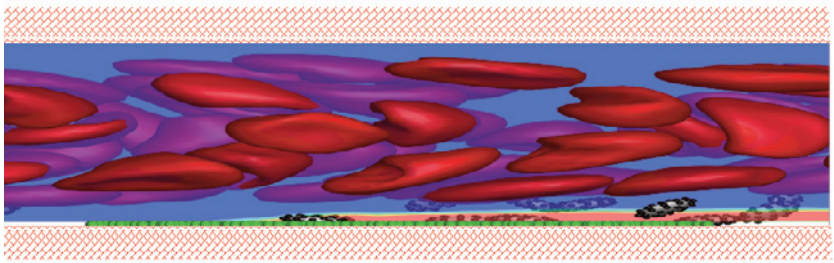

Figure Caption: Multiscale simulation of platelet aggregation.

Acknowledgments: NIH grant U01 HL116323.

[A-03.2]

MULTISCALE MODELING OF BLOOD FLOW AND PLATELET MEDIATED THROMBOSIS

Danny Bluestein[1], *Peng Zhang*[2], *Jawaad Sheriff*[2], *Prachi Gupta*[2], *Yuefan Deng*[2]

1 *PolyNova Cardiovascular, Inc., Stony Brook, USA; Stony Brook University, Stony Brook, USA*
2 *Stony Brook University, Stony Brook, USA*

We developed multiscale particle-based methods, incorporating dissipative particle dynamics (DPD) and coarse-grained molecular dynamics (CGMD), to describe blood flow in cardiovascular pathologies and ensuing mechanotransduction events that may induce initiation of thrombosis via flow-induced platelet activation[1-5]. Our multiscale model (MSM) covers the vast range of spatio-temporal scales required to describe the complex phenomena of flow-induced thrombosis, bypassing inherent limitations of continuum-based methods. Our model is tightly integrated with extensive in vitro measurements of platelet shape change[1], mechanical properties[4], and motion under flow[3]. Our improved model now describes platelet recruitment in early shear-induced aggregation.

Our MSM model, which describes the nanoscale mechanotransduction and biophysics of two deformable platelets under viscous blood flow[3], was adapted for recruitment aggregation simulations of marginated platelets. Simulations were validated with in vitro microchannel experiments using gel-filtered platelets obtained from consenting adult subjects under an IRB-approved protocol. Images, recorded at 200 fps on a DIC microscope (Nikon Ti-Eclipse), were analyzed to obtain platelet geometric parameters, meshed and integrated to determine contact area, and input into a neural network machine learning-based model to predict inter-platelet contact area (Fig. 1B). Our previous multiple time-stepping (MTS) scheme2,5 was improved by using reinforcement learning-based adaptive time stepping (ATS) to intelligently adapt to platelet dynamics (Fig. 1C).

We simulated the recruitment process of marginated platelets and initiation of platelet aggregation (Fig. 1A). A molecular-level hybrid force field was constructed to mimic tbinding of GPIIb-IIIa and fibrinogen during platelet recruitment. This force field was parametrized for reproducing morphologic characteristics as contact area at aggregation. We observed that a rigid platelet model significantly underestimated the contact area of aggregated platelets, compared to deformable platelets. The contact area measured in vitro increased from 1.59 to 2.00 μm^2, while platelet surface area increased slightly (21.56 to 21.89 μm^2), as shear stress increased from 1 to 10 dyne/cm^2. Numerically simulated contact areas correlated well with in vitro measurements in this shear stress range. The platelet-platelet rupture force of our simulated aggregation is measured as 15.6 nN, which correlates well with in vitro measurements (8.1-16.2 nN), given the debonding force for a single GPIIb-IIIa-fibrinogen bond[8] and that 10% of GPIIb-IIIa membrane receptors are capable of binding fibrinogen[9].

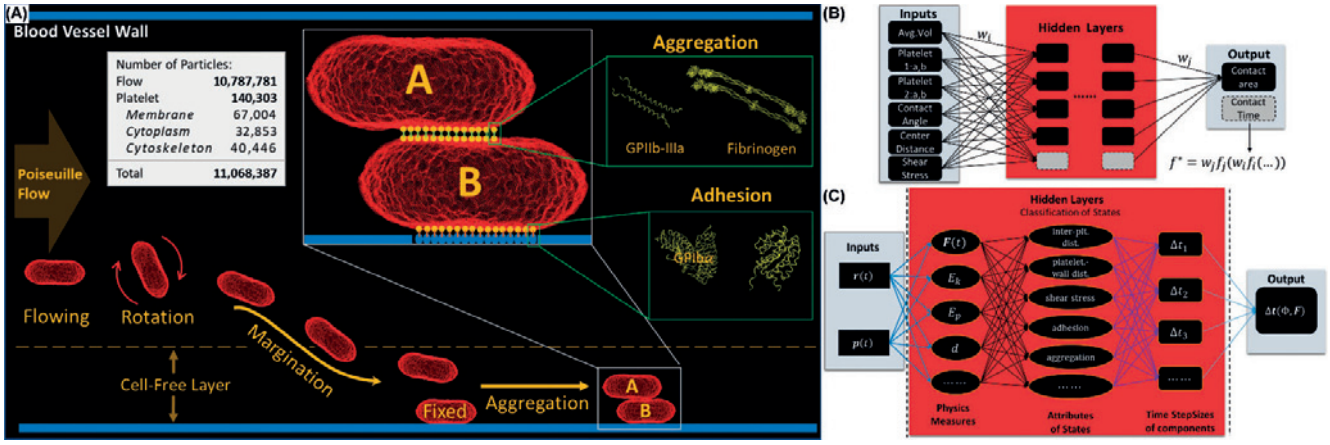

Figure 1. (A) Recruitment of marginated platelets and initiation of platelet aggregation. (B) Neural network for predicting contact area during aggregation. (C) MSM adaptive time stepping reinforcement learning framework.

Conclusions: Our multiscale numerical approach offers a computationally affordable, highly resolved, and validated method for modeling platelet activation, aggregation, and adhesion in flow. Biophysical properties of deformable platelets are accurately described down to the nanoscale, with hemodynamic stresses mapped on membrane and intra-platelet components. Ongoing simulations and experiments incorporate GPIIbIIIa-vWF for aggregation, and GPIb-vWF for adhesion, at high shear stresses. We utilize MSM to analyze impact of clinically relevant shear generated via a range of devices and pathologies to predict cellular response driving thrombosis.

Acknowledgements: This project was funded by the National Institutes of Health (NIBIB U01 HL131052, NHLBI-R21 HL096930-01, NHLBI U01 EB012487).

References:

[1] *Pothapragada, S., et al, Int J Numer Meth Biomed Engng, 2015.*
[2] *Zhang, N. et al, J Comput Phys, 2014.*
[3] *Zhang, P., et al, J Biomech, 2017.*
[4] *Zhang, P., et al, Cell Mol Bioeng, 2014.*
[5] *Zhang, P., et al, Comput Phys Commun, 2016.*
[6] *Litvinov, R., et al, J Biol Chem, 2016.*
[7] *Smyth, S., et al, Biochem J. 1993.*

[A-03.3]

MULTI-SCALE INVESTIGATION OF CELLULAR FLOW CONDITIONS AT THE INITIAL STAGE OF THROMBUS FORMATION

Gabor Zavodszky[1], *Britt van Rooij*[1], *Alfons Hoekstra*[2]

1 *University of Amsterdam, Amsterdam, Netherlands*
2 *University of Amsterdam, Amsterdam, Netherlands; Itmo, St. Petersburg, Russia*

Platelet aggregate formation is part of the primary hemostasis, which is one of our essential defensive mechanisms to prevent blood loss in case of a vascular injury. In high shear-rate cases, this mechanism is initiated by an ultralarge protein, the von Willebrand Factor (vWF). In this work, we study the conditions appearing at the initial platelet aggregation in a high shear rate environment. For a successful plug formation, the first important component is the availability of platelets at the site of the formation. This is a function of the complex trafficking and margination of platelets inside the dense suspension of red blood cells. The second component is the presence of vWFs in the proper conformation. They have to be uncoiled and activated in order to be able to catch and bind the platelets from the fast flow stream. This in turn depends on the local flow environment, i.e. the appearance of high shear rates or elongational flow patterns.

We perform large-scale simulations using our validated HemoCell framework[1] with two major aims. Firstly, to evaluate the trafficking and margination trajectories of platelets under various flow conditions and hematocrit levels, which helps to quantify the intensity of margination and assess the local availability of platelets. Secondly, to acquire accurate shear rates and shear stresses in the vicinity of the aggregate formation. This requires a cellular flow representation as the presence of cells changes the flow profile and creates higher shear-rates at the wall. Furthermore, cell collisions can introduce an effective environment for protein elongation [2].

In addition, we couple cellular simulations to modelled vWF chains to compute the tension forces in the chains appearing in various cellular flow scenarios. In these simulations, vWFs are represented as chains of cylindrical monomers. The mechanical model of these chains is validated using existing experimental data on vWF uncoiling in free-flow[3] and while grafted[4].

We found that in high shear rate cases the local margination intensity of platelets is strongly linked to the gradient of the hematocrit level across the flow channel. What is more, cells cause fluctuation in the local fluid shear stress that can uncoil large chains (50+ monomers) even in case of shear rates below 5000 s^-1.

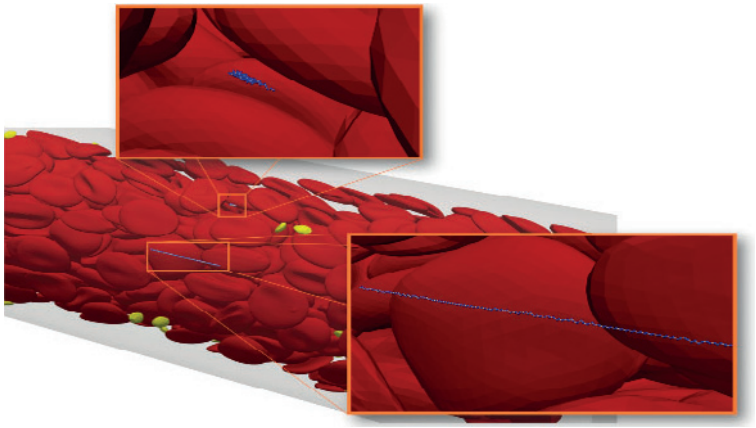

Figure Caption: Visualization of two vWF chains of 187 monomers in cellular flow in two different conformations.

References:

[1] Závodszky et al., Frontiers in Physiology, 2017
[2] de Haan et al., Applied Sciences, 2018
[3] Schneider et al., PNAS, 2007
[4] Fu et al., Nature Communications, 2017

[A-03.4]

COMPUTATIONAL FLUID DYNAMICS WITH SOLUTE TRANSPORT IN FEBIO

Jay Shim[1], *Steve Maas*[2], *Jeffrey Weiss*[2], *Gerard Ateshian*[1]

1 *Columbia University, New York, USA*
2 *University of Utah, Salt Lake City, USA*

A novel framework for computational fluid dynamics (CFD) with solute transport was implemented in FEBio, a free, open-source finite element software specialized for biomechanical applications.[1] Modeling solute transport and chemical reactions in fluids is becoming increasingly necessary in different areas of biomechanics, including cardiovascular mechanics, cellular mechanics, and mechanobiology, among many others, but most modeling tools are not well suited for these applications. Traditionally, the convection-diffusion equation is used as a governing equation. However it suffers from poor numerical convergence when the problem is convection dominated. To remedy this issue, stabilization methods such as streamline upwind Petrov-Galerkin and characteristic methods are utilized[2,3] Recently, as CFD models also suffer from the same problem, a new CFD solver was formulated in FEBio that did not require stabilization methods, modeling the fluid as slightly compressible with a realistic bulk modulus and employing the fluid dilatation as a nodal degree of freedom.[4] The same approach was utilized here with solutes to ensure good convergence. Solutes are incorporated using the framework of mixture theory, which was previously used in FEBio for multiphasic domains.[5]

The FEBio CFD solute solver can currently support multiple neutral solutes with a nearly incompressible, isothermal, and viscous fluid solvent. The degrees of freedom employed are the fluid velocity, fluid dilatation, and the concentration of each solute species. The virtual work equation enforces the momentum balance of the fluid, the kinematic constraint between the fluid velocity and dilatation, and the mass balance of the solutes, where the integrated fluid mass balance relates fluid dilatation with its density. The virtual work equation is then linearized, discretized, and solved using Newton's method. For consistency, all material time derivatives were formulated to follow the fluid. Constitutive models are needed for the fluid properties and the solute diffusivity. Figure 1 shows the cross-section of a 3D example of a solute flowing through a bifurcated carotid artery at different times. The model prescribes an inlet velocity and outlet pressure resistance with properties detailed previously.6 For the solute, a concentration of 0.01 mol/m^3 is prescribed at the inlet with a realistic constant diffusivity of 10-9 m^2/s. The solution showed good convergence even though the Peclet number was on the order of 107. This CFD solute solver greatly expands the modeling capabilities of FEBio and it will be extended to include charged solutes, osmotic effects, and chemical reactions. Eventually, interactions between the solvent-solute mixture and multiphasic domains will be allowed where fluid flow and solute transport are continuous between the two, which will lead to even more general and versatile biomechanical models.

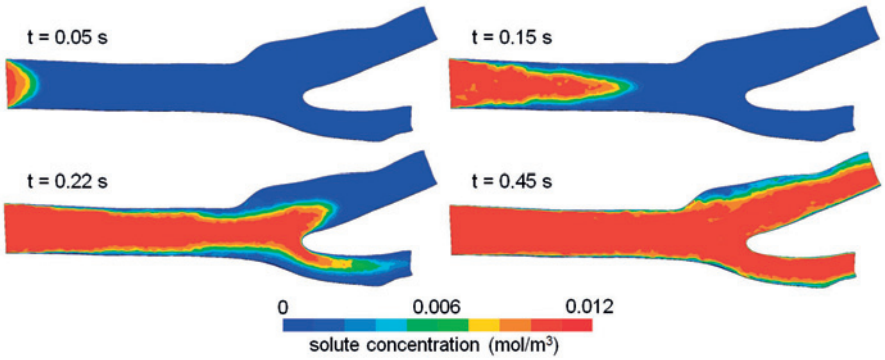

Figure 1: Solute concentration within a bifurcated carotid artery at selected time points.

Acknowledgments: National Science Foundation (Grant No. NSF GRFP DGE-16-44869).

References:

[1] Maas SA et al., Annu Rev Biomed Eng, 19:279-99, 2017.
[2] Brooks AN et al., CMAME, 32(1-3):199-259, 1982.
[3] Kaazempur-Mofrad MR et al., CMAME, 192(11-12):1281-98, 2003.
[4] Ateshian GA et al., J Biomech Eng, 140(2):0210011-02100117, 2018.
[5] Ateshian GA et al., J Biomech Eng, 135(11):1110011-11100111, 2013.
[6] Shim JJ et al., J Biomech Eng, In Press.

[A-03.5]

COMPUTATIONAL MODELING OF BLOOD COMPONENT TRANSPORT RELATED TO CORONARY ARTERY THROMBOSIS IN KAWASAKI DISEASE PATIENTS

Noelia Grande Gutierrez[1], *Mark Alber*[2], *Alison Marsden*[1]

1 *Stanford University, Stanford, USA*
2 *University of California, Riverside, USA*

Computational studies aiming to model thrombosis often rely on an arterial wall injury that exposes collagen and other extra-cellular matrix components to the bloodstream, which facilitates platelet adhesion to the wall and subsequent clot formation. However, these models are not adequate to explain thrombosis in other settings where even in the absence of wall injury blood clots may still form under certain flow conditions in the veins as well as the arteries. Experimental data suggests the role of hemodynamics in thrombus initiation and growth is two-fold: shear forces can contribute to platelet activation and flow stagnation facilitates platelet aggregation, thus thrombus formation and growth [1]. In addition, platelets can be activated by either mechanical (shear induced activation) or biochemical stimuli, which suggest different potential targets for thromboprophylaxis [2]. We present a new model that incorporates information from a patient-specific simulated velocity field to track platelet activation and accumulation in Kawasaki disease coronary artery aneurysms.

We used a Reaction-Advection-Diffusion (RAD) equations stabilized finite element solver to compute the evolution of non-activated platelets and activated platelet concentrations [AP], local concentrations of Adenosine Diphosphate (ADP), a platelet agonist, and Thrombin. Activation of platelets is modeled as a function of shear-rate exposure, local concentration of activated platelets and Thrombin. Activation rates were set to literature values [3]. We compared the distribution of activated platelets in a healthy right coronary artery vs. two cases with coronary artery aneurysms caused by Kawasaki disease, one with confirmed thrombosis. Figure 1 shows the distribution of [AP] in the three coronary artery models. In the case b2, thrombus was still visible on the CMRI images; results show spatial correlation between regions of higher [AP] and the location of the thrombus. The concentration of activated platelets in the aneurysmal regions reached values substantially higher than in the healthy case where [AP] remained close to the initial value for the simulation, which assumed a 5% level of platelet activation. Levels of [AP] were above the initial concentration of non-activated plates (10nM/l) at the specific location were thrombus developed. We also compared the different contributions to platelet activation and we observed that in regions of flow stagnation, the dominant reaction term represented the contribution due to local [AP].

This study provides a new framework to investigate thrombus initiation from a patient specific perspective, which could help identify regions at higher risk of thrombosis as well as the best strategies for thrombosis prevention that target the appropriate pathways. Future work will expand this application to larger patient cohorts.

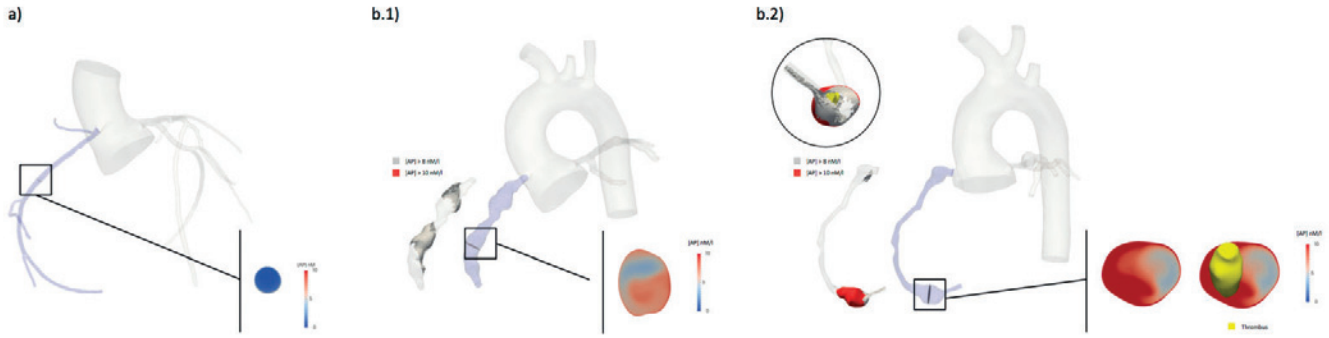

Figure Caption: Comparison of activated platelet concentration distribution averaged over one cardiac cycle in three Kawasaki disease patients a) normal right coronary artery, b1) right coronary artery with proximal and medial aneurysms, highest accumulation of activated platelets is observed only near the wall, b2) right coronary artery with proximal and distal aneurysms, confirmed thrombus location at distal aneurysm, highest accumulation of activated platelets is observed at the wall and also within the vessel lumen. High concentration of activated platelets in the aneurysm lumen corresponds to location of the thrombus extracted using CMRI image segmentation.

References:

[1] *Bluestein et al. (1996)*
[2] *Fogelson and Neeves (2015)*
[3] *Kuharsky and Fogelson (2001)*

[A-03.6]

EXPERIMENTS AND MODELS OF VENOUS THROMBUS EVOLUTION & DAMAGE

Manuel Rausch[1], *Jay Humphrey*[2]

1 *University of Texas at Austin, Austin, USA*

2 *Yale University, New Haven, USA; Department of Biomedical Engineering; Yale University, New Haven, USA*

Thrombus plays a diametrical role in our bodies. On the one hand, thrombus is vital as it prevents excessive bleeding after vascular injury. On the other hand, thrombus is responsible for many devastating diseases such as stroke, heart attack, and deep vein thrombosis. Thrombus mechanical properties play a critical role in its interaction with our body and are critical for its fate including its pathophysiology. For instance, thrombus occluding the deep veins of our extremities may fracture and dislodge when subjected to forces. Once dislodged, thrombus may travel downstream and occlude our pulmonary arteries, leading to hypoxia and death. Thus, thrombus damage behavior determines its likelihood of embolization and its risk potential. Surprisingly, relatively little is known about thrombus mechanics. This is particularly true for venous thrombus mechanics, i.e., thrombus formed in the venous circulation. The goal of our work is to fill some of the existing gaps and to characterize venous thrombus mechanics, including its damage mechanics and to cast venous thrombus mechanical behavior into an appropriate constitutive model. To this end, we study repeated uniaxial tensile loading data on venous thrombus samples from mice [1]. Specifically, our data is based on 2-week-old thrombus that was created via venous ligation. Upon explantation, those thrombus samples were glued to the tips of glass pipettes and displacement cyclically, consecutively to 1g, 2g, 3g etc. up to 10g. Those data showed not only the classic J-shaped stress-stretch behavior of most fibrous soft tissues, but also hysteresis, and a distinct damage pattern resembling Mullin's effect. Based on experimental observation, we formulate a microstructurally-inspired hyperelastic constitutive model that considers fiber uncrimping during loading. Additionally, we endow this model with a novel damage mechanism that accounts for changes in the reference configuration of the distributed fibers as thrombus undergoes damage. We also compare our microstructurally-based approach to two classic continuum damage approaches, those by Simo and by Ogden. We find that for venous thrombus data, our approach performs superiorly, while requiring fewer material parameters than those alternative models [2]. Moving forward, we hope to develop a model that also accounts for changes in thrombus microstructural composition as it evolves from a fibrin dominated material immediately after formation to a collagen dominated material after weeks and months of residing in the venous vasculature [3]."

References:

[1] Y-U Lee, AY Lee, Humphrey JD, Rausch MK. Histological and biomechanical changes in a mouse model of venous thrombus remodeling. Biorheology, 2015; 52:235-245.

[2] Rausch MK, Humphrey JD. A microstructurally inspired damage model for early thrombus. Journal of the Mechanical Behavior of Biomedical Materials, 2015; 55:12-20.

[3] Rausch MK, Humphrey JD. A computational model of the biochemomechanics of evolving occlusive thrombus. Journal of Elasticity, 2017; 129: 125-144."

[A-04.1]

COMPUTATIONAL TOOLS FOR IN-SILICO TRIALS OF MECHANICAL THROMBECTOMY

Kevin Moerman[1], *Behrooz Fereidoonnezhad*[2], *Patrick McGarry*[2]

1 *Massachusetts Institute of Technology, Cambridge, USA; National University of Ireland, Galway, Ireland*
2 *National University of Ireland, Galway, Ireland*

Acute ischemic stroke is a major cause of death worldwide. Mechanical thrombectomy (MT) is a surgical procedure to remove clots using a catheter guided device. The success of the procedure depends on many factors, including the geometry and mechanical properties of the clot and the local vasculature. Since rapid intervention is required following the onset of stroke, there is little time for detailed investigations. Computational models on the other hand offer detailed information and enable iterative investigation of device and procedure variations. The purpose of this study is to create computational tools for in-silico trials of the MT procedure. Here we present two such tools: 1) a method for the generation of subject-specific and population based geometries of the intra-cranial vasculature, and 2) a framework for finite element analysis (FEA) of clot occlusion prediction. Fig.1A shows the performance of two geometry creation algorithms, the top image is for a method relying in levelset descriptions, and produces an unstructured mesh, the bottom image is for a method relying of mesh lofting, and produces a structured mesh. Fig.1B presents the successful application of these methods to cranial MRI data of a human subject. Fig.1C presents FEA simulation of blood clot occlusion. The occlusion location, is seen to vary as mechanical conditions (such friction, and the effective shear and bulk modulus) are altered. Novel methods are presented here for the creation of unstructured and quasi-structured meshes for vascular geometries. The input for these methods may be vessel center lines, and local tortuosity and radii. Statistical population data on such metrics can be used to expand these methods to create not only subject-specific geometries but also custom simulated population models required for in-silico trials. The FEA of clot occlusion can be performed for a set of population models allowing for the analysis of risk factors in terms of vasculature and clot geometry and mechanical behavior.

Figure 1: Levelset (top A) and mesh lofting (bottom A) based vessel geometry creation, application to cranial vasculature reconstruction (B), and FEA based occlusion site prediction.

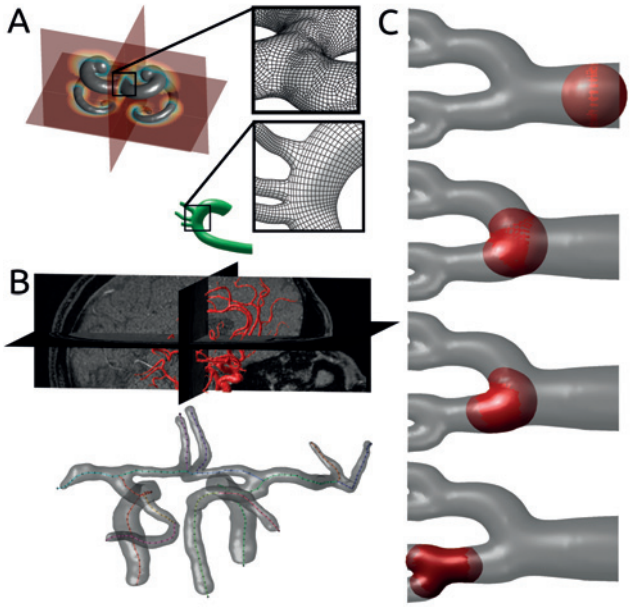

Acknowledgments: Study partially funded by EU Horizon 2020 grant 777072 INSIST.

References:

[1] *Maas et al., J.Biomech.Eng., vol. 134, no. 1, 2012.*
[2] *Moerman et al., J.Mech.Behav.Biomed.Mat., vol. 56, 2016.,*
[3] *Moerman et al., Journal of Open Source Software, vol. 3, no. 22, 2018.*

[A-04.2]

ROLE OF FIBRIN FIBERS ON THE FRACTURE PROPERTIES OF THROMBUS

Behrooz Fereidoonnezhad[1], ***Kevin Moerman***[2], *Patrick McGarry*[1]

1 *National University of Ireland, Galway, Ireland*

2 *Massachusetts Institute of Technology, Cambridge, USA; National University of Ireland, Galway, Ireland*

Thrombus material is a critically important diseased tissue component associated with acute ischemic stroke and a range of vascular disease conditions, such as myocardial infarction, atherosclerosis and deep vein thrombosis. A thrombus, or blood clot, consists of a network of fibrin, platelets and other blood components [1]. Fibrin fibers are observed to be randomly aligned throughout a blood clot. However, if the clot is subjected to large deformation, as occurs during thrombectomy procedures, fibers may become aligned, resulting in the development of anisotropic material behavior. In terms of the fracture toughness of blood clots, fiber alignment can potentially act as a toughness enhancing mechanism. Therefore, the ability of fibrin fibers to align must be considered in the development of a constitutive modeling for blood clots. Modelling of blood clots as an isotropic material may result in significant under-prediction of the fracture resistance. This will result in incorrect predictions of clot fragmentation during thrombectomy procedures. In the current study we perform a series of fracture tests on compact tension shaped clot specimens. Fibrin rich and fibrin free clots are considered. Figure 1 (A-C) illustrates typical results for a contracted clot with 20% red blood cells and shows that a high level of deformation is required for crack growth. This demonstrates the high toughness for these types of clots. A finite element framework is developed to simulate these fracture tests. We propose a hyperelastic constitutive model for thrombus material that includes fibrin alignment. The model is implemented in the finite element software Abaqus via user defined material subroutine (UMAT) where a discrete fiber dispersion approach is employed to represent asymmetry of fiber stress in tension and compression. [2]. Results suggest that significant fiber alignment occurs at the crack tip, as shown in Figure 1(D,E). This results in a significant increase in fracture toughness compared to clots that do not contain fibrin fibers. The model is then used to simulate clot fracture during aspiration into a catheter during a thrombectomy procedure, as shown in Figure 1F.

Clot fragmentation during mechanical thrombectomy is of significant clinical concern as it may cause distal embolization, incomplete microvascular reperfusion, and infarction. The computation prediction of clot fracture as a function of clot composition can potentially guide the design of thrombectomy and aspiration devices, resulting in reduced risk of fragmentation.

Figure 1: Typical results for fracture test of a contracted clot with 20% red blood cells (A-C), fibre alignment around crack tip in computational model (D,E) and computational result of clot fracture during aspiration into a catheter during a thrombectomy procedure (F).

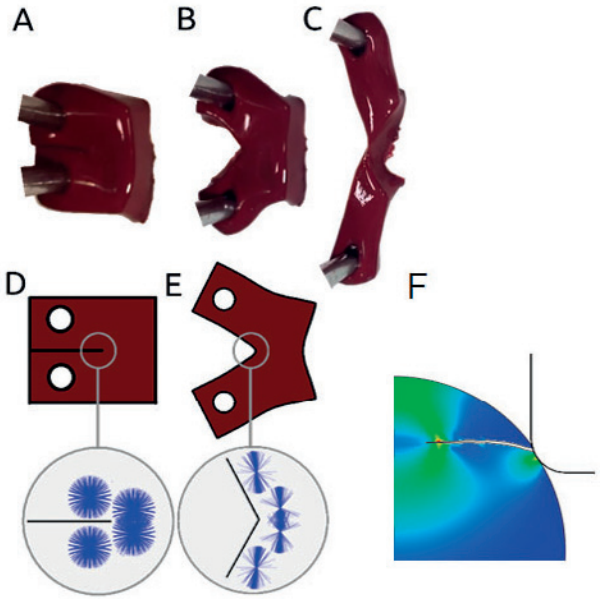

Acknowledgments: This project was funded by a European Union Horizon 2020 Research and Innovation Program, under grant agreement No. 777072.

References:

[1] *Johnson, S., et al. "Review of Mechanical Testing and Modelling of Thrombus Material for Vascular Implant and Device Design." Annals of biomedical engineering 45.11 (2017): 2494-2508.*

[2] *McEvoy, et al. "Compressibility and Anisotropy of the Ventricular Myocardium: Experimental Analysis and Microstructural Modeling." Journal of Biomechanical Engineering 140.8 (2018): 081004.*

[A-04.3]

COMMON GEOMETRIC FEATURES CAN INTERACT SYNERGISTICALLY TO GENERATE HIGH FREQUENCY OSCILLATIONS IN CEREBRAL VASCULATURE FLOWS

Michael Durka[1], *Hessam Babaee*[1], *Anne Robertson*[2]

1 *Swanson School of Engineering University of Pittsburgh, Pittsburgh, USA*
2 *University of Pittsburgh, Pittsburgh, USA*

Introduction: Many investigations of blood flow within cerebral aneurysms have assumed purely laminar flow [1]. High-resolution numerical approaches have detected high-frequency velocity oscillations (HFVOs) within the cerebral vasculature [2,3] and conjectured that HFVOs could impact endothelial biology and hence aneurysm pathology [4]. The present numerical study revisits this topic with the aim to identify geometric conditions that produce HFVOs. The impact of HFVOs on time averaged wall shear stress (WSS) is analyzed by comparing results from studies of different resolution.

Methods: The current study reconsiders a computational study reporting HFVOs in complex internal carotid artery geometry (Case0002) [2]. Here, we introduce idealized models and systematically identify geometric characteristics of the vasculature responsible for HFVO production. The hp-spectral elements solver Nektar with fourth-order elements [5] was used to obtain the flow field and results were compared to solutions obtained using finite-volume solver Ansys CFX. CFX was then used to solve for flow in a non-idealized model of Case0002.

Results: When a constriction greater than 50% was introduced in a straight segment model, HFVOs were generated and intensified with downstream distance. Neither a sudden expansion nor a small radius of curvature independently initiated HFVOs; though when combined they synergized to produce HFVOs. Using spatial resolution of 0.075mm and maximum CFL number of 0.25, Ansys CFX was capable of capturing HFVO in the full Case0002 model. HVOs were seen to initiate after a highly-curved segment preceding a rapid expansion. A coarser 0.15mm resolution mesh with maximum CFL number 20 displayed a solution without HVOs. Additionally, HFVOs had minimal qualitative impact on time-averaged or systolic WSS magnitude.

Discussion/Conclusion: In the idealized models, HFVOs were initiated simply by a constriction or expansion when they were more severe than in Case0002. However, the synergistic effects of combining curvature and expansion found in Case0002 could generate HFVOs in less severe constrictions. These results suggest a series of less-pronounced geometric perturbations (e.g. curvature, constriction, expansion) are capable of HFVO generation in the absence of a sufficiently severe single geometric factor. However, HFVOs minimally impact the time averaged WSS distribution, showing little difference compared to a lower-resolution solution. Therefore, at least in some geometries, if HFVOs impact endothelial biology, they may do so through mechanisms other than the high and low WSS-based mechanisms that are commonly studied.

Acknowledgements: Research reported in this work was supported by the National Institutes of Health under award number 1R01NS097457-01.

References

[1] Xiang, J et al. J Biomech 47:3882–3890, 2014
[2] Valen-Sendstad, K et al., J Biomech, 47:3210-3216, 2014
[3] Baek, H et al., Ann Biomed Eng 36:1496–1514, 2008
[4] Davies, PF et al., Proc. Natl. Acad. Sci. USA. 83:2114-2117, 1986
[5] Karniadakis, GE et al, NY: Oxford University Press, 2005

[A-04.4]

QUANTIFYING TRANSIENT FLOW PATTERNS IN PATIENT-SPECIFIC SIMULATIONS

Simona Hodis[1]

1 *Texas A&M University, Kingsville, USA*

Introduction: Robust quantification of complex and transient patterns of blood flow inside brain aneurysms is needed in assessing the likelihood rupture of aneurysms and treat only those that are at a higher risk to rupture, therefore avoiding unnecessary risks to the patient.

Transient and turbulent-like flow patterns of intra-aneurysmal blood flow make the hemodynamic quantification more challenging. Time-averaged analysis of the hemodynamic parameters washes out the intra-cycle variations, while discrete time points examination provides limited information about flow instabilities. Currently, here is no consensus in the literature on how to robustly quantify such turbulent-like flows.

Methods: We introduced a kinematic parameter that quantifies the complexity of flow patterns in steady cases, based on the calculated curvature and torsion of the velocity field [1] and recently, we generated an analytic solution of the flow complexity parameter [2] in order to facilitate its implementation in the current software used to solve fluid dynamics problems. The advantages of this kinematic parameter are multiple: is a local parameter calculated at each grid point of the computational mesh, requires only the velocity vector field without generating flow lines or delineating control regions, and provides the element size distribution of an adaptive grid based on the complexity of the vector field. The current flow complexity parameter is suitable for steady states, but requires intensive post-processing time to extract the complexity of the flow at different time points in transient cases. The purpose of the current study was to extend the applicability of the flow complexity parameter to the transient and turbulent-like flow cases.

We proposed to use our steady state flow complexity parameter together with the frequency-based operator developed by Khan in [3], which was demonstrated to detect and quantify the high-frequency instabilities on surface and volume-averaged parameters. We demonstrated the efficacy of the local flow complexity parameter in transient cases using the frequency-based operator.

Results and Conclusion: We have quantified the complex patterns of the intra-aneurysmal blood flow that are changing during the cardiac cycle in a way that allows for easy and robust spatial and temporal analysis of aneurysm hemodynamics.

References:

1. *S Hodis, 2018. Correlation of flow complexity parameter with aneurysm rupture status, International Journal for Numerical Methods in Biomedical Engineering, Nov; 34(11): e3131.*
2. *S. Hodis, D.F. Kallmes and D. Dragomir-Daescu, 2013. Adaptive grid generation in a patient-specific cerebral aneurysm, Physical Review E 88, 052720.*
3. *OM. O. Khan, C. Chnafa, D. Gallo et al, 2017. On the quantification and visualization of transient periodic instabilities in pulsatile flows, Journal of Biomechanics 52, 179-182.*

[A-04.5]

ILLUSTRATION-INSPIRED TECHNIQUES FOR VISUALIZING 4D BLOOD FLOW DYNAMICS

Thangam Natarajan[1], *Daniel MacDonald*[1], *Peter Coppin*[2], *David Steinman*[1]

1 *Biomedical Simulation Lab, University of Toronto, Toronto, Canada*
2 *Perceptual Artifacts Lab, Ocad University, Toronto, Canada*

Recent research suggests that highly disturbed blood flow instabilities that appear in cardiovascular flows harbor high-intensity fluctuations up to 1 kHz and these fluctuations could be linked to various vascular pathologies. A key research challenge in understanding these pulsatile, inhomogeneous flows and their corresponding flow structures is producing an effective visualization of the underlying data obtained from high-resolution CFD. However, traditional engineering visualization techniques alone are often insufficient to produce perceptually-optimal visualizations. The resulting visuals are often occluded and rely on complex rendering techniques and animations to convey the 4D (3D + time) nature of the flow. Therefore, to address the problem of depicting the complex 4D cardiovascular flows effectively, we make use of Illustrative flow depictions and other high-level abstraction strategies.

In the current work, we explore these challenges while trying to represent the spatiotemporal evolution of complex flow structures in a single static image. In order to achieve this, first, the "features" of interest are extracted from the CFD velocity data, then subjected to a visual abstraction and eventually, illustrative touches are applied to these abstracted flow features. The "features" of interest are the vortical structures from the high-intensity flow fluctuations. A heuristic technique is used to filter the flow features relevant to the frequency band(s) of interest thus providing further insight into their spatial correspondence. We then use a high-level abstraction strategy such as "exploded views" to communicate the different structures arising from different frequency bands. The flow patterns are conventionally visualized with particle trajectories and isosurfaces. We emphasize the shape and depth perception of the obtained features with cues from illustration-inspired techniques such as silhouettes, outlines, halos, saturation, and toon-shading as shown in Figure 1. The image shows a snapshot with the illustrative touches on the extracted "features" (isosurfaces of filtered Q-criterion) for a middle cerebral artery aneurysm.

Viewing the resulting data as individual snapshots incrementing in time can be cumbersome and hardware intensive, and often results in information overload to the viewer. The visual representation of such time-varying 3D data in a single static image is largely unaddressed in the literature. Informed by visual science and psychophysics, we explore strategies such as sequential art, caricature and careful compositing to guide the user's attention to only the most "important" details in order to overcome the visual overload. The principles of visual art such as "symbolization" (use of symbols such as arrows, strokes) and "ghost" images to represent sequential transitions (past, current, and future) between the extracted features are explored to depict motion in a static image. Speed lines or motion lines amplify the motion and increase the perception of speed and direction when depicting motion.

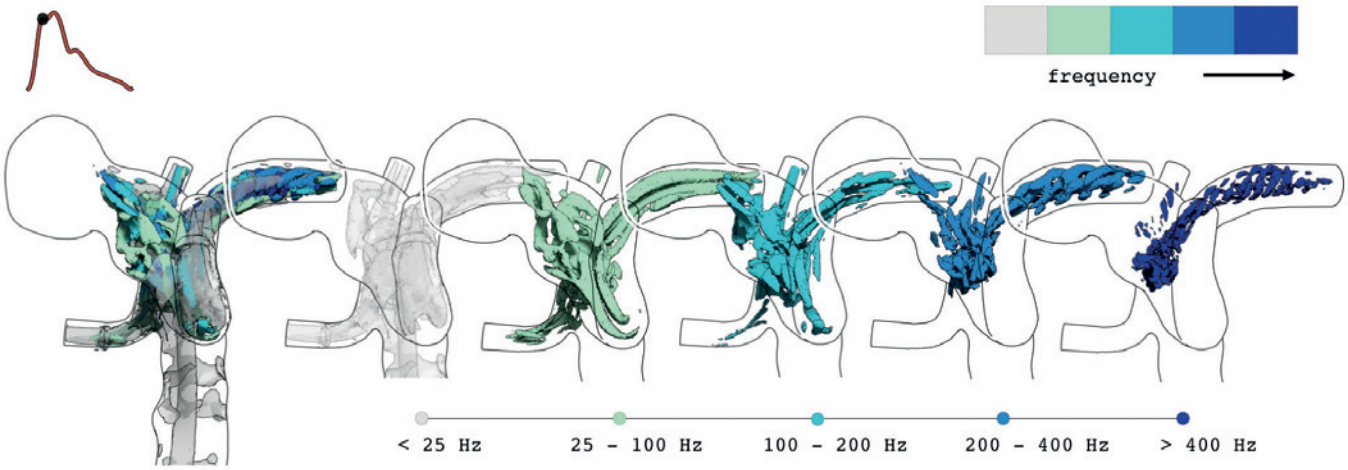

Figure Caption: Instantaneous isosurfaces of Q-criterion for different bandwidths.

[A-04.6]

SURFACE STIFFNESS CORRELATION WITH STENT EXPANSION IN A PATIENT-SPECIFIC SUPERFICIAL FEMORAL ARTERY MODEL BASED ON PLAQUE INHOMOGENEITY

Sean Doherty[1], *Erica Neumann*[1], *Ahmet Erdemir*[1], *Melissa Young*[2]

1 *Cleveland Clinic, Cleveland, USA*
2 *Division of Cardiovascular Diseases, Mayo Clinic, USA*

Atherosclerosis remains a leading cause of vascular disease, specifically for the peripheral artery [1]. Mechanical stents are attractive treatment options given the limited invasiveness of stent insertion, yet stents do not always perform optimally. Health complications can stem from eventual stent fracture and restenosis. In this study, expansion of a stent in an artery accommodating plaque inhomogeneity was simulated. The goal was to understand the interplay between stent performance and localized arterial wall stiffness. Given such a relationship, physicians may infer selection and placement of a stent based on artery properties without the need to simulate stent expansion in new patients. This would be beneficial clinically as simulations of stent expansion are computationally costly compared to simulations that can determine arterial surface stiffness [2].

A Python-based automated procedure was utilized with intravascular ultrasound virtual histology to build a finite element model of the superficial femoral artery [2]. The artery and plaque components were defined as hyperelastic and nearly-incompressible with plaque inhomogeneity accommodated as in Neumann et al. [2]. Artery-only pressurization simulations provided local arterial wall stiffness, with this study utilizing results from systolic pressure (120 mmHg) [2]. The stent was modeled with a superelastic Nitinol material model using a built-in Abaqus UMAT. A stent expansion simulation was performed in the same artery model to quantify arterial diameter expansion induced by the stent. All simulations were performed in Abaqus/Standard 6.12.3.

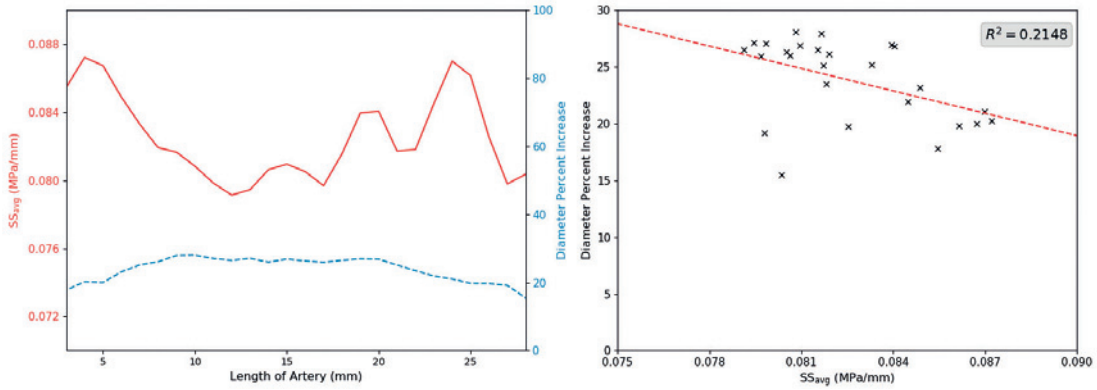

Figure 1: (left) Averaged arterial surface stiffness (SSavg) and percent increase in the diameter of the lumen after stent expansion (dashed line) along the length of the artery. (right) Correlation between arterial diameter percent change and averaged arterial surface stiffness.

Figure 1 examines the influence of average arterial surface stiffness on the expansion of the arterial lumen during the last simulation time point. The overlay of average surface stiffness across artery length indicates the influence of this metric (or lack of it) on diameter change. An expected but weak negative correlation was observed between arterial diameter change and its surface stiffness (R2 = .2148). This suggests that there may be some influence, but that other factors may be more influential in expansion of the lumen radially, e.g. initial diameter. Alternatively a stronger correlation may be observed in other calcification levels, as surface stiffness varied relatively little in this artery model [2]. Future work will include running the same stent expansion in other artery models of varying calcification, and expanding this work to include other performance metrics, such as peak stent stress.

Acknowledgments: This study has been supported by National Institutes of Health (R01EB018965: PI – Young).

References:

1. *Herrington, William, et al. Circulation research (2016) 118:535-546.*
2. *Neumann, Erica et al. CMBBE (2019) in press.*

[A-05.1]

CALCIFIC AORTIC VALVE DISEASE AND TRANSCATHETER AORTIC VALVE REPLACEMENT (TAVR) - A BIOMECHANICS PERSPECTIVE

Matteo Bianchi[1], Ram P. Ghosh[1], Brandon Kovarovic[1], Oren M. Rotman[1], ***Danny Bluestein***[2]

1 *Stony Brook University, Stony Brook, USA*
2 *PolyNova Cardiovascular, Inc., Stony Brook, USA; Stony Brook University, Stony Brook, USA*

Calcific aortic valve disease (CAVD) may lead to severe aortic stenosis and heart failure. TAVR has emerged as an effective therapy for inoperable CAVD patients, often as their only life-saving alternative. However, complications such as calcification, valve migration, cardiac conduction abnormalities in heart rhythm, and paravalvular leaks (PVL) leading to increased stroke risk have limited TAVR utility and its anticipated expansion into lower-risk and younger patients. We aim to expand TAVR utility by combining imaging, computational, and experimental techniques into an optimization approach to guide TAVR procedures for reducing their ensuing complications to achieve better patient outcomes. We are also developing next generation polymeric valves specifically optimized for TAVR.Characterizing the interaction between TAVR and the calcified tissues can guide procedural planning for minimizing TAVR complications. The effect of TAVR deployment on valve migration risk and its performance during heart beating was studied using the Simulia beating electromechanical Living Heart Model (LHM) in balloon and self-expandable TAVR devices. Patient-specific model geometries with the diseased aortic root were reconstructed from CTA images and TAVR crimping into the catheter and deployment were simulated. PVL was quantified for each investigated scenario by computational fluid dynamics (CFD). Self-expandable TAVR performance during the heart beating was evaluated for Medtronic Evolut R and a novel polymeric valve developed by our group (PolyNova Cardiovascular, Inc., Stony Brook, United States). Our simulations predicted the migration risk and PVL, informing which deployment configurations offer optimal positioning and minimizes PVL on a patient-specific basis. Deployment in the LHM further demonstrated the effect of heart beating on the valves and highlighted potential complications such as contact stability and interference with the atrioventricular node that can cause TAVR recipients to develop conduction abnormalities that may require permanent pacemaker implantation. It indicated that the stress induced by the TAVR stent on the membranous septum appears to be correlated with atrioventricular (A-V) block.Prototypes of our polymeric TAVR valves were tested in vitro for hemodynamics performance in the Vivitro Left Heart Simulator, with effective orifice area and transvalvular regurgitant fraction calculated (ISO 5840-3 2013). Durability of the valves was tested in the Vivitro HiCycle and their thrombogenicity measured in the Berlin LVAD and compared to other valves such as our polymeric surgical valve and the Edwards Sapien valve.

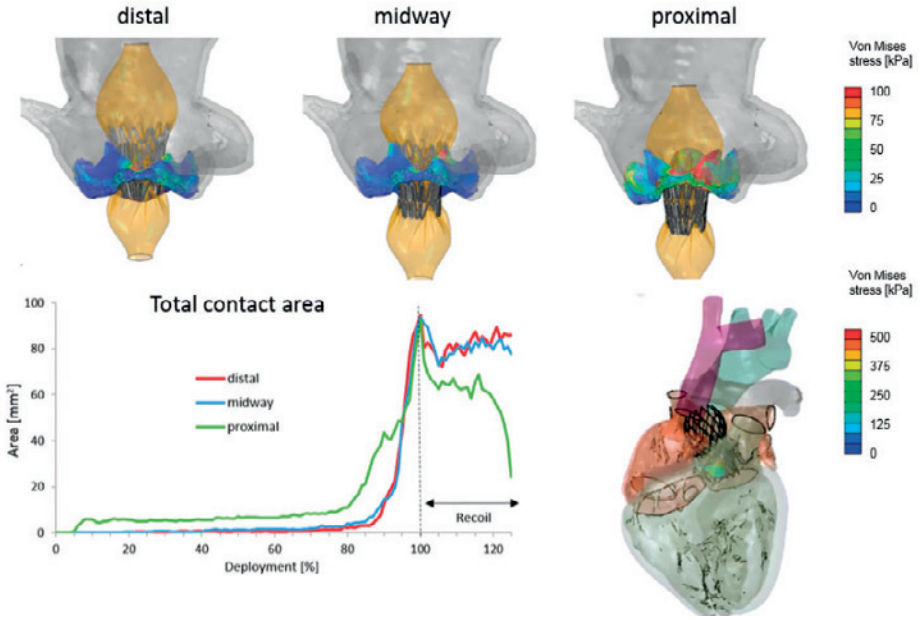

Figure Caption: (Top) Stresses on the native leaflets at 50% of the Edwards Sapien deployment. (Left bottom) Contact area between native leaflets and stent over the time for the three configurations. (Right bottom) CoreValve Evolut R deployed in the beating LHM showing stresses on the native leaflets.

Acknowledgements: This study is supported by the NIH-NIBIB Quantum Award Phase II-U01EB012487 (DB), NHLBI-STTR Phase I R41-HL134418 (DB), and NIBIB-BRP U01EB026414 (DB). ANSYS, Inc. and Simulia are in academic partnership with Prof. Bluestein.

[A-05.2]

IMPACT OF TRANSCATHETER AORTIC VALVE SIZE ON THE ESTIMATION OF PARAVALVULAR LEAKAGE: AN FSI STUDY

Laura Iannetti[1], *Francesco Migliavacca*[2], *Giulia Luraghi*[3], *Claudio Chiastra*[4], *José Félix Rodriguez Matas*[3]

1 *BETA CAE Italy Srl, Turin, Italy*
2 *Politecnico DI Milano; Labs, Dept. of Chemistry, Materials and Chemical Engineering, Milano, Italy*
3 *Labs, Dept. of Chemistry, Materials and Chemical Engineering*
4 *Politecnico DI Milano; Politobiomed Lab, Dept. of Mechanical and Aerospace Engineering, Politecnico DI Torino, Milano, Italy*

Transcatheter aortic valve implantation (TAVI) is a minimally invasive treatment for high-risk patients with aortic diseases. Despite its increasing use, uncertain influential factors require continuous investigation. TAVI "sizing" [1] is an important aspect to be considered for the procedure success. This choice, along with the positioning strategy, strongly affects the onset of paravalvular leak (PVL), a frequent TAVI complication with increased mortality [2]. From a modeling viewpoint, the Fluid-Structure Interaction (FSI) methodology represents the best numerical approach capable of reproducing the loading on the valve leaflets due to the fluid coupling [3]. The aim of this work is to estimate by means of FSI simulations how the choice of the transcatheter valve size affects the PVL after TAVI procedure. A parametric anatomical-resembling model of the aortic root was realized with the morphing tool in ANSA pre-processor (BETA CAE Systems International AG). In particular, a patient with an annulus diameter of 26 mm of and a severe grade of stenosis was selected to virtually implant both 29 and 34 Medtronic Corevalve Evolut R® sizes. The solid parts of the numerical model include the anisotropic hyperelastic aorta, the calcified native valve, the Nitinol frame of the device and its pericardium leaflets and skirt, while the fluid parts were created based on the configuration of the aorta, which was totally immersed in the blood domain. The FSI analyses were then performed using the non-boundary fitted method implemented in LS-DYNA 971 (LSTC). Results from the FSI simulations have been analyzed by means of META post-processor (BETA CAE Systems International AG) and predicted different outcomes for the different implanted valve sizes in terms of the final configuration of the released device in the implantation site, the aorta and calcification stresses, the pericardium leaflets kinematics, the PVL estimations, the regurgitation volume and the effective regurgitation orifice area.

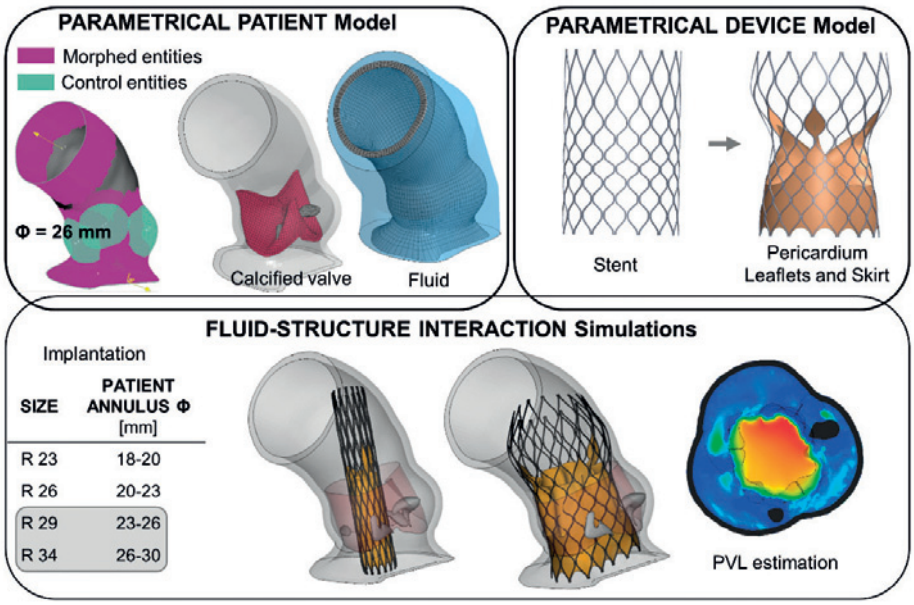

Figure Caption: Parametrical Patient Model: parametrical aorta, calcified valve and fluid domain; Parametrical Device Model: stent in the cylindrical configuration and the complete device with pericardium parts in the final configuration; FSI Simulation: Implantation step and hemodynamics with PVL evaluation.

References:

[1] *Kasel et al., Standardized Imaging for Aortic Annular Sizing, JACC: Cardiovascular Imaging, 2013.*
[2] *Généreux et al., Paravalvular Leak After Transcatheter Aortic Valve Replacement, JACC, 2013.*
[3] *Luraghi et al., Evaluation of an aortic valve prosthesis: Fluid-structure interaction or structural simulation, J Biomech,*

[A-05.3]

HEMODYNAMICS OF THE AORTIC SINUS AND THE CORONARY PERFUSION - NUMERICAL AND EXPERIMENTAL STUDY

Alex Liberzon[1], Shaily Wald[1], Barak Even Hen[1]

1 *Tel Aviv University, Tel Aviv, Israel*

During diastole, coronary perfusion depends on the pressure drop between the myocardial tissue and the coronary origin located at the aortic root. This pressure difference is influenced by the flow field near the closing valve leaflets. Clinical evidence is conclusive that patients with severe aortic stenosis (AS) suffer from diastolic dysfunction (low coronary flow reserve, CFR) during hyperemia, but show increased coronary blood flow (CBF) during rest [1]. Transcatheter aortic valve implantation (TAVI) was shown to decrease rest CBF along with its main purpose of improving the aortic flow and reducing the risk of heart failure [2]. Physiological or pathological factors do not provide a clear explanation for the increase of rest CBF due to AS and its decrease immediately after TAVI.

In this study, we present numerical and experimental studies that examines the impact of AS and TAVI on CBF during rest conditions and on CFR during various HR conditions.

The experiments (figure 1) use simultaneous pressure measurements in three locations in a transparent flexible model of the aortic root, combined with flow measurements to coronary arteries and visualization. The flow is driven by a hemodynamic pump using pulse duplicator, and contains a synchronized controlled resistance in the coronary arteries.

The study compares the hemodynamics of three different models: Healthy, AS and TAVI cases. The experimental study is compared with a numerical analysis [3] The numerical simulations (figure 2) used time-dependent computational fluid-structure interaction (FSI) of blood flow in the aortic root including the dynamics of the flexible valve leaflets and the varying resistance of the coronary arteries. The comprehensive study succeeded to capture the major effects that dominant the hemodynamics in the aortic root, and to explain the hemodynamic effect that leads to the changes CFR and in CBF found in in-vitro and clinical studies.

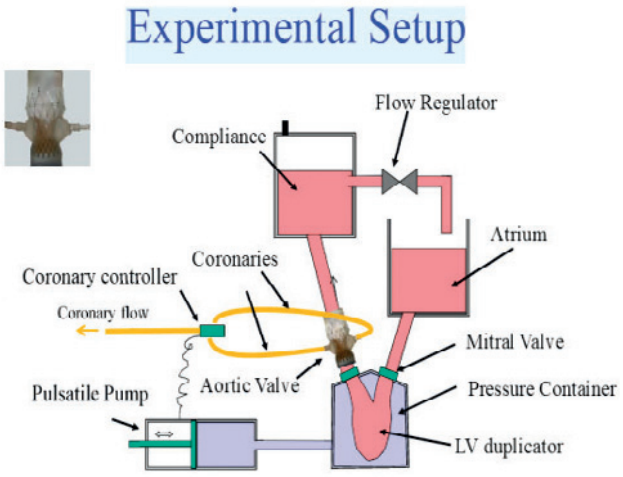

Figure 1: Experimental Setup

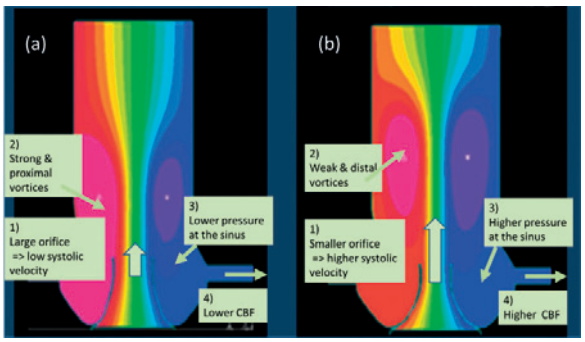

Figure 2: Numerical Results

Acknowledgments: This work was conducted in Ariel Biomechanics Center (ABMC) in Ariel University, Ariel, Israel and supported by scholarship provided by Ariel University, Ariel, Israel. The research was partially supported by Nicholas and Elizabeth Slezak grant, Tel Aviv University, Tel Aviv, Israel.

References:

1. *Cao, C. al. (2015). "A systematic review and meta-analysis of clinical and cost-effective outcomes of transcatheter aortic valve implantation versus surgical aortic valve replacement." Heart, Lung and Circulation 24: S258.*
2. *Meimoun, P.et al., (2012). "Factors associated with noninvasive coronary flow reserve in severe aortic stenosis." Journal of the American Society of Echocardiography 25(8): 835-841.*
3. *Wald, S.et al., (2018). "A numerical study of the hemodynamic effect of the aortic valve on coronary flow." Biomechanics and modeling in mechanobiology 17(2): 319-338.*

[A-05.4]

NUMERICAL MODELS OF VALVE-IN-VALVE DEPLOYMENT: EFFECT OF LEAFLET LACERATION ON ANCHORAGE

*Halit Yaakobovich[1], Romina Plitman-Mayo[2], Uri Zaretsky[1], Ariel Finkelstein[3], Shmuel Einav[1], **Gil Marom**[1]*

1 *Tel Aviv University, Tel Aviv, Israel*
2 *School of Mechanical Engineering, Tel Aviv University, Tel Aviv, Israel*
3 *Division of Cardiology, Tel Aviv Medical Centre, Tel Aviv, Israel*

Coronary artery obstruction is fatal complication of transcatheter aortic valve replacement (TAVR) that occurs in up to 3.5% of the implantations inside a failed surgical bioprosthetic valve (valve-in-valve, ViV).1 A recently developed new technique to address this problem is intentional laceration of the bioprosthetic leaflet, which is more commonly known by the name BASILICA.2 In this technique, one or two leaflets are lacerated to prevent coronary obstruction, but since it is assumed that this technique can also help reducing the incidence of leaflet thrombosis, in the future it may be used to lacerate all the three bioprosthetic leaflets. However, this technique harm the circumferential (hoop) stress in the surgical valve, and may lead to weaker support and anchorage for the TAVR device. This study aims to compare the anchorage post-ViV implantations, with and without lacerations, by numerical modeling. Finite element analysis of surgical bioprosthetic valve (Sorin Mitroflow) implantation was followed by deployment models of the latest version of TAVR devices (Medtronic Evolut PRO, Edwards Sapien 3). The Mitroflow valve was investigated because of its high susceptibility to early degeneration and because it was previously used to demonstrate the BASILICA technique.2 TAVR valve deployments inside the surgical valve, with and without lacerations, were modeled as superelastic expansion and deployment by balloon inflation, for the Evolut and Sapien devices, respectively. All the models were solved in in Abaqus Explicit (Simulia, Dassault Systèmes). The results show that lower stress magnitudes in the surgical leaflets after BASILICA leads to smaller contact area with the TAVR stent, especially in the Sapien 3. In the intact surgical valves, the Sapien anchorage heavily relied on the circumferential stress in the leaflets, while the Evolut contact with the Mitroflow was mainly with the plastic stent, possibly because of contact between the Evolut and the aortic root. It can also explain the lesser effect of the BASILICA technique on the anchorage of Evolut compared to Sapien. The basic understanding this study provides can help expanding the use of leaflet laceration by choosing a better matched TAVR device.

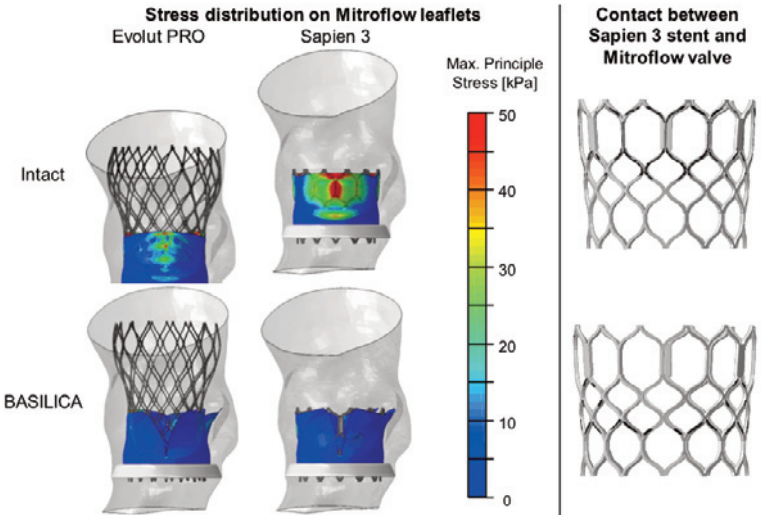

Figure Caption: Deployment of Evolut and Sapien in intact (top) and lacerated (bottom) Mitroflow valve. The right column compares the contact (in black) between Sapien stent and the Mitroflow valve.

References:

1. *Dvir D, et al. Circ Cardiovasc Interv. 2015; 8:e002079. doi: 10.1161/CIRCINTERVENTIONS.114.002079.*
2. *Khan JM, et al. JACC Cardiovasc interv. 2018; 11:677-89. doi: 10.1016/j.jcin.2018.01.247.*

[A-05.5]

DETERMINATION OF PATIENT-SPECIFIC AORTIC VALVE LEAFLET STRAINS FROM IN-VIVO IMAGES

Bruno Rego[1], *Samuel Potter*[1], *Alison Pouch*[2], *Robert Gorman*[2], *Michael Sacks*[1]

1 *James T. Willerson Center for Cardiovascular Modeling and Simulation, Austin, USA; Oden Institute for Computational Engineering and Sciences, Austin, Texas; The University of Texas at Austin, Austin, USA,*
2 *University of Pennsylvania, Philadelphia, USA*

The potential clinical benefit of patient-specific biomechanical models of cardiovascular disease remains an unrealized goal, often due to difficulties in non-invasively acquiring necessary kinematic data. This is particularly true in assessing bicuspid aortic valve (BAV) disease, the most common cardiac congenital defect in humans which leads to premature and severe aortic stenosis/insufficiency (AS/AI) [1]. However, assessment of BAV risk for AS/AI to determine treatment on a patient-specific basis is hampered by large anatomic variations that remain largely unquantified. There is thus a need for simulation techniques that can directly integrate individualized BAV geometry and deformation data from in-vivo images. Toward this goal, we have extended an approach recently developed for the human mitral valve [2] to determine tri-leaflet aortic valve (TAV) and BAV leaflet deformations based on clinically obtained in-vivo imaging data. Imaging data was collected on a patient-specific basis for individuals with TAV and for those with BAV (see figure). To acquire diastolic deformation fields across the entire aortic valve (AV) leaflet surface non-invasively, we utilized a previously validated image-based strain estimation method developed by our group [2], which yields local strain information directly from clinical-quality in-vivo images. To further validate our method, we applied the strain estimation method to a computationally generated geometry of a bioprosthetic TAV implant, with locally prescribed collagen fiber orientation distributions and material properties. The technique was able to capture the complex, heterogeneous leaflet deformation field of the AV. Moreover, our non-invasive method was able to yield strain estimates within 5% of their ground truth value over the entire leaflet surface (see figure). Resulting strain fields also corresponded well with results of structural simulations based on population-averaged fiber structural data and in-vivo measurements from previous studies [3]. Based on the observed spatial resolution of the resultant strain field, this approach is sufficiently sensitive to capture the patient-specific heterogeneity in the in-plane deformations of both TAV as well as BAV leaflets. Deformation is a key parameter in the clinical assessment of valvular function, and serves as a direct means to determine regional variations in structure and function. This study is an essential step toward patient-specific assessment of BAV based on correlating leaflet deformation and AS/AI progression, as it provides a means for assessing patient-specific strain patterns.

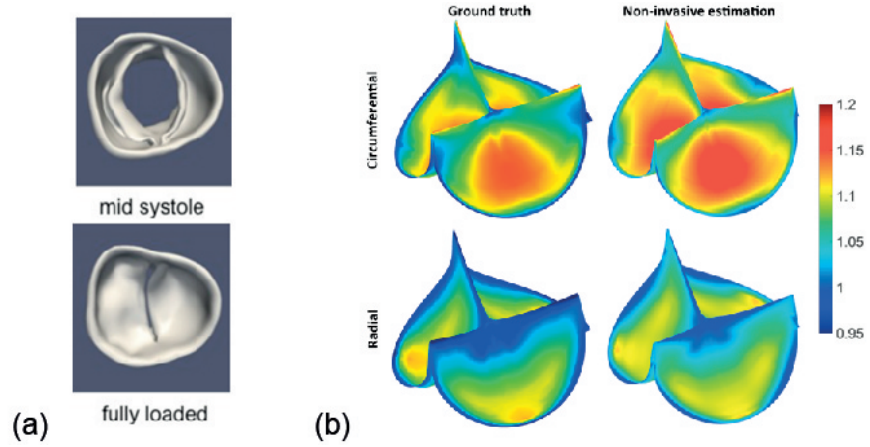

Figure Caption: (a) Representative segmented image of a BAV. (b) In-plane stretch in the bioprosthetic TAV compared with ground-truth strains, showing the ability of the method to capture substantial regional heterogeneity as well as directional differences in strain.

References:

[1] *Brown JM et al. (2009) J Thorac Cardiovasc Surg, 137(1):82–90.*
[2] *Rego BV et al. (2018) Int J Numer Meth Biomed Engng. e3142.*
[3] *Aggarwal A et al. (2016) J Biomech, 49(12):2481-2490.*

[A-05.6]

THE REVERSE CALCIFICATION TECHNIQUE AND ITS IMPACT ON SIMULATIONS OF TRANSCATHETER IN BICUSPID AORTIC VALVE REPLACEMENT

Karin Lavon[1], *Gil Marom*[1], *Adi Morany*[1], *Danny Bluestein*[2], *Rami Haj-Ali*[1]

1 *School of Mechanical Engineering, Tel Aviv University, Tel Aviv, Israel*
2 *Department of Biomedical Engineering, Stony Brook University, Stony Brook, USA*

Calcific aortic valve disease (CAVD) is characterized by stiffened aortic valve leaflets, which rapidly leads to aortic stenosis (AS). Bicuspid Aortic Valve (BAV) is a congenital heart disease, where the valve is composed of two leaflets. Half of the patients with diagnosed AS has a BAV, which progresses in an accelerated rate than patients with a tricuspid aortic valve. The Reverse Calcification Technique (RCT) generates spatial calcified densities (identified from the HU range) based on computed tomography (CT) scans from pre-intervention AS patients. The RCT is capable of predicting the CAVD progression that lead to the current stage [1,2]. Transcatheter aortic valve replacement (TAVR) is a treatment approach for CAVD where a stent with mounted bioprosthetic valve is deployed on the stenotic valve. Performing TAVR in calcified BAV patients has been recently performed on a wider scale, in part because it is associated with preprocedural complications due to the BAV asymmetrical structure.

This study aims to extend the RCT for predicting CAVD progression in calcified BAVs. In addition, refined computational models were developed in order to simulate the deployments of Evolut R and PRO TAVR devices for the different stages of the CAVD progression, predicted from the RCT of the calcified BAV. The paravalvular leakage (PVL) was also calculated for all cases by computational fluid dynamics (CFD) simulations. The RCT was employed to generate the 3D calcification deposits for several stages of the disease. The calcium deposits were embedded inside a parametric model of the BAV 3. Deployments of the Evolut R and PRO inside the calcified BAV were simulated for the several stages of the disease, along with five bioprosthesis leaflets orientations for the severe case. The progression of the disease was found to be accompanied by narrower asymmetric and elliptic stent deployment. Positioning the bioprosthesis commissures aligned with the native commissures was found to yield the lowest PVL. The Evolut PRO reduced the PVL in half compared with the Evolut R. The proposed biomechanical computational model could help assess the functionality of TAVR in BAVs.

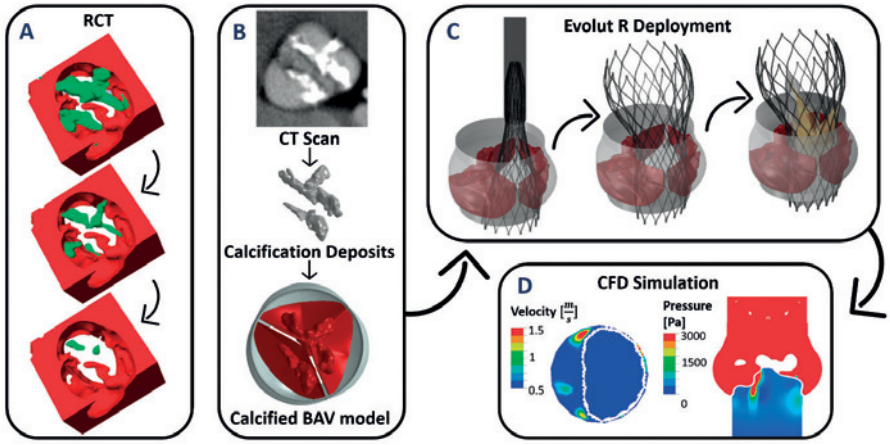

Figure Caption: CT scan of severely stenotic BAV patient was acquired. The RCT was employed to generate the 3D calcification deposits for several stages of the disease (A) and were embedded inside a parametric model of the BAV (B). Deployments of the Evolut R and PRO inside the calcified BAV were simulated (C). CFD simulations were performed to calculate the paravalvular leakage (D).

Acknowledgments: This study is supported by NIH-NIBIB BRP U01EB026414 grant.

References:

1. *Halevi, R. et al. J. Biomech. 48, 489–97 (2015).*
2. *Halevi, R. et al. Med. Biol. Eng. Comput. 54, 1683–1694 (2016).*
3. *Lavon, K. et al. J. Biomech. Eng. 140, 31010-31010–7 (2018).*

[A-06.1]

DEVELOPMENT OF INTEGRATED PATIENT SPECIFIC MODELS OF THE MITRAL VALVE AND THE LEFT VENTRICLE

Michael Sacks[1]

1 *The University of Texas at Austin, Austin, USA*

The mitral valve (MV) regulates blood flow into the left ventricle (LV). In situations where the MV fails to fully close the resulting blood regurgitation into the left atrium causes pulmonary congestion, leading to heart failure and/or stroke. There is now agreement that adjunctive procedures are required to treat IMR, yet there is no consensus regarding the best procedure. There is thus an urgent need for quantitative assessments of MV function to better design surgical solutions. We demonstrate state-of-the-art means to produce patient-specific MV computational models to develop quantitatively optimized devices and procedures for MV repair that incorporate LV geometry. Three patients were randomly selected from the Cardiothoracic Surgical Trial Network (CTSN) for this study. We processed real-time 3D echocardiographic (rt-3DE) images for these patients from before and after undergoing the annuloplasty surgery to extract patient-specific leaflet geometries. For each patient, the pre-operative open valve model was converted into a 3D triangulated mesh using Poisson disk resampling and ball pivoting algorithms. The acquired mesh was then morphed to the closed leaflet geometry through a hyperelastic shape-warping technique that enforced the closed leaflet shape through a level-set penalization. The simulation results showed that our modeling approach can be used to reliably predict the closing behavior of the MV following annuloplasty surgery using pre-operative imaging data (Figure 1). In addition, we computed the leaflet deformation fields in the local surface directions which demonstrated the effects of undersized annuloplasty ring on the entire leaflet. Interestingly, the comparison of pre- and post-operative deformation patterns revealed that the circumferential strain and stress decreased significantly in the entire leaflet while radial components of the strain and stress remained mostly the same before and after the annuloplasty repair surgery. We have also integrated this technique with complete LV to be able to gain insight into the role of LV geometry on the onset and progress of IMR (Figure 1). Simulating the MV response to surgery from clinical imaging data allows for refinements to treatment planning and optimization of repair surgery procedures. To conclude, we present a pipeline that allows for patient-specific modeling of the MV to predict the valvular response to annuloplasty repair with high predictive power. Our framework only relies on the clinically obtainable imaging data prior to the MV repair operation and thus can be extended into a virtual surgery tool that provides surgeons with additional insight into the patient-specific valvular response to different treatment options.

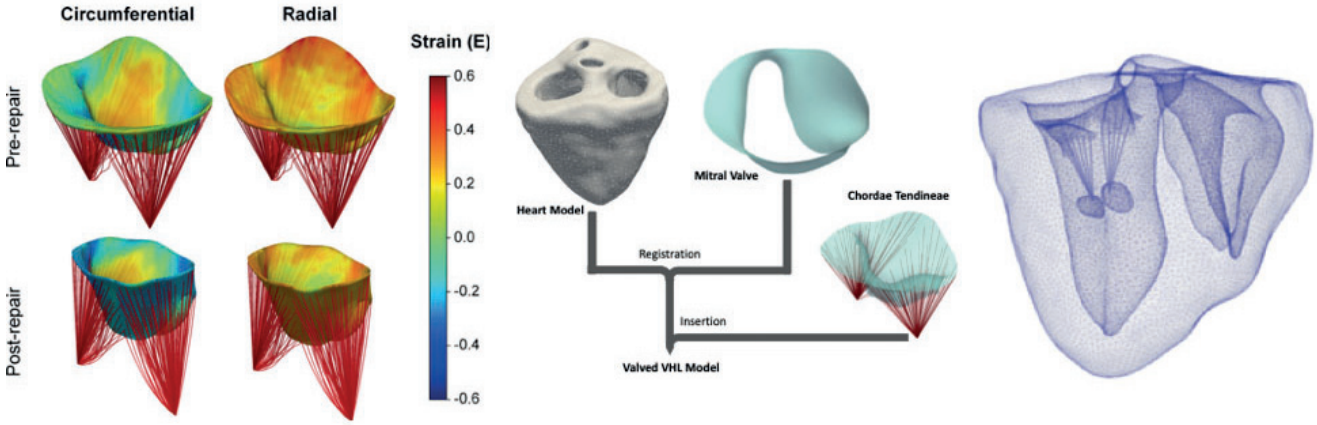

Figure Caption: In-vivo human results for the pre- and post-surgical states. Note that the post-surgical states was accurately predicted from the pre-surgical data alone. Current work is focused on integration of the patient-specific MV pipeline into the left ventricle.

Acknowledgments: NIH

[A-06.2]

BIOPROSTHETIC VALVE MECHANICS AND THE ONSET OF TURBULENT SYSTOLIC BLOOD FLOW

*Barna Becsek[1], Dario De Marinis[1], Maria Nestola[2], Rolf Krause[2], **Dominik Obrist**[1]*

1 *ARTORG Center for Biomedical Engineering Research, University of Bern, Bern, Switzerland*
2 *Institute of Computational Science, Center for Computational Medicine in Cardiology, Lugano, Switzerland (Ccmc), Universita Della Svizzera Italiana, Lugano, Switzerland*

Aortic stenosis is one of the most common valvular heart diseases. In severe cases, the native valve must be replaced by an aortic valve prosthesis which may be either made of technical materials (mechanical valves) or of biological tissue (bioprosthetic valves). Although bioprosthetic valves offer better hemodynamics than mechanical valves, they are nevertheless known to lead to turbulent systolic blood flow which has been connected to blood trauma, leaflet fluttering and adverse events in the ascending aorta due to unphysiological stimulation of the endothelium. Therefore, it is desirable to reduce or even eliminate the production of turbulent systolic flow past bioprosthetic valves.

In this study, we aim at developing a better understanding of the mechanisms leading to turbulent flow past bioprosthetic valves which is a prerequisite for developing strategies to reduce turbulence. To this end, we have devised a computational model for fluid-structure interaction (FSI) in cardiovascular configurations (Nestola et al., 2018). The model comprises a finite-element solver for the full elastodynamics equations of the structure (aortic root, ascending aorta, bioprosthetic valve) and a high-order finite-difference solver for the Navier–Stokes equations for the direct numerical simulation of laminar and turbulent blood flow. The flow solver and the structural solver are coupled with the immersed boundary method where the fluid velocities and the mechanical responses of the structure are transferred between a Cartesian fluid grid and an unstructured finite element mesh by a variational approach.

We will present numerical results that were obtained with this FSI solver. We will discuss and quantify several mechanisms leading to turbulent flow, such as FSI instabilities between the soft leaflet tissue and blood flow resulting in leaflet fluttering, hydrodynamic instabilities of the systolic jet issuing from the valve orifice, and the interaction between the turbulent systolic jet and the confining wall of the ascending aorta. We will relate these mechanisms to the morphology of the bioprosthetic valve and the aortic root, and to the mechanical properties of the valve leaflets.

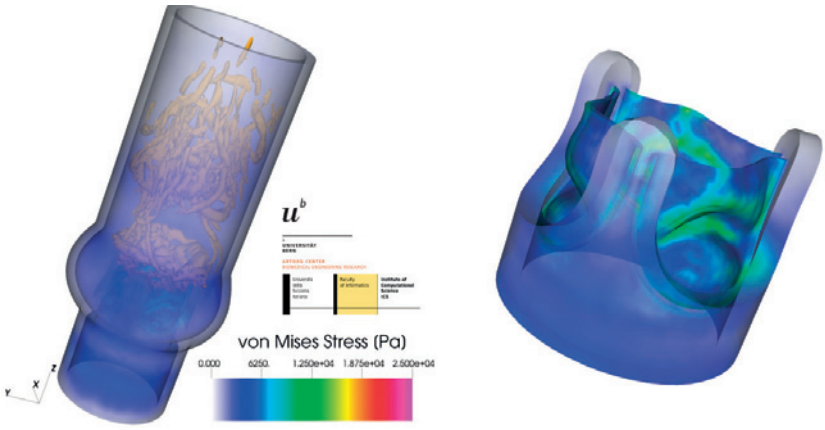

Figure Caption: Visualization of vortical flow structures in systolic flow (left) through a bioprosthetic heart valve exhibiting leaflet fluttering (right). (Colors on the structure indicate von Mises stress levels)

Acknowledgments: The authors acknowledge financial support by the Platform for Advanced Scientific Computing PASC for the project AV-FLOW, and computational resources provided by the Swiss National Supercomputing Centre CSCS.

References: Nestola, M. G. C., Becsek, B., Zolfaghari, H., Zulian, P., De Marinis, D., Krause, R., & Obrist, D. (2018). An immersed boundary method for fluid-structure interaction based on overlapping domain decomposition. arXiv preprint arXiv:1810.13046.

[A-06.3]

COMPUTATIONAL FLUID-STRUCTURE INTERACTION MODELS OF HEART VALVE DYNAMICS IN VITRO AND IN VIVO

Boyce Griffith[1], *Jae Ho Lee*[1], *Charles Puelz*[2], *Robert Hunt*[1], *Margaret Anne Smith*[1], *Simone Rossi*[1]

1 *University of North Carolina at Chapel Hill, Chapel Hill, North Carolina, USA*
2 *Courant Institute of Mathematical Sciences, New York, USA; New York University, New York, USA*

Each year in the United States, there are approximately 70,000 aortic valve replacement procedures to treat severe aortic stenosis. Worldwide, there are nearly 300,000 valve replacement operations performed each year, and it is projected that this number will rise to 850,000 per year by 2050. Heart valves are thin elastic structures that move with the blood flow, but at the same time, they apply forces to the flow that alter the fluid motion. Modeling heart valve performance across the full cardiac cycle requires a fluid-structure interaction approach. This presentation will describe work to develop and to validate fluid-structure interaction models of native and bioprosthetic heart valves in vitro and in vivo. These models are based on an immersed boundary formulation for simulating the dynamics of elastic structures immersed in a viscous incompressible fluid that describes the elasticity of the immersed structures using the framework of large deformation continuum mechanics. We will present in vitro and in vivo models developed using this framework and their application to modeling heart valve performance. In vitro models allow for the acquisition of detailed experimental data in a controlled, reproducible environment. We will describe models based on the ViVitro Labs, Inc. pulse duplicator, which is an experimental flow loop that mimics the conditions of the left heart. Experimental data available from the pulse duplicator system can be used both to calibrate the computational model and to validate the model predictions. We will present initial validation results showing excellent agreement between simulated and experimental flow, pressure, and valve kinematics data. We also will present recent work that is developing a complete fluid-structure interaction model of the heart that includes anatomically and biomechanically realistic descriptions of the atria, ventricles, the four cardiac valves, and the nearby great vessels. Reduced-order models provide the driving and loading conditions in which the heart operates, but all motion within the model is generated through the equations describing fluid-structure interaction.

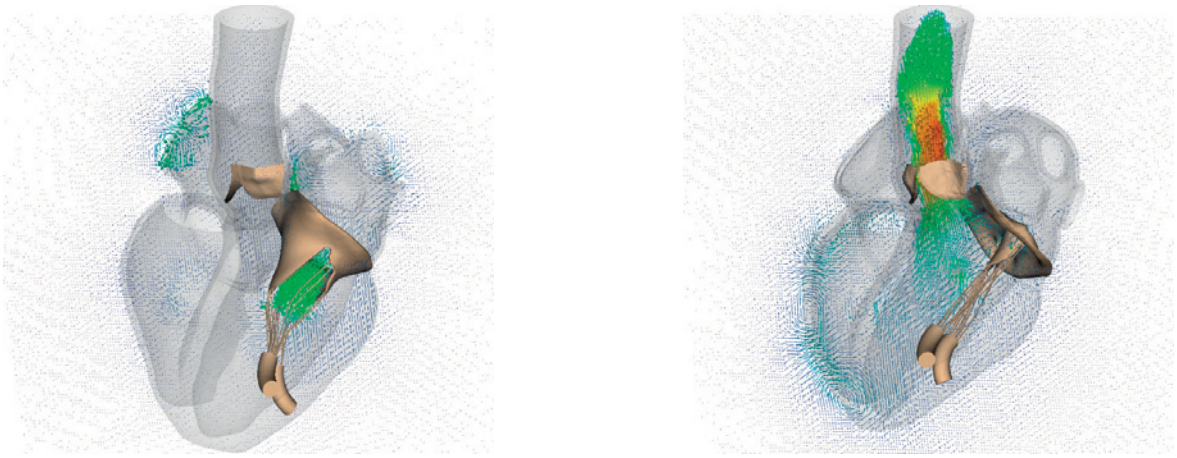

Figure Caption: Initial results from a new fluid-structure interaction model of the heart that includes descriptions of the four chambers of the heart, the four cardiac valves, and the great vessels. Left panel: mitral flow during atrial systole. Right panel: flow through the aortic valve in ventricular systole.

Acknowledgments: We gratefully acknowledge research funding from NSF awards OAC 1450327, OAC 1652541, and CBET 1757193 and NIH awards HL117063 and HL143336.

References:

1. *B. E. Griffith and X. Y. Luo. Hybrid finite difference/finite element version of the immersed boundary method. Int J Numer Meth Biomed Eng, 33(11):e2888 (31 pages), 2017*
2. *J. H. Lee, A. D. Rygg, E. M. Kolahdouz, S. Rossi, S. M. Retta, N. Duraiswamy, L. N. Scotten, B. A. Craven, and B. E. Griffith. Fluid-structure interaction models of bioprosthetic heart valves: Initial in vitro experimental validation. Submitted*

[A-06.4]

PATIENT-SPECIFIC MODELING OF REVASCULARIZATION AND MITRAL REPAIR THERAPIES IN FUNCTIONAL MITRAL REGURGITATION ASSOCIATED WITH CORONARY DISEASE

Vicky Wang[1], *Yue Zhang*[1], *Liang Ge*[1], *Jonathan W. Weinsaft*[2], *Mark Ratcliffe*[1]

1 *San Francisco Veteran Affairs Medical Center, San Francisco, USA*
2 *Weill Cornell Medicine, New York, USA*

Mitral regurgitation (MR) is backward flow of blood from the left ventricle (LV) to the left atrium that occurs during LV contraction. Functional mitral regurgitation (FMR) is MR caused by leaflet restriction that is in turn caused by adverse LV remodeling where the most common cause is coronary disease (CAD). Revascularization (REVASC) alone reduces FMR-CAD by approximately 30% [1]. In those without a REVASC effect, a number of mitral repair options exist, the most common being surgical undersized annuloplasty (UA) and the percutaneous edge-to-edge MitraClip. A key issue with mitral repair is recurrence of MR. In the Cardiothoracic Surgery Network trial, 58% of patients treated with UA developed recurrent advanced (≥ 2+) MR [2]. Similarly, advanced MR recurs in nearly half of FMR-CAD patients treated with MitraClip [3-4]. Among these patients, continued enlargement of the LV is the common denominator. Consequently, there is an urgent need for investigating the mechanistic linkage between REVASC and mitral valve therapies and LV remodeling in FMR-CAD patients in order to better optimize treatment options.

We developed a patient-specific modeling framework driven by clinical images to (i) perform personalized analysis of LV mechanics before and after REVASC and mitral valve therapies; (ii) model remodeling of LV; (iii) predict the effects of mitral therapies on LV remodeling using the population-based growth parameters derived from (ii). Our patient-specific finite element (FE) modeling framework integrates in vivo LV geometry obtained from cardiac MRI, infarct and ischemia measured using delayed contrast enhancement and stress perfusion MRI, respectively, and 3D motion of the LV measured using tagged MRI. For each patient, an AHA 17-sector based score system was used to quantify the degrees of infarction and ischemia. To register those information with the geometric data, the patient-specific LV FE model was also divided into 17 sectors whereby microstructural information (e.g. fiber angles) were specified and mechanical properties were personalized to match LV volume and 3D motion at end-diastole and end-systole after taking infarction and ischemia into account. Remodeling of the LV was simulated by integrating the growth formulation proposed by [5] into our modeling framework.

This type of personalized framework is capable of investigating the acute and chronic effects of REVASC and mitral valve repairs on LV myocardium on a subject-specific basis therefore providing an objective platform to determine the optimal therapeutic strategies for FMR-CAD patients.

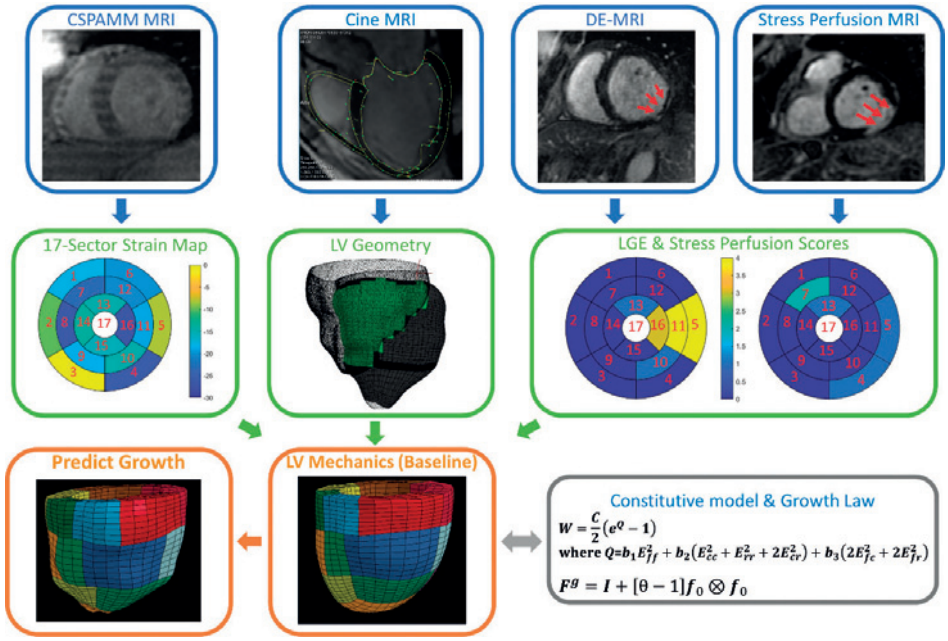

Figure Caption: Image-driven modeling framework for personalized evaluation of mitral valve repairs

References:

[1] *Goyal P et al., Coronary Artery Disease. 2015;26(8):642-50.*
[2] *Kron IL et al., J Thorac Cardiovasc Surg. 2015;149(3):752-61.*
[3] *Franzen O et al., Eur J Heart Fail. 2011;13(5):569-76.*
[4] *Maisano F et al., J Am Coll Cardiol. 2013;62(12):1052-61.*
[6] *Göktepe S, et al., J Theor Biol. 2010;265(3):433-42.*

[A-07.1]
MODELING CARDIAC GROWTH AND REMODELING

Tim Hermans[1], Nick van Osta[1], Eric Chen[1], Emanuele Rondanina[1], ***Peter Bovendeerd[1]***

1 Eindhoven University of Technology, Eindhoven, Netherlands

Patient-specific mathematical models of cardiac electromechanics might be used to assist in diagnosis and treatment selection in cardiac disease [1]. Adding models of cardiac growth and remodeling might assist in both personalizing generic models and estimating the long term effect of potential interventions. A typical clinical example is the heart supported by a left ventricular assist device (LVAD), leading to different growth responses in the left (LV) and right (RV) ventricle.

We evaluated the effect of the LVAD on hemodynamic and tissue function in a generic biventricular finite element (FE) model of cardiac mechanics. Myofiber orientation was estimated using a model of remodeling of fiber orientation in response to tissue strain [2]. As compared to the unsupported heart, in the LVAD supported heart tissue work density changed by -80% in the LV free wall, -70% in the septum and +40% in the RV free wall.

As a first step towards estimating the growth response in the LVAD heart, induced by the change in tissue load, we investigated growth in an FE model of the LV only. In the growth model, a growth stimulus was converted into a desired amount of growth, typically realized if tissue elements would not experience mechanical interaction with their neighboring tissue elements. The actual, realized growth was obtained by including this interaction [3]. When using the deviation of active work density from a homeostatic value as a stimulus for growth, we found the model to progress towards a homeostatic state initially, but to diverge eventually. To distinguish between fundamental issues in the growth law and numerical issues due to element deterioration in the FE model, we investigated growth driven by fiber stress and/or strain in an even simpler model of LV mechanics, the one fiber model [4]. Several combinations of stress and strain based stimuli were found to yield stable growth, suggesting ways to improve the FE growth model.

References:

[1] N Smith et al. euHeart: Personalized and integrated cardiac care using patient-specific cardiovascular modelling. Interface Focus 1, 349-364, 2011.
[2] MH Pluijmert et al. Determinants of biventricular cardiac function: a mathematical model study on geometry and myofiber orientation. Biomech Mod Mechanobiol 16, 721-729, 2017.
[3] W Kroon et al. Constitutive Modeling of Cardiac Tissue Growth. In: F Sachse, G Seemann (eds) FIMH, LNCS, vol. 4466, 340-349, Springer, 2007.
[4] PHM Bovendeerd et al. Dependence of Intramyocardial Pressure and Coronary Flow on Ventricular Loading and Contractility: A Model Study. Ann Biomed Eng 34, 1833-1845, 2006.

[A-07.2]

A NEW ROBUST 3D CONSTITUTIVE MODEL FOR THE PASSIVE PROPERTIES OF LEFT VENTRICULAR MYOCARDIUM

David Li[1], *Reza Avazmohammadi*[2], *Edward Hsu*[3], *Joseph Gorman*[4], *Robert Gorman*[4], *Michael Sacks*[2]

1 *The University of Texas at Austin, Austin, USA*
2 *Willerson Center for Cardiovascular Modeling and Simulation, Austin, USA; The University of Texas at Austin, Austin, USA*
3 *University of Utah, Salt Lake City, USA*
4 *Gorman Cardiovascular Research Group, Philadelphia, USA; University of Pennsylvania, Philadelphia, USA*

Myocardium exhibits complex behavior that demands a comprehensive constitutive formulation in order for its mechanical properties to be captured in a computational model. Current modeling efforts remain limited in that they are not based on full 3D datasets, do not use optimal loading paths, and have not defined the optimal form of the strain energy function and determined its associated material parameters. To this end, we employed a novel numerical-experimental methodology to determine the optimal form of the strain energy function for passive ventricular myocardium. Full 3D structural-mechanical measurements were obtained from cuboidal specimens cut out from the left ventricles of Dorset sheep. We modeled the myocardium as an orthotropic material with material directions f (myofiber), s (sheet or cross-fiber), and n (normal to the fiber-sheet plane), using an initial form by Holzapfel and Ogden [1]. The model was fitted to both a set of simple shear loading paths [2], and a set of optimally selected paths consisting of simple shear and pure shear deformations [3], using a finite element tetrahedral mesh whose elements were assigned spatially varying material directions. Model parameters were estimated with nonlinear least-squares regression via a trust-region-reflective algorithm in order to fit all optimal paths simultaneously. While the model fit the simple shear paths well, it was unable to capture the mechanical anisotropy in the optimal paths. Relative stretching and shearing of fiber, sheet, and normal directions in the myocardium, which could be explained by interactions (shearing in particular) between myofibers and their surrounding collagen matrix. The initial model was extended accordingly to reflect these coupling modes. We used this extended model to successfully fit the optimal datasets for multiple specimens with r^2=0.80–0.99 and used the fitted parameters to accurately predict the myocardium response in other paths outside of the optimal set. This extended constitutive model has particular relevance in the simulation of myocardium in non-physiological states like myocardial infarction. Ultimately, development of more robust models in this manner will make them better suited for clinical evaluation and for simulating treatment of cardiac diseases.

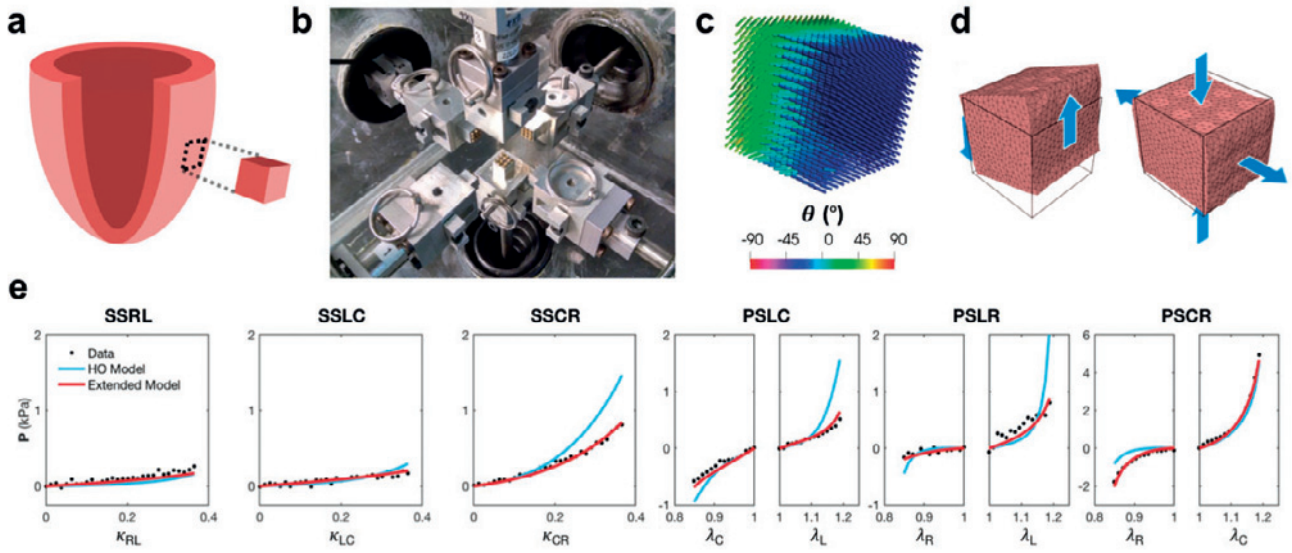

Figure Caption: (a) Harvest, (b) triaxial mechanical testing, and (c) structural measurements (fiber angle θ) of myocardium specimens. (d) Finite element simulations of simple shear and pure shear triaxial tests. (e) Fits of the initial and extended models to the optimal data.

Acknowledgments: NIH T32 EB007507 and F31 HL139113 to D.S.L., NIH K99 HL138288-01A1 and AHA 18CDA34110383 to R.A., and NIH R01 (HL068816, HL089750, HL070969, HL108330, HL063954) to M.S.S.

References:

[1] *Holzapfel et al., Philos Trans Royal Soc A, 367:3445-3475, 2009.*
[2] *Dokos et al., Am J Physiol Heart Circ Physiol, 283:H2650-9, 2002.*
[3] *Avazmohammadi et al., Biomech Model Mechanobiol, 17:31-53, 2018.*

[A-07.3]

3D STRAIN MAPPING OF MURINE LEFT VENTRICULAR REMODELING POST INFARCTION

Arvin Soepriatna[1], *Abigail Clifford*[1], *Kevin Yeh*[1], *Craig Goergen*[1]

1Purdue University, West Lafayette, USA

Introduction: Heart failure is a common sequela of myocardial infarction (MI). Despite a strong positive correlation between infarct size and heart failure, the mechanical factors that drive infarct expansion remain unclear. The majority of ultrasound studies still rely on 2D approaches to quantify global reductions in left ventricular (LV) function post-MI. Here, we integrated 4D ultrasound imaging[1] with a strain mapping technique[2] to longitudinally characterize LV mechanics and its contribution to post-MI remodeling.

Methods: Fifteen mice were separated to three surgery groups: 1) sham (n=5), 2) 30-minutes ischemia-reperfusion (n=5), and 3) permanent ligation of the left coronary artery (n=5). We acquired 4D images of the LV with a Vevo2100 ultrasound at baseline and on days 1,2,3,5,7,14,21, and 28 post-surgery. We estimated the deformation gradient tensor F and the maximum principal component of the 3D Green-Lagrange (GL) strain tensor E_1 using both non-rigid registration and optimization of image warping functions.[2] We segmented LV boundaries to evaluate LV function and present myocardial strain maps according to AHA's 17-segment model. Statistical analyses were conducted using one-way ANOVA with Tukey post-hoc.

Results: Fig.1 highlights LV morphological changes in the permanent ligation (PL) group over a 28-day period. Reduction in 3D myocardial strain (dark blue region) was observed in the infarcted myocardium when compared to the contractile, remote myocardium ($E_{1,infarct}$=0.06±0.03 vs. $E_{1,remote}$=0.39±0.05; p<0.01). Regions of low strains, marked by chamber dilation and wall thinning, continued to expand as heart failure progressed. Compared to the PL group, mice in the ischemia-reperfusion (I/R) group exhibited significantly smaller degrees of remodeling with smaller infarct sizes ($IS_{I/R}$=11±4% vs. IS_{PL}=46±15%; p<0.01) and improved ejection fraction ($EF_{I/R}$=50±7% vs. EF_{PL}=23±12%; p<0.05). No changes in either geometry or function were observed in the sham group when compared to baseline. Discussion: This study demonstrates a novel approach to longitudinally characterize 3D myocardial strain during LV remodeling post-MI. Results suggest that spatial strain gradients may play a role in determining infarct expansion and LV remodeling severity. Future work will focus on quantifying how regional myocardial strain gradients influence the directionality of infarct expansion.

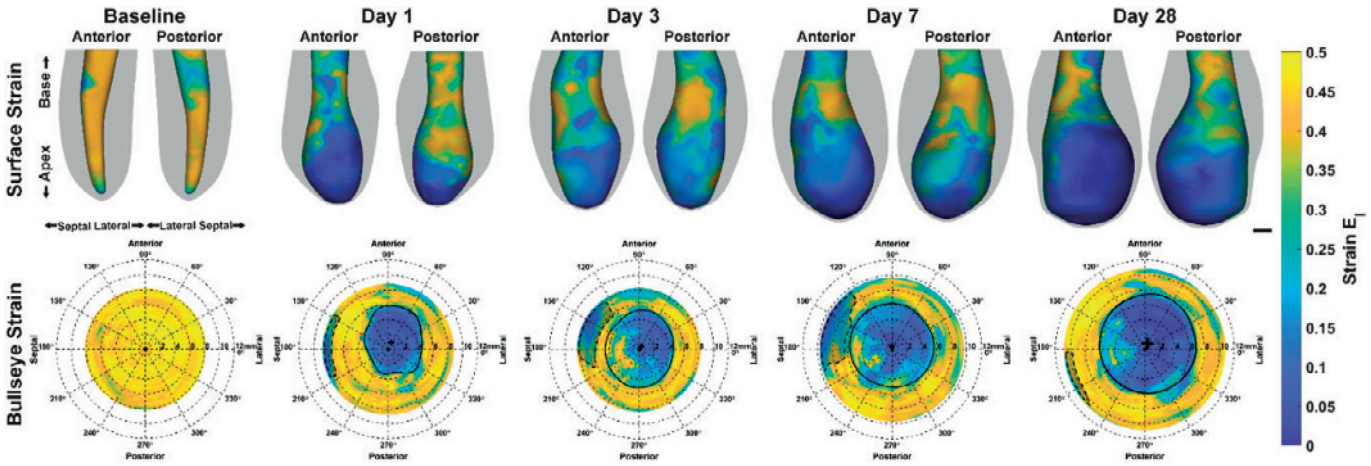

Figure Caption: Fig.1: Maximum principal 3D GL strain (El) maps of a mouse LV in the permanent ligation group over a 28-day period. Top: 3D peak-systolic LV volumes with strains overlaid to endocardial boundaries. Scalebar=1mm. Bottom: Bullseye maps of myocardial strain. Infarct zones are outlined with solid black lines, and sternal artifacts are outlined with black dashed lines.

Acknowledgments: This work was funded by the Donnan Fellowship and AHA (14SDG18220010). We thank John Boyle, Guy Genin, and Stavros Thomopoulos for their advice in the strain code development.

References:

[1] *Soepriatna, A.H., et al. Int J Cardiovasc Imaging, 2018.*
[2] *Boyle, J.J., et al. J Biomech Eng. 2018.*

[A-07.4]

CARDIAC GROWTH AND REMODELING IN HEART FAILURE: CORRELATING CELL AND ORGAN SCALES USING MULTISCALE MODELING AND MACHINE LEARNING

Mathias Peirlinck[1], *Francisco Sahli Costabal*[2], *Kevin L. Sack*[3], *Patrick Segers*[1], *Ellen Kuhl*[2]

1 *Ghent University, Ghent, Belgium*
2 *Stanford University, Stanford, USA*
3 *University of California at San Francisco, San Francisco, USA*

With a 5-year mortality rate of 50%, heart failure remains one of the most common, costly, disabling and deadly medical conditions. Predictive cardiac growth models are a potentially important clinical tool to assess disease progression and optimize pharmacological, device or surgical treatment strategies in heart failure patients. However, considerate debate on the exact mechanistic stimuli that drive the hypertrophic response of myocardial tissue and the lack of validation currently still prevent their clinical adoption. To quantify the predictive power of any of these growth models, the highly patient-specific time course and extent of disease progression, the multiscale nature of the disease and the intrinsic uncertainty on working with experimental data needs to be accounted for. We therefore propose a systematic approach combining a unique experimental chronic volume overload animal model with computational subject-specific continuum growth modeling and machine learning tools.

Left ventricular (LV) volume overload was induced in six Yorkshire domestic pigs through controlled mitral valve regurgitation and animals were followed up over a period of 8 weeks. Bi-weekly echocardiograms characterized organ level changes (volume, mass, wall thickness), whilst bi-weekly endomyocardial biopsy samples characterized cell scale changes (myocyte width and length). Subject-specific finite element models were set up and tuned to incorporate each pig's elastic myocardial tissue response at baseline. Subsequently, a transversely isotropic stretch-driven growth law was implemented in Abaqus and the LV models were subjected to the measured organ scale volumetric overload which caused regional overstretching of the heart cell. The computationally predicted cellular response of the heart cell to this overstretching was compared to the experimentally observed cellular response. Due to large inter-animal variability in measured organ and cell level variables, we decided to use machine learning tools to quantify the uncertainty on the measurements and to propagate this uncertainty through the computational models.

Without tuning the growth law to any experimental observation, implementation of a stretch-driven growth law predicted the changing myocyte morphology with an average accuracy up to 62.0%. Surprisingly, implementation of somatic growth slightly deteriorated this result, which calls for further studies on the relative influence of naturally-induced and overload-induced growth patterns. The developed approach will also be used to further elucidate the predictive power of other mechanistic growth laws.

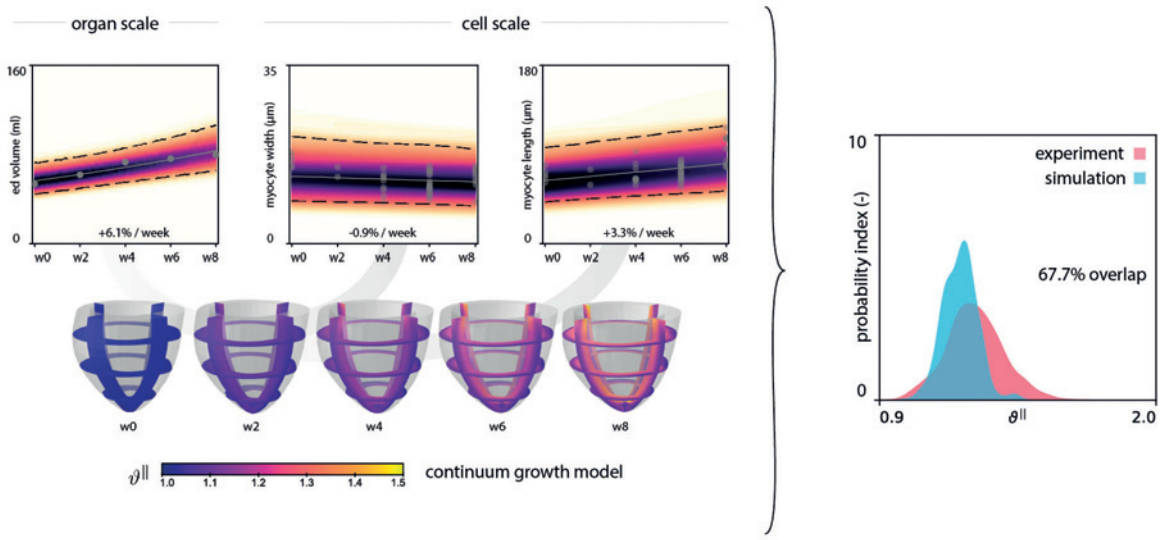

Figure Caption: Set-up of the top-down approach where experimental organ scale volume overload data is propagated through subject-specific finite element models implementing a stretch-driven growth law, to eventually compare the computationally predicted to the experimentally observed changes in myocyte morphology. The blue and red probability density functions represent the simulation and experimental results respectively where the overlap is a quantitative measure of the agreement between both. Results are shown for pig #6.

[A-07.5]

A COMPUTATIONAL APPROACH ON SENSITIVITY OF LEFT VENTRICULAR WALL STRAINS TO FIBER ORIENTATION AND GEOMETRY

Luca Barbarotta[1], *Peter Bovendeerd*[1]

1Eindhoven University of Technology, Eindhoven, Netherlands

Modern techniques of data assimilation have been recently applied to computational models of the heart to achieve model personalization. The patient specific model can then be used as a physics based interpretation of measured data into patient pathology. These data assimilation techniques typically rely on measured strains. Generally in these models, much effort is put in the reconstruction of the geometry, which can be assessed with common imaging techniques. Fiber orientation is typically modeled using generic rules, presumably because in vivo assessment via DT-MRI is not feasible in clinical practice. Yet, it is well known that an accurate description of the fiber architecture of the myocardial wall is required to reliably determine its deformation and to assess its function. It is therefore important to assess how the uncertainty related to geometry and fiber orientation affects those quantities that can be observed in a data assimilation process.

In this work, we investigated the sensitivity of left ventricular wall strains to geometry and fiber orientation.

We varied the geometry of the left ventricle one standard deviation around the average geometry along the six shape modes identified by the principal component analysis conducted in [1]. We modeled the fiber field using five parameters, three describing the transmural and longitudinal variability of the helix angle and two for the longitudinal variability of the transverse angle. We varied the parameters of this model to comply with the ranges of angles found in ex-vivo DT-MRI measurements for a population of healthy human hearts [2] and for a population of healthy goat hearts [3].

Our results show that longitudinal strain, circumferential-transmural shear strain, and longitudinal-transmural shear strain are affected by the variation of fiber and geometry most. For those strains, the mean effect of varying the geometry is well below 15% of the characteristic value of the average of our virtual population. However, the perturbation of the fiber orientation is responsible of a variation in the range 32%-55%. Our results also demonstrate the major role played by the transverse angle as compared to the helix angle.

References:

[1] *Zhang, Xingyu. Atlas Based Analysis of Heart Shape and Motion in Cardiovascular Disease. Diss. ResearchSpace@ Auckland, 2016.*
[2] *Lombaert, Herve, et al. "Human atlas of the cardiac fiber architecture: study on a healthy population." IEEE transactions on medical imaging 31.7 (2012): 1436-1447.*
[3] *Geerts, Liesbeth, et al. "Characterization of the normal cardiac myofiber field in goat measured with MR-diffusion tensor imaging." American Journal of Physiology-Heart and Circulatory Physiology 283.1 (2002): H139-H145.*

[A-07.6]

MYOCARDIAL MATERIAL PAREMETER ESTIMATION: OVERCOMING THE EFFECT OF UNKNOWN BOUNDARY TRACTIONS IN ENERGETICS ANALYSIS

Anastasia Nasopoulou[1], *David Nordsletten*[2], *Steven Niederer*[3], *Pablo Lamata*[3]

1 *King's College London, London, UK; Department of Biomedical Engineering; 5th Floor Becket House, London, UK*
2 *University of Michigan, Ann Arbor, USA*
3 *King's College London, London, UK*

Myocardial stiffness is a proposed biomarker for the stratification of heart failure but its direct measurement in vivo is not available and material parameter estimation from personalized biomechanical models of the heart can provide a valuable surrogate. However, the associated computational cost of current approaches involving multiple simulations or 'heavy' nonlinear optimization techniques, modelling limitations in reproducing the clinical observations and identifiability-related problems inherent in material models can impede the development of fast and robust enough pipelines for implementation in the clinic. Data-based approaches can thus provide powerful alternatives and recently a parameter estimation pipeline was proposed based on an energetics analysis in the passive myocardium, which can also guarantee unique parameter estimation [1,2]. In this work we highlight a hidden pitfall in such an analysis, namely the existence of unknown boundary tractions which participate in the energy balance within the myocardium. A new method is proposed based on the principle of virtual works which addresses this problem in the presence of large basal deformations that can occur within the cardiac cycle. The comparative results of the proposed method using the concept of virtual fields (VF) against the original energy-based pipeline (EB) along with a sensitivity analysis of the VF-method to modelling assumptions and data noise are shown in Fig. 1.

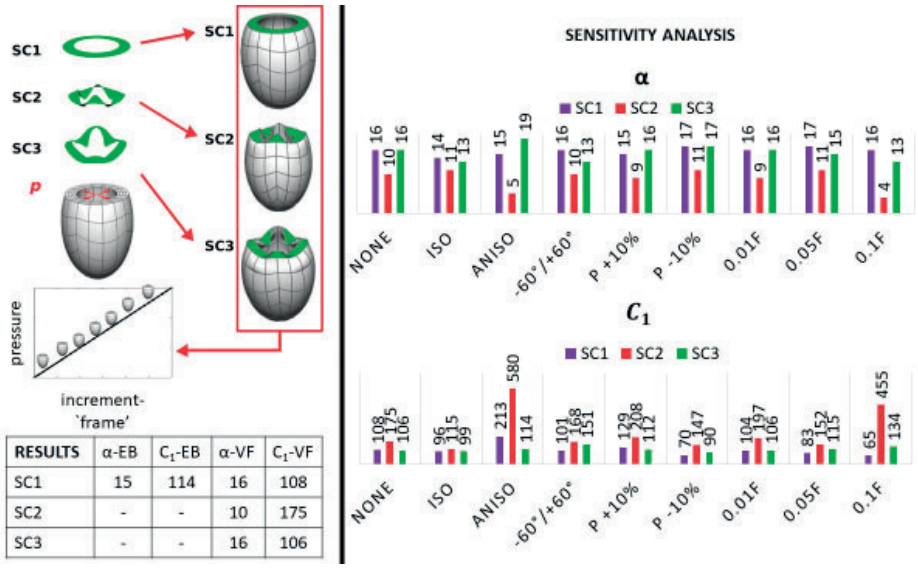

RESULTS	α-EB	C_1-EB	α-VF	C_1-VF
SC1	15	114	16	108
SC2	-	-	10	175
SC3	-	-	16	106

Figure 1: Synthetic data set generation and parameter estimation results for a popular transversely isotropic model [3]. A. (top): Synthetic data sets with varying levels of basal deformation (SC1, SC2, SC3), against which the original energy-based (EB) and the new virtual fields based (VF) parameter estimation pipeline is tested. (bottom): Results of the analysis comparing the performance of the EB pipeline (α-EB, C1-EB) [1] against the VF one (α-VF, C1-VF). For data sets SC2 and SC3 the EB pipeline could not identify the material parameters. B: Results of the sensitivity analysis of the identified parameters (α-VF, C1-VF) against sources of possible model-data incompatibility and data noise. Legend for sensitivity analysis: NONE: no modification, the original results of the analysis. ISO: assumed isotropic behavior of material, ANISO: assumed high anisotropy of the material, -60°/+60°: the assumed mean myofiber orientation in the model, P +/-10%: pressure data are increased/decreased by 10% of mean value, 0.01F, 0.05F, 0.1 F: white Gaussian noise with standard deviation: 0.01, 0.05 and 0.1 respectively was independently applied to each deformation gradient (F) component of the synthetic deformation field [1,2].

References:

[1] *Nasopoulou et al. Improved identifiability of myocardial material parameters by an energy-based cost function. BMMB (2017).*
[2] *Nasopoulou, et al. Feasibility of the Estimation of Myocardial Stiffness with Reduced 2D Deformation Data. FIMH (2017).*
[3] *Guccione et al. Passive material properties of intact ventricular myocardium determined from a cylindrical model. J Biomech Eng (1991).*

[A-08.1]

IMAGE TRACKING AND FLOW MODELLING OF HUMAN FETAL AND ANIMAL EMBRYONIC HEARTS

Choon Hwai Yap[1], *Wei Xuan Chan*[1], *Hadi Wiputra*[1], *Sheldon Ho*[1], *Ching Kit Chen*[2]

1 *National University of Singapore, Singapore, Singapore*
2 *National University Health System, Singapore, Singapore*

The developing fetal / embryonic heart is a fascinating organ, being the first organ to form, and undergoing tremendous amount of growth over gestation. In some cases, however, it can be congenitally malformed (0.6-1.9% of pregnancies), resulting in Tetralogy of Fallot (TOF) or Hypoplastic Left Heart Syndrome (HLHS). During pregnancy diseases such as Intrauterine Growth Restriction (IUGR), mal-remodelling and functional deterioration can also occur and persist after birth, elevating mortality and morbidity rates. Based on small animal studies, an ongoing hypothesis is that the biomechanics force environment directly influences growth and development of the prenatal heart. Pediatric cardiologists have also performed fetal heart intervention, and were able to rescue fetuses from the single ventricular outcome by restoring flow to the undergrown ventricle. We thus strive to understand the biomechanics of the prenatal heart and its impact on heart development.

Towards this goal, we studied human fetal hearts via 4D clinical ultrasound scans, and developed a novel 4D high-frequency ultrasound scan technique for chick embryonic hearts. Our chick embryonic scan technique was non-invasive, had great resolution to reveal fine features like aortic arches, and could scan embryos that were too large for OCT. To track the cardiac motions clinical and in vitro ultrasound images, we developed an algorithm that models cyclic cardiac motion as a B-spline-Fourier mathematical equation, which was curvefitted to pair-wise image-registration displacement fields. The result worked especially well in noisy and inconsistent ultrasound images, and had better accuracies than all participants in a previous cardiac motion analysis challenge.

In our human fetal heart studies, we have discovered that a similar pair of diastolic vortices characterized the diastolic intra-cardiac flow field for both the left ventricle (LV) and right ventricle (RV), and were the primary mechanism for elevated wall shear stress stimuli on the ventricles. Comparing normal to TOF hearts, there were chaotic RV inflow and RV-to-LV shunting that elevated RV wall shear stresses, and this could have caused the observed RV hypertrophy. In the embryonic heart, we discovered a two helical flow structures that rotated about each other in the embryonic outflow tract, which bore similarities to the spiral manner of eventual outflow tract septation, suggesting that flow might have guided the septation. Our whole heart simulations further revealed interesting biomechanics features of the embryonic atria. The atrial appendages were found to be highly contractile, having out-sized contributions to atrial stroke volume, suggesting that it may have a functional role in ejection. At the same time, however, they have high blood retention and low washout, and experiences oscillatory wall shear stresses.

Acknowledgments: National University of Singapore, Singapore, Singapore Young Investigator Award (2015, PI: Yap), Singapore Ministry of Education Tier 2 grant (MOE2018-T2-1-003, PI: Yap) for funding.

[A-08.2]

MULTISCALE MODELING OF NON-OHMIC CONDUCTION IN CARDIAC TISSUE: UPSCALING THE NON-LINEAR BEHAVIOR OF GAP JUNCTIONS

Daniel Hurtado[1], *Grigory Panasenko*[2], *Javiera Jilberto*[1]

1 *Pontificia Universidad Católica de Chile, Santiago, Chile*
2 *Institute Camille Jordan, Université Jean Monnet de Saint-Étienne, Lyon, France*

Electrical conduction in cardiac tissue is key for the normal function of the heart, as the contraction of the cardiac muscle is triggered by electrical impulses that travel throughout the heart domain in a synchronized manner. Under certain cardiac diseases, the electrical conduction is altered, which induces arrhythmias in the heart that can have deadly consequences. The relevance of conduction in the heart has prompted the development of mathematical models for the conductivity in the cardiac tissue to account for cell-level conduction mechanisms [1]. At the cellular level, intercellular conduction is mediated by the gap junctions, which are intercellular channels that control the passage of ions between cardiomyocytes. While the electrical behavior of gap junctions is highly non-linear, most models of electrical conduction in cardiac electrophysiology assume a linear electrical behavior of tissue, which is typically justified on phenomenological arguments [2]. In this work, we introduce a non-linear conduction model for cardiac electrophysiology. Our starting point is the consideration of two scales that govern the electrophysiology problem: a microscopic cell-level scale where the nonlinear behavior of gap junctions is carefully considered, and a macroscopic tissue-level scale where conduction takes place. Using the framework of two-scale non-linear asymptotic homogenization theory, we develop a model for effective conductivity at the tissue level that accounts for cell-level mechanisms of conduction mediated by gap junctions. We validate the proposed model by comparing the resulting travelling waves in terms of conduction velocity and wave profiles, using as a baseline a discrete model of conduction based on cell-to-cell interactions [3]. In particular, we show that the proposed model is able to capture the baseline simulations even in cases where the junctional coupling is severely reduced, outperforming standard models based on linear homogenization on these extreme regimes of conduction which are commonly found in infarcted cardiac tissue.

Acknowledgments: The authors acknowledge the support of the FONDECYT Grant #1180832, and from the Millenium Nucleus in Cardiovascular Magnetic Resonance.

References:

[1] J. C. Neu and W. Krassowska, "Homogenization of syncytial tissues," Crit. Rev. Biomed. Eng., vol. 21, no. 2, pp. 137–199, 1993.
[2] P. Colli Franzone, L. F. Pavarino, and S. Scacchi, Mathematical Cardiac Electrophysiology, vol. 13. 2014.
[3] J. P. Kucera, S. Rohr, and Y. Rudy, "Localization of sodium channels in intercalated disks modulates cardiac conduction," Circ. Res., vol. 91, no. 12, pp. 1176–1182, 2002.

[A-08.3]

SIMULATING VENTRICULAR GROWTH CAUSED BY ABNORMALITIES IN CARDIAC ELECTROMECHANICS

Jayavel Arumugam[1], Joy Mojumder[1], Ghassan Kassab[2], ***Lik Chuan Lee***[1]

1 *Michigan State University, East Lansing, USA*
2 *California Medical Innovations Institute, San Diego, USA*

Asynchronous electrical activation of the heart such as left bundle branch block with prolonged QRS complex can cause mechanical dyssynchrony. Over a period of time, dyssynchronous behavior of the heart can lead to progressive asymmetrical remodeling of the left ventricle (LV) with local increase and decrease in wall thickness at different regions. Motivated by a recent experiment [1] showing in real time both longitudinal elongation and lateral extension occurring in the myocyte in response to longitudinal stretching, we seek to determine whether having myofiber stretch as a single stimuli that controls growth in the myofiber and transverse directions (with different sensitivity) can quantitatively reproduce long term changes in ventricular geometry associated with mechanical dyssynchrony. To do so, we developed an anisotropic growth constitutive model that is coupled to an electromechanics (EM) modeling framework to simulate the effects of asynchronous activation associated with pacing at the LV free wall (LVFW). In the growth constitutive model, local changes in length in 3 material directions are driven locally by the deviation of maximum elastic myofiber stretch over a cardiac cycle from its corresponding homeostatic set point value. In the EM framework, cardiac electrical conduction is described by the modified FitzHugh-Nagumo equations and is coupled to a cardiac mechanics model comprising of a Fung-type passive constitutive model and an active stress constitutive model. A separation of timescale is invoked to couple the growth constitutive model with the EM modeling framework. Homogeneous growth and reverse growth rates related to the myofiber and transverse directions (4 parameters) were calibrated based on experimental data with similar chronic LVFW pacing protocol [2]. The calibrated model is able to quantitatively reproduce local and global measurements from the experiments, namely, an increase in septum wall thickness, a decrease in LVFW thickness and an increase in LV end-diastolic volume (Figure). We conclude that the prescription of elastic myofiber stretch as the sole growth stimulant can quantitatively reproduce long-term changes in ventricular geometry associated with mechanical dyssynchrony.

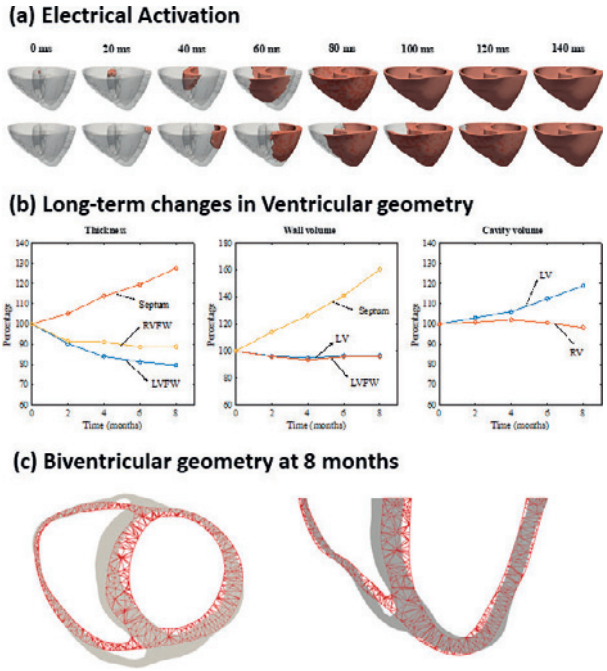

Figure Caption: (a) Electrical activation pattern of normal (top) and LVFW pacing (bottom). (b) Long term changes in ventricular geometry. (c). Resulting geometry at 8 months compared to baseline (red).

Acknowledgments: This work was supported by NIH (R01 HL134841, U01 HL133359-01A1), NSF 1702987, AHA 17SDG33370110, Burroughs Wellcome Fund.

References:

[1] *Yang H, Schmidt LP, Wang Z, et al. Dynamic Myofibrillar Remodeling in Live Cardiomyocytes under Static Stretch. Sci Rep. 2016;*
[2] *van Oosterhout MFM, Prinzen FW, Arts T, et al. Asynchronous Electrical Activation Induces Asymmetrical Hypertrophy of the Left Ventricular Wall. Circulation. 1998;98(6):588-595.*

[A-08.4]

COMPUTATIONAL CARDIAC MODELING: APPLICATION TO PULMONARY ARTERIAL HYPERTENSION

Reza Avaz[1], *Emilio Mendiola*[1], *Michael Sacks*[1]

1The University of Texas at Austin, Austin, USA

The development of integrated computational-experimental models of normal and impaired hearts offers novel ways to better understand the pathophysiology of heart remodeling in response to structural heart diseases and to design and personalize cardiac interventions. Pulmonary arterial hypertension (PAH) is a progressive structural heart disease that imposes a chronic pressure overload in the right ventricle (RV), leading to substantial remodeling events including hypertrophy of muscle cells, reorientation and alignment of muscle fibers (myofibers), and dilation of the RV [1,2]. Many studies, including ours, suggest that the fate of a patient with PAH is not determined by the degree of pressure overload but rather by how the RV responds to it. However, the question of how to predict whether the RV remodeling in response to PAH stabilizes or rapidly transitions to RV failure remains largely unanswered.

We recently developed a high-fidelity finite-element (FE) heart model of PAH using extensive time-course datasets from a normal (control) rat heart and from a post-PAH rat heart [3]. In this work, we extended our model to study time-course multiscale RV remodeling in response to PAH from control to post-PAH time points. We used our model to understand how the volumetric growth and structural remodeling events at multiple scales in the heart influence and interact with each other during the development of PAH. In particular, our model results suggest that augmentation of the intrinsic contractility of myofibers accompanied by an increase in passive stiffness of RV free wall is among the first remodeling events through which the RV strives to maintain the cardiac output. In contrast, we found that the reorientation and alignment of the fibers towards the longitudinal (apex-to-base) direction is rather a maladaptive mechanism that does not improve the overall contractility of the RV and advances together with RV dilation (Fig. 1) at the later stages of PAH development. Along these lines, we demonstrated the capability of our model to predict the compensatory level of the remodeling mechanisms and the possible transition of them to a mal-adaptive state. In conclusion, this research serves as an important step towards creating a robust computational platform to accurately predict the current stage and progression path of PAH, and accordingly guide patient-specific pharmaceutical and surgical interventions.

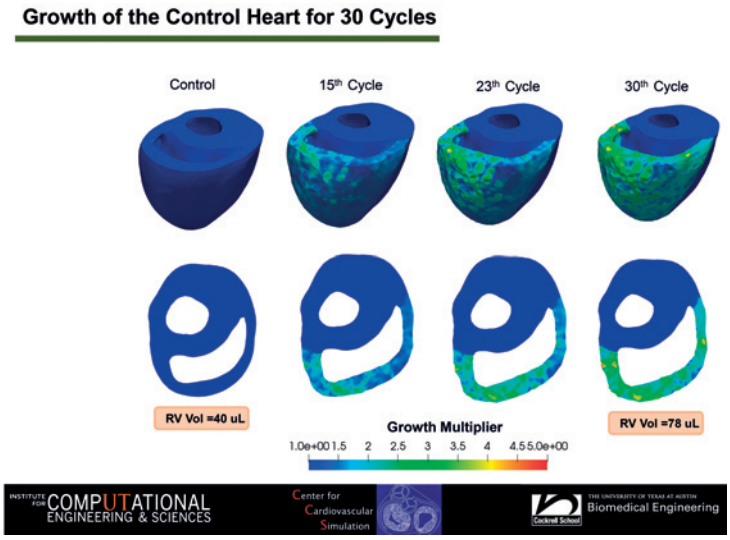

Figure 1. Figure Caption: Short-axis views of the evolution of the rat-specific FE model from the control to post-PAH state simulated by 30 growth cycles.

References:

[1] Hill, MR et al, Ann Biomed Eng, 42:2451-65, 2014.
[2] Avaz, R et al, APL Bioeng, 1:016105, 2017.
[3] Avaz, R et al, Ann Biomed Eng, 47:138-53, 2019.

[A-08.5]

THE RESPONSE OF INTEGRATED PARAMETRIC AORTIC VALVE IN A MECHANO-ELECTRICAL FULL HEART MODEL

Adi Morany[1], *Karin Lavon*[1], *Ashraf Hamdan*[2], *Danny Bluestein*[3], *Rami Haj-Ali*[1]

1 *School of Mechanical Engineering, Tel Aviv University, Tel Aviv, Israel*
2 *Department of Cardiology, Rabin Medical Center, Petah Tikva, Israel*
3 *PolyNova Cardiovascular, Inc., Stony Brook, USA; Stony Brook University, Stony Brook, USA*

The aortic valve (AV) is located between the left ventricle and the aorta. It is responsible for maintaining an outward unidirectional flow. Many hemodynamic and structural aspects of the AV have been extensively studied, however, more refined and multi-physics models are needed in order to better understand the AV bio-mechanical behavior.

This study deals with integrating a new parametric AV structural model with the electro-mechanical Living Heart Human Model ©(LHHM). The LHHM is a finite element robust and integrative model simulating human heart function capable of realistic electro-mechanical simulations. We have introduced and examined different parametric geometries of AV configurations and associated pathologies in the LHHM. New integrated structural AV models within the LHHM can predict the local stresses, during the cardiac cycle, more accurately due to the realistic boundary condition derived from the integration within the LHHM. It was found that ellipticity index, associated with min and max AV diameters, value correlates well to measured clinical data, while the AV perimeter matches the same trend. This increases the confidence in the predicted kinematic behavior including the leaflets coaptation and overall stresses. The new proposed coupled and integrated AV modeling, from the clinical point of view, can serve as a platform for design and implementation of pre-transcatheter aortic valve replacement procedures.

The second part of this study deals with two AV-FSI modeling approaches. The first FSI employs classical CFD-Structural modeling [1-3]. The second AV-FSI deals with using the Lettice Boltzmann (LB) technique for the fluid part of the simulations. Results from the two approaches are compared in order to gain better understanding over their impact on future clinical outcomes.

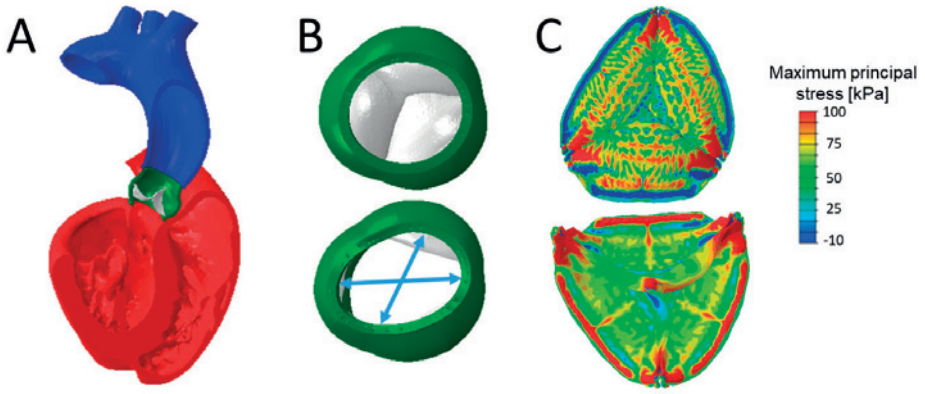

Figure Caption: (A) Integrated parametric aortic valve in a full heart model (B) Parametric aortic valve model during diastole (upper) and geometric max/min diameters during systole peak (lower) (C) Full coaptation and stress distribution over the leaflets during full diastole.

Acknowledgments: This study is supported by NIH-NIBIB BRP U01EB026414 grant.

References:

1. *Marom, G. et al. Medical & Biological Engineering & Computing, vol. 50, no. 2, pp. 173–82,2 (2012)*
2. *Halevi, R. et al. Medical & Biological Engineering & Computing, vol. 54, no. 11, pp. 1683–1694, (2016)*
3. *Lavon, K. et al. J. Biomech. Eng. 140,31010-31010–7 (2018)*

[A-08.6]

A MULTIPHYSICS MODEL OF CARDIAC FUNCTION: METHODS AND VALIDATION

Vijay Vedula[1], *Ju Liu*[1], *Oguz Tikenogullari*[1], *Ellen Kuhl*[1], *Alison Marsden*[1]

1Stanford University, Stanford, USA

The heart is a complex organ sustained by continuously interacting biochemical and physical processes. These include propagation of subcellular ionic currents in the electrophysiological system and activation potential dynamics, coupled with myocardial contraction, and its interaction with blood flow, each represented using complex mathematical models. [1] Although there have been significant independent developments in the respective communities, only recently has attention been drawn towards developing fully integrated cardiac models. The main challenges include large separation of time and length scales between electrophysiology and mechanics, feedback, tissue incompressibility, and valvular fluid-structure-interaction (FSI).

We present a novel multiphysics model of cardiac function that includes cardiac electrophysiology, tissue mechanics, intraventricular blood flow dynamics, and valve FSI. We employ a mono-domain model of myocyte activation and an operator-splitting based technique to integrate the reaction-diffusion type equations for cardiac conduction, coupled with the tissue mechanics using an active stress approach with feedback via stretch activated currents. [2] Our mechanics model is based on a unified variational multiscale formulation for solving hyper-elastodynamics. [3] The method can be used to solve fully incompressible structural dynamics using linear tetrahedral elements, which are typically used to represent patient-specific myocardium geometries. FSI with blood flow is modeled using the Navier-Stokes equations for incompressible flows written in arbitrary Lagrangian-Eulerian (ALE) coordinates. [3] We also present a novel implementation of a variational finite element-based immersed boundary method (FEIBM) to model the FSI with cardiac valves. The complex system of equations is integrated in time using the predictor-corrector algorithm based on generalized-alpha time integration scheme.

The current work focuses on developing each module in a segregated and weakly coupled manner within a single open-source finite element software framework. [4] We emphasize verification of each module using established benchmarks. Our ultimate goal is to create a fully integrated multiscale-multiphysics heart model that will open the door to new research directions in patient-specific modeling of congenital and acquired cardiovascular diseases including heart failure, remodeling, valve dysfunction, and device design.

Acknowledgments: The authors acknowledge technical discussions with Dr. Francisco Sahli and clinical data support from Dr. Ian Chen. The authors acknowledge financial support received through grants NSF SSI grant#1663747, NIH R01 grant#R01HL129727, Stanford CHRI and the Stanford NIH-NCATS-CTSA (grant UL1-TR001085), and computational resources received through NSF XSEDE grant ACI-1053575.

References:

[1] Quarteroni, A., et al., CMAME, 314, pp.345-407, 2017.
[2] Costabal, FS., et al. J. Biomechanics, 49(12), pp.2455-2465, 2016.
[3] Liu, J. & Marsden, AL., CMAME, 337, pp.549-597, 2018.
[4] Updegrove, A., et al., Annals Biomed. Eng., 45(3), pp.525-541, 2017.

[A-09.1]

CONSISTENT BIOMECHANICAL PHENOTYPING OF MURINE ARTERIES - LESSONS LEARNED, FUTURE NEEDS

Jay Humphrey[1]

1Yale University, New Haven, USA; Department of Biomedical Engineering; Yale University, New Haven, USA

Central arteries – mainly the aorta and common carotids – are fundamental to cardiovascular, neurovascular, and cerebrovascular health and disease for they dictate the hemodynamics that provides blood to these various organ systems. Congenital connective tissue, cytoskeletal, and nuclear disorders as well as hypertension, diabetes, natural aging, and other conditions can all adversely affect central artery hemodynamics via changes in arterial geometry, structure, properties, and function. There is, therefore, a pressing need to quantify and compare such changes as a function of the underlying condition. Towards this end, there is a pressing need for consistent methods of experimentation and data analysis.

Mouse models have been the model of choice in vascular research for many reasons, but the small size of these vessels demanded technological advances to enable rigorous and reproducible studies. In this presentation, we will first consider specific computer-controlled devices developed by our lab for this purpose and then use these methods to examine central arterial behaviors from myriad mouse models to glean general understanding of the effects of different extracellular matrix components, cytoskeletal constituents, and nuclear constituents on overall biomechanical behavior. Moreover, we will examine effects across different regions of the central vasculature to gain insight into the means by which local mechanics / mechanobiology affects global hemodynamics / physiology. Notwithstanding the longstanding appreciation in engineering for consistent methods – that is, standards such as those identified via ASTM – we renew the call for consistency within our field to broaden our ability to learn across many laboratories, not just within individual laboratories.

Acknowledgments: The murine data discussed herein were collected and/or analyzed by a host of talented Ph.D. students and post-doctoral fellows over the years, including Rudy Gleason, Seungik Baek, John Eberth, Art Valentin, Luca Cardamone, Heather Hayenga, Jacopo Ferruzzi, Matt Bersi, Paolo Di Achille, Sara Roccabianca, Kristin Miller, Chiara Bellini, Arina Korneva, Guangxin Li, Alex Caulk, Sae-Il Murtada, Bart Spronck, Manuel Rausch, Hossein Ahmadzadez, and Marcos Latorre. This work has been supported over the years largely by grants from the NIH, but also by generous support by Tommie E. and Carolyn S. Lohman (Texas A&M) and John C. Malone (Yale University, New Haven, United States).

[A-09.2]

BIOMECHANICS OF THE AORTA IN MOUSE MODELS OF AORTIC DISSECTION: FROM SYNCHROTRON IMAGING TO COMPUTATIONAL MODELING

Bram Trachet[1], Mauro Ferraro[2], Lydia Aslanidou[2], Gerlinde Logghe[1], Nikos Stergiopulos[2], ***Patrick Segers****[3]*

1 *Ghent University, Ghent, Belgium*
2 *Ecole Polytechnique Federale de Lausanne, Lausanne, Switzerland*
3 *Ghent University, Ghent, Belgium; Ibitech-Biommeda, Ghent, Belgium; Ghent University; IBiTech-bioMMeda, Ghent, Belgium*

Over the past 5 years, we have explored synchrotron-based X-ray phase-contrast imaging of the aorta excised from various mouse models of cardiovascular disease [1,2]. The technique yields 3D images with an isotropic resolution close to 1µm. This, together with the excellent soft tissue contrast, allows for the visualization of aortic elastic lamellae and hence provides 3D insight into the microstructure of soft tissue [2]. We used this technique to visualize the aorta of ApoE-/- knock-out mice infused with angiotensin II, a then well-established mouse model of abdominal aortic aneurysm. Based on our observations we proposed an elaborate hypothesis that explains how aortic side branches (i) affect the initiation and propagation of medial tears and the subsequent adventitial dissection and (ii) affect the variability in shape of dissecting aneurysms. The work led us to the conclusion that angiotensin II-infused mice are more clinically relevant for the study of aortic dissections than for the study of abdominal aortic aneurysms [3]. To reveal potential links between these sites of disease initiation and biomechanical stress, a computational study was set up whereby the aortic geometry of an animal exposed to 3 days of angiotensin II infusion was scanned both in vivo (contrast-enhanced micro-CT) and ex-vivo with phase-contrast X-ray tomographic microscopy (PCXTM). An automatic morphing framework was developed to map the non-pressurized, non-stretched PCXTM geometry onto the pressurized, stretched micro-CT geometry. The output of the morphing model was a structural FEM simulation where the output strain distribution represents an estimation of the wall deformation, not only due to the pressurization, but also due to the local axial stretch field. Hotspots of principal strain co-located with hotspots of early vascular damage as detected on PCXTM [4]. Our most recent synchrotron research has focused on ex-vivo imaging of the deforming 3D arterial microstructure of the mouse carotid artery under quasi-static pressure inflation up to 120 mmHg. We developed a method for the automated segmentation of individual lamellae and demonstrated how the three elastic lamellae stretch and unfold simultaneously as luminal pressure is increased. We did not find any differences in unfolding or stretching behavior between wild-type and ApoE-/- mice. Pressure-inflation experiments will be expanded to the aorta and will provide further insight in the aortic microstructure, particularly near side branches, and contribute to a better understanding of the mechanics of the arterial micro-structure.

References:

[1] Trachet B. et al. Cardiovascular Research 2015;105:213–222.
[2] Logghe G. et al. Scientific Reports 2018;8:2223.
[3] Trachet B. et al. Cardiovascular Research 2017;113:1230-1242.
[4] Ferraro M. et al. Annals of Biomedical Engineering 2018;46:159-170.

[A-09.3]

MULTI-SCALE ECM MECHANICS AND TRANSMURAL INTEGRITY OF THE ARTERIAL WALL

Yanhang (Katherine) Zhang[1]

1 *Boston University, Boston, USA*

Elastin and collagen fibers form the primary load-bearing extracellular matrix (ECM) components in the arterial wall. In arteries, elastic fibers form concentric layers of elastic lamella that are subjected to billions of stretch cycles during a lifetime. Alternating layers of smooth muscle cells anchor on either side to the adjacent lamellar layers that forms a contractile-elastic lamellar unit. Medial collagen fibers are closely associated with the elastin fibers. Large bundles of collagen fibers in the adventitia layer play an important role in preventing artery rupture at high pressures. The ECM not only provides structural support, but also acts as cellular microenvironment and plays important roles in modulating cell function. In this talk I will present our recent studies integrating multi-photon imaging and physiological mechanical loading to understand the multi-scale ECM mechanics in large elastic arteries. Contributions of different ECM constituents, elastic and collagen fibers, to arterial wall mechanics and transmural integrity, and the important role of micromechanical deformation of elastic lamellar layers in maintaining tissue homeostasis will be presented. Potential implications of these findings in several cardiovascular diseases will also be discussed.

Considering the structural and mechanical contributions of the ECM constituents, a multi-scale model was developed to directly incorporate information obtained from quantitative multi-photon imaging and analysis to study the mechanics and the transmural integrity of the arterial wall. A discrete fiber network model was created to incorporate the ECM structural properties (fiber orientation, fiber diameter, and areal density) as well as inter-fiber crosslinking of the elastin network. Such model was used to study tissue-level stress-stretch behavior and fiber-level deformation and kinematics in order to understand the role of inter-fiber crosslinking properties in the response of elastin network at multiple scales.

Acknowledgments: We would like to acknowledge the funding support from NIH (R01HL098028).

[A-09.4]

TISSUE RE-MODELING DURING THE PATHOGENESIS OF ABDOMINAL AORTIC ANEURYSMS

Justyna Anna Niestrawska[1], *Peter Regitnig*[2], *Christian Viertler*[2], *Tina U. Cohnert*[3], *Gerhard A. Holzapfel*[4]

1 *Institute of Biophysics, Graz, Austria; Medical University of Graz, Austria*
2 *Institute of Pathology; Medical University of Graz, Austria*
3 *Clinical Department of Vascular Surgery; Medical University of Graz, Austria*
4 *Institute of Biomechanics; Graz University of Technology*

Soft biological tissues such as arterial walls can be seen as composites consisting of a matrix and several collagen fiber families. It has been shown that the remodeling of structural components in these tissues plays a significant role in their pathogenesis. Therefore, there is a need to understand the changes in structural components of arteries during diseases in detail. We systematically examined changes in microstructure, histology and mechanics of abdominal aortic aneurysms (AAA) and correlated them to disease progression.

AAA walls were subjected to biaxial tension tests, second-harmonic generation imaging after optical clearing [1] and histological staining using Elastica van Giesson, Sudan Red and Hemotoxylin and Eosin. Structural data was analyzed via fitting to a bivariate von-Mises distribution which yielded the main fiber directions and two dispersion parameters for in-plane and out-of-plane dispersion. Both structural and mechanical parameters were incorporated into an existing constitutive model [2]. Mechanical data was used to define the point of collagen recruitment, i.e. the point where the non-linear stress-strain curve stiffens, yielding three disease progression stages. Lastly, 14 parameters were determined analyzing the histological data, such as ratios of layers, content of smooth muscle cells, elastin and abluminal adipocytes. In total we obtained 26 parameters which were statistically compared.

Levels of disease progression were defined in three stages depending on the point of collagen recruitment. Stage 1 had a recruitment point similar to healthy tissues, stage 2 was significantly more compliant and stage 3 showed the stiffest behavior.

Differences were found to be significant between the stages in, e.g., collagen orientation, elastin and abluminal lipid content. Nerves in the middle of the walls (see Figure) indicated a significant deposition of new collagen adjacent to inflammatory cells only on the abluminal side of AAA walls, increasing throughout the stages. Stage 3 showed two kinds of remodeled walls: Walls which seemed to be remodeled 'safely', exhibiting thick struts of collagen and almost no adipocytes inside the wall, and 'vulnerable' walls, exhibiting significant amounts of adipocytes throughout the wall, adjacent to inflammatory cells (see Figure, Stage 3).

The proposed study resulted in a novel hypothesis describing AAA disease progression, which was derived by a systematic comparison of histological, structural and mechanical changes.

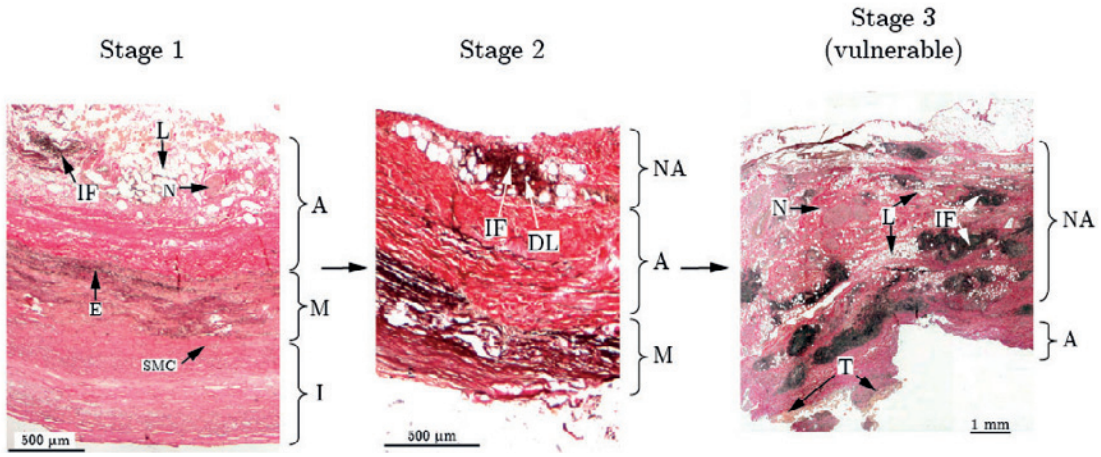

Figure Caption: Micrographs representing the three proposed disease stages. IF: inflammatory cells, N: nerves, L: adipocytes, A: adventitia, NA: neo-adventitia

References:

[1] J.A. Niestrawska et al., J. R. Soc. Interface, 2016.[2] G.A. Holzapfel, J.A. Niestrawska et al., J. R. Soc. Interface, 2015.

[A-09.5]

COLLAGEN REMODELING IN SACCULAR ANEURYSMS: A STUDY IN AN ELASTASE INDUCED ANIMAL MODEL

Chao Sang[1], *David Kallmes*[2], *Simon Watkins*[1], *Anne Robertson*[3]

1University of Pittsburgh, Pittsburgh, USA
2Mayo Clinic, USA
3Department of Mechanical Engineering and Material Science, University of Pittsburgh, Pittsburgh, USA; University of Pittsburgh, Pittsburgh, USA

Intracranial aneurysm (IA) rupture followed by subarachnoid hemorrhage has high morbidity and mortality rates (40-65%) [1]. Improved risk assessment and treatment of IAs needs to be developed to avoid the substantial risks associated with current treatments to prevent rupture. It is essential to gain better understanding of the temporal development of IAs to meet these needs. Although effective collagen fiber remodeling is a critical factor in avoiding IA rupture, little data is available [2]. A central challenge is that human samples can only be obtained at a single time point and therefore, animal models are needed to study the progression of collagen remodeling in IAs.

In this study, we use an elastase-induced saccular aneurysm model in rabbits to study collagen remodeling under saccular flow conditions [3]. The clinical relevance has been previously demonstrated [4,5]. Aneurysm tissue along with control vessels were harvested at 4 time points (2, 4, 8 and 12 weeks) after creation. Computational studies of the intramural loads demonstrated a shift to a more biaxial load state following aneurysm creation, resulting from increased longitudinal load. To assess the remodeling response, samples of aneurysm and control were uniaxially tested simultaneous with multiphoton microscopy imaging. Specimens were then tested to failure [6]. Tissue specific fiber dispersion constitutive models were developed using fiber orientation distributions obtained from multiphoton data.

In control arteries, collagen fibers are largely circumferentially aligned in the media and more tortuous and disperse in the adventitia. Under axial load, these fibers remained largely unrecruited even at nearly 100% strain. In the remodeled aneurysm, a new layer developed between the media and adventitia that displayed a multi-directional distribution of fibers. The new layer was found in all cases by four weeks and seen at all subsequent time points. These fibers were capable of longitudinal load bearing and recruited to axial load bearing by 40% strain. Even at 12 weeks, the remodeled aneurysm walls showed a distribution of strength, a characteristic of unruptured human aneurysms [2], suggesting the rabbit model could be a useful platform for evaluating pharmacological treatments. The time dependent constitutive models developed here can be utilized in computational studies of aneurysm progression [7].

Acknowledgments: The authors are grateful for support from National Institutes of Health under NINDS grant 1R21NS088256.

References:

[1] Fennell, V.S., et al., Front Surg, 3:43, 2016.
[2] Robertson, A.M. et al., Ann Biomed Eng, 43(7): 1502–1515, 2015.
[3] Altes, T.A. et al., Am J Roentgenol, 174(2): 349–354, 2000.
[4] Zeng, Z. et al., Am J Neuroradiol, 32(3):595–601, 2011.
[5] Wang, S. et al, J Neurointerv Surg, neurintsurg-2017, 2017.
[6] Sang, C. et al., J Biomech Eng, 140: 1–10, 2018.
[7] Watton, P.N. et al, J Biomech, 42(9): 1320-1325., 2009.

[A-09.6]

PATIENT-SPECIFIC COMPUTATIONAL PREDICTIONS OF HUMAN ASCENDING THORACIC ANEURYSM GROWTH

Stéphane Avril[1], *Jamal Mousavi*[2]

1 *University of Lyon - Mines Saint-Etienne, Saint-Etienne, France; École des Mines de Saint-Étienne, Université de Lyon, Saint-Etienne, France*
2 *University of Lyon - Mines Saint-Etienne, Saint-Etienne, France*

Recently, growth and remodeling (G&R) has been increasingly approached based on the constrained mixture theory (CMT) to predict a variety of arterial mechanobiological behaviors [1, 2]. Most of previously published work has been limited to simplified cases as isotropic growth, axisymmetric motions, mono-layer wall and/or membrane approximations. Although such models have increased our insights in vascular adaptation, a 3D anisotropic bilayer model has the potential of considering more complex cases of arterial G&R such as aortic root enlargement. Therefore, herein, a 3D numerical model based on homogenized CMT is implemented in ABAQUS through a coupled UEL to predict anisotropic G&R of arteries. At the Gauss points level, the passive behavior is assumed hyperelastic and a strain energy function (SEF) is assumed for each constituent with decoupled contributions of the purely volumetric and isochoric parts. Although the same SEF is assumed for every element across the geometry of the artery, different material properties and mass fraction can be applied at each layer. It is considered that the arterial wall is composed of a constrained mixture of elastin, collagen fibers and smooth muscle cells (SMC) and includes the in situ stresses existing in the reference configuration. Four collagen fibers with different mass fractions in media and adventitia in the axial, circumferential and angular directions are considered. The contractility of SMC and turnover of collagen fibers are assumed stress dependent. Simulations are performed on a bilayer thick-wall geometry reconstructed from the CT scan of patients harboring an ascending thoracic aortic aneurysm (ATAA), subjected to boundary conditions in homeostatic conditions. Two different mechanisms are considered for the initiation of aneurysm enlargement, namely loss of SMC contractility and proteolytic injury. The regional distribution of these effects is related to local wall shear stress obtained from computer fluid dynamics. Different gain parameters for collagen turnover are considered. The models are able to predict realistic aortic root enlargement as confirmed by a follow-up MRI performed on the same patient. Our findings indicate the determinant role of SMC contractility during ATAA growth.

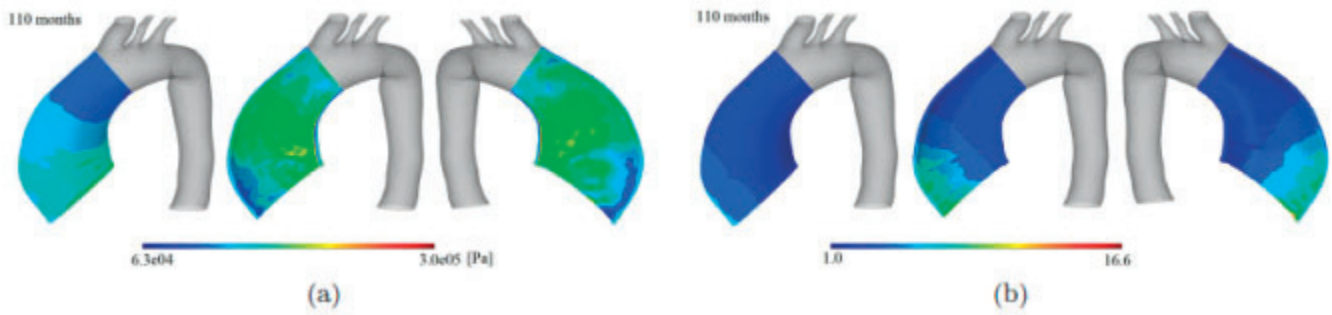

Figure Caption: Evolution of the distribution of the maximum principal stress and normalized collagen mass density in a two-layer patient-specific human ATAA

Acknowledgments: The authors are grateful to the European Research Council for grant ERC-2014-CoG BIOLOCHANICS.

References:

[1] *F.A. Braeu, A. Seitz, R.C. Aydin and C.J. Cyron. Holzapfel. Homogenized constrained mixture models for anisotropic volumetric growth and remodeling. Biomech Model Mechanobiol, 29(8): 16(3):889–906, 2017.*
[2] *A. Valentín, J.D. Humphrey and G.A. Holzapfel. A finite element-based constrained mixture implementation for arterial growth, remodeling, and adaptation: theory and numerical verification. Int J Numer Method Biomed Eng, 29(8):822–49, 2013.*

[A-10.1]

DISSECTION POTENTIAL INDEX (DPI): A BIOMECHANICS-BASED RISK PREDICTION METRIC FOR AORTIC DISSECTION

David Vorp[1], Spandan Maiti[2], Leonid Emerel[3], Thomas Gleason[4]

1 *University of Pittsburgh, Pittsburgh, USA; Department of Bioengineering; Department of Ct Surgery*
2 *University of Pittsburgh, Pittsburgh, USA; Department of Bioengineering*
3 *Department of Ct Surgery; University of Pittsburgh, Pittsburgh, USA*
4 *Division of Cardiac Surgery, School of Medicine, University of Pittsburgh, Pittsburgh, USA; Upmc Heart and Vascular Institute, Pittsburgh, USA; Upmc Center for Thoracic Aortic Disease, Pittsburgh, USA*

Type A Aortic Dissection (AoD) is a highly lethal disease initiated by a tear in the intima of the ascending aorta. Current clinical guidelines are inadequate predictors of the dissection risk [1] necessitating the need of improved evidence-based risk prediction metrics. While preceded by biologic changes and degeneration, AoD is a biomechanical delamination of the aortic wall layers. We have previously defined a "Rupture Potential Index" for abdominal aortic aneurysm based on point-wise predictions of wall strength compared to wall stress [2]. Our objective in this work was to establish the dissection potential index (DPI), a metric for early adjudication of AoD risk based on the failure biomechanics of the ascending aorta. AoD patients with pre-AoD CT imaging (n=10), and a control set of patients without AoD but matched by age, sex, body mass index, heart valve type, aortic diameter and blood pressure (n=8) were chosen as study groups. Thoracic CT scans were taken and the segmentation software Volume Viewer (GE Healthcare, Chicago, IL) was used to generate solid models of the aorta that were subsequently smoothed using Meshmixer (Autodesk, San Rafael, CA). Resulting models were meshed by Trelis (csimsoft, American Fork, UT) and were analyzed using a custom finite element software to produced wall stress mappings. The DPI relating the stress to population-specific aortic wall strength (from previously published uniaxial tensile experiments [3]) was mapped over the entire aorta. Locations of dissection origin were identified by direct evaluation of perioperative contrast CT scans by clinicians blinded to the DPI mapping and compared to the regions of high dissection potential. There was significant difference ($p<0.005$, Student's t-test) in the peak DPI of the control set (0.30±0.04,mean±std) and the AoD set (0.49±0.06). Peak DPI revealed a monotonic increase for patients with multiple CT scans taken over a period of time. We also found that DPI was >0.30 in regions of clinically observed dissection for 8 patients. In general, there was elevated DPI on the greater curvature of the ascending thoracic aorta compared to the rest of the aorta. Our findings support using this new, biomechanics-based approach to predicting aortic dissection potential using multiple patient-specific imaging data points. Our paradigm using patient-specific non-invasive clinical data points will likely improve our ability to predict AoD and thus better direct elective aortic intervention relative to the current guidelines that are based on maximal orthogonal aortic dimensions.

References:

[1] Emerel, L et al., J Thorac Cardiovasc Surg, In Press, 2019.
[2] Vande Geest, JP et al., Ann N Y Acad Sci. 1085:11-21, 2006.
[3] Pichamuthu, JE et al., Ann Thorac Surg, 96:2147-54, 2013.

[A-10.2]

UNDERSTANDING FAILURE MECHANISMS IN TUNICA ADVENTITIA: MULTI DIRECTIONAL EXPERIMENTS AND A UNIFYING MICROSTRUCTURAL FINITE ELEMENT MODEL

Venkat Siva Radha Krishna Ayyalasomayajula[1], *Baptiste Pierrat*[2], *Pierre Badel*[1]

1 *Mines Saint Etienne, Saint Etienne, France; Inserm U1059, Saint-Priest-en-Jarez, France*

2 *University of Lyon - Mines Saint-Etienne, Saint-Etienne, France; Inserm U1059, Saint-Priest-en-Jarez, France; Center for Biomedical and Healthcare Engineering, Mines Saint-Étienne, Saint-Etienne, France*

Tunica adventitia is the outer most layer of the arterial wall. It stands as the last barrier, acting as a protective sheet preventing the artery from overextension at loads much higher than physiological level. Current rupture risk assessment indicators are not always reliable suggesting the need for more information about multi-scale failure behavior of the tissue. In this study, we investigated the mechanical response of the adventitia under uniaxial tension to be eventually realized by a unified microstructural model.

Porcine aortas procured from a local butchery were used in this study. The medial layer of the artery was carefully peeled off from each excised section and the resulting adventitial strips were frozen until the day of the experiment. A TA ElectroForce tensile machine was used to conduct the uniaxial tensile tests. The samples were stretched either until failure or until the limit of the tensile machine. On the other hand, collagen fiber networks were numerically reconstructed for finite element analysis based on morphological parameters extracted from SHG microscopy images previously obtained on similar samples [1]. Each morphological parameter was identified with a probability distribution, using which a range of initial morphological arrangements had been created. The resulting mechanical response from the generated networks was numerically pre-computed to build a surface response. This was used to accelerate an inverse identification procedure yielding morphological and mechanical parameters for experimental responses where a direct morphological analysis of images was not possible.

The validation against experimental data until the point of rupture showed good agreement of the proposed modelling approach. For the moment, damage propagation was not included in the model. However, an examination of the mechanical state of the fibers at the point of rupture reveals interesting details. It shows that at the point of rupture, tensile strain in fibers is close to their tensile strain limit of 0.2-0.25 [2] for a significant number of them in each case. These results highlight the role tensile strain limit of collagen fiber plays in adventitial rupture under uniaxial extension, which should be investigated under more physiological loading conditions. In conclusion, the microstructural model provides better insights into failure mechanisms of complex fiber based tissues, which could be used to replace the existing rupture risk indicators.

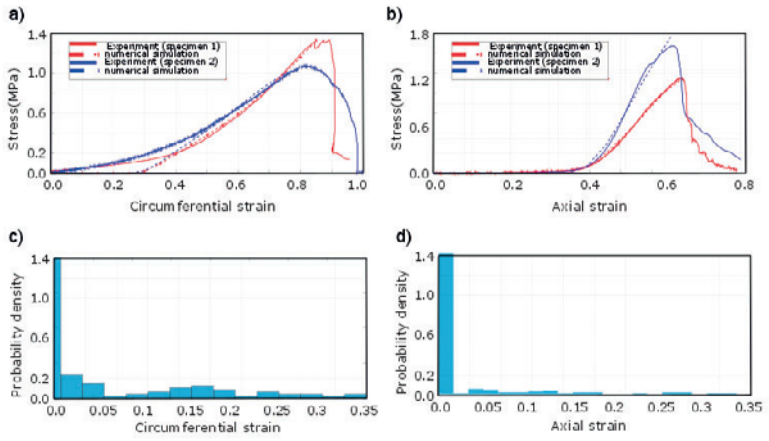

Figure 1 Comparison of numerical simulation to experimental data a) Circumferential specimens, b) axial specimens; Fiber tensile strain distribution at rupture in c)Circumferential specimen, d) axial specimen

Acknowledgements: This work was supported by the European Research Counsil [starting grant n°638804, AArteMIS]

References

[1] C. Cavinato, C. Helfenstein-Didier, T. Olivier, S. R. du Roscoat, N. Laroche, and P. Badel. J. Mech. Behav. Biomed. Mater., vol. 74, pp. 488–498, Oct. 2017.

[2] E. Gentleman, A. N. Lay, D. A. Dickerson, E. A. Nauman, G. A. Livesay, and K. C. Dee. Biomaterials, vol. 24, no. 21, pp. 3805–3813, Sep. 2003.

[A-10.3]

MULTISCALE BIOMECHANICAL INVESTIGATION OF HUMAN AORTAS: EXTRACELLULAR MATRIX ULTRASTRUCTURE UNDER LOAD

Anna Pukaluk[1], *Anna Wittgenstein*[1], *Gerd Leitinger*[2], *Dagmar Kolb-Lenz*[2], *Gerhard A. Holzapfel*[3], *Gerhard Sommer*[4]

1 *Institute of Biomechanics, Graz University of Technology, Graz, Austria*
2 *Gottfried Schatz Research Center, Medical University of Graz, Graz, Austria; Center for Medical Research, Medical University of Graz, Graz, Austria*
3 *Institute of Biomechanics, Graz University of Technology, Graz, Austria; Norwegian Institute of Science and Technology, Trondheim, Norway*
4 *Institute of Biomechanics, Graz University of Technology; Institute of Biomechanics, Graz University of Technology, Graz, Austria*

In aortic tissues, the components of the extracellular matrix (ECM) play a crucial role in withstanding applied force, which results in a nonlinear exponential response with noticeable stiffening effects at higher pressure [1]. This behavior indicates mutable contribution of the ECM constituents to the applied load. Moreover, the response to load is influenced by diseased conditions such as atherosclerosis triggered by tissue remodeling, which is observed at all levels of the hierarchical structure of the aorta [2]. Therefore, the identification of the changes of the aortic tissue ultrastructure in health and disease under loading is crucial to understand, how the components of the ECM interact and contribute to the mechanical deformation.

To reveal the structure alteration under load, an intact aortic wall was biaxially tested and chemically fixed at a defined stretched state by means of glutaraldehyde. Subsequently, the specimen was post-fixed in cuprolinic blue to visualize proteoglycans, stained in uranyl acetate, dehydrated in graded alcohol and embedded in resin [3]. Ultra-thin sections were contrasted with platinum blue and lead. Afterwards, sections were investigated by electron tomography. The SerialEM software was used for tilt series acquisition and IMOD for 3D reconstruction [4]. Image segmentation and visualization was performed by Matlab and Amira, respectively.

As an example, an image of tilt series (left figure) and the spatial reconstruction of an unloaded healthy human aortic media (right figure) disclose long straight collagen fibers and short bacillar structures of proteoglycans, which are nearly perpendicular to the collagen fibers.

Biaxial extension tests in combination with electron tomography allow visualization, reconstruction, and quantification of structural changes in healthy and diseased samples caused by the applied load. The investigation of the correlation between the alteration of the tissue architecture, health status and stretch is a step forward to understand the development, growth and remodeling principle, and the response to pathological conditions.

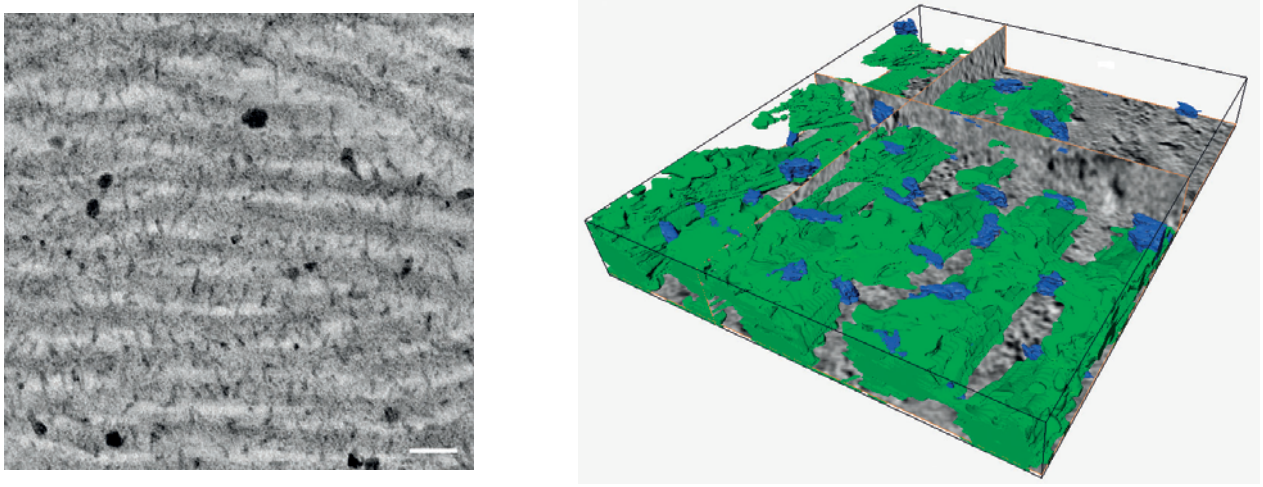

Figure: Left: TEM image from tilt series shows the medial layer of a healthy unloaded aortic wall. Collagen fibrils appear as long light gray strips, while proteoglycans occur as short bacillar dark grey structures. White bar indicates 100 nm. Right: 3D visualization of collagen fibrils and proteoglycans in the human aortic media. The long green structures correspond to collagen fibrils and the blue structures represent proteoglycans.

Acknowledgments: We thank Augustin Donnerer from the Institute of Pathology, Medical University Graz, for his valuable support during tissue harvesting. Furthermore, we gratefully acknowledge the financial support from the Austrian Science Funds (FWF) with grant no. P30260.

References:

[1] *Holzapfel, Gasser and Ogden, J Elasticity, 61:1–48, 2000.*
[2] *Cranford and Buehler, Nanotechnol Sci Appl, 3:127–148, 2010.*
[3] *Williams, et al., Acta Biomat, 5:993–1005, 2009.*
[4] *Mastronarde, J Struct Biol, 152:36–51, 2005.*

[A-10.4]

NUMERICAL IMPLEMENTATION OF FIBER DISPERSION IN A GROWTH AND REMODELING MODEL

Nino Horvat[1], *Gerhard A. Holzapfel*[2], *Igor Karšaj*[1]

1 *Faculty of Mechanical Engineering and Naval Architecture; University of Zagreb, Zagreb, Croatia*
2 *Norwegian University of Science and Technology, Trondheim, Norway ; Graz University of Technology, Graz, Austria*

Human aortas can be viewed as fibrous composites with three layers (intima, media, and adventitia) and three main load-bearing constituents (elastin, collagen fibers, and smooth muscle cells). Collagen fibers are grouped into several families with different mean directions and dispersion that vary from layer to layer. Furthermore, diseased aortas (e.g., abdominal aortic aneurysms) are characterized with local loss of elastin and an increased dispersion when compared with healthy aortas [1].

Numerical studies that focus on the modeling of healthy arterial walls and aortic aneurysms often use growth and remodeling (G&R) models that can describe processes within the aortic wall and responses of the aorta to different mechanical and chemical stimuli. To the best of the authors' knowledge none of the studies so far has combined fiber dispersion with a constrained mixture G&R model. Our aim here is to extend a current G&R model by integrating fiber dispersion, and to study the influence of fiber dispersion on abdominal aortic aneurysm (AAA) evolution.

For modeling AAA growth, we use a constrained mixture G&R model, slightly adapted from [2], and a fiber dispersion model presented in [3]. The dispersion model is based on the generalized structure tensor approach and can capture non-symmetric fiber dispersion (i.e. different dispersions in tangential plane and out-of-plane). Numerical models were implemented in the finite element analysis program FEAP using subroutines for user-defined material models. The aortic wall was modeled as a three-layer structure. Each layer was defined by different mass ratios of main constituents, mean fiber angles of the two collagen fiber families, and dispersion parameters.

The influence of fiber dispersion was analyzed using an arterial cylindrical model and an axisymmetric model of a fusiform aneurysm. In order to initiate the formation of an aneurysm, elastin was locally degraded. Results have shown that collagen fiber dispersion has a significant influence on the aortic wall behavior, and the outcome of aneurysm growth. Hence, we suggest that fiber dispersion should be taken into account in future G&R studies.

Acknowledgments: This work was supported by a grant from the Croatian Science Foundation (project IP-2014-09-7382 I. Karšaj) and by the project Training of New Doctoral Students (DOK-2015-10-3164).

References:

[1] *J.A. Niestrawska, C. Viertler, P. Regitnig, T.U. Cohnert, G. Sommer, and G.A. Holzapfel, "Microstructure and mechanics of healthy and aneurysmatic abdominal aortas: experimental analysis and modelling", Journal of the Royal Society Interface, 13:20160620, 2016.*
[2] *I. Karšaj, J. Sorić, and J.D. Humphrey, "A 3-D framework for arterial growth and remodeling in response to altered hemodynamics", International Journal of Engineering Science, 48:1357-1372, 2010.*
[3] *G.A. Holzapfel, J.A. Niestrawska, R.W. Ogden, A.J. Reinisch, and A.J. Schriefl, "Modelling non-symmetric collagen fibre dispersion in arterial walls", Journal of the Royal Society Interface, 12:20150188, 2015.*

[A-11.1]

COMPUTATIONAL ASSESSMENT OF RISK OF SUBDURAL HEMATOMA ASSOCIATED WITH VENTRICULOPERITONEAL SHUNT PLACEMENT

Milan Toma[1], *Sheng-Han Kuo*[2]

1 *New York Institute of Technology, New York, USA*
2 *Columbia University, New York, USA*

Hydrocephalus is an accumulation of cerebrospinal fluid (CSF) within the brain. The condition yields increased pressure inside the skull. When excess CSF collects in the ventricles of the brain, ventriculoperitoneal (VP) shunt is routinely implanted. A VP shunt redirects fluid from the ventricles to the abdominal cavity. However, the VP shunt is sometimes associated with several complications, e.g. subdural hematoma. A subdural hematoma is a collection of blood outside the brain caused by the sudden shrinkage of the brain as the CSF is drained away by the shunt implant. However, the mechanism of the development of subdura hematoma remains not entirely clear as dynamic alterations between CSF, intraparenchyma, and ventricular pressure. Therefore, we aim to establish a model to simulate this interaction to understand the mechanism.

A comprehensive and validated fluid-structure interaction (FSI) model of the head, Fig. 1, is used [1,2]. The smooth-particle hydrodynamics (SPH) method is used to simulate the CSF flow when redirected from the ventricles. Fluid motion and boundary interaction calculations were solved with the IMPETUS Afea gamma-SPH Solver® (IMPETUS Afea AS, Norway), and large deformations in the solid parts were simultaneously solved with the IMPETUS Afea Solver®. Both the solvers use a commodity GPU for parallel processing.

The areas with decreased CSF pressure upon removal of CSF by simulating VP shunt are identified. The interaction between the CSF and all the brain structures is analyzed. The CSF-brain interaction shows distinct areas with higher stress values. Different rates of the speed by which the CSF is drained away are used to compare the resulting stress and pressure values.

The exact mechanisms that govern the occurrence of the subdural hematoma associated with the VP shunt placement are not fully understood. Computational simulations allow us to look closer at what is happening in the outermost layers of the brain where the hematoma occurs during the drainage of the CSF. A correct recognition of predictive outcome factors can help us to assess the risk of VP shunt placement and also towards the development of individualized algorithm for risk assessment of subdura hematoma.

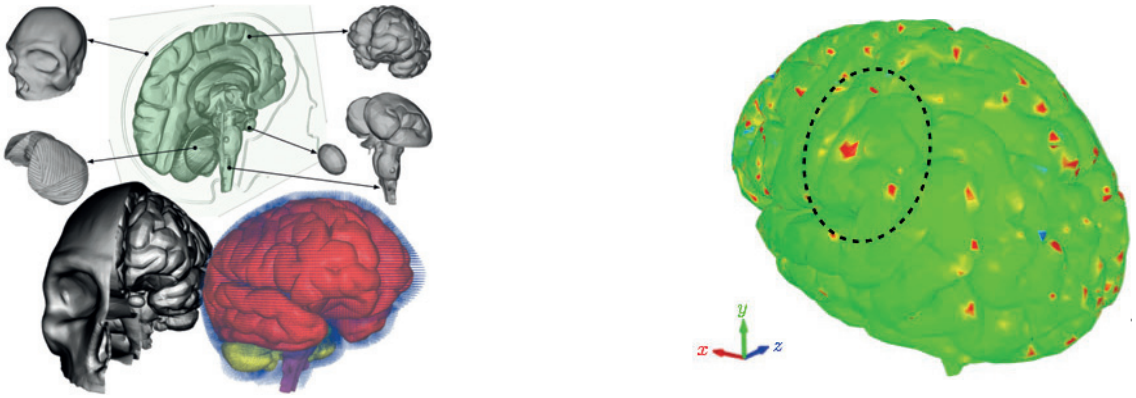

Figure Caption: (Left) The five distinct anatomical structures used in this model are shown. The skull, cerebrum, cerebellum, pituitary gland, and brainstem each have unique material properties. (Right) The higher stress values observed in the outermost layer of the brain.

References:

[1] *M. Toma, P. D. H. Nguyen, "Fluid-structure interaction analysis of cerebrospinal fluid with a comprehensive head model subject to a rapid acceleration and deceleration", Brain Injury, 2018, Volume 32, Issue 12, pp 1576-1584, doi: 10.1080/02699052.2018.1502470.*
[2] *M. Toma, P. D. H. Nguyen, "Coup-Contrecoup Brain Injury: Fluid-Structure Interaction Simulations", International Journal of Crashworthiness, 2019, [Online ahead of print], doi: 10.1080/13588265.2018.1550910*

[A-11.2]

SHEAR WAVE SPEED IS SENSITIVE TO TENSIOMETER-TISSUE INTERACTIONS: A PARAMETRIC MODELING STUDY

Joshua Roth[1], *Jonathon Blank*[1], *Darryl Thelen*[1]

1University of Wisconsin, Madison, USA

Background: Shear wave tensiometers are novel sensors that enable the direct non-invasive measurement of soft tissue loading in vivo by measuring shear wave propagation speed [1]. In general, a shear wave tensiometer consists of one actuator that induces a shear wave in the tissue of interest and two sensors that track shear wave propagation (Figure 1). Because tensiometer design factors (e.g., mass, stiffness) and user factors (e.g., application force) might alter the shear wave speed-load relationship, the objective of this study was to develop and demonstrate the utility of a parametric finite element model to investigate tensiometer-tissue interactions.

Methods: We created a parametric finite element model of the interaction between a tensiometer and a representative tendon (FEBio version 2.8.5.0 [2]). We modeled the tendon as an incompressible, transversely isotropic hyperelastic (Mooney-Rivilin model) cylinder [1] and the actuator and sensors of the tensiometer as rigid cylinders. We modeled the stiffness and damping of the tensiometer with a spring and damper in parallel behind the actuator and each sensor. To demonstrate the utility of our parametric finite element model, we used a three-factor Box-Behnken design resulting in 13 total models to investigate how shear wave speed changes with changes in (1) the force with which the actuator and sensors were pressed into the tendon, (2) the stiffness of the springs behind each sensor, and (3) the mass of the sensors. We performed multiple linear regression with interaction to characterize the sensitivity of the shear wave speed to all three factors.

Results and Discussion: The predicted wave speeds ranged from 62-69 m/s (Figure 1), which are similar, on the lower end, to the those predicted by a tensioned beam model [1]. The wave speeds were most sensitive to application force and spring stiffness with the higher wave speeds observed when spring stiffness was high and application force was low. It is likely that the springs increase the net effective stiffness, by supplementing the restoring forces that arise from axial tension and the shear modulus of the tissue.

Conclusions: Our parametric finite element model provides a platform for investigating how user factors and novel tensiometer designs can alter wave propagation. Our next step is to perform a large-scale sensitivity study by launching 1000's of instances of the model on a high-throughput computing grid. Such large-scale studies are important to determine the extent that sensor components, user factors, and even surrounding tissue alter the dynamics of the system. Understanding this and how well controlled ex vivo results translate to in vivo measurements is critical to utilizing shear wave tensiometry in medical applications.

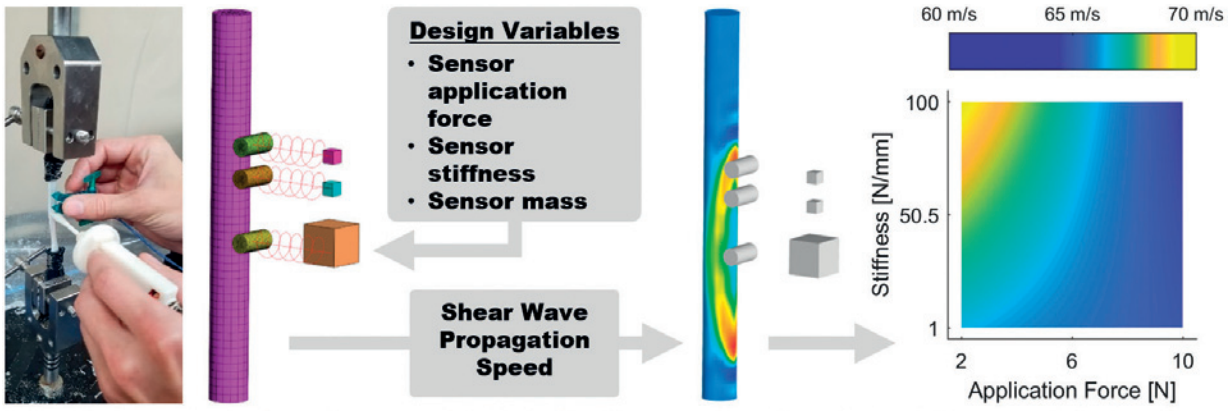

Figure 1. Our ex vivo testing setup was modeled in FEBio. The general workflow of a simulation was a static step of tensile ramp loading to 5 MPa followed by another static step of "pressing" the tensiometer against the surface of the ligament. Next, a dynamic step began with a rapid displacement of the actuator into the ligament (0.1 mm in 0.1 msec) followed by 0.9 msec of tracking wave propagation of the induced shear wave. The transverse accelerations of the sensor bodies during the dynamic step were extracted and cross-correlated to determine shear wave speed [1].

Acknowledgments: NIH (2 T32 AG 213-27)

References:

[1] Martin, Nat Comm, 2018; [2] Maas SA, J Biomech Eng, 2012

[A-11.3]

ESTIMATION OF PATIENT-SPECIFIC CENTRAL HEMODYNAMIC QUALITIES FROM BRACHIAL PRESSURE AND PULSE WAVE VELOCITY

Vasiliki Bikia[1], *Stamatia Pagoulatou*[1], *Dimitrios Soulis*[2], *Athanase D. Protogerou*[3], *Theodore G. Papaioannou*[2], *Nikolaos Stergiopulos*[1]

1 *Swiss Federal Institute of Technology, Laboratory of Hemodynamics and Cardiovascular Technology, Lausanne, Switzerland*
2 *National and Kapodistrian University of Athens, "Hippokration" Hospital, Medical School, Biomedical Engineering Unit, 1st Department of Cardiology, Athens, Greece*
3 *National and Kapodistrian University of Athens, "Hippokration" Hospital, Medical School, Department of Pathophysiology, Athens, Greece*

Introduction: Central hemodynamic qualities, such as cardiac output (CO) and central blood pressure, are believed to contain more clinically relevant information than the corresponding peripheral measurements [1]. Estimation of central aortic pressure is often achieved by the use of generalized transfer functions which do not necessarily reflect the state of the cardiovascular system in a patient-specific way. In the case of CO, monitoring requires an ultrasound device and trained clinician to be present, and thus is rather expensive. Here, we introduce a novel approach to estimate CO and central systolic blood pressure (cSBP) from brachial pressure measurement and carotid-to-femoral pulse wave velocity (cf-PWV). We do so by effectively tuning a generalized mathematical model of the arterial tree to patient-specific measurements. Methods: The tuning of the previously validated one-dimensional arterial tree model [2] is achieved via a two-layer optimization algorithm. In a first internal optimization loop, compliance and resistance of the generic arterial tree model are adjusted so that simulated brachial systolic and diastolic pressures converge towards the measured brachial systolic and diastolic pressures. In a second external optimization loop, aortic flow is modified in order to capture the measured cf-PWV value. The process is repeated until full convergence in terms of both brachial pressures and PWV is reached. To appraise the accuracy of our method, we implemented the algorithm on in vivo anonymized data from 20 subjects [3] and compared our method-derived CO and cSBP estimates to patient-specific measurements obtained with Mobil-O-Graph apparatus (central pressure) and two-dimensional transthoracic echocardiography (aortic blood flow). Results: Precise estimates of both CO (Figure 1) and cSBP (Figure 2) were obtained with an RMSE of 0.38 L/min and 4.36 mmHg, respectively. CO estimates were found to be sensitive to measurement errors (±10%) in both brachial SBP and cf-PWV. In contrast, cSBP estimates were rather insensitive to measurement errors in cf-PWV (less than 2 %). Conclusion: The in vivo validation demonstrated that this method can accurately yield patient-based central aortic hemodynamic qualities, without the need for generalized transfer functions.

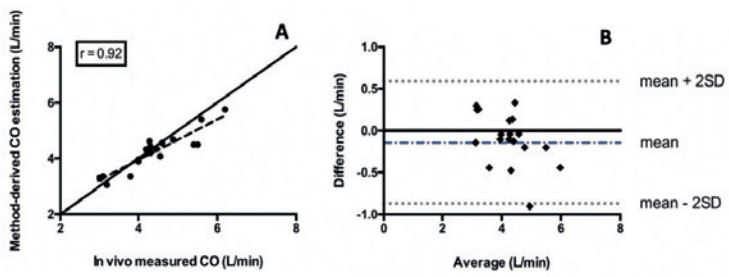

Figure Caption: Figure 1: (A) Model-CO versus reference CO. (B) Bland-Altman plot.

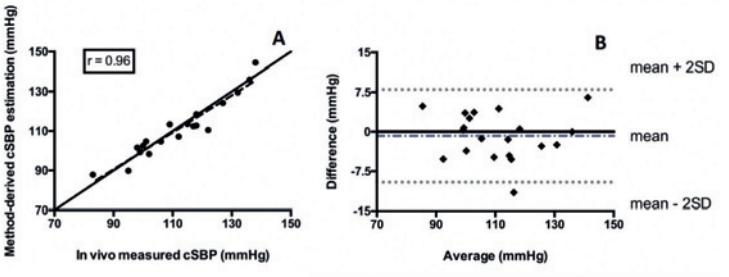

Figure 2: (A) Model-cSBP versus reference cSBP. (B) Bland-Altman plot.

References:

[1] T. K. Waddell et al., "Carotid pressure is a better predictor of coronary artery disease severity than brachial pressure," Hypertension, vol. 38, no. 4, pp. 927–931, Oct. 2001.
[2] P. Reymond et al., "Validation of a one-dimensional model of the systemic arterial tree," Am. J. Physiol. Heart Circ. Physiol., vol. 297, no. 1, pp. H208-222, Jul. 2009.
[3] T. G. Papaioannou et al., "First in vivo application and evaluation of a novel method for non-invasive estimation of cardiac output," Med Eng Phys, vol. 36, no. 10, pp. 1352–1357, Oct. 2014.

[A-11.4]

MODELING SKIN AND SOFT TISSUE VIBRATIONS GENERATED BY PRESSURE PULSE PROPAGATION IN THE COMMON CAROTID ARTERY

Daniela Tommasin[1], *Annette Caenen*[2], *Benedict Verhegghe*[3], *Stephen Greenwald*[4], *Patrick Segers*[5]

1 *Ghent University, Ghent, Belgium; Ibitech-Biommeda, Ghent, Belgium*
2 *Department of Biomedical Engineering, Thoraxcenter, Erasmus MC, Rotterdam, Netherlands*
3 *Ghent University, Ghent, Belgium; Ibitech-Biommeda, Ghent, Belgium;*
4 *Blizard Institute, Queen Mary University of London, London, UK*
5 *Ghent University, Ghent, Belgium; Ibitech-Biommeda, Ghent, Belgium; Ghent University; IBiTech-bioMMeda, Ghent, Belgium*

Introduction: Previous studies have demonstrated the technical feasibility of laser Doppler vibrometry (LDV) to assess pulse wave velocity (PWV) from skin vibrations generated by the pressure pulse traveling inside the underlying artery [1]. We have developed a finite element model to gain insight into the complex wave physics determining the transmission from arterial lumen to skin that could further improve LDV wave analysis.

Methods: Soft tissues surrounding the common carotid artery were modelled as a cuboidal domain with a cylindrical cavity in Abaqus 14.1 (Abaqus Inc. Providence, RI), as shown in Fig.1.

The top surface was modelled as a free surface (skin) whereas the other boundaries were bounded by infinite elements to prevent wave reflection. A viscoelastic material law [2] was used to mimic the behavior of soft tissue. Two pressure conditions (magnitude 40 mmHg) in the arterial lumen were considered: i) a shock impulse (0.1 ms) to simulate free wave propagation, and ii) a traveling pulse (PWV of 4, 7 and 10 m/s). We also investigated the effect of arterial depth, d, (5, 10 and 15 mm) on wave propagation. Out-of-plane displacements were analyzed using time-of-flight plots for wave paths of the lumen and skin surface (Fig. 1). Wave speed at the skin surface (Vs) was calculated by tracking the maximal displacements in time using the Radon transform [3] .

Results: Simulated wave propagation (d 10 mm, PWV of 7 m/s) is visualized in Fig 1, showing a Vs of 6.91 m/s (-1.3% of imposed PWV). Altering d to 5 and 15 mm resulted in Vs values of 7.01 m/s (+0.1%) and 7.23 m/s (+3.3%), respectively. For imposed PWVs of 4 and 10 m/s (d 10 mm), the correspondence between PWV and Vs diminished, resulting in an overestimation (+38.5%) and slight underestimation (-7.8%), respectively. Simulated free waves travelled with different velocities (wave speed at the lumen 4.53 m/s and Vs of 8.16 m/s).

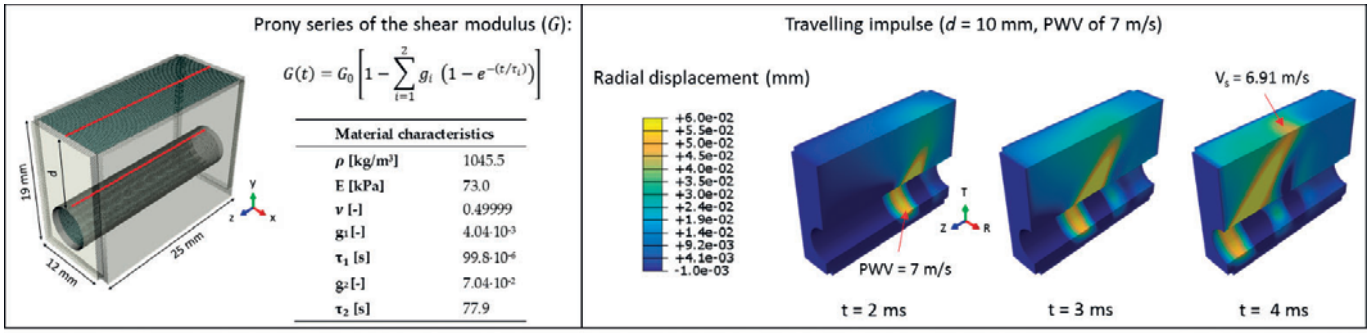

Figure 1: Model features and radial displacement depicting wave propagation at three time instances.

Discussion: The model showed larger deviations in estimated skin wave speed (up to 38.5%) when PWV approached the free wave propagation speed (4.53 m/s). Decreasing arterial depth resulted in a better correspondence between estimated Vs and imposed PWV, however, these effects were small (0.1-3.3%). To conclude, this study showed that the propagation of a pressure pulse inside the artery evokes complex displacement patterns below and at the skin surface due to the combination of different types of mechanical waves.

Acknowledgment: EU Horizon 2020 programme (CARDIS, project 644798)

References:

[1] *Li et al., Opt. Express 26(3), p. 3638, 2018.*
[2] *Caenen et al., IEEE TUFFC 64(2), pp. 349–361, 2017.*
[3] *Rouze et al., IEEE IUS, pp. 21–24, 2010.*

[A-11.5]

MODELLING PULSE WAVE PROPAGATION IN STENOTIC ARTERIES WITH FLUID-STRUCTURE INTERACTION: COMPARISON WITH PULSE WAVE IMAGING

*Vittorio Gatti[1], **Pierre E. Nauleau**[1], Grigorios M. Karageorgos[1], Jay J. Shim[2], Gerard Ateshian[3], Elisa E. Konofagou[1]*

1 *Columbia University, Department of Biomedical Engineering New York, USA*
2 *Columbia University, Department of Mechanical Engineering New York, USA*
3 *Columbia University, New York, USA*

Accurate staging of risk for plaque rupture in atherosclerotic patients is critical to reduce morbidity and mortality. Pulse wave imaging (PWI) is an ultrasound-based elastography method that allows quantification of arterial mechanical properties, by estimating the velocity of the pulse wave (PW) propagation [1]. PWI method can potentially quantify plaques mechanical properties and contribute to the detection of vulnerable plaques, helping the diagnosis and treatment of atherosclerotic disease [2].

In this study, we used a fluid-structure interaction (FSI) tool developed in FEBio (febio.org) to simulate PW propagation in an artery with a stenotic plaque [3,4]. The aim of this work was to validate the simulated results with PWI acquisitions obtained from synthetic phantoms. Finite element (FE) models of carotid walls with stenotic plaques (50 and 70 percent stenosis) were meshed with 10-node tetrahedral elements, adding a gelatin-like surrounding material (Fig. 1). Time varying pressure boundary conditions were imposed on the inlet and outlet surfaces of the fluid. Both the arterial walls and the plaques were modeled as hyperplastic viscoelastic materials, with constants that were estimated from mechanical testing. Phantoms were fabricated with PVA, embedded in a surrounding, tissue-mimicking, gelatin medium, and connected to a peristaltic pump that moved blood-mimicking fluid. PWI was performed on a customized ultrasound system (Verasonics) [5]. Spatiotemporal (ST) maps of the pulse wave propagation were obtained by tracking the wall distension velocity, and pulse wave velocity (PWV) was then calculated by fitting a linear relationship at the foot of the distension wave [5].

The simulated ST maps demonstrated agreement with those experimentally obtained (Fig. 2). PWV calculated at the stenotic segment from the simulated ST maps was in agreement with the experimental estimation for both the 50 percent stenosis and the 70 percent stenosis. These results illustrate that FE-FSI is an accurate tool to quantify pulse wave propagation in stenotic arteries. In addition, the FSI methodology was found to be useful to predict local stresses induced by blood flow, helping to advance the study of atherosclerotic disease.

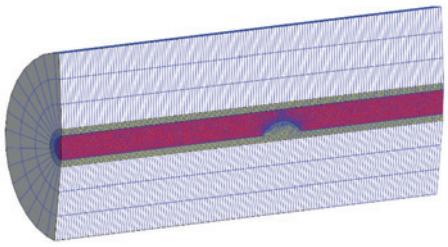

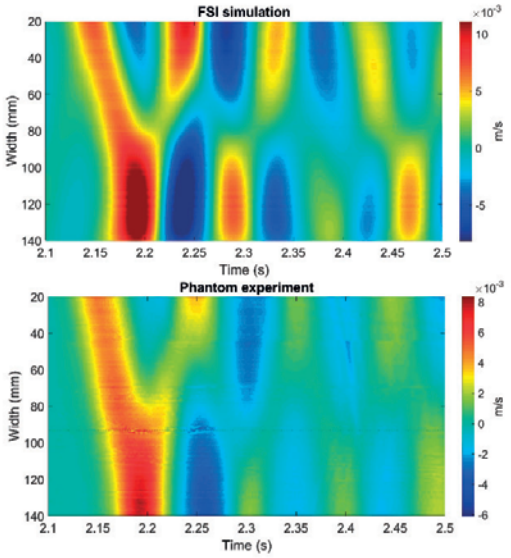

Figure 1. FE model with 50 percent stenotic plaque. Wall is shown in yellow, blood in red, and gelatin surrounding in grey (length=150 mm, lumen-diameter=8 mm, wall-thickness=2 mm).

Figure 2. Spatiotemporal maps of the 50 percent stenosis model from the simulations (Top) and experiments (Bottom).

References:

[1] *Fujikura K et al., Ultrasonic Imaging 29, no. 3 (2007).*
[2] *Li RX, et al., Ultrasound in Med. & Biol 45, no. 2 (2019).*
[3] *Maas SA et al., J of Biomech Eng, 134 no. 1 (2012).*
[4] *Shim JJ et al., J Biomech Eng, In Review.*
[5] *Apostolakis IZ, et al., Physics in Med & Biol, 62 no. 5 (2016).*

[B-01.1]

APPLICATION OF STATISTICAL SHAPE MODELING IN OSSEOINTEGRATED IMPLANT DESIGN

Alex Drew[1], *Adam Shallenberg*[1], *Bryan Kirking*[1]

1 *DJO Surgical, Austin, USA*

Successful orthopaedic implant design depends on comprehensive understanding of bone morphology, but variation in individual anatomy poses a significant challenge for engineers attempting to balance design needs with the requirement that solutions be inclusive of a broad population. Statistical shape modeling (SSM) has emerged as a tool that enables identification of key variations in morphology and rapid interrogation of design concepts against population data. This technology has become an integral part of new product development within DJO Surgical, Austin, United States (Austin, TX) where it was first utilized in development of the TaperFill™ hip stem. Recently, SSM has been utilized for design of a percutaneous osseointegrated docking system (PODS) for skeletal attachment of prosthetic limbs in above elbow amputees. Cementless fixation of PODS devices within the medullary canal of the humerus is especially challenging as, unlike arthroplasty, placement along the length of the bone can vary with the level of individual amputation.

A statistical shape model of the humerus was generated from 43 male cadaver humeri using the ShapeWorks platform (Scientific Computing Institute, University of Utah, Salt Lake City, United States) [1]. The first 5 modes (0-4) were identified as significant by parallel analysis [2]. Modes 0 and 2 were determined to be most strongly associated with variation along the medullary diaphysis including the overall length, medullary diameter, and cortical thickness. Virtual implantation was performed on the mean shape as well as +/-2 standard deviations along modes 0 and 2 (3-Matic, Materialise). Porous coating contact area and bone removal was assessed at 5 amputation levels for each instance. Amputation levels were equally spaced from 20-80% of biomechanical length.

The use of SSM allowed the team to determine an implant taper angle, porous ingrowth engagement length, and distal collar width that produced acceptable levels of bone-implant contact without excess bone removal. Importantly this could be accomplished with assessment in a compact set of humerus shapes. The design could then move forward into additional verification activities, including use in cadaveric tissue to evaluate initial stability under axial, torsional, and bending loads.

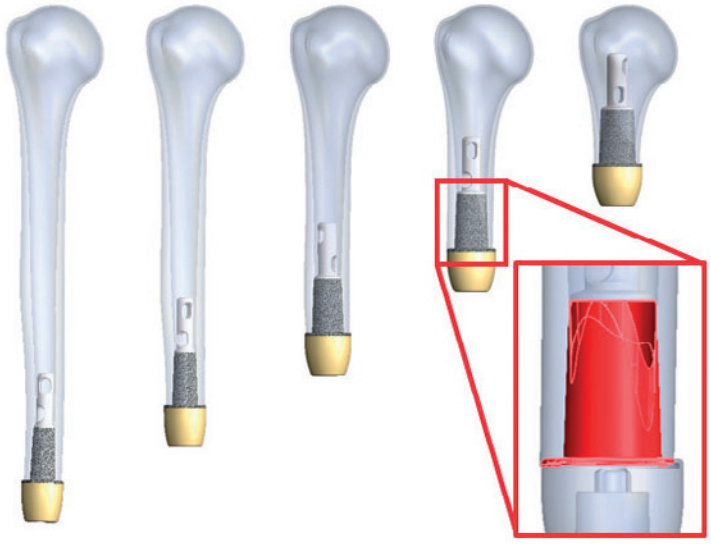

Figure 1: Virtual implantation of an upper extremity percutaneous osseointegrated docking system in a mean humerus model. Implant contact (red) and volume bone loss, assessed at 80 (left), 65, 50, 35 and 20% amputation levels.

Acknowledgments: Work presented here is supported by DJO Surgical, Austin, United States (Austin, TX). Additional support provided by Materialise (Leuven, Belgium), University of Utah, Salt Lake City, United States, Department of Orthopaedics (Salt Lake City, UT), and the Joint Warfighter Medical Research Program - W81XWH-15-C-0058.

References:

1. *Cates, J., et al., ShapeWorks: Particle-based Shape Correspondence and Visualization Software. 2011, Salt Lake City, UT: Scientific Computing and Imaging Institute, Salt Lake City, United States.*
2. *Franklin, S.B., et al., Parallel analysis: a method for determining significant principal components. J Veg Sci, 1995. 6: p. 99-106.*

[B-01.2]

COMPUTATIONAL PARAMETRIC STUDIES FOR PRECLINICAL EVALUATION OF TOTAL KNEE REPLACEMENTS

Hannah Lundberg[1], *Steven Mell*[1]

1 *Rush University Medical Center, Chicago, USA*

Aseptic loosening remains the leading cause of total knee replacement (TKR) failure in the long term, of which much is attributable to osteolysis from the biological consequences of polyethylene wear debris. TKR design innovations are constant, and preclinical wear testing is performed to ensure that contemporary designs meet the standards for wear set by their predecessors. Because of the time and expense of using mechanical simulators, increased usage of computational modeling of the wear process for TKR may help speed up the process. One of the most valuable aspects of computational models is the ability to perform large parametric studies to complement experiments and help guide the design process before experimental testing is performed. With that in mind, we developed a computational framework that could efficiently predict the effect of many sources of variability on TKR wear—including design, surgical, and patient variability.

Our objective was to create and validate a computational framework that is predictive, can handle large numbers of variables, and is scalable to patient-specific, population-specific, or generic in scope. The framework combines finite element analysis (FEA), an execution engine (Isight, Waltham, MA), and a frictional energy-based wear model. The frictional energy-based wear model is coupled with FEA in a Fortran user subroutine (UMESHMOTION) so that at every model time increment linear wear is calculated for each contact node, and material removal is simulated as the loading cycle progresses. The Isight execution engine coordinates a workflow to automatically set up and run design of experiments studies based on a defined sample space. After completion of FEA runs, Isight then builds a statistical model based on the output parameters and design of experiments. The framework has been validated at various levels, from validation of patient-specific loading inputs, to validation of volumetric wear produced on mechanical wear simulators.

To date we have performed studies encompassing two broad categories of sources of variability in TKR wear tests: 1) component alignment, and 2) kinematic and kinetic loading parameters. For component alignment, TKR wear was most sensitive to transverse plane alignment. For kinematic and kinetic loading parameters, volumetric wear was most sensitive to variation in flexion/extension peaks, although no single kinematic factor dominated TKR volumetric wear variability. In the future, the framework could be directly used in the design process to reduce the number of physical prototypes, allow for the adjustment of material and design features to minimize wear debris, and increase the number of physical activities a new design could be tested under before being implanted in patients.

Acknowledgments: This work was supported by the National Institutes of Health (R01 AR059843, R03 AR052039, and F32 AR057297, HJL). Zimmer-Biomet (Warsaw, IN) provided CAD models for FEA analysis.

[B-01.3]

EFFECT OF THE FIXATION OF TOTAL ANKLE REPLACEMENTS ON THE BURDEN PLACED ON THE BONE-IMPLANT SYSTEM

Fernando Quevedo[1], *Brett Steineman*[1], *Dan Sturnick*[1], *Constantine Demetracopoulos*[1], *Timothy Wright*[1]

1 *Hospital for Special Surgery, New York, USA*

Total ankle replacements (TAR) exhibit a wide variety of design features for component fixation, compared to total knee or hip replacements, where designs share common features across manufacturers. Moreover, early failure of TAR can be as high as 32.3%, with the most common complications being subsidence and aseptic loosening [1]. The lack of convergence in fixation features and high incidence of failures indicate that the optimal fixation design has not been determined. Therefore, we asked the question: how does the fixation design of the tibial component of TAR affect the burden placed on the bone-implant system?

We developed a finite element (FE) model based on the experimental implantation of a cadaveric ankle (65 years old, female) with a modern TAR design by a board-certified surgeon (CAD). To isolate the effect of the fixation features, we kept the baseplate unchanged. We modeled three simplified geometries that represent the main fixation features of TAR (Fig.1). The models were meshed with linear tetrahedral elements of sizes increasing from 0.5 mm for the fixation features to 3 mm at the most proximal end of the tibia. Bone's elastic modulus was non-homogeneous and derived from the CT data using relationships specific to the tibia [2]. The implant was assumed to be titanium alloy with E=110 GPa and v=0.33 [3], and with a friction coefficient with bone of 0.6 [4]. Loads and moments during gait were obtained by a musculoskeletal model developed in OpenSim [5], driven by the kinematics of the individual hindfoot bones and ground reaction forces measured through experimental testing of the cadaveric specimen on a validated robotic simulator [6]. Micromotion was computed as the difference in displacement between each pair of bone-implant closest nodes with respect to the unloaded condition.

Joint reaction loads and moments throughout the stance are provided in figure 2. For all three designs, the magnitude of micromotion (Fig.3) was driven by the moments, rather than the axial force. In this way, the highest micromotion for the stem fixation occurred at the beginning of the cycle, with low axial force and high internal moment; while for the spike and keel designs it occurred at the peak varus moment, also with moderate axial load.

These results indicate not only that different fixation designs impose different burden in the bone-implant system, but more importantly, that the load combination that generates such burden is dependent on the fixation design. Therefore, evaluation of different kinds of fixation should include a variety of loading conditions to ensure capturing the worst-case scenario.

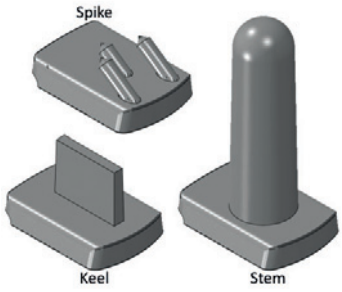

Fig. 1 – Fixation feature designs compared

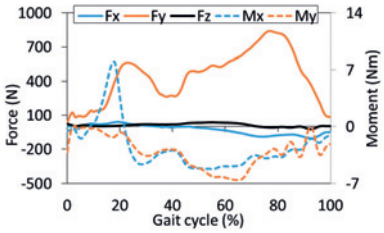

Fig. 2 – Joint forces and moments during gait applied to the FE model

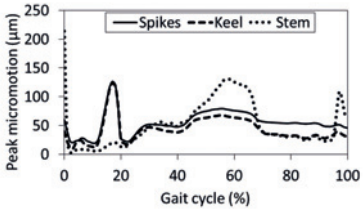

Fig. 3 – Peak bone-implant micromotion during gait

Acknowledgments: This work was supported by the generosity of American Iron & Metal (USA) Inc.

References:

[1] Glazebrook et al., Foot Ankle Int, 2009. 30: 945-949;
[2] Morgan et al., J Biomech, 2003;
[3] Burstein and Wright, Fundamentals of Orhopedic Biomechanics, 1994;
[4] Hashemi et al., J Biomed Mater Res, 1996. 33:257-267;
[5] Malaquias et al., Comput Methods Biomech Biomed Engin 2017;
[6] Baxter et al., J Orthop Res, 2016. 34:1663-1668

[B-01.4]

HOW COMPUTER MODELS CAN OPTIMIZE SHOULDER JOINT REPLACEMENT IMPLANTATION

Andreas Kontaxis[1], *Lawrence Gulotta*[2]

1 *Hospital for Special Surgery, Leon Root Motion Analysis Laboratory, New York, USA*
2 *Hospital for Special Surgery, Sports Medicine Division, New York, USA*

Complex computational musculoskeletal models have allowed non-invasive prediction of multivariate parameters that cannot be easily measured. Over the past years, shoulder models have been used to investigate and understand the biomechanical consequences of Reverse Shoulder Arthroplasty (RSA). However, despite the advancements in knowledge, there are still concerns over limited range of motion (ROM) and impingement. In recent years Patient Specific Instrumentation (PSI) were introduced to improve glenoid implantation accuracy and studies have shown that PSIs can help surgeons achieve accurate glenoid placement. However, it is not well understood how accuracy alone can result in better functional outcomes, or whether placing the glenoid in neutral version and tilt will increase functional ROM for every subject.

To understand how glenoid and humeral placement can affect impingement, a computer shoulder model and a rich kinematic data set of Activities of Daily Living (ADLs) was used to identify all the possible intra and extra-articular impingement sites (Fig.1). The data showed that there are multiple impingement sites that can limit ROM and increase risk of dislocation. However, the wide variability of impingement within a group of 30 osteoarthritic specimens also suggested that optimum placement is highly depended on the bony morphology of each individual.

Next, using the shoulder model we performed a pre-operative plan to a group of cadaveric specimens, based on an expert algorithm that minimizes impingement. Then a single surgeon performed RSA surgery in 20 cadaveric specimens with two methods: i)'traditional' surgery, where the glenoid baseplate placement was determined with standard surgical instrumentation, ii)'guided' surgery, where a 3-D printed, cadaver-specific PSI was used to guide the surgeon based on the expert pre-operative plan that was defined by the model.

In-vivo motion analysis to the cadavers confirmed that when the pre-operative plan and the PSI surgery was used the impingement free ROM was increased compared to the group of cadavers that had received traditional RSA surgery. However, the PSI surgeries did not achieve the functional outcomes that were expected by the pre-operative model (Fig. 3). That was because the pre-operative model and the surgeries were focused only on glenoid placement and did not account for muscle tensioning and humeral implantation.

Overall computer models together with PSI for accurate implantation can be beneficial for RSA. However there is a need for further development of the pre-operative planning models in order to account for multiple factors such as glenoid and humeral implantation accuracy, soft tissue balancing and bone quality.

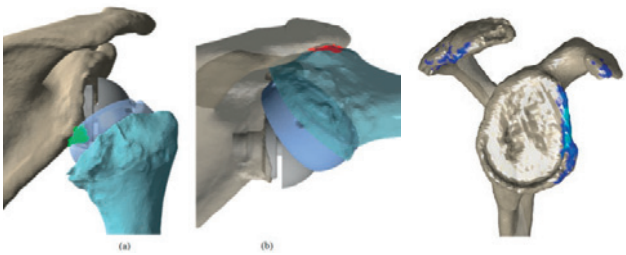

Figure 1: Frequent impingement sites during ADL

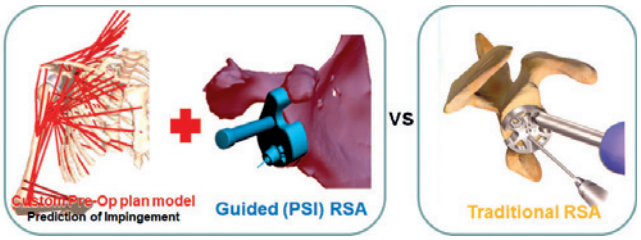

Figure 2: Two groups of cadavers i)pre-op plan with PSI, ii)traditional RSA

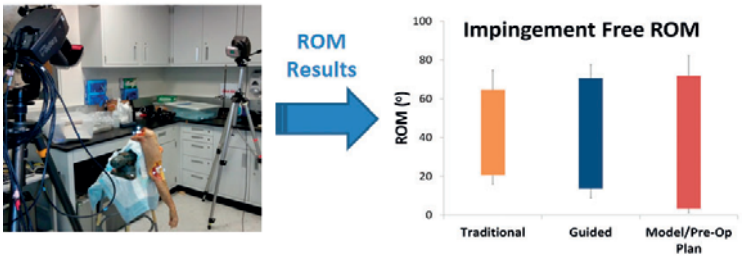

Figure 3: Motion analysis on the guided vs traditional RSA cadavers

[B-01.5]

TRADE-OFFS BETWEEN RANGE OF MOTION AND STABILITY IN REVERSE TOTAL SHOULDER ARTHROPLASTY

Josie Elwell[1], *George Athwal*[2], ***Ryan Willing***[2]

1 *Binghamton University, New York, USA*
2 *Western University, London, Ontario, Canada*

There is still controversy surrounding the optimal design and surgical placement of reverse total shoulder arthroplasty (rTSA) implant components. Previous parametric studies have demonstrated that these factors have a strong influence on the resulting range of motion (ROM) and stability of the prosthesis, but a single unique solution has not been widely accepted. We hypothesized that there is a competing relationship between these two biomechanical factors, meaning that improved ROM could only come at the cost of sacrificed stability, and vice versa. Therefore, the objective of this research was to characterize this trade-off using multiobjective design optimization of implant shape and surgical parameters.

Computational models capable of predicting the performance of any candidate implant design (and surgical placement) with respect to our defined objective functions (ROM and stability) were developed. The ROM objective function was based maximizing overall ROM considering impingement (evaluated using Boolean operations in Blender), muscle capabilities (musculoskeletal modeling using OpenSim 3.31), and non-subluxation (based on an analytical model2 considering contact forces and implant geometry). The stability objective function was based maximizing the ratio of compressive to shear forces across the allowable ROM. These two objective functions, denoted JROM and JStability, were both functions of implant shape and positioning parameters (xi: neck-shaft angle, glenosphere lateralization, glenosphere inferiorization and humeral lateralization). To perform multiobjective design optimization, we used a weighted-sum approach, minimizing the objective function JMDO(x,w) = JROM(x)[w] + JStability(x)[1-w]. The optimal solution (xopt) therefore varied depending on w, the relative importance of the two objective functions (ROM and stability).

The performance of the entire set of optimal solutions, with respect to both ROM and stability, are shown in the figure. The results define a Pareto curve describing a trade-off between ROM and stability. Thus, the optimal design for ROM is different than the optimal design for stability, differing mainly in terms of glenosphere inferior/superior positioning and humeral component lateralization. Ongoing work aims to incorporate robustness to surgical misalignment and durability as additional optimization objectives.

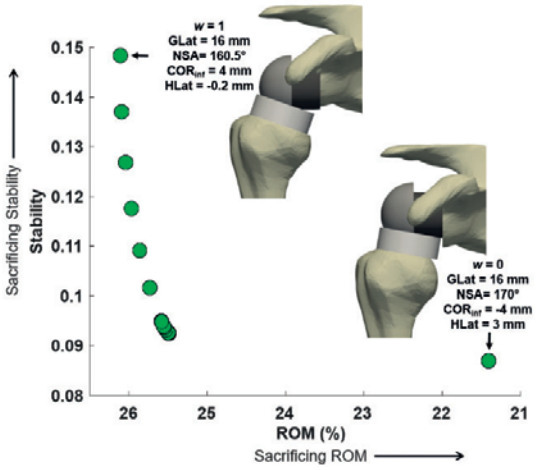

Figure Caption: The Pareto curve representing the trade-off between ROM and stability of rTSA. Optimum designs corresponding to w = 1 and w = 0 are shown.

Acknowledgments: Research reported in this publication was supported by the National Institute of Arthritis and Musculoskeletal and Skin Diseases of the National Institutes of Health under Award Number R03AR066841. The content is solely the responsibility of the authors and does not necessarily represent the views of the NIH.

References:

[1] *Holzbaur et al. Ann Biomed Eng 2005, 33, 829-40.*
[2] *Gutiérrez et al. Clin Orthop Relat Res 2008; 466: 670-676.*

[B-01.6]

COMPUTATIONAL MODELLING AND CLINICAL VALIDATION OF TOTAL WRIST ARTHROPLASTY

Magnus Gislason[1], *Duncan McDonald*[2], *Paolo Gargiulo*[3], *Marc Bransby-Zachary*[2], *David Nash*[4]

1 *Reykjavik University, Reykjavik, Island*
2 *Queen Elizabeth University Hospital, Department of Orthopedics, Glasgow, UK*
3 *Reykjavik University, Institute for Biomedical and Neural Engineering, Reykjavik, Island*
4 *University of Strathclyde, Department of Mechanical and Aerospace Engineering, Glasgow, UK*

Revision rates for total wrist arthroplasty are high compared to the ones seen in total hips and total knees. Little is known about the load transfer characteristics through the implanted wrist and the remodeling behavior within the carpal bones that occurs over a period of time. Aseptic loosening in the distal carpal bones is the main cause for revision and due to the complexity of the anatomy and biomechanics of the wrist joint, few studies have looked at the mechanics of the implanted wrist opposed to the hip and knee, where the collaboration between engineers and surgeons have formed the basis of one of the most successful orthopedic procedures carried out worldwide. In the presented study, a finite element model of the Universal2 implant inserted into the wrist was created simulating gripping and the results compared against follow up clinical data of wrist arthroplasty patients. The finite element model consisted of 1.6 million 4-node tetrahedral elements, incorporating 8 carpal bones and 5 components of the Universal2, total wrist implant. Contact formulation was established between each component and the model was solved using a quasi-static explicit solution algorithm. The stress distribution between the carpal bones and the implant was calculated and compared with clinical data collected with mean follow up of 7 years [1]. The clinical data demonstrated that the area around the central peg and the ulnar screw showed the highest level of aseptic loosening. The finite element model demonstrated the same behavior with a high stresses absorbed by the titanium central peg and the ulnar screw, thus relieving the surrounding bone tissue of the required mechanical stimulus required for bone remodeling. Understanding the mechanics of the total wrist implants can provide a basis for the design of the next generation prostheses.

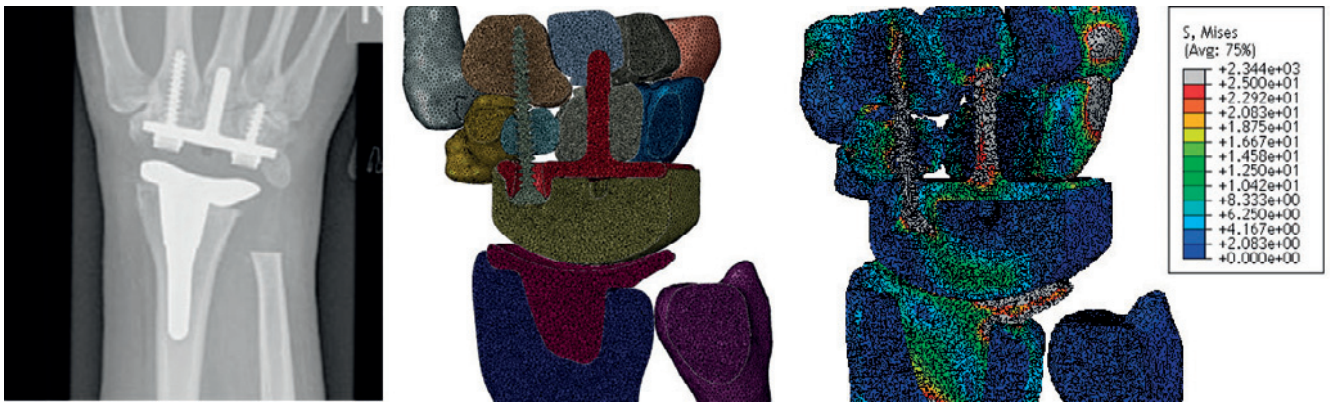

Figure Caption: Figure 1: 3D model construction and solution of the implanted wrist. From the stress plots it can be seen how the radial screw and the central peg of the distal component of the implant absorb high stresses and therefore reducing the mechanical load in the surrounding bone tissue.

References:

1. *Kennedy JW, Ross A, Wright J, Martin DJ, Bransby-Zachary M and MacDonald DJ. Universal*
2 *total wrist arthroplasty: high satisfaction but high complication rates. Journal of Hand Surgery (Eur), 2018, vol 43(4), pp: 375-379*

[B-02.1]
MUSCULOSKELETAL ADAPTATION IN RESPONSE TO JOINT INSTABILITY

Clare Fitzpatrick[1], *Grace McConnochie*[1], *Paul Rullkoetter*[2]

1Boise State University, Boise, USA
2University of Denver, Denver, USA

Introduction: During daily activity, an unstable knee joint can result in altered activation of muscles surrounding the knee [1]. Co-contraction of these muscles can compensate for joint instability and reduce tibiofemoral (TF) motion through increased compressive forces across the joint. However, muscular co-contraction can be mechanically inefficient and can hinder joint mobility. In the implanted knee, instability is a leading cause of dissatisfaction following total knee arthroplasty [2]. Implant geometry can play a substantial role in determining knee stability and, subsequently, musculoskeletal efficiency. The purpose of this work is to develop an objective measure to quantify the relationship between joint stability/laxity and musculoskeletal response.

Methods: Marker-based whole-body motion capture, ground reaction force, and CT imaging data from a subject who had undergone a knee replacement was sourced from the Fourth Grand Challenge Competition data set [3]. Data from five activities of daily living were included: level walking, lunge, stair-ascent/descent, and step-up. Using rigid-body musculoskeletal software (OpenSim [4]), joint kinematics and muscular loads were extracted during these activities. A finite element model with a detailed knee joint and lower limb musculature was developed to represent the same implanted subject.

A series of anterior-posterior (A-P) and internal-external (I-E) laxity tests were performed in the finite element model at key instances in each activity – muscle forces (from the rigid-body simulations) were applied and held fixed while TF A-P (± 500 N) and I-E loads (± 20 Nm) were simulated and resulting motions were recorded. These motions were used as "target" kinematics. Subsequently, the conformity of the tibial insert was modified to create a series of implants with TF conformity ratios which varied from 0.1 to 0.6. The laxity test simulations were repeated, however, this time muscle forces were allowed to vary, using a feedback control system, to match the target kinematics. Muscle forces were compared between implant conformities and activities.

Results: Increased implant conformity required less muscle force to achieve the same target kinematics profile – on average, as implant conformity increased by 0.1, muscle force requirements were reduced by 10.4%. The strength of this correlation varied between activities, with level walking having the lowest R-squared value (R2 = 0.27). Other activities had R-squared values between 0.58 and 0.72.

Discussion: Joint geometry plays in role in determining musculoskeletal requirements to maintain stability. The computational analysis described here provides a method to account for the muscle force adaptations necessary to prevent excessive joint motion during dynamic activity.

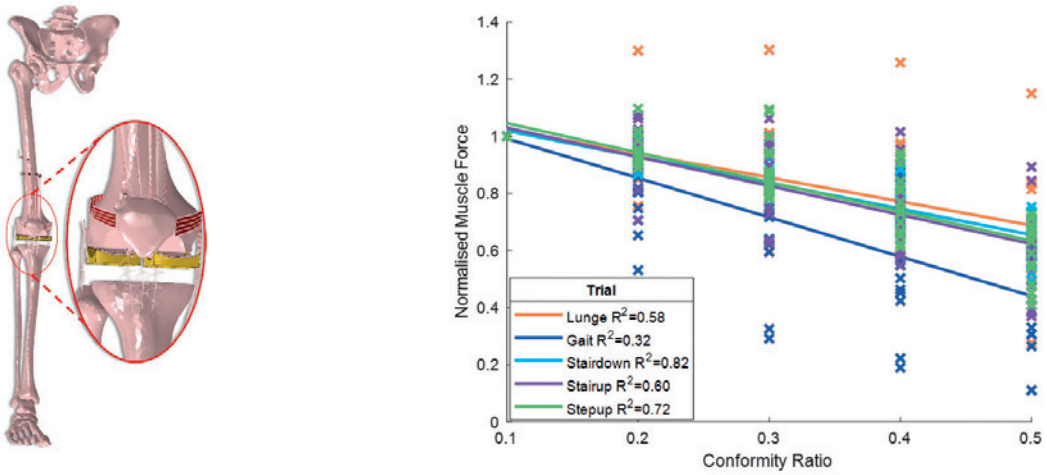

Figure 1: Left: Finite element model of the lower leg. Right: Normalized muscle force regression analysis for all trials

Acknowledgments: Supported in part by a grant from the NIH National Institute on Aging (R15AG059655).

References:

[1] Davidson et al, 2013. J Electromyo Kinesiol, 23:1485-93.
[2] Bourne et al, CORR, 468:57-63.
[3] Fregly et al, 2012. JOR, 30:503-13.
[4] Delp et al, 2007. IEEE Trans Biomed Eng, 54:1940-50.

[B-02.2]

SIMULATION AND IN VIVO VALIDATION OF KNEE MECHANICS DURING WALKING FOLLOWING TOTAL KNEE ARTHROPLASTY

Colin Smith[1], *SH Hosseini Nasab*[1], *Philipp Damm*[2], *Pascal Schütz*[1], *William R Taylor*[1]

1Institute for Biomechanics; Eth Zürich, Zürich, Switzerland
2Julius Wolff Institute; Charité-Universitätsmedizin Berlin, Berlin, Germany

Simulations of knee mechanics during functional movements have great potential to provide insight into total knee arthroplasty (TKA) component designs and surgical techniques. However, functional knee mechanics are governed by multiscale interactions between full-body dynamics, muscle coordination, ligament loads, and articular contact. While novel musculoskeletal simulations incorporate these complex interactions, substantial model uncertainty necessitates comprehensive validation of predicted knee mechanics.

The CAMS-Knee datasets provide simultaneous measurements of ground reaction forces, motion capture, tibiofemoral contact forces and tibiofemoral kinematics [1]. Contact forces were measured using an instrumented implant and kinematics using a novel moving fluoroscope. For this study, a musculoskeletal model was personalized to a single subject based on CT scans. The tibiofemoral joint included six degrees-of-freedom (DOF). Contact between the tibial and femoral components was represented using an elastic foundation model. Fourteen ligaments were modeled using bundles of nonlinear springs.

The Concurrent Optimization of Muscle Activations and Kinematics (COMAK) simulation routine was used to predict muscle forces, ligament loads, and contact pressures during level walking using only motion capture and ground reaction force inputs [2]. COMAK simultaneously optimizes muscle activations and secondary knee kinematics (5 tibiofemoral DOF) to satisfy both whole-body and joint-level dynamics, while minimizing a squared muscle activation objective function. Simulated tibiofemoral contact forces and kinematics were compared against in vivo measurements.

The predicted tibiofemoral adduction and translations closely matched the measurements. Larger errors were found for tibial rotation. The predicted contact force showed good agreement through the first half of stance. During late stance, the model over predicted the contact forces.

We performed a comprehensive validation of simulated tibiofemoral contact forces and kinematics during walking. Tibiofemoral DOF that were constrained by the implant geometry were accurately predicted. Greater errors were present in tibial rotation, which is predominately governed by ligament and muscle forces. Substantial uncertainty in the ligament constitutive properties and resolution of muscle redundancy remain likely sources for these errors. The over prediction of knee contact force at push-off is likely due to preferential activation of the gastrocnemii over the soleus to generate the plantarflexor moment, which results in greater compression at the knee. The ability to predict knee mechanics during functional movements based on standard motion capture data now enables future studies to investigate TKA component designs and surgical techniques.

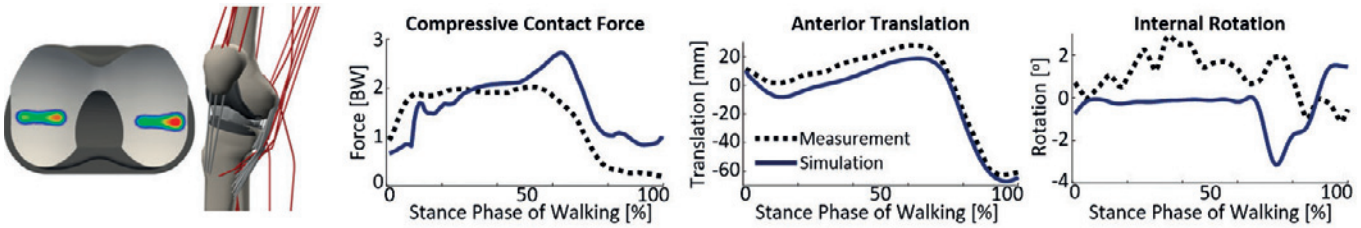

Figure Caption: Validation of simulated knee mechanics during the stance phase of walking.

Acknowledgments: RMS Foundation

References:

[1] Taylor et al, J Biomech, 2017, 65:32-39
[2] Smith et al, J Biomech, 2019, 82:124-133

[B-02.3]

EFFECT OF AN INTERNAL UNLOADING IMPLANT ON TIBIOFEMORAL JOINT STRESS DURING STAIR DESCENT

Rajshree Hillstrom[3], *Oliver Morgan*[1], *S Robert Rozbruch*[2], *Austin Fragomen*[2], *Anil Ranawat*[3], *Howard J Hillstrom*[3]

1Anglia Ruskin University, Chelmsford, UK
2Hospital for Special Surgery, New York, USA
3Hospital for Special Surgery, New York, USA; Anglia Ruskin University, Chelmsford, UK

Introduction: Joint malalignment1, obesity2 and tissue injury3 are primary factors associated with osteoarthritis onset and progression. Excessive joint stress is the common pathway that damages joint tissues, irrespective of the specific biomechanical aetiology. Internal unloading implants, placed subcutaneously upon the medial aspect of the knee joint, are designed to offload the medial knee compartment without violating natural joint tissues. This was confirmed during walking in our in silico studies4,5. Our aim is to investigate the effect of the Atlas™ unloading implant on tibiofemoral compartment stress during stair descent.

Methods: A three-dimensional computer-aided design of an Atlas™ knee system (Figure 1) was virtually fixed to a validated finite element knee model6 in CATIA (Dassault Systèmes, Velizy Villacoublay, France). The construct was meshed and assigned material properties and boundary conditions, as per manufacturer's instructions, in Abaqus (Dassault Systèmes, Velizy Villacoublay, France). The femur was mechanically grounded and the tibia was subjected to loading conditions corresponding to the stance phase of stair descent of a healthy 22-year-old 65-Kg male with similar anthropometrics to those of the cadaver. Finite element analyses were run to compute Tresca and von Mises stress in the tibiofemoral compartments pre- and post-implant fixation.

Results: Von Mises and Tresca stress in the cartilage-cartilage and meniscus-cartilage interfaces spanned 0.45 to 2 MPa while the knee was in 20 o of flexion (Table I). These stress values were lower in the lateral compartment and higher in the medial compartment post-Atlas (Figures 2 & 3). Medial meniscus von Mises stress increased from 4.59 MPa to 5.93 MPa. Lateral compartment von Mises stress decreased from 11.48 MPa to 7.19 MPa while Tresca reduced from 9.84 MPa to 7.54 MPa.

Discussion: The Atlas, an internal unloading implant, reduced maximal von Mises and shear stress values in the tibiofemoral joint. However, peak von Mises and Tresca stress values were higher in the medial knee compartment while lower in the lateral compartment throughout stair decent post Atlas. This may be due to the laterally directed ground reaction force during stair descent compared with level walking. When evaluating implants, it is important to analyse other functional tasks, in addition to level walking, such as stair descent.

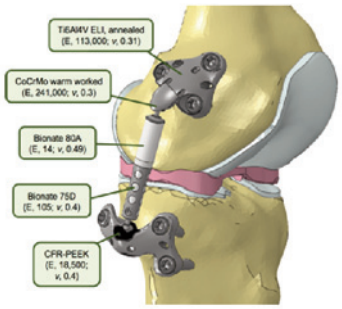

Figure 1: Virtual surgical fixation of an internal unloading implant to a validated knee model

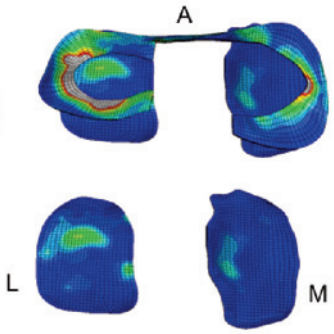

Figure 2: Von Mises stress distribution on tibial cartilage and meniscus before virtual fixation of internal unloading implant

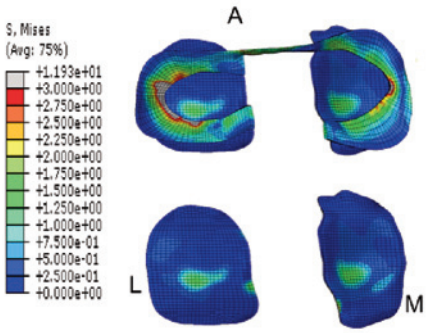

Figure 3: Von Mises stress distribution on tibial cartilage and meniscus after virtual fixation of internal unloading implant

Acknowledgments: Internship students from École des mines d'Albi-Carmaux, Université de Lorraine and Université de Franche-Comté. This study was funded by the Chelmsford Medical Education and Research Trust.

Table I Stress (MPa)	Medial			Lateral		
	Cartilage - cartilage	Menisus-cartilage	Meniscus	Cartilage - cartilage	Menisus-cartilage	Meniscus
Pre-atlas Von mises	1.09	0.45	4.59	1.91	0.88	11.48
Post-atlas Von mises	1.41	0.54	5.93	1.40	0.85	7.19
Pre-atlas Tresca	1.18	0.48	4.42	2.01	0.96	9.84
Post-atlas Tresca	1.48	0.56	4.44	1.46	0.95	7.54

References:

1. *Sharma et al., JAMA. 2001;286(2):188-195.*
2. *Potter et al., Am J Sports Med. 2011;*
3. *Lo et al., 2009;17(6):743-747;*
4. *Morgan et al.,2018, ORS;*
5. *Hillstrom et al.,2018 ISTA;*
6. *Mootanah et al., 2014, CMBBE 17(13):1502-17.*

[B-02.4]

COMPARISON OF DIFFERENT METHODS FOR UNCERTAINTY PREDICTION OF TF-KINEMATICS AND CL-STRAINS USING A BIOMECHANICAL RIGID BODY KNEE MODEL

Laura Bartsoen[1], *Roel Wirix-Speetjens*[2], *Matthias Faes*[1], *David Moens*[1], *Ilse Jonkers*[3], *Jos Vander Sloten*[4]

1KU Leuven, Mechanical Engineering, Heverlee, Belgium
2Materialise NV, Leuve, Belgium
3Ku Leuven, Department of Kinesiology, Leuven, Belgium
4KU Leuven, Mechanical Engineering, Heverlee, Belgium; Biomechanics Section

Computer simulations are commonly used in research to investigate biomechanical problems. These simulations rely on a set of patient-specific input parameters that are often hard to quantify, resulting in the use of average values representative for a certain population. For most models it is however unknown how uncertainty on these input parameters affects the outcome of the simulation. This research evaluates different methods to quantify the effect of uncertainty in the input parameters on the non-deterministic response of the model outputs. The test case of choice is the estimation of uncertainty on tibio-femoral (TF) kinematics and collateral ligament (CL) strains after total knee replacement given the uncertainty in implant position used as an input.

We studied the performance of two different techniques to quantify simulation output uncertainty, namely Fast Probability Integration (FPI) and Response Surface Modeling (RSM). For FPI one method was studied, namely Advanced Mean Value (AMV) [1]. For RSM, three different methods are studied, namely Support Vector Regression (SVR), Artificial Neural Networks (ANN) and Gaussian Process Regression (GPR). With FPI methods a direct approximation of the statistical output distribution is computed, whereas with RSM, an approximation of TF-kinematics and CL-strains as predicted by the knee model is made. Uncertainty on the output is quantified by performing a Monte Carlo analysis on this approximate model (metamodel). Each metamodel was trained and validated on the same set of data, which contains 1500 training samples generated using the Halton sequence and 150 validation samples generated using Latin Hypercube sampling.

The AMV method was found to be unusable for these kind of models, as the model turned out to be too non-linear to perform an accurate approximation of the statistical distribution of the model outputs. In contrast, the RSM methods are all capable of modeling a good approximation of the knee model and resulting errors are comparable for different implementations. The Mean Absolute errors as a percentage of total parameter uncertainty for SVR, GPR and ANN are respectively 1.63%, 1.96% and 1.83% for TF-kinematics and 0.76%, 0.98% and 1.17% for CL-strains. These errors are computed using the same validation samples for each model. Training times are respectively 30min, 23min and 7min and average model evaluation times are respectively 4.3ms, 6.7ms and 1.4ms.

To conclude, the AMV method is inapplicable on this knee model, whereas comparable accuracy is found for the three RSM methods. The ANN model seems to be most performant for the studied application given its computational efficiency compared to SVR and GPR models.

Acknowledgments: Funded by the Materialise chair for image based, patient-specific biomechanics

References:

[1] Wu, Y-T., H. R. Millwater, and T. A. Cruse. "Advanced probabilistic structural analysis method for implicit performance functions." AIAA journal 28.9 (1990): 1663-1669.

[B-02.5]

PEAK AXIAL LOADS DO NOT SUFFICE TO EVALUATE THE BIOMECHANICAL BURDEN PLACED ON TOTAL ANKLE REPLACEMENT FIXATION

Brett Steineman[1], *Fernando Quevedo*[1], *Dan Sturnick*[1], *Timothy Wright*[1], *Constantine Demetracopoulos*[1]

1 *Hospital for Special Surgery, New York, USA*

Most finite element (FE) studies to evaluate the bone-implant interaction of total ankle replacements (TAR) consider a single load case, consisting of a high axial load and no shear forces or moments [1, 2]. Similarly, current standards for evaluating TAR consider only an axial load [3]. However, in larger joints, like the knee, we recently showed that the highest burden for the bone-implant system arises for sub-maximal loads [4]. Moreover, we found that activity cycles should be simulated as opposed to single load cases to ensure the worst-case scenario is considered [4]. Currently, it is unclear whether axial loads alone suffice to capture the most critical case for TAR. Therefore, our objective was to evaluate the bone-implant interaction of a modern TAR throughout the most common activity, gait, to determine whether the simplified loads often considered to evaluate TAR suffice to capture worst-case scenarios.

A cadaveric ankle (65 years old, female) was implanted with a modern TAR design by a board-certified surgeon (CAD). We utilized a previously validated robotic simulator [5] to determine the kinematics of the individual hindfoot bones during gait. The ankle kinematics were calculated using data from motion capture cameras and intracortical bone pins with reflective markers. We adapted a foot-ankle musculoskeletal model developed in OpenSim [6] to reproduce the test performed on a single-limb on the robotic simulator. We then utilized the experimental kinematics and ground reaction force to compute the net forces and moments at the ankle joint throughout the stance phase of gait. An FE model of the implanted specimen was developed to evaluate bone-implant micromotion and the risk of bone failure adjacent to the tibial component as a result of the calculated multi-axial forces and moments throughout stance. The model included non-homogeneous bone material properties derived from the CT data using relationships specific for the tibia [7]. Bone failure was computed using a strain-based failure criterion [8].

The axial force was the primary contributor to reaction loads with small shear forces during midstance and toe-off (Fig. 1). The peak moment was a varus moment at initial flatfoot. The largest applied axial force was accompanied by low shear forces and moments at toe-off. However, the largest peak micromotion (Fig. 2) and largest amount of interfacial bone at risk of failure (Fig. 3) did not arise from the largest axial force. Instead, peak micromotion and risk of bone failure occurred at initial flatfoot, for a moderate axial load and high varus moment.

Our results support the inclusion of multi-axial loads and multiple-load cases to ensure that the worst-case scenario is considered when evaluating the interaction of TAR with the surrounding bone.

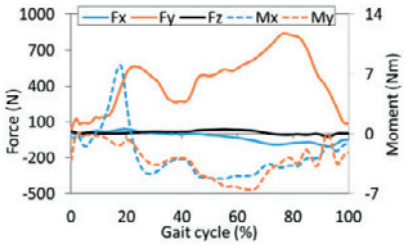

Fig. 1 – Joint forces and moments during gait

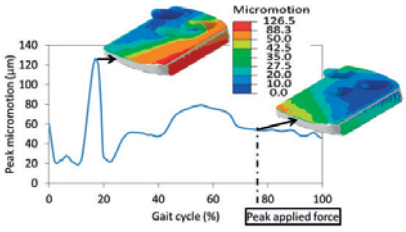

Fig. 2 – Peak bone-implant micromotion during gait

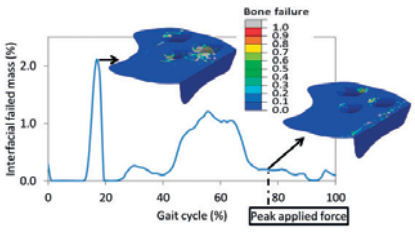

Fig. 3 – Bone failure during gait

Acknowledgments: This work was supported by the generosity of American Iron & Metal (USA) Inc.

References:

[1] *Sopher et al., Med Eng Phys, 2017. 42:80-90;*
[2] *Terrier et al., Clin Biomech, 2017. 48:57-62;*
[3] *ASTM F2665-09;*
[4] *Quevedo Gonzalez et al., J Orthop Res, 2018. In press;*
[5] *Baxter et al., J Orthop Res, 2016. 34:1663-1668;*
[6] *Malaquias et al., Comput Methods Biomech Biomed Engin 2017;*
[7] *Morgan et al., J Biomech, 2003;*
[8] *Bayraktar et al., J Biomech, 2005. 126: 677-684*

[B-02.6]

PERFORMANCE INDICATORS FOR PROSTHESIS SURFACE INTEGRITY AFTER DENTAL CAD/CAM MILLING

Lebon Nicolas[1], *Tapie Laurent*[1], *Vennat Elsa*[2]

1 *URB2i EA4462, Montrouge, France; Faculty of Dental Surgery; Paris Descartes-Paris 13 Universitie, France*
2 *MSSMat (UMR-CNRS8579), Centrale-Supélec, Gif sur yvette, France;*

Various dental diseases lead to prosthetic rehabilitation. Today, prostheses can be manufactured from prefabricated biomaterial raw blocks, which are milled with a CAD/CAM process. The quality of these prostheses can be assessed using roughness, a major surface integrity (SI) component in dentistry [1]. SI is the characteristic signature of the milling process on the generated prosthesis shape [2]. The major challenge in restorative dentistry is to manufacture prostheses, which are able to rehabilitate the teeth in order to fulfil functional performance and aesthetic requirements. For each requirement, a specific SI might be manufactured in different anatomical area of the prosthesis. Aesthetics, biological response and restoration lifetime require a low surface roughness. On the contrary, the surface to be bonded on the remaining dental tissues needs to be sufficiently rough. The main difficulty for prosthesis manufacturers is to integrate the different expected SI during CAM process and to choose the milling process parameters in accordance with the expected prosthesis functionalities. This paper aims to evaluate and quantify the influence on SI of milling tools characteristics, biomaterials properties, and milling process parameters. A comparison to the clinically desired SI is conducted with two performance indicators (PI). a) a weighted relative mean PI named MSI. b) a weighted relative standard deviation PI named SISD. Based on milling experimental results capitalization and the clinically desired SI, the PI are locally computed among the prosthetic shape and displayed on a 3D mapping of the prosthesis shape (figure 1). The mapping results, applied on a crown prosthesis study case, show a limited influence of the tool feedrate parameter, whereas the tool diamond grit size, the tool/prosthesis inclination, and the biomaterials are more significant factors. The use of the PI during the CAM step emphasizes that a topological decomposition of the crown shape is necessary to associate reliable local milling process parameters. The PI provide a valuable assistance to the prosthesis manufacturers to choose efficiently milling parameters according to the prosthesis roughness requirements or to anticipate the post-processing polishing process. These PI can be enriched by new milling experimental results and new relevant SI components.

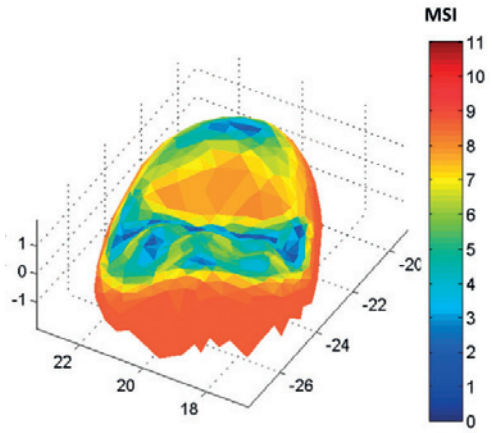

Figure 1: MSI 3D map.

References:

[1] *Ghinea R, Ugarte-Alvan L, Yebra A, Pecho OE, Paravina RD, del Mar Perez M. Influence of surface roughness on the color of dental-resin composites. Journal of Zhejiang University Science B. 2011 1;12(7):552-62.*
[2] *Jawahir IS, Brinksmeier E, M'saoubi R, Aspinwall DK, Outeiro JC, Meyer D, Umbrello D, Jayal AD. Surface integrity in material removal processes: Recent advances. CIRP Annals-Manufacturing Technology. 2011 1;60(2):603-26.*

[B-03.1]

INITIATION AND PROPAGATION OF MICROCRACKS IN COLLAGEN NETWORKS OF ARTICULAR CARTILAGE

David Pierce[1], *Stephany Santos*[1], *Franz Maier*[1], *Jonathan Kaplan*[1], *Bilal Kaleem*[1], *Corey Neu*[2]

1 *University of Connecticut, Storrs, USA*
2 *University of Colorado Boulder, Boulder, USA*

Osteoarthritis (OA) is a debilitating disease that afflicts nearly 20% of people in the US, costing more than $185.5 billion a year (in 2007 dollars), with a projected increase in prevalence of ~40% in the next 25 years [1]. We recently demonstrated that low-energy impact usually considered non-injurious can in fact cause micrometer-scale cracks (widths < 30 μm) in the collagen network of visually pristine human cartilage [2]—distinct from the well-characterized microcracks in bone and sub-millimeter-scale surface fissures in cartilage of early to advanced OA [3]. Furthermore, we showed cartilage microcracks diminish the functional response of cartilage [4] and propagate under progressive cyclic loading. While pre-clinical OA may originate with microcracks in the network of collagen, the extent of initiation and propagation of microcracks during repetitive mechanical loads to cartilage (normal daily activities) is unknown. To quantify the initiation of microcracks, we completed low-energy impact tests on healthy human cartilage using full-thickness osteochondral plugs (specimens) [2]. We found that impact energy density and nominal stress/stress rate were significant ($P < 0.05$) predictors of microcracking, while strain and strain rate were not. In our test configuration, an impact energy density of 1.0 mJ/mm3 corresponded to a ~20% probability of microcracking, yet no specimens presented visible (macroscopic) damage following impact. To quantify the propagation of microcracks, we tested healthy bovine cartilage specimens from lateral and medial femoral condyles. We assigned specimens to three low-energy impact groups (none, low, high), and thereafter to three cyclic compression groups (none, low, high) which mimic walking. We found that changes in overall microcrack width correlate significantly with loading conditions, and that microcracks propagate by increasing in both length and width, but not depth. By combining patient-specific finite element models and longitudinal Magnetic Resonance Images, studies of cartilage microcracks will aid us in linking quantifiable in vivo mechanical loads to mechanisms of damage in cartilage and to aspects of the initiation of OA, potentially enabling new diagnostic tools and treatments.

References:

[1] *H. Kotlarz, C.L. Gunnarsson, H. Fang, and J.A. Rizzo. Insurer and out-of-pocket costs of osteoarthritis in the US: evidence from national survey data. Arthritis Rheum., 60:3546–3553, 2009.*
[2] *B. Kaleem, F. Maier, H. Drissi, and D.M. Pierce. Low-Energy Impact of Human Cartilage: Predictors for Microcracking the Network of Collagen, Osteoarthritis Cartilage, 25(4):544-553, 2017.*
[3] *K.P.H. Pritzker, S. Gay, S. A. Jimenez, K. Ostergaard, J.-P. Pelletier, P.A. Revell, D. Salter, and W.B. van den Berg. Osteoarthritis cartilage histopathology: grading and staging. Osteoarthritis Cartilage, 14:13–29, 2006.*
[4] *J.T. Kaplan, C.P. Neu, H. Drissi, N.C. Emery, and D.M. Pierce. Cyclic Loading of Human Articular Cartilage: The Transition from Compaction to Fatigue, J. Mech. Beh. Biomed. Mat., 65(0):734-742, 2017.*

[B-03.2]

COLLAGEN DESTRUCTURING BASED ON FIBER AND CROSSLINK RUPTURE IS CONSISTENT WITH LOSS OF MECHANICAL PROPERTIES IN AGING ARTICULAR CARTILAGE

Elmer Middendorp[1], Wouter Wilson[1], Keita Ito[1], ***Corrinus van Donkelaar[2]***

1 *Orthopaedic Biomechanics, Department of Biomedical Engineering, Eindhoven University of Technology, Eindhoven, Netherlands*
2 *Dept Biomedical Engineering; Gemz 1.106; Eindhoven University of Technology, Eindhoven, Netherlands*

Prior to clinically observable symptoms of osteoarthritis, ultrastructural changes in the collagen network of articular cartilage occur (Nickien, 2013). This entails destructuring of the collagen network, involving reduced interfibrillar crosslinking and thicker fiber bundles. This is a slow, irreversible process believed to cause a reduction of cartilage functionality. This theory is yet unproven and its importance still unknown. Computationally modelling these effects enables investigation of the impact of destructuring and its effect on the mechanical functionality and susceptibility to damage of cartilage. In this study, the effects of collagen fiber and crosslink damage were introduced into a matrix based constitutive model of articular cartilage to determine whether destructuring based on these phenomenae was consistent with loss of mechanical functionality.

A validated cartilage model (Wilson, 2007) was extended with a collagen degeneration algorithm that contained two failure modes. First, an individual fiber could rupture when overstrained. The consequent inability to resist force was implemented by reducing collagen fiber density in the overstrained direction. Secondly, interfibrillar crosslinks could fail after excessive shearing. This disentangles the network and was implemented by modifying the associated structural organization of collagen. Without modifying mechanical properties of matrix constituents, these structural alterations changed the mechanical behavior.

Results of this algorithm (using parameters from literature) were corroborated against an experimental study (Nickien, 2017) where deep-zone cartilage of different ages was evaluated for transversal stiffness and transversal swelling potential. In silico, age was replicated by different percentages of initial interfibrillar crosslink damage. Stiffness and swelling potential were monitored similar to Nickien (Fig.1).

Excellent agreement between experiments and simulations demonstrated that our degeneration algorithm captures mechanical effects of collagen destructuring in early osteoarthritis and allows studying the circumstances by which cartilage degeneration could occur beyond the possibilities of experimental studies.

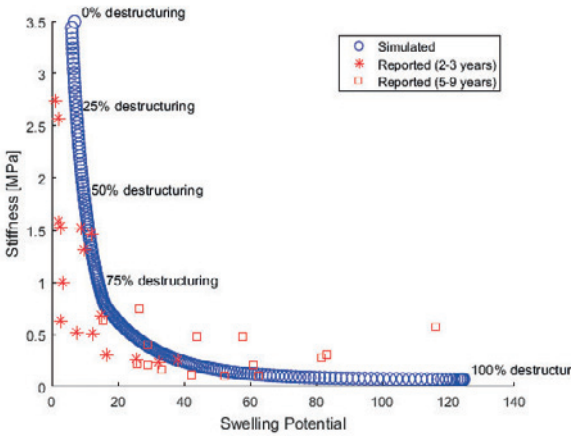

Figure Caption: Stiffness and swelling in cartilage of various ages (red symbols)(Nickien et al., 2017) and simulations (blue) of cartilage with various degrees of initial interfibrillar crosslink damage (percentages in graph).

References:

Nickien, M., Thambyah, A., and Broom, N. (2013). How changes in fibril-level organization correlate with the macrolevel behavior of articular cartilage. Wiley Interdiscip. Rev. Syst. Biol. Med. 5, 495–509.
Nickien, M., Thambyah, A., and Broom, N.D. (2017). How a decreased fibrillar interconnectivity influences stiffness and swelling properties during early cartilage degeneration. J. Mech. Behav. Biomed. Mater. 75, 390–398.
Wilson, W., Huyghe, J.M., and Donkelaar, C.C. van (2007). Depth-dependent Compressive Equilibrium Properties of Articular Cartilage Explained by its Composition. Biomech. Model. Mechanobiol. 6, 43–53.

[B-03.3]

A THREE-DIMENSIONAL ROTATIONALLY NONSYMMETRIC CONTINUOUS FIBER DISTRIBUTION FOR ARTICULAR CARTILAGE

Brandon Zimmerman[1], *Gerard Ateshian*[1]

1Columbia University, New York, USA

The collagenous solid matrix of articular cartilage is known to be anisotropic and inhomogeneous, which strongly influences the mechanical behavior of cartilage. Fibrils are primarily oriented parallel to the surface in the superficial zone and transition to a more random orientation in the middle zone before aligning perpendicular to the subchondral bone in the deep zone. Additionally, the fibrils exhibit a preferred direction at the surface, which can be seen through split lines. This complex network of collagen fibrils is commonly modeled with continuous fiber distributions which are rotationally symmetric, a framework which neglects the fully three-dimensional physiological orientation of fibrils. Although rotationally nonsymmetric models have been proposed for other tissues,1,2 none appear to have been formulated specifically for cartilage based off experimental results. This study constructs a three-dimensional rotationally nonsymmetric continuous fiber distribution (RNCFD) which fits experimental data in two orthogonal planes from each zone in cartilage.

Based on x-ray diffraction data obtained from both the cross-section of cartilage and normal to the articular surface,3 we formulated the RNCFD as a separable function of polar and azimuthal spherical angles. In the polar direction, a bimodal von Mises distribution accounts for the presence of two predominant fiber orientations. The offset angle between the two predominant orientations and the degree of alignment are controlled through adjustable parameters selected to match experimental data. In the azimuthal direction, where the preferred alignment of fibers can be qualitatively seen by examining split lines, the dependence of the RNCFD on the azimuthal angle was constrained to be elliptical, with two parameters indicating the degree of eccentricity. Assembling and normalizing these two functions produces a three-dimensional RNCFD which was implemented in the finite element software FEBio.4

A spherical plot of the proposed fiber distribution suggestive of the middle zone of cartilage is shown in Fig. 1, along with corresponding plots of the projected distribution along polar and azimuthal angles. By adjusting parameters, this model can fit data from all zones of cartilage. To examine whether this increased accuracy in fibril orientation improves the ability to predict mechanical testing, a classic compression study5 was replicated in FEBio. In this study, a cartilage cube was subjected to three separate unconfined compression tests to calculate Young's modulus in all three coordinate directions. The RNCFD model produced anisotropic results in agreement with experiment (not shown).

To improve the accuracy of computational models of cartilage, this study developed a three-dimensional RNCFD via a composition of two independent functions of spherical angles. The proposed RNCFD can be fit to experimental x-ray diffraction data measured in two orthogonal planes at several depths through the tissue, capturing collagenous anisotropy to a high degree. Future work will apply discrete versions of this rotationally nonsymmetric distribution to computational models of fibrous fatigue and damage.

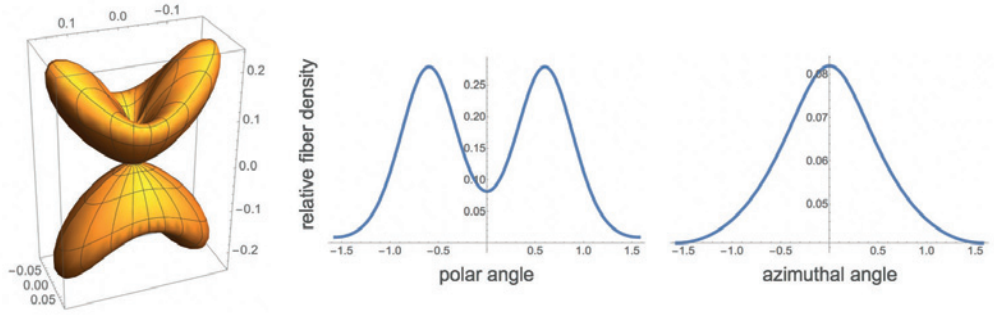

Figure 1: The proposed RNCFD for parameters reminiscent of the middle zone of cartilage. (Left) Spherical plot, where distance from the origin indicates probability of finding a fiber; (Middle) Fiber density as a function of polar angle, at zero azimuthal angle; (Right) Fiber density as a function of azimuthal angle, at zero polar angle.

Acknowledgments: NSF GRFP DGE-16-44869

References:

[1] Holzapfel, GA et al., J. R. Soc. Interface, 12:2015-0188.
[2] Gizzi, A et al., J Eng Math, 109:211, 2018.
[3] Aspden, RM & Hukins, DW, Proc. R. Soc. Lond. B, 212:299-304, 1981.
[4] Maas, SA et al., J Biomech Eng, 134(1):011005, 2012.
[5] Chahine, NO et al., J Biomech, 36(3):339-353.

[B-03.4]

COMPUTATIONAL MODELS OF GROWTH FACTOR DELIVERY TO ENGINEERED CARTILAGE TISSUES

Michael Albro[1]

1Boston University, Department of Mechanical Engineering, Boston, USA

Tissue engineering is a promising strategy to treat of myriad of degenerative conditions, whereby live, cell-incorporated replacement tissues are fabricated for clinical tissue repair. Anabolic growth factors have become ubiquitous in tissue engineering applications due to their well-established ability to promote critical extracellular matrix (ECM) synthesis rates. Generally, growth factors are administered in culture medium during phases of in vitro tissue growth or directly loaded into scaffolds where they can act on cells in vivo after implantation. There is a growing appreciation for the importance of optimizing growth factor delivery regimens to cells, as growth factor excesses can lead to quality limitations of engineered tissues (fibrosis or hypertrophy) or off-target pathology in vivo after implantation. However, this optimization remains a considerable challenge, as growth factors undergo a series of complex molecular interactions with scaffolds, ECM proteins, and cell receptors [1]. Consequently, limited work has been performed on mechanistic models that describe the transport and distribution of administered growth factors in engineered tissues.

Here, we explore the ability of reaction-diffusion models (FEBio implemented) to predict the distribution of a commonly employed growth factor, TGF-beta, in engineered cartilage tissues. Models account for salient TGF-beta-tissue interactions, including reversible binding kinetics (to scaffolds and synthesized ECM) and receptor-mediated internalization by seeded cells. Here, our models are used to depict the TGF-beta tissue distribution for two unique tissue engineering systems: 1) TGF-beta supplemented in medium to diffuse into tissues during in vitro culture (Fig1), and 2) TGF-beta loaded directly into affinity-based scaffolds designed to promote long-term TGF-beta retention in vivo (Fig 2). Results demonstrate that our reaction-diffusion models can account for gradients of media supplemented TGF-beta in engineered tissues. Models further demonstrate the critical influence of binding interactions and cellular receptor internalization on the uptake and retention of different doses of TGF-beta in engineered tissues. We anticipate that this work sets the foundation for critical optimizations of growth factor delivery protocols, leading to improved outcomes in tissue engineering platforms.

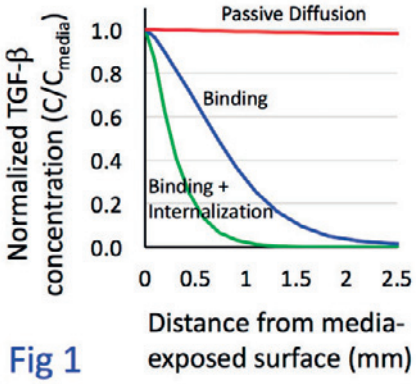

Fig 1

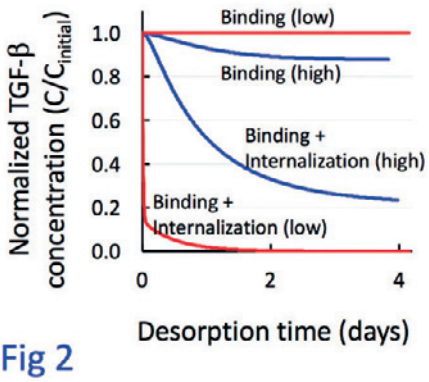

Fig 2

Fig 1: Theoretical model of distribution of media supplemented active TGF-beta (3-day exposure) in an engineered cartilage tissue when accounting for passive diffusion, reversible binding kinetics, and receptor-mediated cellular internalization. Reversible binding and internalization kinetics give rise to highly pronounced concentration gradients in tissues [1].

Fig 2: Theoretical model of retention of high (100ng/mL) and low (1ng/mL) doses of active TGF-beta loaded into heparin affinity-binding retention scaffolds when accounting for reversible binding kinetics, and receptor-mediated cellular internalization. While affinity binding can prolong the retention of high TGF-beta doses, for lower doses, affinity binding is unable to compete with cellular internalization, leading to a short half-life in the tissue.

Acknowledgments: This work is supported by the Boston University, Boston, United States Dean's Catalyst Award and Materials Science & Engineering Innovation Grant.

References:

[1] Albro MB + 2016 Biomaterials 77: 173-185.

[B-03.5]

COMPUTATIONAL MODELS FOR OPTIMIZING ENGINEERED CARTILAGE GEOMETRY FOR GROWTH AND THERAPEUTIC DRUG DELIVERY

Robert J. Nims[1], *Kelsey H. Collins*[1], *Lara Pferdehirt*[1], *Yun-Rak Choi*[2], *Farshid Guilak*[1]

1Washington University in Saint Louis, Saint Louis, USA; Shriners Hospitals for Children, Saint Louis, USA
2Yonsei University Health System, Seoul, Republic of Korea

Recent advances in regenerative medicine have led to the development of multifunctional engineered tissues designed to not only restore tissue function but to also provide for cell-based delivery of biologic drugs. However, recapitulating tissue mechanical properties in combination while optimizing the potential for therapeutic drug delivery results in complex and often competing design criteria. In this regard, testing a broad range of experimental design variables is an expensive, iterative, and time intensive endeavor with a number of complex biologic and mechanical parameters to be considered. An attractive alternative to experimental optimization is using finite element models that match the biological growth, remodeling, and kinetics involved in modeling tissue engineering systems, an achievement brought about by the application of chemical kinetics to the finite element framework. We present two applications of chemical kinetic modeling to finite elements, illustrating the power of models for predicting nutrient consumption and drug production. First, to grow large, mechanically-robust cartilage constructs, it is essential to ensure adequate nutrient availability throughout the engineered tissue. Data from early experiments had implicated that chondrocyte biosynthesis was strongly dependent on glucose availability [1]. Using this insight, we developed finite element models based on experimental measurements of the glucose consumption to optimize our tissue culture protocols for growing anatomically-sized tissue constructs [2]. Our analysis indicated increasing glucose levels by threefold the standard culture levels enhanced tissue growth and remodeling through the deposition of glycosaminoglycans and collagens. Secondly, our ongoing work aims to determine the optimal tissue geometry for maximizing anti-cytokine therapeutic drug production from bioengineered cartilaginous implants for disease modifying applications. Using CRISPR-Cas9 genome engineering, our group has developed stem cells containing a synthetic gene circuit that sense and respond to the potent pro-inflammatory cytokine interleukin-1 (IL-1) and produce the anti-inflammatory biologic drug interleukin-1 receptor antagonist (IL-1Ra) downstream of the endogenous Ccl2 promoter [3,4]. This synthetic gene circuit suppresses IL-1 signaling via closed loop feedback. The geometry of the engineered tissue constructs influences molecular transport to and from the cells, thereby modulating how cells within the engineered tissue sense and respond to IL-1 and therefore the overall production and delivery of IL-1Ra. Here, we used experimental data to model engineered tissue constructs of three different geometries challenged with 1 ng/mL IL-1α, a physiologically relevant dose representing chronically inflamed arthritic joints to determine and manipulate the production and responsiveness of IL-1Ra production in response to IL-1 bioavailability. Our subsequent computational models fit for the biokinetic properties of IL-1Ra production in response to IL-1α concentrations will inform the optimal design of engineered tissue geometries for IL-1Ra production. Together, these approaches can optimize engineered tissue culture and geometries for producing functional replacement tissues in a number of disease applications.

Acknowledgments: Supported by grants from the NIH, NSF, Nancy Taylor Foundation for Chronic Diseases, Arthritis Foundation, AO Foundation, and the Shriners Hospitals for Children.

References:

[1] Cigan+ Tissue Engineering Part A 2013,
[2] Nims+ Tissue Engineering Part C 2015,
[3] Brunger+, Stem Cell Reports 8:2012, 2017,
[4] Choi+, ORS Transactions, 2019.

[B-04.1]

ISSUES TO CONSIDER IN VALIDATION OF NUMERICAL MODELS OF DIARTHRODIAL JOINTS THROUGH EXPERIMENT

Nigel G. Shrive[1], *P. A. Vakil*[1], *M. M. Shekarforoush*[1], *J. E. Beveridge*[1], *M. Atarod*[1], *J. Rosvold*[1]

1 *University of Calgary, Calgary, Canada*

The validation of any numerical model of a diarthrodial joint is difficult. A primary consideration is that humans are individuals and we all have different gait and motion of our bodies: animals are the same (Figure 1). Therefore, experiments on a single joint will only provide data for that joint under the imposed experimental conditions and will not necessarily be generally applicable to other conditions or the same joint from another individual. Using the ovine stifle joint as an example, we will show the variation in individual responses in normal gait and after joint injury to demonstrate the variability that can occur even when animals do something supposedly consistent like walking normally. From the data, we will show that ligament loads change in terms of point to point direction between bones during gait as different parts of the ligaments become taut or slack. Thus, modelling a ligament as a tension-resisting member between single points on the femur and tibia will be inadequate to capture the complex interaction between ligament load and the 3-D relative positions of the bones. Similarly, the stress distribution over the joint surface varies throughout the gait cycle, with different animals having different patterns both spatially and temporally throughout the gait cycle. Modeling of a joint must therefore consider the purpose of the model – what is the model to provide in terms of understanding in relation to functioning of a joint – and from that, what experiments need to be performed in order to validate the conclusions drawn from the modelling. For, example, modeling will show that the menisci transfer load between the femur and the tibia because they have high circumferential stiffness and develop hoop stresses when resisting motion pushing them outwards from the center of the knee, as the femur approaches the tibia. This general, high-level principle holds for menisci and labra in other joints. The fact that circumferential tension develops can easily be shown experimentally by measuring radial movements under load and subsequent to a radial cut across the meniscus. Removing the meniscus completely and displacing the bones as before will reveal a minimum value of how much load the meniscus transferred in that particular joint under that particular displacement scheme, but would not necessarily mean a model will show correctly the loading under a different displacement scheme.

Modeling of joints is not restricted to those being developed to provide understanding of how a joint works, but also includes macroscopic joint properties in multi-body dynamic models. In this case, the stiffness and damping of the joint as a whole are of interest, and how these properties change with joint position, load and activity. "Contact" is particularly problematic as it is load dependent. Suitable data are very scarce, as they are also for Artificial Intelligence models being considered to try and predict ligament loads (for example) from kinematic data. For this latter problem, actual loads in the joint structures are needed together with the simultaneous kinematic data. Such information can be obtained from comprehensive animal studies, but translation to the human case adds another level of complexity.

The models above are all structural/mechanical in context. If the objective of a model is to assess what happens in a compromised joint, then even more information should be considered – genetic and biological biomarkers will be needed and integrated somehow with the mechanical changes to assess the potential of someone developing osteoarthritis for example, or predict potential outcomes of surgical intervention. Of importance in all models will be the level of accuracy needed in the data, for meaningful outputs to be obtained.

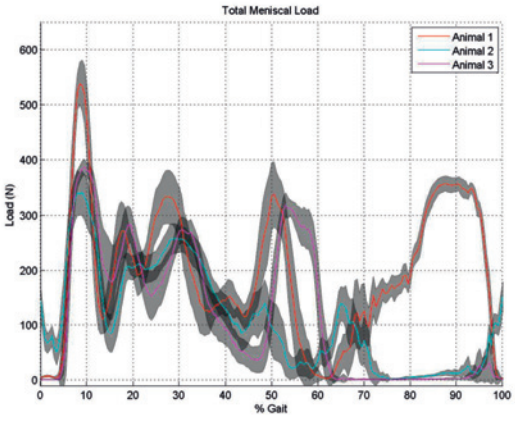

Figure 1: Loads (mean and std deviation over 20 strides) in the menisci of the knee for 3 different sheep during normal gait.

Acknowledgments: Funding for the research by the Canadian Institutes for Health Research, The Arthritis Society, the Natural Sciences and Engineering Research Council and the University of Calgary, Canada is gratefully acknowledged.

[B-04.2]

UNDERSTANDING APPROACHES TO CREATING FINITE ELEMENT MODELS OF OSTEOCHONDRAL GRAFTS IN JOINTS

Gavin Day[1], *Robert Cooper*[1], *Alison Jones*[1], *Marlène Mengoni*[1], ***Ruth Wilcox***[1]

1 *Institute of Medical and Biological Engineering, University of Leeds, Leeds, UK*

Osteoarthritis (OA) is the most prevalent chronic rheumatic disease worldwide with knee OA having an estimated lifetime risk of approximately 14 % [1]. Autologous osteochondral (cartilage-bone) grafting has demonstrated positive outcomes in terms of pain and function in some patients [2], however, currently there is a lack of understanding as to how the treatment can be optimised. The aim of this study was to establish a methodology for the development of finite element models of the graft-host interface with the capability of implementation into models of the whole knee joint. These models will allow us to understand the primary factors affecting the short-term graft stability.

Methods of creating finite element (FE) models of the graft-host interaction were investigated for oversized cylindrical grafts, initially using geometric models built in Abaqus (v.2017 Simulia), these were then recreated in image-space using Simpleware ScanIP (Synopsis) and finally within a full specimen specific porcine knee joint model (Fig. A & B). This full knee joint model was developed in parallel with the current study. Three methods of describing the graft-host interaction due to the oversize of the graft were also investigated; the first utilised an interference fit model. The second used a negative radial pressure on the graft. The final method used an oversized graft, initially separate from the host, then displaced to the correct depth within the host allowing the contact interaction to establish itself progressively with displacement. The push-in force was measured and the sensitivity to mesh quality, material properties, coefficients of friction and graft oversizing was investigated.

The model results were highly sensitive to the quality of meshing and hence simplified models (both geometric and image-space based) had little in common with the full knee joint model, where the meshes at the surfaces were less uniform. Models were found to be non-repeatable using interference fit and unrepresentative using negative pressure graft-host interactions. Displacing the graft to the correct depth provided a robust method that preserved the sensitivity to graft-host moduli seen in our experimental work [3].

The different approaches required for increasingly complex models has shown that there is little value in more simplified approaches, at least when the dependence on the mesh is high. The choice of graft-host interaction gives a repeatable method with greater control than the other tested approaches. These results will allow for an investigation into the effect the intervention has on the biomechanical function of the knee joint.

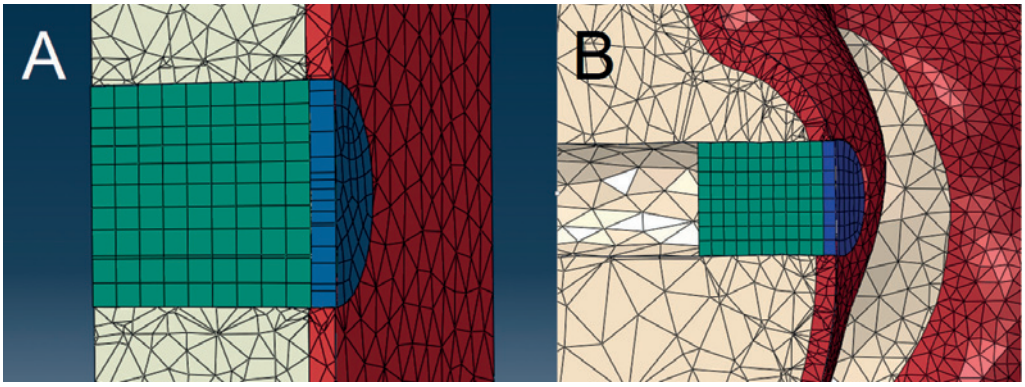

Figure Caption: A: Simplistic geometry based model. B: Graft implemented into a full knee joint model.

Acknowledgments: EPSRC EP/P001076/1

References:

[1] Bortoluzzi, A. et al., 2018. Autoimmunity reviews.
[2] Pareek, A. et al. 2016. Arthroscopy.
[3] Casper-Taylor et al., 2019 Proceedings, World Congress on Osteoarthritis

[B-04.3]

IMPACT OF PERSONALISATION OF GEOMETRY ON THE PASSIVE KINEMATIC RESPONSE OF THE KNEE JOINT IN FLEXION-EXTENSION

Bhrigu Kumar Lahkar[1], *Pierre-Yves Rohan*[1], *Pillet Hélène*[1], *Patricia Thoreux*[2], *Wafa Skalli*[1]

1 *Institut de Biomécanique Humaine Georges Charpak, Arts et Métiers ParisTech, Paris, France*
2 *Université Paris 13 Sorbonne Paris Cité, Paris, France*

In an effort to improve diagnostics and treatment of knee joint laxity and to minimize post-operative complications, development of patient-specific computational models of the knee joint is subject of current interest and investigation. A key strength of computational models is that they can provide an insight on the relative contributions of the musculoskeletal components on the passive biomechanical response. This knowledge is paramount for improving surgery outcomes. In vivo personalization of geometry and mechanical properties however still represents a significant challenge in daily clinical setup. The objective of this contribution was therefore to investigate relative contribution of geometry and material properties on the passive kinematic response of the knee joint in Flexion-Extension using Finite Element (FE) modelling.

Experimental data of passive knee Flexion–Extension tests of 8 fresh frozen lower limbs previously acquired [1] were used to generate the associated subject-specific FE geometrical models. During the experiment, each ligament attachment location had been marked with radio opaque paint and bone segments had been CT-scanned. These data were used to personalize the geometry of both the bones (femur, tibia and patella) and ligament insertions in the FE model. A previously described method was used to get a regular subject specific mesh. First, generic material properties obtained in a previous study were assigned to the ligaments and the static response was computed using an implicit solver in ANSYS. Second, an inverse procedure was used to calibrate the material properties of the ligaments to improve the experimental-numerical agreement.

Preliminary results regarding the femoro-tibial kinematic response are given in the figure below. Analysis of the individual responses with generic material properties showed that the deviation between the experimental and numerical responses (reported as median(interquartile range)) of Rx, Ry, Tx, Ty and Tz were 1.2° (2.3°), 9.8° (8.8°), 5.6mm (2.7mm), 1.7 mm(1.9mm) and 1.9mm (2.3mm) respectively. Personalization of the ligament allowed to improve the goodness-of-fit resulting in the following femoro-tibial kinematic results respectively: 1° (1.4°), 2.9° (2.6°), 4.4mm (1.2mm), 1.1mm (1.9mm) and 1.9mm (2mm).

Results obtained in this contribution on eight specimens strongly suggest that personalization of both geometry and mechanical properties are paramount in order to properly assess and analyze the individual passive kinematic response of the knee joint. Perspective work include assessing the response in other clinically relevant loading scenarios (AP drawer, internal-external rotation, and varus-valgus).

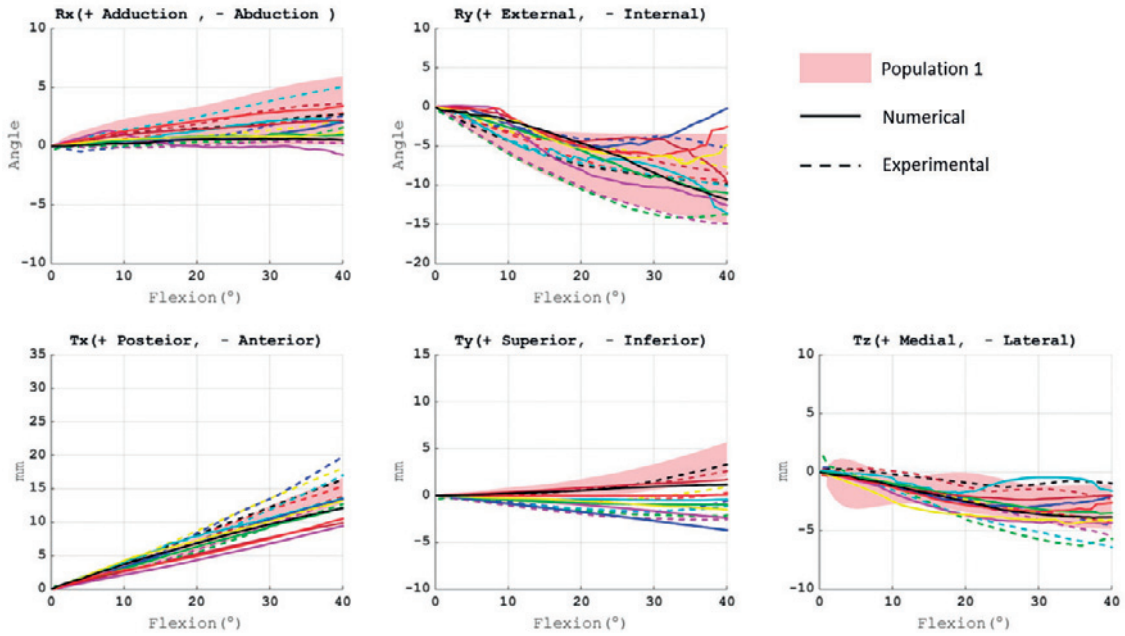

Figure Caption: Femoro-tibial kinematics of the knee joint.

Acknowledgments: The authors are deeply grateful to the BiomecAM chair for the financial support.

References:

[1] *Rochcongor, G., Pillet, H., Bergamini, E., Moreau, S., Thoreux, P., Skalli, W., Rouch, P., 2016. A new method for the evaluation of the end-to-end distance of the knee ligaments and popliteal complex during passive knee flexion. The Knee. 23(3), 420–425*

[B-04.4]

KNEE MODELING - A FIRST HAND EXPERIENCE IN DOCUMENTING FOR REPRODUCIBILITY

William Zaylor[1], *Neda Abdollahi*[1], ***Jason Halloran***[1]

1Cleveland State University, Cleveland, USA

The growth of modeling and simulation in biomechanics, and in particular knee mechanics, warrants study of the potential for reproducibility in this process. From development of geometry to application of boundary conditions, specification of material responses and finally, validation against experimental data, this process requires numerous modeling decisions. Within this, a modeler's decisions may change with time, be open to interpretation, and be influenced by intended model use. We hope to capture this 'art', and as a consequence the potential for reproducibility, in knee simulation. Cleveland State University, Cleveland, United States (CSU) is one of five that is developing detailed modeling specifications, based on the same source data of two knees1,2, for comparative analysis across group-specific models. The purpose of this abstract was to provide a commentary on development of two models, with a focus on differences between a priori developed modeling specifications and what was realized in actual use of those specifications. As the processes are generally similar, this work not only provides a platform to assess knee modeling, but has implications across musculoskeletal modeling as whole.

CSU's modeling specifications were written for development of explicit finite element models of the two data sets chosen for this study. The first step was to write and then utilize detailed specifications for development of two initial models (Fig. 1.a). Here, "initial models" are ones that simulate 0-90° flexion with a nominal compressive force. Like the other four groups, our specifications are currently disseminated on a simtk.org project site3. CSU's documents encompass 90+ pages that outline the development of each model. Importantly, the procedure included documentation of "protocol deviations", which summarize changes or details that were overlooked in the specifications.

CSU's modeling process includes seven stages and protocol deviations were documented (Fig. 1.c). Deviations occurred in the image segmentation and reconstruction (i.e. creation of solid or surface models) and the reference simulation steps. In particular, the perceived quality of the images and the imaging plane used by the modeler appeared to influence the geometric representation. Additionally, modeling parameters were updated to realize stable solutions. Possible consequences are yet to be determined and exploration of these observations will be evaluated as the project progresses. While numerous modeling decisions will likely influence predictions, protocol deviations may highlight areas where even experienced modelers had difficulty defining appropriate steps for model creation.

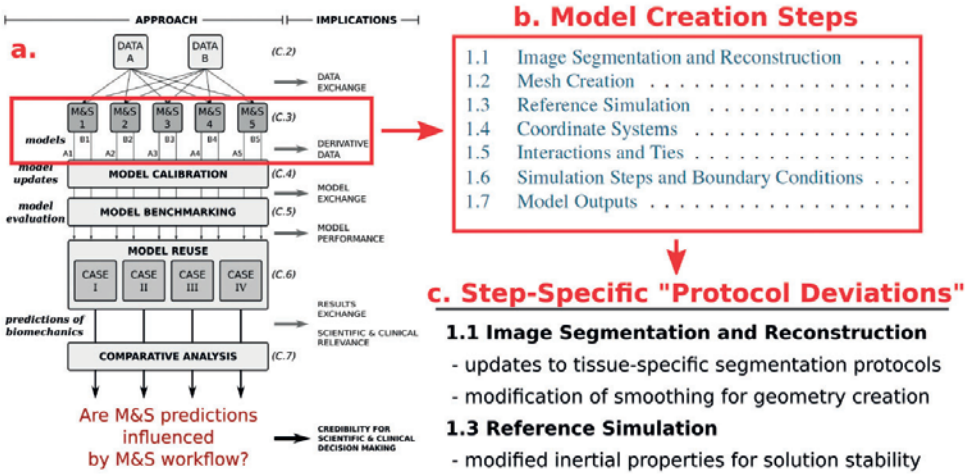

Figure 1: (a) Overall workflow of the study, where the red box highlights the current stage. (b) CSU's model creation specifications and (c) protocol deviations.

Acknowledgments: R01EB024573 (NIBIB-NIH)

References:

1) *Harris, etal., JBiomechEng., 138(8), 2016.*
2) *Erdemir, JKneeSurg, 29, 107-116, 2016.*
3) *https://simtk.org/projects/kneehub*

[B-04.5]

WHAT WE SAID, WHAT WE DID: UNDERSTANDING SUBJECTIVE DECISIONS DURING DEVELOPMENT OF KNEE MODELS

Ariel Schwartz[1], *Snehal Chokhandre*[1], ***Ahmet Erdemir***[1]

1 *Cleveland Clinic, Cleveland, USA*

Development of computational models require several critical decisions which can significantly affect the reproducibility of models and induce uncertainties in predictions. Modeling of the knee joint is not an exception. Modeler needs to decide which mesh density to use, the material properties to assign, and representation of anatomical joint coordinate systems, and so on. Ideally, all of these decisions would be made based on the physical properties of the system being modeled and the scientific question asked. In reality however, many of these decisions are influenced by many factors including skills of the modeler, resource constraints, convergence requirements, etc. In the scope of a collaborative project (Reproducibility in simulation-based prediction of natural knee mechanics [1]), five research teams were asked to use the same anatomical data to build models of the knee and simulate passive flexion. All teams are asked to write and disseminate model development specifications, a-priori, before executing their workflow. They were also asked to document protocol deviations as they moved towards the end goals of the modeling. We present here our experience, i.e., how we said we would do the modeling vs. what we really ended up doing. This document an example of the "art" of modeling, and how some of the subjective modeling decisions significantly impact the simulation outcome. Ideally, the modeling decisions should be based purely on physical characteristics of the knee, and model convergence was expected. However, in reality, changes are likely to get the model complete a simulation, i.e., to converge. One example of a part causing unexpected convergence problems was the medial collateral ligament (MCL). Material properties were initially chosen from literature for a transversely isotropic fiber based model with ground substance. However, during simulations, the MCL was buckling in a fashion preventing convergence (Figure 1). To reconcile this issue, the bulk modulus of ground substance was reduced first. This time, the MCL was twisting unexpectedly (Figure 1). In another iteration, the femoral insertion origin of the MCL was modified, which prevented unrealistic twisting of the ligament. This example demonstrates one of many modeling decisions that needed to be made to achieve model convergence. As of now, it is unknown how these changes will affect the actual model predictions, and is something that will be considered in evaluating the quality of model outputs with further model calibration and validation. This exercise underscores the idea that finite element modeling procedures are not rigid and require a fair amount of "art".

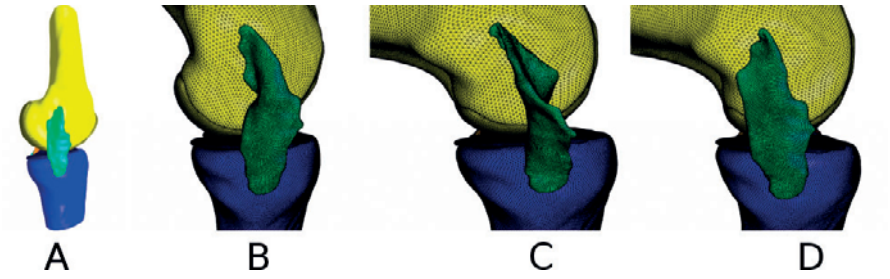

Figure 1: A) Model. B) Failed simulations with MCL of a-priori specifications. C) After reduction of ground substance bulk modulus. D) After changing the insertion origin.

Acknowledgments: R01EB024573, R01GM104139.

References:

[1] https://simtk.org/plugins/moinmoin/kneehub/

[B-04.6]

IDENTIFYING BONE AND LIGAMENT GEOMETRIES OF THE KNEE FOR COMPUTATIONAL MODELING: EASIER SAID THAN DONE

Shady Elmasry[1], *Hamidreza Jahandar*[1], *Donya Jahandar*[1], *Thomas Fraychineaud*[1], ***Carl Imhauser***[1]

1 *Hospital for Special Surgery, New York, USA*

A common and critical aspect of building computational models of the knee is extracting bone and ligament geometries from medical images. This process is complex due to variations in image quality, use of special scanning protocols, heterogeneity in knee morphology, the need to understand knee anatomy, and the expertise required to implement protocols as well as skillfully use a variety of software packages. Consequently, there are numerous opportunities for protocol deviations. Identifying key sources of uncertainty in model predictions is an important step towards using computation models of the knee for clinical decision-making. The goal of this abstract is to discuss the ability to generate knee model geometries using a previously-documented protocol focusing on the medial collateral ligament (MCL) as an example. An open-source, magnetic resonance imaging (MRI) data set was used; the methods for extracting the geometries of the bones and ligaments were prospectively documented and are available for download [1]. Two medical students followed our protocol to define the MCL insertions from the aforementioned image data (25 years old female, oks003) [2]. First, the protocol called for identifying the proximal and distal MCL insertions using bony landmarks from the anatomical literature [3]. Two protocol deviations arose. First, we planned to use a Proton Density-Turbo Spin Echo (PD-TSE) sagittal MRI to segment the femur and the tibia. After creating the 3D model, however, we found that the bony landmarks were not distinct enough to be used to determine the insertions of the ligaments (Fig. 1A). After reviewing all image data, we found that the PD-TSE coronal MRI, which had a resolution of 0.35 mm2 in the coronal plane, more distinctly captured these landmarks (Fig. 1B). Therefore, we decided to use the coronal MRI to segment the femur and the tibia. Second, the femoral attachments of the MCL were placed 4 mm proximal to the designated insertion site (Fig. 1C) due to a lack of specificity in our protocol. Finally, the tibial attachments of the MCL fibers were placed 3.5 cm from the tibial joint line, not 6 cm, despite clear instructions in the protocol. The findings suggest a need for sensitivity analyses to identify those decisions that are most critical to model outcomes. These deviations demonstrate that following a protocol to identify knee model geometries can be fraught with uncertainty despite detailed protocols.

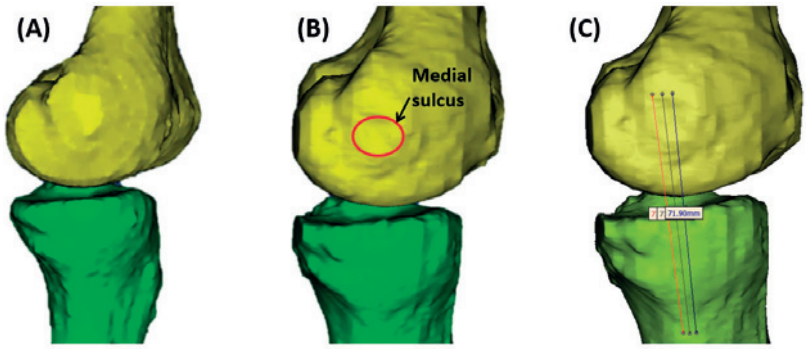

Figure 1: Tibial and femoral geometries extracted from sagittal (A) and coronal (B) MRI scans. The MCL with incorrectly identified proximal and distal insertions (C).

Acknowledgements: R01EB024573 (NIBIB, NIH)

References:

[1] *https://simtk.org/docman/view.php/1061/11493/Earmarked+ protocol_ OpenKnee_HSS.pdf*
[2] *https://simtk.org/frs/download_confirm.php/latestzip/2070/DataforMC-oks003-latest.zip?group_id=1061*
[3] *LaPrade RF, et al. J Bone Joint Surg 2007; 89(9): 2000-2010.*

[B-05.1]

FOCAL CHONDRAL DEFECTS IN THE DYSPLASTIC HIP CAUSE ACTIVITY- AND SIZE-DEPENDENT INCREASES IN STRESS AND STRAIN

Jocelyn Todd[1], *Jeffrey Weiss*[1], *Travis Maak*[2]

1 *University of Utah, Department of Biomedical Engineering, Salt Lake City, USA*
2 *University of Utah, Department of Orthopaedics, Salt Lake City, USA*

Introduction: In the hip, bony pathomorphology such as dysplasia produces abnormal loading of the cartilage, often leading to focal chondral defects and the subsequent development of osteoarthritis (OA)[1]. Focal chondral defects present as partial- or full-thickness voids in the articular cartilage. Although mechanical factors influence the initiation and progression of OA[2], the alterations in mechanics leading to and caused by focal chondral defects are not well-understood and treatment methods remain unclear. A clear understanding of the mechanical effects of focal chondral defects could separate stable defects from those which are likely to expand and should be treated more aggressively. The objective of this study was to assess the effects of focal chondral defects on the response of articular cartilage in a patient-specific finite element model of the dysplastic hip during activities of daily living.

Methods: A validated patient-specific finite element model of a dysplastic hip was used for this study[3] (Fig. 1A). The cartilage layers were represented as anisotropic biphasic materials. An intact case was compared to cases with chondral defects of 3, 7 and 15 mm in diameter at a clinically relevant location on the chondrolabral boundary[4] (Fig. 1A). Single-leg stance (SLS), gait, and squatting were simulated using three-dimensional loading and kinematics from Bergmann et al[5]. All models were analyzed with FEBio (www.febio.org). For each kinematic scenario, the region around the defect (Fig 1B) was analyzed throughout the motion. Maximum tensile strain on the articular surface (E1) and maximum shear stress at the osteochondral interface (τ_{max}) were examined within the acetabular cartilage, due to the potential for collagen fibril fissuring and delamination of the cartilage from the bone, respectively.

Results: Regardless of the activity performed, the presence of a chondral defect increased E1 and τ_{max} in the defect region compared to the intact case (Fig. 1B-C). The 15-mm defect case experienced the highest magnitude for E1 and τ_{max}. For SLS and gait, E1 and τ_{max} increased with increasing defect size. During squatting, E1 and τ_{max} were highest for the 3-mm case and decreased slightly for the 7- and 15-mm cases.

Discussion: Presense of a defect increased damage potential in the defect region. However, the magnitude and trend of damage potential based on defect size differed based on the simulated activity. Therefore, damage progression likely depends on the applied loading and kinematics. The largest defect experienced tensile strain within the reported range for collagen fibril failure in articular cartilage[6], which may indicate a threshold size beyond which more aggressive treatment strategies should be recommended. More cases must be tested to verify this trend and to determine the threshold size.

Acknowledgments: Supported by an LS Peery Investigator Research Grant, Dept. of Orthopaedics, University of Utah, Salt Lake City, United States.

Figure 1: A) Patient-specific hip and close-up of 7 mm defect case. B) Comparison of E1 during gait, showing the concentration in the defect region. The defect region analyzed is indicated by the black dashed line in the 15 mm case. C) Peak values of E1 and τmax during SLS, gait, and squatting.

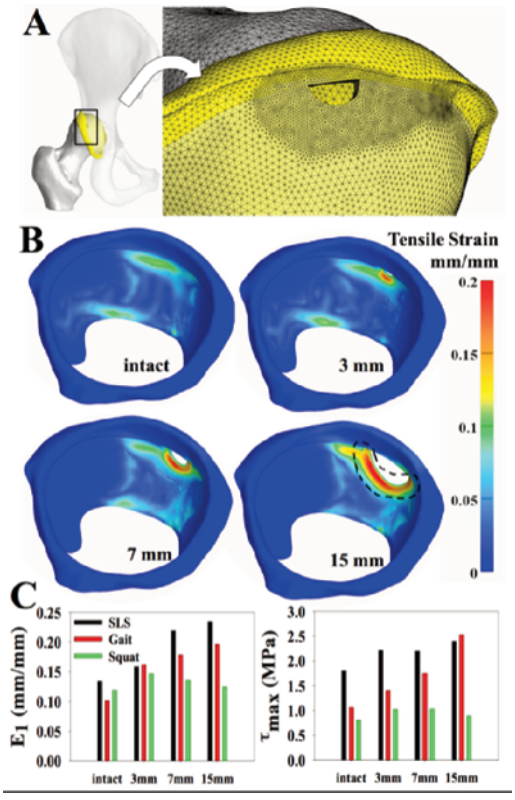

References: [1] Ganz, R., *Clin Orthop Relat Res*. 466: 264-72, 2008. [2] Guilak, F., *Best Pract Res Clin Rheumatol*. 25: 815-23, 2011. [3] Anderson, A.E., *J Biomech Eng*. 130: 051008, 2008. [4] Kapron, A.L., *Knee Surg Sports Traumatol Arthrosc*, 2018. [5] Bergmann, G., *J Biomech*. 34: 859-71, 2001. [6] Sasazaki, Y., *J Anat*. 208: 681-94, 2006.

[B-05.2]

CARTILAGE AND JOINT MECHANICS: NEW INSIGHTS INTO THE CONDITIONS OF THE BURIED INTERFACE

Axel C. Moore[1], *Brian T. Graham*[1], ***David Burris1***, *Chris Price*[1]

1 *University of Delaware, Newark, USA*

After nearly a century of research, we have yet to answer the most basic questions about how cartilage and joints work. For example, it is unclear if friction forces can be attributed to classical adhesive interactions or fluid shear stresses; it is unclear if fluid films are common, rare, or impossible; it is unclear how cartilage recovers and retains interstitial fluid to maintain joint space within loaded contacts. In this talk, I will present our work to address these questions using in-situ measurements to more directly probe the buried interface. In a recent study [1], we replicated a classic hydrodynamic experiment in which decreasing friction with increased speed following equilibration in the cSCA (Fig. 1c) has been interpreted as hydrodynamic fluid film lubrication. Contrary to the long-standing assumption that pore pressure remains zero during sliding while the contact remains loaded (no migration), our in-situ displacement measurements revealed clear evidence that interstitial hydration, pressure, and lubrication were restored by sliding at 60 mm/s (Fig. 1a). Our observation that the greatest rehydration rates accompanied the greatest friction forces suggests that 'tribological rehydration' occurred despite intimate contact (no fluid film) and that interstitial lubrication (via rehydration) was the most likely cause of reduced friction. These observations and our more recent solute transport results [2] (Fig. 1b) are consistent with the hypothesis that hydrodynamic pressures created a rehydration front that reduced friction gradually as it spread across the contact interface (Fig. 1c) [3]; this interpretation explains why friction-speed trends mimic the Stribeck curve for hydrodynamic lubrication. We have quantified tribological rehydration rates (5N) and find that they rival free-swelling rates (1,000 nm/s); both were more than an order of magnitude greater than loaded exudation and static swelling in an unloaded contact. Movement appears to dominate the maintenance and recovery of joint space (compared to static unloading) via comparable contributions from free swelling outside the contact and tribological rehydration inside the contact. Finally, our recent adhesion measurements suggest that cartilage produces virtually no traditional adhesion and yet clings to opposing surfaces with astonishing strength due to the development of substantial negative interstitial pressures at non-zero separation speeds. Our results consistently suggest that cartilage, despite its enormous roughness, conforms to opposing surfaces to eliminate the interfacial gap as the preferred flow pathway. In summary, we report the following repeatable yet unexpected results: (1) rapid tribological rehydration in the cSCA; (2) maximal rehydration rates during maximal friction; (3) negligible interface permeability. These results are unanticipated based on current understanding, highlight specific deficiencies in our current modeling capabilities, provide benchmarks for model validation, and suggest new opportunities for cartilage and joint modeling (e.g. how movement patterns affect the dynamics of joint space loss and recovery).

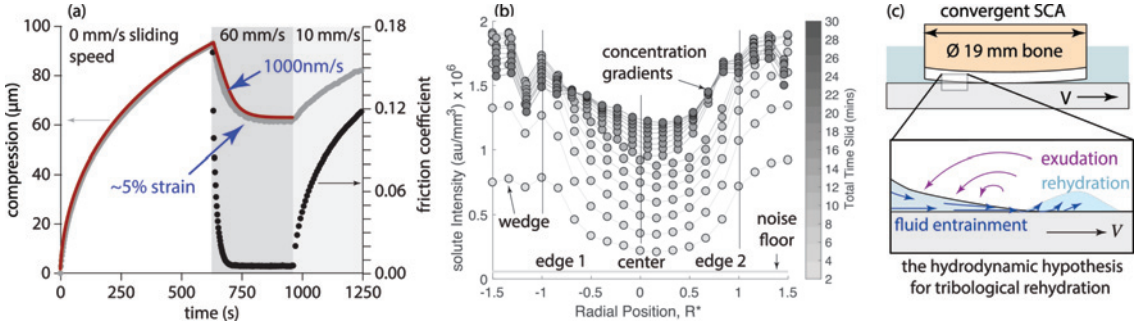

Figure 1: Tribological rehydration in the convergent stationary contact area (cSCA). (a) Compression and friction coefficient during static loading, sliding at 60 mm/s, and sliding at 10 mm/s (5 N). Rehydration at 60 mm/s led to low initial friction at 10 mm/s via tribological rehydration. (b) Solute (AlexaFluor 633) intensity from in-situ confocal microscopy measurements as a function of location within the contact region (the contact area spans -1 to 1) as a function of time during sliding at 60 mm/s and 5N of load. The gradient suggests flow from the bath (source) toward the center. (c) Schematic of the cSCA illustrating our hydrodynamic hypothesis for tribological rehydration.

Acknowledgments: We gratefully acknowledge support from NSF BMMB 1635536.

References:

[1] Moore & Burris, Osteoarthr. Cartil., (1), 99-107, 2017;
[2] Graham et. al., J. Biomech., (71), 271-276, 2018;
[3] Moore & Burris, Biotrib. (12), 8-14, 2017

[B-05.3]

TIME-DEPENDENT IN VITRO VALIDATION OF FIRST METATARSOPHALANGEAL JOINT BIPHASIC FINITE ELEMENT MODELS

Oliver Morgan[1], *Howard J Hillstrom*[2], *Xiang Chen*[2], *Matthew F Koff*[2], *Jennifer Martay*[1], *Rajshree Hillstrom*[1]

1Anglia Ruskin University, Chelmsford, UK
2Hospital for Special Surgery, New York, USA

To date, no published FE model of the foot has validated 1st MTP joint contact mechanics.1 There may be uncertainty regarding the predictive capability of such models and hence, their application to clinical problems. To address these gaps in knowledge, we developed and validated eight 1st MTP joint FE models pre- and post-3-mm Moberg osteotomy.

Eight cadavers were used. A TekScan K-Scan 6900 transducer (TekScan, Boston, USA) was inserted into each 1st MTP joint pre- and post-3-mm Moberg osteotomy to derive measurements of contact pressure (MPa), contact area (mm^2), and change in COP location (mm). Vertical loads of 28N and 40N were applied to the distal phalanx and sesamoid bones. Static equilibrium was achieved by tensioning the plantar fascia by 145 ± 16 N for 30 s.

3D 1st MTP joint FE models were created from MRI datasets of each cadaver. Tissues were segmented in Mimics (Materialise, Lueven, Belgium). The proximal phalanx geometries were modified to simulate a 3-mm Moberg osteotomy in CATIA V5, (Dassault Systèmes, Vélizy-Villacoublay, France) creating two model variations: (1) pre-3-mm Moberg osteotomy; (2) post-3-mm Moberg osteotomy. The assemblies were meshed in ABAQUS (Dassault Systèmes, Vélizy-Villacoublay, France), and analyzed using FEBio 2.8.5 (FEBio, Utah, USA). Bones (E=7.3 GPa, v=0.3) were modelled as linear elastic materials and the plantar fascia (E=350 MPa, v=0.4) as a hyperelastic material. Fourteen 1D tension-only springs represented the ligaments (E=260 MPa, v=0.4). Articular cartilage (φ^s =0.25, $E_{1,3}$ =16 MPa, E_2 =0.98 MPa, $v_{12,31}$ =0.42, v_{23} =0.07, G =0.45 MPa, K =2.02 10^{-15} m^4/N.s) was modelled as a transversely isotropic, poroelastic material. Identical loads to the experimental testing were transiently applied to each FE model.

First, the validation outcomes were quantified by calculating RMSE% between the experimental and FE results (i.e. pre- and post-3mm Moberg osteotomy). Second, the ability of each FE model to reproduce the effect of the 3-mm Moberg osteotomy was evaluated (i.e. pre- to post-3-mm Moberg osteotomy). Bland-Altman analysis plots compared the differences and 95% confidence intervals (CI) between each method.

The RMSE are shown in Table 1. The Bland-Altman plots are shown in Figure 1. A constant bias was demonstrated for contact pressure (bias, -0.9 MPa, 95% CI -2.4 – 0.6 MPa) and contact area (bias, -4.7 mm^2, 95% CI -21.5 – 12.1 mm^2), while there was no bias for change in COP location (0.0 mm, 95% CI -0.8 – 0.8 mm).

The known range in 1st MTP joint cartilage material properties may explain some of the inter-specimen variability in the RMSE% for contact pressures and contact areas. This work expands on existing FE modelling strategies of the forefoot and provides a methodological framework to investigate 1st MTP joint contact mechanics following surgical interventions.

	Specimen	1	2	3	4	5	6	7	8
Contact Pressure	**RMSE%**	22.9	28.7	47.4	40.6	4.6	25.0	50.7	30.2
Contact Area	**RMSE%**	44.4	20.2	37.7	31.5	4.8	47.9	32.3	49.3

Table 1. RMSE% between experimental and FE results

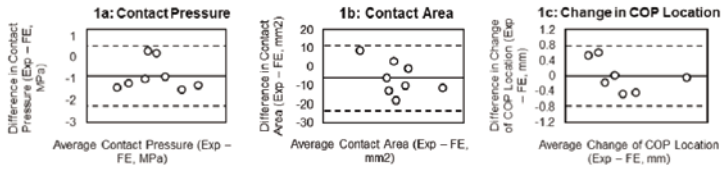

Figure 1a-c. Bland-Altman plot analyses for the change in contact pressures (left), contact areas (middle), and COP locations (right).

Acknowledgments: We would like to acknowledge Mark Lenhoff, BS, Scott J. Ellis, MD, Jonathan T. Deland, MD, of Hospital for Special Surgery, New York, United States, and Josh Baxter, PhD, of University of Pennsylvania, Philadelphia, United States as co-authors of this abstract. We also acknowledge contributions from Internship groups: École des mines d'Albi-Carmaux; Université de Franche-Comté. Hospital for Special Surgery, New York, United States, Foot and Ankle Research Grant.

References:

Behforootan et al, Med Eng Phys, 39:1-11. 2017.

[B-05.4]

FINITE ELEMENT ANALYSIS OF PATELLOFEMORAL JOINT CONTACT USING A TRIPHASIC MODEL FOR CARTILAGE

Brian Jones[1], *Gerard Ateshian*[2]

1 *University of Virginia, Dept of Biomedical Engineering, Charlottesville, USA*
2 *Columbia University, New York, USA*

Introduction: The response of articular cartilage to physiologic loading is dependent upon the Donnan swelling and mechanical pressure of its interstitial fluid and the stresses in its solid matrix. Triphasic models of cartilage can predict separately these pressures and stresses, but formulations useful for modeling articular contact have only recently become available5. Such methods are of interest, for example, in research examining the altered contact mechanics of osteoarthritic cartilage, where aggrecan and collagen are known to be degenerated. The objective of this study was to examine the stress within the collagen matrix of osmotically swelled patellofemoral articular cartilage using an anatomically faithful triphasic model subjected to physiologic loads.

Methods: Finite element models were created from four cadaver knees measured previously1 and imported into FEBio2. Cartilage layers were modeled as triphasic mixture materials consisting of interstitial water, charged solutes, and a charged porous solid matrix. Interstitial fluid transport was modeled using a constant, isotropic hydraulic permeability. Depth-varying material properties for cartilage were obtained from the literature3 and prior data from our lab4. The patella tendon was modeled using linear springs, and the quadriceps muscle applied physiologic loads approximately equivalent to a body-weight squatting motion (534 N). Bones were modeled as rigid bodies. The femur was spatially fixed and tibia motion was prescribed based on experimental measurements of knee flexion ranging from 45° to 75° at 15°/s. A frictionless triphasic contact interface was used at the articular surfaces of the patella and femur5.

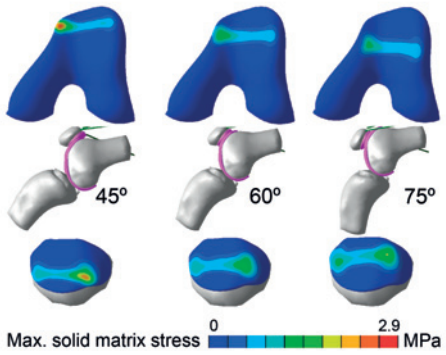

Figure 1. Representative variation of the maximum principal solid stress in the collagen matrix, with knee flexion for the femur (top) and patella (bottom).

Conclusions: The solid matrix swelling strains produced by Donnan osmotic pressure remained below 0.5%. Upon loading, the contact stress was nearly indistinguishable from the fluid pressure at the articular surface, and collagen matrix stresses were predominantly tensile (Fig.1). Principal directions of collagen matrix tensile stresses were also primarily aligned with known orientations of cartilage collagen fibrils. Future work will address modeling pathologies such as osteoarthritis, where the progressive loss of proteoglycan occurs in a depth-dependent manner.

References:

1. *Kwak SD, Ahmad CS, Gardner TR, Grelsamer RP, Henry JH, Blankevoort L, et al. J Orthop Res 2000;18:101-8.*
2. *Maas SA, Ellis BJ, Ateshian GA, Weiss JA. J Biomech Eng 2012;134:011005.*
3. *Ficat C, Maroudas A. Ann Rheum Dis, 1975 34(6):515–519.*
4. *Krishnan R, Park S, Eckstein F, Ateshian GA. J Biomech Eng 2003;125:569-77.*
5. *Ateshian GA, Maas SA, Weiss JA. 2012 45(6):1023-7.*

[B-05.5]

POROMECHANICAL MODELING OF PORCINE KNEE JOINT USING INDENTATION MAP OF ARTICULAR CARTILAGE

LePing Li[1], *Mojtaba Zare*[1]

1 University of Calgary, Department of Mechanical and Manufacturing Engineering, Calgary, Canada

The mechanical response of the knee joint to compressive loading is greatly influenced by the fluid pressurization in articular cartilages and menisci, which may play an important role in the mechanobiology of the joint. Great progresses have been made in understanding the creep and relaxation response of tissue explants from the knee joints [1]. We are interested to advance these understandings to the joint level. The joint as an organ experineces complex interplays among several soft and hard tissues of irregular geometries [2], making it difficult for both computational modeling and experimental determination. The long-term goal of this research is to understand the joint mechanics associated with fluid pressurization in cartilages and menisci during joint compression using both computational and experimental approaches. One interesting behavior of the joint simulated in the present study is the compression-rate-dependent mechanical response observed in lab tests with fresh porcine joints [3].

Fresh porcine stifle joints with intact joint capsules were obtained from a local meat market within 24 hours of slaughter of the animal. Hydration was maintained during all measurements [3]. High-resolution CT images of the joint were obtained at the Micro-CT laboratory and used to reconstruct the geometry of the bones. Cartilage surfaces and thickness were mapped with the Mach-1 system (Biomomentum, Quebec, Canada). Indentation stiffness was also obtained from the test. A finite element model of the porcine joint was constructed using a similar process that was previously used for human knee joints [4], which featured fluid-pressure driven fibril-reinforcement in cartilages and menisci. However, at this moment, the menisci have not yet been included in the porcine model, because only cartilages were mapped during the indentation test.

The numerical results were compared with mechanical testing results of similar porcine joints when the menisci were carefully removed but synovial fluid was conserved in the joint [3]. Preliminary results showed a reasonable match in the reaction force when the joint was compressed by 800 microns using, respectively, three different compression rates (Figure 1). The force-compression relationship of the joint was substantially affected by the compression-rate. The poromechanical joint model was able to capture the rate and time-dependent response of the joint. A strong rate-dependent nonlinear response was also seen: the load response was almost linear at the static compression while it became strongly nonlinear at a fast compression. The implication of site-specific cartilage stiffness will be further investigated using the stiffness obtained from indentation tests.

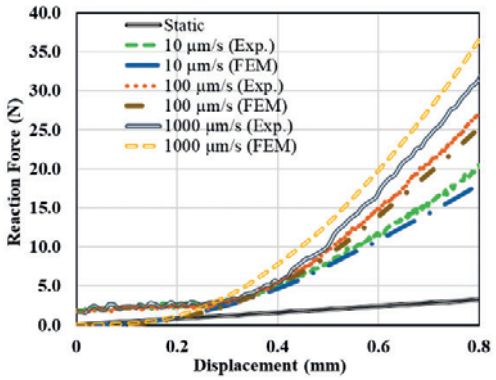

Figure 1: Predicted and measured reaction force in a meniscectomized porcine stifle joint as a function of compression for three compression rates. The static response from finite element static analysis is included as a reference (FEM stands for finite element method, while Exp. stands for experiment).

Acknowledgments: The present research was supported by the Natural Sciences and Engineering Research Council of Canada. The indentation test was performed at Biomomentum (Quebec, Canada) with a Mach-1 tester. The bone images were obtained at the Micro-CT Laboratory (Dr. Steven Boyd's lab at the University of Calgary, Canada).

References

[1] Soltz MA, Ateshian GA, 2000, J Biomechanical Eng 122, 576-586.
[2] Andrews S, Shrive N, Ronsky J, 2011, J Biomech 44, 2737-2740.
[3] Rodriguez ML, Li LP, 2017, BMC Musculoskeletal Disorders 18, 447.
[4] Kazemi M, Li LP, 2014, Med Eng Physics 36, 998-1006.

[B-05.6]

FIBRIL-REINFORCED POROELASTIC AND POROVISCOELASTIC MODELING OF CARTILAGE, MENISCUS AND LIGAMENTS

Petri Tanska[1], *Aapo Ristaniemi*[1], *Elvis Danso*[2], *Mohammadhossein Ebrahimi*[1], *Rami K Korhonen*[1]

1 *University of Eastern Finland, Kuopio, Finland*
2 *Tulane University, New Orleans, USA*

Knee joint cartilage, meniscus and ligaments are mainly composed of highly organized collagen network, proteoglycans and fluid. Fibril-reinforced poroelastic (or biphasic) models have been developed to account for the contribution and effect of these constituents on the mechanical response of tissues. Here we characterize constituent-specific material parameters of cartilage, meniscus and anterior cruciate ligament.

Multi-step stress-relaxation tests were conducted for human cadaver cartilage (osteochondral plugs, n = 5) and meniscus (n = 77) in indentation, and for bovine anterior cruciate ligaments (n = 10) in tension. Finite-element models of the experiments were constructed. Cartilage and meniscus were modeled using the fibril-reinforced poroelastic material model [1,2] while the fibril-reinforced poroviscoelastic model was applied for ligaments. In the ligament model, the collagen matrix was modeled using a nonlinear spring (strain-dependent collagen modulus E_t) parallel with two Maxwell viscoelastic elements (moduli E_1 and E_2 and dashpot viscosities η_1 and η_2). The choice of the poroviscoelastic model for ligaments was based on the observation that poroelasticity alone cannot replicate the experimental relaxation behavior under tension (as fluid has negligible contribution to the mechanical response in tension). The material parameters were obtained by fitting the model to the experimental data with a non-linear optimization routine in MATLAB. For cartilage and meniscus, the optimization was conducted for each sample, while for ligaments, it was conducted for the average data of 10 ligaments.

Human cartilage and meniscus exhibited a strong non-linear stress-relaxation response which is mainly caused by the non-linear behavior of collagen fibrils and deformation-dependent permeability. The nonfibrillar matrix modulus was greater in cartilage (0.35 ± 0.28 MPa) than in meniscus (0.08 ± 0.04 MPa). The initial collagen fibril network modulus was greater in cartilage than in meniscus (0.41 ± 0.37 vs. 0.08 ± 0.10 MPa), while the strain-dependent collagen fibril network modulus was smaller in cartilage (15.42 ± 12.34 vs. 26.0 ± 28.0 MPa). Tissue permeability was also greater in cartilage than in meniscus (1.19 ± 0.33 vs. 0.08 ± 0.10 × 1015 $m^4 N^{-1} s^{-1}$), while the constant describing the deformation-dependency in permeability was smaller in cartilage (3.36 ± 2.07 vs. 12.1 ± 10.0). In ligaments, the non-linear stress-relaxation response was related to viscoelasticity of the collagen fibrils, which is governed by slow and fast damping coefficients. The strain-dependent fibril network modulus was greater in ligaments (429.5 MPa) compared to cartilage and meniscus. The mechanical parameters of the Maxwell elements were E_1 = 188.9 MPa and η_1 = 546.5 MPa·s ("short" relaxation) and E_2 = 251.8 MPa and η_2 = 4698.1 MPa·s ("long" relaxation).

These constituent-specific material properties of cartilage, meniscus and ligament can be useful in tissue engineering approaches. Moreover, the characterization of these properties will help us to develop more accurate computational models of the knee joint.

Acknowledgments: The Academy of Finland.

References:

[1] Ebrahimi M et al. (2019), Ann. Biomed. Eng., doi:10.1007/s10439-019-02213-4.
[2] Danso E et al. (2015), J. Biomech. 48:1499-507.

[B-06.1]

A COMBINED MUSCULOSKELETAL MODEL OF THE TRUNK AND FINITE ELEMENT MODEL OF LUMBOSCRAL PASSIVE SPINE TOWARDS INDIVIDUALIZED MUSCLE FORCES AND STRESS/STRAIN PROFILES

Tao Liu[1], *Marwan El-Rich*[1]

1 *Khalifa University, Abu Dhabi, United Arab Emirates*

The lumbosacral spine plays an important role in supporting the upper body, transmitting loads from the thorax to the pelvis, and contributing to the stability of the body. Accurate determination of loads along the lumbosacral spine is of importance to injury prevention, implant design and the understanding of spinal disorders. In recent decades, computational models emerged as an indispensable and efficient tool that predicts spinal load, stress and strain distribution in the spinal structures which cannot be measured non-invasively in-vivo. The musculoskeletal type of these models allows modeling of the whole body to predict the muscle forces, yet fail to determine stress and strain distribution at the spinal structure level as they use simple rigid body-joint connections. On the other hand, the FE models can be detailed, account for the 3D geometry and detailed tissue properties, hence estimate stress and stress distribution. However, the FE models require longer computational time and their convergence is more difficult particularly for large deformation scenarios. The current study aims to develop a new computational tool that combines a musculoskeletal model of the trunk with a FE model of the ligamentous lumbosacral spine to investigate the spinal loads under in-vivo loading conditions. The proposed model can be individualized using anthropometric and imaging data such as MRI to predict a subject-specific muscle forces and stress/strain profiles.

The musculoskeletal model of the trunk was modified by changing the flexural stiffness of the spherical joints simulating the disc from linear and constant at all spinal levels to nonlinear and level dependent based on literature. The model was then validated by indirectly comparing the compressive force in the joint L4-L5 to the in-vivo intradiscal pressure (IDP) [1]. The muscle forces and joint loads predicted by the musculoskeletal model in standing posture were then applied to a 3D nonlinear FE model of the spine that was created based on the geometry of the spine of the musculoskeletal model. The FE model which includes the vertebrae, intervertebral discs, articular facet joints and surrounding ligaments was also validated using in-vivo and in-vitro data. The FE model predicted the spinal loads such as ligament forces, shear and compression in the discs as well as IDP.

The developed model is a powerful computational tool that can be used to predict subject-specific muscle forces, spinal load-sharing and stress/strain profile under various postures and loading scenarios."

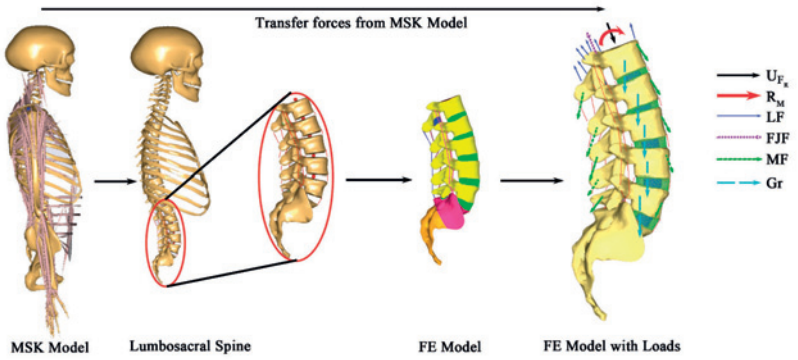

Figure Caption: Flowchart of the steps involved in the creation of the combined musculoskeletal and FE model

References:

[1] Wilke, H. et al.,2001. Intradiscal pressure together with anthropometric data-a data set for the validation of models. Clin. Biomech. Bristol Avon 16 Suppl 1, S111-126.

[B-06.2]

GEOMETRY AND MECHANICS OF DIARTHRODIAL JOINTS WITH EMPHASIS ON THE TALUS JOINT

Samer Adeeb[1], *Mehrdad Palizi*[2], *Yousef Algohary*[2], *Alexandra Trovato*[2], *Kamrul Islam*[3], *Mason Kim*[2], *Nadr Jomha*[4]

1 *University of Alberta, Department of Civil and Environmental Engineering, Edmonton, Canada*
2 *University of Alberta, Edmonton, Canada*
3 *Ecole Polytechnique de Montreal, Montreal, Canada*
4 *University of Alberta, Faculty of Medicine & Dentistry - Surgery Dept, Edmonton, Canada*

Finite Element Anlysis models of diarthrodial joints rely on two pillars for generating accurate predictions of the mechanics: Geometry and material properties. This walk will focus on three aspects of the geometry of diathrodial joints for the prediction of mechanical behaviour. First, we will discuss the methods of generating geometry for diathrodial joints and the expected accuracy associated with the process(1). The implications of specific geometry on the stresses within diarthrodial joints is then reviewed for general diarthrodial joints with labrum like structures(2) and in the patello-femoral joint(3) with the latter showing a need to fully investigate the variation of the geometry among individuals. The third aspect of geometry is the qualification and quantification of the geometric variations among individuals. For this, two techniques are reviewed and presented; one relying on simple geometric manipulations (scaling and registration)(4) and the other relying on statistical shape analysis(5). The application of the first approach to quantify the symmetry of the talus joint(6) and to identify an average talus shape among individuals(7) will be presented along with its clinical application. While the first approach is simple and intuitive, it might fail to identify consistent patterns of deviation. Examples of the comparison between the two approaches in quantifying the variation of the talus joint among individuals will be presented.

References:

1. *Kim, M. et al.(2017). Intra-Operator and Inter-Operator Reliability, and CT scan repeatability in 3D Modeling of Talus Bone Using CT Imaging. Computer Methods in Biomechanics and Biomedical Engineering: Imaging & Visualization, DOI: 10.1080/21681163.2017.1340193.*
2. *Adeeb, S.M. et al.(2004). Congruency Effects on Load Bearing in Diarthrodial Joints. Computer Methods in Biomechanics and Biomedical Engineering, 7(3), 147-158.*
3. *Islam, K. et al.(2015). A Geometric Approach to Study the Contact Mechanisms in the PatelloFemoral Joint of Normal versus PatelloFemoral Pain Syndrome Subjects. Computer Methods in Biomechanics and Biomedical Engineering, 18(4), 391–400.*
4. *Islam, K. et al.(2014), "Three-Dimensional Geometric Analysis of the Talus for designing Talar Prosthetics", Proceedings of the Institution of Mechanical Engineers, Part H: Journal of Engineering in Medicine, 228(4): 371-8.*
5. *van de Giessen M., et al.(2012) An Efficient and Robust Algorithm for Parallel Groupwise Registration of Bone Surfaces. In: Ayache N., Delingette H., Golland P., Mori K. (eds) Medical Image Computing and Computer-Assisted Intervention – MICCAI 2012. Lecture Notes in Computer Science, vol 7512. Springer, Berlin, Heidelberg*
6. *Islam, K. et al.(2014). Symmetry Analysis of Talus Bone: Geometric Morphometric Approach. Bone and Joint Research, 3(5):139-45.*
7. *Trovato, A. et al.(2017). Geometric Analysis of the Talus and Development of a Generic Talar Prosthetic. Foot and Ankle Surgery, 23(2):89-94.*

[B-06.3]

DISPLACEMENT-ENCODED MAGNETIC RESONANCE IMAGING OF TISSUE AND INTERFACE BIOMECHANICAL BEHAVIOR

Deva Chan[1]

1 *Rensselaer Polytechnic Institute, Troy, USA*

Displacement encoding with stimulated echoes (DENSE) is a phase contrast magnetic resonance imaging (MRI) technique that enable the visualization of motion at physiologic frequencies. This talk will discuss prior implementation of DENSE MRI for noninvasive assessment of tissue mechanics and ongoing research to utilize this and other biomechanical imaging techniques to evaluate interface mechanics.

With DENSE MRI [1], the phase of the MRI signal is proportional to the displacement of each pixel. Spatial preparation of magnetization (SPAMM) is performed while a tissue is in the desired reference configuration, while data is acquired – as either single-frame or cine (multi-frame) images – during the current configuration(s). During the SPAMM preparation, the phase of protons in the tissue are sensitized to their material locations using a gradient magnetic field. Then, protons are sensitized to their spatial location before acquisition, so that the acquired phase information of each pixel is proportional to the displacement. Although DENSE MRI [1] was initially developed for the heart, which produces its own deformation, the technique can be implemented in soft tissues so long as external application of cyclic loading is possible. This has led to applications of DENSE MRI in osteoarthritic articular cartilage [2], intact ex vivo joints [3-5] and intervertebral discs [6], as well as in vivo studies of knee cartilage in healthy human volunteers [3]. Because cyclic loading must be synchronized to multiple image acquisitions, biomechanical engineers can either cyclically load tissues until they have reached a quasi-steady state load-deformation response [7] or permit enough time between loading events to neglect the role of loading history on the measured tissue mechanics[8].

Since volumetric imaging modalities such as MRI are ideally suited to visualize internal structures and behaviors of tissues, DENSE MRI can be utilized to examine interface mechanics without destruction of the tissue nor disruption of boundary conditions. Additionally, DENSE MRI can be paired with other MRI techniques, including quantitative MRI of biomolecular correlates, such as glycosaminoglycan content or collagen fiber alignment, to inform the development and validation of computational biomechanics models.

References:

1. *Aletras, et al., J Magn Reson, 1999.*
2. *Griebel, et al., Magn Reson Med, 2013.*
3. *Chan, et al., Sci Rep, 2016. 6: p. 19220.*
4. *Chan, Neu, and Hull, Osteoarthritis Cartilage, 2009.*
5. *Chan, et al., J Biomech, 2017.*
6. *Chan, et al., Spine (Phila Pa 1976), 2011.*
7. *Neu and Hull, J Biomech Eng, 2003.*
8. *Knutsen, et al., J Biomech, 2014.*

[B-06.4]

MULTISCALE FINITE ELEMENT INVESTIGATION OF THE RABBIT MEDIAL COLLATERAL LIGAMENT FEMORAL ENTHESIS MICROSCOPIC LOAD RESPONSE

John Sevick[1], *Ziad Abusara*[2], *Mehdi Shekarforoush*[1], *Stephen Andrews*[1], *David Hart*[1], *Nigel Shrive*[3]

1McCaig Institute for Bone and Joint Health, University of Calgary, Calgary, Canada
2Human Performance Laboratory, University of Calgary, Calgary, Canada
3Schulich School of Engineering, University of Calgary, Calgary, Canada

The point of attachment of a ligament or tendon to bone (the enthesis) is a thin region adapted to perform load transfer between these tissues. The region is of interest given the body's inability to repair or form an adequate attachment after injury, such as at the rotator cuff and anterior cruciate ligament [1,2]. Thus, understanding of enthesis load transfer mechanisms is of importance to developing repair strategies. Attempts to assess enthesis mechanics have been hindered by difficulties of visualization. Moreover, an investigation of fibril pull-out has not been performed. The main objective of this study therefore was to use a multi-scale finite element (FE) analysis of the rabbit medial collateral ligament femoral enthesis (partly validated by a separate, novel visualization study) to assess the effects of material gradations, as suggested in the literature [3,4], on fibril shear and bending stresses, thereby providing insight to fibril pull-out. A 2D, linear elastic, transversely isotropic "macroscale" FE model with approximately the same gross geometry as one experimental specimen was developed in ABAQUS. The deformation of a small (500x500 µm) rectangle at the ligament/bone boundary was compared to microscopic images with the same field of view and location (approximately) captured during experimentation, as a means of partial validation. The stress inputs from a small portion comprising the ligament/bone boundary were then applied to a 2D, linearly elastic, isotropic "microscale" model, consisting of 40 individual fibrils assumed to be embedded in matrix with perfect bond. Four different modulus gradations (linear, bi-linear, power, exponential) were implemented between ligament and bone. Results indicated that the more (initially) gradual gradations permitted greater fibril deformation and lower bending stress (more gradual bending). However, no obvious difference in shear stress distribution could be discerned. This work constitutes a first attempt at validating a FE model of the enthesis through the use of imaging techniques, and provides some evidence for the benefit of the material gradation between ligament and bone. However, further work is required to elucidate pull-out mechanics more fully, and to capture the true complexity of load transfer across the enthesis (e.g. 3D, imperfect fibril-matrix bond).

References:

[1] Thomopoulos S. Tendon to Bone Healing: Differences in Biomechanical, Structural, and Compositional Properties Due to a Range of Activity Levels. J Biomech Eng 2003, 125:106.
[2] Lazarides et al. Histological Evaluation of Tendon-Bone Healing of an Anterior Cruciate Ligament Hamstring Graft in a 14-Year-Old Boy. Am J Sports Med 2015, 43:1935–40.
[3] Genin et al. Micromechanics and structural response of functionally graded, particulate-matrix, fiber-reinforced composites. Int J Solids Struct 2009, 46:2136–2150.
[4] Deymier et al. Micro-mechanical Properties of the Tendon-to-Bone Attachment. Acta Biomater 2017.

[B-06.5]

3D SUBJECT-SPECIFIC FINITE ELEMENT FOOT MODELING WITH AUTOMATIC LIGAMENTS POSITIONING AND BONE REGISTRATION ON GLOBAL SKELETON

Nicolas Kroupa[1], *Baptiste Pierrat*[2], *Jérôme Molimard*[3], *Woo Suck Han*[3]

1 *University of Lyon - Mines Saint-Etienne, Saint-Etienne, France; Inserm U1059; Center for Biomedical and Healthcare Engineering, Mines Saint-Étienne, Saint-Etienne, France*
2 *University of Lyon - Mines Saint-Etienne, Saint-Etienne, France; Inserm U1059; Center for Biomedical and Healthcare Engineering, Mines Saint-Étienne, Saint-Etienne, France*
3 *Ecole Nationale Supérieure des Mines de Saint-Etienne, Cis-Emse, F-42023 Saint Etienne, France; Inserm U1059, Sainbiose, F-42023 Saint Etienne, France; Université de Lyon, France, F-69000 Lyon, France*

Biomedical modeling of the foot in association with motion capture, is a promising technique to study the foot in various loading situations. In the literature both aspects are treated with diversity; modeling is mostly done with finite element (FE) models. Foot motion capture is done through multiple techniques which can give an internal or external point of view.

The aim of this study is to model soft-tissue deformations within the foot in various loading conditions by constraining a 3D FE model, with bone motion acquired from CT scans. Also a dedicated protocol for patient specific studies based on a mesh morphing technique allowing automatic ligaments positioning was developed.

A generic, source geometry of the bones with their ligament attachment sites was manually segmented from the Visible Human Project data.

CT scans from cadaveric feet were acquired in an unloaded reference configuration, and various loaded configurations. For each subject, a specific target mesh is first constructed using classic semi-automatic segmentation and 3D reconstruction from the unloaded CT scan. As this mesh is missing the specifications required for FE simulations, a mesh-morphing technique was used to deform the high-quality source model to match each corresponding target bone, also allowing positioning of the source ligaments attachment sites on the target bones.

The subject specific displacement-controlled FE model is built with the integration of the target bone geometries, the ligaments by joining attachment sites with cable elements, the surrounding soft tissues (muscle, fat and skin) considered as one homogeneous material.

During the acquired loaded configurations, each bone position was updated from the reference configuration using SLSQP minimization.

Figure Caption:
(a). Ligament positioned by mesh-morphing *(b). Bone position in feet skeleton* *(c). Soft Tissue deformations*

The FE simulation was then used to study the soft tissue deformation and ground interactions using bone displacements as boundary conditions. The soft tissues constitutive parameters are identified by minimization of the ground reaction force. The mesh-morphing method provides ligament attachment points which follow the source geometry assumptions and do not require target image ligament segmentation or user positioning.

The soft tissue stiffness was identified with a coefficient of determination (R^2) of 0,986 between simulated and measured reaction forces. Simulated pressure maps had a RMSE of 0.152 MPa when compared to measurements.

The simplification of the foot model allowed us to accelerate its generation time with a good agreement between simulated and measured ground reaction forces. Future work will take advantage of the proposed method to study larger samples of feet constrained by different environments (device, shoe, insole and sole).

Acknowledgments: We thank Mr Florian Bergandi and Dr. Sylvain Grange, University Hospital of Saint-Etienne, for their help in the experiments.

[B-06.6]

VALIDATION OF PORCINE KNEE FINITE ELEMENT MODELS WITH VARIED FLEXION ANGLES AND TIBIAL FREEDOMS

Robert Cooper[1], *Gavin Day*[1], *Ruth Wilcox*[1], *Alison Jones*[1]

1 *Institute of Medical and Biological Engineering, University of Leeds, Leeds, UK*

Efforts are increasing to develop early-stage interventions to prevent knee degeneration due to osteoarthritis. This requires an understanding of the mechanical environment of the knee. Computational finite element (FE) models can play an important role in non-invasively understanding knee mechanics, allowing rapid investigation of different loading scenarios for multiple subjects, but such specimen-specific models require individual validation [1]. The aim of this study was to develop a robust specimen-specific knee model development methodology and compare predictions to corresponding specimens tested in the laboratory under different loading scenarios.

Bones of two porcine knees were segmented from CT scans using Simpleware ScanIP. Cartilage layers of uniform thickness were generated by dilating out bone masks, and meniscus geometry was generated by adjusting masks of the segmented tissue to ensure conformity of contact surfaces. Tissue masks were meshed with quadratic tetrahedral elements and modelled as linearly elastic materials. The menisci were assigned a higher modulus in the circumferential direction and meniscal attachments were simulated using linear springs [2]. FE models were developed in Abaqus 2017, with frictional contact defined between surfaces and enforced using the penalty method. For each specimen, there were six loading scenarios: 0o, 10o and 20o femoral flexion, each with the tibia fixed and freed. Experimental data for model validation was obtained using contact pressure sensors with the knees axially loaded in a material testing machine.

During the model development process it was found to be crucial to export cartilage and meniscus geometry from ScanIP as a single meshed part in order to ensure sufficient conformity required for the models to run and converge robustly in Abaqus. Contact pressures predicted by the models were of similar magnitude to experimental values. When the tibia was fixed in vitro, the contact region shifted to the medial plateau with increasing flexion. This did not occur when the tibia was free to translate and rotate in response to loading. These trends in the balance of the forces transferred through the medial and lateral plateaus were replicated in the FE models (Figure 1).

It is challenging to ensure stability of models featuring multiple soft tissue contacts. Furthermore, model calibration to match experimental results does not imply the model is validated under alternative conditions. This study demonstrated the ability of specimen-specific models to replicate trends in load sharing between the two tibial plateaus of the knee, providing confidence in the capture of bone shape and alignment. The model development process will next be applied to human knees and used to evaluate osteochondral interventions.

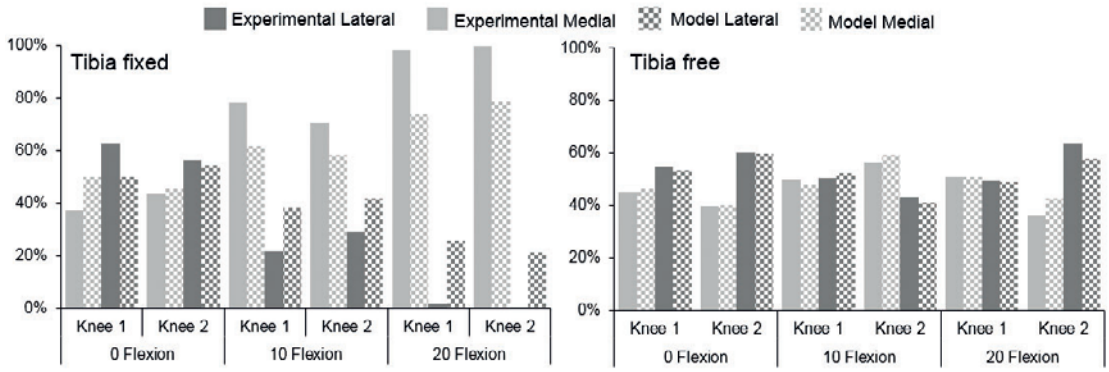

Figure Caption: Percentage of the total force transferred through the medial and lateral tibial plateaus.

Acknowledgments: EPSRC [EP/P001076/1]

References:

1. *Mootanah et al, CMBBE, 17(13):1502-1517, 2014*
2. *Meng et al, RoyalSocOpenSci 4(8):170670, 2017*

[B-06.7]

SIMULATIVE METHOD FOR EVALUATING PASSIVITY FOR CELL'S MIGRATION IN ECM FIBER NETWORK

*Yongrou Zhang[1], Zetao Huang[2], **Liqun Tang**[3], Shoubin Dong[2], Zejia Liu[2]*

1 *Guangdong Institute of Intelligent Manufacturing, Guangzhou, China*
2 *South China University of China, Guangzhou, China*
3 *Department of Engineering Mechanics, South China University of Technology, Guangzhou, China*

The microstructure of the ECM plays a key role in affecting cell behaviors, including growth, propagation, and migration, but some micro properties including the mechanical properties of fibers and microstructure are difficult to be measured experimentally. Further, during the non-proteolytic migration, the cell changes its shape and expands the network pore, and it is hard to learn how much energy is demanded for the cell, i.e. how to evaluate the passivity of the ECM network for cell's migration is uncertain. Based on a network model of collagen fiber in ECM, which has been used to simulate the mechanical behavior such as stress-strain relation well [1], we proposed methods to study the microstructure properties, containing pore size and pore stiffness, and to search the possible migration paths for cells. Especially, in the search of the migration paths, two important techniques were developed: an algorithm for searching the migration path (Fig. a); an approach for calculating the stiffness of a pore in the network (Fig. b). Taking the total pore expansion energy in passing the migration path as a criterion, we evaluate the difficulty of cell migration in the ECM network. This work provides a quantitative method to evaluate the passivity of ECM network for cell's migration.

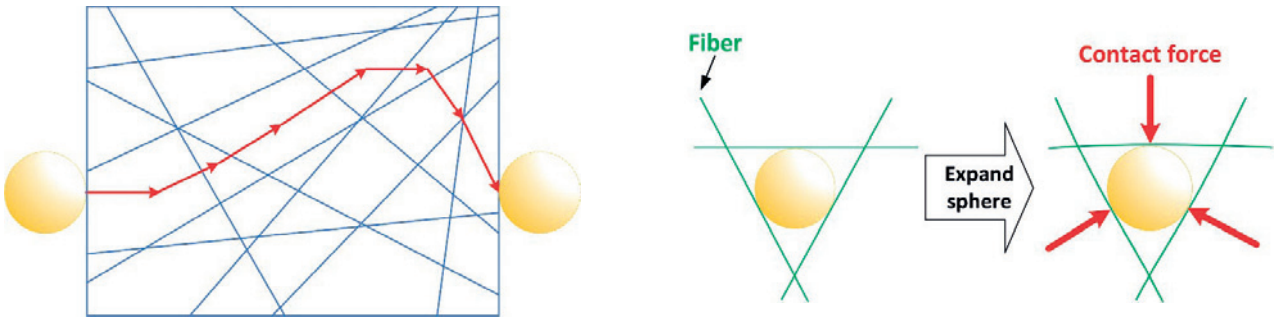

(a) *(b)*

Figure Caption: Schematic diagram of simulative method for evaluating passivity for cell's migration in ECM fiber network: (a) from the starting point to the destination, the cell migration in a path with large pore size; (b) the pore stiffness is measured with an expanding sphere.

Acknowledgments: This work was financially supported by the National Natural Science Foundation of China (NSFC no. 11802062, 11772134, 11772132, 11772131).

References:

[1] *Dong, S., Huang, Z., Tang, L., Zhang, X., Zhang, Y., Yi, J., 2017. A three-dimensional collagen-fiber network model of the extracellular matrix for the simulation of the mechanical behaviors and micro structures. Computer Methods in Biomechanics & Biomedical Engineering, 20, 991-1003.*

[B-07.1]

MICROSTRUCTURAL ANALYSIS OF NUTRITION CANALS IN THE HUMAN LUMBAR VERTEBRAL ENDPLATE

*Cheng-LI Lin[1], Jing-Yao Wang[1], Yu-Hua Fang[1], Howard S. An [2], Nozomu Inoue[2], **Alejandro Espinoza**[2]*

1 National Cheng Kung University, Tainan, Taiwan
2 Rush University Medical Center, Chicago, USA

Introduction: The vertebral endplate balances conflicting requirements of being strong to maintain vertebral integrity and porous to facilitate nutrition transport from vertebral capillaries to disc cells. Accurate knowledge of the endplate morphology will help to explain spinal degeneration pathogenesis as well as diagnosing or treating degenerative disc disease. The purpose of this study is to develop a quantitative microstructural analysis technique to describe the three-dimensional (3D) canal networks of nutrition canals in human vertebral endplates, and report the preliminary results.

Methods: Lumbar spines from cadavers were obtained from a tissue bank. Five endplate samples, a disco-vertebral core with 4 mm in diameter, were obtained from the central portion of the superior surface of two L4 and three L5 endplates. Specimens were imaged using micro-Computed Tomography (µCT 50, Scanco Medical, Switzerland) at 2 µm resolution. Segmentation and reconstruction of the canals were performed using in-house custom-developed software. 3D model representing the vascular canals was obtained (Figure 1). The nutrition canal segments were identified and their orientation as reported in previous work with the rabbit model [2]. Mean diameter, length and volume were determined using a custom Matlab program.

Results: More transverse canals (62%, mean angle 6.3±8.0 degrees) were identified than longitudinal canals (38%, mean angle 37.1±19.3 degrees). The mean diameters (µm) of transverse and longitudinal canals were 115.8±68.4 and 145.8±88.3, respectively. The mean lengths (µm) of transverse and longitudinal canals were 379.5±525.1 and 327.1±313.6, respectively. The average volume of all the canals was 47,842.1 µm3.

Discussion: A technique to determine the quantitative microstructure of the 3D vascular canal networks in human vertebral endplates was described. Using a high-resolution micro CT scanner, it was feasible to segment small vascular canals, demonstrating the complex 3D canal structures. In previous study, Crock et al. have demonstrated that the capillary system drain either directly into the network of veins of the subadjacent marrow spaces or into the subchondral postcapillary venous network [1]. In the present study, we further analyzed the microstructures of nutrition canals in human vertebral endplates, which appears to be a conduit for the epiphyseal subarticular collecting vein. Such structures may play a role for collecting and redistributing the nutrient within the vertebral endplate. Information of the 3D canal structure could provide essential information to understand nutrient pathways through the vertebral endplate and the pathogenesis of disc degeneration.

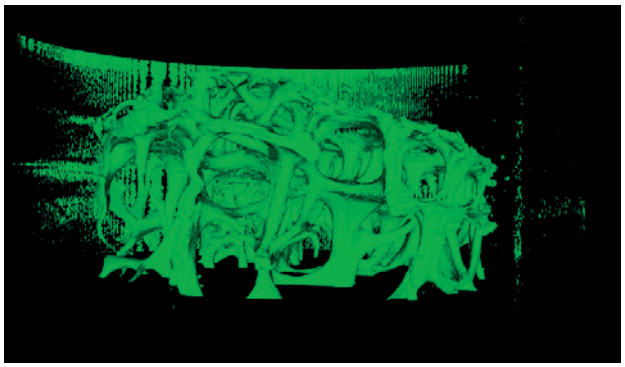

Figure Caption: Fig. 1 Representative 3D microCT model of the the nutrition canals within the endplate.

Acknowledgments: This study was funded by the Rush Scientific Leadership Council

References:

[1] Crock H.V., et al., Anatomic studies of the circulation in the region of the vertebral end-plate in adult Greyhound dogs. Spine 1984;9:702–706.
[2] Yamaguchi T, et al. Microstructural analysis of three-dimensional canal network in the rabbit lumbar vertebral endplate. J Orthop Res. 2015 Feb;33(2):270-6.

[B-07.2]

MECHANICAL EFFECTS OF ENZYMATIC DIGESTION OF THE TISSUES COMPOSING THE INTERVERTEBRAL DISC

*Liam Fleming Nicol[1], Ruth Coe[1], James Warren[1], Ruth Wilcox[1], **Marlène Mengoni**[2]*

1Insitute of Medical and Biological Engineering, University of Leeds, Leeds, UK
2Institute of Medical and Biological Engineering, University of Leeds, Leeds, UK

Globally, back pain causes more disability than any other condition, with intervertebral disc (IVD) degeneration being the major causal diagnosis (Urban and Roberts, 2003). New treatments to repair or augment the IVD have been proposed, but there are challenges in examining their efficacy in vitro due to high inter-specimen variability. An enzymatic method is sometimes employed to artificially degenerate healthy IVD tissue in a controlled manner, but there are still large variations in outcome. Rationalizing the range of required preclinical tests could be attained by using a systematic in silico approach, however this requires an accurate representation of the mechanical changes due to enzymatic digestion. The aim of this work was to develop and calibrate an in silico model of enzymatically digested IVDs when the functional spine unit is subject to compression testing.

Bovine caudal tissue (N=8) was prepared in bone-IVD-bone specimens (Sikora et al. 2018) to undergo a longitudinal testing protocol comprising microCT imaging; mechanical testing (pre-loading 24h and cyclic loading in a PBS bath) defining an "healthy behavior"; enzymatic degradation with papain over 24h at 42°C; microCT imaging and final mechanical testing defining a "degenerated behavior". Image-based finite element models were developed from each set of microCT images. Models of the "healthy behavior" were generated using a previously developed and validated process (Sikora et al 2018). Models of the "degenerated behavior" were generated using by adjusting material parameters for the nucleus of the IVD in such a way that the relative increase in final mechanical stiffness between the healthy and degenerated behavior was similar (i.e. within 10% of each other) in both the experimental and the computational models.

The bone-disc-bone experimental stiffness significantly increased due to enzymatic digestion (by 10% to 30%), with a decrease in height due to digestion of 0.6 to 2.2 mm. In the FE models, these changes were achieved by increasing the material parameters describing a Mooney-Rivlin model of the nucleus by an amount (ranging 7%-18%) proportional to the reduction in disc height.

These results suggest that the degeneration by enzymatic digestion stiffens the tissue composing the disc, both by reducing the disc height and increasing the aggregate elasticity of the tissue. The bigger the change in disc height, the bigger the change in tissue elasticity. In in vitro models which need the systematic creation of different level of degeneration, attention should therefore be paid to selecting homogeneity in disc height across samples in order to achieve a homogeneous level of degeneration.

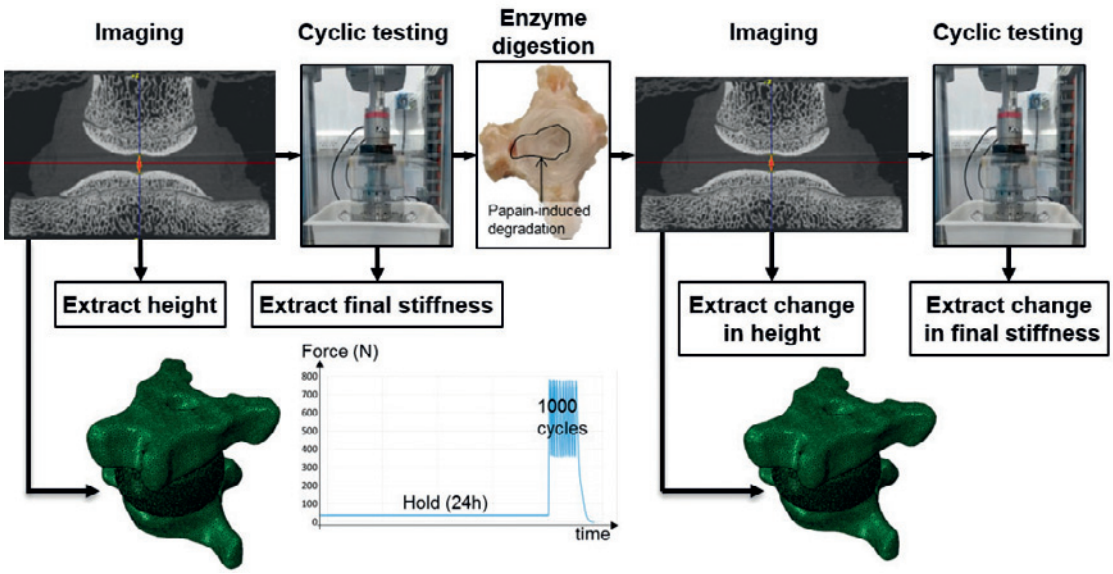

Figure Caption: Longitudinal process (micro-CT imaging and experimental testing) and FE models

Acknowledgments: Funding by EPSRC grant EP/K020757/1; support by University of Leeds' Engineering Summer Internship Scheme

References:

Urban and Roberts, 2003, Arthritis Research & Therapy; Sikora et al, 2018, IMech-E/H

[B-07.3]

NUMERICAL MODELING OF INTERVERTEBRAL DISC FAILURE DURING HYPERFLEXION AND HYPERFLEXION-COMPRESSION INJURIES

Marie-Helene Beausejour[1], *Yvan Petit*[1], *Pierre-Jean Arnoux*[2], *Eric Wagnac*[3]

1 *École de Technologie Supérieure, Ilab Spine, Montreal, Canada*
2 *Iffstar; Ilab Spine; Laboratoire de Biomecanique Appliquee, Aix-Marseille Universite – Ifsttar, Marseille, France*
3 *École de Technologie Supérieure, V2r Biomédical, Montreal, Canada*

Flexion-distraction injuries represents 35% of injuries at the cervical spine and are associated with neurological deficits in 61% of the cases (Blauth et al. 2007). However, the mechanism of injury and the lesion dynamic propagation are still misunderstood. Finite elements studies have been interested in the mechanism of flexion-extension or compression injuries. However, they generally do not model the intervertebral disc (IVD) rupture, while the IVD is an important structure for spinal stability. The aim of this study was to characterize the mechanism of injury in hyperflexion and hyperflexion-compression using a finite elements model of C4-C5 incorporating an IVD failure model. Failure models based on maximal deformation were applied to the ligaments and the IVD. Loading in flexion (500 deg.s-1) and a combination of flexion (500 deg.s-1) and axial compression (0.2 m.s-1) were applied at C4 while C5 was fixed. Loads at failure were computed and dynamic injuries patterns were reported. In flexion, simulated failure moment had a difference of 4% compared to in vitro results (Nightingale et al. 2007). Peak load corresponded with the interspinous ligament and ligamentum flavum rupture. Posterior elements disruption in the annulus followed. All soft-tissues structures were disrupted except the capsular and anterior longitudinal ligaments. In hyperflexion-compression, moment at rupture was 19% higher and axial force at rupture was 17% lower compared to experimental data (Carter et al. 2002). Both values were inside one standard deviation of experimental results. Peak load corresponded to IVD disruption. The posterior longitudinal ligament was damaged, but not ruptured. The capsular ligaments and the anterior longitudinal ligament were intact. Simulations without IVD failure model resulted in higher moment at segment failure: 2% higher for hyperflexion and 22% higher for flexion-compression. Without failure model, the ligaments were disrupted in the same sequence in flexion as with the failure model. However, in flexion-compression, high deformation of IVD elements forced the simulation interruption. Failure model implementation for the IVD is important to achieve a realistic representation of injury mechanisms. Absence of failure models can lead to excessive elements deformations and numerical aberrations.

Acknowledgments: This research was funded by the Canada research chair in biomechanics of head and spine injuries

References:

Blauth, M., Mair, G., Schmid, R., Reinhold, M. and Rieger, M. 2007. Classification of injuries of the subaxial cervical spine. AO Spine Manual: Clinical Applications. 2: 21-38.
Carter, J. W., Ku, G. S., Nuckley, D. J. and Ching, R. P. 2002. Tolerance of the cervical spine to eccentric axial compression. SAE CONFERENCE PROCEEDINGS P, SAE; 1999.
Nightingale, R. W., Chancey, V. C., Ottaviano, D., Luck, J. F., Tran, L., Prange, M. and Myers, B. S. 2007. Flexion and extension structural properties and strengths for male cervical spine segments. Journal of biomechanics. 40(3):535-542.

[B-07.4]

PRECISE MEAN AXIS OF ROTATION (MAR) ANALYSIS FOR CLINICAL AND RESEARCH APPLICATIONS

Mayar Abbasi[1], *Aslam Khan*[2], *Karim Bayanzay*[3]

1 *McGill University, Center for Intelligent Machines, Center for Intelligent Machines, Montreal, Canada;*
2 *Kkt Orthopedic Spine Center*
3 *Jersey Shore University, Neptune City, USA*

It is estimated that approximately 80% of the global population will experience some form of back pain in their lifetime. However, back pain is difficult to diagnose with traditional X-rays, CT and MRIs, as they do not correlate well with clinical symptoms. In other words, patients with severe, debilitating symptoms will often have normal imaging and patients with considerably abnormal image findings may be completely asymptomatic. Therefore, currently, clinicians and researchers have no objective way of measuring the degree of back pain a patient may be experiencing.

Mean Axis of Rotation (MAR) analysis was first proposed by Penning (Penning, 1964) to analyze the cervical spine movement from full extension to full flexion. It was subsequently utilized by many studies thereafter. However, in 1991, Amevo et al evaluated the reliability of the MAR Analysis technique used by Penning and others, and determined it is not precise enough to be used in research due to large interobserver and intraobserver differences, with relative variances up to 35%. (Amevo, 1991)

Amevo et al proposed an optimized MAR analysis technique, achieving a relative variance of 3%-11% (Amevo, 1991), which was precise enough to be utilized in back and neck pain research. Subsequent studies were performed to accurately determine normal MAR (Amevo & Worth, 1991), and abnormal MAR (Amevo & Aprill, 1992). These studies demonstrated that abnormal MAR correlates with neck or back pain, while normal MAR correlates with absence of pain. Desmoulin et al utilized this technique to measure the efficacy of KKT Orthopedic Spine Treatment (Desmoulin, Szostek, & Khan, 2011). MAR Analysis can require up to 2-3 hours and therefore despite its scientific reliability and promise, it is not practical to use in the research or clinical setting.

To overcome this obstacle, Abbasi et al designed a software, incorporating computer vision to semi-automate Amevo's optimized MAR technique (Abbasi, Desmoulin, & Khan, 2013). The accuracy of the MAR Analysis software was evaluated (Abbasi, 2015) which yielded a relative variance of 6%-26%. A further review of the design and processes of Abbasi's MAR Analysis software revealed that it did not exactly replicate every decision point in Amevo's manual technique, and therefore failed to achieve a similar degree of precision.

The MAR Analysis software has been redesigned, with added intelligence and decision-making capabilities, revised algorithms, and more advanced software engineering architectures. Initial evaluation of this present MAR software demonstrates a reliability on par with Amevo's optimized technique. Furthermore, a single MAR analysis requires under 20 minutes to complete, making this MAR software suitable for general clinical adoption.

References:

Abbasi et al (2013). SEMI AUTOMATION OF MEAN AXIS OF ROTATION (MAR) ANALYSIS USING COMPUTER VISION. Proceedings of the 11th Int Symposium, CMBBE, (p. 515). Salt Lake City, Utah.
Abbasi et al (2015). Reliability of a Semi-Automated Mean Axis of Rotation (MAR) Analysis Tool. CMBBE International Symposium (p. 54). Montreal: https://mccaig.ucalgary.ca/cmbbe.
Amevo et al (1991). Instantaneous axes of rotation of the typical cervical motion segments: Optimization of Technical Errors. Clinic Biomech.
Amevo et al (1992). Abnormal instantaneous axes of rotation in patients with neck pain. Spine.
Amevo et al (1991). Instantaneous axes of rotation of the typical cervical motion segments: a study of Normal volunteers. Clinic Biomech.
Amevo et al (1991). Instantaneous axes of rotation of the typical cervical motion segments: an empirical study of errors. Clinic Biomech, 31-37.
Desmoulin et al (2011). Spinal Intervention Efficacy on Correcting Cervical Vertebral Axes of Rotation and the Resulting Improvements in Pain, Disability and Psychsocial Measures,. J. Musculoskeletal Pain.
Penning. (1964). NONPATHOLOGIC AND PATHOLOGIC RELATIONSHIPS BETWEEN THE LOWER CERVICAL VERTEBRAE. AJ Roentgenology, 91

[B-07.5]

INVESTIGATION OF FRACTURE PATTERNS AFTER PURE COMPRESSION IN THE SPINAL THORACIC REGIONS. AN EXPERIMENTAL AND ANALYTICAL BIO-MECHANICAL STUDY

Sacha Guitteny[1], Amir Beltagi[1], Giovanni Solitro[2], Farid Amirouche[1]

1 *University of Illinois College of Medicine, Chicago, USA*
2 *Louisiana State University Health Sciences Center, New Orleans, USA*

Background: It has been shown in previous studies that the spine, especially the thoracolumbar region, is vulnerable to high energy impact and trauma.[Waterloo et al.] A high frequency of abnormalities affecting the thoracolumbar spine has been found among athletes in sports with high back impact, lifting and any sport that demands great exertion force on the back. Compression wedge fracture is one example where these abnormalities are still being investigated.

Purpose: The aim of the study was to describe the resulting fracture patterns after compression loading in the spinal thoracic regions, analyze the mechanical response in terms of strength of stiffness, and develop their corresponding FEA models for validation.

Methods: Sixteen vertebrae obtained from four adolescent pigs and twenty thoracic cadaver vertebrae from humans were used. They were all exposed to compression loading using an apparatus designed for the MTS machine. A displacement of 3mm/min was chosen for loading to failure with a maximum displacement of 1/3 of the vertebrae height. Each vertebra 3D model was obtained using CT images and an FE analysis was performed for validation and for analyzing the stress strain component and assess the fracture pattern and its relation to loading.

Results: Fractures/separations were seen in the anterior and lateral zones. Two main fractures patterns were observed: the first ones are vertical lines in the lateral sides and the other is a horizontal line in the anterior wall causing the failure of the superior or inferior endplates. Only large fractures could be seen on plain videography. With FEA macroscopically, fracture/separation could be seen in all cases and seems to follow similar patterns observed experimentally. The stiffness values obtained numerically are within 8-42 percent of the experimental values (with a correlation of 0.71, $p<0.01$). The median ultimate compression peak load in the compression was 9.7 kN (range, 9.6-10 kN) for the porcine and 3.1 kN (range 2.5-3.9) for the human cadaver.

Conclusions: The weakest part of the porcine thoracic spine, when compressed, was the anterior and lateral zones. Only the anterior zone was deteriorated for the human spine. The FE model established in this study predicts with a high level of accuracy the mechanical behavior under a pure compression loading. The model can be adapted to a wide range of clinical applications, including osteoporosis, fusion and spine implant designs.

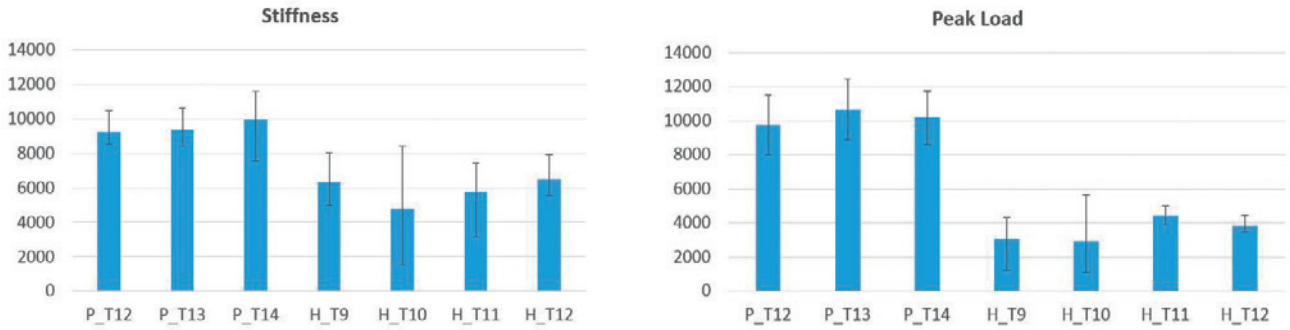

Figure Caption: Figure 1: Stiffness (a) and Peak Load (b) experimental values by vertebral level

References:

1. *[Waterloo et al - 2012] Waterloo, S., Ahmed, L. A., Center, J. R., Eisman, J. A., Morseth, B., Nguyen, N. D., ... & Emaus, N. Prevalence of vertebral fractures in women and men in the population-based Tromsø Study. BMC musculoskeletal disorders, 13(1), 3. 2012*

[B-07.6] S

UBJECT-SPECIFIC VERTEBRAL FRACTURE RISK ASSESSMENT: WHAT'S MISSING?

Simon Cataño Jimenez[1], *Sebastian Saldarriaga*[1], ***Hugo Giambini***[1]

1 *University of Texas at San Antonio, San Antonio, USA*

Low bone mineral density and changes in bone material properties as a result of osteoporosis or cancer metastasis to the spine lead to reduced skeletal strength and an increase in fracture risk. Despite fracture risk increasing with age, and affecting both men and women, there is no clear prevention for vertebral fractures. Quantitative computed tomography-based finite element analysis (QCT/FEA) is a popular tool used for fracture prediction. Material assignment to the finite element is dependent on the gray scale values of the CT image and based on empirical equations obtained experimentally which relate grey values to Young's modulus. However, previous experimental observations did not include the whole vertebral body, endplates, cortical bone, and other important characteristics of the modeling process. The purpose of this study were twofold: 1) to develop an optimum density-elastic modulus equation, incorporating the whole vertebral body and accounting for all variables used during FE modeling; 2) to evaluate the effect of tumor size and location on the fracture properties of vertebrae. We developed a semi-automated QCT/FEA modeling process to evaluate fracture properties. We obtained 54 cadaveric vertebrae and CT-scanned them using a clinical protocol and a calibration phantom. The vertebrae were experimentally compressed to obtain stiffness and failure loads. 3D-FE models were developed and stiffness outcomes were determined. A power-law material model equation was used to relate density-elastic modulus with two unknown coefficients ($E = \alpha \times \rho_{ash}^{b}$). An objective function was defined between experimentally-measured stiffness (Ki) and QCT/FEA-estimated stiffness ($\hat{K}_i$) values as

$$J = \sqrt{\sum_{i=1}^{n} \left(K_i - \hat{K}_i \right)^2}$$

Using the optimized material and a pre-defined failure criterion equations, the effect of tumor size and location was investigated. Spherical lesions of 16 and 20mm in diameter were created on the center (Fig. 1), anterior region, and on a pedicle. A lesion was assigned a modulus of 0.05 MPa. The optimization processes yielded the equation $E = 970 \times \rho_{ash}^{0.84}$. Linear regression analysis between experimental outcomes and QCT/FEA optimized stiffness and fracture loads were R^2=0.5 and R^2=0.4, respectively. Lesion location affected the strength of the vertebra to a wider extent than size. As imaging techniques continue to improve, we will be able to obtain advanced three-dimensional information and properties of bone. However, can we evaluate the in-vivo contribution of muscle to fracture risk? Improvement of imaging modalities and approaches will allow for evaluation of not only bone properties, but muscle health and overall spinal alignment. As they continue to improve, robust clinical subject-specific fracture risk methodologies will include muscles, ligaments, discs, and other anatomy that are currently hindered either by imaging techniques, computer power, or the complexity of the model validation.

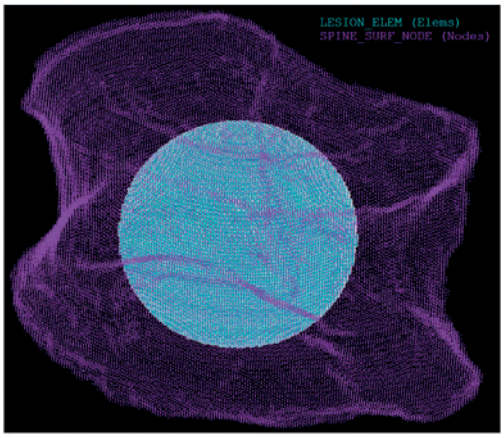

Fig. 1. Metastatic vertebral lesion representation

Acknowledgments: We would like to acknowledge the University of Texas at San Antonio, San Antonio, United States (UTSA) for the support.

[B-08.1]

POSTOPERATIVE EFFECT OF LUMBAR FUSION ON ADJACENT SEGMENT BIOMECHANICS- A PERSONALIZED PARAMETRIC FINITE ELEMENT STUDY

Kinda Khalaf[1], *Mohammad Nikkhhoo*[2], *Chih- Hsiu Cheng*[3], *Chi-Chien Niu*[4], *Zahra Khoz*[5]

1 *Khalifa University, Abu Dhabi, United Arab Emirates of Science and Technology; Health Engineering and Innovation Center*
2 *Department of Biomedical Engineering, Science and Research Branch, Azad University, Tehran, Iran*
3 *Department of Orthopaedic Surgery, Chang Gung Memorial Hospital, Linkou, Taiwan*
4 *Bone and Joint Research Center, Chang Gung Memorial Hospital, Linkou, Taiwan*
5 *Department of Biomedical Engineering, Science and Research Branch, Azad Universit, Tehran, Iran*

In alignment with the continued technical advancement in spinal instrumentation and surgical techniques, spinal fusion is increasingly employed in the treatment of various lumbar diseases [1]. Post-operative images of patients, however, indicate that lumbar fusion can often alter the alignment, lordosis angle and adjacent intervertebral disc heights [2], adversely affecting spinal biomechanics, and potentially clinical outcomes. Finite element (FE) modeling provides a time-and cost-effective tool for quantitatively assessing the detailed spinal biomechanics that are typically unattainable in vivo. This study aimed to investigate the biomechanics of the lumbar spine following one-level-fusion, short and long term post-surgery, using a parametric subject-specific FE model.

Ten subject-specific osteoligamentous FE models were developed using pre-surgery, 3 months, and 12 months post-surgery images from 10 patients (30 models in total), obtained form the Chang-Gung Memorial Hospital in Taiwan. A signed informed consent had been acquired a priori. The geometries (L1-S1) were automatically updated by inputting 125 independent parameters from lateral and AP X-Ray images by a user-defined code. The validity of the pre-surgery FE models was evaluated using pure moments of 1 to10 Nm in different directions, subsequent to compressive preloading with a follower load. Biomechanical responses, including intersegmental ranges of motion (ROM), intradiscal pressure (IDP), facet joint forces (FJF), and annulus fibrosus (AF) stress, were analyzed under the same loading/boundary conditions. The results were compared using one-way ANOVA (significance set at $p<0.05$).

The results of the ROMs, IDP, and FJF for pre-operation models were consistent with literature [3-5]. The average ROM and stress of adjacent levels were significantly higher at 3 months post-op in flexion, extension and axial rotation, as compared to pre-operation. However, all parameters significantly decreased from 3 months to 12 months post-operation, although not to the same pre-surgical level. The FJF of adjacent levels significantly decreased for 3 months post-op in extension and axial rotation, as compared to pre-operation. Nonetheless, the forces slightly increased ($p=0.073$) from 3 months to 12 months post-operation. No significant changes were seen for the IDP between pre, 3 months and 12 months post-operation.

This study provides clinicians with quantitative biomechanical data towards subject-specific informed clinical evaluation. The results confirm that the biomechanics (intersegmental motions and load-sharing) of the lumbar spine are altered after fusion. Short-term and long-term post-op models revealed different ROM, FJF and stress distribution, which may differentiate the spinal response during recovery, hence influencing clinical strategies. Ongoing/future work includes expanding the studied population to investigate different spinal diseases and diverse surgical techniques.

References:

[1] Lee et al., Asian Spine J., 2015 (9);
[2] Wang et al., Medicine, 2017 (96);
[3] Panjabi et al., J. Bone Joint Surgury, 1994(76);
[4] Brinckmann et al., Spine, 1991 (16);
[5] Wilson et al., J. Biomechanics, 2006 (39).

[B-08.2]

IMAGE-BASED FINITE ELEMENT MODELLING AS A PRE-CLINICAL EVALUATION TOOL FOR SPINAL INTERVENTIONS

Marlène Mengoni[1], *Alison Jones*[1], ***Ruth Wilcox***[1]

1 *Institute of Medical and Biological Engineering, University of Leeds, Leeds, UK*

Four out of five adults will suffer from low back pain during their lifetime. The disorder often affects people of working age, placing high economic burdens on society, estimated to be as high as 1-2% of gross domestic product [1]. Despite the scale, the surgical treatment for late-stage back pain is not as effective as interventions for other musculoskeletal joints. This is partly due to the lack or robust preclinical testing available for the spine, meaning new innovations cannot be adequately screened and optimized prior to clinical use.

We have developed a range of preclinical testing methodologies for new spinal interventions by combining in silico and in vitro models. Our approach has been to generate image-based finite element models of individual specimens that are tested in parallel laboratory experiments. We have applied this approach to derive properties and validate models of individual vertebrae, intervertebral discs, facet joints and ligaments [e.g. 2, 3] (Figure 1a). The methods developed have then been combined to simulate the full functional spinal unit, and specimen-specific models have again been validated against corresponding experimental tests for a range of local and global measurements (Figure 1b) [4].

We have then applied the models to examine interventions including vertebroplasty [5] and nucleus augmentation [6], which has involved further refinement of the models to capture the biomaterial-host interactions (Figure 1c). These models have helped inform the device and clinical requirements for specific interventions, as well as the potential risks, such as adjacent vertebral failure in the case of vertebroplasty. More recently, we have used statistical shape and appearance modelling to capture variances in a population with the aim of better defining patient characteristics that would indicate positive or negative outcomes.

The potential for image-based modelling to be used as a preclinical testing tool continues to grow, especially when coupled with statistical methods to evaluate performance across the variances seen in the patient population. However, careful consideration of the research question and required level of accuracy is needed to identify the necessary sensitivity, verification and validation steps required to produce robust and efficient models.

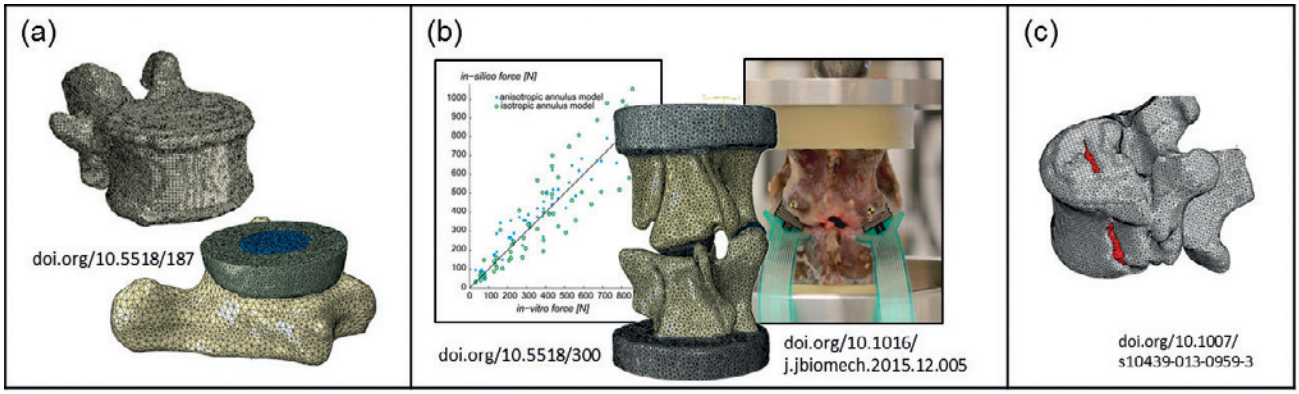

Figure Caption: Finite element models of (a) individual components, b) functional spinal unit, showing experimental comparison and (c) vertebroplasty analysis

Acknowledgments: Funded by grants from EPSRC and ERC

References:

[1] Norlund AI & Waddell G. In: Nachemson AL & Jonsson E. Neck and back pain (2000), Lippencott, Williams & Wilkins.
[2] Zapata-Cornelio FY et al (2017) Annals Biomed. Eng, 2451-2460.
[3] Mengoni M et al (2017) Royal Soc. Open Sci., 170807.
[4] Mengoni M et al (2016) J. Biomech.,259-266.
[5] Tarsuslugil SM et al. (2014) Annals Biomed. Eng., 751-762,
[6] Sikora SNF et al (2018) J. Eng. Med., 230-240.

[B-08.3]

METHODS TO INVESTIGATE THE EFFECTS OF VERTEBRAL VARIATION ON THE MECHANICAL OUTCOMES OF VERTEBROPLASTY USING STATISTICAL SHAPE AND APPEARANCE MODELLING

Gavin Day[1], *Alison Jones*[1], *Ruth Wilcox*[1]

1 *Institute of Medical and Biological Engineering, University of Leeds, Leeds, UK*

Patient variation is an important factor for a range of spinal interventions; the variance in morphology and properties of vertebrae may explain the large differences in outcomes for treatments such as vertebroplasty. In previous work [1], a statistical shape and appearance model (SSAM) has been created to identify modes of variation across a set of intact vertebrae. Here, the effects of variation on the mechanical outcomes of vertebroplasty are investigated.

Fourteen cadaveric lumbar vertebrae were µCT-scanned and tested under axial compression before and after vertebroplasty. Finite element (FE) models were created and validated against their experimental stiffness in both the intact and post-vertebroplasty states. A statistical shape modelling tool was used to characterise the shape and material property variation within the input set. The tool was then used to generate vertebral FE models at points along the three most significant modes of variation. Nineteen "spawned" FE models were validated against the input set. These vertebrae were then artificially augmented using relevant volumes and positions of cement based on the experimental results. The effect that the modes of variation had on the mechanical outcomes of augmentation were then investigated.

The PCA algorithm captured 69% of the total variation in the first 5 principal components (PC). Good agreement was found between the input set and spawned models. Percentage difference between the mean of the input set and mean generated model for volume, mean greyscale and FE compressive stiffness were 10%, 3% and 10% respectively. The first PC captured the majority of variation in the greyscale (both distribution and mean). Variation in the second and third components described more specific geometric variations (Fig.A,B).

Both the geometry and material properties (density and density distribution) had a large effect on the response to augmentation (Fig.C). The stiffness following augmenation was mainly controlled by combinations of shape (anterior/posterior wedge shapes) in addition to shifting posterior to anterior density distributions.

The results show effects of vertebral variation on the mechanical response to loading. Importantly, this variation is often not directly measurable or obvious without such techniques, such as the shifting density from anterior to posterior in the L1-like to L5-like vertebrae of PC2. The results emphasise the relationship between the density distribution and the response to augmentation that was found experimentally. The inclusion of larger input sets will allow the extension of vertebroplasty procedure advice and patient suitability to the wider population.

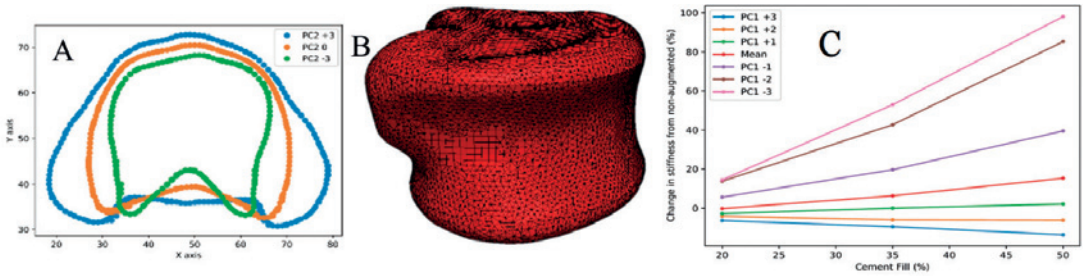

Figure Caption: A: The shape variation found in the axial-mid-slice of models generated from PC2 the mean generated FE model. B: the mean generated FE model. C: The response to augmentation fill volumes in PC1.

Acknowledgments: ERC (2012-StG-306615) and EPSRC (EP/L014823/1).

References:

[1] *Day,G., Jones,AC., Wilcox,RK. Understanding Vertebral Variation using PCA and SSAM, WCB 2018*

[B-08.4]

A PRELIMINARY SENSITIVITY STUDY OF VERTEBRAL TETHERING CONFIGURATIONS USING A PATIENT-SPECIFIC FINITE ELEMENT MODEL OF IDIOPATHIC SCOLIOSIS

J Paige Little[1], *Robert Labrom*[2], *Geoffrey Askin*[3]

1 *Biomechanics and Spine Research Group, South Brisbane, Australia; Ihbi at Centre for Children's Health Research; Queensland University of Technology, Brisbane, Australia*
2 *The Wesley Hospital Brisbane, Brisbane, Australia*
3 *Mater Health Services, Brisbane, Australia*

There is a growing interest in the use of Vertebral Body Tethering (VBT) surgery for skeletally immature idiopathic scoliosis (IS) patients. Anteriorly placed vertebral screws secure a deformable Polyethylene-Terephthalate (PET) tether. Before securing the tether, compressive force is applied between the screw heads along the axis of the spine. There are no clear guidelines regarding the force magnitude required to optimize deformity correction. In the current study, a validated, patient-specific finite element (FE) model of IS was analysed to investigate the effect of four different VBT loading scenarios on spinal alignment and biomechanics.

Custom-software (VirtuSpine) reconstructed the osseo-ligamentous anatomy of the thoracolumbar spine and ribcage for a 10-year-old IS patient [1]. The patient-specific FEM was previously validated using clinical results for pre-/post-operative deformity [1]. Linear elastic continuum elements (PET material) tethered laterally oriented screws at spinal levels T5-T12, with roughened contact simulating the screws when locked onto the tether. Compressive forces measured intra-operatively during anterior scoliosis fusion surgery (FS) [4] defined the first loadcase. In this preliminary series of VBT analyses, four loading scenarios were investigated: i) Tethered all levels T5-T12 & Level-wise compressive forces=FS (T5toT12_100%Force); ii) Two tethered regions, T5-T9 and T9-T12 (levels in between unconstrained) & Total force equivalent to FS (T5T9T12_100%Force); iii) Tethered all levels T5-T12 & Level-wise compressive forces=75%FS (T5toT12_75%Force); iv) Tethered correction all levels T5-T12 & No compressive forces (T5toT12_TetherOnly, Baseline loadcase). The inferior L5 endplate was fixed. After surgical loadcase, patient-specific, level-wise gravitational loads at all vertebral levels simulated standing.

Model predictions for Corrected Cobb angle/Kyphosis angle/Axial trunk rotation and reaction moments at L5 were compared to determine how surgical loading strategy affected deformity correction/spinal loading (Table 1).

Coronal plane correction decreased slightly after standing. The larger deformity correction for the T5T9T12_100%Force loadcase was promising and demonstrated that marked differences in deformity correction can be achieved with different patterns of tethering loads. However, resultant loads on surrounding anatomy must be considered, with associated high moments active on the spinal tissues. Further analyses of additional loading scenarios will consider the mechano-biological effect of compressive vertebral tethering.

TABLE 1	*T5toT12_100%Force*		*T5T9T12_F00%Force*		*T5toT12_75%Force*		*T5toT12_TetherOnly*	
	Change in Angle from pre-operative condition (degrees)							
Coronal Cobb	10	9	25	23.5	8	7	0	0
Axial Trunk rotation	-4	-4	-7	-7	-3	-3	0	0
Sagittal Kyphosis	1	0	2	1	1	0	1	0
	Change in Reaction moments from pre-operative condition (Nmm)							
Coronal Cobb	-6,900	9	-20,200		-5400		15	0
Axial Trunk rotation	-4	-4	-7	-7	-3	-3	0	0
Sagittal Kyphosis	1	0	2	1	1	0	1	0

Figure Caption: Grey shaded columns are surgical loadcase results; Hashed columns are standing loadcase results

References:

[1] Little, J. P., Adam, C. J. Spine, 2009, 34(2)

[B-08.5]

EXPERIMENTAL IN-VITRO EVALUATION PF A NUMERICAL MODEL OF THE SPINE AND ITS APPLICATION FOR THE COMPARISON OF DIFFERENT APPROACHES TO SCOLIOSIS CORRECTIVE SURGERY

*Claudio Vergari[1], Mathilde Gaume[2], Sylvain Persohn[1], Lotfi Miladi[2], **Wafa Skalli**[3]*

1 *Arts et Métiers ParisTech, LBM/Institut de Biomécanique Humaine Georges Charpak, Paris, France*
2 *Pediatrics Orthopedics Department, Necker Hospital, Paris Descartes University, Paris, France*
3 *Institut de Biomécanique Humaine Georges Charpak, Arts et Métiers ParisTech, Paris, France*

Design and testing of spinal implants to correct scoliosis is a classical application of numerical modeling. Nevertheless, models often lack validation due to the paucity of cadaveric samples and the difficulty of implementing in-vivo situations. The aim of this work was to evaluate a numerical model against mechanical testing, and to apply it to an in-vivo situation to compare two constructs.

The numerical model consisted of vertebral bodies, transverse processes, articular facets, intervertebral discs and ligaments. Nonlinear mechanical behavior of the discs was modeled with 3rd order polynomials which were fit to the experimental data below, while mechanical properties of the other components were retrieved from the literature. The model was first validated against in-vitro mechanical tests: six T1-T5 segments were loaded in flexion-extension (FE), torsion (TO) and lateral bending (LB). Specimens were tested both intact and with a bipolar instrumentation with thoracic hook claws, where strain was measured with a strain gage on the implant's rod at the level of T6. Tests were replicated in silico to compare range of motion (ROM) and implant's strain.

In a second step, a model of a T1-L5 spine, pelvis and ribcage was built from a typical subject geometry. A T1-to-pelvis bipolar instrumentation was added to the model and attached with sublaminar hooks from T1 to T5 vertebrae, and with ilio-sacral screws. Simulation of the thoracic segment was compared to the experimental data. A second configuration was simulated by adding pedicle screws at T6 to L5 vertebral levels. The two configurations were loaded with imposed rotations to T1 vertebra in FE, TO and LB to simulate in-vivo conditions. Maximal rods' Von Mises stress was compared between configurations.

Figure 1 shows experimental and numerical ROMs of the intact thoracic specimens. Instrumentation reduced experimental ROM between 70% and 98% depending on loading, with consistent model results. Strain gages and numerical model both yielded a strain of 0.01% of the instrumentation's rod. Simulation of in-vivo conditions showed that all-screws instrumentation had maximal stresses of 35, 40 and 95 MPa in FE, LB and TO, respectively. Bipolar instrumentation showed 38, 44 and 75 MPa for the same imposed displacements.

The main limitation is that full spines were not tested, but only thoracic and lumbar segments. Nevertheless, this conceptual model appeared consistent with experimental data, and it allowed comparing in-vivo instrumentations.

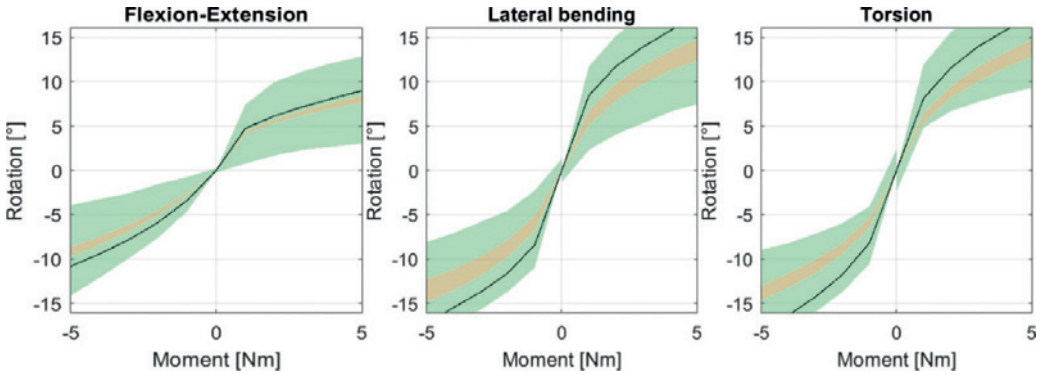

Figure Caption: Experimental (green, mean ± 2SD) and numerical (red) mobility corridors of T1-T5 segment (green). Black line is the simulation based on subject geometry.

Acknowledgments: This study was financed by EUROS company and the ParisTech BiomecAM chair program (with the support of ParisTech and Yves Cotrel Foundations, Société Générale, Proteor and Covea).

[B-08.6]

TRANSPOSITIONS OF INTERVERTEBRAL CENTROIDS IN ADOLESCENTS SUFFERING FROM IDIOPATHIC SCOLIOSIS OPTICALLY DIAGNOSED

Sasa Cukovic[1], *William R. Taylor*[2], *Christoph Heidt*[3], *Goran Devedzic*[1], *Vanja Lukovic*[4], *Tito Bassani*[5]

1 *University of Kragujevac, Faculty of Engineering, Kragujevac, Serbia*
2 *Swiss Federal Institute of Technology Eth, Department of Health Sciences and Technology, Institute for Biomechanics, Zürich, Switzerland*
3 *Pediatric Orthopaedic Department, Children's Hospital, University of Basel, Base, Switzerland*
4 *University of Kragujevac, Faculty of Technical Sciences, Cacak, Serbia*
5 *Irccs Istituto Ortopedico Galeazzi; Irccs Galeazzi Orthopaedic Institute, Labs - Laboratory of Biological Structures Mechanics, Milano, Italy*

Adolescent idiopathic scoliosis (AIS) is the most frequent spinal deformity type, diagnosed in about 80% of all scoliosis cases. Besides preliminary diagnosis, regular radiological follow-ups are required to monitor the deformity every 3-6 months. In order to reduce ionizing radiation of AIS patients, we recently developed a 3D non-invasive method aiming to calculate a number of deformity indicators and to visualize patient-specific skeletal distortion, based only on a 3D virtual dorsal surface [1].

Using optically scanning, we digitalised the dorsal surfaces of 372 patients (141 males and 231 females) in a clinical environment from 2014-2017. Patient datasets were processed using our in-house "ScolioSIM" tool to generate over 100 extrinsic and intrinsic deformity parameters, along with 3D deformity visualizations. This method relies on a multiscale and registerable 3D generic spinal model developed in Materialise Mimics and KAx technologies, and implemented within the PLM system CATIA v5 (Fig.1). We focused our attention towards the positions of intervertebral disks' centroids from the DM-C7 line in the AP plane, located on a 5th degree B-Spline that represents middle spinal line.

Transpositions of all intervertebral centroids (L5/L4 to T1/C7) from the DM-C7 line (Tab.1) revealed that the most transposed intervertebral disc (apex disc) in AIS patients was located between T7-T6 in (left) thoracic curvatures (-43.3mm) followed by a right-transposed disc between T10-T9 (49.6mm).

The clinical relevance of the presented study is high, since the degree of the deformity and the localization of the apex vertebra or intervertebral disk on AIS middle spines define a range as well as the horizontal boundaries of AIS spinal curves, and may be the basis for investigating the range of motion and flexibility of the spine. We demonstrated that our radiation-free imaging method enables a reliable 3D visualisation of deformity and detection of subtle postural changes in a large cohort affected by the most translated vertebrae in the primary AIS curve. Due to its non-ionizing nature, the integrated method of data acquisition and analysis has enormous potential to be safely used in clinical settings, for monitoring AIS, and to predict important indicators of the underlying structures and the associations between the intervertebral transpositions and other parameters of spinal deformity.

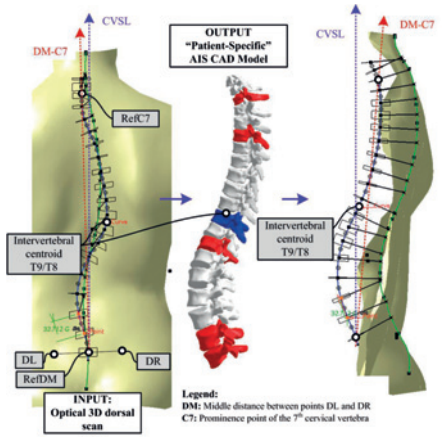

Parameters	Females, n=231			Males, n=141		
	min	max	mean	min	max	mean
T1/C7	-5.8	2.8	-0.2±0.9	-3.2	1.9	-0.3±0.8
T2/T1	-10.6	9.3	-0.4±3.0	-10.4	6.6	-0.9±2.8
T3/T2	-174.	19.4	0.5±5.6	-20.4	13.4	-0.8±5.1
T4/T3	-25.3	28.2	2.5±8.3	-27.5	24.9	-0.2±7.5
T5/T4	-33.2	33.9	4.4±10.5	-30.0	34.9	0.4±9.2
T6/T5	-38.4	40.5	6.1±12.2	-28.9	42.7	1.1±10.3
T7/T6	-43.3	45.4	7.4±13.4	-24.1	46.6	1.8±10.9
T8/T7	-39.4	47.8	8.2±13.7	-20.2	48.2	2.2±11.2
T9/T8	-41.5	49.0	8.2±13.5	-22.4	48.0	2.2±11.1
T10/T9	-39.6	49.6	7.5±12.9	-25.5	46.8	1.9±10.9
T11/T10	-35.4	44.2	6.0±12.1	-29.1	51.9	1.2±10.8
T12/T11	-31.0	42.9	3.9±11.8	-32.5	55.1	0.3±11.1
L1/T12	-30.9	38.1	1.7±11.7	-33.4	55.4	-0.3±11.4
L2/L1	-33.3	34.8	0.0±10.9	-30.3	44.4	-0.8±10.6
L3/L2	-25.0	27.4	-0.8±8.8	-24.5	30.2	-0.8±8.6
L4/L3	-12.2	20.4	-0.9±5.8	-17.1	17.3	-0.4±5.5
L5/L4	-6.7	9.3	-0.3±2.2	-9.5	12.0	-0.0±2.5

Figure Caption: 3D optical diagnosis of AIS and intervertebral centroids' positions from DM-C7 line in frontal plane.

Table Caption: Descriptive statistics on intervertebral centroids' positions from C7-DM line [mm] in 372 AIS cases; ("-") assigns left and ("+") right oriented scoliosis (frontal plane).

Acknowledgments: Presented research is supported by the Swiss-SERI-SGES grant [2017.0024] and by the Serbian Ministry of Science grant III-41007.

References:

1. *Cukovic S, Non-rigid registration of sculptured surfaces in internet environment, UniKg, PhD-thesis, Serbia, 2015.*

[B-09.1]
BONE CELL CROSS TALK UNDER MECHANICAL LOADING

Lidan You[1]

1 University of Toronto, Toronto, Canada

Bone is able to adapt its composition and structure in order to suit its mechanical environment. Osteocytes, bone cells embedded in the calcified matrix, are believed to be the mechanosensors and responsible for orchestrating the bone remodeling process. However, detailed cellular and molecular mechanism underlying osteocyte mechanobiology is not well understood. In this talk, osteocyte intracellular response under pressure and shear stress were presented. Furthermore, inter cell-population communications under mechanical loading and its implication in bone disorder management such as bone metastasis prevention is discussed.

Bone metastases are common and severe complications of cancers. It is estimated that 65-75% of patients with breast and prostate cancer develop bone metastasis [1] and an estimate of 350,000 people in the United States die annually from bone metastases [2]. Metastasized cancer cells have devastating impacts on bone quality due to their ability to alter bone remodeling by interacting with other bone cells such as osteoblasts and osteoclasts. Exercise, often used as an intervention for patients suffering from cancer, regulates bone remodeling. We hypothesize that mechanical loading may regulate bone metastases via osteocyte signaling. We observed that significantly more breast cancer cells (MDA-MB-231) and prostate cancer cells (PC3 cells) migrated towards the conditioned media (CM) from MLO-Y4 cells with exposure to flow in comparison to CM from MLO-Y4 cells not exposed to flow. The preferential migration is abolished with the application of anti-VEGF antibodies. MDA-MB-231 cells apoptosis rate was slightly lower in CM from MLO-Y4 cells exposed to flow, while proliferation rate was slightly higher. On the other hand, we found that less MDA-MB-231 cells migrated towards CM from RAW264.7 cells conditioned in CM from MLO-Y4 cells stimulated with flow in comparison to those conditioned in CM from MLO-Y4 cells not stimulated with flow. TRAP staining results confirmed that there were less differentiated osteoclasts when RAW264.7 cells were cultured in CM from MLO-Y4 cells exposed to flow in comparison to those not exposed to flow [3].

Overall, results from our studies suggest that osteocytes are highly sensitive to mechanical loadings. Physiologically relevant mechanical loading and high frequency and low magnitude loading can induce signals inhibit bone resorption and promot bone formation. Loading on osteocyte also have major impact on cancer cell migration and proliferation, provides insights into the impact of exercises on bone metastases.

Acknowledgement: Natural Sciences and Engineering Research Council of Canada Discovery Grant.

Reference:

[1] Coleman. Cancer Treatment Rev. 2001. 27(3):165.
[2] Mundy. Nat. Rev. Cancer. 2002. 2(8):584.
[3] Ma. 2016 ORS abstract 1570.

[B-09.2]

OSTEOCYTE PRIMARY CILIA MECHANOSENSING: INTRACILIARY SIGNALS, EXTRACILIARY DYNAMICS, AND BEYOND

Michael Duffy[1], *Milos Spasic*[2], *Emily Moore*[3], *An Nguyen*[1], *Kristen Lee*[1], *Christopher Jacobs*[1]

1 *Columbia University, New York, USA*
2 *Harvard Medical School, Brigham and Women's Hospital, Boston, USA*
3 *Harvard Medical School, Developmental Biology, Boston, USA*

Osteoporosis or low bone mass affects over half of the US population over 50 and can lead to a significant loss of quality of life. [1]. Current therapeutics, while somewhat efficacious, have risks that are perceived to be high, leading to suboptimal patient compliance [2]. Therefore, the continued development of pharmaceutical targets to enhance bone strength is critical. Osteocytes are described as bone's mechanosensor, likely by detecting fluid flow through the lacunar-canalicular system, and help orchestrate bone response to mechanical loading [3]. We focus on how the primary cilium – a solitary, immotile, microtubule-based organelle [4,5] – helps coordinate mechanotransduction from initial intraciliary signals to influencing cellular response and tissue level changes. Within the cilium, we show that calcium signaling is an early response, peaking within 10 seconds of flow initiation (Fig1A), and is followed by a sustained increase in cAMP signaling (Fig1B). Downstream of these intraciliary signals, we show that the primary cilium regulates actin cytoskeletal response to fluid flow, whereby inhibiting cilia formation prevents an increase in the area of F-actin staining in response to fluid flow (Fig1C) and alters cell morphology. This also leads to a decrease in Taz, a transcriptional co-activator, translocation to the nucleus – an actin-dependent mechanoresponse. At the tissue level, we employ Cre-Lox technology to knockdown IFT88, a protein required for cilia formation, in late osteoblasts and osteocytes. We find that ciliary impairment abrogates load-induced bone formation in a murine ulnar loading model (Fig 1D). We then injected mice with fenoldopam, which has been shown to increase primary cilium length, and found that the treated mice had an increased osteogenic response to ulnar loading (Fig1E). Based on these data that span scales from the intraciliary to whole tissue level, we propose that the primary cilium contributes to osteocyte mechanotransduction and is a promising therapeutic target for bone disease.

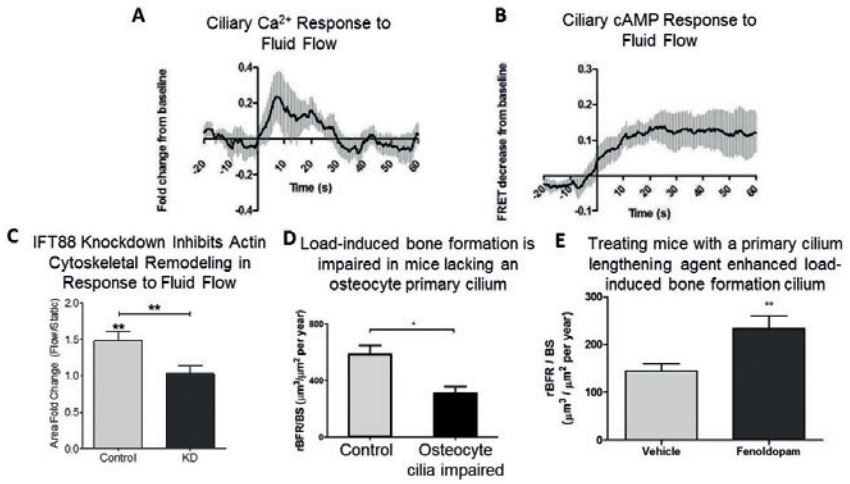

Figure 1: A) FRET-based measurement of intraciliary calcium demonstrates that the primary cilium is a calcium-responsive mechanosensor. B) Primary cilia respond to fluid flow and, possibly, intraciliary calcium signaling with a sustained increase in cAMP production as measured with a ciliary-localized FRET-based biosensor. C) Inhibiting primary cilia formation with an siRNA-mediated KD of IFT88 prevents actin cytoskeletal reorganization in response to mechanical stimulation. D) Osteogenic response to ulnar loading is diminished in mice lacking osteocyte primary cilia. E) Treating mice with an agent that lengthens primary cilia increases the osteogenic response to loading.

Acknowledgments: We thank the NIH for funding under AR062177 and AR045989.

References:

1. US Dept of Health Services: 2004 "The Burden of Bone Disease."
2. Khosla et al. Lancet Diabetes Endorinol. 2017.
3. Bonewald. J Bone Miner Res. 2011.
4. Nguyen & Jacobs. Bone 2013.
5. Hoey et al. Frontiers in Endocrinology. 2012.

[B-09.3]

TARGETING MECHANOBIOLOGICAL CUES TO DRIVE STEM CELL OSTEOGENESIS AND BONE REGENERATION

David Hoey[1]

1 *Trinity College Dublin, Dublin, Ireland*

Osteoporosis affects millions globally and current anti-catabolic treatments are limited by undesirable side-effects. Osteoporosis arises in part when skeletal stem cells (SSC) no longer sufficiently replenish osteoblasts, leading to net bone loss. A key regulator of SSC recruitment, proliferation and osteogenic differentiation is physical loading, yet the mechanisms by which SSCs sense and respond to changes in their mechanical environment are virtually unknown. This paper will explore two mechanisms by which SSCs are mechanically regulated in bone. Initially, it will be shown that fluid shear can directly drive SSC osteogenic lineage commitment and the mechanistic role of the primary cilium in this process will be explored. Primary cilia are nearly ubiquitous 'antennae-like' cellular organelles that have very recently emerged as extracellular chemo/mechano-sensors and thus, are strong candidates to play an important role in regulating SSC responses in bone. This study will also demonstrate a second indirect mechanism whereby mechanically stimulated lineage committed bone cells coordinate SSC recruitment and osteogenic differentiation in a paracrine manner, through the release of mechanically activated extracellular vesicles. Finally, it will be shown that targeting these direct and indirect mechanisms of biophysical regulation of SSC behaviour represent novel mechanotherapeutic avenues to enhance SSC contributions to bone and new anabolic treatments for osteoporosis. These mechanotherapeutics can also be combined with bone mimetic fibrous scaffolds produced through Melt Electrospinning Writing, resulting in novel mechano-biomimetic materials which have great potential as an effective strategy to guide bone regeneration

Acknowledgments: The author would like to acknowledge the European Research Council (n°336884), Science Foundation Ireland (n°SFI/13/ERC/L2864) and the Irish Research Council (GOIPG/2014/493) for funding

[B-09.4]

OSTEO-ANGIO COUPLING DURING MECHANICALLY-REGULATED BONE REPAIR

Alesha Castillo[1]

1 *New York University, New York, USA; Nyu Bioengineering Institute, New York, USA*

Elucidating the effects of mechanical stimulation on bone repair is crucial for optimization of the healing process. Specifically, the regulatory role that mechanical loading exerts on the osteogenic stem cell pool and vascular morphology during healing is incompletely understood. We recently showed that crosstalk between osteoprogenitors and endothelial cells was regulated by mechanical stimulation. Because dynamic loading has been shown to enhance osteogenesis and repair, we hypothesized that loading induces the expansion of the osteoprogenitor cell population within a healing bone defect, leading to an increased presence of osteogenic cells. We further hypothesized that loading during the repair process regulates vascular and collagen matrix morphology and spatial interactions between vessels and osteogenic cells. To address these hypotheses, we used a mechanobiological bone repair model, which produces a consistent and reproducible intramembranous repair response confined in time and space. Bilateral tibial defects were created in adult C57BL/6 mice, which were subjected to axial compressive dynamic loading either during the early cellular invasion phase on postsurgical days (PSDs) 2 to 5 or during the matrix deposition phase on PSD 5 to 8. Confocal and two-photon microscopy was used to generate high-resolution three-dimensional (3D) renderings of longitudinal thick sections of the defect on PSD 10. Endomucin (EMCN) positive vessels, paired related homeobox 1 (Prrx1+) stem cell antigen-1 positive (Sca-1+) primitive osteoprogenitors (OPCs), and osterix positive (Osx+) preosteoblasts were visualized and quantified using deep tissue immunohistochemistry. New bone matrix was visualized with second harmonic generation autofluorescence of collagen fibers. We found that mechanical loading during the matrix deposition phase (PSD 5 to 8) increased vessel volume and number, and aligned vessels and collagen fibers to the load bearing direction of bone. Furthermore, loading led to a significant increase in the proliferation and number of Prrx1+Sca-1+ primitive OPCs, but not Osx+ preosteoblasts within the defect. Together, these data illustrate the adaptation of both collagen matrix and vascular morphology to better withstand mechanical load during bone repair, and that the mechanoresponsive cell population consists of the primitive osteogenic progenitors. Ongoing work is focused on signaling pathway crosstalk between osteoprogenitors and endothelial cells in the context of mechanically-regulated bone repair.

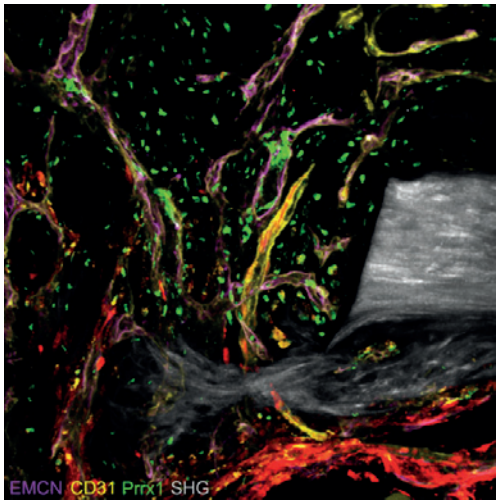

Figure Caption: Tibial monocortical defect at postsurgical day 5 showing physical interactions between vessels [endomucin (EMCN, purple) and CD31 (yellow)] and Prrx1+ (green) osteoprogenitors. Collagen fibers are visualized by the second harmonic generation signal (SHG, gray).

Acknowledgments: We gratefully acknowledge the support of a VA Career Development Award (ABC), a VA Merit Review Award 1I01RX001500 (ABC), and an NYU Clinical and Translational Science Institute Postdoctoral Fellowship 5TL1TR001447-03 (PCZ). We thank Emily Fang for assistance in vessel quantification methodology development; Ralph Adams for assistance in immunofluorescence deep-tissue imaging methodology; the NYU Microscopy Core for confocal and two-photon microscopy; and the NYU Histopathology Core for assistance in cryosectioning.

[B-09.5]

EXTREME BIOMECHANICAL ADAPTATIONS OF BONE AND BIOINSPIRED MATERIAL DESIGN

Seth Donahue[1]

1 *University of Massachusetts, Amherst, USA*

Bone evolved to serve many mechanical and physiological functions including adaptations to unique and extreme mechanical and physiological conditions (Doherty, 2015). Krogh's principle of using the best adapted animal for solving a particular problem in physiology can be used for musculoskeletal physiology and pathology (Donahue, 2018). For example, hibernating bears and rodents can prevent disuse-induced losses of bone structure and strength. Krogh's principle can be extended for translating the biomechanical adaptations of biological materials to extreme mechanical environments. For example, bighorn sheep ram heads with impact forces that would cause severe brain trauma if not death in humans. To help protect the brain in this extreme mechanical environment bighorn sheep have bone-filled spiral horns to absorb much of the impact energy. Dynamic finite element modeling has shown that the unique porous bone architecture that fills the horn plays a significant role in reducing brain cavity linear and angular accelerations during impact (Drake, 2016). The porous bone that fills the horn has approximately the same volume fraction as typical trabecular bone, however, the solid parts of the material are more sail-like than strut-like. Furthermore, the bone sails have a considerably larger size scale than trabecular bone struts. The bighorn bone sails are about 7-fold thicker than trabeculae and can be as long as 5 cm. This raises the possibility this unique bony architecture is adapted for absorbing energy during extreme mechanical impacts. An iterative design process utilizing finite element modeling, additive manufacturing, and mechanical testing is being used to develop new bioinspired material architectures, inspired by bighorn porous bone, for energy absorbing polymers that can be used in helmets, running shoes, etc. Similarly, dinosaur bone architecture is being used to design bioinspired material architectures for mechanically supporting gigantism.

Acknowledgments: I am grateful for my mentors Neil Sharkey, Bruce Martin, Chris Jacobs, and Hank Donahue (no relation, thankfully), and to Hannah Carey for immersing me in the field of comparative physiology, and Brian Barnes, Hal Black, and Greg Florant for giving me the opportunity to study wild animals in wild places.

References:

Doherty AH, Ghalambor CK, and Donahue SW (2015), Evolutionary physiology of bone: bone metabolism in changing environments, Physiology, 30(1):17-29. Donahue SW (2018), Krogh's principle for musculoskeletal physiology and pathology, J Musculoskelet Neuronal Interact,18(3):284-291. Drake A, Donahue TL, Stansloski M, Fox K, Wheatley BB, Donahue SW (2016), Horn and horn core trabecular bone of bighorn sheep rams absorbs impact energy and reduces brain cavity accelerations during high impact ramming of the skull, Acta biomaterialia, 44: 41-50.

[B-09.6]

DEEP PHENOTYPING IN THE ZEBRAFISH SKELETON ENHANCES SOMATIC MUTANT DETECTION AND MOSAIC PATTERN RECOGNITION

Claire Watson[1], Adrian Monstad-Rios[1], Rehaan Bhimani[1], Yi-Hsiang Hsu[2], ***Ronald Kwon***[1]

1 *University of Washington, Seattle, USA*
2 *Harvard University, Boston, USA*

Because CRISPR-based rapid-throughput biology often entails analysis of G0 somatic mutants, there is a need to improve our ability to discern and interpret variable phenotypes arising from mosaicism. Here, we examine mechanisms underlying mosaic patterns in "crispant" zebrafish, and assess the benefits of phenomics—i.e., in depth phenotyping at a large number of sites—in discerning variable phenotypes arising from mosaicism. We characterize spatial and size characteristics of loss-of-function cell clusters in the skeleton. Despite inter-animal differences in mutation efficiency, we identify a distinctive size distribution in bones of separate developmental lineages, replicating that predicted from clonal fragmentation and merger events. Using a microCT-based workflow enabling hundreds of measures per animal [1], we describe diverse phenotypic manifestations in mosaic models of brittle bone diseases (plod2 and bmp1a). At the population level, we show convergence between somatic and germline mutant phenomes. We demonstrate that vertebral patterns confer heightened sensitivity in discriminating somatic mutant populations compared to single readouts. We also establish a framework to quantify spatial phenotypic variation, and show this is differentially altered in disease models. Finally, we detect a low bone mass phenotype in adult somatic mutants for wnt16, a gene implicated in heritable risk for osteoporosis, and validate this phenotype in germline mutants. Our studies demonstrate mosaic analysis and phenomic approaches to help detect and interpret spatially variable phenotypes in G0 animals. Applied to the skeleton, microCT-based phenomics, in concert with CRISPR-based G0 screens, is a promising direction for the identification of causal genes and targeted therapies for mono- and multigenic skeletal diseases.

References:

1. *Hur M, Gistelinck CA, Huber P, Lee J, Thompson MH, Monstad-Rios AT, Watson CJ, McMenamin SK, Willaert A, Parichy DM, Coucke P, Kwon RY. MicroCT-based phenomics in the zebrafish skeleton reveals virtues of deep phenotyping in a distributed organ system. Elife. 2017 Sep 8;6. pii: e26014. doi: 10.7554/eLife.26014.*

[B-10.1]

HARNESSING CHONDROCYTE MECHANOTRANSDUCTION TO DRIVE THERAPEUTIC TRANSGENE PRODUCTION VIA A SYNTHETIC MECHANOGENETIC CIRCUIT

Robert J. Nims[1], *Lara Pferdehirt*[1], *Alireza Savadipour*[1], *Jeremiah Lorentz*[1], *Alison K. Ross*[1], *Farshid Guilak*[1]

1 *Washington University in Saint Louis, Saint Louis, USA; Shriners Hospitals for Children - Saint Loui, USA*

Articular cartilage maintains its normal physiology in response to dynamic changes in the mechanical and inflammatory environment within the joint. Chondrocytes within cartilage integrate and respond to their local mechanical environment through specific ion channels that respond to different magnitudes of tissue or cell deformation. Chondrocytes use the ion channel transient potential vanilloid 4 (TRPV4) to interpret their mechanical environment as an osmotic gradient to the cell. Prior computational and experimental work in our lab has shown that deformations to the cartilage tissue are converted through each chondrocyte's osmotically-active pericellular matrix, provoking a local change in the osmotic environment which in turn directly activates the TRPV4 channel. Our previous studies have suggested that in vivo, TRPV4 is critical in the development, growth, and maintenance of cartilage, suggesting a purely anabolic role of the ion channel. Using a model system of tissue-engineered cartilage consisting of primary porcine chondrocytes in agarose gel, we show that physiologic levels of strain activate TRPV4, eliciting intracellular calcium signaling and other intracellular signaling cascades. Microarray analyses show that TRPV4 activation elicits both a transient anabolic and inflammatory signaling pathways and gene transcript regulation [1]. With this enhanced understanding of the signaling pathways evoked by TRPV4 activation, we have developed synthetic circuits which respond to the intracellular signaling pathways downstream of TRPV4 activation. In particular, we repurposed the TRPV4-induced activation of NF-κB signaling within chondrocytes and developed a NF-κB-responsive synthetic promoter [2,3,4]. Activation of this circuit drives therapeutic drug delivery, specifically here we use the anti-inflammatory biologic drug interleukin-1 receptor antagonist (IL1-Ra), an inhibitor of IL-1 activity. Transducing chondrocytes with this lentiviral synthetic circuit utilizes the endogenous chondrocyte mechanobiological machinery and intracellular response to loading to drive a prescribed output. To test this system, we applied both deformational and osmotic forms of mechanical loading as well as direct, pharmacologic stimulation of the TRPV4 ion channel using the specific agonist GSK101, and measured increases in circuit activation through increased IL-1Ra production [5]. Moreover, using an antagonist to inhibit TRPV4 during deformational mechanical loading significantly reduced circuit activation, implicating the role of TRPV4 in stimulating the circuit. Together, this work demonstrates a framework for developing engineered tissues that can autonomously respond to their environment to drive therapeutic drug production or other outputs. Here, we utilized our extensive knowledge and new molecular insights of chondrocyte mechanobiology to develop a mechanically-responsive tissue engineered cartilage for implantation into the inflammatory and robust mechanical environment of the diseased joint. A better understanding of the impact and molecular consequences of activation of different mechanosensitive receptors and ion channels may be used to develop nested and more complex signaling circuits that respond to different presentations of mechanical loading.

Acknowledgments: Supported by grants from the NIH, NSF, Nancy Taylor Foundation for Chronic Diseases, Arthritis Foundation, AO Foundation, and the Shriners Hospitals for Children.

References:

[1] Ho+, ORS Transactions 43:453, 2018.
[2] Pferdehirt+, ORS Transactions 43:66, 2018.
[3] Brunger+, Stem Cell Reports 8:2012, 2017.
[4] Salmon and Trono, Curr Protoc Hum Genet Ch. 12, 2007.
[5] Nims+, ORS 2019 Transactions.

[B-10.2]

ACTOMYOSIN CONTRACTILITY AND INFLAMMATION MEDIATES MECHANOBIOLOGY IN DD

Nadeen Chahine[1], *Timothy Jacobsen*[1]

1 *Columbia University, New York, USA*

Intervertebral disc (IVD) degeneration (DD) is characterized by elevated levels of pro-inflammatory cytokines, and inflammatory stimulation of nucleus pulposus (NP) cells within the disc has been previously shown by our group to lead to significant changes in cellular properties. Since actomyosin contractility is a well-established regulator of cell morphology, here we investigate its role in mediating cellular biophysical properties in an inflammatory environment. We treated NP cells with TNFα for 24 hours in 3D culture and examined phosphorylated Myosin Light Chain (pMLC) levels as an indicator of actomyosin contractility, and single cell elastic modulus (E) with AFM. Our results show that TNFα decreases pMLC levels (Fig1), promotes formation of actin extensions (Fig4), and decreases E (Fig2). Decreasing actomyosin contractility with a ROCK inhibitor (Y27632) or a myosin-II inhibitor (Blebbistatin) phenocopied the morphological and cell biomechanical changes observed with TNFα (Fig2). Conversely, constitutive activation of RhoA (CN03) mitigated the effects of TNFα stimulation on E and morphology (Fig 3&4). In a NP explant ex-vivo culture system TNFα significantly reduced explant GAG content after 2 weeks in culture, however CN03 co-treatment mitigated this inflammatory induced GAG loss (Fig 5). Lastly, we observed changes in cell biophysical properties in cells from clinical disc degeneration samples as defined by Pfirrmann grade. E was found to decrease with increasing degree of degeneration, with cells from patients with degeneration above Pfirrmann grade 3 having moduli akin to that seen with decreased contractility or inflammatory stimulation. Our findings here indicate that loss of actomyosin contractility induced by a pro-inflammatory environment alters NP cell biophysical properties and promotes degradation of the ECM. Cell biophysical properties have been seen to change in DD. Importantly, preventing changes in these properties by protecting myosin contractility is effective at maintaining ECM integrity, and may be a novel therapeutic strategy for DD.

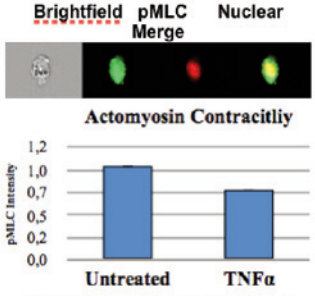

Figure 1: (A) Representative pMLC staining. **(B)** Actomyosin contractility decreases w/ TNFα. (* p<0.05)

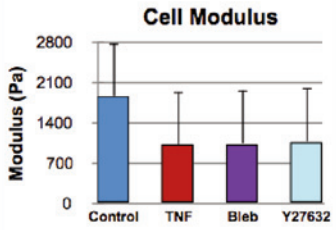

Figure 2: Cell modulus decreases with TNFα, Bleb, and Y27 treatment. (* p<0.05)

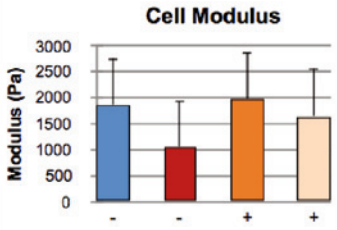

Figure 3: CN03 protects against TNFα induced decrease in cell modulus (* p<0.05)

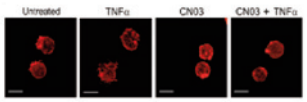

Figure 4: Actin (phaloidin) staining of NP Cells. TNFα stimulation disrupts actin cytoskeleton and promotes formation of punctate actin structures. CN03 prevents TNFα induced actin changes

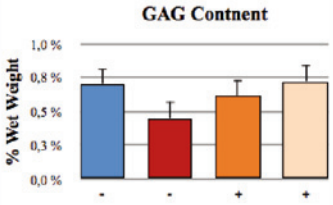

. **Figure 5:** GAG content of NP explants decreases w/ TNFα stim. CN03 mitigates TNFα induced GAG loss (* p<0.05).

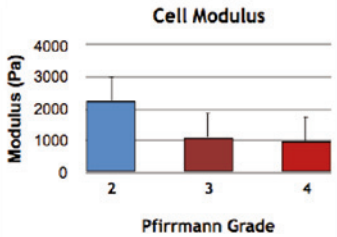

. **Figure 6:** Cell modulus decreases with increased degree of DD (* p<0.05).

Acknowledgments: Funded in part by NSF CAREER Award 1151605, NIH R01AR069668.

[B-10.3]

MECHANOBIOLOGY OF EMBRYONIC DEVELOPMENT TO INFORM ADULT TENDON REGENERATION

Catherine K. Kuo[1]

1 *Department of Biomedical Engineering, University of Rochester, Rochester, USA; Department of Orthopaedics, University of Rochester Medical Center, Rochester, USA*

Tendons transfer forces from muscle to bone to enable skeletal movement and stability. These tissues commonly sustain injuries, which is problematic as their inability to heal regeneratively compromises their mechanically demanding function. Rapidly rising incidence of tendon injuries due to increasing lifespans and participation in recreational sports has led to a critical need to regenerate new tendon during healing and in tissue engineering. We are focused on understanding how tendons develop naturally in the embryo to inform a rational tendon regeneration strategy. To that end, we are applying materials science techniques to characterizing structure-property relationships of developing embryonic tendons. We have generated a profile of embryonic tendon mechanical properties from early-to-late developmental stages and examined the spatial and temporal correlation of these properties with cellular and extracellular matrix (ECM) tissue components. Our studies have revealed that ECM components are unreliable predictors of mechanical properties. In contrast, we have found that enzymatic crosslink density is highly correlated with tendon mechanical properties, and that lysyl oxidase is a key regulator of collagen crosslink-mediated mechanical property elaboration. Using novel animal models and custom-bioreactor systems, we have shown that embryonic movements directly regulate lysyl oxidase activity and tendon mechanical properties during development. Our current efforts are focused on elucidating these mechanisms of mechanoregulation and developing new therapeutics for tendon regeneration based on these novel targets.

[B-10.4]

SYNOVIUM MECHANOBIOLOGY AND JOINT INFLAMMATION

Robert M. Stefani[1], Lance A. Murphy[1], Andy J. Lee[1], Lianna R. Gangi[1], Eben G. Estell[1], Roshan P. Shah[1], Clark T. Hung[2]

1 *Departments of Biomedical Engineering, Columbia University, New York, USA*

2 *Departments of Biomedical Engineering, Columbia University, New York, USA; Orthopaedic Surgery, Columbia University, New York, USA*

In addition to synthesizing lubricants and cytokines in synovial fluid, the synovium serves to govern bidirectional transport of the joint space, which defines the synovial fluid composition. Proinflammatory cytokines are upregulated with osteoarthritis (OA) and affect synovial transport properties in addition to synovium production of extracellular matrix (ECM), cell proliferation, and protein secretion [2, 8]. Fibroblast-like synoviocytes (FLS), CD14-, and macrophage synovial macrophages (SM), CD14+, [18] reside in synovium. Normal synovium is comprised predominantly of FLS, but SM number increases with joint inflammation and OA [19]. Joint flexion and extension results in changes to intra-articular pressure that result in fluid shifts into and out of the joint [13, 15]. Joint articulation gives rise to physical stimuli that influence synovial expression and production of MMPs [4, 20, 21], as well as hyaluronan secretion [10]. The mechanisms underlying synovium mechanobiology are not well-defined. Using 2D cultures and 3D biofidelic models of the synovium, we have gained insights to the influence of applied mechanical loading and pro-inflammatory cytokines on synovium function. We have observed that isolated FLS are extremely mechanosensitive to shear induced by fluid flow [4] as well as to cartilage particulates [17]. As macrophage activation and migration are altered by the physical environment [1, 7, 16], changes to synovium ECM composition and mechanical loading are likely to modulate SM function. Gap junctions are permit direct cell-to-cell communication in the synovium [11], Figure 1A. Connexin 43 expression impacts the function of FLS by contributing to the production of catabolic and inflammatory factors that exacerbate joint destruction in arthritis [12, 14]. The presence of gap junctions increases in OA synovium [6] and in synovial cells in culture subjected to interleukin [12]. Our preliminary data indicate differential shear stress sensitivity (via fluid flow [5]) as measured by intracellular calcium waves [9], where the addition of 10% SM to 90% FLS cultures significantly increased the percentage of shear-responsive cells, Figure 1B. A such, gap junction communication is preserved in vitro and that changing cell ratios may influence synovium mechano-chemical regulation [3, 19].

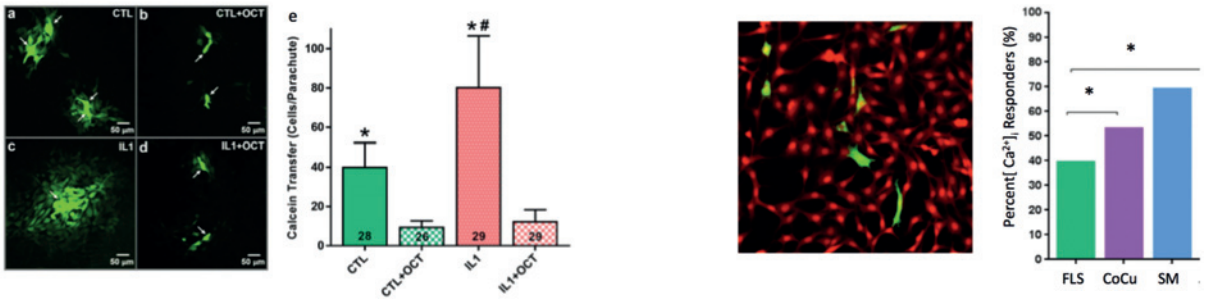

*Figure 1. A) Cell connectivity assay [22] for engineered synovium for (a) control (CTL) and (c) cultured with IL-1 where "parachuted" cells (DiI membrane staining, red, also co-stained with calcein in the cytoplasm) were dropped over layer of unlabeled synovial fibroblasts. (b,d,) Same studies with octanol (gap junction inhibitor). Interleukin (IL-1) increases bovine synovial fibroblast connectivity (4 hours). *p<0.05 vs. respective octanol group. #p<0.05 vs. untreated control. From [42]. B) SM potentiate FLS calcium response to fluid shear. Inclusion of SM (green) to FLS (red) (CoCu) increased the population percentile Ca2+ response versus FLS-only controls (FLS), but less than SM-only [119].*

Acknowledgments: OSRF and NIH/NIAMS.

References:

1. *Blakney+ J Biomed Mater Res A, 2012. 100(6): p. 1375-86.*
2. *Bondeson+ Arthritis Res Ther, 2006. 8(6): p. R187.*
3. *D'Andrea+ Biochem J, 1998. 329 (Pt 3): p. 681-7.*
4. *Estell+ J Biomech, 2017. 60: p. 91-99.*
5. *Estell+ Trans Orthop Res Soc, 2018: p. 248.*
6. *Gupta+ BMC Musculoskelet Disord, 2014. 15: p. 425.*
7. *Hind+ Integr Biol (Camb), 2015. 7(4): p. 447-53.*
8. *Hui+ Wiley Interdiscip Rev Syst Biol Med, 2012. 4(1): p. 15-37.*
9. *Hung+ J. Biomechanics, 1996. 29(11): p. 1403-1409.*
10. *Ingram+ J Physiol, 2008. 586(6): p. 1715-29.*
11. *Kolomytkin+ J Cell Physiol, 2000. 184(1): p. 110-7.*
12. *Kolomytkin+ Am J Physiol Cell Physiol, 2002. 282(6): p. C1254-60.*
13. *Levick and McDonald, Ann Rheum Dis, 1995. 54(5): p. 417-23.*
14. *Marino+ Clin Orthop Relat Res, 2004(422): p. 224-32.*
15. *Myers+ Arthritis Rheum, 1995. 38(8): p. 1085-91.*
16. *Patel+ PLoS One, 2012. 7(9): p. e41024.*
17. *Silverstein+ Osteoarthritis Cartilage, 2017. 25(8): p. 1353-1361.*
18. *Smith, Open Rheumatol J, 2011. 5: p. 100-6.*
19. *Stefani+ Tissue Eng Part A, 2019. 25(7-8): p. 538-553.*
20. *Sun and Yokota, Matrix Biol, 2002. 21(3): p. 263-70.*
21. *Sun+ Connect. Tissue Res., 2003. 44(1): p. 42-49.*
22. *Yellowley+ J Bone Miner Res, 2000. 15(2): p. 209-17.*

[B-11.1]
MACHINE LEARNING IN DRUG DEVELOPMENT

Francisco Sahli Costabal[1], Jiang Yao[2], Paris Perdikaris[3], ***Ellen Kuhl[1]***

1 *Stanford University, Stanford, USA*
2 *Dassault Systemes Simulia Corporation, Johnston, USA*
3 *University of Pennsylvania, Philadelphia, USA*

Prolonged QT intervals are a major risk factor for ventricular arrhythmias and a leading cause of sudden cardiac death [1]. Various drugs are known to trigger QT interval prolongation and increase the proarrhythmic potential [2]. Yet, how precisely the action of drugs on the cellular level translates into QT interval prolongation on the whole organ level remains insufficiently understood. Here we use machine learning techniques to systematically characterize the effect of 30 common drugs on the QT interval [3]. We combine information from high fidelity three-dimensional human heart simulations [4] with low fidelity one-dimensional cable simulations to build a surrogate model for the QT interval using multi-fidelity Gaussian process regression. Once trained and cross-validated, we apply our surrogate model to perform sensitivity analysis and uncertainty quantification. Our sensitivity analysis suggests that compounds that block the rapid delayed rectifier potassium current have the greatest prolonging effect of the QT interval, and that blocking the L-type calcium current and late sodium current shortens the QT interval. Our uncertainty quantification allows us to propagate the experimental variability from individual block-concentration measurements into the QT interval and reveals that QT interval uncertainty is mainly driven by the variability in IKr block. Our study shows an excellent agreement between predicted QT interval changes and changes observed in a randomized clinical trial for the drugs dofetilide, quinidine, ranolazine, and verapamil. We anticipate that both the machine learning methods and the results of this study will have great potential in the efficient development of safer drugs.

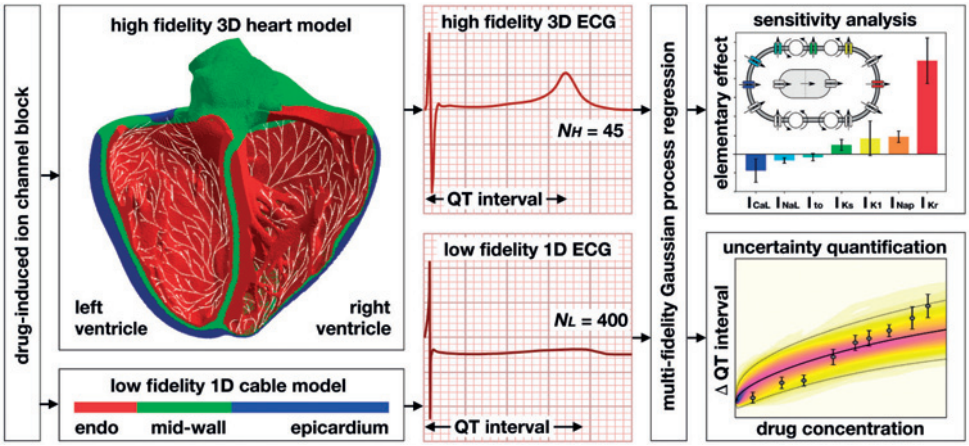

Figure Caption: Using machine learning techniques, we combine data from different levels of fidelity and characterize the effect of drugs on the QT interval.

Acknowledgments: This model was developed within the Dassault Systemes Living Heart Project as part of a collaboration with Pfizer Inc. This study was supported by the Stanford SoE Fellowship, the Becas Chile-Fulbright Fellowship, a Stanford Bio-X IIP Seed Grant, and the National Institutes of Health Grant U01-HL119578.

References:

[1] *Sahli Costabal F, Yao J, Kuhl E. Predicting the cardiac toxicity of drugs using a novel multiscale exposure-response simulator. Comp Meth Biomech Biomed Eng. 2018; 21:232-246.*
[2] *Sahli Costabal F, Yao J, Kuhl E. Predicting drug-induced arrhythmias by multiscale modeling. Int J Num Meth Biomed Eng. 2018; 34:e2964.*
[3] *Sahli Costabal F, Matsuno K, Yao J, Perdikaris P, Kuhl E. Machine learning in drug development: Characterizing the effect of 30 drugs on the QT interval using Gaussian process regression, sensitivity analysis, and uncertainty quantification. Comp Meth Appl Mech Eng. 2019; in press.*
[4] *Sahli Costabal F, Yao J, Sher A, Kuhl E. Predicting critical drug concentrations and torsadogenic risk using a multiscale exposure response simulator. Prog Biophys Mol Bio. 2019; doi:10.1016/j.pbiomolbio.2018.10.003.*

[B-11.2]
OPEN SOURCE SOFTWARE FOR SIMULATION OF HUMAN MOVEMENT

Scott Delp[1]

1 *Stanford University, Stanford, USA*

We launched the OpenSim project in 2007 to provide biomechanists with open-source tools for simulating musculoskeletal dynamics [1]. Since then, the OpenSim software has become widely used in a wide variety of disciplines (Fig 1). We recently introduced OpenSim version 4.0, which includes methods for modeling biological joints, muscles, and robotic actuators [2]. The methods are implemented in C++; their functions form the OpenSim application programming interface (API). The API is accessible via MATLAB and Python, where users can create custom models, simulations, and workflows that leverage OpenSim's algorithms. The graphical user interface (GUI) enables users to execute algorithms in the API and to visualize musculoskeletal models and simulations. OpenSim has helped researchers from diverse fields examine the functional roles of muscles in generating movement and to understand the effect of treatments on patients with gait disorders. Biomedical engineers and roboticists are using OpenSim to design and analyze assistive devices. Furthermore, OpenSim is being integrated into larger simulation and experimental projects for studying ergonomics, assistive robotics, and neurorehabilitation, where a model of human movement is essential. Our vision for OpenSim is to provide anyone with tools to gain biomechanical insights from measurements of movement and computational models. Under a permissive Apache 2.0 open-source license, everyone is welcome to use and adapt OpenSim for research and commercial endeavors.

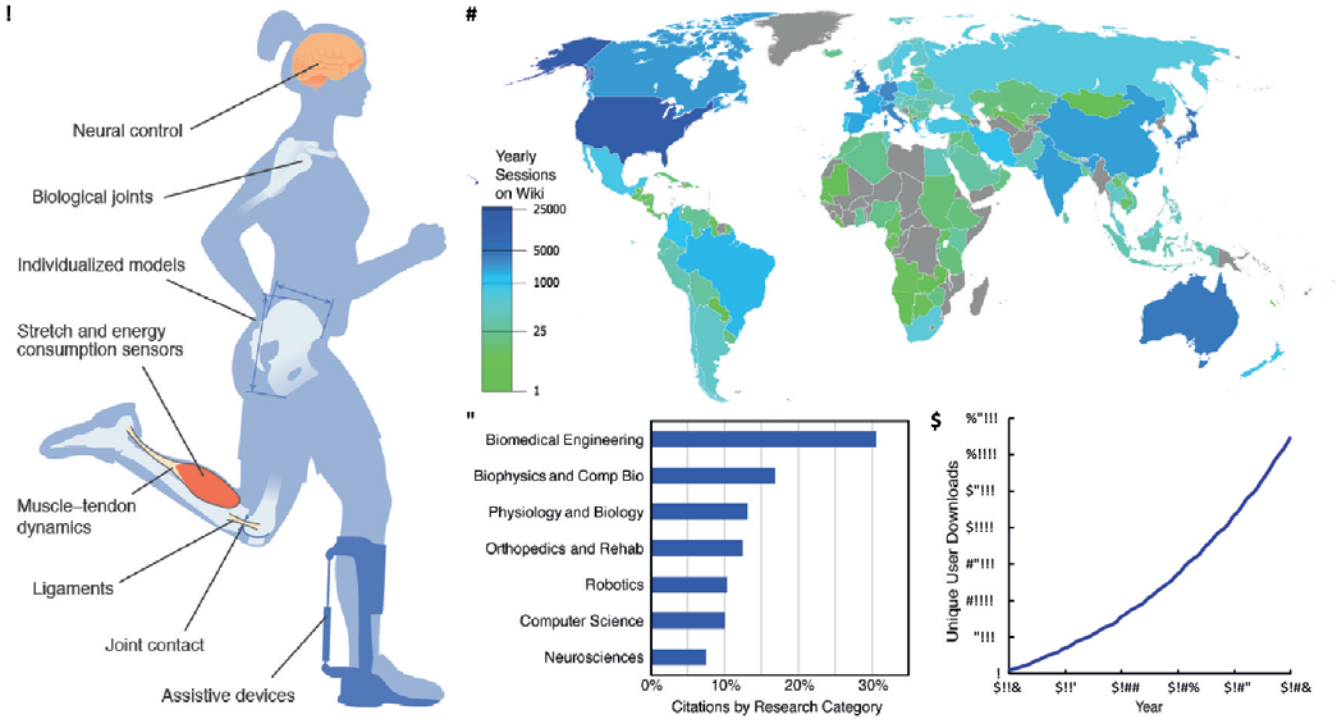

Figure 1: OpenSim components and user base. (A) OpenSim components for modeling neuromusculoskeletal and mechatronic systems. (B) Locations of users. (C) Usage of OpenSim (Web of Science). (D) Cumulative OpenSim users since its release.

Acknowledgments: I thank Ajay Seth, Thomas Uchida, Jennifer Hicks, Ayman Habib, Christopher Dembia, Nicholas Bianco, Mazen Al Borno, James Dunne, Carmichael Ong, Apoorva Rajagopal, Joy Ku for important contributions to the software and abstract and NIH P2C HD065690 for financial support.

References:

[1] *Delp, S.L., et al., (2007). IEEE Trans Biomed Eng, 54:1940.*
[2] *Seth A, et al. (2018) Plos Comp Biol 14:e100622.*

[B-11.3]
HISTORY AND OVERVIEW OF THE FEBIO SOFTWARE PROJECT

Jeffrey Weiss[1], *Steve Maas*[1], *Gerard Ateshian*[2]

1 *University of Utah, Salt Lake City, USA*
2 *Columbia University, New York, USA*

Computational modeling in biomechanics and biophysics has become a standard methodology, and the finite element (FE) method is by far the most common numerical technique that is used. Historically, the lack of a software environment that was tailored to the needs of the field hampered research progress, dissemination of research and sharing of models and results. Investigators previously relied on commercial software, but these packages were not geared toward biological applications, were difficult to verify, and precluded the easy addition, extension and sharing of new features. To address these issues, we developed the FEBio software suite, a FE framework designed specifically for analysis in biomechanics and biophysics. FEBio employs mixture theory to account for the multi-constituent nature of soft and hard tissues, unifying the classical fields of irreversible thermodynamics, solid mechanics, fluid mechanics, mass transport, chemical reactions and electrokinetics. FEBio is a true multiphysics code, tailored to the biomechanics community.

The FEBio project has been supported by NIH funding since 2007. This has provided the means to develop new computational algorithms and methodologies to meet the research needs of our target user community, and to document and distribute the software. New developments have included contact for biphasic materials [1], new element formulations [6], automatic mesh generation, chemical reactions between constituents of a mixture [2], shell elements that support passive and active solute transport [4], a plugin framework for extending FEBio and coupling it to other analysis codes [7], parallelization of key computational steps, and a novel fluid mechanical finite element formulation [3] and a fluid-solid interaction formulation. The project has met with great success, with over 10,000 registered users and over 60 citations each year to our primary reference [5].

This presentation will provide an overview of the FEBio software, its development history and the guiding principles that we follow for development, the current capabilities of the software and plans for future development.

Acknowledgments: NIH #R01GM083925, R01HL131856, and R01AR069297.

References:

[1] Ateshian GA, Maas S, Weiss JA, Journal of Biomechanical Engineering, 132(6):061006, 2010.
[2] Ateshian GA, Nims RJ, Maas S, Weiss JA, Biomechanics and Modeling in Mechanobiology, 13(5):1105-1120, 2014.
[3] Ateshian GA, Shim JJ, Maas SA, Weiss JA, Journal of Biomechanical Engineering, 140(2), 2018.
[4] Hou JC, Maas SA, Weiss JA, Ateshian GA, Journal of Biomechanical Engineering, DOI: https://doi.org/10.1115/1.4041043, 2018.
[5] Maas SA, Ellis BJ, Ateshian GA, Weiss JA, Journal of Biomechanical Engineering, 134(1):011005, 2012.
[6] Maas SA, Ellis BJ, Rawlins DS, Weiss JA, Journal of Biomechanics, 49(5):659-667, 2016.
[7] Maas SA, LaBelle SA, Ateshian GA, Weiss JA, Biophysical Journal, 115(9):1630-1637, 2018.

[B-11.4]

A FOUNDATIONAL REACTIVE MIXTURE THEORY FRAMEWORK FOR COMPUTATIONAL BIOMECHANICS

Gerard Ateshian[1], *Brandon Zimmerman*[1], *Jay Shim*[1], *Steve Maas*[2], *Jeffrey Weiss*[2]

1 *Columbia University, New York, USA*
2 *University of Utah, Salt Lake City, USA*

The field of biomechanics typically addresses the modeling of living biological tissues, fluids, and cells while accounting for mostly nonlinear phenomena, often in anisotropic and inhomogeneous media. The field of computational biomechanics today is focused on modeling such materials using multiphysics frameworks. In our approach, which has been embodied in the free finite element software FEBio (febio.org), we have used the foundational framework of reactive mixture theory to systematically model multiphysics phenomena with an increasing range of complexity. This presentation reflects on our experiences, including the challenges we have met, our milestones of success, and the future developments that we envision with this approach.

Mixture theory was formulated within the framework of rational mechanics between the late 1950s and early 1980s. Some of its earliest applications in biomechanics occurred in the late 1970s, primarily as a means of modeling porous media mechanics, with biphasic theory serving as an alternative to classical consolidation theory (poroelasticity). Starting in the 1990s, mixture theory was extended to the modeling of coupled fluid and solute transport in porous-deformable biological tissues, via the triphasic and multiphasic theories, confirming the suitability of this framework for modeling complex tissue responses.

Biphasic theory was implemented in FEBio starting in the mid-2000s, followed by multiphasic theory in the following decade. These implementations were soon extended by incorporating reactive processes, such as chemical reactions, and tissue growth and remodeling. We also came to realize that reactive processes may be used to describe the viscoelasticity of tissues, by modeling breaking and reforming of weak bonds in a reactive mixture framework. This has led us to also formulate reactive frameworks for damage mechanics in anisotropic tissues, plasticity and elastoplastic damage in metals, and fatigue failure in metals and biological tissues, using reactions to describe the yielding and damage of molecular bonds.

Moreover, a systematic reexamination of classical theories of continuum mechanics within the context of mixture theory has allowed us to formulate computational frameworks for fluid dynamics, fluid-structure interactions, and solute transport in CFD using a very succinct set of equations, leading to streamlined and robust computational implementations. Our ongoing theoretical investigations aim to extend these formulations to account for additional multiphysics phenomena, such as active transport across cell membranes, phase transformations across moving interfaces, and other similar phenomena.

These advances suggest to us that reactive mixture theory is a foundational framework for a wide range of phenomena that span classical fields as well as the multiphysics of living tissues. Our implementations in the FEBio finite element code serve as a practical application of the benefits of this framework.

Acknowledgments: FEBio is partially funded by NIH/NIGMS R01 GM083925

[C-01.1]

HYBRID AGENT-BASED/TRANSPORT MODELING OF IMMUNE CELL INTERACTIONS IN LYMPH NODES

Sarah Johnson[1], *Lowell Edgar*[1], *Daniel Watson*[1], ***James Moore***[1]

1 *Imperial College London, London, UK*

Adaptive immunity relies on a combination of biological and physical actions being carefully coordinated inside lymph nodes. Antigen-presenting cells (APCs) arriving in afferent lymph are distributed around the periphery of the node in the subcapsular sinus, and then are directed into the porous structure of the cortex by gradients in chemokine concentrations. Chemokines are produced by resident lymph node cells and rely on a combination of diffusion, advection, extracellular matrix binding, and cell-mediated modifications to establish and maintain concentration gradients. Within the cortex, APCs must then communicate effectively with T cells in sufficient numbers to generate the appropriate distribution of activated T cell subtypes. A commonly observed characteristic of this adaptation process is lymph node swelling, in which the node might grow to several times its baseline volume. However, the effects of this volume change on immune cell trafficking and chemokine transport are largely unknown. Therefore, we have developed a hybrid agent-based model – transport model to provide a better understanding of the coupled cellular/biophysical aspects of adaptive immunity. Node swelling was varied as an input parameter of maximum volume change allowed. Under baseline conditions, the dynamics of experimentally observed random walk-like behavior of T cells were reproduced. Following the initiation of a stimulus of an incoming antigen or vaccination (total duration of four days), T cell numbers increased within hours, peaked at 2.5X on day 3, and remained elevated for 10 days. T cell activation peaked at day 2, and was sustained through day 6. The differentiation and subsequent proliferation of activated T cells into effector cells began in day 4, and peaked in day 5. Production of CD4+ and CD8+ cells showed similar dynamics, and all of these behaviors corresponded well to experimental data. Allowing the node to expand up to 2.8X its baseline volume resulted in proportionally greater numbers of activated T cells. The number of effector T cells was reduced at higher maximum volumes, but this result was not robust to parameter variations. The number of CD4+ cells present in the cortex at any given time was not increased, but the total number that exited the node increased. These results indicate a potentially important role for lymph node swelling as a means for allowing not only for increased T cell numbers, but also enhanced T cell activation and subsequent differentiation. The increase in volume appears to delay the exit of the additional cells until the processes required for adaptive immunity have had time to run their course.

[C-01.2]

A CELL-BASED MODEL OF DRUG-ORIENTED TREATMENT DURING INITIAL STAGES OF PANCREATIC CANCER

Jiao Chen[1], *Daphne Weihs*[2], *Fred Vermolen*[3]

1 *Delft University of Technology, Delft, Netherlands*
2 *Technion – Israel Institute of Technology; Faculty of Biomedical Engineering, Technion-Israel Institute of Technology*
3 *Delft Institute of Applied Mathematics / Delft University of Technology, Delft, Netherlands*

Keywords: Computational modeling; Monte Carlo simulations; Pancreatic cancer; Cancer therapy

Pancreatic cancer is a fatal disease with a roughly 20% cumulative 5-years survival rate. The curable treatment for pancreatic cancer is resection, however, the surgical resection rate is 15-20%. Since pancreatic cancer is typically diagonalized late, therapeutic methods supplemented by radiotherapy and chemotherapy are the main methods to improve the prognosis. However, due to the drug toxicity as well as ethical issues in animal-based experiments, computational methods are an attractive alternative to assess the patient's prognosis.

In this study, we have developed a mathematical model of drug therapy on pancreatic cancer in the early stage. Initially, cancer cells are less invasive and they are more likely to grow into dense clusters, where they remodel the surrounding extracellular matrix into a stiff barrier from immune cells and drug delivery. The chemotaxis or/and mechanotaxis migration is simulated by setting up a large system of stochastic differential equations. Firstly, we consider the PEGPH20 treatment that enzymatically degrades the cancer-related extracellular matrix. Subsequently, the administration of the chemotherapy drug gemcitabine is modeled. Both concentrations of PEGPH20 and gemcitabine are based on Green's fundamental solutions of the reaction-diffusion equation. In addition, the impact of several input parameters is quantitatively investigated by performing Monte Carlo simulations. This results into a prediction of likelihoods of cancer cure.

The front-line therapy of pancreatic cancer normally involve the administration of gemcitabine combined with other drugs. Our simplified model is able to be extended to other drug-oriented combinations, which can benefit the extensive drug testing in clinical use. Furthermore, the time to start cancer treatment is also taken into account in the current model, and thereby it provides a possible length of the time period of administration of various therapies.

[C-01.3]

PROBING THE MECHANISMS OF MUSCLE DEGENERATION IN CEREBRAL PALSY USING AGENT-BASED MODELING

Stephanie Khuu[1], *Kelley M. Virgilio*[2], *Justin W. Fernandez*[3], *Geoffrey G. Handsfield*[1]

1 *Auckland Bioengineering Institute, The University of Auckland, Auckland, New Zealand*
2 *Department of Biomedical Engineering, University of Virginia, Charlottesville, USA*
3 *Auckland Bioengineering Institute, The University of Auckland, Auckland, New Zealand; Department of Engineering Science, University of Auckland, Auckland, New Zeland*

Cerebral palsy (CP) is a neuromusculoskeletal disorder that commonly affects movement and posture. Structural changes in CP muscles include reduced cross-sections, lengthened sarcomeres, and the development of contractures [1].

Satellite stem cells (SSCs) are essential for healthy skeletal muscle regeneration. A ~70% decline in SSCs in muscles with contracture, compared to typically developing muscles has previously been shown [1]. But SSC dynamics at the muscle level are complex and nonlinear, and a thorough understanding of these dynamics is required prior to the development of cellular level interventions. Computational modeling techniques can test levels at which SSC loss begins to impair muscle regeneration, as well as elucidate interactions between SSCs and other cellular components of skeletal muscle. Agent-based modeling (ABM) is a technique used to represent tissue adaptation at cellular and molecular levels, with the potential to depict emergent phenomena [2].

Here we demonstrate the alteration of SSC levels in an existing ABM for muscle fiber regeneration (Fig. 1), and the construction of a finite element model (FEM) from a histological section, used to provide mechanical feedback to the ABM (Fig. 2). Mechanical stimulus from a FEM was used to localize the actions of the cells present in the ABM. The macro-scale results from the ABM, following regeneration, can be used to inform the next iteration of the FEM geometry, creating a mechanobiological feedback loop.

The existing ABM was created in Repast Simphony and seeded using experimental murine studies on muscle regeneration obtained from literature. Cellular components in the ABM include inflammatory cells, SSCs, fibroblasts, and ECM. SSC levels were altered by decreasing the number of SSCs per fiber between 0.25 (healthy control) and 0, with a 0.05 decrement. SSC levels were tested at baseline and double levels of initial injury. Simulations represented injury-induced muscle regeneration over 28 days. End-point fiber count was used as a measure of muscle regeneration.

ABM was used to explore the cellular pathophysiology of CP. An 80% reduction in SSC count led to a 10% decline in regeneration in otherwise healthy muscle (Fig. 1B). Double injury altered recovery profiles and prevented full recovery at all SSC levels. The interactions between other cell types in the muscle milieu, such as fibroblasts and inflammatory cells, will be explored during the development of this model.

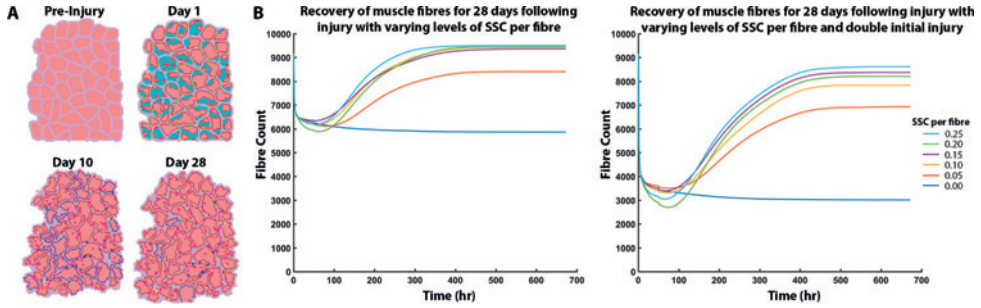

Figure 1 A) Simulation of healthy mouse muscle regeneration. B) Regeneration of muscle following typical injury and double initial injury, at different levels of SSCs per fiber.

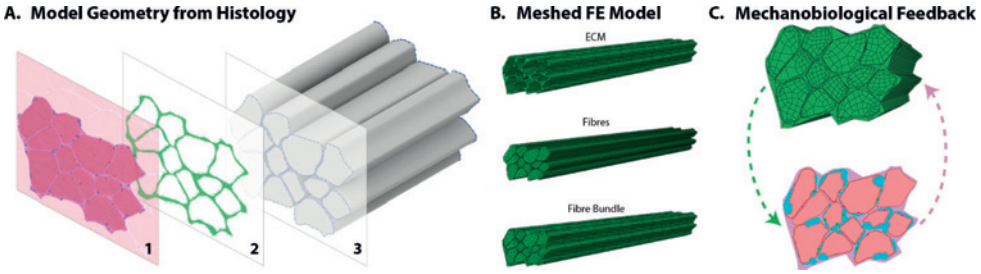

Figure 2 A) Construction of FEM geometry from histological images. B) FE meshes combined to form a fiber bundle. C) Mechanical and geometric feedback loop for the ABM and FEM.

References:

[1] Graham et al., Nat. Rev. Dis. Prim., 2:p15082, 2016.
[2] Gorochowski, Essays Biochem., 60:p325, 2016.

[C-01.4]

COMBINING IMAGING AND IN VITRO DATA WITH MATHEMATICAL MODELS TO UNDERSTAND CHEMOKINE BIOLOGY: A BAYESIAN PARAMETER INFERENCE APPROACH.

*Dimitris Kalogiros[1], Willy Bonneuil[2], Francesca Fasanella Masci[3], **Bindi Brook**[1], Matthew Russel[1]*

1 *University of Nottingham, Nottingham, UK*
2 *Imperial College, South Kensington Campus, London, UK; Royal School of Mines, London, UK*
3 *University of Glasgow, Glasgow, UK*

All protective and pathogenic immune and inflammatory responses rely heavily on leukocyte migration and localisation. Chemokines are secreted chemoattractants that orchestrate the positioning and migration of leukocytes through concentration gradients. How these gradients are formed, maintained and regulated remains unclear.

A variety of transport and biological processes are involved in the establishment, stabilisation and regulation of gradients of the chemokine CCL21 in interstitial tissue in vivo. These include CCL21 production by endothelial cells in lymphatic vessels, CCL21 transport via diffusion and advection via interstitial fluid flow, binding to the extracellular matrix (ECM) and truncation by dendritic cells (DCs). DCs exhibit both chemotaxis (by migrating up gradients of soluble chemokine) and haptotaxis (by migrating up immobilised chemokine gradients). The truncation of CCL21 and consequent unbinding from ECM modifies the gradients as the leukocytes migrate, possibly influencing subsequent DC migration.

A full mathematical model accounting for all of these processes results in a large number of parameters, most of which are currently unknown. We have thus formulated a strategy with which to systematically reduce the system both experimentally and from a modelling viewpoint. In this study we focus on CCL21 transport and CCL21-DC interactions:

(i) To estimate the transport parameters of the system we consider an advection-diffusion model of CCL21 combined with imaging data of spatio-temporal CCL21 gradients from microfluidic experiments;

(ii) To estimate the maturation rates of immature to mature DCs and truncation rates of CCL21 by DCs we develop a model of CCL21-DC interactions combined with data from an in vitro assay. Despite the seemingly simple nature of the experimental setup, the multiple interactions between cell types and CCL21 result in a system of 5 ODEs and 20 parameters.

We present a computational framework that integrates experimental data, mathematical modelling and Bayesian inference approaches. Numerical optimisation techniques and computational Bayesian methods are implemented to infer underlying parameters as well as to quantify uncertainty of the parameters.

We employed sequential Bayesian inference, in which the posterior distribution for the previous time-step used as a prior distribution for the next time-step to estimate transport parameters from the measured concentration profiles. This provides consistently tight gamma posterior distributions for both advection and diffusivity over time. The approach also allows us to quantify the uncertainty, and thus design experimental protocols that minimises inherent noise.

Application of these processes to other reductionist experiments (e.g. assays that include CCL21 binding to ECM) will enable us to build up a comprehensive parameter set underlying the relevant biological processes. Ultimately, this approach will generate a fully parametrized model which will provide broader insights into chemokine gradient formation and leukocyte migration.

[C-01.5]

COUPLING AGENT-BASED AND FINITE-ELEMENT MODELS TO SIMULATE CELL-CELL SIGNALING IN ARTERIES AND TISSUE-ENGINEERED VASCULAR GRAFTS

Tommaso Ristori[1], *David R. Nolan*[2], *Caitríona Lally*[2], *Cecilia M. Sahlgren*[1], *Sandra Loerakker*[3]

1 *Department of Biomedical Engineering, Eindhoven University of Technology, Eindhoven, Netherlands; Åbo Akademi University, Faculty of Science and Engineering, Biosciences, Turku, Finland*
2 *School of Engineering and Trinity Centre for Bioengineering, Trinity College Dublin, Dublin, Ireland*
4 *Department of Biomedical Engineering, Eindhoven University of Technology, Eindhoven, Netherlands*

The growth and remodeling of arteries in response to surrounding mechanical stimuli is largely mediated by vascular smooth muscle cells (VSMCs), which acquire a synthetic or contractile cell phenotype based on changing demands. In turn, the VSMC phenotype is regulated by Notch signaling; activation of Notch receptors on a cell membrane by Jagged ligands present on neighboring cells leads synthetic VSMCs to become contractile. Loerakker et al. [1] have recently demonstrated that Notch and Jagged expression in VSMCs decreases with cyclic strain. By incorporating this phenomenon in a one-dimensional (1D) agent-based model for Notch signaling [2], they could predict the homeostatic wall thickness of arteries at different locations of the arterial tree, indicating Notch mechanosensitivity as a fundamental mechanism regulating arterial growth and remodeling. However, in that study, the number of neighbors and local mechanical stimuli experienced by VSMCs in arterial walls were only approximated, thereby limiting the predictive potential of the agent-based model.

In the present study, we extended the 1D agent-based model to a 2D formulation, enabling the investigation of Notch signaling for VSMCs with 4 and 6 neighbors (Fig. 1A). Furthermore, the agent-based model was coupled with finite-element simulations of arteries, modeled as a fiber-reinforced Neo-Hookean material. These simulations were adopted to compute the local mechanical stimuli experienced by VSMCs in arteries and inform the agent-based model accounting for Notch mechanosensitivity (Fig. 1B).

The comparison between 1D and 2D results revealed that the number of cell neighbors does not have significant effects on the phenotype predicted for VSMCs in different arteries. This conclusion was corroborated by performing a sensitivity analysis of the model parameters. The simulations with the coupled agent-based and finite-element models revealed that, when arteries have uniform transmural mechanical properties, specific wall thicknesses induce VSMCs in the inner layer of arterial walls to acquire a synthetic phenotype, while VSMCs in the outer layer are contractile. By tuning the transmural stiffness gradient of arterial walls, while keeping the thickness constant, we could identify conditions leading to a uniform VSMC phenotype, which can be relevant for vascular graft tissue engineering.

Concluding, we developed a computational framework coupling agent-based and finite-element simulations, to simulate Notch signaling among VSMCs in arterial walls accounting for local mechanics. This framework is not only relevant to understand native arterial morphogenesis; it could also be used as a design tool for tissue-engineered vascular grafts.

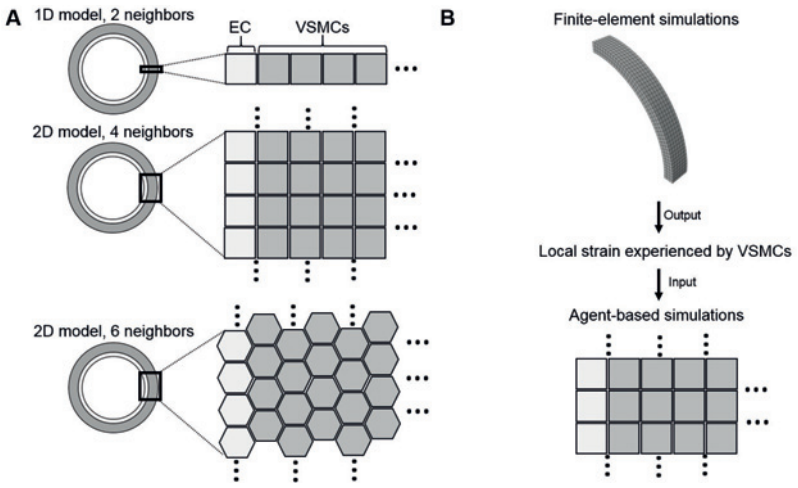

Figure Caption: (A) Scheme of the extension of the previous 1D agent-based model [1] to 2D. (B) Scheme of the coupling between the agent-based and finite-element models.

Acknowledgments: This work has been supported by the Academy of Finland, the ERC-CoG ForceMorph, and the ERC-StG MechanoSignaling.

References:

[1] *Loerakker et al., PNAS, 115(16):E3682-E3691,2018.*
[2] *Boareto et al., PNAS, 112(5):E402-E409,2015.*

[C-01.6]

LARGE SCALE TISSUE SLICE SIMULATIONS OF CORTICAL SPREADING DEPRESSION AND THE EFFECTS OF CEREBRAL CURVATURE

Allanah Kenny[1], *Michael Plank*[1], *Tim David*[1]

1 *University of Canterbury, Christchurch, New Zealand*

Neuronal activity evokes a localised increase in cerebral blood flow in a response known as neurovascular coupling (NVC), achieved through communication via the neurovascular unit (NVU). Dysfunctional NVC can lead to pathologies such as cortical spreading depression (CSD), a slow moving wave of neuronal depolarisation and high extracellular potassium levels that travels through the cortex. CSD is associated with several neurological disorders such as migraine, stroke, and traumatic brain injury.

Our research group has developed a large scale numerical model able to simulate NVC in a vascularised cortical tissue slice [1], where "In silico" experiments can be performed which are impossible in the wet-lab.

The model has been designed to run on parallel architectures with a view of building simulation size up to macro scale tissue slices. The model is extended with a spatial curvature mapping that can simulate the highly folded nature of the human cortex, where the effective extracellular diffusion rate of various ions changes depending on the curvature of the medium.

For a flat surface corresponding to a smooth murine cortex the model can simulate propagating waves of high extracellular potassium travelling radially outwards from a stimulated area at approximately 6.7 mm/min, corresponding well with experimental results [2]. The high potassium concentration induces a corresponding wave of vasoconstriction (with decreased blood flow) then slight vasodilation, achieved through cellular communication via the NVU.

For a surface with spatially varied curvature comparable to a section of human cortex, areas of positive Gaussian curvature inhibit wave propagation due to decreased extracellular diffusion rate, whereas areas of negative curvature promote propagation. Consequently extracellular potassium is observed travelling as wave segments (as opposed to radial waves seen on a smooth surface) through flat or negatively curved areas, and the CSD wave is less able to spread far throughout the cortex (see Figure). These results may provide some insight into the differences seen between human and animal experiments.

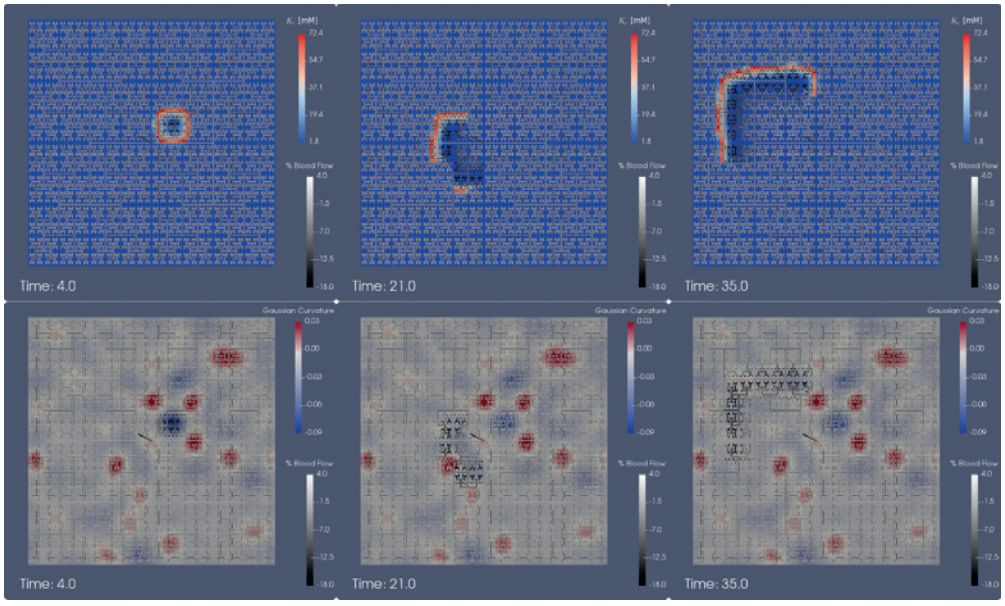

Figure Caption: An 8mm x 8mm tissue slice with spatially varied curvature simulating a curved section of a human cortex, following a stimulation input current at t=0. Top: extracellular potassium [mM], bottom: Gaussian curvature and change in blood flow.

Acknowledgments: The authors wish to thank the University of Canterbury, Christchurch, New Zealand and Brain Research New Zealand for providing funding for this project.

References:

[1] *Kenny, A., Plank, M. J. M. J., & David, T. (2018). Macro scale modelling of cortical spreading depression and the role of astrocytic gap junctions. Journal of Theoretical Biology, 458, 78–91.*
[2] *Chen, S., Feng, Z., Li, P., Jacques, S. L., Zeng, S., & Luo, Q. (2006). In vivo optical reflectance imaging of spreading depression waves in rat brain with and without focal cerebral ischemia. Journal of Biomedical Optics, 11(3), 034002.*

[C-02.1]

MACHINE LEARNING IN HUMAN MOVEMENT BIOMECHANICS: LESSONS, CHALLENGES, AND OPPORTUNITIES FOR THE FIELD

Eni Halilaj[1]

1 *Carnegie Mellon University, Pittsburgh, USA*

The recent proliferation of wearable sensors is generating large amounts of data, which, in addition to traditional laboratory experiments, offer musculoskeletal biomechanists a wealth of information on healthy and pathological human movement. Robust machine learning models could facilitate patient monitoring and optimal delivery of therapy out of the clinic, accurate prediction of treatment outcomes, and detection of gait pathologies earlier than currently possible. While the application of machine learning toward these goals is rising in recent years, rigorous reporting standards have not been established within the biomechanics community. In this talk I will highlight a set of best practices that we recently proposed after reviewing the movement biomechanics literature and encountering a few common pitfalls. These include recommendations for feature engineering and selection, parameter and hyperparameter selection, validation and testing procedures, model evaluation metrics, and steps that we can take to leverage open source libraries in Python, which are lowering the barrier to entry. These recommendations should enable critical evaluation of the published literature and make machine learning more accessible to the biomechanics community at large. I will also discuss the potential that several underexplored approaches, including deep learning, transfer learning, and semi-supervised learning, have in advancing biomechanics research. Deep learning is especially applicable and leads to better performance when large datasets are available. A related paradigm, transfer learning, allows models that have been trained on large data to be transferred to similar applications with smaller training data. Similarly, semi-supervised learning and weak supervision are paradigms that allow users to build robust models even if labels are available for only a small subset of a large dataset. These approaches are especially useful with movement data being generated through mobile devices, most of which are unlabeled. After reviewing the potential of these emerging approaches with concrete examples of biomechanics challenges to which they could contribute, I will end the talk by highlighting recent work in my research group to facilitate real-world gait analysis from wearable sensors using deep learning. This highly desirable outcome is currently limited by the reliance of traditional sensor fusion algorithms on magnetic data, which are often distorted by ferromagnetic interferences. We are leveraging data from thousands of subjects to train deep neural networks that can predict joint angles directly from inertial data, without relying on magnetic data or prior knowledge on sensor body-to-segment alignment.

Acknowledgments: I would like to thank Apoorva Rajagopal, Jennifer Hicks, Madalina Fiterau, Trevor Hastie, Scott Delp, Wolf Thomsen, and Reed Ferber for collaborating with me on this work.

[C-02.2]

DETERMINATION OF CARTILAGE BIOMECHANICS FROM TISSUE BIOMARKERS USING ARTIFICIAL NEURAL NETWORKS

Joe Rexwinkle[1], *Nicole Werner*[2], *Aaron Stoker*[2], *Muhammad Salim*[2], *Ferris Pfeiffer*[2]

1 *Army Research Laboratory, Aberdeen Proving Ground, USA*
2 *University of Missouri, Columbia, USA*

Articular cartilage provides a low-friction, damage-resistant interface between articulating bones. Arthritic diseases, in particular osteoarthritis, progress through the degradation of this tissue. The ability to accurately predict the in vivo mechanical properties of articular cartilage and to model the relationship between cartilage biology and biomechanics would have important implications for osteoarthritis diagnosis and treatment. However, these properties and their interactions are difficult to assess clinically due to the invasive nature of mechanical testing and the complexity of cartilage biology and metabolism, which is why we employed artificial neural networks. Artificial neural networks are a machine learning method capable of taking large amounts of input and target data and forging complex equations to predict the target values from the given inputs. In the current study, the tibial plateau and/or femoral condyle were collected from six patients undergoing total knee arthroplasty and 6mm osteochondral plugs were created from these samples. These samples were subjected to compressive stress relaxation testing, histological analysis, and assays for tissue composition and proteomics. Optimization in FEBio calculated the collagen modulus, ground substance modulus, and permeability of the tissue samples. Two neural networks were created: a "clinical" and "non-clinical" network. The clinical network utilized only data from non-destructive proteomics assays while the non-clinical network included data from destructive histologic and composition analysis, which would prohibit clinical application. Both networks treated the biomechanical properties as the target values. The non-clinical neural network produced a moderate correlation between the predicted and experimentally derived ground substance modulus, though it had no predictive ability for the other properties. The clinical network produced weak correlations between the predicted and experimental mechanical properties of the cartilage samples. While the predictive values of these neural networks were relatively weak, the ability to predict mechanical properties between patients with a low sample size, small homogeneous patient population, and low number of features is a promising indication for the future of machine learning methods in the field.

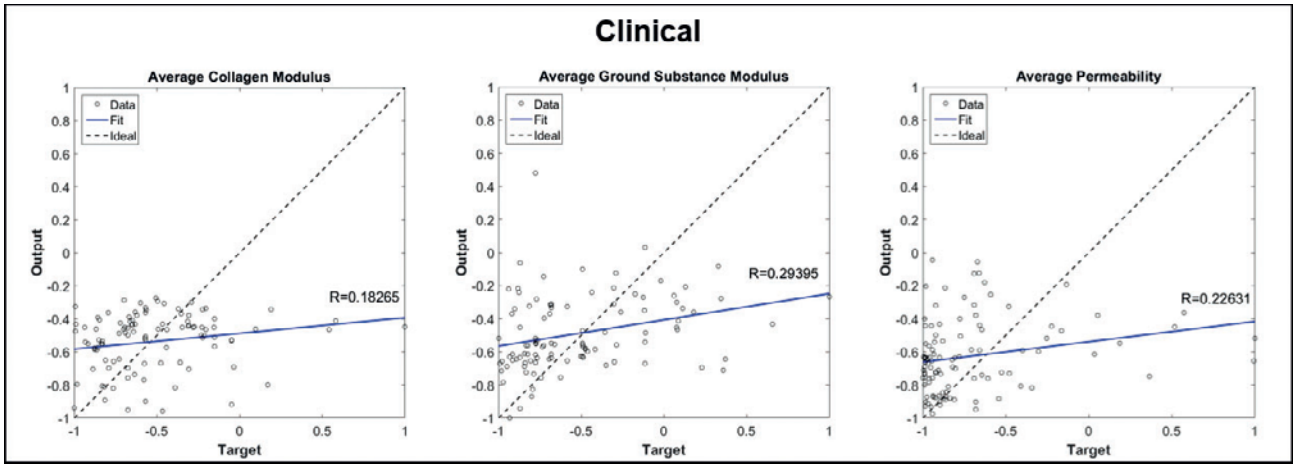

Figure Caption: Regression plots showing the fit between predicted and experimentally determined mechanical properties. The R-value represents the closeness of the fit for each mechanical property. The dashed line represents an idealized perfect match between the predicted and measured values, while the blue line shows the actual trendline of the samples. (Figure from Rexwinkle et al., 2018)

Acknowledgments: This study was funded by the Thompson Laboratory for Regenerative Orthopaedics.

References:

Rexwinkle, J.T., Werner, N.C., Stoker, A.M., Salim, M., Pfeiffer, F.M., 2018. Investigating the relationship between proteomic, compositional, and histologic biomarkers and cartilage biomechanics using artificial neural networks. J. Biomech. 80, 136-143.

[C-02.3]

A MACHINE LEARNING MATERIAL MODEL FOR SOFT TISSUE REMODELING

Wenbo Zhang[1], *Tan Bui-Thanh*[1], *Michael Sacks*[1]

1 *The University of Texas at Austin, Austin, USA*

When complex mechanical behaviors are involved, the high-fidelity multiscale methods for soft tissue constitutive modeling are attractive and predictive but are also computationally very demanding. Traditional phenomenological models have simple forms based on physical insight, but they often lack the ability to be predictive. For example, for remodeling of the bioprosthetic heart valve (BHV) leaflet biomaterials, predictive structural constitutive models have been developed for time independent and time evolving properties of exogenously crosslinked collagenous soft tissues under cyclic loading [1,2]. To simulate novel BHV designs or further identify underlying mechanisms, efficient computational methods are crucial.

Neural networks approaches are an attractive alternative attention because of their high representation capability, flexible designs, and high speed when properly trained. To this end, we investigated possible approaches to build a neural network (NN) model that can replicate the responses of detailed structural models for soft tissue with manageable computational costs. The fact that the NN model was trained on analytical model instead of experimental data helped to implicitly impose proper regularization so that the fitting problem was well-defined.

In this work, we considered a particular constitutive model; a recently developed full structural model for cross-linked soft tissue [1]. We have, for the first time, examined the possibility of constructing a NN model as a surrogate constitutive model for a high-fidelity but computationally efficient soft tissue model. We show that the results for the NN model fits the data, i.e., the strain-to-stress mapping, and it has reasonable convergence. The present NN with only 21 neurons can serves as an efficient surrogate model for detailed structural model. Therefore, the present work serves as a proof-of-concept for the use of neural networks in replicating the same response as the predictive structural model with improved efficiency. Thanks to the flexibility of the NN model, it paves the way for applying machine learning methods for simulation of soft tissues and identification its mechanical properties to much broader applications. We are currently extending it to time dependent models that include fatigue and growth for simulating the long-term behavior of soft tissues.

Acknowledgments: The authors gratefully acknowledge support of this work by NIH R01 HL142504 and R01 HL129077

References:

[1] Sacks MS et al. (2016) Interface Focus, 6(1):20150090.
[2] Zhang W & Sacks MS. (2017) J. Mech Behav Biomed Mater, 75:336–350.

[C-02.4]

DEEP LEARNNING-BASED SEGMENTATION OF MINERALIZED CARTILAGE VERSUS BONE ON HIGH-RESOLUTION MICRO-CT IMAGES

Jean Léger[1], *Lisa Leyssens*[2], *Christophe De Vleeschouwer* [1], *Greet Kerckhofs*[3]

1 *Icteam, Uclouvain, Louvain-la-Neuve, Belgium*
2 *Institute of Mechanics, Materials, and Civil Engineering, UCLouvain, Louvain-la-Neuve, Belgium*
3 *Biomechanics Lab, Institute of Mechanics, Materials, and Civil Engineering, UCLouvain, Louvain-la-Neuve, Belgium; Institute of Experimental and Clinical Research, Uclouvain; Dept. Materials Science and Engineering, Ku Leuven*

High-resolution 3D contrast-enhanced microCT (HR CE-CT) is, thanks to its high spatial and contrast resolution, powerful for the visualization of both unmineralized and mineralized cartilage, along with the bone [1]. However, it remains challenging to discriminate automatically the mineralized cartilage from the bone in both HR micro-CT and CE-CT images, as they have similar grey values. Indeed, when using only greyscale-based segmentation, it is very difficult to detect accurately the boundaries between these two mineralized tissues. Currently, manual delineation is still used to allow 3D structural analysis of both tissues. Nevertheless, this is very time consuming, user-biased and prone to errors. Interestingly, mineralized cartilage has a discriminant porous texture in comparison to bone, because of the presence of chondrocyte lacunae. Consequently, our goal was to develop an automatic mineralized cartilage segmentation tool exploiting its texture, shape and 3D consistency. This was done using a 3D convolutional neural network [2], named u-net, which is state-of-the-art for the semantic segmentation in biomedical images [3].

The datasets consisted of a 3D stack of HR microCT images of the murine bone-to-Achilles tendon interface, and we manually labeled the mineralized cartilage as ground truth. The volumes were automatically cropped around a region of interest and downsampled. The u-net model was trained using an 8-fold cross-validation (6 training sets, 1 validation set and 1 test set). Data augmentation with rotations was performed to make the algorithm robust to the mineralized cartilage orientation. The model was trained using the Dice loss, 150 epochs, a 1e-4 learning rate and a mini-batch size of two.

In Figure 1, the proposed segmentation is compared to the manual segmentation. The proposed method fits the manual segmentation well, but still shows small differences, mainly on the mineralized cartilage extremities, and few isolated false positive pixels. Nevertheless, the overlap between the proposed and manual segmentations, as measured with the 3D averaged Dice similarity coefficient on all datasets, reached 0.84. Further work will focus on addressing the remaining limitations.

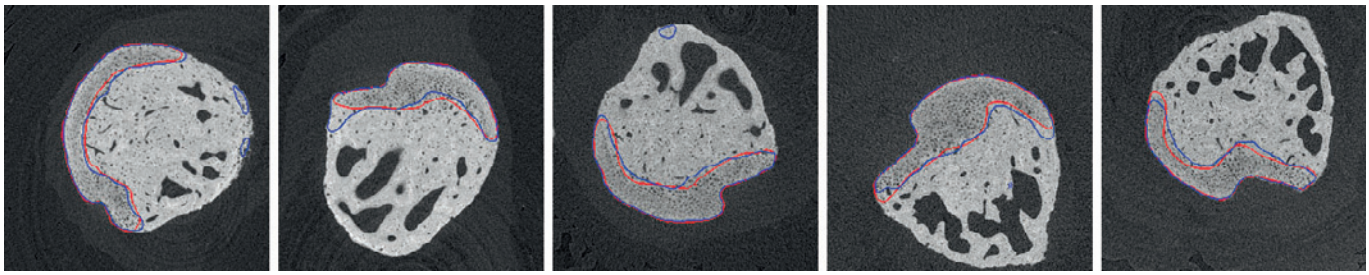

Fig.1: Qualitative comparison between proposed (blue) and manual (red) segmentations.

Acknowledgments: J.L. is a Research Fellow of the Fonds de la Recherche Scientifique (FNRS). CDV is Senior Research Associate with the Belgian F.R.S.-FNRS.

References:

1. *Kerckhofs G. et al. Eur Cell Mater. 2013. Feb 7; 25: p. 179-89.*
2. *Long, J., Shelhamer, E. and Darrell, T. 2015. Proceedings of the CVPR, p. 3431-3440.*
3. *Ronneberger, O., Fischer, P. and Brox, T. 2015. Proceedings of MICCAI, p. 234-241.*

[C-02.5]

STATISTICAL FINITE ELEMENT ANALYSIS OF THE MECHANICAL RESPONSE OF THE INTACT HUMAN FEMUR USING A WIDE RANGE OF INDIVIDUAL ANATOMIES

Mamadou Bah[1], *Reynir Snorrason*[2], *Markus Heller*[2]

1 *University of Winchester, Winchester, UK*
2 *University of Southampton, Southampton, UK*

This paper attempts to obtain an improved and more physiological distribution of the applied joint and muscle forces on the intact human femur and to gain an understanding of inter-subject variability on the mechanical response. To this end, a set of 109 CT-based femur models of individual anatomies were simulated using the Finite Element (FE) method. Heterogeneous material properties, physiological boundary and loading conditions were applied to each femur model to form a reference initial load configuration [1]. To correct the imbalance in the force system, an optimisation scheme was adopted for each model. It iteratively updated the locations of both muscle and joint attachments across a 5-mm radius circle centred at the initially defined node in the reference load configuration [2, 3]. Across the considered patient population, a 28–48% reduction in the resultant reaction force magnitude measured at the femoral head was achieved (Figure 1a – left plot). This implies that varying the nodes at which soft tissue forces were applied reduced the imbalance in the force system. A clear gender bias was present in terms of reaction forces and strains in both the initial and optimised FE models. The optimisation scheme mostly affected the medial-lateral component of the reaction force (FX) in both females and males rather than the anterior-posterior component (FY), see Figure 1a (middle and right plots). The change in the average strain was found to be highly dependent upon the percentage reduction achieved in the optimisation process. This reduction was higher for males than females and is most likely due to size differences (Figure 1b). Inter-subject variability showed that body weight and bone density highly influenced reaction forces and strains. Femoral anteversion linearly increased with reaction forces; other anatomical parameters such as neck length, neck offset, and functional femoral length or CCD angle did not have a clear influence on these forces. The present work can help in understanding the possible variability bound that can occur between patients and its impact on the design and analysis of hip replacements.

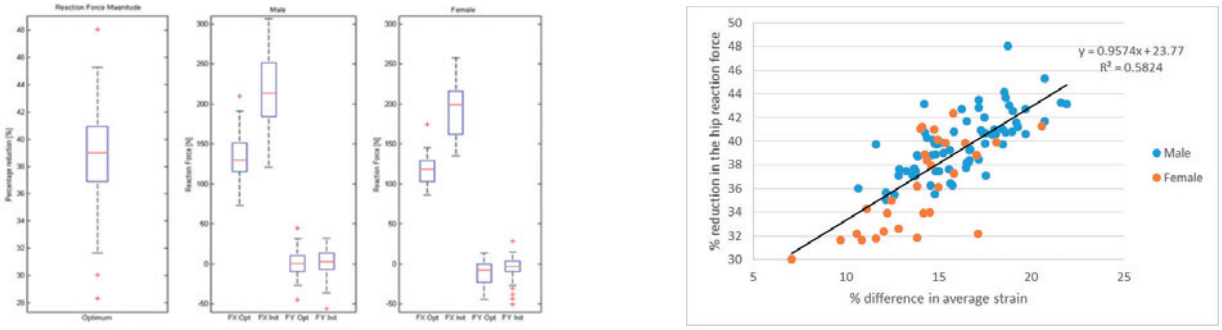

(a) *(b)*

Figure 1: Percentage reduction of hip reaction force in the optimised load configuration (a); Relationship between percentage reduction in hip reaction force and bone average strain (b).

Acknowledgments: The authors would like to acknowledge Southampton University General Hospital for providing CT scans.

References:

[1] *Speirs A. D. et al., 2007. J. Biomechanics 40(10), 2318-2323.*
[2] *Kepple T. M. et al., 1994. J. Biomechanics, 365–371.*
[3] *Matias R. et al., J. Biomechanics, 331–335.*

[C-03.1]

SHRINKING WINDOW OPTIMIZATION ALGORITHM APPLIED TO PNEUMATIC ARTIFICIAL MUSCLE POSITION CONTROL

William Scaff[1], *Marcos de Sales Guerra Tsuzuki*[1], *Oswaldo Horikawa*[1]

1 *Escola Politécnica da Universidade de São Paulo, Brazil*

The usage of robotics in the rehabilitation field is becoming more popular. But whenever a robot interacts with a human, a safety concern takes place. In this sense, Pneumatic Artificial Muscles (PAMs) are compliant actuators that can be safely used to interact with humans. Additionally, they can be made compatible with functional Magnetic Resonance Imaging (fMRI) for neurorehabilitation procedures and MRI-guided surgery. A major drawback of PAMs, however, is the precise positioning control due to its highly nonlinear dynamics. This control problem can be solved using an optimal control approach, defining an objective function and solving for the controller parameters that minimizes this function. The objective function can be evaluated using a nonlinear model of the system or the real system. Optimizing the parameters using the real system to evaluate the objective function may produce higher quality parameters, but the noise of the objective function can make this optimization difficult. The computational cost of the algorithm execution, the objective function evaluation and the type of objective function are three essential features when deciding which algorithm to use. Bayesian Optimization (BO) is a common choice for optimizing noisy objective functions with few evaluations, but is very computational intensive and does not scale well with the growing size of parameters and evaluations. This paper describes the Shrinking Window (SW) optimization algorithm, which is a gradient-free Monte Carlo method. This algorithm is used to optimize noisy objective functions without the computational overhead of the BO with a few more evaluations. The SW algorithm is compared with the BO implementation of the scikit-optimize Python library on synthetic noisy functions and in a positioning system powered by a PAM. With 100 evaluations on the synthetic noisy function, the BO algorithm takes about 2.4 hours to perform 100 optimizations in contrast with the SW algorithm which takes about 0.2 seconds. In terms of quality of the solution, the BO is about 8% better when 100 evaluations are taken with the synthetic function. In a "wall time" comparison with both synthetic functions and real system parameter optimization, the SW algorithm outperforms the BO in quality of solution. After 500 evaluations with both algorithms on the real system, SW was capable of finding the controller's optimal parameters in half of the time and with a result 5% better compared to BO.

[C-03.2]

STATISTICAL LEARNING FOR ESTIMATING CENTRAL SYSTOLIC BLOOD PRESSURE FROM CUFF-BASED BRACHIAL PRESSURE

Vasiliki Bikia[1], *Stamatia Pagoulatou*[1], *Patrick Segers*[2], *Nikolaos Stergiopulos*[1]

1 *Swiss Federal Institute of Technology, Laboratory of Hemodynamics and Cardiovascular Technology, Lausanne, Switzerland*
2 *Ghent University, Ghent, Belgium; Ibitech-Biommeda; IBiTech-bioMMeda, Ghent, Belgium*

Introduction: Central aortic pressure is an important hemodynamical quantity, carrying significant value for disease prognosis and management. The gold standard method for central pressure is a catheter-based measurement; however, its use is severely hampered by its invasive nature [1]. Available hemodynamical data have been exploited to build a regression function that maps noninvasive measurements (e.g., peripheral pressure) to central blood pressure approximations using statistical learning techniques [2]. Nevertheless, the state-of-the-art often requires recordings of the entire peripheral pressure waveform. In this study, we propose a novel method for predicting central systolic blood pressure (cSBP) using alone cuff-based brachial blood pressure from the large Asklepios study [3]. Methods: Our approach lies on cuff-based brachial systolic blood pressure (SBP) and diastolic blood pressure (DBP), and heart rate (HR) which are used to train a regression model. Concretely, the analysis was performed using a Random Forest model (RFm) and an artificial neural network (ANN). To appraise the performance of the two prediction models, we applied ten-fold cross validation on in vivo anonymized data from 1445 healthy individuals. Results: RFm achieved an RMSE of 3.19±0.03 mmHg and a correlation coefficient equal to r=0.97 (Figure 1). For the ANN, RMSE and r were reported equal to 2.74±0.02 mmHg and 0.98, respectively (Figure 2). Variability of the difference was found to be slightly higher in the case of the RFm (±3.21 mmHg, p<0.001) in comparison with the ANN (±2.79 mmHg, p<0.001). The RMSE values obtained from the two models were gathered and compared (Figure 3). Conclusion: Our results suggest that easily obtained cuff-based brachial SBP and DBP, and HR can be used to yield precise estimates of cSBP using a statistical learning model. ANN demonstrated an overall better performance compared to RFm. Further extensive validation in special conditions or disease should be conducted to allow us to deduce that our method may be potentially embedded in a clinical monitoring device.

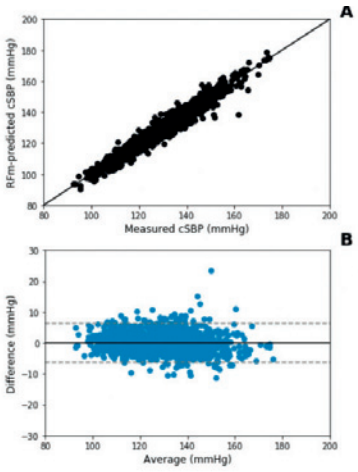

Figure 1

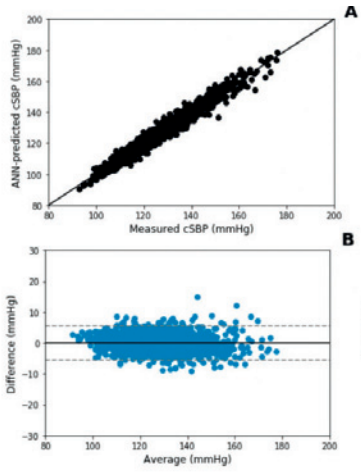

Figure 2

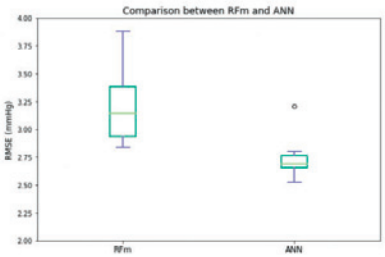

Figure 3

Figure Caption: Figure 1: (A) RFm-predicted cSBP versus measured cSBP (solid line represents equality). (B) Bland-Altman plot. Figure 2: (A) ANN-predicted cSBP versus measured cSBP. (B) Bland-Altman plot. Figure 3: Boxplot representing the RMSE values of the ten-fold cross-validation for the two prediction models.

References:

[1] *C. M. McEniery et al., "Central blood pressure: current evidence and clinical importance," Eur Heart J, vol. 35, no. 26, pp. 1719–1725, Jul. 2014.*
[2] *H. Xiao, A et al., "Estimation of aortic systolic blood pressure from radial systolic and diastolic blood pressures alone using artificial neural networks," J. Hypertens., vol. 35, no. 8, pp. 1577–1585, Aug. 2017.*
[3] *E.-R. Rietzschel et al., "Rationale, design, methods and baseline characteristics of the Asklepios Study," Eur J Cardiovasc Prev Rehabil, vol. 14, no. 2, pp. 179–191, Apr. 2007.*

[C-03.3]

PATIENT SPECIFIC CARDIOVASCULAR FLOW RESOLUTION IMPROVEMENT USING 4D FLOW MRI, COMPUTATIONAL FLUID DYNAMICS, AND MACHINE LEARNING

David Rutkowski[1], *Kevin Johnson*[2], *Shiva Rudraraju*[3], *Alejandro Roldán-Alzate*[1]

1 *University of Wisconsin, Madison, USA; Mechanical Engineering ; Radiology*
2 *University of Wisconsin, Madison, USA; Medical Physics; Radiology*
3 *University of Wisconsin, Madison, USA; Mechanical Engineering*

Hemodynamic metrics can be of great value in clinical cardiovascular disease diagnosis and treatment planning [1]. Such metrics can be derived from three-dimensional, time-resolved, velocity information that is measured with four dimensional (4D) flow magnetic resonance imaging (MRI) [2]. Yet, the flow field information provided by 4D flow MRI is often flawed due to image noise and the relatively low spatial resolution in small vascular geometries. Another flow analysis method, computational fluid dynamics (CFD), can provide much higher spatial and temporal flow resolution in even the smallest of vascular geometries. Furthermore, its basis in the governing equations of fluid flow leads to a more physics-bounded solution. However, the validity of CFD can also be limited by its heavy reliance on accurate patient specific geometries and input boundary conditions. The purpose of this work is to utilize the advantages of both 4D flow MRI and CFD, along with neural network training, to provide high resolution, physics-based, physiological flow fields in patient-specific vascular geometries. To do this, five cerebral vascular geometries were derived from high-spatial-resolution digital subtraction angiography (DSA) data. These five vascular geometries were then manually modified in 3-matic (Matrialise, Leuven, Belgium) to create 25 physiologically-plausible vascular geometry iterations. Additionally, five mock vessels were designed in Solidworks (Dassault Systèmes) to represent a wider variety of flow path configurations. The 30 vascular geometries were then imported into CONVERGE CFD Software (Convergent Science, Madison, WI), where blood flow simulations were performed at 6 different physiological-based pulsatile inlet flow waveforms, for a total of 180 simulations (Figure 1a,b). Simulation velocity output data was converted on to a Cartesian grid to be representative of a "simulated MR image". The resolution of the simulated images was then reduced and imaging "noise" was added. In current work, both the high resolution CFD flow fields and noisy, low resolution simulated MR flow fields are input to a neural network that will learn key flow features of the simulated MR data based on the high resolution flow field (Figure 2c). In the future, such data may be utilized to improve 4D flow MR images with the trained network, therefore improving the quality of flow results that can be obtained with 4D flow MRI.

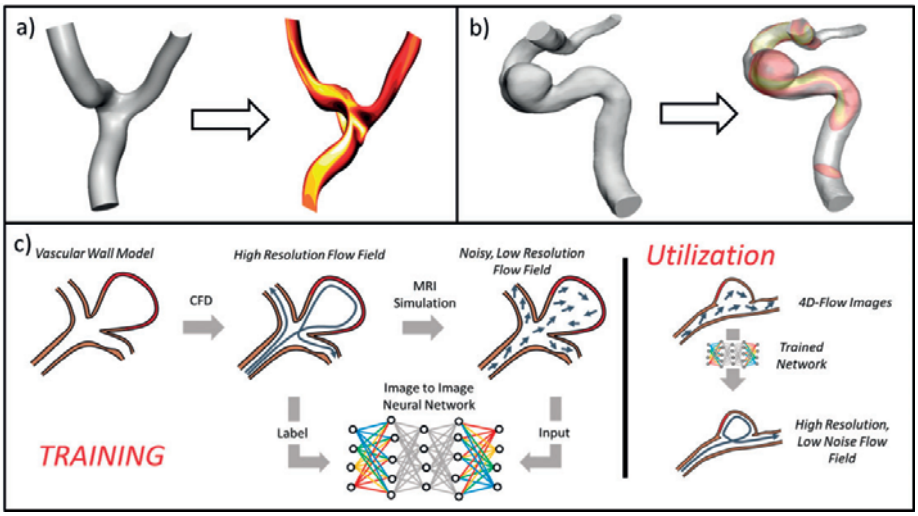

Figure Caption: Machine learning strategies will be used to improve 4D flow MRI flow data with computed flow fields from CFD. a) Mock vessel geometry and simulated flow results b) patient-specific aneurysm geometry and simulated flow field c) neural network training and utilization method overview

References:

[1] Sengupta, P. et al., 2012, JACC Cardiovasc Imaging, 5(3), pp. 305-316.
[2] Markl, M., et al., 2012, "4D flow MRI," J Magn Reson Imaging, 36(5), pp. 1015-1036.

[C-03.4]

DEVELOPMENT OF A MRI-BASED STATISTICAL SHAPE MODELLING BONE MORPHING WORKFLOW FOR THE ANYBODY GLASGOW-MAASTRICHT FOOT MODEL

Zach Welshman[1], *Claire Brockett*[1], *Graham Chapman*[2], *Michael Backhouse*[3], *Anthony Redmond*[4]

1 *Institute of Medical and Biological Engineering, University of Leeds, Leeds, UK*
2 *Leeds Institute of Rheumatic and Musculoskeletal Medicine, University of Leeds, Leeds, UK; Leeds Biomedical Research Centre, Leeds, UK*
3 *York Trials Unit, Department of Health Sciences, University of York, York, UK*
4 *Leeds Institute of Rheumatic and Musculoskeletal Medicine, University of Leeds, Leeds, UK; Nihr Leeds Biomedical Research Centre, Leeds, UK*

Introduction: Current patient-specific modeling with the AnyBody Glasgow-Maastricht (GM) foot model [1],[2] exploits computed tomography (CT) and 3D surface scans for dynamic movement analysis. This work demonstrates a magnetic resonance image (MRI) based statistical shape modeling (SSM) workflow to generate patient-specific data for the GM foot model.

Methods: MR images were acquired on 3 patients with varying Foot Posture Index (FPI) scores [3] using a 3D proton density sequence in a Siemens 3T Magnetom Verio scanner with an 8-channel foot and ankle coil and slice thickness of 0.5 mm. The talus, calcaneus, navicular, three cuneiforms, cuboid and metatarsals 1-5 were segmented using the robust statistic segmentation algorithm [4] in 3DSlicer[5]. GM foot model bones were exported from the AnyBody modelling system and converted to binary image volumes. Patient bone images were then registered to GM bone images using an iterative closest point (ICP) algorithm (shown visually in figure 1A). Using the ShapeWorksStudio[6] SSM workflow, binary image volumes were aligned using their center of mass and signed distance transforms were generated using the fast marching method. A particle based correspondence initialization and optimization algorithm was applied to the images. Principal component analysis (PCA) was initiated and meshes were then reconstructed from the optimized corresponding points, (figure 1B). The corresponding points generated from the SSM were used as the initial source and target points for the morphing. SSM mesh reconstructions and optimized points were implemented into the AnyBody GM model (figure 1C). Finally, the root mean square (RMS) error was used to measure the quality of the morphing process.

Results: A comparison of shape model meshes to patient meshes showed a minimum RMS error of 0.1 mm and a maximum RMS error of 1 mm.

Conclusion: This work demonstrates an MRI-based SSM workflow, which does not require the ionizing radiation exposure of CT, to generate representative bone geometries for patient-specific modeling. Further work could consider the sensitivity on GM model outputs including, kinematics, muscle and joint reaction forces.

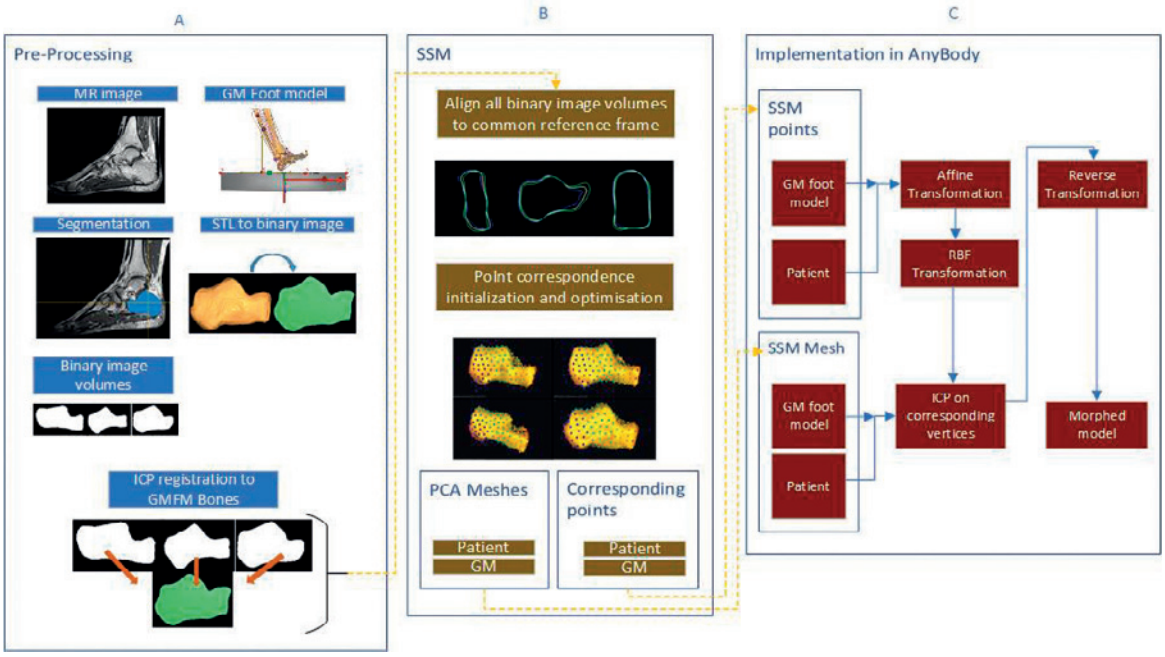

Figure 1A Pre-processing steps taken to generate binary image volumes from MR images generating STL files into binary image format for shape modeling; 1B An overview of the shape modeling process; 1C An overview of the processes involved in morphing a template geometry into a patient specific one.

Acknowledgments: This work was supported by the EPSRC grant (EP/L014823/1).

References:

[1] *Carbes, S., et al. 2011 Proc. ISB Congr. XXIII, 1–2.*
[2] *Oosterwaal M., et al. 2011 BMC Musculoskelet. Disord, 12:256*
[3] *Redmond, A. C., et al. 2008 Foot Ankle Res, 1:6.*
[4] *Gao Y., et al 2012 Med. Image Anal, 16: 1216–1227*
[5] *Fedorov, A., et al. 2012 Magn. Reson. Imaging, 30: 1323–41*
[6] *Elhabian, S., et al. 2012 ShapeWorksStudio v2.2*

[C-03.5]

IMPLEMANTATION OF DEEP DETERMINISTIC POLICY GRADIENTS FOR CONTROLLING DYNAMIC BIPEDAL WALKING

Roger Quinn[1], *Chujun Liu*[2], *Andrew G. Lonsberry*[2], *Mark J. Nandor*[2], *Musa L. Audu*[3], *Alexander J. Lonsberry*[3]

1 *Case Western Reserve University, Cleveland, USA*
2 *Department of Mechanical and Aerospace Engineering; Case Western Reserve University, Cleveland, USA*
3 *Department of Biomedical Engineering; Case Western Reserve University, Cleveland, USA*

We are developing a cyber-physical walking system (CPWS) that seamlessly integrates: (1) a person with a spinal cord injury (SCI) with intact and excitable lower motor nerves; (2) an exoskeleton with controllably locked/unlocked joints; (3) DC motors for need-dependent joint power assistance; and (4) computational algorithms that continuously and automatically learn to improve standing and walking stability.

To stabilize the CPWS, we developed a controller for bipedal walking in the sagittal plane and demonstrated it in simulation. The model is based on anthropometric data for a 1.8 m tall male of average build. At the core of the controller is a deep deterministic policy gradients (DDPG) neural network that was trained in GAZEBO, a physics simulator, to predict the ideal foot location to maintain stable walking despite external disturbances. The complexity of the DDPG network is decreased through carefully selected state variables and a distributed control system. State variables were estimated via a simulated IMU sensor attached to the torso. The step length was calculated from the relative position of the foot, and combined with accelerations to yield the ZMP. Although the biped is in a simulated environment, the acceleration measured by the IMU has noise due to the surface contact model from the physics engine and is Kalman filtered. The state is updated at the moment when the front foot contacts the ground, then it is passed to the network which returns an action. Decaying noise is added to the action chosen to promote initial exploration. The trained network decides the distance and speed of the next step based on the walking speed, torso pitch angle, step length, and ZMP position of the previous step. Additional controllers for pelvis joint movement during stance phase, and ankle joint torque during toe-off, help to stabilize the CPWS during walking. The simulated biped can walk at a steady pace of approximately 1 m/s, and can maintain stability during nominal locomotion despite a 30 N-s impulse applied forward on the torso or a 40 N-s applied rearward. A forward impulse increases its speed and step length and decreases step duration accordingly to counter the impulse. When a rearward impulse is applied, the DDPG network shortens the step length with a longer step duration to adapt to a slower speed. It also maintains stable walking with a 10 kg backpack or a 25 kg front pack. The controller is trained on a 1.8 m tall model, but also stabilizes models 1.4 m to 2.3 m tall (with mass and length properties scaled accordingly) with no changes. Furthermore, it stabilizes the 1.8 m tall model walking with 10 kg masses attached to its legs representing the exoskeleton's mass.

[C-03.6]

AGING HEALTH BEHIND AN IMAGE QUANTIFYING SARCOPENIA AND ASSOCIATED RISK FACTORS FROM CT ANALYSIS AND MACHINE LEARNING TECHNOLOGIES

Paolo Gargiulo[1], *Kyle J. Edmunds*[2], *Marco Recenti*[2], *Magnús K. Gíslason*[2]

1 *Institute for Biomedical and Neural Engineering, Reykjavík University, Reykjavík, Iceland; Department of Science, Landspítali, Reykjavík, Iceland*
2 *Institute for Biomedical and Neural Engineering, Reykjavík University, Reykjavík, Iceland*

The growing field of translational myology continually seeks to identify and optimize the generalizability of muscle assessment to clinical practice. While there are many distinct challenges in this field of research, quantifying the precise physiological impacts of mobility loss presents a current strategic priority. Despite its increasing prevalence in an ever-aging world, precise quantitative definitions for both the ætiology and health implications of sarcopenia remain debated in literature. Identifying a gold standard in this regard remains a crucial step in ultimately proving how aging health can be interrogated.

From this motivation, we developed and validated a novel method for soft tissue radiodensitometric distribution profiling, which we entitled nonlinear trimodal regression analysis, or collectively, the NTRA method for soft tissue CT profiling. This work show a comparative analysis using the NTRA method and standard soft tissue CT analysis modalities, which was implemented on parameter assemblies from the 3,162-patient AGES-Reykjavík dataset [1]. Furthermore we use machine learning approach to find connections between amplitude, location, width and skewness in fat, muscle and connective tissue and link these data to biomechanical measurements, BMI and Cholesterol. Our preliminary results highlight the specificities of each muscle quality metric to Lower Extremity functions and sarcopenic comorbidities. Machine learning approach shows predictive value for Body mass index, having as most significant features: connective and fat amplitude.

Standardizing a quantitative methodology for myological assessment in this regard would allow for the generalizability of sarcopenia research to the indication of compensatory targets for clinical intervention.

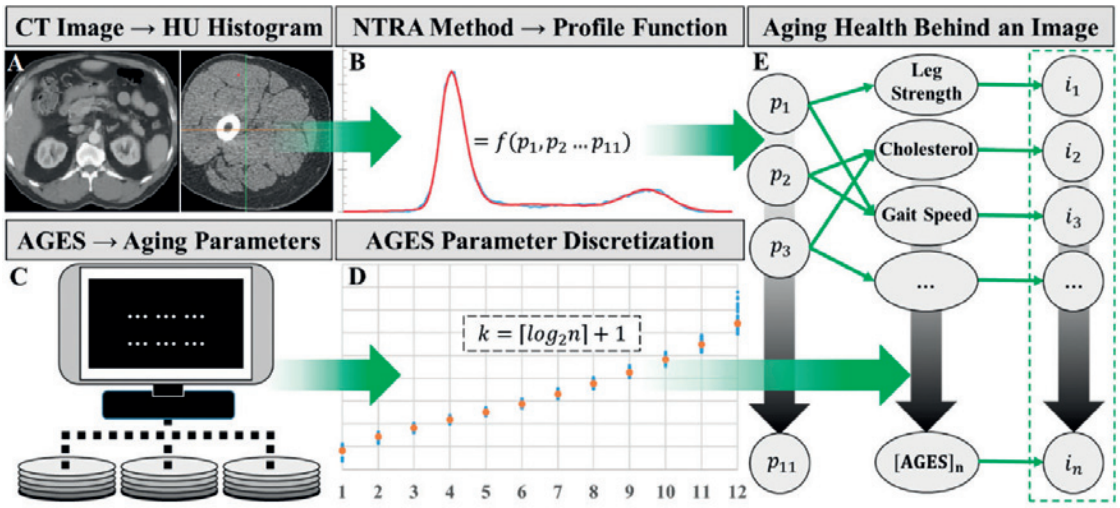

Figure Caption: Fig. 1: Workflow, illustrating the principle behind quantifying indices for aging health using our novel NTRA method for CT image HU distribution analysis. A) We begin with the linear transformation of CT images to constituent HU absorption histograms, followed by B) employing the NTRA method to generate distribution profile functions defined by 11 patient-specific coefficients ( ). C) Aging comorbidities and physiological measurements are defined from the AGES-Reykjavík dataset and D) discretized into subject groups for logistic regression. Finally, E) NTRA parameters are compared to discretized AGES parameters, implicating novel indices ( ) for aging health.

References:

1. *Edmunds K, GõÂslason M, Sigurðsson S, Guðnason V, Harris T, Carraro U, et al. (2018) Advanced quantitative methods in correlating sarcopenic muscle degeneration with lower extremity function biometrics and comorbidities. PLoS ONE 13(3): e0193241. https://doi.org/ 10.1371/journal.pone.0193241*

[C-05.1]

TOWARD A PATIENT-SPECIFIC IMAGE DATA-DRIVEN PREDICTIVE MODELING FRAMEWORK FOR GUIDING MICROWAVE ABLATIVE THERAPY

Michael Miga[1], *Jarrod Collins*[1], *Jon Heiselman*[1], *Daniel Brown*[2]

1 *Vanderbilt University, Nashville, USA, Department of Biomedical Engineering*
2 *Vanderbilt University, Nashville, USA Medical Center, Department of Radiology*

In this work, we report on a preliminary effort toward a novel multi-physics framework that combines computational approaches in soft-tissue biomechanics, and biotransport to create a patient-specific, image-data driven, guidance platform to improve localization and predict thermal dose delivery for microwave thermal ablation. More specifically, the approach begins with the use of standard preoperative magnetic resonance imaging that allows for the modeling of patient-specific organ shape followed by the acquisition of an additional fat quantification sequence (mDixon Quant) which allows for the establishment of patient-specific dielectric and thermal properties. With bioelectric and bioheat patient-specific planning models established, accurate predictions of thermal dose can be created. With dose prediction capabilities realized, the process moves on to an image-guided approach for delivery. In order to translate preoperative dose estimates to guide procedures, it is important to be able to deliver a microwave antenna to the appropriate position determined by planning. Within open, laparoscopic, or percutaneous ablative procedures, often deformation of soft-tissue organs during the procedure can compromise guidance accuracy. As part of this multiphysics framework, a soft-tissue biomechanical model is then used in combination with sparse geometric digitization data to account for deformation and provide an accurate image-to-physical registration.

To investigate, we demonstrate the novel framework in realistic liver phantoms. Briefly, phantoms were created with varying fat content between 0-10%, a range quite similar to that found in fatty liver disease. Microwave ablations were then created physically and in silico with the latter being 'tuned' by previously acquired fat quantification images. To evaluate, overlap of the physical ablation and computationally predicted were measured. The model-predicted ablation zones showed compelling overlap with observed ablations in both the validation phantoms (93.4 ± 2.2%) and the leave-one-out cross validation study (86.6 ± 5.3%). With respect to localization, our biomechanically-driven image-to-physical registration methodology to correct for deformation has been equally encouraging. In the case of partial surface availability for registration, the average target registration error was 6.0 ± 2.3 mm and 3.7 ± 1.4 mm for rigid, and nonrigid registration. When the full surface of the liver could be used, the average target registration error was 5.6 ± 2.3 mm and 2.5 ± 1.1 mm for rigid, and nonrigid registration (see Figure 1). Similarly, when comparing the predicted ablation relative to ground truth, the volumetric overlap was 67.0 ± 11.8%, and 85.6 ± 5.0% for rigid, and nonrigid registration, respectively. This multiphysics framework demonstrates, as a proof-of-concept, that physical modeling parameters can be linked with quantitative medical imaging to improve the utility of predictive procedural modeling for microwave ablation as well as improve localization.

Acknowledgments: This work was supported by the National Institutes of Health with awards R01CA162477 from the National Cancer Institute and T32EB021937 from the National Institute of Biomedical Imaging and Bioengineering.

[C-05.2]

COMPUTER-ASSISTED SURGERY FOR EVAR PROCEDURES: COUPLING 2D PERIOPERATIVE IMAGES WITH 3D MECHANICAL MODELS

Aymeric Pionteck[1], *Baptiste Pierrat*[2], *Sébastien Gorges*[3], *Jean-Noël Albertini*[4], *Stéphane Avril*[5]

1 *University of Lyon - Mines Saint-Etienne, Saint-Etienne, France; Inserm U1059*
2 *University of Lyon - Mines Saint-Etienne, Saint-Etienne, France; Inserm U1059; Center for Biomedical and Healthcare Engineering, Mines Saint-Étienne, France*
3 *Thales, France*
4 *Chu Saint-Etienne, France*
5 *University of Lyon - Mines Saint-Etienne, Saint-Etienne, France; 2école des Mines de Saint-Étienne, Université de Lyon, Lyon, France*

Abdominal aortic aneurysms are major cardiovascular diseases. Minimally invasive procedures such as Endovascular Aneurysm Repair (EVAR) are particularly well adapted to their treatment and are performed daily in modern-hospitals. However, complications and reinterventions are still prevalent because of endograft misplacement or misalignment [1]. The following work aims at improving the procedure outcome by simulating and displaying a full spatial 3D configuration of the stent-grafts inside the aorta before and during deployment, in real time throughout the surgery, based on constraints derived from the perioperative imagery.

Methods: In this research, we present a fast 3D simulation of the deployment of a stent-graft based on a finite element model and a single 2D perioperative image of the stent graft. The deformed configuration of each stent is parametrized by a combination of 7 parameters corresponding to rotation, translation and radial expansion. Some of these features can be found directly on perioperative images. The other parameters are determined with a combination of geometric assumptions and a mechanical model. The equilibrium configuration of the structure is computed by a finite element model built from the preoperative CT-scan and constrained with data extracted from perioperative images. To validate our method, EVAR surgery was simulated in a hybrid room: a stent graft was deployed in a 3D printed phantom of an abdominal aorta aneurysm. Then, the configuration of the stent-graft obtained from our method is compared to the reconstructed stent graft generated from rotational angiography.

Results: For these preliminary results, three types of errors are used to measure the precision of the simulation.

The mean stents position error in the perioperative images projection plane is 1.0±0.5mm; the mean stents position error out of the projection plane is 2±1mm. The mean relative diameter error is 5±6 %. Computation time is under 30s.

Discussion: According to surgeons, the acceptable accuracy for stent positioning is less than 5mm. Our method therefore offers a high precision on the positioning of stents in the projection plane. Accuracy is lower outside the projection plane but still acceptable. Our method provides a reliable visual rendering that can be used by surgeons to efficiently assist the surgeon and improve the precision of the stent-graft deployment. Thanks to its very low computational cost, our method can be run in real time which will be essential for clinical applications.

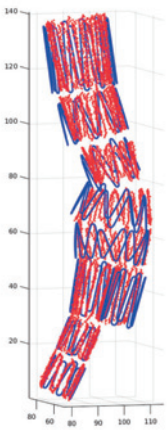

Fig. 1. In red the target from the phantom, in blue the reconstruction. Qualitative comparison of the segmented stents and reconstructed stents

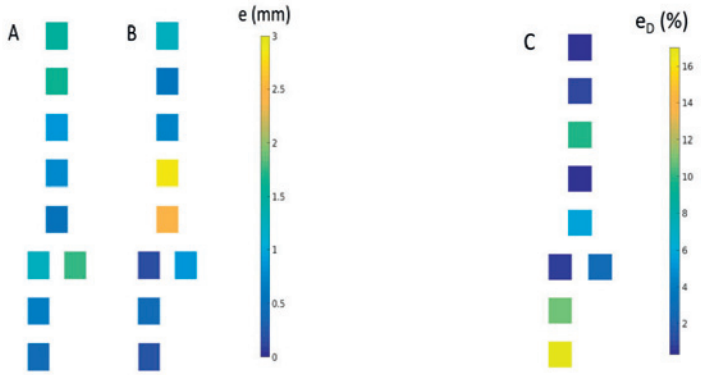

Fig. 2. Stent by stent errors: errors (e) in projection plan (A), depth errors out of the projection plan (B) and relative diameters errors (eD) (C). Each square is one stent. The error for each stent is coded by the color of the square

References:

[1] „Endovascular versus Open Repair of Abdominal Aortic Aneurysm". The United Kingdom EVAR Trial Investigators. N Engl J Med, 362:1863-1871, 2010

[C-05.3]

TEMPLATE-BASED RECTIFICATION AND REGISTRATION FOR IMAGE-GUIDED SPINE SURGERY

*Yunliang Cai[1], Xiaoyao Fan[2], Sohail Mirza[2], Keith Paulsen[2], **Songbai Ji**[1]*

1 *Worcester Polytechnic Institute, Worcester, USA*
2 *Dartmouth College, Hanover, USA*

Accurate and efficient patient registration is critical for surgical image guidance. Spine patient registration is particularly challenging because of the spine's complex geometry, limited options for intra-operative imaging, and vertebral motion during surgery. Recently, an intraoperative stereovision (iSV) system was developed [1][2] to provide low-cost, fast intra-operative imaging. However, registration between iSV and pre-operative CT is cross-modality and surface vs. volumetric, making conventional iterative registration methods ineffective [1]. Our previous approach using non-linear principal component analysis [3] achieved sufficient registration accuracy. However, it was computationally inefficient. Here, we present a template-based technique to improve efficiency while maintaining the same level of accuracy.

The proposed method includes the following key steps, which are graphically summarized in Fig. 1.

- Template Registration: A CT volume and 5 iSV images are manually segmented (one-time effort) to serve as vertebral templates for rigid registration with target CT and iSV of interest, respectively.
- Transverse Process (TP) Identification: TPs on a target image are identified by mapping those on the templates.
- Plane Approximation: A 3D plane is fitted using points of the extracted TPs. This step significantly improves efficiency relative to our prior method [3] (from 5-10 min to <10 seconds).
- Rectification: Spine surface points from iSV/CT are projected onto the plane to obtain 2D projection images, whose intensity encodes the topological surface heights [3].
- Image Registration: The projected 2D images are rigidly registered via cross-correlation [3] to provide iSV-CT point-to-point correspondences.
- 3D Registration. The point-wise correspondences allow direct, closed-form 3D registration.

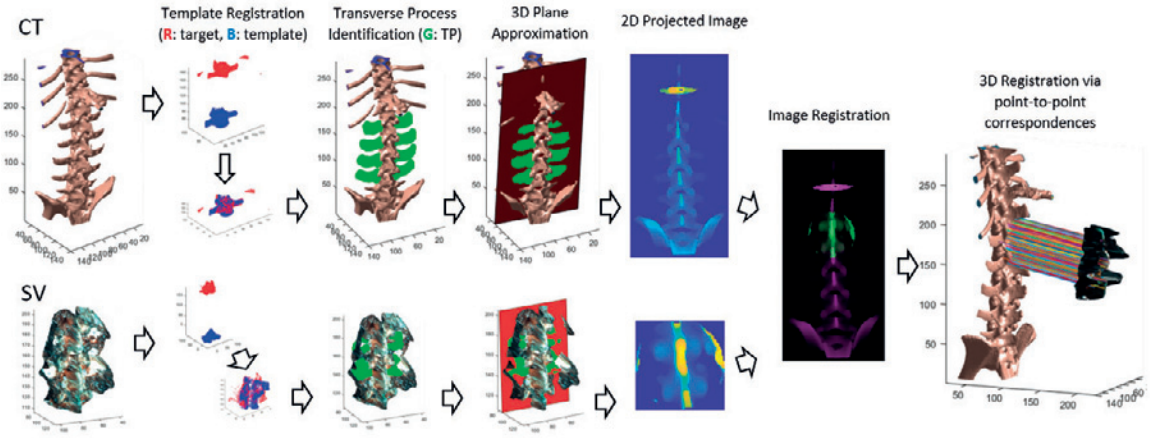

Figure 1. Summary of the iSV-CT spine patient registration procedure.

The technique was tested on five live porcine experiments (IRB approved). Mini screws were implanted in the porcine vertebra to measure target registration error (TRE), which is summarized below.

	Case 1	Case 2	Case 3	Case 4	Case 5
# of screws	20	21	24	18	22
Avg. TRE (mm)	1.63	1.87	2.01	1.76	1.79

Acknowledgments: NIH Grants R01 EB025747, R21 NS078607.

References:

[1] *L. Evans, et al, Stereovision Co-Registration in Image-Guided Spinal Surgery: Accuracy Assessment Using Explanted Porcine Spines, Operative Neurosurgery, Vol.15, Issue 6, Dec 2018, p686–691.*
[2] *S. Ji, et al. Patient Registration Using Intraoperative Stereovision in Image-guided Open Spinal Surgery. IEEE TBE. 2015;62(9):2177-86.*
[3] *Y. Cai, et al, Automatic geometric rectification for patient registration in image-guided spinal surgery, Proc. SPIE 9786, Medical Imaging, 2016*

[C-05.4]

FINITE ELEMENT ANALYSIS FOR GUIDING INTERSTITIAL LASER THERAPY OF BONE TUMORS IN AN ANIMAL MODEL - A COMPUTATIONAL STUDY

Emily Oakley[1], *Yekutiel Katz*[2], *Gal Dahan*[2], *Zohar Yosibash*[2], *Gal Shafirstein*[1]

1 *Photodynamic Therapy Center at the Department of Cell Stress Biology, Roswell Park Comprehensive Cancer Center, Buffalo, NY , USA*
2 *Computational Mechanics and Experimental Biomechanics Lab, School of Mechanical Engineering, The Iby and Aladar Fleischman Faculty of Engineering, Tel Aviv University, Tel Aviv, Israel*

About 50% of advanced cancer metastasize to bones and induce sever pain. Radiation therapy, the standard of care for these tumors, is associated with a risk of bone fracture. Local thermal ablation can significantly reduce pain and provide local tumor control. Interstitial light thermal therapy (ILTT) may be used to minimize morbidity and pain, but its impact on bone strength is unknown. Computed tomography (CT)-based finite element (CTFE) methods have been shown to well determine bone strength in human femurs [1,2]. Image-based finite element method (FEM) modelling has been shown to guide interstitial laser light therapy in preclinical studies [3]. The goal of this computational study was to explore the possible use of New Zealand White (NZW) rabbits with VX2 bone tumors to study ILTT. This talk presents preliminary results on the CTFE analysis (Figure 1) that determines the bone strength in the presence of tumors, and FEM computation of the temperature distribution in New Zealand white rabbit femur induced by ILTT (Figure 2). Preliminary results on the determination of NZW femur mechanical properties will also be presented.

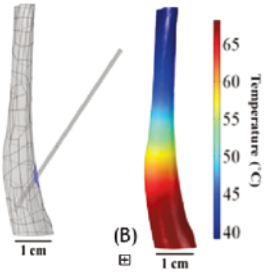

Figure 2. (A) The FEM mesh of the bone including a laser fiber. (B) The corresponding temperature distribution. The laser settings: 665-nm, 200 mW and 540 Joule. Optical properties: absorption coefficient = 11.4 [1/m], reduced scattering coefficient = 765 [1/m].

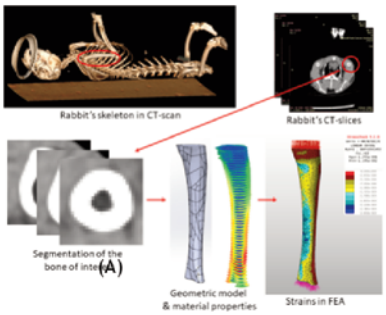

Figure 1. CT scan of a rabbit, segmentation of one of its humeri and CTFEA simulation of a compressive load – color bottom left figures show material distribution in each CT slice and compressive principal strains.

Acknowledgments: Supported in part by Roswell Park Comprehensive Cancer Center Support Grant P30CA16056. We thank Diane Filippini and Raymond Wasielewski for their assistance in obtaining the CT scans. We thank Drs. Sexton and Curtin and the staff of Laboratory Animal Shared Resource at Roswell Park. We thank M. Habitzruther, H. Cooper and L. Tworek for assisting us in collecting discarded rabbit bones.

References:

[1] *Yosibash Z, Plitman Mayo R, Dahan G, Trabelsi N, Amir G, Milgrom C. Predicting the stiffness and strength of human femurs with real metastatic tumors. Bone. 2014;69:180-90.*
[2] *Sternheim A., Giladi O., Gortzak Y., Drexler M., Salai M., Trabelsi N., Milgrom C. and Yosibash Z., "Pathological fracture risk assessment in patients with femoral metastases using CT-based finite element methods. A retrospective clinical study", Bone, 2018;110:215-220.*
[3] *Shafirstein G, Bellnier DA, Oakley E, Hamilton S, Habitzruther M, Tworek L, Hutson A, Spernyak JA, Sexton S, Curtin L, Turowski SG, Arshad H, Henderson B. Irradiance controls photodynamic efficacy and tissue heating in experimental tumours: implication for interstitial PDT of locally advanced cancer. Br J Cancer. 2018;119(10):1191-9.*

[C-05.5]

ASSESSING NASAL SYMMETRY USING MOBILE 3D SCANNING TECHNOLOGY FOR RECONSTRUCTIVE PLASTIC SURGERY

Zachary Fishman[1], *Amanda Hope*[2], *Allan Billig*[3], *Jeff A Fialkov*[4], *Cari Whyne*[5]

1 *Sunnybrook Research Institute, Toronto, Canada; University of Toronto, Canada*
2 *Sunnybrook Research Institute, Toronto, Canada*
3 *Sunnybrook Health Sciences Center - Plastic Surgery, Toronto, Canada*
4 *Department of Surgery, University of Toronto, Canada; Sunnybrook Health Sciences Center - Plastic Surgery, Toronto, Canada*
5 *Sunnybrook Research Institute, Toronto, Canada; Institute of Biomaterials and Biomedical Engineering, University of Toronto, Canada; Department of Surgery, University of Toronto, Canada*

Symmetry of the facial anatomy is key to both form and function. As such, symmetry restoration is an essential goal in facial reconstructive surgery secondary to severe traumatic injury (e.g. vehicular accidents or military trauma). In particular, the nose is a focal point of a patient's face and an unsatisfactory restoration of symmetry can impact an individual's psycho-social wellbeing and breathing. Currently, the ability to intraoperatively accurately measure nasal symmetry and displacement is limited to visual assessment with rulers yielding errors in the range of up to 2-3 mm. In this work, an algorithm was developed to use new mobile 3D scanning technologies that enable intra-operative quantification of facial and nasal symmetry. The iPhoneX has introduced miniaturized infra-red facial depth sensing cameras (i.e. FaceID) into a portable form factor at a relatively low cost compared to existing systems. Bellus3D's FaceApp is a mobile software application developed to leverage the iPhoneX's FaceID camera to rapidly capture 3D faces scans. The measurement workflow developed automatically evaluates nasal symmetry from a facial 3D scan generated from the iPhoneX's FaceID camera and the FaceApp output. The scan geometry was tilt corrected with iterative closest point registration to an average face aligned to the orthogonal planes. The nasal region was magnified for the surgeons' viewing and the asymmetry is evaluated as the maximum distance from the medial plane along the dorsum to the nose tip. The measured nasal asymmetry with the mobile scanning tools was compared against a surgeon's qualitative assessment of asymmetry as well as quantifiably compared against non-mobile clinical 3D scanners (Vectra M3, Canfield Scientific), which cannot be used intraoperatively. Real time assessment of nasal symmetry enables the plastic surgeon to rapidly adjust their work in progress and the algorithms developed provide a low cost, accessible mobile tool to help restore symmetry for improved nasal reconstruction.

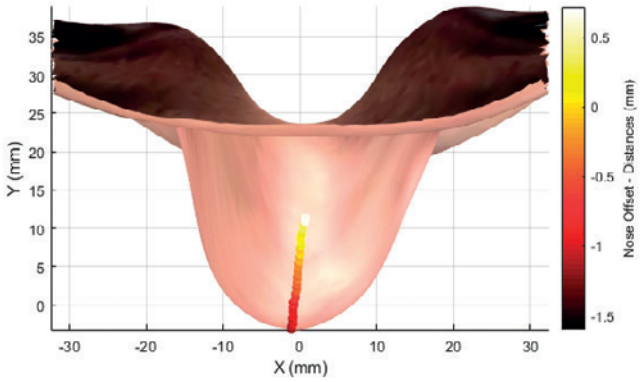

Figure Caption: Top view of nasal asymmetry distance measurement algorithm on 3D scan captured from iPhone X. Color scale corresponds to millimeters away from medial plane.

[C-06.1]

INVESTIGATION OF PELVIC SYMMETRY AND THE DEVELOPMENT OF 3D PELVIC MODELS USING CAD SOFTWARE

Maha Ead[1], ***Lindsey Westover***[1], *Kajsa Duke*[1]

1 *University of Alberta, Edmonton, Canada*

Introduction: Fractures in the pelvic bone are often quite complex, as the bone may be split into several small pieces, making it difficult to distinguish them from surrounding matter. Treatments of such fractures involve fitting metal plates, but in severe cases, where the bone may be shattered, customized plates need to be designed. In order to assist with the development of these custom plates, patient-specific 3D pelvic models must be developed. This can be done by modelling the fractured bones and connecting them to recreate the pelvis. The assumed symmetry of the intact pelvis may be useful in reconstructing a fractured pelvis in cases where one side is unaffected.

Objectives:

- Evaluate left-right symmetry of the intact pelvis.
- Virtually reconstruct fractured pelvis models using the assumed symmetry.

Method: CT scans of n=14 intact pelvises were imported into Materialise-Mimics software to segment the pelvic bone and create a 3D model. The 3D models were then exported to Geomagic in order to compare symmetry of the left and right sides. The left side of each pelvis was reflected across the sagittal plane and aligned with the right side by minimizing the distance between two parts. Geometrical deviations between both surfaces (reflected left side and right side) were then determined by conducting a 3D deviation analysis.

A CT scan of one patient case study with a fractured pelvis was imported into Materialise-Mimics to create 3D models of the fractured bone pieces. The unbroken side of the pelvis was exported to Geomagic and reflected to serve as a template for reconstructing the broken side. The broken side was also exported to Geomagic and reconstructed by using the "N-point Alignment" function where points on either of the broken pieces are selected and mated together. A 3D deviation analysis was then conducted between the reconstructed side and the reflected side to evaluate symmetry of the reconstructed pelvis.

Results: The average RMS value for the intact pelvises and fractured pelvis was 1.16 mm and 1.73 mm, respectively. The average percentage of points between a ± 2 mm deviation for the intact pelvises and fractured pelvis was 91.4% and 80.1%, respectively.

Conclusion: Results show that most deviations in both cases are within 2 mm. This suggests that the pelvis is indeed symmetric, and this concept can be used to model a fractured pelvis.

Patients with pelvic fracture often endure delayed treatment due to time taken in analyzing their specific cases. This work will provide a better treatment for these patients by offering quicker treatment proposals and easing the design process of the custom plates.

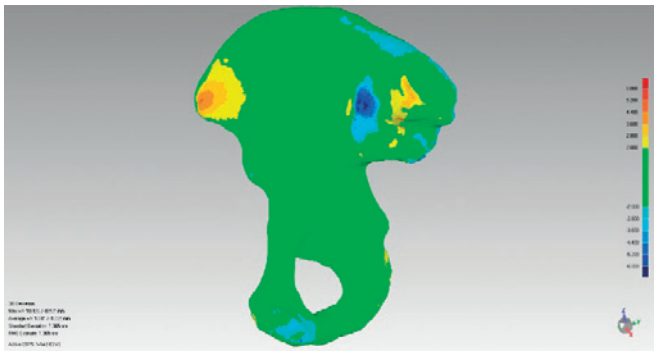

(a)

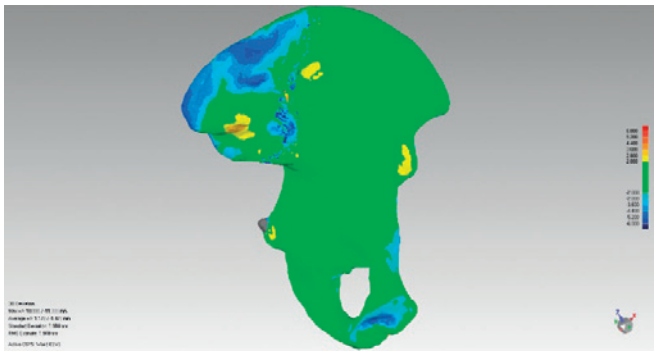

(b)

Figure Caption: Deviation Color Map for Intact Pelvis (a) and Fractured Pelvis (b)

Acknowledgments: Funding provided by NSERC

[C-06.2]

BIOMECHANICAL STRESS CHANGES ON FOREFOOT AND HINDFOOT CAUSED BY THE MEDIALIZING CALCANEAL OSTEOTOMY AS ADULT ACQUIRED FLATFOOT DEFORMITY TREATMENT

Christian Cifuentes[1], *Ricardo Larrainzar-Garijo*[2], *Javier Bayod*[1]

1 *Applied Mechanics and Bioengineering Group (AMB), Aragón Institute of Engineering Research (I3A), Universidad de Zaragoza, Zaragoza, Spain*
2 *Orthopedics and Trauma Department, Surgery Department – Hospital Universitario Infanta Leonor - Madrid, Spain*

The medializing calcaneal osteotomy (MCO) is one of the most common treatments applied to correct adult acquired flatfoot deformity (AAFD) in stages II and III [1, 2]. The structural correction that is achieved with this procedure is widely known [2]. However, changes of the biomechanical stress that this procedure causes in both forefoot and hindfoot have not been sufficiently studied. The objective of this study was to evaluate the biomechanical stress generated by MCO in these foot regions, using a validated computational model of the human foot [1-3]. The finite element model was reconstructed from computerized tomography images of a healthy patient. A 10mm-MCO was generated, modifying the geometry of the calcaneus bone. The model includes the geometry of all the foot bones, the plantar fascia, cartilages, plantar ligaments, Posterior tibialis tendon (TPT), Peroneus tendons and Achilles tendon, respecting their anatomical distribution and biomechanical properties [3]. The simulations were carried out emulating mid-stance support phase of the gait cycle and generating some pathological scenarios related with the AAFD before and after applying MCO: TPT failure and TPT, plantar fascia (PF) and Spring ligament (SL) failures [3-4]. The tissues failures were simulated removing each one to the model. The simulations were evaluated comparing the stress maximum values of each simulations with the bone stress generated in a healthy foot. Results show that MCO reduces the biomechanical stress in both forefoot and hindfoot. However, it generates some stress concentrations around the osteotomy region, which increases when it is used to treat the AAFD caused by failure of soft tissues that support the plantar arch (fig.-1). Additionally, MCO generates a notable stress increase in both third and fourth metatarsals (fig.-2). Therefore, we conclude that MCO helps to reduce both forefoot and hindfoot bones stresses caused by itself, because this procedure increases the foot supination, reducing the pronation of the hindfoot. However, it should be applied carefully in patients with diagnosis of failure/weakness of the soft tissues that supports the plantar arch, because there is a higher risk of bone fracture around the osteotomy region. Finally, increment of the metatarsals stress could explain the long-term pain that patients report after applying MCO as treatment to correct AAFD.

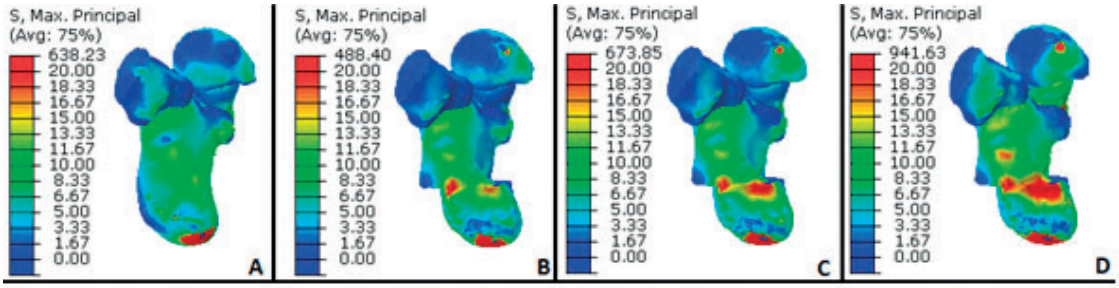

Figure 1: Stress maximum in hindfoot. A) Healthy, B) MCO, C) MCO-TPT-failure. D) MCO-TPT-PF-SL-failures.

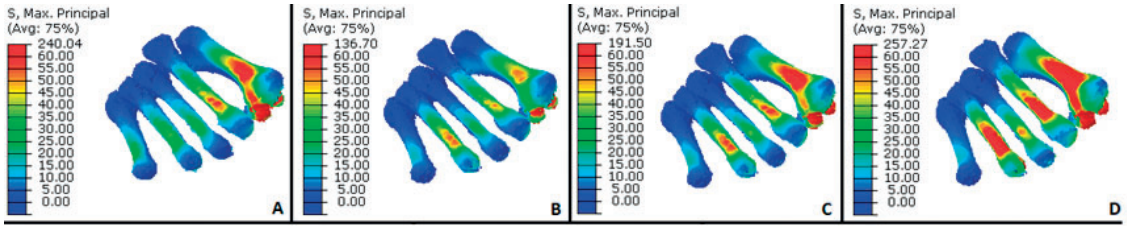

Figure 2: Stress maximum in forefoot. A) Healthy, B) MCO, C) MCO-TPT-failure. D) MCO-TPT-PF-SL-failures.

Acknowledgments: The authors gratefully acknowledge of the Ministry of Economy and competitiveness of the Spain-Government support through the project DPI2016-77016-R.

References:

Larrainzar-Garijo R, et al. DOI: 10.1016/j.recot.2018.04.003. (2018)
Arangio GA, et al. DOI: 10.1016/S0268-0033(01)00011-0 (2001)
Cifuentes-De la Portilla C, et al. DOI: DOI: 10.1016/j.jbiomech.2018.12.047 (2018)
Vora AM, et al. DOI: 10.2106/JBJS.E.00045 (2006)

[C-06.3]

THE ROLE OF PHYSIOLOGICAL LOADING ON BONE FRACTURE HEALING UNDER ILIZAROV CIRCULAR FIXATOR : THE EFFECTS OF LOAD DURATION AND LOADING FREQUENCY

Ganesharajah Ganadhiepan[1], *Saeed Miramini*[1], *Priyan Mendis*[1], *Lihai Zhang*[1]

1 *The University of Melbourne, Parkville, Australia*

In the recent decades, minimally invasive techniques to treat bone defects, such as the use of external fixators has gained interest in the field of orthopaedics [1]. Besides being, minimally invasive, these devices allow some degree of external control over the mechanical microenvironment of the fracture site which significantly affects the healing outcome. This provides more flexibility to surgeons in treating bone fractures; because, the fixator could be adjusted throughout the healing period depending on the progress of healing. Ilizarov circular fixator (ICF) is one such external fixator which is used to treat a variety of bone defects such as fractures, non-union, bone length discrepancies etc. [2] One of the main advantages of ICF is that it enables early weight bearing which is beneficial in terms of patient's mobility. In addition, it is believed that early weight bearing could lead to faster and more stronger fracture callus development and thus enhancing the healing progression [1]. However, the exact mechanism by which early weight bearing enhance fracture healing under ICF remains unclear. In this study, it was hypothesised that dynamic loading resulting from physiological activities (e.g. walking) could significantly enhance the bone cell and growth factor concentrations within the early callus and thus, enhance the healing progression. In addition, we hypothesised that, duration of the physiological activities and their frequencies have significant effect on these concentrations. The hypotheses were tested using a computational model of a tibial fracture site (Fig.1), which was developed to simulate the interactions, transport and differentiations of bone cells (i.e. mesenchymal stem cells, osteoblasts chondrocytes and fibroblasts) and the growth factors (i.e. osteogenic growth factor and chondrogenic growth factor) within the early callus. The changes in cell and growth factor concentrations due to different load durations (1 – 4 hours) and load frequencies (1-4 times/day) were parametrically studied and the findings of this study are presented in this paper.

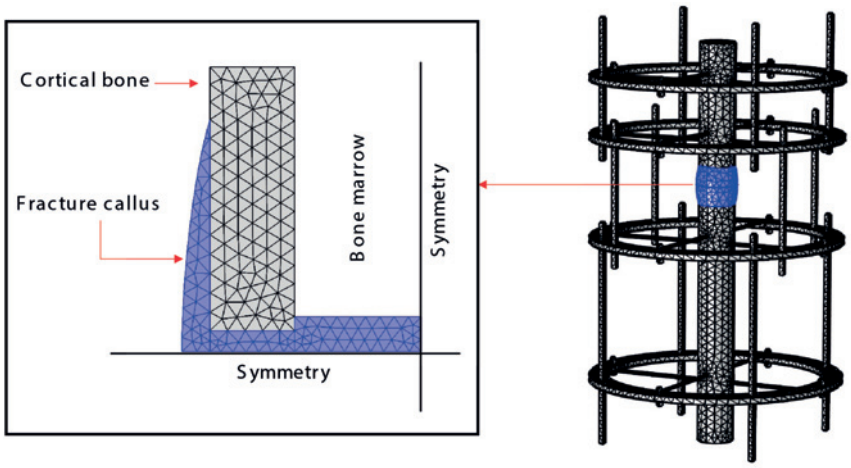

Figure.1 Computational model of the fractured tibia

References:

[1] *A. T. Fragomen and S. R. Rozbruch, "The mechanics of external fixation," HSS Journal, vol. 3, no. 1, pp. 13-29, 2007.*
[2] *K. Erler, C. Yildiz, B. Baykal, A. S. Atesalp, M. T. Ozdemir, and M. Basbozkurt, "Reconstruction of defects following bone tumor resections by distraction osteogenesis," Archives of orthopaedic and trauma surgery, vol. 125, no. 3, pp. 177-183, 2005.*

[C-06.4]

DECISION SUPPORT SYSTEM IN CRANIAL IMPLANTOLOGY BASED ON RESULTS FROM COMPUTATIONAL MODELING - A FEASIBILITY STUDY

Jakub Chamrad[1], *Petr Marcián*[1], *František Mazura*[2]

1 *Brno University of Technology, Brno, Czech Republic; Faculty of Mechanical Engineering; Institute of Solid Mechanics, Mechatronics and Biomechanics*
2 *Brno University of Technology, Brno, Czech Republic; Faculty of Information Technology*

A cranial defect can result from many different causes, e. g. car accidents, assaults, falls or tumor. Such an injury entails side complications, which may include coma, headaches, loss or deterioration of senses, such as hearing, vision, smell or taste [1].

The cranial defects are repaired by a cranioplasty. The functions of the cranioplasty are to restore the protective function of cranium and its aesthetics [2]. Cranioplasty is performed by surgeons, who decide during the pre-operation planning about important aspects of the surgery. The decision-making process covers implant material selection, a location and an amount of fixation mini-plates. It is a common practice that performing surgeons decide based on their experiences.

In case of alloplastic cranioplasty, synthetic biomaterials (e. g. PolymethylMethacrylate, PolyetherEtherketone or titanium alloy) are used instead of autografts, patient-specific approach is employed for designing and manufacturing of cranial implants.

Understanding of the interaction of the artificial objects (such as implant, fixation mini-plates and micro-screws) with the bone tissue is highly important and biomechanical assessment brings view from another perspective. Computational modeling (CM), more specifically finite element method (FEM), are employed as successful tool for such an analyses and simulations.

CM consists of several steps (as shown in Fig. 1), model of geometry, material, loads and boundary conditions, discretization and calculation. Today, it is a common practice, that a geometry of computational models is based on medical imaging techniques, e. g. computed tomography (CT) or Magnetic resonance imaging (MRI). In this study, CT dataset was used to define CM geometry. Material of bone [3] and artificial components were modeled as linear elastic homogeneous material models. Cranial bone with implant were loaded by physiological value of intracranial pressure (2 kPa) [4]. Implant was loaded by a static force 100 N, which corresponds to hard pressing with a finger [5].

The aim of this study was a creation of parametric study about cranial implants, which were analyzed using FEM. The results of performed analyses were collected to result database. Another aim is a feasibility study of decision support system in cranial implantology based on database of FEM results. Difficulties and obstacles were explored and discussed.

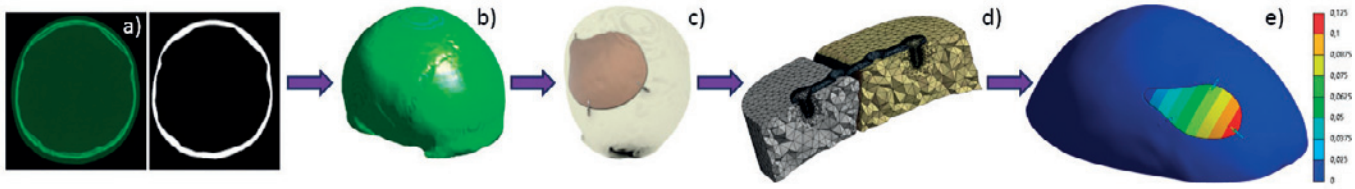

Figure 1: The steps of creation of CM: a) processing CT data and segmentation; b) STL file creation; c) volume model creation and implant design; d) discretization and pre-calculation tasks; e) analysis of results.

Acknowledgments: This research was funded by research project FSI/FIT-J-19-XXXX.

References:

[1] *Halabi et al, J Mech Behav Biomed Mater, 4:1819–1832, 2011.*
[2] *Bogu et al, Acta Bioeng Biomech, 19:125-131, 2017.*
[3] *Chamrad et al, Applied and Computational Mechanics, 12:5-16, 2018.*
[4] *Czosnyka et al, J Neurology, 75:813-821, 2004.*
[5] *Persson et al, J Cranio Maxill Surg, 46:418-423, 2018.*

[C-06.5]

CLINICAL DECISION SUPPORT MODEL TO GUIDE FLUID ADMINISTRATION IN INTENSIVE CARE PATIENTS

Tilai Rosalina[1], *Jan Willem Sels*[2], *Arthur Bouwman*[3], *Frans van de Vosse*[4], *Peter Bovendeerd*[1]

1 *Eindhoven University of Technology, Eindhoven, Netherlands*
2 *Maastricht University Medical Center, Maastricht, Netherlands*
3 *Catharina Ziekenhuis Eindhoven, Netherlands; Technische Universiteit Eindhoven, Eindhoven, Netherlands*
4 *Eindhoven University of Technology, Eindhoven, Netherlands, Dept. of Biomedical Engineering*

During surgery patients can lose significant amounts of fluid, due to bleeding, evaporation and diuresis, and redistribution of fluid can occur, due to capillary leakage. To avoid hypovolemia, and thereby hypoperfusion, they can be treated with intravenous fluid administration. However, exact estimation of fluid loss and redistribution is difficult, frequently leading to over resuscitation and thus hypervolemia, which causes tissue edema and organ failure and is associated with impaired outcome [1]. Mathematical models might be able to assist in determining the optimal fluid administration protocol for individual patients, by translating available measurements into quantitative information on the fluid status. In this project we are developing such a clinical decision support model to guide fluid administration.

We developed a cardiorespiratory model including capillary fluid exchange and urine production. The model contains a systemic and pulmonary circulation, with the left and right ventricle modeled with the one-fiber model [2]. Transcapillary fluid exchange is modeled by the Starling equation. The cardiovascular circulation is coupled to a simple model for urine production which is driven by vascular volume [3].

First, we tested the model on a healthy volunteer dataset [4] where cardiovascular response and fluid redistribution were recorded in healthy volunteers after infusion of 2.3 L of saline in 23 minutes. Typically, at the end of the experiment heart rate (+3 bpm) and interstitial volume (11 mL/kg) and urine production (9.2 mL/kg) remain elevated. Upon fitting of 5 parameters, a good match between model output and measurements was obtained. Without additional fitting, equally good results were obtained for a second dataset of healthy volunteers [5]. This shows that the model is capable of describing the healthy volunteers after infusion of saline.

Next, to evaluate the applicability of the model in a clinical environment we tested the predictive capability of the model in ICU patients. Patients were followed for 4 hours post cardiac surgery and all fluid intake and losses were recorded. Cardiovascular responses and diuresis were compared to the model.

To conclude, we developed a model which may be the first step towards a clinical decision support tool. Eventually the model must be tested on different patient data sets and a systematic sensitivity analysis must be performed to evaluate the uniqueness of the solutions.

Acknowledgments: This project was performed within the IMPULS II framework in collaboration with Philips Research.

References:

1. *Holte et al., (2002) Br. J. Anaesthesia, 89(4), 622-632.*
2. *Bovendeerd et al., (2006) Ann. Biom. Eng., 34(12), 1833–1845.*
3. *Gyenge et al., (2003) Ann. Biom. Eng., 31(7), 823-839.*
4. *Watenpaugh et al., (1992) J. of Appl. Phys., 73(4), 1218-1226.*
5. *Drobin et al., (1999) Anesthesiology, 90(1), 81-91.*

[C-07.1]

MICROPHYSIOLOGICAL SYSTEMS FOR MODELING NEUROLOGICAL DISEASE

Roger Kamm[1], *Cynthia Hajal*[1], *Marco Campisi*[2], *Yoojin Shin*[1], *Tatsuya Osaki*[1], *Giovanni Offeddu*[1]

1 *Massachusetts Institute of Technology, Cambridge, USA*
2 *Politechnico DI Torino, Torino, Italy*

Introduction: With the wide availability of human iPS cells and their cell type specific derivatives, it is now possible to develop microphysiological systems (MPS) that replicate aspects of real organ physiology and human disease. Such systems have now been developed for a wide range of tissues and organs, and are beginning to bear fruit, bringing new insights into disease processes and as drug screening platforms. Here, we focus on neural tissue models developed in our lab over the past few years: the blood-brain barrier (BBB)1 and a motor unit including motor neurons and skeletal muscle2.

Methods: Microfluidic platforms are fabricated using standard soft lithography, from a single SU-8 wafer. Channels and chambers are produced by bonding the PDMS substrate to a glass coverslip. The BBB model consists of a single gel region, flanked by two media channels. Three cell types – endothelial cells, astrocytes and pericytes, either primary or iPSC-derived – are mixed with a fibrin gel and injected into the gel region. Within 4-7 days, vascular networks form with the pericytes and astrocytes having physiological morphology and function (Fig. 1A). Barrier integrity is assessed by leakage of fluorescent dextrans of various size from the lumens.

The motor unit model consists of iPSC-derived motor neurons and skeletal muscle cells, separately differentiated over times up to one month. Muscle cells undergo the final stages of differentiation after being injected into a muscle compartment and coalescing around two flexible posts; later, the differentiated motor neuron neurospheroid is injected into the adjacent compartment, the entire gel region is filled with collagen gel. Functionality is assessed by optogenetically-induced excitation of the motor neurons producing contractile force by the muscle, and tissue viability is assessed over time (Fig. 1B).

Results and Discussion: Both in terms of morphology and functionality, the BBB model recapitulates many aspects of barrier function in vivo. The endothelial cells express many transporter proteins that are specific to the BBB, and both diffusive and convective molecular transport across the endothelium can be modeled in the system, recapitulating physiological values.

The motor model exhibits normal muscle contractile function for up to 2 weeks, allowing assessment of interactions between the neurons and muscle along with the neuromuscular junction. Two models, one obtained from healthy iPSCs and the other from an ALS patient show distinct differences in performance and viability with respect to muscular contraction force and response to activation by light. Initial experiments also demonstrate the potential application of this model for drug screening.

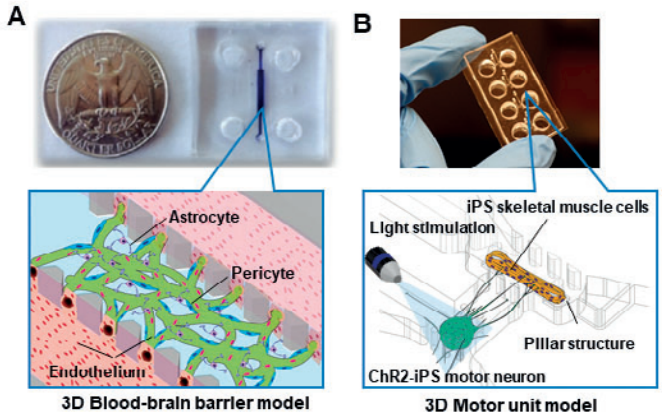

Figure 1. (A) Microphisiological blood-brain barrier model in microfluidic device using endothelial cells, pericytes, and astrocytes. (B) Optogenetically controlled motor unit model with Channelrhodopsin-2 motor neuron and skeletal muscle cells along with neuromuscular junction.

Acknowledgments: Support from the National Science Foundation and Amgen are gratefully acknowledged. G.S.O. is also supported by an AICF fellowship. T.O. was supported by an overseas research fellowship from the Japan Society for the Promotion of Science and Biogen. Y.S. was supported by the Cure Alzheimer's Fund. C.H. was supported by the Ludwig Center for Molecular Oncology Graduate Fellowship.

References:

1. *M. Campisi, Y. Shin, T. Osaki, C. Hajal, V. Chiono, R.D. Kamm, "3D self-organized microvascular model of the human blood-brain barrier with endothelial cells, pericytes and astrocytes." Biomaterials, 180:117-129, 2018*
2. *T. Osaki, S. G.M. Uzel, R.D. Kamm, "Microphysiological 3D model of amyotrophic lateral sclerosis (ALS) from human iPS-derived muscle cells and optogenetic motor neurons", Science Advances, Vol. 4, no. 10, eaat5847, 2018*

[C-07.2]

ILLUMINATING HUMAN FUNCTION: DEVELOPMENT OF A SMART MICRO-PHYSIOLOGICAL BIOANALYZER

Yaakov Nahmias[1]

1 *The Hebrew University of Jerusalem , Jerusalem, Israel; Tissue Dynamics Ltd., Jerusalem, Israel*

Organ-on-chip technology aims to replace animal toxicity testing, but thus far demonstrated few advantages over traditional methods. Indeed, current methods to evaluate product safety still rely on end-point assays measuring tissue damage and cell death, resulting in little to no mechanistic information. This inability to learn from failure makes the drug development process Sisyphean rather than iterative in nature. To address this problem, we developed a platform technology capable of tracking the dynamics of tissue function from the very onset of the initiative event, gaining critical information about compounds mechanism of action. This data rich approach enables the use of deep learning algorithms to track and identify risk factors without a priori information. Our microfluidic platform is capable of maintaining vascularized three-dimensional liver, cardiac, kidney and neural micro-tissues for over a month in vitro. Micro-tissues acquire the native architecture, physiological activity and show complex metabolic zonation of in vivo organs. Tissue-embedded metabolic sensors for oxygen, glucose, lactate and glutamine permit the real-time quantification of intracellular fluxes and tissue level function. Change in metabolic function is the first indication of physiological stress, preceding any detectable damage. Using the Tissue Dynamics bioanalyzer, we already explained the idiopathic nephrotoxicity of acetaminophen (Tylenol), and the idiosyncratic hepatotoxicity of valproate (Depakine) and troglitazone (Rezulin) whose post-market withdrawal cost upwards of $1B in legal settlements. Importantly, we will present a newly discovered mechanism of drug-induced nephrotoxicity for cyclosporine (Neoral) and cisplatin (Platinol). Our platform allows us to screen therapeutics to block the pathway, increasing the safety of the drugs through combination treatments. Our work marks the importance of tracing human organ function in real-time, demonstrating its specific advantages in lead optimization as well as predicative toxicology.

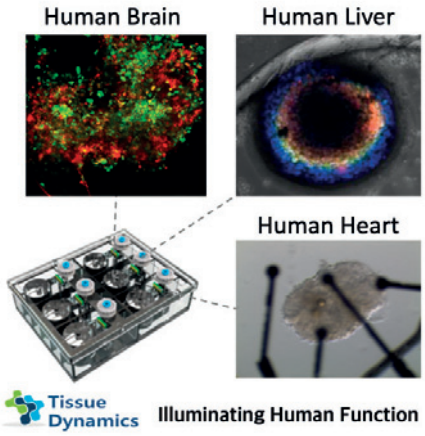

Figure Caption: Tissue Dynamics organ on chip platform

Acknowledgments: This work was supported by the European Research Council (ERC) and SME Instrument under H2020 program. Additional funding was provided by L'Oreal Research and Innovation.

References:

1. *Prill et al. Real-time monitoring of oxygen uptake in hepatic bioreactor shows CYP450-independent mitochondrial toxicity of acetaminophen and amiodarone. Arch Toxicol. 90(5):1181-91. (2016)*
2. *Bavli et al. Real-time monitoring of metabolic function in liver-on-chip microdevices tracks the dynamics of mitochondrial dysfunction. PNAS 113(16):E2231-40. (2016)*
3. *Ehrlich et al. Microphysiological flux balance platform unravels the dynamics of drug induced steatosis. Lab Chip, 18, 2510-2522 (2018)*

[C-07.3]

PDMS-FREE ORGAN ON CHIP PLATFORMS FOR MODELING HUMAN DISEASE

Ashutosh Agarwal[1]

1 University of Miami, Miami, USA

We report the design and fabrication of robust fluidic platforms that are optimal for culturing and interrogating 3D organoid cultures. The optimized design of convective fluid flows, use of bio-inert and non-absorbent materials, reversible assembly of the platform, manual access for loading and unloading of cultures, and straightforward integration with commercial imaging and fluid handling systems are major improvements over conventional PDMS-based low volume microfluidics. The platform has been used for perfusion interrogation of (1) human pancreatic islets, and (2) engineered spheroid cultures that mimic the metastatic niche of the bone marrow.

(1) Human pancreatic islets were tested for dynamic secretion of hormones, concomitant live-cell imaging, and optogenetic stimulation of genetically engineered islets. We are currently integrating immunological features into the islet MPS. With a significant knowledge gap in the development and progression of most autoimmune diseases, engineering an MPS platform capable of supporting the dynamic interactions between immune cells and their target antigens would not only provide new insights into pathways, but allow for high content screening intervention screening. The efforts to evaluate ex vivo function of islets are informing the clinical trials currently underway to transplant human islets in Type 1 Diabetic patients.

(2) The platform is also being tested for long term culture of spheroids composed of primary human cells of the bone marrow along with vascular cells and supporting pericytes. The efforts to recreate the metastatic niche are enabling in vitro maintenance and propagation of circulating tumor cells derived from the blood of breast cancer patients. An in vitro recapitulation of the metastatic bone microenvironment could provide new insight into the metastatic cascade and aid in developing new therapeutic strategies. The efforts to maintain and propagate circulating tumor cells sourced from a liquid biopsy sample are informing the precision management of cancer patients.

Research is supported by NIH (1UC4DK104208, U01CA233363, 1 F31 DK118860, 5U01DK104162), Early stage commercialization grants from Wallace H. Coulter Foundation, and a Sponsored research project from Mallinckrodt Pharmaceuticals.

[C-08.1]

BODY-ON-A-CHIP HUMAN SYSTEMS FOR DRUG DEVELOPMENT USING PBPK/PD MODELS

Michael Shuler[1]

1 *Cornell University, Ithaca, USA; 101 Weill Hall; Biomedical Engineering*

"Body-on-a-Chip" or micro physiological systems (MPS) represent a developing technology that holds great promise to increase the effectiveness of the drug development process to yield new human pharmaceuticals. Current pre-clinical studies rely typically on in vitro studies of static, single organ human modules or on animals; only 11% of drugs exiting preclinical studies end up as approved drugs due to lack of efficacy in humans or to off-target toxicity in other organs. A microscale, human, multiorgan "Body-on-a-chip" system can potentially identify issues of lack of efficacy or toxic side effects in humans at the preclinical level which should lead to increase success in clinical trials. An increase from 11% to 33% success could have significant impact on development cost and provide society with many more useful drugs. We began to develop such multiorgan human based microscale model over 15 years ago as analogs to physiologically based pharmacokinetic (PBPK) pharmacodynamics (PD) models. By making these systems, analogs to PBPK/PD models we can better emulate the action of a drug and its metabolites and the exchange of metabolites and signal molecules between organs. A multiorgan system that is not physiologically-based cannot mimic the exchange of compounds between organs at relevant levels and be unable to predict toxic side effects as well as efficacy. Here I will describe aspects of the design and use of such micro fabricated systems in combination with PBPK/PD models and provide examples of applications with drugs such as doxorubicin, Tegafur and terfanadine. These examples will demonstrate how these systems can predict efficacy and toxicity and, in some cases, how such systems could have identified issues with compounds which had passed preclinical studies, but had to be withdrawn from the market after approval.

Acknowledgments: Support in part, from NIH Grants R44 TR001326 and U01 CA 214300

References:

Sung, J. H., C. Kam, M.L. Shuler. 2010. A microfluidic device for pharmacokinetic-pharmacodynamic (PK-PD) model on a chip. Lab Chip. 10: 446-455.
Sung, J.H., Srinivasan, B., Esch, M.B., McLamb, W.T., Bernabini, C., Shuler, M.L., and J.J. Hickman. 2014. Using physiologically-based pharmacokinetic-guided "body-on-a-chip" systems to predict mammalian response to drug and chemical exposure. Experimental Biology and Medicine. 239:1225-1239.
Abaci, H.E., and M.L. Shuler. 2015. Human-on-a-chip design strategies and principles for physiologically based pharmacokinetics/pharmacodynamics modeling. Integr Biol, 7:383-391
Sung, J.H., Y.I Wang, N.N. Sriram, M. Jackson, C. Long J.J. Hickman and M.L. Shuler. 2019. Recent advances in body-on-a-chip systems. Anal Chem 91:330-351.

[C-08.2]

HUMAN-ON-A-CHIP SYSTEMS FOR USE IN EFFICACYAND TOXICOLOGICAL INVESTIGATIONS IN PRE-CLINICAL DRUG DISCOVERY FOR APPLICATIONS IN NEUROLOGICAL DISEASES

James Hickman[1]

1 Hesperos, Inc, Orlando, USA

One of the primary limitations in drug discovery and toxicology research is the lack of good model systems between the single cell level and animal or human systems. This is especially true for neurodegenerative diseases such as ALS and Alzheimer's as well as spinal cord injury. In addition, with the banning of animals for toxicology testing in many industries body-on-a-chip systems to replace animals with human mimics is essential for product development and safety testing. Our research focus is on the establishment of functional in vitro systems to address this deficit where we seek to create organs and subsystems to model motor control, muscle function, myelination and cognitive function, as well as cardiac and liver subsystems. The idea is to integrate microsystems fabrication technology and surface modifications with protein and cellular components, for initiating and maintaining self-assembly and growth into biologically, mechanically and electronically interactive functional multi-component systems. Our advances in culturing adult rat, mouse and human mammalian spinal cord, hippocampal neurons, muscle and cardiac cells in a defined serum-free medium, suggest outstanding potential for answering questions related to maturation, aging, neurodegeneration and injury. A specific embodiment of this technology is the creation of a functional human NMJ system to understand ALS. We have investigated four mutations found in ALS patients; SOD1, FUS, TDP43 and C9ORF72. The models have demonstrated variations of the disease phenotype compared to WT for NMJ stability and functional dynamics. Results of these studies will be presented as well as preliminary results for reversal of the deficits. Examples will be given of some of the more advanced human-on-a-chip systems being developed for CNS and PNS disease applications as well as the results of six workshops held at NIH to explore what is needed for validation and qualification of these systems.

[C-08.3]
ORGANS ON A CHIP: A NEW TOOL FOR THE STUDY OF BRAIN PHYSIOLOGY

Ben Maoz[1]

1 *Tel Aviv University, Tel Aviv, Israel*

Micro-engineered cell culture models, termed Organs-on-Chips, have emerged as a new tool to recapitulate human physiology and drug responses. Multiple studies and research programs have shown that Organs-on-Chips can capture the multicellular architectures, vascular-parenchymal tissue interfaces, chemical gradients, mechanical cues, and vascular perfusion of the body. Accordingly, these models can reproduce tissue and organ functionality and mimic human disease states to an extent thus far unattainable with conventional 2D or 3D culture systems. Here we exploit the micro-engineering technology in a novel system-level approach to decompose the integrated functions of the neurovascular unit into individual cellular compartments, while retaining their paracellular metabolic coupling. Using individual, fluidically-connected chip units, we have created a system that models influx and efflux functions of the brain vasculature and the metabolic interaction with the brain parenchyma. Results of proteomic and metabolic assays indicate that this system mimics the effect of intravascular administration of the psychoactive drug methamphetamine observed in vivo. Moreover, this model reveals a previously unknown role of the brain endothelium in neural cell metabolism: In addition to its well-established functions in metabolic transport, the brain endothelium secretes metabolites that are directly utilized by neurons. This discovery would have been impossible to achieve using conventional in vitro or in vivo measurements.

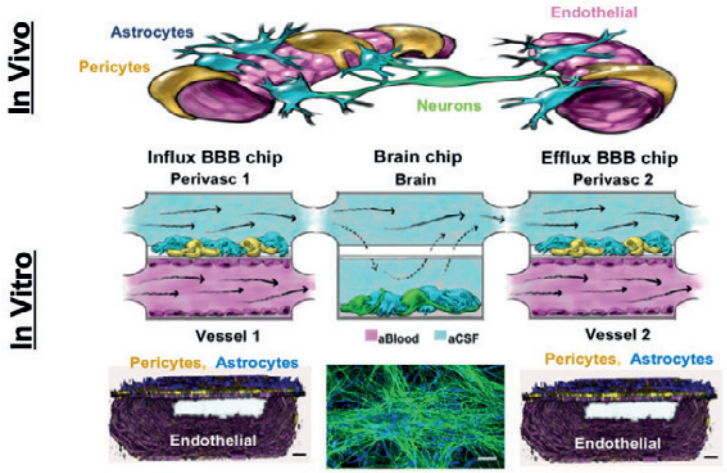

Figure Caption: Simplified anatomical illustration of the NVU in vivo (top) and the new human in vitro Organ-on-a-Chip platform that emulates the in vivo system (middle). The bottom shows immunohistochemistry of human brain microvascular endothelial cells (magenta) a mixture of brain astrocytes (blue) and pericytes (yellow) in the top compartment of both BBB chips and human brain neuronal cells (green) and astrocytes (blue) are cultured in the lower compartment of the brain chip

Acknowledgments: This research was supported by the Wyss Institute for Biologically Inspired Engineering at Harvard University, Defense Advanced Research Projects Agency (DARPA) under Cooperative Agreement Number W911NF-12-2-0036 (D.E.I & K.K.P.), and Sverige-Amerika Stiftelsen, Carl Trygger Stiftelse, Erik och Edith Fernstrom's stiftelse (A.H.).

References:

B. M. Maoz, A. Herland*, E. A. FitzGerald*, T. Grevesse*, C. Vidoudez, A. R. Pachenco, S. P. Sheehy, T-E. Park, S. Dauth, R. Mannix, N. Budnik, K. Shores, A. Cho, J. C. Nawroth, D. Segré, B. Budnik, D. E. Ingber, and K. K. Parker; "A linked organ-on-chip model of the human neurovascular unit reveals the metabolic coupling of endothelial and neuronal cells;" Nature Biotechnology, 2018*

[C-09.1]

IDENTIFICATION OF POROVISCOELASTIC MATERIAL PROPERTIES OF HYDROGELS

Michelle Oyen[1]

1 *East Carolina University, Greenville, USA*

Indentation techniques have recently been adapted for the study of hydrated materials, including natural and synthetic hydrogels. Both single component and composite hydrogels have been characterized using indentation and nanoindentation across a wide range of experimental length-scales. The material response is shown to be greatly dependent on the chemical bonding within the hydrogel, i.e. whether the network is physically or chemically cross-linked. Based upon knowledge of the properties of each individual component, composite hydrogels can be created to mimic the overall response of complex biological materials to create multi-component tissue engineering scaffolds (1). Multiple experiments are required for a thorough characterization of hydrogel response, particularly when both viscoelastic and poroelastic deformation mechanisms are active in the material simultaneously. Varying the length-scale of the experiment, by changing the indenter geometry, allows for decomposition of the different time-dependent mechanisms from simple indentation creep or relaxation curves, since there is no intrinsic length-scale in the viscoelastic response but there is in the poroelastic constitutive response. Parameter identification utilizes analytic expressions combined with forward and inverse finite element modeling, and relies on the empirical observation that the viscoelastic and poroelastic relaxation responses are separable (2, 3). Results from indentation tests are compared with those from compression tests and from direct permeability measurements for validation.

References:

(1) Strange DGT and Oyen ML, Composite hydrogels for nucleus pulposus tissue engineering. J. Mech. Behav. Biomed. Mater. 11 (2012) 16 - 26.
(2) Strange DGT, Fletcher TL, Tonsomboon K, Brawn H, Zhao X, Oyen ML, Separating poroviscoelastic deformation mechanisms in hydrogels. Appl. Phys. Lett. 102, (2013) 031913.
(3) Wang Q-M, Mohan AC, Oyen ML, Zhao X-H, Separating viscoelasticity and poroelasticity of gels with different length and time scales. Acta Mechanica Sinica 30 (2014) 20 - 7.

[C-09.2]

THE EFFECT OF MODEL DISCRETIZATION ON PARAMETER IDENTIFICATION. APPLICATION TO REAL-TIME FINITE ELEMENT SIMULATIONS

Nava Schulmann[1], *Stephane Cotin*[2], *Igor Peterlik*[2]

1 *University of Strasbourg, Strasbourg, France; Inria, Valbonne, Francie*
2 *Inria, Valbonne, Francie*

Identifying the elastic parameters of a finite element model from a dynamically acquired set of observations is a fundamental challenge in many data-driven medical applications going from soft surgical robotics to image-guided per-operative simulations.

While various strategies exist to tackle the parameter-identification inverse problem (Aster et al. 2013), the effect of sub-optimal discretization, as often required in real-time applications, is largely overlooked. Indeed, the need to tune the parameter values in order to account for discretization-induced stiffening in specific models is reported in different works (e.g. Chen et al. 2015; Mira et al. 2018). However, to the best of our knowledge, neither a systematic study of this phenomenon exists, nor a strategy to select optimal effective values has been developed.

Our work addresses the issue of parameter identification in coarsened meshes with special attention to performance differences between classical and Bayesian identification methods.

We focus on the estimation of Young's moduli in various systems and show that the estimated stiffnesses are underestimated in a systematic manner when reducing the number of degrees of freedom. We also show that the effective stiffness of a given coarse mesh, when associated with an undersampled mesh discretization, is not constant but strongly depends on the prescribed deformations. These results show that the estimated parameters should not be considered as the true parameter value of the organ or tissue but instead are model-dependent values.

Through examination of the shape prediction accuracy obtained by different inverse approaches, we argue that Bayesian methods present a clear advantage w.r.t. classical minimization methods due to their capacity to locally adapt the model parameter values.

In conclusion, by studying the impact of spatial resolution on parameter inference, this work sheds new light on the nature of the effective stiffness in coarsened meshes and provides a strategy to handle system-specific, real-time parameter identification.

References:

Desai Chen, David I. W. Levin, Shinjiro Sueda, and Wojciech Matusik. Data-driven finite elements for geometry and material design. ACM Trans. Graph. 34, 4, Article 74, 2015
Mîra Anna, Ann-Katherine Carton, Serge Muller, Yohan Payan. Breast biomechanical modeling for compression optimization in digital breast tomosynthesis. A. Gefen and D. Weihs. Computer Methods in Biomechanics and Biomedical Engineering, Lecture Notes in Bioengineering, Springer International Publishing, pp.29-35, 2018
Richard C. Aster, Brian Borchers, and Clifford Thurber. Parameter Estimation and Inverse Problems. Elsevier, 2004

[C-09.3]

IDENTIFICATION OF A CEREBRAL CONTUSION INJURY THRESHOLD BY MEANS OF COUPLED EULERIAN-LAGRANGIAN FINITE ELEMENT ANALYSIS OF A PORCINE BRAIN MODEL

Andrea Menichetti[1], *Bart Depreitere*[2], *Jos Vander Sloten*[1], *Nele Famaey*[1]

1 *KU Leuven, Mechanical Engineering, Heverlee, Belgium; Dept. - Biomechanics Section, Leuven, Belgium*
2 *KU Leuven, Department of Neurosurgery,Leuven, Belgium; University Hospital Gasthuisberg, Leuven*

Cerebral contusion is a frequent type of focal traumatic brain injury and is often associated with lifelong disability and mortality. A series of in-vivo controlled cortical impact (CCI) tests was performed in our research group [1] on pigs to investigate the mechanopathogenesis of cerebral contusions. This study aims to identify a local injury threshold that best predicts the volume of the induced brain damage. This is done by comparing the post-CCI MRI to the outcome of a 3D finite element (FE) analysis that simulates the trauma sustained by the pig brain during the CCI.

The porcine brain FE model (Fig.a) includes the fluid-structure interaction of the cerebrospinal fluid (CSF) with the cerebrum and the dura mater by means of a coupled Eulerian-Lagrangian approach (Abaqus/Explicit). The cerebrum (one hemisphere) and the dura mater were considered as Lagrangian deformable elements and modeled with two Neo-Hookean-based hyperviscoelastic material definitions [2-3]. The CSF was treated with an Eulerian formulation, assuming water-like mechanical properties. The brain geometry was segmented (Mimics) from the MRI of a pig brain atlas [4], rescaled and finally meshed in ANSA. A representative case of the CCI test cohort was simulated. The internal response of the brain in terms of principal logarithmic strains was computed and compared to different threshold values in the range of 5-30%. The lesion volume, calculated as the total volume of elements exceeding the threshold, was compared to the reference contusion volume segmented from the MRI that was collected 48 hours post-trauma.

For this representative case the experimentally obtained reference contusion volume amounted to

762.6 mm^3. An iterative procedure identified the threshold value that yielded a computed contusion volume that corresponded as close as possible to the reference. Results (Fig.b) show that for a strain injury threshold of 13.1%, the FE model is able to predict the contusion volume with an accuracy of 99.6%.

Future work will include the simulation of all other cases of the CCI test cohort. Next, the predictive capability of other mechanical variables such as strain rate, strain energy density, shear strain or a combination of them will be investigated. This will bring new insights towards the definition of a more reliable, mechanically quantifiable, lower injury threshold for cerebral contusion.

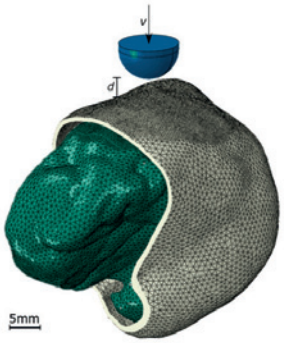

a

	Upper threshold		Lower threshold	
Iter.	Value [-]	ΔRef [mm3]	Value [-]	ΔRef [mm3]
1	0.050	3080.9	0.300	-660.9
2	0.050	3080.9	0.175	-411.8
3	0.113	349.5	0.175	-411.8
4	0.113	349.5	0.144	-158.9
5	0.129	34.8	0.144	-158.9
6	0.129	34.8	0.137	-81
7	0.129	34.8	0.133	-25.8
8	***0.131***	*2.9*	0.133	-25.8

b

Figure Caption: a) FE model of the pig brain. The space between the cerebrum (green) and the dura mater (grey, sectioned) is filled with CSF; b) Critical compressive principal strains and the corresponding deviations from the reference volume, for each iteration.

Acknowledgments: FWO SB Doctoral Grant - Project no.1S25918N; EU's Horizon2020 Marie Skłodowska-Curie Grant no.642662.

References:

[1] *DeKegel et al., Proc. 22nd ESB Congress, 2016;*
[2] *MacManus et al., ActaBiomater, 57:384-394, 2017;*
[3] *MacManus et al., JMechBehavBiomedMater, 87:256-266, 2018;*
[4] *Saikali et al., JNeurosciMethods, 192:102-109, 2010.*

[C-09.4]

HYPERELASTIC BIOMECHANICAL MODEL OF A TRANSTIBIAL RESIDUUM FROM IN-VIVO INDENTATION USING INVERSE FEA AND 3D DIGITAL IMAGE CORRELATION

Dana Solav[1], *Kevin Moerman*[2], *Aaron Jaeger*[3], *Hugh Herr*[3]

1 *Massachusetts Institute of Technology, Cambridge, USA, Cambridge, USA; Media Lab, Cambridge, USA*
2 *National University of Ireland, Galway, Ireland; Massachusetts Institute of Technology, Cambridge, Massachusetts, USA*
3 *Massachusetts Institute of Technology, Cambridge, USA*

The socket is the most critical component of the lower limb prosthetic system. Predictive patient-specific biomechanical models of the residuum are essential for a repeatable and quantitative computational socket design process. This study presents a novel framework for obtaining such a model using an experimental-numerical approach. The model geometry of the femur, tibia, fibula, and patellar tendon were derived from segmented MRI data, and the skin geometry was measured using 3D digital image correlation (3D-DIC). A custom designed 360° multi-camera system, featuring 21 RaspberryPi camera modules, was built for capturing synchronized image sets of an entire residuum [1]. Additionally, a synchronized custom hand-held indentation device featuring two 6DOF force/torque transducers was fabricated.

The DIC images were analyzed using MultiDIC, an open-source 3D-DIC MATLAB toolbox developed by the authors [2]. The toolbox features custom algorithms specifically tailored to accurately reconstruct 3D point clouds and triangular meshes, automatically merge data obtained from multiple views into continuous surfaces, and calculate the full-field 3D displacements, deformations, and strains [2]. The MRI and 3D-DIC derived surfaces were aligned in a common coordinate system using the iterative closest point algorithm.

The bones were modelled as rigidly supported voids, and the bulk soft-tissue mechanical behavior was modeled using a 2nd order Ogden hyperelastic formulation. The spherical head of the indenter was modelled as a rigid body. The indenter position and orientation at each time step were determined from the 3D-DIC data. The indentation simulation boundary conditions were derived from the experimental data. A sticky contact interface was assumed between the indenter and skin.

To determine the material parameters, an inverse finite element analysis (FEA) based optimization routine was used, which minimizes the combined differences between simulated and experimental force and surface deformation data. The iterative parameter optimization was done using custom MATLAB software [3] designed for: 1) producing FEBio (http://febio.org/) input files with the appropriate geometry, material parameters, and boundary conditions for the residuum-indenter model, 2) Starting FEA analysis by calling FEBio solver in C++, 3) Importing and analyzing the FEA results in MATLAB, 4) Comparing FEA results to the experimental results to formulate the objective function, and 5) Performing inverse FEA based optimization of the objective function using Levenberg-Marquardt algorithm.

This novel framework provides a promising solution for the in-vivo evaluation of the residuum soft-tissue mechanical properties. These data may be used to describe the residuum's biomechanical behavior and interaction with the prosthetic socket, leading to improved data-driven algorithms for prosthetic socket design.

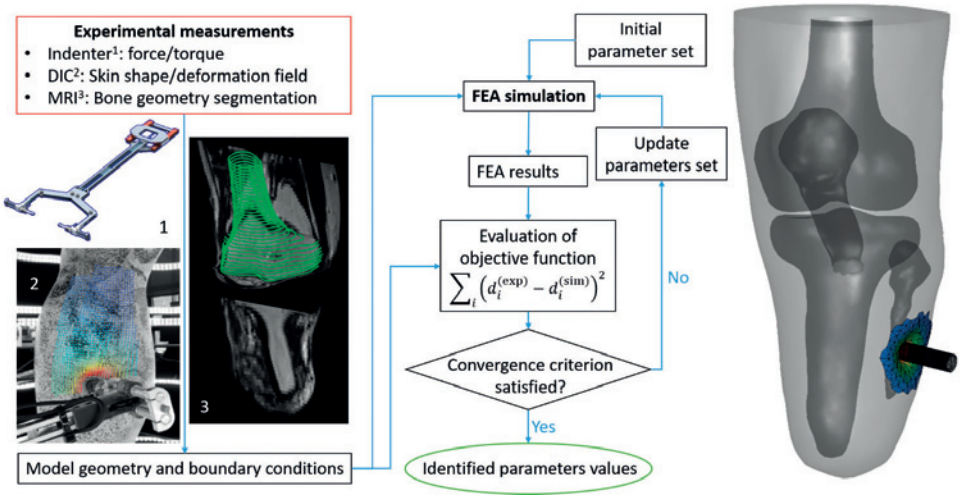

References:

1. *Solav D. et al. (2019). IEEE Trans Biomed Eng, DOI:10.1109/TBME.2019.2895283*
2. *Solav D. et al. (2018). IEEE Access, 6: 30520-30535. DOI:10.1109/ACCESS.2018.2843725*
3. *Moerman K. (2018). J. Open Source Softw., 3(22): 506, DOI: 10.21105/JOSS.00506*

[C-09.5]

LOCAL STIFFNESS ESTIMATION OF THE HUMAN EARDRUM VIA THE VIRTUAL FIELDS METHOD

Felipe Pires[1], *Stéphane Avril*[2], *Steve Vanlanduit*[1], *Joris Dirckx*[3], *Julio Cordioli*[4]

1 *University of Antwerp, Antwerp, Belgium; Vrije Universiteit Brussel, Belgium*
2 *Mines Saint-Étienne, Université de Lyon, Lyon, France*
3 *University of Antwerp, Antwerp, Belgium*
4 *Federal University of Santa Catarina, Santa Catarina, Brazil*

The human eardrum is a soft membrane that contains organized fibers in a large area of its structure. These fibers contain a heterogeneous stiffness distribution and several were the attempts to estimate their material properties. The published results vary greatly among each other and examples of methods that were employed to perform such estimations are tensile experiments on tissue strips, characterization by nanoidentation and finite element updating, just to name a few. Apart from the obtained results still being a matter of debate, most of them just provide the stiffness in specified regions of the membrane or assume the measured sample to have a homogeneous stiffness distribution. Such simplifications became necessary due to the difficulty of analyzing a sample with such small dimensions. However, the development of non-contact and full-field measurement techniques in combination with the Virtual Field Method (VFM) made it possible to develop an approach to estimate heterogeneous stiffness distributions on an eardrum. It is the purpose of this work to present a method from which heterogeneous constitutive parameters of the referred sample can be estimated. Here, the sample's behavior is not assumed to be dominated only by bending or membrane strains. Instead, both strains are taken into account in the derivation of the principle of virtual work, since these parameters are considered to be of equal importance in the current case. With measured full-field displacements at hand, their projection on a triangular finite element mesh can take place and both the bending and membrane strains are computed. Moreover, to account for the stiffness' heterogeneity, local bulge functions, which respect the sample's boundary conditions of null displacements and rotations were created and used as the virtual out-of-plane displacements. Lastly, local stiffnesses are extracted for each element of the mesh by assigning the virtual fields in the equilibrium equation. The method was validated on the basis of finite element model of an eardrum with known material properties. By comparing the assigned heterogeneous stiffness of the model with what was estimated via the VFM, it could be seen that the extracted stiffness distribution was in agreement with the reference of the model.

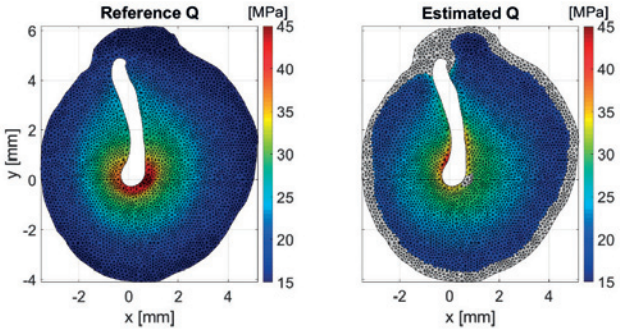

Figure Caption: Comparison between the assigned constitutive parameter of the finite element model and the estimated parameter by using the proposed approach

Acknowledgments: Financial support for this work was supplied by the Research Foundation of Flanders 536 (FWO), (grant No. G049414N).

References:

Volandri, G., Di Puccio, F., Forte, P., & Carmignani, C. (2011). Biomechanics of the tympanic membrane. Journal of biomechanics, 44(7), 1219-1236.
Farzaneh, S., Trabelsi, O., & Avril, S. (2018). Inverse identification of local stiffness across ascending thoracic aortic aneurysms. Biomechanics and modeling in mechanobiology, 1-17.

[C-10.1]

INVERSE IDENTIFICATION OF REGIONAL MATERIAL PROPERTIES IN A MOUSE MODEL OF SUPRARENAL AORTIC DISSECTIONS

Matthew R Bersi[1], Victor Acosta Santamaria[2], Paolo Di Achille[3], Craig J Goergen[4], Jay D Humphrey[3], ***Stéphane Avril[5]***

1 *Vanderbilt University, Nashville, USA*
2 *University of Lyon - Mines Saint-Etienne, Saint-Etienne, France*
3 *Yale University, New Haven, USA*
4 *Purdue University, West Lafayette, USA*
5 *University of Lyon - Mines Saint-Etienne, Saint-Etienne, France; 2école des Mines de Saint-Étienne, Université de Lyon, France*

The objective of this study is to quantify the multiaxial mechanical properties in a murine model of dissecting aneurysms [1-3] by combining in vivo ultrasound data with in vitro distension-extension data and full-field multimodality measurements of wall strain. Specifically, deformations experienced by the outer surface of the lesion are measured by tracking motions of a speckle pattern using a custom panoramic digital image correlation system while deformations throughout the wall and thrombus are measured using optical coherence tomography and digital volume correlation [4]. These measurements are registered and combined one with another to reconstruct the 3D reference geometry and to compute the 3D strain fields throughout the specimen. Prior experience with similar murine arteries revealed that a microstructurally motivated constrained mixture model describes the constitutive behavior well [5]. Such a hyperelatic model is considered for every material position, including the arterial wall and thrombus, which permits reconstruction of 3D stress fields from the 3D strain fields. The optimal set of nonlinear constitutive parameters is obtained across the whole artery by minimizing a cost function according to the virtual fields method [6]. Following mechanical testing, the dissected aortic segments were fixed in formalin, embedded in paraffin, sectioned, and stained with standard histological stains, including Movat's Penta-chrome (MOV), to assess the composition of the extracellular matrix, thereby allowing point-wise comparisons of inferred properties and underlying microstructure. From the identified material parameters fields, we show the distributions of circumferential material stiffness linearized at a pressure of 140 mmHg and the in vivo value of axial stretch for an illustrative cross section of a dissected SAA (Figure 1). Results reveal for the first time point-wise correlations between local material stiffness and constituent area fractions obtained from histology. Because matrix remodeling is critical to the formation and growth of these lesions, we submit that the associated material properties will help tremendously in increasing our understanding of the local patho-mechanical mechanisms underlying aortic dissection initiation and progression.

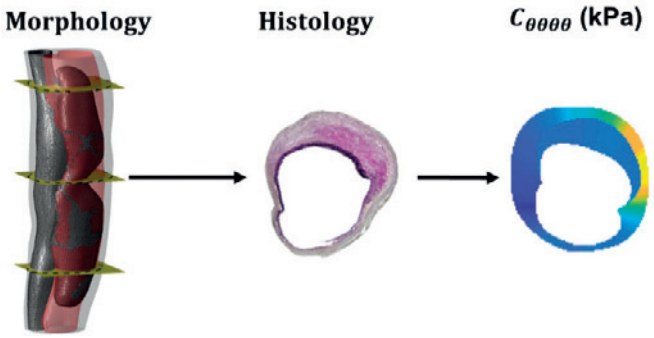

Figure Caption: left - 3D representation of the internal morphology of a dissected SAA, lumen (dark-red), thrombus (red); middle – histological cross-section showing thrombus (fibrin; red), elastin (black), and collagen (yellow-grey); right - distribution of the reconstructed circumferential material stiffness

Acknowledgments: The authors are grateful to the European Research Council for grant ERC-2014-CoG BIOLOCHANICS.

References:

[1] *Trachet et al, Cardiovasc Res, 113(10), 1230-1242, 2017.*
[2] *Bersi et al, Ann Biomed Eng, 42(6), 1207-1223, 2014.*
[3] *Bellini et al, J R Soc Interface, 14(130), 20161036, 2017.*
[4] *Acosta et al, Frontiers Mech Eng, in press, 2019.*
[5] *Bersi et al, J Biomech Eng, 138(7), 071005, 2018.*
[6] *Bersi et al, Biomech Model Mechanobiol, 18:203–218, 2019.*

[C-10.2]

RECONSTRUCTION OF LOCAL CONTRACTILITY OF THE HEART BASED ON VISIBLE KINEMATICS

Simone Pezzuto[1], *Davide Ambrosi*[2], *Rolf Krause*[3]

1Center for Computational Medicine in Cardiology, Lugano, Switzerland; Institute of Computational Science; Università Della Svizzera Italiana, Lugano, Switzerland
2Dipartimento DI Scienze Matematiche; Politecnico DI Torino, Torino, Italy
3Institute of Computational Science; Università Della Svizzera Italiana, Lugano, Switzerland

The in-vivo quantification of the mechanical function of the heart is a most relevant issue in clinical cardiology. Local contractility of the tissue, that is the ability of the myocardium to pump blood, is indeed clinically relevant for therapeutic planning (e.g., lead placement in cardiac resynchronization therapy) and outcome prediction (reverse remodeling), especially in presence of a scar.

Current imaging techniques, however, only provide an indirect assessment of contractility. Abnormal regional wall motion (or strain), obtained from echocardiography, cardiac MRI or even electroanatomic mapping [1], has been associated to a loss of contractility. Nonetheless, regions with low contractility may still move, due to the dynamic of the surrounding tissue. Additionally, absence of wall motion is not necessarily associated with absence of contractility.

From a mathematical perspective, we can predict the displacement of the myocardium on the basis of the equations the stress balance due to external forces, passive stress and local contraction of the tissue. It is therefore, tempting to address the above problem of measure indirectly the contractility by means of an inverse procedure, that is reconstructing the contractility field by minimizing the mismatch between simulated and measured displacement.

To this aim, we have been inspired by the recent literature on this subject [2] and applied an adjoint-based approach to solve the PDE-constrained parameter identification problem. In this work, however, we have also considered Total Variation (TV) regularization and compared it to standard Tikhonov regularizations for the scar identification problem. We found that TV performs very well in this context, yielding an accurate reconstruction of the contractile region even when observation is limited to the boundary of the domain (e.g., known kinematics of the endocardium only).

We also show that the standard zeroth-order Tikhonov regularization may lead to non-physiological reconstruction of the contractility in the presence of fibers non-tangent to the boundary. While this may sound uncommon in realistic heart geometries, this observation sheds some light on the poor stability of the reconstruction near the boundaries.

We conclude the presentation with an application of clinical interest reconstructing the contractility of the whole cardiac muscle from endocardial displacement, using data obtained from catheter-based mapping.

References:

[1] *Maffessanti, F. et al. (2018). Integrated Assessment of Left Ventricular Electrical Activation and Myocardial Strain Mapping in Heart Failure Patients. JACC: Clinical Electrophysiology, 4(1), 138-146.*
[2] *Balaban, G. et al. (2018). In vivo estimation of elastic heterogeneity in an infarcted human heart. Biomechanics and Modeling in Mechanobiology, 17(5),1317–1329.*

[C-10.3]

INVERSE ELASTOSTATICS TO COMPUTE THE IN VIVO LOADED STRESS STATE OF HUMAN CARDIOVASCULAR TISSUE

Mathias Peirlinck[1], *Matthieu De Beule*[1], *Patrick Segers*[1], *Nuno Rebelo*[2]

1 *Ghent University, Ghent, Belgium*
2 *Dassault Systèmes Simulia Corp.*

Upon building complex patient-specific biomechanical models of the cardiovascular system, the presence of a constant physiological pressure load remains a complicating factor given that the imaged tissue is in a pre-stressed and -strained state. Neglect of this prestressed state into solid tissue mechanics models leads to erroneous metrics (e.g. wall deformation, peak stress, wall shear stress) which in their turn are used for device design choices, risk assessment and surgery planning. It is thus of utmost importance to incorporate this deformed and loaded tissue state into the computational models, which implies solving an inverse problem (calculating the undeformed geometry given the load and the deformed geometry).

Methodologies to solve this inverse problem can be categorized into iterative and direct methodologies, both having their inherent advantages and disadvantages. Whilst iterative approaches offer the advantage of straightforward implementation in combination with any existing finite element (FE) solver, they suffer from high computational costs and convergence issues, especially for fiber-embedded anisotropic, hyperelastic and quasi-incompressible materials (as all cardiovascular tissues). Direct methodologies are typically based upon the inverse elastostatics (IE) approach and offer a computationally efficient single shot methodology to compute the in vivo stress state. However, cumbersome and problem-specific derivations of the formulations and non-trivial access to the FE code, especially for commercial products, refrain a broad implementation of these methodologies. For that reason, we developed a modified, modular IE approach and implemented this methodology in the commercial FEA solver Abaqus with minor user subroutine interventions.

The accuracy of this modified approach was assessed in two test cases, an arterial tube model with two families of collagen fibers embedded into the lumen wall and a porcine biventricular myocardium model with a complex architectural distribution of myocytes anchored in a connective collagen and elastic fiber embedded tissue network. The roundtrip (inverse deflation simulation followed by a forward inflation simulation) stress and displacement accuracy for the arterial model amounted to 99.43% and 98.74%, respectively, and to 99.07% and 99.53% for the cardiac model. Subsequently, we successfully applied the methodology on models containing multiple interacting incompressible, anisotropic (fiber-embedded) and hyperelastic material behaviors (see Figure). In conclusion, the developed methodology proved to be a computationally efficient and stable approach to incorporate the in vivo stress and strain state in complex patient-specific arterial and cardiac FE models.

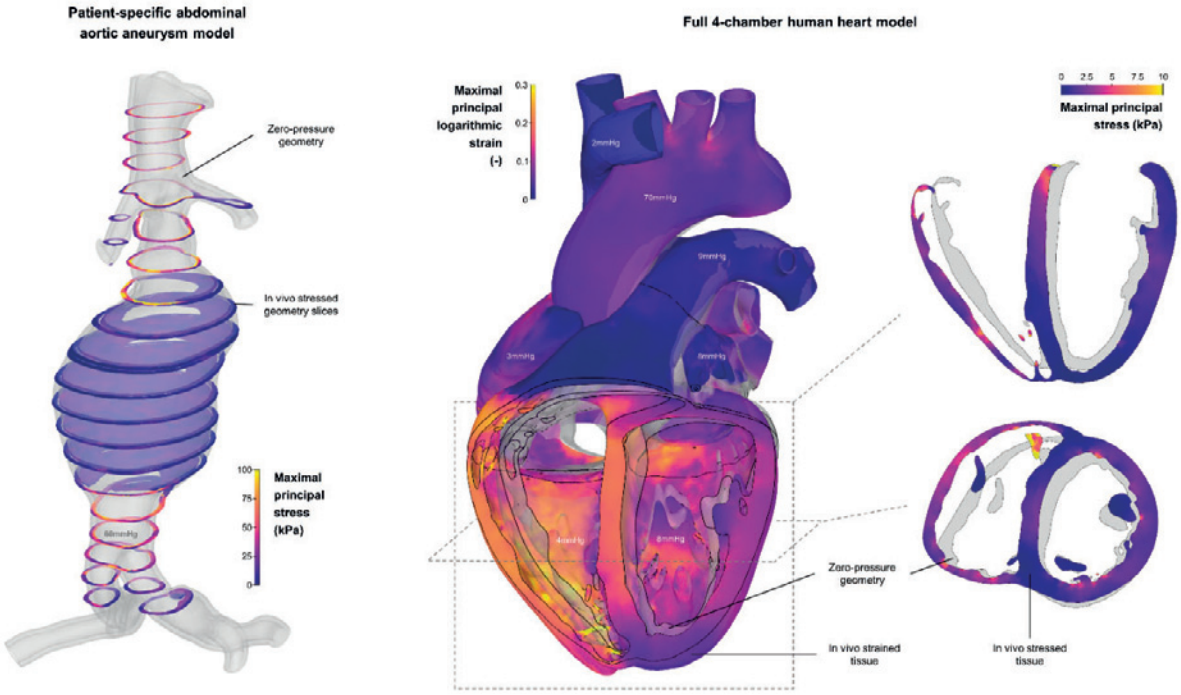

Figure Caption: Arterial and cardiac application of the modified, modular inverse elastostatics methodology. (left): computed zero pressure geometry (transparent gray) and in vivo stress state (sliced visualization) of a complex patient-specific AAA model. (mid & right): computed zero pressure state (transparent gray) and in vivo strained state of a full patient-based human heart model in diastole (computed in vivo stress state depicted in a short and long axis slice).

[C-10.4]

IDENTIFICATION OF DAMAGE CRITERIA IN PRESSURE ULCERS USING THE VIRTUAL FIELDS METHOD

Bethany Keenan[1], *Stéphane Avril*[2]

1 *Cardiff School of Engineering, Cardiff University, Soft Tissue Mechanics, Cardiff, UK*
2 *École des Mines de Saint-Étienne; Université de Lyon, France*

Soft tissues undergo large changes as a result of injury, repair and adaptation processes. The mechanics of these processes, and the ways that they adapt themselves are not well understood [1]. Although some progress has been made in understanding soft tissue mechanics under normal conditions, very little progress has been made in understanding damage and injury mechanisms or the circumstances in which they occur. In the heel, the tissue is damaged through localised overloading, which can result in the form of a pressure ulcer. The estimated cost of pressure ulcers in the UK is £1.4bn-£2.1bn [2]. There is therefore a clear need to better understand the mechanics of soft tissue damage and develop new methods to improve the efficiency of constitutive model identification and consequently guide critical clinical decisions.

The virtual fields method (VFM) is an approach to inversely identify material parameters using full-field deformation data [3]. Whilst care is needed to choose an appropriate VFM for non-linear constitutive models, the VFM is a computationally faster technique than finite element modelling updating. Automated virtual fields are now routinely used to solve linear elasticity problems but currently no automated approach exists for non-linear models. To the authors' best knowledge, this is the first study to implement the VFM for the soft tissue in the heel.

A custom virtual fields method was developed in MATLAB and evaluated using simulated data from a 3D MRI-based finite element model (Figure1). This was achieved by simulating the data that would be collected during an actual experiment (e.g. DIC). More specifically, the resultant force of the foot in contact with the mattress and the strain in the fat pad were exported from the FE solver, FEBio, for each loading step. Deviatoric stresses were directly calculated from the measured strains and expressed as functions of the unknown material properties. Stress equilibrium was evaluated by the principle of virtual work and parameters adjusted until this equilibrium was reached.

This study has proposed and verified a novel technique based on VFM aimed to extract the constitutive parameters of the heel fat pad. Results show that the proposed technique is able to accurately capture the non-linearity and anisotropy of the heel fat pad. The methods developed in this study could be applied to other soft tissue studies or foot related pathologies to better understand how injury occurs.

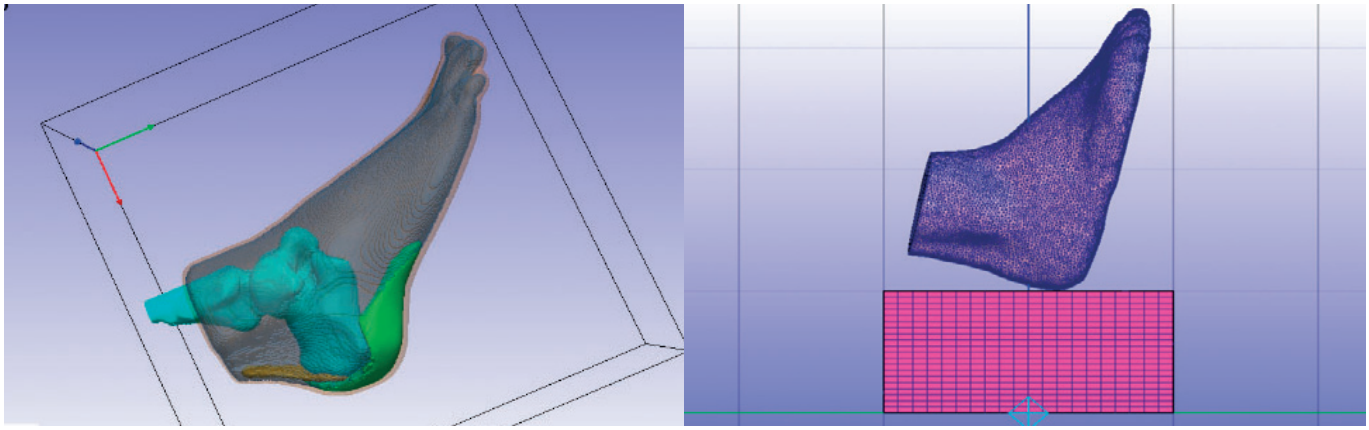

Figure1: 3D MRI-based FEM

References:

[1] Gasser TC, Damage in Vascular Tissues and its Modelling, Material Parameter Identification and inverse problems in soft tissue biomechanics. CISM 2016.
[2] Dealey, C et al. 2012. The cost of pressure ulcers in the UK. J. Wound Care 21(6).
[3] Grédiac, M et al. 2006. The VFM for extracting constitutive parameters from full field measurements. Strain 42.

[C-10.5]

OPTIMIZATION-DERIVED GLENOHUMERAL CAPSULE PROPERTIES FROM IN-VIVO LAXITY DATA

Andrew Kraszewski[1]

1 *Hospital for Special Surgery, New York, USA*

The contribution of the glenohumeral capsule to joint loading is generally understood in terms of reduced cadaveric experiments. Upper extremity musculoskeletal models do not typically represent this tissue. Parameters describing such a complex tissue are difficult to obtain. The objective was to indirectly estimate constitutive properties of a discrete mesh model through optimization from in-vivo laxity measurements.

The dataset was based on 12 experimentally tested cadaveric shoulder specimens. Each was CT-scanned, dissected, and underwent rotational laxity tests in baseline condition. A test was a rotation direction and abduction position. Internal and external axial rotation was conducted at 5°/s up to 2,000N-mm axial torque while recording 6-DOF glenohumeral kinematics and torque. This was done at 0°, 20°, 40°, and 60° of scapular abduction. Mesh origin and insertion points were selected from CT-reconstructed 3D bony geometries. The humeral head was modelled as a best-fit sphere fit to the articular surface.

The mesh consisted of 1D elements connected by nodes. It had 12 longitudinal and 5 transverse strands, where a strand is composed of serial elements with the same properties (Figure 1A). Element behavior was governed by a hyperelastic force-length model $f(x)=C1*(e^{(C2*x)}-1)$ (N). Quasi-static simulations were done in MATLAB 2018b. The optimization was performed using fmincon() to minimize a cost function, which was the sum of: i) total mesh strain-energy-density $\sum w(x)=C1*(e^{(C2*x)}/C2-x)$ (N-mm), and ii) sum-squared error between the mesh torque and experimental torque $\sum(\tau_{mesh}-\tau_{exp})^2$.

Per specimen, 3-4 frames per test were selected, totaling 24-30 frames. A frame included a joint kinematic position and corresponding torque value. Per frame, thirty-four constitutive parameters, seventeen slack length parameters, and 120 3D node coordinates were solved for simultaneously. Constraints: i) strand constitutive parameters < ±30% of adjacent strands [1,2], ii) element strain < 22.5% [1], and iii) nodes not allowed to penetrate sphere. Slack length could vary but only ±1% of predetermined values. Optimization concluded when constraint violation was between 0.1 and 1, and when the cost function was less than 106.

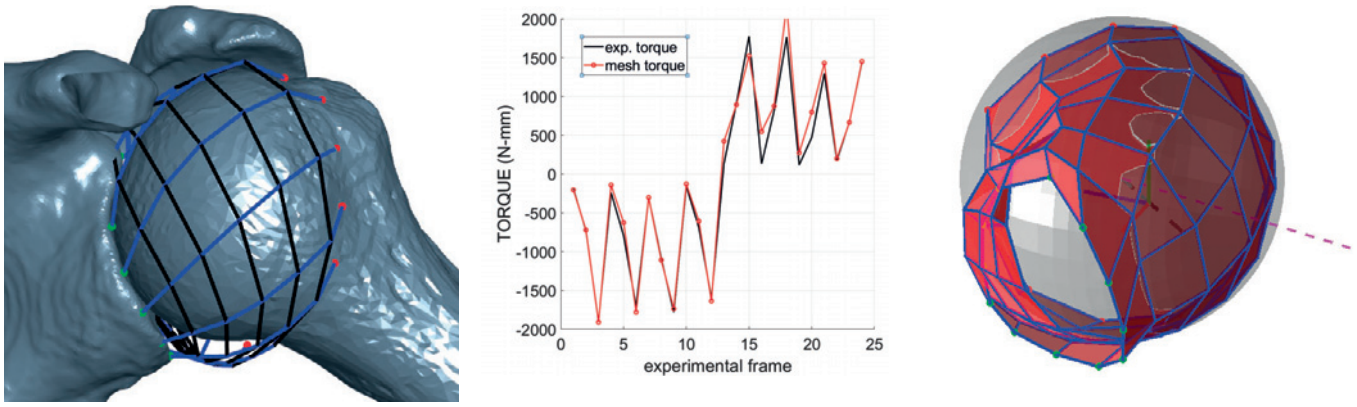

Figure 1: A – Computational mesh showing elements, strands, and nodes. B – Torque profiles across test frames, from one specimen, where the mesh (red lines) closely matches experimental values (black lines). C – Mesh solution for the ninth test frame, crimping indicates the mesh was locally slack.

Average results from 5 specimens are presented, with the study ongoing. The torque root mean square error was 272N-mm. Longitudinal strand constitutive parameters were 1.28N (C1) and 1.46 (C2), and transverse parameters were 0.66N (C1) and 1.22 (C2). C1 findings are marginally similar to published values obtained through mechanical testing, but C2 findings are much lower. This approach may yield an effective model for simulating end-range-of-motion activities like overhead sports. The model is sensitive to slack length and future work will explore obtaining slack length parameters through optimization.

References:

1. *Bigliani, LU et al. Tensile Properties of the Inferior Glenohumeral Ligament, J Ortho Res, 1992.*
2. *Ticker, JB et al. Inferior glenohumeral ligament: Geometric and strain-rate dependent properties, J Shouler Elbow Surg, 1996.*

[C-10.6]

IN VIVO IDENTIFICATION OF THE MECHANICAL PROPERTIES OF THE THIGH TISSUES FROM FREEHAND ULTRASOUND FOR THE NUMERICAL INVESTIGATION OF LOADS AT THE SOCKET/RESIDUAL LIMB INTERFACE OF AMPUTEE PEOPLE

Fougeron Nolwenn[1], *Bonnet Xavier*[2], *Rose Jean-Loïc*[3], *Pierre-Yves Rohan*[4], *Pillet Hélène*[4]

1 *Institut de Biomécanique Humaine Georges Charpak, Arts et Métiers ParisTech, Paris, France; Proteor, Recherche et Développement, Dijon, France*
2 *Institut de Biomécanique Humaine Georges Charpak, Arts et Métiers ParisTech, Paris, France, Arts et Metiers Paristech*
3 *Proteor, Recherche et Développement, Dijon, France*
4 *Institut de Biomécanique Humaine Georges Charpak, Arts et Métiers ParisTech, Paris, France*

Prosthetic sockets are custom-designed and are decisive for functionality and comfort of limb prosthesis. To ensure load transmission and stability, high interface stresses are applied. Several computer models of the socket/residual limb assembly have been designed to identify critical stress accumulations that may induce discomfort or trauma. However, clinically relevant personalized Finite Element (FE) models represent a bottleneck. While material definition of tissues is critical for the evaluation of socket/tissues interactions, personalization of deep Soft Tissue (ST) material properties remains challenging. For clinical purpose, it has to be simple, in vivo and thus non-invasive. This work explores the feasibility of freehand ultrasound with an inverse method for assessing mechanical properties of the ST of the thigh. To be relevant for socket design, the residual strain from donning socket was simulated by compressing tissues (5% of initial circumference).

Force-displacement curves acquired during localized compressions of the anterior thigh of one non-amputee subject was measured with a custom-made set-up combining freehand ultrasound and a force sensor (fig 1A). Two configurations were investigated, for which three acquisitions of ten loading/unloading cycles were acquired. From the ultrasound images, an idealized geometry of the thigh was designed. A FE model was designed to model the response of tissues in large displacement (>20 mm) with Ogden constitutive model (fig 1B). Material parameters were calibrated against mean experimental data for each configuration. A membrane was added in the compressed model.

Experimental and simulation curves of both configurations are provided below (fig 1C). The optimized shear modulus are 1.3 and 7.4 kPa, with RMSE of 2.4 and 3.2, for configurations 1 and 2, respectively.

A simple non-invasive method to identify the in vivo mechanical properties from FreeHand Ultrasound was developed. Results are only presented for one of the six subjects that will participate to the study, but preliminary results are encouraging. In fact, although being freehand, the proposed method allows fitting simulations to experimental data. Moreover, resulting shear modulus are consistent with literature [1]. To authors' knowledge, this is the first attempt to compare uncompressed and compressed tissues in vivo material properties, in order to consider the compressed state of ST in sockets. Configurations in large deformation allow capturing the response of tissues in domains compatible with the use of prosthesis. These results contrast with previous studies where methods were cumbersome and/or not sufficient to assess the mechanical properties of ST.

Figure Caption: A) Studied configurations: relaxed and uncompressed versus relaxed and B) FE simulation C) mean experimental results (continuous lines) and simulation curves (dotted lines). Green: compressed, red: uncompressed.

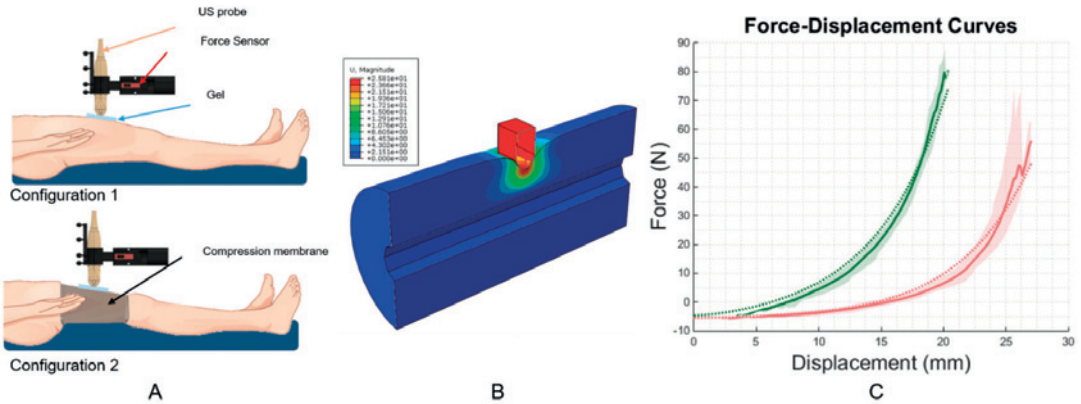

References:

G. Dubois et al., "Reliable Protocol for Shear Wave Elastography of Lower Limb Muscles at Rest and During Passive Stretching," Ultrasound Med. Biol.,41(9), 2284–2291, 2015.

[C-11.1]

TOWARD AN EXPRESSIVE BIPEDAL ROBOT: VARIABLE GAIT GENERATION AND VALIDATION ON A PLANAR COMPASS BIPED AND A CORE-DRIVEN PLANAR BIPED ACROSS MULTIPLE ENVIRONMENTS

Amy LaViers[1]

1 *University of Illinois at Urbana-Champaign, Illinois, USA*

Movement seems to encode information. How does this work? We know that animals, including humans, use the motion of counterparts to produce coordinated, social behaviors. But how do we resolve the discrete measures of communication and information theory with the continuous laws of motion and mechanics? Answering these questions is critical to developing expressive robotic systems that integrate seamlessly with natural counterparts – a goal that has increasing urgency as robots move out of factories and into workplaces and homes. This talk presents work in generating variable bipedal gait via parameters embedded as constraints in an optimization and predicting perceived affect when human viewers observe artificial gait across multiple environments. This work includes projects spanning hardware, algorithm design, and human perception prediction. In particular, the design of a core-driven bipedal robot is developed from study of Bartenieff Fundamentals, an embodied movement practice that emphasizes the role of the falling pelvis in human gait; hundreds of feasible gaits for two planar biped designs are found in simulation and a small subset is labeled with human viewers; and further human subjects studies shows that modeling context is critical in predicting human perception of gait. In addition to traditional tools in dynamics, control, and empirical measurement, these projects leverage qualitative observation, embodied movement practice, and artistic creation. Thus, the talk will also highlight how dancing with robots is critical to developing automation that functions correctly in human-built spaces.

Acknowledgments: This work has been sponsored by NSF grants #1701295 and #1528036 and performed by members of the Robotics, Automation, and Dance (RAD) Lab at the University of Illinois at Urbana-Champaign and its collaborators.

References:

U. Huzaifa, C. Maguire, and A. LaViers. "Toward an Expressive Bipedal Robot: Variable Gait Synthesis and Validation in a Planar Model." arXiv:1808.05594 [cs.RO] (under review – revision requested and in progress)

M. Heimerdinger and A. LaViers. "Modeling the Interactions of Context and Style on Affect in Motion Perception: Stylized Gaits Across Multiple Environmental Contexts." International Journal on Social Robotics (SORO). 1875-4791 1-19. 2019.

A. LaViers. "Programmed Improvisation Inspired From Autonomous Humanoids." 513-526, Chapter in Handbook of Improvisation in Dance. Vida Midgelow (Ed.) Oxford University Press. 2019.

I. Pakrasi, N. Chakraborty, C. Cuan, E. Berl, W. Rizvi, and A. LaViers. "Dancing Droids: An Expressive Layer for Mobile Robots Developed Within Choreographic Practice." International Conference on Social Robotics (ICSR). 410-420. Qingdao, China, 2018.

A. LaViers, et al., "Choreographic and Somatic Approaches for the Development of Expressive Robotic Systems," Arts (Special Issue on Machine as Artist for the 21st Century). MDPI. 7(2) 1-11. 2018.

M. Heimerdinger and A. LaViers. "Influence of Environmental Context on Recognition Rates of Stylized Walking Sequences." Ninth International Conference on Social Robotics (ICSR). 272-282. Tsukuba, Japan. 2017.

T. Marino, C. Widdowson, A. Oetting, A. Lakshmanan, H. Cui, N. Hovakimyan, R. Wang, A. Kirlik, A. LaViers, D. Stipanovic. "Carebots: Prolonged Elderly Independence Using Small Mobile Robots." ASME Mechanical Engineering Magazine. 138(9) S8-S13. 2016.

U. Huzaifa and A. LaViers. "Control Design for Planar Model of a Core-located Actuation Walker." 6th IEEE International Conference on Biomedical Robotics and Biomechatronics (BioRob). 170-175. Singapore. 2016.

U. Huzaifa, C. Bernier, Z. Calhoun, C. Kohout, J. Heddy, B. Libowitz, A. Moenning, J. Ye, C. Maguire, and A. LaViers. "Embodied Movement Strategies for Development of a Core-located Actuation Walker." 6th IEEE International Conference on Biomedical Robotics and Biomechatronics (BioRob). 176-181. Singapore. 2016. (Best Poster Finalist)

A. LaViers, A. Bashiri, Y. Sheng, J. Heddy, and L. Bai. "Abstractions for Design- by-Humans of Heterogeneous Autonomous Behaviors." 237-262, Chapter in Dance Notations and Robot Motion Springer Tracts in Advanced Robotics (STAR). 2015.

[C-11.2]

WALKING PRINCIPLE FROM BALANCE STABILITY PERSPECTIVE: FROM ROLLING WHEEL TO HUMAN TO ROBOT

Carlotta Mummolo[1], *William Z. Peng*[2], ***Joo H. Kim***[2]

1 *New Jersey Institute of Technology, Newark, USA*
2 *New York University, New York, USA*
**These authors contributed equally to this work.*

Legged systems, such as biped robots and humans, are generally unstable. In this work, a theoretical-algorithmic framework that estimates the balanced and unbalanced states of a biped system is introduced and is used to evaluate the relevant walking principle. Comprehensive and univocal definitions of the states of balance of a generic legged system are introduced with respect to the system's contact with the environment. Theoretical models of joint-space and center of mass (COM)-space dynamics under multiple contacts, distribution of contact wrenches, and system parameters are established for their integration into a nonlinear programming problem. In the proposed approach, the balance stability capabilities of a biped system are quantified by a partition of the state space of COM position and velocity. The boundary of such a partition provides a threshold between balanced versus unbalanced states of the biped system with respect to a specified contact configuration. For a COM state to be outside of the stability boundary represents the sufficient condition for unbalanced, from which a change in the system's contact is inevitable. Through the calculated stability boundaries, the effects of different contact configurations (single support and double support with different step lengths) and angular momentum on the system's balance stability capabilities can be quantitatively evaluated. Using the boundary results, the principle of bipedal walking is discussed from balance stability perspective for locomotion systems with various levels of performance: rolling wheel, human, biped robot, and wearable robot. The discussion will also include the trade-off between balance stability and energetic efficiency of bipedal walking.

[C-11.3]

MULTIMODAL FOOT-GROUND CONTACT INTERACTION IN HUMAN POSTURAL STABILITY

Giulia Vicentini[1], ***Carlotta Mummolo***[2]

1New York University, New York, USA
2New Jersey Institute of Technology, Newark, USA

The human foot structure endures complex contact interactions with the ground, allowing the body to move with remarkable agility and stability. During balancing tasks, the recovery action from a perturbed posture could benefit from intermittent heel and toe lifting, as compared to the flat-foot fixed contact configuration. The proposed unified approach generates balancing trajectories of a human posture model recovering from velocity perturbations in the anterior-posterior direction, while exploiting the multimodal nature of the foot-ground contact interaction.

A six-link planar mechanism represents the human body in sagittal plane (Fig. 1). Left and right lower-body joints are modeled in parallel through one equivalent joint for hip, knee, ankle, and toe motion, with equivalent rotation and actuation limits. The upper body is modeled by the HAT body segment (head-torso-arms), connected to the hip by a torso joint and a pelvis segment.

The proposed foot model can establish multiple contact modes with the ground. The contact interaction is modeled through one equivalent resultant force applied at the system's time-varying center of pressure (COP), to mimic heel-to-toe ground pressure distribution. A contact mode detection algorithm is established to map at each time the foot angles θ_1 and θ_2 into to corresponding contact modes and associated COP lower and upper limits (Fig. 1). The transition between discrete modes is approximated by two surface functions, $f^L(\theta_1, \theta_2)$ and $f^U(\theta_1, \theta_2)$, that provide continuous values for COP lower and upper limits.

Joint-space and center of mass (COM)-space dynamics are used to formulate joint torques, COM motion, ground reaction forces, and COP position, as functions of joint motion. Balancing trajectories that drive the system's COM from a perturbed state (position and velocity) to a rest state (upright static posture) are generated through a constrained optimization problem, to investigate the maximum allowable COM velocity perturbation along the anterior-posterior direction (Mummolo et al. 2018). The optimal joint motion and control trajectories resulting from optimization are subject to:

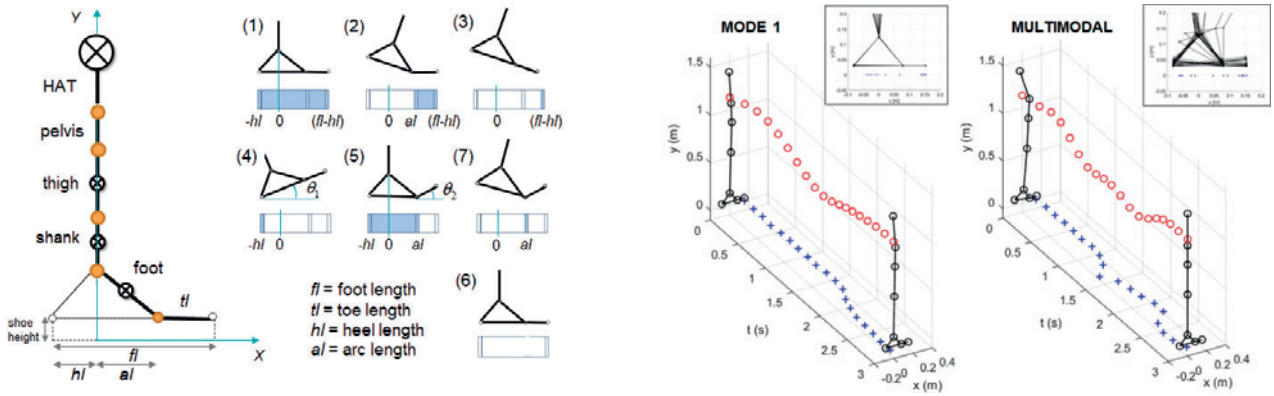

Kinematics Constraints: anatomical ranges of motion; mode 6 exclusion, by constraining the toe joint position on an arc centered on the heel, and vice versa; ground penetration avoidance; COM initial position and final rest state. Kinetics Constraints: anthropometric torque limits; positive normal ground reaction force; friction cone; COP position within $f^L(\theta_1, \theta_2)$ and $f^U(\theta_1, \theta_2)$.

The multimodal contact interaction allows for greater COM velocity perturbation in the anterior/posterior directions (+0.788/-0.411 m/s), as compared with flat-foot interaction (i.e., mode 1; +0.483/-0.284 m/s). The multimodal foot-ground contact schedule naturally arises from optimization results, leading to greater balancing capabilities in the human postural model (Fig. 2).

References:

Mummolo, et al. Journal of Mechanisms and Robotics. 2018;10(2):021009.

[C-11.4]

PREDECTIVE MODELS OF ENERGY EXPENDITURE FOR ACTUATED DYNAMIC SYSTEMS: HUMAN VERSUS ROBOT

Joo H. Kim[1], *William Z. Peng*[1]

1 *New York University, New York, USA*

Energy expenditure—as the consumption of an energy source—of actuated dynamic systems, such as machines and humans, is an important performance criterion but is complicated to measure and difficult to predict. The objective of this study is to establish rigorous mathematical models of energy expenditure for actuated dynamic systems as functions of state variables, control inputs, and system parameters. The model forms are derived theoretically using the laws of thermodynamics, the principles of multibody system dynamics, and the working principles of actuators and energy supplies, while the model parameters are estimated experimentally. The internal energy for chemical reactions (e.g., battery and food) and heat are formulated in terms of kinematic and dynamic variables. The work components for actuation (e.g., electric motor and muscle), dissipation, restoration, and reaction are formulated with respect to generalized coordinates. The reversibility/irreversibility of the energy transformations in actuators (regenerative vs. non-regenerative) and energy supplies (rechargeable vs. non-rechargeable) are taken into account to address negative as well as positive and zero work. The predictive models are developed to reliably and accurately evaluate instantaneous energy expenditure without limitations inherent in experimental measurements or other approximation methods. Experimental and computational results of robotic and human task (such as walking) energetics will be used as illustrative examples.

[C-11.5]

DESIGN AND EVALUATION OF EXOSKELETONS WITH NEUROMUSCULOSKELETAL MODELING

Xianlian Zhou[1]

1 *New Jersey Institute of Technology, Newark, USA*

Design and evaluation of exoskeletons is often a time consuming and costly process that involves prototype fabrication, human testing, and several design iterations. For active exoskeletons, the primary challenge is to detect movement intent of the wearer and provide potent assistance, which often requires sophisticated control algorithm implementation. The goal of this study is to integrate human neuromusculoskeletal modeling with robot modeling and control for human-in-the-loop simulations. We will present several exoskeleton designs and demonstrate utilization of this integrated approach for virtual evaluation of exoskeletons in terms of their functionalities and biomechanical effects on the wearer' musculoskeletal system. One of the exoskeletons is a lower extremity exoskeleton that is elastically strapped onto human body. It has 3 rotational DOF on each side of the body and contains 6 idealized actuators that can generate both positive and negative (i.e. push and pull) forces. Two different torque compensation controllers of the exoskeleton were introduced, aiming to 1) minimize the interaction forces between the exoskeleton and the wearer and 2) provide maximum assistive torques to help the wearer's motion, respectively. The effects of these two controllers on the wearer's biomechanical loadings were studied with a running motion, in which the ground reaction forces were predicted. By examining the interaction forces between the exoskeleton and the wearer, the wearer's joint torques, joint reaction forces, and muscle activations (i.e. neuro control) and comparing them with those of the purely passive exoskeleton, we showed sound evidence of the efficacy of these two controllers on reducing the wearer's musculoskeletal loadings. The second assistive controller in particular reduced both hip and knee joint torques significantly. The first controller, despite of providing less assistance, is much easier to implement in practice as it needs only sensory information from the exoskeleton (i.e. exo-joint angles), whereas the second controller requires additional information on human kinematics and derived dynamics quantities. Other examples including hand and upper arm exoskeletons and their interaction with human body will also be presented. In summary, the proposed human-in-the-loop simulation paradigm can be utilized for virtual design and evaluation of exoskeletons and pave the way to build optimized exoskeleton prototypes for experimental evaluation.

[C-11.6]

OPTIMIZATION OF THE KINEMATIC CHAIN OF THE THUMB FOR A HAND PROSTHESIS BASED ON THE KAPANDJI OPPOSITION TEST

Antonio Pérez-González[1], ***Immaculada Llop-Harillo***[2]

1 *Universitat Jaume I, Castellón, Spain (Uji)*
2 *Universitat Jaume I, Castellón, Spain (Uji); Universitat Jaume I, Castellón, Spain; Departamento de Ingeniería Mecánica Y Construcción*

The human hand is a marvelous tool optimized in an evolutionary process since our ancestors. Thumb opposition is said to be one distinctive feature of the human hand. The Kapandji opposition test (KOT) [1] was proposed as a simple method for assessing the opposition of the thumb in pathological hands. The design of artificial hands, both prosthetic and robotic, is moving in last decades towards devices more anthropomorphic, to improve the functionality and the cosmetic appearance. However, their thumb's kinematic chain (TKC) is normally simplified with respect to that of the human hand. This simplification is mainly guided by the difficulty of obtaining adequate mechanical solutions for reproducing the geometry and mobility of the carpometacarpal (CMC) and metacarpophalangeal (MCP) joints, but also by the attempt to simplify the artificial hand control.

Here we tested a method for optimizing the TKC of a prosthetic hand based on the KOT. A simplified model of the IMMA hand [2], a 3D-printed 5-digit prosthetic hand designed by the authors, was created in Matlab (Figure 1). The model has four straight links for each digit. The joints range of motion (ROM) was defined based on the hand prototype. The TKC was optimized in order to minimize the mean position error (MPE) when trying to adopt the nine first positions of the KOT. The variables for the optimization were the orientation of the CMC and MCP joints, the thumb's links length and the position of the CMC joint. The position error for each position of the KOT was defined as the minimum achievable distance between the thumb tip and the corresponding finger point (obtained by a nested optimization process where the variables were the joint angles, constrained by their ROM). The Matlab genetic algorithm was used for the optimization of the TKC whereas fmincon function was used for the nested optimization for each position of the KOT.

The results indicate that the method allowed decreasing the MPE relative to the hand length from 0.13 to 0.04. However, additional simulations in Matlab for the original and improved designs when grasping primitive shape objects suggest that the improvement of the TKC based on KOT does not guarantee better grasping postures. Future work should address the improvement of the optimization objective and the inclusion of the kinematic chain of other digits as variables.

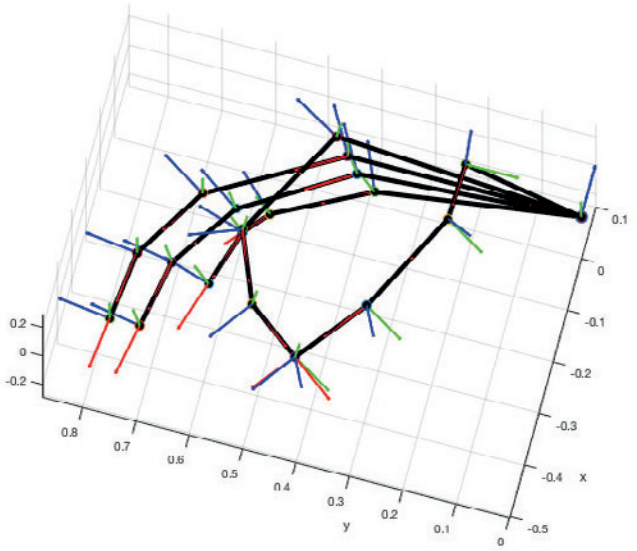

Figure 1: Prosthetic hand model in position 3 of the Kapandji opposition test

Acknowledgments: This work was supported by grants DPI2017-89910-R and BES-2015-076005 from the MINECO, ERDF and ESF, and by grant UJI-B2017-70 from Universitat Jaume I, Castellón, Spain.

References:

[1] Kapandji, Annales de Chirurgie de la Main 5(1),67-73,1986.
[2] Llop-Harillo et al., International Biomechanics 4(2):50-59,2017.

[D-01.1]

EXPERIMENTAL CHARACTERIZATION, CONSTITUTIVE MODELING, AND COMPUTATIONAL SIMULATIONS OF LIGAMENTS OF THE KNEE

Ellen Arruda[1]

1 *University of Michigan, Ann Arbor, USA*

Injuries in soft tissues of the knee such as the anterior cruciate ligament (or ACL) occur in elite athletes and weekend warriors alike. A long-term goal of my work in this area is to prevent many of these injuries. Not enough work has been done to understand the finite deformation response of these non-linear, anisotropic, poro-visco-elastic tissue structures - not to mention how they fail. This talk will focus on our recent efforts to characterize the ACL response utilizing full-field displacement measurement techniques that offer more accurate, repeatable, and comprehensive experimental data than traditional testing methods. We've pioneered full-volume characterization techniques that provide much needed insight into the inaccuracies associated with many current experimental protocols and also the shortcomings of some popular constitutive models in capturing the full 3D response of the ACL. I will describe how we use these data to develop constitutive models for soft tissues and implement them into computational models of the knee for gait analysis and impact loading simulations. Accurate computational models of the knee such as ours may one day be used to guide clinical practice to determine the best course of action to repair an injury.

[D-01.2]
MATHEMATICAL MODEL OF AGE-SPECIFIC TENDON HEALING

Akinjide Akintunde[1], *Daniele Schiavazzi*[2], ***Kristin Miller***[1]

1 *Tulane University, New Orleans, USA*
2 *University of Notre Dame, Notre Dame, USA*

Tendons perform unique functions in the body—transmit muscle generated force to bones for joint motion. However, decreased mechanical response is observed post-injury and during aging, which in turn limits functional capacity. While there are many strategies aimed at restoration of pre-injury mechanical properties, they fail typically because of lack of understanding of tendon healing mechanisms, particularly at the extracellular matrix level. Toward this end, mathematical models, especially those with microstructural details can be insightful. In prior study, we evaluated the ability of three constitutive models to describe uniaxial mechanical test data from murine patellar tendons excised pre- and post-injury from multiple age groups [1]. The chosen models range from simple i.e. the Freed-Rajagopal (FR) model, to complex i.e. the Gasser-Ogden-Holzapfel (GOH) and Shearer (SHR) models. Least-squares optimization was performed to obtain model parameter values, while the models fitted the experimental data adequately, the relatively complex models exhibited low parameter identifiability evidenced by high correlation. To address the limitations observed in the prior study, we adopted a Bayesian approach using an adaptive Markov chain Monte Carlo (MCMC) to compute the posterior distribution of model parameters [2]. Local identifiability of the model parameters was assessed through the rank of the Fisher information matrix, and the correlation identified from stationary posterior samples. Global sensitivity analysis was performed using Monte Carlo estimates of the Sobol indices. Learning factor—depends on the ratio of posterior to prior marginal variance—was used to assess how well MCMC performed between fitting model using all data (ALL) versus the average (AVG) per age-healing timepoints. Agreement of two approaches was observed only in the FR model parameters. Also, while high negative correlation values were recorded between structural parameters of the GOH and SHR models, the FR model parameters were all identifiable. In the upcoming talk, we highlight the trade-off between model complexity and confidence level of inferred parameters, the critical need for structural data to motivate clinical relevance of mathematical model for tendons. Addressing these needs would enhance translational research and motivate the rational design of tissue engineering strategies for better treatment outcomes."

Acknowledgments: "We thank Dr. Lou Soslowsky of the University of Pennsylvania, Philadelphia, United States for the experimental data and NIH P20GM103629 (KSM) for support."

References:

[1] Akintunde & Miller 2018 Biomech model mechanobiol [2] Akintunde et al. (in review) J Mech Behav Biomed.

[D-01.3]

ULTRASOUND STRAIN MAPPING FOR MEASURING TENDON COMPRESSION IN PATIENTS WITH TENDINOPATHY.

*Ruth Chimenti[1], A. Samuel Flemister[2], John Ketz[2], Mark Buckley[3], **Michael Richards**[4]*

1 *University of Iowa Carver College of Medicine, Iowa, USA; Department of Physical Therapy and Rehabilitation Science*
2 *University of Rochester, New York, USA, Medical Center; Department of Orthopaedics & Rehabilitation*
3 *University of Rochester, New York, USA; Department of Biomedical Engineering*
4 *Rochester Institute of Technology, Rochester, USA*

One of the most frequent sites of tendon pathology is the Achilles, which connects the calf muscles (gastrocnemius, soleus) to the heel bone (calcaneus). It is estimated that the cumulative lifetime incidence of Achilles tendon pathology in the general population is between 6 and 15% [1]. Approximately 1/3 of cases of Achilles tendon pathology involve the tendon insertion [2] and are classified as insertional Achilles tendinopathy (IAT). IAT causes intense foot pain focused near the heel that is exacerbated by activity and more than 50% of people with IAT fail conservative care and require surgery. To improve clinical outcomes for IAT patients, there is a need to develop new and effective conservative treatments for IAT and we hypothesize that understanding the role of tendon compression will aid in the development of these therapies. The purpose of this study was to: 1) to quantify tendon compression using ultrasound and examine the effects of heel lifts on tendon compression during dorsiflexion; 2) Assess the compressive strain at the Achilles tendon insertion in individuals with IAT during dorsiflexion compared to healthy subjects. Tendon compression in ten adults with no Achilles tendinopathy was measured during three weight-bearing tasks: 1) Lowering via a controlled removal of a heel lift, 2) Performing a partial squat to a tibial inclination of 15o, and 3) Combined lowering and partial squat (Fig 1). Subjects Achilles tendons were imaged with a SonixTouch Ultrasound system (Analogic, Boston, MA) with RF image capabilities (Fig 1,2). An image registration algorithm [3] was adapted to cumulatively (over 50-100 image frames) measure the total strain over each exercise using the US image sequences. The tendon compression was defined as the absolute value of the minimum principal strain in the region of Achilles tendon overlying the bursal prominence, which was subdivided into superficial and deep regions (Fig 2). Tibial inclination during the partial squat was independently measured via video. Ten adults with IAT were also tested during task 3 to compare to healthy subjects. There was significantly greater compression during task 3 compared to the individual tasks and greater compression on the deep tendon compared to the superficial region for all tasks (Fig 3a). Note that heel lowering to a neutral ankle position induces substantial compression, comparable to a partial squat. Compressive strains were lower in the IAT group and lowest in the subjects who experience pain (Fig 3b). These preliminary findings suggest that IAT tendons experience lower compression due to some biomechanical stiffening induced within the tendon and that it may be transferred compression in the surrounding tissues which causes pain during dorsiflexion.

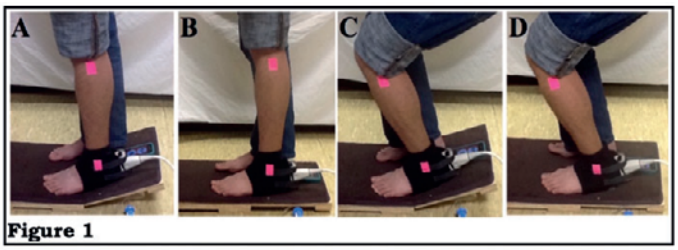

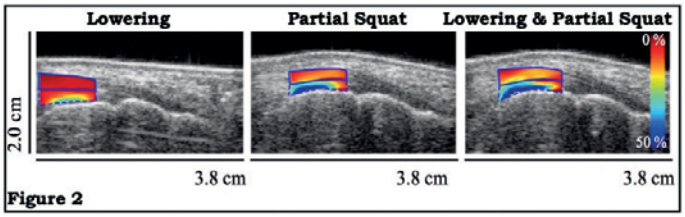

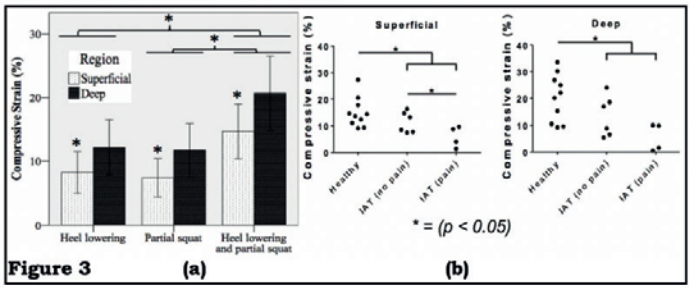

Figure 1. Task 1: A to B, Task 2: A to C, Task 3: A to B to D

Figure 2. Compressive strain in the Achilles insertion for 1 subject, 3 tasks.

Figure 3. (a) Compression in deep and superficial Achilles tendon regions for three tasks in healthy subjects. (b) Compressive strain during task 3 in Achilles tendon comparing healthy controls to individuals with IAT. IAT (pain) denotes subjects who experienced pain during task [4].

Acknowledgments: This work was partially supported by NIH-funded study (R03 AR067484) and (R01 AR070765).

References:

1. *Kujala UM, et al. Cumulative incidence of AT rupture and tendinopathy in male former elite athletes. CJSM. 2005;15(3):133-5.*
2. *Karjalainen PT, et al. MR imaging of overuse injuries of the Achilles tendon. AJR, 2000;175(1):251-60.*
3. *Richards MS, et al. Non-rigid image registration-based strain estimator for IVUS elastography. Ultrasound Med Bio, 2013;39(3):515-33.*
4. *Chimenti, Ruth L., et al. "Ultrasound strain mapping of Achilles tendon compressive strain patterns during dorsiflexion." Journal of biomechanics 49.1 (2016): 39-44.*

[D-01.4]

ULTRASOUND STRAIN MAPPING OF TRANSVERSE COMPRESSIVE STRAINS IN THE MOUSE ACHILLES TENDON INSERTION DURING DORSIFLEXION

Keshia Mora[1], *Samuel Mlawer*[1], *Michael Richards*[2], *Alayna Loiselle*[1], *Mark Buckley*[1]

1 *University of Rochester, New York, USA*
2 *Rochester Institute of Technology, Rochester, USA*

Introduction: Although tendon predominantly experiences tensile forces, extreme transverse compression, due to contact from neighboring bony structures, has been implicated in the development of tendon pathologies including rotator cuff disease and insertional Achilles tendinopathy [1]. Previous studies in mice have demonstrated that static dorsiflexion leads to the development of insertional tendon pathology [2]. However, the mechanical strain environment in the Achilles tendon insertion associated with this loading condition is unknown. Here we implement high frequency ultrasound elastography to test the hypothesis that passive dorsiflexion produces high magnitudes of transverse compressive strain in the mouse Achilles tendon under passive dorsiflexion. By describing the strain pattern in a scenario known to cause insertional tendinopathy, this study is taking a key step towards connecting aberrant mechanical cues with pathological alterations in tendons.

Methods: Hindlimb explants of skeletally mature mice (N=3), were embedded below the knee and loaded onto a custom 3D-printed platform. A cord tied across the mouse paw, was used to apply passive dorsiflexion across ankle angles beginning at 90° and ending at 130°. A high frequency ultrasound system (Vevo 3100, FUJIFILM VisualSonics) set to collect raw radiofrequency image data with a 30-70 MHz transducer was used to collect image sequences. Average transverse compressive strain (defined as the minimum principal strain) was calculated in a region of interest within the Achilles tendon insertion (above the superior aspect of the calcaneus), implementing a previously described non-rigid image registration-based algorithm [3].

Results: Under static dorsiflexion, large magnitudes (up to -27%) of transverse compressive strain were measured in the mouse Achilles tendon insertion (Fig, 1, Table 1).

Discussion: The large compressive strains observed in the Achilles tendon insertion as a result of passive ankle rotation are consistent with our hypothesis and with previous ultrasound-based assessments of multiaxial strains in the human Achilles tendon insertion during different activities [3]. Since static dorsiflexion is known to induce pathological alterations in the mouse Achilles tendon insertion [2], this study suggests a possible link between transverse compressive strain and insertional disease.

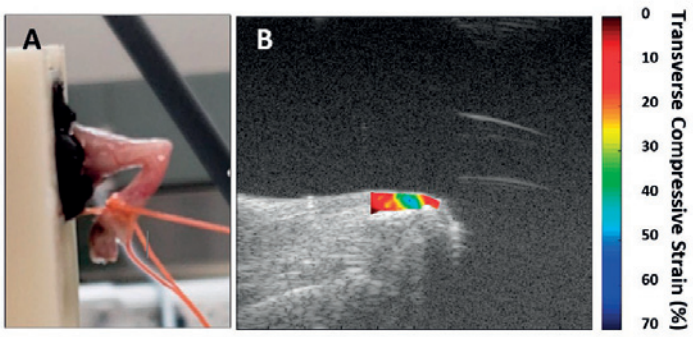

FIG 1. A) Image of representative a mouse hindlimb explant undergoing passive dorsiflexion in our custom 3D-printed platform. B) Representative transverse compressive strain map in a region of interest within the Achilles tendon insertion overlaying a b-mode image of the mouse hindlimb.

Specimen	Transverse Compressive Strain
Specimen 1	-27.2%
Specimen 2	-27.1%
Specimen 3	-25.0%

TABLE 1. Average transverse compressive strain due to static dorsiflexion in a region of interest within the mouse Achilles tendon insertion.

References:

[1] *Cook at al. 2011, Br J Sports Med;*
[2] *Wang et al. 2018, Journal Clin Invest;*
[3] *Chimenti et al. 2016, J Biomech*

[D-01.5]

HELICAL GROUPING IS A POTENTIAL MECHANISM OF INTERFIBRILLAR LOAD TRANSFER: A FE STUDY BASED ON SERIAL BLOCK-FACE SEM OF TENDON

Babak Safa[1], *John Peloquin*[1], *jessica natriello*[1], *jeffrey caplan*[1], *Dawn Elliott*[2]

1 *University of Delaware, Newark, USA*
2 *University of Delaware, Newark, USA; Dept of Biomedical Engineering*

Load transfer between tendon's fibrillar elements occurs at multiple length scales. The micro-scale is especially important, because it includes the cells and their surrounding collagen fibrils. The interactions between these elements can have potentially important physiological and pathological effects. However, the three-dimensional microstructure and the microscale mechanisms of load transfer are not known. Interfibrillar matrix shear and direct load transfer via the fusion/branching of small fibrils are postulated to be responsible for microscale load transfer, but the significance of these mechanisms is still unclear [1,2]. The helical tendon fibrils, alternatively, may also mediate load transfer [3], however, these structures are not well studied due to the lack of a three-dimensional visualization of tendon microstructure. In this study, we studied rat tail tendon fascicles using serial block-face scanning electron microscopy (SBF-SEM) over a 86.2 µm scan depth, and developed a finite element (FE) model to investigate the mechanical implications of helically wrapped fibrils [4].

We found that tendon fibrils have a complex architecture with many groups of helically wrapped fibrils, where the helices had a pitch of 39 ± 18 µm and were both left-handed (13 out of 20) and right-handed (7 out of 20) (Fig.1). Further, FE modeling indicated that frictional contact between helical fibrils can induce load transfer even in the absence of matrix bonding or fibril fusion/branching. This was shown by simulating two helical fibrils sliding past each other with frictional contact (Fig.2). Increased the frictional coefficient in the contact surface increased both axial stress and deformation. In conclusion, we showed that the interfibrillar friction should be considered as an additional mechanism for interfibrillar load transfer. This study is significant in that it provides a three-dimensional view of the tendon microstructure and suggests friction between helically wrapped fibrils as a mechanism for load transfer, which is an important aspect of tendon biomechanics.

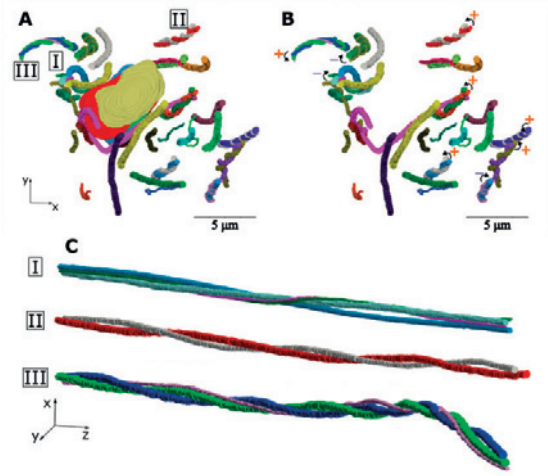

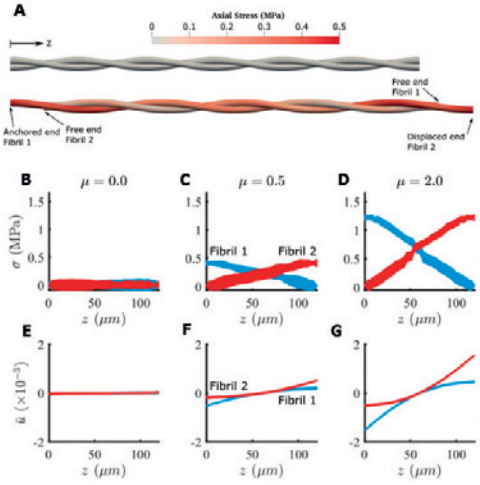

Fig.1: 3D segmentation of fibrils around the tendon cells (A), showing both left- and right-handed helices (B). Example of the helical groups (C)

Fig.2: FE model of a pair of helical fibrils showing that increasing frictional coefficient increases both axial stress (B-D) and normalized axial deformation (E-G)

Acknowledgments: Delaware Biotechnology Institute (DBI) and the Thermo Fisher Scientific Company for SBF-SEM imaging. NIH-NIBIB grant R01-EB002425, NIH-NIGMS P20-GM103446, NSF IIA-1301765 and the State of Delaware.

References:

[1] *Fessel et al., Matrix Biol., 28: 503–10, 2009.*
[2] *Szczesny et al., J. Orthop. Res., 35: 2127–2134, 2017.*
[3] *Kalson et al., Elife, 4: 2015. [4] Safa et al., bioRxiv, 547281, 2019.*

[D-03.1]

MECHANICAL PREDICTORS OF ATHEROSCLEROTIC PLAQUE RUPTURE: BEYOND 'WHERE STRESS, THERE RUPTURE'

Daniel Rutten[1], ***Frank Gijsen***[1], *Ali Akyildiz*[1]

1 *Erasmus MC, Rotterdam, Netherlands*

Introduction: Plaque rupture occurs when plaque's structural integrity is compromised by a mechanical load. Seminal biomechanical modelling studies demonstrated colocalization of rupture and circumferential stress [1]. Subsequent research has mostly focused on improving modelling techniques and the acquisition of imaging data. However, there has been little-to-no investigation into the rupture-predictive power of alternative mechanical metrics. This study performed colocalization-analyses for a comprehensive selection of mechanical metrics to identify their rupture prediction power.

Methods: A total of ten mechanical stress, strain, and energy metrics (Table 1) were selected for computational finite element (FE) modelling, based on a unique histopathological dataset of ruptured carotid plaques (n=35) obtained from 20 patients [2]. The plaques presented minimal morphological change due to rupture, enabling accurate replication of pre-rupture geometry. Segmentation of the histology images for the mechanically relevant components produced plaque geometries for the FE models (Figure 1). In addition, the histology images were processed to detect collagen fibers, enabling implementation of both local fibre orientations and dispersions (Figure 1). The anisotropic material behaviour was incorporated in the FE models trough Holzapfel-Gasser-Ogden hyperelastic model, using material constant values from literature [3]. The 2D, plain-strain FE models simulated quasi-static intraluminal pressurization of 140 mmHg. Colocalization analyses of rupture sites at the lumen with the location of the max computed value of each mechanical metric were performed.

Metric	Types
Stress	1. von Misses, 2. max principal, 3. fiber-parallel, 4. fiber-transverse, 5. fiber-shear
Strain	1. max principal, 2. fiber-parallel, 3. fiber-transverse, 4. fiber-shear
Energy	1. strain energy density

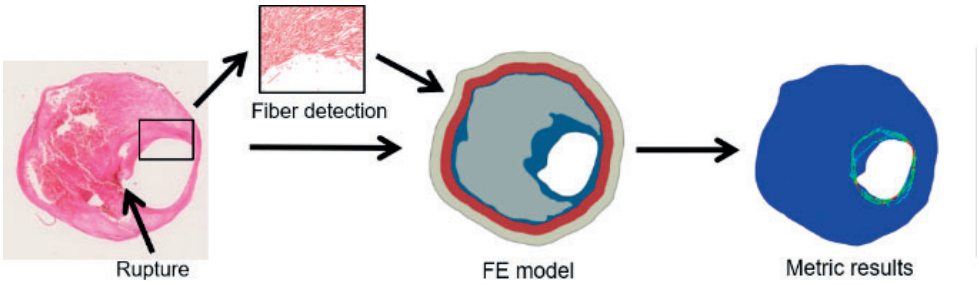

Figure 1: Workflow from histology to fiber detection, plaque geometry assessment, and metric computation with FEM.

Results: It was observed that the stress concentrations were mainly located at the regions with thin plaque cap and high lumen curvature, confirming previous findings [7], and low-dispersion fiber regions, not reported before. Colocalization analyses demonstrated that each rupture colocalized with at least one mechanical metric. Two metrics ("fibre-parallel" and "fiber-transverse" strains) showed sensitivity below 50% and the average sensitivity of all the metrics was 58% (64% without the two metrics <50% sensitivity). The "fibre-shear strain" had the highest sensitivity (75%). Furthermore, "fibre-shear strain" was the only predictor for one rupture case.

Conclusion: The overall success of the mechanical metrics for rupture colocalization highlights once more the great role of the local mechanics in plaque rupture. The high sensitivity of the anisotropic "fibre-shear strain" supports the previously-posited delamination-based damage mode in atherosclerotic plaques [4].

References:

1) Richardson et al. 1989, The Lancet, 334(8669):941-944. 2) Daemen et al. 2016, Atherosclerosis, 254:102-108.
3) Heiland et al. 2013, J Mech Behav Bio Mat, 27:226-2238. 4) Akyildiz et al., 2016, Comp Meth Biomech Biomed Eng, 19(7): 271.

[D-03.2]
MECHANICAL DAMAGE IN CEREBRAL ARTERIES

Ken Monson[1]

1 *University of Utah, Salt Lake City, USA*

Cerebral arteries are commonly damaged as a result of both accidental trauma and surgical manipulation. Because the vessels play a key role in the maintenance of brain tissue, such damage can put neural tissue at risk, but little is known about the mechanics of vascular damage or about how damage processes affect subsequent vessel function. It may be that chronic conditions associated with traumatic brain injury, including increased risk of stroke,[1,2] are at least partially mediated by persisting structural deficiency in the vasculature. Similarly, vessel damage in angioplasty likely influences restenosis. Improved understanding of vessel damage mechanisms and responses is critical to the development of more advanced strategies for injury prevention and treatment.

In order to characterize the mechanics of this damage, we have investigated the response of isolated cerebral arteries to overstretch. Experiments show that axial overstretch induces persistent softening of the stress-stretch response of the vessels, with larger overstretch producing more extensive softening.[3] Tests similarly show that arterial regulatory function is altered by overstretch, particularly by large deformations imposed at high rates,4 though it is not yet known whether the dysfunction is a result of smooth muscle cell injury or damage to the surrounding extracellular matrix.

To better understand these observations of both mechanical and functional alteration, we have also investigated microstructural changes in overstretched arteries. As part of this, we recently showed that collagen hybridizing peptide can be used to identify mechanically-induced collagen molecule damage.5 Not surprisingly, collagen damage only occurs above a supraphysiological level of stretch but appears to then increase linearly with additional stretch until failure. Interestingly, the stretch threshold of collagen disruption appears to be greater than the threshold of both mechanical and functional alteration, suggesting that other damage mechanisms may also contribute to changes in behavior. Our research on microstructure also shows that both the intima and the internal elastic lamina commonly rupture at overstretch levels below those required for complete vessel disruption.

The described research shows that cerebral arteries are susceptible to damage at deformations that are less severe than those required to produce bleeding. The resulting damage may have important implications in disease progression. The observed changes in microstructure may offer a starting point for treatment of damaged vessels.

Acknowledgments: The primary contributors to the reported research were David Bell, Matt Converse, Kevin Nye, Jake Sullivan, and Ray Walther.

References:

1. *Chen Y-H et al. Stroke 2011*
2. *Burke JF et al. Neurology 2013*
3. *Bell ED et al. Frontiers in Bioeng Biotech 2015*
4. *Bell ED et al. J Mech Behav Biomedl Mat 2017*
5. *Converse MI et al. Acta Biomat 2018*

[D-03.3]

STRUCTURAL MODELING OF THE BIOMECHANICAL FAILURE OF CEREBRAL ARTERIAL WALL TISSUE

Ronald Fortunato[1], *Anne Robertson*[1], *Chao Sang*[1], *Spandan Maiti*[2]

1 *University of Pittsburgh, Pittsburgh, USA*
2 *Department of Bioengineering, University of Pittsburgh, Pittsburgh, USA; Department of Mechanical Engineering and Materials Science, University of Pittsburgh, Pittsburgh, USA; Department of Chemical and Petroleum Engineering, University of Pittsburgh, Pittsburgh, USA*

Biomechanical failure of cerebral aneurysms, a pathology of cerebral arteries (CAs), is a catastrophic clinical event with a fatality rate of 45% [1]. Thus, there is a pressing need to understand the mechanisms of failure in CAs as well as other soft tissues. However, the interplay between tissue extracellular matrix structure and mechanical failure is not fully understood. Here, we develop a computational framework to quantify the relationship between collagen fiber architecture and failure response of the CA wall using a cohesive volumetric finite element approach. We apply this framework to uniaxial testing of CA tissue to understand the relationship between collagen fiber properties and uniaxial failure response.

The CA wall was modeled as a nonlinear, anisotropic [2] finite thickness composite. Supported by multiphoton imaging of collagen in CA tissue [3], two families of fibers with small dispersion about the circumferential direction were used. To simulate spontaneous initiation and propagation of tears, we inserted zero thickness cohesive elements in the unloaded state at the 3D element interfaces and employed a failure law relating traction and displacement jump across these elements. Away from the tear, standard hexahedral finite elements were used. The failure law incorporated strength and toughness of individual collagen fibers as failure parameters, and the volume fraction and orientation of the collagen fibers as structural parameters. Specimen material and geometric properties were drawn from prior experiments [3]. We simulated uniaxial loading, of the CA tissue, investigating the influence of failure and structural parameters on the pre- and post-failure biomechanical behavior of CA tissue.

Collagen fiber failure properties did not influence pre-peak uniaxial response, while the peak stress and post-peak regime was correlated with fiber strength, orientation and volume fraction. A precipitous drop in the post-peak response was observed for rapid tear of collagen fibers with high strength and low fracture toughness. Parametric variation of the fiber reinforcement direction resulted in corresponding changes in strength and tear propagation path.

In summary, we developed and preliminarily tested a structural cohesive volumetric finite element framework that incorporates collagen fiber structure. The inclusion the fiber structure-failure property relationship within a fiber network model enabled mechanistic insight of the tissue failure process that would not be possible with phenomenological failure models. Hence this approach can have important ramifications in future studies aimed at identifying the structural factors in healthy and diseased vascular tissues that influence tear propagation and wall rupture.

Acknowledgments: Research reported in this work was supported by the National Institutes of Health under award numbers 1R01NS097457-01 and T32-HL076124.

References:

[1] Kelly, P et al., Stroke, 32(2):530-534, 2001
[2] Gasser, T. C. et al., J R Soc Interface, 3:15-35, 2006.
[3] Sang, C et al., J of Biomech. Eng., 140(6): 061010, 2018.

[D-03.4]
ON CRACKS IN ARTERIES

Pullela Mythravaruni[1], ***Konstantin Volokh***[1]

1 *Technion - Israel Institute of Technology, Haifa, Israel*

We present a theoretical approach to study the onset of failure localization into cracks in arterial wall. The arterial wall is a soft composite comprising hydrated ground matrix of proteoglycans reinforced by spatially dispersed elastin and collagen fibers. As any material, the arterial wall material cannot accumulate and dissipate strain energy beyond a critical value. This critical value is enforced in the constitutive theory via energy limiters. The limiters automatically bound reachable stresses and allow examining the mathematical condition of strong ellipticity. Loss of the strong ellipticity physically means inability of material to propagate superimposed waves. The waves cannot propagate because material failure localizes into cracks perpendicular to a possible wave direction. Thus, not only the onset of crack can be analyzed but also the direction of its localization.

We use the recently developed constitutive theories of the arterial wall including 8 and 16 structure tensors to account for the fiber dispersion. We enhance these theories with energy limiters. We examine the loss of strong ellipticity in uniaxial tension in circumferential and axial directions of the arterial wall. We also study the effect of the incompressibility constraint on the analysis of strong ellipticity in uniaxial tension, pure shear and equibiaxial tension. We find that the enforcement of the incompressibility constraint can significantly affect the crack direction.

Acknowledgments: The support from the Israel Science Foundation (ISF-198/15) is gratefully acknowledged.

[D-03.5]

DIGITAL IMAGE CORRELATION FOR STUDIES OF ARTERIAL FAILURE MECHANICS

Susan Lessner[1], *Liya Du*[1], *Brooks Lane*[1], *Xiaoying Wang*[2], *Naren Vyavahare*[2], *John Eberth*[1]

1 *University of South Carolina, Columbia, USA; School of Medicine; Dept. of Cell Biology and Anatomy*

2 *Clemson University, Clemson, USA; Dept. of Bioengineering*

Failure of vascular tissues can result in life-threatening clinical consequences including aneurysm rupture and arterial dissection. Digital image correlation (DIC) is a non-contact optical technique to measure deformation and strain, based on tracking the displacements of a high-contrast speckle pattern on the material surface. DIC offers advantages for strain measurement in soft tissues, since it provides full-field data and can be used for large strain measurements, typical of soft tissues taken to failure. Our recent studies have focused on developing new tools for DIC-based evaluation of local failure mechanics in mouse models of abdominal aortic aneurysm (AAA).

Colloidal gold nanoparticles were synthesized by reducing chloroauric acid in ascorbic acid. Nanoparticle aggregation was controlled by adjusting pH, time, and capping agent to obtain particle size of 1-10 µm. Mouse aortic rings were incubated in colloidal gold aggregate (CGA) suspension to form random speckle patterns by spontaneous adsorption.1 Patterned samples were subjected to uniaxial mechanical tensile tests with a CCD camera tracking displacements and VIC2-D software for strain analysis. Error analysis was conducted by calculating pseudo-strains in a series of static specimen images. To prevent loss of correlation, strain analysis during uniaxial failure experiments was performed in stepwise fashion, with the first image in each set of 20 chosen as reference.

Preliminary pressurization-to-failure studies were conducted on mouse AAAs. Suprarenal AAAs were induced in low density-lipoprotein receptor (LDLr) knockout mice by Western diet feeding and angiotensin II infusion.2 Excised AAAs were cannulated within a panoramic DIC-capable device and pressurized 1-3 mmHg/s to failure.

Mean pseudo-strain errors in static tests of CGA-speckled aorta specimens ranged from 0.6 millistrain in εyy to 4 millistrain in εxy. These errors were considered acceptable for strain tracking during failure tests, as failure of aortic rings occurred at strain values exceeding 200%. Stepwise DIC analysis of image series acquired during uniaxial failure tests of aortic rings was successfully applied to track local strains up to the point of material failure at ~200-300% strain. Burst testing of 11 mouse AAA samples demonstrated material failure at pressures ranging from 141-540 mmHg.

The use of aggregated colloidal gold particles to create speckle patterns shows potential in DIC applications to soft tissue failure analysis. These speckle patterns remain adherent on tissue even at 200-300% strain. We plan to apply CGA to pattern mouse AAA specimens for both ring failure tests and burst testing.

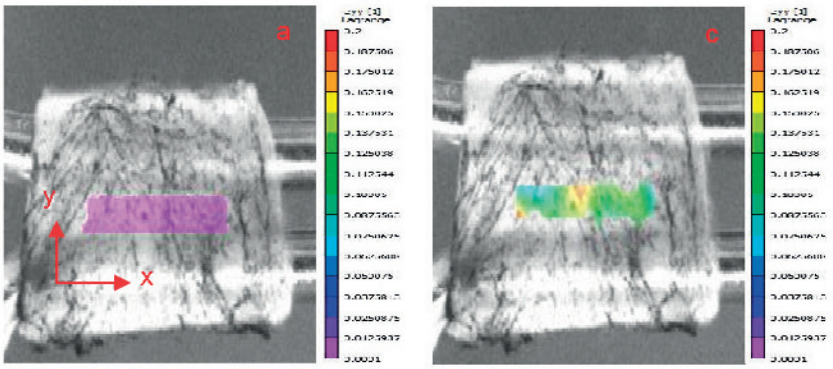

Figure Caption: DIC-based local strain measurement of mouse aortic ring sample with CGA speckle pattern. Left: reference image.

Acknowledgments: This work has been supported by NIH HL133662, NIH HL145064 and NSF CMMI-1760906.

References:

[1] *Lessner SM, Du L, Patent Application US 62/743,874, 10/10/2018*
[2] *Cassis LA, Gupte M, et al. Am J Physiol Heart Circ Physiol., 296:H1660-5 (2009).*

[D-03.6]

STRUCTURAL MODELING OF ASCENDING AORTIC TISSUE FAILURE USING A FIBER-EMBEDDED FINITE ELEMENT METHOD

Spandan Maiti[1], *Ronald Fortunato*[2], *Thomas Gleason*[3], *David Vorp*[4]

1 *Department of Bioengineering, University of Pittsburgh, Pittsburgh, USA; Department of Mechanical Engineering and Materials Science, University of Pittsburgh, Pittsburgh, USA; Department of Chemical and Petroleum Engineering, University of Pittsburgh, Pittsburgh, USA*
2 *Department of Mechanical Engineering and Materials Science, University of Pittsburgh, Pittsburgh, USA*
3 *Division of Cardiac Surgery, University of Pittsburgh, Pittsburgh, USA School of Medicine; Upmc Heart and Vascular Institute; Upmc Center for Thoracic Aortic Disease*
4 *University of Pittsburgh, Pittsburgh, USA; Department of Bioengineering; Department of Ct Surgery*

Acute aortic dissection, a disease associated with very high mortality, is mediated by the biomechanical failure of the aortic wall. Yet, current clinical guidelines are inadequate predictors of the dissection risk [1] necessitating the need of improved evidence-based risk prediction metrics. Towards that end, the knowledge of the failure biomechanics of the aortic wall is a must. However, the failure mechanisms of the aortic wall tissue is not well understood. Our objective in the current work was to develop an image-based structural finite element model of the aorta that directly incorporated the organization of load-bearing components (collagen and elastic fibers), and quantify the structure-failure property relationship for the wall tissue.

Two patient populations were considered: control non-aneurysmal (n=7), and aneurysmal (n=13). Sample collection and uniaxial testing was conducted with IRB approval. A Representative Volume Element (RVE) of the lamellar unit of the aortic media with elastin sheets (EL) surrounding an interlamellar space (IL) was constructed [2]. Two collagen networks, with population-relevant fiber density and orientation distribution obtained from multiphoton microscopy [3], were directly embedded within 3D continuum. RVE constituents were modeled as isotropic neoHookean materials (EL and IL) and 1D rods (collagen fibers) with an embedded-fiber finite element framework. Resulting models were stretched uniaxially using a custom nonlinear finite element software. Strength of the tissue was computed from the peak of the stress-strain curve, and was contrasted against experimentally cohort-specific uniaxial strength [4].

Simulation derived uniaxial strength for both circumferential and longitudinal directions agreed with their experimentally measured values ($p<0.05$). Tissue stress was uniform under low applied strains, but became heterogeneous after collagen fiber recruitment. Existence of high stress paths through collagen fibers spanning in the loading direction were identified. With increasing loading, tissue failure was initiated from the collagen fibers comprising the high stress paths. Collagen fibers oriented in the loading direction and non-collagenous matrix both contributed to the tissue strength. Presence of high stress regions within the elastic sheets adjacent to fiber failure locations suggested a master-slave relationship between collagen and non-collagenous tissue components with collagen fiber failure driving total tissue failure.

In summary, we have developed a fiber-embedded finite element method to directly incorporate and elucidate the role of load-bearing fibers on the tissue failure biomechanics. Albeit the methodology was demonstrated on aortic tissue, the protocol is general enough and is expected to explain failure mechanisms of soft fibrous tissues in other organs. In the future, we will utilize this model to quantify failure properties under physiologically relevant loading scenarios.

References:

[1] Emerel et al., J Thorac Cardiovasc Surg, In Press, 2019.
[2] Pasta et al. Med Eng Phys, 38:121-30, 2016.
[3] Thunes et al. J Biomech, 71:84-93, 2018.
[4] Pichamuthu et al., Ann Thorac Surg, 96:2147-54, 2013.

[D-04.1]
DISCRETE MODELS OF FIBROUS SOFT TISSUE FRACTURE

Michelle Oyen[1], *Ching Theng Koh*[2]

1 *East Carolina University, Greenville, USA*
2 *Universiti Tun Hussein Onn, Parit Raja, Johor, Malaysia*

Soft tissues are fibrous composites, in which the fibers can realign under mechanical stress. Electrospun scaffolds mimic the microstructure of structural collagenous tissues and have been widely used in tissue engineering applications. Both brittle cracking and ductile failure have been observed in scaffolds and tissues with similarly random fibrous morphology. Finite element analysis can be used to qualitatively examine the mechanics of these differing failure mechanisms. The finite element modeling demonstrates that the noncontinuum deformation of the network structure results in fiber bundle formation and material toughening via fiber bridging of the crack tip. Such toughening is accommodated by varying fiber and matrix properties, including allowing for large failure strains and significant microstructural rearrangement. Dynamic models capture the physics of fracture as individual fibers reach a peak strength and fail.

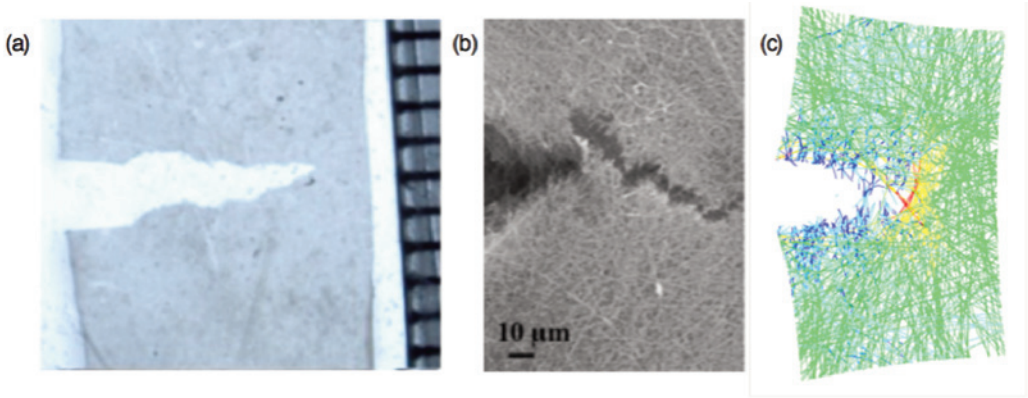

Figure Caption: Experimental fracture in a (a) fibrous soft tissue, (b) an electrospun scaffold, and (c) a computational noncontinuum model.

References:

(1) Koh CT and Oyen ML, Toughening in Electrospun Fibrous Scaffolds, APL Mater. 3 (2015) 014908.
(2) Koh CT, Strange DGT, Tonsomboon K, Oyen ML, Failure mechanisms in fibrous scaffolds. Acta Biomater. 9 (2013) 7326 – 34.
(3) Koh CT and Oyen ML, Branching toughens fibrous networks. J. Mech. Behav. Biomed. Mater. 12 (2012) 74 - 82.

[D-04.2]

ON MODELING SOFT TISSUE DAMAGE AND FAILURE USING SMOOTHED PARTICLE HYDRODYNAMICS

Manuel Rausch[1], *Hossein Ahmadzadeh*[2], *Jay Humphrey*[3]

1 *University of Texas at Austin, Austin, USA*
2 *Yale University, New Haven, USA*
3 *Yale University, New Haven, USA; Department of Biomedical Engineering*

Soft tissues are ubiquitous in our bodies and are subject to forces while fulfilling their physiological function, or during disease and surgery. Because of their vital importance to our health, understanding soft tissues' response to mechanical forces is critical. Unfortunately, soft tissues are complex, hierarchical structures, that demonstrate myriads of nonlinear phenomena making modeling their behavior difficult. This is particularly true during damage and failure, when tears or cuts disrupt their natural continuity. While important for many disciplines, computational models of soft tissue failure are rare owing to the mathematical and numerical challenges of discontinuous behaviors. Here we discuss our attempt of using a hybrid continuum/particle approach toward modeling soft tissue failure. Specifically, we combine a large deformation smoothed particle hydrodynamics (SPH) framework with classic continuum damage mechanics introduced by Simo. While originally formulated for astrophysical problems, SPH has proven a robust and versatile numerical method. Recent developments toward a total Lagrangian formulation with an "hourglass control algorithm" have now made SPH a viable option for modeling soft tissues. Here we adopt the total Lagrangian approach and implement a nonlinear hyperelastic material model as per Holzapfel et al within this framework. In SPH, instead of discretizing the geometry of interest using finite elements, particles represent the spatial domain of the soft tissue, while connectivity is ensured through lists of neighboring particles. Based on these neighbor lists, physical quantities are approximated using kernel functions that have a finite support radius. Thus, failure may be modeled as loss of connectivity between particles, which can be easily implemented by removing neighboring particles form their respective neighbors' lists. In our formulation, the point at which particles disconnect is determined by a damage evolution law that is driven by a damage history variable which depends on the maximum principal stretch at each particle. Thus, once a particle is critically damaged, i.e., the damage variable has reached the maximum value, the particle is removed from all its neighbors' lists. First, we demonstrate the method's accuracy against the analytical solution for homogeneous uniaxial extension and against a numerical solution for heterogeneous clamped uniaxial extension. Finally, we demonstrate our methods capabilities by modeling failure of an anisotropic soft tissue strip during clamped uniaxial extension for various fiber distributions. In conclusion, we adopted and enhanced a total Lagrangian SPH framework to model soft tissue damage and failure and believe our approach shows great potential for solving a difficult problem is soft tissue mechanics.

References:

Ahmadzadeh H, Rausch MK, Humphrey JD. Particle-based computational modelling of arterial disease. Royal Society Interface, 2018.
Rausch MK, Karniadakis GE, Humphrey JD. Modeling soft tissue damage and failure using a hybrid particle/continuum approach. Biomechanics and Modeling in Mechanobiology, 2017; 16:249-261.

[D-04.3]

DEVELOPMENT OF PVA MODELS FOR BIOMECHANICAL AND BIOPHYSICAL IN-VITRO SIMULATIONS

Rosaire Mongrain[1], *He Zinan*[1], *Leask Richard*[2], *Raymond Cartier*[4], *Bertrand Olivier*[5], *Soulez Gilles*[6]

1 *McGill University, Montreal, Canada; Department of Mechanical Engineering*
2 *McGill University, Montreal, Canada; Department of Chemical Engineering; Wong Building*
4 *Montreal Heart Institute, Montreal, Canada; Surgery Department*
5 *Quebec Heart-Lung Institute, Quebec, Canada*
6 *Department of Radiology; Centre Hospitalier Universitaire de Montréal (Chum), Montreal, Canada*

Vascular phantoms are useful means to investigate various mechanical properties and phenomena reproducing healthy or pathological situations as they provide reproducible mechanical parameters and well controlled conditions (flow regimes, loading) and have the capacity to be shaped into complex anthropomorphic structures [1, 2]. Indeed, the synthetic models can reproduce precisely the biomechanical behavior of the various structures of interest (hyperelastic, anisotropic and fracture toughness) [3]. Hydrogels are capable of absorbing much of their weight in water and exhibit non-linear and viscoelastic properties. They are constructed from long-chain hydrophilic molecules that form semi-crystalline matrices. As living tissue largely consists of organized water-imbibed cells within fibrous extracellular matrices, hydrogels appear as a natural surrogate. PVA's long-chain matrix network is formed by slowly rearranged hydrogen bonds formed during the thermal cycles of freezing and thawing [4]. PVA's mechanical properties, can then be tailored with specific freeze-thaw processing cycles (number of cycles, PVA concentration, temperatures, temperature gradients). We experimentally characterized the mechanical properties of the biological tissue of interests (veins, arteries) in the arterio-venous access (tissue preparation, sample gripping, hyperelastic, strength, viscoelastic models) and identified the native mechanical parameters to be matched with the PVA phantoms using a Levenberg-Marquardt approach. A reproducible methodology was elaborated for the phantom fabrication with an optimized PVA material preparation and the 3D printing of anthropomorphic molds based on 3D imaging modalities segmentations. The global structure is imbedded in a visualization box mimicking surrounding tissues effects and subsequently used for technology assessment (navigation, deployment, implantation) and given their adjusted fracture toughness can be used to investigate tissue rupture and perforation [5]. The PVA phantoms are also suitable for chemical compound transport assessment given the hydrates state of the hydrogel (drug diffusion, compound dispersion). The phantoms provide reproducible and realistic testing conditions for various vascular technologies.

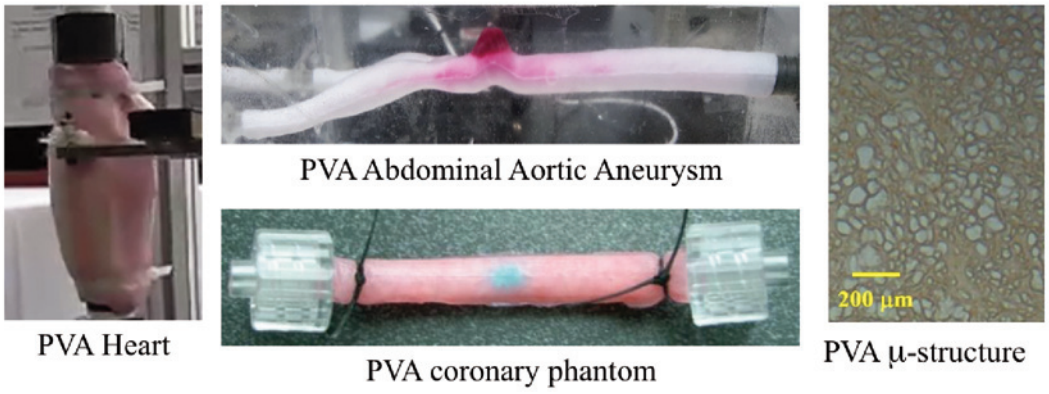

Figure 1: Illustration of PVA structures

References:

[1] *Garcia J et al, 3D printing materials and their use in medical education: A review of current technology and trends for the future, BMJ Simulation & Technology Enhanced Learning, 4(1): 27-40, 2018*
[2] *Yazdi SG et al. A Review of Arterial Phantom Fabrication Methods for Flow Measurement Using PIV Techniques, An Biomed Eng, 46(11): 1697–1721, 2018*
[3] *Pazos V et al. Polyvynil alcohol cryogel: Optimizing the parameters of cryogenic treatment using hyperelastic models, J Mech Behav Mat, 2(5):542-549, 2009*
[4] *Adelali M et al., Cap buckling as a potential mechanism of atherosclerotic plaque vulnerability: a numerical, experimental and analytical study with clinical preliminary insights, J Mech Behav Biomed Mater, 32:210-24, 2014*
[5] *He Z et al., Tissue-mimicking mockup for abdominal aortic aneurysm – effect of surrounding tissue, Abstract P4631, World Congress of Biomechanics, Dublin Ireland, July 8-12, 2018*

[D-04.4]

COLLAGEN MOLECULAR DAMAGE EVOLVES WITH CREEP STRAIN DURING FATIGUE LOADING

*Jared Zitnay[1], Gang Sub Jung[2], Allen Lin[1], Zhao Qin[2], Markus Buehler[2], **Jeffrey Weiss**[1]*

1 *University of Utah, Salt Lake City, USA*
2 *Massachusetts Institute of Technology, Cambridge, USA*

Although the mechanisms and structures involved in load-induced micro-damage are still under investigation, it is clear that damage to collagen, the primary structural component of tendon, is involved in the micro-damage process. The objectives of this study were to investigate the role of molecular-level collagen damage during tendon fatigue, and to identify possible molecular level mechanisms of triple-helical fatigue damage using steered molecular dynamics (SMD) simulation.

Rat tail tendon fascicles were subjected to fatigue loading at three strain rates. Cyclic loading was applied until peak cyclic strain reached one of three predefined levels, representing increasing levels of fatigue, or failure occurred. Unloaded samples served as controls. Following fatigue testing, samples were removed from the test system and the amount of denatured collagen was measured using a CHP based microplate assay [1]. Data for peak cyclic strain and percent denatured collagen were plotted as a function of normalized number of cycles (cycle number divided by cycles to failure).

SMD simulations were performed using a representative homotrimeric collagen peptide comprised of twenty [Gly-Pro-Hyp] triplets in explicit water solution. Periodic boundary conditions were applied to all directions. Each simulation was performed in the isothermal-isobaric ensemble (pressure = 1 atm and temperature = 310 K) with 1 fs simulation time step. The SMD method was used to deform the molecule between 350 pN and 2085 pN with a constant loading speed of 3, 5, or 10 m/s. Simulations were performed with either tension dominant loading that stretches the whole triple-helical collagen molecule or shear dominant loading that corresponds to pulling a single strand out of the triple helix.

Tendon fatigue loading caused the accumulation of denatured collagen even at early levels of loading, suggesting that mechanical unfolding of the collagen triple-helix is a critical feature of fatigue damage (Figure 1). Both tissue level fatigue, indicated by creep strain, and fatigue damage to the collagen molecule evolve with increasing loading cycles. The SMD results mirror the experimentally observed strain-rate dependent increase of creep strain and triple-helical unfolding with increased loading cycles. This demonstrates a possible molecular mechanism for tissue-level rate dependence of fatigue damage accumulation, and strongly indicates triple-helical unfolding as a foundational mechanism of tissue creep.

Our results support the hypothesis that molecular level collagen damage is fundamental to the initiation and progression of fatigue damage in tendon. Furthermore, progressive accumulation of collagen damage throughout fatigue supports the hypothesis that overuse injuries involve loading-induced damage to collagen that outpaces the remodeling capacity of the tissue, providing both a mechanistic explanation for micro-damage accumulation and a potential clinical target for the treatment and prevention of overuse injuries.

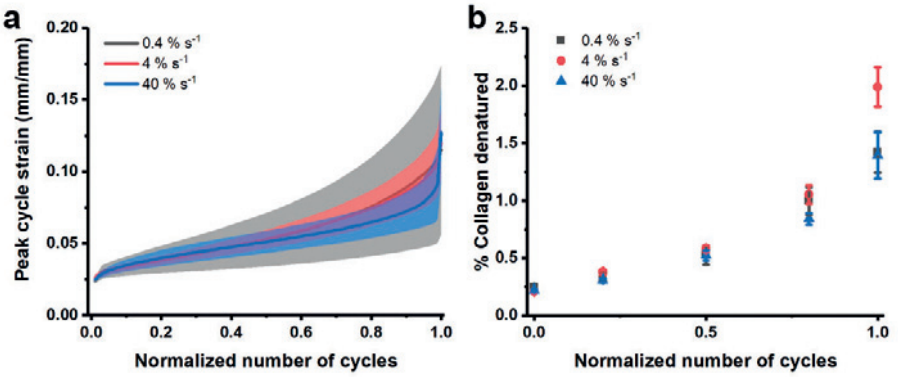

Figure 1. Normalized tissue creep (a; mean ± SD, n=10 each) and molecular damage (b; mean ± SEM, n≥5 each) due to fatigue loading. Neither the mean peak strain nor the amount of denatured collagen, as a function of normalized number of cycles, was significantly affected by strain rate.

Acknowledgments: NIH #R01AR071358

References:

[5] Lin, A. H. et al. J Orthop Res, 2018.

[D-04.5]

COMPUTATIONAL SIMULATIONS FOR ENGINEERING OF BIOMIMETIC SOFT TISSUE STRUCTURES USING ULTRA-LONG COLLAGEN FIBERS

Mirit Sharabi[1], *Rami Haj-Ali*[2]

1 *Ariel University, Ariel, Israel*
2 *Tel-Aviv University, Tel-Aviv, Israel*

Soft tissues can be seen as fiber-reinforced composites with very effective structures and superior mechanical properties. They are constructed as anisotropic laminates with varied collagen fiber orientations and graded fiber volume fractions (FVFs). From mechanical point of view, collagen fibers serve as the load bearing element of the tissue, reinforcing a softer matrix. Soft tissues are characterized in hyperelastic mechanical behavior, where the matrix governs the initial part of the stress-strain curve followed by strain stiffening that is dominated by the collagen fibers.

Our research is aimed in biomimetics of soft tissues' structure and mechanical function by fabricating collagen fiber reinforced biocomposites 1-3. The ultra-long collagen fibers are extracted from soft corals and embedded in alginate hydrogel to mimic different tissue structures such as the intervertebral disc, blood vessels and ligaments. The mechanical behavior of the biocomposites was investigated experimentally and computationally in different FVFs and fiber orientations. It was found to be hyperelastic with large deformations, similar to varied soft tissues. We have developed compatible 3D hyperelastic and heterogeneous models with refined representation of the fibers to aid the engineering process of the biocomposites and to get better understanding of the relation between the structure and the mechanical function in these biocomposites and in soft tissues in general. Different computational models were built to explore the mechanical behavior of the biocomposites in several length scales: from the laminate level to more complex tissue structures such as the full intervertebral disc (IVD), its functional spinal unit (FSU) and their physiological loading modes 3,4 in order to investigate the biocomposite's mechanical compatibility with the native tissue.

Our goal is to understand the mechanical behavior of soft tissue structures and to mimic them using our biomimetic composites, towards engineering novel materials with tailor-designed mechanical behavior for soft tissue repair and replacement.

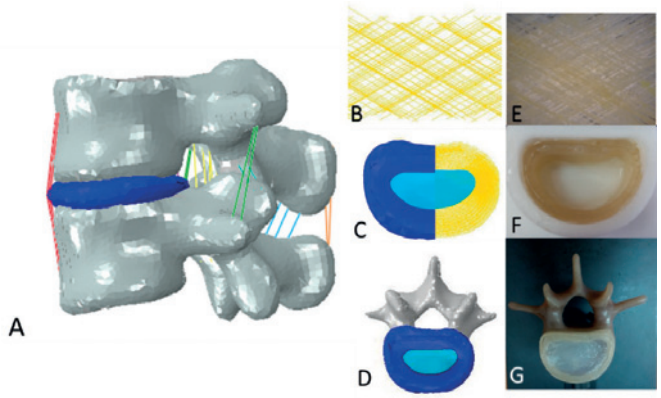

Figure: Finite element model of the FSU and IVD(A-D) and biocomposite laminates with ultra- long collagen fibers in a ±30º orientation (B, E).

Acknowledgments: This study is supported by NIH-NIBIB BRP U01EB026414 grant.

References:

1. *Sharabi, M., et al. Composites Science and Technology 117, 268-276 (2015).*
2. *Sharabi, M. et al. Journal of the Mechanical Behavior of Biomedical Materials 36, 71-81 (2014).*
3. *Sharabi, M. et al. Composite Structures 153, 392-400 (2016).*
4. *Sharabi, M. et al. Journal of biomechanical engineering 141, (2019).*

[D-04.6]

DEVELOPMENT OF A NEW VISCO-ELASTIC HEMOLYSIS MODEL WITH SUBLETHAL HEMOGLOBIN RELEASE

Amy McKean[1], *Rosaire Mongrain*[1], *Catherine Pagiatakis*[2], *Renzo Cecere*[1]

1 *McGill University, Montreal, Canada*
2 *National Research Council Canada Industrial Materials Institute, Boucherville, Canada*

Flow-induced hemolysis is a major concern when developing blood interacting medical devices. Hemolysis is defined as the rupture of a red blood cell membrane and the release of the cell's hemoglobin content. When the extracellular hemoglobin concentration is high enough, it can impair organ function and impede gas-exchange in the cardiovascular system. The unphysiological flow conditions caused by blood interacting medical devices create high shear stresses which can initiate hemolysis as well as cause the formation of reversible pores in the membrane. It has been hypothesized that these pores can contribute to hemoglobin release from the cell by diffusion.

While many numerical models have been developed to assess the hemolytic potential of devices, these models produce largely qualitative results. A major shortcoming of many of the initial models is that they only consider hemoglobin release due to rupture events and do not account for diffusion of hemoglobin through membrane pores. While some models incorporate this phenomenon, these methods involve simulating local membrane strains on regions of individual cells and do not scale well to whole blood volumes [1].

In this work, a relationship between the global area strain on a membrane and pore formation is proposed. Pore number and size is restricted using membrane properties, empirical work from constant shear studies and area strain above a threshold strain equaling pore area. The resulting number and size of pores is used as an input into the diffusion equation across the membrane to predict sublethal hemoglobin release. Additionally, rupture events are incorporated by including a critical membrane strain that causes complete membrane rupture. The model is used with the red blood cell morphology model, developed by Arora et al. [2], that is used to compute the global area strain of the membrane. This is tested in three different scenarios: constant shear flow studies, flow through a simple cannula and flow through a left ventricular assist device. The first scenario is implemented in Matlab (The MathWorks Inc., Natick, MA) while the latter studies use ANSYS FLUENT (ANSYS Inc., Canonsburg, PA). The plasma hemoglobin concentration predictions are compared against both experimental data and predictions from other empirical models such as the Giersiepen-Wurzinger equation. The model developed herein balances both computational cost and predictive ability, and therefore has the potential to improve the efficiency of prototyping blood interacting medical devices.

References:

[1] S. Sohrabi and Y. Liu, "A Cellular Model of Shear-Induced Hemolysis," Artif. Organs, vol. 41, no. 9, pp. E80–E91, 2017.
[2] D. Arora, M. Behr, and M. Pasquali, "A tensor-based measure for estimating blood damage," Artif. Organs, vol. 28, no. 11, pp. 1002–1015, 2004.

[D-05.1]

INCORPORATING MATERIAL RESIDUAL STRESS USING A MULTIGENERATIONAL GROWTH APPROACH IN AN INTERVERTEBRAL DISC FINITE ELEMENT MODEL

Dawn Elliott[1], *John DeLucca*[2], *John Peloquin*[2], *Edward Vresilovic*[2]

1 *University of Delaware, Newark, USA; Dept of Biomedical Engineering*
2 *University of Delaware, Newark, USA*

INTRODUCTION: Residual stresses and strains arise in the disc from both osmotic swelling and growth & remodeling processes, and they contribute to disc mechanical behavior. For example, the "unloaded" disc has significant internal pressure and annulus fibrosus fiber tension. While swelling-induced residual stresses are well described in disc finite element models (FEM), no FEMs of the disc include residual stresses in the AF fiber material properties. Indeed, when AF material properties are measured, the AF is cut from the disc, releasing its residual stresses, therefore, they are not incorporated into the constitutive models used in the disc FEM. The objective of this study was to apply a multigenerational growth approach to incorporate residual stresses arising from both swelling and fiber tension in a disc FEM and to validate the model using experimental disc segment testing in all six degrees of freedom.

METHODS: FEBio was used to develop FE models that included residual stress due to both swelling and growth. Residual stresses from swelling were modeled using Donnan osmotic swelling pressure via fixed charge density. Residual stresses from growth were modeled using a multigeneration approach applied to the AF. This approach allows for fiber populations to be added as 'generations' that are in a different reference state, enabling greater tensile stresses in the AF. To achieve this, the first fiber family (generation) was deposited with the disc rotated +α° in torsion, the second fiber family was deposited at –α°, and then the disc was returned to the 0° position, resulting in AF fibers that are residually stressed. In addition, the disc model was given an initial outward bulge (b, mm) to represent the effects of internal pressure. A parametric study on these two multigenerational parameters (α and b) was performed. Model simulations were run to simulate disc loading and compared to experimental measures.

RESULTS: The models that included both osmotic and growth residual stresses matched the experimental nonlinear loading response curves and the stiffness better than osmotic swelling alone for all loading directions.

DISCUSSION: This study demonstrated that including residual stresses arising from both osmotic loading and fiber tension are needed to model physiological multi-axial loading. Moreover, for the first time, multigenerational approach of growth & remodeling achieved these residual stresses based. This approach improves model predictions of multiaxial mechanics. The disc experiences large multidirectional loading under daily activity and simulating the disc's mechanical response to these loadings is vital to the design and evaluation of implants and therapies. This study provides a methodology to apply multigenerational growth & modeling to achieve physiological residual stresses and improve the predictive capabilities of disc FEM.

Acknowledgments: NIH R01AR050052

[D-05.2]
CONSTITUTIVE MODELING OF LUNG BRONCHI

Mona Eskandari[1], *Grace O'Connell*[2]

1 *University of California Riverside, Riverside, USA*
2 *University of California Berkeley, Berkeley, USA*

Each year millions of lives are claimed by pulmonary disease, motivating research advancements to investigate the underlying mechanical physiology of the lung and alterations caused by disease. The lung is both a fluid and structural system, necessitating fundamental exploration of bronchial mechanics to connect breathing forces to airway tissue deformation. However, experimental testing of bronchial tissue mechanics has been a significant challenge, hindering development of accurate computational models for predicting lung biomechanical function. Recent work by Eskandari and coworkers characterized uniaxial tensile mechanical properties throughout the healthy porcine airway; in this study, we develop a constitutive model of extra- and intra-parenchymal bronchi informed by experiments. Region- and direction-dependent material behavior motivates the formulation of a structure-based constitutive model, and further exploration of each constituents' contribution (e.g., fibers or extrafibrillar matrix) to bulk tissue deformations. Moreover, relationships between mechanical properties and tissue composition are assessed through biochemical analyses and histology. Common strain-energy functions are evaluated to describe the mechanical behavior of the matrix (compressible NeoHookean, unconstrained Ogden, uncoupled Mooney-Rivlin, incompressible Ogden, incompressible Demiray, and incompressible NeoHookean) and fibers (exponential and polynomial). Model parameters are determined by curve fitting to experimental data. Model uniqueness and sensitivity is also considered. All bronchial regions are best represented by an incompressible Demiray function describing the extrafibrillar matrix, and exponential strain energy function describing the fibers. The role of tissue composition (glycosaminoglycan and collagen content) is examined in light of bulk tissue mechanics and constitutive relations. Microstructural observations suggest bronchial heterogeneity is prominently explained by regional evolution of fiber undulation. To the authors' best knowledge, this is the first study to formulate a structurally-motivated bronchial constitutive model representative of proximal and distal airway mechanics. Our systematic pulmonary tissue characterization enables future fluid-structure interaction simulations, ultimately aiming to advance disease diagnosis and clinical translation through computational techniques.

References:

O'Connell, G. D., Sen, S., & Elliott, D. M. (2012). Human annulus fibrosus material properties from biaxial testing and constitutive modeling are altered with degeneration. Biomechanics and modeling in mechanobiology, 11(3-4), 493-503.
Eskandari, M., Arvayo, A. L., & Levenston, M. E. (2018). Mechanical Properties of the Airway Tree: Heterogeneous and Anisotropic Pseudoelastic and Viscoelastic Tissue Responses. Journal of Applied Physiology.

[D-05.3]

RESPIRATORY MECHANICS IN HEALTHY AND CIGARETTE EXPOSED APOE-/- MICE

Dongyang Yi[1], *Yasmeen Farra*[1], *Emma Lloyd*[1], *Chiara Bellini*[1], ***Jessica Oakes***[1]

1 *Northeastern University, Boston, USA*

"Exposure to fine particulate matter promotes atherosclerosis and chronic obstructive pulmonary disease (COPD) by enhancing lipid imbalance1 and systemic inflammation2 through an increase in oxidative stress3. Deficiency of apolipoprotein E expression in ApoE-/- mice leads to a macrophage-specific lipid imbalance that fosters inflammation and matrix degradation through cytokine and protease secretion4. As a result, chronic cigarette smoke exposure in ApoE-/- mice yields airspace enlargement and changes in lung mechanics in ApoE-/- mice5. Here, we speculate that apolipoprotein E deficiency will enhance airway hyperreactivity and mucin gene expression in cigarette exposed mice. Female ApoE-/- mice (n=6) were nose-only (InExpose, Scireq) exposed to cigarette smoke for one hour a day, five days a week, over six months following developed protocols, which incorporated blood cotinine concentrations, detected with ELISA analysis, with delivered particulate matter concentrations (1.2-1.6 g/mL). Following exposure, we quantified and identified inflammatory cells from bronchial alveolar lavage (BAL) fluid, tissue structure and composition from perfusion-fixed lungs (Fig. 1A, B, and D), and respiratory mechanics (FlexiVent, Scireq). To test bronchiole hyperresponsiveness, we delivered increasing amounts of nebulized methacholine (0-50 mg/mL of PBS, of 2-3 µm diameter particles) to the mice and collected time-dependent pressure and volume tracings with single phase and low-frequency forced oscillation techniques. Normalized by baseline values, airway resistances (Rn) increased with methacholine dosage, with the cigarette-exposed mice being more hyper-responsive than the controls (Fig. 1C). In addition, the respiratory compliance was higher in the cig-exposed mice (Crs, exposed: 2.85E-2 ± 0.19E-2 mL/cmH2O, Crs, control: 2.17E-2 ± 0.04E-2 mL/cmH2O). This work suggests that lung degradation is exacerbated with cigarette exposure in ApoE-/- mice, with enhanced bronchial hyper-responsiveness to methacholine challenges, uncovered by respiratory mechanics analysis and modeling."

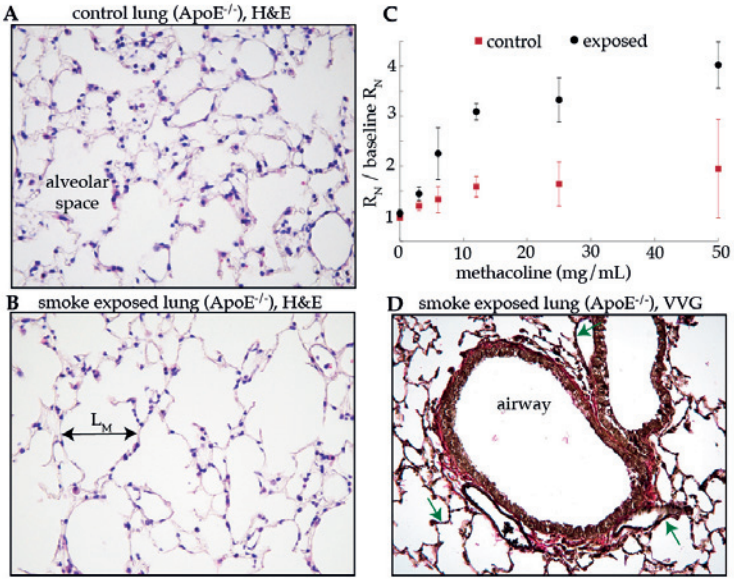

Figure Caption: "Lung histological images (H&E stain) of a control (A) and smoke-exposed (B) ApoE-/- mouse. VVG stain of two airways and surrounding parenchyma (D). Green arrow indicates elastic fibers. Panel C shows normalized airway resistance (RN) with increasing doses of methacholine."

Acknowledgments: "This work was supported by a Northeastern Tier 1 grant and NIH-NHLBI 1R03HL142472-01"

References:

1. *Mirzaie, M., Kheradmand, F. & DeBakey, M. E. Bioactive Lipids in Emphysema: Decoding Fat to Reveal COPD Phenotypes. Am. J. Respir. Crit. Care Med. 191, 1210–1210 (2015)*
2. *Eapen, M. S., Myers, S., Walters, E. H. & Sohal, S. S. Airway inflammation in chronic obstructive pulmonary disease (COPD): a true paradox. Expert Rev. Respir. Med. 11, 827–839 (2017).*
3. *Rao, X., Zhong, J., Brook, R. & Rajagopalan, S. Effect of particulate matter air pollution on cardiovascular oxidative stress pathways. Antioxid. Redox Signal. 28, 797–818 (2017).*
4. *Lo Sasso, G. et al. The Apoe-/- mouse model: A suitable model to study cardiovascular and respiratory diseases in the context of cigarette smoke exposure and harm reduction. J. Transl. Med. 14, 1–16 (2016).*
5. *Arunachalam, G., Sundar, I. K., Hwang, J.-W., Yao, H. & Rahman, I. Emphysema is associated with increased inflammation in lungs of atherosclerosis-prone mice by cigarette smoke: implications in comorbidities of COPD. J. Inflamm. (Lond). 7, 34 (2010).*

[D-05.4]

NOVEL STRUCTURE-BASED MODEL FOR INVESTIGATING DAMAGE IN THE ANNULUS FIBROSUS

Minhao Zhou[1], *Grace OConnell*[1]

1 *University of California, Berkeley, USA*

An extensive understanding of the causes for disc herniations requires investigations on failure mechanics of the annulus fibrosus (AF).[1] Our recent work showed that changes in water and glycosaminoglycans contents redistributed stress bore by the extrafibrillar matrix (matrix) and fibers, greatly reducing AF energy absorption capacity before failure.[2] Mechanical testing of sub-tissue components is experimentally challenging; however, finite element models (FEM) provide a powerful tool for investigating sub-tissue interactions.[3] Therefore, the objective of this study was to develop and validate a structure-based FEM of the AF that replicated the native tissue architecture and to use the model to investigate fiber-matrix interactions during tensile loading till failure.

The matrix and the fibers were described as two separate materials to replicate the outer AF (OAF) native tissue architecture (Fig.(a)). Uniformly distributed cylindrical fibers and a welded fiber-matrix interface was assumed.[4-6] The triphasic material framework was applied with the model parameters calibrated to single lamellar uniaxial AF experimental data.[7-9] Reactive damage mechanics[10] was incorporated, and predicted bulk tissue properties were validated with data in the literature.[11-14]

Multi-lamellar OAF subfailure mechanics agreed well to reported experimental data under biaxial and uniaxial loading modalities (Fig.(b)-(d)). Tissue damage initiated in the fibers and propagated to the adjacent matrix, radiating from the tissue's outer surface to the interior (Fig.(e)). Moreover, bulk tissue failure occurred at ~11% strain and was not affected by hydration conditions; however, increases in average local strains during tensile loading was more dramatic with dehydration, where local strains increased by ~50% in hydrated samples and ~500% in dehydrated samples.

The structure-based FEM developed using single lamellar experimental data accurately predicted multi-lamellar AF mechanical behaviors. Findings from this study suggest that fiber-matrix interactions play a pivotal role in maintaining bulk tissue failure properties. Future work will evaluate the effect of degenerative changes in sub-tissue properties on AF failure mechanics and damage progression. While computationally more expensive, the model provides an excellent tool for studying AF sub-tissue interactions and failure mechanics, which is important for further studies that aim to understand the failure progression during disc herniations.

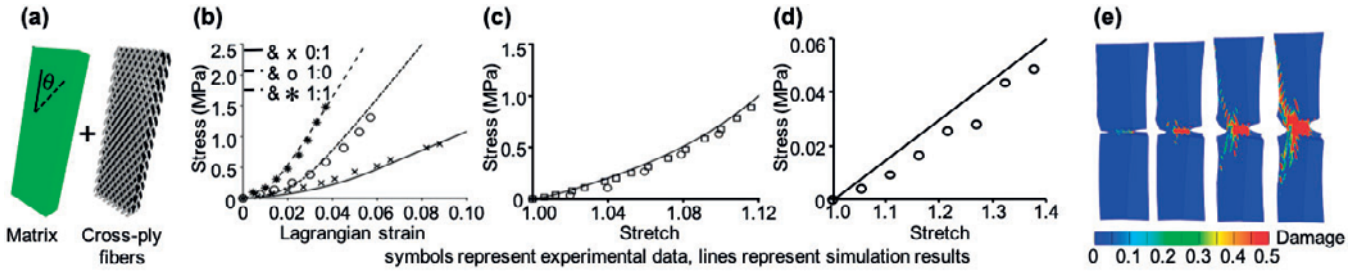

Figure Caption: (a) Model schematics (represents fiber angle; 30o for OAF). (b) Model validation to biaxial tension[11] (strain ratios: circumferential strain:axial strain). Model validation to uniaxial tensile data along the (c) circumferential[12-13] and (d) axial directions.[13] (e) Uniaxial tension damage profile.

Acknowledgments: NSF CMMI Grant No. 1760467; Iain Finnie Fellowship; Graduate Division Block Grant

References:

[1] Dang+, Eur. Spine. J., 2010;
[2] Werbner+, JBM, in review;
[3] Guo+, JMBBM, 2012;
[4] Marchand+, Spine, 1990;
[5] Pezowicz+, J. Anat., 2006;
[6] Schollum+, J. Anat., 2010;
[7] Lai+, JBME, 1991;
[8] Ateshian+, JBM, 2004;
[9] Holzapfel+, BMMB, 2005;
[10] Nims+, Interface Focus, 2017;
[11] O'Connell+, BMMB, 2012;
[12] Ebara+, Spine, 1996;
[13] Elliott+, JBME, 2001;
[14] Rausch+, BMMB, 2016.

[D-05.5]

SIMULATION AND PREDICTION OF HUMAN INTERVERTEBRAL DISC DEGENERATION AND REPAIR

Weiyong Gu[1], *Qiaoqiao Zhu*[2]

1 *University of Miami, Miami, USA; Department of Mechanical and Aerospace Engineering*
2 *University of Miami, Miami, USA*

Introduction: Degenerative intervertebral disc (IVD) disease is related to low back pain which affects more than 500 million people worldwide. Understanding degenerative processes in human IVD is challenging, due mainly to the complicated interactions among biological, chemical, electrical, and mechanical signals. Simulation and characterization of these signals are crucial for developing effective treatment strategies for degenerated discs. Thus, the objective of this study was to develop a novel multi-physics model for human IVD for simulating and predicting disc degeneration and repair.

Methods: A 3D finite element model for IVDs was developed based on a recently developed, cell-activity-coupled mechano-electrochemical mixture theory. In this model, the disc was considered as an inhomogeneous, porous, mixture consisting of a charged solid phase (with cells), an interstitial fluid phase, and a solute phase (with multiple species of solutes, e.g., Na+, Cl- , glucose, oxygen, and lactate). The governing equations were cast in terms of solid matrix displacement, cell density, and (electro)chemical potentials of the constituents. The material properties, such as tissue fixed charge density, hydraulic permeability, solute diffusivities were nonlinearly coupled with tissue deformation (or tissue hydration), and cell metabolism and viability were nonlinearly related to nutrient levels in the disc. The degenerative disc disease caused by poor nutrition supply was simulated. The repair of degenerated discs with biological therapies was also investigated.

Results: Changes in cell density, nutrients concentration, swelling pressure, glycosaminoglycan (GAG) content, water content, mechanical stress and strain, and disc height during tissue degeneration (up to 55 years) process and tissue repair were investigated. The cell number needed for disc repair, the nutrition level needed for survival of implanted cells, timing for treatment, and long-term outcomes of the therapies were predicted. Moreover, the relationship between cell number and the time needed for degenerated disc to recover to its original height was obtained.

Discussion: The findings from this study provide new insights into nonlinear interactions among biological, chemical, electrical, and mechanical events in the disc during its degenerative or repairing progression. This model can be used to develop new strategies for treating degenerative disc disease and to evaluate their long-term efficacy of therapeutic strategies.

[D-06.1]

MULTISCALE AND MULTIPHASE MODEL OF THE HUMAN LIVER FOR DESCRIPTION OF PERFUSION, METABOLISM AND FAT DEPOSITION

Tim Ricken[1], *Lena Lambers*[1]

1 *University of Stuttgart, Institute of Mechanics, Structural Analysis and Dynamics, Stuttgart, Germany*

The liver is the most important human organ responsible for metabolic homeostatis like glucose metabo-lism or fat storage. A further central task of the human liver is the detoxification of the blood since toxic substances or excessive medication can cause damage in the liver structure which can lead to acute liver failure.

In previous publications a computational model with a multicomponent/multiphasic/multiscale approach to simulate important functionalities which are directly coupled with the blood perfusion is presented, see [1-2]. Now, the growth in the liver tissue and its influence on the metabolism is examined. Furthermore, the development of the fatty liver disease which occurs of lipid inclusions and growing cells is presented.

The main functions of the liver take place at the smallest cells of the liver, the hepatocytes, which are embedded in the liver lobules. Nutrient, oxygen and other substances are transported with an anisotropic blood flow via a delicate system of capillaries, so called sinusoids. The inner structure of the lobule is highly complex due to the inhomogeneous distribution of the sinusoidal network and the complex arrangement of the hepatocytes. For a homogenization of the complex geometry we use a multiphasic mixture theory based on the Theory of Porous Media (TPM).

The intended full liver model consists of three scales, namely the organ-, lobuli hepatis- and cell-scale. Each scale is connected via energy based homogenization conditions (Hill condition). In this study we will focus on the scale bridging between the loboli hepatis (meso-) and cell-scale. Regarding the processes on the cell scale in the hepatocytes a system of ordinary differential equations (ODE) for the calculation of the metabolism is included. The input for the ODE-system results from the overlying FEM meso-scale and contains information about external glucose and lactate concentrations that are solved and carried in the blood whereas the glycogen is stored stationary in the hepatocytes. In addition, the agglomeration of lipid contents has been included in the model which impacts the perfusion and metabolic equilibrium.

Acknowledgments: We thank the Cluster of Excellence SimTech (PN 4-27) for funding.

References:

[1] *RICKEN, T., et al. Modeling function-perfusion behavior in liver lobules including tissue, blood, glucose, lactate and glycogen by use of a coupled two-scale PDE-ODE approach. Biomechanics and modeling in mechanobiology, 2015, 14 (3), 515-536.*

[2] *RICKEN, Tim; DAHMEN, Uta; DIRSCH, Olaf. A biphasic model for sinusoidal liver perfusion remodeling after outflow obstruction. Biomechanics and modeling in mechanobiology, 2010, 9.(4), 435-450.*

[D-06.2]

MODELLING OF ABDOMINAL WALL UNDER UNCERTAINTY OF MATERIAL PROPERTIES

Katarzyna Szepietowska[1], *Izabela Lubowiecka*[1], *Benoit Magnain*[2], *Eric Florentin*[2]

1 *Gdansk University of Technology, Gdansk, Poland*
2 *Lamé, Insa Cvl, Univ. Orléans, Univ. Tours*

The study concerns modelling of the abdominal wall including uncertainties. Understanding mechanical behaviour of abdominal wall is important in the context of ventral hernia repair. Prediction of behavior of abdominal wall – implant system by numerical simulations is needed to optimize the hernia treatment. The shell or membrane models [1] can be useful in patient-specific approach due to relatively easy geometry generation when compared to models based on MRI or CT scans (like one in [2]). However, one of difficulties in the modelling is uncertainties of mechanical properties of abdominal wall, e.g. to natural variability of abdominal wall mechanical properties and challenges in accurate identification of these properties in vivo. Global sensitivity analysis enables investigation of influence of input uncertainties on the uncertainty of the output. Previously, we investigated [3] an influence of uncertainties on the response of model of healthy abdominal wall and abdominal wall with hernia and implant. In that case material models of abdominal wall was linear orthotropic. However, soft tissues exhibit nonlinear behavior and abdominal wall tissues were in the literature also modeled with hyperelastic constitutive laws [2]. In [4] Gasser-Ogden-Holzapfel (GOH) model [5] was used in the shell model of abdominal wall. In the paper we study the influence of uncertainties of parameters of GOH material model on the output of abdominal wall model.

Finite element (FE) model is taken from previous study [3]. The model is composed of shell elements with fixed translations on the edge of the model. The model is subjected to a pressure simulating intraabdominal pressure during cough. The FE calculations are performed in MSC.Marc. Rregression-based polynomial chaos expansion [6] is used to propagate uncertainties and calculate the Sobol' indices with low computational cost. The parameters of GOH model including fiber orientation are treated as random variables. Displacement of chosen point in the center of abdominal wall is the quantity of interest in the analysis.

Uncertainties have been propagated and the distribution of the output has been obtained. The calculated Sobol indices indicate that the uncertainty of C10 parameter has the highest contribution to the variance of quantity of interest. Second in terms of importance, but with much smaller influence, is κ describing dispersion of fibers. The outcomes of global sensitivity analysis will be useful in the identification of properties of abdominal wall based on an inverse approach.

Acknowledgments: This work was partially supported by grant UMO-2017/27/B/ST8/02518 from the National Science Centre, Poland and by subsidy for young scientists given by the Faculty of Civil and Environmental Engineering, Gdansk University of Technology, Gdansk, Poland. Computations were performed partially in TASK Computer Science Centre, Gdańsk, Poland.

References:

[1] *I. Lubowiecka, A. Tomaszewska, K. Szepietowska, C. Szymczak, M. Lichodziejewska-Niemierko, M. Chmielewski, Membrane model of human abdominal wall. Simulations vs. in vivo measurements, in: Shell Struct. Theory Appl., 2018: pp. 503–506.*
[2] *B. Hernández-Gascón, A. Mena, E. Peña, G. Pascual, J.M. Bellón, B. Calvo, Understanding the passive mechanical behavior of the human abdominal wall., Ann. Biomed. Eng. 41 (2013) 433–44.*
[3] *K. Szepietowska, I. Lubowiecka, B. Magnain, E. Florentin, Global sensitivity analysis of membrane model of abdominal wall with surgical mesh, in: Shell Struct. Theory Appl., 2018: pp. 515–518.*
[4] *B. Borzeszkowski, T.X. Duong, R.A. Sauer, I. Lubowiecka, Isogeometric Shell FE Analysis of the Human Abdominal Wall, Submitted. (2019).*
[5] *T.C. Gasser, R.W. Ogden, G.A. Holzapfel, Hyperelastic modelling of arterial layers with distributed collagen fibre orientations, J. R. Soc. Interface. 3 (2006) 15–35.*
[6] *B. Sudret, Global sensitivity analysis using polynomial chaos expansions, Reliab. Eng. Syst. Saf. 93 (2008) 964–979.*

[D-06.3]

SIMULATING CEREBRAL EDEMA AND DELAYED FATALITY AFTER TRAUMATIC BRAIN INJURY USING TRIPHASIC SWELLING BIOMECHANICS

Andrew Basilio[1], *Peng Xu*[1], *Yukou Takahashi*[2], *Toshiyuki Yanaoka*[2], *Gerard Ateshian*[3], *Barclay Morrison III*[1]

1 *Columbia University, New York, USA; Biomedical Engineering*
2 *Honda R&d Co., Ltd.*
3 *Columbia University, New York, USA; Mechanical Engineering*

Finite element (FE) methods have been used to assist in the development of safety systems to reduce injuries due to motor vehicle crashes (MVCs), including traumatic brain injury (TBI). Although FE models have been useful for studying TBI during a MVC, a large proportion of TBI-related mortality occurs hours or days after a MVC. One reason for this delay in death is because a severe TBI can lead to cerebral edema where the brain begins to swell within the rigid skull, increasing intracranial pressure (ICP). An increase in ICP can have devastating consequences for the patient, limiting cerebral blood flow and leading to ischemia. Using triphasic biomechanics and FE methods, this study modeled the sustained elevated levels of ICP following an impact scenario and the percent mortality associated with it.

Triphasic biomechanics can explain the brain swelling that occurs during cerebral edema by modeling the brain, or any other similar biological tissue, as an aggregate of different components: a charged deformable porous solid matrix with a fixed charge density (FCD) and monovalent counter-ions present in the cerebrospinal fluid. After a mechanical insult, dying brain cells expose their FCD and the resulting Gibbs-Donnan osmotic pressure causes water to flow into the brain. FEBio (febio.org) was used to simulate cerebral edema following an impact scenario. Once the FE mesh of the brain from the Global Human Body Models Consortium (GHBMC) was imported into FEBio, each element was assigned a FCD value based upon the maximum principal strain (MPS) that the element experienced within a crash simulation in LS-DYNA using the stock GHBMC model. As an element experienced a higher MPS, it was assigned a higher FCD indicative of a higher degree of cell death. Elements within the FEBio mesh swelled depending on the magnitude of their assigned FCD value, causing adjacent elements to compress. This compression was assumed to cause reduced blood flow and represent ischemic cell death that occurs in biological tissue. These compressed elements would then be assigned a new FCD value and subsequently swell, mimicking the swelling response that occurs in the brain following ischemia.

Our model successfully produced increasing ICP values as a greater number of elements in the FEBio mesh experienced a larger MPS, demonstrating that more severe crash scenarios lead to increasingly higher ICP, and therefore, a higher probability of death.

To the best of our knowledge, this is the first study to model sustained elevated ICP after an impact scenario. With the potential capability to capture delayed mortality after a MVC, we believe our model will assist researchers in developing new safety systems.

Acknowledgments: Honda R&D

[D-06.4]

COMPUTATION OF IN-PLANE LEFT VENTRICULAR MYOCARDIAL STRAIN VIA IMAGE REGISTRATION

Miguel Rodriguez[1], *Shawn Shadden*[1], *Moriel Vandsburger*[2]

1 *Mechanical Engineering, University of California, Berkeley, USA*
2 *Bioengineering, University of California, Berkeley, USA*

The 2015 Annual Data Report from the US Renal Data System indicates that sudden cardiac death and arrhythmias are the leading cause of mortality for patients on routine hemodialysis for end-stage renal disease (ESRD) [1]. Given the reduced kidney function in such patients, gadolinium-based contrast agents used during standard cardiac magnetic resonance imaging are contraindicated in patients with ESRD [2]. Driven by this limitation, and the increased risk of adverse cardiac events [3], Stromp et al. developed a gadolinium-free imaging method to identify diseased myocardium [4]. Subsequently, a strong correlation between initial fibrotic burden and subsequent loss of contractile function was shown [5].

In this study, we aim to further augment gadolinium-free imaging of ESRD patients by considering the mechanics of the left ventricle. To validate our framework, we first generate synthetic images based on analytical shapes. Specifically, we sinusoidally vary the ratio of the major and minor axes of an ellipse, such that the initial image is of a circular domain. We apply the image registration technique known as the Large Deformation Diffeomorphic Metric Mapping (LDDMM) [6] to these synthetically generated images. The LDDMM provides a map between a target and source image, such that the target image is reproduced when the mapping is applied to the source image. To compute the deformation, a triangular mesh is used as the discrete representation of the circular reference domain. The displacement field provided by LDDMM is then interpolated at the mesh nodes and used to update their coordinates throughout the entire cycle. We are able to reproduce the corresponding elliptic domains, and our preliminary tests show that, though fairly robust, the quality of results indubitably depends on the image resolutions.

Being able to compute the displacement of the domain enables us to compute the transmural strain of the left ventricular myocardium. We will present the resulting myocardial strain throughout the cardiac cycle at multiple locations along the long axis of the left ventricle for seven patients. The strain field can then serve as an additional diagnostic tool to identify loss of contractile function for patients under routine surveillance, such as those with ESRD.

References:

1. *Saran, R. et al. Am J Kidney Dis 67, A7-8, 2016.*
2. *US FDA, Public Health Advisory, 2006.*
3. *Wu, K.C. et al. J Am Coll Cardiol, 51(25):2414-21, 2008*
4. *Stromp, T.A. et al. J Cardiovasc Magn Reson, 17, 2015.*
5. *Stromp, T.A. et al. Scientific Reports, 8(1), 2018.*
6. *Beg, M.F. et al. Int J Comput Vision, 61(2):139-157, 2005.*

[D-06.5]

IN-VIVO MEASUREMENTS OF HUMAN TONGUE ELASTICITY UNDER GENERAL ANESTHESIA USING A VOLUME BASED ASPIRATION METHOD

Kilian Kappert[1], *Sander Boonstra*[1], *Fons Balm*[1], *Nathanael Connesson*[2], *Maarten van Alphen*[1], *Yohan Payan*[2]

1 *Netherlands Cancer Institute, Amsterdam, Netherlands*
2 *Université Grenoble Alpes, Grenoble, France*

Treatment of locally advanced head and neck cancer, in particular tongue cancer, often results in impaired speech, swallowing, or mastication. Due to the complex structures and systems involved in oral functions, it is difficult for a clinician to predict the functional consequences after surgery or chemoradiation. Effective patient counseling and choosing the right treatment is therefore often an arduous task. Simulating the effect of treatments using biomechanical computer models can help the patient and the treating physician to understand the effects and impact of the intervention. Therefore, we are currently developing a Finite Element tongue model that can simulate these postoperative functions.

To simulate the deformations of tissue in the tongue, accurate measurements of the elastic properties are essential. Furthermore little is known regarding inter-person variability. Techniques such as magnetic resonance elastography, shear wave elastography, and ex-vivo measurements have not provided us with sufficient information yet. Recently Elahi et al. (2019) introduced a new measurement technique to estimate elasticity using a volume-based aspiration method (Figure 1). The device was slightly modified to estimate in-vivo tongue tissue stiffness (Figure 2). The method relies on an inverse Finite Element Analysis (FEA) of the aspiration experiment using the Gent hyperelastic material model. The aspirated volume over time is translated to the Young's modulus and the strain limiting factor Jm.

To test the feasibility of this technique for clinical measurements, we measured 16 healthy volunteers ten times, and subsequently estimated their Young's modulus at rest. While the inverse FEA procedure is still in development, the first identified values range from 3 to 5 kPa, with a mean standard deviation of 1.73 kPa within every subject.

However, under normal circumstances, it is hypothesized that muscle tonus will cause the tongue to be stiffer, even if the volunteers were asked to keep their tongue "at rest". In order to measure the tongue with and without muscle tonus, we have started the inclusion of 19 urology and gynecology patients scheduled for surgery under general anesthesia. In the final paper, we will present the results of both the measured elastic properties in normal circumstances and under general anesthesia.

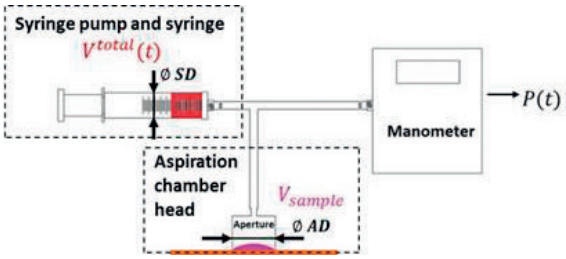

Figure 1: Schematic overview of the setup. By removing a known volume of air, a vacuum is created inside the aspiration chamber. The pressure is measured using a manometer. (Image from: Elahi et al. 2019)

Figure 2: Placement of the aspiration chamber head at the lateral side of the tongue.

References:

Elahi, S. A., N. Connesson, G. Chagnon, and Y. Payan. 2019. "In-Vivo Soft Tissues Mechanical Characterization: Volume-Based Aspiration Method Validated on Silicones." Experimental Mechanics. Retrieved (https://doi.org/10.1007/s11340-018-00440-9).

[D-06.6]

A COMPUTATIONAL FRAMEWORK FOR PREDICTION OF BIOPROSTHETIC HEART VALVE FUNCTION UNDER LONG-TERM CYCLIC LOADING

Rana Zakerzadeh[1], *Will Zhang*[2], ***Michael Sacks***[1]

1 *The University of Texas at Austin, Austin, USA*
2 *University of Michigan, Ann Arbor, USA; University of Texas at Austin, Austin, USA*

Bioprosthetic heart valves (BHV) remain the design of choice for most clinical applications due to their low thrombogenicity and excellent hemodynamics. However, durability remains to be the central issue hindering BHV designs and even marginal improvements to the current lifespan of 10-15 years can have significant clinical impacts. Recently, we developed a novel, mechanism-based mathematical model of BHV leaflet responses to long-term valve operation via a permanent set mechanism [1-2]. The focus of the present study was to utilize this material model to predict BHV evolving geometry, microstructure, and mechanical property changes under simulated in-vivo conditions. Simulations were conducted using the standard BHV valve geometry and collagen fiber distributions aligned with the circumference direction with the standard deviation of 30◦. There are four main stages in simulating permanent set: 1) modeling the initial state composed of BHV geometry, material properties and mapped collage fiber architecture, 2) quasi-static simulation of the BHV using finite element method under physiological transvalvular pressure, 3) updating the material properties for the next time step, and 4) updating the BHV geometry for the next time step. Steps 2-4 are repeated for each subsequent time step until we reach the prechosen maximum number of cardiac cycles. We observed that permanent set induces major changes, especially in the belly region, center of the free edge, and the regions near the commissures where the leaflets make contact. These regions are also the most common regions of failure in BHVs. Due to the change in reference configuration, the collagen fibers in these regions recruit more quickly and may even held in a constant extended state. This can have dramatic consequences on the likelihood of failure of these collagen fibers due to their low extensibility and could be a major failure mechanism. We note too that these effects slow down after 20 million cycles and nearly cease after 50 million cycles. This important structural response allows us to predict the final reference geometry of the BHV. Because collagen fibers have high rates of failure after being extended by 7-8%, more evenly distributing the stresses can reduce this mode of failure. Thus, by optimizing the initial BHV design so that the peak stress is minimal in the configuration after permanent set has seized, we can potentially improve the durability of BHVs by minimizing the load on the collagen fibers (Figure 1). What is novel here is the ability to predict permanent set effects on BHV geometry in-silico and develop means to compensate for it in a design setting.

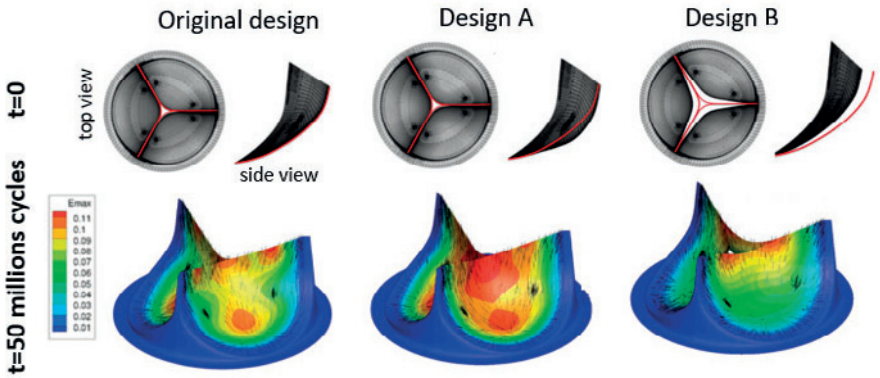

Figure Caption: Predicted shape of the valve leaflet at 50 million cycles form different starting geometries. Note that here we show the max strains, where a simple extension of the leaflet (Design B) produces smaller permanent set strains, which could lead to lower stress concentrations and potentially extended durability.

References:

[1] *Zhang, W., et al. J Mech Behavior Biomed Mat, 2017. 75: p. 336-350.*
[2] *Sacks, M., et al. Interface focus, 2016. 6(1): p. 20150090.*

[D-08.1]

THE MECHANICAL BEHAVIOUR OF SKIN: A STRUGGLE FOR THE APPROPRIATE TESTING METHOD

Cees Oomens[1]

1 *Eindhoven University of Technology, Eindhoven, Netherlands*

The first serious biomechanical experiments to study properties of skin were published in the early seventies by Lanir and Fung (1974). Their biaxial tests on rabbit skin and the formulation of the pseudo-elastic strain energy equation had a major impact on later studies. Over the years many different testing methods to measure skin mechanical properties were developed, many of these were non-invasive, in-vivo test methods, like suction tests, indentation tests, uniaxial, biaxial and multi-axial strain tests and often a numerical/experimental inverse method to obtain the parameters. Until 10 years ago most tests were focused on the skin as a whole. Because in-vivo testing does not allow making small samples with a controlled shape, this inverse method was the only feasible approach. However, the success of these testing methods was severally hampered by the quality and detail of the constitutive models and appeared to be quite elaborate.

In the last decade the interest has shifted to the individual top-layers of the skin like stratum corneum and viable epidermis. The incentive for this was an interest in trans-epidermal drug delivery and advanced developments in personal skin care. This led to a revival of in-vitro testing of human skin samples or skin equivalents. Methods for extraction, conserving and preserving during testing of very small samples has benefitted a lot from developments in the area of tissue engineering and techniques to follow the skin structure during testing are also available. In the presentation an overview will be given of this research and it will end with a discussion on a single skin model to describe, biaxial testing, shear as well as indentation behavior of human skin.

References:

1. *Lanir, Y., Fung, Y.C. Two-dimensional mechanical properties of rabbit skin, Journal of Biomechanics, 7, pp. 29 – 34, 1974a.*
2. *Lamers, E et al., Large amplitude oscillatory shear properties of human skin. J Mech Behav Biomed Mat, 28, 462-470, 2013.*
3. *A model of human skin under large amplitude oscillatory shear T J.F.J. Soetens, M. van Vijven, D.L. Bader, G.W.M. Peters, C.W.J. Oomens, JMBBM, 86, 423-432, 2018.*

[D-08.2]

DESIGNING EXPERIMENTS FOR IDENTIFYING MECHANICAL PROPERTIES OF SOFT TISSUES

Thiranja Babarenda Gamage[1], *Poul Nielsen*[2], *Martyn Nash*[2]

1 *Auckland Bioengineering Institute, The University of Auckland, Auckland, New Zealand,*
2 *Auckland Bioengineering Institute, The University of Auckland, Auckland, New Zealand; Department of Engineering Science*

Determining the mechanical properties of soft tissues using biomechanical models is useful for a wide range of applications, ranging from improving breast cancer diagnosis and treatment, to developing realistic facial avatars for the animation industry. Computer models of tissues typically require many parameters to represent their nonlinear, anisotropic mechanical properties. Attempting to identify these parameters using ad-hoc experimental protocols often results in unreliable estimates of the mechanical properties. This is due to a lack of understanding of whether a given experimental protocol provides sufficiently rich information to determine the parameters. Poorly designed experiments may yield little useful information, resulting in highly correlated and/or inaccurate model parameter estimates [1]. To address this challenge, we have developed software tools for determining experimental protocols that maximise the identifiability of mechanical parameters using design of experiments (DOE) techniques. This approach was validated by performing controlled experiments on silicone gel cantilever phantoms under gravity loading. The approach was then applied to determine breast tissue mechanical properties from the changes in skin surface shape that occurs when the breast is repositioned from the prone position (where the 3D structure of the breast can be quantified using magnetic resonance imaging) to a given target orientation (where a surface scan of the breast can be obtained). This allowed us to determine the optimal target orientation to image the breast surface to maximise identifiability of breast tissue mechanical properties. DOE techniques are applicable to a wide range of biomechanics applications. Our current research efforts are aimed at designing experiments for identifying the nonlinear, anisotropic, and viscoelastic properties of the skin, breast, and the lung using a 3-axis force and torque sensitive micro-robotic indenter and phase-based digital image correlation techniques [2]

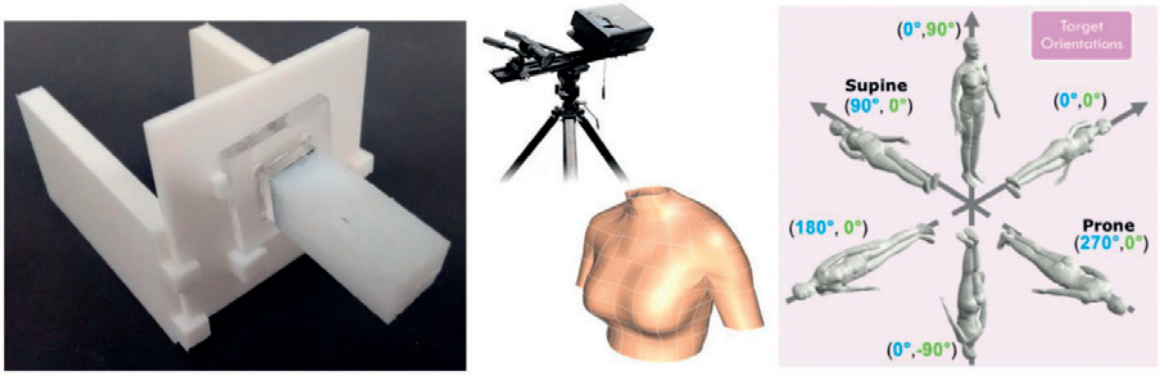

Figure Caption: "Silicone gel cantilever experiments (left panel), and target orientations considered for designing experiments to identify breast mechanical properties (middle and right panels)"

Acknowledgments: New Zealand Ministry for Business, Innovation and Employment and the University of Auckland Foundation

References:

[1] *Babarenda Gamage, T. P., et al., Int. J. Numer. Meth. Biomed. Engng., 27: 632, 2011*
[2] *Parker et al., 2019, Biomech Model Mechanobiol, DOI 10.1007/s10237-019-01127-3*

[D-08.3]
COLLAPSE OF VESSELS IN SOFT TISSUES

Sam Evans[1], *Lucie Pecheur*[1], *Hayley Wyatt*[1], *Bethany Keenan*[1]

1 *Cardiff University, Cardiff, UK*

Introduction: The collapse of vessels in soft tissues is important in many clinical situations. Compression of a tissue can occlude blood vessels causing ischaemia, either deliberately induced to prevent blood loss or seal vessels, or accidentally leading to pressure injuries. On the other hand, the veins in the leg collapse due to pressure from contraction of the surrounding muscles, which helps to pump blood back up to the heart.

The unstable behaviour of a vessel with internal pressure embedded in tissue undergoing large deformations presents a very complex problem of mechanics. The objective of this study was to simulate and investigate it, with the aim of better understanding the factors that determine whether or not a vessel collapses and hence to understand and if possible alleviate the risks of ischaemia and tissue damage.

Methods: A variety of vessels with different diameters, wall thicknesses and material properties embedded in a block of homogenous soft tissue were modelled. The analysis proceeded in two stage, firstly ramping the internal pressure in the vessel up to a physiological level and secondly applying confined compression to the surrounding tissue. The dimensions, material properties and loading were systematically varied in order to evaluate their effect on buckling and collapse of the vessel.

Results and Discussion: An embedded tube with internal and external loading undergoing large deformations can behave in a variety of different ways, with several possible bifurcations and instabilities. The unstable inflation of a tube is well known and occurs clinically in aneurysms. An embedded tube under external load can buckle and collapse with a variety of possible modes. Another interesting instability is that under internal pressure the inside of the tube can wrinkle. The interior of the tube would like to expand longitudinally with the result that its surface buckles. To our knowledge this mode has never previously been identified.

There are several other curious and anomalous behaviours that emerged in this study. During inflation, the wall thickness first decreases but then increases again. This may be because of a shift from behaving like a thick walled cylinder where the load is carried by radial compression of the wall, to a thin walled cylinder where the load is carried by the hoop stress. It was found, for a realistic range of material properties, that the expansion of the vessel depended far more on the properties of the tissue around it than on the properties of the vessel wall. This suggests that the typical approach of analysing a vessel in isolation may be misleading, and that the tissue around the vessel contributes more than is generally appreciated.

Simulating vessels with realistic dimensions and material properties confirmed that collapse does occur at physiologically relevant pressures and external stresses. This demonstrates the potential to predict and avoid unwanted vessel occlusion. The vessels have evolved to an optimal design with little surplus strength, which is efficient but leaves them vulnerable when the circumstances change.

[D-08.4]

ULTRASOUND-BASED BIOMECHANICAL MODELING OF ABDOMINAL AORTIC ANEURYSMS FOR CLINICAL DECISION SUPPORT

Richard Lopata[1], *Emiel van Disseldorp*[1], *Niels Petterson*[1], *Marc van Sambeek*[1], *Frans van de Vosse*[1]

1 *Eindhoven University of Technology, Eindhoven, Netherlands, Dept. of Biomedical Engineering*

Cardiovascular disease is still the number one killer worldwide. Abdominal aortic aneurysms (AAAs), local dilatations in the aorta, lead to a life-threatening hemorrhage when ruptured. Current clinical practice comprises of watchful waiting until the diameter reaches 5.0 – 5.5 cm. This criterion is evidence-based but not tailored to the individual patient. Over the years, image-based wall stress analysis of AAAs has been investigated extensively. Finite element (FE) analysis is used to assess peak wall stresses in a patient-specific geometry. However, translation to the clinic is hampered by the use of either costly (MR) or harmful (CT) imaging modalities. Moreover, individual differences in wall properties are not considered, nor are these modalities suitable for patient follow-up.

Ultrasound (US) functional imaging has many advantages for AAA characterization. One can perform multiple measurements at low cost without the use of ionizing radiation or contrast. The high spatial and temporal resolution allows for not only the assessment of a patient-specific geometry but also the measurement of wall motion and strain. However, US has some disadvantages such as the anisotropy in image quality and contrast, and the limited field-of-view. Still, US provides a powerful tool for personalized modeling of AAAs.

In recent years, we have developed an US-based modeling framework that starts with transabdominal, 3-D, US acquisition, followed by automatic segmentation based on 3-D deformable contours and image registration, geometry discretization and FE analysis to assess peak wall stresses. In case the aneurysm did not fit a single 3-D volume acquisition, or contrast was too low for segmentation, a novel multi-perspective method was applied, merging separate volumes into one. A model of the artery and its surroundings is generated automatically. Additionally, the FE models are further personalized by calibrating the FE output to the actual motion, measured with an in-house developed 3-D US speckle tracking technique. The method was verified experimentally in a mock loop using porcine aortas in vitro.

The methodology has been validated in 40 AAA patients in vivo by comparing geometry and wall stress results to CT-based methods and arterial stiffness to US elastometry. Furthermore, a study between age-matched volunteers (n = 30) and AAA patients (n = 65) showed the reproducibility and sensitivity. Large differences in arterial stiffness were observed between age-matched healthy volunteers and patients with relatively small aneurysms, whereas several small AAAs revealed peak stresses similar to larger AAAs (> 5.5 cm). Addition of surrounding tissue (and a spine) reduced the residual errors after the calibration process significantly. A longitudinal study of these parameters is currently ongoing in a cohort of over 310 AAA patients. The first results (n = 70) show that on the onset of growth, AAAs tend to be weaker and regain their stiffness during growth.

[D-08.5]

MULTIPLE SCALES BROAD BAND-WIDTH FREQUENCY (0.1 -1 KHZ) STUDY ON DYNAMIC POROVISCOELASTICITY OF NEUTRAL AND POLYELECTROLYTE HYDROGELS

Yin Chang[1], *Ronan Daly*[2]

1 *University Of Cambridge, Department of Chemistry, Cambridge, UK; Department of Engineering; Institute for Manufacturing*
2 *University Of Cambridge, Institute for Manufacturing*

Cell-matrix interactions are determined for successful cell culture. Cells can passively be affected by matrix relaxation [1], and can actively respond to dynamically properties of matrix over a 10 μm lateral thickness [2]. Hydrogels are widely used to culture cells due to their biocompatibility and similarities with the natural extracellular matrix. Static mechanical and transport properties of neutral hydrogels have been widely studied but this has not yet been extended to polyelectrolyte hydrogels, which are important because the charged functional groups potentially encourage active responses to external stimuli. In this study, oscillation indentation with frequency 0.1- 100 Hz) and PAV rheometer (with frequency 0.1- 1kHz) are used for characterizing local and global dynamic mechanical properties of hydrogels. This is coupled with molecular dynamic simulations to reveal the likely molecular interactions, and finite element analysis (FEBio Software suit [3] and GIBBON [4]) to study the poroviscoelasticity of polyelectrolyte hydrogels. We characterized shear modulus and permeability of neutral and polyelectrolyte hydrogels from a single relaxation test. Rheological analysis using oscillation indentation was developed and applied to neutral hydrogels, with a significant benefit in enabling in-depth local rheological studies. The negatively charged hydrogels show a different relationship between modulus and permeability compared with neutral hydrogels, and we conclude that the charge density provides independent tuning of the mechanical and transport properties. The development of a local rheology detection technique and the investigation into polyelectrolyte hydrogel poroviscoelasticity provides new design strategies for future tissue replacements. This cross-scales experiments and simulation methods provide a better understanding local and global mechanical properties of hydrogels and provides new strategies for tuning tissue replacement matrices properties.

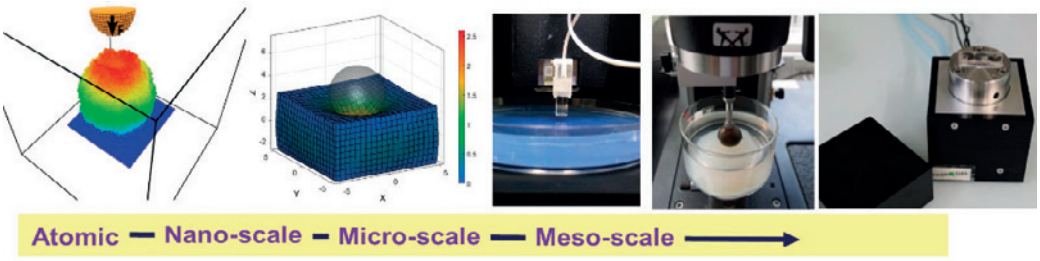

Figure 1 Cross-scales mechanical properties characterization by using MD simulation, FEM analysis, nanoindenter, microindenter, and PAV rheometer.

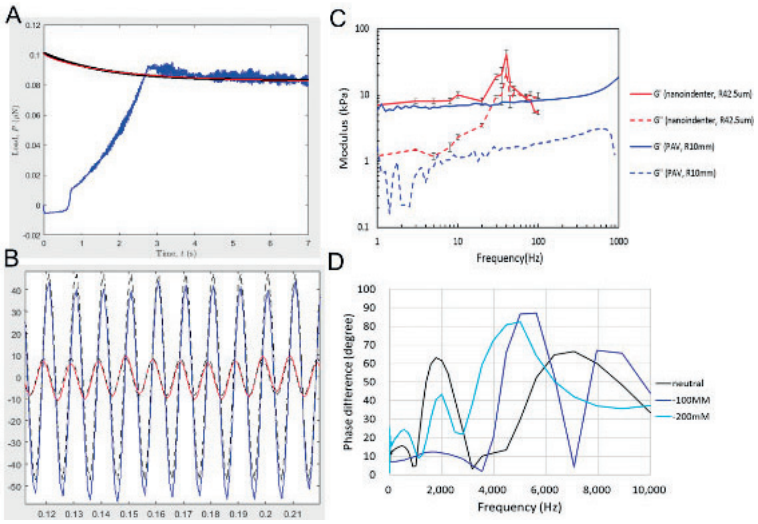

Figure 2 Nano- and micro-mechanical property and rheology of 10 wt% neutral and PEGDMA hydrogels (A) are indentation relaxation curve and simulation fitted results. (B) shows the dynamic responses of stress (red solid line) and strain (blue solid line) and simulation fitted results (black dash line) (C) Comparison of G' and G" measured by indenter and PAV rheometer. (D) Charges effects on the hysteresis and phase difference.

Acknowledgments: The authors acknowledge the financial support from Taiwan-Cambridge Trust Scholarship provided by Cambridge Trust.

References:

1. *Chaudhuri et al., Nature materials, 15(3), 326, 2016.*
2. *Sen et al, Cellular and molecular bioengineering, 2(1):39–48, 2009*
3. *Maas SA et al., Journal of Biomechanical Engineering, 134(1):011005, 2012*
4. *Moerman, Journal of Open Source Software, 3(22), 506, 2018*

[D-08.6]

COMPUTATIONAL MODELING INSPIRED VALVE DESIGN ENABLES LONG-TERM FUNCTIONALITY OF TISSUE-ENGINEERED HEART VALVES

Sandra Loerakker[1], *Bart Sanders*[1], *Maximilian Emmert*[2], *Simon Hoerstrup*[2], *Frank Baaijens*[1]

1 *Eindhoven University of Technology, Eindhoven, Netherlands*
2 *University of Zurich, Zurich, Switzerland*

Tissue-engineered heart valves (TEHVs) have the capacity to grow and remodel over time in line with the recipient's demands, and hence the potential to last for a life-time. Still, pre-clinical studies have demonstrated that the mid- to long-term functionality of TEHVs is often suboptimal as a consequence of adverse tissue remodeling, e.g. leading to leaflet thickening or retraction. To improve the performance and reliability of TEHVs and hence accelerate clinical translation, it is essential to understand the underlying remodeling mechanisms, and design TEHVs such that remodeling leads to physiological adaptation.

Previously, we used computational modeling to propose a valve design that could aid in the prevention or minimization of leaflet retraction [1], and we developed a computational framework to predict cell-mediated tissue remodeling in response to dynamic mechanical cues [2-5]. The goal of the present study [6] was to evaluate in a pre-clinical study (1) if the suggested improvement in valve design indeed leads to improved tissue remodeling and functionality, and (2) whether we could understand and predict the observed remodeling response with our computational model, given the properties of the valves upon implantation.

Eleven valves were implanted in the pulmonary position of sheep, with a follow-up period of one year. Valve functionality was frequently monitored during the implantation period, and appeared to be excellent for most of the valves throughout the complete follow-up period. This was due to the fact that leaflet retraction was only limited and stable within six months of implantation. In terms of tissue organization, the initially isotropic collagen network remodeled during implantation towards a more circumferentially aligned configuration.

With the material properties on non-implanted valves derived from mechanical tests, we used our computational framework to analyze the in vivo remodeling process of the valves. The model predicted that, with the current parameters, the valves were indeed able to preserve their functionality due to limited retraction, and the predicted tissue structure was in good agreement with the experimental results. Furthermore, via incorporating valve specific properties as determined after explantation, our model could explain certain differences in observed collagen organization.

In summary, our integrated computational-experimental study confirmed that TEHVs can maintain their functionality during a one-year implantation period in sheep. Computational modeling was essential for defining the superior valve design and enabling the successful one-year pre-clinical follow-up.

Acknowledgments: This research was supported by the European Union's FP7 program (LifeValve), and the Dutch Heart Foundation (CVON, 1Valve).

References:

[1] Loerakker et al., J Biomech 2013;
[2] Obbink-Huizer et al., BMMB 2014;
[3] Loerakker et al., BMMB 2014;
[4] Ristori et al., CMBBE 2016;
[5] Loerakker et al., JMBBM 2016;
[6] Emmert, Schmitt, Loerakker, Sanders et al., Science Transl Med 2018.

[D-09.1]
THE MODELLING AND MECHANICS OF POSITIONAL BRAIN SHIFT

Nicholas Bennion[1], *Stefano Zappala*[1], *Matthew Potts*[1], *David Marshall*[2], *Sam Evans*[1]

1 *School of Engineering; Cardiff University, Cardiff, UK*
2 *School of Computer Science & Informatics; Cardiff University, Cardiff, UK*

Introduction: Positional brain shift (PBS) is the relative movement of the brain within the skull which results from reorientation of the head with respect to gravity. Within this highly constrained scenario exists boundary conditions dissimilar to typical areas of computational brain modelling; predominantly high strain rate impact or craniotomy during surgery. Compared to these areas of study, little is known about the mechanics of PBS and as such the important modelling considerations in similar areas. Additionally, PBS is clinically significant in a range of procedures and is often unaccounted for.

Methods: Using ScanIP, Matlab and FEBio, a combined CFD/FEA model was developed incorporating the pia mater, fluid filled subarachnoid space and spring element representation of the arachnoid trabeculae. Material properties were varied over a realistic range using the Latin Hypercube method within GEM-SA to yield 60 unique combinations. Each combination was loaded with acceleration due to gravity in prone and supine orientations. In a parallel study, corresponding MR images in human subjects were obtained and analysed to extract a 3D displacement field. Sensitivity analysis of material properties was performed in GEM-SA, comparing the displacement field of the FE predictions and human subjects.

Results: Displacement was predominantly in the direction of gravity, with an average magnitude of less than 1mm. Greatest displacements were found in central regions indicating non-rigid deformation. Of the materials varied, the bulk modulus of the brain and stiffness of the arachnoid trabeculae were found to be most influential in PBS. For bulk modulus, optimised values in all cases were below 200 KPa. The spring stiffness and distribution equated to a tensile stiffness of approximately 30 KPa. The supine load distribution of the trabeculae is shown.

Discussion: The displacement pattern found in this study fell broadly in line with previous studies of PBS (1). Notably, we have shown the bulk modulus to be integral in the accurate capture of this process; a factor that is often not considered in similar studies. We suggest that careful selection of the bulk modulus for single phase representations is an appropriate simplification when considering consolidation of brain tissue in time-independent scenarios. To the best of the authors knowledge, this is the first implementation of a fluid-filled, spring-spanned PAC. The similarity between the stiffness calculated in this study and direct tensile testing (2) suggests this to be a highly efficacious representation, with promise for other areas of modelling. This human-validated model can now be developed for the prediction of PBS for use in a range of clinical procedures.

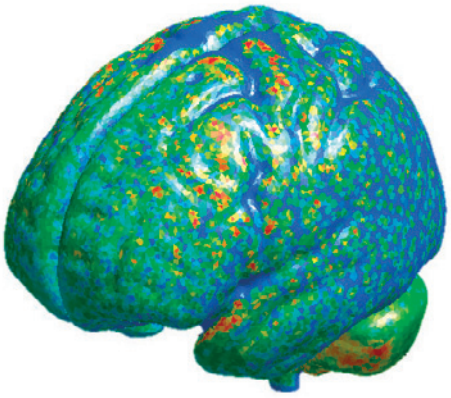

Figure Caption: Colour plot depicting spring force over the brain surface in the supine position

Acknowledgments: This research is funded by the EPSRC and Renishaw Plc. as part of an iCase Studentship. The authors acknowledge the assistance of Rob Harrison, Renishaw Plc.

References:

1. *Schnaudigel S, Preul C, Ugur T, Mentzel HJ, Witte OW, Tittgemeyer M, et al. Positional brain deformation visualized with magnetic resonance morphometry. Neurosurgery. 2010;66(2):376-84; discussion 84.*
2. *Jin X, Mao H, Yang KH, King AI. Constitutive modeling of pia-arachnoid complex. Ann Biomed Eng. 2014;42(4):812-21.*

[D-09.2]
IMAGING OF POSITIONAL BRAIN SHIFT IN A DEFORMABLE PHANTOM

Matthew Potts[1], *Nicholas Bennion*[1], *Stefano Zappala*[2], *David Marshall*[2], *Sam Evans*[1]

1 *School of Engineering; Cardiff University, Cardiff, UK*
2 *School of Computer Science & Informatics; Cardiff University, Cardiff, UK*

Stereotactic surgery and radiotherapy of the brain often present with a very low margin for spatial error. For some surgeries, this margin can be as small as 1 mm. Planning for these surgeries is traditionally done using pre-operative scans taken with the head in the supine position, however, in the operating theatre, the patients head is often positioned differently with the brain loaded in a different anatomical direction by gravity. The purpose of this study was a) to develop a phantom capable of simulating positional brain shift (PBS) in transitions for which brain shift has already been measured (e.g. supine to prone in humans) and then, b) to take the validated phantom and investigate whether other, non-studied, transitions (e.g. supine to 45° elevated supine) elicit a similar degree of brain shift. This will provide information for transitions in which in-vivo measurement is difficult due to impracticalities in MRI/CT measurement (e.g. head coil design in MRI) and help in the validation of a finite element model of PBS being concurrently developed at Cardiff University.

To study PBS, a mechanically realistic phantom of the brain and skull was developed for CT imaging, consisting of [polyvinyl alcohol - phytagel - sucrose - deionised water] hydrogel brain with embedded glass bead markers, deionised water cerebrospinal fluid, elastomer dural septa and rigid plastic skull.

In development, the mechanical properties of the hydrogel brain were tuned to produce a phantom that best reproduced reported in-vivo supine to prone brain shift. Once validated against this transition, brain shift was then measured upon transition to seven other positions from the supine position. In measuring brain shift, non-supine scans were each rigidly registered to the initial supine scan and the displacements of the markers between the scans were determined.

The repositioning of the phantom from the supine position produced non-negligible brain shift in a majority of the transitions.

For transitions in which in-vivo data was available, comparable brain shift was found within the phantom.

Given the difficulty of imaging humans in non-standard head positions, a well validated phantom provides the means to investigate PBS beyond what can be measured in humans. For a majority of the studied transitions, non-negligible brain shift was observed in the phantom. Applied to surgery, these shifts represent a sizeable starting error that encroaches on the error margin even before the skull is opened, further demonstrating the need for PBS prediction tools in surgical planning.

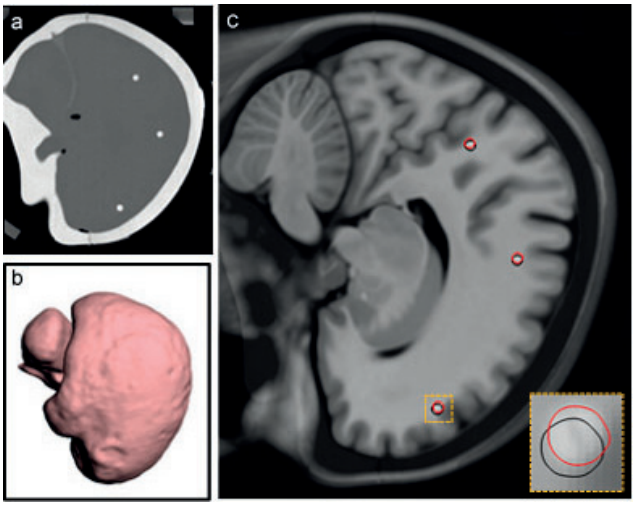

Figure Caption: a) Prone CT image of phantom (sagittal); b) Segmentation of phantoms brain; c) Prone phantom CT fused with registered human MRI dataset showing shifting of three markers upon transition from the supine position.

Acknowledgments: The authors acknowledge the assistance of Rob Harrison, Renishaw Plc.

[D-09.3]

DIGITAL VOLUME CORRELATION VIA MAGNETIC RESONANCE IMAGING: AN IN-VIVO INVESTIGATION OF POSITIONAL BRAIN SHIFT

Stefano Zappala[1], *Nicholas Bennion*[2], *Derek Jones*[3], *Sam Evans*[4], *David Marshall*[5]

1 *Cardiff University, School of Computer Science and Informatics, Cardiff, UK*
2 *School of Engineering; Cardiff University, Cardiff, UK*
3 *Cardiff University Brain Research Imaging Centre, Cardiff, UK*
4 *School of Engineering; Cardiff University; Cardiff University School of Engineering, Cardiff, UK*
5 *School of Computer Science and Informatics; Cardiff University; Cardiff University School of Computer Science and Informatics, Cardiff, UK*

Image-guided neurosurgical systems (IGNS) are common routine in the surgical planning for deep brain stimulation, local drug delivery and biopsy. Current IGNS are based on the rigid alignment of pre-operative scans to the surgical head orientation (determined through a stereotactic frame or skull markers). However, being a soft tissue, the brain sags non-linearly against the skull under the effect of gravity (positional brain shift (BS)). Such non-uniform deformation is not modelled in the rigid transformation, making the location of the target structures differ from the one planned, depending on the actual positioning of the patient on the surgical table.

Finite element (FE) head models predicting such complex deformation field can be integrated with IGNS systems, increasing the targeting accuracy (~ 2 mm)1. However, a thorough validation of such models is still needed before any clinical use. To the best of our knowledge, there is no comprehensive study of positional BS on a volumetric scale to validate these models against.

Eight young healthy participants were scanned in supine and prone positions with the same 7T scanner. Three consecutive images were acquired in order to extract the time evolution of positional BS. Global affine registration was used to align the skulls of each image, so that positional BS remained as the only difference left in the scans. The displacement field and its time evolution were measured through digital volume correlation, via local elastic registration of consecutive scans.

The protocol successfully quantified positional BS, finding an average magnitude of around 1.6 mm. The largest BS occurred along the anterior to posterior direction, with rotational components in both sagittal and axial planes. The volumetric analysis showed numerous local variations, according to the distribution of the regions in the brain (see Figure below). The ROI-analysis showed deformation up to 4 mm of deeper structures (common surgical targets), being more affected by the momentum created by gravity. More externally, positional BS resulted influenced by structures enclosing the brain. Regarding the time evolution, positional BS resulted rather a fast process, stabilised before 10 minutes.

The study showed that positional BS is a complex interaction of gravity, anatomical boundaries and tissue mesostructure. Indeed, the magnitude of positional BS was found to be comparable with the accuracy of IGNS systems, indicating that its prediction on such systems is critical to guarantee the success of a procedure.

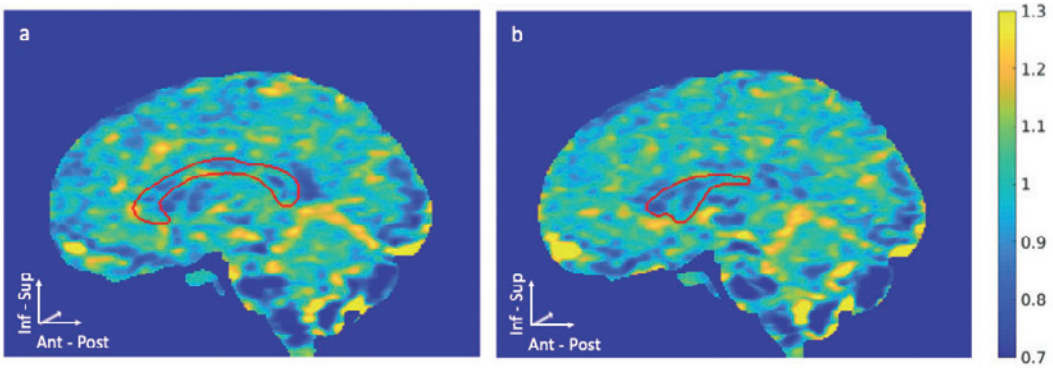

Figure Caption: Average Jacobian map for a sagittal slice at the level of the corpus callosum (a) and the right ventricle (b) (regions outlined in red).

Acknowledgments: This work is supported by Renishaw plc.

References:

1. *Miga, M. et al., "Computational Modeling for Enhancing Soft Tissue Image Guided Surgery: An Application in Neurosurgery". Annals of Biomedical Engineering (2016).*

[D-09.4]

ENRICHED HYDROGELS AS REGENERATIVE SCAFFOLDS FOR NEURONAL REGROWTH

Orit Shefi[1], *Merav Antman Passig*[1], *Jonathan Giron*[2]

1 *Faculty of Engineering and Institute of Nanotechnologies and Advanced Materials, Bar Ilan University, Ramat Gan, Israel*

2 *Faculty of Engineering and Institute of Nanotechnologies and Advanced Materials, Bar Ilan University, Ramat Gan, Israel; Augmanity Nano Ltd*

Controlling cell navigation, organization and growth has great importance in engineering regeneration platforms, for a wide range of tissues. Here we present our recent studies of collagen-based scaffolds for nerve regeneration. Techniques to control cell growth include bio-mimetic scaffolds, nano-fibrous constructs, structured gels, etc., offering a mechanical guide to the regenerating cells. We have developed a novel approach of injectable hydrogels combined with magnetic functionalized nanoparticles (MNPs), that can be incorporated directly into the injured site. We show that gel fiber structure can be aligned in situ dynamically and remotely in response to an external magnetic field. We optimized the gel remodeling to the extracellular environment presenting the gel fibers as mechanical topographical cues for cells. We demonstrated promoted and directed growth combined with effective regeneration of neurons embedded in the aligned gels. Several model systems were examined in vitro and ex-vivo including dorsal root ganglion (DRG) cells. In addition, we enriched the gel by adding growth factors and by functionalizing the MNPs by coating with nerve growth factors. Thus, we present a 'smart' delivery system of biomolecules, together with integral guidance cues within the regenerative scaffold. The combined system has been modified for in vivo implantation. Cross-linkers were added to control degradation and for optimizing mechanical properties and stability of the gel along time. The enriched hydrogel was examined as a scaffold for neurons in an injured peripheral nervous system (PNS) model in rats, leading to promoted growth. Our study presents an emerging biomimetic approach using magneto-chemical scaffolds for promoted nervous tissue regeneration.

Acknowledgments: This work was supported by KAMIN program, Most, Israel #59041 (O.S.) and was partially supported by the Israel Science Foundation Individual grant #1053/15 (O.S.) The authors thank Dr. Hadas Schori with DRG experiments.

References:

Alon, N., Havdala, T., Skaat, H., Baranes, K., Marcus, M., Levy, I., Margel S., Sharoni A. and Shefi, O., Magnetic micro-device for manipulating PC12 cell migration and organization. Lab on a Chip, 15(9), 2030-2036, 2015

Antman-Passig, M., Levy, S., Gartenberg, C., Schori, H., and Shefi, O., Mechanically Oriented 3D Collagen Hydrogel for Directing Neurite Growth. Tissue Engineering Part A, 23(9-10), 403-414, 2017

Antman-Passig, M., and Shefi, O., Remote magnetic orientation of 3D collagen hydrogels for directed neuronal regeneration. Nano letters, 16(4), 2567-2573, 2016

Baranes, K., Hibsh, D., Cohen, S., Yamin, T., Efroni, S., Sharoni, A. and Shefi, O., Comparing transcriptome profiles of neurons interfacing adjacent cells and nano-patterned substrates reveal fundamental neuronal interactions. Nano Letters, doi: 10.1021/acs.nanolett.8b03879, 2019

Marcus, M., Smith, A., Maswadeh, A., Shemesh, Z., Zak, I., Motiei, M., Schori H., Margel S., Sharoni A. and Shefi, O., Magnetic Targeting of Growth Factors Using Iron Oxide Nanoparticles. Nanomaterials, 8(9), 707, 2018

[D-09.5]

THE ANISOTROPIC MATERIAL PROPERTIES OF HUMAN CERVICAL TISSUE IN TENSION AND COMPRESSION

Lei Shi[1], Joy Vink[2], Ronald Wapner[3], ***Kristin Myers***[1]

1 *Columbia University, New York, USA*
2 *Columbia University, New York, USA, Irving Medical Center; Obstetrics and Gynecology*
3 *Columbia University, New York, USA, Irving Medical Center*

The cervix is crucial to a healthy pregnancy by sustaining the increasing load caused by the growing fetus during pregnancy. Premature cervical remodeling and tissue softening is hypothesized to contribute to preterm birth [1]. To understand the role of cervical material properties and tissue architecture during pregnancy, the overall goal of our work is to formulate material models to account for the anisotropic nature of cervix. Here, we formulate an anisotropic constitutive model for human cervical tissue, and we conduct indentation and tension tests on non-pregnant and pregnant cervical tissue to measure material parameters. We model the tissue as a composite material with a compressible neo-Hookean ground-substance embedded with nonlinear fibers following a 3D von Mises distribution. To determine the material parameters of this model, axial slices of human cervical tissue are indented with a spherical indenter at different anatomical regions. Dominant fiber orientation is determined from our previous optical coherence tomography (OCT) study [2]. The displacement and strain fields of the speckled bottom surface are measured by digital image correlation (DIC) using images of the bottom of the specimen against a clear rigid substrate (Fig. A1&2). The indentation force response is recorded using a universal material tester (Instron Inc. Microtester 5948, Norwood, MA). An optimized inverse finite element analysis (IFEA) is performed using Matlab and FEBio (https://febio.org/) to fit the material mode to the strain and force experimental data (Fig. B1, B2, C&D), and material parameters are compared between anatomical locations and specimens from patients with different obstetric histories. To validate this model, predictions are made for the uni-axial tensile response parallel and perpendicular to the direction of the fiber using the optimized material properties from the indentation IFEA. The predicted tensile response is compared to the experimental strain and stress response of the tension test. Results of these mechanical tests and material model validation will be presented.

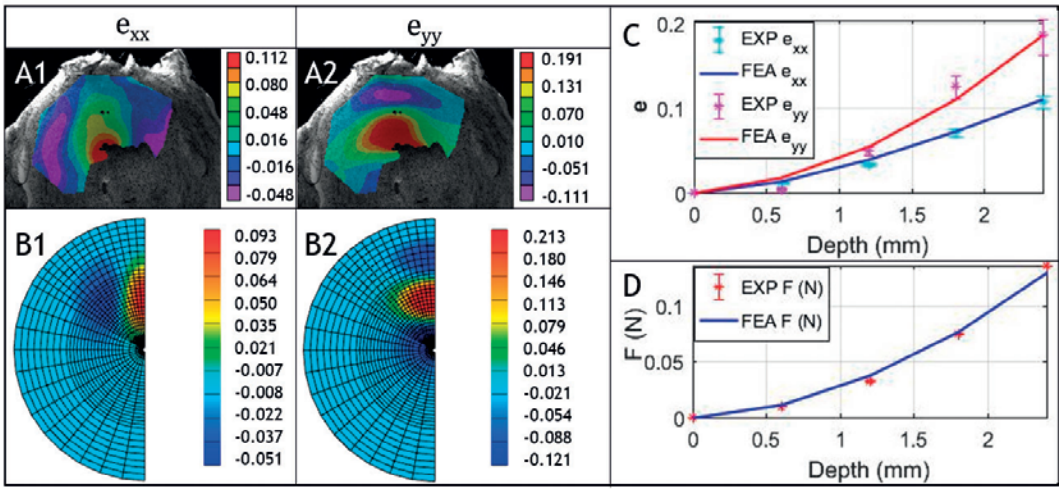

Figure Caption: A1 and A2 are experimental Lagrangian strains e_{xx} and e_{yy} of of the indentation test, respectively. B1 and B2 are the corresponding e_{xx} and e_{yy} of the FEA simulation. C and D are the fitting results of the equilibrium e_{xx}, e_{yy} and force response.

Acknowledgments: Research reported in this publication was supported by the NIH R01HD091153 to KM. The content is solely the responsibility of the authors and does not necessarily represent the official views of the NIH.

References:

[1] *Vink, J et al., 2016, Semin Fetal Neo. Med., 106-112.*
[2] *Yao, W et al., 2014, J. Mech. B. Biom. Mat., 18-26.*

[D-09.6]

MECHANOBIOLOGY CONTROLLED BY DISSIPATION IN HYDROGEL

Dominique Pioletti[1]

1 *Laboratory of Biomechanical Orthopedics - Epfl; Lbo, Ecole Polytechnique Federale de Lausanne (Epfl), Lausanne, Switzerland*

Dissipation plays an essential role in the mechanical behavior of materials under cyclic loading. In particular for soft materials, an insufficient dissipative capacity is known as the main reason for the low toughness and inability to resist defect growth in hydrogels. In parallel, a new paradigm on the role of dissipative phenomena in soft tissues and biomaterials recently emerged with experimental observations correlating dissipation and mechanobiology. Dissipation may therefore be related to two different but complementary objectives in the development of hydrogels: increase their fatigue resistant properties and induce new mechanobiological features. As example for the development of an hydrogel, we will focus on the clinical situation related to a focal defect in cartilage. In that situation, a fairly stiff and tough hydrogel is required to sustain the particular mechanical behavior of this tissue. As a supplemental constraint, adhesion of the hydrogel to the cartilage is key to avoid its premature delamination. Dissipation also plays a central role for adhesion related process. In this talk, it will be presente how by carefully controlling the sources of dissipation, hydrogels with enhanced mechanical and mechanobiological properties can be obtained and can be proposed for functional tissue engineering.

[D-10.1]

REGULATION OF NUCLEAR ARCHITECTURE, MECHANICS AND NUCLEO-CYTOPLASMIC SHUTTLING OF EPIGENETIC FACTORS BY CELL GEOMETRIC CONSTRAINTS

Farid Alisafaei[1], *Doorgesh Sharma Jokhun*[2], *Shivashankar*[2], ***Vivek Shenoy***[1]

1 *University of Pennsylvania, Philadelphia, USA*
2 *National University of Singapore, Singapore*

Cells sense mechanical signals from their microenvironment and transduce them to the nucleus to regulate gene expression programs. To elucidate the physical mechanisms involved in this regulation, we developed an active three-dimensional chemo-mechanical model to describe the three-way feedback between the adhesions, the cytoskeleton, and the nucleus. The model shows local tensile stresses generated at the interface of the cell and the extracellular matrix (ECM) regulate the properties of the nucleus, including nuclear morphology, levels of lamin A,C and histone deacetylation, as these tensile stresses (i) are transmitted to the nucleus through cytoskeletal physical links, and (ii) trigger an actomyosin-dependent shuttling of epigenetic factors. We then show how cell geometric constraints affect the local tensile stresses and subsequently the three-way feedback and induce cytoskeleton-mediated alterations in the properties of the nucleus such as nuclear lamina softening, chromatin stiffening, nuclear lamina invaginations, increase in nuclear height and shrinkage of nuclear volume. We predict a phase diagram that describes how the disruption of cytoskeletal components impacts the feedback and subsequently induce contractility-dependent alterations in the properties of the nucleus. Our simulations show that these changes in contractility levels can be also used as predictors of nucleo-cytoplasmic shuttling of transcription factors and the level of chromatin condensation. The predictions are experimentally validated by studying the properties of nuclei of fibroblasts on micropatterned substrates with different shapes and areas.

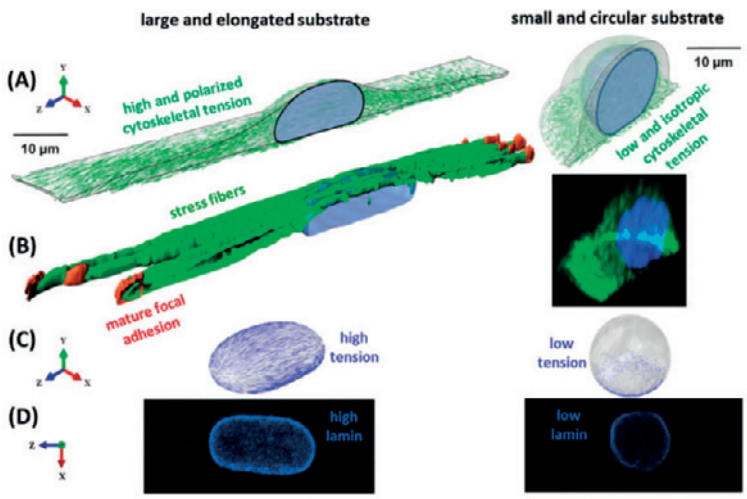

Figure 1: Cell geometric constraints regulate cell contractility, actin organization, and nuclear envelope lamina stiffness.

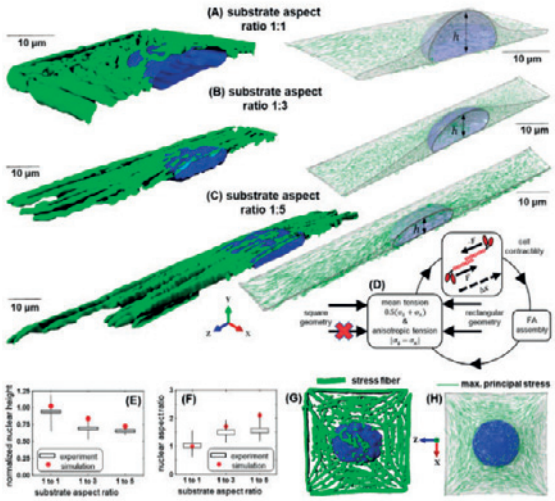

Figure 2: Substrate aspect ratio induces alterations in prenuclear actin organizations and nuclear morphology.

Acknowledgments: This work is supported by the National Cancer Institute awards U01CA202177 and U54CA193417 (to V.B.S.), National Institute of Biomedical Imaging and Bioengineering award R01EB017753 (to V.B.S.), and the NSF Center for Engineering Mechanobiology (CMMI-154857).

References:

[1] *Damodaran, K et al., MBoC, 29:3039-3051, 2018.*
[2] *Li, Q et al., Biomaterials, 35:961-969, 2014.*
[3] *Jain, N et al., PNAS, 110:11349-11354, 2013.*

[D-10.2]

MATHEMATICAL MODEL OF OSTEOBLAST GROWTH KINETICS IN A MICROCARRIER CULTURE

Iva Burova[1], *Ivan B Wall*[2], *Rebecca J Shipley*[1]

1 *Department of Mechanical Engineering, University College London, London, UK*
2 *Aston Medical Research Institute and School of Life and Health Sciences, Aston University, Birmingham, UK; Institute of Tissue Regeneration Engineering (Itren), Dankook University, Gyeonggi-do, South Korea*

Bone tissue engineering is a promising treatment for bone injury when self-regeneration is impaired due to extensive trauma or compromised by diabetes or osteoporosis1, increasingly prevalent in an aging population. Regenerative bone cell therapies have the potential to deliver clinically-relevant cell numbers without the drawbacks of current treatments (allo or auto-grafting), such as fracture at the donor site, chronic pain, or revision surgery. Translation of engineered bone tissues to the clinic requires protocols capable of producing functional grafts with uniformly-spread, clinically-relevant cell numbers. Using microcarriers to seed osteoprogenitors in a bioreactor is a promising bottom-up tissue engineering technique which preserves cell phenotype by providing 3D cell-to-cell interaction and supplies sufficient nutrients and mechanical stimulation.

Characterising and controlling the multiple factors in these cultures (fluid flow, shear force and nutrient concentration) can be aided by mathematical modelling. A highly time and cost-effective tool to simulate outcomes of different operating conditions, it can improve experimental trial-and-error by selecting operating settings which promote the functionality of engineered tissues and inform culture scale-up. Building on our previous mathematical model of a microcarrier culture in static conditions2, here we present a CFD model capturing the flow induced by an orbital shaker. The aim is to parameterise the simulations to experimental data on cell number at different rotation speeds3 to obtain a cell growth function dependent on shear stress.

A centrifugal volume force is applied to the culture domain to represent the movement of the shaker platform. The Navier-Stokes equations for incompressible laminar flow alongside the level set two-phase flow method are adopted to track the free surface developed due to the shaking. Advection-reaction-diffusion equations model mass transport of oxygen, glucose and lactate in the system. A modified logistic growth law models cell number as a function of local oxygen concentration and shear force. The model is solved using finite-element methods in COMSOL Multiphysics.

The CFD model is first validated against PIV experiments published in literature4 (Fig.1A&B), showing a good agreement for the free surface position at all points during the orbital period. The same method is then applied to the culture set-up under investigation. This is used to evaluate mass transport of the nutrients and the wall shear stress (Fig.1C) exerted at the bottom of the well (acting on the microcarrier-seeded cells). This model can then be parameterised to the experimental data to obtain a cell-specific shear stress-dependent growth function, enabling us to predict flow settings which maximise cell yield by improving nutrient availability at non-damaging stress levels.

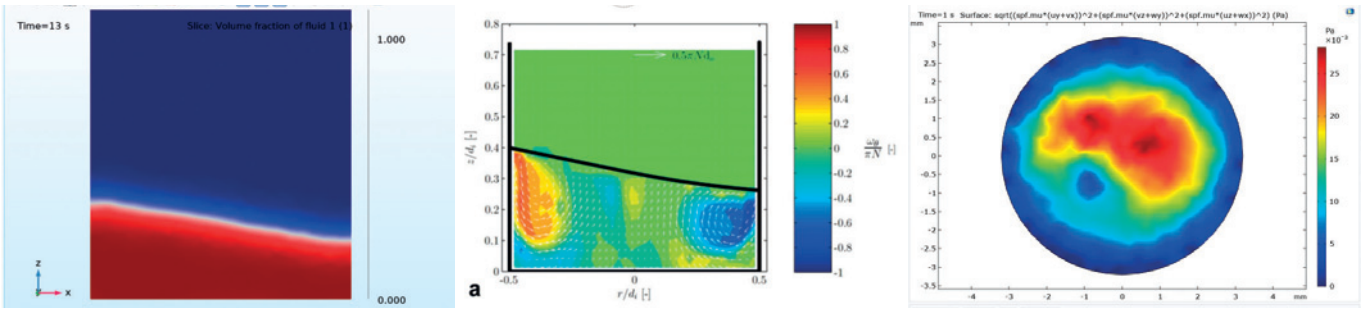

Fig.1: A) Simulation results of free surface position in a position equivalent to that used in B. B) PIV experimental results4. C) Wall shear stress (mPa) exerted at the bottom of the culture well as found for the investigated culture at 150 rpm orbiting frequency.

Acknowledgments: IDB thanks the Rosetrees Trust for kindly funding this work.

References:

1. *Burova, I., et al., 2019. Mathematical and computational models for bone tissue engineering in bioreactor systems. J. TissueEng., 10, p.2041731419827922.*
2. *Burova, I., et al., 2019. A parameterised mathematical model to elucidate osteoblast cell growth in a phosphate-glass microcarrier culture. J. TissueEng, accepted.*
3. *De Silva Thompson, D., et al., 2019. Assessing behaviour of osteoblastic cells in dynamic culture conditions using titanium-doped phosphate glass microcarriers. J. TissueEng, 10, p.2041731419825772. 4. Weheliye, W., et al., 2013. On the fluid dynamics of shaken bioreactors—flow characterization and transition. AIChE Journal, 59(1), pp.334-344.*

[D-10.3]

MICROSTRUCTURAL HETEROGENEITY INFLUENCES ON THE FLEXURAL RIGIDITY OF THE AXON.

Lucy Wang[1], *Rijk de Rooij*[1], *Ellen Kuhl*[1]

1 *Stanford University, Stanford, USA*

The cytoskeleton of the axon has a unique structure in which microtubules are arranged in parallel bundles and crosslinked by microtubule-associated proteins such as tau. Rather than continuously spanning the entire length of the axon, these microtubules are broken up into shorter segments [1]. This results in the presence of discontinuities along the bundle. In the axon, the microtubule bundle is thought to bear compressive loads [2]. Therefore, the bundle's resistance to bending and buckling is important for maintaining the structural integrity of the axon. Using a finite element model [3], we studied the impact of discontinuities on the mechanical behavior of the microtubule bundle. In bending, we found that the flexural rigidity of the microtubule bundle decreases with increasing number of discontinuities. As the number of discontinuities is increased, the bundle transitions between two behavioral regimes. At low numbers of discontinuities, strain energy is stored in both the microtubules and crosslinks. Deformation in the bundle is split between bending of microtubules and stretching of crosslinks. At high numbers of discontinuities, most of the strain energy is stored in the crosslinks. In this regime, deformation in the bundle is dominated by stretching of the crosslinks, while the microtubules remain relatively rigid. In buckling, we found that increasing discontinuities resulted in decreasing critical buckling load in accordance with the decrease in flexural rigidity. These results show that having continuous microtubule filaments would provide the greatest resistance to bending and buckling. However, bending in such a structure would result in high stresses within the microtubules, possibly leading to fracture. For an axon that undergoes bending during normal physiological function, it may then be beneficial to have discontinuities to decrease the stress in the microtubules.

Figure Caption: (left) A major component of the axonal cytoskeleton is a bundle of microtubules (green and blue) linked together by tau proteins (red) [4]. (right) For a given axon length and crosslink density, the flexural rigidity of the axon decreased with increasing number of discontinuities.

Acknowledgments: This work was supported by the NSF CMMI-1727268 grant.

References:

[1] Coles CH, Bradke F. Coordinating neuronal actin-microtubule dynamics. Curr Biol. 2015; 25:R677-R691.
[2] Dennerll TJ, Joshi HC, Steel VL, Buxbaum RE, Heidemann SR. Tension and compression in the cytoskeleton of PC-12 neurites. II: Quantitative measurements. J Cell Biol. 1988; 107:665-674.
[3] de Rooij R, Kuhl E. Microtubule polymerization and cross-link dynamics explain axonal stiffness and damage. Biophys J. 2018; 114:201-212.
[4] de Rooij R, Kuhl E. Physical biology of axonal damage. Front Cell Neurosci. 2018; 12:144.

[D-10.4]

THE IMPORTANCE OF MESH AND ANALYSIS TYPE IN CELLULAR MODELLING

Evangelos Karatsis[1], *Vasilis Mazis*[2], *Lambros Papadakis*[3], *Konstantinos Michalakis*[4], *Alexander Tsouknidas*[3]

1 *Beta Cae Systems Sa*
2 *Beta Cae Systems International AG*
3 *Department of Mechnical Engineering; Faculty of Engineering; University of Western Macedonia, Parko Agiou Dimitriou, Greece*
4 *Division of Postgraduate Prosthodontics; School of Dental Medicine; Tufts University, Medford, USA*

The notion of interplay between physical forces and cell function, was devised in 1926 [1]. Since then, it has become clear that nearly every biological process, is modulated by how these forces are decoded intracellularly. Several cellular components have been suggested as mechanosensing molecules, translating these mechanical cues into biochemical ones [2]. The nucleus has recently dominated the interest of researchers [3], as it has been argued to offer a more direct and rapid pathway to cellular events [4]. Encouraged in part by this and the abundance of modelling techniques, we try to determine which one is preferable in drawing an analog between force and sensory mechanisms that could activate the nucleus.

A 3D osteoblast was reverse-engineered, with the nucleus covering about 25% of the cell's volume. The nucleus, cytoplasm and cellular membrane were considered as non-linear materials, whereas actin network (resembling a 2,5μm thick filamentous layer), cytoskeleton (consisting of 300 polymerized microtubules) and all 26 mitochondria modelled as linear elastic ones.

The model's mesh grid was verified as to its conceptual soundness through convergence studies and validated against AFM experiments. The model was then subjected to three types of analyses (FE modelling, Fluid–Structure Interaction and Smoothed-Particle Hydrodynamics) and the results compared as to their capacity to transduce external loads (compression and shear) into the nucleus.

The application of mechanical loads on the cell membrane, resulted in all cases in their non-linear transduction to the cell's inner structures (see Figure 1). This was less pronounced in the FE analysis, showing a reduced capacity of the method to simulate the cell's domain exhibiting fluid-like properties.

Regardless of the applied methodology, the results presented, were consistent with recent observations, that forces of 5pN are sufficient to decondense single chromatin fibers [5]. However, the extent to which mechanical loads can elicit conformational changes at cell entities, distant to their point of application, varied significantly among both, the computational approach and across the force magnitude. In conclusion, Fluid–Structure Interaction showed the most promising potential in applications involving cellular mechanobiology.

Figure Caption: Characteristic stress filed transduced into the nucleus.

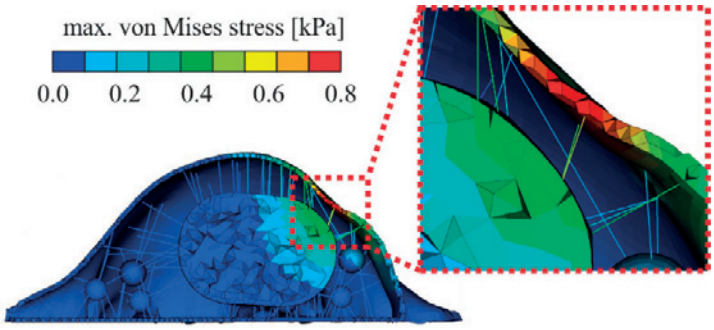

References:

[1] *Murray CD (1926). Proc. Natl Acad. Sci., 12: 299–304.*
[2] *Muehlich S et al. (2016). Nucleus, 7: 121–125.*
[3] *Kirby TJ & Lammerding J (2018). Nat Cell Biol 20(4): 373-381.*
[4] *Chambliss AB et al. (2013). Sci. Rep. 3: 1087.*
[5] *Cui Y & Bustamante C (2000). Natl Acad. Sci. 97: 127–32.*

[D-11.1]

EFFECT OF SKIN MODEL AND MATERIAL PARAMETERS IN FINITE ELEMENT MODELLING INDENTATION

Hayley Wyatt[1], *Miffy Arnold*[1], *Rhys Pullin*[1], *Sam Evans*[1]

1 *School of Engineering, Cardiff University, Cardiff, UK*

Skin is a complex structure comprised of three distinct layers, each with their own unique mechanical properties. The mechanical properties are typical of many other soft tissues in that they exhibit a non-linear stress strain relationship, are anisotropic and hyperelastic. In addition, the properties of skin are highly variable and can depend on testing methods and conditions as well as the natural variation that occurs. As such there are a wide variety of material parameters, models, and general approaches used when modelling skin.

A review of literature was conducted to investigate a range of modelling approaches, including modelling the skin as a single layer structure, as a three layer structure, with isotropic and anisotropic material properties, and varying the thickness of the hypodermis layer. As such a three layer model, including the epidermis, the dermis and the hypodermis, for simulating indentation tests, was developed in the FEBio software suite. The study aimed to investigate and compare a number of different modelling approaches and understand the significance of modelling parameters on the behaviour of the skin and also in the reaction force of the indenter.

Results from the study found that varying the thickness of the hypodermis layer had a significant effect on the reaction force through the indenter, with the force decreasing as the thickness of the layer increased. Additionally, when comparing a single layer skin structure, the stress was significantly higher in the skin, when compared to a three layer skin structure. This led to an increase in the indenter reaction force for the three layer structure. Furthermore the strain distribution clearly varied between the three distinct layers highlighting the importance of modelling the individual layers of the skin.

Additionally, seven models were created based on the data of Groves et al 2012, where a total of seven patients skin properties were tested using the same methods. Using this data it was possible to gain a small insight into the natural variation of skin properties to understand how this varies the stress and strain distributions through the different layers of skin and also the indenter reaction forces.

These results highlight the limitations of finite element modelling as a tool for evaluating medical device design. For example, if these results were used to help optimise the design of microneedles, the modelling approach selected for the skin could significantly alter needle reaction forces and influence the optimal design. Researchers modelling skin need to be aware of this variation caused by the modelling approach.

References:

Groves et al, (2012) Quantifying the mechanical properties of human skin to optimise future microneedle device design, Computer Methods in Biomechanics and Biomedical Engineering, 15:1, 73-82

[D-11.2]

FROM DEEP LEARNING TOWARDS FINDING SKIN LESION BIOMARKERS

Xiaoxiao Li[1], ***Junyan Wu***[2]

1 *Yale University, New Haven, USA*
2 *Cleerly Inc, Colorado Springs, USA*

Melanoma is a type of skin cancer with the most rapidly increasing incidence. Early detection of melanoma using dermoscopy images significantly increases patients' survival rate. However, accurately classifying skin lesions by eye, especially in the early stage of melanoma, is extremely challenging for the dermatologists. Hence, the discovery of reliable biomarkers will be meaningful for melanoma diagnosis. In recent years, the value of deep learning empowered computer-assisted diagnose has been shown in biomedical imaging-based decision making. However, much deep learning research focuses on improving disease detection accuracy but not understanding the features deep learning use to determine the evidence of pathology. We aim to make sure the features used by deep learning methods are the reasonable clinical features for skin lesions diagnosis, rather than artifacts. Further, we aim to discover new biomarkers, which may not have been included in clinical criteria but do make sense to the dermatologists. In this study, we propose a method to interpret the deep learning classification findings. Firstly, we propose an ResNet [1] and VGG [2] based ensemble neural network architecture to classify 7 kinds of skin lesions. The dataset was extracted from the open challenge dataset of Skin Lesion Analysis Towards Melanoma Detection (ISIC2018) [3]. The deep learning model achieved high accuracy (0.85), precision (0.84) and sensitivity (0.85). Secondly, we utilize a prediction difference analysis method that examines how much each patch on the image contributes to the classifier. Specifically, we applied patch-wised corrupting and compare the classifier probability output between original and corrupted images. We investigated the suitable window size for interpretation and presented the biomarkers heightened by the deep-learning classifier in each class. Lastly, we validate that our biomarker findings are corresponding to the patterns in the literature and double confirmed the biomarkers with dermatologists. Our proposed pipeline can find biomarkers for identifying melanoma, nevus, basal cell carcinoma, actinic keratosis, pigmented benign keratosis, dermatofibroma and vascular lesions. The patterns are agreed with dermatologists. Surprisingly, we find surround skins also can be used as evidence for skin lesion diagnosis, which has not been included in traditional diagnosis rules, such as ABCD rules and 7-points checklist. The biomarkers discovered from deep learning classifier can be significant and useful to guide clinical diagnosis.

References:

[1] Kaiming He and et al., "Deep residual learning for image recognition," in Proceedings of the IEEE conference on computer vision and pattern recognition, 2016.
[2] Karen Simonyan and Andrew Zisserman, "Very deep convolutional networks for large-scale image recognition," arXiv:1409.1556, 2014.
[3] Rosendahl C and et al., "The ham10000 dataset: A large collection of multi-source dermatoscopic images of common pigmented skin lesions," Sci. Data 5, doi.10.1038/sdata.2018.161, 2018.

**The authors contributed equally*

[D-11.3]

MULTISCALE AND MULTIPHYSICS MODELING OF PRESSURE ULCERS AND WOUND HEALING IN THE SKIN

Adrian Tepole[1], *Vivek Sree*[1], *Manuel Rausch*[2]

1 *Purdue University, West Lafayette, USA, West Lafayette, USA*
2 *University of Texas at Austin, Austin, USA*

Pressure ulcers are devastating injuries that disproportionately impact older adults. These injuries form when compressive loads at the skin surface cause occlusion of blood vessels and lack of blood supply or ischemia. Then, as oxygen concentration reduces, native skin cells react to this hypoxic condition by initiating a self-sustained inflammatory cascade which culminates in ulceration [1]. However, even though we understand the general mechanisms of pressure ulcer formation, several gaps remain: i) the mechanics of pressure-driven ischemia at the microscale are not well understood, ii) the interaction of the cell regulatory network dynamics with the tissue mechanics in realistic spatial domains remains understudied. Crucially, skin anatomy, mechanical properties, microvascular anatomy, and inflammation signaling, all change with aging. Therefore, predictive models of this complex system could hold the key to better understand the increased susceptibility of ulcers in the older population. Here we build a multiscale and multiphysics model of pressure ulcer that combines a cell signaling network, tissue scale mechanics, oxygen transport, and microvascular collapse.

First, based on microvascular anatomy from the literature we implemented a fractal generation code that creates vascular trees with the same statistics as the dermal microvasculature [2]. We generate several solid 1x1mm3 RVEs with a microvascular inclusion based on the fractals. We apply compression or shear to the RVE and impose periodic boundary conditions on the lateral surfaces. The vessels undergo non-affine changes. The homogenized variable of interest is the change in volume fraction of the blood vessel inclusion. We find that a compressive stretch of 0.8 leads to more than 40% reduction in blood volume fraction. We use this variable in a tissue scale axisymmetric finite element model of skin mechanics and oxygen transport. We couple the source term of the oxygen transport model to the volume fraction of blood vessels. Compressing skin in the tissue scale model leads locally to a reduction in vessel volume based on the RVE model, which reduces the oxygen source. In this manner we predict partial oxygen pressures indicative of hypoxia when a 50kPa load is applied to the skin, which is not an uncommon value.

We further incorporate the knowledge of a regulatory network implicated in pressure ulcers. The different elements of the system are modeled with logistic growth functions connected via Hill functions for the interactions, common in systems biology models of inflammation [3]. The coupled model allows us to predict ulcer pattern formation in response to applied loads to the skin.

In conclusion, we present a multiscale multiphysics model of pressure ulcer formation. Further work on model calibration will likely enable a better understanding of pressure ulcer dynamics and will hopefully enable the next generation of diagnostic and treatment technologies.

References:

[1] Coleman et al. J Adv Nurs, 2014, 70:2222-34.
[2] Cevc and Vierl. J Control Release, 2007, 118:18-26.
[3] Vodovotz et al, PLoS Comput Biol, 4:e1000014.

[D-11.4]

APPLICATION OF DIGITAL VOLUME CORRELATION TO THE IN-VIVO DEFORMATION OF THE SUB-DERMAL TISSUES IN THE HUMAN BUTTOCK

Stefano Zappala[1], *Bethany Keenan*[2], *Sam Evans*[3], *Rami Al-Dirini*[4]

1 *Cardiff University School of Computer Science and Informatics, Cardiff, UK*
2 *Cardiff School of Engineering, Soft Tissue Mechanics, Cardiff University, Cardiff, UK*
3 *School of Engineering, Cardiff University*
4 *College of Science and Engineering, Flinders University, Bedford Park, USA*

High pressure states due to prolonged seating can cause discomfort, soreness, and ultimately pressure ulcers. Finite element (FE) models predicting soft tissue deformation and strains are an invaluable tool for the design of seating systems aimed at reducing the consequent pressure state. To the authors' best knowledge, there are no in-vivo rich volumetric datasets representing such deformation to validate these models against.

Digital volume correlation was applied to an existing dataset of magnetic resonance (MR) images for ten subjects, whereby each subject was scanned in three conditions (full, partial and non-weight-bearing conditions) while in a semi-recumbent posture1. The following regions of interest were manually segmented: the greater trochanter and the ischial tuberosity bones as well as the gluteus maximum muscle and the fat and skin layers beneath it. Global affine registration allowed to firstly align the scans at the level of the segmented bones, so that the only difference left between the scans was the deformation of the soft tissues. The volumetric displacement field was evaluated through elastic registration of the previously aligned scans. Volumetric strain maps were extracted to better correlate the deformation with the mechanical properties of the muscle and the fat layers beneath it.

The analysis successfully captured the deformation, and results were in line with previous 2D analysis on the same dataset1. Results show a general compression of the buttock area along the direction perpendicular to the seat surface (anterior-poserior) of around 14±30%, as shown in Figure 1 below. Along this direction, higher deformation (strain values of 40%) was located closer to the contact area, affecting mainly the fat layer. Moving to the partially deformed conditions, the tissues beneath the greater trochanter extended, whereas the ones beneath the ischial tuberosity extended back to the undeformed state only in the non-weight-bearing condition. This is in accordance with the hypothesis under which most of the load is borne by the ischial tuberosity.

The method developed resulted capable of capturing the complexity of the phenomenon in-vivo and on a volumetric scale, thanks to the analysis of MR images. Such rich dataset is an invaluable workbench for the validation of FE models designed to replicate such complex scenario.

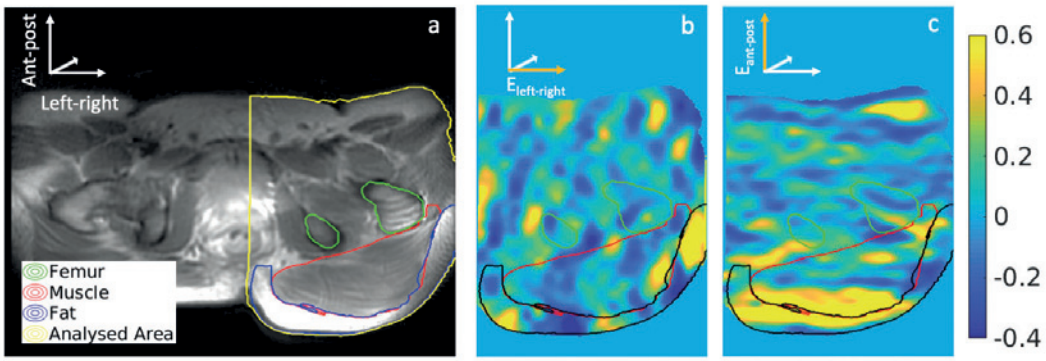

Figure 1: (a) Axial slice showing the investigated area, in particular the right buttock (enlightened in yellow), where the bone, muscle and fat regions are drawn. (b) Map of the left to right component of the strain tensor over the right buttock. (c) As before, but for the anterior to posterior component.

References:

1. *Al-Dirini, R. M. A. et al. (2017). Quantifying the in vivo quasi-static response to loading of sub-dermal tissues in the human buttock using magnetic resonance imaging. Clinical Biomechanics, 50(September), 70–77.*

[D-11.5]

MRI BASED 3D FINITE ELEMENT MODELLING TO INVESTIGATE HEEL PRESSURE ULCERS - IS HAGLUND'S A RISK FACTOR?

Bethany Keenan[1], *Peter Hobden*[2], *Stefano Zappala*[3], *Sam Evans*[4]

1 *Cardiff School of Engineering, Soft Tissue Mechanics, Cardiff University, Cardiff, UK*
2 *Cardiff University Brain Research Imaging Centre (Cubric); Cardiff University, Cardiff, UK*
3 *School of Computer Science and Informatics, Cardiff University, Cardiff, UK*
4 *School of Engineering, Cardiff University, Cardiff, UK*

Pressure ulcers are localised areas of injury to the skin or underlying tissue; caused by external forces such as pressure and/or shear. Ulcers often occur at the skin covering bony prominences, but are most common on the back of the heel. Large deformations (strains >50%) lead to soft tissue injury within minutes [1]. In the UK alone, pressure ulcers are estimated to cost the NHS more than £1.4 million every day [2]. Research on pressure ulcers is complex and requires a good understanding from both an engineering and clinical perspective.

There are numerous medical devices available, but it is not clear which is the most effective for preventing the formation of pressure ulcers. With a better understanding of the mechanics of soft tissue damage many of these problems could be avoided through better treatment and medical devices or mattresses. There is therefore a need for accurate and realistic models that can predict these processes to enable the development of effective treatments (or prevention) and guide critical clinical decisions.

Novel MRI techniques were developed to clearly identify the anatomical geometry in the foot in an unloaded and loaded state. Healthy volunteers were recruited with and without Haglund's deformity (an enlargement of the posterosuperior part of the calcaneus). Image-processing software was used to create 3D subject-specific finite element (FE) models to investigate the internal strains in the soft tissue surrounding the heel when in contact with a support surface (Figure 1). Digital volume correlation was applied to quantify the soft tissue deformation and strain map from the MRI data. The FE model was then validated against the measured data.

High internal strains are observed in the soft tissues of the Haglund's foot compared to the healthy foot. A 3D foot FE model is a valuable tool in predicting the sites of excessive internal strains on the heel when in contact with a support surface. The different FE models allow for the simulation of the foot with a realistic behaviour (in terms of surface and internal pressures).

This study is part of an ongoing project that will lead to guidelines or a test method that can determine which products are effective in preventing ulcers. This will potentially aid clinicians and carers to ensure that patients receive the best possible care.

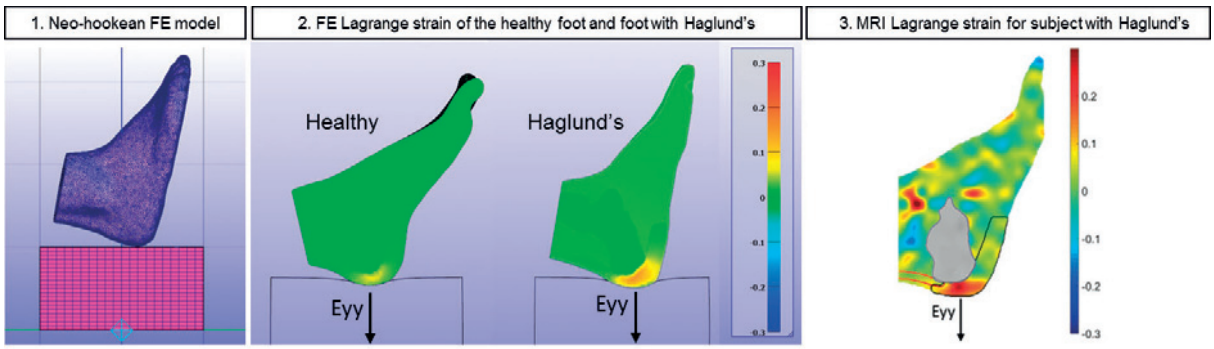

Figure 1: MRI-based FE model with Lagrange strain (anterior-posterior) and corresponding Lagrange strain from the MRI measured data, for subject with Haglund's deformity.

References:

[1] *Loerakker, S. et al. (2011). Journal of Applied Physiology, Vol. 111(4), pp.1168-1177*
[2] *Guest JF, Fuller GW, Vowden P, et al (2018) Cohort study evaluating pressure ulcer management in clinical practice in the UK following initial presentation in the community: costs and outcomes BMJ Open 2018;8:e021769.*

[E-01.1]

SYSTEMATIC ANALYSIS OF THE INFLUENCE OF THE FRAMEWORK MATERIAL CHOICE ON THE BIOMECHANICAL BEHAVIOR OF A DENTAL BRIDGE ON FOUR IMPLANTS

Ludger Keilig[1], *Arozo Ahmadi*[2], *Istabrak Hasan*[3], *Helmut Stark*[3], *Christoph Bourauel*[4]

1 *Oral Technology and Department of Prosthetic Dentistry, Preclinical Education and Materials Science; Dental School; University of Bonn, Germany*
2 *Oral Technology; Dental School; University of Bonn, Germany*
3 *Department of Prosthetic Dentistry, Preclinical Education and Materials Science; Dental School; University of Bonn, Germany*
4 *Endowed Chair of Oral Technology; Dental School; Rheinische Friedrich-Wilhelms University Bonn, Germany*

The "All-on-four" protocol offers implant-supported restorations for the edentulous mandible, and similar procedures are currently transferred to the maxilla. Aim of this study was to investigate the biomechanical behavior of such a maxillary bridge depending on the choice of its framework material.

Based on the CT data of an edentulous patient a finite element model of the maxilla was created, and four implants with customized abutments were inserted in the model using CAD data. A full anatomical bridge (framework and veneering) was constructed on the implants and integrated in the FE model. In a last step, separate, regularly shaped thrust dies were modeled above of each unit (tooth) of the bridge. Two different situations were considered, early loading of the implants (sliding contact between implants and bone) and late loading (direct connection between implants and bone). A vertical force of 500 N was applied separately to each unit, either directly to some nodes on the upper side of the units or by using the modeled thrust dies (200 GPa). Material parameters for the framework were varied between 4.5 GPa (high performance polymer, HPP), 110 GPa (Ti alloy), and 200 GPa (CoCr alloy). Resulting stresses and strains within the framework and the veneering as well as in the bone were registered and compared depending on the point of load application, loading mode, implant status and framework material.

Differences between direct and indirect loading were mainly visible in the veneering. For indirect loading, the number of contact points changed with the (allowed) transversal movement of the thrust dies when they moved to fit the morphology of the occlusal surface. With indirect loading, stresses in framework and bone decreased slightly by approximately 10 %. Displacement varied depending on the loading location, especially when the loading location was not directly supported by an implant. They increased more than twofold for the incisors where the point of force application was located on the labial side of the framework compared to the molars where it was located directly above the framework (e.g. 117 (261) µm, 38 (142) µm and 48 (171) µm for the second incisor, first premolar and first molar, all with CoCr (HPP) framework and indirect, late loading). Decreasing the material stiffness of the framework increased the deflection of the bridge. In all cases, the increased deformation in turn resulted in increased stresses within the framework as well. The determined material reactions increased in all components when assuming early compared to late loading situation.

The simulations showed that the choice of the framework material has a strong influence on the resulting loads in the restoration. Nonetheless the correct clinical conditions – implant/bone interface, loading method – need to be considered to get valid and realistic results.

[E-01.2]

IMAGE-BASED EXPERIMENTS AND MODELING OF IMMEDIATELY-LOADED DENTAL IMPLANTS

*Qiyuan Mao[1], Kangning Su[2], Yuxiao Zhou[2], Mehran Hossaini-Zadeh[3], Gregory Lewis[4], **Jing Du**[5]*

1 *Department of Mechanical Engineering; Changzhou Vocational Institute of Light Industry*
2 *Department of Mechanical Engineering; Penn State University, University Park, USA*
3 *Department of Oral Maxillofacial Pathology Medicine and Surgery; Temple University, USA*
4 *Department of Orthopaedics and Rehabilitation; College of Medicine and M.S. Hershey Medical Center; Penn State University, University Park, USA*
5 *Penn State University, University Park; Department of Mechanical Engineering, USA*

The success of dental implant treatment is related to the complex 3-dimensional (3D) biomechanics of the implant-bone interaction. In this work, the biomechanics of immediately-loaded dental implants are studied using their micro X-ray computed tomography (micro-CT) images. Dental implants are placed in cadaveric mandibles and loaded in an in situ mechanical tester coupled with micro-CT scanner. Micro-CT images are taken before and after forces are applied on the implants. The 3D full-field strain mapping in alveolar bone were obtained through digital volume correlation (DVC) of micro-CT images of no-load and loaded specimens. The experimental results reveal high strain concentration at bone-implant contact areas and, more importantly, in the buccal (lip-side) bone that is not making contact with the implant.

Voxel-based 3D micro-finite element models are also built based on the micro-CT images. The simulation results show that the computed strain values in bone are affected by the choice of trabecular tissue modulus. A bone-volume-fraction (BV/TV) based method is proposed to assign the tissue moduli of bone elements based on their BV/TV. The method can also increase the connectivity of the mesh as well as to improve the accuracy of the models. The computed strain concentration patterns are found to be in good agreement with the observations from the experiments. The buccal bone is thinner and less stiff than other areas of bone and is also the commonly observed area of bone resorption after dental implant treatment.

Acknowledgments: The project described was supported by the National Center for Advancing Translational Sciences, National Institutes of Health, through Grant UL1TR002014. The content is solely the responsibility of the authors and does not necessarily represent the official views of the NIH. The support was made available through Penn State Clinical and Translational Science Institute (CTSI). Mr Qiyuan Mao was supported by the Education Department of Jiangsu Province. The authors would also like to express gratitude to the Institute for CyberScience (ICS) at Penn State University, University Park, United States for providing software, computing cores and storage.

[E-01.3]

EFFECT OF CUTTING FLUTE ON DENTAL IMPLANT INSERTION PROCESS WITH THREE-DIMENSIONAL ELEMENT ANALYSIS

Baixuan Yang[1], *Kelly Vazquez*[2], *Ainara Irastorza Landa*[3], *Peter Heuberger*[3], *Heidi-Lynn Ploeg*[1]

1 *Mechanical and Material Engineering, Queen's University, Kingston, ON, CAN*
2 *Mechanical Engineering, University of Wisconsin, Madison, USA-Madison, Madison, WI, USA*
3 *Nobel Biocare Services AG, Balz-Zimmermann-Str. 7, 8302 Zürich, Switzerland*

Dental implants have made great progress over the last several decades.[1] The insertion process strongly affects and associates with secondary stability and success rates of dental implants. Finite element analysis (FEA) is a powerful tool to assess insertion process mechanics.[2] The objective of this study was to improve the understanding of dental implant insertion mechanics by conducting mechanical testing and FEA in parallel. Implants (with and without cutting flute, NobelActive NP 3.5 x 13 mm, Nobel Biocare AB, Göteborg, Sweden) were inserted into bone surrogate (20 PCF, Sawbones®) under controlled angular and axial displacement rates using a mechanical testing machine (TA Electroforce 3230-AT Series III, New Castle, DE). Axial force, torque and surface deformation of the bone surrogate (digital image correlation, DIC) were measured during experimental testing. Multiple implicit non-linear FEAs of the insertion process were conducted (Figure 1). FEA results were evaluated against DIC data and stress distributions at the bone-implant interface were compared between different implant designs. FEAs predicted higher strain values than those measured by DIC. For an implant without a cutting flute, von Mises stresses near the bone-implant interface were more uniformly distributed during the insertion and higher than those for an implant with a cutting flute (Figure 2). High-stress level at the bone-implant interface may be associated with bone damage and inferior clinical results.[3]

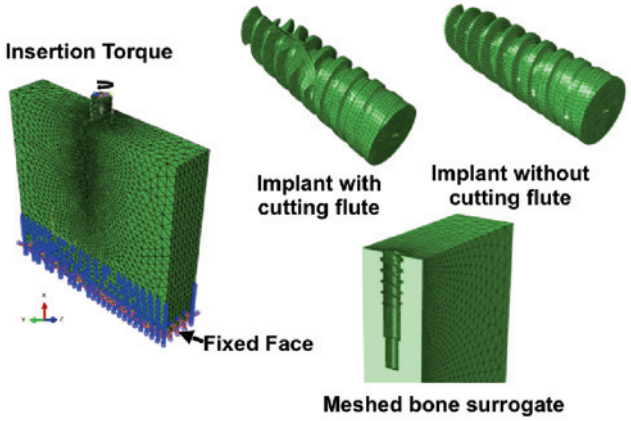

Figure 1.Finite element models, loading and boundary conditions

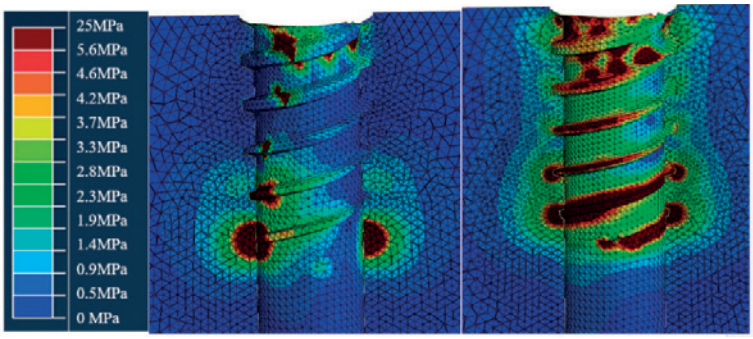

Figure 2. Contour plot of von Mises stress (MPa) with insertion depth of 7.2mm; left: implant with cutting flute, right: implant without cutting flute.

Acknowledgments: Prof. Corinne Henak provided me access to her laboratory's materials testing machine.

References:

American Academy of Implant Dentistry. "Dental Implants Facts and Figures." Dental Implants Facts and Figures - AAID: American Academy of Implant Dentistry. Accessed November 06, 2018. https://www.aaid.com/about/Press_Room/Dental_Implants_FAQ.html.
Rittel, D, and A Dorogoy. 2017. "Modelling Dental Implant Extraction by Pullout and Torque Procedures." Journal of the Mechanical Behavior of Biomedical Materials 71 (April): 416–27. https://doi.org/10.1016/j.jmbbm.2017.04.010.
Guazzi, Paolo, Tommaso Grandi, and Giovanni Grandi. "Implant site preparation using a single bur versus multiple drilling steps: 4-month post-loading results of a multicenter randomised controlled trial." Eur J Oral Implantol 8, no. 3 (2015): 283-290.

[E-01.4]

FATIGUE AND WEAR ANALYSIS FOR TEMPOROMANDIBULAR JOINT PROSTHESIS BY MEANS OF FINITE ELEMENTS METHOD

Edwin Rodriguez[1], *Angelica Ramirez-Martinez*[2]

1 *Universidad Central; Universidad Jorge Tadeo Lozano, Bogota, Colombia*
2 *Universidad Central; Universidad Central, Bogota, Colombia*

Temporomandibular joint (TMJ) prosthesis consists of two elements: one which is solidary with the temporal bone (fossa component) and the other which replace part of the jaw bone (condylar plate). Main problem on this joint replacement is mechanical fail of the mandibular plate| due the cyclic muscular [1] and the wear between the mandibular condyle and the temporal fossa [2], [3]. With the aim of supporting the virtual assessment of personalized prosthesis, this paper presents a finite element study of the fatigue and wear of the Temporomandibular Joint (TMJ) prosthesis, under the forces generated by the masticatory muscles during the clenching process. The 3D finite element model has three stages to solve the whole statement. The first one is a multistep static model that describes the response to the masticatory forces pattern including the sliding and bonded contact behavior between all the parts of the assembly. Materials used were Ultra High Molecular Weight Polyethylene (UHMWPE) for the fossa component, Titanium alloy (Ti6AlV4) for the condylar plate and temporal component and cortical bone for the mandible, all of them were considered as isotropic linear materials. The second stage has as input data the stresses calculated from the finite element analysis of the first model and evaluates the high-cycle, constant amplitude fatigue for each component of the TMJ prosthesis. Due to the mean stress calculated is not equal to zero in this analysis, the specific stress-life curves of the materials including the mean stress effects in the fatigue life were used. The third model was developed to evaluate the effect of wear phenomena on the components of the TMJ prosthesis, in this case the Archard linear wear model was used to calculate the lost volume during the contact interaction between the condylar plate and the fossa component. The tribological pair characteristics like wear rate were taken from experimental data available on literature. The velocity effect was simulated as an increased wear rate in a quasi-static model. The simulation showed the critical zone under fatigue considerations and provide an understanding of the remaining life of the components and makes possible to promote geometrical modifications that improve the durability of the TMJ prosthesis before its construction. The wear model gives the quantity of lost volume and a preliminary calculation of the affected surface that allows an evaluation of the durability of the fossa component"

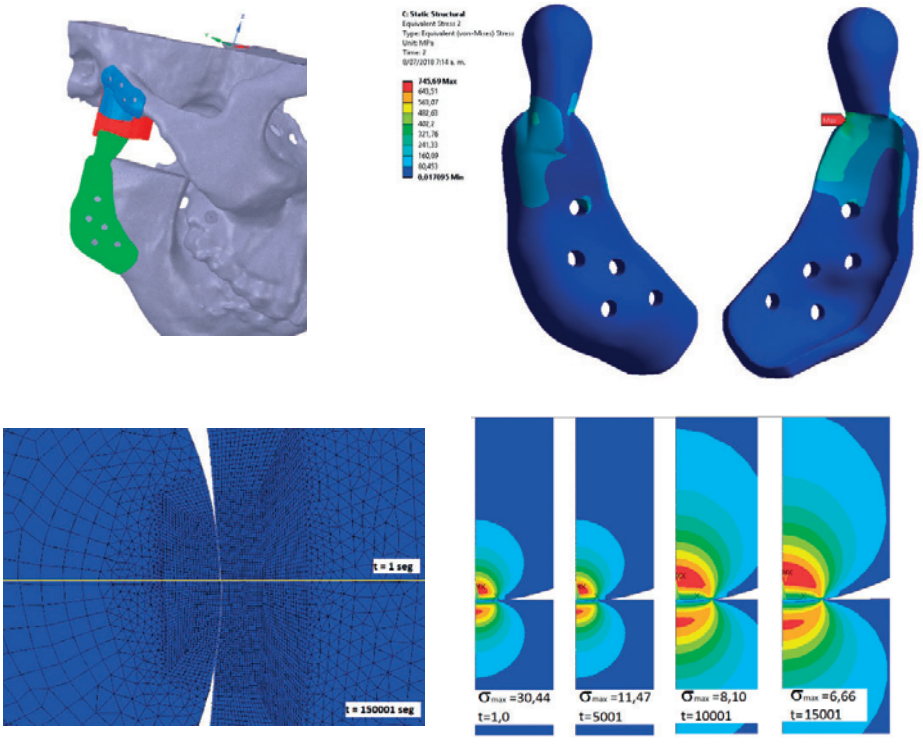

Figure Caption:" a) CAD Model of the TMJ prosthesis adapted to the skull. b). Results of the 3D fatigue analysis. d) and e) Wear analysis between the condylar plate and the fossa component.

References:

[1] Mercuri, L. G. The role of custom-made prosthesis for temporomandibular joint replacement. Revista Española de Cirugía Oral y Maxilofacial 35, 1 – 10 (2013).
[2] Van Loon, J.-P., Verkerke, G., De Vries, M. & De Bont, L. Design and wear testing of a temporomandibular joint prosthesis articulation. Journal of Dental Research. 79, 715–721 (2000).
[3] Wolford, L. M. Factors to consider in joint prosthesis systems. Proc (Bayl Univ Med Cent). 19, 232–238 (2006). "

[E-01.5]

NONINVASIVE MEASUREMENT OF TOOTH STABILITY AND PERIODONTAL LIGAMENT STIFFNESS

Lindsey Westover[1], *Gary Faulkner*[2], *William Hodgetts*[3], *Don Raboud*[4]

1 *University of Alberta; Department of Mechanical Engineering, Edmonton, Canada;*
2 *Glenrose Rehabilitation Hospital; University of Alberta, Edmonton, Canada*
3 *University of Alberta; Institute for Reconstructive Sciences in Medicine, Edmonton, Canada*
4 *University of Alberta, Edmonton, Canada*

Introduction: The periodontal ligament (PDL) is an important structure in tooth stability, connecting the tooth root to the surrounding bone. Changes in tooth stability or PDL stiffness can occur due to periodontal disease, orthodontic treatment, or trauma. The Advanced System for Implant Stability Testing (ASIST) is a noninvasive measurement system for estimating interface stability1. The application of the ASIST to natural teeth provides a method to noninvasively measure the PDL stiffness2-4.

Objectives: The objective of this study is to provide an overview of the ASIST application to natural teeth for evaluation of PDL stiffness. We present the method development and two clinical applications.

Methods: The ASIST is an experimental-numerical technique to estimate tooth stability (Fig. 1). A handpiece is used to impact the tooth and measure the acceleration response. Combined with this, an analytical model of the tooth and surrounding structure is developed using the theory of vibrations. The geometry and inertia properties are estimated and the PDL is modeled as a stiffness and damping distributed along the tooth root. The PDL stiffness is estimated by matching the model response to the experimental measurement. The ASIST was evaluated on two sets of patients undergoing orthodontic treatment. (1) n=12 patients were followed for one year during movement of maxillary canines into an extraction space and ASIST measurements were used to estimate changes in PDL stiffness during treatment. (2) n=5 patients underwent 5-7 weeks buccal root torque of all 4 first premolars to induce root resorption prior to extraction. ASIST measurements were taken before and after buccal root torque to investigate changes in stability associated with root resorption.

Results: The ASIST model provided an adequate representation of the physiological system with good agreement between the experimental measurements and the model response. The ASIST detected a decrease in PDL stiffness during extraction space closure with some recovery at the end of the study period. Both teeth in individual patients tended to follow the same pattern of stability changes throughout treatment. Secondly, the ASIST was able to detect a decrease in stability following buccal root torque of first premolars, which was meant to induce root resorption.

Conclusions: The ASIST is a promising technique of evaluation of PDL stiffness and tooth stability. The ASIST has been able to detect expected changes in PDL behavior in two clinical applications of orthodontic treatment. The ASIST has the potential to be a valuable tool for noninvasive assessment of the tooth root interface.

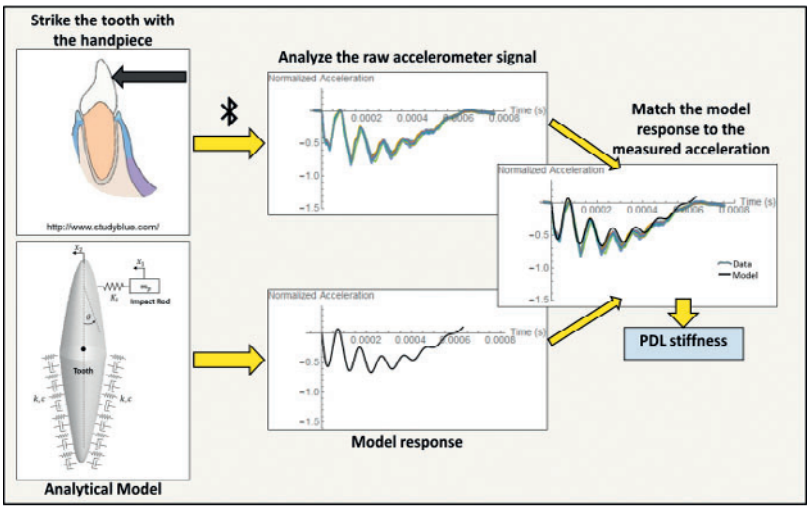

Figure Caption: Fig. 1. ASIST Overview

References:

1 *L. Westover et al. J. Biomech. 49:3651-9, 2016. 2 L. Westover et al. J. Biomech. 69:129-37, 2018. 3 L. Westover et al. Angle Orthod. doi 10.2319/031918-218.1. 4 L. Westover et al. AADR/CADR Annual Meeting Mar 21-24, 2018.*

[E-02.1]

SIMULATION AND VISUALIZATION OF LONG-TERM ORTHODONTIC TOOTH MOVEMENT USING THE FINITE ELEMENT METHOD

Noriaki Yoshida[1]

1 *Department of Orthodontics and Dentofacial Orthopedics Nagasaki University Graduate School of Biomedical Sciences, Nagasaki, Japan*

The prediction and planning of orthodontic tooth movement have largely depended on clinical experiences. If the long-term tooth movement can be accurately predicted, the treatment results will be greatly improved. Although many attempts have been made to simulate orthodontic tooth movement, most of finite element (FE) studies have been limited to simulation of initial tooth displacement. However, long-term tooth movement occurs after going through bone remodeling. It is therefore difficult to precisely predict overall tooth movement from the initial displacement. The purposes of the present study were to develop a method to simulate long-term orthodontic tooth movement using a bone remodeling algorithm based on the FE method and to determine the force system acting on each tooth.

A three-dimensional (3D) model of a maxillary dentition including teeth and the surrounding periodontal tissues was developed based on the images of micro-computed tomography. The PDL was modeled as a nonlinear (bilinear) isotropic material. To develop a more simplified model for reducing the analysis time, the tooth material was assumed to be a rigid body. The simulation of long-term tooth movement was accomplished on the assumption that bone remodeling correlates with the initial tooth displacement. As the first step, an orthodontic force is applied to the tooth model. Then the initial displacement is produced reflecting the deformed PDL. Displacements are constrained at the outer surface of the PDL on the assumption that the alveolar bone is assumed to be a rigid body. As the second step, each node forming the outer surface of the PDL is displaced so that the PDL is restored to its original configuration and thickness of 0.2 mm. That procedure is iterated to carry out long-term tooth movement.

An analysis of tooth movement during space closure was performed on the assumption that the case model was diagnosed as maxillary protrusion. The extraction space was completely closed after the bone remodeling steps were iterated. In case no power arm was used in combination with sliding mechanics, anterior and posterior teeth were remarkably tipped into the extraction site, and bowing occurred as an undesirable side effect. When a power arm length was increased, tipping tendency was decreased.

We developed a novel method that could simulate the long-term orthodontic tooth movement and accurately determine the force system in the course of time using FE method. Also, the tooth movement pattern was visualized.

[E-02.2]

ASSESSMENT OF ALVEOLAR BONE REMODELING AND RELAXATION PHENOMENA IN ORTHODONTIC EXTRUSION PROCEDURES

Grzegorz Milewski[1]

1 *Cracow University of Technology, Cracow, Poland*

Orthodontic extrusion is a method of choice in modern dentistry in teeth preparation for further prosthetic treatment. An application of an additional tensile force coming from a special elastic traction produces eruptive tooth movement in an occlusion plane. It stimulates periodontal ligament, surrounding bone tissues and finally leads to a bone remodeling of both alveolar process and bone area close to the root apex. The main advantage of the method is that it allows to maintain the own tooth root together with the periodontal ligament and adjacent bone tissue. Orthodontic extrusion enables avoiding tooth extraction as well as following bone resorption and dental arch disorders.

Elastomeric products, applied as elastic ligatures, despite their popularity and undoubted advantages, exhibit large load losses due to the relaxation phenomenon. This seems to be a dominant feature badly influencing the dentition corrections.

The aim of the paper was to estimate the extrusion force values, which result in a positive remodeling of the bone in the areas close to the alveolar process and tooth root apex. The local strain distribution changes were considered as the most important factor for stimulating an adaptive bone material response to the mechanical loadings. Numerical simulations were performed with regards to the analysis of the rheological properties of biocompatible orthodontic elastomeric ligatures.

The upper mesial incisor was a subject of the numerical simulations. The tooth model consisted of enamel, dentine, pulp, periodontal ligament and surrounding alveolar bone structures. Periodontal ligament was modeled both as a continuous membrane and as a set of 3600 longitudinal and tangential collagen fibers. Calculations were done for the various extrusion force values in a range (20 – 50) cN.

Numerical simulations showed that the value of the extrusion force for a positive remodeling phenomena started from 40 cN and produced strain intensity values in a range of (2 – 40) x 10-4. On the other hand, the maximal stress of a periodontal ligament did not exceed 0.55 MPa, which was a safe stress level for collagen fibers, which are able to carry at least 1.6 – 1.7 MPa.

The results of the relaxation experiments proved that a power-law description is the best fit for the time-dependent behavior of ligatures during orthodontic procedures. Power-law model produces the most intensive initial relaxation, which is typical for elastomeric ligatures. The proper assessment of their rheological properties enables dentists to predict a degree of load/stress loss due to the relaxation and leads to a precise control of treatment progress in various orthodontic procedures.

[E-02.3]

EXPERIMENTAL AND NUMERICAL ANALYSIS OF ORTHODONTIC ALIGNERS MADE OF A NOVEL SHAPE MEMORY POLYMER

Tarek Elshazly[1], *Ludger Keilig*[1], *Sherif Kandil*[2], *Christoph Bourauel*[1]

1 *Oral Technology - Bonn University, Bonn, Germany*
2 *Research and Development - K Line Europe, Düsseldorf, Nordrhein-Westfalen, Germany*

Objective: Aligner treatment is an almost invisible option to correct misalignement of teeth. Recently, several improvements to aligner materials have been proposed to overcome the drawbacks of conventional aligner treatment. One recent approach is the incorporation of shape memory polymers (SMPs). The aim of this study was to experimentally assess the effectiveness of an orthodontic aligner made of a novel SMP, to quantify the forces and moments delivered by two different aligner thicknesses and to biomechanically evaluate the capability of bodily movement by SMP. Additionally, a 3D finite element (FE) numerical model was developed to be used for understanding limits and real effectiveness of clear aligners.

Methods: An upper arch typodont model with a movable tooth 21 was prepared. A reproducible palatal movement of 3 mm was planned in the typodont experiment. A set (n=5) of two thicknesses of SMP aligner (0.8 and 1.0 mm) were fabricated. Each aligner was rinsed in boiling water for 2 minutes for softening and then adapted to a misaligned model with the 3 mm displacement. The aligner on the model was put in a hot water bath (55 °C) for 5 minutes. The model was scanned before and after each treatment. Using Onyx Ceph software, superimpositions and measurements were done to evaluate tooth 21 movements by the thermal recovery of the aligner. The force quantification of the two sets was measured in customized biomechanical Orthodontic Measurement and Simulation System (OMSS) at different temperatures (55, 45 and 37 °C). A prepared resin model was mounted in OMSS. For each aligner, force systems and movements were measured experimentally until no further forces or moments were generated by the aligner. Using FE system Marc/Mentat, an idealized numerical model of teeth and the aligner was developed. Parameters of SMPs were used to simulate force delivery of aligner. Results were compared with the experimental results.

Results: Aligners succeeded to achieve a significant bodily tooth movement (2.5±0.5 mm) on the typodont model, with insignificant difference between different thicknesses. The mean forces delivered by (0.8 mm) aligners for palatal displacement of tooth 21 were 0.70±0.22 N at 55 °C, 0.18±0.09 N at 45 °C, and 0.34±0.08 N at 37 °C. The mean forces delivered by (1.0 mm) aligners were 0.58±0.19 N at 55 °C, 0.26±0.14 N at 45 °C, and 0.28±0.07 N at 37 °C. A good concordance with numerical results could be shown for selecting appropriate material parameters for the SMP aligner.

Conclusion: SMPs can be used for fabrication of orthodontic aligners that are capable to move teeth by biocompatible forces within orthodontic forces' range.

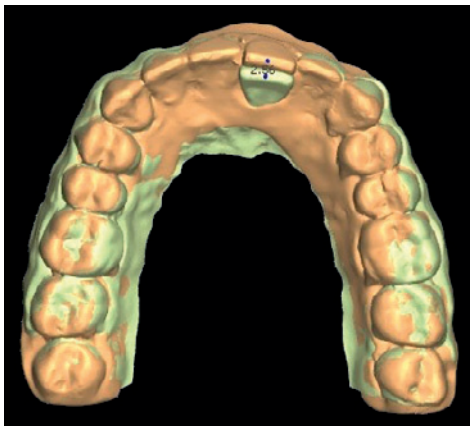

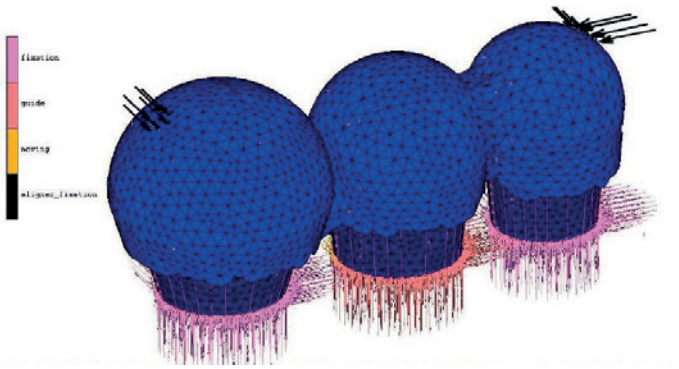

Figure Caption:
Left: Superimposition of scanned typodont before and after using SMP aligner.
Right: Idealised model of an aligner segment on three teeth.

[E-02.4]

INFLUENCE OF THE MULTISCALE TUBULAR NETWORK ONT THE MECHANICAL PROPERTIES OF THE DENTINE

Vennat Elsa[1], *Aubry Denis*[1]

1 *MSSMat (UMR-CNRS8579), Gif sur yvette, France; Centrale-Supélec*

The dentinal tissue is the main anchorage tissue of restorative dental biomaterials. However, its microstructure and nanostructure and their influence on its mechanical properties are not so well known (Vennat 2017, Kinney 2003).

The dentin is a hierarchical porous media (Vennat 2009). At the tissue scale, it is described as a composite made of three main structures: the tubules (micrometric cylindrical holes filled with physiological fluids and oriented from pulp cavity to enamel), the peritubular collar (a highly mineralized cuff surrounding the tubules) and intertubular dentin. However, another structure has to be mentioned: some channels (of a few hundred nanometers diameter) are linking those tubules in a transverse direction (Mjör & Nordahl 1996). Their density varies within the depth of dentin and the existence of a "perichannel" collar is not often discussed. It has also been observed that most of those channels seem to be arched (thus lowering stress concentration compared to straight channels, Vennat 2017). At a lower scale, intertubular dentine is itself a composite made of collagen fibrils and hydroxyapatite crystals with characteristics length of tenth of nanometers order of magnitude. As in bone tissue, the fibers and crystals arrangement is still unclear but it is accepted that collagen fibrils are lying in planes perpendicular to the tubule axes (Elbaum 2007).

Mathematical homogenization analyses (Cioranescu & Saint-Jean Paulin 1999) have shown that when a fiber network is built from segments with different scales diameters, the resulting homogenized material model is different from classical ones. Here, we develop this idea by considering a periodic network of tubules plugged inside the dentin material and connected by microchannels. A multiscale expansion considering both the scale of the tubule and the one of the channels shows that the latter may be modeled as slender beams inside the dentin itself and connecting the tubules. An original homogenized model is obtained especially showing the influence of the microchannels on the effective anisotropic properties of the dentin taking into account the density of microchannels inside the periodic reference cell. The proposed geometries are deduced from our microscopic observations using FIB-SEM and CLSM (Vennat 2017) of dentin at different locations in the tooth.

References:

Vennat et al. (2017), Acta biomaterialia, 51, 418-432.
Kinney et al. (2003), Critical Reviews in Oral Biology & Medicine, 14(1), 13-29.
Mjör & Nordahl (1996), Archives of oral biology, 41(5), 401-412.
Elbaum et al. (2007), Journal of dentistry, 35(2), 150-155.
Vennat et al. (2009), Dental Materials, 25(6), 729-735.
Cioranescu & Saint-Jean Paulin (1999), Homogenization of reticulated structures, Springer.

[E-03.1]

PEAK TRABECULAR BONE MICROARCHITECTURE PREDICTS RATE OF ESTROGEN-DEFICIENCY-INDUCED BONE LOSS

*Yihan Li[1], Wei-Ju Tseng[1], Chantal de Bakker[1], Hongbo Zhao[1], **X. Sherry Liu**[1]*

1 University of Pennsylvania, Philadelphia, USA

Reduced estrogen levels during menopause lead to accelerated bone remodeling, resulting in low bone mass and increased fracture risk. Peak bone mass is a significant predictor of postmenopausal osteoporosis. However, it is not clear if rates of postmenopausal bone loss depend on peak bone mass and bone microarchitecture. To establish this relationship, we used in vivo μCT to longitudinally track tibial bone changes in 62 rats (4-5 month old) from 0 to 4 weeks post-OVX.

Bone volume fraction (BV/TV) decreased 57% over 4 weeks post-OVX. There was no correlation between baseline BV/TV and percent decrease in BV/TV. Among all the baseline bone microarchitecture parameters, only trabecular thickness (Tb.Th) showed a trend of correlation with the extent of post-OVX bone loss (r=-0.21, p=0.097). Stepwise multiple linear regressions suggested that the combination of baseline Tb.Th and connectivity density (Conn.D) was an important predictor for percent decrease in BV/TV, Tb spacing (Tb.Sp), Tb number (Tb.N) and Conn.D (adjusted r=0.41-0.67,Table 1).

To further examine the influence of Tb.Th regardless of BV/TV on OVX bone loss, rats were stratified by the relative baseline Tb.Th (adjusted by BV/TV) into 3 groups: Low, Medium, and High relative Tb.Th (Fig1A-D). No difference of baseline BV/TV was found among the 3 groups. In contrast, bone loss rate was 15% lower in the High and 5% lower in the Medium compared to the Low relative Tb.Th group, respectively (Fig1E). Similar results were found for % decrease in Conn.D, Tb.N, and Tb.Sp (Fig1F-H). Next, we used individual trabecular dynamics (ITD) analyses to track bone loss that occurred in each individual trabecula based on precisely aligned pre- and post-OVX μCT images (Fig1I). 11,862 trabeculae from 24 rats were analyzed and categorized to 6 groups based on their Tb.Th (Fig1J). ANOVA test showed significant difference between all Tb.Th groups, suggesting thicker trabeculae led to less bone loss. Moreover, trabeculae that went through connectivity deterioration (Fig1I) had 14% lower Tb.Th than trabeculae that remained intact post-OVX.

In summary, the extent of OVX bone loss was affected by peak bone microarchitecture, most notably the trabecular thickness. Thicker trabeculae are less likely to be disconnected or perforated in response to OVX, resulting less degree of bone loss. Given the same bone mass (BV/TV), a trabecular bone phenotype with thin trabeculae may be a risk factor toward accelerated postmenopausal bone loss

Table 1: Correlation coefficients (*r*) and independent baseline predictors by stepwise multiple linear regression for % decrease in trabecular parameters. Minus sign indicates negative correlation. *:p<0.05, ⁺:p<0.01, #:p<0.001.

% decrease	*r*	*Adjusted r*	*Independent predictors*
BV/TV	0.46	0.41	-Tb.Th⁺, Conn.D⁺
Tb.Th	0.66	0.66	-BS/BV#
Tb.Sp	0.51	0.48	-Conn.D#, Tb.Th⁺
Tb.N	0.66	0.64	-Tb.Th⁺, Conn.D⁺
SMI	0.26	0.23	-SMI*
Conn.D	0.69	0.67	-Tb.Th⁺, Conn.D⁺, SMI*

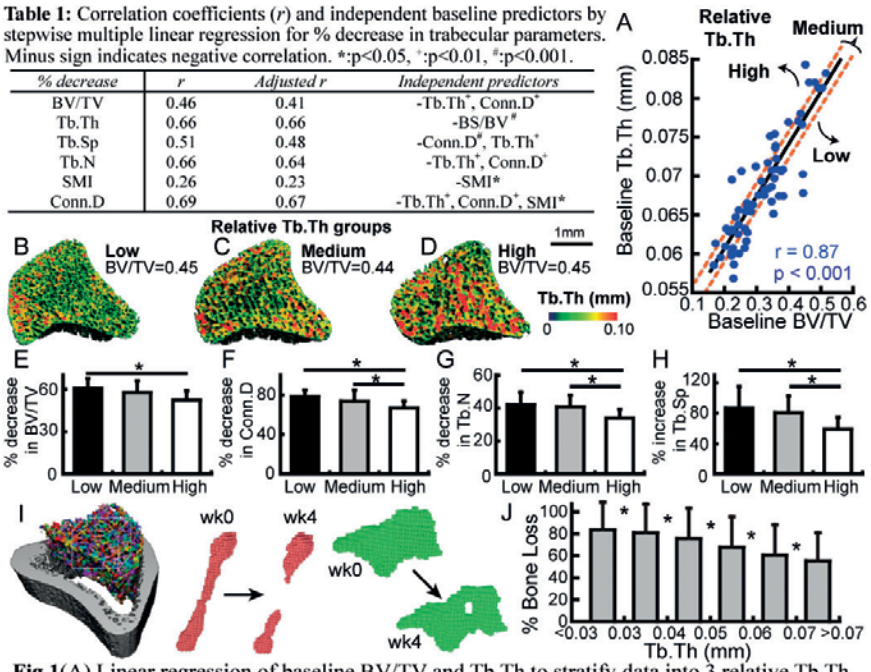

Fig 1(A) Linear regression of baseline BV/TV and Tb.Th to stratify data into 3 relative Tb.Th groups.(B-D) Representative trabecular bone images and (E-H) % changes in bone parameters in Low, Medium, and High relative Tb.Th groups. (I) Schematics of individual trabecular dynamics analysis; (J) % bone loss in individual trabeculae stratified by thickness. *: p<0.05

*Figure Caption: (A) Linear regression of baseline BV/TV and Tb.Th to stratefy data into 3 relative Tb.Th groups. (B-D) Representative trabecular bone images and (E-H) % changes in bone parameters in Low, Medium, and High relative Tb.Th groups. (I) Schematics of individual trabecular dynamics analysis; (J) % bone loss in individual trabeculae stratified by thickness. *: p<0.05*

Acknowledgments: NIH R03-AR065145, K01-AR066743, P30-AR069619

[E-03.2]

SEVEN LABORATORIES PERFORMING BIOMECHANICAL CALCULATION OF THE SAME HUMAN FEMUR: A ROUND-ROBIN FINITE ELEMENT ANALYSIS WITH EXPERIMENTALLY ACHIEVED GROUND TRUTH

*Daniel Klüß[1], Ehsan Soodmand[2], **Hans-E. Lange**[1], Maeruan Kebbach[2]*

1 *Department of Orthopaedics, Biomechanics and Implant Technology Research Laboratory (FORBIOMIT), Rostock University Medical Center, Rostock, Germany*
2 *Department of Orthopaedics, Rostock University Medical Center, Germany*

In musculoskeletal biomechanics, finite element analysis is a fundamental tool that has been used for the past four decades to predict the mechanical behavior of bone. However, to our knowledge, there are no round-robin finite element analyses of long human bones with more than two participating biomechanics laboratories published yet, where the results of the experimental tests were not known in advance. Owing to this gap in the numerical biomechanical research, we decided to conduct a round-robin FEA that was organized within the Cluster "Numerical Simulation" of the Musculoskeletal Biomechanics Network (MSB-Net), which is part of the Basic Research Section of the German Society for Orthopaedics and Traumatology (DGOU).

We prepared a fresh-frozen human femur for a compression test in a universal testing machine measuring the strains at 10 bone locations as well as the deformation of the bone in terms of the displacement of the loading point at a static load of 2 kN. The computed tomography data of the bone with a calibration phantom as well as the orientation of the bone in the testing machine with the according boundary conditions were delivered to seven participating laboratories. These were asked to perform a finite element analysis simulating the experimental setup and to deliver their results to the coordinator without knowing the experimental results a priori.

The experimental strain measurements were successfully performed with a repetition of n = 5. After the evaluation of the measured strains, these were compared to the strains calculated by the FEA from the partnering seven laboratories of the round-robin test. Resultantly, four laboratories had deviations from the experimentally measured strains of less than 40 %, and three laboratories had deviations of their numerically determined values compared to the experimental data of more than 120 % (Figure 1).

These deviations are thought to be based on different material laws and material data, as well as different material mapping methods. It was shown that the precision of finite element models of the human femur is not yet as developed as desired by the biomechanics community. Our results are to be understood as a review of the current situation at various research laboratories. Next, basic research for the cause of the high deviation is to be done on the different models

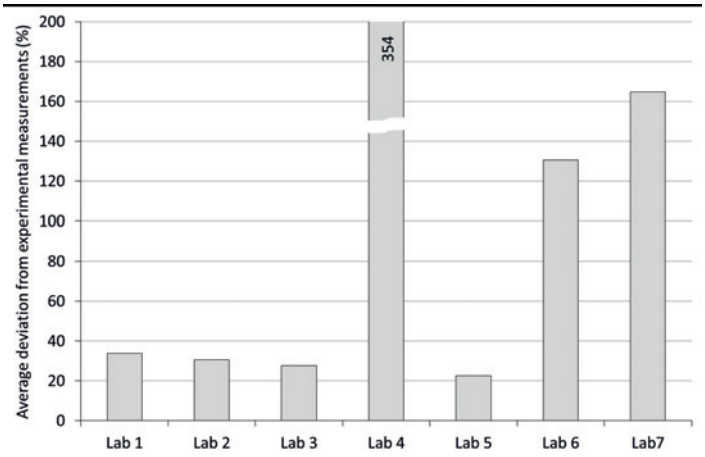

Figure 1: Average deviation from the experimental measurements of all partnering laboratories

Acknowledgments: We acknowledge the internal funding program of University Medical Center Rostock ('Förderung zur Vorbereitung von Anträgen der Verbundforschung') to financially support this project.

[E-03.3]
MICRO-SCALE NUMERICAL MODEL OF CANCELLOUS BONE

*Mohammad Salem[1], Lindsey Westover[2], **Samer Adeeb**[3], Kajsa Duke[1]*

1 *Department of Mechanical Engineering, University of Alberta, Edmonton, Canada*
2 *University of Alberta; Department of Mechanical Engineering, University of Alberta, Edmonton, Canada; 3Department of Civil and Environmental Engineering; University of Alberta, Edmonton, Canada*

Introduction: It is important to understand the material characteristics of cancellous bone after initial damage accounting for any residual plastic strain. In a large scale model, it is not practical to include the porous microstructure of cancellous bone, but instead it is desired to determine an equivalent macro-scale model. The XFEM technique can be used to model the micro-scale tissue. The obtained material behavior, including the plastic behavior captured with the hysteresis graph, can help to implement a material model to estimate the behavior of cancellous bone in the macro-scale.

Objective: To estimate the behavior of cancellous bone after initial damage in the anatomical longitudinal direction using XFEM.

Method: A 3D XFEM model of a cancellous bone specimen with side lengths of 1.75mm was developed from the micro-CT scan data of a human forearm. The material properties of the bone tissue were assigned as well as the other XFEM parameters like maximum principle strain and fracture energy. The developed 3D XFEM model of bone specimen was loaded cyclically between tension and compression. The unloading was applied at 0.046 and 0.057 strains in tension and 0.075, 0.1 and 0.1436 strains in compression.

Results: As can be seen in Figure 1, Young's modulus of the specimen was determined to be the same in loading and unloading (572MPa), which is similar to the metal plasticity model. Also, the strength and failure strain are higher in compression than tension which were found to be in a good agreement with literature [1]. This characteristic of cancellous bone can be seen in the cast iron plasticity model as reported in the literature [2]. The strength and failure strain in compression were determined to be 25.74MPa and 0.1436 respectively and in tension were equal to 21.31MPa and 0.057 respectively.

Conclusion: The hysteresis graph of a cancellous bone specimen behaves similarly to the cast iron plasticity model. The parameters of cast iron plasticity model can be modified by the hysteresis graph and can be utilized in macro-scale FE modeling of bone instead of modeling the large volume of porosity. Also, XFEM of cancellous bone has the potential to be a valuable tool to predict the mechanical characteristics of cancellous bones as a function of the microstructure.

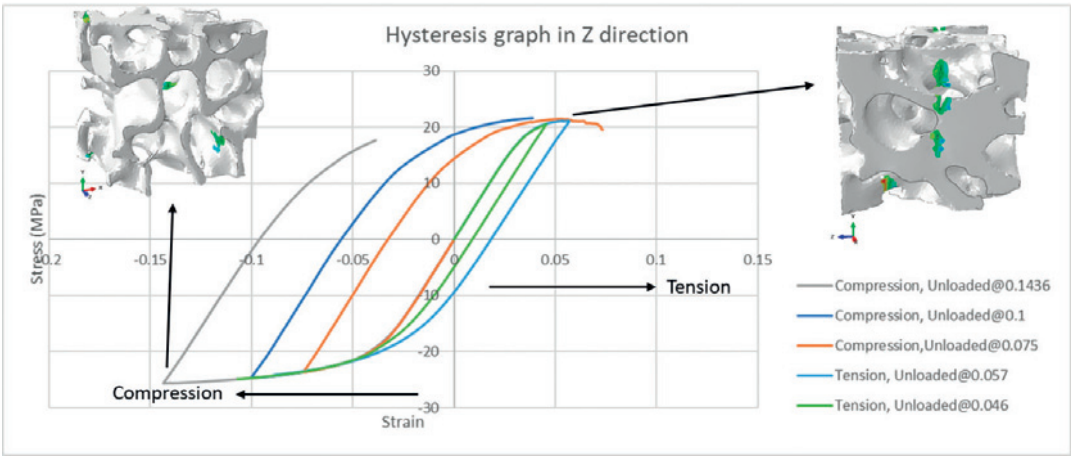

Figure 1: Hysteresis graph of cancellous bone in longitudinal direction

References:

[1] *Keaveny, Tony M., et al. "Biomechanics of trabecular bone." Annual review of biomedical engineering 3.1 (2001): 307-333.*
[2] *Bayraktar, Harun H., and Tony M. Keaveny. "A computational investigation of the nonlinear behavior of human trabecular bone." Transactions of the 12th annual pre-ORS symposium on computational methods in orthopaedic biomechnics. Vol. 2. 2004.*

[E-03.4]

DEVELOPMENT AND CALIBRATION OF MICRO-FINITE ELEMENT MODELS OF PORCINE ANKLE SUBCHONDRAL BONE

Lekha Koria[1], *Claire Brockett*[1], *Marlène Mengoni*[2]

1 *Institute of Medical and Biological Engineering; University of Leeds, UK*
2 *Institute of Medical and Biological Engineering, University of Leeds, UK*

An ever-increasing younger population are seeking treatment for ankle osteoarthritis (OA). One in five treatments for OA in the UK are foot and ankle related [1]. For a disease affecting over 1.77 million people annually, it is highly understudied and the full impacts of the disease on the mechanical properties of bone in the joint are relatively unknown. Improved understanding of bone quality changes to the joint would increase the use of early-stage treatments, such as talar dome resurfacing. These minimally-invasive devices help to delay the progression of OA, whilst preserving healthy bone that may otherwise be lost during late-stage OA surgical treatments. Changes to the stiffness of osteoarthritic bone may be observed on the apparent level, but if this is observed on lower hierarchical levels of subchondral bone remains unclear. To address this question, this study developed specimen-specific micro-finite element (µFE) models of porcine talar subchondral bone.

A cubic volume of interest (4x4x4 mm) was extracted from a µCT image dataset (16 µm resolution) of porcine talar subchondral bone cylindrical specimens (N=10, 6 mm Ø). Morphological indices (BV/TV, DA, Tb.th and Conn.D) were evaluated using BoneJ [2]. Specimen-specific continuum (hFE) models (N=10) were developed with greyscale-based material properties using relationships previously validated on whole specimens [3]. Specimen-specific µFE models were calibrated (N=5) and validated (N=5) against their corresponding hFE stiffness to produce an average tissue Young's modulus (Etiss). All hFE and mFE models were non-linear static analysis, run in Abaqus CAE 2017.

Average Etiss for calibration specimens was 428.38 ± 45.82 MPa and average calibrated stiffness was 711.97 ± 62.21 N/mm. An 11.6% RMS error was found using the validation set (N=5), which was of similar order to the calibration dataset, with a corresponding CCC value of 0.32. Average values for BV/TV and anisotropy (DA) were 0.376 and 0.67, respectively. From all key morphological indices measured, DA correlated the most with stiffness (r2 = 0.347).

Calibrated, greyscale-based hFE models could be used to assess mechanical properties of bone in silico, but showed high intra-specimen variation in stiffness. Contrastingly, calibrated µFE models showed little intra-specimen variation of material properties. This suggests that the variation in stiffness is mostly due to a variation in morphology rather than tissue properties. Though it is unclear whether this remains true for non-diseased human ankle tissue, these in silico models could provide a good control group to assess differences in tissue stiffness when evaluating osteoarthritic bone specimens.

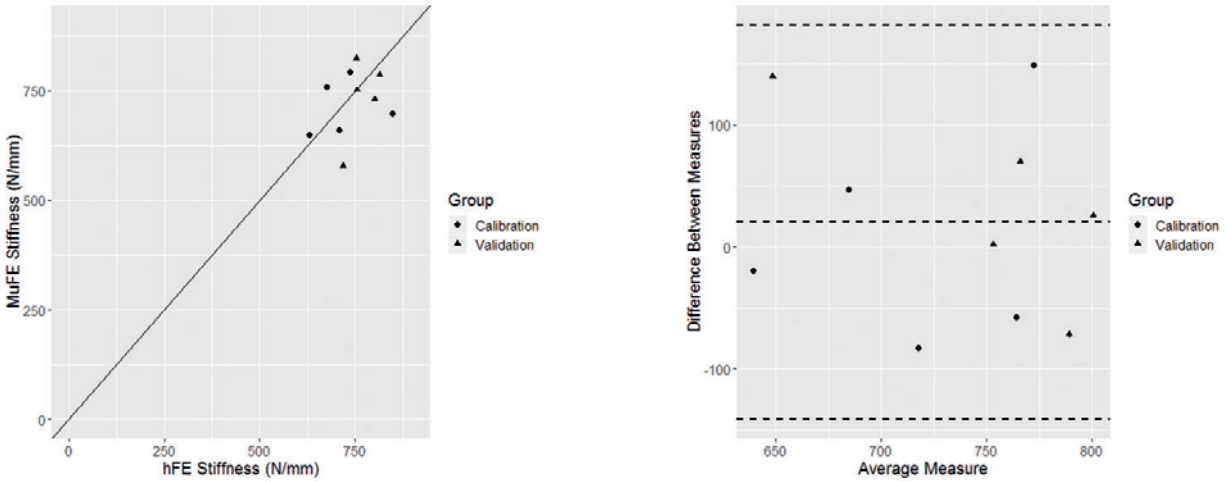

Figure Caption:"(Left) Good correlation of stiffness values observed for both groups. (Right) Bland-Altman plot showing moderate agreement."

References:

1. *Arthritis Research UK, Med Press. 222:253–8, 2013*
2. *Doube, M, Bone 47:1076-9, 2010*
3. *Koria, L, Orthopaedic Proceedings, 101-B (SUPP_2), 41-41, 2019*

[E-03.5]

3D SEGMENTATION AND CHARACTERIZATION OF THE SUBCHONDRAL MINERALIZED ZONE OF MOUSE FEMUR CONDYLES, A NEW OPPORTUNITY FOR ADRESSING MORPHOLOGICAL CHANGES DURING MUSCULOSKETAL PATHOLOGIES

Brahim Mehadji[1], *Yoseph Ahmed*[2], ***Jean-Philippe Berteau***[3]

1 *Aix Marseille Univ, CNRS/IN2P3, CPPM, Marseille, France; Department of Physical Therapy, City University of New York - College of Staten Island, Staten Island, USA*
2 *Department of Physical Therapy, City University of New York - College of Staten Island, Staten Island, USA*
3 *Department of Physical Therapy, City University of New York - College of Staten Island, Staten Island, USA; New York Centre for Biomedical Engineering, City University of New York – City College of New York, USA; Nanosciences Initiative, City University of New York – Advance Science Research Center,New York, USA*

One of the most-scanned joints in preclinical animal models dealing with musculoskeletal pathologies is the mouse knee (B. Poulet et al., 2013). While three-dimensional (3D) characterization of bone tissue porosity have previously been performed on cortical bone (B. Jokihaara, et al.; 2010), it has not yet been comprehensively performed for the subchondral mineralized zone (SMZ) which is composed of the subchondral bone (SB) and the calcified cartilage (CC) of femur condyles. Thus, it remains challenging to assess changes that occur in the SMZ during pathologies such as osteoarthritis. One of the keys to addressing this challenge is to segment each layer to measure their material properties, morphologies, and porosity.

We present a novel approach for measuring Tissue Mineral Density, 3D porosity, and the thickness of SB and CC in mice femur condyles using High-Resolution Micro Tomography (HR-µCT). We have segmented the Vascular Porosity network, the osteocytes' lacunae of the SB, and the chondrocytes of the CC by using multi-thresholding (Figure 1). Regarding porosity and geometrical properties of both CC and SB, our results spread in the range of the literature.

Interestingly and for the first time, our 3D reconstructions show some vascular porosity infiltrations (superior to 1.2 µm) within numerous chondrocytes forming chambers (Figure 2). These infiltrations are due to SMZ damages and might be of interest to assess during the progression OA (D. Burr and E. Radin 2003).

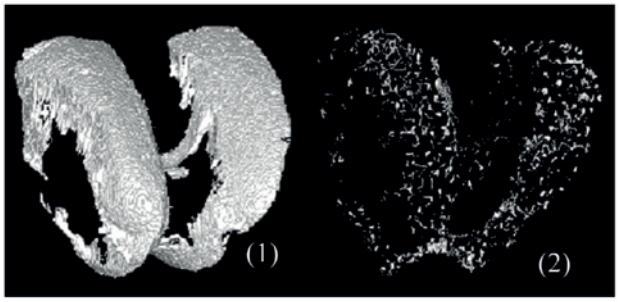

Figure 1: Mask of the segmented SMZ (1) and segmented vascular porosity within SMZ (2)

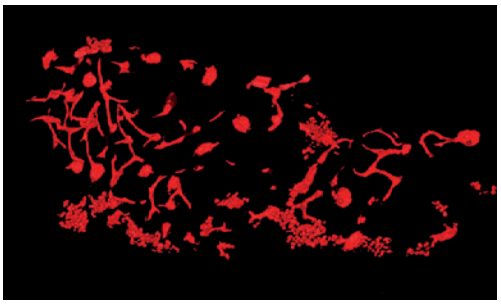

Figure 2: Vascular porosity on top of the lateral condyle. We observe some grainy regions close to the intercondylar fossa which correspond to infiltrations in chondrocytes.

Acknowledgments: The authors want to thank SCANCO for performing the imaging, and the College of Staten Island – Willowbrook campus for the startup funds that supported this research.

References:

B. *Poulet et al.,Osteoarthritis and Cartilage, 21(5), 756–763 (2013)*
B. *H. M. Jokihaara et al., Journal of Microscopy, 240(1), 32–37 (2010)*
D. *Burr and E. Radin, Rheumatic Dis Clin North Am, 29(4), 675–85 (2003)*

[E-03.6]

PREDICTING FEMORAL GROWTH PLATE SHAPE: A SURFACE OF MINIMUM SHEAR?

Mahsa Sadeghian[1], *Sandra Shefelbine*[1]

1 *Northeastern University, Boston, USA*

The proximal femur is particularly prone to changes in bone growth, resulting in bone deformities such as coxa valga, slipped capital femoral epiphysis, and femoroacetabular impingement. Alterations in bone morphology can be caused by changes in hip joint loading patterns. Considering that growth plate cartilage has low shear strength and shear stress at the proximal growth plate reduces hip joint stability, we hypothesized that the growth plate orients in the direction that minimizes shear stress on its surface. A computational model was developed to predict the orientation of proximal femoral growth plate under different hip joint loads.

Hip joint contact force was parameterized to describe upright standing and bilateral hip flexion. Also, a posteriorly directed and a laterally directed forces were defined on sagittal and frontal planes to detect the influence of alterations in loading direction on predicted growth plate shape. An algorithm was developed to predict the shape of the femoral growth plate along the principle stress vectors using the stress field of the growth region, resulting in minimized shear stress within the growth plate. Initially a finite element model of the proximal femur was generated with a flat growth plate. For each hip contact force, a corresponding growth plate was predicted by iteratively determining the surface of the minimum shear stress in the growth region. We characterized the growth plates by measuring the height of the growth plates from a reference plane perpendicular to the neck axis and tangent to the femoral head, plotted as two-dimensional contours.

The shape of the growth plate predicted for standing load correlated closely with morphological properties of the growth plane of a typically developing child. Also, the bilateral hip flexion shifted the growth plate in a way that mimics the traits of the growth plates in children with femoroacetabular impingement. The laterally directed parameterized force tilted the growth plate medially (the medial side moved inferiorly) and the posteriorly directed parameterized force tilted the growth plate anteriorly (the anterior side moved inferiorly). Subject-specific models and more realistic loading condition will help to predict abnormalities corresponded by specific activities in future work.

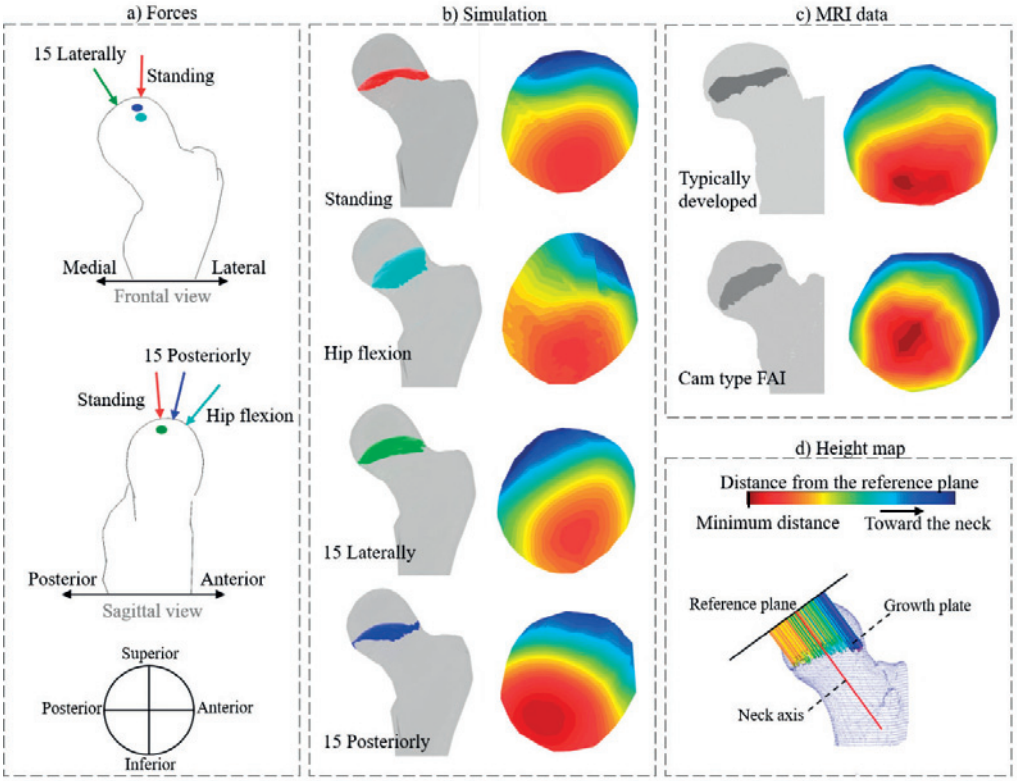

Figure Caption: "a) Force: The load vectors for standing, hip flexion and two parametric forces (15 degrees shift laterally and 15 degrees shift posteriorly) passing through the head center are shown in the sagittal and frontal view. b) Simulation: the 3D growth plate geometries and 2D contour plots of growth plate height is indicating the difference of the growth plates orientation under different loading conditions. c) MRI data: the contours for two subjects were plotted to compare with the simulation geometries. d) Height map: the reference plane and definition of height and colors."

[E-04.1]

MRI MEASURES OF BONE FRAGILITY: OPPORTUNITIES FOR COMPUTATIONAL MODELING

Mark Does[1], *Jeffry Nyman*[2]

1 *Vanderbilt University, Nashville, USA*
2 *Vanderbilt University, Medical Center, Nashville, USA*

Increased bone fragility is a consequence of normal aging and numerous diseases, and results in debilitating and costly fractures. However, the clinical standard for evaluating bone health, dual energy X-ray absorptiometry (DXA), does not fully predict increased fracture risk with age or disease. Thus, there is a need for improved diagnostics to guide the clinical decisions of when and how to treat patients for bone fragility. Unlike X-ray based imaging, which is sensitive only to the mineral content of bone, magnetic resonance imaging (MRI) is sensitive to water, which exists in both the pore spaces of bone mineral (pore water, PW) and bound to the collagen matrix (bound water, BW). The collagen matrix is critical for providing toughness and fracture resistance to bone, and thus, in comparison to X-ray, MRI has the potential to offer additional insight into bone health and biomechanical properties. Recently developed MRI methods provide quantitative maps bound and pore water concentrations (Cbw and Cbw, respectively – see Fig below). These measures have been shown to predict mechanical properties of isolated cadaver bone specimens, but the relationships between 2D or 3D maps of Cbw & Cpw and whole-bone biomechanics remains an open question. Experimental MRI and biomechanical tests of cadaver bones are being used to explore these relationships, but there is an opportunity to accelerate this exploration through in silico experimental studies, such as those based on finite element models of bone.

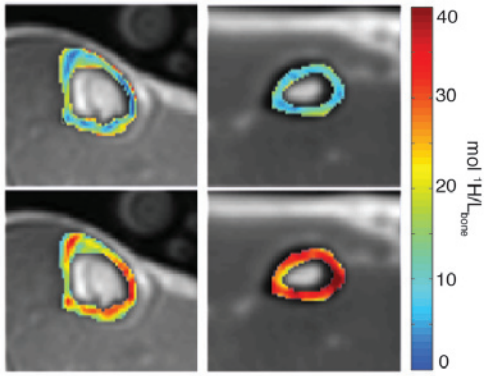

Figure Caption: Representative In Vivo Cpw (top) and Cbw (bottom) maps; tibia (left) and radius (right), extracted from 3D volumes.

Acknowledgments: NIH funding R01EB014308, R01AR063157

[E-04.2]

PHASE-CONTRAST NANO-CT REVEALS POROUS NETWORK IN INTERMUSCULAR BONES OF HERRING FISH

Imke A.K. Fiedler[1], *Murielle Salome*[2], *Max Langer*[3], *Cécile Olivier*[3], *Francoise Peyrin*[3], *Jean-Philippe Berteau*[4]

1 *University Medical Center Hamburg-Eppendorf, Department of Osteology and Biomechanics, Hamburg, Germany; Department of Physical Therapy, City University of New York - College of Staten Island, Staten Island, USA*
2 *European Synchrotron Radiation Facility, X-Ray Microscopy Beamline Id21, Grenoble, France*
3 *Univ Lyon, Insa-Lyon, Univ Claude Bernard Lyon 1, Cnrs, Inserm, Creatis Umr 5220, U1206, France*
4 *Department of Physical Therapy, City University of New York - College of Staten Island, Staten Island, USA; New York Center for Biomedical Engineering, City University of New York – City College of New York; Nanosciences Initiative, Advanced Science Research Center, City University of New York, USA*

Introduction: There is an increasing interest in understanding the skeletal properties of teleosts, i.e. bony fish. Within the teleost skeleton, intermuscular bones (IB) grow within the muscles and originate from mineralized tendons1. Whereas IB consist of collagen type I and carbonated hydroxyapatite similar to other bone tissues, a simpler hierarchical structure compared to mammalian bones has been attributed to these bones2, making them an interesting candidate to study structure-function relationships in mineralized composite tissues. The goal of this research is to investigate the structural properties of IB at the sub-microscopic level.

Methods: IB of two fish groups with different growth status (3 IB of small fish (21 cm body length), 3 IB of large fish (28 cm body length)) were investigated using phase contrast imaging at the beamline ID16A at the European Synchrotron Research Facility. Phase nano-computed tomography (CT) was performed with 33.6 keV at an isometric voxel size of 100 nm for overview images and 30 nm for imaging of specific regions of interest. Phase retrieval, tomographic reconstruction and morphometry were performed using ESRF in-house software and imageJ.

Results: Phase nano-CT revealed that small and large IB had a rod-like fiber shape with a mean ellipsoidal diameter <200 µm. Both groups featured patterns of concentric layer-like mineralization, where layers of low mineralization were visible in the form of darker rings (Figure). In IB from larger fish, higher mineralized patches were distributed across the cross-sections. Moreover, lacuna-like porous structures of up to 2 µm diameter (Figure) with attached canalicular structures in the range of 100 nm were present, indicating a more intricate network of channel-like structures in IB from larger fish.

Discussion: Previous own data assessing the mechanical tensile properties and mineral-related properties of intermuscular bones at the whole bone level showed that IBs showed a peculiar behavior compared to mammalian cortical bone, including a distinct ability for post-yield deformation, and an elastic modulus in the range of tendons but strength in the range of mammalian cortical bone. Interestingly, the elastic modulus of IB from smaller fish (lower growth status) was higher than in IB from larger fish, which could not be explained by changes in mineralization or porosity at the microscale. Here, the data gained from nano-CT showed additional sub-microscopic tissue porosity, which could be an important factor of elasticity in IB. This porosity shows aspects of a cellular and/or vascular network that is different from a typical osteocyte-lacunar network. Finally, the acquired data also revealed specific patterns of tissue mineralization in IB.

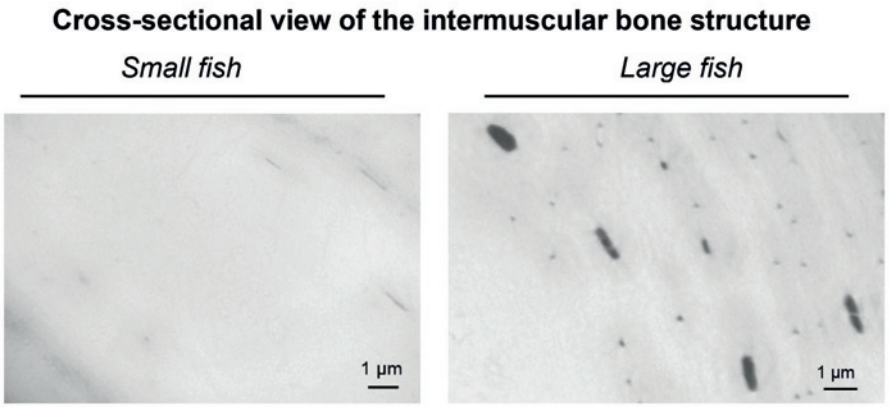

Figure Caption: Nano-CT reveals more porous structures in intermuscular bones of larger fish compared to smaller fish.

References:

1) *Yao et al., 2015;*
2) *Burger et al., 2008*

[E-04.3]

UNDERSTANDING THE MODIFICATIONS IN MICROSCALE FRACTURE TOUGHENING MECHANISMS OF BONE DUE TO AGING, DISEASE, AND TREATMENTS USING COMPUTATIONAL MODELING

Ani Ural[1]

1 *Villanova University, Villanova, USA*

Bone derives its fracture resistance from the toughening mechanisms that exist at multiple length scales. These toughening mechanisms may be altered due to aging, osteoporosis, and therapeutic treatments such as bisphosphonates. Recent studies showed that microscale material heterogeneity, which may be altered as a result of aging, osteoporosis or long term bisphosphonate treatment, is an important factor affecting the fracture resistance of cortical bone. These observed compositional changes may also interact with the underlying bone microstructure and existing microcracks altering the fracture toughening mechanisms of cortical bone. As a result, this study aims to evaluate the influence of material heterogeneity, microstructure, and microcracks on crack initiation and propagation in cortical bone using a three-dimensional finite element modeling approach.

Finite element models with homogeneous and heterogeneous material properties were generated for different bone microstructures based on human cortical bone images. Additional models that incorporate microcracks were also generated with both homogeneous and heterogeneous material properties. Both the initiation and propagation fracture resistance were assessed in all models. The results showed that initiation fracture resistance was higher in models with homogeneous material properties compared to heterogeneous ones. On the other hand, an opposite trend was observed for propagation fracture resistance. The increase in material heterogeneity increased the propagation fracture resistance up to a certain level beyond which a decrease was observed while still remaining higher than the homogeneous material distribution. In addition, homogeneous models demonstrated extensive crack formation with limited areas of damage whereas, heterogeneous models showed an increased amount of damage with a more variable distribution of damage and with smaller areas of crack formation. The fracture response was also significantly influenced by the microstructure. An increase in percent osteonal area and evenly distributed osteons led to a lower amount of crack growth for all levels of material heterogeneity. When microcracks were introduced in the models, a combination of low material heterogeneity and high microcrack density led a higher initiation toughness compared to high material heterogeneity and low microcrack density. An opposite trend was observed at later stages of crack growth.

These results show that microscale structural and material properties significantly influence the fracture resistance and toughening processes in cortical bone. The computational modeling approach presented in this study elucidated how possible microscale modifications due to aging, disease, and bisphosphonate treatment may influence the initiation and propagation fracture resistance of cortical bone. The computational simulations provided new information that cannot be captured by experiments due to the simultaneous existence of these factors in bone specimens and improved the understanding of the influence of material and structural changes on the fracture resistance of cortical bone.

Acknowledgments: National Science Foundation CMMI-1434412 and XSEDE MSS-160001.

[E-04.4]

IN SILICO PLATFORM FOR PERTURBATION EXPERIMENT IN MECHANO-BIOCHEMICAL COUPLING SYSTEM OF BONE REMODELING

Taiji Adachi[1], *Yoshitaka Kameo*[1]

1 *Kyoto University, Kyoto, Japan*

Bone structure is maintained by mechanical adaptation via remodeling, in which osteoclastic bone resorption and osteoblastic bone formation are in harmony with each other under the regulation by mechanosensory network of osteocytes in bone matrix. An imbalance between bone resorption and formation due to disuse results in metabolic bone disorders such as osteoporosis. Cell and molecular biology studies have identified many signaling pathways that regulate these cellular activities; however, the physiological and pathological conditions of bone as a system remain difficult to understand because of the complexity of the signaling networks including mechano-biochemical couplings. In this study, we have developed a novel mathematical model of bone remodeling that enables us to conduct in silico experiment by which the effects of perturbation of the biochemical and mechanical factors on the spatiotemporal dynamics of bone remodeling can be observed.

To demonstrate the capability and reproducibility of the proposed in silico experiment platform, effects of disruption of the signaling molecules were investigated through computational simulations for cancellous bone remodeling using image-based cancellous bone models. Mechano-adaptive behaviors of trabecular bone under mechanical loading were investigated by considering a mechano-sensory network of osteocytes in bone matrix, in which the pathological bone states due to low mechanical loadings and abnormal expression of signaling molecules were reproduced. The developed platform were applied to conduct in silico perturbation experiment to observe the effects of specific signaling molecules on bone remodeling dynamics over time including distribution of signaling molecules, cell behaviors, and trabecular microstructure. Furthermore, the capability of the platform as an in silico experimental tool to predict the effects of drug treatment for osteoporosis was discussed.

Acknowledgments: The authors thank Yuki Miya (Kyoto University, Kyoto, Japan) for his contribution in in-silico experiment and Tomoki Nakashima and Mikihito Hayashi (Tokyo Medical & Dental University) for their discussion. This work was partially supported by CREST (Mechanobiology) from the AMED, Japan.

[E-04.5]

CHANGES IN TRABECULAR BONE APPARENT DENSITY UNDER CYCLIC LOADING THROUGHOUT LIFE IN MEN AND WOMEN: FINITE ELEMENT SIMULATION

Rabeb BEN KAHLA[1], *Abdelwahed Barkaoui*[2], *Moez Chafra*[1]

1 *Applied Mechanics and Systems Research Laboratory (LASMAP), Tunisia Polytechnic School, University of Carthage, La Marsa, Tunisia*
2 *Laboratory of Renewable Energy and Advanced Materials (Lerma), School of Renewable Energy, International University of Rabat, Morocco*

Bone is a highly dynamic tissue, able to self-adapt its density and microarchitecture to changes in long term loading. This adaptation process is known as bone remodeling, which includes the resorption of old bone and the formation of new bone. Any imbalance between these two phases leads to bone diseases, such as osteoporosis, considered as one of the major health problems worldwide. Using the finite element (FE) method, the current work provides a numerical investigation of the evolution of trabecular bone apparent density according to changes in the initial mineral density and the mineral Young's modulus, in addition to the changes in sex hormones, based on a more accurate description of testosterone evolution in men and estradiol evolution in women. Bone tissue was assumed as an elastic isotropic material, and the remodeling process was mathematically described, taking into account the mechanical parameters and the cell activities at the microscopic level [1], [2]. Boundary conditions were set up to simulate walking, where the proximal femur head was subjected to a succession of charge/discharge cycles, resulting in bone fatigue damage. The FE algorithm was implemented in FORTRAN language, using UMAT as a subroutine, and the numerical simulations were performed using ABAQUS software. According to the obtained results, a decrease by 20% in the initial mineral density of trabecular bone affects the resorption and the formation processes. In addition, trabecular bone apparent density is strongly related to its Young's modulus. Thus, when the Young's modulus increases, the apparent density increases. It was also noticed that the formation process is greater when bone has a higher stiffness. Moreover, the difference in trabecular bone behavior between men and women starts being noticeable from the age of 20 years. However, bone strength in men remains almost the same until the age of 50 years, unlike women, in whom the damage rate starts increasing at about the age of 40 years.

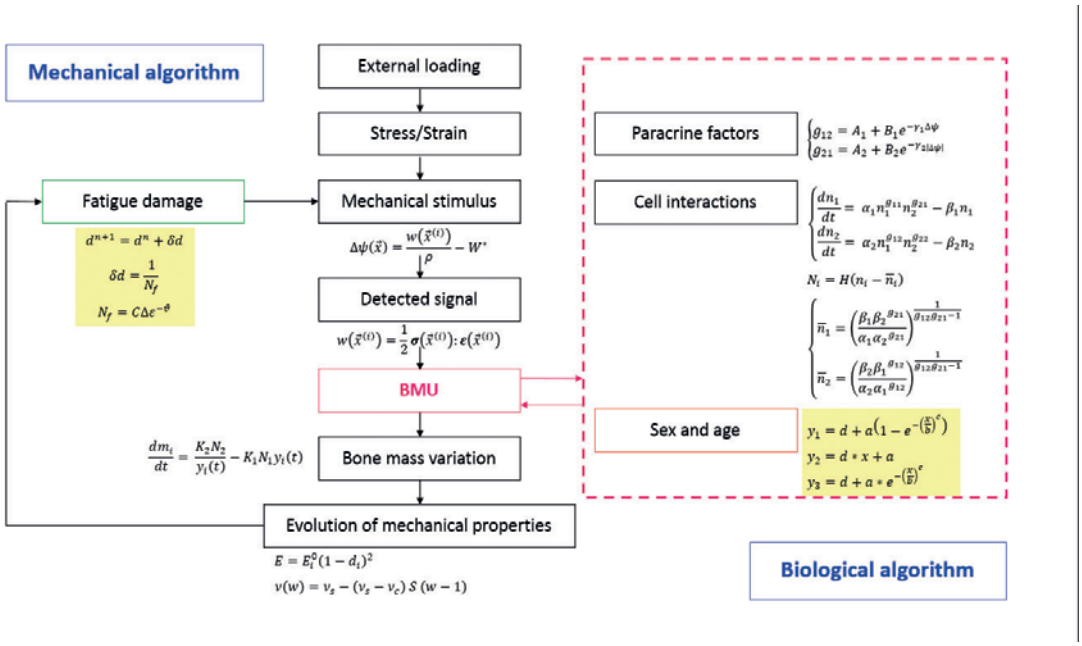

Figure Caption: Organization chart of the bone remodeling algorithm implemented in UMAT using ABAQUS 6.12®EF.

References:

[1] *A. Barkaoui, R. Ben Kahla, T. Merzouki, R. Hambli, Age and gender effects on bone mass density variation: finite elements simulation, Biomech. Model. Mechanobiol. 16(2) (2017) 521– 535*
[2] *R. Ben Kahla, A. Barkaoui, T. Merzouki, Agerelated mechanical strength evolution of trabecular bone under fatigue damage for both genders: fracture risk evaluation, J. Mech. Behav. Biomed. Mater. (2018)*

[E-04.6]

BONE HEALING SIMULATION IN THE MANDIBLE AFTER ORTHOGNATHIC SURGERY

Maria Hilvert[1], *Mariska Wesseling*[2], *G. Harry van Lenthe*[3], *Roel Wirix-Speetjens*[2], *María José Gómez-Benito*[4]

1 *University of Zaragoza, Zaragoza, Spain; Materialise NV, Belgium*
2 *Materialise NV, Leuven, Belgium*
3 *KU Leuven, Belgium*
4 *University of Zaragoza, Spain*

Introduction: Orthognathic surgeries using titanium plates to correct teeth malalignment are frequently performed. However, the interactions between the bone healing process and stiffness of the plate has yet to be fully understood. The aim of this study was to simulate the bone healing process of the mandible after orthognathic surgery to gain more insight about long-term bone healing simulation.

Methods: A finite element model of the mandible was developed using real-case data. CT-data of an orthognathic surgery patient was segmented and the surgery was planned in-silico. The model was meshed using 3-matic (Materialise NV). The bone was fixed in the mandible joint and biting forces resulting from muscle activity were introduced [1]. An orthodontic surgery was simulated by introducing a transverse fracture gap and realigning the ramus of the mandible parallel. In future simulations the real wedge-shaped gap will be applied. The FEM model consisted of 210428 linear tetrahedral elements and bone was considered linear elastic. Material properties of the bones were assigned according to the Hounsfield Units (HU). The following relation between bone density ρ and young's modulus E was assigned: $E=0.013\rho-13.05$ [2]

Stiff connectors were introduced to simulate mechanical fixation of ramus and mandible after surgery. To simulate the bone healing within the fracture gap, the model of Alierta was used [3]. A UMAT subroutine was therefore implemented in Abaqus. Low normal and shear strain within the fracture gap was simulated to result in bone formation, higher strain to result in cartilage formation. If the stimulus was too high, only connective fibrous tissue was formed [3]. The model was qualitatively validated in one patient using CT follow-up data at two intervals (4 and 12 weeks) after the surgery.

Results: The results resemble qualitatively the bone healing process as can be seen in the CT data. After 4 weeks an initial bone healing process can be observed in both, the simulation (Figure 1) and on the image data. After 12 weeks bone growth could be seen in the model and in the CT data. The model showed that the mandible healed after about 6 months, which is the time frame surgeons are commonly referring to for the healing process in CMF surgeries.

Discussion and conclusion: The developed model allowed to simulate the long-term bone healing process in a mandible. The model is capable of predicting the time frames regarding bone healing that were also observed in the CT scans and are in line with surgeons' findings.

In this case study, only one patient-specific case of a mandible surgery was simulated. In further studies, more cases will be included to gain further insight into simulation process. In addition, the effect of different realignment angles of mandible and ramus will be investigated.

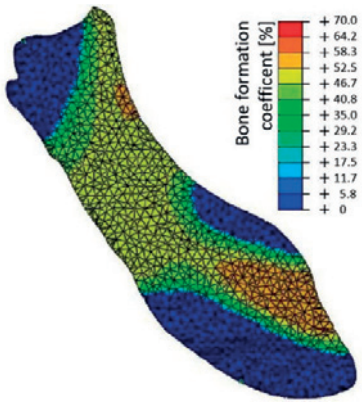

Figure Caption: Figure 1: Simulated bone formation [%] after 12 weeks

Acknowledgments: The authors would like to thank the Marie Skłodowska-Curie grant CuraBone Project MSCA ITN-EID GA no 722535 for providing financial support.

References:

[1] *Korioth, T. W. P. et al: Three-Dimensional Finite Element Stress Analysis of the Dentate Human Mandible. Am. J. Phys. Anthropol. 1992 [2] Rho, J:Y: et al: Relations of mechanical properties to density and CT numbers in human bone. Med. Eng. Phys. 1995, [3] Alierta, J. A. et al. An interface finite element model can be used to predict healing outcome of bone fractures, 2013*

[E-06.1]

CONNECTION BETWEEN GAIT AND BALANCE FUNCTIONS IN PEDIATRIC PATIENTS WITH EITHER NEUROLOGICAL OR SENSORY INTEGRATION PROBLEMS

Malgorzata Syczewska[1], *Ewa Szczerbik*[2], *Malgorzata Kalinowska*[1], *Anna Swiecicka*[1]

1 *The Children's Memorial Health Institute, Warszawa , Poland*
2 *The Children's Memorial Health Institute, Kinesiology Lab, Warszawa , Poland*

Introduction: Gait and balance are often assessed in patients with performance problems of various functional tasks. Patients with gait deficits may manifest balance problems, and vice versa [1, 2]. Patients with many neurological illnesses demonstrate both gait and balance problems [3, similarly to children with coordination problems and sensory integration deficits [4]. Aim of this study: to evaluate gait parameters and indices in patients with neurological diseases (ND) and sensory integration (SI) problems.

Material and Methods: Patients with ND (30) and SI (17) underwent gait analysis on VICON system and balance tests with eyes open on Biodex Balance System on stable and unstable base. From gait data the selected spatio-temporal and kinematic parameters were extracted. Gait Deviation Index (GDI), Movement Analysis Profiles (MAP) and Gait Profile Score (GPS) were calculated as general indices reflecting the level of gait pathology. From Biodex tests the overall stability indices were used to assess the patients' balance. The data were analyzed using discriminant analysis (StatSoft), and logistic regression (MedCalc) to see the influence of disease, abnormal balance on stable base or unstable base on gait parameters.

Results: Disease: Logistic regression did not show any difference in gait parameters between the groups, discriminant analysis indicated variability of GDI and pelvis MAP in sagittal plane as classification parameters. Median values were 2,3 and 3,818 for ND, and 2,8 and 5,225 for SI, respectively, 67,7 % of cases were properly classified.

Balance on stable base: Both methods indicated MAP foot progression as classification variable. Median values were 8,029 for good balance group, 7,782 for abnormal balance group, 87 % of cases were properly classified.

Balance on unstable base: Discriminant analysis did not show and difference in gait parameters between the groups, logistic regression indicated pelvis MAP in transverse plane as classification variable. Median values were 13,789 for good balance group, and 8,817 for bad balance group, 78,3 % of cases were properly classified.

Discussion: The results point to the connection between the ability to maintain proper balance and the gait. The division according to clinical problems suggested that the gait of the SI patients is less repeatable than ND patients. The division according to stability indices pointed to the position of the foot in respect the direction line and control of the pelvis as the differentiating parameters.

Shortcoming: low number of subjects. In all three divisions one of the subgroups was smaller than the other, making the conclusions less reliable.

Acknowledgments: STRATEGMED3/306011/1/NCBR/2017

References:

1. *K.Guffey, et al. – Gait & Posture 2016; 43: 165 – 169*
2. *R.de Souza Melo – Gait & Posture 2017; 57: 109 – 114*
3. *M.Smith, M.Kurian –Paediatric and Child Health 2018; 28: 454 – 458*
4. *B.Bril, A.Ledebt – Neurosci Biobeh Rev 1998; 22: 555 - 563*

[E-06.2]

DETERMINING OPTIMAL BIOMECHANICAL PARAMETERS FOR CLASSIFICATION OF ELDERLY FALLERS DURING BALANCE AND GAIT TASKS

Ashirbad Pradhan[1], *Usha Kuruganti*[1], *Victoria Chester*[1]

1 *Andrew and Marjorie McCain Human Performance Laboratory, University of New Brunswick, Fredericton, Canada*

A major health concern in older adults is accidental falls [1]. Previous studies for classifying elderly faller/non-fallers have focused on the postural sway measured by centre of pressure (COP) data and have neglected other biomechanical parameters, such as ground reaction force (GRF) and plantar pressure (PP) [3,4]. Research on optimal combinations of biomechanical parameters for classifying elderly fallers is warranted. As previous classification studies have incorporated both gait and balance tasks [2], it was important to compare classification accuracy using parameters from these tasks. The purpose of the study was to analyse the accuracy of classifying elderly fallers using biomechanical parameters measured during balance and gait tasks. 59 non-fallers (NF) and 41 fallers (F) performed balance and gait tasks on a walkway with embedded force plates (Kistler Instruments, Winterhur, Switzerland), and pressure mats (Tekscan Inc., Boston, MA, USA). Balance tasks involved semitandem stance with eyes open and a narrow stance with eyes closed for 30 seconds and gait tasks involved the participants walking 6 times on the walkway. The biomechanical parameters extracted from the devices included 3D GRF-time data, COP displacement/velocity data, and PP data unique to pressure mats. Fisher Linear Discriminant Analysis Classifier models were built using the biomechanical parameters from the balance and gait tasks as input. The classification model using COP, GRF and PP data from combined gait and balance tasks resulted in a maximum accuracy of 86.02% for classifying faller/non-faller categories. High accuracies were also obtained for classification using COP and GRF (84.95%), and COP alone (80.65%). The inclusion of PP parameters to COP had mixed effects for balance, gait and combined tasks (Table 1). The accuracies were competitive when compared to previous studies [3]. Biomechanical parameters from combining gait and balance tasks resulted in higher accuracy than the respective individual tasks (Table 1). The results suggest that accurate classifications of faller/non-fallers can be obtained using biomechanical parameters obtained from force plates and pressure mats. The results of this study demonstrate that the classification accuracy is improved by adding GRF parameters (84.95%) to the more commonly used COP parameters [3,4]. This approach may aid in improving the identification of fallers and have applications in fall prevention programs.

	Gait (41F, 58NF)	Balance (39F, 54NF)	Combined (39F, 54NF)
PP	64.52	65.59	72.05
GRF	78.50	61.29	78.50
COP	80.65	65.59	80.65
COP + GRF	82.05	64.52	84.95
COP+PP	78.50	74.19	80.65
COP+GRF+PP	82.05	74.19	86.02

Table 1 Classification Accuracy (%) from biomechanical parameters during gait and balance tasks

Acknowledgments: The authors acknowledge the valuable help of Sana Oladi, M.Sc who contributed to data collection in this work.

References:

1. *Delbaere, K. et al. (2010) J Amer Geri Soc, 58(9), 1679-1685.*
2. *Ejupi, A. et al. (2014) Cu Op Clin Nutri & Meta, 17(5), 407-411.*
3. *Sun, R. et al. (2018) BMC geriatrics, 18(1), 14.*
4. *Bizovska, L. et al. (2014) Gait & posture, 40(3), 399-402.*

[E-06.3]

ACCURACY OF ANTHROPOMETRIC MEASUREMENTS BY A VIDEO-BASED 3D MODELLING TECHNIQUE

Chuang-Yuan Chiu[1], *Michael Thelwell*[1], *Simon Goodwill*[1], *Marcus Dunn*[1]

1 *Centre for Sports Engineering Research, Sheffield Hallam University, Sheffield, UK*

The use of anthropometric measurements, to understand an individual's body shape and size, is an increasingly common approach in health assessment, product design, and biomechanical analysis. Non-contact, three-dimensional (3D) scanning applied specific sensors such as depth-cameras, stereo-cameras, to obtain individual human models and has been widely used as a tool for automatic anthropometric measurement. Recently, Alldieck, et al. [1] developed a video-based 3D modelling technique, enabling the generation of individualised human models for virtual reality purposes. As the technique is based on a standard video images, hardware requirements (e.g. depth camera, turntable, etc.) are minimal, increasing the flexibility of the technique's application. However, whilst good accuracy for point-to-point distances has been demonstrated [1], the accuracy of anthropometric measurements derived by this technique must be examined before its use in kinanthropometric applications. The aim of this study was to determine the accuracy of anthropometric measurements obtained using this video-based, 3D modelling technique. Five male and six female participants were recruited (stature: 1.71 ± 0.09 m; mass: 77.2 ± 13.8 kg). Participant anthropometry was measured manually by accredited operators according to the International Society for the Advancement of Kinanthropometry (ISAK) protocols. Sequential images for each participant were captured and used as input data to generate personal 3D models, using the video-based 3D modelling approach. Bespoke scripts were then applied to obtain corresponding anthropometric data from generated 3D models. When comparing manually measured and video-based 3D modelled anthropometric data, root-mean-square errors for waist and hip girths were both larger than 5 cm. As such, the accuracy of video-based 3D modelled anthropometric data was lower than existing commercial solutions (e.g. Styku or Fit3D scanners). Further, typical processing time (Azure virtual machine F1s) for generating one individual model exceeded two hours; limiting applications for general purpose or research studies. Whilst computational cost and anthropometric modelling error was relatively high; the use of video cameras represents a unique and flexible opportunity for estimating human morphometrics. Therefore, further development, aimed at improving modelling accuracy and processing speed, is warranted.

Acknowledgments: The author would like to thank Terry Senior for helping to develop the data capture system.

References:

[1] *T. Alldieck, M. Magnor, W. Xu, C. Theobalt, and G. Pons-Moll, "Video based reconstruction of 3d people models," in Proceedings of the IEEE Conference on Computer Vision and Pattern Recognition, 2018, pp. 8387-8397.*

[E-06.4]

BIOMECHANICAL MODEL FOR DYNAMIC ANALYSIS OF THE HUMAN GAIT

Claysson Bruno Santos Vimieiro[1], *Jordana Simões Ribeiro Martins*[2], *Diego Henrique Antunes Nascimento*[3], *George Schayer Sabino*[4], *Gabriel Mudadu Carmona Machado*[5]

1 *Graduate Program of Mechanical Engineering, Pontifícia Universidade Católica de Minas Gerais, PUC-Minas, Belo Horizonte, Brazil; Graduate Program of Mechanical Engineering, Universidade Federal de Minas Gerais - Ufmg*
2 *Graduate Program of Mechanical Engineering, Pontifícia Universidade Católica de Minas Gerais, PUC-Minas, Belo Horizonte, Brazil*
3 *Graduate Program of Mechanical Engineering, Universidade Federal de Minas Gerais – Ufmg, Brasil*
4 *Graduate Program in Rehabilitation Sciences, Universidade Federal de Minas Gerais – Ufmg, Brasil*
5 *Department of Mechanical Engineering, Pontifícia Universidade Católica de Minas Gerais, Puc-Minas, Brasil*

Biomechanical models are important tools in the study of human motion. The human body can be defined as an articulated system in complete static or dynamic equilibrium, where internal forces produce joint movements in the body segments. This work proposes a biomechanical model for the dynamic analysis of the lower limbs during human gait, with continuous cycle. The model uses kinematic and kinematic data collected from seven volunteers, with no history of pathology related to human gait, walking under an instrumented treadmill with controlled speed. The proposed model was developed in MotionView software (Altair Hyperworks) and is based on a kinematic chain to represent the segments of the body, connected by rotational joints with defined viscoelastic parameters (Fig 1). The geometry of the model is similar to the human skeleton, with dimensions based on the anthropometric data of the volunteers, and agglomerates in 8 segments, upper limbs, hips, thighs, legs and feet. The kinematic data were captured by Qualisys® motion analysis system with 8 cameras and were used to determine the joint angles, using Cardan's angular theory. The ground reaction forces were collected by force platforms installed under the belt of the instrumented treadmill. The model is able to dynamically analyze joint movements to identify variations in gait pattern and to evaluate the resulting forces and torque in the joints. To validate the model, the results was compared with previously published data in the literature. The results show the same pattern and range of values found in the literature for human gait movement.

Figure Caption: Figure 1 - Representation of the body segments in the MotionView model.

Acknowledgments: The authors are grateful for the financial support by PUC-Minas, FAPEMIG and CAPES (Coordenação de Aperfeiçoamento de Pessoal de Nível Superior – Brazil) - Finance Code 001.

References:

VIMIEIRO, C., ANDRADA, E., WITTE, H., PINOTTI, M. "A computacional model for dynamic analysis of the human gait". Computer Methods in Biomechanics and Biomedical Engineering, 2015.
RIBEIRO, J. S.; VIEIRA, F. G.; RIBEIRO, J.M.S., VIMIEIRO, C. B. S. "Analysis of forces and angles of the lower member's articulations during the human gait". In: 24rd ABCM International Congress of Mechanical Engineering, Curitiba, Brazil. 2017.
LIU, T., INOUE Y., SHIBATA, K., SHIOJIMA, K. "A Mobile Force Plate and Three-Dimensional Motion Analysis System for Three-Dimensional Gait Assement". IEEE Sensor Journal, Vol. 12. 2012.

[E-06.5]

THE EFFECT OF NON-LINEAR SPRING-LOADED KNEE ORTHOSIS ON LOWER EXTREMITY BIOMECHANICS

*Christine Walck[1], Tyler Farnese[2], **Yeram Lim**[2], Victor Huayamave[2], Todd Furman[3], Daryl Osbahr[3]*

1 *Embry-Riddle Aeronautical University, Daytona Beach; U.S. Naval Research Laboratory, USA*
2 *Embry-Riddle Aeronautical University, Daytona Beach, USA*
3 *Department of Sports Medicine, Orlando Health, USA*

The current solutions to common knee problems consist of total knee replacement, and use of knee orthotics [1]. However, the biomechanical effects of various knee orthotics have not been quantified. Our study aims to quantify the biomechanical response of the tibiofemoral joint complex to a newly proposed non-linear spring-loaded knee joint orthosis (KJO).

For this study, electromyography (EMG) sensors, marker based motion capture, and a single force plate were used to evaluate the lower extremity dynamics of a subject during a squatting motion. The computational study used a customized Opensim musculoskeletal model (Figure 1) to analyze the effect of the KJO on lower extremity joints range of motion using inverse kinematics. Static optimization allowed the individual forces around the knee joint to be estimated.

Preliminary results show anterior translation of the knee axis during descent and posterior translation during ascent without the KJO. Although similar, a decrease of anterior translation during descent is observed with the KJO, as well as a posterior translation of the pelvis. An increase in tension in the gluteus maximus (Figure 2) may explain this difference, to which the pelvis translates to maintain balance.

A forward knee translation of the knee joint axis as the subject descends is observed without the KJO, while, with the KJO, the axis translates forward during descent, then stabilizes as the pelvis translates posteriorly. At 60° of knee flexion, the tension in the quadriceps is neutralized by the posterior chain musculature, like the hamstrings and gluteus muscles. At angles deeper than 60°, the posterior chain controls the movement. The hallmark feature of this movement synergy is a more posteriorly oriented pelvis at angles below 60°, whereas a quadriceps dominant strategy will bring the pelvis into a more anteriorly oriented position.

One additional effect of a quadriceps dominant synergy will be increased soleus forces to stabilize the tibia on the talus due to the anteriorly displaced center of mass (Figure 3). A synergy that employs more posterior chain musculature will reduce soleus activation due to a posterior shift in the subjects weight.

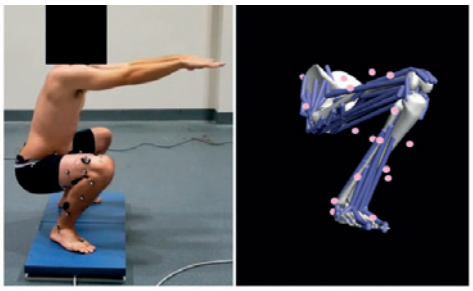

***Figure 1:** Subject and Opensim Musculoskeletal model comparison*

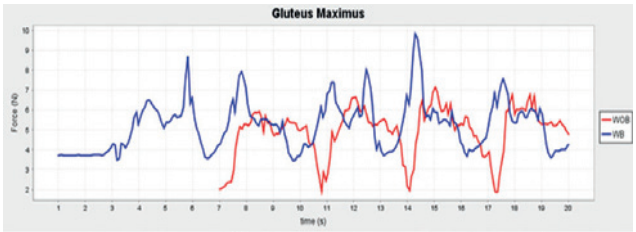

***Figure 2:** Forces of the Gluteus Maximus with and without the brace (w/ brace starts at 3.4 s and w/o brace starting at 7 s)*

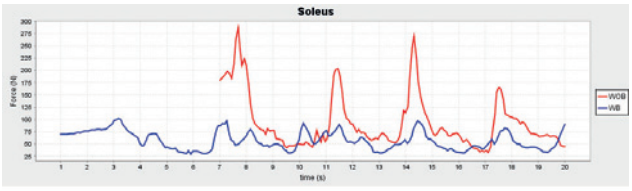

***Figure 3:** Forces of the Soleus with and without the brace (w/ brace starts at 3.4 s and w/o brace starting at 7 s)*

From the data collected, a change in muscle forces is observed. Such results show the KJO decreases the muscle forces surrounding the tibiofemoral joint, while creating an increase elsewhere, proving effective in aiding muscular offloading about the knee joint. Further research will show the effects of the knee orthosis on a larger population, and, with periodic re-evaluations, a difference in further augmentation.

References

1. *B. S. Gardiner et al, "Predicting Knee Osteoarthritis," Annals of Biomedical Engineering, vol. 44, (1), pp. 222-23*
2. *Dahlkvist, N J, et al. "Forces during Squatting and Rising from a Deep Squat." Engineering in Medicine, vol. 11, no. 2, 1982, pp. 69–76., doi:10.1243/emed_jour_1982_011_019_02.*

[E-06.6]

SCAPULAR AND HUMERAL ELEVATION PATTERNS USED BEFORE VS. AFTER REVERSE TOTAL SHOULDER ARTHROPLASTY

Antonia Zaferiou[1], *Christopher Knowlton*[2], *Sukhwan Jang*[3], *Bryan Saltzman*[4], *Gregory Nicholson*[2], *Anthony Romeo*[5]

1 *Stevens Institute of Technology, Hoboken, USA*
2 *Rush University Medical Center, Chicago, USA*
3 *Inje University Seoul Paik Hospital, South Korea*
4 *Orthocarolina Sports Medicine Center, North Carolina, USA*
5 *Rothman Orthopaedic Institute, Pennsylvania, USA*

The purpose of this study was to develop robust ways to non-invasively measure and evaluate shoulder muscle activation and kinematics used by reverse total shoulder arthroplasty (RTSA) patients before and after surgery during activities of daily living (ADL). Among additional hypotheses, we expected that during arm elevation tasks performed post-operatively: (1) the "shrug compensation" would be used less, quantitatively identified with less scapulothoracic (ST) upward rotation at low humerothoracic (HT) elevation angles and (2) there would be greater HT elevation range of motion (ROM) vs. pre-operatively. 15 pre-operative RTSA patients volunteered in accordance with the IRB to undergo optical motion analysis during scapular-plane arm elevation "scaption" ROM tasks and ADL (Optitrack, OR, USA). To date, four of these patients returned to the lab six months post-operatively. Patients were asked to perform each task three times and pain scores were monitored using a visual analog scale. An acromion marker cluster (AMC) was used to track the scapula [1,2]. ISB-recommended conventions were used to calculate HT and ST orientations [3]. 1-D statistical parametric mapping (via paired t-test) compared ST upward rotation before vs. after surgery for each patient across the common range of HT elevation measured both before and after surgery.

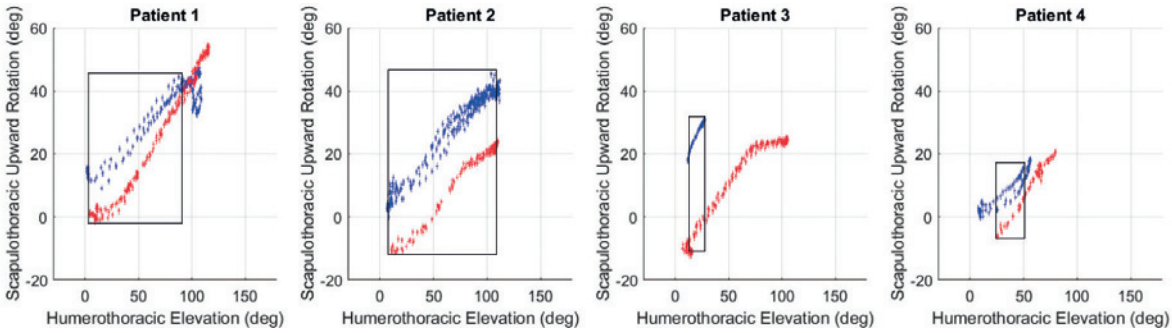

Figure Caption: ST upward rotation vs. HT elevation during the elevation phase of three repetitions of scaption performed by four patients pre-operatively (blue) and post-operatively (red). +/- 1 degree bars are displayed about each data point and 0.1s elapsed between each data point. Boxed subphases indicate p<.001 differences in ST upward rotation before vs. after surgery.

All four patients used statistically lower ST upward rotation at <50° HT elevation angles post-operatively vs. pre-operatively. This could be attributed to successful rehabilitation to avoid the shrug compensation strategy, even during resting posture. Further testing is needed to confirm this hypothesis as more patients participate post-operatively. Post-operatively, Patients 3 & 4 achieved greater HT elevation ROM vs. pre-operatively. Patients reported lower pain scores post-operatively vs. pre-operatively. Pain scores may not be qualitatively robust, however, the diversity in pain scores vs. shoulder ROM measured in this study merits further research about how pain affects motion in this population. Additional research within the scope of this study is focused on: muscle activation patterns (and corresponding normalization methods), AMC measurements vs. calibration poses, and how shoulder control and dynamics differ across ADL.

Acknowledgments: The authors thank the research participants, research coordinators, research assistants and funding from: the Cohn Fellowship (PI: Zaferiou), philanthropic donations to Rush University Medical Center, Chicago, United States, Mid-America Orthopaedic Association (PI: Saltzman).

References:

[1] *Warner M. et al. (2012). Hum Movement Sci, 31: 386-396.*
[2] *Rapp E. et al. (2017) J Biomech, 61: 269-274.*
[3] *Wu G. et al. (2005). J Biomech, 38: 981-992.*

[E-07.1]

EVALUATION OF A 1-DOF HAND EXOSKELETON FOR NEUROMUSCULAR REHABILITATION

Xianlian Zhou[1], ***Ashley Mont***[1], *Sergei Adamovich*[1]

1 *New Jersey Institute of Technology, Newark, USA*

Recently, many robotic hand rehabilitation systems have been introduced to help stroke patients recover hand function through repetitive training1-3. We developed a low-cost 1-DOF hand exoskeleton for neuromuscular rehabilitation of individual fingers. This exoskeleton consists of a base equipped with a servo motor, an index finger part, and a thumb part, connected through gears (Figure 1). The index and thumb parts have rings for the fingers and a tri-axial load cell is attached to the index ring. To help users with muscle weakness during training, an admittance control paradigm is designed for providing intuitive control and positive force amplification to assist the user's finger movement. This admittance control transfers the force measured from the load cell into motion of an end-effector mass (at the index ring) in the task space, through a step-wise integration of the forced acceleration. To evaluate the effects of different control parameters on neuromuscular response of the fingers, such as mass and damping coefficients of the end-effector and feedback control parameters of the motor control torque, we built an integrated hand and exoskeleton model as shown in Figure 1b. The hand model has five index finger muscles including: flexor digitorum superficialis (FDS), flexor digitorum profundus (FDP), extensor digitorum communis (EDC), extensor indicis (EI) and first dorsal interosseous (FDI). The exoskeleton is controlled by a proportional derivative (PD) controller that computes a joint torque ( ) to track a desired joint angle ( ), which is obtained from an inverse kinematics calculation based on the end-effector mass position. We conducted parametric simulations of the exoskeleton in action, driven by the fingers' closing and opening movements, with different proportional gains and end-effector mass and damping coefficients. We compared the interaction forces between the index finger and the ring in both passive and active modes. The passive mode has the largest force close to 4N while the best active case has a maximum force less than 1N, clearly indicating substantial assistance. As a result, the muscle activations of the flexors and extensors were reduced significantly. Currently, an experimental study is being conducted to calibrate model parameters and validate the simulation predictions. The fingers' angular displacement, force measured from the load cell, and muscle EMG are being collected for model calibration and validation.

Figure 1 Caption: (a)The hand exoskeleton and (b) its model; Muscle activation during finger (c) closing and (d) opening.

(a) *(b)* *(c)* *(d)*

Acknowledgments: NIDILRR Grant #90RE5021-01-00.

References:

1. *Adamovich SV, et al. JNER, 2009, 6:28*
2. *Heo P. et al. IJPEM, 2012;13(5):807-824*
3. *Thielbar, KO, et al. JNER, 2014, 11:171*

[E-07.2]

COMPUTATIONAL PREDICTION OF GRASP PERFORMANCE ON A COMPLIANT SURFACE DURING ALTERED VISUAL OPERATION

Raviraj Nataraj[1], *Sean Sanford*[1], *Mingxiao Liu*[1], *Samuel Wilder*[1], *Corrine Rybarski*[1]

1 *Stevens Institute of Technology, Hoboken, USA*

Introduction: The objective of this study is to verify accurate prediction of grasp force performance on a compliant surface under systematic changes in visualized operation. Characterizing dependence of grasp performance and visual operation would indicate how best to present operation to the user for improving function. This work would have implications to visual-based rehabilitation involving virtual-reality (VR) to accelerate motor function or operational tuning of sensorimotor-activation devices for amputation [1] or spinal cord injury [2].

METHODS – Grasp force data were collected from 18 able-bodied subjects (age = 20.9+/-3.1 years) consented for this protocol approved by the local institutional review board. Subjects applied precision pinch (index finger and thumb) grasp onto a force-sensing apparatus with compliant surface [3]. The compliant surface motivated greater dependence on visual feedback by introducing proprioceptive uncertainty in grasp posture. The task-objective was to visually match a real-time trace of total grasp force to a target force ramp (5 N over 4 sec). Performance was assessed as minimizing the average error between the force trace and ramp. The force trace was displayed under five different operational conditions: (1) matching actual applied force, (2) lagging actual force by 50%, (3) increased by 50% over actual force, (4) having noise (bounded over –/+ 0.5N), (5) increasingly follows ramp regardless of subject force-input. Data for agency, subject perception of control, were also collected [4].

RESULTS and DISCUSSION (current and future work) – Greatest agency and performance were observed for condition (5), which differs from our findings for a solid grasp surface [5]. Agency and performance were still positively related ($p < 0.05$, linear regression slope) just as previous force and VR motion experiments [5]. Currently, we are creating computational constructs using machine learning (e.g., artificial neural network) to predict future force errors from windows (10 to 100 msec) of visualized force trace and previous force errors. We expect this study to inform how operational control of an assistive device may be modified online to improve functional performance and augment cognitive agency across user and device.

Acknowledgments: Shaefer School of Engineering and Science at Stevens Institute of Technology, Hoboken, United States. Grant #PC 53-19 from New Jersey Health Foundation.

References:

[1] Marasco et al, Sci Trans Med, 2018
[2] Nataraj et al, IEEE TBME, 2013
[3] Nataraj et al, J Biomech, 2015
[4] Moore et al, Consc Cogn, 2012
[5] Sanford & Nataraj, Annual Meeting for ASB, 2018

[E-07.3]

MODEL BASED PREDICTIVE CONTROL APPLIED TO PROSTHETIC HANDS

Jose Vicente García Ortiz[1], *Jesús Cantero-Ramis*[1], *Marta C Mora Aguilar*[1], *Antonio Pérez-González*[1]

1 *Universitat Jaume I (Uji), Castellón, Spain*

In this study, a comparison between different model based predictive control algorithms (MBPC) for prosthetic hands and the PID controllers is presented. Simulations were carried out in MATLAB Simulink, using an identified CARIMA model of the movement of the proximal phalange of the index finger. The movement data were registered by using a BruJa prosthetic hand [1], which was actuated by a bar mechanism, and optical sensors were placed in the hand's phalange. The obtained model consists of a two-order system with a zero and an integrator (type I system). From the step response of this system, a classic PID controller is set by the Ziegler-Nichols [2] tuning parameters method. The performance of the PID control is evaluated and compared to the performance of the system when using the Generalized Predictive control (GPC) [3]. The GPC controller is implemented with the future set point considered unknown as well as with this set point included in the optimization process. However, the GPC control algorithms are based on linear models and the system has not a linear behavior. Thus, a linear schedule algorithm is programmed based on a piecewise linear system identification. For the evaluation of the different control algorithms, a cost function (J) considering the error and the control effort is used. In addition to the cost, the temporal response of the different control strategies including a white noise disturbance (Figure 1) is studied. Results show that GPC controllers with no future reference provide a much lower overall cost (J=9.67) than classic PID controllers (J=69.69) but It is slightly slower and provide a greater error but lower control effort. Furthermore, GPC controllers with the future set point included in the optimization process present even lower overall cost (J=5.308) while improving the temporal response of the classic PID controllers. Concerning the noise response, the GPC controllers show the best performance regardless of whether the future set point is unknown or if this set point is included in the optimization process.

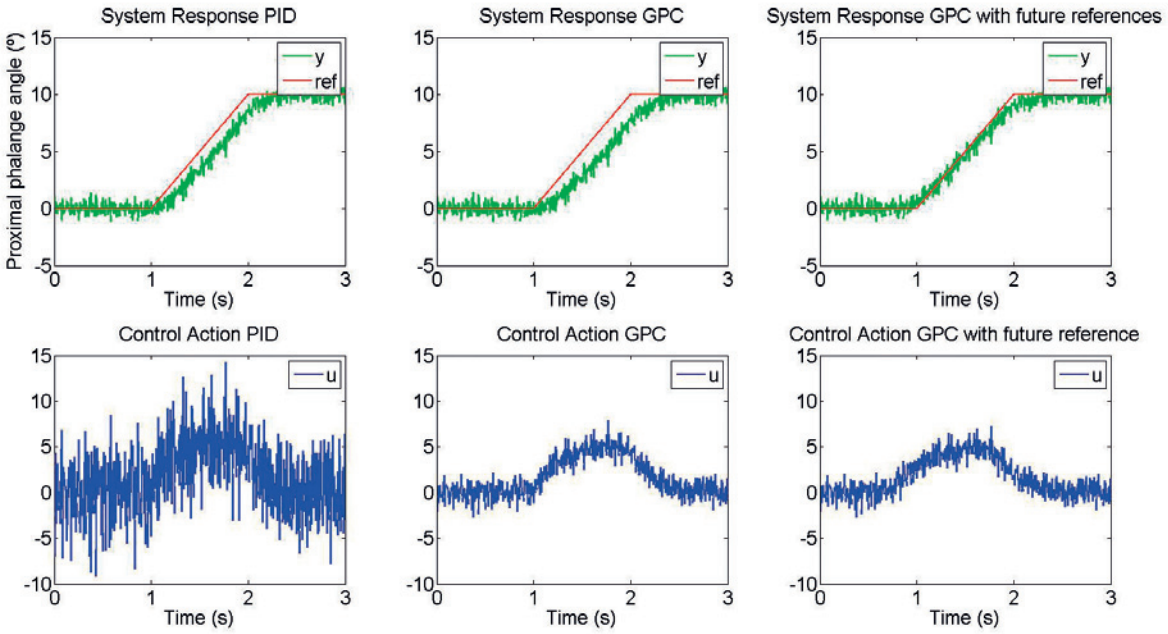

Figure 1: Temporal response of the system with PID control (left), GPC control (center) and GPC control with future reference (right.)

Acknowledgments: This work was financed by the Valencian Community and the Spanish Ministry of Economy and Competitiveness through the GV/2018/125 and DPI2017-89910-R projects respectively.

References:

1. *F. Javier Andrés et al., J.Mechanisms Robotics 11(1), 011018, 2018*
2. *J. B. Ziegler et al., ASME Transactions, v64 (1942), pp. 759-768.*
3. *Clarke D.W. et al., Automatica, Vol. 23 No.2, pp. 137–160, 1987.*

[E-07.4]

A NEW MUSCULOSKELETAL ANYBODY DETAILED HAND MODEL VALIDATED BY ELECTROMYOGRAPHY

Maximilian Melzner[1], *Lucas Engelhardt* [2], *Linda Havelkova* [3], *Ulrich Simon*[4], *Sebastian Dendorfer*[5]

1 *Laboratory for Biomechanics, Ostbayerische Technische Hochschule (OTH); Regensburg Center of Biomedical Engineering, Oth and University Regensburg, Germany*
2 *UZWR, Ulm University, Germany*
3 *New Technologies Research Centre, University of West Bohemia (Uwb), Czech Republic*
4 *Scientific Computing Center Ulm (Uzwr), Ulm University, Germany*
5 *Laboratory for Biomechanics, Ostbayerische Technische Hochschule (OTH); Regensburg Center of Biomedical Engineering, Oth and University Regensburg; Laboratory for Biomechanics, Ostbayerische Technische Hochschule (OTH) Regensburg, Germany*

The AnyBody™ Modelling System (AMS) is an universally used musculoskeletal simulation software using inverse dynamics. Until now, no complete human hand model is realized in the AMS. Considering other musculoskeletal hand models [1], no validation based on dynamic movements has been investigated yet. The aim of this work is to implement a full detailed hand model for the AMS including all extrinsic and intrinsic muscles using data from an anatomic study. For validation purposes, the calculated muscle activities are compared to electromyographic (EMG) data.

Muscle are modelled using 3-Element Hill type representation. Obstacle methods, which utilize tori and spherical ellipsoids, are used for anatomical modeling of the muscle paths. Moreover, a unique feature of the model is the origin point of the lumbrical muscles within the tendons of the flexor digitorum profundus. A study with 47 patients was elaborated to determine the average relation between each phalangeal bone and the hand length to provide a subject specific scaling of the model. To express the strong dependence between the distal and proximal interphalangeal joint a finger rhythm according to van Zwieten [2] can be utilized, if motion data lacks information. For motion capturing (MoCap) a Vicon system with a new marker setup was used (Figure 1). The EMG-sensors recorded ten extrinsic and intrinsic muscles during muscle specific activation movements.

For each movement the calculated on- and offset of the muscle activities were compared to the experimental data. Figure 2 shows exemplarily the investigated activation of the extensor carpi ulnaris muscle during an abduction of all fingers (three times). The results indicate that not only the on- and offset timing correlates well, but also the trend validation shows comparable outcomes.

Nevertheless, the EMG measurements, which are only a possible rejection and not a verification of a model [3], show no reason to decline our model due to the good correlation of muscle activity. To prove the stability of the proposed model, future work will include a Monte Carlo sensitivity analysis of parameter variations.

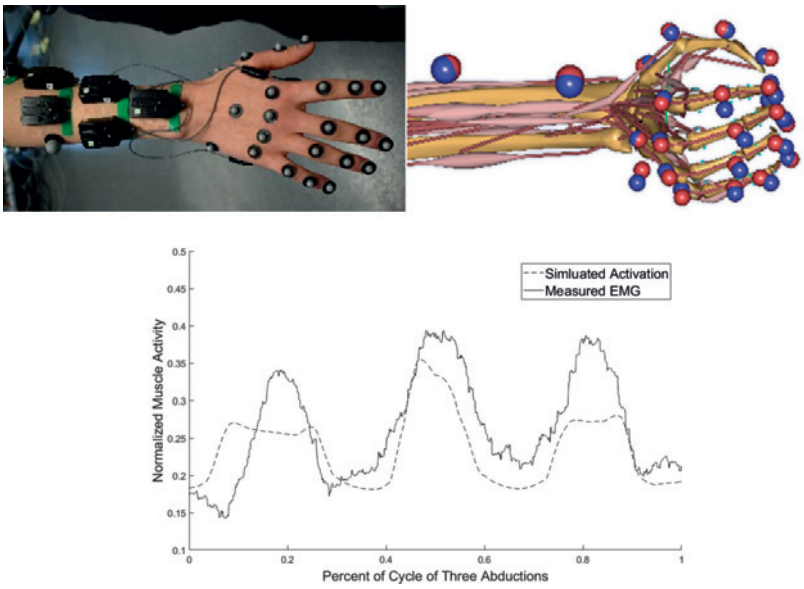

Figure Caption:
Figure 1: Experimental marker and sensor placement and MoCap model of the human hand.
Figure 2: Muscle activation of the extensor carpi ulnaris muscle during abduction of all fingers three times in a row.

Acknowledgments: Maximilian Melzner and Lucas Engelhardt contributed equally to the abstract and share first authorship. Funding from the SNF (320030L_170205), DFG (SI 2196/2-1, IG 18/19-1) and FWF (I 3258-B27) for the DACHFX Project and funding from the EFRE, Ziel ETZ BY-CZ 2014-2020 (Interreg V) (Pr. 182) BayWISS is gratefully acknowledged.

References:

[1] Mirakhorlo et al., Int Biomech, 3:1, 40-49, 2016
[2] Van Zwieten et al., Acta Bioeng Biomech, 17:1, 2015
[3] Lund et al., Proc Inst Mech Eng, 226:82–94, 2012

[E-07.5]

RECURSIVE ESTIMATION OF THE HUMAN BODY'S CENTER OF MASS AND ANGULAR MOMENTUM DERIVATIVE

François Bailly[1]

1 Laas-Cnrs, Toulouse, France

Introduction: Estimating the body's center of mass (CoM) and angular momentum derivative (AMD) is of great interest in biomechanics. Methods commonly rely on kinematic or kinetic signals [1]. We propose to estimate both the CoM and AMD simultaneously, by recursively fusing kinematic and kinetic signals (Fig.1). We first demonstrate the accuracy of the method in simulation by adding noise to measurements. Then, its efficiency is shown on real human walking data.

Methods: The coupling between the CoM and the AMD computed at the CoM is expressed by: $\mathcal{L}^c=\tau^0+f\times c$ (1).

Where $\mathcal{L}^c$ denotes the AMD, τ^0 and f are the external moments and forces applied to the body and is the CoM. Our recursive algorithm is based on Eq.1, which guarantees that a better estimation of c leads to a better estimation of $\mathcal{L}^c$ and vice-versa. The different sources of information used for estimation are fused together using complementary filtering [2]. The CoM estimation is the combination of: kinetic data, using the double integration of the contact forces; kinematic data using reflective markers and anthropometric tables; the use of the central axis of contact wrench, which links $\mathcal{L}^c$ and c [3]. The $\mathcal{L}^c$ estimate is the combination of: kinematic data using the velocities and moment of inertia of each segment; kinetic data using Eq.1. At each step, the equations are recomputed and c and $\mathcal{L}^c$ are updated using the new estimates.

Results: In simulation, the average absolute error of the kinematic estimate on the vertical axis was of 3.6cm, whereas it was reduced to 1.1cm thanks to our method. In the lateral direction, the average absolute error was reduced from 2.1cm to 0.29cm. On human walking data, the difference between kinematic estimation of the CoM and our method was of the same order of magnitude, suggesting an improvement towards ground truth.

Discussion-Conclusion: Simulations show that using the proposed scheme, a precise estimation of both the AMD and the CoM can be obtained. The application of the method on real data is promising for future biomechanics studies or for benchmarking anthropometric tables which are currently the most common approach for estimating the CoM.

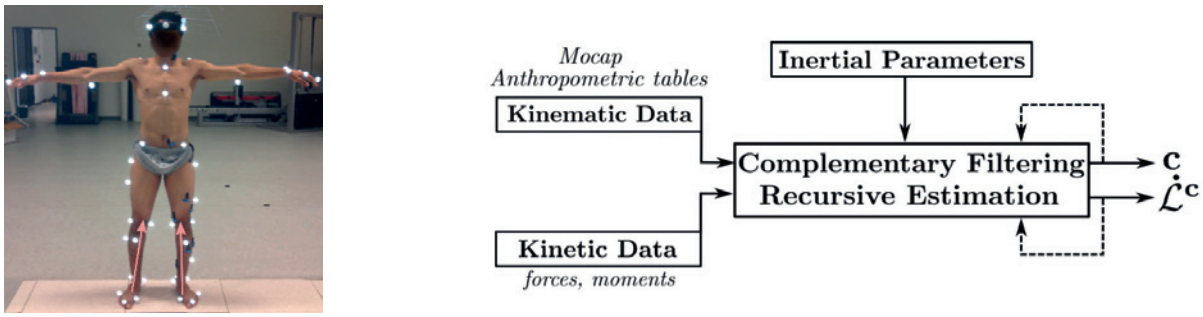

Figure Caption: Fig. 1: a) Picture of the experiment. b) Simplified sketch of the estimation framework.

References:

[1] Lafond D, Duarte M, Prince F. Journal of biomechanics 37(9), 2004: 1421-1426. https://doi.org/10.1016/S0021-9290(03)00251-3
[2] Higgins WT. Transactions on Aerospace and Electronic Systems, 11(3), 1975: 321–325. https://doi.org/10.1109/TAES.1975.308081
[3] Bailly F, Carpentier J, Pinet B, Souères P, Watier B, 7th IEEE International Conference on Biomedical Robotics and Biomechatronics (Biorob), 2018: 350-356. https://doi.org/10.1109/BIOROB.2018.8488125

[E-08.1]

A FORWARD DYNAMICS APPROACH TO EXPLORE THE MECHANICS OF MUSCLE SIZE SCALING IN HUMANS

Geoffrey Handsfield[1], *Marie Balas*[2], *Thor Besier*[3]

1 *Auckland Bioengineering Institute, The University of Auckland, Auckland, New Zealand*
2 *Auckland Bioengineering Institute, The University of Auckland; Sigma-Clermont*
3 *Auckland Bioengineering Institute, The University of Auckland; Dept of Engineering Science, University of Auckland, New Zealand*

The allometry of lower limb muscle sizes in mammals has been of interest for decades [1]. In a study on lower limb muscle volumes in healthy humans in vivo, Handsfield et al. [2] showed that the product of mass and height served as a strong predictor of lower limb muscle volume. In that study, it was hypothesized that a biomechanical relationship governed mass-height scaling: with incremental changes to either mass or height, a proportional increase in muscle volume was necessary to preserve biomechanical function. Forward dynamics simulations offer an opportunity to investigate the underlying mechanics of muscle size scaling in humans. An approach of this nature would allow for an exploration of the relationship between body size, muscle size, and physical or mechanical outputs such as gait speed, jump height, or movement energetics. This could be used to test hypotheses such as the one posed here: that movement similarity (e.g. jump height per body height) is preserved under a mass-height relationship of muscle size scaling, suggesting this relationship is based in the underlying physics of movement.

In this study, we used a jumping model simulated in OpenSim (https://opensim.stanford.edu/) to assess mechanical similarity (jump height per body height) of a standardized jump across variations of height, mass, and lower limb muscle volumes. We used a jumping model scaled to the heights, masses, and muscle architectures of the 24 individuals observed in [2]. Muscle activation profiles were maintained across all models. Muscle lengths were scaled according to model geometry and maximum isometric muscle forces (Fmax) were scaled to preserve the muscle volumes from [2]. We assessed the jump height of each model with and without mass-height scaling of Fmax.

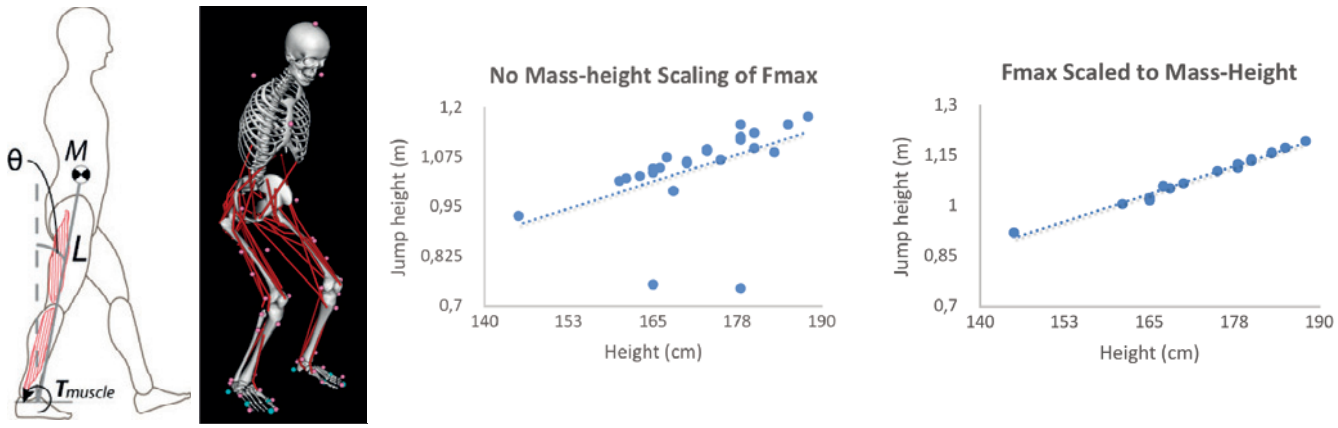

Figure Caption: When Fmax values of the lower limb muscles were unchanged from the default values, there was a poor relationship between jump height and participant height (movement dissimilarity). When Fmax values of the lower limb muscles were scaled according to mass-height, a strong similarity of movement was observed, indicating that the scaling law is consistent with the physical requirements underpinning the movement.

In this study, we performed forward dynamic simulations of jump height to explore the effects of scaling muscle size to the mass and height of the model. Our results suggest that there is a physics-based underpinning to a mass-height scaling of muscle volumes. Further exploration of other potential relationships is warranted. Forward dynamics is a useful tool to explore biomechanical size scaling relationships in humans and animals.

Acknowledgments: We would like to thank Thorben Pauli for his assistance and code for Fmax scaling of lower limb muscle volumes.

References:

[1] R.M. Alexander et al., J Zoology 194(4): 539-552, 1981.
[2] G.G. Handsfield et al., J Biomech 47(3):631-638, 2014.

[E-08.2]

VALIDATION OF MICROMECHANICAL MUSCLE MODELLING TECHNIQUE TO PREDICT MUSCLE MEMBRANE STRAIN

Emily Miller[1], *Rachel Bour*[1], *Kate Bukovec*[2], *Daniel Fathalikhani*[2], *Robert Grange*[2], *Silvia Blemker*[1]

1 *Department of Biomedical Engineering, University of Virginia, Charlottesville, USA, Charlottesville, USA*
2 *Department of Human Nutrition, Foods, and Exercise, Virginia Tech, Blacksburg, USA*

Introduction: Computational models provide a powerful paradigm to understand muscle degeneration and explore possible treatment approaches for Duchenne muscular dystrophy (DMD). Recently, finite element (FE) models of skeletal muscle microstructure were developed to explain the susceptibility of DMD muscles to contraction-incurred damage[1]. However, validation of micromechanical models to predict damage from muscle contractions in both healthy and diseased muscle has yet to be completed. The goals of this study were to: (i) create histological-based FE models of healthy and diseased muscle cross-sections, and (ii) compare the muscle membrane strains derived in the FE models to a histological measure of membrane disruption.

Methods: Intact soleus and EDL muscles from wild type (wt) and mdx (model of DMD) mice were subjected to an in vitro eccentric contraction injury protocol. After the protocol, muscles were incubated with the fluorescent dye procion orange and sectioned to assess uptake through leaky fiber membranes as an index of membrane damage. Sections were also stained with laminin-α2 antibody to define fiber sarcolemmal membranes. An image segmentation algorithm was developed to outline the membranes to distinguish the individual fibers. The number of fibers displaying dye uptake was quantified using a custom thresholding algorithm and validated within the error of a manual count. Muscle fiber and ECM areas from the segmented image were mapped onto an initialized FE mesh. Nonlinear elastic springs were incorporated into the models to represent both the presence (in wt) and loss (in mdx) of transmembrane proteins[1]. Boundary conditions were assigned to the FE model to prescribe a simple shear deformation experienced during an eccentric muscle contraction[1]. FE models were run in FEbio, averaged 350,000 elements and required approximately 30 minutes of solution time on a 240 GB computing cluster. Membrane strain was calculated using methods described in [1]. The number of fibers that demonstrated uptake of procion orange dye served as the experimental index of muscle damage[2].

Results and Conclusions: There was a positive correlation (Fig. 1D) between predicted membrane strain and procion orange dye uptake ($p < 0.01$). The results suggest that micromechanical muscle models are predictive of membrane damage in both healthy and diseased muscles. This model-experiment integration provides a framework to determine micro-scale damage from microstructure images and could be used to ultimately predict the effects of pharmacological treatments on the susceptibility of DMD muscles to damage.

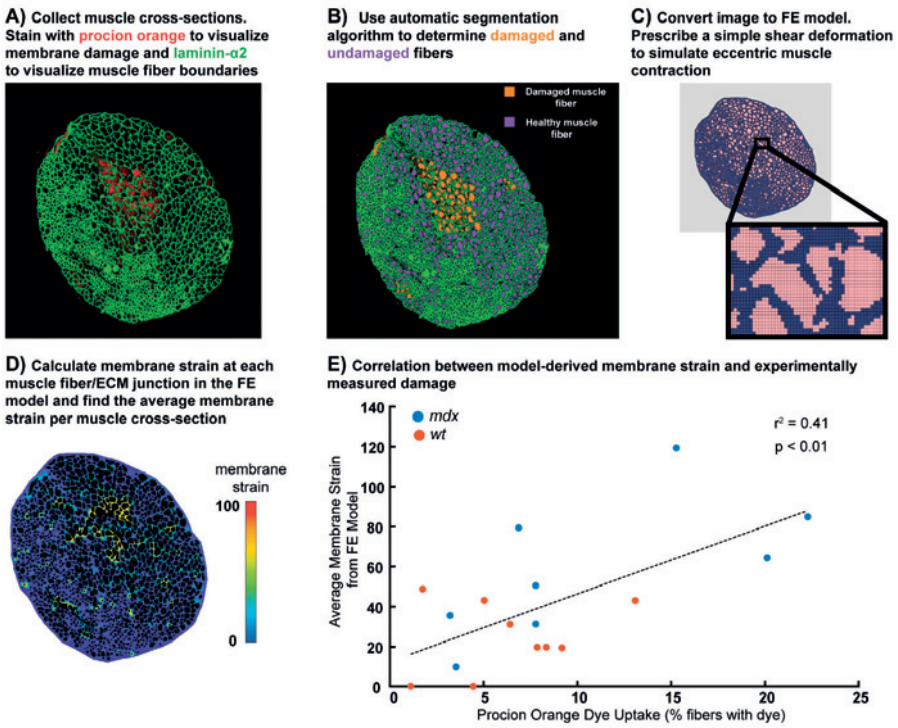

Figure 1: A) Muscle cross-sectional images were B) segmented to determine dye uptake and C) image-based FE models were created to calculate D) membrane strain and E) simulation derived membrane strain was compared to dye uptake.

Acknowledgements: The authors acknowledge Shayn Peirce-Cottler and grant #1U01AR069393.

References:

[1] *Virgilio et al. (2015). Interface Focus, 5(2),20140080.*
[2] *Consolino and Brooks. (2003). J Appl Physiol, 96:633–638.*

[E-08.3]

LEADING THE MUSCLE PATH: A VIA-ELLIPSE APPROACH FOR THREE-DIMENSIONAL MUSCULOSKELETAL MODELS

Maria Hammer[1], *Michael Günther*[2], *Daniel F.B. Haeufle*[3], *Syn Schmitt*[4]

1 *Computational Biophysics and Biorobotics, University of Stuttgart; Stuttgart Centre for Simulation Sciences (Sc Simtech), University of Stuttgart, Germany*
2 *Computational Biophysics and Biorobotics, University of Stuttgart, Stuttgart, Germany*
3 *Multi-Level Modeling in Motor Control and Rehabilitation Robotics, Eberhard-Karls University Tübingen*
4 *Computational Biomechanics and Biorobotics, University of Stuttgart; Stuttgart Centre for Simulation Sciences (Sc Simtech), University of Stuttgart, Germany*

Representing anatomical muscle paths is a key factor in physiological musculoskeletal modeling when describing muscles as strands. Muscle routing largely affects the torque exerted by a muscle about the joints it spans: On the one hand, muscle length and length changes influence the muscle force along the muscle's line of action, and, on the other hand, the path geometry has a major impact on the muscle moment arm. Consequently, a correct representation of muscle paths is mandatory in every biomechanical simulation containing strand-like muscles. The path modeling is particularly challenging for three-dimensional and high-amplitude motions, as the use of current muscle routing methods, which are commonly based on muscle wrapping around obstacles and the use of body-fixed via-points, is often restricted to essentially two-dimensional motions or can only represent anatomical muscle moment arms in small amplitude motions.

We, thus, introduce the via-ellipse approach, a novel computational algorithm for three-dimensional modeling of the muscle path. This algorithm overcomes some of the current limitations of muscle routing whilst being easy to implement even for complex muscle path geometries. It is based on the premise that muscle strands can move freely in a certain volume during motion. Anatomical constraints on the muscle path may be imposed by bones, surrounding soft tissue such as underlying muscles, tendon sheaths and the skin. These constraints are modeled as elliptical areas the muscle has to pass [1], see Figure 1a. Muscles are assumed to be massless, viscoelastic elements, moving frictionless in the ellipses and along the ellipses' inner edges. Being under permanent tension, the muscle's line of action is defined as the shortest path from origin to insertion through all ellipses. Whenever the path is redirected by an ellipse (in the current joint configuration), a via-point is set at the ellipse edge. The via-points are dynamical, i.e. they may change in number, and their relative position to a body segment with the joint angular configuration whilst ellipses keep their position and orientation constant relative to the body they are attached to.

This approach was used to model the muscles of the human lower limbs, see Figure 1b. We demonstrate for different complexities of muscle path geometries that – by only adjusting ellipse parameters – we are able to achieve physiologically realistic muscle moment arms and lengths for all degrees of freedom of joints and for a large range of angular configurations of uniarticular as well as multiarticular muscles.

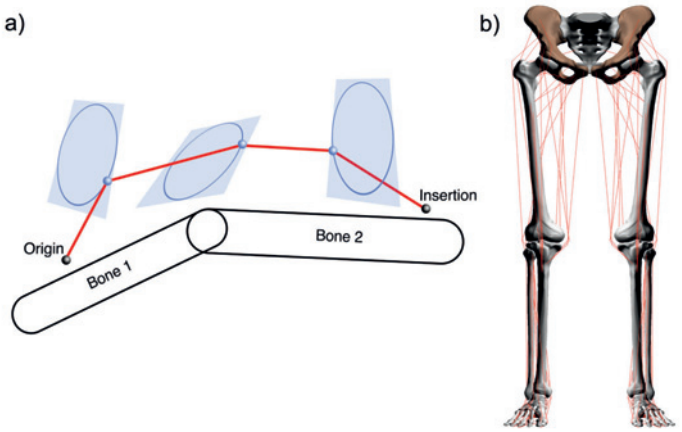

Figure 1: a) Illustration of the via-ellipse approach, leading the muscle path (red) from origin to insertion through elliptical areas. b) Detailed human lower limb model including 122 muscles, which were modeled using up to two via-ellipses per muscle.

References:

[1] Hammer, M. et al., Mathematical Biosciences (in press)

[E-08.4]
INDEX FINGER MUSCULOSKELETAL DYNAMIC MODEL

Jumana Ma'touq[1]

1 *Institute of Automatic Control; Gottfried Wilhelm Leibniz Universität Hannover, Germany*

Introduction: Modelling and simulating the dynamic behaviour of a musculoskeletal system requires a musculoskeletal force model and the transformation from musculotendon forces to joint torques; i.e., the matrix of musculotendon excursion moment arms $\mathbf{R^T(q)}$. In a previous work a musculotendon kinematic model that provides $\mathbf{R^T}$ for a given joint configuration **q** has been proposed [1]. The aim of this work, therefore, is to extend the previous models [1-2] and develop an index finger musculoskeletal dynamic model that serves as a plant in studying human motor control. In particular, the focus of this work is to develop a musculotendon dynamic model and skeletal inverse dynamic model (Figure 1).

Methods: The proposed musculotendon model consists of Hill-type model, which estimates musculotendon force for a given musculotendon lengths $\mathbf{l(q)}$, length change rates $\mathbf{R^T(q)}$, muscle activation $\mathbf{\dot{l}(q, \dot{q})}$, and an activation **u** estimation model, which estimates **u** for a given musculotendon force, joint torque $\boldsymbol{\tau}$, and $\mathbf{R^T(q)}$. In Hill-type model, the parameters were estimated so that the resulted normalised muscle length $\mathbf{\tilde{l}_m}$ is within the operating muscle length and the resulted forces/torques are comparable to experimental data from the literature. In activation estimation model, the summation of $\mathbf{u^2}$ is minimised subject to the minimum difference between the torque resulted from muscle force model $\boldsymbol{\tau}^*$ and the torque from the inverse dynamic model $\boldsymbol{\tau}$. In the inverse dynamic model, the passive torque due to the passive joint properties $\boldsymbol{\tau_p}$ and the link torque due to gravitational and inertial forces $\boldsymbol{\tau_l}$ are modelled.

Results: Using the estimated Hill-type model parameters, the resulted $\mathbf{\tilde{l}_m}$ for all index muscles ranged between 0.97 and 1.03 in resting posture and between 0.5 and 1.5 in flexion/extension task. The resulted $\mathbf{u}^*$ ranged between 0 and 1 and related to the activation/deactivation of muscles during the motion task. The preliminary results show only a little difference **E** between modelled torques ($\underline{\boldsymbol{\tau}^*}$ and $\underline{\boldsymbol{\tau}}$) and previously published measured/modelled torques.

Conclusion: The proposed index finger musculoskeletal dynamic model estimates joint torques, musculotendon forces, and muscle activation for a given motion. A possible reason for **E** is the differences between subjects in this model and in the literature models. These differences affects $\mathbf{R^T(q)}$ and $\boldsymbol{\tau_p}$. Therefore, future work will address 1) enhancing the model to compensate for subjects differences, and 2) modelling and validation of the complete hand musculoskeletal dynamics and human motor control.

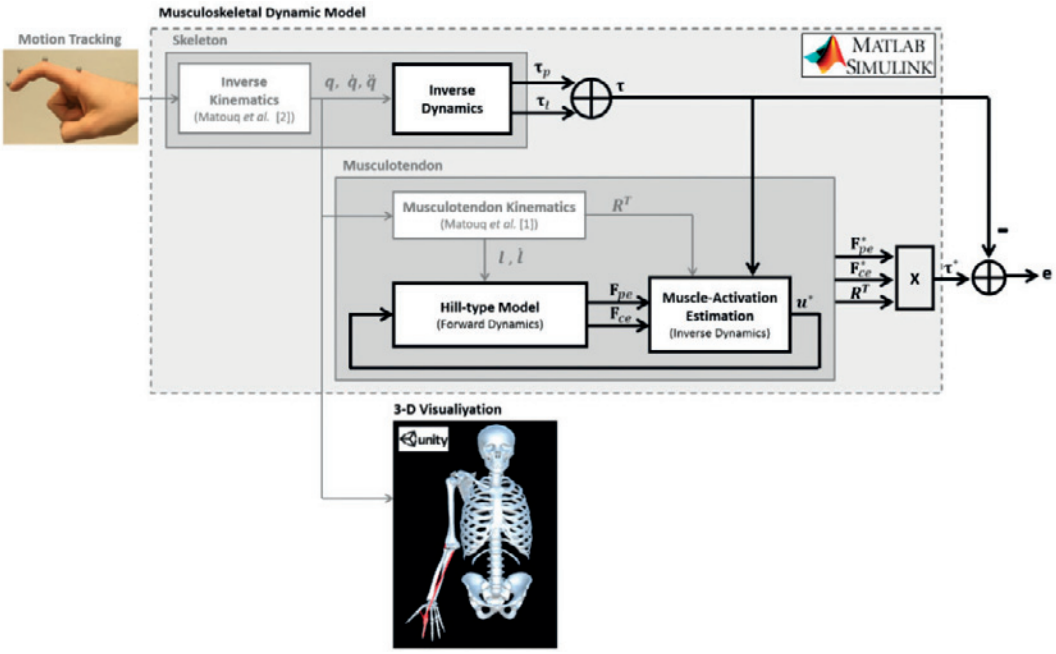

Figure1: The overall musculoskeletal dynamic model of the index finger. The bold blocks represent the models of the current work."

References:

[1] *Ma'touq et al. (2019). A validated combined musculotendon path and muscle-joint kinematics model for the human hand. Revision submitted to CMBBE.*
[2] *Ma'touq et al. (2018). Sub-millimetre accurate human hand kinematics: from surface to skeleton. CMBBE, 21(2):113-128.*

[E-08.5]

MULTIMODAL IMAGE-BASED FINITE ELEMENT MODELING OF THE CRANIOMAXILLOFACIAL SKELETON: THE IMPACT OF 3D MUSCLE ANATOMY

Hanieh Arjmand[1], *Cristina Falcinelli*[2], *Jeffrey Fialkov*[3], *Cari Whyne*[1]

1 *Orthopaedic Biomechanics Laboratory, Sunnybrook Research Institute; Biomaterials and Biomedical Engineering, University of Toronto, Canada*
2 *Orthopaedic Biomechanics Laboratory, Sunnybrook Research Institute, Toronto, Canada*
3 *Institute of Biomaterials and Biomedical Engineering, University of Toronto; Department of Surgery, University of Toronto; Division of Plastic Surgery, Sunnybrook Health Sciences Centre, Canada*

Introduction: Computed tomography (CT)-based finite element (FE) models can accurately represent the complex anatomy and material distributions in the craniomaxillofacial (CMF) skeleton, however, multimodal imaging data may be required for sufficient visualization of the CMF muscular anatomy to enable simulation of physiologic load transmission from muscle to bone. This study aimed to create CMF FE models from integrated CT, magnetic resonance imaging (MRI) and diffusion tensor imaging (DTI) data to evaluate the effects of 3D muscle geometry and fibre architecture on bone stress patterns.

Methods: CT, MRI and DTI were acquired for a single fresh-frozen cadaveric head and co-registered. CT images were deblurred and segmented to reconstruct the CMF skeleton and mandible. The masseter and temporo-mandibular joint (TMJ) disc were segmented from MRI. DTI and fibre tractography were used to reconstruct the 3D fibre bundle arrangement in the masseter. Mesh generation was performed using 10-noded tetrahedra for bone, 4-noded tetrahedra with mixed u-P formulations for the masseter and 4-noded tetrahedra for the TMJ disc. NMAP process-flow was used to map the image-based bone densities to nodal elastic moduli[1]. The mandible was modelled as a rigid body. Transversely isotropic nearly incompressible hyperelastic material properties were assigned to masseter elements with the fibre axis showing the plane of symmetry[2]. Linear elastic isotropic material properties were assigned to the TMJ disc[3]. Bonded contact pairs were defined and boundary conditions applied to restrain the skull. A 5mm displacement was applied to the mandible at the canine teeth. To evaluate the effect of 3D masseter geometry and fibre directions on bone stress patterns, the 3D muscle model was reanalyzed with 2-noded tensile-only link elements (line segments spanning from the origin to the insertion of the masseter, E=2kPa, ν=0.49)[1,4].

Results: Notable differences in compressive and tensile stress patterns were observed in the 3D muscle vs link element loading. The zygomatic arch alone was under tensile stress in the link muscle model whereas high tensile stresses were apparent across the muscle origin in the 3D muscle model. High compressive stress was seen in the zygoma in the 3D muscle model due to bending.

Conclusions: Fibre directionality and muscle-bone contact integrated in the 3D muscle representation impact load transfer to CMF bone. Experimental validation and analysis of a larger cohort of CMF specimens will verify the need for 3D muscle modelling generated from multimodal imaging in accurately representing CMF biomechanical behaviour.

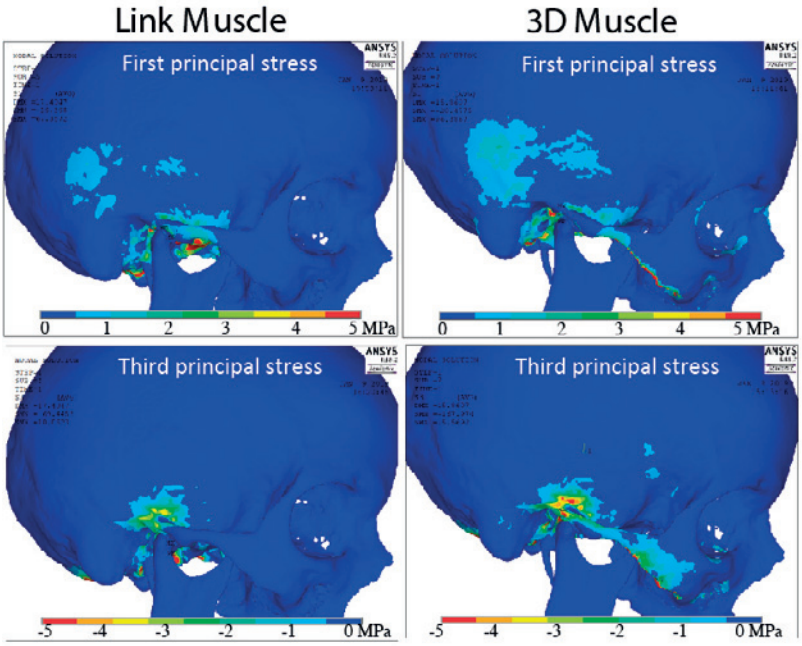

Figure Caption: Figure 1 - Tensile (top) and compressive (bottom) stress results from the link and 3D muscle representations.

References:

Pakdel et al., J Biomech, 49:1454-1460, 2016
Morrow et al.,CMBBE, 13:247-256, 2010
Tanne et al., J Dent Res, 70:1545-1548, 1991
Chen et al., EEE Trans Freq Control, 43:191-194, 1996

[E-08.6]

ASSESSMENT OF A SHOULDER FINITE ELEMENT MODEL TO PREDICT MUSCLE TRAJECTORIES

Marion Hoffmann [1], *Sonia Duprey*[2], *Yoann Lafon*[2], *Mickael Begon*[1]

1 *Laboratoire de Simulation et Modélisation du Mouvement, Faculté de Médecine, Université de Montréal, Laval, Canada*
2 *University Lyon, Université Claude Bernard Lyon, France*

Knowing muscle forces and activations helps to provide a musculoskeletal assessment and thus improve diagnosis and treatment. Since measuring muscle forces is an invasive process, musculoskeletal models can advantageously provide an estimate of muscle forces. In these models, muscle geometry is often reduced to lines of action modeling the main muscular functions. Several shoulder muscles have broad attachment area and complex fibre arrangements that make them challenging to represent only using lines of action. Especially for the deltoid, the use of via-point and wrapping methods is essential but technically difficult for constraining the muscle path for all motions [1]. Three-dimensional finite element (FE) modelling allows to represent muscles with broad attachment areas, to model muscle-muscle and muscle-bone contacts, while accounting for muscle deformation while preserving muscle volume. Thus, we hypothesized that FE model would represent more physiologically the muscular function. Our purpose was to validate a 3D FE model of the shoulder to study moment arm variations within each muscle-tendon unit by predicting their lines of action based on the FE mesh.

A shoulder FE model including major muscles was created based on medical imaging of a participant without history of shoulder pathology or injury. Bones (humerus, scapula and clavicle) were defined as rigid bodies. Muscles (infraspinatus, supraspinatus, subscapularis and deltoids) were modelled using Mooney Rivlin material law [2] and tendons with a linear elastic material law [3]. Automatic contact between surfaces was used to prevent muscles to penetrate the surrounding structures. Muscle fibres were defined as lines of action passing through the middle of the muscle volume. Six lines of actions were included into each rotator cuff muscle and twelve into the deltoid (four lines for anterior, middle and posterior parts each). Movements of abduction, flexion and internal-external rotation were simulated. No muscle activation was considered in these simulations. Moment arms and muscle lengths were calculated and qualitatively compared to a review of literature data [4]. Results were also compared to MRI data from the same shoulder obtained in six additional configurations [5].

Range of moment arms obtained with the FE model matches with those from the literature (see Figure). When comparing with MRI data, a maximum error of 31 mm for moment arms and 14.9% for muscle lengths was observed, except for the configurations higher than 90° in abduction where the errors were up to 36.5 mm for moment arms and 33.4% for muscle lengths. This current FE model, partially validated, could be used to estimate the range of moment arms for motion under 90° elevation. As a perspective, a sensitivity study could be performed to evaluate the impact of tendon insertion area on range of moment arms prediction.

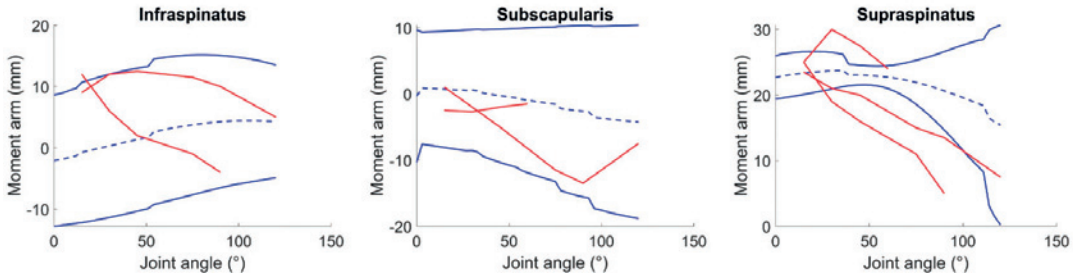

Figure Caption: "Moment arm in abduction from various studies [4] (red line, mean values) and the mean (blue dashed line) and the standard deviation (blue line) from the model".

References:

1. *Webb, J.D. et al,. CMBBE, 2014. 17(8):829-837.*
2. *Stelletta, J., et al.. In Biomechanics of Living Organs: Hyperelastic Constitutive Laws for Finite Element Modeling (Elsevier, pp. 497–521).*
3. *Itoi, E., et al., J. Orthop. Res., 1995. 13(4):578-584.*
4. *Hik, F. et al., J. Anat. 2019. 234(1):1-15.*
5. *Hoffmann, M., et al., CMBBE, 2017. 20(11):1175-1181.*

[E-10.1]

COMBINING COMPUTATIONAL AND EXPERIMENTAL STUDIES IN INJURY BIOMECHANICS: TOWARDS PREVENTION OF SCI, TBI AND HIP FRACTURE

Peter Cripton[1], *Ingmar Fleps*[2], *Tom Whyte*[3], *Duane Cronin*[4], *Matthew B. Panzer*[5], *Benedikt Helgason*[2]

1 *Department of Mechanical Engineering; School of Biomedical Engineering; University of British Columbia, Vancouver, Canada*
2 *ETH Zürich, Switzerland*
3 *University of British Columbia, Vancouver, Canada*
4 *University of Waterloo, Canada*
5 *University of Virginia, Charlottesville, USA*

Researchers in the field of injury biomechanics use experimental and computational approaches to establish the tolerance of biological tissues to injury and in the design and optimization of devices and techniques to prevent injuries. The promise of computational models is that they will one day allow researchers to study any injury using a human body model or a detailed FE model of a segment of the body and to have these models verified and validated to the point that no additional experiments are necessary in order to trust the results. Unfortunately, computational models are not yet validated to the point that an arbitrary injury event can be simulated and the result trusted. Nor is there enough good quality experimental data available to allow this level of validation for the many FE, multi-body dynamic and other computational models that are currently in use. In the setting of injury biomechanics, the materials and structures are undergoing complex, high-rate, nonlinear material and structural responses and failure mechanics. In this setting, one approach that shows promise to accelerate the availability of computational models that are fully validated for injury biomechanics experiments is to combine experimental and computational modelling approaches in a single research project. This has advantages over the more traditional approach where computational modelers use published experimental data for calibration in the development of the model. This requires establishing a collaborative research group that is in frequent communication and includes advanced researchers and facilities capable of both advanced computational and advanced experimental investigations. In our experience, these collaborations often involve multiple institutions. Another advantage of this approach is that it enables researchers to take an iterative process that involves preliminary protocol development experiments and/or computational simulations and these studies can optimize overall experiment and model design and also optimize the applicability of the experiments to the model validation.

We have applied this approach to combined experimental and computational studies in the following contexts which will be presented:

1) Hip fracture: We have conducted matched experimental and computational models of hip fractures under sideways falls. (Figure 1) [1], [2]
2) We have designed matched experiments and theoretical models of the cervical spine under shear load.
3) We have studied brain motion in head impacts of a ferret and used this to validate brain FEM
4) We have studied brain injury associated with skull deformations in a rat model of brain injury and used this to compare to results from and explicit FEM of the skull and brain.

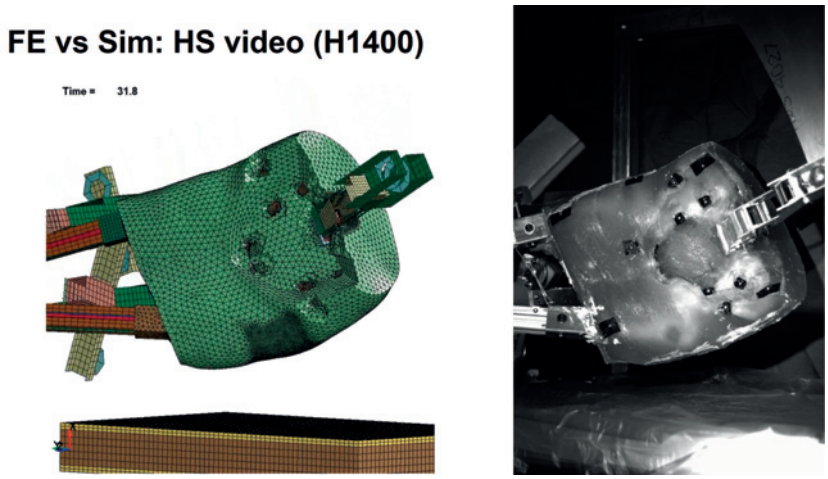

Figure 1: Hip fracture experiment and Explicit FE model.

Acknowledgments: The authors thank the many staff and students at our centres that have contributed to this work but are too numerous to list on this abstract.

References:

[1] *B. Helgason et al., "Development of a balanced experimental–computational approach to understanding the mechanics of proximal femur fractures," Med. Eng. Phys., vol. 36, no. 6, pp. 793–799, Jun. 2014.*
[2] *I. Fleps et al., "A novel sideways fall simulator to study hip fractures ex vivo," PLOS ONE, vol. 13, no. 7, p. e0201096, Jul. 2018.*

[E-10.2]

HUMAN BODY MODELING: A PRIORITY FOR FUTURE VEHICLE SAFETY LANDSCAPE

Saeed Barbat[1]

1 *Ford Motor Company; Research and Innovation Center, USA*

Current vehicle safety landscape and future safety regulatory and technology trends pose significant challenges to the automotive manufactures, policy makers and regulatory agencies. This lecture will briefly touch on trends such as demographics (increasing aged populations and vulnerable vehicle occupants), future mobility, and future regulations and consumer safety rating programs associated with partially or fully automated modern vehicles. These vehicles, fully autonomous ones in particular, will drive new innovations in vehicle interior cabins and a paradigm shift from today's conventional seating configurations. This will demand new state-of-the-art development of restraint, comfort, and convenience technologies. Some of the current safety standards (e.g., FMVSS and ECE), associated protocols, and safety performance evaluations may require revisions or interpretations from regulatory agencies. In addition, the Anthropomorphic Test devices (ATD)s and their associated injury metrics used in current safety evaluations and regulatory certification may not be fully capable in evaluating occupant responses in seating, postures, and orientation different than those in conventional seating. Regulatory agencies, vehicle manufacturers and ATD manufacturers are initiating research and testing with existing and modified ATDs, and Post Mortem Human Surrogates (PMHS), to better understand biomechanical responses and to help develop new or modified ATDs and associated injury criteria. This research is ongoing and may not be completed in the near term.

Human Body Models (HBM), enabled by Finite Element Analysis (FEA), may have the potential to help better understand the biomechanical responses of occupant's in future autonomous vehicles with and without non-conventional seating configurations. These HBMs may also help research ways to reduce the risk of injuries to those occupants in crashes through the development and evaluation of new restraint innovations. Future U.S. and Euro NCAPs (New Car Assessment Program) may include additional body regions and new injury criteria in safety performance evaluations. HBM applications in developing risks curves and research into new injury criteria are deemed necessary to address future safety evaluations, the increasing aged population with increasing exposures, and exploring new injury criteria for vulnerable occupants (e.g., elderly, obese, children).

[E-10.3]

SCALABLE HUMAN BODY MODEL FOR MULTI-MODAL SAFETY

Ludek Hyncik[1], *Jan Vychytil*[2], *Ludek Kovar*[3]

1 *University of West Bohemia, Pilsner, Czech Republic*
2 *University of West Bohemia, Pilsner, Czech Republic*
3 *Mecas Esi S.R.O., Czech Republic*

Current trends in mobility bring new challenges for active and passive safety. Multi-modal transport including non-standard seating configurations is concerned. Whilst the mechanical dummies are usually composed to assess an injury risk in a single direction impacts, virtual human body models are able to reflect the situation in a multi-directional scenario using the computational biomechanics approaches. The work presents a hybrid scalable virtual human body model, which skeleton is formed as a multi-body structure coupled to deformable segments representing the outer skin. Thus, the deformation of soft tissues is taken into account using a fast calculation process. The model is validated in a wide spectrum of impact configurations. The model is scalable to be able to represent any occupant or pedestrian of gender, height and weight, all depending on age. The performance of the model is demonstrated in several non-standard impact configurations.

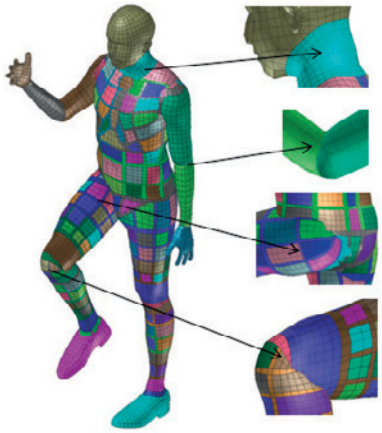

Figure 1: Hybrid human body model

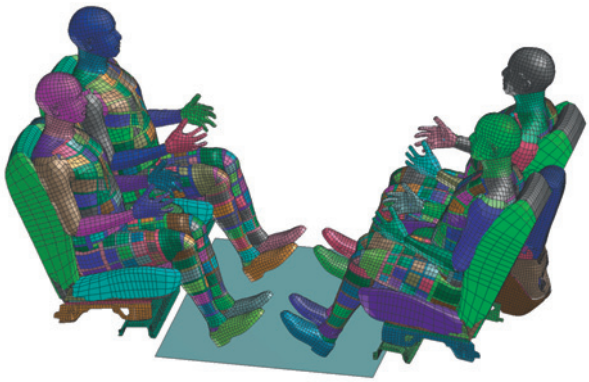

Figure 2: Non-standard seating configuration

Acknowledgements: The work was supported by the European Regional Development Fund-Project „Application of Modern Technologies in Medicine and Industry" (No. CZ.02.1.01/0.0/0.0/17_048/0007280).

References:

Hynčík, L., Čechová, H., Kovář, L. and Bláha, P., "On Scaling Virtual Human Models," SAE Technical Paper 2013-01-0074, 2013, doi: 10.4271/2013-01-0074.
Vychytil, J., Maňas, J., Čechová, H., Špirk, S., et al., "Scalable Multi-Purpose Virtual Human Model for Future Safety Assessment," SAE Technical Paper, 2014-01-0534, doi: 10.4271/2014-01-0534.
Yang, K.H., Hu, J., White, N.A., King, A.I., "Development of Numerical Models for Injury Biomechanics Research: A Review of 50 Years of Publications in the Stapp Car Crash Conference," Stapp Car Crash Journal 50:429-490, 2006, doi: 10.4271/2006-22-0017.

[E-10.4]

EVALUATION OF OCCUPANT RESPONSE IN SIDE IMPACT CRASH SCENARIOS USING HUMAN BODY MODELS

Donata Gierczycka[1]

1 University of Waterloo, Canada

Side crashes constitute 25% of road deaths in North America. While the effectiveness of side curtain airbags in reducing head injury was confirmed by epidemiological studies, the expected reduction of chest trauma due to thoracic side airbags has not been observed. To improve the effectiveness of side restraints, a novel methodology to assess the sensitivity of occupant surrogates to pre-crash parameters, and to examine the limitations of current experimental vehicle compliance tests is required. Human Body Models provide new insight into occupant response during vehicle crash scenarios. For the purpose of this study two Human Body Models were integrated with a mid-sized sedan and restraint models, and subjected to vehicle side crashes with different combinations of restraints and occupant pre-crash positions. Simulations identified potential improvements for interaction between the occupant and thoracic side airbags.

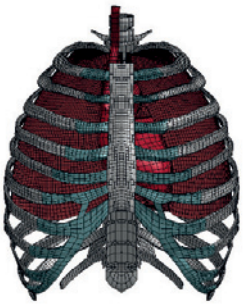

Figure 1: Detailed thorax of the Human Body Model.

Figure 2: Vehicle side crash scenario.

Figure 3: Varying pre-crash arm positions of the Human Body Model.

Acknowledgements: The author would like to acknowledge the Global Human Body Models Consortium for use of the HBM, the National Crash Analysis Centre for the vehicle model, and the Natural Sciences and Engineering Research Council of Canada for funding.

References:

Gierczycka, D., Cronin, D.S., "Influence of the Chest Compression Measurement Method on Evaluation of Side-impact Restraint Performance in Side Impact Crash Scenarios", Journal of Biomechanics, Vol. 75, pp. 53-57, 2018, doi: 10.1016/j.jbiomech.2018.04.044.

Gierczycka, D., Cronin, D.S., "Occupant Thorax Response Variation Due to Arm Position and Restraint Systems in Side Impact Scenarios", Journal of Accident Analysis and Prevention, Vol. 106, pp. 173-180, 2017, doi: 10.1016/j.aap.2017.05.017.

Gierczycka, D., Watson, B., and Cronin, D.S. "Investigation of Occupant Position and Door Properties on Thorax Kinematics in Side Impact Crash Scenarios, Comparison of ATD and Human Models". International Journal of Crashworthiness, Vol. 20(3), pp. 242-269, 2015, doi: 10.1080/13588265.2014.998000.

[E-10.5]

VIRTUAL ASSESSMENT OF ADVANCED SAFETY SYSTEMS FOR NEW MOBILITY MODES

Jan Spicka[1], *Ludek Hyncik*[1], *Ludek Kovar*[2], *Alojz Hanuliak*[3]

1 *University of West Bohemia in Pilsen, Pilsen, Czech Republic*
2 *Mecas Esi S.R.O., Czech Republic*
3 *EB Safety System, Czech Republic*

Current trends in the automotive industry regarding future mobility bring new challenges for active and passive safety technology. Non-traditional seating configurations in autonomous vehicles and complex crash scenarios including multi-directional loading are to be considered. Since the dummies can usually assess unidirectional impact, the expected future scenarios will cover complex and highly unpredictable loading in various directions. Thus, the numerical simulations using human body models are great importance in this field.

The aim of this work is to exploit human body model Virthuman [Vychytil] for assessing injury risk of a brand new concept of the interior safety systems for front and back seats made of thin elastic ultralight materials. The system called nanobag [Hanuliak] concerns a curtain folded in front of the passenger to protect the passenger in a similar way as the airbag. The system is built in the way that it can be easily adopted for side impact.

The main advantages of this new technology are the minimization of volume of the folded airbag, simplicity of the technology production and maintenance, low cost of materials, including the assembly and the multidirectional impact crashes (non-standard configurations), which is going to be a critical issue within new technologies of autonomous cars.

This work presents the numerical model Virthuman in the standard frontal crash scenario within the defined acceleration pulse simulating the 30 km/h and 50 km/h collision [Vezin]. The Virthuman model is seated in the seat as a driver, fastened with the seatbelts and the three scenarios are analyzed. Firstly, the model only with the seatbelt, secondly the model that includes seatbelt and airbag and finally the model with the new system nanobag with the seatbelt are compared one to another. The injury risk of the most threatened body parts is monitored within the criterion such as Head Injury or Neck Injury Criteria [Schmitt].

Figure Caption: Figure 1: Airbag versus nanobag

Acknowledgments: This work is supported by the John H. and Amy Bowles Lawrence Foundation and by the European Regional Development Fund-Project "Application of Modern Technologies in Medicine and Industry" (No. CZ.02.1.01/0.0/0.0/17_048/0007280).

References:

Hanuliak, Alojz. Safety Restraint System for Motor Vehicles. Radali Spol. s.r.o., Mátl, Roman, Havlík, Martin. PV 2017-307 (CZ). B60R 21/08 (2006.01). WO2018/219371. Valid from 19 November 2018. Signed 06 December 2018.
Schmitt, Kai-Uwe, et al.: Trauma biomechanics: Introduction to accidental injury. Springer Science & Business Media, 2013.
Vezin, P., Garnier, K., Bermond, F. and Verriest, J. P.: Comparison of Hybrid III, Thor-alfa and PMHS response in frontal sled tests. Stapp Car Crash Journal, Vol. 46, pp. 1-26, 2002.
Vychytil J., Maňas J., Čechová H., Špirk S., Hynčík L. and Kovář, L.: Scalable multi-purpose virtual Human model for future safety assessment, (No. 2014-01-0534), SAE Technical Paper, 2014.

[E-11.1]

THE CURRENT STATE OF IN-GAME MARKERLESS MOTION CAPTURE

Scott Selbie[1], *Marcus Brown*[2]

1 *C-Motion, Inc, Kingston, Canada*
2 *Theia Markerless Inc., Canada*

This presentation is an introduction to the state of the art in Motion Capture applicable to in-game recording. I will focus on 3D motion tracking solutions that are based on recording a game using temporally and spatially synchronized commercial video cameras mounted in the stadium or arena. These technologies passively observe the field of play, can be used indoors and outdoors, and do not require that sensors or markers be attached to the players; thus do not require the player's or team's cooperation, and do not influence the game directly.

All athletes in the field of view are represented by a personalized multibody skeletal model comprising rigid segments and physiologically meaningful joint constraints. The motions of the athletes are described as a time series of 3D poses (position and orientation) of all segments. The display of the activity can be an overlay of the underlying skeletal model back projected onto the video images, or an animation of an avatar of each athlete.

The state of the art motion tracking for live game recording is based on using Deep Neural Networks to identify the location of anatomical features of the subject from video images. Pose estimation for each player is based on an Inverse Kinematics optimization of the anatomical features constrained by a personalized biomechanical model.

Analyzing game strategy can be divided into two categories; the tendencies of an individual player, and the tendencies of a team. For an individual player, the objective may be to identify cues that allow the opposing team to predict an action. For example, predicting a fastball based on subtle distinctions in posture during the delivery. For a team, the objective may be to predict changes in strategy based on the movement of one or all players.

In order for the data analysis to make sense in a game situation we need to identify the activity being performed, and to define precisely, and consistently between subjects, the start and the end of any particular movement sequence (e.g. kicking). Most biomechanical assessments neglect the issues of segmentation because they are based on movement sequences that have already been parsed manually.

I will present recent approaches to segmentation. Recognizing one movement sequence from a game in which multiple movements occur based on the 3D pose is challenging because of the high dimensionality of the input and the variability in pose within and between subjects. When many different movement sequences exist in the data, the challenge of identifying each different sequence increases dramatically. For automated assessment of a game, however, this segmentation issue is a critical limitation in reducing the time for collection and analysis.

[E-11.2]

MARKERLESS MOTION CAPTURE FOR IN-GAME BASEBALL BIOMECHANICS ASSESSMENT

Steven Cadavid[1], *Katie Bradley*[2], ***Thomas Kepple***[2]

1 *Kinatrax Inc., USA*
2 *C-Motion, Inc, Kingston, Canada*

For many major league baseball teams, it is accepted that 3D analyses of player performance can be used to evaluate performance, predict musculoskeletal injuries, inform training and rehabilitation strategies, and influence game strategy. Recent advances in computer vision, machine learning, and graphical processing units (GPUs) have made possible the development of human motion tracking algorithms that function in indoor and outdoor environments without the need of subject cooperation. This presentation will focus on a 3D motion markerless motion capture solution for major league baseball using standard video cameras (Kinatrax Inc., Fla).

Video cameras (8 - 16 in our implementation) are mounted in the ballpark outside of the field of play and the vision of the players. Camera data are synchronized and sampled at 300 Hz. Between 2016 and 2018 data was recorded in 11 ballparks for pitchers and/or batters resulting in the motion of >1,000 pitchers for >700,000 pitches and >100,000 at bats and quantified using Kinatrax software. In step 1 a space carving algorithm was used to generate 3D visual hulls of the player at multiple keyframes of the throw (or swing) for every player. The locations of anatomical joints with respect to the visual hulls were hand digitized for 16 joints of the player model, and a multibody skeleton was defined from these joints. Using these keyframes as a seed solution to an optimization algorithm, the pose was estimated for all frames. Prior to the 2018 season the hand digitized data were used to train a 32 layer Convolutional Neural Network (CNN) to automatically recognize joint center probability distributions on the 2D images for both hitters and batters. From the 2D joint center distribution maps, 3D reconstructions of the players were obtained via traditional stereo photogrammetric techniques.

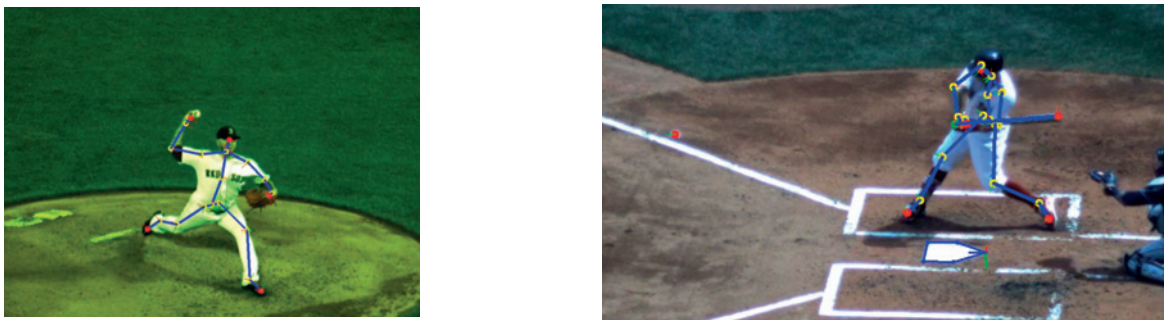

Figure 1 Caption: 3D skeletal model back projected on the video image for a typical pitch and at bat.

Visual3D software (C-Motion Inc., MD) was used to automatically generate and store team-proprietary kinematic analyses and biomechanical metrics for each pitch and each swing in the team's analytics database.

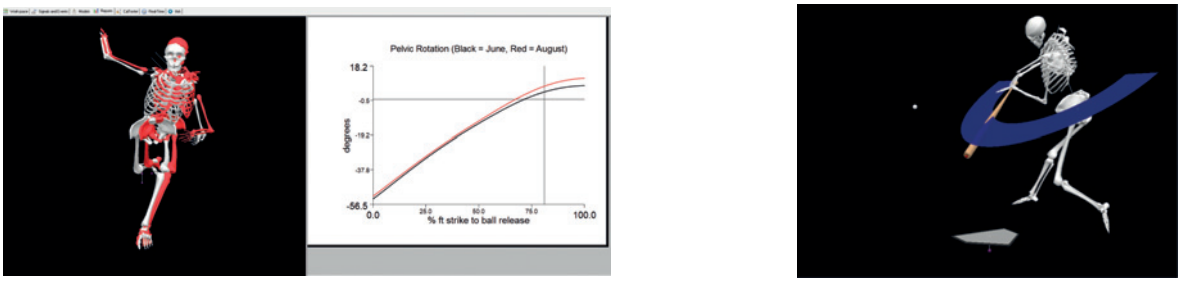

Figure 2 Caption: Left shows a pitcher overlaid from pitches thrown in mid (white) vs late season (red). Right the batter's swing plane is an added visual available for hitting analysis.

[E-11.3]

ON FIELD ASSESSMENT OF ELITE GOALKEEPERS MOVEMENT STRATEGIES FOR PENALTY KICKS IN FOOTBALL

António Veloso[1], *Silvia Cabral*[1], *João Brito*[2]

1 *Faculdade de Motricidade Humana , University of Lisbon., Cruz-Quebrada, Portugal*
2 *Federação Portuguesa de Futebol, Portugal*

The purpose of this presentation is to describe our pilot work evaluating the performance of the top Portuguese Football Goalkeepers selected for the Under 21 Portuguese National Team. 6 goalkeepers selected for the U21 Portuguese Football Federation (FPF) training Camp are participating in the study. All the participants were injury free and signed an informed consent form approved by the Ethics Committee of FMH University of Lisbon. The study is being carried out by request of the Portuguese FPF Performance Unit and the FPF U21 Technical Staff. The goal is to optimize goalkeeper movement patterns for stopping balls kicked to the lateral side of the goals when the goalkeeper is positioned on the center of the goal. The coaching doctrine of Portuguese postulates that for balls directed to the top corner of the goal the best solution would be to use the contralateral hand to stop the ball but this is still a matter of dispute. In order to address this hypothesis in a way that is meaningful to the coaches and players, it is essential that we collect data on a football pitch, and eventually during live games.

To describe the goalkeeper movement patterns we are recording the action using multiple temporally and spatially synchronized video cameras recording at 85 frames per second. In order that we do not interfere with the action, and taking advantage of the fact that most of the motion is directed laterally by the player, the 8 cameras are arranged behind the goal viewing through the net. Each player is represented by a personalized mathematical multibody model consisting of fourteen rigid segments constrained by physiologically representative joints. The movement of the player is quantified as a time series of the 3D pose (position and orientation) of this mathematical model during the activity. The 3D pose estimation of the multibody model is computed using the Theia3D markerless tracking solution (Theia Markerless, Canada). Theia3D employs a Deep Neural Network, and in conjunction with the intrinsic and extrinsic camera parameters, estimates the 3D pose of the model by inferring the probable location of 3D anatomical salient features constrained to an Inverse Kinematics optimization.

In order to evaluate the performance of the top goalkeepers in a controlled situation a 2 Victa ball launcher is used to precisely manage ball speed, elevation, direction and spinning allowing us to control ball target and position. The ball is directed to the lateral sides of the goal varying the elevation, velocity and side in a randomised order. For this study the most common successful movement solutions used by the top goalkeepers will be established as training guides for future studies.

Acknowledgments: This work was supported by CIPER-FCT (PEST-OE/SAU/UI447/2014 & UID/DTP/00447/2013).

[E-11.4]

GENERATING MEANINGFUL BIOMECHANICAL DATA DURING LIVE TRACK AND FIELD EVENTS

Athanassios Bissas[1]

1 *Leeds Beckett University | LEEDS MET, Carnegie School of Sport, UK*

Biomechanics and athletics go hand in hand. From running and hurdling to jumps and throws, all key parameters affecting performance have a clear mechanical basis. Capturing such variables "live" during competition is challenging. These challenges include securing tens of camera vantage locations, calibrating several spaces infield between official sessions, and operating in a scientific and experimental manner alongside tens of thousands of spectators and hundreds of officials, stadium staff and TV crews.

Our two projects with the IAAF (London World Championships 2017 and Birmingham World Championships 2018) created history in applied sport biomechanics. For instance, in London, a total of 21 events were captured with 17 events included in the final report. Taking into account semi-final rounds and men/women grouping we recorded over 70 individual races/events and over 730 world class athletes. This translated into over 3000 individual video files of a total unedited size of 2.86 TB. The project was conducted by a team of 42 researchers who deployed 49 HD cameras across 22 stadium locations, most of them operating at high-speed. This is unprecedented not only in terms of any previous IAAF Biomechanics project but also in terms of any sports science project ever conducted during official competitions.

Central to our data collection protocols was the deployment of three-dimensional motion techniques to analyze all the events. The plan was to deploy as many cameras as possible per event so all key aspects are captured. For instance, we deployed 23 high-speed cameras to capture the 100 m race, something unprecedented in the world of athletics.

The London (38 reports, >1500 pages) and Birmingham (13 reports, >500 pages) reports have received unparalleled attention and acclamation. Tens of thousands of downloads in 204 countries signify the demand for this type of data within the world of athletics and beyond.

So, what type of innovations would the future require from sport biomechanists as the model described above seem to be very successful? Without doubt, the production of fast data with immediate feedback, something that is possible under laboratory conditions, is a vital need for official competitions. However, these fast data have to be accurate but without needing thousands hours of manual digitizing.

In this presentation we will describe our experience using deep learning based markerless motion capture software; Theia3D (Theia Markerless, Canada) estimates the 3D position and orientation of a personalized multibody biomechanical model of athletes automatically from multiple synchronized video recordings based on anatomical feature recognition and optimal control theory. These algorithms do not require the cooperation of the athletes to don wearable sensors or stand in any required pose. We anticipate that live action recording is poised to change the way sports biomechanics is conducted.

[E-11.5]

INTEGRATING FE ANALYSIS AND T2 MRI RELAXATION TIMES REVEALS DIFFERENT RESPONSES TO BAREFOOT RUNNING IN NOVICE AND EXPERIENCED ATHLETES

Hyun Kyung Kim[1], Ali Mirjalili[2], Anthony Doyle[3], ***Justin Fernandez[4]***

1 *Faculty of Medical and Health Sciences; University of Auckland; New Zealand*
2 *Faculty of Medical and Health Sciences ; University of Auckland; New Zealand*
3 *Radiology Department; Auckland District Health Board; New Zealand*
4 *Auckland Bioengineering Institute, The University of Aucklan; New Zealand*

Biomechanical studies have advocated barefoot running as it may lower impact force [1, 2]. However, the effect of long distance barefoot running on ankle cartilage stress for different athlete types has yet to be investigated. The objective of the study was to integrate MRI T2 relaxation times (a measure of inflammation), plantar pressure and finite element (FE) modelling to compare novice and experienced runners before and after a 5km barefoot run.

Ten novices and ten experienced runners with equal split in gender participated. All participants were free from lower-limb injury and first-time barefoot runners who ran with conventional heel strike techniques. This study was approved by the human ethics committee in our institution (ref: 016488). Dynamic plantar pressure (Novel Emed®) was measured before and after 5km unshod running on a treadmill. Before and after running, MRI data of the right foot and ankle were acquired with a 3.0-T scanner (Siemens) using a foot coil. Two experienced radiologists quantified T2 relaxation times of the tibiotalar cartilage in the anterior, central, and posterior zones. A previously validated Abaqus FE model of the foot [3] was customised to the MRI shape data of each individual and loaded using participant plantar pressure

The novice and ME runners both showed similar spatial patterns with high von Mises stress and higher T2 relaxation times in the anterior and posterior sagittal zones of the tibiotalar cartilage (Figure 1). Between pre- and post-run measurements, ME runners decreased tibiotalar von Mises stress by 17% ($P<0.05$) while maintaining similar pre-run T2 values. In contrast, novice runners maintained the same level of tibiotalar stress and increased T2 values ($P<0.02$). ME and novice responses may be partly due to different foot strike strategies. ME runners decreased plantar pressure across the medial metatarsals by 29% and increased lateral midfoot loading by 32%. In contrast, novice runners reduced toe pressure by ~30% and increased lateral foot loading by 22%. Novice and ME runners exhibit different T2 MRI relaxation times and cartilage stress responses to barefoot running that may play a role in observed novice ankle pathology

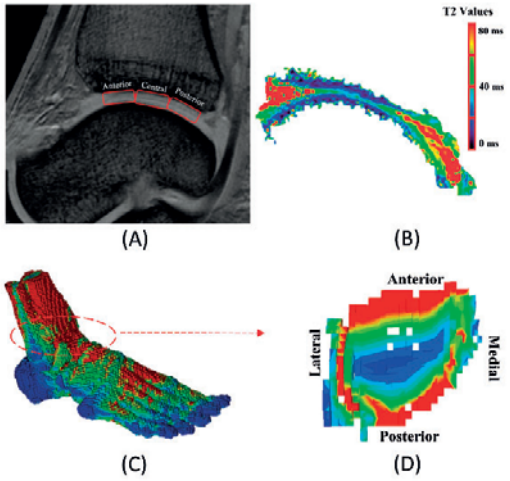

Figure Caption: Figure 1: (A) Sagittal ankle MRI; (B) T2 relaxation times; (C) Finite element foot model; and (D) Tibiotalar cartilage von Mises stress.

References:

[1] *Jenkins DW et al. (2011). J Am Podiatr Med Assoc, 101(3): 231-46.*
[2] *Lieberman DE et al. (2010). Nature, 463: 531-5.*
[3] *Fernandez JW et al. (2012). Int J Num Meth Bio Eng, 28(10): 1056-70.*

[E-11.6]

COMPARISON OF ENERGY AND POWER DURING MUSCLE-UP AND PULL-UP

Galo Maldonado[1], Philippe Soueres[2], ***Bruno Watier[2]***

1 *Institut National des Invalides; CERAH, France*
2 *Laas-Cnrs, Toulouse, France; Université de Toulouse, France*

Introduction: Pull-up and muscle-up techniques provide a way for enhancing strength and endurance training for the upper body and can contribute to prevent injuries. While many studies in the literature focus mainly on the lower limb's capabilities, few of them have studied upper limbs performance. Commonly, push-up variations have been investigated in the context of sports training and injury prevention of the upper limbs [1]. The results of these researches shown that push-ups are well suited for the aforementioned purposes and factors such as hand placement, execution speed and instability induced by training suspension devices affect the muscular recruitment and intensity levels. In this research, we propose to investigate the maximal power and the total work of pull-up and muscle-up techniques executed by parkour practitioner (Fig.1).

Methods: Male traceurs (age: 20.5±2.3 years, body mass: 68.04±9.93 kg, height: 1.73±0.05 m) volunteered for this study. Each subject realized at least two trials of pull-ups and muscle-ups. A motion capture system equipped with 14 cameras (Vicon – 400Hz) was used to obtain the 3D trajectory of markers.

Two six axis sensors were used to record reaction forces and moments and allowed for motion segmentation. Inverse kinematics and a whole-body inertial model [2,3] were used to compute the center of mass trajectory. The power developed by the participants was computed as follows:

$$P = m \times g \times V^G \quad (1)$$

The total work done was calculated as the scalar product of the center of mass displacement between the lower (G_l) and the upper position (G_u) and the body weight as:

$$W = m \times \vec{G_l G_u} \quad (2)$$

Results: Both, work and maximal power developed by the participants are significantly ($p<0.05$) lower with the pull-up technique than with the muscles-up technique (6.0±0.6 vs. 10.5±0.5 J/kg and 10.1±1.4 vs. 17.2±2.2 W/kg). In both techniques, the maximal power was higher than 500W.

Discussion-Conclusion: The results demonstrate that muscle-ups could be preferred to strengthen upper limbs conditioning. However, due to high mechanical constrains, pain prevention studies are needed to better understand the possible benefits and risks of these techniques. The muscle-up technique can be also better suited to challenge not only upper body muscles but also the trunk and lower body ones. Lastly, progression sequences for upper body conditioning can incorporate push-up and muscle up variations but more research is still needed. The authors are currently working in a whole-body 3D study of inverse dynamics and in a muscular recruitment analysis.

Figure Caption: Fig. 1: Initial and final postures of the pull-up (A) and the muscle-up (B)

References:

[1]. S.L. Delp et al. IEEE Transactions on Biomedical Engineering 54, 2007: 1940-50. https://doi.org/10.1109/TBME.2007.901024.
[2]. W. Dhahbi et al. Sports Biomechanics, 2018, 1-40. https://doi.org/10.1080/14763141.2018.1512149.
[3]. G. Maldonado et al. Journal of Sports Sciences 36, 2018: 2551-57. https://doi.org/10.1080/02640414.2018.1469226.

[E-11.7]

OPTIMIZING PADDING THICKNESS IN FOOTBALL HELMETS TO MINIMIZE ANGULAR ACCELERATION

Michael Fanton[1], *Jake Sganga*[1], *David Camarillo*[1]

1 *Stanford University, Stanford, USA*

American football is one of the leading causes of the 3.8 million sports-related traumatic brain injuries (TBI) that occur in the US each year[1]. The introduction of foam padding to football helmets in the 1970's nearly eliminated severe head trauma (e.g. skull fracture) from the sport[2]. However, diffuse brain trauma, resulting primarily from head rotation[3], remains a major problem, causing acute neurological dysfunction and increasing the risk of long-term neurodegeneration. Here, we optimize the distribution of helmet padding to minimize head impact angular acceleration.

We determined the head's rotational vulnerability to impacts on the helmet using the force-rotational admittance (FRA)[4]. The FRA is an analytical solution to the initial angular acceleration of the head resulting from an input force. Using a 20 degree-of-freedom head-neck model[5], we derived the FRA at 4795 points on the skull covered by the helmet shell6, assuming an input force normal to the surface of the skull. To account for the cervical spine's range of motion, we calculated the FRA over 216 neck configurations and averaged them to create a single measure for the head's rotational vulnerability to an impact, $\mathbf{FRA_i}$ (Fig 1B). We validated the FRA-predicted angular acceleration against the peak angular acceleration from 1000N, 10ms half-sine forces simulated in the upright configuration (Fig 1A).

As a baseline, we found the thickness of a Riddell Speed finite element model[6] at each skull point ($\mathbf{t_i}$). To constrain the optimization, we ensured the total pad volume remained constant. We assume the pads exhibit a constant force over the full thickness. We set up the following optimization, where $\mathbf{\Delta t_i}$ is the change in thickness at each point:

$$\min_{\Delta t_i} \sum_i \frac{FRA_i}{t_i + \Delta t_i} \quad s.t. \quad \sum_i \Delta t_i = 0$$

In the optimized helmet, padding was redistributed from the top, where the head is less sensitive to angular acceleration, to the sides and jaw pad (Fig 1C). Using this methodology, the maximum head angular acceleration was reduced by 28%, while the sum of the acceleration over all points was reduced by 6.4%. This analysis identifies opportunities for redesigning helmet geometries to reduce angular acceleration.

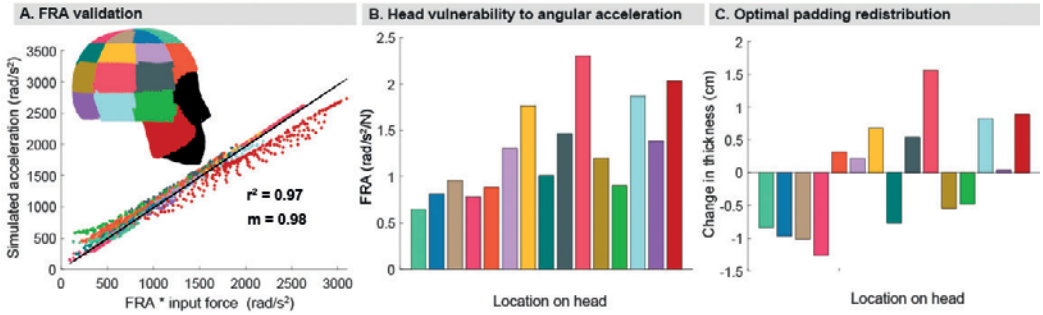

Figure 1: A) The FRA-predicted angular acceleration and the simulated angular acceleration is well correlated with r2 of 0.97. B) The FRA for 15 sections of the skull. C) Optimization distributes padding from top of head to other locations.

References:

[1] *Lincoln Am. J. Sports Med. 2011.*
[2] *Bishop, et al Am. J. Sports Med. 1984.*
[3] *Gennarelli, et al. The Neuroscientist 1998*
[4] *Fanton et al, IEEE TBME. 2018.*
[5] *Kuo. et al. J. Royal Soc. Interface. In review.*
[6] *Biocore LLC, biocorellc.com/resources/*

[F-01.1]
IN VIVO MEASUREMENTS OF BRAIN BIOMECHANICS

Philip Bayly[1]

1 *Washington University in Saint Louis, Saint Louis, USA; Mechanical Engineering and Materials Science*

Traumatic brain injury (TBI) is a widespread and important medical problem that may lead to chronic deficits in cognition, memory, or emotional control. Chronic traumatic encephalopathy (CTE) is a specific brain pathology associated with multiple impacts to the head, and characterized by localized accumulations of hyperphosphorylated tau. The causes of TBI and CTE are believed to be rapid deformation of the brain in response to high skull accelerations, typically due to impact. The specific magnitudes and locations of strain that lead to injury remain unknown, as do the mechanisms by which strain leads to neuropathology. This lack of knowledge is partly due to the difficulty of visualizing how the intact, living, human brain deforms, and also to the challenges in modeling and simulating the biomechanics of the brain: a soft, heterogeneous, anisotropic, nonlinear, viscoelastic, mechanical system. In this presentation I will present two approaches to improving our understanding of brain biomechanics through MR imaging. In one approach, tagged magnetic resonance imaging (tagged MRI), we track tissue deformations through synchronizing image acquisition with voluntary, transient head motion. In a second approach, magnetic resonance elastography (MRE), shear waves in the brain are induced by low-amplitude vibration of the skull, and imaged using specialized MR imaging pulse sequences. I will discuss how these imaging-based measurements of skull and brain motion provide insight into the structural dynamics and material properties of the human brain.

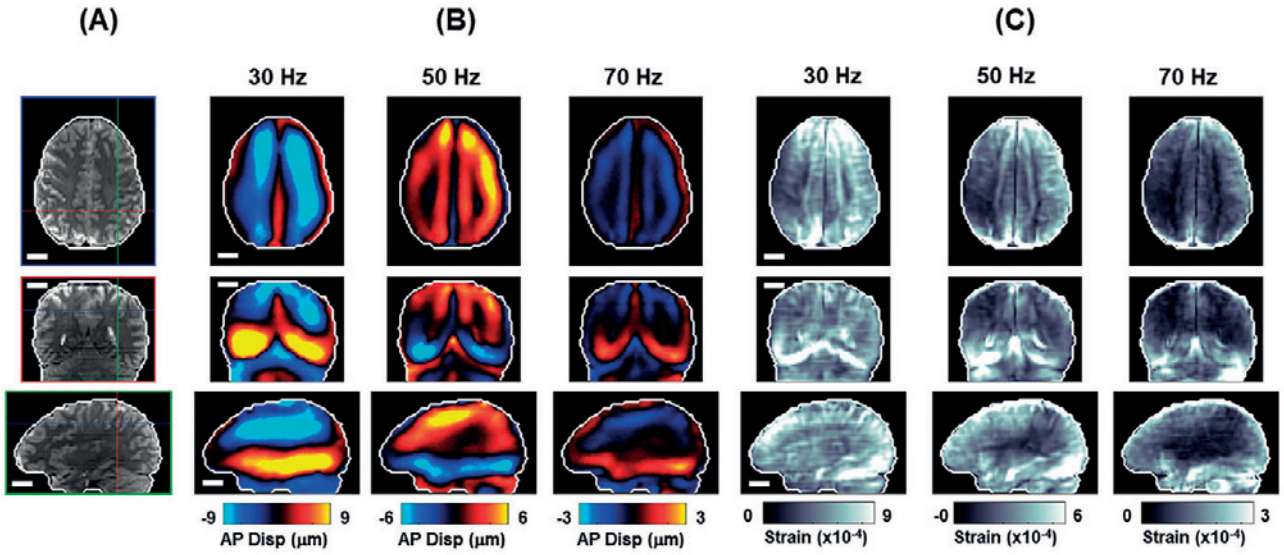

Figure Caption: Structural dynamics of the human brain in vivo from MRE. Shear wave displacement and strain at multiple frequencies for a representative subject at three different vibration frequencies: 30 Hz, 50 Hz, and 70 Hz. Shear waves attenuate less (penetrate deeper into the brain) at the lowest frequency, 30 Hz, compared to 50 Hz and especially 70 Hz. (A) Anatomical images (masked MRE magnitude), (B) anterior-posterior (AP) wave displacement, and (C) octahedral shear strain (OSS) magnitude. Note that displacement and strain scales differ for each frequency. Scale bar equals 2 cm in all images.

Acknowledgments: NIH Grants R01/R56-NS055951 and R01-EB027577 and NSF Grant CMMI-1727412.

References:

[1] Bayly et al. (2005) Deformation of the human brain induced by mild acceleration. J Neurotrauma. 22(8):845-56.
[2] Sabet et al. (2008) Deformation of the human brain induced by mild angular head acceleration. J Biomech. 41(2):307-15.
[3] Clayton et al. (2012) Transmission, attenuation and reflection of shear waves in the human brain. J R Soc Interface. 9(76):2899-910.
[4] Knutsen et al. (2014). Improved measurement of brain deformation during mild head acceleration using a novel tagged MRI sequence. J Biomech. 47(14):3475-81.
[5] Gomez et al. (2018). 3D Measurements of Acceleration-Induced Brain Deformation via Harmonic Phase Analysis and Finite-Element Models. IEEE Trans Biomed Eng. In press.

[F-01.2]

PATTERNS OF AXONAL FIBER STRETCH DURING MILD AXIAL AND SAGITTAL ACCELERATION IN THE LIVE HUMAN BRAIN

Andrew Knutsen[1], *Arnold Gomez*[2], *Philip Bayly*[3], *John Butman*[4], *Dzung Pham*[1]

1 *The Henry M Jackson Foundation, Bethesda, USA*
2 *Johns Hopkins University, Baltimore, USA*
3 *Washington University in Saint Louis, Saint Louis, USA*
4 *National Institutes of Health, Bethesda, USA*

The rapid stretching of axonal fibers in response to impulsive loading of the brain can lead to diffuse axonal injury [1]. Measurements of strain along white matter fiber bundles in the live, human brain may predict regions susceptible to injury in response to such loading. In this study, we used tagged Magnetic Resonance Imaging (MRI) to measure strain in the brains of healthy volunteers and Diffusion Tensor Imaging to calculate strain along white matter fibers.

Seven healthy volunteers were enrolled in a protocol to measure brain deformation in response to mild head acceleration in either the axial (4 scans) or sagittal (4 scans) plane; 1 subject was imaged during both head motions. A series of tagged MRI slices, covering the entire brain, were acquired in 3 orthogonal orientations at 18 ms temporal resolution. A total of 120–156 were required to acquire the data. Three-dimensional Lagrangian strain over time was computed using the harmonic phase finite element (HARP-FE) method [2]. Diffusion weighted images were also acquired (2x2x2 mm, b=1000 s/mm2, 30 directions), and diffusion tensors were calculated and registered to the tagged image space. Using the principal eigenvector from the diffusion tensor to infer fiber orientation, axonal strains were calculated. The diffusion tensors were segmented into various white matter tracts [3]. Positive fiber strain was analyzed in white matter voxels with fractional anisotropy greater than 0.2.

Average values of peak angular velocity and acceleration ranged from 3.2–3.7 rad/s and 214–238 rad/s2 for axial acceleration, and from 1.8–2.0 rad/s and 309–347 rad/s2 for sagittal acceleration. Figure 1 shows images of fiber strain in response to mild head acceleration. Overall, average and maximum (99th percentile) positive fiber strains were larger during axial acceleration than sagittal acceleration – 0.010 to 0.007, and 0.037 to 0.026. Maximum strains were larger (>0.01) during sagittal acceleration in the cortico-spinal tract, inferior cerebellar peduncle, and medial lemniscus, whereas, for example, the corpus callosum, posterior thalamic radiation, and inferior fronto-occipital fascicle experienced larger strain during axial acceleration.

The measurement of fiber strain during non-injurious loading in the live, human brain provides an important data set for evaluation of computer models of brain biomechanics. Local fiber strains may also provide insight into patterns of axonal injury in animal models and humans caused by higher-amplitude insults.

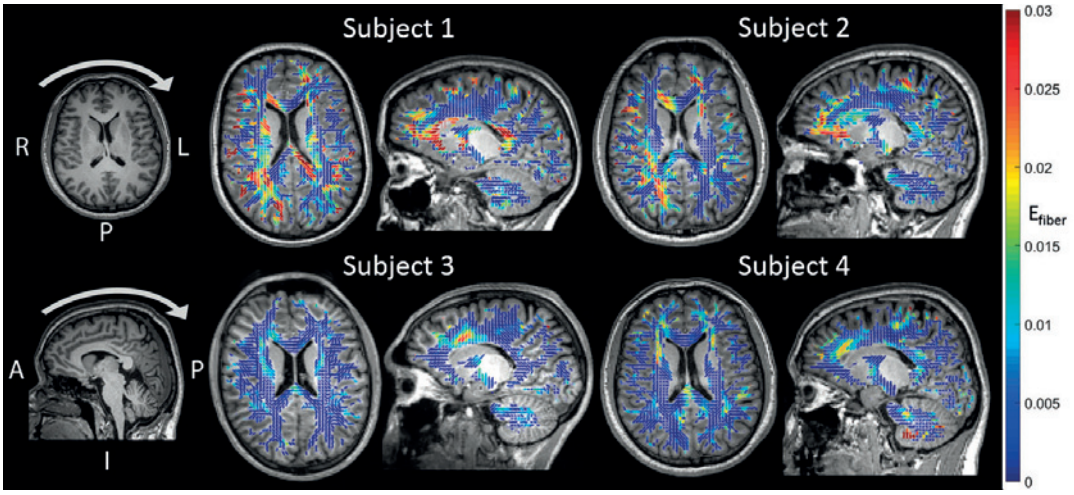

Figure 1: Positive fiber strain values in response to acceleration in the axial (top row) or sagittal (bottom row) planes were mapped to 3D ellipsoids that indicate the orientation of white matter.

Acknowledgments: We acknowledge funding from NINDS (R01/R56NS055951), the CNRM, and the NIH Intramural Research Program.

References:

[1] Meaney et al. 1995 J. Neurotrauma 12:4;
[2] Gomez et al. 2018 IEEE TBME;
[3] Bazin et al. 2011 NeuroImage 58

[F-01.3]

IN VIVO DEFORMATION MAPPING OF THE HUMAN OPTIC NERVE HEAD USING OPTICAL COHERENCE TOMOGRAPHY AND DIGITAL VOLUME CORRELATION

Dan Midgett[1], ***Thao Nguyen***[1]

1 *Johns Hopkins University, Baltimore, USA; Mechanical Engineering*

We developed a novel method to analyze radial optical coherence tomography (OCT) scans of the optic nerve head (ONH) in patients before and after a change in intraocular pressure (IOP) to characterize the in vivo strain state of the human ONH. Twenty-four radial OCT scans were taken of the ONH of 5 eyes from 5 glaucoma patients immediately before and after laser suturelysis, an IOP-lowering surgery, and from 5 eyes from 3 glaucoma suspect patients before and after wearing tight-fitting swimming goggles without lenses for 15 minutes. A custom digital volume correlation (DVC) algorithm was developed to calculate the 3D displacement field within the ONH volume between images taken at high and low IOP. The method has subpixel displacement correlation errors and strain errors less than 0.37%. The lamina cribrosa (LC) anterior limit and Bruch's membrane opening (BMO) were marked to segment the LC volume, and the LC anterior depth (ALD) was defined as the distance from the BMO to the LC anterior limit. Changes in ALD and strains were calculated from the DVC displacement field and analyzed for associations with each other and with IOP. In this presentation, I will describe the development of the image processing and DVC method to estimate strains from radial OCT scans and present results regarding the relationship between strain components and changes in IOP and between strains and ALD change. Suturelysis caused the IOP to decrease by 9 - 20 mmHg and produced significant anterior-posterior strains Ezz in the anterior LC, which indicated less compression at the lower IOP (i.e., strain relief). Likewise, wearing goggles caused the IOP to increase by 0 - 4 mmHg and produced significant compressive strains Ezz in the anterior LC. ALD increased at lower IOP, which indicated that increasing IOP caused ALD to move anteriorly towards the front of the eye. A larger posterior change in ALD and greater strain relief were measure for a larger IOP change; however the association between ALD change and IOP change as highly variable for small IOP changes, less than 5 mmHg. A greater posterior ALD change as also associated with a greater Ezz; however the relationship was highly variable also for small IOP changes. These results showed that the DVC method can measure strains and ALD changes for IOP changes as low as 3 mmHg. Increasing IOP causes on average significant anterior-posterior compression of the anterior LC volume and anterior motion of the anterior LC limit.

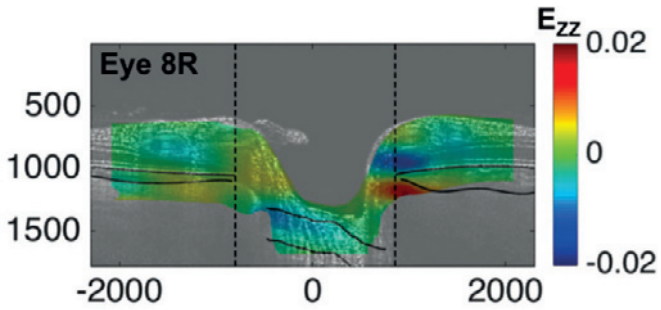

Figure 1: Contour of the anterior-posterior strain Ezz in the inferior-superior section of the optic nerve head obtained from DVC analysis of in vivo radial OCT scans of subjects experiencing an increase in the intraocular pressure (IOP). An increase in IOP caused compressive Ezz in the lamina cribrosa

[F-01.4]

SENSING THE BRAIN DURING MECHANICAL TRAUMA: FROM BIOMECHANICS TO FUNCTIONAL OUTCOMES

Lyndia Wu[1], *Kaveh Laksari*[2], *Mehmet Kurt*[3], *Calvin Kuo*[1], *David Camarillo*[4]

1 *University of British Columbia, Vancouver, Canada*
2 *University of Arizona, Tucson, USA*
3 *Stevens Institute of Technology, Hoboken, USA*
4 *Stanford University, Stanford, USA*

Mild traumatic brain injury (mTBI), commonly referred to as concussions, is a major public health concern. Globally, about 42 million people (0.6%) are diagnosed with mTBI annually [1]. Among different types of traumatic brain injuries, the injury mechanism and pathology of mTBI is least understood, resulting in ineffective prevention, diagnosis and treatment. The dominating theory is that trauma results from a single severe blunt impact to the head, but how the mechanical inputs damage the brain within a closed skull remains a mystery. Ideally, we would like to look inside the skull at the moment of injury, and observe potential brain deformations as well as subsequent brain changes. But this is not yet achievable with current technology, especially in human injury cases. Here we describe wearable technology and data analytics techniques to help observe the mechanobiological cascade occurring in human mTBI in real time. To measure the biomechanics (input) of mTBI, we developed a head impact sensor in the form factor of an instrumented mouthguard that can record full six-degree-of-freedom head kinematics during contact sports [2]. To detect head impacts among other activity on the field, we designed a head impact detection system using infrared sensing and machine learning algorithms [3]. This technology enables real-time head impact measurements from sports impacts that may result in mTBI, and with tools such as finite element models of the head and brain, we are able to simulate brain deformations occurring during these field head impacts. To measure the brain changes (output) of mTBI, we explored the application of non-invasive brain electrophysiology sensors to detect immediate physiological and functional disturbances in the brain after head impact. Combining wearable head impact biomechanics and brain electrophysiology sensors, we have an opportunity to open a window into the human brain and observe mTBI in real-time.

References:

[1] R. C. Gardner and K. Yaffe, "Epidemiology of mild traumatic brain injury and neurodegenerative disease," Mol. Cell. Neurosci., vol. 66, no. PB, pp. 75–80, 2015.
[2] F. Hernandez et al., "Six Degree-of-Freedom Measurements of Human Mild Traumatic Brain Injury.," Ann. Biomed. Eng., vol. 43, no. 8, pp. 1918–34, Dec. 2015.
[3] L. C. Wu et al., "Detection of American Football Head Impacts Using Biomechanical Features and Support Vector Machine Classification," Sci. Rep., vol. 8, no. 1, pp. 1–14, 2018.

[F-01.5]

BIOMECHANICS OF THE RAT PIA-ARACHNOID COMPLEX THROUGH MULTIMODAL IMAGING

*Zeynep Melis Suar[1], **Gloria Fabris**[1], Luke Langner[1], Javid Abderezaei[1], Mehmet Kurt[1]*

1 Stevens Institute of Technology, Hoboken, USA

To better understand the onset of damage occurring in the brain upon traumatic events, it is essential to analyze how external mechanical loads propagate down to the brain cortex. However, despite their putative role as structural dampers protecting the brain, the mechanical behavior of the meningeal layers are still poorly understood [1]. Here, we characterized the deformation characteristics following a multimodal imaging technique, where we observed the local mechanical heterogeneity of rat pia-arachnoid complex (PAC) at the microscale via atomic force microscopy (AFM) indentation experiments and the deformation response of intact PAC via optical coherence tomography (OCT).

Tissue stiffness probed at the microscale revealed large local heterogeneities, with a distribution mean of 4.7 ± 2.8 kPa. In particular, the Young's modulus (E) of vascularized tissue resulted significantly higher than that of non-vascularized PAC. We therefore hypothesize that the microanatomy of tissue causes differential load propagation properties in different regions of the pia-arachnoid complex.

Higher trabecular density area showed higher stiffness values and longer relaxation times, supporting the hypothesis that the trabecular structure of the PAC is an enclosing structure around the brain with higher stiffness and damping values, possibly contributing to protect the brain against impacts.

The OCT images were obtained for intact PAC on the brain and peeled-off PAC. The following scanning settings for imaging are used: 800 A-scans per B-Scan, 200 B-scans, and 3 volume repetitions over a field of view of 3x3x1.2 mm. The observation of trabecular structure suggests that the PAC preserve its form after removing the dura and peeling-off the PAC.

It is known that mammalian PAC displays a high regional variability both in arachnoid trabeculae density and subarachnoid vasculature distribution [2], [3]. Our data highlight strong local variations in the mechanical response of this tissue, possibly relating to the differences in local vulnerability to TBI reported by [4]. Future work will attempt to better quantify the most relevant microanatomical parameters (e.g., cellular density, local trabecular orientations) and correlate them with the deformation and recovery response of tissue via coupled AFM-confocal microscopy experiments and OCT imaging.

Exploring the mechanics of this peculiar bridging structure would also be highly relevant for a number of computational applications. From a biomechanical perspective, a popular hypothesis considers the random three-dimensional structure of the collagen sheets and pillars that make up the trabeculae as a mechanically redundant structure, contributing to damping and constraining brain deformation following head rotation and movement despite the small volumetric contribution of the PAC to the intracranial space [5]. The multi-phasic (liquid, solid, ions, etc.) nature of bio-interfaces make their characterization a rather challenging task. Lack of accurate experimentally-derived material parameters characterizing the brain-skull interface is a key part in TBI research. Obtaining a comprehensive quantification of the mechanical response of the meningeal interfaces would therefore bring us one step closer to accurately modeling and understanding the nature of this complex biomaterial.

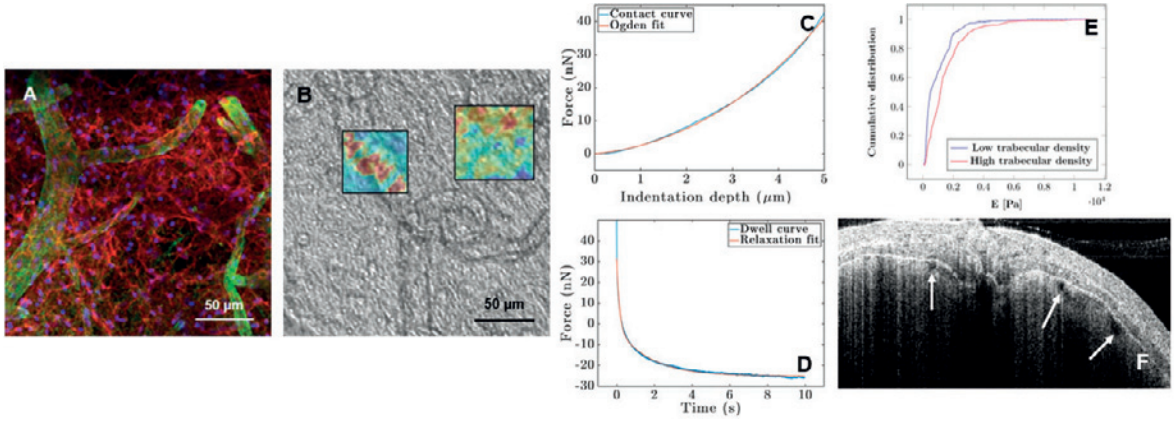

Figure Caption: A. Fluorescent imaging of peeled-off PAC (Green: collagen-I; red: vimention; blue: nuclei) B. Phase contrast image with AFM force maps overlay. C. Example F-d curve. D. Example relaxation curve. E. Cumulative distribution of stiffness values comparing low- and high- density trabecular areas. E. Intact PAC anatomy observed via OCT through skull.

Acknowledgments: We thank Dr. Kevin Costa (Icahn School of Medicine, Mount Sinai, NY) for AFM access.

References:

[1] X. Jin et al., J. Biomech., 2011.
[2] J. A. Siegenthaler et al., Curr. Opin. Genet. Dev., 2011.
[3] G. G. Scott et al., IEEE Trans. Med. Imaging, 2015.
[4] G. G. Scott et al., Biomech. Model. Mechanobiol., 2016.
[5] M. M. Mortazavi et al., World Neurosurg., 2018.

[F-02.1]

PRECISION MEASUREMENT OF MILD BRIAN TRAUMA USING AN INSTRUMENTED MOUTHGUARD

David Camarillo[1]

1 Stanford University, Stanford, USA

Mild traumatic brain injury (mTBI) affects 55 million people worldwide and can lead to neurodegeneration. My goal is to enable early detection and prevention of mTBI. My laboratory has pioneered instrumented mouthguard technologies that precisely measure the acceleration of the head during impact, which we use to drive finite element (FE) models of the brain. In this talk, I will share preliminary data that suggests that blood brain barrier disruption, a potential initiator of neurodegeneration, may be very common in contact sports and is detectable in real-time with the mouthguard. Finally, I will present data on early prototypes of a compact shock absorber that has the potential to prevent mTBI in helmets for football and other high-risk activities.

[F-02.2]

AN OPTIMIZED WORCESTER HEAD INJURY MODEL VERSION 2.0

Wei Zhao[1], *Songbai Ji*[1]

1 *Worcester Polytechnic Institute, Worcester, USA*

Head injury models are important tools to study traumatic brain injury (TBI). Rigorous validations are critical for their effective use. To date, most head injury models are validated against high-rate cadaveric head impacts using relative brain-skull displacements [1], [2]. Few of them considered validation against in vivo brain biomechanics [3]–[5] relevant to sub-concussive impacts. In addition, they do not typically optimize brain material properties to maximize validation performance. Here, we upgraded the Worcester Head Injury Model (WHIM) by optimizing its brain material properties. We reported its validation performances across the full spectrum of blunt impact conditions for the brain.

Specifically, a high-resolution, re-meshed brain [6] was used to implement white matter anisotropy [7] using an HGO anisotropic model and a simplified viscoelastic model. Nine high-rate cadaveric head impacts (major rotational acceleration impulse duration ($\mathbf{\Delta t}$) of ~3–5 ms) were used to optimize $\mathbf{G_5}$ (shear modulus at 5 ms), as $\mathbf{G_t}$ was most relevant to brain responses for impacts at the corresponding loading rate [8]. The average Correlation Analysis Score (CORA) served as an objective function for maximization. The optimized WHIM was then cross-validated against cadaveric cluster strains [2], [9] as well as relative brain-skull displacements from eight mid-rate cadaveric head impacts ($\mathbf{\Delta t}$ of ~14.4–34.4 ms). Seven of the cases were non-contact, pure rotations based on neural density targets [10], [11] or sonomicrometry [12]). Finally, it was cross-validated against strains from three in vivo head rotations ($\mathbf{\Delta t}$ of ~40 ms) [3]–[5] that represent the lower spectrum of impact severity.

The optimized WHIM achieved an average CORA of 0.707 from high-rate impacts and 0.567–0.879 for mid-rate impacts, with the highest CORAs from the sonomicrometry data (Figure 1). It also achieved reasonable strains compared to the experiments. The comprehensive validations of the optimized WHIM Version 2.0 across the full spectrum of blunt impact conditions for the brain using data from 20 cases offered a robust foundation for its future applications.

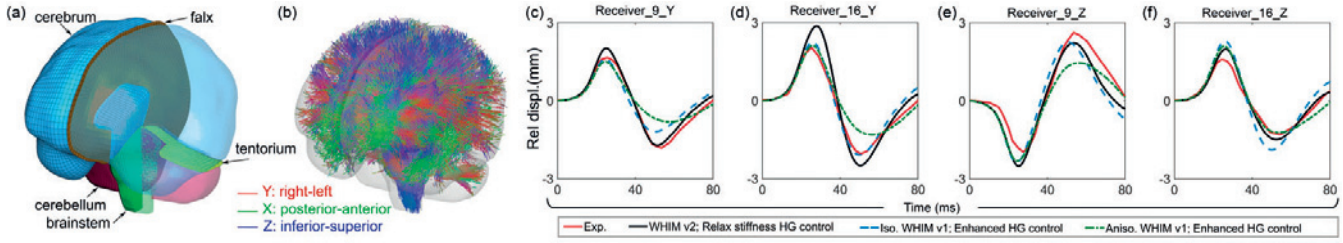

Figure 1 (a) Re-meshed and upgraded WHIM Version 2.0; (b) element-wise fiber orientations; (c–f) predicted relative brain-skull displacements from the upgraded and previous WHIMs compared against measurements from a case with the highest CORA using the sonomicrometry technique.

Acknowledgement: Funding is provided by the NIH grant R01 NS092853.

Reference:

[1] Hardy et al., 2001.
[2] Hardy et al., 2007.
[3] Sabet et al., 2008.
[4] Knutsen et al., 2014.
[5] Chan et al., 2018.
[6] Zhao and Ji, 2019.
[7] Zhao et al., 2016.
[8] Zhao et al., 2018.
[9] Zhou et al., 2018.
[10] Guettler et al., 2018.
[11] Guettler, 2017.
[12] Alshareef et al., 2018.

[F-02.3]

USING FUNDAMENTAL FRACTURE MECHANICS TO PREDICT INFANT SKULL FRACTURE PATTERNS

Junyan He[1], Jiawei Yan[1], Robert M Metcalf[1], Ashley Spear[1], ***Brittany Coats****[1]*

1 University of Utah, Salt Lake City, USA

Accidental falls are the leading cause of non-fatal injury in infants and the most common explanation given by caretakers suspected of abuse. Distinguishing a truthful history of a fall from a false one proves to be a difficult but important task for a clinician. Skull fracture is a common finding for both accidental falls and abusive injuries, but it is unknown how to distinguish fracture from accidental or abusive scenarios. Careful biomechanical investigations can determine characteristics of trauma that lead to specific skull fracture patterns in infants. The purpose of this study was to develop and validate a computational framework for predicting skull fracture patterns in infants based on fundamental principles of fracture mechanics.

Human infant parietal and occipital bone specimens were obtained from autopsy and tested in a custom three-point bending high-rate impact system to identify rate-, region-, and direction-dependent material properties. Using the resulting properties, we developed a high-fidelity computational framework to predict crack propagation following a head impact. The framework integrates three-dimensional crack growth software (Franc3D) with explicit dynamic simulations (ABAQUS) to identify patterns of crack growth from low-height falls. Occipital and parietal infant cranial bones were 10 times stiffer when tested parallel to trabecular fibers compared to perpendicular to the fibers, indicating high anisotropy of the material. The computational framework incorporated this anisotropy with a transversely anisotropic material model and defined localized radial orientations corresponding to trabeculae in infant cranial bone. The framework was validated against a single parietal impact in a 5-month old infant cadaver dropped from 15 cm onto concrete.

When simulating the experimental impact, the framework predicted a crack that initiated from the edge of the right parietal bone, followed by extension along the direction of the trabecular fibers and eventually arresting near the ossification center. This crack initiation site and pattern were similar to the experimental observations. The overall crack length was 9.0% shorter (43.5mm vs 40mm) than the hand-drawn length in the experimental study. The overall kink angle of the crack showed a 1.8° difference compared to the hand-drawn pattern (8.62° vs 6.82°). The close levels of agreement in crack initiation location, crack pattern, crack length, and kink angle illustrate the framework's excellent predictability of skull fracture patterns following impact to the infant skull. Additional validation is ongoing with additional cadaver data and simulations of real-world impacts in children. Our computational framework is the first to predict crack propagation in the infant skull using fracture mechanics theory. Future studies with the framework will parametrically evaluate the effect of impact energy and impact direction on skull fracture patterns in children, and provide the medical and legal communities with empirical data to improve medical and judicial accuracy in child abuse cases.

Acknowledgments: This project was supported by Award No. 2016-DN-BX-0160, awarded by the National Institute of Justice, Office of Justice Programs, U.S. Department of Justice. The opinions, findings, and conclusions or recommendations expressed in this presentation are those of the authors and do not necessarily reflect those of the Department of Justice.

[F-02.4]
UNDERSTANDING BRAIN INJURY MECHANISMS THROUGH MODELLING

Haojie Mao[1], *Kewei Bian*[1], *Yanir Levy*[1], *Lihong Lu*[1], *Kathy Xu*[1], *Arthur Brown*[1]

1 *Western University, London, Ontario, Canada*

The fundamental mechanisms of traumatic brain injury (TBI) especially mild TBI remain unclear. Meanwhile, to improve protection, diagnostics and treatment of this challenging health problem, it is critical to understand the mechanisms of TBI and hence take appropriate measures to target these mechanisms. Two essential steps toward understanding TBI mechanisms are needed including: 1) investigating brain internal forces during traumatic impacts that eventually lead to various brain damage, and 2) replicating real-world-relevant TBI in controlled lab settings that allow comprehensive observation of brain damage process and accurate measurement of impact parameters.

In this invited talk, we discuss in vivo mouse concussion experiments1 that were designed to mimic real-world concussive impacts. In our animal neurotrauma experiments, the strain distribution as evaluated by cumulative strain damage measure (CSDM), which counts brain regions experiencing strains exceeding a pre-set value, were close between laboratory mouse and real-world human head impacts with differences less than 15%. Such comparison ensured that laboratory animal models could represent real-world impacts rather than generate an artificial injury such as contusion from the open-skull animal models. From our mouse neurotrauma experiments and associated mouse computational simulations, we found that diffuse brain strains, especially strains in the cerebrum and several deep brain structures correlated to mild TBI. Using brain strain as a bridge between laboratory animal work and real-world human brain injury, we further discuss our recent work in using and improving advanced human head models to predict brain responses during helmeted impacts2. We then discuss how these brain responses help to guide new helmet designs that can reduce the risk of mild TBI besides reducing the risk of severe damage such as skull fracture or contusion. Our data demonstrated that traditional injury metrics were not sufficient for brain protection. Also, traditional scaling laws3,4 between animal and human, which have been heavily relied on to develop injury tolerances, might not be valid given the significant correlations between brain strains and brain damage.

Briefly, in this talk we discuss the significance of modelling head impacts5 through both computational models and animal models. In the future, by leveraging accurate material constitutive equation development, advanced neuroimaging, and complex neuropathological studies, we will be eventually in a position to fully understand the injury mechanisms of TBI.

Acknowledgments: We acknowledge NSERC Discovery and Canada Research Chairs program for support.

References:

1. *Namjoshi et al. Molecular Neurodegeneration 2014 9:55.*
2. *Panzer et al. Neurotrauma 2018, Toronto, Canada.*
3. *Takhounts et al. Stapp Car Crash J 2003 107-134.*
4. *Ommaya et al. Stapp Car Crash J 1967 73-80.*
5. *Yang et al. Modeling of the Brain for Injury Simulation and Prevention 2019.*

[F-02.5]

HUMAN BRAIN TISSUE TESTING AND MODELING ACROSS TIME SCALES

Silvia Budday[1], *Gerhard A. Holzapfel*[2], *Paul Steinmann*[3], *Ellen Kuhl*[4]

1 *Friedrich-Alexander Universität Erlangen-Nürnberg, Erlangen, Germany*
2 *Norwegian University of Science and Technology, Trondheim, Norway ; Graz University of Technology, Graz, Austria*
3 *University of Glasgow, Glasgow, USA; Friedrich-Alexander Universität Erlangen-Nürnberg, Erlangen, Germany*
4 *Stanford University, Stanford, USA*

Neurological disorders, including dementia, epilepsy, multiple sclerosis or long-term effects of traumatic brain injury, have been identified as one of the major public health challenges by the world health organization. While long underestimated, more and more evidence confirms that mechanics play a critical role for brain function and dysfunction. Therefore, computational simulations based on the field equations of nonlinear continuum mechanics can provide important insights into the underlying mechanisms of brain injury and disease that go far beyond the possibilities of traditional diagnostics. Those, however, require mechanical models capable of capturing the complex and unique characteristics of the ultrasoft, highly heterogeneous, and adaptive brain tissue. In recent years, however, contradictory experimental results, mostly attributed to the time and length dependence of brain tissue properties, have hindered continual progress.

Here, we carefully assess the challenges associated with brain tissue testing and modeling. Based on the evaluation of previously published experimental data [1], complemented by new experimental and numerical analyses, we work out the most important characteristics of brain tissue behavior on different length and time scales. We further try to disentangle seemingly contradictory experimental results in the literature. We then present mechanical models that capture the experimentally observed time-independent and time-dependent characteristics of brain tissue [2]. Finally, we propose application-specific modeling approaches, which are as complex as necessary but as simple as possible. The presented considerations will, on the one hand, facilitate well-designed future experiments and, on the other hand, help to choose the appropriate constitutive law for a specific application at hand. The appropriate choice of constitutive models and material parameters is key to performing predictive simulations useful for the biomedical and clinical communities - to assist diagnosis of disease and its progression, estimate risk of injury, and plan surgical procedures.

References:

[1] *S. Budday, G. Sommer, C. Birkl, C. Langkammer, J. Haybaeck, J. Kohnert, M. Bauer, F. Paulsen, P. Steinmann, E. Kuhl and G.A. Holzapfel, Mechanical characterization of human brain tissue. Acta Biomater., 48:319–340, 2017.*
[2] *S. Budday, G. Sommer, J. Haybaeck, P. Steinmann, G.A. Holzapfel and E. Kuhl, Rheological Characterization of Human Brain Tissue. Acta Biomater., 60:315–329, 2017.*

[F-03.1]
MODELING DEMENTIA

Ellen Kuhl[1]

1 *Stanford University, Stanford, USA*

Prions diseases are characterized by a chain reaction in which infectious misfolded proteins force native proteins into a similar pathogenic structure. Recent studies reinforce the hypothesis that the prion paradigm, the templated growth and spreading of misfolded proteins, can explain the progression of a variety of neurodegenerative disorders [1]. However, our current understanding of prion-like growth and spreading is rather empirical. We show that physics-based reaction-diffusion models can explain the growth and spreading of misfolded protein in Alzheimer's disease, Parkinson's disease, and amyotrophic lateral sclerosis [2]. To characterize the spreading of misfolded proteins across the brain, we combine local kinetic models of protein misfolding with global network models of protein diffusion. Our whole brain models correctly predict amyloid-beta deposits and tau inclusions in Alzheimer's disease, alpha-synuclein inclusions in Parkinson's disease, and TDP-43 inclusions in amyotrophic lateral sclerosis and display excellent agreement with the histological patterns in diseased human brains [3]. To reduce computational complexity, we apply reduced order modeling and represent the brain through a connectivity-weighted Laplacian graph created from 418 brains of the Human Connectome Project [4]. Our brain network model correctly predicts the neuropathological pattern of Alzheimer's disease and captures the key characteristic features of our whole brain models at a fraction of its computational cost. When integrated across the brain, both models result in biomarker curves that display a striking similarity with the sigmoid shape and qualitative timeline of clinical biomarker models. Our results suggest that misfolded proteins in various neurodegenerative disorders grow and spread according to a universal law that follows the basic physical principles of nonlinear reaction and anisotropic diffusion. Our findings substantiate the notion of a common underlying principle for the pathogenesis of a wide variety of neurodegenerative disorders, the prion paradigm. A more quantitative understanding of the growth and spreading of misfolded amyloid-beta, tau, alpha-synuclein, and TDP-43 will allow us to establish a prognostic timeframe of disease progression.

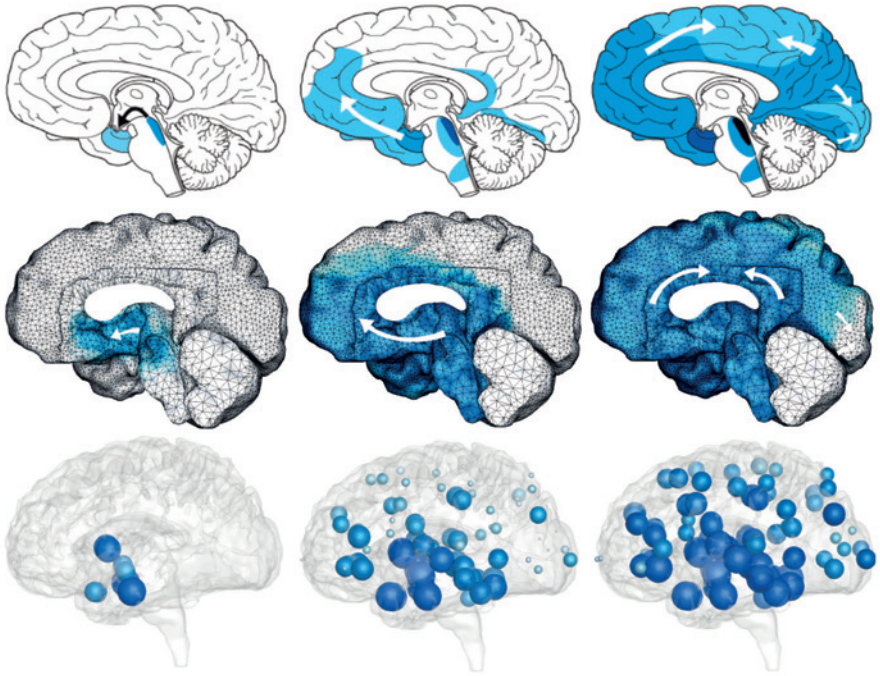

Figure Caption: Typical pattern of tau protein misfolding in Alzheimer's disease. Neuropathological observation [1], continuum model [2,3], and network [4].

Acknowledgments: This work was supported by the NSF CMMI-1727268 grant.

References:

[1] *Jucker M, Walker LC. Self-propagation of pathogenic protein aggregates in neurodegenerative diseases. Nature 2013;501:45-51.*
[2] *Weickenmeier J, Jucker M, Goriely A, Kuhl E. A physics-based model explains the prion-like features of neurodegeneration in Alzheimer's disease, Parkinson's disease, and amyotrophic lateral sclerosis. Journal of the Mechanics and Physics of Solids. 2019;124:264-281.*
[3] *Weickenmeier J, Kuhl E, Goriely A. The multiphysics of prion-like diseases: progression and atrophy. Physical Review Letters. 2018;121:158101.*
[4] *Fornari S, Schafer A, Jucker M, Goriely A, Kuhl E. Prion-like spreading of Alzheimer's disease within the brain's connectome. 2019; submitted.*

[F-03.2]
A NETWORK-BASED BRAIN INJURY METRIC

Shaoju Wu[1], *Wei Zhao*[1], ***Songbai Ji***[1]

1 *Worcester Polytechnic Institute, Worcester, USA*

Traumatic brain injury (TBI) is a major public health problem in the United States (US) [1]. To date, much of the biomechanical work has centered on developing a scalar injury metric to describe head impact severity, based on which to further predict the occurrence of injury. For example, the use of impact linear and/or rotational acceleration is ubiquitous. An FE model of the human head provides unparalleled rich information about brain mechanical responses such as strain. However, the most widely used responses from head impact simulation are either the peak maximum principal strain of the entire brain, or the percentage of brain volume experiencing strains above a certain threshold (i.e., cumulative strain damage measure; CSDM) [2]. They cannot inform the location or distribution of brain strains that are likely important to study mild TBI, given the widespread neuroimaging alterations and a diverse spectrum of clinical signs and symptoms.

To account for inherent limitations with scalar injury metrics, here we established a structural network-based "response feature matrix" to characterize brain response magnitude and distribution in both gray matter (GM) regions of interest (ROIs) and their white matter (WM) interconnections. Specifically, we employed the LONI Probabilistic Brain Atlas (LPBA40 [3]) to identify 54 cortical GM ROIs. They were used as seeding nodes to construct a brain structural network. Interregional connections between each pair of GM ROIs were identified by testing each WM fiber (obtained from the whole-brain tractography) whether it traversed the two GM ROIs under scrutiny. A global density-based thresholding was applied to the resulting connectivity matrix [4] to retain the top strongest links while removing weaker and spurious interconnections. The resulting binarized connectivity matrix was used to encode strain responses.

For illustration, reconstructed NFL head impacts [5] were used to simulate brain strains with the anisotropic Worcester Head Injury Model (WHIM [6]). For network nodes or GM ROIs, we choose to use the peak maximum principal strain to encode their responses. For network edges, injury susceptibility at a threshold level of 0.09 [7] based on WM fiber strains was used for encoding. The structural network-based feature response matrix is shown in Fig. 1 for one concussive head impact.

The resulting features enabled a machine learning approach to perform a feature-based concussion classification. We show that with support vector machine classifier, the network-based injury metric outperformed conventional head impact kinematics via logistic regression in injury prediction. This supported the use of a network-based brain injury metric and a feature-based machine learning classifier for injury prediction in the future.

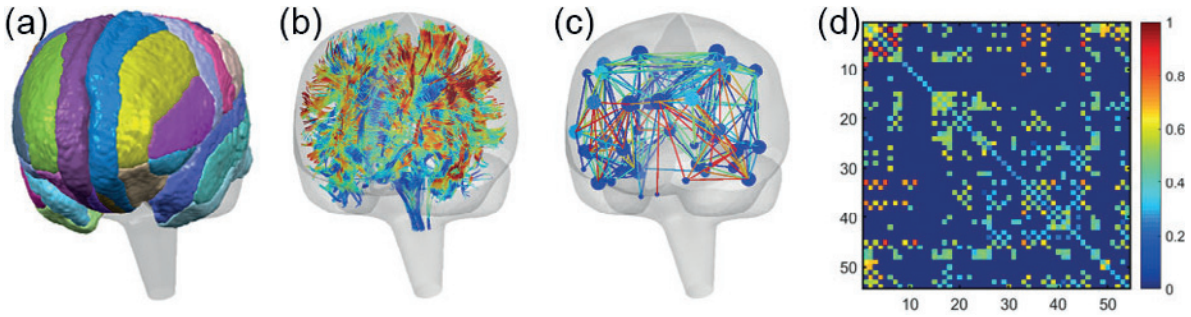

Figure 1 Strain responses of the 54 cerebral GM ROIs (a) and WM fiber strain-encoded tractography (b) are used to construct a brain structural network (c) in order to encode the magnitude of maximum principal strains in GM ROIs and the injury susceptibilities between each pair of GM ROIs. The strain-encoded brain structure network is represented in the form of a feature response matrix (d).

Acknowledgement: Funding is provided by the NIH grant R01 NS092853.

Reference:

[1] *CDC, 2015.*
[2] *Takhounts et al., Stapp 2008.*
[3] *Qi et al., J. Neurosci. Methods, 2015.*
[4] *Fornito et al., 2016.*
[5] *Sanchez et al., Clin. Biomech. 2018.*
[6] *Zhao and Ji, J. Neurotrauma 2019.*
[7] *Zhao et al., Biomech. Model. Mechanobiol 2017.*

[F-03.3]

NONLINEAR BIOMECHANICS OF THE HUMAN BRAIN WITH IMPLICATIONS FOR MECHANISMS OF BRAIN INJURY

Javid Abderezaei[1], Wei Zhao[2], Carissa Grijalva[3], Songbai Ji[2], Kaveh Laksari[3], ***Mehmet Kurt****[1]*

1 *Stevens Institute of Technology, Hoboken, USA*
2 *Worcester Polytechnic Institute, Worcester, USA*
3 *University of Arizona, Tucson, USA*

Traumatic brain injury (TBI) is a major cause of death and disability, affecting approximately 2.8 million people each year across the US [1]. Despite substantial research, however, our physical insight into the cause of injury is limited. Such a physical understanding could be helpful to improve the injury metrics which are currently based on kinematics or brain finite element criteria [2]. However, these measures lack the sufficient mechanical understanding of the characteristics of the brain and the question remains as to why some specific sub-regions of the brain, such as corpus callosum (CC) are more prone to injury [2].

To address this issue, it is important to consider the intricate geometry of the brain, and its nonlinear material properties. Such characteristics, could result in nonlinear dynamical behavior. In a recent study, Laksari et al., identified localized modes and multimodal behavior in the brain, a common characteristics of nonlinearity [3]. Sabet el al., also found disrupted strain fields using tagged MRIs which hint at nonlinear behavior around gray-white matter junction and CC [4]. Considering the importance of nonlinear effects and its possible role on the injury metrics, here we combined FE simulations and modal analysis to study the nonlinear behavior of deep regions of the brain.

We implemented Worcester Head Injury Model (WHIM) [5] to simulate the brain responses under a range of coronal rotations. A half-sine acceleration impulse was applied to the center of gravity of the head by varying the amplitude between 1-10 and the duration between 5-25 ms. Next, proper orthogonal decomposition (POD) was performed on the brain's displacement field to find the corresponding proper orthogonal modes (POMs) of each acceleration as well as their contribution to the energy of the system (eigenvalues). We then studied the possible link between the nonlinear effects and FE criteria.

We observed nonlinear effects in the deep regions of the brain in the vicinity of dural folds and CC with 30.3% decrease of the dominant mode (Fig. 1A, B). We then compared the nonlinear region with , which corresponds to brain volume experiencing strains higher than 35% (Fig. 1C). We observed that deep regions of the brain with such high principal strains are connected to the identified nonlinear regions. This hints at possible correlation of the nonlinear dynamical behavior of the brain with the injury metrics.

A) B) C)

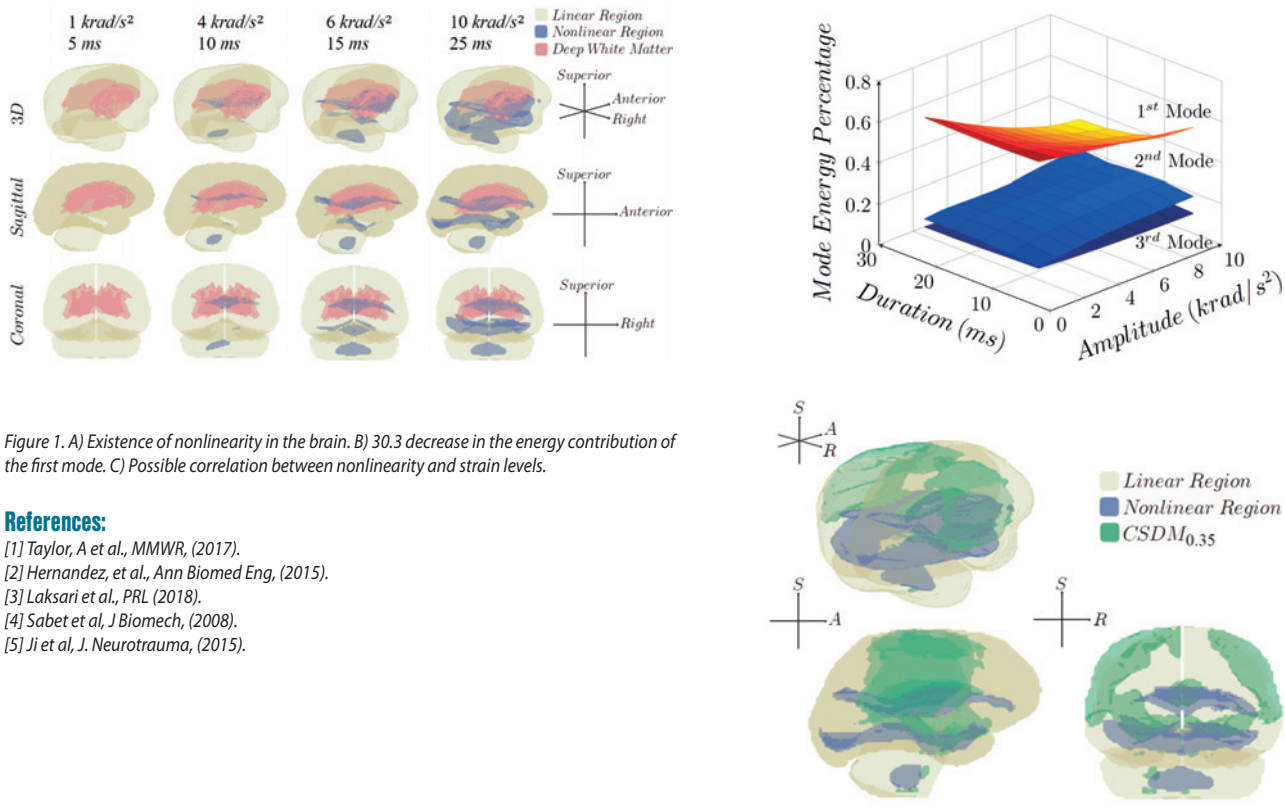

Figure 1. A) Existence of nonlinearity in the brain. B) 30.3 decrease in the energy contribution of the first mode. C) Possible correlation between nonlinearity and strain levels.

References:

[1] Taylor, A et al., MMWR, (2017).
[2] Hernandez, et al., Ann Biomed Eng, (2015).
[3] Laksari et al., PRL (2018).
[4] Sabet et al, J Biomech, (2008).
[5] Ji et al, J. Neurotrauma, (2015).

[F-03.4]

BRAIN STRUCTURE INFLUENCES STRESS TRANSFER PATTERNS AFTER TBI

Vickie Shim[1], *Justin Fernandez*[1], *Tae-rin Lee*[2], *Mike Dragunow*[3], *Shaofan Li*[4]

1 *Auckland Bioengineering Institute, The University of Auckland, Auckland, New Zealand*
2 *Seoul National University, Seoul, South Korea*
3 *Centre for Brain Research; The University of Auckland, Auckland, New Zealand*
4 *Department of Civil and Environmental Engineering; Uc Berkeley*

Introduction: Traumatic brain injury (TBI) is a major public health challenge that is on course to become the third leading cause of death worldwide by 2020(1). Yet, we still do not have a capability to objectively identify injury threshold for brain concussion(2). One main reason is that a clear link between the mechanical factors of the concussion and subsequent downstream cellular events have not been established. We do not know how the mechanical energy from concussion is transferred to the cellular and vessel network causing damages in the tissue. Our aim is to create a multiscale framework to analyze how mechanical impacts from TBI are transferred to the tissue and eventually to the cells.

Method: The existing human brain model is from the International Union of Physiological Society (IUPS) Physiome Project (3), which contains the scalp, skull and the brain. This model has been further developed into to have tissue anisotropy of the white matter, an important mechanical feature of the brain(4) by embedding the fibre orientation of the white matter to the model [Figure 1]. We used the microstructurally based material coordinate system in our FE software (5) (www,opencmiss.org, freely available for academic use), which has been used to describe anisotropy of human tissues (6). A parametric study was performed with this model to identify the pattern of damage in the brain after TBI. Boundary conditions were from the literature(7), which was applied to a parameterized model of the brain and the resulting stress pattern was observed.

Results and Discussion: Two brain impact scenarios - frontal and occipital impacts were used to simulate stress propagation after impact. The type of loading as well as the internal tissue structure influenced the resulting stress pattern [Figure 2]. We have built a cell mechanical device capable of applying identified strain fields directly to cells. By combining the model with the device, we will characterize downstream cellular events after TBI to find potential therapeutic targets.

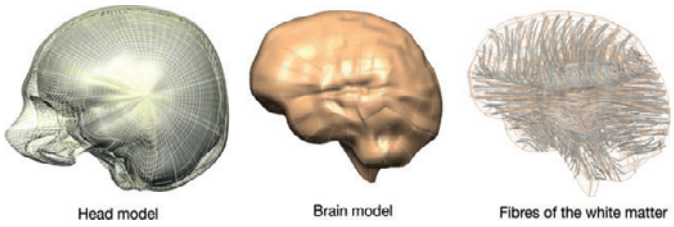

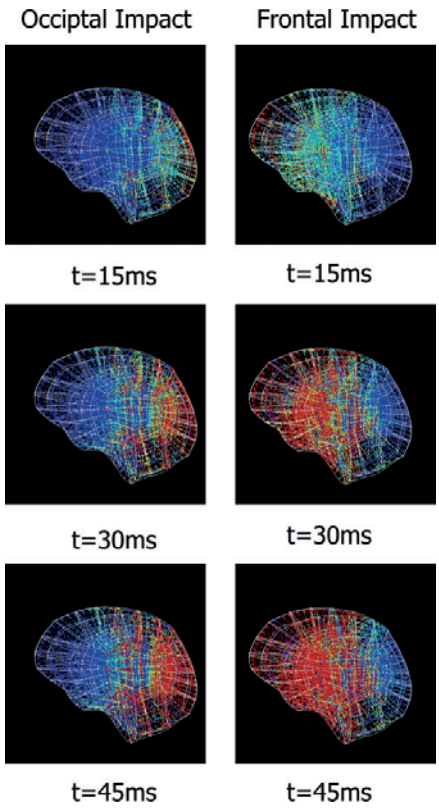

Figure Caption:
Figure 1: Brain model including skull and white matter fibre tracts,
Figure 2. Resulting stress pattern from different impact scenarios.

Acknowledgments: This work was funded by New Zealand Ministry of Business, Innovations & Employment grant (55749-INTCS-UOA)

References

1. *Young et al. Lancet Neurol. 2010;9(4):331.*
2. *Sharp DJ, Jenkins PO. Pract Neurol. 2015;15(3):172-86.*
3. *Hunter PJ, Borg TK. Nature reviews Molecular cell biology. 2003;4(3):237-43.*
4. *Giordano C et al. 2014;47(5):1052-9.*
5. *Shim VB et al. BMMB. 2016;15(1):195-204.*
6. *Shim VB et al. Scientific Reports, 8 (1) 13856*

[F-03.5]

A MULTI-MODALITY CHARACTERIZATION OF INJURED BRAIN TISSUE

*Suhao Qiu[1], Wenheng Jiang[2], Mohammad Shah Alam[1], Shaoxuan Chen[1], Xiaowei Li[1], **Yuan Feng**[1]*

1 *Shanghai Jiao Tong University, Shanghai, China*
2 *Soochow University, Jiangsu Sheng, China*

Traumatic brain injury (TBI) is one of the leading causes of death and disability worldwide [1]. biomechanical properties of brain tissue are of great importance to establish and validate finite element (FE) models, and to understand the mechanism of TBI [2]. Many studies have been dedicated to investigate biomechanical properties of brain tissue, ether in vivo [3] or ex vivo [4]. However, most of them focused on healthy brain tissues and few studies investigated the properties of injured tissues [5]. In this study, we characterized the injured brain tissue with macro-scale biomechanical testing and micro-scale vasculature imaging. Characterization of the injured brain tissue could help understand injury mechanism, verify computational results, and provide pivotal information for TBI detection and treatment evaluation.

In this study, a custom-built controlled cortical impact (CCI) device was used to induce injury to a mouse. Three different impact velocities (0.6 m/s, 0.8 m/s, and 1.0 m/s) with three different impact angles (0°, 30°, 50°) were introduced to the mouse brain after craniotomy. After the impact, the brain tissue was sliced for indentation. Viscoelastic properties of four regions of the brain were estimated with 2-term Prony series, based on a ramp-hold test. To investigate the structural changes after the injury, confocal imaging of the injured tissue were carried out after perfusion of the brain. Structural details of the brain vasculature were revealed with an imaging resolution of 1.2μm.

Results showed that the impact angles had a more significant role than the impact velocities in terms of the changing viscoelastic properties, especially for the injured regions. We also found that the vasculature of the injured brain had a denser distribution than that of the control sample. The measurements from two different modalities provided insights into the biomechanical changes of the injured tissues.

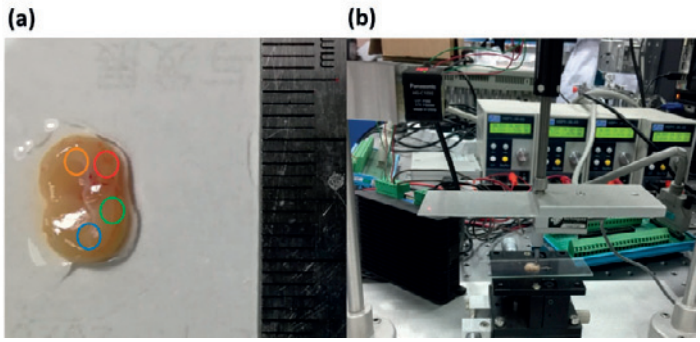

Figure Caption: Fig. 1. (a) Four regions of the brain were tested, which are the injured region, the ipsilateral hippocampus region, and the two corresponding contralateral regions. (b) A custom-built indentation test device.

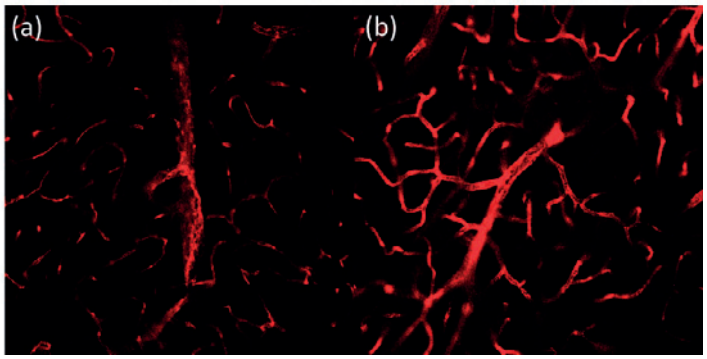

Fig. 2. Confocal imaging of the vasculature of the (a) injured tissue and (b) non-injured tissue.

Acknowledgments: Grant 31870941 (YF) from National Natural Science Foundation of China (NSFC). We thank Prof. Philip V. Bayly for helpful discussions.

References:

1. *Tagge, C.A., et al., Brain, 2018. 141(2): p. 422-458.*
2. *Zhao, W., et al., JMBBM, 2018. 80: p. 222-234*
3. *Bayly, P.V., et al., Ann Rev Bio Eng, Vol 14, 2012. 14: p. 369-396.*
4. *Budday, S., et al., JMBBM, 2017. 74: p. 463-476.*
5. *Feng, Y., et al., JMBBM, 2017. 71: p. 407-415.*

[F-04.1]

COMPUTATIONAL MODEL VERSUS KINEMATIC MOTION BASED METRICS IN SUBCONCUSSION: WHICH IS SUPERIOR?

Joel Stitzel[1], *Logan Miller*[1], *Joseph Maldjian*[2], *Elizabeth Davenport*[2], *Christopher Whitlow*[1], *Jillian Urban*[1]

1 *Wake Forest University, Winston-Salem, USA*
2 *University of Texas Southwestern, Dallas, USA*

Most head impacts in football are subconcussive impacts, which do not result in clinical signs and symptoms of a concussion, and recent studies suggest repetitive subconcussive head impacts are of increasing concern. This study examines different biomechanical metrics to quantify the effects of cumulative head impacts over the course of a season, derived from both kinematic measures and finite element volumetric strain-based computational measures. The performance of biomechanical metrics was evaluated by examining their relationship with measurable changes in the brain through magnetic resonance imaging (MRI) metrics. The study cohort is part of the Imaging, Telemetry, and Kinematic Modeling (iTAKL) study of youth football players. Subjects were recruited from a local youth football organization and outfitted with the Head Impact Telemetry System during all practices and games to collect biomechanics associated with each head impact experienced. The approach seeks to evaluate whether the cumulative effects of head impacts over the course of a single season of youth football are better quantified, correlated and discriminated using kinematic-based or computational model-based measures.

Biomechanics and imaging data from pre and post season for 107 athletes over 138 athlete seasons are used to demonstrate the concept. Diffusion tensor imaging (DTI) metrics including fractional, linear, planar, and spherical anisotropies as well as mean diffusivity were evaluated on the basis of total number of abnormal white matter voxels. Biomechanical data collected was used to calculate five kinematic-based exposure metrics: number of impacts, impacts per session, summed linear acceleration, summed rotational acceleration, and risk-weighted exposure (RWE), including three subcategories of linear, rotational and combined probability RWE. Finally, seven biomechanically distinct and less correlated types of a possible 32 finite element (FE) strain-based metrics based on principal strain were calculated using the atlas-based brain model (ABM) [1]. These metrics will be introduced and are based on strain, strain rate, strain*strain rate, cumulative strain damage measure area (CSDMA), CSDMA*strain, CSDMA*strain rate, and CSDM strain rate area.

The strain-based metrics are less skewed than the kinematic-based exposure metrics, and as a result, there are fewer influential points affecting the relationship with imaging metrics. Linear regression analyses revealed a statistically significant relationship between MPS, strain rate, and multiple DTI metrics. Previous investigations have observed statistically significant relationships between RWE and DTI metrics. Since the RWE metrics are highly skewed, however, outliers or influential points may play a significant role in the strength of the relationship observed. We will demonstrate a novel method of quantifying cumulative exposure using strain-based metrics. While the clinical implications of these metrics are not well understood, they demonstrate great possibility. There is significant potential for such metrics to better discriminate exposure as it correlates with medical imaging. This approach and these findings will serve as the foundation for enhanced inquiry into location-based analyses and for correlation between biomechanics and imaging as well as biomechanics and neurocognitive testing, and biomechanics and biomarkers. They may also in the future provide the foundation for better prediction of concussion, and also discrimination of the many and varied clinical presentation of signs and symptoms related to concussion.

Acknowledgments: This work was supported by the National Institutes of Health (NIH) grant R01NS082453 (JM,JS), and R01NS091602 (CW,JM,JS). Special thanks to the Childress Institute for Pediatric Trauma at Wake Forest Baptist Medical Center for providing support for this study. National Science Foundation Graduate Research Fellowship under Grant No. DGE-0907738.

References:

[1] Miller et al, Biomech Model Mechan, 2016

[F-04.2]
MULTISCALE MODELING OF AXONAL FIBER BUNDLES IN THE BRAIN

Reuben Kraft[1], *Ritika Menghani*[1]

1 *Penn State University, University Park, USA*

Computational brain medicine is an emerging field that has the opportunity to impact numerous clinical applications. From morphogenesis to injury to repair, computer methods have potential to revolutionize diagnostics and care of brain-related disorders. This talk will focus on novel computational methods being applied to understand and model the neuronal tract bundle level in the brain. There will be two major parts of the presentation. The first revolves around continuum approaches to extend our modeling capability from the organ level (full brain) to the mesoscopic level of the brain – the level at which magnetic resonance imaging diffusion tractography can be used to describe the structural architecture of the tissue. To bridge this gap, we have applied the embedded element method1 to model the axonal fiber tracts explicitly. An application of the method for modeling axonal injury will be discussed. The second part of the presentation involves beginning at the cell level and extending numerical methods to reach up to the bundle or tract level. The ultimate goal is to develop a simulation platform which can be used for the design and optimization of micro-tissue engineered neural networks in rehabilitation applications. The presentation will discuss techniques, currently under development, that capture bundle growth and the bioelectric response. Ultimately, we hope to link these two scales and enable both a structural and functional models of the brain's physiological activity. Some comments will be made towards this goal. Such a multiscale, Multiphysics approach may elucidate mechanisms of injury, disease, and repair.

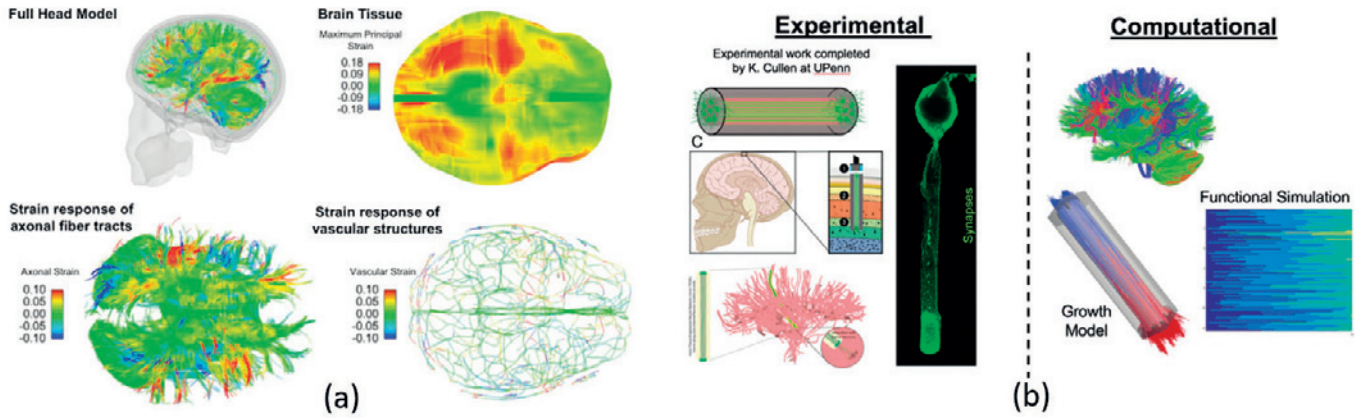

Figure Caption: (a) Finite element model showing how embedded element method can be applied to included axonal fiber tractography and vasculature. (b) Computational framework for designing and optimizing micro-tissue engineered neural networks.

Acknowledgments: The authors acknowledge support provided by the U.S. Army Research Laboratory, Aberdeen Proving Ground, United States under contracts W15P7T-10-D-D416 and DOTC-17-01-INIT0086, and CFD Research Corporation under a subcontract funded by the Department of Defense, Department of Health Program through contract W81XWH-17-C-0216 and NSF CAREER Award # 1846059. The authors thank Dr. Sam Slobounov, Dr. Brian D. Johnson, Dr. Kacy D. Cullen for the data provided.

References:

Garimella, H. T. & Kraft, R. H. Modeling the mechanics of axonal fiber tracts using the embedded finite element method. Int. J. Numer. Methods Biomed. Eng. 33, (2017).

Conflict of Interest: Dr. Kraft has a financial interest in Digital Brain Technologies, LLC. a company which could potentially benefit from the results of this research. This interest has been reviewed by Penn State University, University Park, United States in accordance with its Individual Conflict of Interest policy for the purpose of maintaining the objectivity and integrity in research and is being managed.

[F-04.3]

SPATIO-TEMPORAL DYNAMICS OF HUMAN BRAIN DURING HEAD IMPACTS IN CONTACT SPORTS

Kaveh Laksari[1], *Carissa Grijalva*[1], *Hessam Babaee*[2], *Ryan Black*[2], *Mehmet Kurt*[3]

1 *University of Arizona, Tucson, USA*
2 *University of Pittsburgh, Pittsburgh, USA*
3 *Stevens Institute of Technology, Hoboken, USA*

Traumatic brain injury (TBI) is a major cause of death and disability in the United States, contributing to about 30% of all injury-related deaths [1,2]. Every year, millions of Americans are diagnosed with TBI [3], 80% of which are categorized as mild [2]. Undiagnosed cases, due to either lack of clinical expertise or underreporting, might be twice as high [4]. Given that mild TBI (mTBI), or concussion, has become a serious health concern in society, the burden of understanding and preventing it has become ever more indisputable for clinicians and physicists alike. Until now, only weakly statistical correlations between mechanical parameters, such as head kinematics and more recently brain strain, and brain injury have been proposed. However, there remains a need for deeper understanding of the underlying biomechanical characteristics of brain's response to head impacts in order to be able to develop smart protective technology. Here, we applied a data mining technique, namely Dynamic Mode Decomposition, to local brain displacements derived from finite element simulations of over 180 football head impact. First, by investigating MRI measured brain displacements under mild head motions and comparing those to moderate head motions, we showed that other spatially informed data compression techniques are unable to capture the rich dynamics of the human brain deformations during highly transient phenomena such as head impacts. After analyzing over 40,000 snapshots of close to 5,000 three-dimensional nodal displacements, we showed that 95% of brain's displacement can be explained by temporal modes that have frequencies under 65Hz, contrary to the TBI community's emphasis on much higher frequencies as potentially being dangerous. More importantly, we discovered that strain in brain tissue is amplified in frequencies close to 25Hz, with strain concentration in the parasagittal brain region. We attributed this effect to the significant variation of dynamical characteristics of adjacent brain regions, which could explain high strain concentrations and possibly cause of injury. Most notably, corpus callosum, known to correlate best with diagnosed injuries, has dominant frequencies close to the 25Hz strain amplification mentioned above. Finally, by analyzing the largely-unknown relationship between the helmet dynamics and brain motion, we speculate that softer and bigger helmets can be more effective in attenuating the high temporal differentials between brain regions. This framework in designing smarter protective helmets based on the understanding of the complex dynamics of brain deformation rather than ad hoc injury correlations is unprecedented [4].

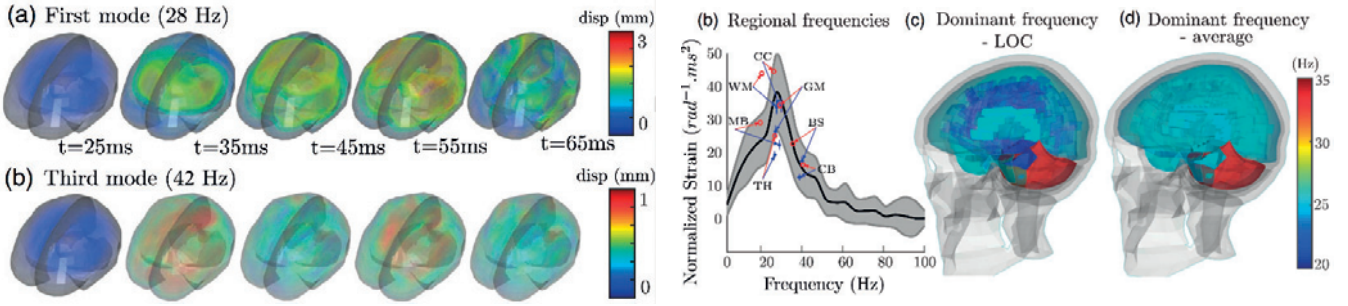

Figure 1 - (a) Propagation of the first displacement mode oscillating at 28 Hz. (b) Propagation of the third displacement mode oscillating at 42 Hz showing out of phase oscillation with the first mode, (c) Strain values derived from each mode normalized by the peak rotational acceleration of the corresponding head kinematics. Here, we superimpose regional dominant frequencies for each brain part for the LOC case (red circles) and the average and standard deviations (blue solid dots) for all cases. Brain part abbreviations: corpus callosum (CC), gray matter (GM), brain stem (BS), midbrain (MB), white matter (WM), thalamus (TH), corpus callosum, cerebellum (CB). (d) Structural distribution of the dominant frequency of brain regions for the LOC case, indicating out of phase oscillation due to significant discrepancy between regions especially in the periventricular region. (e) Structural distribution of dominant frequencies for an average head impact case, which indicates a lower dynamic range.

Acknowledgments: We thank Dr. David Camarillo for sharing the Stanford data.

References:

[1] *M. Faul, et al, Centers for Disease Control and Prevention (2010).*
[2] *C. L. MacDonald, et al, J. Neurotrauma (2014).*
[3] *J. A. Langlois, et al, J. Head Trauma Rehabilitation (2006).*
[4] *K. Laksari, et al, Physical Review Letters (2018).*

[F-04.4]

COMPUTATIONAL MODELLING OF FLUID AND TRACER MOVEMENT IN BRAIN PERIVASCULAR SPACES

Adam Martinac[1], *David Fletcher*[2], *Lynne Bilston*[3]

1 *Neuroscience Research, Sydney, Australia*
2 *University of Sydney, Sydney, Australia*
3 *Neuroscience Research, Sydney, Australia ; University of New South Wales, Kensington, Australia*

Circulation of fluid through the brain and spinal cord maintains fluid homeostasis and solute clearance from the central nervous system (CNS). The 'glymphatic' system is hypothesised to provide a distinct waste clearance system in the brain driven by bulk flow[1]. This proposed flow is the movement of cerebrospinal fluid from periarterial spaces, through the parenchymal interstitium, to perivenous spaces, facilitated by water channels located in astrocytes. The driving force for this mechanism is still unknown, although arterial pulsations and pressure gradients have been suggested. Previous CFD modelling in the spinal cord suggests that timing offsets between arterial and spinal subarachnoid space pressure pulses can give rise to a net inflow[2]. This mechanism is akin to a 'leaky valve' where a mismatch of cardiac and external pulse timing causes a varied resistance to perivascular flow.

In this study, we adapted this approach to the brain, including tracer particles (Dextran 70kDa) to simulate experiments[1]. We applied either a steady pressure drop or intracranial pressure pulses[3] to one end of a 500µm long perivascular space (PVS), and modelled both pressure-driven bulk flow and diffusion, with a moving arterial wall simulating arterial pulsations. Tracer penetration into the brain parenchyma was simulated with permeability values of 5x10-15 m^2 and 1.5x10-13 m^2 for the parenchyma and astrocytes respectively.

The simulations confirmed the feasibility of this 'leaky valve' mechanism in the brain, and increased ICP increases net flow. The results also suggest that arterial pulse amplitude can restrict tracer penetration. Tracer particles driven by bulk flow can penetrate through the PVS with a net velocity of ~90µm/s when there is no arterial wall displacement. With an arterial pulse, the particles become trapped in recirculating flow where instantaneous velocities increase, yet net movement of particles is reduced (~50µm/s). The amplitude of artery wall displacement determines where these zones occur. Results also suggest a diffusive component to tracer particle movement might be required for them to pass these zones and penetrate deeper into the parenchyma. Particles driven solely by the bulk flow of the fluid can reach the parenchyma, but the resistance is too high due to the low permeability of brain.

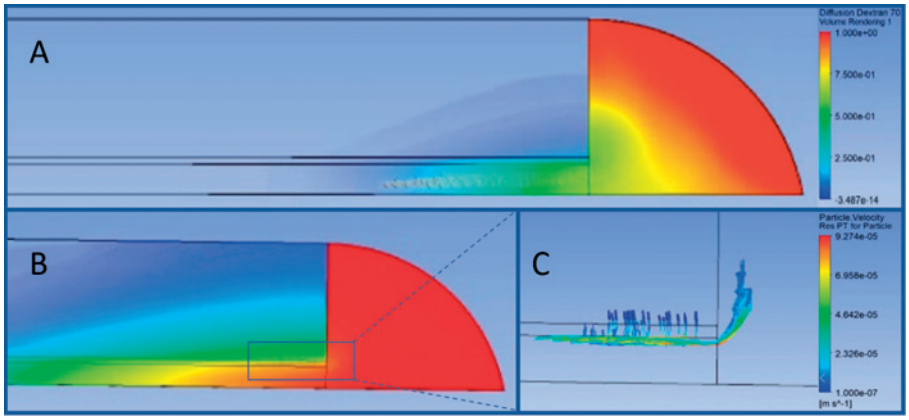

Fig 1. (A) With arterial pulsations, tracer (grey spheres) becomes trapped in recirculation zones. (B) Diffusive modelling of tracer manages to clear both the PVS and parenchyma while bulk flow modelling stays trapped. (C) An inset of (B). Tracer driven solely by bulk flow reaches parenchyma but does not penetrate deeply.

Acknowledgments: Project supported by the Australian Government Research Training Program Scholarship, UNSW POWCS Scholarship, and a NHMRC project grant.

References:

1. Iliff JJ et al., Sci Transl Med. 2012;4(147):147ra11.w;
2. Bilston LE et al., J Neurosurg. 2010;112(4):808-13.;
3. Penn RD et al., Pediatr Neurosurg. 2009;45:161–174.

[F-04.5]

MECHANICAL INJURY THRESHOLDS AND MECHANISMS FOR A RODENT FINITE ELEMENT MODEL OF BLAST-INDUCED TRAUMATIC BRAIN INJURY

Molly Townsend[1], *Namas Chandra*[1]

1 *New Jersey Institute of Technology, Newark, USA; Center for Injury Biomechanics, Materials, and Medicine*

The too-frequent exposure of military and law enforcement servicemembers to a blast-induced shock wave results in a diffuse traumatic brain injury (TBI). This phenomenon is widely studies through animal models, which enables the investigation of injury biomechanics, mechanisms, prevention methods, and diagnostics in a way that is beyond the scope of human testing. However, anatomical differences between animal models and human create additional complexities in applying the extensive findings of animal models towards warfighter combat readiness. Computational models offer a unique opportunity to tie the injury mechanisms and responses of these species together, bridging that gap. This work seeks to understand existing mechanical injury thresholds, proposed for TBI in humans, using a computational animal model. A validated rodent head finite element model was used to simulate a wide variety of loading conditions corresponding with mild to moderate shock exposures (peak overpressure of 130, 180, and 230 kPa). Rodent simulation results were compared to human TBI mechanical injury thresholds developed. These mechanical injury thresholds were developed based upon human blunt injuries through the correlation of computer simulations with clinical injury definitions and accident reconstructions. Simulation results were investigated to identify areas of the brain which exceeded each threshold value, indicating that a theoretical injury takes place. It was found that injury thresholds were largely non-discriminatory and without a neuropathological basis in the animal model, it offers little to no insight into the severity of injury observed in shock exposure. Of the fifteen injury criteria investigated, seven reported an injured brain volume of over 99% in the lowest severity blast investigated, 130 kPa (Figure 1A). Seven of the remaining eight reported an injured volume of under 1%. The five most severe strain-based injury criteria were not triggered for the highest severity shock simulated, 230 kPa (Figure 1B). This highlights the lack of sensitivity that existing mechanical injury thresholds have in predicting the subtle nature of blast injury in a rodent model. Although blast is known as a diffuse injury, a mechanical injury threshold should identify some spatial variability, as seen in the neuropathology of blast injuries at varying injury severity (Kuriakose 2018). Therefore, a more sensitive injury marker is proposed which offers higher specificity for blast-induced TBI in a rodent model. This work marks an important step towards the development of mechanically-based, inter-species injury levels.

(A) 130 kPa Incident Overpressure

(A) 230 kPa Incident Overpressure

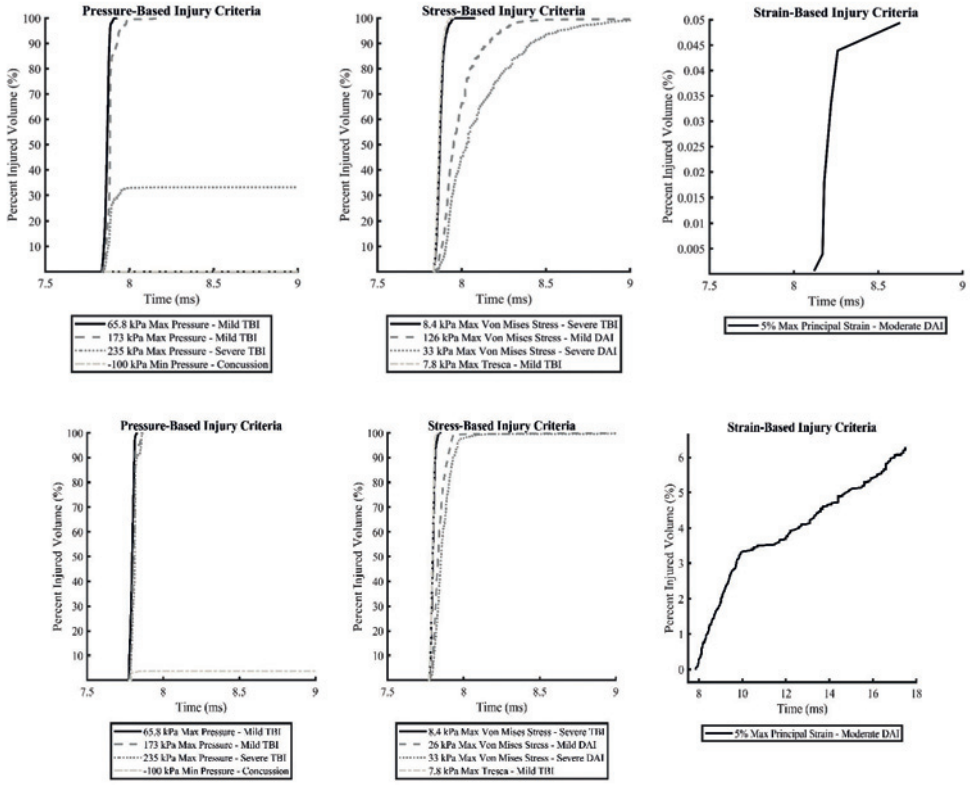

Figure 1: The percent injured volume of the brain for (left) four pressure-based, (middle) four stress-based, and (right) one strain-based injury criteria in a (A) 130 kPa and (B) 230 kPa exposure.

References:

Kuriakose M, Rama Rao KV, Younger D, Chandra N. 2018. Temporal and spatial effects of blast overpressure on blood-brain barrier permeability in traumatic brain injury. Sci Rep. 8(1):8681.

[F-04.6]

A NOVEL NONLINEAR DYNAMIC REDUCED ORDER MODEL OF THE HUMAN BRAIN UNDER CORONAL ROTATION FOR STUDY OF TRAUMATIC INJURY

Alireza Mojahed[1], *Javid Abderezaei*[2], *Mehmet Kurt*[2], *Songbai Ji*[3], *Lawrence Bergman*[4], *Alexander Vakakis*[1]

1 *Department of Mechanical Science and Engineering, University of Illinois, Illinois, USA*
2 *Stevens Institute of Technology, Hoboken, USA*
3 *Worcester Polytechnic Institute, Worcester, USA*
4 *Department of Aerospace Engineering, University of Illinois, Illinois, USA*

Despite substantial research, there is no consensus as to the biomechanical mechanisms underlying traumatic brain injury (TBI), a leading cause of mortality and morbidity. The current criteria, developed to analyze the effect of head impacts, are based either on kinematics (e.g., head injury criteria (HIC)) or brain finite element (FE) models (e.g., cumulative strain damage measures (CSDM)). It has been observed that TBI usually affects the deep region of brain, and recent studies have shown that to be the area of the brain exhibiting strong nonlinear behavior perhaps explaining why the deep region is more susceptible to injuries. Inspired by these observations, we propose a planar reduced order model (ROM) to represent the dynamics of the deep region of the brain in the coronal plane. The model consists of discrete masses, linear springs and dampers, with kinematics accounting for the strong nonlinearity. To reconcile this model with a FE model of human brain – the Worcester Head Injury Model (WHIM) – system identification analyses were performed to determine the unknown stiffness and damping coefficients. Then, in order to ensure the validity of the identified parameters and capability of the proposed model to predict the response of the brain under impact-like excitations, the following steps were taken: First, the time-responses of the model under impact-like excitations were compared with those of WHIM to verify the good agreement between the response of the ROM and that of the FE model. Following that, injury tolerance curves suggested by Margulies and Thibault [1] and by Ommaya [2] were compared with the iso-strain curves produced by our proposed ROM. These thresholds appeared to be in good agreement with the results from our model. Finally, by employing the proper orthogonal decomposition (POD) method, it was shown that the proposed model exhibits nonlinear behavior similar to that of the deep region of the brain. As noted previously, that the model exhibits nonlinear behavior, while all of the elements in the proposed model are linear, implies that the nonlinearity originates from the geometry and the kinematics of the model. Keeping this in mind, and recalling that the nonlinear behavior exhibited by the brain FE model and the ROM are similar, one can conclude that the hardening nonlinearity observed in the deep region of the brain is likely a result of the special configuration of the human brain. Having similar characteristics as linear reduced order models of the brain in the literature and being capable of exhibiting similar nonlinear behavior as FE models of human brain with a relatively simple and basic design, it is conjectured that the proposed reduced order model can be used effectively in injury-prediction and research applications.

Acknowledgments: We thank Sonbai Ji and Wei Zhao for providing us with numerical data from their FE model of the human brain.

References:

[1] *Margulies, S. S., & Thibault, L. E. (1992). A proposed tolerance criterion for diffuse axonal injury in man. Journal of biomechanics, 25(8), 917-923.*
[2] *Ommaya, A. K. (1985). Biomechanics of head injuries: Experimental Aspects,‖ Biomechanics of Trauma. Nahum and Melvin, eds. Appleton-Century-Crofts, East Norwalk, CT, 249-269.*

[F-05.1]
IMAGE-BASED BIOMEDICAL VISUALIZATION

Chris Johnson[1]

1 *Scientific Computing and Imaging Institute, Salt Lake City, USA; University of Utah, Salt Lake City, USA*

Computers are now extensively used throughout science, engineering, and medicine. Advances in computing allow researchers to build and test models of increasingly complex phenomena and thus to generate unprecedented amounts of data. These advances have created the need to make corresponding progress in our ability to understand large amounts of data and information arising from multiple sources. In fact, to effectively understand and make use of the vast amounts of information being produced is one of the greatest scientific challenges of the 21st Century. Visual computing, which relies on and takes advantage of, the interplay among techniques of visualization, large-scale computing, data management, and imaging, is fundamental to understanding models of complex phenomena, which are often multi-disciplinary in nature. In this talk, I will provide examples of visual computing as applied to important problems in biomedicine and discuss solving important research and clinical problems in biomechanics, cardiology, and genetics.

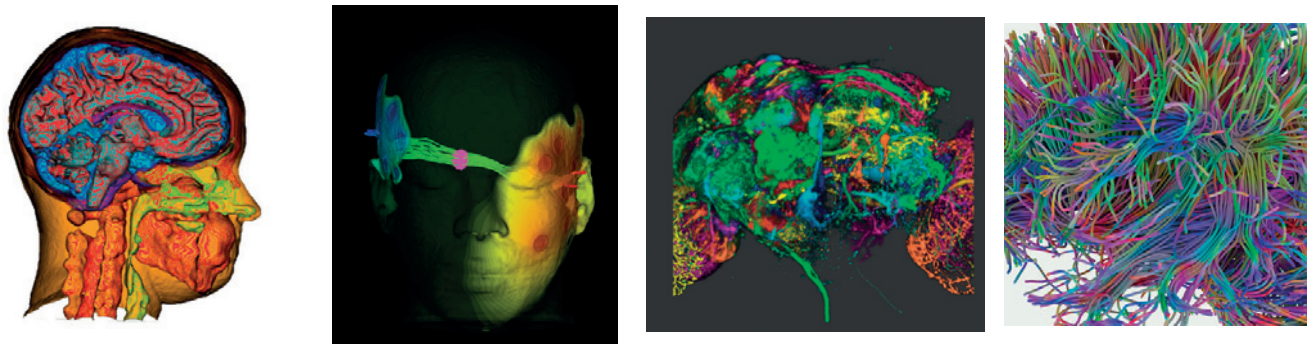

Figure Caption: Biomedical visualizations (left to right) of a large-scale head and brain finite element model; neurostimulation simulation streamlines; multichannel confocal imaging; semi-transparent white matter tracts from an MR-DTI.

Acknowledgments: This project is supported in part by the National Institute of General Medical Sciences of the National Institutes of Health under grant number P41 GM103545-18 and by the Intel Parallel Computing Centers Program.

References:

1. *M. Chen, H. Hagen, C. Hansen, C.R. Johnson, and A. Kauffman, editors. Scientific Visualization: Uncertainty, Multifield, Biomedical, and Scalable Visualization. Springer-Verlag, 416 pages, 2014.*
2. *X. Tong, J. Edwards, C. Chen, H. Shen, C. R. Johnson, P. Wong. View-Dependent Streamline Deformation and Exploration, In IEEE Transactions on Visualization and Computer Graphics, vol. 22, no. 7, pp. 1788-1801, 2016.*
3. *C.R. Johnson. Biomedical Visual Computing: Case Studies and Challenges, IEEE Computing in Science and Engineering, Volume 14, Issue 1 pp. 12-21, 2012.*
4. *C.R. Johnson and X. Tricoche. Biomedical Visualization. In Advances of Biomedical Engineering, P. Verdonck, Editor, Elsevier Science, pp. 209-272, 2008.*

[F-05.2]
CARDIOVASCULAR BIOMECHANICS USING 4D FLOW MRI

Alejandro Roldán-Alzate[1]

1 *University of Wisconsin, Madison, USA; Department of Mechanical Engineering, Department of Radiology*

Cardiovascular disease accounts for approximately one-third of mortality world-wide, and often requires invasive diagnostic and treatment methods [1, 2]. However, the development of medical imaging methods have greatly improved diagnosis and treatment, often in a non-invasive manner [3]. One imaging method, four-dimensional (4D) flow magnetic resonance imaging (MRI), has been particularly useful in non-invasive analysis and treatment planning of complex cardiovascular conditions due to the time-resolved, three-dimensional flow data that it can provide [4, 5]. Not only can complex flow patterns be visualized in nearly any anatomical region of the body, but the 4D flow MRI-derived velocity data can also be used to quantify and calculate a number of clinically valuable fluid dynamic parameters. For example, velocity information can be used to calculate energy losses across and within vascular regions, such as the cardiac ventricles and vasculature (1a), giving an indication of the efficiency of the system. Flow rotation metrics such as vorticity and helicity can be used to analyze the flow patterns in abnormal vascular anatomy, such as in cerebral aneurysms (1b). Flow magnitude changes can be analyzed across varying physiological conditions, such as occur in the liver after eating a meal (1c). Other derived metrics, like pulse-wave velocity, can be quantified to give an idea of the stiffness of blood vessels (1d). Furthermore, the effects that a surgical procedure has on essential blood flow can be analyzed, as is done in the total cavopulmonary connection (TCPC) (1f). Finally, validation experiments can be conducted to compare these metrics to real fluid flow measurements. With appropriate scientific and clinical collaboration, and strong validation and application methods, 4D flow MRI has immense potential for improving biomechanical analysis in a wide variety of cardiovascular conditions and procedures.

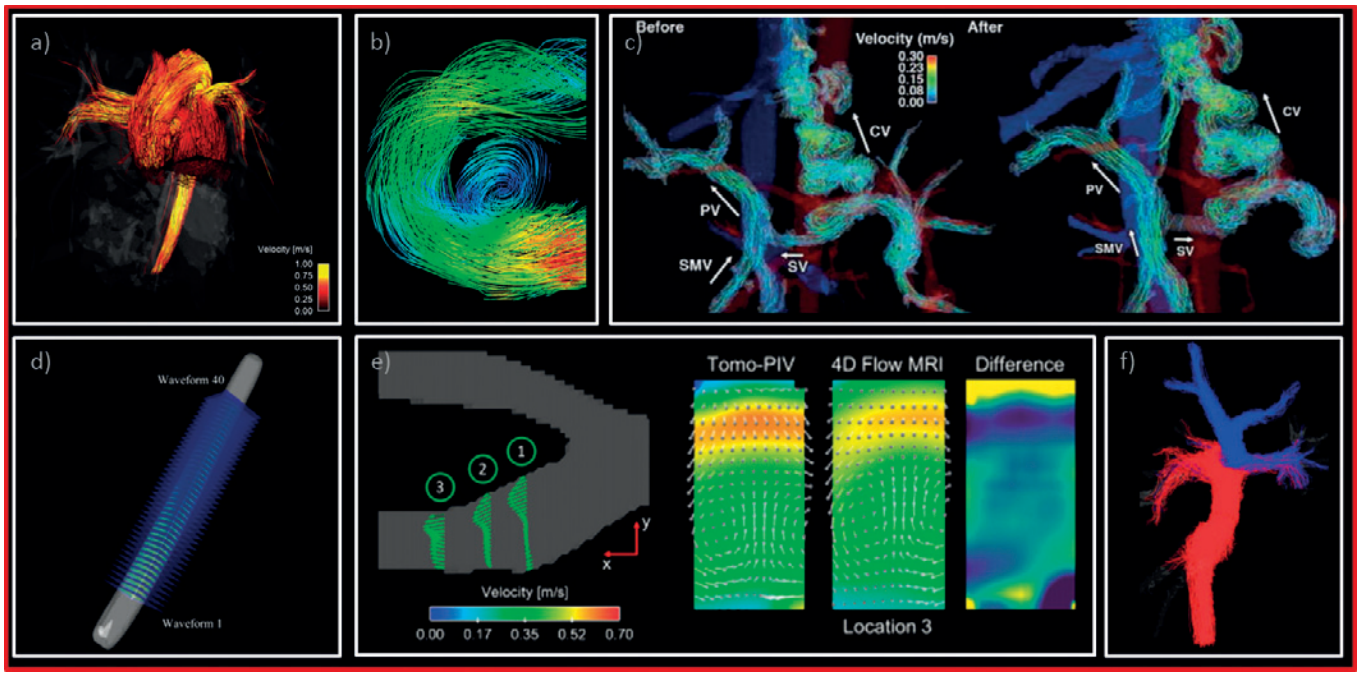

Figure 1 Caption: 4D flow MRI can be used to analyze a wide variety of cardiovascular biomechanics problems. a) Cardiac analysis of ventricular and great vessel flow b) helical flow in a cerebral aneurysm c) meal challenge flow data in hepatic vasculature d) pulse wave velocity measurement in an MRI blood vessel phantom e) 4D flow validation experiment with particle image velocimetry f) flow distribution in a TCPC.

References:

[1] *Stewart, J., et al., 2017, JRSM Cardiovasc Dis, 6, p. 2048004016687211.*
[2] *Perk, J., et al, E. A. f. C. P. R., 2012, Int J Behav Med, 19(4), pp. 403-488.*
[3] *Nerem, R. M., 2013, Glob Cardiol Sci Pract, 2013(1), pp. 29-36.*
[4] *Markl, M., et al, 2012, "4D flow MRI," J Magn Reson Imaging, 36(5), pp. 1015-1036.*
[5] *Roldán-Alzate, A., et al., 2016, AJR Am J Roentgenol, 207(1), pp. 58-66.*

[F-05.3]
RECENT ADVANCES IN CARDIOVASCULAR PHOTOACOUSTIC IMAGING

Craig Goergen[1]

1 *Purdue University, West Lafayette, USA*

Photoacoustic (PA) imaging is an emerging modality which uses pulsed laser light to induce acoustic waves that can be used to quantify the location and density of biological components [1]. When used in combination with traditional ultrasound (US), this technique can be used to obtain structural, hemodynamic, and compositional information. For example, because oxy- and deoxyhemoglobin absorb light at unique characteristic wavelengths, multispectral imaging can be used to noninvasively quantify oxygen saturation within tissue. Similarly, peak absorption of lipid at 1210nm can be utilized to create label-free images of tissue that are relevant to atherosclerosis. The purpose of this talk will be to highlight multiple studies that reflect the recent advancements in PA imaging with special emphasis on small animal techniques where much of the initial work has been applied. First, we developed a novel motorized PA probe capable of tuning the depth in which light is focused, effectively reducing probe-skin artifacts while overcoming many of the challenges associated with high-resolution in vivo PA imaging (Fig. 1 left/middle). An improvement in signal-to-noise ratio (SNR) and penetration depth was observed due to the optimized photon density within deeper regions of interest [2]. Second, the potential for PA imaging of atherosclerosis will be highlighted via a study quantifying lipid accumulation within atherosclerotic lesions using a partial carotid ligation model of apolipoprotein E-deficient mice fed a high fat diet (Fig. 1 right; [3]). Third, parametric maps of myocardial O2 saturation within murine hearts, which can beat up to 600 beats per minute, were created via PA signals at 750nm and 850nm. This study utilized a model of myocardial infarction to develop and optimize a retrospectively gated multispectral 4D PA/US technique for high-resolution volumetric cardiac imaging in mice [4]. While not yet broadly used in the clinic, PA imaging approaches have the clear potential to image deep internal structures, longitudinally monitor atherosclerotic plaque progression, and more effectively diagnose acute myocardial infarction.

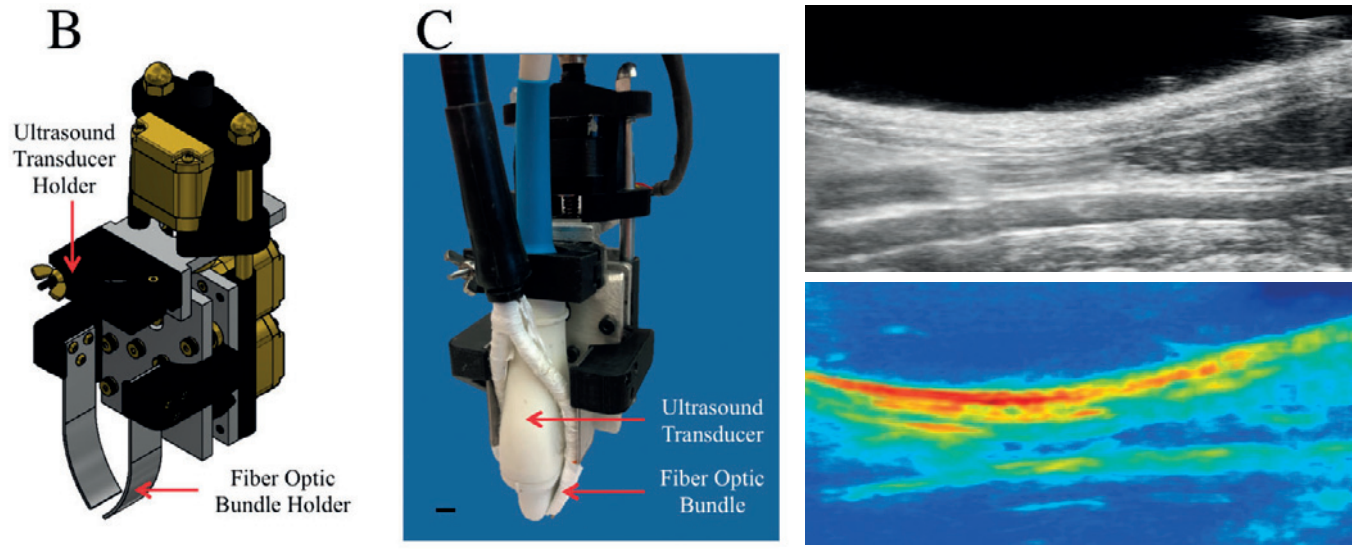

Figure Caption: Photoacoustic transducer holder CAD drawing (left), picture (middle), and murine images of a mouse aorta with subcutaneous and perivascular lipid accumulation (right).

Acknowledgments: Gurneet S. Sangha contributed to the studies highlighted in this presentation.

References:

1. *Sangha GS, Goergen CJ. Photoacoustic Tomography: Applications for Atherosclerosis Imaging. Journal of Optics. 2016 Jul 14; 18(4):084005.*
2. *Sangha GS, et al. Adjustable photoacoustic tomography probe improves light delivery and image quality. Photoacoustics. 2018 Aug 22; 12:6-13.*
3. *Sangha GS, et al. In Vivo Photoacoustic Lipid Imaging in Mice Using the Second Near-Infrared Window. Biomedical Optics Express. 2017 Feb; 8(2): 736-742.*
4. *Sangha GS, et al. Photoacoustic Imaging Of Myocardial Oxygen Saturation Changes Using Retrospective Gating. European Molecular Imaging Meeting. Glasgow, Scotland. 2019 March 19-22.*

[F-05.4]

ESTABLISHMENT OF AN ANALYSIS AND VISUALIZATION FRAMEWORK TO INTERROGATE THE IN VIVO VASCULAR BIOMECHANICAL ENVIRONMENT WITH 4D FLOW CMR

Elliott Hurd[1], *David Jiang*[1], *Chris Johnson*[2], *Edward DiBella*[3], *Lucas Timmins*[4]

1 *Department of Biomedical Engineering, University of Utah, Salt Lake City, USA*
2 *Scientific Computing and Imaging Institute, Salt Lake City, USA, University of Utah, Salt Lake City, USA; School of Computing, University of Utah, Salt Lake City, USA*
3 *Department of Radiology and Imaging Sciences, University of Utah, Salt Lake City, USA; Department of Biomedical Engineering, University of Utah, Salt Lake City, USA*
4 *Department of Biomedical Engineering, University of Utah, Salt Lake City, USA; Scientific Computing and Imaging Institute, Salt Lake City, USA, University of Utah, Salt Lake City, USA*

Four-dimensional (4D) flow cardiovascular magnetic resonance (CMR) permits comprehensive evaluation of the flow field in the cardiac chambers and large vessels. While 4D flow CMR has provided further insight on the role of hemodynamics in cardiovascular physiology and pathophysiologies, limitations in advanced flow visualization strategies to interact and interrogate the image data has limited the clinical utility of this modality to mostly a research tool. Thus, the aim of this project was to establish an analysis and visualization framework utilizing fully open-source software platforms to provide high-fidelity visualization and data quantification approaches to evaluate 4D flow CMR data.

4D flow CMR image data were collected in experimental and clinical settings (3T Prisma scanner). Patient-specific arterial phantoms (carotid, type B aortic dissection) were imaged while being subjected to physiologic flow conditions with the aid of a custom computer-controlled MR-compatible experimental flow circuit, and the thoracic aorta of healthy volunteers were imaged using sagittal oblique slices and prospective respiratory gating (Fig. 1A,B). Image data were segmented (Seg3D) to isolate the fluid volume, converted from raw to velocity data using defined VENCs, and imported into ParaView, which included the OSPray ray tracing framework plugin for high-quality rendering [1]. Data were processed to create flow streamlines, velocity profiles, and particle tracings for qualitative analysis and extract quantitative data on temporal velocities, flow rates, vorticity, and helicity at specific anatomic positions.

We successfully integrated the OSPray ray tracing framing to create high-fidelity visualizations of the 4D flow CMR data. Evaluation of flow streamlines encoded with velocity magnitude and vorticity demonstrated strong heterogeneity in the flow field across the imaged volume (Fig. 1C-F). For example, quantification of data in a representative volunteer aorta showed anatomic differences for several hemodynamic metrics. While significant differences in values at the aortic arch and descending aorta were not observed in time-average velocity (32.0±12.3 vs. 36.4±11.0 cm/s, respectively) and vorticity (1.5±1.0 vs. 1.6±1.2 s-1, respectively), significant differences were observed in helicity (20.9±16.8 vs. 11.6±9.8 s-1, respectively, $p<0.05$), which suggest increased flow disturbances at the site of the complex anatomy.

In our preliminary study, we demonstrate the utility of establishing a visualization framework to examine the in vivo mechanical environment via 4D flow CMR. We highlight the use of fully open-source software platforms for image analysis towards increasing the use of 4D flow CMR in the research and clinical communities.

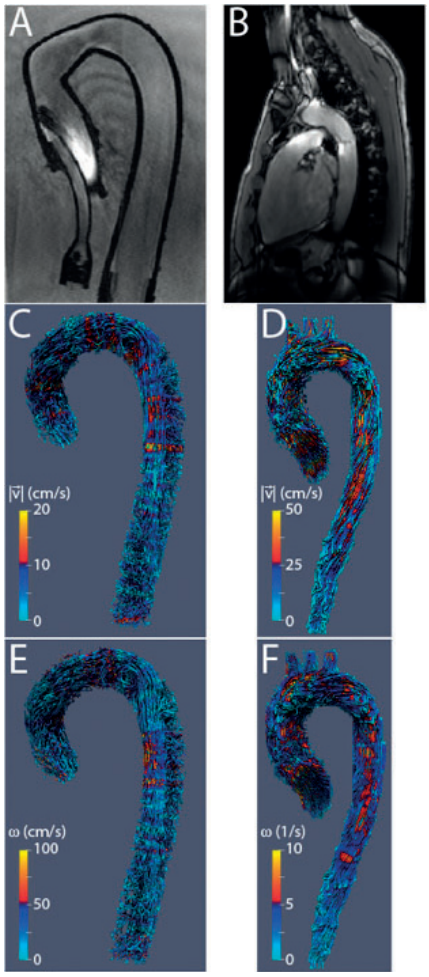

Figure 1: Magnitude images of aortic phantom (A) and volunteer thoracic aorta (B). Streamlines encoded with velocity (C,D) and vorticity (E,F).

Acknowledgments: The Authors thank John Oshinski, PhD, Jason Mendes, PhD, and Mengjiao Han for their assistance in conducting the study.

References:

[1] Wald, I. et al., 2017, IEEE Trans. Vis. Comput. Graph., vol. 23(1).

[F-05.5]

DEEP LEARNING BASED SUPER-RESOLUTION OF 4D FLOW MRI IN BRAIN ANEURYSMS

Augusto Sanches[1], *Suprosanna Shit*[2], *Judith Zimmermann*[2], *Thomas Liebig*[3], *Bjoern Menze*[2]

1 *Department of Informatics, Technical University of Munich (Tum), Munich, Germany; Department of Neuroradiology, University Hospital Munich (Lmu), Munich, Germany*
2 *Department of Informatics, Technical University of Munich (Tum), Munich, Germany*
3 *Department of Neuroradiology, University Hospital Munich (Lmu), Munich, Germany*

Cerebral aneurysms are a life-threatening clinical condition that can produce severe intracranial bleeding, a subarachnoid hemorrhage, with an estimated prevalence of between 2% and 5% of the population. Most of the aneurysms are discovered only after rupture. Furthermore, due to the current advance of diagnostic imaging access worldwide, there are an increasing number of incidentally discovered aneurysm patients who will require a fast evaluation for potential treatment or follow-up. Thus, the equilibrium between rupture risk and treatment risk, to be considered in the orientation of the clinical decision, became a challenge.

The assessment of the intracranial hemodynamics seems to play to a major role for the understanding and management of this lesion and the appraisal of the blood flow can be crucial and influence positively on the patients' management. Four-dimensional (4D) flow magnetic resonance imaging (MRI) is a noninvasive phase contrast technique with additional temporal resolution that has been developed to assess qualitatively and to measure quantitatively the hemodynamics in vascular diseases. It has a great potential if followed by further technical improvements and comprehensive and systematic clinical studies.

Flow sequences improvements and higher magnetic fields enable 4D flow MRI to access vascular structures with smaller diameters such as intracranial vessels. However, there is a trade-off between the signal-to-noise ratio, spatio-temporal resolution and acquisition duration. For instance, an increase in resolution deteriorates SNR drastically. Furthermore, an inadequate spatial resolution leads to an inaccurate and unstable numerical estimation of the local blood flow parameters. Thus, noise-suppressed and high-resolution 4D flow MRI data is essential in order to perform stable and reliable inferences of the blood flow quantification.

In the present work, we address the problem to super-resolve (SR) three dimensional velocity field data obtained from 4D flow MRI. Recently, deep neural network based SR became popular in computer vision due to its fast processing time and high accuracy [1]. We develop a novel deep learning architecture to super-resolve 3D vector fields and show its application in spatial SR of 4D flow MRI in intracranial aneurysms. We validate our super resolution technique in comparison with patient-specific computational fluid dynamics simulations using segmented intracranial vessels and boundary conditions obtained from 2D phase contract-MRI sequence.

The proposed network is computationally efficient and outperforms the conventional cubic spline based up-sampling in quantitative reconstruction metrics such as peak-signal-to-noise ratio and flow divergence. This network delineates flow patterns in the intracranial vessels more accurately.

Reference:

[1] J. Yu, Y. Fan, J. Yang, N. Xu, Z. Wang, X. Wang, and T. Huang. Wide activation for efficient and accurate image super-resolution. arXiv preprint arXiv:1808.08718, 2018.

[F-06.1]

4D POINT CLOUD REGISTRATION FOR TUMOR VASCULAR NETWORKS MONITORING FROM ULTRASENSITIVE DOPPLER IMAGES

Emmanuel Cohen[1], *Thomas Deffieux*[2], *Charlie Demene*[2], *Laurent Cohen*[3], *Mikael Tanter*[2]

1 *CEREMADE, Université Paris Dauphine, PSL Research University, CNRS, UMR 7534, Paris, France; Institut Langevin, Espci Paristech, Psl Research University, Cnrs, Umr 7587, Inserm U979, Paris, France*
2 *Institut Langevin, Espci Paristech, Psl Research University, Cnrs, Umr 7587, Inserm U979, Paris, France*
3 *University Paris Dauphine, Psl Research University, Cnrs, Umr 7534, Ceremade, 75016 Paris, France; Université Paris Dauphine, Psl*; CEREMADE, Université Paris Dauphine, PSL Research University, CNRS, UMR 7534, Paris, France*

Numerous diseases find their origin and their diagnosis in the physiological behavior of vascular networks [1]. In particular, to understand the architecture and growth of a tumor the study of blood flows is crucial. Recently, ultrasensitive Doppler has enabled 4D ultrasound imaging of tumor micro-vasculature in mice [2]. In this study, we propose new computational tools to monitor the growth of a tumor vascular network by registering in time and space this new highly sensitive temporal data. We first quantify the acquired data using the minimal-path based framework we introduced in [3]; the vascular network paths around the tumor are segmented from images obtained for four days of observation; local geometrical parameters such as diameters are also estimated. Then, using a point cloud representation of the segmented vascular networks, we develop point cloud registration algorithms that automatically align similar vascular structures, thus allowing a better visualization of the growth and the evolution of the tumor vascular network. A rigid registration model is first considered by manually selecting similar features from two temporal different observations of the tumor. More accurate results are then obtained by automatically extracting invariant vascular patterns. Finally, combining rigid transformations to non-linear deformation models produce a very accurate time matching between invariant vascular structures.

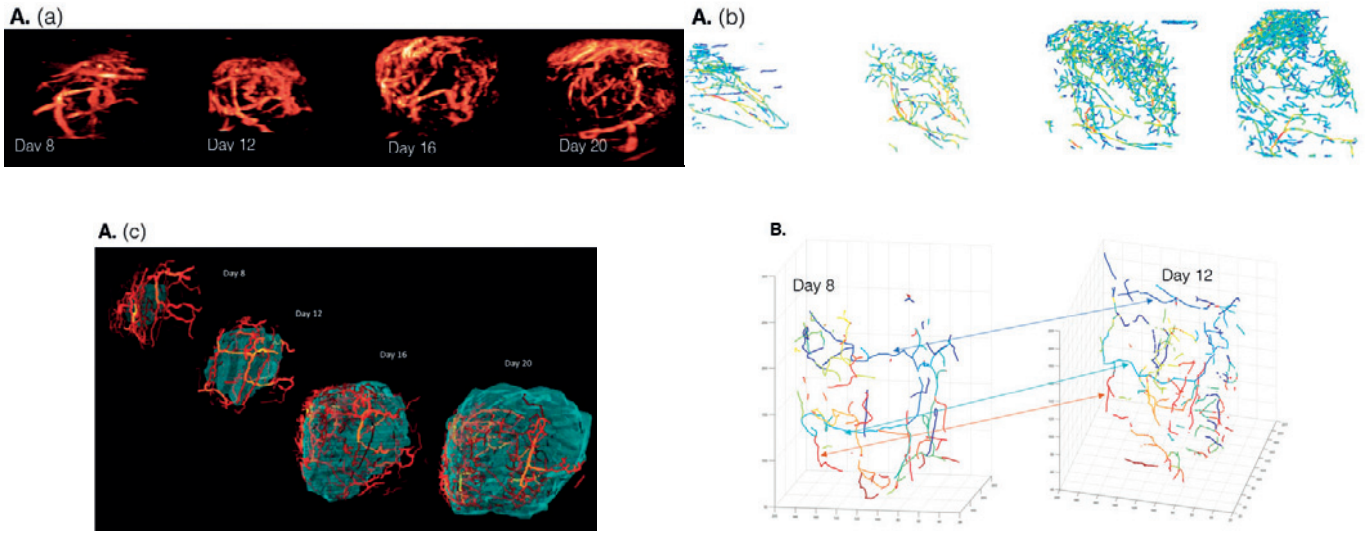

Figure Caption: A. Tumor growth reconstruction and visualization over four days of observations after implantation in a mouse back using our segmentation and registration pipeline. (a) Ultrasensitive Doppler original data. (b) Segmented vascular networks. (c) Registered vascular networks with tumor tissue in blue. B. Matching of vascular structures from temporal tumor data. Left: day 8. Right: day 12. Matching structures are drawn with the same color on both graphs.

References:

[1] *Folkman, J. (1971). "Tumor angiogenesis: therapeutic implications". In: New England Journal of Medicine 285.21, pp. 1182-1186.*
[2] *Demene, C., et al. (2014). "Comparison of tumor microvasculature assessment via ultrafast Doppler tomography and dynamic contrast enhanced ultrasound". In: Ultrasonics Symposium (IUS), 2014 IEEE International. IEEE, pp. 421-424.*
[3] *Cohen, E., et al. (2017). "An isotropic minimal path based framework for segmentation and quantification of vascular networks". In: International Workshop on Energy Minimization Methods in Computer Vision and Pattern Recognition. Springer, pp. 499-513.*

[F-06.2]

MATHEMATICAL CHALLENGES IN DIFFUSE OPTICAL TOMOGRAPHY: ENHANCING ACCURACY AND SPEED

Paola Causin[1], *Marina Giulia Lupieri*[2], *Giovanni Naldi*[2], *Rada Maria Weishaeupl*[2]

1 *Department of Mathematics, University of Milan, Milano, Italy*
2 *University of Milano, Milano, Italy*

Qualitative diagnoses via reflected or transmitted light through biological tissues are very familiar to physicians. Diffuse Optical Tomography (DOT) provides instead a quantitative tool. In this technology, light injected in the tissue from several near infrared sources is collected and tomographic reconstruction of the optical coefficients distribution is performed. This task implies the solution of an inverse problem consisting in the minimization of the discrepancy between the observed data and the corresponding mathematically modeled field. While several literature works and computer software address the inverse problem solution (see [1] for a review), we believe that space is still open to produce the accurate and fast approaches requested to market light imaging instruments. In this presentation, we will discuss our efforts to overcome the speed bottlenecks as well as the severe ill-conditioning phenomena occurring in the inverse problem solution. A first contribution stems from the observation that much computational time is spent in solving the light propagation model. Adopting the steady diffusion approximation and using for its solution free space Green's functions yields a fast approach, albeit at the expense of accuracy where it is needed most, i.e. at the boundary. We propose to adopt the method of fundamental solutions (MFS, [2]), a boundary discretization technique which makes use of the Green's functions basis, enforcing correct boundary conditions via a collocation approach on a virtual exterior domain, preserving high speed. Another contribution stems from the need for a proper regularization of the inverse problem. Tikhonov (L2) as well as LASSO (L1) penalizations have been generally advocated in DOT. Here we originally consider for DOT a combination of the two techniques, known as "elastic net", which shares the desirable properties of both [3]. This procedure provides a robust regularization -thanks to the L2 norm- and can single out areas of interest in the domain -due to L1 norm. We assess the potentialities of these approaches in the context of DOT used for breast cancer screening, presenting simulations carried out on several 2D and 3D cases."

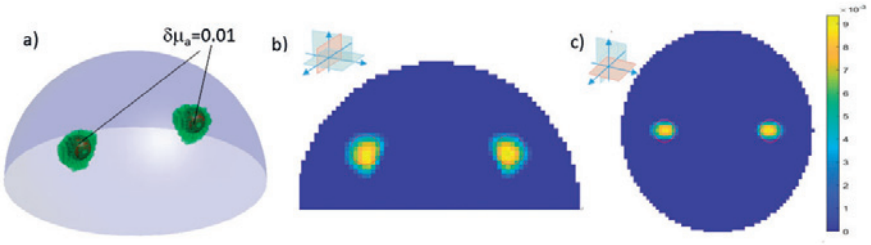

Figure Caption: Domain with two inclusions: a)localization; b),c)slices showing the intensity of the reconstructed variation of absorption coefficient

References:

[1] H. Jiang, Diffuse Optical Tomography: Principles and Applications. CRC Press, 2018
[2] G. Fairweather, A. Karageorghis, "The method of fundamental solutions for elliptic boundary value problems", Adv. Comput. Math. 9, pp.69-95, 1998
[3] H. Zou, T.Hastie, "Regularization and variable selection via the elastic net", J.R. Stat. Soc. Series B, 67(2), pp.301-320, 2005

[F-06.3]

BREAST CANCER CATEGORIZATION USING CONVOLUTIONAL NEURAL NETWORKS

*Clayton Pereira[1], Claudio Santos[2], Luis Afonso[2], Leandro Passos[1], **Joao Papa**[1]*

1 *UNESP - Sao Paulo State University, Bauru, Brazil*
2 *Ufscar - Federal University of Sao Carlos, São Carlos, Brazil*

Breast cancer is one of the most common types of cancer among women worldwide, and its diagnosis is based on the appearance, structure, and reproductive behavior of the affected cells. Besides, its severity can be measured mainly by the development stage of the cells. The tumors are classified as either benign or malignant, where the former is not considered hazardous to health. Nonetheless, the benign tumors must be periodically monitored to control their activity and to prevent them to eventually become malignant. Although the dominant test used for diagnosis is the analysis of microscopic cells images from the tissue, this method depends on professional evaluation. Several automated techniques have been proposed to aid diagnosis by indicating potential tumor locations or by providing a broader insight, but they only indicate the type of tumor (i.e., benign or malignant). This work provides a framework able to distinguish between eight types of tumors, being four benign: Adenosis (Ad), Fibroadenoma (Fi), Tubular Adenoma (Ta) and Phyllodes Tumor (Pt); and four malignant: Ductal Carcinoma (dc), Lobular Carcinoma (lc), Mucinous Carcinoma (mc) and Papillary Carcinoma (pc). The proposed architecture relies on the fusion of traditional convolution kernels with dilated convolutions before pooling, thus increasing the learning capacity with more spatial information. The experiments were carried out in a relatively small data set comprised of around 1,820 images [1], and the results were compared against the state-of-art architectures ResNET50 [2] and MobileNET [3]. The proposed framework outperformed the state-of-art techniques by reaching over 94% accuracy, and in some specific cases grasping over 99.8% efficiency. Figure 1 presents an example of a cancerous image and its convolved versions. The technique showed promising results primarily because of the relatively small dataset since most state-of-art techniques require several thousand images for better performance. It is worth mentioning that the experimental dataset is unbalanced with one of the classes containing around 40% of the samples.

(a) *(b)* *(c)*

Figure 1: Examples: (a) cancerous image and its convolved versions in (b) and (c).

Acknowledgments: The authors are grateful to CNPq grants 307066/2017-7 and 427968/2018-6, as well as FAPESP grants 2013/07375-0, 2014/12236-1 and 2016/19403-6.

References:

[1] *B. R. N. Matheus and H. Schiabel, "Online mammographic images database for development and comparison of cad schemes," Journal of Digital Imaging, vol. 24, no. 3, pp. 500–506, Jun 2011.*
[2] *A. G. Howard, M. Zhu, B. Chen, D. Kalenichenko, W. Wang, T. Weyand, M. Andreetto, and H. Adam, "Mobilenets: Efficient convolutional neural networks for mobile vision applications," CoRR, vol. Abs/1704.04861, 04, 2017.*
[3] *K. He, X. Zhang, S. Ren, and J. Sun, "Deep residual learning for image recognition," in 2016 IEEE Conference on Computer Vision and Pattern Recognition (CVPR), 2016, pp. 770–778.*

[F-06.4]

LIVER TUMOUR SEGMENTATION WITH CONVOLUTIONAL NEURAL NETWORKS

*Jessica Delmoral[1], Diogo Faria[2], Durval Costa[3], **Joao Tavares**[4]*

1 *Faculdade de Engenharia, Universidade do Porto, Porto, Portugal*
2 *Universidade de Aveiro, Aveiro, Portugal*
3 *Fundação Champalimaud, Lisbon, Portugal*
4 *Faculdade de Engenharia, Universidade do Porto, Porto, Portugal; Instituto de Ciência e Inovação Em Engenharia Mecânica e Engenharia Industrial*

The 3D segmentation of the liver can provide doctors with meaningful and reliable quantitative information, which can facilitate the diagnosis of liver abnormalities. However, this segmentation is challenging due to the usually low contrast among liver/lesions/and nearby organs [1]. Convolutional neural networks (CNNs) have become the state of the art in several fields of computational vision. Particularly, CNNs have successfully addressed segmentation problems toward hierarchical representations build from image data. The purpose of this study was to develop a CNN to build 3D liver and tumour shapes from abdominal CT scans. A total of 130 CT scans obtained from the publicly available 2017 MICCAI Lits dataset were used to assess the developed segmentation approach, which aims the identification of the: liver, liver tumor and background. The annotation of the objects was performed in each scan by trained health professionals. We used cascaded CNN architecture, which starts by segmenting the liver in order to establish a target region of interest (ROI), followed by a second step concerning the segmentation of the lesion in the ROI. This segmentation is complemented with a segmentation refinement step performed using a statistical modeling method: 3D Conditional Random Fields (CRF). We designed a variation of the standard U-Net by including a dilated pyramid pooling module as the encoding path. Two CNNs were trained end-to-end, with a He norm weight initialization, and a weight function was integrated into the loss function so as to strengthen the supervision of the tumor boundaries. Our approach was able to successfully extract the liver and tumors in a subset of 30 scans, Figure 1, outperforming two state-of-the-art approaches in terms of the quantitative metrics: Dice coefficient, sensitivity (SE), and specificity (SP), Table 1.

Method	Dice (%)		SE		SP	
	liver	tumor	liver	tumor	liver	tumor
[2]	96.3	65.7	-	-	-	-
[3]	95.9	50.0	-	-	-	-
Ours	94.4	59.6	90.5	50.7	93.8	59.9

Table 1. Performance metrics result.

Figure 1. Original CT slice, target annotations and obtained segmentations.

Acknowledgments: The authors gratefully acknowledge the funding from Project NORTE-01-0145-FEDER- 000022, cofinanced by NORTE2020/FEDER. The authors also thank Nvidia, for providing one NVIDIA Titan Xp GPU board.

References:

1. *A. Gotra, et. al, Liver segmentation: indications, techniques and future directions. Insights into imaging,8(4): 377-392, 2017.*
2. *Yading Y, Hierarchical convolutional-deconvolutional neural networks for automatic liver and tumor segmentation. Arxiv: 1704.02703, 2017.*
3. *Lei B., et al, Automatic liver lesion detection using cascaded deep residual networks. Arxiv: 1704.0270, 2017.*

[F-06.5]

QUANTIFICATION OF 3D COLLAGEN FIBER DISTRIBUTIONS FROM SHG IMAGE DATA USING Q-BALL ALGORITHM

Adam Rauff[1], *Jeffrey Weiss*[1]

1 *University of Utah, Salt Lake City, USA*

Introduction: Collagen fibrils define the local mechanical response of many biological tissues. Second Harmonic Generation (SHG) imaging has provided an unprecedented tool for imaging supramolecular structural details of collagen fibrils in 3D living tissues [1]. Yet, a review of the literature demonstrated that algorithms to quantitatively and objectively analyze 3D SHG image data and extract structural information are not available. These data could be used in constitutive models that rely on fiber distributions to characterize tissue structures and thus advance research on biological structure-function relationships. Our objective was to develop an algorithm that can objectively analyze SHG image data to quantify 3D distributions of type I collagen fibrils.

Methods: We developed our method by generalizing the 2-dimensional Fourier transform method (2DFTM) algorithm [2] to 3 dimensions, and utilizing the Q-ball algorithm from diffusion MRI. The main difference with the 2DFTM was the relationship of fiber direction corresponding to frequency components of 3D space. In the 2DFTM, pixels of the power spectrum contribute to an orientation perpendicular to the pixel's position. With 3 degrees of freedom, this leads to a plane of solutions of fiber orientations. Thus, our algorithm projects the 3D power spectrum onto the unit sphere, and uses the Q-ball algorithm to iterate over spherical directions and compute the contribution from the orthogonal plane [3]. The orientation distribution function (ODF) of fibers was fitted to a structure tensor using covariance matrix of coordinates and a subsequent Eigen decomposition to obtain anisotropy index (AI). The algorithm was tested on synthetic datasets with varying distributions. Then, the algorithm was applied to real 3D SHG image data obtained from time series imaging of 3D microvascular constructs in collagen gels.

Results and Discussion: The algorithm accurately obtained 3D distributions from single family, multi-family, crossing, and isotropic fibers, with varying from synthetic images with pre-defined ODFs (Figure 1). The AI of ideal single family fibers was larger than 0.99, while randomly aligned fibers had AI smaller than 0.05. This approach enables quantification of 3D fiber distributions from SHG image data that can be used in computational models with continuous fiber distributions, and facilitate investigation of dynamic changes in tissue structures.

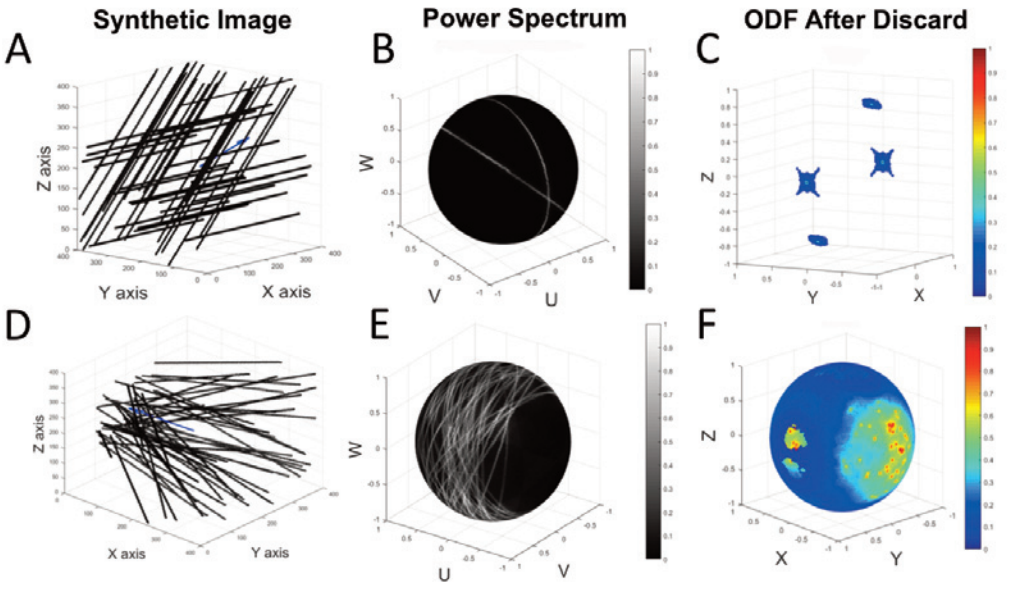

Figure Caption. A –Synthetic image of two-family fibers. **B** –The power spectrum of the image in A, filtered and projected onto the unit sphere. **C** – ODF of two-family fibers after discarding non-significant fiber directions. **D** – Synthetic image of a single fiber family with variance along the x-direction. **E** – The power spectrum of the image in D. **F** – ODF of the fibrous image in D.

Acknowledgments. This research was supported by NIH grant #R01HL131856.

References: 1. Campagnola, P.J. and L.M. Loew, *Nature biotech*, **21**(11): 1356, 2003. **2.** Sander, E.A. and V.H. Barocas, *J Biomed Mater Res*, **88**(2): 322-331, 2009. **3.** Tuch, D.S., *Q-ball imaging. Mag Res Med*, **52**(6): 1358-1372, 2004.

[F-07.1]

MECHANICALLY MAPPING THE HUMAN BRAIN WITH MAGNETIC RESONANCE ELASTOGRAPHY

Curtis Johnson[1]

1 *University of Delaware, Newark, USA; Department of Biomedical Engineering*

Mechanical properties of the human brain can provide sensitive information about the microstructural health of neural tissue in vivo. Parameters such as viscoelastic shear stiffness and damping ratio are affected by aging, neurodegeneration, and rehabilitation, and can reflect cognitive performance1. Magnetic resonance elastography (MRE) provides the ability to noninvasively measure such properties in the living brain, and the pursuit of accurate and robust maps of brain tissue viscoelasticity is of interest to improve the utility of these measures in neurology, neurosurgery, and neuroscience.

MRE is a shear wave imaging technique that uses externally-applied harmonic motion to generate deformations in the brain that can be imaged with phase-contrast MRI sequences. The resulting full vector, complex displacement fields across the entire brain are input to an inversion algorithm to estimate the spatial distribution of the complex shear modulus. The brain has considerable heterogeneity in mechanical properties owing to the spatial organization of white and gray matter structures. As such, accurately resolving the regional properties of these structures requires imaging and inversion schemes with sufficiently high spatial resolution.

Here we will present our solutions for performing high-resolution brain MRE in short scan times. These acquisitions are based on multishot spiral imaging, field inhomogeneity correction, and correction for motion-induced phase errors during iterative reconstruction2,3. Through these developments we have achieved the highest reported spatial resolution in the shortest scan times on a clinical 3T MRI scanner while maintaining sufficient signal-to-noise ratio4. Recent developments include 3D multiband k-space sampling and subspace-based image reconstruction to further push the limits of achievable resolution and shorten acquisition times. We will demonstrate how this higher resolution data improves property estimates with the nonlinear inversion algorithm5. Lastly, we will share our recent efforts at using MRE data from a large sample of young adults to construct a high-resolution template of healthy brain viscoelasticity. This template will be useful in understanding the normal brain, differences in properties between regions, and expected population variability.

Acknowledgments: NIH/NIA R01-AG058853, NIH/NIBIB R01-EB027577, NIH/NIGMS P20-GM103446, ONR N00014-17-P-7001, and University of Delaware, Newark, United States Research Foundation.

References:

[1] Hiscox, et al, Phys Med Biol, 2016;61(24):R401-R437;
[2] Johnson, et al, Magn Reson Med, 2013;70(2):404-412;
[3] Johnson, et al, Magn Reson Med, 2014;71(2):477-485;
[4] McGarry, et al, Phys Med Biol, 2011;56(13):N153-N164;
[5] McGarry, et al, Med Phys, 2012;39(10):6388-6396.

[F-07.2]

PRION-LIKE PROPAGATION OF TOXIC PROTEINS ALONG THE AXON NETWORK IN NEURODEGENERATIVE DISEASES

Johannes Weickenmeier[1]

1 *Stevens Institute of Technology, Hoboken, USA*

The pathogenesis of neurodegenerative diseases such as Alzheimer's disease (AD), Parkinson's disease (PD), amyotrophic lateral sclerosis (ALS) or Lou Gehrig's disease, and chronic traumatic encephalopathy (CTE) is characterized by prion-like spreading of toxic proteins in the brain [1]. Prion diseases themselves are associated with abnormal folding of specific cellular proteins in the brain leading to neuronal damage and ultimately death [2]. Prions infest healthy tissue and trigger a cascade of plaque formation leading to a progressive spreading throughout the brain. Several neurodegenerative diseases follow a very similar mechanism. For example, AD is known for the aggregation of misfolded amyloid-beta and tau forming extracellular plaques and intracellular neurofibrillary tangles, respectively [3]. The proteins' spatial propagation patterns are increasingly understood, although a unifying model describing the spatio-temporal propagation of toxic proteins does not exist to this day [4].

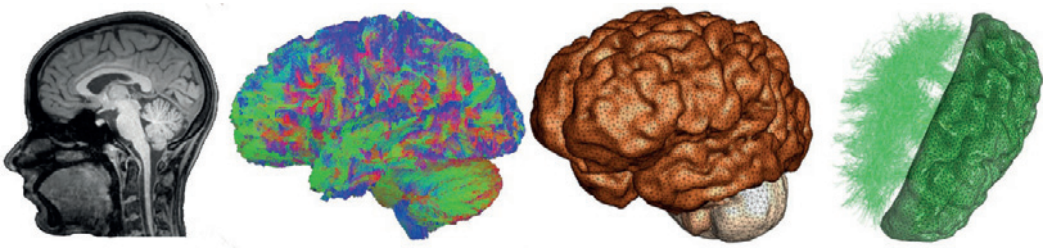

Figure 1: (A) Magnetic resonance images and 7T diffusion tensor images (B) were used to create (C) an anatomically accurate three-dimensional finite element model of the brain that (D) incorporates the axon fiber network obtained through tractography.

Here, we present a multi-scale approach to study competing hypotheses for the propagation of amyloid-beta plaques and neurofibrillary tangles. We demonstrate that a simple reaction-diffusion model for protein spreading and a realistic representation of brain anatomy are necessary to recover known spatial propagation patterns. Figure 1 shows the anatomically accurate finite element model of the brain reconstructed from magnetic resonance images as well as an axon fiber model created from tractography data. Our model demonstrates the roles of proximity-based spreading of amyloid-beta plaques and connectivity-based propagation of toxic tau. Our model recovers clinically observed propagation patterns and allows us to systematically test different propagation mechanisms observed in vivo [5].

Acknowledgments: We would like to thank Priti Balchandani and Kuang-Han Huang from the Icahn School of Medicine at Mount Sinai for providing the diffusion tensor images.

References:

[1] *Jucker, M. and Walker L., Nature, 501:45, 2013.*
[2] *Jack, C. et al., Lancet Neurol, 12:207-216, 2013.*
[3] *Walker, L. and Jucker, M. Annu Rev Neurosci, 38:87-103, 2015.*
[3] *Braak, H. and Braak, E., Acta Neuropathol, 82:239-259, 1991.*
[4] *Weickenmeier, J. et al., PRL, 121:158101, 2018.*
[5] *Zeshan, A. et al., Acta Neuropathol, 127:667-683, 2014.*

[F-07.3]

INVESTIGATING THE PULSATILE MOTION OF THE BRAIN THOROUGH 3D PHASE-BASED AMPLIFIED MRI

Javid Abderezaei[1], *Itamar Terem*[2], *John Martinez*[1], *Samantha Holdsworth*[3], *Mehmet Kurt*[1]

1 *Stevens Institute of Technology, Hoboken, USA*
2 *Stanford University, Stanford, USA*
3 *University of Auckland, Auckland, New Zealand*

Brain as a complex biomechanical system with soft material properties and intricate boundary condition with vasculature, cerebrospinal fluid (CSF) and dual folds, is under constant motion and deformation inside the skull. With each heartbeat, the periodic blood pressure variation, causes the movement of this tissue [1]. Evaluating this intrinsic motion could potentially be used as an indicator for pathologies such as Chiari I malformation that has been shown to affect the motions of the brain [3]. Recently, with the introduction of 2D amplified MRI (aMRI), which uses a phase-based algorithm to amplify the subtle spatial variations in cardiac-gated brain MRI scans, better visualization of such motions became possible [3,4].

Here we extended the 2D aMRI to a 3D which lets us quantify 3D micro-level tissue displacement during each cardiac cycle. In order to track a 3D voxel volume, we extended the 2D steerable pyramid to 3D and transformed the spatial filters from circular into a spherical domain. To equally partition the full range in the space, we formed 6 cuboctahedron geometries with 60 degrees angle difference between each filter [5]. The temporal filters and Fourier analysis were also extended to 3D, which allows for the detection of the pixel intensity changes in the voxels.

In order to identify the limits of the 3D aMRI algorithm to achieve the minimum artifacts, a phantom model was created and amplified in MATLAB. A Gaussian-filtered phantom disk with a radius of 10 mm was created. The displacement of with amplitude , harmonic number n = 1, and time t was imposed on the phantom. With varying amplification factor (α) between 1-7 we observed a linear correlation between the amplified displacement and α (, Fig. 1A) which hints at linear dependence of amplified displacement on true displacement [3]. In the next step we implemented the developed technique on an acquired cardiac-gated CINE MRI. A 3T whole-body GE MR750 Discovery MRI system (GE Healthcare) was used to capture videos of the brain during a heart pulse via a cardiac-gated balanced steady state free precession (bSSFP) sequence with the following imaging parameters: matrix size = 192-192, flip angle = 45°, TR/TE = 3.6/1.18 ms, bandwidth = 127 KHz, slice thickness = 5 mm. Data collection was triggered by external photoplethysmography (PPG) gating. We then amplified the acquired video with amplification factor (α) of 7 and evaluated the normalized temporal variance map of the out-of-plane motion of the brain (Fig. 1B, also see here). We observed subtle out-of-plane motion near midbrain, which hints at the correlation of brain movement with the contraction of major cerebral arteries in that region.

A) *B)*

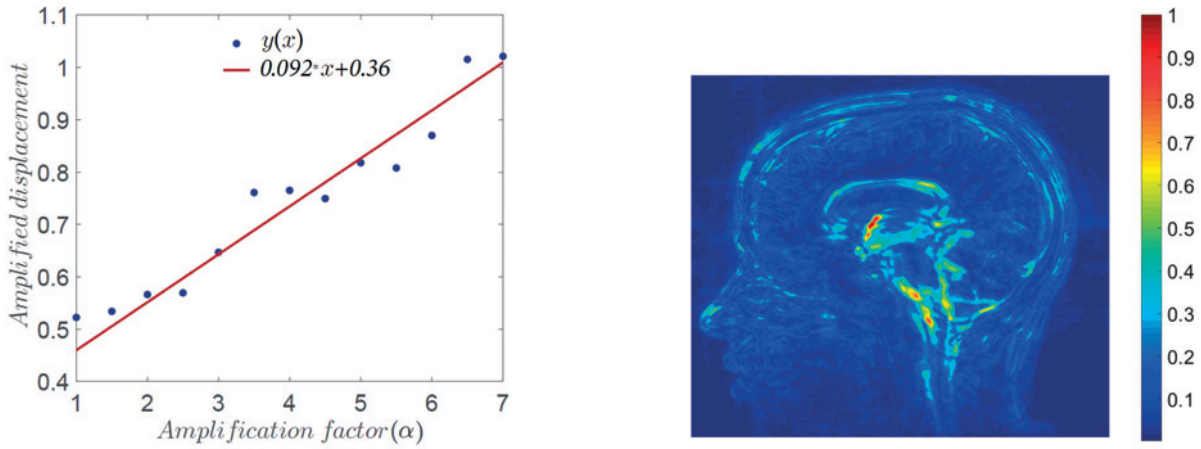

Figure 1. A) Linear correlation of the amplified displacement and α. B) Normalized standard deviation maps for the out-of-plane motion of each voxel over time

References:

[1] Wagshul, E., et al., Fluids and Barriers of the CNS, (2011).
[2] Pujol, J et al., Neurology, (1995).
[3] Terem, I. et al., Magn Reson Med, (2018).
[4] Holdsworth SJ et al. Magn Reson Med, (2016).
[5] Mathewson, J., et al., SEG Technical Program Expanded Abstracts (2008).

[F-07.4]

THE SIGNIFICANCE OF ABDOMINAL PRESSURE ON RESPIRATORY CEREBROSPINAL FLUID DYNAMICS

Robert Lloyd[1], *David Fletcher*[2], *Jane Butler*[1], *Simon Gandevia*[1], *Lynne Bilston*[1]

1 *Neuroscience Research, Sydney, Australia; University of New South Wales, Kensington, Australia*
2 *School of Chemical and Biomolecular Engineering, University of Sydney, Sydney, Australia*

Magnetic resonance imaging (MRI) studies have shown that voluntary deep inhalation commonly results in a large cranial displacement of CSF [1,2]. It is accepted that this flow compensates for the loss of cranial blood volume, caused by epidural drainage in response to reduced intrathoracic pressure [1]. However, this mechanism does not explain why cases of caudal CSF displacement were also measured during voluntary deep inhalation [1,2]. Determining the drivers of respiratory CSF flow is crucial for understanding transport mechanisms of intrathecal drug injections, and the pathophysiology of CSF flow disorders.

To quantify the influence of respiration on CSF flow, real-time phase-contrast MRI was used to record CSF and blood flow, while healthy subjects (5:5 M:F, 25-50 years) performed either an expiratory (cough) or inspiratory (sniff) effort between breaths. Scans were acquired on a 3T MRI scanner (Philips Achieva 3TX). Transverse images were taken at mid C3 and L2. Later the participants performed the same maneuvers with a pressure transducer used to measure the trunk pressures.

The Figure shows the relationship between CSF displacement and the trunk pressures in both the cervical and lumbar spine. With elevated abdominal pressure, epidural blood flow into the lumbar spinal canal was increased, and CSF was displaced cranially. Similarly, when the thoracic pressure was elevated there was an increase of blood flow into the cervical epidural veins, and a cranial displacement of CSF. With a negative thoracic pressure there was an increase in venous drainage through the cervical epidural veins, and CSF was displaced both cranially and caudally. A stepwise multiple regression was performed to determine how thoracic and abdominal pressure were associated with CSF displacement. Cervical CSF displacement was only significantly associated with the abdominal pressure (R^2=0.59), whereas, lumbar CSF displacement was significantly associated with both the thoracic and abdominal pressures (R^2_{adj}=0.52).

The results of this study indicate that respiratory CSF flow is primarily driven by the lumbar spinal pressure and not venous drainage. Additionally, the thoracic spinal canal acts as a variable reservoir, being less compliant with increased thoracic pressure (resulting in a larger cranial displacement of cervical CSF), and a sink under negative pressure (hindering cranial displacement in the cervical spine). This mechanism allows for caudal flow to occur during inhalation, when the thoracic spine becomes sufficiently negative relative to lumbar spinal canal (Fig.).

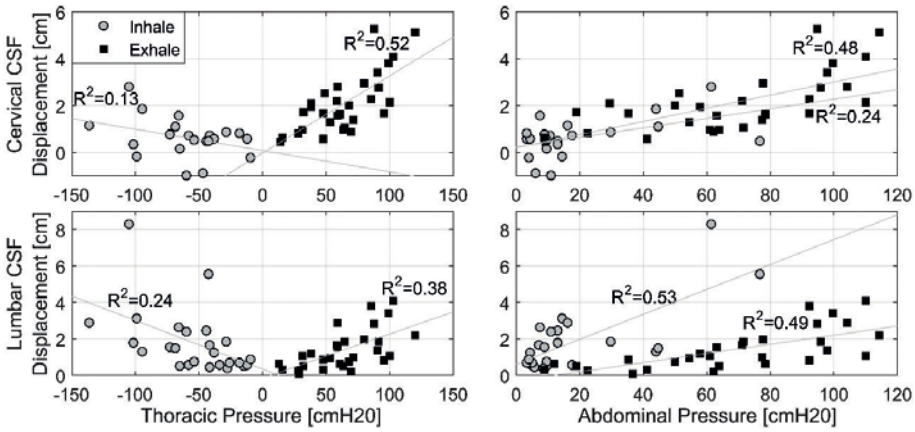

Figure: Peak CSF displacement plotted against the peak thoracic and abdominal pressures generated during the inspiratory and expiratory efforts. Where cranial and caudal CSF displacement are shown as positive and negative, respectively.

Acknowledgments: This research was funded by the Column of Hope Foundation & NHMRC project grant.

References:

1. *Dreha-Kulaczewski, S., et al., (2017). J Neurosci, 37(9) p2395; 2. Dreha-Kulaczewski, S., et al., (2018). Sci. Rep., 8(1) p5594*

[F-07.5]

EVALUATION OF FACIAL SYMMETRY AFTER HEAD AND NECK RECONSTRUCTION

Jade Duchscherer[1], ***Daniel Aalto***[2], *Lindsey Westover*[1]

1 *Department of Mechanical Engineering, University of Alberta, Edmonton, Canada*
2 *Institute for Reconstructive Sciences in Medicine, Misericordia Community Hospital, Edmonton, Canada ; Department of Communication Sciences and Disorders, Faculty of Rehabilitation Medicine, University of Alberta, Edmonton, Canada*

Introduction: Reconstruction of the head and neck restores anatomy and function after acquired defects. In addition to functional benefits, aesthetic outcomes play a role in quality of life and social perception. Symmetry of facial features after reconstruction is a significant component of aesthetics. Previous methods to quantify symmetry after this type of surgery typically include the placement of anatomical landmarks, which requires highly trained operators and introduces measurement inaccuracies1. However, a method using the "best plane of symmetry" has been used to objectively quantify asymmetry associated scoliosis without the use of anatomical landmarks2. The current study proposes a similar 3D objective method of evaluating symmetry at the craniofacial surface and soft tissue surface after jaw reconstruction surgery. Furthermore, this study aims to investigate potential relationships of asymmetry between reconstructed and non-reconstructed areas.

Methods: The study protocol was approved by the Heath Research Ethics Board of Alberta Cancer Committee. A waiver of consent was granted to include eight head and neck cancer patients in the study. 3D models were created using CT scans from four patients who underwent maxilla reconstruction and four patients who underwent mandible reconstruction. A hard tissue (skull, mandible), and soft tissue model (face) were created for each patient. The 3D model was reflected about the midsagittal plane. The original and reflected models were then aligned by minimizing the distance between the two models using the Geomagic software. A deviation colour map (DCM) was created indicating the difference between the two models, quantitatively highlighting areas of asymmetry. In the DCM, green indicates areas of relative symmetry (2mm) while blue and red indicate areas of asymmetry. Grey areas indicate that the original model does not have a corresponding point on the reflection.

Results: Fig. 1 shows an example of the DCM for the soft tissue surface (A) and corresponding hard tissue surface (B) for one patient. Across all patients, the reconstructed regions (maxilla or mandible) showed greater levels of asymmetry at both the bone level and the soft tissue level in comparison with unaltered regions. Furthermore, grey areas on the hard tissue surface in which there are no corresponding points on reflected model display the highest levels of asymmetry at the soft tissue surface.

Conclusions: The developed method effectively highlights areas of asymmetry. This promising tool can help evaluate aesthetic outcomes of facial reconstruction surgery. Additionally, this method can be used to investigate the relationship between the local areas of asymmetry following surgery and the global perception of facial symmetry.

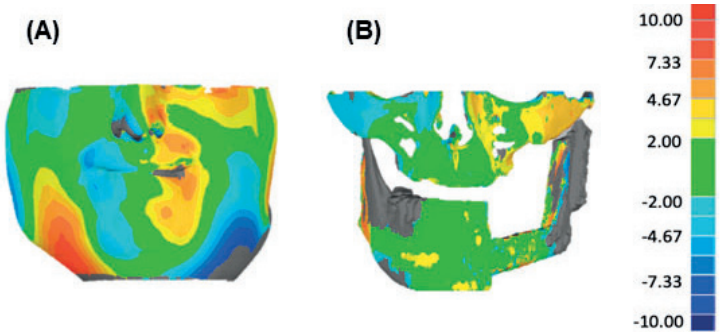

Figure Caption: Fig. 1. DCM for soft tissue surface (A) and corresponding hard tissue surface (B)

References:

1 *G.O. Ramirez-Yanez et al. Eur. J. Orthod. 33(3):236-242, 2011.*
2 *A. Komeili et al. Spine Deform. 3(4):303-311, 2015.*

[F-08.1]
MURINE CARDIAC AND VASCULAR 4D ULTRASOUND

Craig Goergen[1]

1 *Purdue University, West Lafayette, USA*

The lack of accurate and sensitive cardiac imaging techniques remains a prominent issue when diagnosing heart failure. While recent imaging development efforts are improving diagnostic capabilities for patients in the early stages of heart disease, current approaches have limitations. Conventional methods, including standard echocardiography for example, rely on geometric assumptions from 2D cardiac images to evaluate global metrics of cardiac function, often leading to inaccurate measurements with large variability. While ultrasound is useful for monitoring disease progression due to its short acquisition times, lack of ionizing radiation, and clinical availability, there is a clear need to develop a more sensitive method for evaluating cardiac function that is fast, robust, label free, and independent of geometric assumptions. The purpose of this presentation is to highlight recent advancements in gated volumetric ultrasound imaging (4DUS) that can effectively evaluate volumetric cardiac function in mice. The results suggest that 4DUS provides comparable information to cine MRI through spatiotemporally synced imaging of cardiac motion. Murine models of cardiac hypertrophy [1] and myocardial infarction [2] further highlight the precision of 4DUS compared with standard ultrasound as the data have narrower groupings of cardiac metrics based on health status. These findings suggest that murine cardiac 4DUS can be used as a reliable, accurate, and cost-effective technique for longitudinal studies of cardiac function and disease progression.

A second study utilized 4DUS to characterize abdominal aortic aneurysm (AAA) pulsatility and strain in vivo [3]. Current rupture risk strategies focus on maximum aortic diameter and its growth rate, but AAAs often have complex vessel geometries, heterogeneous wall composition, and surrounding structures that can all influence aneurysm rupture risk. Improved understanding of the complex kinematics of the aorta has the potential to increase our ability to predict aneurysm disease progression. Here we show that 4DUS data can be combined with a direct deformation estimation approach to compute in vivo 3D Green-Lagrange strain in murine angiotensin II-induced dissecting aortic aneurysms. Regions of intramural thrombus formation and focal breakage in medial elastin were observed in areas of reduced aortic strain. These results suggest that in vivo measurements of 3D strain may provide improved insight into aneurysm disease progression. While further work is needed with both preclinical animal models and human imaging studies, this initial murine work indicates that vessel strain may help when developing an improved metric for predicting aneurysm growth and rupture.

Acknowledgments: Hannah Cebull, Frederick Damen, and Arvin Soepriatna contributed to the studies highlighted in this presentation.

References:

1. *Damen FW, et al. Tomography. 2017 Dec; 3(4):180–187.*
2. *Soepriatna AH, et al. International Journal of Cardiovascular Imaging. 2018 May; 34(5)713-24.*
3. *Cebull HL, et al. Journal of Biomechanical Engineering. 2019 (Accepted).*

[F-08.2]

COMPUTATIONAL MODELLING OF VALVE INTERSTITIAL CELLS

Emma Lejeune[1], *Alex Khang*[1], *Michael Sacks*[1]

1 *The University of Texas at Austin, Austin, USA*

Heart valve interstitial cells (VICs) are situated within the leaflet tissue where they play a critical role in tissue maintenance and the progression of valve disease. At present, it is not well understood how changes in macroscale valve loading conditions alter VIC behavior or how specific changes in VIC behavior influence macroscale heart valve tissue. In this work, we describe the first steps towards a combined experimental/computational framework to understand how the behavior of VICs traverses scales. First, we describe computational tools from spatial statistics that we use to interpret experimental data on the geometric and material properties of VICs in vitro (Fig. 1a). Spatial statistics, unlike traditional statistics, does not assume that observations are independent. By measuring the spatial autocorrelation of different experimentally observed quantities, we are able to better detect change in cell behavior and construct improved models of how cell properties vary in space. Second, we focus on the initial steps of creating a robust three-dimensional computational cell model. This cell model is constructed in conjunction with experiments conducted in a three-dimensional hydrogel environment (Fig. 1b,c). In the computational cell model, we include sub-cellular components of VICs, and run simulations on suites of representative cell geometries (Fig. 1d). Then, we use meta-modeling and sensitivity analysis to interpret the results of the cell model and draw conclusions about critical cell behavior (Fig. 1e). Looking forward, we anticipate that this work will be meaningful for both the analysis of experimental data (Fig. 1b,c), and for creating a computational framework that will be capable of connecting cellular scale behavior observed in vitro to cell-driven changes in tissue properties in the in vivo environment.

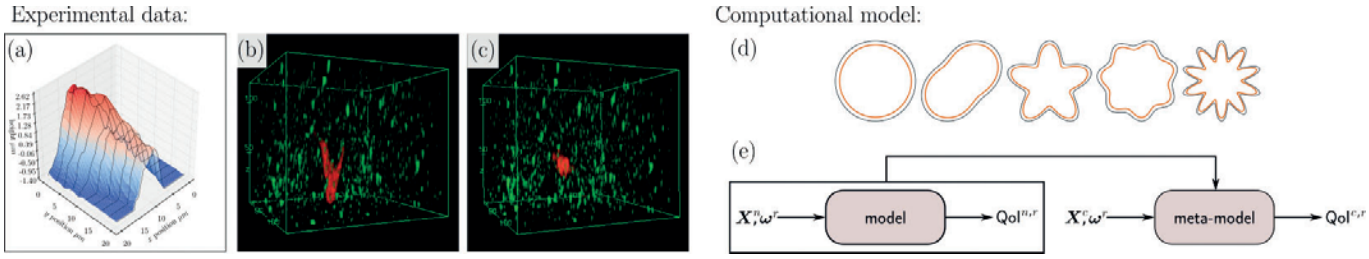

Figure Caption: (a) Traction force microscopy, normal state; (b) Traction force microscopy hypertensive state; (c) Cell shape reconstruction with Gaussian Process Regression; (d) Toy example of a computational cell model; (e) Meta-modeling and sensitivity analysis are used to interpret the results of the cell model.

Acknowledgments: This work was supported by the Peter O'Donnell, Jr. Postdoctoral Fellowship in Computational Engineering and Sciences.

References:

[1] *Butcher, JT et al., Journal of Heart Valve Disease, 17:62, 2008.*
[2] *Ayoub, S et al., Cellular and Molecular Bioengineering, 1-16, 2018.*
[3] *Merryman, DW et al., Tissue engineering, 13:2281, 2007.*
[4] *Goodchild, MF, Geo Books, 37, 1986.*
[5] *Rasmussen, CE and Williams CK, MIT press, 2006.*
[6] *Hart, JL et al., SIAM Journal on Scientific Computing, 39:A1514, 2017.*

[F-08.3]

MURINE CARDIAC HYPERTROPHY REDUCES IN VIVO GREEN-LAGRANGE STRAIN QUANTIFIED FROM 4D ULTRASOUND

Alycia Berman[1], *Arvin Soepriatna*[1], *Adrienne Scott*[2], *Corey Neu*[2], *Craig Goergen*[1]

1 *Purdue University, West Lafayette, USA*
2 *University of Colorado, Boulder, USA*

Cardiac hypertrophy is the abnormal enlargement of the heart, driven by myocardial thickening and eventual dilation. One factor that can lead to cardiac hypertrophy is increased cardiac afterload, which can be driven by hypertension. Herein, we used hypertension to induce hypertrophy in mice in order to explore the relationship between in vivo strain and the resultant hypertrophic state.

Male C57BL/6J mice were surgically implanted with mini-osmotic pumps containing either saline (n=5) or angiotensin II (AngII; n=10). AngII infusion led to hypertension-induced hypertrophy. Two weeks post-surgery, pumps were removed from half of the AngII mice to assess cardiac recovery post-insult (AngII D14/14 group; n=5). Weekly tail cuff measurements (CODA; Kent Scientific) were used to quantify systemic blood pressure and verify effectiveness of the AngII. Mice were also imaged weekly by ultrasound (Vevo2100; VisualSonics) to collect 2D short-axis and long-axis images, as well as 4D data (3D+time) using a linear stepper motor. All mice were euthanized 4 weeks post-surgery. Standard metrics of left ventricular mass were calculated from the 2D slices. Additionally, using 2D short-axis slices at the mid-papillary, the heart was divided into 4 quadrants (anterior, posterior, medial, lateral). First principal Green-Lagrange strain was calculated using a direct deformation estimation (DDE) approach [1] and results averaged for each quadrant (Figure 1A-B).

Mice receiving constant AngII infusion had increased blood pressure by Day 14 ($p<0.05$ vs. saline), which remained increased for the duration of the study. In contrast, after removal of the pump, the blood pressure in AngII D14/14 mice returned to normal levels ($p=0.97$ vs. saline). Similarly, left ventricular mass was increased in AngII mice by Day 14, while removal of the pump led to recovery (Figure 1C). Strain also indicated improved cardiac function in AngII D14/14 mice on Day 28 (Figure 1D). Intermediate strain timepoints as well as 3D strain analysis is currently underway. Ultimately, we aim to determine if changes in strain precede increases in cardiac mass.

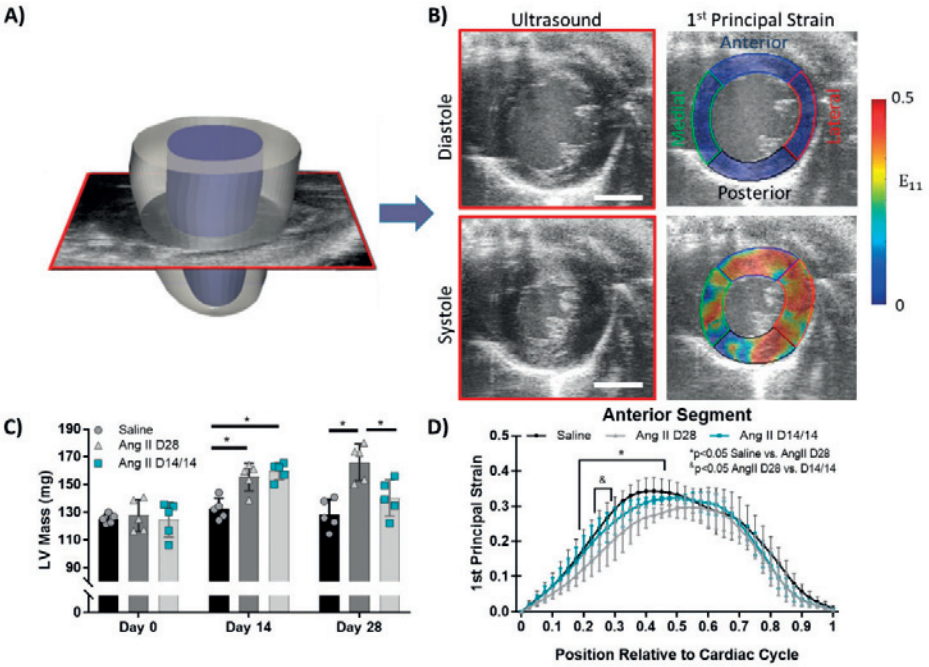

Figure Caption: A) 4D ultrasound data (3D+time) was collected weekly for each mouse, from which 2D slices at the mid-papillary were obtained. B) These slices were used to calculate 1st principal Green-Lagrange strain with end-diastole as the reference. The heart was divided into four quadrants, and values of each quadrant were averaged for each mouse. C) Left ventricular mass was significantly increased in the AngII mice by Day 14, while removal of the pump enabled significant recovery by Day 28. D) Analysis of the anterior quadrant strain at end of study showed reduced values during contraction in AngII D28 mice, but not AngII D14/14. Scale bar: 2 mm.

Acknowledgments: We would like to thank Jennifer Anderson and Elizabeth Niedert for image acquisition.

References:

[1] *Boyle, JJ, et al. (2014). JRSI, 11(100):20140685.*

[F-08.4]

AN IMAGE-BASED MODELING PIPELINE FOR PREDICTING PATIENT-SPECIFIC MITRAL VALVE REPAIR OUTCOMES

Harshita Narang[1], *Amir Khalighi*[1], *Bruno Rego*[1], *Robert Gorman*[2], *Michael Sacks*[1]

1 *James T. Willerson Center for Cardiovascular Modeling and Simulation, Austin, USA; Oden Institute for Computational Engineering and Sciences, Austin, USA; The University of Texas at Austin, Austin, USA, Austin, USA*

2 *University of Pennsylvania, Philadelphia, USA*

Ischemic mitral regurgitation (IMR) is a highly prevalent heart valve disorder that afflicts up to half of the population that has suffered a myocardial infarction. Unfortunately, current IMR treatments still have less than optimal long-term patient survival outcomes and a high rate of recurrence. It is believed that IMR surgical treatments need to become more personalized to account for patient-specific variations in valvular structure and disease progression path. Computational models provide excellent resources to predict valvular response to repair and explore novel repair scenarios. In the present study, we developed a computational modeling pipeline to predict mitral valve (MV) annuloplasty outcomes on a patient-specific basis and validated the method using pre- and post-surgical 3D echocardiographic MV images from 10 patients (5 with recurrent IMR, 5 without). The images were processed to develop geometrical representations of the MV leaflets for both end-diastolic (fully open) and end-systolic (fully closed) states. We then applied a hyperelastic registration technique implemented within a finite element framework to build consistent correspondence between the open and closed MV leaflets [1]. Next, functionally equivalent chords were constructed and attached to the MV leaflets following our recent work on the development of such models through topology optimization [2]. Finally, we performed finite element simulations of MV closure in the pre-surgical and post-surgical states. Our predictive post-surgical simulations showed agreement with previously reported observations on the effect of annuloplasty ring implantation on MV leaflet strain patterns. In particular, the results revealed significant reduction in circumferential Green strains while the radial component of the strain tensor remained mostly the same (see figure). This pattern has been shown to trigger cell biosynthetic pathways in the direction of deleterious remodeling of the MV tissue. We believe that our modeling framework can be applied to patients in the clinic pre-surgery to quantitatively compare the performance of different annuloplasty rings, and may be extended to evaluate auxiliary repair methods such as leaflet clipping or augmentation. In addition to guiding the optimization of MV repair devices, results from the present study could also guide the development of novel treatment options that target the MV and left ventricle simultaneously. For example, post-infarction interventions involving the injection of shear-thinning hydrogels into infarcted myocardium are currently under development with the aim of slowing and possibly reversing the progression of maladaptive post-infarction remodeling. Since the MV is an integral part of the left heart, the successful application of such approaches must take into account the intimate connection between left ventricular and MV function as well as the MV's strain-driven remodeling potential, so that they may be designed to optimally curb the recurrence and severity of IMR.

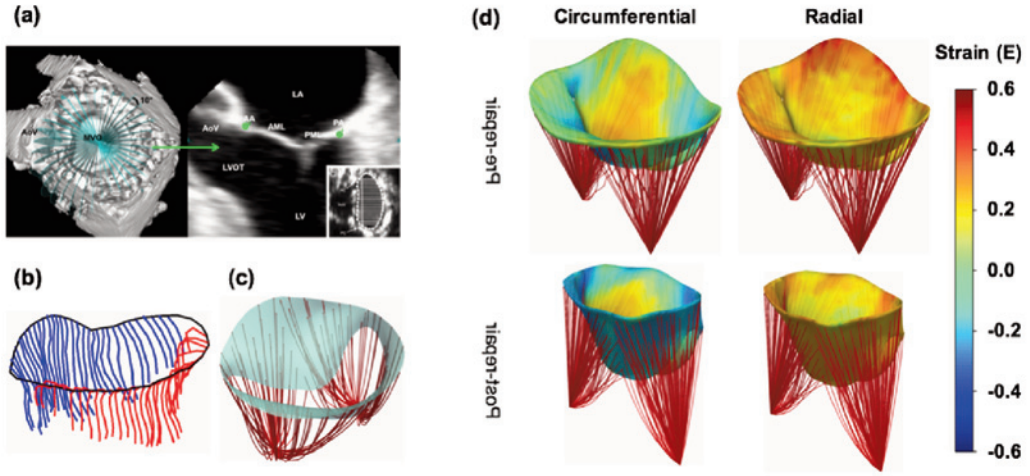

Figure Caption: (a) shows clinical imaging data that was processed to extract MV leaflet geometry (b). We developed functionally equivalent chords (c) to build a full MV that was used to simulate the MV's closing behavior pre- and post-surgery (d).

References:

[1] *Rego BV et al. Int J Numer Meth Bio, 2018, https://doi.org/10.1002/cnm.3142*

[2] *Khalighi AH et al. Ann Biomed Eng, 2019, https://doi.org/10.1007/s10439-018-02122-y*

[F-08.5]

OPTIMIZATION OF CONTRAST-ENHANCED MICRO-CT FOR CHARACTERIZATION OF THE IN VIVO BEHAVIOR OF BIODEGRADABLE METALLIC INTRAVASCULAR STENTS

Lisa Leyssens[1], *Carole Verhaegen*[2], *Sandrine Horman*[2], *Pascal Jacques*[1], *Greet Kerckhofs*[3]

1 *Institute of Mechanics, Materials, and Civil Engineering, UCLouvain, Louvain-la-Neuve, Belgium*
2 *Institut de Recherche Expérimentale et Clinique, UCLouvain, Louvain-la-Neuve, Belgium*
3 *Biomechanics Lab, Institute of Mechanics, Materials, and Civil Engineering, UCLouvain, Louvain-la-Neuve, Belgium; Institute of Experimental and Clinical Research, UCLouvain, Louvain-la-Neuve, Belgium; Dept. Materials Science and Engineering, KU Leuven, Leuven, Belgium*

Artery obstruction, a leading cause of death in the world, can be treated by implanting an intravascular stent to reopen the narrowed or blocked artery. During the past decade, bioresorbable intravascular stents have appeared. They are advantageous compared to the currently used permanent stents, as the latter ones can cause secondary effects such as thrombosis or the formation of blood clots. Moreover, the role of stenting is only temporary as the artery is expected to heal within 6 to 12 months after stenting. Metallic biodegradable stents are popular because of their good mechanical properties (1). The optimal design and alloy with the appropriate degradation rate has, however, not yet been found. Micro-computed tomography (micro-CT) has shown its potential for assessing the 3D microstructural properties of materials. Visualization of soft tissues by micro-CT is, however, challenging due to the inherently poor contrast in standard absorption mode. To achieve sufficient X-ray attenuation, contrast agents, containing high atomic number molecules, are adopted. In this study, contrast-enhanced micro-CT (CE-CT) was optimized for imaging implanted metallic alloys inside rat arteries, which is highly challenging because of their greatly distinct difference in X-ray attenuation.

First, arteries alone were imaged with CE-CT to find the optimal contrast agent. This allowed to analyze the blood vessel microstructure in great detail (Fig.1A). Next, instead of implanting stents directly, a simplified, low-cost approach was used. A sterilized wire was punctured into the abdominal aorta, which was then led into the lumen before puncturing the wall a second time to exteriorize the wire from the artery (2). The aorta with the wire was then harvested, and CE-CT was performed (Fig.1B). Scanning parameters were optimized for visualization of both the soft tissue and the metal. Pure iron wires were used for optimization, and will later be replaced by in-house developed iron alloys.

Further work will focus on evaluation of the surface roughness of the metal, its degradation rate and the interactions between the metal and the artery, in view of finding an optimized stent design. This newly emerging imaging method for in vivo evaluation of stent behavior tackles all the shortcomings of standard histology.

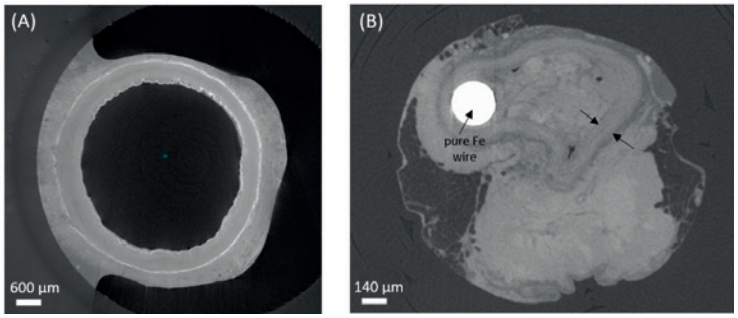

Figure Caption: Fig.1: CE-CT image of (A) human artery and (B) rat aorta (between arrows) implanted with iron wire

References:

(1) *Moravej M., et al. International Journal of Molecular Sciences, vol. 12, no. 7, 2011, pp. 4250–4270*
(2) *Pierson D. et al. J Biomed Mater Res Part B 2012:100B:58–67*

[F-09.1]

DENSE AND HARP: TWO SIDES OF THE SAME ELASTOGRAPHY COIN

Deva Chan[1]

1 Rensselaer Polytechnic Institute, Troy, USA

Displacement encoding with stimulated echoes (DENSE) and harmonic phase (HARP) are magnetic resonance imaging (MRI) techniques that enable the visualization of motion at physiologic frequencies. This talk will discuss the shared MRI physics of both techniques [1], considerations for experimental design in biomechanics, and examples of their implementation in tissues that require exogenous loading.

MRI data is complex in that signals consist of both magnitude and phase. DENSE [2] and HARP [3] are phase contrast techniques, wherein the phase of the MRI signal is proportional to the displacement of each pixel. Spatial preparation of magnetization (SPAMM) is performed while a tissue is in the desired reference configuration, while data is acquired – as either single-frame or cine (multi-frame) images – during the current configuration(s). During the preparation, the phase of protons in the tissue are sensitized to their initial location using a gradient magnetic field. With cine HARP, images are then acquired of the deformed tissue, and the phase information is used to track each pixel back to its location in the first frame. With DENSE, protons are sensitized to their new location before acquisition, so that the phase of each pixel is proportional to the change in displacement.

Differences in these sequence of imaging events may dictate how useful these techniques may be for a particular tissue of interest. DENSE requires only one acquisition to measure the change in displacement so may be selected in cases where measuring deformation at only one time point is desired. On the other hand, HARP requires an initial image to which motion in subsequent images can be tracked and is often more practical for visualizing motion over time.

Application of these techniques also must consider their limitations. SPAMM is accompanied by imaging artifacts that can only be removed by subtracting information from complementary scans [4, 5]. Because multiple acquisitions are required for both techniques, the repeatability of the tissue deformations being measured is of utmost consideration. To address this in applications requiring exogenous loading, researchers have either cyclically loaded tissues until they have reached a quasi-steady state [6] or permitted enough time between loading events to allow tissues to neglect the role of loading history [7].

Acknowledgments: The presenter acknowledges the many insightful conversations with numerous colleagues in the field on this topic, including Corey Neu, Dzung Pham, Andrew Knutsen, David Arnold Gomez, and David Prince.

References:

1. *Kuijer, et al., J Magn Reson Imaging, 2006.*
2. *Aletras, et al., J Magn Reson, 1999.*
3. *Osman and Prince, Phys Med Biol, 2000.*
4. *Fischer, et al., Magn Reson Med, 1993.*
5. *Epstein and Gilson, Magn Reson Med, 2004.*
6. *Neu and Hull, J Biomech Eng, 2003.*
7. *Knutsen, et al., J Biomech, 2014.*

[F-09.2]

INTERFACE AND CONSISTENCY CHARACTERIZATION OF MENINGIOMA THROUGH MRE AND AMRI

Efe Ozkaya[1], *Dominic Nistal*[2], *Zeynep Melis Suar*[1], *Priti Balchandani*[2], *Raj Shrivastava*[2], *Mehmet Kurt*[1]

1 *Stevens Institute of Technology, Hoboken, USA*
2 *Department of Neurosurgery, Icahn School of Medicine at Mount Sinai, New York City, USA*

In brain tissue it is found that change in shear modulus can be related to pathology [1]. In the case of meningioma, mechanical characterization of it ahead of surgery is crucial for the surgical planning [2]. Meningiomas are primarily treated by surgical resection. Two important determinants to a complete resection for meningioma is its degree of firmness and adhesiveness to the surrounding healthy brain tissue. Recently, with the emerging non-invasive technique called magnetic resonance elastography (MRE) these two determinants for resection success are tackled [3]. Especially, with the slip interface imaging technique, meningioma-brain interface adhesiveness is tried to be quantified [4,5]. In this study, we performed a broadband mechanical characterization protocol for meningioma through multi-frequency MRE. Multi-frequency MRE data has been transformed into frequency-independent domain through standard linear solid (SLS) model fitting by using the global mean and loss modulus values under three different actuation frequencies of meningioma and healthy brain regions. The purpose of this is to create a consensus among neurosurgeons. Furthermore, we applied a phase-based video amplification technique on meningioma patients' data collected by cardiac gated balanced steady-state free precision (bSSFP) sequence which utilizes the heart as an intrinsic actuator [6]. Through the acquired phase offset time frames, tracking the relative motion of meningioma with respect to the surrounding healthy brain tissue boundary is targeted. After IRB approval, nine meningioma patients aged between 35-68 (3 Female & 6 Male) underwent MRI scans in which a 3T whole-body GE MR750 Discovery MRI system (GE Healthcare, Milwaukee, WI) is used. MRE data is acquired via multi-slice spin echo EPI pulse sequence. As an MRE actuator, a head pillow (Mayo Clinic) is used under actuation frequencies of 40, 60, and 80 Hz. Through the bSSFP sequence, a short cine MRI movie capturing the meningioma regions' movement with respect to surrounding healthy brain tissue over different phases of cardiac cycle is created. Amplification of the cine MRI dataset is done by using a bandwidth having a lower cutoff frequency of 0.01 Hz and a higher cutoff frequency of 3.0 Hz with an amplification factor of 20 [6]. On a single sagittal slice, meningioma boundary and the nearby brain-meningioma interface boundary were manually drawn to create binary masks. This was followed by the use of minimum eigenvalue detection algorithm from MATLAB computer vision toolbox to tag traceable corner points inside these binary mask regions. A thorough examination of the link between aMRI relative displacement and neurosurgeon's resection assessment is pending. However, if we consider Patient 7 (Figure 1), the neurosurgeon assessment revealed a well-preserved arachnoid region after resection, implying a loose connection. Our aMRI tracking results with an amplification factor of 20 demonstrate that for this patient, the maximum relative motion between the tumor and the brain is on the order of several pixels.

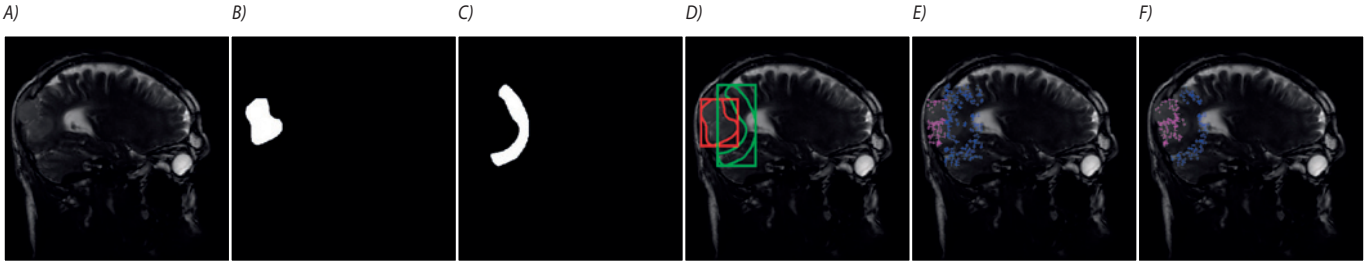

Figure Caption: Relative motion tracking between meningioma and the surrounding healthy brain interface boundary region. A) Original image. B) Meningioma region. C) Interface boundary region. D) Manually selected boundaries. E) Traceable tagged points inside the rectangular regions generated by the minimum eigenvalue detection algorithm. F) Traceable tagged points inside the masked rectangular regions.

References:

[1] *Wuerfel, Jens et al., Neuroimage, 49(3):2520-2525, 2010,*
[2] *Shiroishi, Mark S. et al., Neurosurgery Clinics, 27(2):145-154, 2016,*
[3] *Oertel, Joachim et al., Neurosurgical review, 26(26-4):168-174, 2003,*
[4] *Murphy, Matthew C. et al., Journal of neurosurgery, 118(3): 643-648, 2013,*
[5] *Hughes, Joshua D. et al., Neurosurgery, 77(4):653-659, 2015,*
[6] *Terem, Itamar et al., Magnetic resonance in medicine, 2018*

[F-09.3]
REGULARIZATION-FREE STRAIN MAPPING IN THREE DIMENSIONS

John J Boyle[1], Arvin Soepriatna, Frederick Damen, Craig Goergen[2], Roger A Rowe, Attila Kovacs[3], Robert B Pless[4], Stavros Thomopoulos[1], ***Guy Genin***[5]

1 *Columbia University, New York, USA*
2 *Purdue University, West Lafayette, USA*
3 *Washington University in Saint Louis, Saint Louis, USA*
4 *George Washington University, Washington, D.C., USA*
5 *Washington University in Saint Louis, Saint Louis, USA; Nsf Center for Engineering Mechanobiology*

Quantifying dynamic strain fields from time-resolved volumetric medical imaging and microscopy stacks is a pressing need for radiology and mechanobiology. A critical limitation of all existing techniques is regularization: because these volumetric images are inherently noisy, the current strain mapping techniques must impose either displacement regularization and smoothing that sacrifices spatial resolution, or material property assumptions that presuppose a material model, as in hyperelastic warping. Here, we present a three-dimensional (3D) method for estimating mechanical strain directly from raw 3D image stacks without either regularization or assumptions about material behavior. We apply the method to high-frequency ultrasound images of mouse hearts to diagnose myocardial infarction, and show that strain concentrations arising from structural features on the order of a few voxels can be resolved (Figure 1).

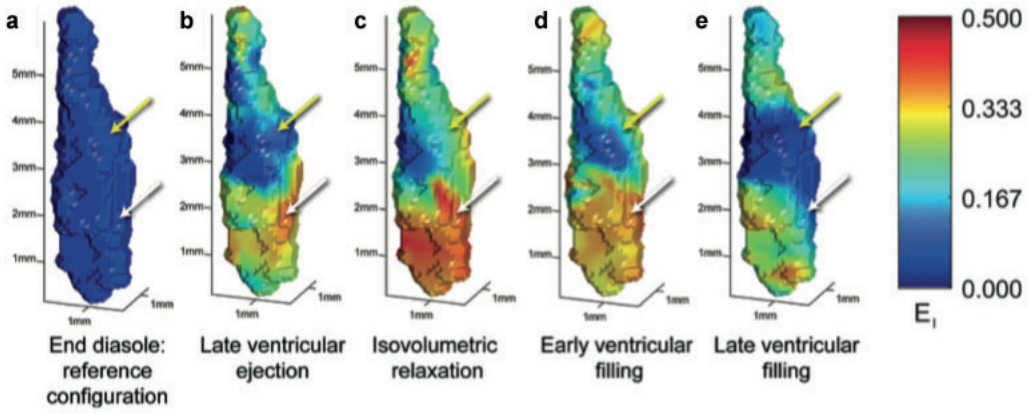

Figure Caption: Peak principal strain fields estimated from high frequency ultrasound imaging of a beating mouse heart, showing spatial variations associated with the structure of the heart. Volumetric ultrasound data were acquired over several cycles of a beating mouse heart, then analyzed using our method, 3D-DDE, to detect spatial variations in Green–Lagrange strain fields. These strain fields were segmented to reveal 3D strains in the left ventricle papillary muscle and to track how the myocardial first prin- cipal component of the 3D strain fields varied near the insertions of the chordae tendinae. (a) End diastole was taken as a refer- ence configuration. (b) The heart developed strains in the left ventricle as it contracted and blood was ejected from the heart, while the papillary muscles remained unstretched. (c) As the heart cycle reached peak systole and entered isovolumetric relaxa- tion, principal strains in the heart wall reached maximum levels on the order of 0.5. (d) As the heart relaxed during early ventricu- lar filling, strain levels reduced, approaching baseline levels after (e) late ventricular filling. Throughout the cardiac cycle, strains in the papillary muscles (upper arrows yellow online) were lower than those in the surrounding myocardium in the apex (white, lower arrows).

Acknowledgments: This work was sponsored in part by the American Heart Association (14SDG18220010), the NIH (R01HL109505, U01EB016422, and DK101001-01), and the National Science Foundation Science and Technology Center for Engineering Mechanobiology (CMMI-1548571).

[F-09.4]

STRAIN IMAGING WITH SUBSAMPLE DISPLACEMENT ESTIMATION USING A PROJECTION METHOD

Mohamed Almekkawy[1], *Brandon Rebholz*[1]

1 *Penn State University, University Park, USA*

Elastography has been a rapidly developed field in recent years to increase the information presented by ultrasound imaging. In order to estimate the strain, accurate displacement estimation is required. Additionally, it is useful to have subsample level estimation in the dimension of the strain kernel, otherwise the quantization of the estimates will cause high magnitude strain estimates along the transition line.

Normalized cross correlation (NCC) has been proven to be an accurate method of speckle tracking, however, due to the nature of the tracking, the estimates are locked to the sample grid. This results in integer value displacements, so, the high magnitude lines mentioned previously will often occur. The Loupas algorithm, however, cannot estimate motion when the displacement is large. When elastography is performed by manual palpation of the transducer there is great difficulty controlling the speed of the motion.

Our proposed algorithm first correlates on the sample level to find the peak of maximum correlation. Then the B-Mode image is interpolated in a constrained region around the displacement peak. An interpolated kernel is then passed over this region to provide subsample accurate estimates in the lateral dimension. To achieve subsample accuracy axially and to improve the lateral estimate, the interpolated peak is then projected onto the zero phase contour. This method generates the accuracy on large displacements that the Loupas algorithm would fail on, while also reducing the quantization effect of a standard correlation method, particularly at low displacement.

Experimental RF data was captured with Telemed (ArtUs) Scanner from a CIRS 040GSE elastography phantom while manually palpating around a 10kpa inclusion situated 1.5 cm deep in a low attenuation background material. The first row of images is from large displacement. Fig.1A shows the strain result from NCC displacement estimation, here the inclusion is visible and there are few high magnitude estimates (shown in yellow). Fig.1B is the result of our algorithm, noting that the high magnitude estimates are less present than in the NCC method. Fig. 1C presents the Loupas result, where the large magnitude displacements lose all accuracy and the strain is unreadable. The opposite effect is seen under small displacement in the second row. Here, Fig.2A shows the high magnitude lines resulting from the quantization of the displacement estimates. In Fig. 2B our method maintains the strain estimation, similar to the resolution and accuracy of Fig.1B. The Loupas algorithm in Fig.2C shows the inclusion, yet less clearly than our method in Fig.2B.

Our algorithm provides the accurate displacement estimates for strain imaging under both large and small displacement, where the Loupas and NCC methods fail respectively.

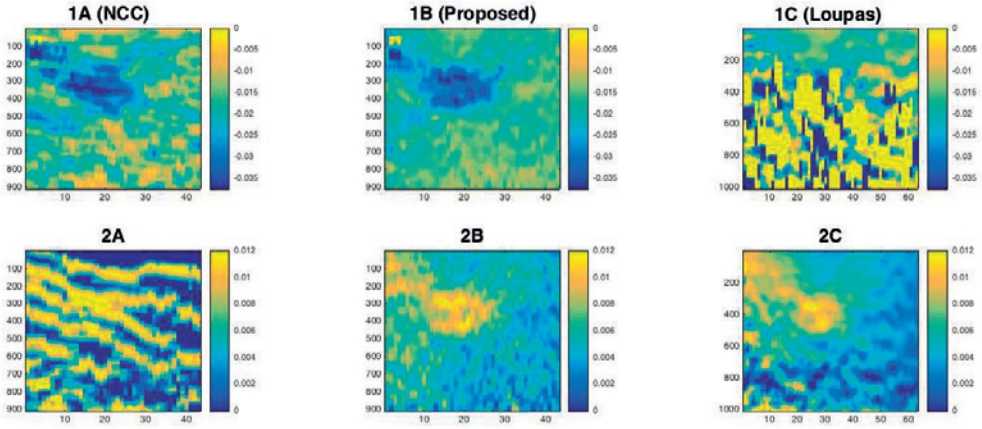

Figure Caption: Strain images. The first row is from capturing large displacement, and the second row is from small displacement.

[F-09.5]

NARROW-BAND SHEAR WAVE GENERATION AND DETECTION USING A SINGLE ULTRASOUND CLINICAL TRANSDUCER

Daniel Cortes[1], *Seyedali Sadeghi*[1]

1 *Pennsylvania State University, University Park, USA*

Ultrasound shear wave elastography (SWE) can be classified as transient or harmonic based on its temporal characteristics. Most transient ultrasound elastography methods use high-intensity ultrasound "push" pulses that generate a shear wave with a wide frequency spectrum [1]. However, it is difficult to control how the wave energy (i.e., amplitude) of the wave is distributed within that spectrum. For this reason, the shear-wave group velocity of transient methods may not match that of harmonic methods like magnetic resonance elastography (MRE). Additionally, several studies have shown biases in the shear wave group velocity measurements of transient methods related to imaging depth, type of transducer and pulse frequency. The objective of this study was to introduce a narrowband shear wave generation method produced by "push" pulses with sinusoidally modulated intensity. The method, named harmonic shear wave imaging (HSWI), successively transmits a series of push pulses with a periodic change in duration. The excited shear waves form a continuous shear wave with a known main frequency that can be controlled by the user. Push pulses are interleaved with imaging pulses so only one clinical transducer is used to generate and record the shear waves. The wave data was processed by using local frequency estimation (LFE) to obtain the 2D quantitative map of shear wave speed. HSWI was validated on a CIRS homogeneous elasticity phantom and agarose gels with different concentrations. HSWI was also performed in the rectus femoris muscle of a healthy male individual to evaluate the HSWI performance in vivo. Frequency domain analysis showed that most of the ultrasound energy concentrates at a single frequency. Therefore, HSWI produces narrowband waves with a speed that closely matches that measured by MRE (Figure). Measurement of the acoustic output parameters indicated that the acoustic intensities in HSWI are suitable for clinical applications. Phantom experiments showed that the shear wave speeds obtained using HSWI and MRE were comparable. The results from HSWI in the rectus femoris muscle of a healthy male individual showed an increase in speed with frequency, as expected, due to the viscoelasticity of the tissue. The ability of HSWI to generate narrowband shear waves using a single linear array transducer makes it amenable for clinical translation. HSWI can potentially use the same thresholds as MRE for diagnosis of diseases affecting the stiffness of soft tissues.

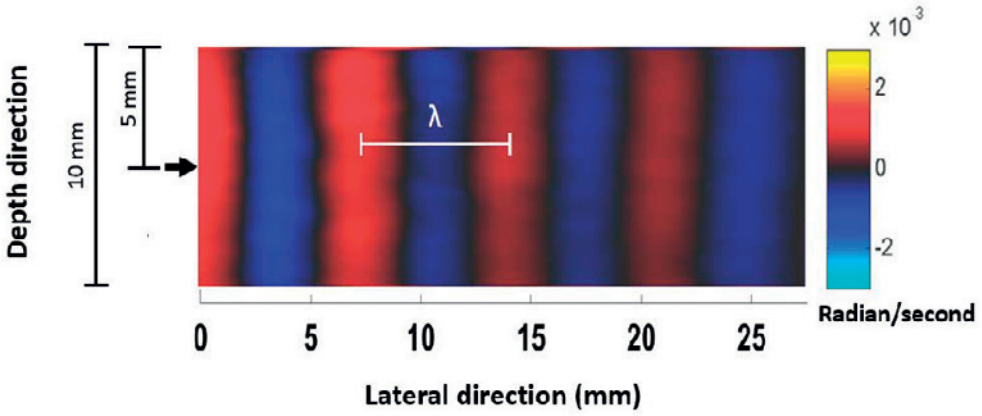

Figure Caption: Representative shear wave pattern at 200 Hz. Detection pulses can be post-processed to obtain a 2-D image showing the wave propagation through the tested material.

Acknowledgments: This work was performed using start-up funds provided by Penn State University, University Park, United States.

References:

[1] Palmeri M et al., Interface Focus, 1: 553-564, 2011.

[F-10.1]

DEFORMATION MICROSCOPY FOR DYNAMIC MAPPING OF INTRACELLULAR AND INTRANUCLEAR MECHANICS

Corey Neu[1], *Soham Ghosh*[1], *Benjamin Seelbinder*[1], *Adrienne Scott*[1]

1 *University of Colorado Boulder, Boulder, USA*

Tissues, cells, and nuclei exhibit exquisite structural heterogeneity that drives local mechanical properties and dynamic cellular responses, including adhesion, gene expression, and differentiation [1]. Despite the ubiquitous influence of mechanics on biology, robust quantification of mechanics at intracellular or intranuclear scales are lacking from conventional methods [2-3]. We describe a development of deformation microscopy that leverages conventional imaging and an automated hyperelastic warping algorithm to investigate strain history, deformation dynamics, and changes in structural heterogeneity within the interior of cells and nuclei. Using deformation microscopy, we found that partial or complete disruption of LINC complexes in cardiomyocytes in vitro, and Lamin A/C deficiency in myocytes in vivo, abrogate dominant tensile loading in the nuclear interior. We also found that cells cultured on stiff substrates or in hyperosmotic conditions displayed abnormal strain burden and asymmetries at interchromatin regions, which are associated with active transcription, compared to controls. Additionally, using deformation microscopy as a foundation, we propose a noninvasive image texture-based elastography technique that can elucidate relative stiffness of euchromatin and heterochromatin regions. Initial studies indicate that for cardiomyocytes cultured on soft substrates that match their native environment, the ratio of heterochromatin to euchromatin stiffness was ~10, while for stiff (aberrant, pathology-like) substrates, the ratio was ~0.05. The reversal of the stiffness is most likely caused by the altered mechanobiological response through mechanisms that require further studies. Our technique and methodological framework can be applied to broader application areas on any images that have inherent texture with an assumption that the local image intensity is a function of the stiffness. Deformation microscopy represents a foundational approach toward intracellular elastography, with potential utility to provide new mechanistic and quantitative insights in diverse mechanobiological applications.

References:

[1] *Wang, N., Tytell, J.D. & Ingber, D.E., 2009. Mechanotransduction at a distance: mechanically coupling the extracellular matrix with the nucleus. Nature reviews. Molecular cell biology, 10, 75–82.*

[2] *Henderson J.T., Shannon G., Veress A.I., Neu C.P., 2013. Direct measurement of intranuclear strain distributions and RNA synthesis in single cells embedded within native tissue. Biophysical journal 105 (10), 2252-2261.*

[3] *Ghosh S., Seelbinder B., Henderson J., Watts R., Veress A., Neu C.P., 2018. Deformation microscopy for dynamic intracellular and intranuclear mapping of mechanics with high spatiotemporal resolution. bioRxiv, 403261.*

[F-10.2]
IMAGE-BASED CONSTITUTIVE MODELING OF ARTICULAR CARTILAGE

David Pierce[1], *Tim Ricken*[2], *Xiaogang Wang*[3], *Thomas Öst*[4], *Magnus Lilledahl*[5], *Corey Neu*[6]

1 *University of Connecticut, Storrs, USA*
2 *University of Stuttgart, Institute of Mechanics, Structural Analysis and Dynamics, Stuttgart, Germany*
3 *University of Connecticut, Mansfield, USA*
4 *Swedish Defense Research Agency, Stockholm, Sweden*
5 *Norwegian University of Science and Technology, Trondheim, Norway*
6 *University of Colorado Boulder, Boulder, USA*

Both computational mechanics and medical imaging play an increasingly significant role in the study of biological systems at the scales of the organism, organ system, organ, tissue, cell, and molecule [1]. Imaging can provide a non-invasive assessment of tissues such as cartilage and can guide selection of material parameters, define boundary conditions or morphology, or enable precise validation studies. We propose virtual human cartilage—an analysis framework combining medical imaging, image analysis, biology, and experimental and computational mechanics. By design, our modeling framework accepts structural data on patient-specific networks of collagen fibers as determined via imaging, e.g. confocal microscopy [2] or diffusion tensor MRI [3], to inform both the solid (reinforcement) and fluid (permeability) dependence of cartilage's mechanical response on the patient-specific collagen network. Sample-specific results show that the fiber network dramatically increases interstitial fluid pressure and focuses it near the surface. Heterogeneity in the tissue's composition also increases fluid pressure. We establish methods to include osmotically induced prestretch/prestress in image-driven virtual human cartilages and investigate the influence of the prestretched/prestressed state when fitting constitutive models of cartilage that include osmotic swelling and when simulating cartilage responses [4]. Our results highlight the importance of determining the prestretched/prestressed state within cartilage in the imaged configuration prior to solving boundary value problems. Patient-specific computational analysis of virtual human joints and cartilage enables a unique opportunity to couple the in vivo solid and fluid biomechanics of cartilage at the joint and tissue levels with cell-mediated changes in cartilage structure, properties, and geometry. Our framework expands our capacity to integrate diverse patient-specific data and enables the testing of hypotheses on virtual human cartilage – connecting in vivo mechanobiology at the cellular, tissue and joint levels. Improved simulations can thus provide medical researchers with new information often unavailable in a clinical setting and may offer better insight into the pathophysiology of cartilage diseases.

References:

[1] *D.M. Pierce, T. Ricken, C.P. Neu, Image-Driven Constitutive Modeling for FE-Based Simulation of Soft Tissue Biomechanics, In: M. Cerrolaza, S. Shefelbine, D. Garzón-Alvarado (Eds), Numerical Methods and Advanced Simulation in Biomechanics and Biological Processes, 55-76, Elsevier, Cambridge, MA, 2018.*
[2] *M.B. Lilledahl, D.M. Pierce, T. Ricken, G.A. Holzapfel and C. de Lange Davies, Structural Analysis of Articular Cartilage Using Multiphoton Microscopy: Input for Biomechanical Modeling, IEEE Trans. Med. Imaging, 30(9):1635-1648, 2011.*
[3] *D.M. Pierce, M.J. Unterberger, W. Trobin, T. Ricken and G.A. Holzapfel, A Microstructurally Based Continuum Model of Cartilage Viscoelasticity and Permeability Incorporating Measured Statistical Fiber Orientations, Biomech. Model. Mechanobiol., 15(1):229-244, 2016*
[4] *X. Wang, T.S.E. Eriksson (Öst), T. Ricken, D.M. Pierce, On Incorporating Osmotic Prestretch/Prestress in Image-Driven Finite Element Simulations of Cartilage, Journal of the Mechanical Behavior of Biomedical Materials, J. Mech. Beh. Biomed. Mat., 86(0):409-422, 2018.*

[F-10.3]

HIGH-RESOLUTIONCONTRAST-ENHANCED MICRO-CT FOR SPATIAL ASSESSMENT OF BIOLOGICAL TISSUES

Greet Kerckhofs[1]

1 *Biomechanics Lab, Institute of Mechanics, Materials, and Civil Engineering, UCLouvain, Louvain-la-Neuve, Belgium; Institute of Experimental and Clinical Research, UClouvain, Louvain-la-Neuve, Belgium; Dept. Materials Science and Engineering, KU Leuven, Leuven, Belgium*

As biological tissues have a complex architecture and spatial heterogeneity, measurements made in 2D only partially reveal their full 3D morphology and interconnectivity. Indeed, conventional and even digital histology are largely unsatisfactory for spatial assessment of biological tissues, because of the restricted sectioning orientation and limited depth resolution. Also, they lack reproducibility on a large scale (sample destruction). In this overview, the potential of contrast-enhanced microfocus computed tomography (CE-CT) is presented.

CE-CT is a very recent development in the micro-CT imaging field and allows quantitative virtual 3D histology of both soft and mineralized tissues. Over the past decade, different CAs have been reported for CE-CT of specific soft tissues [1]. However, it is important that the CA staining and the image acquisition are non-destructive, having no effect on the tissue integrity. As most of the currently applied CAs are destructive, in our research we focus on the development of non-invasive tissue-specific CAs. Recently, we reported an in-house synthesized Hafnium-substituted Wells-Dawson polyoxometalate (Hf-WD POM), which allowed visualizing, apart from bone, the bone marrow adipocytes at the single cell level, and the vascular network allowing full 3D blood vessel network assessment (i.e. branching and spatial distribution) [2]. In a follow-up study, we explored whether similar POM formulations, including the much less expensive precursors of the metal-substituted Hf-WD POM, could also be efficient CAs for soft tissue visualization. Based on their staining capacity and speed of diffusion, we concluded that monolacunary POMs are highly suitable CA candidates.

Because of their capacity to bind electrostatically to collagen and connective tissues, as well as to blood, we successfully used the POMs for several applications: developmental changes of murine placentas and embryos (unpublished data), effect of an anti-angiogenic drug on tumor angiogenesis [3], quantitative analysis of the fiber orientation in tendons and the bone-tendon interface (unpublished data), and many others. In future research, we will further develop and validate novel, tissue-specific CE-CT CAs, and we will focus on the combination with deep learning image analysis for improved quantitative 3D analysis of the CE-CT datasets.

References:

1. *de Bournonville, S. et al. Contrast-enhanced microCT for virtual 3D anatomical pathology of biological tissues: A literature review. In Press at 'Contrast Media & Molecular Imaging'*
2. *Kerckhofs, G. et al. Simultaneous three-dimensional visualization of mineralized and soft skeletal tissues by a novel microCT contrast agent with polyoxometalate structure, Biomaterials 159 (2018) 1-12*
3. *Kerckhofs, G. et al. Contrast-enhanced microCT to visualize and quantify the 3D vasculature in biological tissues without the need for perfusion. Bruker User Meeting Brussels 2017.*

[F-10.4]

CONTRAST-ENHANCED MICRO-CT REVEALS ALTERATIONS IN THE CASCADE OF FRACTURE HEALING IN OBESITY-DRIVEN DIABETIC MICE

Carlos Marin[1], *Jolien Tuts*[2], *Katleen Vandamme*[2], *Greet Kerckhofs*[3]

1 *keletal Biology and Engineering Research Center, Department of Development and Regeneration, KU Leuven, Leuven, Belgium; Prometheus - Division of Skeletal Tissue Engineering Leuven, KU Leuven, Leuven, Belgium; Biomaterials – Biomat, Department of Oral Health Sciences, KU Leuven, Leuven, Belgium*

2 *Biomaterials – Biomat, Department of Oral Health Sciences, KU Leuven, Leuven, Belgium*

3 *Biomechanics Lab, Institute of Mechanics, Materials, and Civil Engineering, UCLouvain, Louvain-la-Neuve, Belgium; Institute of Experimental and Clinical Research, UCLouvain, Louvain-la-Neuve, Belgium; Dept. Materials Science and Engineering, KU Leuven, Leuven, Belgium*

Bone healing after trauma is a complex and long process, in which many different mechanical and biological conditions must be met for proper tissue repair [1]. A compromised micro-environment, such as a diabetic micro-environment, could alter these conditions at any of the described phases of the cascade of fracture healing: i.e inflammation, repair and remodeling [1]. Type 2 diabetes mellitus (T2DM) accounts for 90% of the total diabetes cases and it is associated with obesity and hyperglycemia. The potential impact of T2DM on bone fracture healing represents an important problem, since the T2DM patients are prone to an increased fracture risk. Even though efforts have been made to understand the detrimental effects of T2DM on the fracture healing process, the exact mechanisms and pathophysiological events involved still remain unclear.

The aim of this study was to assess the alterations in the cascades of tibial fracture healing (i.e inflammation, repair and remodeling) of high fat diet-induced obese (DIO) mice. To achieve this, contrast-enhanced microfocus computed tomography (CE-CT) was used to evaluate both soft (unmineralized cartilage and adipocytes) and hard (mineralized cartilage and new bone) tissues. To corroborate the CE-CT results, gene expression and trilineage differentiation of periosteum-derived cells were assessed, after treatment with hyperglycemic (HG) vs normoglycemic (NG) media.

For the first time, using CE-CT we were able to evaluate not only the bone formation, but also the cartilage (mineralized and unmineralized) and the adiposity, simultaneously, within fractures. Compared to aged-matched controls, the DIO mice presented delayed fracture healing, evidenced by a trend towards a decreased bone volume fraction, and an increased volume of the callus, adipose tissue and cartilage at day 14 post-fracture. Our in vitro results confirmed that the osteogenic, adipogenic and chondrogenic differentiation of the osteoprogenitors were altered by HG treatment. In addition, elevated PPARγ expression confirmed the observed increase in adipocytes in vivo. Finally, chondrogenesis-related genes SOX9 and COL2 were downregulated for osteoprogenitors treated with HG medium, confirming the compromised chondrogenic differentiation in vitro and contributing to the delay of the fracture healing process in vivo.

These results are evidence for the T2DM-driven alterations in the cascades of tibial fracture healing, and reveal the potential link between HG-induced dysfunctionality of osteoprogenitors and fracture healing delay under T2DM conditions.

References:

1. *Claes L, Recknagel S, Ignatius A. Fracture healing under healthy and inflammatory conditions. Nat. Rev. Rheumatol. 2012;8(3):133–43.*

[F-10.5]

RESIDUAL LIMB SHAPE AND DEFORMATION USING MULTI-CAMERA 3D DIGITAL IMAGE CORRELATION

Dana Solav[1], *Kevin Moerman*[2], *Aaron Jaeger*[3], *Hugh Herr*[3]

1 *Massachusetts Institute of Technology, Cambridge, USA; Media Lab, Massachusetts Institute of Technology, Cambridge, USA*
2 *National University of Ireland, Galway, Ireland; Massachusetts Institute of Technology, Cambridge, USA*
3 *Massachusetts Institute of Technology, Cambridge, USA*

The residual limbs of lower-limb amputees undergo considerable changes in volume and shape as a result of stresses applied by the prosthetic socket, muscle activation, and knee angle changes. These changes often lead to compromised limb-socket interface stress distributions, which is critical for ensuring a comfortable and stable load transfer between the residuum and the prosthesis.

The aim of this work was to develop a system for providing high-resolution and accurate measurement of the time-varying shape, as well as full-field deformations and strains of residual limbs. Other considerations for the system were its non-invasive nature, low cost and relatively small size.

A 360° camera rig was designed and fabricated to hold 21 synchronously controlled Raspberry Pi camera modules. The residual limbs of seven transtibial amputees were scanned in multiple configurations: knee flexions and extensions, swelling upon socket removal, and muscle contractions. The images were analyzed using MultiDIC, an open-source 3D digital image correlation (3D-DIC) MATLAB toolbox developed by the authors [1]. The toolbox features unique stereo calibration procedures tailored to allow 3D reconstruction of points and triangular meshes from multi-view images (Figu 1). The 3D displacement vectors at each triangle vertex were used to calculate the full-field 3D stretches and strains, as well as the enclosed volumes and cross-sectional areas [2].

Strains in the range of -0.45-0.25 were measured as a result of knee flexion and muscle contraction, with respect to the reference configuration. Doffing resulted in an immediate and fast increase in the residuum volume followed by a slower monotonic increase, which reached 30.2ml 10 minutes post-doffing. The cross-sectional area increase was non-uniform along the length of the residuum.

It was shown that the proposed 3D-DIC framework can be employed to quantify the time-varying residuum shapes and strains, and the enclosed volumes and cross-sectional areas. This framework also provides a promising solution for the in-vivo evaluation of the mechanical properties of the underlying soft-tissues, which may inform data-driven algorithms for prosthetic socket design and other biomechanical interfaces.

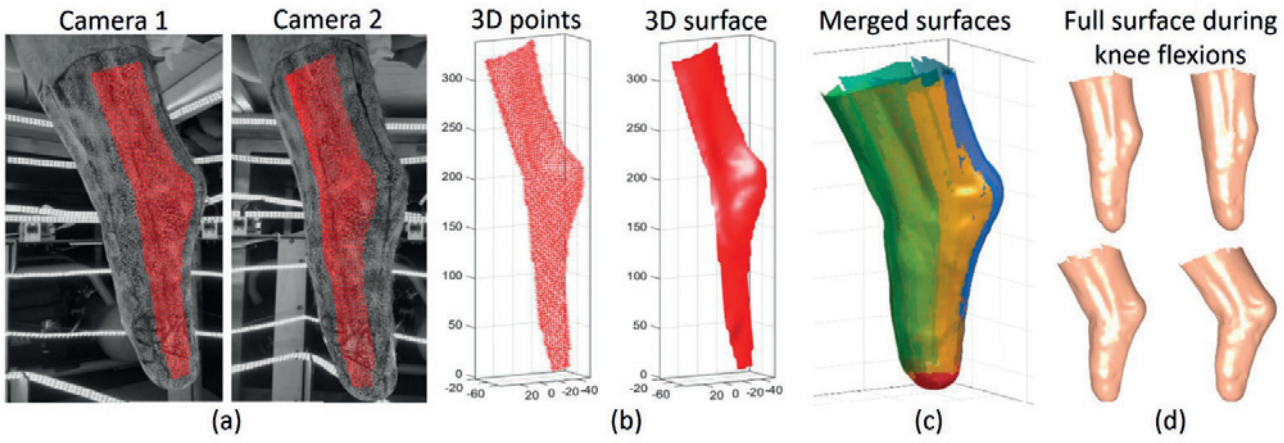

Figure Caption: Workflow of residual limb surface reconstruction using 3D-DIC. (a) Portions of the speckled residual limb imaged by camera 1 and 2 are shown with the correlated points plotted in red on top of the images. (b) The resultant 3D point cloud and triangular meshes for the camera-pair shown in (a). (c) The reconstructed surfaces from all camera-pairs. (d) The merged surfaces in different knee flexion configurations.

References:

1. Solav D. et al. (2018). IEEE Access, 6: 30520-30535. DOI:10.1109/ACCESS.2018.2843725
2. Solav D. et al. (2019). IEEE Trans Biomed Eng, DOI:10.1109/TBME.2019.2895283

[F-11.1]
IMAGING DATA FUSION AND SUBJECT SPECIFIC SPINE MODELLING

Wafa Skalli[1], *Maxim Van Den Abbeele*[2], *Christophe Muth Seng*[3], *Sebastien Laporte*[3], *Dominique Bonneau*[4]

1 *Institut de Biomécanique Humaine Georges Charpak, Arts et Métiers ParisTech, Paris, France*
2 *Ecole Nationale Superieure Darts et Metiers, Châlons-en-Champagne, France*
3 *Arts et Métiers Paristech, Institut de Biomécanique Humaine George Charpak, Paris, France*
4I *nstitut Supérieur de Thérapeutique Manuelle, Avignon, France*

Spine finite element modelling is widely used for a better understanding of mechanisms of injury, and for spinal implants analysis. However, taking into account subject specificity is still a bottleneck. Methods for direct generation of regular subject specific meshes have been proposed, either from CT scans, or from low dose biplanar X-Rays (BPXR). Ultrasound elastography appears as a promising modality to estimate, even grossly, the intervertebral discs material properties [1]. Estimating subject specific loads in clinical routine is still one of the more challenging issues, because their require both subject specific free body diagrams to assess gravity loads acting on a specific body segment, and relevant personalized muscle control models to manage muscles redundancy.

This presentation will focus on recent advances in methods using image data fusion to get subject specific models that could be built in clinical routine. Low dose BPXR and associated barycentremetry models [2] now yield fast generation of subject specific free body diagrams. From BPXR data, geometric transformation of generic musculoskeletal models allows first estimate of subject specific models. Then a very limited set of MRI images, that could be obtained in clinical routine, allow further model adjustment, allowing to run a proprioceptive control model for subject specific loads estimation [3] . Such approach opens the way for a better understanding of spine instrumentation clinical outcome, in relation with postural troubles and muscle status. Recent results and their clinical implications will be presented.

Acknowledgments: This work was performed with the founding of ParisTech BiomecAM chair program on subject specific musculoskeletal modelling, with the support of ParisTech foundation, COVEA and Société Générale.

References:

[1] *Amabile C, Choisne J, Nérot A, Pillet H, Skalli W., J Biomech. 2016 3;49(7):1162-1169*
[2] *Vergari C, Rouch P, Dubois G, Bonneau D, Dubousset J, Tanter M, Gennisson JL, Skalli W. Eur Radiol. 2014 24(12):3210-6.*
[3] *Van den Abbeele M, Li F, Pomero V, Bonneau D, Sandoz B, Laporte S, Skalli W. Clin Biomech. 2018 51:58-66.*

[F-11.2]

EFFECT OF CT-BASED PATIENT-SPECIFIC DATA IN EVALUATION OF JOINT REACTION FORCE AFTER TOTAL SHOULDER ARTHROPLASTY

*Ehsan Sarshari[1], Yasmine Boulanaache[1], Fabio Becce[2], Alain Farron[2], **Alexandre Terrier**[1]*

1 *Laboratory of Biomechanical Orthopedics; Ecole Polytechnique Fédérale de Lausanne (Epfl), Lausanne, Switzerland*
2 *Centre Hospitalier Universitaire Vaudois (Chuv), Lausanne, Switzerland*

Patient-specific musculoskeletal models (MSM) in which all model's parameters are adapted to specific patients can potentially best address inter-patient variability [1]. However, it is not yet feasible to personalize all models' parameters to each patient, given that it is highly demanding [2]. Alternatively, applications of scaling techniques on generic MSMs, known as scaled-generic modeling, provided promising results [3]. On the other hand, a CT-scan of patients' glenohumeral (GH) joint is often acquired during the routine clinical examination of total shoulder arthroplasty (TSA). The objective of this study is to evaluate effects of incorporating CT-scan based patient-specific data in a scaled-generic MSM model on reaction force (JRF) and stability ratio (SR) of GH joint in patients after TSA.

Twenty patients (68±8 years, 6M/14F) planned for TSA were included. We used an EMG-assisted generic shoulder and elbow MSM (MSM-generic) developed based on a healthy male volunteer [4]. Kinematic and EMG data were measured on the same volunteer for two activities: abduction in scapula plane with 2 kg weight in hand (act1), and touching the opposite shoulder (act2). Two modelling alternatives of MSM-generic were compared: MSM-scaled and MSM-CT. The MSM-scaled was obtained from MSM-generic by scaling kinematics, EMG, segment inertia and lengths, and muscle architectures, according to gender, weight, and height. The MSM-CT was obtained from MSM-scaled by accounting for rotator cuff degenerations measured on preoperative CT scans, and by accounting for version/inclination of glenoid implant from preoperative planning. We replicated act1 and act2 with MSM-scaled and MSM-CT, for each patient. JRF was reported in BW% as maximum average of all patients. SR varied from 0 (subluxation) to 1 (fully centered). Variability was reported as average standard deviation over all patients and cycle.

For act1, JRF was 185.3 with MSM-scaled and 169.7 with MSM-CT. SR was 0.9 for both MSM-scaled and MSM-CT. JRF variability was 11.0 with MSM-scaled and 30.4 with MSM-CT. SR variability was 0.1 with MSM-scaled and 0.3 with MSM-CT. For act2, JRF was 27.4 with MSM-scaled and 62.2 with MSM-CT. SR was 0.8 with MSM-scaled and 0.3 with MSM-CT. JRF variability was 4.0 with MSM-scaled and 16.6 with MSM-CT. SR variability was 0.2 for both MSM-scaled and MSM-CT.

Incorporating CT-scan based patient-specific data in a MSM-scaled predicted larger variability in JRF and SR among patients, for both activities. This highlighted the potential importance of considering patient-specific data to improve predications of MSM models. The present results underscored the potential of MSM-CT as an alternative solution to address inter-patient variability. In a next step, this preliminary conclusion would be confirmed with more patients and other activities of daily living.

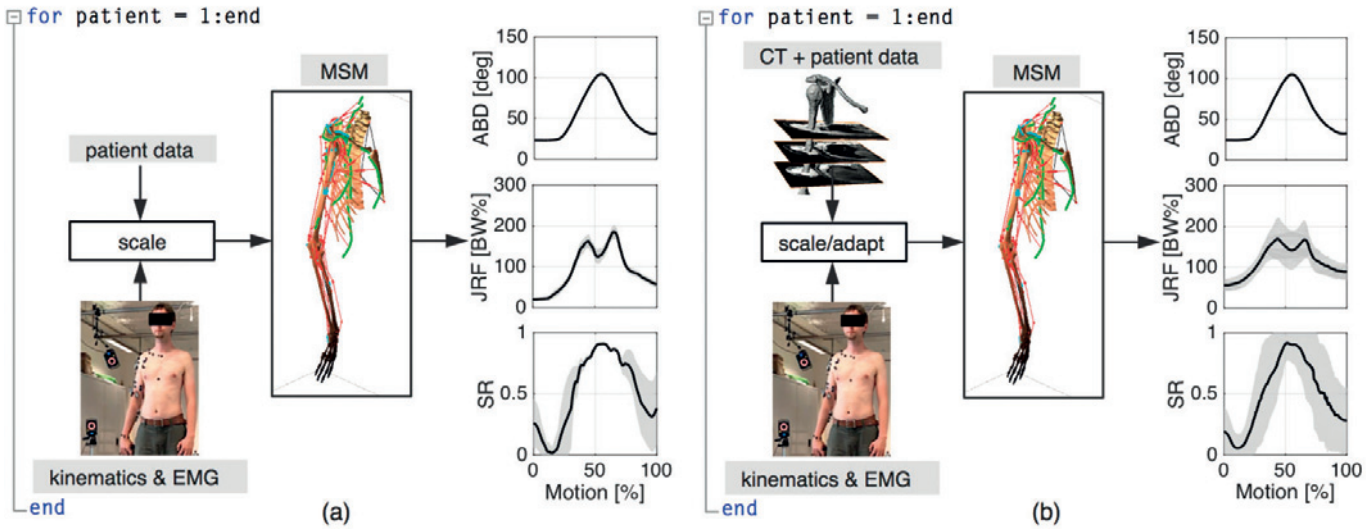

Figure Caption: MSM-scaled (a) and MSM-CT (b) for act1 for all patients.

Acknowledgments: Supported by the Swiss National Science Foundation [K32K1-122512].

References:

[1] *Prinold, JA., J Eng Med, 227(10) 1041-1057, 2013.*
[2] *Martelli S., et al, J Biomech, 48(13) 3615-3624, 2015.*
[3] *Wu W., et al, J Biomech, 49(15) 3626-3634, 201.*
[4] *Sarshari E., EPFL diss, 2018.*

[F-11.3]

DEVELOPMENT AND VALIDATION OF SUBJECT-SPECIFIC PATELLOFEMORAL JOINT KINEMATIC MODELS FOR CHILDREN AND ADOLESCENTS WITH RECURRENT PATELLAR DISLOCATION

Martina Barzan[1], *Simao Brito da Luz*[2], *Luca Modenese*[3], *Michele Conconi*[4], *David Lloyd*[2], *Christopher Carty*[1]

1 *Griffith University, Southport, Australia*
2 *Gcore, Gold Coast, Australia; Menzies Health Institute Queensland, Cold Coast, Australia; Griffith University, Southport, Australia*
3 *Imperial College London, London, UK*
4 *Dept. of Industrial Engineering, Bologna, Italy*

Patellar dislocation is a common paediatric injury, with an estimated incidence rate of 43-77 per 100,000 individuals [1], and an estimated recurrence rate of 38-91% [2]. Clinical tests (e.g., J-sign) and static radiographical measures are commonly used to describe patellofemoral joint (PFJ) kinematics in the assessment of patellar instability. However, these approaches cannot objectively characterize the multi-plane PFJ kinematics throughout the entire tibiofemoral joint (TFJ) range of motion (ROM). The aim of this study was to implement and validate MRI-based PFJ models to estimate PFJ kinematics in paediatric RPD patients.

Four RPD patients (13.0±2.5 years) underwent MRI. Full lower limb and left knee scans were acquired at ~0° TFJ flexion. Three additional knee scans were performed at ~10°, 20° and 30° of TFJ flexion. Three-dimensional lower limb bones, knee ligaments and articular cartilage were reconstructed using Mimics 20.0 (Materialise, Leuven). The passive TFJ motion was modelled as a 6-link parallel mechanism with surface contact conditions and prescribed ligament length variations. Contrarily, the PFJ motion was modelled as a combination of two hinge joints which described the patellar motion in (i)0°-30° TFJ flexion, where the patella is least stable, and (ii)30°-90° TFJ flexion. The first hinge axis was the axis of a cylinder fitted to the femoral surface connecting the pose of the patella at ~0° and 30° TFJ flexion. The pose of the patella at ~0° TFJ flexion was measured from MRI, while its pose at 30° TFJ flexion was estimated by maximising the PFJ congruence [3]. The second hinge axis was the vector connecting the centres of the spheres fitted to the medial and lateral trochlear surfaces [4]. For validation purposes, RMSEs between each patient's predicted and MRI-measured PFJ kinematics were computed and averaged across the four TFJ flexion angles.

RPD1, RPD2 and RPD3 exhibited decreased external rotation and lateral to medial patellar translation in the first 30° of TFJ flexion, while RPD4 exhibited increased external rotation and lateral patellar translation in the first 30° of TFJ flexion (Figure 1). The developed PFJ kinematic models well estimated these different patellar maltracking patterns, allowing to quantify lateral patellar tilt across the entire ROM (Figure 1A) and J-sign patterns (Figure 1B) on an individual basis. Average RMSEs between model-estimated and MRI-measured PFJ kinematics were below 10.2° and 4.5mm for PFJ rotations and translations, respectively.

In conclusion, subject-specific PFJ kinematic models can identify different maltracking patterns in RPD patients and may be used to personalise surgical planning in the treatment of RPD patients.

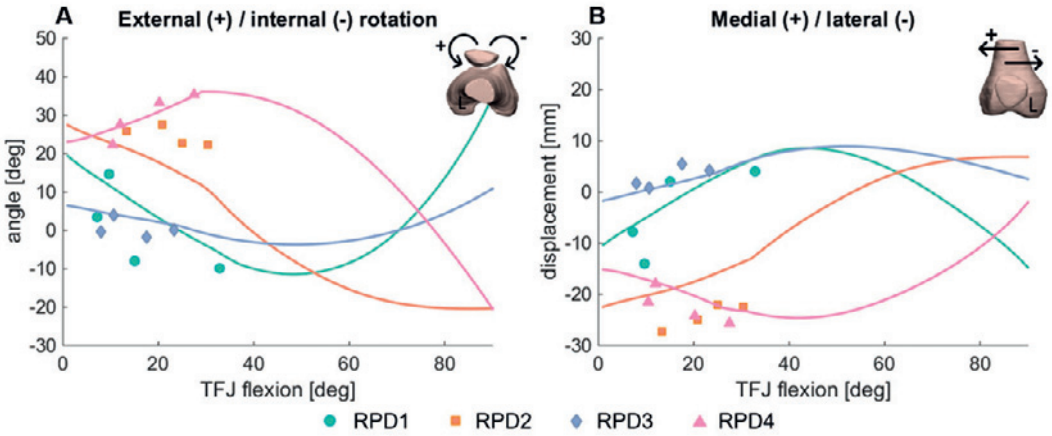

Figure 1: Comparison between model-estimated (solid lines) and MRI-registered (scatter points) external/internal patellar rotation (A) and medio/lateral patellar translation (B) for the four RPD patients.

References:
[1] Fithian DC et al.(2004). Am J Sports Med, 32:1114-21.
[2] Lewallen LW et al.(2013). Am J Sports Med, 41:575-81.
[3] Conconi M et al.(2015). J Biomech, 48:2960-2967.
[4] Brito da Luz S et al.(2017). J Biomech, 53:45-55.

[F-11.4]

FROM SCALING TO MRI DEFINED SUBJECT-SPECIFIC ANKLE JOINT MODELS: A COMPARISON OF THREE APPROACHES WITH INCREASING LEVEL OF ANATOMICAL CONSISTENCY

*Michele Conconi[1], **Erica Montefiori**[2], Nicola Sancisi[1], Claudia Mazzà[2]*

1 *Dept. of Industrial Engineering, Bologna, Italy*
2 *Department of Mechanical Engineering & Insigneo Institute for in Silico Medicine, University of Sheffield, Sheffield, UK*

An implicit assumption in standard musculoskeletal model (MSKM) is that joint constraints, i.e. ligament and contact forces (CFs), do not contribute to the equilibrium of the joint. To be consistent with this assumption, ligament elongation and cartilage co-penetration should be small enough to produce negligible deformation work [1]. In this study, three ankle joint models with increasing level of personalization are compared within a (MSKM) of the lower limb, integrated with individual ligaments and articular surfaces from magnetic resonance images (MRI) to assess their anatomical consistency.

Stereophotogrammetric, force plate, and MRI data were collected for three volunteers. 3D representations of the volunteers' ankles including ligaments and cartilage were obtained from MRI. Subject-specific MSKMs of the lower limb were built [2]. In two cases the ankle was represented as an ideal hinge, whose rotation axis was identified by a marker-based scaling of the gait2392 [3] model (GJ) and by fitting a cylinder to the talar dome (FJ) [2]. The third model is a custom joint (CJ), whose three-dimensional kinematics was determined through maximization of articular congruence, i.e., of load distribution for the specific anatomy [1]. The latter model was also used to identify the most isometric fibres of tibiocalcaneal (TiCa) and fibulocalcaneal (FiCa) ligaments [1]. Joint kinematics, kinetics and CFs, and muscle forces from the three models using Opensim [3] were compared. Elongations of the TiCa and FiCa ligaments and articular co-penetration were also evaluated.

Whereas the MSKMs' output was similar in terms of joint range of motion (ROM), kinetics and CFs estimates (inter-model standard deviation, SD, below 2°, 0.05 Nm/kg and 0.4 BW, respectively), they differed for joint kinematics and anatomical consistency. Over the three subjects, maximum estimates of ligament elongations for GJ, F, and CJ were 34%, 12% and 3% for TiCa, and 36%, 16% and 5% for FiCa, respectively, while maximum mean co-penetration was 2.02 mm, 1.34 mm and 0.18 mm, respectively (Fig.1).

Among the three tested ankle models, only CJ was anatomically consistent, while the others resulted in non-negligible and un-physiological ligament and cartilage deformation. Nevertheless, the effect of this inconsistency was not evident on kinetic results of MSKM, since it neglects the contribution of ligament and contact deformation to the joint equilibrium. Anatomical consistency should be verified to guarantee the reliability of MSKMs' outputs, particularly when joint reaction analysis is performed.

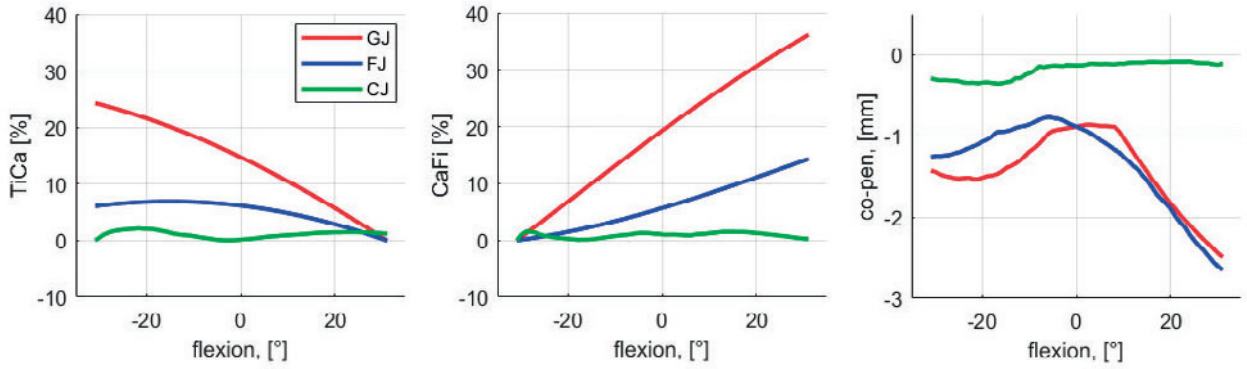

Figure 1: Ligament elongation and articular co-penetration of subject 1.

Acknowledgments: Supported by the EU (FP7, 600932), the UK EPSRC (EP/K03877X/1) and the NIHR Sheffield BRC.

References:

[1] *Conconi M et al. (2015) J Biomech 48(12):2960-7*
[2] *Montefiori et al. (2019) J Biomech https://doi.org/10.1016/j.jbiomech.2018.12.041*
[3] *Delp SL et al. (1990) IEEE Tran. Biomed Eng 37:757-767*

[F-11.5]

SUBJECT-SPECIFIC MODEL WITH HIP MUSCLES' PATHWAYS DETERMINED USING OPTIMIZED WRAPPING SURFACES

Simao Brito da Luz[1], Bryce Killen[1], David Saxby[1], Thor Besier[2], ***David Lloyd***[1]

1 *Gcore, Gold Coast, Australia; Menzies Health Institute Queensland, Gold Coast, Australia; Griffith University, Southport, Australia*
2 *Auckland Bioengineering Institute, The University of Auckland, Auckland, New Zealand; Department of Engineering Science, The University of Auckland, Auckland, New Zealand; Auckland Bioengineering Institute, The University of Auckland, Auckland, New Zealand*

Introduction: Generic musculoskeletal (MSK) Opensim models use via points and 3D wrapping surfaces to constrain musculotendon (MTU) pathways1. However, when generic models are individually scaled, MTU can penetrate bones and have discontinuous lengths and moment arms, producing inaccurate predictions of MTU and joint contact forces2. Thus, building MSK models can be a slow manual process that is tedious and error prone.

The Musculoskeletal Atlas Project (MAP) can automatically create personalized Opensim MSK models using motion capture and sparse medical imaging data using statistical shape models3. We now describe a new method to automatically generate and optimize wrapping surfaces that constrain 40 hip MTU pathways to be continuous, follow the patterns of published MTU lengths and moment arms and without penetrating bones.

Method: For one individual, a subject-specific MAP-Opensim model was created using motion capture data, MRI acquisition and the MAP pipeline3, generating full lower-limb personalized bone meshes from statistical shape models. MTU wrapping surfaces, i.e., cylinders, spheres or tori, were automatically defined and fitted to the subject-specific bone surfaces.

Wrapping surfaces' geometric parameters were tuned via multi-objective particle swarm optimization to ensure: 1) continuous hip flex-extension, int-external and add-abduction MTU moment arms vs. hip flexion, 2) no MTU penetration into bones, 3) match patterns of MTU lengths and moment arms to those from Opensim generic models and experimental studies and 4) minimize difference between tori centers and initial via points. Pearson's correlations (ρ) were calculated between optimized MAP-Opensim model's MTU lengths and hip moment arms with those from generic models and experimental studies.

Results: All hip MTU lengths and moment arms were continuous and similar to those from generic models and experimental studies. High correlations were found between optimized and experimental and generic MTU moment arms (all $\rho>0.53$, $p<0.001$) and between MTU lengths and experimental studies (all $\rho>0.8$, $p<0.04$). Furthermore, optimization prevented MTU bone penetration, and small differences between optimized tori centers and Opensim generic model's via points (<1±0.7cm).

Conclusions: We have created subject-specific MAP-Opensim models, using MAP pipeline, with hip MTU pathways solely constrained by wrapping surfaces automatically fitted to individual bone. Finally, these models can potentially improving estimates of MTU and joint contact forces during dynamic simulations.

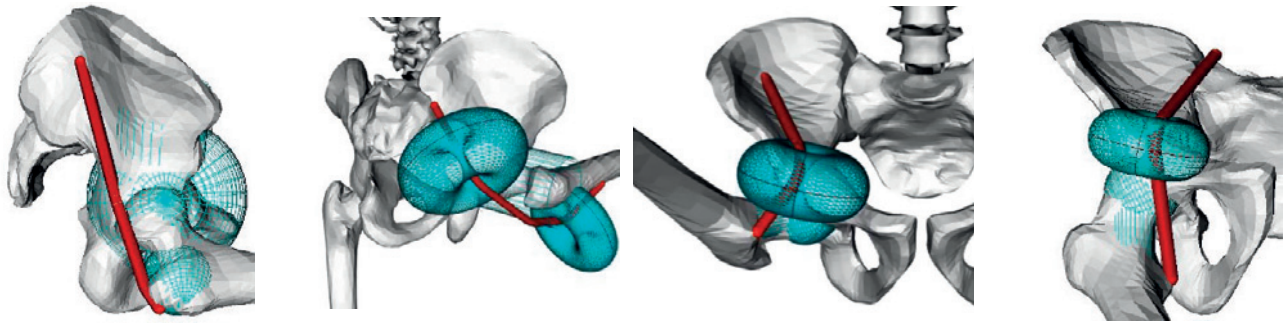

Figure Caption: Optimized wrapping surfaces constraining hip MTU pathways: a) glut med, b) glut max, c) iliacus, and d) psoas

References:

[1] Delp S, et al., IEEE Trans. Biomed. Eng, 54: 1940-1950, 200
[2] Fregly, B.J., et al.,(2012).J. Orthop. Res, 30:503-513
[3] Zhang, J., et al.,(2014).ISBMS 2014,8790:182-192

[F-11.6]

KNEE MEDIAL AND LATERAL CONTACT FORCES COMPUTED ALONG SUBJECT-SPECIFIC CONTACT TRAJECTORIES

Raphael Dumas[1], *Ali Zeighami*[2], *Rachid Aissaoui*[2]

1 *Université de Lyon, Lyon, France; Ifsttar, France; Laboratoire de Biomécanique et Mécanique des Chocs, Lyon, France*
2 *Centre de Recherche du Chum, Montreal, Canada; École de Technologie Supérieure, Montreal, Canada; Laboratoire de Recherche En Imagerie et Orthopédie*

Knee medial and lateral contact forces estimated from musculoskeletal modelling depend on the location of contact points [1-3]. Patient-specific contact point trajectories can be obtained from weight-bearing medical imaging systems which give access to both joint anatomy and joint alignment either in a set of postures (i.e. pseudo-kinematics) or during a continuous movement [4-5].

The medial and lateral contact point trajectories are obtained during quasi-static squat for 10 healthy and 12 severe osteoarthritis (OA) subjects using bi-plane low-dose radiography. The contact forces are estimated using a lower limb musculoskeletal model at each point of the trajectories corresponding to a given knee flexion angles during gait [3]. The contact forces were generally found slightly lower in OA subjects and applied more medially on the tibial plateaus but with high inter-subject variability. The positions of the medial contact points were ones of the linear predictors (together with external knee moments) of the amplitude of the medial contact force.

The lower limb musculoskeletal model with generic contact points has been previously validated with data from instrumented prosthesis [6]. Updated validation of the model taking into account subject-specific prosthetic contact points is currently under progress.

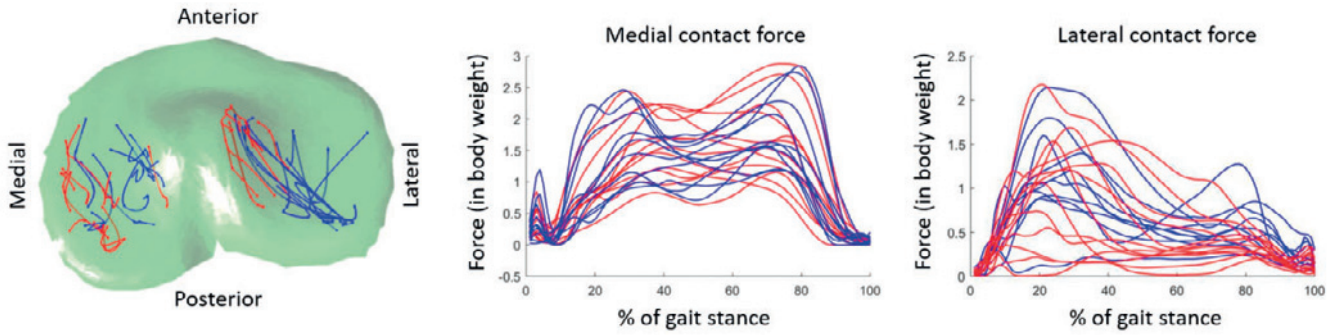

Figure Caption: Contact point trajectories and contact forces for healthy (blue) and OA (red) subjects

Acknowledgments: Fonds de Recherche du Quebec en Sante (FRQ-S), Fonds de Recherche du Quebec en Nature et Technologie (FRQNT), Natural Science and Research Council of Canada (NSERC), LABEX PRIMES (ANR-11-LABX-0063) of Université de Lyon, France.

References:

[1] Lerner et al. (2015). How tibiofemoral alignment and contact locations affect predictions of medial and lateral tibiofemoral contact forces, J Biomech 48(4): 644-650.
[2] Saliba et al. (2017). Sensitivity of medial and lateral knee contact force predictions to frontal plane alignment and contact locations, J Biomech 57: 125-130.
[3] Zeighami et al. (2018). Knee medial and lateral contact forces in a musculoskeletal model with subject-specific contact point trajectories, J Biomech 69: 138-145.
[4] Gray et al. (in press). Three-dimensional Motion of the Knee-joint Complex during Normal Walking Revealed by Mobile Biplane X-ray Imaging, J Orthop Res.
[5] Zeighami et al. (2017). Tibio-femoral joint contact in healthy and osteoarthritic knees during quasi-static squat: A bi-planar X-ray analysis, J Biomech 53: 178-184.
[6] Moissenet et al. (2014). A 3D lower limb musculoskeletal model for simultaneous estimation of musculo-tendon, joint contact, ligament and bone forces during gait, J Biomech 47(1): 50-58.

[G-01.1]

THE MECHANICS OF INTER-TISSUE ADHESION AND PREDISPOSITION TO SPINA BIFIDA

Scott Holley[1], *Emilie Guillon*[1], *Dipjyoti Das*[1], *Dörthe Jülich*[1], *Hannah Geller*[1]

1 *Yale University, Cellular and Developmental Biology, Department of Molecular, New Haven, USA*

An extracellular matrix of Fibronectin adheres the neural tube to the two flanking columns of paraxial mesoderm and is required for normal vertebrate development. Here, we find that the bilaterally symmetric interfaces between the neural tube and paraxial mesoderm function as optimally engineered adhesive lap joints with rounded edges, a graded adhesive and an arced adhesive spew filet. Fibronectin is a 'smart adhesive' that remodels to the lateral edges of the neural tube-paraxial mesoderm interfaces where stress is highest. This Fibronectin remodeling is mechanically responsive to contralateral variation morphogenesis. Fibronectin mediated adhesion to the paraxial mesoderm also constrains neural tube convergence. Perturbation of the Fibronectin matrix rescues the neural tube convergence defect of cadherin 2 mutants, but bilaterally symmetric morphogenesis of the paraxial mesoderm is lost. Therefore, Fibronectin mediated inter-tissue adhesion mechanically coordinates bilaterally symmetric morphogenesis but predisposes the neural tube to convergence defects that lead to spina bifida.

Acknowledgments: Research support provided by NIH Grants R01GM107385 and R01HD092361.

[G-01.2]

SPATIOTEMPORAL CONTROL OF THE MECHANICAL FORCES THAT BUILD AND SHAPE TISSUES DURING MORPHOGENESIS

Karen Kasza[1]

1 *Columbia University, Department of Mechanical Engineering, New York, USA*

Mechanical forces generated by cells drive changes in tissue shape and structure that are essential to building functional tissues and organs during embryonic development. One of the primary force-generating machines inside cells is the contractile actomyosin network, an assembly of myosin II motor proteins and actin filament biopolymers. Mechanical forces generated by actomyosin are likely to have multiple roles in development: driving cell movements and cell shape changes, tuning tissue mechanical properties, and influencing biochemical processes that control cell behavior. Yet, due to the strong coupling between mechanical and biochemical factors during morphogenesis and the lack of experimental tools for manipulating mechanical forces in vivo, it has remained an experimental challenge to dissect the roles of mechanical forces during morphogenesis. To address this, my lab combines live imaging and genetics with emerging optogenetic technologies for manipulating forces inside cells to study the mechanics of morphogenesis in the model organism Drosophila melanogaster. We investigate how mechanical forces and genetic factors conspire to determine epithelial tissue shape, structure, mechanics, and remodeling during Drosophila morphogenesis. Here, we studied how the balance between mechanical tension, mediated by actomyosin to generate forces inside cells, and cell-cell adhesion, mediated by E-cadherin to transmit forces between cells, influences the mechanical behavior of epithelial tissues. We find that systematically shifting the balance between tension and adhesion modulates cell shapes and packings within epithelial tissues, which tunes the ability of tissues to remodel and flow during morphogenesis. Together, these studies shed light not only on how mechanical forces shape tissues during normal development but also on how mechanical factors might contribute to improper tissue movements associated with birth defects and other disease states.

[G-01.3]

SYNTHETIC MORPHOGENESIS BY RECONSTITUTION OF EMBRYONIC CONNECTIVE TISSUE BIOMECHANICS

Alex Hughes[1]

1 *University of Pennsylvania, Philadelphia, USA*

Many tissues fold into complex shapes during development, defining the geometry of emerging stem cell and tissue niches. In vitro control over this process would represent an important advance for tissue engineering, by enabling spatial niche arrays with an engineered developmental "history" encoded in the local ECM composition and mechanical properties. We use embryonic tissue explants, finite element modeling, and 3D cell-patterning techniques to show that mechanical compaction of the extracellular matrix during mesenchymal condensation is sufficient to drive tissue folding along programmed trajectories. The process requires cell contractility, generates strains at tissue interfaces, and causes patterns of collagen alignment around and between condensates. Aligned collagen fibers support elevated tensions that promote the folding of interfaces along paths that can be predicted by modeling. We demonstrate the robustness and versatility of this strategy for sculpting tissue interfaces by directing the morphogenesis of a variety of folded tissue forms from patterns of mesenchymal condensates. These studies provide insight into the active mechanical properties of the embryonic mesenchyme and establish engineering strategies for more robustly directing tissue morphogenesis ex vivo.

[G-01.4]

ROBUSTNESS IN THE MORPHOGENESIS OF VASCULAR NETWORKS AND DEVELOPMENTAL MORPHOGEN PATTERNS

Jason Gleghorn[1], *Saurabh Modi*[1], *Zachary Sexton*[1]

1 *University of Delaware, Department of Biomedical Engineering, Newark, USA*

Stochasticity in biological systems appears at the cellular and multi-cellular tissue scales with gene expression noise, diffusion/degradation/secretion of morphogens appearing in the former and spatio-temporal fluctuations in growth factors, cell movement, proliferation and death appearing in the latter. We focus on two biological systems in which these sources appear: 1) During early embryonic development, the early vasculature resembles a random unorganized plexus of blood vessels. The plexus perfuses with blood and remodels into a hierarchical network providing the tissue with necessary nutrients. We use the chorioallantoic membrane (CAM) from the chicken embryo to study the remodeling of vasculature. We then use time-lapse imaging to observe remodeling. To understand the probabilistic rules that govern remodeling, we developed a multiscale computational framework. The framework combines hydraulic equations of blood flow at the scale of a single vessel that connect to the overall flow distribution in the vasculature. This distribution, along with hydraulic resistances are coupled onto directed graphs that guide the pruning and remodeling of vessels in the network. Allowing for a single input and output of blood flow, we observe that the initial random plexus is primarily pruned at the periphery and blood velocities within each branch tend to slow at the end of the remodeling process. In order to validate the model, we compare graph-theory based metrics in silico to experiments. Finally, we quantify network robustness to the random initial plexus and stochasticity in the system. 2) In order to achieve appropriate biological function, cells with specialized functions must be spatially patterned. Such patterning is a key developmental feature and is governed by external morphogen gradients. We developed a computational tool to infer the minimal structure and parameters of intracellular gene regulatory network (GRN) and intercellular interactions within interacting cell types to explain experimentally observed spatial gene expression patterns. To validate the framework, a bacterial system is used with a sender cell that secretes a morphogen, which diffuses through the medium into a receiver cell to activate a particular gene expression. Reporter genes are used to image and quantify gene expression intensities in both the cell types. Stochasticity can be disadvantageous to cell fate patterning as the cells must transduce the morphogen gradient and reliably lock into a particular cell fate and prevent random switching. This feature is encoded in the interplay of the GRN and the external morphogen concentration. Hence, we simulate the pattern in silico and rank order the inferred networks based on the robustness of their generated patterns against stochastic gene expression and random spatial distribution of cell-types.

[G-01.5]

MODELING THE INFLUENCE OF LOCAL MECHANICAL STIMULI ON JOINT MORPHOGENESIS IN REGENERATING AXOLOTL LIMBS

Ester Comellas[1], *Johanna Farkas*[2], *James R. Monaghan*[2], *Sandra J. Shefelbine*[3]

1 *Northeastern University, Department of Mechanical and Industrial Engineering, Boston, USA*
2 *Northeastern University, Department of Biology, Boston, USA;*
3 *Northeastern University, Department of Mechanical and Industrial Engineering; Department of Bioengineering, Boston, USA*

Understanding the roles of motion and mechanotransduction in joint formation holds promise for the study and treatment of joint deformities in humans. Joint development is driven by the proliferation and subsequent hypertrophy of chondrocytes, which transduce and respond to mechanical stimuli such as changes in osmotic pressure.

In this research we use axolotls to explore the role of mechanics in joint formation. Axolotls can regenerate whole limbs throughout their life, the limbs are morphologically similar to human limbs, and regeneration utilizes the same biological rubrics as ontogenic growth. To draw from the therapeutic potential of these similarities, we are developing a multi-scale computational model for the prediction of joint development. Our model will be based on in vivo data obtained using a click chemistry to label both proliferating and differentiating chondrocytes combined with light sheet microscopy to obtain 3D images of the whole joint [1]. We will combine experimental results and computational modeling to determine the physical mechanisms of normal and pathological joint morphogenesis.

To this end, we have developed a finite element biomechanical model of growth at tissue level in deal.II [2] to study how specific changes in limb motion regulate joint morphology. The tissue is modelled as a biphasic poroelastic material consisting in a fluid-saturated nonlinear porous solid. Pressure-driven growth is modelled via the multiplicative decomposition of the deformation gradient tensor of the solid component [3]. The governing equations are linearized using automatic differentiation and solved monolithically for the unknown solid displacements and fluid pressure value.

Initial results show the model developed can account for the effect of different mechanical stimuli on the final joint morphology, matching our experimental observations of neurectomized limbs. The next steps are towards the incorporation of the biochemical stimuli on joint development by integrating a molecular-level biochemical model [4] into our tissue-level growth response. A computational model that links the biomechanics and biochemistry of normal and pathological limb development across scales is a powerful predictive tool for the study of joint morphogenesis.

Acknowledgments: This work was funded by NSF grant #1727518.

References:

[1] *J. Farkas, J. Monaghan and S. Shefelbine, Visualizing joint morphogenesis and mechanobiology in the regenerating axolotl salmander limb. 8th World Congress of Biomechanics; July 8-12, 2018; Dublin, Ireland.*
[2] *G. Alzetta et al. (2018), The deal.II Library, Version 9.0. Journal of Numerical Mathematics, 26(4):173-183.*
[3] *E. Comellas, S. Budday, J.-P. Pelteret and P. Steinmann, Probing the mechanisms for brain tissue growth via a biphasic nonlinear poro-viscoelastic material model. 55th Annual Technical Meeting Society of Engineering Science, October 10-12, 2018; Madrid, Spain.*
[4] *K.M. Márquez-Flórez, J.R. Monaghan, S.J. Shefelbine, A. Ramirez-Martínez and D.A. Garzón-Alvarado (2018), A computational model for the joint onset and development. Journal of Theoretical Biology, 454:345-356.*

[G-01.6]

MOLECULAR CONTROL OF FORCES DRIVING VERTEBRATE MORPHOGENESIS

Nandan Nerurkar[1]

1 *Columbia University, New York, USA*

Even the most complex organs and organisms have their origins during embryonic development as seemingly simple configurations of stem cells. The intervening process of embryonic development requires careful orchestration of gene expression and downstream regulation of physical forces that sculpt the embryo in a precise and stereotyped fashion. While the past several decades of developmental biology have been driven by a gene-centric view of embryogenesis, there has been a recent resurgent interest in understanding the mechanics of development, and how physical and molecular aspects of development are integrated. One area that – particularly among vertebrates – has received less attention is how developmental signals specify forces to shape the embryo. The present work studies this broader question in the context of early gastrointestinal development, using live imaging together with molecular and biomechanical approaches in the chick embryo to study how the gut tube forms. The gut tube is a cylindrical epithelial tube in the early embryo that will give rise to the lining of the entire respiratory and gastrointestinal systems. We find that formation of the posterior gut tube, the hindgut, occurs by collective movement of epithelial cells in the endoderm, and that this collective cell movement is an emergent property that arises through conversion of a gradient in a diffusible signal, fibroblast growth factor 8 (FGF8), into an active force gradient in the endoderm. This results in a positive feedback such that active cells pull non-contractile cells from low to high levels of FGF8, inducing them to contract, begetting an additional increase in tension pulling more cells into the contractile zone, and so on. This positive feedback is what allows cell movements in the posterior endoderm to outpace axis elongation, and in doing so, to fold from a sheet into a tube. These findings provide insight into a fundamental, yet severely understudied aspect of early embryonic development, and demonstrate how developmental signals modulate tissue-scale forces to drive vertebrate morphogenesis.

Acknowledgments: Work was supported by the NICHD

[G-02.1]

BIOMECHANICAL MODELING OF VASCULAR TISSUE WITH APPLICATION TO THE ANEURYSMATIC AORTA

T.Christian Gasser[1]

1 KTH Royal Institute of Technology, Stockholm, Sweden

Mechanical stimuli influence cell function at the level of gene expression and thereby contribute to the overall control of vascular tissue structure and function. The Extra-Cellular Matrix defines the micromechanical environment within which vascular cells are embedded and to which they respond. Its mechanical properties are governed by the delicate interaction of constituents such as elastin, collagen, proteoglycans, fibronectin and fibrilin. These constituents are synthesized by vascular cells and degraded mainly by Matrix MetalloProteinases. Very much like other biological tissues, vascular tissues seem to adapt towards stable homeostatic mechanical conditions, and failure of reaching homeostasis may result in pathologies, such as aneurysm formation. Tissue Growth and Remodeling (G&R) has to obey basic physical principles, and even within these constraints, a large number of models have been proposed [1,2,3]. Despite adaptation models being based on very different hypotheses, many of them lead to physically reasonable results.

This talk discusses the structural organization of the vessel wall towards the multi-scale mechanical characterization of the aneurysmatic aorta. It is assumed that aneurysmatic vessel wall properties are mainly governed by collagen fibrils, with their undulation and orientation being the most influential micro-histological parameters. Purely passive constitutive descriptions are further complemented by collagen turnover kinetics, and all models are set-up such that they may be used for organ-level vascular biomechanics simulations. The G&R description follows a kinematics-based growth approach [3] and addressed the length scales of individual tissue constituents, which in turn allowed for the linking of biomechanical and biochemical adaptation.

The implementation of the model is based on the general theory of fibrous biological tissues, and uses spherical t-designs to integrate over dispersed fiber orientations [4,5]. To ensure the sufficiently accurate integration of the governing equations, a 'look-ahead' technique was used, where the highest collagen density rate controlled the time step of the numerical problem [6]. Whilst example simulations show plausible results, much more interdisciplinary experimental work is required to support the underlying modeling assumptions. Predictive biomechanical G&R models would not only be of considerable scientific interest, but would also have a large number of practical applications.

References:

[1] TC Gasser, A Grytsan. Current Opinion in Biomed. Eng. 1, 71-77, 2017.
[2] JD Humphrey, KR Rajagopal. Math. Model. Methods Appl. Sci. 2002, 12:407–430
[3] EK Rodriguez, A Hoger, AD McCulloch. J. Biomech. 1994, 27: 455–467.
[4] Y Lanir. J. Biomech. 16, 1–12 (1983)
[5] S Federico, TC Gasser. J. R. Soc. Interface. 7 (47), 955-966, 2010.
[6] TC Gasser. In: P Wriggers and T Lenarz (eds.) Biomedical Technology; Lecture Notes in Applied and Computational Mechanics, Springer Science+Business Media, 2017.

[G-02.2]

AN ACTIVE REMODELING APPROACH TO CARTILAGE FATIGUE MECHANICS CAN PREDICT EXPERIMENTAL RESULTS

Brandon Zimmerman[1], *Gerard Ateshian*[1]

1 *Columbia University, New York, USA*

Osteoarthritis (OA) is a debilitating disease characterized by degeneration and damage to articular cartilage. Idiopathic OA is primarily attributed to natural wear and tear brought on by aging, manifesting as an increase in joint friction and concomitant swelling of the articular cartilage and culminating in a loss of tissue. Although mechanisms of OA initiation remain an active area of study, it is well accepted that mechanical loads mediate OA progression. Previous experimental studies1 have shown fatigue failure of cartilage in a lens-on-strip model, even under physiologic sliding conditions which maintain low friction. The rate of wear was drastically accelerated with a glass counterface, despite only minor increases in friction relative to a cartilage counterface. To investigate the role of friction and evaluate potential mechanisms of fatigue failure, this study develops a theoretical framework for fatigue mechanics that couples tissue remodeling with damage evolution. A computational model of cartilage fatigue including frictional interactions is then used to simulate lens-on-strip experiments in FEBio2.

Cartilage is modeled as a fiber-reinforced multiphasic tissue which includes Donnan osmotic swelling due to proteoglycans and their intrinsic stiffness. Damage to collagen fiber bundles is modeled by our framework for fatigue mechanics of fibrous tissues,3 based on a reactive mixture theory framework originally developed for simulating growth and remodeling (G&R).4 In this framework, a finite number of fiber bundles may be spatially oriented according to experimentally characterized fiber distributions. Each bundle sustains damage independently, allowing fiber recruitment as damage evolves. Our finite element algorithm for frictional contact between multiphasic tissues5 was used to probe the role of surface forces in damage initiation and progression, by including/neglecting friction between the lens and strip. Simulations were performed with both glass and cartilage counterfaces.

FEBio results show a progressive damage process; as collagen bundles become fatigued and fail, other bundles are recruited and loaded (Fig. 1). Investigating the role of friction with a glass counterface demonstrates that significant damage occurs under frictionless conditions (D = 0.63), compared to D = 0.70 with friction included, suggesting friction plays a lesser role than previously thought in damage mechanics. When a cartilage counterface was employed, stresses decreased and the resultant damage was D = 0.08, considerably less than the glass counterface model.

This study is able to predict experimental cartilage damage results by incorporating a novel G&R reactive model of fibrous fatigue mechanics into a finite element simulation. The use of reaction kinetics-based fatigue accumulation to guide the evolving composition of the tissue correctly identifies different regimes of accelerated wear, and provides a computational platform for evaluating hypotheses regarding fatigue in fibrous tissues.

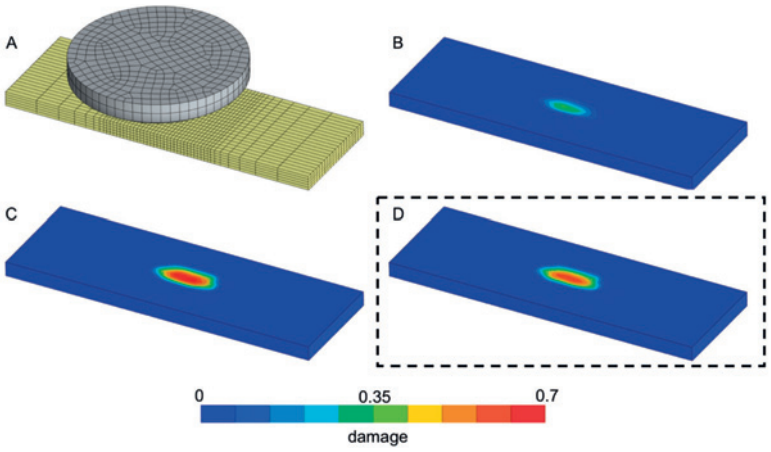

Figure 1: Fatigue evolution during lens-on-strip sliding with glass lens. Mesh (A) matches experimental configuration of Ref. 1; Damage after 5 (B) and 10 (C) cycles of frictional sliding; Damage after 10 cycles of frictionless sliding (D). Note: the damage rate was increased in this preliminary study.

Acknowledgments: NSF GRFP DGE-16-44869

References:

[1] *Durney, KM et al., SB3C 2015-1160.*
[2] *Maas, SA et al., J Biomech Eng, 134(1):011005, 2012.*
[3] *Zimmerman, BK & Ateshian, GA, SES 2018-494.*
[4] *Nims, RJ & Ateshian, GA, J Elast, 129:69-105, 2017.*
[5] *Zimmerman, BK et al., SB3C 2017-179.*

[G-02.3]

STRAIN-INDUCED APPARENT COLLAGEN DENSITY FAILS TO PREDICT NEOVESSEL GROWTH IN COLLAGEN CONSTRUCTS UNDER COMPRESSIVE LOADING

Steven LaBelle[1], *Marissa Ruehle*[2], *Robert Guldberg*[3], *Jeffrey Weiss*[1]

1 *University of Utah, Salt Lake City, USA; Scientific Computing and Imaging Institute, Salt Lake City, USA*
2 *Emory University, Georgia Institute of Technology, Atlanta, USA*
3 *University of Oregon, Eugene, USA*

Introduction: Compression affects in vivo bone healing in a time-dependent manner; loading early in the healing process inhibits growth while delayed loading enhances vascularization [1]. Similar behavior was found in the absence of bone mineralization by seeding collagen gels with angiogenic microvessels [2]. Local collagen density has been shown to affect neovascular growth [3]. The objective of this study was to determine if strain-induced changes in apparent collagen density predict the time-dependent response of neovessels to compression observed in vitro.

Methods: Rat microvessels were suspended in cylindrical 3 mg/mL collagen type-I gels and grown for 10 days [2, 4]. Gels were cultured either unloaded, under 30% unconfined compression (+C), or unconfined compression and shear (+S) for the first 5 days (early) or last 5 days (delayed) of culture (Fig A-B). The total vascular length of the resulting microvascular network was measured from confocal images. Compressive stress relaxation data from avascular gels were fit to a biphasic constitutive model. Gel mechanics during loading were simulated using FEBio [5]. Mechanical models were coupled with AngioFE, a plugin that simulates neovessel growth from parent microvessels based on in vitro data. Growth is scaled by the local apparent collagen density predicted in FEBio based on previously published data [3].

Results and Discussion: In vitro growth was reduced during early +C and +S (Fig C). Delayed +C had no observable effect on growth and delayed +S slightly improved growth despite the predicted increase in apparent collagen density. Growth under shear increased slightly compared to compression for each loading scheme. Simulations predicted homogeneous equilibrium stress/strain fields during +C and inhomogeneous distributions for +S (Fig D). AngioFE simulations failed to predict the experimental results for microvascular growth as early loading had little effect on growth while late loading reduced growth (Figs C, E).

Reduced growth after early loading could be explained by disrupted sprout formation or tip cell quiescence. We previously demonstrated that vessel growth decreases with increasing collagen concentration beyond 3 mg/mL. The predicted apparent collagen density exceeds this threshold, yet in vitro growth is uninhibited. Thus, strain-induced increases in collagen apparent density fail to hinder growth in the same way that we have observed previously. In silico results are explained by the scaling of the growth curve. Early loading occurs when the growth is slow while delayed loading occurs during the rise of the sigmoidal curve.

Further simulations and experiments will investigate the mechanism for reduced growth during early loading and determine when loading ceases to be inhibitory. The effects of apparent and referential collagen density will be distinguished by comparing growth in low density gels compressed to an apparent density that matches the density of unloaded controls.

Acknowledgments: NIHR01AR069297, NIHR01HL131856
References: 1) Boerckel, J.D., et al., PNAS, 108(37): E674-80, 2011. 2) Ruehle, M.A., et al., MRS Commun, 7(3): 466-471, 2017. 3) Edgar, L.T., J.B. Hoying, J.A. Weiss, Ann Biomed Eng, 43(7): 1531-42, 2015. 4) Hoying, J.B., C.A. Boswell, S.K. Williams, In Vitro Cell Dev Bio Anim, 32(7): 409-19, 1996. 5) Maas, S.A., et al., J Biomech Eng,134(1): 011005, 2012.

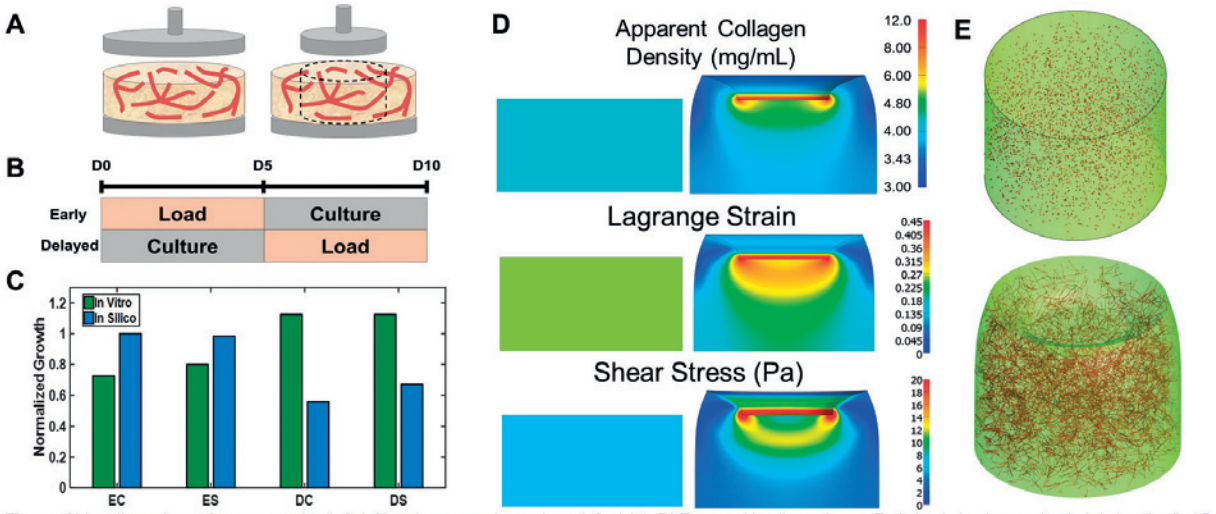

Figure: A) Loading scheme for compression (+C, left) and compression + shear (+S, right). **B)** Temporal loading scheme. Early loaded gels were loaded during the first 5 days of culture then allowed to culture in the absence of load until day 10. Delayed loaded gels were cultured in the absence of loading for 5 days then load was applied for the remaining 5 days. **C)** Normalized growth. Along the bottom E denotes early load, D denotes delayed load, C and S denote compression or compression and shear respectively. *In vitro* growth was normalized by growth in unloaded in vivo constructs. *In silico* growth was normalized by unloaded simulations. **D)** Cross-section of cylindrical gels at equilibrium. Heat maps of predicted mechanical distributions for +C (left) and +S (right). Apparent collagen density was determined from the local deformation and the initial 3 mg/mL concentration. Lagrange strain and shear stress included as well. **E)** AngioFE model of gels grown with delayed compression + shear. Top: seeded vessels in unloaded configuration at day 0. Bottom: Vessel growth at day 5 just after compression is applied.

[G-02.4]

ON THE PRESERVATION OF BRANCHED NETWORK STRUCTURE DURING DEVELOPMENTAL VASCULAR REMODELLING

Lowell Edgar[1], *Miguel Bernabeu*[1]

1 *Usher Institute of Population Health Sciences and Informatics, Edinburgh, UK; University of Edinburgh, Edinburgh, UK*

Angiogenesis occurs as two phases: an early sprouting phase, and a late remodelling phase which involves the pruning of superfluous connections. Recent experiments show that this remodelling phase is driven by vascular endothelial cells (ECs) responding to shear stress by polarising/migrating against blood flow [1-3]. Based on these observations, questions arise as to how vascular integrity is preserved: for any vessel segment to remain stable, a net flux of zero should be achieved between incoming, outgoing, proliferating, and apoptotic cells. How do vessel networks preserve their branched structure and satisfy this zero flux condition within this highly dynamic migratory environment?

Towards answering this, we have implemented an agent-based model (ABM) of flow-regulated migration in a simplified model of the mouse retina consisting of a high-pressure artery connected to a low-pressure vein by proximal and distal branches. Individual ECs are modelled as independent agents. During each time step, ECs migrate against the direction of flow. Vessel diameter is calculated using 3D approximations of the lumen based on the number of cells in the vessel, directly linking flow to migration.

With this model we have determined that cells must make a decision upon reaching a bifurcation (see Figure). Cells that choose to migrate along either the path of highest flow or continuing along polarity alignment result in a loss of either the distal or proximal branch, respectively, as these choices do not satisfy the zero flux condition in both branches. However, if cells randomly choose one of the two paths upon encountering a bifurcation, the incoming cells are split evenly and both branches remain. Alternatively, if cells slightly prefer one branch over the other, both branches remain but with unequal diameter, effectively implementing a form of diameter control: a key outcome of vascular remodelling.

Thus, any persistent bifurcation within a vessel network must include a mechanism to split the flux of incoming cells between its two branches. ECs in vessels are joined by dynamic adherens junctions [4], and ECs must migrate with these junctions intact in order to maintain the epithelium [1]. Force is transmitted amongst neighbouring cells which coordinate and migrate as a supracellular unit, known as collective cell migration (CCM). We hypothesise that at stable vessel bifurcations, cells within each branch transmit force to incoming cells and "pull" them inside, ensuring a constant supply of new cells and satisfying the zero flux condition within each branch. Currently, we are expanding our ABM with representations of adherens junctions to fully demonstrate that force transmission during CCM stabilizes vessel bifurcations and preserves branched networks during vascular remodelling.

References:

1. *Franco CA, PLoS Biol 2015*
2. *Franco CA, Elife 2016*
3. *Vion AC, J Cell Biol 2018*
4. *Bentley K, Nat Cell Biol 2014*

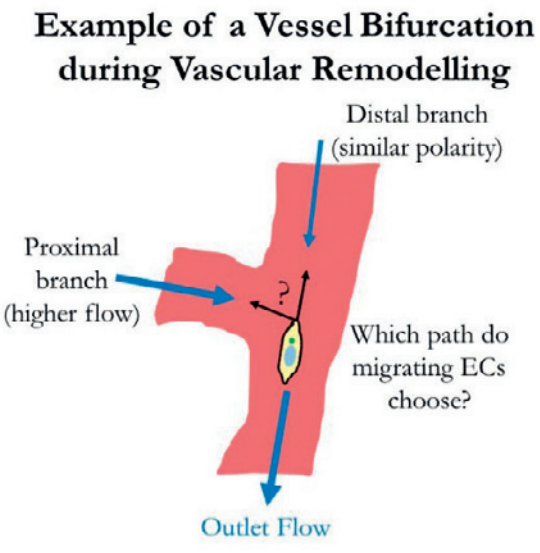

[G-02.5]

GRAPHICAL ANALYSIS OF DEVELOPING TRABECUAR ARCHITECTURE: AN APPLICATION OF DIJKSTRA'S ALGORITHM.

Nicholas Roberts[1], *Richard Abel*[2], *Richard Trask*[3], *Kate Robson Brown*[1]

1 *University of Bristol, Bristol, UK*
2 *Imperial College London, London, UK*
3 *University of Bath, Bath, UK*

In this study we quantitatively analyzed trabecular network development by creating trabecular graphs from micro-computed tomography images of human vertebrae at different stages of development. Graphs in this sense are mathematical objects that deal with nodes (trabecular junctions) and their connections (trabeculae), in computer science graphs and networks are synonymous. Once a graph has been constructed it opens up a range of analysis tools that can be used to categorize trabecular networks and their development. Here we focus on degree distribution and an application of Dijkstra's algorithm.

The lumbar vertebrae (L1 – L5) from 5 historic human skeletons, ranging from 6 month fetal to 5 years post natal, were micro-CT scanned. The images were processed and skeletonised (Arganda-Carreras et al 2010) using BoneJ (Doube et al 2010). The results of the skeletonization were then converted into undirected weighted graphs with a bespoke multithreaded Python code using the Numpy numerical library (Travis & Oliphant 2006).

The degree of a node/trabecular junction is the number of links/trabeculae that node has. The degree distribution is a histogram of node degrees taken over the whole network. We found that in the pre-natal specimens there was a mean probability of 59.8% ± a standard deviation of 0.03% that a trabecular junction would have degree 3. In the post-natal specimens we found that the mean probably for a junction to be of degree 3 rose to 69.19% ± 0.05%.

Dijkstra's algorithm (Dijkstra 1959) was used to analyze changes in network connectivity during development. This implementation of the algorithm calculated the minimum number of links between any 2 nodes in the trabecular networks. We randomly selected 1000 nodes from each vertebrae and calculated the shortest path back to the chosen node. We found a mean path length of 4.93 ± 0.44 for the pre-natal specimens and 6.0 ± 0.77 for the post-natal specimens.

From the preceding results it can be seen that graphical analysis can be used to characterize trabecular network changes over time. This method may also be of use in tracking the development of pathologies such as multiple myeloma where trabecular architectures are disrupted.

References:

Arganda-Carreras, I., Fernández-González, R., Muñoz-Barrutia, A., and Ortiz-De-Solorzano, C. (2010). 3D reconstruction of histological sections: application to mammary gland tissue. Microsc. Res. Tech. 73, 1019–1029. doi:10.1002/jemt.20829
Doube, M., Kłosowski, M. M., Arganda-Carreras, I., Cordelières, F. P., Dougherty, R. P., Jackson, J. S., et al. (2010). BoneJ: free and extensible bone image analysis in ImageJ. Bone 47, 1076–1079. doi:10.1016/j.bone.2010.08.023
Travis E, Oliphant. A guide to NumPy, USA: Trelgol Publishing, (2006)
Dijkstra, E. W. (1959). "A note on two problems in connexion with graphs" (PDF). Numerische Mathematik. 1: 269–271. doi:10.1007/BF01386390.

[G-02.6]

GLYCOLYTIC INHIBITION LEADS TO A GLOBAL METABOLIC SHIFT IN A GENOME-SCALE ENDOTHELIAL CELL MODEL

Jonathan Garcia[1], *Sarah Basehore*[1], *Alisa Morss Clyne*[2]

1 *Drexel University, Philadelphia, USA*
2 *University of Maryland, Fischell Department of Bioengineering, College Park, USA*

Endothelial cells (ECs) form a single layer lining the interior of blood vessels. Under physiological conditions these cells display an anti-proliferative phenotype which changes in response to environmental stimuli. For example, an adjacent cancerous tumor can cause ECs to assume a proliferative phenotype. EC proliferation was experimentally shown to depend on glucose metabolism via glycolysis [1]. Glycolytic inhibition with 3-(3-pyridinyl)-1-(4-pyridinyl)-2-propen-1-one (3PO) reduce EC proliferation, pathological angiogenesis, and tumor metastasis [2]. However, glucose metabolism involves a complex network of reactions, and changes in the entire cell metabolic network have not yet been determined in proliferative vs. growth-inhibited ECs. We therefore constructed a genome scale metabolic model of human umbilical vein ECs (HUVECs) to investigate endothelial metabolism in proliferative and growth-inhibited phenotypes.

We constrained Recon3D, a generic genome scale model (GEM) of a human cell, using publicly available transcriptomic data [3,4]. The model generated captures EC core metabolic features, including predicting correct ATP production from energy sources such as glucose, fructose and palmitic acid. To further constrain the model, ECs were experimentally exposed to 13C6-glucose for 24 hours with or without 3PO. Intracellular metabolites were extracted and quantified using ultra-high-performance liquid chromatography (UHPLC). Metabolic fluxes were estimated via 13C metabolic flux analysis (13CMFA) and used to constrain the GEM. 13CMFA uses nonlinear optimization to predict fluxes based on known carbon atom transitions, iteratively updating the predicted fluxes to reduce the error between experimental and predicted 13C labeling.

The base model predicts that 98% of glucose is processed into lactate through glycolysis and shuttled out of the cell. To simulate glycolytic inhibition via 3PO, the flux through phosphofructokinase was set to zero. The model predicted a significant decrease in NADH and lactate production due to decreased glycolysis. The model further predicted that several mechanisms are used to bypass 3PO inhibition. There is a predicted increase in the pentose phosphate pathway (PPP) and uptake of glutamine (GLN), which is processed through the tricarboxylic acid (TCA) cycle. These predictions were partially verified using mass spectrometry data, in which we observed a significant decrease in lactate and NADH production and increased 13C labeled glycerol 3-phosphate in 3PO-treated cells.

These findings suggest that glycolytic inhibition changes redox balance by altering NADH production. Increased TCA flux can also increase oxidative stress. Understanding the complex network of reactions in glucose metabolism will help us better connect metabolism and endothelial phenotypes, improving our ability to develop new metabolic therapies. The newly developed model will be expanded and verified with other metabolic inhibitors so that in the future, it can be used as a tool for understanding experimental data and generating new hypotheses.

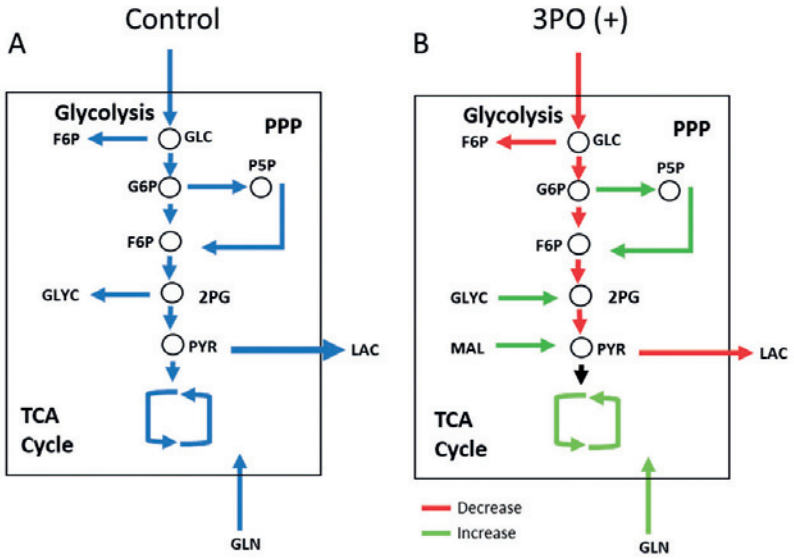

Figure Caption: Control and 3PO (+) models predict distinct flux distributions. (A) in the control model most of the glucose is processed into lactate. (B) 3PO causes a decrease in NADH and lactate production and increases TCA, PPP and glutamine uptake. GLC, glucose; F6P, fructose 6-phosphate; G6P, glucose 6-phosphate; P5P, pentose 5-phosphates; GLYC, glycine; 2PG, 2-phosphoglycerate; PYR, pyruvate; LAC, lactate.

References:

[1] *Doddaballapur, A., et al, Arteriosclerosis, thrombosis, and vascular biology, 2014*
[2] *Brunk, E., et al, Molecular cancer therapeutics, 2008*
[3] *Kolesnikov, N., et al, Nucleic acids research, 2014*
[4] *Brunk, E., et al, Nature biotechnology, 2018*

[G-03.1]

A GENERAL MODELING FRAMEWORK FOR PHENOMENA OF MATERIAL EVOLUTION

Marcelo Epstein[1]

1 *University of Calgary, Calgary, Canada*

Processes of material evolution can be placed under the general umbrella of continuum theories involving internal state variables. Within this context, the definition and demarcation of the terms remodeling, growth, aging, and morphogenesis can be precisely established by invoking mathematically and physically identifiable criteria. Beyond the terminological distinction, this classification may have important repercussions in both the epistemological and computation realms. Significantly, the symmetry group of the material is shown to play a somewhat unexpected role in our ability to draw a clear distinction between the various phenomena, and thus in our ability to assign separate causes to various simultaneously occurring effects. These considerations extend also to possible computational models, as will be demonstrated with the help of examples.

[G-03.2]

THEORIES OF GROWTH AND STRUCTURAL EVOLUTION OF BIOLOGICAL MATERIALS: A REVIEW OF EXISTING LITERATURE AND AN OUTLOOK ON NEW METHODOLOGIES

Alfio Grillo[1]

1 *Dipartimento di Scienze Matematiche (DISMA) "G.L. Lagrange", Politecnico di Torino, Turin, Italy*

In this contribution, I would like to present the main results of two studies concerning the growth of tumors in their avascular growth stage [1,2]. To formalize these processes, I will briefly review the biomechanical framework within which they are typically described [3,4]. For this purpose, I will put together concepts taken from the mechanics of porous media and multiphasic materials as well as from the theory of inelastic processes. After an introduction on the subject, I will discuss a model, inspired by [5], in which the inelastic distortions brought about by growth are assumed to influence the spatiotemporal evolution of growth itself by their being inhomogeneously distributed inside the tumor [1]. In this respect, growth is said to be "self-influenced" [1], and the inhomogeneities of the growth-induced distortions are resolved by hypothesizing a growth evolution law depending on the curvature associated with such distortions. I would also like to report on a more recent model [2], based on [6], in which the picture of growth depicted in [1] is extended to include a two-scale, plastic-like remodeling process, possibly triggered by growth, but independent from it. Such process, studied within a strain-gradient approach, is assumed to occur when the mechanical stress in the tumor overcomes a critical value, and is said to be "two-scale" because it should capture both the plastic distortions at the tissue scale and those associated with the tissue's structural reorganization occurring at the intercellular level. In conclusion, and as an element of novelty, I would like to propose a partial reformulation of the theoretical framework developed in [2], in which tumor growth close to interfaces is investigated.

Acknowledgments: "The Department of Mathematical Sciences (DISMA) 'G.L. Lagrange' of the Politecnico di Torino 'Dipartimento di Eccellenza 2018-2022' (Project code: E11G18000350001) is kindly acknowledged"

References

[1] *Di Stefano, S., Ramírez-Torres, A., Penta, R., Grillo, A.: "Self-influenced growth through evolving material inhomogeneities". International Journal of Nonlinear Mechanics, 106 (2018) 174-187.*
[2] *Grillo, A., Di Stefano, S., Ramírez-Torres, A., Loverre, M.: "A study of growth and remodelling in isotropic tissues, based on the Anand-Aslan-Chester theory of strain-gradient plasticity". Accepted for publication.*
[3] *Goriely, A.: "The Mathematics and Mechanics of Biological Growth", Springer, New York, 2016.*
[4] *Sadik, S., Yavari, A.: "On the origins of the multiplicative decomposition of the deformation gradient". Mathematics and Mechanics of Solids, 22(4) (2017) 771-772.*
[5] *Epstein, M.: "Self-driven continuous dislocations and growth". In: M.G. Steinmann, P. (Ed.), Mechanics of Material Forces, in: Advances in Mechanics and Mathematics, vol. 11, Springer, Boston, MA, 2005, pp. 129-139.*
[6] *Anand, L., Aslan, O., Chester, S.A.: "A large-deformation gradient theory for elastic-plastic materials: Strain softening and regularization of shear bands". International Journal of Plasticity, 30-31 (2012) 116-143.*

[G-03.3]

THE ROLE OF GRAFT AND MICROENVIRONMENTAL PARAMETERS ON GROWTH AND REMODELING OF IN SITU ENGINEERED VASCULAR GRAFTS

Piyusha Gade[1], *Keewon Lee*[1], *Yadong Wang*[2], *Anne Robertson*[1]

1University of Pittsburgh, Pittsburgh, USA
2Cornell University, Ithaca, USA

There is a persistent clinical need for off-the-shelf small diameter vascular grafts to treat diseases of the coronary and peripheral arterial circulation. In situ tissue engineering of vascular grafts (TEVGs) is a novel technology that uses cell-free, porous, biodegradable grafts to harness host growth and remodeling (G&R) ability to develop a new functional artery (neoartery) in the degrading graft microenvironment. In order to translate this technology to the clinic, there is a need to understand the fundamental bio-mechanical phenomenon governing this process and predict the host-specific long-term remodeling response of the neoarteries. Constrained mixture theory-based models1 provide a platform for predicting long-term biomechanics of these grafts. However, they require three types of constitutive equations pertaining to mass kinetics, turnover kinetics and strain energy responses of each constituent. Using experimental and numerical techniques, we aim to determine these age dependent constitutive relationships and understand how the graft and microenvironmental material parameters drive key features of the G&R process in TEVGs.

We fabricated 800µm inner diameter poly-glycerol(sebacate) PGS grafts and implanted them in a young2,3 and aged rat carotid artery interposition model. Remodeling was tracked up to six months with by biaxial inflation testing, two photon microscopy, histology and biochemical evaluation at pre-determined time points. These data were used to formulate constitutive relationships that informed our G&R model4.

Old neoarteries (ONs) exhibited a stiffer response in comparison with young neoarteries (YNs) (Fig 1A). ONs also demonstrated inward (stenotic) remodeling as opposed to YNs which presented with normal wall thickness (Fig 1B). Both these qualitative features were predicted using our tailored G&R model. Parametric analysis with this tool revealed graft degradation half-life (S0.5), extracellular matrix deposition rate and collagen deposition stretch can be modulated to mitigate stenotic remodeling seen in ONs.

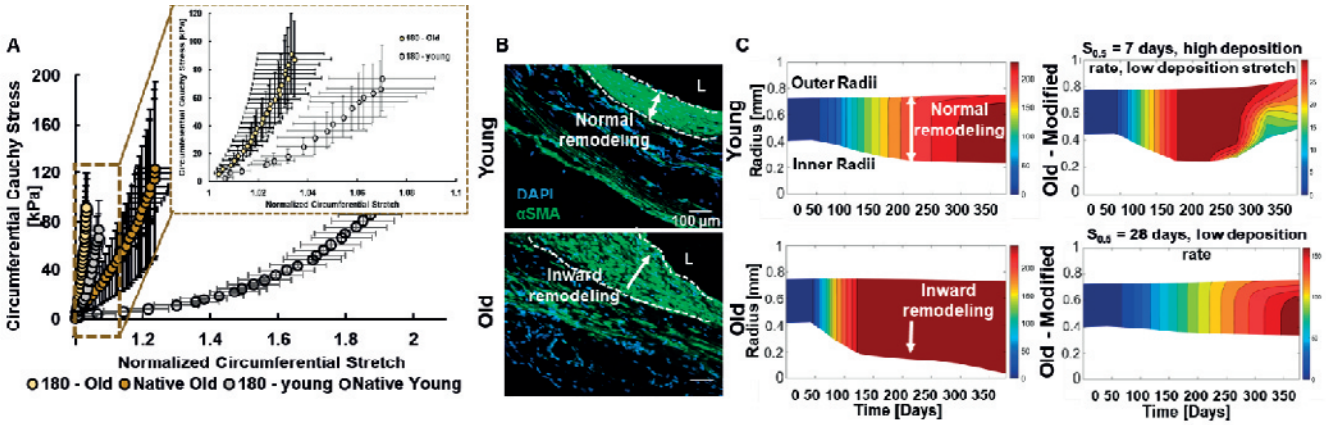

Figure 1: A) Circumferential stress-stretch response and B) outward (normal) versus inward (stenotic) remodeling as seen with αSMA staining in YNs and ONs at six months post-implant. L indicates lumen. C) Predicted inner and outer radius with time in YN and ONs using tailored G&R model. Modulating collagen deposition stretch, degradation half-life ($S_{0.5}$) and extracellular matrix deposition rate in ONs can mitigate the inward (stenotic) remodeling.

Acknowledgments: This work was supported by National Institutes of Health grant NIH/1R21HL124479-01.

References

[1] *Humphrey et al., Math Models Methods Appl Sci, 12:407-430, 2002.*
[2] *Wu et al., Nat Med, 18:1148-1153, 2012.*
[3] *Lee et al., Biomat, 181:67-80, 2018.*
[4] *Gade et al., J. R. Soc. Interface, 14(132): 20170102.*

[G-03.4]

EFFECTS OF HYPERTENSION-INDUCED REMODELING ON THE MECHANICS OF THE LEFT VENTRICLE

Marissa R. Grobbel[1], Gregory D. Fink[2], Stephanie W. Watts[2], Lik Chuan Lee[1], ***Sara Roccabianca[1]***

1 *Michigan State University, Department of Mechanical Engineering, East Lansing, USA*
2 *Michigan State University, Department of Pharmacology and Toxicology, East Lansing, USA*

We have recently shown that the interaction between myocytes and the collagen fiber network plays a key role in defining left ventricle (LV) residual stresses [1]. Furthermore, it is well known that hypertension induces pathological remodeling in the LV, increasing collagen volume fraction and passive stiffness in the heart [2], and affecting the residual stress distribution in the LV [3]. We hypothesize that hypertension could also alter the LV's inter-constituent mechanical interaction. To test this hypothesis, we have isolated the LV constituents of healthy and hypertensive rats, performed opening angle tests on them, and used this data to estimate possible forms of the interaction.

Whole hearts were extracted from healthy (Sprague-Dawley, fed control diet) and hypertensive (Dahl-Salt sensitive, fed 60% high fat diet) adult male rats. The LVs were then split into three groups: intact tissue, isolated collagen fibers, and isolated myocytes. Myocytes and collagen fibers were isolated through previously published protocols [1]. Then, opening angle tests were performed on all samples. A constrained mixture modeling framework was utilized to estimate the interaction between myocytes and collagen fibers in all hearts, as previously published [1], using a range of hypertensive collagen mass fractions.

We found that the opening angle in the isolated collagen fibers was significantly higher compared to the intact tissue for both healthy and hypertensive rats. Additionally, the intact tissue and the isolated collagen fibers of hypertensive LV's had a lower average opening angle than their respective healthy groups. Furthermore, the model solution corresponding to no interaction between constituents was not valid for either the healthy or hypertensive samples. Additionally, no solutions for the healthy and hypertensive were equal.

In this study, for the first time, we have shown that (1) the opening angle in isolated collagen fibers decreases with hypertension, while (2) the opening angle of isolated myocytes seems to not be affected by remodeling. The model showed that the interaction between myocytes and collagen fibers should not be ignored in either healthy or hypertensive LV. Furthermore, it appears that the value of the interaction terms is highly affected by tissue composition.

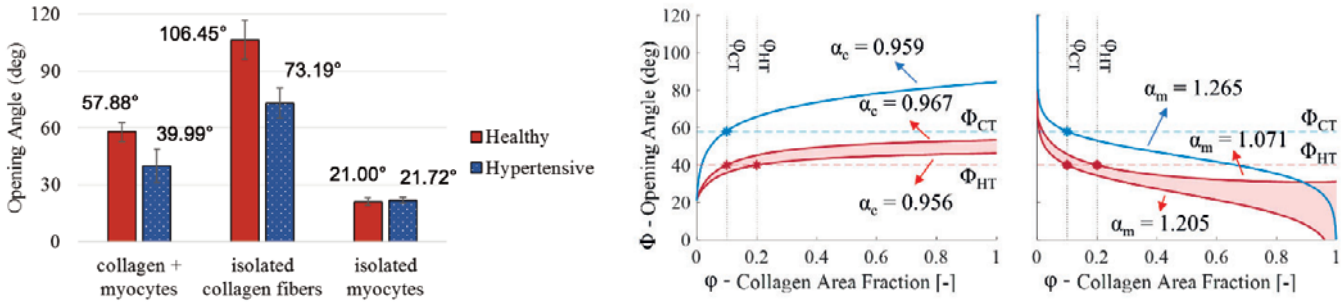

Figure Caption: Comparison of opening angle between each experimental group. Error bars showing standard error (represents $p < 0.05$). Right: Opening angle as a function of collagen inclusion shows the solutions for interactions of healthy (blue, CT) and hypertensive (red, HT) constituents.*

Acknowledgments: We kindly thank Ari Hollander and Analeeza Dubay, for help with the experiments, and Emma Darios Flood and Kibrom M. Alula, for help with the animals.

References:

[1] M.R. Grobbel, et. al. BMMB, 2018.
[2] M.A. Rossi. J Hypertens, 1998.
[3] J.H. Omens, et. al. J Mol Cell Cardiol, 1996.

[G-03.5]

COMPUTATIONAL AND ANALYTICAL METHODS FOR MODELLING THE OVERALL BEHAVIOR OF HETEROGENEOUS TISSUES

Ariel Ramirez Torres[1], *Salvatore Di Stefano*[1], *Alfio Grillo*[1], *Raimondo Penta*[2]

1 *Dipartimento di Scienze Matematiche (DISMA) "G. L. Lagrange", 'Dipartimento di Eccellenza 2018–2022', Politecnico di Torino, Torino, Italy*
2 *University of Glasgow, School of Mathematics and Statistics, Mathematics and Statistics Building, Glasgow, UK*

The study of multi-scale heterogenous tissues is of great interest in biomechanics. Biological materials are often organized across two or more length scales and they present the property of remodelling their internal structure, e.g. to adapt themselves to changes in the chemo-mechanical environment. Multi-scale techniques, such as asymptotic homogenization[1], have been successfully applied to investigate various physical systems due to their potentiality in decreasing the complexity of a problem by averaging and ciphering any geometrical and mechanical micro-scale variation in the effective coefficients of the macro-scale governing equations. In the present work, we aim at exploiting the asymptotic homogenization technique in order to obtain the governing equations of composite tissues that may, or may not, present structural changes of their internal micro-environment. Furthermore, we solve the resulting homogenized partial differential equations as well as the arising relevant cell problems using analytical[2] and computational[3] approaches, and we compare our results with experimental data from the literature. In this way, we provide a computationally feasible multi-scale modelling towards the understanding of the complex interactions taking place in multi-scale tissues.

Acknowledgments: We kindly acknowledge the Dipartimento di Scienze Matematiche (DISMA) "G.L. Lagrange" of the Politecnico di Torino, 795 "Dipartimento di Eccellenza 2018–2022" ('Department of Excellence 2018–2022'), Project code: E11G18000350001.

References:

[1] N. Bakhvalov, G. Panasenko (1989). Homogenization: Averaging Processes in Periodic Media. Kluwer, Dordrecht, The Netherlands.
[2] A. Ramírez-Torres, R. Penta, R. Rodríguez-Ramos, A. Grillo (2019). Effective properties of hierarchical fiber-reinforced composites via a three-scale asymptotic homogenization approach. (Submitted)
[3] A. Ramírez–Torres, S. Di Stefano, A. Grillo, R. Rodríguez–Ramos, J. Merodio, R. Penta (2018). An Asymptotic Homogenization Approach to the Microstructural Evolution of Heterogeneous Media. International Journal of Non-Linear Mechanics. https://doi.org/10.1016/j.ijnonlinmec.2018.06.012

[G-05.1]

COMPUTER METHODS FOR THE UNDERSTANDING AND REPAIR OF PELVIC ORGAN PROLAPSE

Steven Abramowitch[1]

1 *University of Pittsburgh, Pittsburgh, USA*

Pelvic organ prolapse (POP) is a common condition with a 12.6% lifetime risk of surgical repair (1). While there is a lot known about this disorder, its mechanisms—similar to those of other pelvic floor disorders (including urinary and fecal incontinence and obstructed defecation)—still elude us. Many of these pelvic floor disorders (PFDs) are linked to vaginal delivery. In fact, the risk of POP alone goes up 8-fold following just two vaginal deliveries (2). However, the significant time between delivery and the onset of symptoms (often 2 decades or more) limits our ability to perform prospective studies that would help identify the women at greatest risk. Moreover, many animal models have significant anatomical differences that preclude them from use in studies probing the mechanisms of PFDs (3). Those that are similar, e.g. non-human primates, are a limited resource and expensive to study long-term. For these reasons, a significant amount of research has focused on the use of various medical imaging modalities (e.g. MRI and ultrasound) to better understand maternal injuries that result from vaginal delivery and the functional consequences of anatomical defects that can be observed in patients with PFDs. This creates significant opportunities for the application of computer methods to extract quantitative data that will be useful to clinicians. Some of the computer methods being explored include combinations of machine learning, statistical shape modeling, computer vision technologies, and finite element analysis.

Another area where computer methods have become useful is in the study of POP repair. Of the patients undergoing a native tissue repair for POP, 70% will fail after 5 years (4). As a result, many surgeons have turned to biomaterials, most commonly polypropylene mesh, to achieve more durable repairs. Unfortunately, POP meshes started as abdominal hernia meshes that were remarketed under FDA 510K applications for POP repair and thus, were never designed specifically for the vagina. Complications resulting from these meshes, especially those implanted transvaginally, have prompted FDA warnings and significant litigation. Our research group has spent more than a decade trying to understand why these devices are successful in some women and lead to complications in others. We have utilized mechanical testing protocols and an array of computer methods (e.g. photogrammetry, finite element simulations) to identify what we believe to be major limitations of current mesh designs. This talk will describe some of those strategies and the results that are improving our understanding of PFDs and their surgical repairs.

Acknowledgments: NIH R01HD083383, NSF 1511504

References:

1. *Wu J. Obstet and Gynecol. 123(6):1201-6. 2014*
2. *Mant J. British J Obstet Gynaecol. 104(5):579-585. 1997*
3. *Abramowitch S. Eur J Obstet Gynecol Reprod Biol. 144(S1):S1 46-58. 2009*
4. *Jelovsek, J. Obstet Gynecol. 132(2): 298-309. 2018*

[G-05.2]

BIOMECHANICS OF FEMALE PELVIC CAVITY: LESSONS FROM COMPUTATIONAL MODELS

Renato Natal Jorge[1], *Dulce Oliveira*[2], *Maria Vila-Pouca*[2], *Elisabete Silva*[2], *Teresa Mascarenhas*[3], *Marco Parente*[1]

1 *Inegi, FEUP, Faculty of Engineering of University of Porto, Porto, Portugal*
2 *Laeta; Inegi, FEUP, Porto, Portugal*
3 *Fmup; Laeta; University of Porto, Porto, Portugal*

Pelvic floor dysfunction includes different pathological conditions with a common ground related to pelvic structures loss of support or disruption of ligaments, fascia and pelvic floor muscles, like the levator ani complex. The ethiology of those diseases may be influenced by anatomical features, traumatic events such as vaginal delivery [1], hormonal status and heavy work or exercise [2]. As clinical aspects may not be immediately evident, imaging techniques play an important role on diagnosis, follow-up or surgery outcome.

Vaginal delivery is the greatest epidemiological risk factor for the development of pelvic floor disorders (PFD). It is known that parity has the strongest association with the risk of requiring surgery for pelvic organ prolapse. Vaginal delivery is also the most important risk factor for developing stress urinary incontinence.

In this sense, biomechanical models have been applied to estimate the mechanical behavior of the pelvic cavity under several conditions. During the last decade, simulation of the biomechanical behavior of PFM has been developed and implemented in the University of Porto by a multidisciplinary team [3-5]. In this work a summary of those investigations is done including the main conclusions obtained.

Acknowledgments: Funding by Ministério da Ciência Tecnologia, e Ensino Superior, FCT, Portugal, under the project UID/EMS/50022/2013 and also the Project NORTE-01-0145-FEDER-000022 - SciTech - Science and Technology for Competitive and Sustainable Industries, cofinanced by Programa Operacional Regional do Norte (NORTE2020), through Fundo Europeu de Desenvolvimento Regional (FEDER).

References:

[1] *-MPL Parente, RM Natal Jorge, T Mascarenhas, AL Silva-Filho, "Computational modeling approach to study the effects of fetal head flexion during vaginal delivery", American Journal of Obstetrics and Gynecology, 203, Article Number: 217.e1, 2010.*
[2] *-A Carvalhais, RM Natal Jorge, K Bo, "Performing high-level sport is strongly associated with urinary incontinence in elite athletes: a comparative study of 372 elite female athletes and 372 controls", British Journal of Sports Medicine, 52:1586-1590, 2018.*
[3] *-S Brandão, MPL Parente, T Mascarenhas, ARG Silva, I Ramos, RM Natal Jorge, "Biomechanical study on the bladder neck and urethral position: simulation of impairment of the pelvic ligaments", Journal of Biomechanics, 48:217-223, 2015.*
[4] *-DA Oliveira, MPL Parente, B Calvo, T Mascarenhas, RM Natal Jorge, "A biomechanical analysis on the impact of episiotomy during childbirth", Biomechanics and Modeling in Mechanobiology, 15:1523-1534, 2016.*
[5] *-M Vila Pouca, J Ferreira, DA Oliveira, MPL Parente, T Mascarenhas, RM Natal Jorge, "On the effect of labour durations using an anisotropic visco-hyperelastic-damage approach to simulate vaginal deliveries", Journal of the Mechanical Behavior of Biomedical Materials, 88:120-126, 2018.*

[G-05.3]

INVESTIGATION OF MECHANICAL PROPERTIES OF WHOLE PLACENTA TISSUES AND OF USING ULTRASOUND PLACENTA STRAIN ELASTOGRAPHY TO DETECT INTRAUTERINE GROWTH RESTRICTION

Choon Hwai Yap[1], *Shier Nee Saw*[1], *Citra Nurfarah Zaini Mattar*[2], *Arijit Biswas*[2], *Lujie Chen*[3]

1 *National University of Singapore, Singapore, Singapore*
2 *National University Health System, Singapore, Singapore*
3 *Singapore University of Technology and Design, Singapore, Singapore*

Intrauterine Growth Restriction (IUGR) is a pregnancy complication where there is insufficient nutrient and oxygen transport from to the fetal baby, due to excessive flow resistance in the placenta. This causes a 5-10x higher mortality rate, and long-term morbidities such as heart diseases, diabetes, hypertension, and neural maldevelopment. The prevalence is high at 3% in the developed world and 10-15% in the developing world, but to date, we have no proven strategy to prevent or treat the disease. Early detection, however, can enable management strategies, such as optimizing the timing of delivery, which has been shown to improve outcome. There is thus a need for improved understanding of the disease, to lead to better detection and management strategies.

To this end, we performed a series of investigations to understand the whole placenta mechanical properties and to test if ultrasound strain elastography can be a good method to detect IUGR, via non-invasive measurement of the mechanical properties of the placenta. We first performed uniaxial compression mechanical testing on post-delivery human placenta in all 3 axes, and ex vivo strain elastography on the same samples.

We found that placenta tissues had substantial viscoelasticity, having altered stiffness with different compression rates. This suggested the importance of standardizing the palpation rate during strain elastography, such as via a motorized control. We further demonstrated that motorized palpation can significantly increase elastography precision. Secondly, we found that placenta tissues were surprisingly isotropic, and consequently, simpler strain energy functions could be utilized to describe its properties. Thirdly, we found substantial spatial variability in mechanical properties within the same placenta, suggesting that elastography must be conducted across several locations and averaged, as we demonstrated in our ex vivo elastography. Fourthly, we found that IUGR placenta had increased stiffness over normal ones, but the difference was only significant at lower compression rates, providing guidance for elastography settings during disease detection. The differences in mechanical properties could be explained by the change in collagen-to-elastin ratio found via histology. Finally, we introduced an innovation to standardize strain elastography between different subjects, by introducing an external polymeric pad of known stiffness as the reference layer, rather than adopting existing clinical practice of using maternal subcutaneous fats tissue as the reference layer. This solved the problem of fats tissues not being a good reference material as its stiffness can be significantly different from one person to another.

Our investigations show that elastography has promise as a detection tool for IUGR. However, caution and deeper consideration for the biomechanical conditions are necessary to ensure accuracy and precision.

Acknowledgments: National University of Singapore, Singapore, Singapore Young Investigator Award (2015, PI: Yap), Singapore Ministry of Education Tier 1 grant (2017, PI: Yap) for funding.

[G-05.4]

STATISTICAL SHAPE MODELING TO DESCRIBE THE PELVIC FLOOR OF WOMEN WITH OBSTRUCTED DEFECATION

Megan Routzong[1], *Shaniel Bowen*[1], *Ghazaleh Rostami Nia*[2], *Roger Goldberg*[2], *Steven Abramowitch*[1]

1 *University of Pittsburgh, Pittsburgh, USA*
2 *Northshore University Healthsystem, United System*

Background: Obstructed defecation (OD) is a common condition with an estimated incidence of 15-20% in adult females. The pelvic floor requires both functional and anatomical integrity, which can be compromised in women with pelvic floor disorders1. Posterior compartment abnormalities are associated with defecatory disorders, but the relationship between pelvic floor function/anatomy and OD remains undetermined1. Therefore, the goal of this study was to identify differences in pelvic floor shape at rest and peak evacuation and compare control vs case (those with OD symptoms) subjects using statistical shape modeling. Methods: Mid-sagittal pelvic floor traces—from the inferior portion of the pubic symphysis to the tip of the coccyx—from MR images (IRB EH18-19) were converted into 3D curves and normalized by the pubococcygeal line (Figure 1). Subjects were categorized by Group (case (n=6) vs control (n=6)) and each subject had one curve for each State (rest and peak evacuation). DeformetricaTM determined corresponding points across all shapes, then a Principal Component Analysis (PCA) was performed in MathematicaTM. To determine which modes of variation (described by eigenvectors and eigenvalues) explained variance greater than noise, a Monte Carlo analysis determined the noise associated with the size of this dataset2. PCA scores—the projections of original data onto eigenvectors—were calculated for those modes and became the dependent variables in a Two-Way Mixed MANOVA performed in SPSSTM. Results: The first 3 modes described variance greater than noise (Figure 1). Multivariate statistics on their PCA scores showed that the interaction between Group and State was significant (p=0.007). Within-Subject Contrasts revealed that the main effect of State was significant for Mode 1 (p=0.042), while the interaction was only significant for Modes 1 and 3 (p=0.001 and p=0.036, respectively). Conclusions: This study demonstrates that women with OD symptoms have a more relaxed pelvic floor at rest, resulting in minimum shape changes during evacuation. Asymptomatic women, on the other hand, have better support during rest and, therefore, more significant shape changes during evacuation.

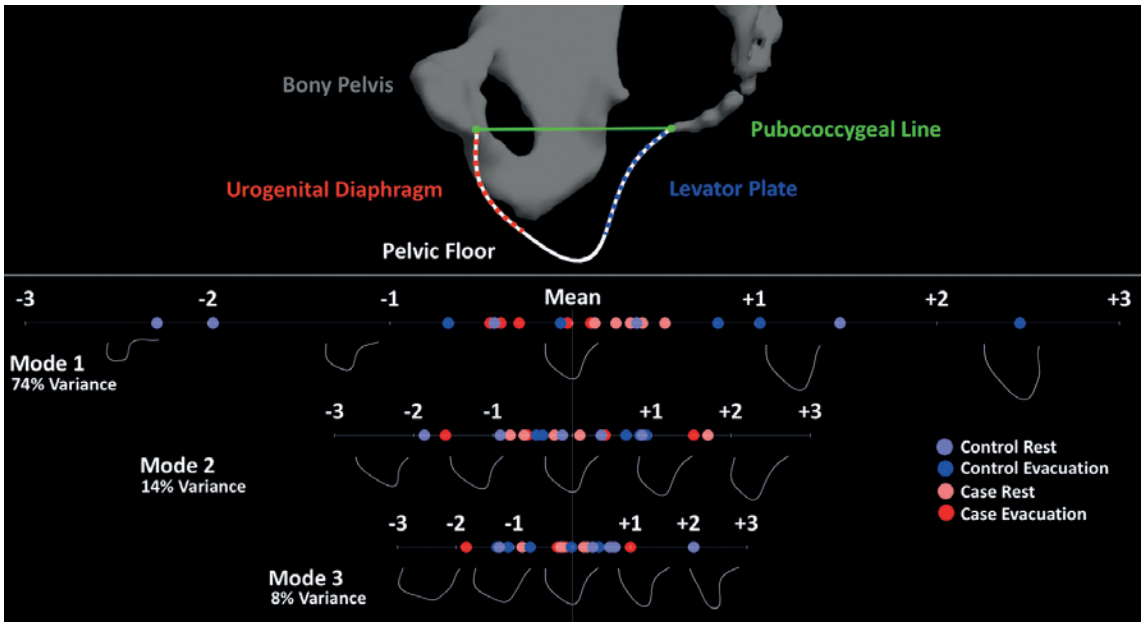

Figure 1: Top) Shows the mean pelvic floor shape within a representative bony pelvis with relevant anatomy labelled. Bottom) Demonstrates the 3 significant modes within ±3 standard deviations of the mean shape and where subjects' PCA scores lie along each mode. Percent of the total variance explained by each mode is given. Qualitatively, Mode 1 seems to describe variation in levator plate angle, Mode 2 variation in urogenital diaphragm angle, and Mode 3 variation in relative inferior pelvic floor width. Across Mode 1, case subjects lie closer to the mean compared to controls.

Acknowledgments: This work was supported by NSF GRFP Grant #1747452.

References:

1. *Guzman Rojas R. Int Urogynecol J. 27(6):939-944. 2016*
2. *Cates J. Math Found Comput Anat Work. 170-181. 2008*

[G-05.5]

IMPACT OF PERFORMING MULTIPLE SMALL INCISIONS ON THE PELVIC FLOOR DURING VAGINAL DELIVERY

Dulce Oliveira[1], *Marco Parente*[2], *Teresa Mascarenhas*[3], *Renato Natal Jorge*[4]

1 *Inegi, Institute of Science and Innovation in Mechanical Ans Industrial Engineering, FEUP, Porto, Portugal;*
2 *Inegi, FEUP, Faculty of Engineering of University of Porto, Porto, Portugal*
3 *Fmup; Laeta; University of Porto, Porto, Portugal*
4 *Inegi, Faculty of Engineering of University of Porto, Porto, Portugal*

Current biomechanical models of childbirth provide some understanding of pelvic floor muscles function during vaginal delivery and allow to address the influence of common obstetric procedures, such as episiotomy [1]. Although recent Cochrane reviews do not recommend the routine use of episiotomy for vaginal delivery irrespective of fetal position, ensuring that the reduction in perineal / vaginal trauma is not justified by current evidence [2], further research is needed in particular situations. In the present work, a 3D biocomputational model previously developed to simulate vaginal deliveries was used to test whether multiple small perineal mediolateral incisions protected the pelvic floor muscles. It was concluded that multiple small incisions are not beneficial for the muscles compared to larger single incisions [1]. Small incisions (10-mm) at 30˚ and 45˚ during vaginal delivery induced 20.1% of tissue damage. Incisions of 20-mm at 30° reduced this damage to 11.1% and even at 60° the damage was 0.7% lower (19.4%). With regard to delivery without episiotomy, the best multi-cut analyzed case reduced the damage by only 9.8%. From the clinical point of view this approach would be quite debatable, from the mechanical point of view it has not proved to be a good option either. In addition, although the results of simple mediolateral episiotomies seem promising for protection of PFM trauma, the model does not include the perineal body, which is the primary structure involved. Therefore, further work that includes the perineal body is necessary.

Acknowledgments: Authors gratefully acknowledge the funding of project 030062 SIM4SafeBirth – A biomechanical approach to improve childbirth outcomes and the support from the Portuguese Foundation of Science under grant IF/00159/2014.

References:

[1] *Oliveira D, Parente M, Calvo B, Mascarenhas T, Natal Jorge R. (2016b) A biomechanical analysis on the impact of episiotomy during childbirth. Biomech Model Mechanobiol 15(6):1523-1534. doi: 10.1007/s10237-016-0781-6*
[2] *Jiang H, Qian X, Carroli G, Garner P. (2017) Selective versus routine use of episiotomy for vaginal birth. Cochrane Database of Systematic Reviews 2: CD000081. doi: 10.1002/14651858.CD000081.pub3.*

[G-06.1]

MECHANICAL BIOMARKERS BY TORSIONAL WAVES FOR GESTATIONAL DIAGNOSIS

Guillermo Rus[1], *Jorge Torres*[2], *Juan Melchor*[1], *Antonio Callejas*[2], *Inas Faris*[2], *Alberto García*[3], *Francisca Molina*[4]

1 *Ultrasonics Group, Biomechanics Group, Biosanitary Research Institute, MNat Excellence Scientific Unit, Ultrasonics Lab, Dpt. Structural Mechanics, University of Granada, Granada, Spain*
2 *Ultrasonics Group, Biomechanics Group, Biosanitary Research Institute, Ultrasonics Lab, Dpt. Structural Mechanics, University of Granada, Granada, Spain*
3 *Innitius, Granada, Spain*
4 *Ultrasonics Group, Biomechanics Group, Biosanitary Research Institute, Ultrasonics Lab, University Hospital San Cecilio, Granada, Spain*

The WHO estimates that in 2017 approximately 15 million babies will be born preterm, this is, a rate above 1 in 10 newborns [1]. Worldwide, complications of preterm births have supplanted pneumonia as the primary cause of child mortality [1; 2]. While progress is being made in identifying socioeconomic risk factors of preterm birth, the biology of cervical ripening that leads to birth is poorly understood. Currently, there is no clinical tool to quantitatively evaluate the cervical biomechanical state, which in words of Feltovich et al. [3] "…likely contributes to the reason [that] the singleton spontaneous preterm birth rate has not changed appreciably in more than 100 years." Ultrasonic characterization and understanding of soft tissue have been developed as a clinical diagnostic tool over the last two decades [4] and evolved through different elastography technologies.

Aims: Towards this problem, we work on enabling new sensor technologies linked to soft tissue biomechanics, to endow a new class of biomarkers that quantify the mechanical functionality of the cervix, and indeed any soft tissue. Beyond labor disorders, abnormalities in the structural architecture of soft tissues are intimately linked to a broad range of pathologies including tumors, atherosclerosis, liver fibrosis or osteoarticular syndromes.

Methods: Existing ultrasonic techniques are restricted to map first order tissue stiffness. In contrast, our recent advances covering (a) torsional waves (shear elastic waves that propagate in quasifluids radially and in depth in a curled geometry), (b) sensors (based on a novel arrangement of concentric sandwiches of piezo- and electro-mechanical elements [5]), (c) propagation models and (d) patient testing, are allowing to quantify the mechanical functionality through relevant parameters beyond linear: dispersive and nonlinear.

Results:

a) To understand how structural architecture of soft tissue is intimately linked and controls a broad range of pathologies, which underpins the foundation of a new diagnostic technology.
b) To develop new sensor technologies capable of effectively sensing tissue elasticity and yield simple and robust diagnostic tests and instruments.

Acknowledgments: This research was supported by the Ministry of Education DPI2017-85359-R, DPI2014-51870-R, DPI2010-17065, and UNGR15-CE-3664, Ministry of Health DTS15/00093, PI16/00339, PI-0107-2017, PIN-0030-2017 projects"

References:

1. *WHO, March of Dimes. 2012. Geneva.*
2. *WHO. Fact sheet - preterm birth. 2016.*
3. *Feltovich H. et al. 2012. Am J Obst & Gyn 207 345-54.*
4. *Barr R., et al. 2012. Ultrasound Quarterly 28 13-20.*
5. *Melchor J and Rus G. Ultrasonics, 54(2014): 1950-1962*

[G-06.2]

BLADDER PHYSIOLOGY AND BIOMECHANICS; FROM BED-SIDE TO BENCH-TOP AND BACK

Michael Chancellor[1]

1 Beaumont Health System, Royal Oak, USA

Michael B Chancellor, M.D., Professor, Director of Aikens Research Center; Department of Urology, Beaumont Health System, Royal Oak, United States and Oakland University William Beaumont School of Medicine (OUWB)

I am a urologist whose clinical specialty is the diagnosis and treatment of patients with urinary tract symptoms, such as incontinence, urinary frequency, urinary obstruction and inability to urinate. During my career I developed a strong interest in translational research and transitioned from a busy urologic surgeon to a physician scientist. I have been fortunate to have been funded by the NIH since mid-1990 and formed collaborations with top biomechanical engineers. Most importantly, I headed a program project (PO1 NICHD HD39768) that studied multiple aspects of bladder dysfunction after spinal cord injury while a faculty member at the University of Pittsburgh, Pittsburgh, United States. Michael Sacks, PhD, faculty in the School of Engineering, headed up one of the project looking at changes in biomechanical function of neurogenic bladder after rat model SCI (1). In addition, we recruited Jiro Nagatomi, PhD to join the study of extracellular matrix changes after SCI (2). Although we all have since moved from Pittsburgh, my interest and respect for bladder biomechanics is very much alive. Drs. Sacks and Nagatomi are now Professors and head world class labs at the University of Texas Austin and Clemson University, respectively. I was recruited to Beaumont Health System, Royal Oak, United States in the Detroit area to help build up transitional research at Beaumont Research Institute in collaboration with the new medical school and recently I was lucky enough to be introduced to Sara Roccabinca, PhD, at Michigan State University, East Lansing, United States. Dr. Roccabinca's lab focus is a perfect fit to study bladder biomechanics and we have started a collaboration that I hope and believe will lead to great results and grant partnership.

The urinary bladder is a pretty cool organ to research. The bladder is the most compliant organ in our body. After micturition, the empty bladder is often no larger than a kiwi. Yet over a few hours, it can fill with urine and reach a capacity of 500 mL, with no increase in filling pressure or involuntary detrusor contractions. During micturition, maximum detrusor pressure can reach approximately 60 cm H20 in a normal adult and sustained for about a minute until the bladder is fully emptied. I will discuss the clinical diagnostic technique of urodynamic testing that assess flow, pressure, power and work of the normal and diseased bladder. A normal adult voids up to about 8 times/24 hrs.

The urinary bladder is also the most impermeable organ in our body with an incredible change in urothelial surface area from 0 to 500 mL that remains water tight to the toxic substances excreted by the kidney. The bladder has tremendous plasticity and can undergo 2-3x increase in weight and bladder wall thickness such as after SCI and bladder outlet obstruction. I will share examples of these.

Lastly, we are working with Dr. Roccabinca on looking at fibrosis and biomechanical changes after pelvic radiation damage to bladder (radiation cystitis) in a mice model. I believe bladder biomechanics is fascinating and there is much to learn. I look forward to the meeting and forum to discuss.

References:

1. *Toosi, K.K., Nagatomi, J., Chancellor, M.B., Sacks, M.S.: The effects of long-term spinal cord injury on mechanical properties of the rat urinary bladder. Annals Biomedical Engineering. 36:1470-80, 2008.*
2. *Nagatomi, J., de Miguel, F., Torimoto, K., Chancellor, M.B., Getzenberg, R.H., Sacks, M.S.: Early molecular-level changes in rat bladder wall tissue following spinal cord injury. Biochemcial & Biophysical Research Communications. 334:1159-1164, 2005.*

[G-06.3]

MODELING THE MULTI-STAGE REMODELING DURING BLADDER OUTLET OBSTRUCTION

Fangzhou Cheng[1], *Paul Watton*[2], *Lori Birder*[3], *Naoki Yoshimura*[3], *Anne Robertson*[4]

1 *Department of Mechanical Engineering and Material Science, University of Pittsburgh, Pittsburgh, USA*
2 *University of Sheffield, Department of Computer Science, Sheffield, UK; University of Sheffield, Insigneo Institute for in Silico Modeling, Sheffield, UK*
3 *University of Pittsburgh, Department of Pharmacology and Chemical Biology, Pittsburgh, USA*
4 *University of Pittsburgh, Department of Mechanical Engineering and Material Science, Pittsburgh, USA*

Lower urinary tract symptoms (LUTS) such as increased urination urgency, frequency, incontinence, and residual volume can significantly lower the quality of life. Benign prostatic hyperplasia and consequent bladder outlet obstruction (BOO) are believed to be major contributing factors to male LUTS and affect 64% of men [1]. The outlet obstruction leads to elevated pressure in the bladder that induces progressive tissue remodeling. BOO involves an initial compensation phase with increased contractility and compliance, and a later decompensation phase with a reduction in bladder contractility and compliance, as well as bladder wall fibrosis [2]. Although morphological changes such as smooth muscle hypertrophy and collagen fibrosis have been commonly observed in obstructed bladders, the effect of these changes on the bladder mechanical function is not understood. This integrative study investigates the underlying mechanisms of multi-stage BOO remodeling by applying a novel mathematical model of bladder microstructure remodeling to describe experimental observations.

Eight young rat bladders (3-month-old, Sprague Dawley) were operated following the surgical procedures described in [3] and harvested after one month of the operation with four sham-operated and four BOO bladders. Biaxial mechanical testing coupled with multiphoton microscopy were performed on 6 1mm square bladder samples to assess bladder mechanical properties while observing the microstructure transformation [4]. This data was interpreted in the context of a growth and remodeling analysis, in which collagen recruitment distribution evolved over time to maintain a homeostatic stretch [5] in response to BOO.

All BOO bladders developed a more compliant, distensible wall and this was successfully predicted by our model. However, half of the BOO bladders showed a delayed collagen recruitment process in the muscular layer. This change was conjectured to be due to a pathological evolution of collagen homeostatic stretch which could initiate the BOO bladder transition from a compensated state to the final decompensation stage. We examined this conjecture in our model by prescribing different evolution patterns of collagen homeostatic stretch in the detrusor layer and found the delayed recruitment is associated with change of bladder compliance through long term remodeling. In the future, we anticipate these findings can be used to tailor LUTS treatment to the different stages of BOO remodeling.

Acknowledgments: This work was supported by NIH grant R01AG056944-01A1.

References:

[1]. Simel, D et al., JAMA & Archives Journals. McGraw-Hill, 2008
[2]. Zderic, S. A et al., World journal of urology, 16(5), 350-358, 1998
[3]. Zvara, P et al., The Journal of Urology, 168(6), 2682-2688, 2002
[4]. Cheng, F et al., Biomechanics and modeling in mechanobiology, 17(2), 403-417, 2018
[5]. Aparicio, P et al., Journal of Biomechanics, 49(12), 2321-2330, 2016

[G-06.4]

EXTRACELLULAR MATRIX REMODELING OF THE DIABETIC URINARY BLADDER

Marissa R. Grobbel[1], Matthew T. Lewis [2], Anne Tonson [2], Robert W. Wiseman [2], ***Sara Roccabianca***[1]

1 *Michigan State University, Department of Mechanical Engineering, East Lansing, USA;*
2 *Michigan State University, Department of Physiology, East Lansing, USA*

Diabetic cystopathy is a form of neurogenic bladder dysfunction that occurs in diabetic patients experiencing peripheral neuropathy. Loss of connection between the urinary bladder and the nervous system dulls the sensation of fullness in the bladder. This causes delays in voiding, leading to chronic over-filling of the bladder. This type of volume overload has been shown to cause changes in extracellular matrix (ECM) content, wall thickness, tissue compliance, and inflammation in the bladder [1, 2, 3]. In this study, we have measured experimentally the mechanical behavior of the ECM of urinary bladders from a lean and an obese rat model of type II diabetes. We then employed a Fung-type exponential isotropic strain energy function to model the experimental data, and quantify material parameters for each model of type II diabetes.

Uniaxial ring tests were conducted using transversely sliced, decellularized rings of urinary bladder tissue from: Goto-Kakizaki rats (lean diabetic, GK-D, n = 5), Zucker diabetic fatty rats (obese diabetic, ZDF-D, n = 4), Wistar as a control for GK-D animals (GK-C, n = 6), and lean ZDF littermate as a control for ZDF-D animals (ZDF-C, n = 4). Additionally, histological analyses were performed to asses changes in the ECM due to remodeling—elastin and collagen fibers—and mast cell activation, which is indicative of immune system activation and inflammation.

Our experimental results showed that the ECM of bladders from both GK-D and ZDF-D diabetic animals presented an increase in compliance when compared to their respective controls. Furthermore, we observed that the ECM of bladders from ZDF animals, both the ZDF-C and ZDF-D, show a higher compliance when compared to GK animals, GK-C and GK-D, respectively. The model proved useful in identifying where differences between the groups are present in regards to the mechanical parameters: significant differences were identified across all test groups except for ZDF-C v. GK-D and ZDF-C v. GK-C.

These results strongly suggest that there is remodeling of the ECM within the bladder wall in both the models studied. The response however seems to be more prominent in the bladder of obese animals. We suggest that inflammation, generally associated with obesity, could play a key role in this difference.

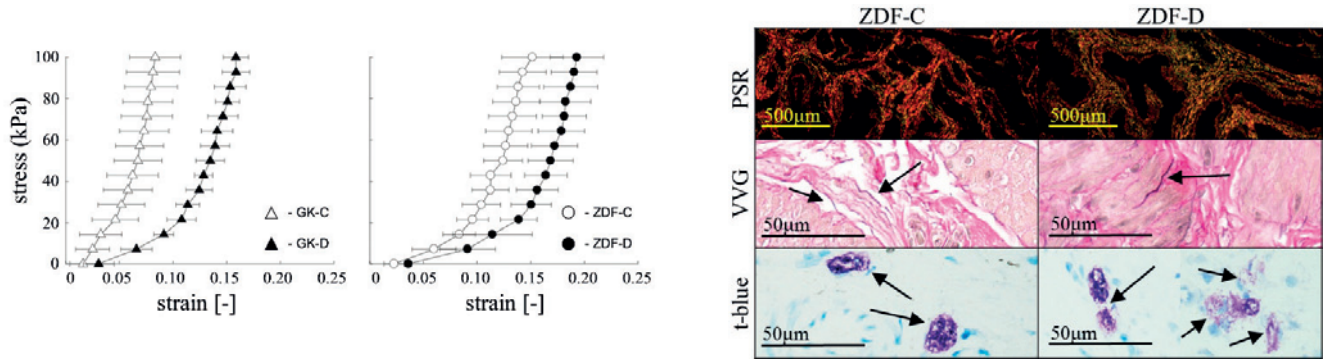

Figure Caption: Left: Stress-strain data from uniaxial ring test. Each point represents average (error bars showing standard deviation) strain from all samples in each group. Data shown is from final loading curve. Histological stains from ZDF-C and ZDF-D groups. Arrows show elastin fibers and mast cells.

References:

[1] G. Liu & F. Daneshgari. Am J Physiol Regul Integr Comp Physiol (2006).
[2] C.C. Wang et. al. Urology (2009).
[3] M.Y. Donath & S.E. Shoelson SE. Nat. Rev. Immunol. (2011).

[G-06.5]

VISCOELASTIC PROPERTIES OF FRESH HUMAN BLADDER TISSUE

Duncan Morhardt[1], *Andrea Poli*[2], *John M. Park*[3], *Ellen M. Arruda*[2]

1 *Department of Urology, Boston Children's Hospital, Boston, USA*
2 *Department of Mechanical Engineering, University of Michigan, Ann Arbor, USA*
3 *Department of Urology, Michigan Medicine, Ann Arbor, USA*

Viscoelastic materials exhibit the properties of a viscous fluid, exemplified as the energy loss of a dashpot, and the restoring effects of elastic solids, exemplified by energy return of a spring. Human bladder deforms dramatically several times a day and its viscoelastic properties, while recognized, are poorly understood. Understanding the mechanical properties of this tissue is critical for understanding both physiology and engineering appropriate tissue replacements. Dynamic mechanical analysis applies a sinusoidal strain to a specimen while stress is measured and allows for characterization of both storage (elastic) and loss (viscous) moduli. Currently, the mechanical properties of human bladder have not been well-characterized both because of limited access to full specimens and scarcity of non-diseased tissue. Furthermore, the contribution of individual tissue components to viscoelastic properties, like elastin and muscle, are unknown. We investigated the viscoelastic properties of fresh, non-diseased human tissue.

Two bladders were procured at death, stored at 25-37°C in phosphate buffered saline (PBS), and tested within 24 hours. Tissue was dissected with a 6mm biopsy punch from the posterior dome of the bladder and transferred to a 37°C PBS bath, pure, dosed with oxybutynin (150um), or dosed with elastase (50U). A dynamic mechanical analyzer was used to determine the storage and loss moduli at 0.12 Hz. A uniaxial compression test was also used to examine creep and recovery by applying force at several levels (900 to 2700 pascal) and determining the resulting strain. This stress was applied orthogonal to the urothelium as it was the most stable and consistent position.

Storage moduli averaged 1.62, 2.30, and 1.729 kPa in untreated, oxybutynin, and elastase treated specimens, respectively. Loss moduli were 0.159, 0.303, and 0.401 kPa in untreated, oxybutynin, and elastase treated specimens, respectively. Creep-recovery testing revealed bladder tissue under all conditions exhibited viscoelastic behavior.

Human bladder tissue has viscoelastic properties that are altered by removing elastic and muscular components. Deactivating muscle with oxybutynin increases the elasticity of specimens. Removing elastin with elastase increases viscous properties. Forces required for tissue relative deformation are generally less than previously reported. These parameters will be critical for directing appropriate mechanical properties in engineered tissues and elucidating mechanical impact of disease processes.

[G-06.6]

TISSUE ENGINEERED ENDOMETRIAL BARRIER EXPOSED TO PERISTALTIC FLOW SHEAR STRESSES

David Elad[1], *Tatyana Kuperman*[2], *Uri Zaretsky*[2], *Oren Zalzhendler*[2], *Ariel Jaffa*[3], *Dan Grisaru*[4]

1 *Tel Aviv University, Department of Biomedical Engineering; Faculty of Engineering, Tel Aviv, Israel*
2 *Department of Biomedical Engineering, Israel*
3 *Department of Obstetrics and Gynecology; Lis Maternity Hospital; Tel Aviv Medical Center, Tel Aviv, Israel*
4 *Gynecological Oncology Unit; Lis Matternity Hospital; Tel Aviv Medical Center, Tel Aviv, Israel*

Background: Cyclic myometrial contractions of the non-pregnant uterus induce intra-uterine peristaltic flows, which have important roles in transport of sperms and embryos during early stages of reproduction. Hyperperistalsis in young females may lead to migration of endometrial cells and development of adenomyosis or endometriosis. We developed a tissue engineered endometrial barrier to study the biological response to peristaltic wall shear stresses (PWSS).

Methods: We co-cultured endometrial epithelial cells (EEC) and myometrial smooth muscle cells (MSMC) in custom-designed wells that can be disassembled for mechanobiology experiments with tissue-engineered models. First, MSMC were cultured on a collagen coated PTFE membrane. Then, EEC were cultured on the MSMC after coating with Matrigel to simulate the stromal tissue. In order to induce PWSS on the in vitro model we developed a new experimental setup with a fluid-filled rectangular flow chamber that can hold 3 well bottoms with the endometrial barrier model. The elastic membrane of the upper wall of the flow chamber underwent local deformations by bumps of a custom-designed 3D printed semi-elastic belt that was driven by a DC motor at a linear velocity of 12 mm/s. The resulted motility of the chamber upper wall induced a peristaltic flow field above the endometrial barrier model. We also conducted a finite element analysis with the ADINA software in order to compute the time dependent PWSS exerted on top of the in vitro endometrial model at the bottom of the flow chamber. Then, we exposed the in vitro biological model to peristaltic flows for 60 and 120 minutes. The co-cultured models were stained with specific and non-specific antibodies for immunofluorescence studies of alternations in the cells cytoskeleton after exposure to PWSS.

Results: The confocal images verified that the 3D co-culture model mimics the structural architecture of the in vivo intrauterine wall. The computational analysis revealed that the peristaltic fluid flow within the flow chamber exerted on the endometrial barrier periodic shear stresses with peaks up to 0.03 Pa. Quantification of the amount of actin fibers in the z-stack of the confocal images revealed a relative increase after exposure to PWSS.

Conclusion: The present study provides for the first time a new tissue engineered model that closely mimics the structural architecture of the uterine endometrial barrier. Exposure of this barrier to PWSS induced polymerization of actin fibers within the layer of MSMC.

Acknowledgments: This work was supported by grant # 2505/16 from the Israel Science Foundation (ISF-NSFC Joint Scientific Research Program).

[G-07.1]
ODONTOID FRACTURE: FROM INJURY TO INTUBATION

Christian Puttlitz[1], *Bradley Hindman*[2], *Brandon Santoni*[3], *Michael Todd*[4], *Vincent Traynelis*[5], *Benjamin Gadomski*[1]

1 *Colorado State University, Fort Collins, USA*
2 *University of Iowa, Iowa City, USA*
3 *Smith and Nephew*
4 *University of Minnesota, Minneapolis, USA*
5 *Rush University, Chicago, USA*

Although cervical spine motion during direct laryngoscopy is well-characterized for the stable spine, the magnitude and location of applied force on spinal cord compression in the presence of injury has not been well understood. In addition, certain patient characteristics are associated with difficult intubation in which laryngoscope forces are applied in an atypical manner. Thus, our group has investigated the role of intubation force location, magnitude, and direction on resultant cervical spinal cord strains in a stable cervical spine and in the presence of a Type II odontoid fracture using finite element (FE) methods. The loading and boundary conditions for these studies were derived from patient and whole cadaver studies (Figure 1). The intact spine data indicate that intubation force magnitude had the greatest effect on spinal cord strain predictions at the C2, C3, and C4 vertebral levels. The angle of applied intubation force had the greatest effect at the C1 level. Maximum changes due to alterations in force magnitude were 71% and 63% for minimum and maximum principal strain predictions, respectively, at the C4 location. Changes due to alterations in force angle were 84% and 80% for minimum and maximum principal strain predictions, respectively, at the C1 location. When an odontoid fracture is imposed on the model, C1-C2 subluxation increased markedly (220%; from -1.0 to -3.2 mm) with the caudal to cranial shift of force. In addition, a Type II fracture markedly increased the minimum principal strain (65%; from 17.0% to 28.1%) with the caudal to cranial shift of force, exceeding the injury threshold (-20%). The peak compressive strain within the spinal cord shifted cranially with the caudal to cranial shift of force (from C3 to C2). To conclude, these simulations show that the intact cervical spine is relatively insensitive to changes in the location of laryngoscope force in terms of both C1-C2 motion and spinal cord strains. In contrast, with an injured spine, intervertebral rotation and cord strain are highly dependent on the location of laryngoscope force. With a Type II odontoid fracture, potentially injurious cord stain occurs as the result of subluxation (cord compression) rather than extension (stretch).

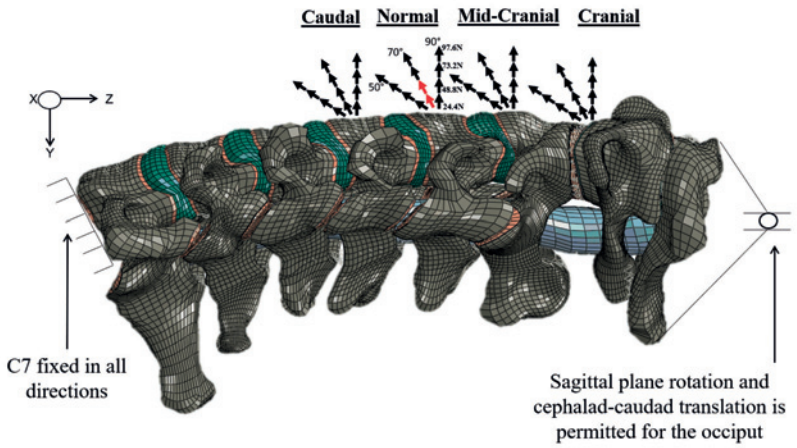

Figure 1. Applied laryngoscope force was applied to the typical in vivo position (Normal, C3), a Caudal position on C4, a Mid-Cranial position on C2, and a Cranial position on C1 of the cervical spinal column. The magnitude and angle of the applied laryngoscope force was varied. A total of 48 simulations were performed.

Acknowledgments: This study was supported by the National Institutes of Health (grant no. R01EB012048 PIs:. Puttlitz, Hindman, and Santoni).

[G-07.2]

ON THE CHALLENGES IN PREDICTION OF HIP FRACTURE RISK CAUSED BY FALL AMONG ELDERLY PEOPLE

Yunhua Luo[1]

1 *University of Manitoba, Winnipeg, Canada*

Fall-induced hip fracture is a major health risk among elderly people worldwide. Hip fracture may cause long-term disability and even lead to fatality. Accurate assessment of fracture risk is a prerequisite step for clinicians to take proper measurements to prevent fractures. There are basically two categories of tools available for clinicians to assess fracture risk, one is based on statistical models; the other is biomechanical modeling. Statistical tools mainly rely on associations between fracture outcome and clinical risk factors, they have shown limited accuracy in both retrospective and prospective clinical studies. Therefore, we have focused on development of biomechanical models, aiming at improving prediction of fall-induced impact force and subject-specific femur strength, which are the two biomechanical determinants of hip fracture risk. However, both of them are challenging to predict. Fall-induced impact force is affected by large number and complicated variables, including instinct and reflex action, type of fall (forward, backward or sideways), body configuration in fall, body height, weight, body mass index, floor or ground hardness, etc. For a clinical assessment of fracture risk, femur strength must be determined in vivo and non-invasively. Finite element modeling based on a hip medical image, e.g. CT (computed tomography) and DXA (dual energy X-ray absorptiometry), is a promising approach to determine subject-specific femur strength. But the accuracy of finite element models is constrained by the limited information captured in medical images, which is far from adequate to fully depict the complicated mechanical properties of bones. Another major challenge is the validation of biomechanical models. Clinical fracture cases are commonly used in validation of various tools for fracture risk assessment. But information required for validating a biomechanical model is often missing in clinical records, for example, the impact force occurred in a clinical fracture case is often unknown.

In the presentation, I will report our recent progresses in meeting the challenges [1-4] and discuss the remaining ones.

References:

[1] *Y. Luo. Image-based Multilevel Biomechanical Modeling for Fall-Induced Hip Fracture. Springer, 2017.*
[2] *Y. Luo, S. Ahmed, et al. Automation of a DXA-based Finite Element Tool for Clinical Assessment of Hip Fracture Risk. Computer Methods and Programs in Biomedicine, 155:75 – 83, 2018.*
[3] *M. Nasiri Sarvi and Y. Luo. Study of sex differences in the association between hip fracture risk and body parameters by DXA-based biomechanical modeling. Bone, 90:90 – 98, 2016.*
[4] *S. Yang, Y. Luo, et al. Comparison of femoral strength and fracture risk index derived from DXA-based finite element analysis for stratifying hip fracture risk: a cross-sectional study. Bone, 110:386 – 391, 2018.*

[G-07.3]

THE ROLE OF CORPUS CALLOSUM MYELINATION IN THE BIOMECHANICS OF TBI

*Javid Abderezaei[1], Gloria Fabris[1], Zachary Lopez[1], Cassandra Gologorsky[2], Johannes Weickenmeier[1], **Mehmet Kurt**[1]*

1 *Stevens Institute of Technology, Hoboken, USA*
2 *Cornell University, Ithaca, USA*

Mild traumatic brain injury (mTBI) is a severe health problem in the U.S, causing approximately 50,000 deaths a year [1]. Out of several structures of the brain that have been found to be vulnerable in mTBI, corpus callosum (CC), has been of particular interest. Hernandez et al. introduced peak principal strain in CC as one of the predictors of mTBI [2]. Such studies hint at the importance of analyzing mechanics of the brain in injury metrics. Weickenmeier et al. showed how brain stiffness is correlated with the myelin content [3]. Considering the effect of myelin in mechanics of the brain, here we demyelinated the CC of mice to investigate its effect on mTBI. We then utilized a finite element (FE) model to analyze the effect of mechanical stiffness variance on strain patterns.

8 young adult C57BL6/J male mice weighing between 25 and 30 g were used. All animal care, surgical and post-surgical procedures were IACUC-approved. The animals were anesthetized with 3% sevoflurane. 1 μL of 1% lysolecithin and 1 μL of PBS was injected into the CC of experimental (n=4) and control group (n=4), respectively. 3 days post injection, a rod with a diameter of 3 mm and mass of 317 g raised to a height of 2.5 cm, was dropped on the head of anesthetized mice (Fig. 1A; [4]). Brain sections were then stained (GFAP: Z0334, Dako) to visualize the patterns of inflammation. Following that, a murine FE model replicating the conditions of the experiment was used to simulate the strain responses for various $\mathbf{k_{WM}/k_{GM}}$ (white matter/grey matter stiffness).

We observed a 27.1% increased astrocyte activation in the body region of CC of subjects that experienced both the PBS injection and weight drop (WD; p=0.01; Fig. 1B). We did not, however, observe substantial increase in the regions above CC and near grey matter (GM) of the lysolecithin injected group (12.4% increase, p=0.72). Furthermore, we observed that by varying $\mathbf{k_{WM}/k_{GM}}$ from 3.0 to 0.3 in the FE model, there is a significant change in the strain response ($\boldsymbol{\varepsilon}$), from $\boldsymbol{\varepsilon = 1.55 \times 10^{-1}}$ to $\boldsymbol{1.93 \times 10^{-1}}$, respectively (Fig. 1C). Considering the significant microstructural changes of the pediatric brain, including myelination [5], studying the role of myelin and its possible shielding effect in TBI could be crucial in understanding the injury mechanisms.

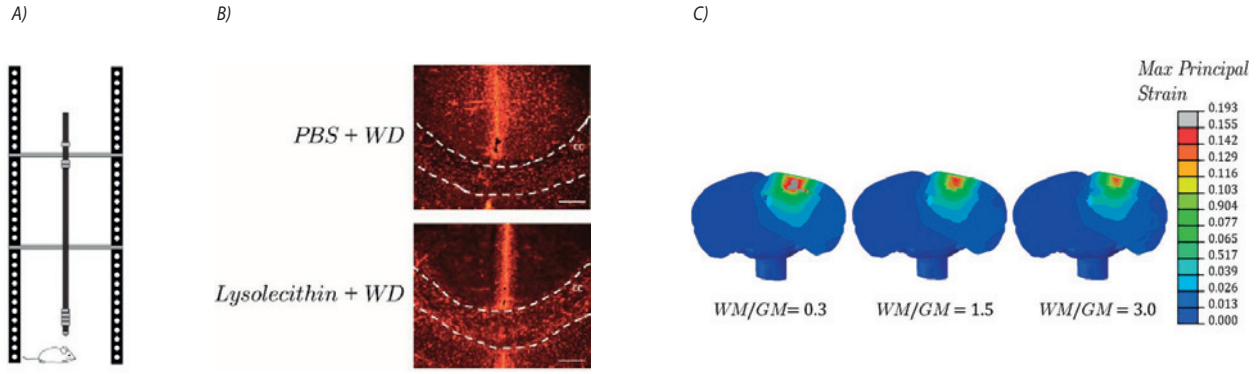

Figure 1. A) Schematics of the WD device. B) Immunofluorescent staining of the area surrounding the CC (Red: reactive astrocytes (GFAP). Scale bar: 200 µm). C) FE simulation of the WD for various $\mathbf{k_{WM}/k_{GM}}$.

References:

[1] Corrigan, D et al., J Head Trauma Rehab, (2010).
[2] Hernandez, F et al., Ann Biomed Eng, (2015).
[3] Weickenmeier, et al., JMBBM, (2017),
[4] Flierl, M et al., Nat. Protoc., (2009).
[5] Kim, G et al., Neuroradiology, (2017).

[G-07.4]

CONSIDERATION OF STRUCTURAL BEHAVIOR OF BONES IN MUSCULOSKELETAL SIMULATION MODELS

Robert Eberle[1], *Dieter Heinrich*[1]

1 *University of Innsbruck, Innsbruck, Austria*

Bone and ligament injuries are one of the most common serious injuries in sports. To prevent such injuries, it is necessary to understand the underlying injury mechanism. In the last decades musculoskeletal simulation models have become popular to investigate injury situations on a computer. Most of the existing musculoskeletal simulation models consist of a rigid multi-body model and muscles. The muscles actuate the movement of the rigid multi-body model [1]. If bones are incorporated as rigid segments and not deformable segments, some mechanical behavior of bones are not considered. Further, bone injuries or effects on the bone structure during human movements cannot be analyzed.

In this study a simulation model of a two-segment arm (for humerus and ulna) has been developed in Matlab that does take into account the structural behavior of bones. The bones were modelled as Euler-Bernoulli beams and were incorporated into the simulation model using the floating frame of reference formulation [2]. The simulation model resulted in a system of differential algebraic equations (DAE):

$$M\ddot{q} + D\dot{q} + Kq + C_q^T\lambda = Q_v + Q_e$$
$$C(q,t) = 0$$

where **M** denotes the mass matrix, **q** the generalized coordinates (including elastic coordinates), **D** the damping matrix, **K** the stiffness matrix, $\mathbf{C^T_q}$ the transposed Jacobian w.r.t. **q** of the constraints **C(Q, T)**, **λ**, the Lagrange multipliers, $\mathbf{Q_v}$ the quadratic velocity vector and $\mathbf{Q_e}$ the vector of external generalized force.

The developed simulation model was used to simulate a fracture of the ulna (i.e., exceeding an assumed ultimate bending stress of 100 MPa). In particular, a drop in which a person landed from a height of 1.7 m on a solid ground with the ulna was simulated (see Figure). The movement of the person's arm during the fall was actuated by joint moments acting on the shoulder and elbow. The impact at the ground was considered in the vector of external generalized force $\mathbf{Q_e}$.

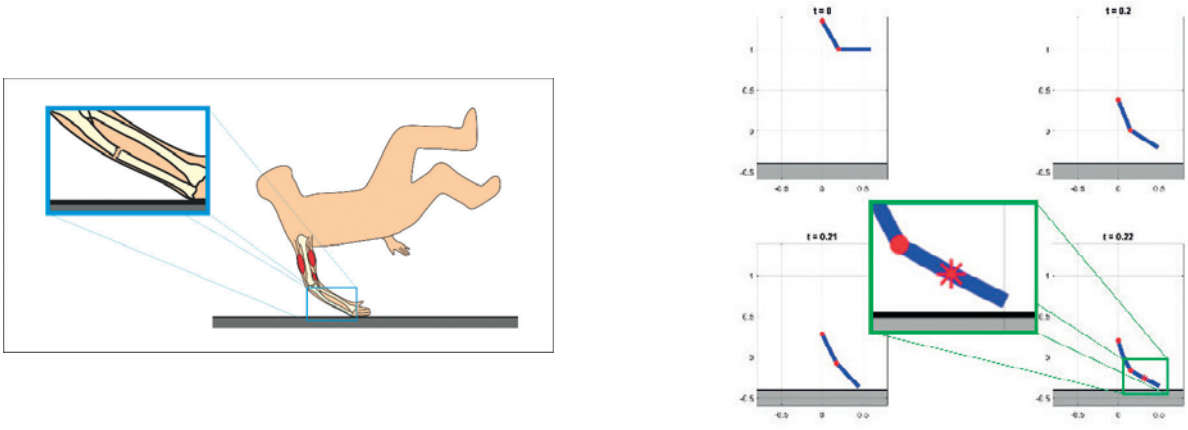

Figure: Person lands on a solid ground with the ulna: schematics (left) and simulation (right).

The right side of the figure shows the stick-figures (blue lines) of the humerus and ulna in the simulated drop at times t = 0, 0.2, 0.21 and 0.22 s. At time t = 0.22 s the red star (*) depicts the position, where the ulna broke with a bending stress of 111 MPa.

The developed computational approach allows for investigation of injuries with a musculoskeletal simulation model considering the structural behaviour of bones.

References:

[1] Van den Bogert AJ et al. (2011). Procedia IUTAM, 2: 297-316.
[2] Shabana AA. (2013). Dynamics of multibody systems; Cambridge University press

[G-07.5]

DEVELOPMENT AND VALIDATION OF A HIGH-FIDELITY HUMAN THORAX MODEL FOR IMPACT SCENARIOS

Wei Zeng[1], *Sayak Mukherjee*[1], *Adrian Caudillo*[1], *J. Sebastian Giudice*[1], *Matthew B. Panzer*[1]

1 *Center for Applied Biomechanics, University of Virginia, Charlottesville, USA*

Thoracic injury resulting from different impact collisions ranks the second leading cause of fatalities and severe injuries. The development and applications of finite element (FE) models of human body have become an indispensable tool in injury biomechanics and automotive safety. High-fidelity human body FE models can accurately describe the human anatomy, biomechanics and variability for injury risk predictions, and develop occupant crash safety measures. This work introduces the development and validation of a human thorax model as part of the development of mid-size adult male occupant (M50-O) FE model for Global Human Body Models Consortium (GHBMC) project (Phase III). Significant improvement has been made in the previous stage of M50-O thorax model development. However, there are many issues reported with regard to thoracic cavity and thoracic musculoskeletal system, which lead to a lack of biofidelity for upper torso simulation. For example, the large voids were created inside and outside of the ribcage. In this work, we incorporated a series of novel sliding interfaces between related organs to restrain unrealistic separations. This prevented gap opening and voids forming for multiple regions of the thorax under various impact scenarios. Other prominent aspects to improve model biofidelity include: 1) the aorta was enhanced through mesh improvement and material updates to better represent aortic laceration injuries; 2) the thoracic musculoskeletal system was enhanced by adding fracture features to the clavicles, sternum and costal cartilage; 3) for thoracic intervertebral joint, better material modeling approaches were utilized to characterize the properties of intervertebral discs. The model was first systematically tested, validated and improved at the component or organ level against experimental data. At the body regional level and full torso level, the biomechanical responses were evaluated and improved under various thoracic validation loading tests. These test conditions contained point loading of the eviscerated ribcage, vertical loading trial, frontal pendulum impacts, shoulder pendulum impact and table-top belt loading tests, etc. The modeling responses were found to be in good agreement with the experimental data using both qualitatively and quantitative assessments. This model will serve as a valuable tool for thorax injury prediction, mitigation and prevention. Moreover, this study provides a framework of modeling and validation for enhancing biofidelity of future computational human body models for injury biomechanics and crash analysis.

Acknowledgments: Data and results demonstrated in this abstract were prepared under the support of the Global Human Body Models Consortium, LLC (GHBMC) by the Thorax and Upper Extremity Center of Expertise and do not necessarily reflect the views of the GHBMC.

[G-07.6]

UNCERTAINTY CHARACTERIZATION OF THE MULTI-BODY RECONSTRUCTION OF REAL-LIFE BICYCLE ACCIDENTS

Lise Gheysen[1], *Michel Woering*[2], *Markos Kapeliotis*[2], *Jos Vander Sloten*[3]

1 *Ghent University, Ghent, Belgium, Ibitech-Biommeda*
2 *Ku Leuven, Biomechanics Section, Leuven, Belgium*
3 *KU Leuven, Mechanical Engineering, Biomechanics Section, Leuven, Belgium*

To predict head injuries caused by bicycle accidents, many criteria have been proposed1. These criteria, often developed with finite element head models, require accurate information of the head impact kinematics. Using real-life accident kinematics, obtainable with multi-body (MB) software, allows gaining insight in severe head injuries in realistic situations2. However, the descriptive accident and injury information is subjective and the pedestrian and bicycle MB models have many variables, which results in uncertainty on the MB simulation outcome2,3. No uncertainty quantification of real-life non-vehicle bicycle accident reconstruction, was found in literature. Therefore, this study aims to characterize the influence of the uncertainty on these initial situations.

For five real-life bicycle accidents, collected at UZ Leuven, an initial simulation based on validated pedestrian and bicycle models was constructed in MADYMO, using trial and error2,3. A simulated impact place corresponding to the description was required. Two types of parametric studies, with six input variables (table 1), were performed. The peak resulting and anterior-posterior angular acceleration ($\alpha_{Peak,Res}$, $\alpha_{Peak,AP}$) were taken as output variables, as they are linked to the injury mechanisms4,5. The influence per input variable was investigated for three cases by considering univariate linear regression and the maximal change in $\alpha_{Peak,Res}$ and $\alpha_{Peak,AP}$ per variable and case, w.r.t. the initial simulation. Multivariate linear regression, using an orthogonal array, was applied to the other cases. For the simulations with the correct impact place, the total uncertainty on $\alpha_{Peak,Res}$ and $\alpha_{Peak,AP}$ was quantified.

Parameter	Range	Step
Position pedal hub	-20° to 20° w.r.t. initial position	10°
Position upper body	Ca. 25° to 60° w.r.t. vertical line	8.64°
Speed	60% to 140% of initial speed	20%
Saddle height	-6 cm to 6 cm w.r.t. initial height	3 cm
Feet-pedals	60% to 140% of initial strain	20%
Hands-handlebars	60% to 140% of initial strain	20%

Table 1: Input variables used in the parametric studies.

Although the maximal change in input variable differed strongly between cases, minimally one case per variable had a maximal change in αPeak,Res and αPeak,AP above 70%. The number of significant univariate relations and significant terms in multivariate relations was, although limited, larger for αPeak,Res. The variables leading to the significant relations and terms were case dependent. For the simulations with the reported impact place, the smallest maximal change was 30%.

In this preliminary study, αPeak,Res was the most appropriate output variable to investigate the effect of uncertainty on the input variables using uni- and multivariate linear regression. Although all input variables were relevant, no general trends in the influence of the uncertainty on the initial situation and the relative importance of the input variables could be established, with the studied cases. The simulations with the reported impact place indicated a minimal total uncertainty of 30%. Including more cases is suggested to gain further insight in the overall influence of the input variables and the expected total uncertainty on the outcome.

References:

1 *Marjoux, D. et al., Accid Anal Prev, 40:1135-1148, 2008.*
2 *Verschueren, P., K.U.Leuven, 2009.*
3 *MADYMO, Human body manuals, 2017.*
4 *Kleiven, S., Stapp Car Crash J, 51:81-114, 2007.*
5 *Kuo, C. et al., Biomech Model Mechanobiol, 17:235-247, 2018.*

[G-08.1]

NONLINEAR FEA FOR DESIGN AND QUALITY CONTROL OF 3D PRINTED PATIENT SPECIFIC MEDICAL DEVICES

Scott Hollister[1], *Sarah Jo Crotts*[1], *Harsha Ramaraju*[1]

1 *Georgia Institute of Technology, Atlanta, USA*

3D printed patient specific medical devices present significant challenges for assess safety and efficacy. Among these challenges are assessment of device mechanical performance when device geometry will change for each patient. Finite Element Analysis (FEA) provides a powerful tool for assessing patient specific device performance if such analyses can be verified with experimental test of 3D printed devices. We developed a design control process1 for assessing 3D printed bioresorbable polycaprolactone (PCL) airway splints that have been used to been implanted in pediatric patients2 to treat life threatening tracheobronchomalacia. A critical part of the design control design inputs require the splints to have specific compression parallel and perpendicular deformation force relationships to protect the collapsing airway in addition to allowing airway growth. Since splint diameter and length vary for each patient, each splint design must be verified to ensure that it meets the force displacement design requirement prior to 3D printing. This design performance is assessed by modeling the parallel and perpendicular behavior as a nonlinear contact problem between the PCL splint and rigid platens of the mechanical testing system. We model the splint by directly meshing the STL design file with 10-node tetrahedral elements in FEBio PreView and modeling the testing system platens as rigid bodies. We modeling mechanical testing using a nonlinear friction contact analysis between the splint and platens (Fig. 1ab). For clearing splint designs for 3D printing, we must verify that the FEBio results can replicate mechanical testing. We compared mechanical testing results from 3D laser sintered, sterilized PCL splints of the same design implanted in patients. We found that the FEBio contact results could closely replicated experimental data from 3D printed, patient specific PCL splints (Fig. 1cd). This verifies the use of nonlinear FEA of 3D laser sintered airway splints for design assessment and clearance for fabrication in the design control process. We are in the process of assessing the effect of splint implantation on airway deformation in idealized, nonlinear elastic airway models3 to further verify splint design on airway reconstruction. We believe these results suggest the importance of experimentally verified nonlinear FEA for assessment of patient specific 3D printed medical devices in a design control process required by the FDA.

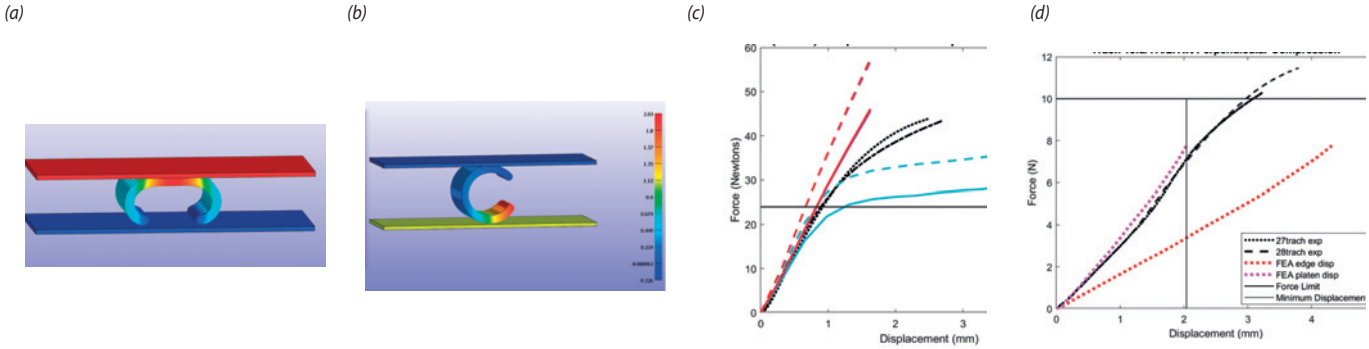

Figure Caption: Figure 1. (a) Platen Splint parallel contact compression in FEBio (b) Patent splint perpendicular contact compression in FEBio. (c) comparison of FEBio (black lines), frictionless contact (blue lines), friction (0.5 coeff) contact. (d) same results as (c) for perpendicular contact

Acknowledgments: This work was supported by NIH NICHD R01 086201. We are grateful to Drs. Kevin Maher, Steven Goudy, April Landry, and Subi Shashidharan from Children's Healthcare of Atlanta who provided clinical image data on which the splints were based.

References:

1 *Hollister et al. (2016) ACS Biomaterial Sci Eng;*
2 *Les et al. (2019) The Laryngosopce;*
3 *Hollister et al. (2017) Resp Res*

[G-08.2]

FINITE ELEMENT MODELLING OF TPMS SCAFFOLDS FOR BONE TISSUE ENGINEERING

Andre Castro[1], *Rui Ruben*[2], *José Miranda Guedes*[3], *Paulo Fernandes*[3]

1 *Instituto Superior Tecnico, Universidade de Lisboa, Lisbon, Portugal*
2 *Estg, Cdrsp, Instituto Politécnico de Leiria, Leiria, Portugal*
3 *Idmec, Instituto Superior Técnico, Universidade de Lisboa, Lisbon, Portugal*

The present work is devoted to the Finite Element (FE) modelling of triply periodic minimal surfaces (TPMS) scaffolds for bone tissue engineering (TE). Different basic structures and the porosity levels are analysed, in order to assess the potential for cells seeded inside TPMS scaffolds to differentiate towards osteoblasts, from the biomechanical point of view. TPMS are defined mathematically as infinite and periodic surface curvatures, which allow for fully controllable homogenous TE scaffolds, parting from the design of the repeatable unit cell. The structures considered in this work are Schwartz D, Schwartz P and Gyroid, which have been previously studied for bone TE, with 50, 60 70 and 80% porosity. The scaffolds were created in STL format with a custom TPMS generator (Castro et al., 2019) and then meshed into FE models. The asymptotic homogenisation method described by Guedes and Kikuchi (1990) allows the calculation of the equivalent elastic coefficients for these periodic porous structures. Scaffold pores were filled with collagen hydrogel, as shown in figure 1a). The poroelastic FE simulations were ran on ABAQUS® and have shown that, under compression, the minimum fluid velocity calculated within the collagen layer in contact with each TPMS scaffold (between 0.1 and 0.5 µm/s) is sufficient for cell differentiation towards bone formation. Figure 1b) shows the fluid concentration spots over the collagen substrate layer in the peak compression stage. It is worth noting that Schwartz P models promoted some irregularities in the fluid distribution that will be further investigated experimentally, namely through MultiJet 3D printing of the scaffolds and subsequent mechanical and permeability tests. This work gives a good perspective over the numerical modelling of scaffolds for bone TE applications, namely in what concerns to scaffold-substrate potential interaction.

a) *b)*

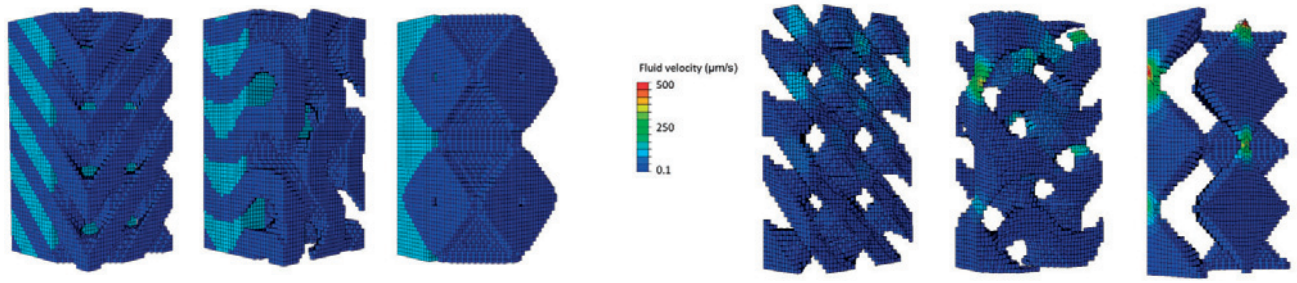

Figure 1. FE models of TPMS Scaffolds: a) Scaffold (dark blue) + collagen substrate (light blue) constructs; b) Fluid velocity calculations for the peak compression stage, over the collagen substrate layer.

Acknowledgments: This work was supported by Fundação para a Ciência e Tecnologia, through project PTDC/BBB-BMC/5655/2014 and also through IDMEC, under LAETA project UID/EMS/50022/2019.

References

Castro APG, Ruben RB, Pinheiro J, Gonçalves S, Guedes JM, Fernandes PR. 2019. Numerical and Experimental Evaluation of TPMS Gyroid Scaffolds for Bone Tissue Engineering. Comput Methods Biomech Biomed Engin. (in press)
Guedes JM, Kikuchi N. 1990. Preprocessing and postprocessing for materials based on the homogenization method with adaptive finite element methods. Comput Methods Appl Mech Eng. 83:143–198.

[G-08.3]

CASE REPORT: DEVELOPING FOREHEAD FLAP TEMPLATES TO GUIDE PARTIAL OR FULL NASAL RECONSTRUCTION FROM 2D AND 3D IMAGES

Zachary Fishman[1], *Mark McRae*[2], *Oleh Antonyshyn* [3], *Jeff A Fialkov*[3], *Cari Whyne*[4]

1 *Sunnybrook Research Institute, Toronto, Canada; University of Toronto, Toronto, Canada*
2 *Department of Plastic Surgery, St. Joseph's Healthcare Hamilton, Hamilton, Canada*
3 *Department of Surgery, University of Toronto, Toronto, Canada; Division of Plastic Surgery, Sunnybrook Health Sciences Center, Toronto, Canada*
4 *Sunnybrook Research Institute, Toronto, Canada; Institute of Biomaterials and Biomedical Engineering, University of Toronto, Toronto, Canada; Department of Surgery, University of Toronto, Toronto, Canada*

The face is a complex three-dimensional (3D) structure that is important to function (i.e. sight, speech, chewing, and sense of smell) and an individual's self-perception (physical appearance). Facial anatomy can be impacted by trauma (i.e. car accidents, sporting and military injuries) or pathology (i.e. cancer or congenital disease). After a traumatic injury or pathologic change to the face, an individual's primary desire is to return to their original state both in terms of function and their appearance. However, there is generally insufficient information regarding the shape of an individual's pre-injury/pathology face and especially the nose shape from front view photographs. This makes accurate restoration of appearance through surgery extremely challenging, with much of the work of a plastic surgeon dependent on their experience and 3D spatial visualization abilities.

This case report highlights the pre-operative planning of forehead flap template with a CAD and CAM process. Planning was performed for five cases, of which three examples are provided to demonstrate a unilateral rhinectomy with design from 3D scan mirroring, a partial bilateral rhinectomy from a 3D scan with aesthetic subunit labelling, and a complete bilateral rhinectomy with nose design from a 3D morphable model. The 3D nose designs of the missing nasal surface were then flattened with digital unwrapping tools to generate a 2D forehead flap template. The 2D design is translated into a physical traceable template via a 1:1 scale paper print-out for a rapid and low-cost CAM tool, which is then transferred to sterilizable metal foil. Intra-operative photos for two cases are presented showing the template applied by tracing it on the forehead as the first stage of nasal soft tissue reconstructions. This digital forehead flap planning and fabrication presents a new patient-specific workflow for plastic surgeons to compliment current their existing experience and practice.

Figure 1. A) Front & profile photos of patient with cancerous regions. B) 3D scan of the patient's nose after mirroring and nostril sculpting. C) 3D modelled nose labelled with according to aesthetic subunits. D) Flattened complete nose template (not to scale) with arranged subunit boundaries.

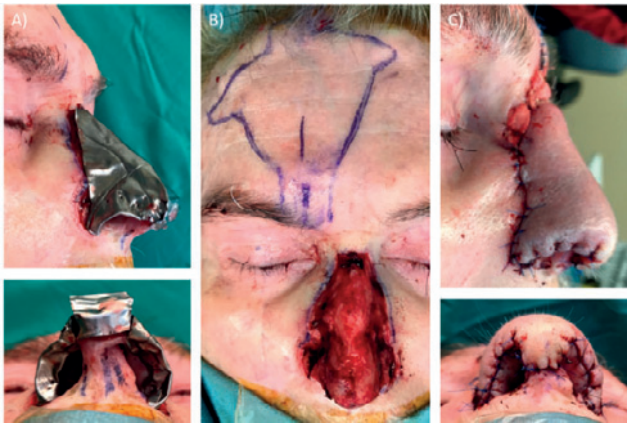

Figure 2. A) Nose template traced in foil and test-fit into the defect after tumor resection (side & bottom view). B) Nose template traced on the forehead. C) Forehead flap transferred to replace missing nasal skin following resection (side & bottom view)

[G-08.4]

IMAGE-BASED 3D PRINTING FOR SURGICAL PREPARATION AND EXPERIMENTAL VALIDATION

David Rutkowski[1], *Alejandro Roldán-Alzate*[1]

1 *University of Wisconsin, Mechanical Engineering, Radiology, Madison, USA*

The use of 3D printing methods in the medicine has increased considerably over the past few decades as a result of the high potential for medical intervention improvement [1, 2]. Rapidly manufactured, case-specific medical products offer many advantages in surgical preparation, surgical intervention, medical equipment validation, disease research, imaging studies, experimental setup, and patient/student education. In this work, we detail the workflow for successful image-based 3D printing in medical applications by giving project examples and discussing the aspects of collaboration and resources. Key components of this process include fielding the needs of physicians, obtaining the anatomical geometry through various imaging methods, designing the requested device or anatomical print structure, collaborating with physicians on design improvements and implementation, fabricating the part, and delivering the finished product in a time frame adherent to surgical schedule requirements. Specific examples of this work include congenital heart disease surgery preparation (1a), small animal urogenital holding devices for imaging research (1b), experimental validation models for liver blood flow (1c), pediatric pulmonary artery stenosis surgical planning (1d), liver and kidney imaging phantom molds (1e), optically clear models for particle image velocimetry validation experiments (1f), ex-vivo blood vessel experimental setups (1g), MRI-based prostate cutter for cancer lesion analysis (1h), spine models and drill templates for surgical use and preparation (1i), aortic dissection experimental analysis (1j), congenital heart disease surgery patient education (1k), visualization of vasculature for educational use (1l), and more. Through each of these examples, not only are case-specific problems and solutions presented, but the immense potential and utility of 3D printing in medicine is displayed.

Figure Caption: 3D-printed models and devices for medical applications.

References:

[1] Martelli, N., et al., 2016. Surgery, 159(6), pp. 1485-1500.
[2] Chepelev, L., et al., 2018, 3D Print Med, 4(1), p. 11.

[G-09.1]
COMPLEX CELLULAR MODELS OF NEUROVASCULAR COUPLING

*Yves Vijgeboom[1], Allanah Kenny[2], **Tim David**[2], Jason Berwick[3]*

1Technical University of Eindhoven, Eindhoven, Netherlands
2University of Canterbury, Christchurch, New Zealand
3University of Sheffield, Sheffield, UK

Neurovascular coupling is the ability of the cortical tissue to regulate the blood supply locally. Blood oxygen level dependent (BOLD) signals represent neuronal activity (via measurement of de-oxyhaemoglobin)and is the gold standard for functional MR protocols. We have developed a complex cellular, numerical model of neurovascular coupling utilising the neurovascular unit (NVU) consisting of neurons, astrocytes, smooth muscle cells and endothelial cells. The neuron model exhibits both excitatory and inhibitory functions whilst the other cells determine the time-dependent ion concentration profiles This model now has the ability to simulate both time-varying cerebral blood flow and the associated fMRI BOLD responses due to continuous neuronal spiking, bursting phenomena and task orientated stimulation [1-4]. Numerical simulations are compared to experiments of the stimulation of awake rat whiskers of varying duration observed in the rat barrel cortex [5]. Comparison shows excellent agreement for both blood flow and haemoglobin profiles. The results support the theory that K+ is the key pathway for providing above baseline levels of oxygen and glucose to the cerebral cortex during local activity. The model is able to conduct in-silico experiments that are either impossible or ethically restrictive in the laboratory.

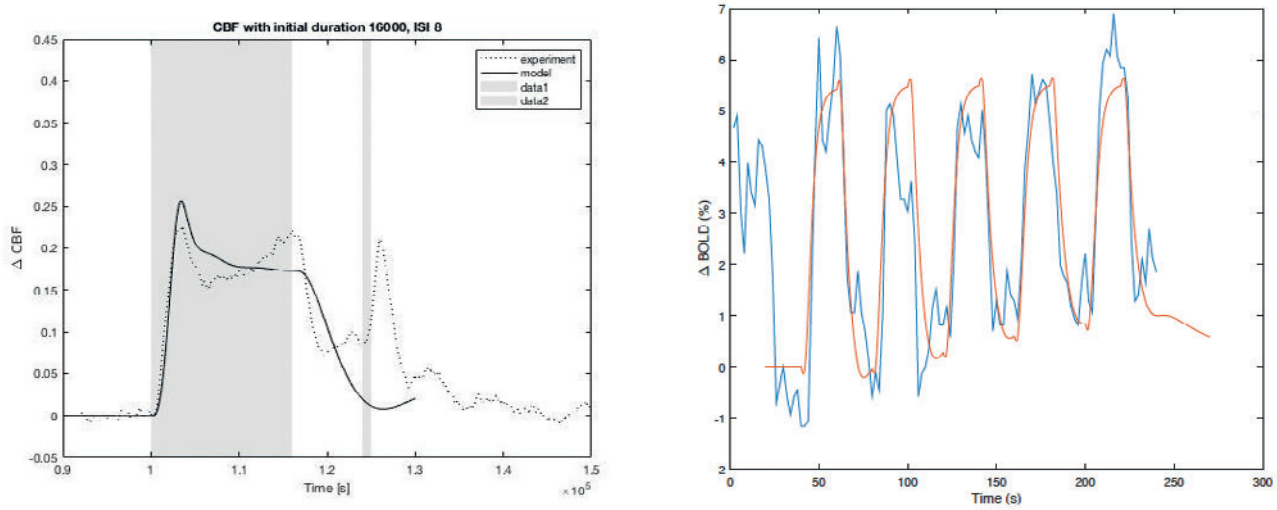

Figure Caption: Left:Cerebral Blood Flow for single pulse compared with experimental data from [5]. Right: simulated BOLD signals (red) compared to experimental (blue) for finger tapping exercise.

Acknowledgments: Funding provided by Brain Research New Zealand

References:

1) *Dormanns, K.; et al (2015): Neurovascular coupling and the influence of luminal agonists via the endothelium, Journal of Theoretical Biology, Vol. 364 pp.49–70.*
2) *Mathias, E. Kenny, A.; Plank, M. J. M. and David, T. (2018): Integrated models of neurovascular coupling and BOLD signals: Responses for varying neural activations, NeuroImage, Vol. 174, pp. 69–86.*
3) *Mathias, E. J.; Plank, M. J. and David, T. (2017): A model of neurovascular coupling and the BOLD response: PART I, Computer Methods in Biomechanics and Biomedical Engineering, Vol. 20, pp. 508–518.*
4) *Kenny, A.; Plank, M. J. M. and David, T. (2018): The role of astrocytic calcium and TRPV4 channels in neurovascular coupling, Journal of Computational Neuroscience, Vol. 44, pp. 97–114.*
5) *Zheng, Y. et al (2010). A dynamic model of neurovascular coupling: implications for blood vessel dilation and constriction. NeuroImage, 235:1135–1147.*

[G-09.2]

TOWARDS A REAL-TIME SOLUTION FOR VIRTUAL SURGICAL PLANNING OF UPPER AIRWAY PROCEDURES, INCLUDING COMPUTATIONAL FLUID DYNAMICS

Rachel Clipp[1], *Jared Vicory*[1], *Julie Kimbell*[2], *Sorin Mitran*[2], *John Rhee*[3], *Andinet Enquobahrie*[1]

1 *Kitware, Inc, Carrboro, USA*
2 *University of North Carolina, Chapel Hill, USA*
3 *Medical College of Wisconsin, Milwaukee, Wisconsin*

Introduction. Upper airway surgery is used to treat a variety of common conditions that lead to breathing difficulties, including airway obstruction and obstructive sleep apnea. However, these procedures have long-term failure rates of 25-50%1 and 40-50%2, respectively. We have previously proposed a low-cost easy to use diagnostic and surgical planning tool to improve outcomes3. Here, we focus on the image segmentation and computational fluid dynamics (CFD) components. Current tools for segmentation and CFD require extensive experience and time, costly licenses, and extensive computational resources. We propose the use of open source tools (3D Slicer) and a customized Lattice Boltzmann Method (LBM) for near real-time CFD. Methods. Patients, selected from the IRB Rhee study cohort4,5, were at least 15 years old and had a diagnosis of non-reversible, surgically treatable nasal obstruction (deviated septum, turbinate hypertrophy resistant to medical treatment, or lateral nasal wall collapse), elected to have surgery, and provided written, informed consent. Five patient CT images were segmented using the semi-automated algorithm, detailed in3, and analyzed with the LBM. A patient-specific flow rate was specified at the inlet with an initial pressure drop of 10 Pa. The computation was then executed until steady state was achieved. The results were compared to previously published Mimics segmentations with CFD analysis in Fluent4,5 and LBM. Results. Figure 1 illustrates that the LBM method produces a valid pressure drop for the Mimics segmentation, 37.6 Pa vs the Fluent calculation, 36.1 Pa. All Slicer segmentations produced 10-60% lower pressure drops, which was proportional to the fluid flowing into the attached sinuses. Discussion. These results demonstrate that LBM can produce an accurate flow and pressure profile compared to Fluent. However, future work will focus on refining the segmentations to remove the sinuses to improve CFD calculations, improving the LBM algorithm to include secondary flow characteristics and heat flux calculations, and improving the parallelization algorithm for improved calculation speed. We will also do a full validation of the ten patient cases by comparing our results to previous work across more parameters4,5

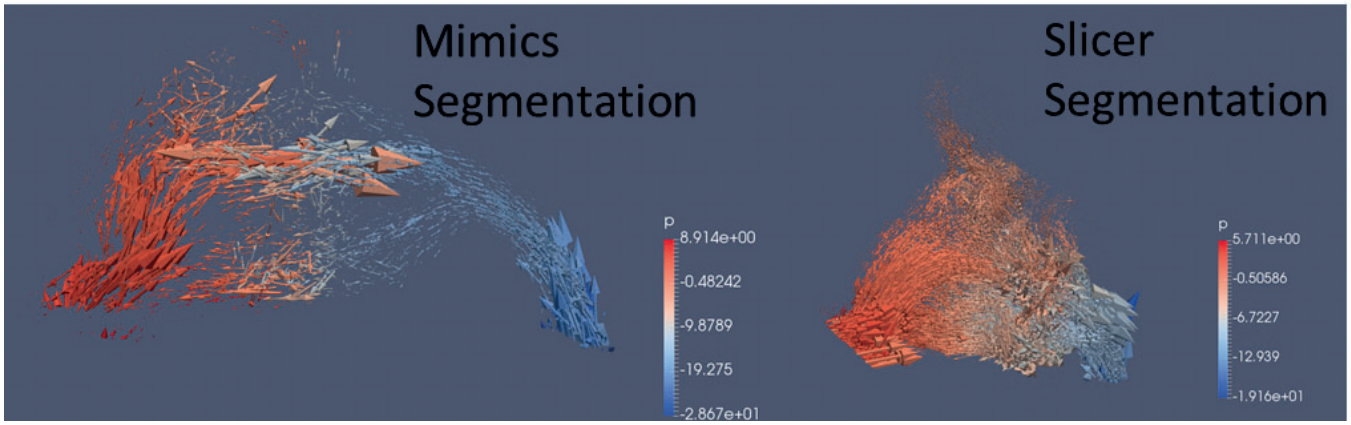

Figure Caption: The original segmentation shown appropriate flow trends and a pressure drop of 37.6 Pa, while the Slicer segmentation shows flow into the sinuses and a pressure drop of 24.8 Pa.

Acknowledgments: Research and patient data collection was supported by the NIBIB of the NIH under Awards R43EB023121 and R01EB009557, respectively.

References:

1. *Won, et al. Proc Am Thorac Soc. 2008;5(2):193-199.*
2. *Frank-Ito et al. Otolaryngol - Head Neck Surg. 2014;151(5):751-759.*
3. *Clipp et al. In: 2018 IEEE EMBC. Vol 2018. IEEE; 2018:5802-5805.*
4. *Kimbell, et al. J Biomech. 2013;46(15):2634-2643.*
5. *Kimbell et al. Am J Rhinol Allergy. 2012;26(3):e94-8.*

[G-09.3]

PATIENT-SPECIFIC PARAMETERIZATION OF PRESSURE-OVERLOADED LEFT VENTRICULAR ELECTRO-MECHANICAL MODELS

Laura Marx[1], *Matthias Gsell*[1], *Armin Rund*[2], *Christoph Augustin*[1], *Gernot Plank*[1]

1 *Medical University of Graz, Graz, Austria*
2 *University of Graz, Graz, Austria*

Stenotic aortic valve disease (AS) or aortic co-arctations (CoA) impose a significant increase in afterload upon the left ventricle (LV) which may impair, by pressure overloading the LV, myocardial energetics and drive adverse remodeling processes leading to heart failure. Computational models of LV electro-mechanics (EM) show promise as a clinical research tool for quantitatively assessing the impact of pressure overload conditions upon mechanics and disease progression and, potentially, also for predicting the acute and chronic outcome of interventions. To be of clinical utility models must be parameterized in a patient-specific fashion, but the personalization of models with clinical data remains a challenging endeavor.

Finite element EM models of LV and aorta of patients suffering from AS (N=12 cases) or CoA (N=7 cases) were built [1,2]. An automated global-local optimization method was developed for identifying parameters of three (Wk3) and four (Wk4) element Windkessel models [3] of afterload from clinical pressure and flow data. Physiological box constraints were used to restrict the global search space within a combined global-local optimization procedure to find globally unique optimal parameter sets. The identified afterload parameters were used in coupled electro-mechanical LV models, after fitting of other model components comprising electrical activation sequence, mechanical boundary conditions as well as passive and active biomechanical properties, to ascertain that the combined model replicates all available clinical observations.

For all AS and CoA cases under study, our optimization approach identified a globally unique set of parameters under the given physiological constraints. Using a minimum number of inputs, parameters were found automatically without any operator interventions within < 2 minutes. Simulation results obtained with the combined LV models of both AS and CoA cases show close agreement, within the limits of clinical data uncertainty, with all available clinical observations in all N=19 cases.

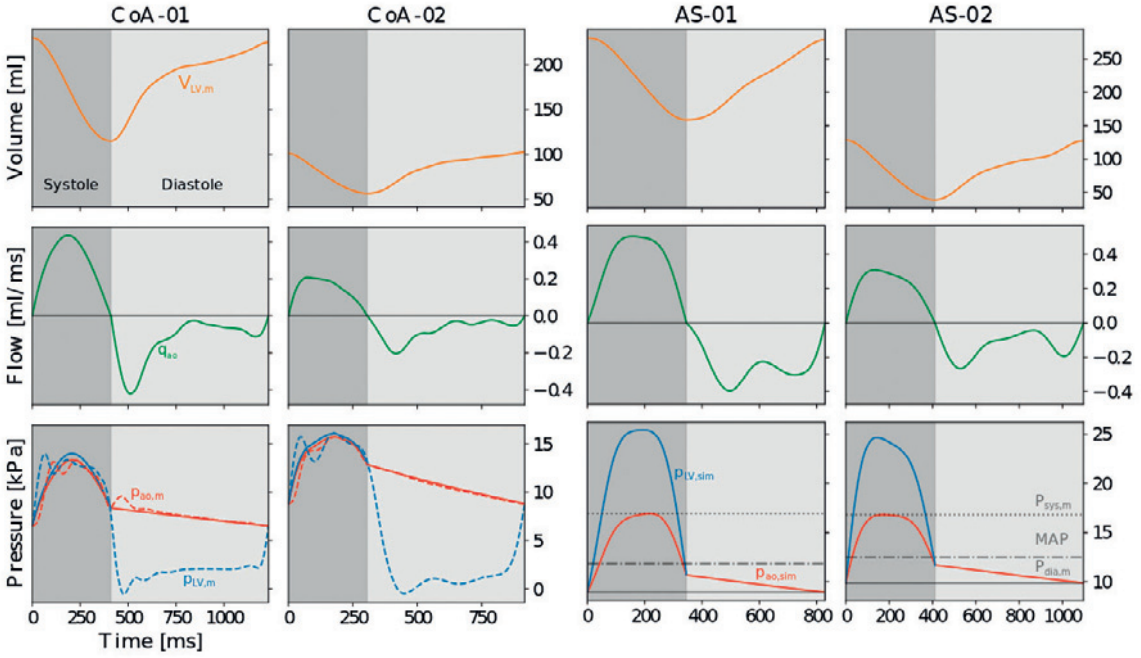

Figure Caption: Shown are four representative results (NCoA=2, NAS=2): First row: Measured and upsampled volume traces in the LV (solid orange line); Second row: the derived flow in the aorta (solid green); Third row: Goodness of fit is illustrated by comparing between simulation results (solid red (aorta) and blue (LV)) and measured pressure traces (invasive for CoA cases (dashed red and blue), and discrete values for AS (gray horizontal lines)) for the respective cases.

Acknowledgments: This research was supported by the grants F3210-N18 and I2760-B30 from the Austrian Science Fund (FWF), the EU grant CardioProof agreement 611232 and the BioTechMed Graz award ILearnHeart to GP.

References:

[1] *Crozier A. et al., Annals of biomedical engineering, 2016.*
[2] *Augustin C.M. et al.,Journal of Computational Physics 2016.*
[3] *Westerhof et al., Medical and biological engineering and computing, 2009.*

[G-09.4]

AN EULERIAN APPROACH TO PATIENT-SPECIFIC HEMODYNAMIC MODELING USING IMAGE-DERIVED LEFT VENTRICLE MOTION

Aaron Goddard[1], ***Sarah Vigmostad***[1]

1 *The University of Iowa, Roy J Carver Dept of Biomedical Engineering, Iowa City, USA*

Patient-specific multi-physics simulations have the potential to improve the diagnosis, treatment, and scientific inquiry of cardiovascular hemodynamics. Modeling of patient-specific hemodynamics continues to require extensive user-input, which hinders high-throughput models or models that include wall motion. Since patient geometry can be captured throughout the cardiac cycle, wall motion can be prescribed a priori as a Dirichlet boundary condition during a simulation.

One challenge in specifying wall motion from medical images stems from the temporal resolution required for CFD calculations, which is orders of magnitude higher than the temporal resolution available from imaging. This discrepancy necessitates the estimation of intermediate positions, and the current work employs a morphing technique that smoothly deforms the interface from one known position to the next known position (i.e. from one image frame to the next) over a finite number of intermediate steps. To maximize computational efficiency, CFD solvers typically adapt the timestep size, requiring morphing to be performed during a simulation's run-time.

This work describes an Eulerian approach to represent cardiovascular geometry, displacement, and motion. This is achieved using levelsets, which are used to segment the medical images and represent the geometry within a Cartesian grid flow solver. Here, morphing is implemented and adapted to accommodate the unique needs of the flow solver, which include adaptive mesh refinement, parallel domain decomposition, a narrow-band approach, and the need to supply local interface velocities to the flow solver which describe both normal and tangential motion. By employing skeletonization, warp and blend operations ensure that tangential wall motion is accurately captured. The framework has been validated on several moving boundary problems and shows sub-grid accuracy. Figure 1 shows streamtraces of a 3D left ventricle simulation throughout the cardiac cycle. The simulation was performed without any meshing, through the morphing of levelset-based interface positions from fifteen time points to describe wall motion and drive flow throughout the cardiac cycle.

Through the use of an Eulerian representation throughout the modeling process, this approach circumvents the need for Lagrangian-based surface or volume meshing. This method has been developed with the long-term goal of integrated imaging-to-flow without user intervention, so that computational modeling can be employed to aid clinical decision-making, and high-throughput computations can be performed on large patient cohorts.

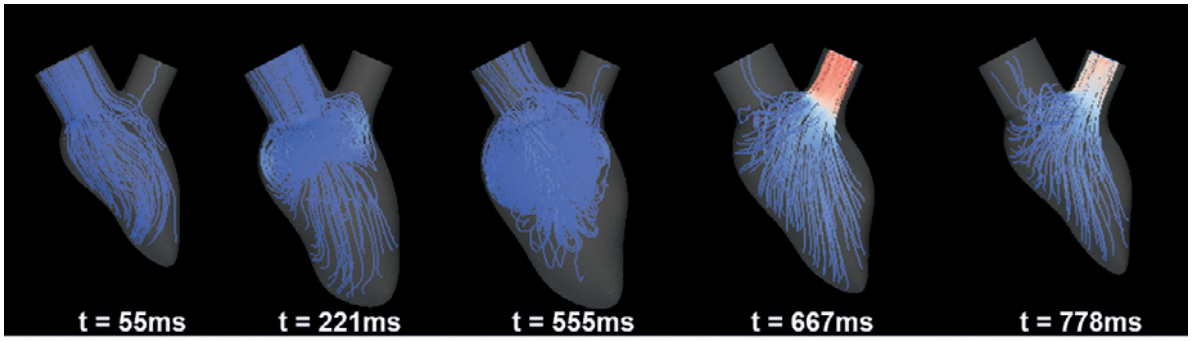

Figure 1: Left ventricle geometry is represented using levelsets, and through morphing and skeletonization, local wall motion drives flow throughout the cardiac cycle.

[G-09.5]

4D FLOW MRI ESTIMATION OF BOUNDARY CONDITIONS FOR PATIENT SPECIFIC CARDIOVASCULAR SIMULATION

Ryan Pewowaruk[1], ***Alejandro Roldán-Alzate***[2]

1 *University of Wisconsin, Madison, USA*
2 *University of Wisconsin, Mechanical Engineering, Radiology Madison, USA*

Accurate cardiovascular simulations require patient specific boundary conditions (BCs) for inlets, outlets and vessel wall mechanical properties. While inlet BCs are typically determined non-invasively, invasive pressure catheterization is often used to determine patient specific outlet BCs and vessel wall mechanical properties [1]. First, pulse wave velocity (PWV) is used to determine the vessel stiffness [2]. Once stiffness is known from PWV, the pulse pressure in the vessel can be calculated from the systole to diastole artery area change using the Law of Laplace [3]. Compliance can then be calculated from flow and the pulse pressure. Lastly, an exponential decay is fit to vessel area during diastole. The exponential time constant ( ) is assumed to be the vasculature time constant and used to calculate resistance. While for area will not be the same as for pressure, vessel area is a function of pressure and should provide an estimate of . Parameters are modulated until measured-simulated error is less than 10%. Both in vitro validation with a latex tube [4] and an in vivo pulmonary artery stenosis (PAS) stent intervention are performed.

Table 1: FSI Validation Against Benchtop Measurements

Measurement	Benchtop [11]	FSI	Error
PWV (cm/sec)	93 ± 2	102	10%
Max Disp (mm)	1.73 ± 0.02	1.98	15%

For in vitro validation, acceptable agreement is found between simulation using BCs from 4D Flow MRI and benchtop measurements. For the PAS virtual intervention, simulation correctly predicts flow distribution with 9% error and RAC with 20% compared to MRI. Using 4D Flow MRI to noninvasively determine patient specific BCs increases the ability to use image based simulations as pressure catheterization is not always performed.

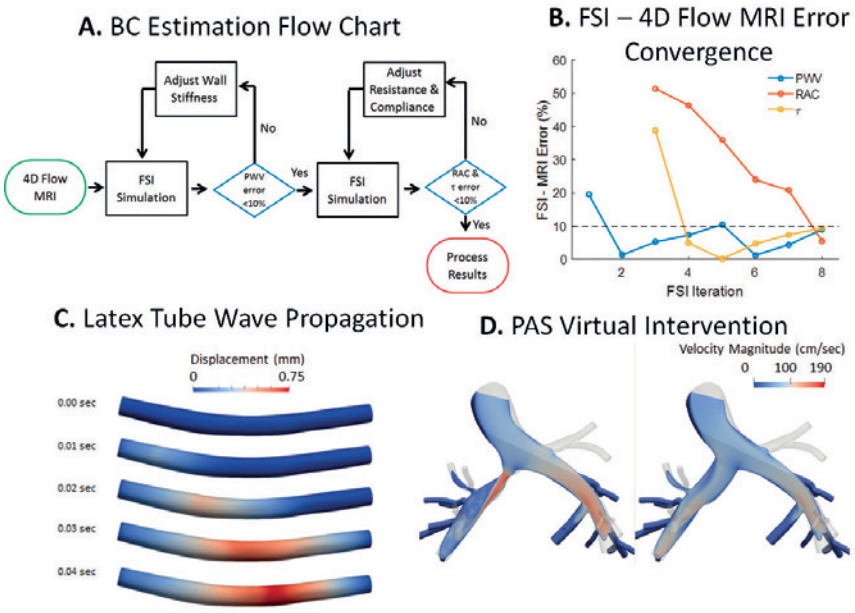

Figure Caption: A. Flow chart describing the algorithm to determine patient specific conditions from 4D Flow MRI. An initial iterative loop is used to match PWV, a second loop matches RAC and τ. B. FSI-4D Flow MRI error plots of the PAS showing the convergence of PWV and RAC over the course of 8 FSI iterations. C. Latex tube displacements show wave propagation from the inlet (left) to outlet (right). D. FSI velocity magnitude is shown on cut planes in MPA, LPA and RPA. A jet is seen impinging on the LPA wall distal to the stenosis which stent intervention is predicted to eliminate.

Acknowledgments: UW Cardiovascular Research Center T32 HL 007936 and used UW Center for High Throughput Computing.

References:

1. *Zambrano, B.A., et al., J Biomech, 2018.*
2. *Quail, M.A., et al., Am J Physiol Heart Circ Physiol, 2015.*
3. *Olufsen, M.S., Am J Physiol Heart Circ Physiol, 1999*
4. *Ruesink, T., et al., Cardiovasc Eng Technol, 2018.*

[G-10.1]

HOW VISION-GUIDED SCLERAL REMODELING SHAPES OUR EYES AND PRODUCES CLEAR VISION OR NOT

Rafael Grytz[1]

1 *University of Alabama at Birmingham, Department of Ophthalmology and Visual Sciences, Birmingham, USA*

During the developmental phase, genetically controlled growth and remodeling mechanisms shape the tissues of our organs. Unlike any other organ, the development of the eye is controlled by genetics and, in addition, by visual environmental factors. The growth and remodeling of the sclera plays a key role during the development of the eye impacting the size and refractive state of the eye. Myopia is the most common type of refractive error. The myopic eye is too long for its own optical system, which is typically caused by an elongated posterior scleral shell. Within the past 60 years, myopia has reached epidemic condition in East and Southeast Asia, with a prevalence of 80-90% in young adults. A deeper understanding of the underlying mechanisms that determine the final size of our eyes is critical for the development of effective myopia treatment modalities. In this lecture, animal experiments and computational multi-scale models are presented to provide insight into the underlying mechanisms that shape our eyes during development and produce clear vision or not. The proposed finite element model assumes that scleral growth and remodeling are two (mostly) independent mechanisms. The results of our model show in agreement with experimental observations that scleral growth is genetically controlled and ceases early in life. In contrast to scleral growth, scleral remodeling is controlled by both, genetics and vison, and remains active until the end of the developmental phase. Consequently, scleral remodeling and not scleral growth determines the final shape of our eyes. Using a mesh-free approach to model the local signaling of the visual stimulus form the retina to the sclera, we investigate the role of locally controlled scleral remodeling on the development of the eye shape. Our results provide evidence that visual signaling in the periphery of the visual field may significantly impact the shape of the eye and promote progressive myopia. Lastly, we will discuss scleral crosslinking as a potential treatment option that targets scleral remodeling for myopia control. Sub-Tenon's injections of genipin were performed at different concentration to crosslinking the sclera of tree shrews with experimentally induced myopia. Our results show that scleral crosslinking can slow myopia development. The extent and duration of this treatment effect is dose dependent. However, some unexpected effects were observed after scleral crosslinking (corneal thickening, reduction of the anterior chamber depth, sham effect). Further development of the crosslinking technique is needed to localize the treatment effect and inhibit scleral remodeling for effective myopia control.

Acknowledgments: The work presented in this abstract was supported in part by the NIH grants R01-EY027759, R01-EY026588 (Bethesda, MD, USA), EyeSight Foundation of Alabama (Birmingham, AL, USA), and Research to Prevent Blindness (New York, NY, USA).

[G-10.2]
PEDIATRIC RETINAL MICROVASCULATURE MECHANICS DURING TRAUMA

Matthew P. Byrne[1], ***Brittany Coats***[1]

1 *University of Utah, Salt Lake City, USA*

Retinal hemorrhage is one of the least understood traumatic injuries associated with pediatric abusive head trauma. In this study, we developed three-dimensional, high-resolution finite element models (FEMs) of the pediatric and adult ovine retinal vasculature. Using these models, we evaluated how stress and strain manifests in microvasculature during shaking and falls, with special consideration to the morphology and material properties of the retinal vasculature. Preterm and adult microvasculature from the posterior retina were imaged using confocal microscopy. Two high-resolution (19-20M nodes), three-dimensional FEMs of the infant and adult complex microvasculature networks were generated from these images. Experimentally obtained shaking and fall data were applied to each model to simulate two common traumatic scenarios in infants. Magnitude and distributions of stress and strain were evaluated as a function of retinal depth and compared between the age groups. The relative contribution of morphology and material properties to the mechanical response was also evaluated. In both the adult and infant models, the stresses and strains in the deeper layers of the retina were 20-74% greater than the superficial layers, respectively. This is likely due to decreased vessel lengths and diameters in this layer. The adult retina had 1.5-2 times the stress and strain of the infant retina. Further investigation revealed the stiffer material properties of the adult retina overshadowed any morphological vulnerabilities of the infant microvasculature. The stresses and strain produced by falls were 2.25 times greater than shaking. The vulnerabilities of deeper layers to the retina correspond with clinical observations that interretinal hemorrhages are more prevalent in pediatric abusive or accidental trauma compared to preretinal or subretinal hemorrhage. These studies highlight the integral role of computational models, such as those developed in this study, to understanding the mechanics and eventual prediction of retinal hemorrhage in children. However, magnitudes of stress and strain capable of causing rupture in infants will be necessary before predictions of injury can be made, and distinctions between abusive and accidental head trauma are identified.

Acknowledgments: Support for this work was provided from the National Eye Institute with the National Institutes of Health award no. R21EY025813.

[G-10.3]

BIOMECHANICAL ASSESSMENT OF THE IRIS IN RELATION TO ANGLE-CLOSURE GLAUCOMA: A MULTI-SCALE COMPUTATIONAL APPROACH

Vineet Thomas[1], *Samuel Salinas*[1], *Anup Pant*[1], ***Rouzbeh Amini***[1]

1 *University of Akron, Akron, USA*

Iris biomechanics plays an important role in the pathophysiology of primary angle-closure glaucoma (PACG). Since abnormalities in the iris and their interference with aqueous humor flow are established contributing factors in the closure or narrowing of the anterior chamber angle, the mechanical response of the iris has been studied extensively in the context of PACG [1]. The collagen fibrils of the iris stroma provide support while undergoing continuous large mechanical deformation [2]. In the microenvironment, stromal cells respond to mechanical stimuli from the surrounding fiber network. As a result, the shape of the nucleus changes, which leads to functional and morphological alterations at the extracellular matrix/cellular level [3]. However, the relationship between micrometer-scale and macro-scale mechanical environment remains unknown. To bridge this knowledge gap, we have used a multiscale computational framework [4] that links the volume-averaged stress in micrometer-scale representative volume elements (RVEs) to a macro-scale finite element (FE) continuum. We fitted the multiscale model response to experimental data obtained from uniaxial tension tests of intact irides [5]. A three-dimensional (3D) FE model of the intact iris was generated (Fig. 1a). A strain value of ~25% was applied to the model by prescribing uniaxial displacement values on the boundary nodes of the sample (Fig. 1b). In this study, we considered the nuclear aspect ratio (NAR) as a measure to quantify cellular deformation, with an average initial NAR value of 2.0. An ellipsoidal geometry was assumed for the cell nucleus [6]. The model fitting parameters (with R2 value of 97.6%) for the intact iris included a shear modulus value of 3.5 kPa and a fiber modulus value of 7.5 kPa. Nuclei deformed and realigned in response to the macro-scale mechanical loading (Fig. 1c). We hope to employ our model in pathophysiological states of the iris to understand how the nuclear deformation may differ in glaucomatous eyes as compared to the normal controls.

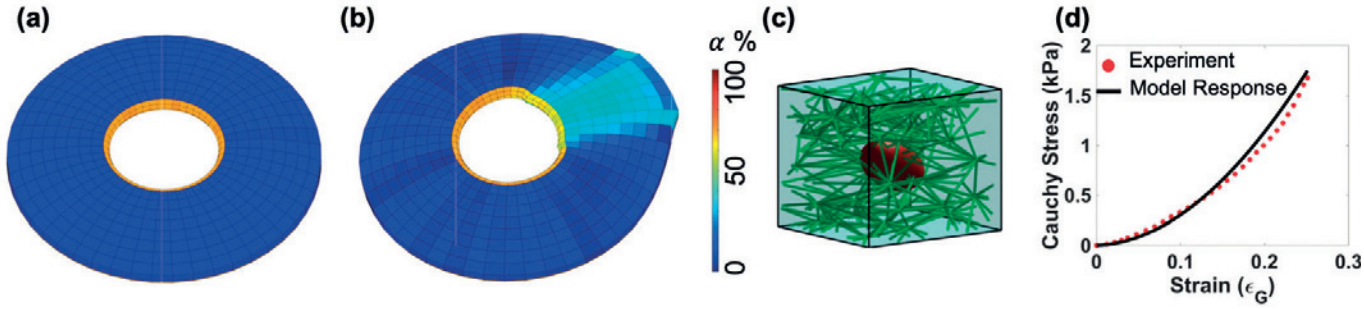

Figure 1: (a) Undeformed and (b) deformed configurations of 3D FE model of an intact iris. (c) Deformed RVE of collagen fibers with a 3D ellipsoidal geometry representing the nucleus (d) Multiscale model response fitted to the experimental data [5].

Acknowledgments: Computational facilities from the Ohio Supercomputer Center and funding from BrightFocus Foundation (G2018177) are acknowledged.

References:

[1] *Amini, R et al., Invest Ophthalmol Vis Sci, 53(3):1188-94, 2012.*
[2] *Marshall, G. E. et al., Br J Ophthalmol, 77:515-524, 1993.*
[3] *Cho, S. et al., J Cell Biol, 216(3): 305, 2017.*
[4] *Stylianopoulos, T. et al., Comput Methods Appl Mech Eng, 196(31-32):2981-90, 2007.*
[5] *Whitcomb, J. E. et al., Exp Eye Res, 89: 456-461, 2009.*
[6] *Huang, H. S. et al., J Biomech Eng, 129(6):880-889, 2007.*

[G-10.4]

UTILIZING FINITE ELEMENT ANALYSIS TO DETERMINE SCLERAL MECHANICAL PROPERTIES AND OPTIC NERVE HEAD STRAIN IN THE RAT EYE

Ross Ethier[1], *Stephen Schwaner*[1], *Bailey Hannon*[1], *Robert Perry*[1], *Alison Kight*[1]

1 *Georgia Institute of Technology, Atlanta, USA*

Glaucoma is the second leading cause of blindness. Although it is well-accepted that elevated intraocular pressure (IOP) leads to biomechanical insult to the optic nerve head (ONH), which in turn contributes to retinal ganglion cell (RGC) death, the mechanism(s) of this process remain unknown. Rodent animal models, such as the rat, provide an opportunity for mechanistic understanding of how biomechanical insult leads to RGC death, and a wealth of data from rat glaucoma studies already exists. However, the biomechanics of the rat ONH have not been characterized, even though the rat ONH anatomy is noticeably different from the human, as summarized elsewhere [1].

Here we summarize a multi-year effort to characterize rat ONH biomechanics using finite element (FE) modeling. This includes construction of individual-specific rat ONH FE models, as well as a generic FE model with parameterized geometry for conducting sensitivity studies. Using these models, we have simulated the effects of elevated IOP, assuming neo-Hookean tissue behavior with material properties previously used in human modeling studies and from the literature. Initial results [1] have revealed strain concentrations in the inferior nerve, which match well with patterns of astrocyte activation observed in previous in vivo rat glaucoma studies, but which conflict with the observation that RGC death often occurs first in the superior nerve. An initial sensitivity analysis performed with the generic model suggested that, like the human ONH, scleral stiffness is the most important factor in rat ONH biomechanics.

Since scleral properties are important, and because rat-specific scleral properties are unknown, we are now focusing on determining the material properties of rat sclera using digital image correlation (DIC) and inverse FE modeling. Briefly, enucleated rat eyes are secured to a mounting block attached to a fluid reservoir that allows for control of IOP. A speckle pattern is applied to the posterior eye and IOP is increased while 3D deformation of the speckled surface is captured by stereo DIC cameras. An FE model of the sclera is built using information about the scleral surface as measured by DIC and the thickness of the sclera as measured with optical coherence tomography. A differential evolution algorithm is then used to drive an optimization loop in which material properties of the sclera are varied until simulated FE model displacements closely match the experimental displacements measured by DIC. Figure 1 illustrates a proof-of-concept test in which the optimization procedure successfully retrieved a known set of material parameters that had been used to generate a set of "pseudo-experimental" data. We will present further inverse FE results and integrate more accurate scleral mechanical properties into an overall rat ONH model.

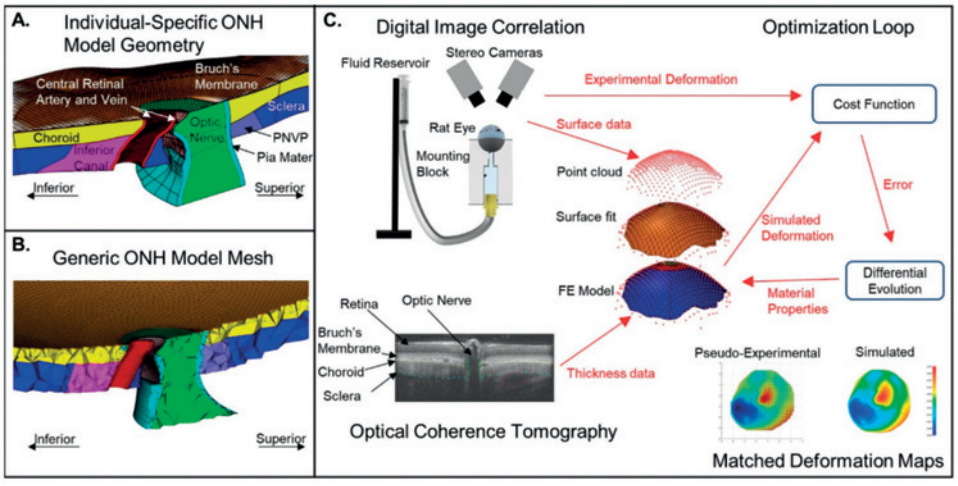

Figure Caption: A. Superior-Inferior cut plan view of individual specific model geometry. B. Superior-Inferior cut plan view of generic ONH model mesh. C. Illustration of inverse FE modeling workflow and proof-of-concept matching of pseudo-experimental and simulated deformation maps (bottom right).

Acknowledgments: Georgia Research Alliance; NEI T32EY007092; NEI F31EY02882

References:

[1] Schwaner et al., J.Biomech.Eng. 140(8), 2018

[G-10.5]

QUANTIFYING THE MECHANICAL PROPERTIES OF THE HUMAN LAMINA CRIBROSA - A PRELIMINARY STUDY

Jonathan Vande Geest[1], *Hirut Kollech*[1], *Reza Behkam*[1]

1 *University of Pittsburgh, Pittsburgh, USA*

Introduction and Background: Glaucoma is the second leading cause of blindness in the world and is expected to affect 80 million people by 2020 [1]. Risk factors include age, race, gender, intraocular pressure and optic nerve head (ONH) mechanics [2-3]. It is more prevalent in those of Hispanic ethnicity (HE) and African descent (AD) than European descent (ED) [5]. Previous studies have shown the biomechanics of the lamina cribrosa (LC) in the ONH plays a major role for developing glaucoma [6-7]. In addition, our team recently showed that strain in the LC of ED is significantly different than that of AD and HE [9]. The objective of this study is to determine the material properties of the LC using samples in the European and Hispanic groups and to compare differences across these groups.

Methods: A total of four non-glaucomatous eyes from donors older than 50 years were used in the study (n = 2, ED and n = 2, HE). Pressure inflation tests were performed capturing the second harmonic generation (SHG) signal of collagen at 5, 15, 30, and 45 mmHg from an anterior view. A non-rigid image registration

technique was utilized to determine the 3D displacement field in each LC [4]. These displacement results were utilized to impose boundary condition and as input into our optimization scheme. Since our recent work [9] showed major differences in the superior quadrant of the LC where ED has higher strain than that of HE and AD, a small LC subdomain was selected from the superior quadrant of each sample for geometry creation (Figure 1). For the purposes of this preliminary work, both the collagen and nerve tissue within the LC were assumed to be incompressible isotropic materials with a Neo-Hookean material strain energy density function with a single material constant (C10). In this work a design of experiments was performed to generate the lower and upper bounds of C10 used in the optimization.

Results and Conclusion: The optimized C10 values for the ED samples were 263 kPa and 76.1 kPa with relative percent error of 9.76 x 10-6 and 4.52 x 10-6, respectively. For the HE samples, the above values were 79.5 kPa and 77.0 kPa, with relative percent error of 1.75 x 10-6, and 1.3 x 10-6, respectively. Although the C10 values are bigger in one of the ED samples more samples need to be studied to report a comprehensive statistical analysis across these groups. In addition, future work will include anisotropic models of the LC as well as consider the entire domain of the LC.

Acknowledgments: This research was supported by the National Institute of Health (NIH) under award number R01EY020890 to JPVG, the University of Pittsburgh, Pittsburgh, United States Center for Research Computing (CRC) and Pittsburgh Supercomputer Center through NSF-XSEDE award number TG-ENG160035.

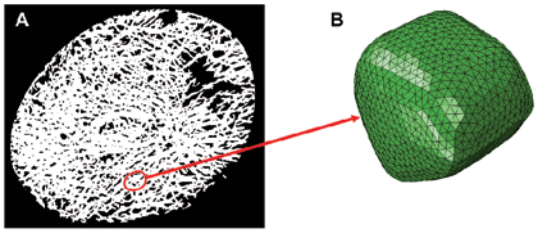

Figure 1A) A representative subdomain region in LC
1B) Subdomain region mesh

References:

[1] *Quigley H et al., J Ophthalmol, 90(3):262–267, 2006*
[2] *Le A et al., IOVS, 44(9): 3783-3789, 2003*
[3] *Rudnicka et al., IOVS, 47(10):4254-4261, 2006*
[4] *Thirion I et al., Medical Image Analysis, 2(3):243–260, 1998*
[5] *Quigley, H et al., A Ophthalmol, 119(12): 1819-1826, 2001*
[6] *Sigal I et al., IOVS, 8(2):85-98 2009*
[7] *Downs J et al., E Eye Research, 93(2):133-140, 2011*
[8] *Midgett D et al., 2017 Acta Biomater, 53:123-139*
[9] *Behkam R et al., Acta Biomater, 2019 (in press)*

[G-11.1]

HORMONE MEDIATED GROWTH AND REMODELING IN MOUSE CERVIX

Nicole Lee[1], *Mala Mahendroo*[2], *Sudeshna Tripathy*[2], *Kristin Myers*[1]

1 *Columbia University, New York, USA*
2 *University of Texas Southwestern Medical Center, Dallas, USA*

One of the most dramatic and unique remodeling events in the human body happens during pregnancy. As the fetus grows, the mother's body evolves to accommodate the increasing fetal volume through uterine growth, pelvic tissue softening, and progressive cervical remodeling. For a successful full-term pregnancy, the cervix must remain closed throughout gestation [1]. Then nearing full-term, the cervix must have softened enough to dilate and deliver the fetus. The process of cervical remodeling and softening remains unknown, but the onset of accelerated cervical remodeling has been hypothesized to cause preterm cervical dilation and preterm birth [2]. Previous mechanical testing data on human and mouse cervical tissue indicate it has nonlinear and time-dependent material behavior, in which its material properties dramatically evolve in parallel with distinct regimes of hormonal control [2,3]. Additionally, previous biochemical investigations support the remodeling behavior might be linked to hormone-mediated extracellular matrix (ECM) turnover of collagen and elastin fibers [3]. In this study, we mechanically characterize cervical remodeling in non-pregnant mouse samples using distinct mechanical tests designed to tease out specific deformation mechanisms controlled by the tissue's hormone-responsive ECM constituents.

Methods: We will mechanically test mouse cervix samples from 4 different groups. All samples will be ovariectomized (ovx), then split equally into the following treatment groups: progesterone (P), estrogen (E), relaxin (R), and no subsequent treatment. Samples will be prepared for whole-specimen ring tensile loading as previously described [4]. Briefly, the sample will first be allowed to swell for 2 hours in phosphate buffered saline with 2 mM ethylenediaminetetraacetic acid. A preload of 0.001 N will be applied to ensure the sample is in contact with threaded sutures. The loading protocol consists of 2 main sections: 1) strain rate sensitivity cyclic load-unloads and 2) stress relaxation ramp-holds (Fig.1). Load levels will be determined using previous loading experiments to ensure the samples can sustain a majority of the loading regimen. Between each loading, the sample will be held at zero displacement for 20 minutes to recover and equilibrate. Images for deformation measurements will be taken 1/s while loading and 1/60s while holding. To describe the material behavior between the different sample groups, the cervix will be modeled as a hydrated fiber composite porous material where the interstitial pore space allows for the growth and removal of solid mass dictated by hormone-mediated compositional state variables. A computational inverse finite element analysis will be employed to aid in finding the best-fit material parameters from the experimental dataset.

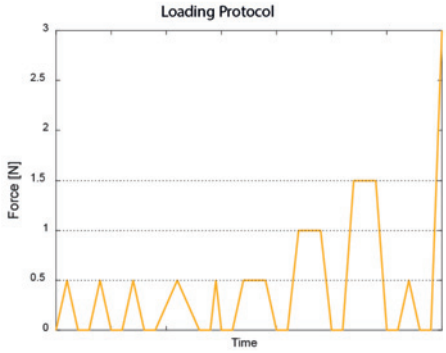

Figure 1: Loading Protocol. Numbers above each load denotes the loading rate for that cycle in mm/s. Time not to scale.

Acknowledgments: This research was funded by the National Science Foundation CAREER award (CMMI 1454412) to K. Myers.

References:

1. *Myers KM, Feltovich H, Mazza E, et al. J of Biomech 2015;48(9):1511-1523.*
2. *Vink J, Feltovich H. Semin Fetal Neonatal Med. 2016;21(2):106-112.*
3. *Nallasamy S, Yoshida K, Akins M, Myers K, Iozzo R, Mahendroo M. Endocrinology. 2017;158(4):950-962.*
4. *Yoshida K, Mahendroo M, Vink J, Wapner R, Myers K. Acta Biomater. 2016;36:195-209. *

[G-11.2]

MODELING LONGITUDINAL PLACENTAL PERFUSION USING MOLECULARLY TARGETED CONTRAST-ENHANCED ULTRASOUND

Dylan Lawrence[1], *Kristie Huda*[1], ***Carolyn Bayer***[1]

1 *Tulane University, New Orleans, USA*

Preeclampsia, affecting 5-8% of all pregnancies, is associated with reduced placental perfusion due to incomplete remodeling of the maternal spiral arteries1. Current understanding is that placental ischemia, resulting from this insufficient placental perfusion, is a major contributor in the progression towards maternal hypertension. Currently, there are no treatments for preeclampsia that increase placental perfusion and alter the course of the disease. The goal of this study is to develop methods to use molecularly targeted contrast-enhanced ultrasound (CEUS) imaging for the longitudinal, in vivo assessment of placental perfusion both during the development and treatment of preeclampsia. CEUS imaging detects gas-filled microbubbles introduced as intravascular tracers in a perfused tissue. Normally, the time-course change in contrast intensity within a region of interest is fit to a mathematical model, generating a time-intensity curve (TIC) which can then be used to calculate perfusion-related parameters2. This approach provides produces limited information about regionally-varying perfusion characteristics in the highly heterogeneous placenta. Using a pixel-wise TIC analysis, we have demonstrated the longitudinal assessment of perfusion in the placenta and surrounding tissue of pregnant Sprague Dawley rats. CEUS images were acquired on gestational days (GD) 14, 16, and 18 after a bolus injection of contrast microbubbles. Hemodynamic parameters were calculated from the TIC in each pixel and used to generate maps of the parametric indices of perfusion. By analyzing the TIC of each pixel in the image data, we are able to quantify changes in mean and variance of blood flow rates in egional anatomy (placental arterial vessels, labyrinth, and maternal spiral arteries). The average blood flow rate in the placenta increased from GD14 to 18, while variance decreased. We are implementing these methods in the reduced uterine perfusion pressure (RUPP) rat model of preeclampsia, using microbubbles targeted to αvβ3, an integrin expressed by endothelial cells during angiogenesis. The developed methods could provide new knowledge of normal and pathological perfusion characteristics of the placenta.

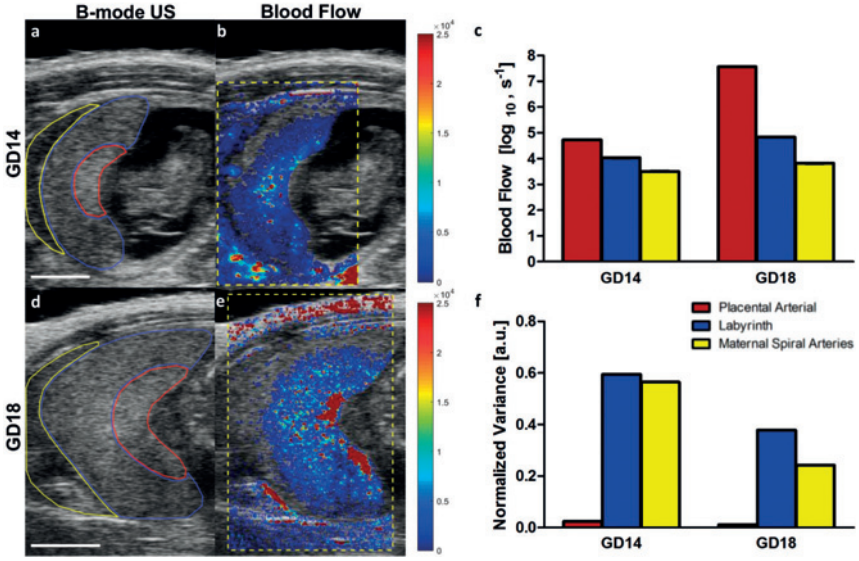

Figure Caption: Representative B-mode ultrasound (a, c) and superimposed pixel-wise CEUS-derived parametric images of relative blood flow (b, d) in the placental vasculature on GD14 (top row) and GD18 (bottom row). (e) Mean of perfusion in specific anatomical regions of interest. (f) Variance of perfusion in specific anatomical regions of interest. Scale bars = 3 mm.

Acknowledgments: We thank funding through the Louisiana Board of Regents Graduate Research Fellowship (DJL) and NIH P20GM109036 (KH, CLB) for support.

References:

1 *Kaufmann, P., et al. Biology of Reproduction, doi:10.1095/bioreprod.102.014977 (2003).*
2 *Strouthos, C., et al. IEEE Transactions on Ultrasonics Ferroelectrics and Frequency Control, doi:10.1109/tuffc.2010.1550 (2010).*

[G-11.3]

COMPUTATIONAL MODELS OF HUMAN PREGNANCY FROM A COHORT OF PATIENTS AT HIGH RISK FOR PRETERM BIRTH

*Andrea Westervelt[1], Joy Vink[2], Mirella Mourad[3], **Kristin Myers**[1], Erin Louwagie[1]*

1 *Columbia University, New York, USA*
2 *Columbia University, Obstetrics and Gynecology, Irving Medical Center, New York, USA*
3 *Columbia University, Irving Medical Center, New York, USA*

One in nine babies are delivered preterm in the US each year, totaling over 450,000 preterm births [1]. The preterm birth (PTB) rate has not significantly decreased in part because not much is known about the mechanics of pregnancy and it is challenging to perform studies during pregnancy. Our ultimate research goal is to reduce the PTB rate and the associated emotional and societal costs by providing a multi-scale computational framework to understand the growth, remodeling, and loading of the soft tissue structures supporting the fetus. In a clinical setting, we aim to predict the potential for stretch-activated onset of early labor, tissue overloading, and mechanical failure given a set of minimally-invasive clinical measures of maternal anatomy and tissue properties.

In this study we measured maternal anatomy and cervical stiffness from a cohort of women at high risk for preterm birth. Deidentified B-mode ultrasound images were obtained from 20 female patients with a high-risk profile, defined as cervical length on transvaginal examination of less than or equal to 20mm. All high-risk subjects were recruited from Columbia University, New York, United States Irving Medical Center (CUIMC). Cervical stiffness measurements were taken using a cervical aspirator device [2]. Each high-risk subject underwent an ultrasound exam at two different gestational timepoints: the first scan at 16-24 weeks and the second scan 4-9 weeks after the first. Six B-mode ultrasound images of the uterus and cervix were obtained to measure maternal anatomical dimensions [3] during each visit with the patient in a supine orientation. The six images included transabdominal sagittal views of the uterus and cervix, transabdominal transverse views of the uterus, and a transvaginal view of the cervix and lower uterine segment.

3D CAD models of each patient's anatomy were built using the patient's ultrasonic measurements from their 1st visit in Trelis 16.1 (csimsoft) using a custom parameterized script. These geometries were meshed in Trelis using tetrahedral (uterus, cervix, abdomen), and hexahedral (fetal membranes) elements. The meshes were then imported to FEBio for finite element analysis. Anatomical boundary conditions and material properties were prescribed [3], and contraction-magnitude intrauterine pressure 8.67 kPa was applied to the inner FM surface. For each patient, cervical material properties were informed by the cervical aspiration measurement. In each patient, a mechanical compliance index of the cervix was measured as a percentage of the cervical tissue above a 1.1 stretch threshold under the uniform IUP. This index reflects the structural response of the maternal anatomy and cervical material properties under a given load. The mechanical compliance index is compared to birthing outcomes, where it is hypothesized patients with a higher compliance index will deliver before patients with a lower compliance index.

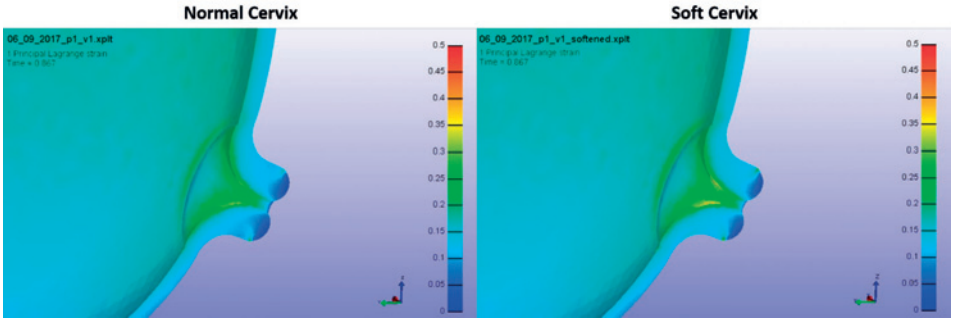

Figure Caption: Finite element analysis results of first principle strain in a single high-risk patient with comparison of normal (left) vs soft cervix (right).

Acknowledgments: The authors would like to thank the clinical team at CUIMC: Ronald Wapner, MD, Chia-Ling Nhan-Chang, MD, and Sabine Bousleiman. Research reported in this publication was supported by the NIH R01HD091153 to KM and 3UG1 HD040485-18S1 to MM. The content is solely the responsibility of the authors and does not necessarily represent the official views of the NIH.

References:

1. *https://www.who.int/news-room/fact-sheets/detail/preterm-birth*
2. *Badir et al, JMBBM 2013, 27: 143-153.*
3. *Westervelt et al. J Biomech Eng 2017; 139 (05).*

[G-11.4]
BURSTING THE VAGINA INTO TEARS

Jeffrey McGuire[1], *Woowon Lee*[2], *Kimani Toussaint*[2], ***Raffaella De Vita***[1]

1 *Virginia Tech, Blacksburg, USA*
2 *University of Illinois at Urbana Champaign, Champaign, USA*

During childbirth, the female pelvic floor endures substantial stretching that frequently results in tearing of the vaginal wall and the surrounding tissues and organs. Childbirth-related maternal trauma is the primary etiological factor contributing to pelvic floor disorders (PFDs). These disorders affect one out of three adult women, representing a major healthcare concern in the U.S. No quantitative methods that predict maternal trauma and the development of PFDs exists. In this study, we aim to determine the mechanical factors that can lead to tear formation in the vagina using rats as animal models. Toward this end, we conduct inflation tests up to rupture in conjunction with digital image correlation (DIC). We also use the second-harmonic generation (SHG) imaging to reveal the micro-mechanical mechanisms of vaginal tear formation.

Vaginal tracts were isolated from virgin Sprague-Dawley rats (n=18). They were then dyed blue and speckled white to create a high contrast pattern for non-contact strain measurements. Specimens were tested using a custom-built experimental setup that pressurized the vaginas via a syringe pump while allowing their free extension in the axial direction. Specimens were pre-conditioned and then inflated up to rupture. High-resolution images were captured during testing. The surfaces of specimens were tracked with a digital image correlation (DIC) system (Correlated Solutions Inc.) to calculate the Lagrangian strains in the hoop and axial directions.

Rupture of the vaginal wall consistently occurred in the central region away from the clamped ends. The major axis of each tear was oriented along the axial direction of the vagina. Hoop strains overall were larger than axial strains such that the average hoop Lagrangian strain at failure was 0.14 ± 0.10 compared to 0.05 ± 0.02 for the average axial Lagrangian strain. The average pressure at rupture was 15.7 ± 3.5 psi, corresponding to an average maximum hoop stress of 1118 ± 253 kPa and an average maximum axial stress of 553 ± 126 kPa. Images collected using SHG microscopy after mechanical testing showed that the collagen fiber orientation changes through the thickness of the specimens. However, fibers seemed to be preferentially aligned along the axial direction of the vagina. In regions that were close to the tear, the fibers appeared to re-orient along the edges of the tears. Moreover, delamination as well as collagen fiber bridging and rupture were observed near the tears.

The findings of this study advance current knowledge about the tear behavior of the vagina. This knowledge is crucial for the development of new prevention and treatment strategies for maternal birth trauma.

Acknowledgments: Funding was provided by NSF Grant No. 1511603.

[P 01]

REPRESENTATIVE KNEE KINEMATIC PATTERNS IDENTIFICATION USING WITHIN-SUBJECT VARIABILITY ANALYSIS

Mariem Abid[1], *Neila Mezghani*[1], *Youssef Ouakrim*[1]

1 *Centre de Recherche LICEF, TELUQ University, Montreal, Canada; Laboratoire Lio, Centre de Recherche du Chum, Montreal, Canada*

The purpose of this study is to perform data processing to identify, for a subject, robust representative knee kinematic patterns from a set of three-dimensional (3D) curves in the sagittal, frontal and transverse planes, recorded throughout several trials during walking on a treadmill. Our analysis takes into consideration the within-subject variability [1]. Indeed, knee kinematics measurements of each subject generate a family of curves that can differ from each other in magnitudes and timings, and are possibly affected by outliers. Standard deviation band [2] and functional boxplot [3] have been used for estimating curve variability. An outlier is any curve that is more than two standard deviations away from the mean or that is outside the maximum non-outlying envelope. However, the mean itself of the data can be greatly affected by outliers and the band-depth computation is very complex. In this study, we identify a representative gait of a given subject using the within-subject's evaluation for outliers' removal and reliable curves' selection. The proposed processing methodology encompasses steps of gait events detection, normalization, outlier detection and cycles' selection. Gait events detection algorithm centers around the location of local maxima values in the sagittal plane curve. Heel strike (HS) points are the first local minima after the local maxima and are specified as the start of each gait cycle. The resulting superposed time-normalized cycles constitute the observations to be considered for representative patterns. The within-subject variability is then estimated using boxplot which allow us to eliminate efficiently any outlier curve (defined outside the upper and lower limits). This is followed by a cross-validation, which consists to keep only the 15 curves having the highest Root mean Square Error (RMSE). These are considered as the most repeatable curves. In order to measure the reliability of the subjects' curves before and after processing, we computed the intraclass correlation (ICC) estimates and their 95% confidence intervals for knee kinematics of a multicentric dataset of 226 knee osteoarthrosis (OA) and asymptomatic subjects. The figure shows, for each plane, the frequency distribution of the ICC computed on the dataset before and after processing, for all the subjects. The graph shows that the subset of the 15 curves selected to represent the gait of the subject are perfectly reliable (ICC ≥ 0.7). The experimental results show that the proposed processing methodology allows to identify representative Knee Kinematic Patterns.

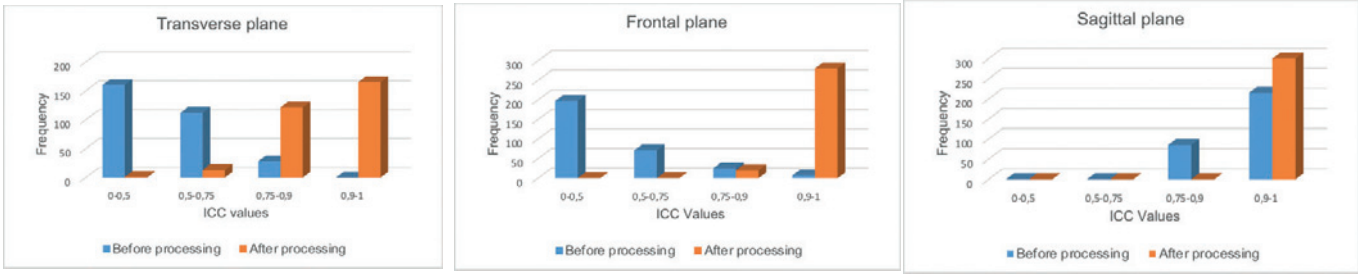

Figure Caption: ICC Values of knee kinematics for all subjects in all three planes.

References:

[1] T. Chau et al., «Managing variability in the summary and comparison of gait data» J Neuroeng Rehabil, vol. 2, 2005.
[2] D.R. Labbe et al., «Reliability of a method for analyzing three-dimensional knee kinematics during gait» Gait Posture, vol. 28, n° 11, pp. 170-174, 2008.
[3] I. Mechmeche et al., «Data correction to determine a representative pattern of a set of 3D knee kinematic measurements» IEEE- EMBC, 2016, p. 884–887.

[P 02]

AUTOMATED DETECTION OF BASAL CELL CARCINOMA IN A REAL-WORLD SAMPLE USING DEEP LEARNING

Julianna Ianni[1], *Rajath Soans*[1], *Sivaramakrishnan Sankarapandian*[1], *Ramachandra Vikas Chamarthi*[1], *Theresa Feeser*[1], *Thomas Olsen*[2]

1 *Proscia, Philadelphia, USA*
2 *Dermatopathology Lab of Central States, USA*

Review of H&E-stained slides is the standard diagnostic procedure for skin lesions and requires inspection under a microscope, performed by a pathologist or dermatopathologist. This process is time-consuming, particularly in cases in which the diagnosis is challenging, and the slide must be sent to an expert for further review. A system which can pre-sort images of scanned slides and route them to the appropriate expert for diagnosis could shorten the time to diagnosis both challenging and typical cases. Deep learning has previously been applied to problems in digital pathology, but typically on datasets which are pre-selected to contain only a small subset of diagnoses or variables present in a lab practice, which does not simulate real world conditions.1-2 Digital pathology presents several challenging aspects for deep learning, namely large image sizes and the wide amount of variation in the data.3 Furthermore, diagnosis in the subfield of dermatopathology presents significant challenges even for humans.4 Basal cell carcinoma (BCC) is one of the most commonly diagnosed pathologies in dermatopathology. Fig. 1a shows an example scanned whole slide image (WSI) from a skin biopsy with regions of basal cell carcinoma (BCC) annotated. A zoomed-in region of the pathology is shown in Fig. 1b. In this study, a convolutional neural network (CNN) for automatic detection of BCC among the diverse caseload of a dermatopathology lab. It is designed to take as input any slide (representing one of the hundreds of pathologies) seen in a dermatopathology practice, and output a classification into two classes: 1) BCC, all subtypes and 2) non-BCC, representing any other pathology, or lack of any pathology present. We collected 4560 WSIs of H&E-stained skin lesion specimens, including 2000 slides consisting of a lab's entire dermatopathology case volume over a period of time. The WSIs were randomly divided into training, validation and testing sets with a 70/15/15 split, and results are reported in the test set, which contains 55 unique diagnoses in the non-BCC class. Class balancing was implemented during training to account for different amounts of data belonging to the two classes. Results of the WSI-level classification demonstrate that the CNN is able to differentiate BCC from other pathologies with a class-balanced accuracy of 92.8%, sensitivity of 92.3% and specificity of 93.3%. Fig. 1c shows the ROC curve, and Fig. 1d depicts example patches from correctly- and incorrectly-classified WSIs. These results demonstrate that CNNs are capable of distinguishing between very similar WSIs, learning a class-separating boundary even in the presence of a wide range of real-world variation, and a very large number of pathologies. Pathology practices can potentially make use of such pre-sorting CNNs to improve lab efficiency, shortening the time to diagnosis and any necessary treatment.

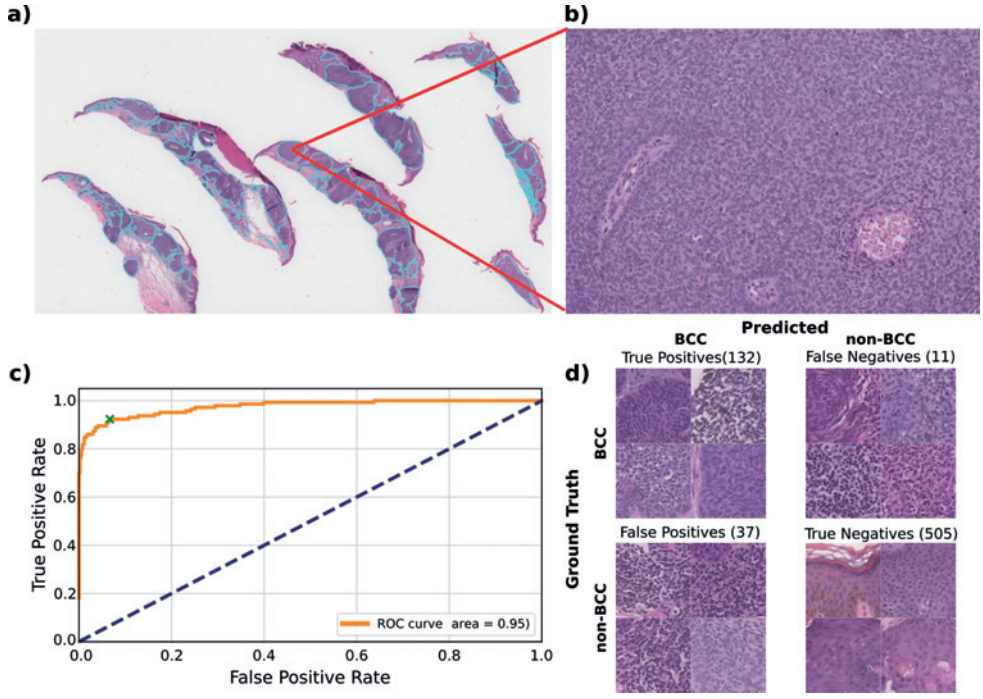

Figure Caption: a) A whole slide image (WSI), with regions of basal cell carcinoma (BCC) annotated. b) zoomed-in region of BCC. c) ROC curve for classification of (BCC) vs. other pathology, with green x indicating the optimal threshold d) Example image patches from WSIs with true positive, true negative, false positive and false negative classification.

Acknowledgments: The authors would like to thank Joel Crockett, MD, for expertise in annotation of images.

References:

1. *Hart SN, et al. Classification of melanocytic lesions in selected and whole-slide images via convolutional neural networks. J Pathol Inform 2019;10:5.*
2. *Olsen, TG, et al. "Diagnostic performance of deep learning algorithms applied to three common diagnoses in dermatopathology." J Pathol Inform 2018;9.*
3. *Simone L. Van Es, Digital pathology: semper ad meliora. Pathology, 2019;51:1, pp. 1-10.*
4. *Claudia Mello-Thoms, et al. Perceptual Analysis of the Reading of Dermatopathology Virtual Slides by Pathology Residents. Arch. Pathol. Lab. Med 2012;136:5, pp. 551-562.*

[P 03]

TOWARDS PARTICLE TRACKING VELOCIMETRY OF CELL FLOW IN DEVELOPING TISSUE USING DEEP NEURAL NETWORK

Yukitaka Ishimoto[1], *Tomoaki Watanabe*[2]

1 *Akita prefectural University, Dept. of Mechanical Engineering, Yurihonjo, Japan*
2 *Akita prefectural University, Yurihonjo, Japan*

In regenerative therapy or, in a broader sense, medical research, measurements of cellular dynamics in living body have been paid much attention in recent years, because they provide deeper insight on tissue engineering and a deeper scientific understanding of living body. Among measurements of such dynamics, those of cell motility or cell flow play a key role for elucidation of tissue/organ morphogenesis. To perform the measurements, or more specifically to track individual cells, it is critical to establish precise detection of individual cell positions and correspondence between them at different timepoints. These demands are reflected in recent developments in the field, for example in the intelligent image-activated cell sorter [1]. Recognition and sorting of cells are becoming tractable through such emerging technologies, yet a general platform for measurements on cell positions and cell tracking have been anticipated.

Difficulties of such measurements lie chiefly on cell heterogeneity and autonomy upon which one may not naively assume linearity of their movements and may assume cell-specific events such as cell divisions and deaths. In addition, in confluent cell system like epithelium, cells are densely packed and even cell nuclei are toughing in acquired images when the resolution is insufficient, which is often the case with live-imaging.

In this work, we aim at establishing a method of particle tracking velocimetry (PTV) for four-dimensional cell flow by using deep neural network model (DNN) of machine learning. We focus on precise detection of cell nucleus positions particularly in a very confluent situation, which would enable us to apply not only to the fly case but to broader morphologically changing tissues. That is, as an example of intriguing cellular dynamics, we consider morphogenesis of fly wing in its pupal stage, when cells nontrivially exhibit inhomogeneous and autonomous behaviours. Nontriviality means that, for instance, Navier-Stokes equation cannot be directly applied onto the cell flow, nor can conventional methods of flow visualisation. An implementation of this spot detection to PTV and an extension of DNN to recurrent neural network model (RNN) will also be discussed.

Acknowledgments: This work is supported by JSPS KAKENHI (Grants-in-Aid for Scientific Research) Grant Number 17K00410 and 17KK0007.

References:

[1] Nitta, N., et al. (2018) Intelligent Image-Activated Cell Sorting, Cell 175, pp. 266.

[P 04]

CLASSIFICATION OF ELDERLY FALLERS AND NON-FALLERS USING FORCE PLATE PARAMETERS FROM GAIT AND BALANCE TASKS

Ashirbad Pradhan[1], *Usha Kuruganti*[1], *Victoria Chester*[1]

1 *Andrew and Marjorie McCain Human Performance Laboratory, University of New Brunswick, Fredericton, Canada*

Accidental falls are a major health concern among older adults [1]. The advent of advanced machine learning algorithms has found its application in different biomedical fields. Previous research classifying elderly fallers and non-fallers using such algorithms have used force platforms to assess postural control [2,3]. Although force plates are considered the "gold standard" for objective balance and gait assessment [4], the studies related to identifying fallers are limited and the results are diverse due to variation in task routines and classification methods [3]. Certiain force plate parameters might be a better classifier of falls [2]. Research analysing the performance of different classification algorithms based on these force plate parameters from balance and gait tasks is warranted to determine optimal classification methods. The purpose of this study was to compare the accuracy of different classification models for identifying elderly fallers using force plate parameters measured during balance and gait tasks. 59 non-fallers (NF) and 41 fallers (F) performed balance and gait tasks on a walkway with embedded force plates (Kistler Instruments, Winterhur, Switzerland). Balance tasks involved semi-tandem stance with eyes open and a narrow stance with eyes closed for 30 seconds and gait tasks involved the participants walking 6 times on the walkway. The force plate parameters included 3D GRF-time data and COP displacement/velocity data. Using these data as input, five different classification algorithms were used to build models: Naïve Bayesian (NB), Artificial Neural Network (ANN), Linear Discriminant Analysis (LDA), Support Vector Machine (SVM) and k nearest neighbours (kNN). The LDA classifier based on parameters from a combined gait and balance tasks resulted in a maximum accuracy of 84.95% for classifying faller/non-faller categories. Combining force plate parameters from gait and balance tasks resulted in higher classification accuracies of elderly fallers (>75%) for all of the algorithms (Table 1). These accuracies are comparable to previous classification studies using force plate parameters [2,3]. The results demonstrate that the LDA classifier which is a simple algorithm without issues of any overfitting has higher accuracy than more complex methods such as SVM and ANN. The findings of this study suggest that high accuracy of identifying elderly fallers can be obtained using force plate parameters.

	Gait (41F, 58NF)	Balance (39F, 54NF)	Combined (39F, 54NF)
LDA	82.05	64.52	84.95
NB	78.79	66.67	80.65
SVM	73.74	68.82	75.27
kNN	75.76	67.74	77.42
ANN	75.76	64.52	82.80

Table 1 Classification Accuracy (%) of different algorithms during gait and balance tasks

Acknowledgments: The authors acknowledge the valuable help of Sana Oladi, M.Sc who contributed to data collection in this work.

References:

1. *Delbaere K et al. (2010). J Amer Ger Soc, 58(9), 1679-1685.*
2. *Pajala, S et al. (2008) J Gerontol Series A: Biol Sci and Med Sci, 63(2), 171-178.*
3. *Piirtola, M et al. (2006). Gerontology, 52(1), 1-16.*
4. *Hamacher, D et al. (2011) J Royal Society Interface, 8(65), 1682-1698.*

[P 05]

PREDICTING JOINT KINEMATICS FROM SENSORS WITH VARYING BODY-SEGMENT ALIGNMENTS

Wolf Thomsen[1], *Reed Ferber*[2], *Eni Halilaj*[1]

1 *Carnegie Mellon University, Pittsburgh, USA*
2 *University of Calgary, Calgary, Canada*

Deep learning shows great promise for solving many problems in biomechanics, such as more robust kinematic measurements from inertial measurement units (IMUs). However, a potential drawback is their reliance on large training datasets in order to avoid overfitting. Data augmentation is a successful approach for synthetically introducing expected real-world variations, thereby training more generalizable models. Specifically, in the case of body-worn IMUs, a significant amount of data heterogeneity is due to differences in sensor-to-segment orientation. Therefore, with this work we demonstrate that data augmentation, which replicates sensor-to-segment orientation variability, leads to more generalizable predictive models.

We used existing optoelectronic data from 1015 subjects running on a treadmill for 20 to 60 seconds [1]. After simulating IMU data for the thigh and shank, we trained two groups of bidirectional long short term memory (LSTM) neural networks to predict knee joint angles from the inertial data. We developed two models: (1) a default model trained on consistent sensor orientations derived from markers, and (2) an augmented model trained on randomly altered sensor orientations. We assigned 812 subjects to the training dataset, 101 to the validation dataset, and 102 to the test dataset. We extracted multiple samples of uniform sequence length from each subject, which led to 5968 training samples, 742 validation samples, and 602 test samples.

The results show that the augmented model performed significantly better than the default model in predicting from different virtual sensor positions ($5.53 \pm 1.93°$ vs. $6.99 \pm 2.99°$, $p < 0.0001$; Figure 1). The augmented model also generalized better to the default data ($4.86 \pm 2.10°$ vs. $5.08 \pm 2.25°$, $p < 0.0001$; Figure 1). We expect the predictive accuracy to improve further after performing thorough outlier detection in order to leave out subjects with unusual gait kinematics (e.g., due to extreme pathology or large differences in data collection protocols).

Other fields, such as computer vision, have demonstrated that data augmentation is essential for robust machine learning models. The augmentation implemented here addresses one of the major forms of uncertainty when using wearable sensors. Additional forms of augmentation (e.g., soft tissue movement) could result in more robust models and accelerate the adoption of IMUs for ubiquitous patient monitoring and studying biomechanics in natural environments.

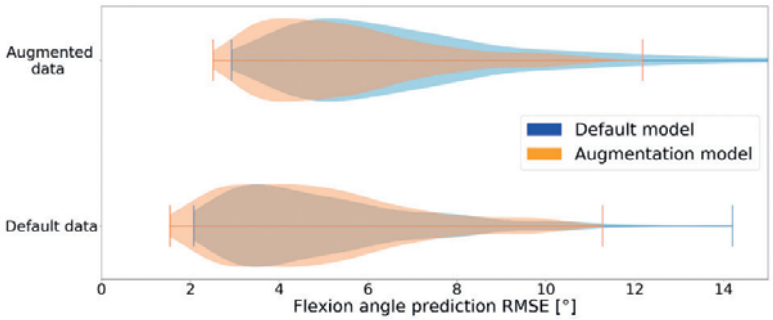

Figure caption: Figure 1: Distribution of the prediction error. The default model was trained on data from the default sensor orientation. The augmentation model was trained on data with randomly rotated measurement axes. Both models were tested on unseen subjects.

Acknowledgments: We thank the Running Injury Clinic from the University of Calgary, Canada for their assistance with the data transfer and the Pittsburgh Supercomputing Center for providing computing resources.

References:

[1] Osis, S.T., et al. (2015) Comput Methods Biomech Biomed Engin. 18.10:1108-1116.

[P 06]

VISUALIZATION OF SYMBOLIC MUSICAL RHYTHMS: RECENT METHODS AND APPLICATIONS

Godfried Toussaint[1]

1 *New York University, Abu Dhabi, United Arab Emirates*

Methods for visualizing symbolically notated musical rhythms are reviewed. Some of these methods were covered in a previous paper [1]. However, the focus here is on comparing methods absent in [1] with the previous methods in terms of their suitability for a wide range of applications. All the methods take as input a binary sequence of symbols, and produce as output a transformation of the input into a higher dimensional geometric representation. The binary symbols of the input correspond to elements that are either sounded or silent, and have unit time duration. The methods covered are the following. Mnemonic notation is perhaps the oldest form of transmitting rhythms from one generation to the next. It is not visual, but is likely the precursor of visual notation. The method uses syllables of language to capture the duration of the elements in the string. An example from the ancient Arabic tradition is Tanan Tanan Tananan Tan Tananan, where the Ta denotes the sounded pulse and the remaining syllables provide the durations between the sounded pulses. Box notation is popular among ethnomusicologists [2] and is a more precise representation of the mnemonic representation. Instead of syllables, it uses two arbitrary symbols, such as "X" and "." to denote the sounded and silent pulses, respectively. The above rhythm becomes [x..x..x…x.x…]. Box notation is also preferred by composers of minimalist rhythmic music such as Steve Reich [2]. Alternating-hands box notation is a variant useful for learning drumming technique. Spectral notation and TEDAS notations are favored in linguistic studies of speech. Schillinger notation codes the durations between sounded pulses and is useful for mathematical analysis of rhythms. Inter-onset-interval histograms display the frequency of each duration interval between pairs of sounded pulses. Circular notation maps box notation onto a circle for cyclic rhythms. Polygon notation extends circular notation by connecting adjacent sounded pulses with lines, converting rhythms to convex polygons. Arc diagrams create semicircular arcs connecting patterns that are repeated in a rhythm. Phase space plots convert a rhythm into a 2-dimensinal polygon by mapping pairs of adjacent duration intervals into points in the plane. Tangle diagrams use concepts from knot theory to convert rhythms into knot diagrams.

Acknowledgments: Research supported by a grant from the Provost's Office of New York University, New York, United States Abu Dhabi, Abu Dhabi, United Arab Emirates in the United Arab Emirates

References:

1. *Y. Liu and G. T. Toussaint, "Mathematical notation, representation, and visualization of musical rhythm: A comparative perspective," International Journal of Machine Learning and Computing, Vol. 2, No. 3, 2012, pp. 261-265.*
2. *G. T. Toussaint, The Geometry of Musical Rhythm, CRC Press, Boca Raton, 2013.*

[P 07]

ESTIMATING SHOULDER MUSCLE FORCES OF THE SHOULDER COMPLEX USING STATIC OPTIMIZATION AND EMG-INFORMED NEUROMUSCULOSKELETAL MODELLING

Najoua Assila[1], *Claudio Pizzolato*[2], *Benjamin Michaud*[1], *David Lloyd*[2], *Mickaël Begon*[1]

1 *École de kinésiologie et des sciences de l'activité physique, Université de Montréal, Montreal, Canada*
2 *Gold Coast Orthopaedic Research, Engineering and Education (Gcore, Gold Coast, Australia), Menzies Health Institute Queensland, Griffith University, Southport, Australia*

The estimation of muscle contribution to joint moments is critical in the understanding of musculoskeletal pathologies. While several computer methods have been developed to estimate these internal loadings, this problem remains one of the major challenges in biomechanics, due to muscle redundancy. This problem is exacerbated in shoulder complex as muscles have the dual role of assuring a large range of mobility while maintaining glenohumeral joint stability. Whereas commonly used approaches (e.g., static optimization (SO)) often rely on predefined optimization criterion, calibrated electromyogram (EMG)-informed neuromusculoskeletal models also account for the excitation pattern of each individual. EMG-informed algorithms have shown more physiologically plausible estimates of hip and knee contact forces during gait [1,2] when compared to SO, but they have not yet been applied to the shoulder complex.

The objective of this study is to compare the EMG-informed algorithm performance to that of SO in the study of the upper limb. Marker trajectories (m=21) and EMG signals (n=10+3, surface and in-dwelling electrodes) were recorded for 40 healthy subjects during the lifting of a box with two different masses (6 or 12 kg). The subjects were asked to transfer the box between three shelves (hip, shoulder and eye levels). An OpenSim 3D upper limb generic model [3] was used to estimate the force distribution in the shoulder. The model included 8 degrees-of-freedom and 29 Hill-type musculotendon units. Joint generalized coordinates were estimated using inverse kinematics from the marker trajectories, and joint moments were calculated using inverse dynamics. The muscles forces were then estimated using SO and the EMG-informed algorithm from the Calibrated EMG-informed neuro-musculoskeletal toolbox (CEINMS) [4]. Since the muscle surrounding the glenohumeral contact are more prone to injury, we focused, as a first step, solely on this joint. The trials used for the model calibration represented a maximal mobility range for two possible loading conditions. For the execution step, we used the EMG-driven mode of CEINMS.

The preliminary results (1 subject) show that the forces obtained through the EMG-informed algorithm were generally larger than those obtained from SO, suggesting that this algorithm might be more representative of muscles co-contraction and their different possible synergies. Additionally, the tracking of the EMG data would implicitly enforce a non-dislocation constraint at the glenohumeral contact level, which would ensure a plausibly more physiological solution. The EMG-informed approach is also corrected with the EMG data, which tends to reduce the effect of errors related with kinematics acquisitions. Accordingly, using EMG-informed algorithms to evaluate muscle forces is promising to have a more comprehensive insight of muscle co-contraction and action around the shoulder, thus improving the understanding of musculoskeletal pathologies.

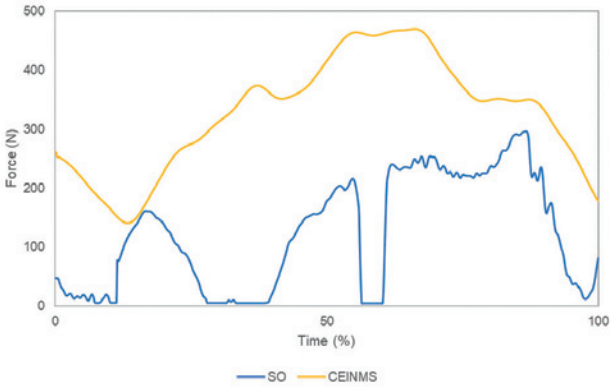

Figure 1: SO and CEINMS EMG-driven mode muscle force estimations for the anterior deltoid muscle.

References:

[1] Hoang, et al. (2018). Journal of Biomechanics, 80, 111-120.
[2] Hoang, et al. (2019). Journal of Biomechanics, 83, 134-142.
[3] Wu, et al. (2016). Journal of biomechanics, 49(15), 3626-3634.
[4] Pizzolato, et al. (2015). Journal of Biomechanics, 48(14), 3929-3936.

[P 08]

THE IMPACT OF THE HILL TYPE MUSCLE MODEL ON THE GLENOHUMERAL JOINT REACTION FORCE

Maximilian Aurbach[1], *Franz Süß*[1], *Sebastian Dendorfer*[2]

1 *Laboratory for Biomechanics, Ostbayerische Technische Hochschule (OTH) Regensburg, Germany; Regensburg Center of Biomedical Engineering, Oth and University Regensburg*

2 *Laboratory for Biomechanics, Ostbayerische Technische Hochschule (OTH) Regensburg, Germany; Regensburg Center of Biomedical Engineering, Oth and University Regensburg; Laboratory for Biomechanics, Ostbayerische Technische Hochschule (OTH) Regensburg, Germany*

Musculoskeletal models of the shoulder complex enable the recruitment pattern prediction of the involved structures and allow insights into the forces acting on the glenohumeral (GH) joint. While these models are valid for abduction up to 90° humeral elevation [1], they show a divergence from experimental data of the muscle activities [2] and forces [3] for angles >90°. With the shoulder complex experiencing one of the largest ranges of motion, the three element Hill type model consequently has a severe impact on the muscle recruitment. The aim of this work is to investigate the resultant GH joint reaction force of a musculoskeletal model of the shoulder (AnyBody™) with a parameter study on several constants of the Hill model for humeral abduction >90°. An experimental study was conducted where 10 subjects performed abduction of the humerus up to 140°. The kinematics were recorded with a motion capture system. An alteration of parameters was computed for each trial: muscle model with constant strength, Hill model, Hill model with shifted onset of the passive element, variation in strength and variation of ideal muscle length ± 20%. All modifications of the Hill model resulted in an increased GH joint reaction force after 90° abduction. Figure 1 exemplifies the reaction force of one subject. The combination of the passive stiffness and increased strength leads to forces up to 150 %BW. With a shift of the onset point of the stiffness, the forces drop to 75 %BW, which correlates with data from literature. The Hill type muscle model has two effects on the GH joint reaction force:

1. The passive stiffness introduces a new set of forces into the equilibrium equations.

2. With a change in strength in dependency of the elongation of each muscle element, the solver distributes the load differently. This shifts the acting moments and thus forces on the joint.

Both factors lead to an increase in the resultant GH joint reaction force for humeral abduction >90°, while the later seems to be the relevant criterion. We propose that the Hill type model is a key parameter for musculoskeletal models of the shoulder.

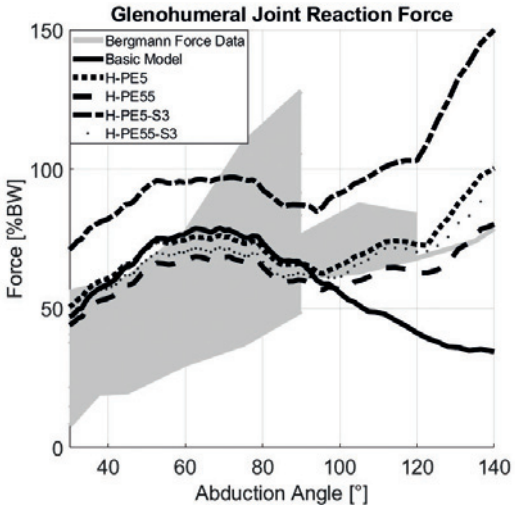

Figure 1: Resultant GH joint reaction force of one subject for five different models. H = Hill Model, PE5 = passive element with standard onset, PE55 = passive element onset shifted by factor ten, S3 = strength index increased by factor three, Grey = reference data [3]

Acknowledgments: Funding from the EFRE, Ziel ETZ BY-CZ 2014-2020 (Interreg V) (Pr. 038) BayWISS is gratefully acknowledged.

References:

[1] Nikooyan AA et al., J Biomech,43:3007–14, 2010.
[2] Wickham J et al., J Electromyogr Kinesiol,20:212–22, 2010.
[3] Bergmann G et al., Charité Universitaetsmedizin Berlin "OrthoLoad"; 2008.

[P 09]

WHAT IS ACCEPTABLE AGREEMENT IN KINEMATICS AND KINETICS FROM TWO INDEPENDENT OPENSIM MODELS OF FES ROWING?

Vishnu Chandran[1], *Rebecca Lambach*[2], *Gary Beaupre*[2], *Saikat Pal*[1]

1 *New Jersey Institute of Technology, Newark, USA*
2 *Va Palo Alto Health Care System*

Introduction: Computational models are widely used to study human movement biomechanics. These models provide additional insights that are difficult or infeasible to obtain using only experimental methods. Ideally, a computer model should be validated with experimental testing; however, such validation is often infeasible in musculoskeletal modeling. When experimental validation is not possible, the effects of modeling choices and assumptions on the accuracy of the results remain unclear. OpenSim, a free software for musculoskeletal modeling, provides best practices for choices and assumptions during the different steps of model development, including scaling, inverse kinematics, and inverse dynamics [1]. However, differences exist in OpenSim models developed by multiple research groups, in part due to differing modeling preferences and priorities. It is important to quantify the range of results due to differing modeling assumptions. The goal of this study was to quantify the range in model-predicted kinematics and kinetics from two independently developed OpenSim models of functional electrical stimulation (FES) rowing. We hypothesized that there is acceptable agreement (difference <20%) in results from the two models.

Methods: We developed two OpenSim models independently (Veterans Affairs, VA and New Jersey Institute of Technology, Newark, United States, NJIT; Figure 1A). The models were created from identical experimental data and a published OpenSim model [2]. The experimental data were from FES rowing of five subjects with spinal cord injury (SCI) [3]. Each site made modeling assumptions based on their experience and preferences. There were differences in geometric representation and definition of the local axes of the rower. The VA model defined the seat-pelvis as a weld joint, whereas the NJIT model defined the seat-pelvis as a custom cardan (rotational) joint. The VA model represented the knee joint with one degree of freedom (flexion-extension), whereas the NJIT model included flexion-extension and internal-external rotations. The models were scaled using different model marker sets and run through Inverse Kinematics and Inverse Dynamics modules in OpenSim.

Results: Average differences in kinematics from the two OpenSim models were <12% for the knee and ankle joints (Figure 2B). At the hip joint, average kinematic differences were larger (up to 49%). Average differences in kinetics were <19% for the hip, knee, and ankle joints. The sources of these differences, ranked according to their contributions, were the definition of the pelvis with respect to the seat, a rower's local axis definitions, scaling factors, and choice of model marker sets.

Discussion: Our results corroborate our hypothesis for the knee and ankle kinematics, and for the hip, knee, and ankle kinetics. However, average kinematic differences were greater at the hip joint due to differences in definition of the pelvis joint. Developing best practices will help define acceptable agreement in results for computer models of FES rowing.

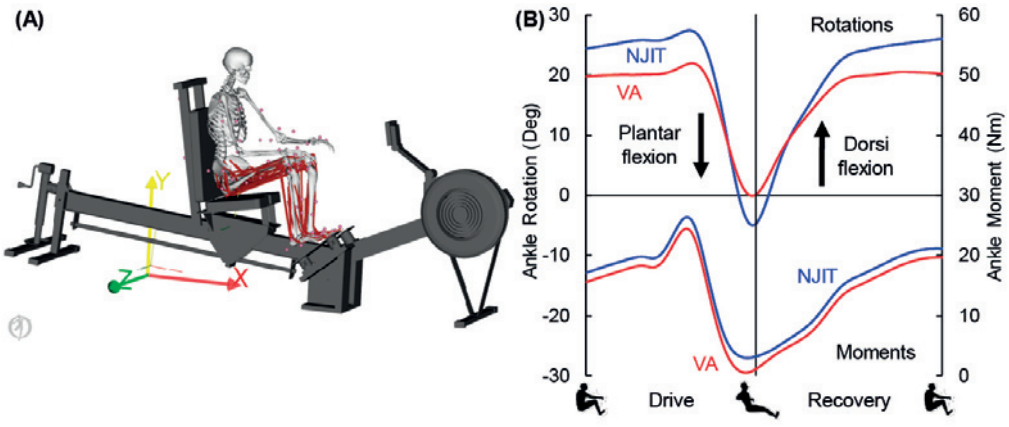

Figure 1: OpenSim model of a representative SCI subject during FES rowing (A), and (B) ankle dorsi/plantar flexion-extension angles and moments from the VA and NJIT models of that corresponding subject.

References:

1) *Hicks J, et al, J Biomech Engr, 137(2), 2015;*
2) *Lai A, et al, Annals of Biomed Engr, 45(12), 2017;*
3) *Lambach R, et al, J Spinal Cord Med, 2018.*

[P 10]

HANDRIM FORCES AND MOMENTS PREDICTION DURING MANUAL WHEELCHAIR PROPULSION USING INERTIAL SENSORS

Aiman Feghoul[1], *Rachid Aissaoui*[2], *Felix Chénier*[3]

1 *École de technologie supérieure, Montreal, Canada; Laboratoire D'imagerie et D'orthopédie*
2 *Centre de Recherche du Chum; École de Technologie Supérieure; Laboratoire de Recherche En Imagerie et Orthopédie, Montreal, Canada*
3 *Université de Québec À Montréal, Montreal, Canada*

Manual wheelchair (MWC) propulsion is a functional activity involving repetitive and strenuous movements, which increases the risk of developing shoulder impairments. During MWC propulsion, shoulder pain and overuse injuries are related to the high level of glenohumeral joint moments [1]. Moreover, there is also a strong correlation between handrim reaction forces and the increase of shoulder joint moments [2]. Load acting at the handrim level can be measured inside laboratory with dynamic force platforms (DFP).

The aim of this study is to predict the vertical and the anterior-posterior component of handrim reaction forces (Fx and Fy), and the medial-lateral component of handrim moment (Mz) during MWC propulsion outside laboratory.

Eleven able-bodied subjects propelled a MWC along a 20-meter corridor. Three inertial measurement units (Xsens, Inc), were used to measure the 3D linear acceleration as well as 3D angular velocity of both wrists and of the pelvis at 120 Hz. Handrim reaction forces and moments were measured by two SmartWheel (Three Rivers, Inc) at 240 Hz. A new method based Hammerstein-Wiener identification has been developed in order to predict the three dependant variables Fx, Fy and Mz from the inertial data. The test and the validation of the new method were assessed using the Leave-one Subject-out approach [3].

The Root Mean Square were equal to 5.8N, 7.6N and 1.6N.m for Fx, Fy and Mz, respectively.

The results obtained by our method will allow monitoring load acting at handrim level during daily activities of MWC users without the need for using DFP.

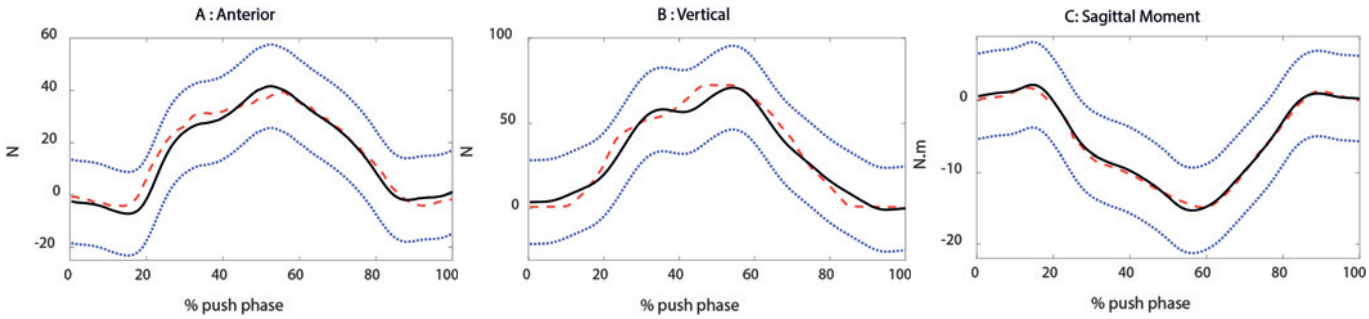

Figure Caption: Predicted (red) and Measured (Black) of a typical subject during MWC propulsion. A in anterio-posterior direction (Fx), B in vertical direction Fy and C in sagittal plane moment (Mz). Standard deviation correspond to the measured variables.

Acknowledgments: Fond de recherche du Québec en nature et technologie (FQRNT). Regroupement stratégique INTER (Ingénierie de technologies interactives en réadaptation).

References:

[1] *Chow J.W., Levy C.E. (2011). Wheelchair propulsion biomechanics and wheelers' quality of life: an exploratory review. Disability and Rehabilitation: Assistive Technology, 6(5): 365-377.*
[2] *Desroches, G., R. Aissaoui and D. Bourbonnais (2008). Relationship Between Resultant Force at the Pushrim and the Net Shoulder Joint Moments During Manual Wheelchair Propulsion in Elderly Persons. Archives of Physical Medicine and Rehabilitation 89(6): 1155-1161.*
[3] *Ding, D., S. Hiremath, Y. Chung and R. Cooper (2011). Detection of Wheelchair User Activities Using Wearable Sensors, Berlin, Heidelberg, Springer Berlin Heidelberg.*

[P 11]

MOMENTS IN THE LOWER LIMBS' JOINTS DURING VOLUNTARY POSTURAL SWAYS IN SAGITTAL AND FRONTAL PLANE

Malgorzata Kalinowska[1], *Malgorzata Syczewska*[1], *Ewa Szczerbik*[2]

1 *The Children's Memorial Health Institute, Warszawa , Poland*
2 *The Children's Memorial Health Institute, Kinesiology Lab, Warszawa, Poland*

Introduction: The voluntary inclinations of the body depend on postural control and cause the load in lower limbs' joints which are estimated by external joints' moments. The aim of the study is to evaluate the range of joints moments, their symmetry and correlations between them and Center of Mass (COM) movements in two directions (in sagittal and frontal plane).

Material and Methods: 17 women (50-62 years old) without any balance problems (all orthopaedic and neurological problems were exclusion criteria) who regularly exercise sport activity participated in this study. All subjects performed two balance tests (lasting 30 sec. each) on two Kistler platforms (one leg in one platform), consisting on maximal voluntary inclinations of the body in sagittal plane (anterio-posterior movements, AP test), and in frontal plane (medio-lateral movements, ML test), both with eyes open, during which ground reaction forces were measured. During these tests also COM movements were measured with VICON System (Full Body Pug-In-Gait) and the hip, knee and ankle moments were calculated by Polygon software. After that the ranges of COM movements and ranges of joint's moments were calculated. As all variables were normally distributed and there were no differences between appropriate parameters for right and left leg, parameters for both legs were pooled together and new ranges of moments and the symmetry index were calculated. Finally Spearman's correlations between joints moments and ranges of COM movements were evaluated. Statistical calculations were performed using Statistica (cut-off level 0.05).

Results: In AP test the greatest moments were in ankles (0,78 Nm/kg) and knees (0,69 Nm/kg) in sagittal plane, these moments were symmetrical (symmetry index about 13%) and the correlations between ankles and hip and ranges of COM movement were significant. In ML test the highest moments were in ankles in sagittal plane (0,57 Nm/kg), but hip moments in frontal plane also occurred to be hight (0,43 Nm/kg), in addition, hip and knee moments in sagittal plane were closed to each other and also high (0,35-0,39 Nm/kg); symmetry was worse than in AP test and generally no correlation between ranges of COM movements in frontal plane and joints moments was found.

Discussion: Regardless of the direction of the sway, the greatest moments are transferred in the ankle in sagittal, but the load on the hip and knee is also high, especially in ML test, where the moments in sagittal and frontal plane are similar. These results may be helpfull while designing the hip and knee endoprostheses and for the selection of exercises during rehabilitation.

Acknowledgments: STRATEGMED3/306011/1/NCBR/2017

[P 12]

ANATOMICAL CORRECT HUMAN HAND NEUROMUSCULOSKELETAL MODEL FOR VIRTUAL REHABILITATION

Jumana Ma'touq[1]

1 *Institute of Automatic Control, Hannover, Germany; Gottfried Wilhelm Leibniz Universität Hannover, Hannover, Germany*

Virtual reality (VR) is defined as an environment consists of interactive computer simulations and sensors that gives the user the feeling of being mentally immersed or present in a virtual word [1]. This technology has opened up entirely new application domains that were not possible before such as applications for physical rehabilitation and motor control research. Using VR in neurorehabilitation provides many advantages such as real-time performance feedback, independent practice, stimulus control and consistency, stimulus and response modifications that are contingent on a user's physical abilities, and a safe testing and training environment [2]. The aim of this work is to develop an anatomical correct human hand neuromusculoskeletal model for neurorehabilitation training in virtual reality. Such models will enhance the performance of the training and the evaluation of patient performance. The complete system consists of a mathematical model integrated in VR environment (Figure 1). The mathematical model consists of three models corresponding to the three anatomical levels; skeletal (kinematic and dynamic), musculotendon (kinematic and dynamic), neural (human motor control). The skeletal kinematic model is a highly accurate model that includes the five digits and the palm arc with a total of 26 degree of freedom [3]. The skeletal dynamic model predicts the passive torque due to the passive joint properties and the link torque due to gravitational and inertial forces are modelled. Musculotendon kinematic model includes all extrinsic and intrinsic hand muscles which are represented by 47 musculotendon paths [4]. The output of musculotendon kinematic model is fed into musculotendon dynamic model to calculate forces, torques, and muscle activation. The mathematical model is implemented in MATLAB/Simulink (The MathWorks Inc., USA) and a 3-D visualisation is implemented in Unity (Unity Technologies, USA). Future work will address 1) the completion and validation of the complete human hand neuromusculoskeletal model and motor control and 2) the integration of the 3-D model and the VR.

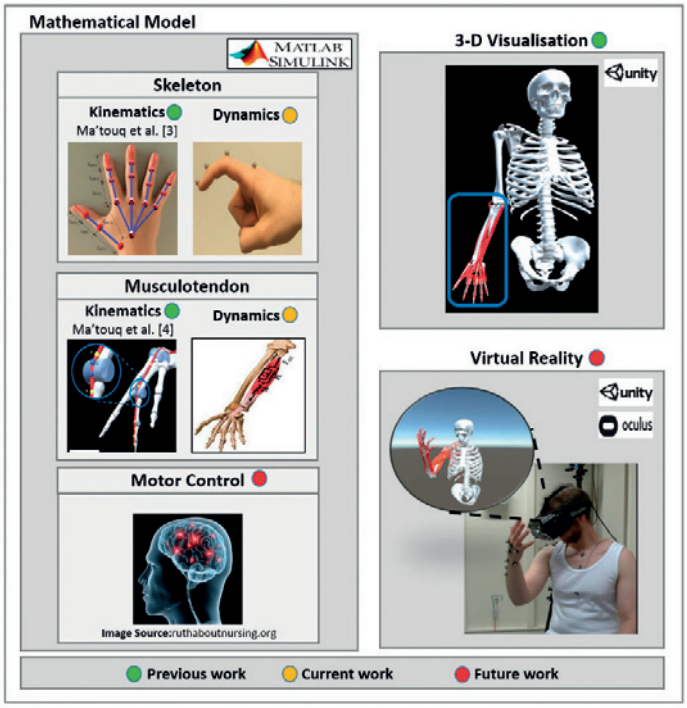

Figure1: " The overall neuromusculoskeletal model for virtual rehabilitation"

References:

[1] Sherman W,and Craig A. (2002). Understanding virtual reality: Interface, application, and design. California: Morgan Kaufmann.
[2] Keshner, EA. (2004). Virtual reality and physical rehabilitation: a new toy or a new research and rehabilitation tool?. J Neuroeng Rehabil. 1:8.
[3] Ma'touq et al. (2018). Sub-millimetre accurate human hand kinematics: from surface to skeleton. CMBBE, 21(2):113-128.
[4] Ma'touq et al. (2019). A validated combined musculotendon path and muscle-joint kinematics model for the human hand. Revision submitted to CMBBE.

[P 13]

ON THE ROLE OF ANGULAR MOMENTUM DAMPING IN FOOT CONTACT STABILIZATION DURING DYNAMIC MOVEMENTS

Kei Kobayashi[1], *Ryotaru Hinata*[1], *Dragomir Nenchev*[2]

1 *Tokyo City University, Graduate School of Engineering, Tokyo, Japan*
2 *Tokyo City University, Department of Mechanical Systems Engineering, Tokyo, Japan*

In a previous work [1] we have proposed the Reaction Null-Space filter as a useful tool for extracting reactionless movement synergies for optimal postural balance during squat, sway and forward bend. In this work, we further develop the method by employing a multi-segment whole-body model in 3D that includes the trunk and the arms. With this model, it becomes possible to extract reactionless movement synergies for complex movement patterns in 3D, such as kicking or throwing a ball. We pay special attention to the body angular momentum and its rate of change. It will be shown that the rate of change stemming from the movements in the upper body, trunk and arms plays an important role in maintaining the stability of the contacts at the feet. We aim to verify the hypothesis that well-trained persons may employ an angular momentum damping synergy to maintain the stability of the foot contacts during highly dynamic movement patterns.

So far, only simple models have been employed to assess dynamic balance in biological motion [2]. Here, a complex model based on the rate of change of angular momentum is employed for the first time. As an experimental setup, we used an OptiTrack motion capture system with a TF-4060 force plate by Tec Gihan. The motion capture and force plate data were integrated via an inverse dynamics analysis software package. We captured and analyzed the data shown in the figure for an in-step kicking motion. The plots show the following contact stability indices: the ground projection of the center of mass (CoM), the extrapolated CoM (exCoM) [3], the center of pressure (CoP) and the enhanced centroidal moment pivot (eCMP) [4]. The rate of change of angular momentum (RCAM) is determined by the difference between the CoP and the eCMP.

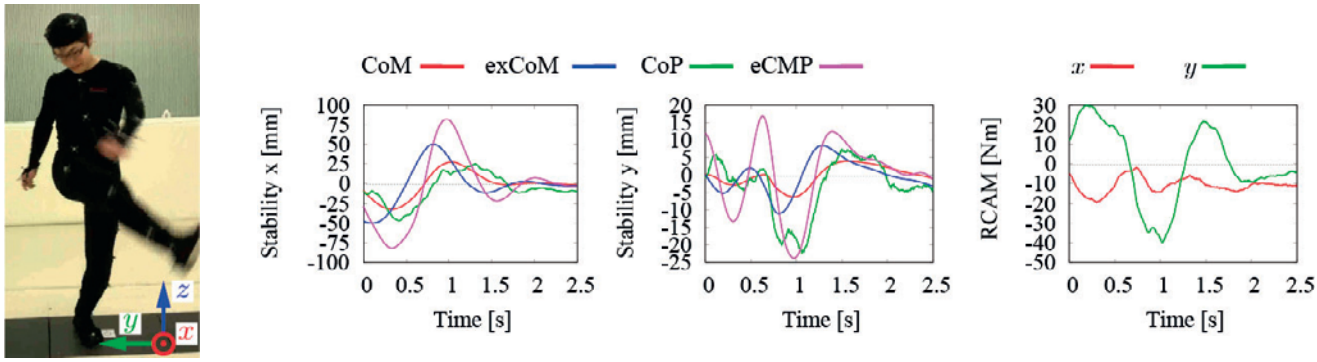

Figure Caption: Experimental data from the motion analysis of a complex dynamic motion pattern.

References:

[1] *Nenchev, D. N., Miyamoto, Y., Iribe, H., Takeuchi, K., & Sato, D. (2015). Reaction null-space filter: extracting reactionless synergies for optimal postural balance from motion capture data. Computer Methods in Biomechanics and Biomedical Engineering, 19(8), 864–874.*
[2] *Hoyet, L., & Multon, F. (2011). Comparison of models of dynamic balance in biological motions. Computer Methods in Biomechanics and Biomedical Engineering, 14(S1), 183–184.*
[3] *Hof, A. L., Gazendam, M. G. J., & Sinke, W. E. (2005). The condition for dynamic stability. Journal of Biomechanics, 38(1), 1–8.*
[4] *Popovic, M. B., Goswami, A., & Herr, H. (2005). Ground reference points in legged locomotion: Definitions, biological trajectories and control implications. The International Journal of Robotics Research, 24(12), 1013–1032.*

[P 14]

ASSESSMENT OF BODY WEIGHT GAIN ON THE PLANTAR PRESSURE DISTRIBUTION DURING GAIT IN PREGNANT WOMEN WITH NORMAL BODY WEIGHT, OVERWEIGHT AND OBESITY.

Dagna Swinarska[1]

1 Bialystok University of Technology, Faculty OF Mechanical Engineering, Bialystok, Poland

Introduction: Pregnancy is a period during which many significant changes occur in the woman's body [1,2]. The aim of the study is to assess the effect of weight gain on the distribution of under foot pressure in pregnant women with normal body weight, overweight and obesity. Material and method: 55 pregnant women participated in the study: 29 women with normal body mass and 26 overweight women and obesity at 11th, 25th and 38th weeks of pregnancy. The pressure distribution under the foot was registered using a pedobarographic system, under the following areas of the foot: forefoot, metatarsal head, lateral arch, medial arch and heel. Results: The BMI index before pregnancy was 21.8±1.3 kg/m^2 for women with normal body weight and 28.6±3.4 kg/m^2 for pregnant women with overweight and obesity. At 11th weeks of pregnancy the BMI index was 22.0±1.2 kg/m^2 in pregnant women with normal body weight and in women with overweight and obesity 28.8±3.2 kg/m^2. In the 25th week of pregnancy the BMI index was higher in both groups and amounted to: 23.5±2.0 kg/m^2 for women with normal body weight and 30.5±3.4 kg/m^2 for women with overweight and obesity. In the 38th week of pregnancy the BMI index was the highest 26.1±2.8 kg/m^2 for women with normal body mass and 32.8±4.0 kg/m2 for women with overweight and obesity. The results show that increased body weight affects changes in pressure distribution under the plantar side of the foot. In the 11th week of pregnancy, the pressure distribution values were higher in pregnant women with overweight and obesity under forefoot by 32.6% and lateral arch by 26.3%. In the 25th week of pregnancy, the pressure distribution values underfoot were average higher in pregnant women with overweight and obesity compared to pregnant women with a normal body mass on the forefoot by 24.5%, the metatarsal head by 30.0%, medial arch by 17.2%, the lateral arch by 19,5%($p<0.05$). During 38th week of pregnancy, changes in pressure values were observed in all anatomical parts of the foot in the group of pregnant women with overweight and obesity($p<0.05$). Conclusion: Research shows that pregnant women with normal weight and overweight use different mechanisms of adaptation that allow maintaining a stable posture of a woman's body while walking.

Acknowledgments: The paper is supported by Bialystok University of Technology, Bialystok, Poland W/WM/17/2017.

References:

[1] AGUIAR, Liliana, et al. Comparison between overweight due to pregnancy and due to added weight to simulate body mass distribution in pregnancy. Gait & posture, 2015, 42.4: 511-517.
[2] BERTUIT, Jeanne, et al. Plantar pressure during gait in pregnant women. Journal of the American Podiatric Medical Association, 2016, 106.6: 398-405.

[P 15]

COMPUTATION OF MUSCLES ACTIVITY DURING BALANCE TESTS ON STABLE AND UNSTABLE PLATFORM IN GROUP OF HEALTHY WOMEN OF AGE ABOUT 50.

Ewa Szczerbik[1], *Małgorzata Syczewska*[1], *Małgorzata Kalinowska*[1]

1 *The Children's Memorial Health Institute, Kinesiology Lab, Warszawa , Poland*

According to WHO fall risk increase of age over 65. The fall's injuries often result in disability and death. To prevent them mechanism of sufficient balance control should be assigned to allow for therapy program implementation. Proper activity of muscles is crucial in movements and balance tasks. Root mean square (RMS) calculations are used for estimation of muscles activity. Most studies focus on shank muscles and influence of different unstable conditions on shunk muscles activity was proved [1]. Also hip joint is important in balance control strategies, but literature describing the contribution of other segments muscles is lacking.

The aim of this study was to determine the activity of shank, thigh and trunk muscles during stance on stable and unstable platform in group of women over 50 (age when first signs of imbalance can appear).

17 healthy women aged 45-62 without balance, neurological or orthopaedic problems, systematically training sport activity were recruited. Surface electromyography was captured simultaneously with Postural Stability tests (Biodex_Balance_System_ SD) in conditions: stable platform eyes opened (PS), stability level 4 eyes opened (PS4_EO) and closed (PS4_EC), stability smoothly reduced levels 12-4 eyes opened (PS12-4). Muscles registered: rectus femoris (RF), biceps femoris (BF), tibialis anterior (TA), gastocnemus (GA), soleus (SOL), peroneus longus (PL), gluteus maximus (GM), erector spinae (ES). RMS values were calculated to estimate their activity. Overall Biodex Index (BI) was regarded to verify balance. Calculations performed: correlations between RMS and BI (CORR), multiply regression (MR1, MR2, MR3) for models consisted of all captured muscles MR1: RMS and BI, MR2: RMS during PS4_EO and PS12-4 normalized on RMS PS, PS4_EC normalized on RMS PS4_EO and BI, MR3: RMS normalized like MR2 and BI normalized on BI under easiest conditions (convention as RMS), to estimate muscles activity changes during more demanding tasks in reference to easier ones.

RMS of left and right side muscles were pooled (no significant differences). Results of computations are presented in Table 1. Results of normalized RMS and BI are plotted on Figure 1.

Computations revealed: no significant muscle activity during PS (CORR and MR1), significant participation of shank and thigh muscles (CORR), significant SOL participation on unstable platform when conditions become more demanding (MR2-normalized RMS) and when balance problems appear (MR3-normalyzed BI). That means that all muscles groups should be strengthened to avoid/delay balance problems.

	PS	PS4_EO or PS4_EO/PS (MR2,3)	PS4_EC or PS4_EC/ PS4_EO (MR2,3)	PS12-4 or PS12-4/ PS (MR2,3)
CORR	ns=no significant	TA(R=0.59)/BF/GA	RF (R=0.36)	RF (R=0.59)/BF
MR1	ns	ns	ns	RF(p=0.0131)
MR2		SOL(p=0.0010)	ns	SOL(p=0.0000)
MR3		SOL(p=0.0053)/BF	ns	SOL(p=0.0016)/ GM

Table 1. Correlation and multiply regression of muscles RMS and BI.

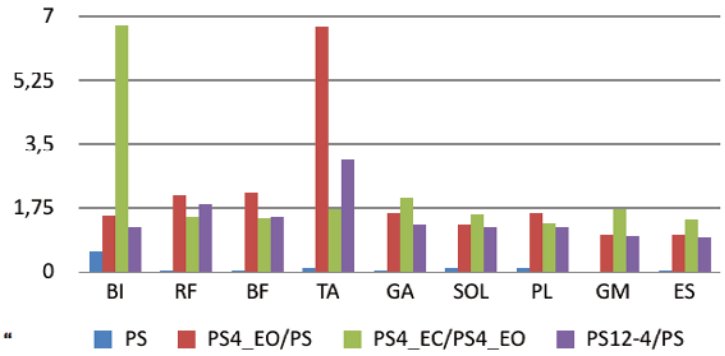

Figure 1 Caption: Raw BI and RMS (PS) and normalized BI and RMS

Acknowledgments: "Study founded by STRATEGMED3/306011/1/NCBR/2017"

References:

[1] Cimadoro_G_et_al._(2013).Neuroscience_Letters,548:228-232.

[P 16]

EXAMINING HETEROGENEOUS OSTEOCYTE ACTIVATION AND BONE MECHANOTRANSDUCTION: 3D MULTIPLEXED IMAGING FOR MULTI-SCALE FINITE ELEMENT ANALYSIS.

Loretta Laughrey[1], *LeAnn Tiede-Lewis*[2], *Sarah Dallas*[2], *Mark Johnson*[2], *Thiagarajan Ganesh*[3]

1 *University of Missouri - Kansas City, Kansas City, USA*
2 *University of Missouri-Kansas City, School of Dentistry, Department of Oral and Craniofacial Sciences, Kansas City, USA*
3 *University of Missouri-Kansas City, Department of Civil and Mechanical Engineering, Kansas City, USA*

Lara-Castillo et al. (2015), observed that cyclic compression loading of a mouse forearm results in heterogeneous activation levels of Wnt/β-catenin in the osteocytes at the mid-shaft of the ulna, indicating that in bone neighboring osteocytes respond differently to the same load. This is in contrast to current bone models which predict a homogeneous response to load.

To develop a more detailed understanding of mechanotransduction between bone loading and Wnt/β-catenin activation, we have created a preliminary, sophisticated, predictive computer model to compute bone strains in lacunar walls in response to macroscopic bone loading and to correlate those strains with Wnt signaling activation.

The forearm of a live TOPGAL mouse was subjected to cyclical compression loading of 2.5 N at 2 Hz for 100 cycles to induce osteocyte activity. The ulnae were stained with Dextran-conjugated Texas Red to label the lacunocanalicular network, LacZ to label activated osteocytes, DiO to identify osteocyte membranes, and DAPI to mark nuclei.

Images were collected using 3D confocal fluorescence microscopy. Figure 1 shows osteocytes containing LacZ stain which indicates Wnt signaling activation. This image was converted into a volumetric finite element model (FEM) using Mimics and 3-Matic.

Finite element analysis of the model was done using FeBio with a compression load applied to the top surface. Figure 2 shows a colormap of resultant 3 Principal Lagrangian strains. The lacunar walls experience a higher strain relative to the surrounding bone matrix.

Strain in the lacunar walls was magnified by a factor of ~1.7 compared to strain in the bone (Figure 3). This strain magnification is lower than previously reported results, which is expected since the lacunar size here is higher relative to the volume of the sample in comparison to previously published experiments. Larger models are being developed to verify this effect.

Multiplexed imaging and FEA allows us to compute amplification of strain in lacunar walls relative to surrounding bone and visualize Wnt signaling activation in the osteocytes contained therein. Strain results will be correlated with osteocyte activation to evaluate the relationship between load and bone formation.

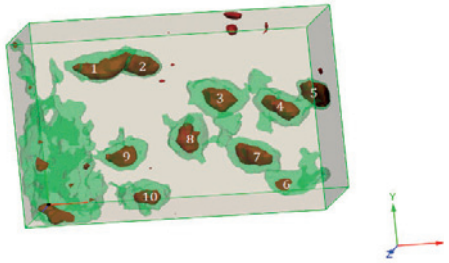

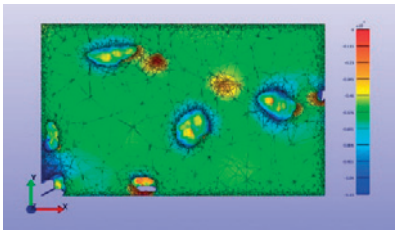

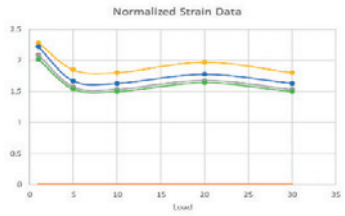

Figure 1: FEM of lacunae in bone. Lacunar space is green and LacZ stain is red, indicating activated osteocytes. Osteocytes 1, 2, 4, and 8 are completely surrounded by bone.
Figure 2: Corresponding FEA of bone from Figure 1 using Tet4 elements. Colormap indicates 3 Principal Lagrangian strains.
Figure 3: Strains in lacunar walls are typically magnified by a factor of ~1.7 relative to surrounding bone.

Acknowledgments: This work was funded by a grant from the National Science Foundation award number NSF-CMMI- 1662284 (PI: Thiagarajan Ganesh) and National Institutes of Health – NIA P01 AG039355 (LF Bonewald-PI).

References:

Lara-Castillo, N., Kim-Weroha, N. A., Kamel, M. A., Javaheri, B., Ellies, D. L., Krumlauf, R. E., Johnson, M. L. (2015). In vivo mechanical loading rapidly activates beta-catenin signaling in osteocytes through a prostaglandin mediated mechanism. Bone, 76, 58-66.

[P 17]

NANOINDENTATION OF SUBCHONDRAL BONE DURING OSTEOARTHRITIS PATHOLOGICAL PROCESS USING ATOMIC FORE MICROSCOPY

Lisa Manitta[1], *Clemence Fayolle*[1], *Lucile Olive*[1], *Jean-Philippe Berteau*[1]

1 *Department of Physical Therapy, City University of New York - College of Staten Island, Staten Island, USA*

Osteoarthritis (OA) is characterized by the alteration of connective tissue in the joints (Wieland, Michaelis, Kirschbaum, & Rudolphi, 2005). The current theory believes that changes to the subchondral bone, such as increased stiffness actually precede and contribute to cartilage loss in the early stages of OA (Amini et al., 2015), however, subchondral bone changes are not yet fully understood (Fang et al., 2018). The goal of this project is to understand the effects of osteoarthritis on the mechanical properties of the subchondral bone femur of mice. The hypothesis is that at the nanoscale the subchondral bone (SB) Elastic Modulus is lower in early OA mice than in control. To test our hypothesis, we investigated the SB of C57Bl6 mice femurs from an early OA group and a control group (n = 6 and n = 6, respectively). We performed eight indentations at three locations on both the medial and lateral condyles for each femur. The averages of these values are reported below. Our results show that the average Elastic Modulus in early OA mice is 3.57E+09 Pa, while that of the control group mice is 1.09E+10 Pa. This indicates a higher average Elastic Modulus in the control group mice than in the early OA mice, which may indicate an initial decrease in Elastic Modulus during the OA pathological process.

	Elastic Modulus in Pa for Early OA group		Elastic Modulus in Pa for Control group	
Sample number	**Medial Condyle**	**Lateral Condyle**	**Medial Condyle**	**Lateral Condyle**
1	2.51E+09	2.75E+09	1.99E+10	2.46E+09
2	2.60E+09	4.66E+08	3.47E+09	5.76E+09
3	7.40E+08	3.23E+08	2.53E+09	5.19E+09
4	3.02E+09	2.07E+09	2.19E+09	9.45E+09
5	9.15E+09	3.39E+09	2.96E+10	3.42E+10
6	6.52E+09	9.29E+09	1.06E+10	5.87E+09
Mean of the Means	4.09E+09	3.05E+09	1.14E+10	1.05E+10

Figure Caption: Average Elastic Modulus Values Reported in Pa

References:

Amini, M., Nazemi, S. M., Lanovaz, J. L., Kontulainen, S., Masri, B. A., Wilson, D. R., … Johnston, J. D. (2015). Individual and combined effects of OA-related subchondral bone alterations on proximal tibial surface stiffness: A parametric finite element modeling study. Medical Engineering and Physics. https://doi.org/10.1016/j.medengphy.2015.05.011

Fang, H., Huang, L., Welch, I., Norley, C., Holdsworth, D. W., Beier, F., & Cai, D. (2018). Early Changes of Articular Cartilage and Subchondral Bone in The DMM Mouse Model of Osteoarthritis. Scientific Reports, 8(1), 2855. https://doi.org/10.1038/s41598-018-21184-5

Wieland, H. A., Michaelis, M., Kirschbaum, B. J., & Rudolphi, K. A. (2005). Osteoarthritis - An untreatable disease? Nature Reviews Drug Discovery. https://doi.org/10.1038/nrd1693

[P 18]

IN SEARCH OF TYPE 2 DIABETES-RELATED DIFFERENCES IN BONE

Sasidhar Uppuganti[1], *Nora Ward*[2], *Mark Does*[2], ***Jeffry Nyman***[1]

1 *Vanderbilt University, Medical Center, Nashville, USA*

2 *Vanderbilt University, Nashville, USA*

Clinical studies conclude that people with type 2 diabetes (T2D) are at higher risk of fracture than non-diabetics [1]. Current tools, such as the online FRAX calculator, underestimate fracture risk for individuals with diabetes [2] suggesting disease-related changes to bone quality are a contributing factor to poor fracture resistance in T2D. We hypothesize that T2D for >10 years reduces the mechanical properties of human bone at the apparent level. To investigate this possibility, we analyzed cadaveric femurs for differences between T2D (15 Males, duration-19.5±10.0-yrs; 23 Females, duration-19.8±9.5-yrs) and age-matched Non-T2D donors (15M/21F). Ten micro-indents were performed along the medial side using reference point indentation (BioDent) with a target force of 10 N for 20 cycles to determine total indentation distance (TotID), averaged creep indentation distance (AvgCID), and average unloading slope (AvgUS) [3]. The mid-shaft (~13.2 mm length) was next scanned by micro-computed tomography (μCT) at 48.4 μm voxel to determine cortical area (Ct.Ar), cortical thickness (Ct.Th), and volumetric BMD (vBMD). Longitudinal strips from the medial quadrant were then machined into tensile (T) or single-edge-notched-beam (SENB) specimens. The test region of each specimen was scanned by μCT (5 μm voxel) to determine local tissue mineral density (TMD) and porosity (Po). The T specimens were loaded-to-failure at 5 mm/min to measure strength and toughness [4]. SENB specimens were loaded at 0.6 mm/min in three-point bending to determine fracture toughness (KJc and J-integral) [5]. Body mass index (BMI) of the donor and vBMD of the mid-shaft were negatively associated with age (Table). Unexpectedly, T.Po and SENB.Po were lower for T2D than for Non-T2D donors when accounting for age and sex of the donor (Table). Tensile strength and toughness as well as fracture toughness properties were not different between the two groups, though T properties were negatively related to age and depended on sex of the donor (Table). T2D donors had larger Ct.Ar and Ct.Th and lower avgCID but higher TotID (especially if male, Table). Individuals with T2D at risk of osteoporosis may be those with other complications that negatively affect porosity (e.g., micro-vascular disease) and the bone tissue (chronic kidney disease). Ongoing work involves separating out donors with complications, increasing the number of donors in both groups balancing sexes, and assessing matrix-sensitive properties (matrix-bound water).

Property	*units*	*Ref. value*	*Add or sub. [Age x coeff.]*	*If F, add or sub. [coeff.]*	*If T2D, add or sub. [coeff.]*	*If M & T2D, add or sub. [coeff.]*	*Adj.-R^2*
BMI	kg/m^2	47.6	- 0.2 *(0.011)*	+6.2 *(0.045)*	- 1.0 *(0.761)*	- 8.6 *(0.047)*	15.5
Ct.Ar	mm^2	6.39	- 0.03 *(<0.001)*	-1.40 *(<0.001)*	+ 0.42 *(0.005)*	NS	54.7
Ct.Th	mm	9.70	- 0.05 *(<0.001)*	-1.42 *(<0.001)*	+ 0.85 *(0.001)*	NS	38.7
vBMD	mm	871	- 1 *(0.007)*	-16 *(0.083)*	+ 30 *(0.003)*	+ 30 *(0.023)*	16.2
TotID	μm	76.4	NS	+1.8 *(0.403)*	+ 0.8 *(0.727)*	+ 6.0 *(0.045)*	15.0
AvgCID	μm	1.67	NS	+0.12 *(0.047)*	- 0.19 *(0.001)*	NS	19.0
AvgUS	N/μm	0.57	NS	NS	NS	NS	0.9
T.Po	%	4.11	NS	+1.14 *(0.412)*	- 4.41 *(0.004)*	- 4.54 *(0.022)*	12.7
T.TMD	$mgHA/cm^3$	1078	NS	-11 *(0.026)*	NS	NS	5.2
Strength	MPa	123.3	- 0.3 *(0.017)*	+7.8 *(0.011)*	NS	NS	17.1
Toughness	N/mm	2.98	- 0.02 *(0.008)*	+0.35 *(0.035)*	NS	NS	16.1
K_{Jc}	$MPa/\sqrt{m}$	9.53	- 0.03 *(0.028)*	NS	NS	NS	6.7
J-integral	KJ/m^2	13.2	NS	NS	NS	NS	6.3
SENB.Po	%	8.33	NS	-13.09 *(0.039)*	- 2.41 *(0.018)*	+ 0.19 *(0.030)*	12.6
SENB.TMD	$mgHA/cm^3$	1004	NS	-13 *(0.004)*	NS	NS	10.5

Table: The coefficients and their p-values from general linear models.

Acknowledgments: NIH-AR067871 and VA-BX004297.

References:

[1] Schwartz. JAMA. 2011.,
[2] Giangregorio. J Bone Miner Res. 2012.,
[3] Granke. J Mech Behav Biomed Mater. 2014.,
[4] Nyman. J Mech Behav Biomed Mater. 2013., and
[5] Granke. J Bone Miner Res. 2015.

[P 19]

EXPERIMENTAL AND COMPUTATIONAL INVESTIGATIONS FOR DAMAGE INITIATION AND CRACK PROPAGATION PHENOMENA OF PERI-IMPLANT BONE UNDER SCREW PULLOUT ACCORDING TO SCREW DESIGN PARAMETERS

Chan-Hee Song[1], *Eun Sun Lee*[2], *Dong-Man Ryu*[2], *Tae Sik Goh*[3], *Jung Hoon Ro*[2], *Chi-Seung Lee*[4]

1 *Department of Biomedical Engineering, School of Medicine, Pusan National University, Busan, Korea, Rep. of South*
2 *Department of Biomedical Engineering, School of Medicine, Pusan National University, Busan, Korea, Rep. of South; Biomedical Research Institute, Pusan National University Hospital, Busan, Korea, Rep. of South*
3 *Department of Orthopaedic Surgery, Pusan National University Hospital, Busan, Korea, Rep. of South; Biomedical Research Institute, Pusan National University Hospital, Busan, Korea, Rep. of South*
4 *Department of Convergence Medicine, School of Medicine, Pusan National University, Busan, Korea, Rep. of South; Department of Biomedical Engineering, School of Medicine, Pusan National University, Busan, Korea, Rep. of South; Biomedical Research Institute, Pusan National University Hospital Busan, Korea, Rep. of South*

The insertion of orthopedic screw is usually involved the risk of damage to the peri-implant bone. The peri-implant bone damage is caused by the insertion and/or pullout of the screw, which is more likely to occur osteoporotic bone than normal bone. As the degenerative osteoporosis progresses after implant surgery, the screw pullout phenomenon is a common complication. According to a number of biomechanical studies, it was found that a lot of factors such as bone-mineral density, surgical procedure, screw insertion condition, and screw design are closely related to the screw pullout phenomenon. Among these, one of the most crucial factors is the screw design such as pitch height, conical angle and core diameter. Due to these parameters, the pullout force of screw and damage/crack characteristics near peri-implant bone can be drastically changed (Lee et al., 2019).

Although the pullout-type load is not a dominant loading condition in human motion after surgery, the pullout test should be carried out to investigate the screw fixation features. In many studies, the pullout test considering various screw design parameters has been conducted experimentally and numerically, and the relationship between screw design parameters and pullout force has been investigated. However, it is difficult to find the literatures that precisely address the damage initiation and crack propagation phenomena of peri-implant bone according to screw design parameters.

Hence, in this study, the damage/crack characteristics as well as the pullout force with respect to the screw design parameters under screw pullout was experimentally and computationally analyzed. In experimental approach, ten types of pedicle screws with various pitch height, conical angle and core diameter were fabricated, and implemented into normal/osteoporotic cancellous/corticocancellous bone analogues. In other words, forty types of different screw-bone combined test specimens were fabricated. The pullout test was repeated five times, namely, the test was carried out 120 times, and each pullout force was measured. The damage/crack features of peri-implant bone analogues after pullout test were investigated using micro-computed tomography (micro-CT) and CT image analysis software.

On the other hand, in computational approach, the modified Tsai-Wu (Keaveny et al.,1999) and modified Hashin (Freerick et al., 2013) failure criteria were adopted to the cancellous and cortical bones, respectively to evaluate/predict the damage initiation of peri-implant bone analogue. In addition, the extended finite element method (XFEM) was adopted to estimate/anticipate the crack initiation and propagation of cortical bone adjacent to screw during screw pullout (Freerick et al., 2013). In particular, the modified Hashin failure criterion was combined with XFEM during crack initiation/propagation analysis. The calculation results were compared to the experimental results of CT images in order to validate the simulation technique.

The introduced simulation technique might be used to design an orthopaedic screw that maximize the pullout force and minimize the bone damage adjacent to screw.

Acknowledgments: This research was supported by Basic Science Research Program through the National Research Foundation of Korea (NRF) funded by the Ministry of Education (NRF-2016R1D1A1B03934304; NRF-2018R1D1A3B07048028).

References:

Lee ES, Goh TS, Heo JY, Kim YJ, Lee SE, Kim YH, Lee CS. Experimental Evaluation of Screw Pullout Force and Adjacent Bone Damage According to Pedicle Screw Design Parameters in Normal and Osteoporotic Bones. Applied Sciences. 2019 Jan;9(3):586.
Keaveny TM, Wachtel EF, Zadesky SP, Arramon YP. Application of the Tsai–Wu quadratic multiaxial failure criterion to bovine trabecular bone. Journal of biomechanical engineering. 1999 Feb 1;121(1):99-107.
Feerick EM, Liu XC, McGarry P. Anisotropic mode-dependent damage of cortical bone using the extended finite element method (XFEM). Journal of the Mechanical Behavior of Biomedical Materials. 2013 Apr 1;20:77-89.

[P 20]

IDENTIFICATION OF MECHANICAL PROPERTIES OF HUMAN ORBITAL WALL BONES

Krzysztof Zerdzicki[1], *Pawel Lemski*[2], *Pawel Klosowski*[1], *Andrzej Skorek*[2], *Marcin Zmuda-Trzebiatowski*[1]

1 *Gdansk University of Technology, Faculty of Civil and Environmental Engineering, Department of Structural Mechanics, Gdansk, Poland*

2 *Medical University of Gdańsk, Departament of Otolaryngology, Gdansk, Poland*

The presented study aims at identification of mechanical properties of the human orbital wall bones. The experimental tests were realized in the Laboratory of Mechanics of Structures and Materials (Faculty of Civil and Environmental Engineering, Gdansk University of Technology, Gdansk, Poland, Poland) after gaining the consent from the bioethics faculty committee of the Medical University of Gdańsk. All human specimens were obtained from cadavers during medicolegal autopsy performed no later than 2-5 days after their death. The biological material has been collected from 63 different patients (age between 20 to 51 years old, 45 males and 18 females). The specimens of orbital bone (without periosteum layer) were obtained directly after the cranial cavity opening and brain's removing for the histological examination. Then the specimen was cut off the orbit as one integral bone piece, both for right and left orbit. Such obtained specimens (all of them having the length range of 3 – 4 cm) have been put in to the 0.9% NaCl at temperature level of -20°C for the next 6 to 36 hours untill the laboratory tests. The procedure is similar to the procedures proposed before by Morgan [1] and Waterhouse [2]. The mechanical tests have been held after defrosting the specimens to the temperature of about 20°C. Then, every specimen has been individually measured, weighted and then tensioned till failure with 0.01 mm/s crosshead speed in the Zwick Roell Z0/20 testing machine (Fig. 1 left). Each specimen has been marked with four white dots in order to follow the specimen deformation by the video extensometer. After the test each specimen was cut in the middle of its length and the cross sections of both parts of the specimen have been imprinted on the paper with ink (Fig. 1 right). Then, scans of mentioned imprints have been imported to the AutoCAD program, and the area of each imprint has been calculated, in accordance to the scale given. Next, the data registered by the TestXpert (software dedicated to Zwick/Roell machine) along with the obtained cross section areas were recalculated using the SigmaPlot Software. The basic mechanical properties like Young's modulus, yield limit and ultimate tensile strength were identified using the least square method. The obtained values are of great importance during FEM analysis of the human skull modes of failure, especially for numerical analysis of the blow out and orbital wall traumas [3].

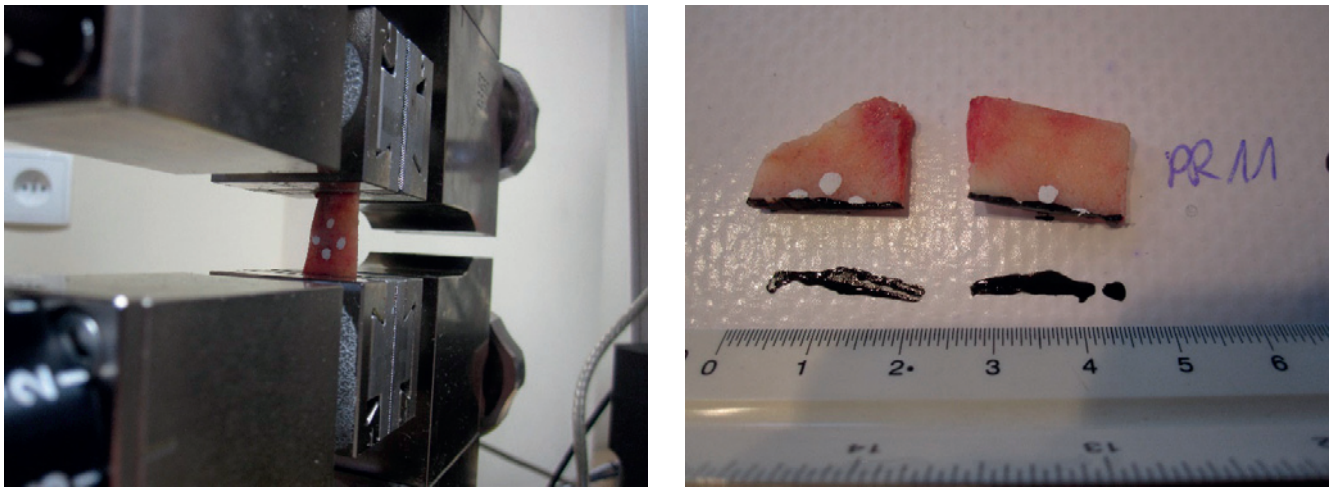

Figure Caption: Orbital wall bones: in the testing machine (left); during imprinting (right)

Acknowledgments: The study was financed within the National Science Center grant No. UMO-2016/23/B/ST8/00115 realized at Faculty of Civil and Environmental Engineering, Gdansk University of Technology, Gdansk, Poland.

References:

[1] *E. F. Morgan, H. H. Bayraktar, and T. M. Keaveny, "Trabecular bone modulus-density relationships depend on anatomic site," J. Biomech., vol. 36, no. 7, pp. 897–904, 2003.*

[2] *N. Waterhouse, J. Lyne, M. Urdang, and L. Garey, "An investigation into the mechanism of orbital blowout fractures," Br. J. Plast. Surg., vol. 52, no. 8, pp. 607–612, 1999.*

[3] *A. Schaller, H. Huempfner-Hierl, A. Hemprich, and T. Hierl, "Biomechanical mechanisms of orbital wall fractures - A transient finite element analysis," J. Cranio-Maxillofacial Surg., vol. 41, no. 8, pp. 710–717, 2013.*

[P 21]

EVALUATING THE EFFECT OF SKULL AND BRAIN STIFFNESS ON SHOCK WAVE PROPAGATION IN A RODENT FINITE ELEMENT MODEL

Rahul Shah[1], ***Molly Townsend***[1], *Namas Chandra*[1]

1 *New Jersey Institute of Technology, Center for Injury Biomechanics, Materials, and Medicine, Newark, USA*

Blast-induced traumatic brain injury (TBI) remains to be a leading cause of combat casualties, with over 15,000 service members experiencing a mild TBI in 2017 [1]. These injuries have lasting effects, with service members exhibiting persisting neurobehavioral deficits [2]. Computational models of blast-induced TBI have the potential to shed light on mechanical injury mechanisms, yet models are crippled by a lack of appropriate experimental validation studies and poorly characterized constitutive models for biological tissues under high strain rate shock loading. To this end, a parametric study of model boundary conditions, loading conditions, and constitutive models is presented. A recently developed finite element model based on radiographic scans of a 10-week-old male Sprague Dawley rat has been validated against experimental measurements from the nine-inch shock tube at the Center for Injury Biomechanics, Materials, and Medicine. This model was shown to accurately predict intracranial pressures (ICPs) under a mild shock (130 kPa). The model was further validated for a wider range of shock exposures consistent with the lower (70 kPa) and upper end (180 kPa) of exposures which are associated with mild TBI. Simulated ICP and ICP impulses exhibited no significant differences with experimental measurements ($n=4$, $p<0.01$). Once validated, constitutive models were varied within the range of reported literature values for the skull and brain. The ICP, intracranial strain fields, and cranial vault strains were reported and validated against experimental data. This results in a robust finite element model shown to be largely insensitive to the viscoelastic brain constitutive model. More compliant bone material models introduce oscillations in the ICP profile, which are associated with increased flexure of the cranium. The developed model demonstrates that a spike in ICP is exhibited, closely following the incident overpressure. Further work will seek to connect observed mechanical loading pathways and patterns to microscale injury cascades.

References:

[1] Department of Defense. 2018. 2017 DoD TBI Worldwide Numbers. Falls Church (VA): Department of Defense.

[2] Combs HL, Berry DTR, Pape T, Babcock-Parziale J, Smith B, Schleenbaker R, Shandera-Ochsner A, Harp JP, High WM Jr. 2015. The effects of mild traumatic brain injury, post-traumatic stress disorder, and combined mild traumatic brain injury/post-traumatic stress disorder on returning veterans. J. of Neurotrauma. 32(13).

[P 22]

GEOMETRIC CONSTRUCTION OF ANATOMICALLY REALISTIC BLOOD CAPILLARY MESHES BY SPACE FILLING CURVES

Marina Bertolini [1], ***Paola Causin***[2], *Cristina Turrini*[1]

1 *University of Milano, Milano, Italy*
2 *Department of Mathematics, University of Milan, Milano, Italy*

Microcirculation is the collective name for the smallest (<150 microns in diameter) blood vessels in the body. Such vessels are usually categorized according to their diameter in arterioles, venules and capillaries [1]. When performing numerical simulations, the geometry of larger vessels may be reconstructed from imaging tools. This operation is much more cumbersome when dealing with capillaries, as capillary beds are composed of thousands (>104) of tiny vessels with diameter ranging from 5 to 9 microns. For this reason, different studies have proposed the use of mathematical algorithms to model capillary structures. In [3] a homogenized perspective is adopted and the geometry of the capillaries in the cubic REV is represented by randomly disposed straight segments. Other studies range from the use of simple concentric rings to more refined models as in [2]. In this latter work, the underlying structure of a portion of the cerebral capillary net is obtained from a Voronoi dual mesh built from a tetrahedral Delaunay triangulation filling the space within a set of terminal arterioles and venules.

Here we propose an alternative technique to generate the capillary geometry in the cubic REV, retaining a more realistic description as in [2]. The idea is based on the recursive and self-similar construction of space-filling curves, like Hilbert or Moore curves [4]. Such curves have the interesting property of displaying a range which, at the limit, fills the entire unit cube. Closed loops, characteristic of the capillary meshes, are obtained by adding, in an automatized way, arcs between neighboring vertexes (nodes) of the curve. Tubular neighborhood of the curve is generated by sweeping a circular section along the curve itself and embedded into a solid cube. Then we mesh the complementary space for computations. The choice of the number of iterations used to construct the tubular neighborhood of the curve allows to control the density of the nodes in the space, between the arterial and venous terminals, and the tortuosity of the structure. Notice that, once the level of the iteration is chosen, the degree of tortuosity may be further altered by constructing arcs which interconnect the nodes by Bézier interpolation with different tension.

References

[1] D. Goldman, A.S. Popel, "A computational study of the effect of capillary network anastomoses and tortuosity on oxygen transport", J Theor Biol 206:181–194, 2000
[2] A.A. Linninger et al, "Cerebral Microcirculation and Oxygen Tension in the Human Secondary Cortex", Ann Biomed Eng 41(11):2264-84, 2013
[3] J. Reichold et al, "Vascular graph model to simulate the cerebral blood flow in realistic vascular networks", J Cereb Blood Flow Metab 29: 1429-1443, 2009
[4] H. Sagan, Space-Filling Curves, Springer-Verlag, New York, 1994

[P 23]

NUMERICAL SIMULATION OF CEREBRAL ANEURYSM HEMODYNAMIC TREATED WITH FLOW DIVERTER STENT

Augusto Sanches[1], *Thomas Liebig*[2]

1 *Department of Informatics, Technical University of Munich (Tum), Munich, Germany; Department of Neuroradiology, University Hospital Munich (Lmu), Munich, Germany*

2 *Department of Neuroradiology, University Hospital Munich (Lmu), Munich, Germany*

Cerebral aneurysms are present in approximately 1% to 5% of the population. The majority of these aneurysms may never rupture, but when they do 40% of patients die and of those that survive, roughly one-third will be permanently disabled.

Endovascular intervention is the treatment of choice for cerebral aneurysms because of safety and efficacy. Recently, flow diverter (FD) stent treatment was proven to be a successful method of endovascular reconstruction particularly for large, wide-neck and complex brain aneurysms. It consists of an overall high-density mesh stent, placed in the parent artery to redirect and reduce blood flow into the aneurysm. Ultimately, it induces a gradual thrombosis and reendothelialization across the neck, which either reduces or ultimately eliminates the risk of further growth and rupture.

Despite the high success rates of aneurysm treatment with FD stents, concerns remain regarding post-procedural complications such as subacute aneurysm rupture, parent artery occlusion, and flow persistence. At this time, there is no method for measuring flow modification reliably and predicting safe and effective aneurysm occlusion after flow diverter treatments. Although many hypotheses have been proposed to explain some of these complications, most of the mechanisms of action of flow diverters remain unanswered.

To avoid the risk of treatment to potentially outweigh the risk of spontaneous rupture, treatment decisions should be based on as much available information on the individual aneurysm as possible. Currently, these decisions are based size, shape and location of the aneurysm, as well as family history and other risk factors such as smoking and hypertension. But these predictors of rupture risk are largely unreliable.

It is widely believed that intra-aneurysmal hemodynamics contributes substantially to the individual rupture risk and should be used during assessment and treatment-planning. Therefore, the availability of a simulation tool that can predict the effect of FD implantation on aneurysm hemodynamic will be extremely useful, either to support the treatment decisions, or to develop and improve new FD designs.

Computational techniques offer new capabilities in healthcare for cerebral aneurysms. In the present study, the blood flow computational fluid dynamics in cerebral aneurysm treated with stents is modeled and analyzed taking into account their design, porosity, and the flow reduction at aneurysm sac. A comparison with particle image velocimetry experiments is conducted for both cases before and after the implant treatment.

It is shown that the hemodynamic changes induced in the system through the stent deployment, provides a realistic insight into the pathological vessel parameters in order to improve the evaluation of the risk of rupture for a given patient.

[P 24]

DESIGN AND DEVELOPMENT OF A DUAL-FLOW BIOREACTOR FOR DRUG TRANSPORT ASSESMENT MIMICKING INTESTINAL PERISTALSIS AND PERMIABILITY IN EPHITELIAL TISSUE BARRIERS

Odin Ramirez-Fernandez[1], *Joana Costa*[2], *Ludovica Cacopardo*[2]

1 *Research Centre "E. Piaggio" Department of Information Engineering, University of Pisa, CDMX, Mexico; Basic Science Department, Tlalnepantla Technologic Institute, Technologics of México*

2 *Research Centre "E. Piaggio" Department of Information Engineering, University of Pisa, CDMX, Mexico*

In this work we present a bioreactor system which combines a semi permeable membrane that simulates the osmotic nutrients interchange in the small intestine circulation and rhythmic peristaltic movement.[1] This custom-designed presents a semipermeable membrane bioreactor, with peristaltic flow and compression variation that allows adjustment of luminal flow rate as shown in figure 1. This dynamic bioreactor can mimic the human small intestine with increased accuracy to overcome many of the limitations and accuracy with the previously small intestinal models, providing a more representative model of the small intestine [2].

To simulate the peristaltic moves we decided to use two helices with six radial blades that allow us to model the compression movement of the intestine to pass nutrients through the lumen of the apical side, we model the system in such a way that the maximum point of compression out of 50% of the total lumen of the pipe, the model can vary the occlusion percentage of the lumen since we simulate and model scenarios with different occlusions and the permeability difference. [3]

The results, summarized in Figure 3, indicated that in dynamic and squish conditions, after 3 weeks, around 12-13% of the compound permeated through the apical chamber and passed to the basal chamber. This indicates that the dialysis tube were effectively permeable with this conditions. [4] At first 7 days the values of some samples in static conditions were even higher than the dynamic ones, while in some cases it was the other way around. In that case, the "barrier effect" could had overcome the effect of the concentration gradient, which potentially is kept high for a longer period in the cases was being diluted by the moving fluid of the basal chamber.

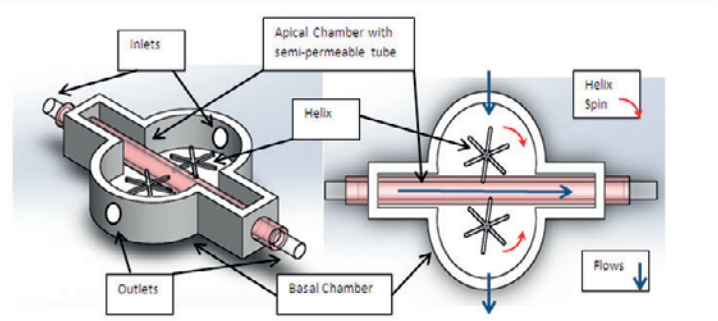

Figure 1 Bioreactor design. The flow goes through the apical chamber where the cell culture

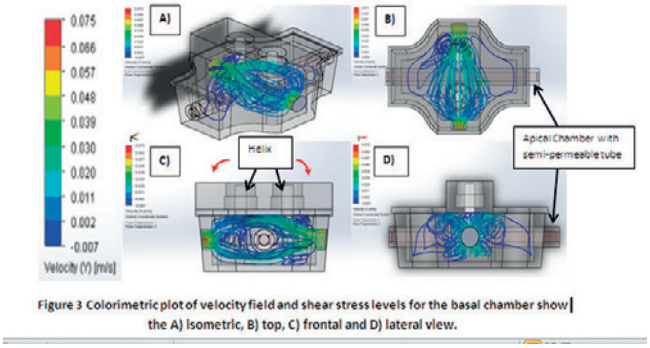

Figure 3 Colorimetric plot of velocity field and shear stress levels for the basal chamber show the A) isometric, B) top, C) frontal and D) lateral view.

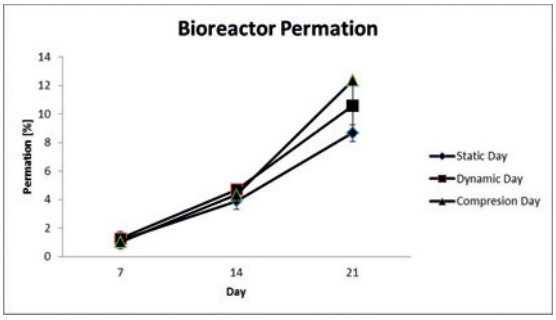

Figure 1. Bioreactor design
Figure 2 Colorimetric plot of velocity field for the basal chamber
Figure 3. Permeability data from dialysis tube in the bioreactors for 3 weeks in 3 different conditions.

References:

[1] Kim HJ.(2013). Gut-on-a-Chip microenvironment induces human intestinal cells to undergo villus differentiation. Integrative Biology, 5 : 1130–40.
[2] Cei D.(2017). A bioreactor with an electro-responsive elastomeric membrane for mimicking intestinal peristalsis. Bioinspiration & Biomimetics , 12: 016001.
[3] Chen Y.(2015). Robust bioengineered 3D functional human intestinal epithelium. Scientific Reports, 5: 13708.
[4] Ramirez-Fernández O.(2017). Cell Cocultures on Coated Scaffolds Applied to Liver Models International Journal of Medical Engineering and Informatics, 37:165.

[P 25]

BIOMECHANICAL EFFECTS OF VARUS AND VALGUS DEFORMITY OF THE KNEE IN ACL RECONSTRUCTION SURGERY

Byeongchan Cho[1], *Dai-Soon Kwak*[2], *Tae Soo Bae*[1]

1 *Department of Biomedical Engineering, Jungwon University, Geosan, Korea, Rep. of South*
2 *Catholic Institute for Applied Anatomy College of Medicine, The Catholic University of Korea*

In case of the varus and valgus deformities of knee joints that exceeds normal range, surgical location of an implanted graft should be considered during the anterior cruciate ligament reconstruction (ACLR). However, clinicians often suffer from difficulties in decision making in the surgical process due to the insufficient related researches. Therefore, the objective of this study was to examine the biomechanical effect of the severity of the varus and valgus deformity of knee joints on the implanted graft through the multi-flexible body dynamics (MFBD) analyses. Left knee model of a man who had no orthopedic diseases in the knee joint was obtained from computed tomography and three-dimensional knee model was reconstructed by image processing (Mimics 20.0, Materialize). To apply continuous knee movement, motions of the main parts of femur and tibia were recorded in 15-degree interval on the coordinates, while maintaining the distance of articular surface between tibia and femur at a constant level of 2 mm. Through the MFBD analysis, stresses of the implanted grafts were calculated from a total of 27 cases were calculated for the combinations of three recommended surgical positions in posteroproximal area (5, 10 and 15mm radii) on the femoral epicondyle and neutral, varus and valgus deformities (Neutral, +5, +10, +15 and +20 degrees). In case of the varus deformity, stress of the implanted graft was 23% lower than the neutral on average where the varus deformity model of 15-degree showed the lowest stress. On the contrary, the valgus deformity model showed that stress of the graft was 27% higher than the neutral on average and stresses were increase as valgus deformity increased. Based on the result, it is recommended that the ACLR surgery for severe valgus deformed knee (more than 10-degree deformity) is implemented after readjusting the alignment of knee for the stability of graft. Furthermore, clinicians should pay close attention to the early alignment of knee joints so that excessive stress is not applied on the graft and then the stress of the ligament around the knee (MCL, LCL, etc) before and after surgery should also be considered. In conclusion, adjustment of varus and valgus deformed knee during ACLR surgery need to be considered for the stability of the implanted graft to increase the success rate of ACLR surgeries. Furthermore, future studies for diverse knee shapes and motions were needed.

Acknowledgments: This research was supported by Basic Science Research Program through the National Research Foundation of Korea (NRF) funded by the Ministry of Education (NRF2017R1D1A3B04033410)

[P 26]

MECHANICAL SKIN BEHAVIOR: NEW NUMERICL APPROACH USING BIO - TENSEGRITY AS A MODELLING

Amaury Guillermin[1], *Meriem Ayadh*[1], *Eric Feulvarch*[2], *Hassan Zahouani*[3]

1 *Laboratoire de tribologie et dynamique des système, Eculy, France; École Centrale de Lyon, France*
2 *Laboratoire de tribologie et dynamique des système, Eculy, Frances; École Nationale D'ingénieurs de Saint Étienne, France*
3 *Laboratoire de tribologie et dynamique des système, Eculy, Frances; École Centrale de Lyon, France*

In the recent decades, minimally invasive techniques to treat bone defects, such as the use of external fixators has gained interest in the field of orthopaedics [1]. Besides being, minimally invasive, these devices allow some degree of external control over the mechanical microenvironment of the fracture site which significantly affects the healing outcome. This provides more flexibility to surgeons in treating bone fractures; because, the fixator could be adjusted throughout the healing period depending on the progress of healing. Ilizarov circular fixator (ICF) is one such external fixator which is used to treat a variety of bone defects such as fractures, non-union, bone length discrepancies etc. [2] One of the main advantages of ICF is that it enables early weight bearing which is beneficial in terms of patient's mobility. In addition, it is believed that early weight bearing could lead to faster and more stronger fracture callus development and thus enhancing the healing progression [1]. However, the exact mechanism by which early weight bearing enhance fracture healing under ICF remains unclear. In this study, it was hypothesised that dynamic loading resulting from physiological activities (e.g. walking) could significantly enhance the bone cell and growth factor concentrations within the early callus and thus, enhance the healing progression. In addition, we hypothesised that, duration of the physiological activities and their frequencies have significant effect on these concentrations. The hypotheses were tested using a computational model of a tibial fracture site (Fig.1), which was developed to simulate the interactions, transport and differentiations of bone cells (i.e. mesenchymal stem cells, osteoblasts chondrocytes and fibroblasts) and the growth factors (i.e. osteogenic growth factor and chondrogenic growth factor) within the early callus. The changes in cell and growth factor concentrations due to different load durations (1 – 4 hours) and load frequencies (1-4 times/day) were parametrically studied and the findings of this study are presented in this paper.

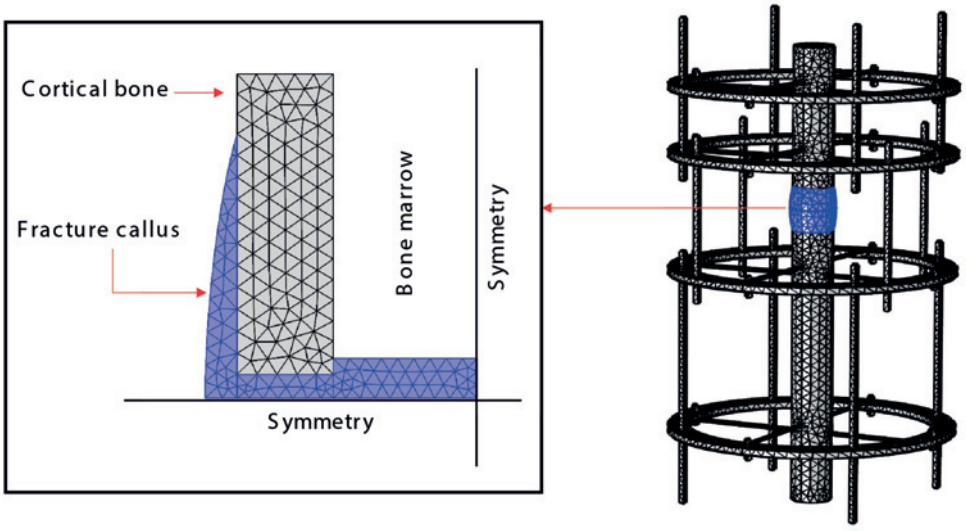

Figure.1 Computational model of the fractured tibia

References:

[1] *A. T. Fragomen and S. R. Rozbruch, "The mechanics of external fixation," HSS Journal, vol. 3, no. 1, pp. 13-29, 2007.*
[2] *K. Erler, C. Yildiz, B. Baykal, A. S. Atesalp, M. T. Ozdemir, and M. Basbozkurt, "Reconstruction of defects following bone tumor resections by distraction osteogenesis," Archives of orthopaedic and trauma surgery, vol. 125, no. 3, pp. 177-183, 2005.*

[P 27]

LINKING PHYSICAL EXPERIMENTS AND COMPUTATIONAL MODELING IN KNEE BIOMECHANICS: ASSESSMENT OF ACCURACY AND REPEATABILITY

Shady Elmasry[1], *Hamidreza Jahandar*[1], *Zaid Zayyad*[1], *Thomas Fraychineaud*[1], ***Carl Imhauser***[1]

1 *Hospital for Special Surgery, New York, USA*

Evaluating knee mechanics, by combining physical and computational models capitalizes on the strengths of each approach. For example, cadaver models allow for well-controlled loads and boundary conditions based on real-world knee physiology. Experimental measurement of contact stress, however, is difficult and error prone. In contrast, computational models allow for efficient estimation of contact stress but need to be driven by real-world kinematics, which can be obtained from cadaver models. Accordingly, the goal of this study was to assess the positional accuracy of a robotic manipulator, used to perform cadaveric testing of the tibiofemoral joint under applied load as calculated using rigid body transforms of the end effector position and orientation. These data will ultimately be used to drive computational models of the knee to assess contact stress. This assessment is important because robotic manipulators have finite compliance, which can affect the accuracy of the measured positions, ultimately affecting the accuracy of the contact stress measurement. To this end, we loaded a cadaveric knee (male, 53 years old) using a robotic manipulator (ZX165U, Kawasaki). The robot flexed the knee to five degrees under 10 N compression; then applied 400 N of compression. A 3D digitizer (accuracy = 0.018 mm, FAROARM®) was used to directly digitize 3 mm diameter glass spheres rigidly fixed to the tibia and the femur with and without compression as a gold standard for comparison. These loading conditions and the digitization were repeated three times. The knee was CT scanned and segmented using Mimics software. CAD software (Geomagic) was used to orient the knee based on the robot and the digitizer transforms. The root mean square (RMS) deviation of the proximal tibia and fibula (which were rigidly fixed together) between the two methods was measured. The RMS error of the tibia without and with compression was 0.6 mm (Fig. 1A) and 1.8 mm (Fig. 1B), respectively. The maximum RMS error for the three times the knee was compressed using the robot was < 0.3 mm. These results demonstrate that robot-driven positions are repeatable, but sensitive to robot compliance, which reduce the positional accuracy of the tibia with applied compression. Next step will be to assess the extent to which these positional errors impact tibiofemoral contact stress in knee computational models.

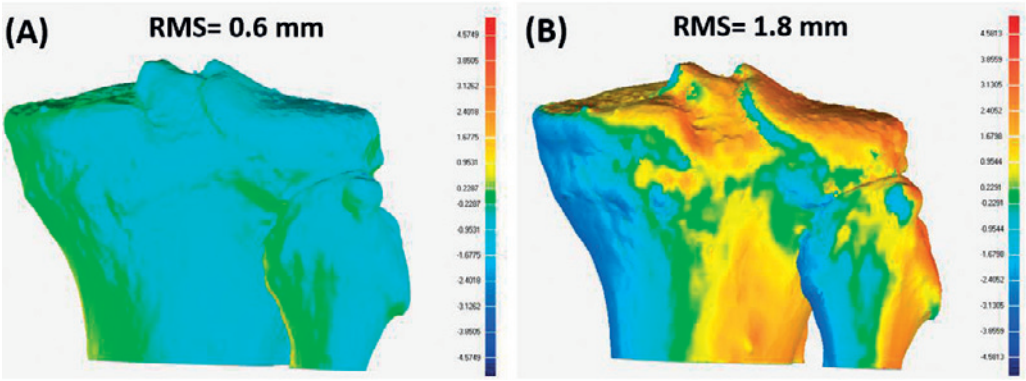

Figure 1: Root mean square (RMS) surface deviation of the proximal tibia and fibula position between robot transformation and direct digitization. (A) with 10 N and (B) with 400 N of compression at 5° of flexion.

[P 28]

EFFECT OF CUTTING PLANE POSITIONS ON THE STRESSES OF LATERAL CORTEX AND TALUS IN THE OPENING-WEDGE HIGH TIBIAL OSTEOTOMY

Heo In Hyuk[1], *Moon Jong Chang*[2], *Seung Baek Kang*[2], *Tae Soo Bae*[1]

1 *Department of Biomedical Engineering, Jungwon University, Geosan, Korea, Rep. of South*

2 *Seoul Metropolitan Government Seoul National University Boramae Medical Center, Seoul, Korea, Rep. of South*

Opening wedge high tibial osteotomy (OWHTO) is a surgery to relieve the pain of patients with arthritis, but can cause a fracture of tibia during the surgery or a pain in the ankle after the surgery. Therefore, effects on the tibial lateral cortex (TLC) and talus should be considered for successful OWHTO. However, scientific basis is insufficient about the effect of the cutting plane positions (CPP) of the medial proximal tibia. Therefore, the aim of this study was to propose a safety zone by analyzing the stresses on the TLC and talus according to the CPP during OWHTO surgeries. The image data of the right knee of a male cadaver was obtained through computed tomography and a three-dimensional varus deformity (10 degree) model was reconstructed through image processing software (Mimics 20.0, Materialize). After selecting 16 CPPs in 2mm intervals between 5 mm and 40 mm near the tibial plateau, the stresses on the TLC and talus were analyzed through static analysis. The stress on the TLC tended to increase as the CPP formed in a distal zone more than in the proximal zone. For the CPP of 5 mm, the stress on the TLC was lower by 52.3% than the average stress (750.11Mpa) of the total models. Furthermore, for the CPP of 18 mm, the stress on the TLC was lower by 44.8% than the average stress of the total models. In contrast, for the CPP of 30 mm, the stress on the TLC was higher by 79.2% than the average stress. For the CPP of 40 mm, the stress on the TLC was higher by 79.9% than the average stress. At this time, the stress on the talus was 25.8% (193.9Mpa) of the stress on the TLC. The CPP did not show a significant difference in the stress on the talus, but the stress on the talus was the lowest at the CPP of 5 mm and the highest at the CPP of 20 mm. This study provided a biomechanical basis for the safety zone in clinical settings by presenting stresses on TLC and talus by applying actual clinical CPPs. In conclusion, this study suggests that when the OWHTO is applied to patients with varus deformity, a fibula region (30 mm or larger) showing an excessive stress should be excluded from the surgery sites in the clinical application step by considering the changes of stress on the TLC and talus according to the CPP.

Acknowledgments: This research was supported by Basic Science Research Program through the National Research Founding of Korea (NRF) funded by the Ministry of Education (NRF2017R1D1A3B04033410)

[P 29]
BIFURCATION ASYMMETRY INFLUENCES MICROFLUIDIC BLOOD FLOW CHARACTERISTICS

Iveta Jancigova[1]

1 University of Zilina, Cell-in-Fluid: Biomedical Modeling & Computation Group, Zilina, Slovakia

Investigation of microfluidic blood flow in bifurcations is important for understanding the blood behavior in capillary network, where the important gas exchange happens. Several computational approaches have been taken to consider 3D red blood cell flow in bifurcations, such as [1]. Such works typically do not take into account that there are other cells suspended in the blood plasma, some of them comparable in size to the diameter of the bifurcating branches, such as white blood cells or circulating tumor cells. These cells occur at much lower frequency than red blood cells, however, when they do, they have a significant effect on the local flow.

We use a 3D computational model described in [2] and its implementation in open-source scientific software ESPResSo [3] to perform a simulation study of a bifurcating microfluidic channel with red blood cells and a larger stiffer rare cell. We observe how the presence of large rare cell, which flows through the wider daughter branch, impacts the red blood cell distribution in both branches and obtain red blood cell distributions in branches of different diameters.

The model also allows us to quantitatively examine the velocity profiles and fluid forces acting on the red blood cells in symmetric and various asymmetric bifurcations and compare them in situations when a rare cell is and is not present.

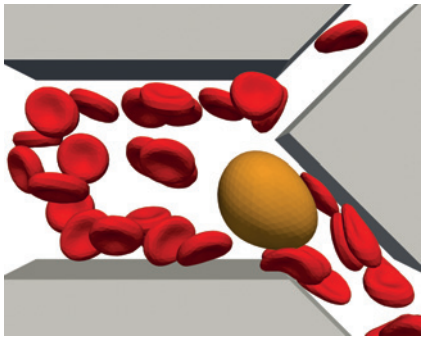

Acknowledgments: This work was supported by the Slovak Research and Development Agency (APVV-15-0751) and by the Ministry of Education, Science, Research and Sport of the Slovak Republic (VEGA 1/0643/17).

References:

[1] T. Ye, L. Peng and Y. Li: Three-dimensional motion and deformation of a red blood cell in bifurcated microvessels, Journal of Applied Physics 123, 064701, 2018.
[2] I. Cimrák and I. Jančigová. Computational Blood Cell Mechanics: Road Towards Models and Biomedical Applications. 1. edition, CRC Press, Taylor & Francis Group, 2019.
[3] F. Weik, R. Weeber, K. Szuttor et al. ESPResSo 4.0 - An Extensible Software Package for Simulating Soft Matter Systems. preprint, 2018.

[P 30]

COMPUTATIONAL STUDY OF CELL-MATRIX INTERACTIONS IN DIFFERENT LOCATIONS OF GROWTH PLATE RESERVE ZONE CARTILAGE

Masumeh Kazemi[1], *John Leicester Williams*[1]

1 *Engineering Technology, Memphis, USA*

Long bones grow by a process in which chondrocytes within growth plate cartilage near the bone ends synthesize and mineralize a cartilaginous matrix that serves as a template for bone cells. The growth plate consists of several distinct zones, including a reserve zone (RZ) that lies between the epiphyseal subchondral bone plate and the proliferative zone. Chondrocytes in the RZ are randomly distributed within an extracellular matrix (ECM), unlike cells in the proliferative zone (PZ) that are arranged in columns. Cells within the RZ seldom divide, but function as stem cells and provide daughter cells to the proliferative zone. Mechanical loading of the growth plate modulates chondrocyte activity and bone growth, but the role of the RZ in relation to this is unclear. To explore this we developed a finite element model of chondrocytes as a function of location in the RZ relative to the epiphyseal and the proliferative zone interfaces.

Based on biomechanical and histological studies of growth plate and mechanobiology theories, an axisymmetric, large deformation model was developed. In this model, chondrocytes were embedded within the RZ/ECM in four different locations. Growth plate cartilage was partitioned into sections to represent the RZ and the proliferative/hypertrophic zones and zone of provisional calcification (PC). Chondrocytes were surrounded by a layer of pericellular matrix (PCM) with a thickness equal to half of the cell radius. By including or excluding the PCM we could examine the influence of the PCM on stress-strain distributions around the chondrocyte. A displacement equivalent to 15% of the overall cartilage thickness was applied at one edge of the model along the long axis of the bone, while the other edge at the PC was fully constrained. First-order axisymmetric hybrid solid elements (CAX4H) were used for all parts. Homogeneous isotropic linear elastic materials properties were assigned to all regions. The average hydrostatic stresses and principal tensile strains in the cells and PCM were calculated as some of the key parameters relating to the mechanobiology of the growth plate.

Our results revealed that the maximum principal strains (tensile) averaged within the chondrocyte increased in magnitude from a value of 6% strain near the epiphyseal subchondral bone to 22% near the proliferative zone. Cellular height and width strains followed a similar trend. However, the opposite pattern was observed for the cell hydrostatic compressive stresses which decreased in magnitude by 45%. The presence of PCM resulted in an approximate 20% increase in the cellular maximum principal strains in all locations and a 7 to 16% decrease in cellular hydrostatic pressure, depending on cell location. The role of the PCM in amplifying cellular strains appears to be similar to what has been reported for articular cartilage.

[P 31]

FINITE ELEMENT MODELLING OF FOUR-POINT BENDING TEST OF PMMA BONE CEMENT WITH PORES

Sunjung Kim[1], *Heidi-Lynn Ploeg*[2], *Aaron Bishop*[3], *Warren Rose*[4], *Suzan Ozgur*[5]

1 *University of Wisconsin, Madison, USA*
2 *Queen's University at Kingstondepartment of Mechanical and Materials Engineering Mclaughlin Hall Room Queen's University, Ontario, Canada*
3 *University of Wisconsin, Madison, USA*
4 *University of Wisconsin, Madison, USA; School of Pharmacy University of Wisconsin, Madison, USA*
5 *Department of Mechanical and Materials Engineering Mclaughlin Hall Room, Queen's University, Ontario, Canada*

Introduction: Polymethyl methacrylate (PMMA) bone cement is a grouting material used for anchoring cemented arthroplasties to contiguous bone. In a previous study, we tested the mechanical properties, drug elution, and efficacy of PMMA with added antibiotics [1]. This study found PMMA mechanical properties (Palacos and Simplex) decreased with increasing amounts of added antibiotics (Vancomycin and Telavancin). After the drug elutes, pores remain, and degrade the PMMA mechanical properties. The purpose of the current study was to investigate the effect of pores on PMMA mechanical properties. Finite element analysis (FEA) was used to calculate the mechanical strength and apparent modulus of PMMA with pores. FEA results were evaluated against the experimental results.

Method: Planar symmetric, plane stress FEA models of PMMA four-point bending specimens (7 samples per group, 75 mm 10 mm 3.3 mm, Palacos® and Simplex P) were developed using geometric tools in Abaqus 6.11 (Dassault Systèmes, Velizy-Villacoublay, France). Pore size and number were quantified from scanning electron and micro computed tomography images. (Fig. 2 and 3). The Young's modulus considering the contact mechanics and Von Mises stress were calculated and compared with the experimental results. Vertical displacement was applied to the top rigid cylinder and the bottom cylinder was fixed (Fig.1). Frictionless contact was assumed. The measured and calculated apparent Young's moduli were corrected for Hertz contact at the load points.

Results and Discussion: The measured apparent elastic modulus of Palacos bone cement with added Telavancin were 2284 ± 164 and 2075 ± 130 MPa, for controls and 2 g added antibiotic, respectively. These measured apparent values were corrected for Hertz contact to 2312 ± 169 MPa and 2103 ± 139 MPa. The calculated corrected modulus from FEA for controls and 2 g of added Telavancin were statistically not different (two tailed paired student t-test, $\alpha = 0.05$) than the measure ones, 2363 ± 160 MPa and 2205 ± 104 MPa. 2 g of Telavancin decreased the apparent modulus by 9.1% when compared with the control group. Flexural strength from the experiment and von Mises stress from FEA were also compared. The measured flexural strength of the PMMA control and with 2 g of added Telavancin from the experiments were 55.3 ± 3.50 MPa and 47.8 ± 5.47 MPa, respectively. The FEA calculated von Mises stress of the PMMA control and with 2 g of added Telavancin were 66.9 ± 1.52 and 61.7 ± 3.72 MPa, respectively. The flexural strength of PMMA with 2 g of added Telavancin was reduced by 13.5 % in comparison to controls. These findings indicate that the PMMA porosity significantly affected the mechanical properties.

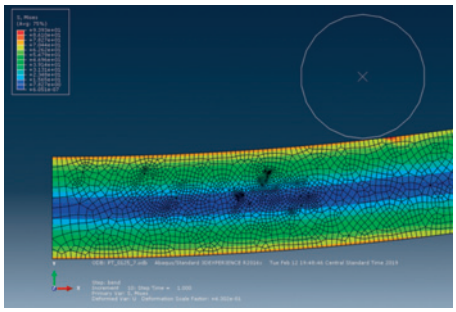

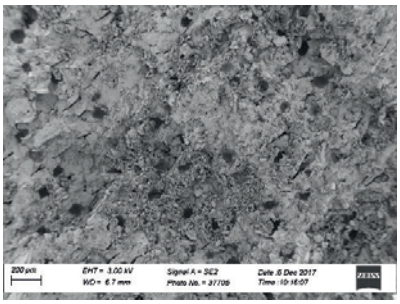

Fig 1. Von Mises stress plot of PMMA sample in four point bending
Fig 2. Micro CT scan of three point bending test sample for fracture toughness
Fig 3. SEM image for 1g of Telavancin in Palacos sample

Acknowledgments: Funding for this study has been provided by Theravance Biopharma. Current results with Vancomycin with later be used as comparison and baseline for the analysis of Televancin. WR has received consulting fees from Theravance

References:

[1] A. R. Bishop, S. Kim, M. W. Squire, W. E. Rose, and H.-L. Ploeg, "Vancomycin elution, activity and impact on mechanical properties when added to orthopedic bone cement," J. Mech. Behav. Biomed. Mater., vol. 87, 2018.

[P 32]

MICRO-CT IMAGING AND DIGITAL VOLUME CORRELATION TO EVALUATE GLENOID DEFORMATION AFTER TOTAL SHOULDER ARTHROPLASTY

*Yasmine Boulanaache[1], Alain Farron[2], Fabio Becce[2], **Dominique Pioletti3**, Alexandre Terrier[1]*

1 *Laboratory of Biomechanical Orthopedics; Ecole Polytechnique Fédérale de Lausanne (Epfl), Lausanne, Switzerland*
2 *Centre Hospitalier Universitaire Vaudois (Chuv), Lausanne, Switzerland*
3 *Laboratory of Biomechanical Orthopedics; Epfl; Lbo, Ecole Polytechnique Federale de Lausanne (Epfl), Lausanne, Switzerland*

After anatomical total shoulder arthroplasty, the fixation of the glenoid implant remains a major source of complication and failure[1-4]. The objective of this study was to develop a technique to measure in vitro bone strain around a typical cemented polyethylene glenoid implant sustaining compressive load on the humeral implant. The method is based on micro-CT and digital volume correlation. A loading device was developed to fit within a micro-CT. Elastix [5] open source toolbox was used to estimate the displacement vector field and Abaqus FE (Simulia, Dassault Systèmes) solver to derive strain tensor field. A parametric study provided optimal non-rigid transformation parameters. Systematic and random errors of displacement and strain were evaluated with three pairs of unloaded scans. In addition, accuracy and precision of the method were defined by mean absolute error and standard deviation of absolute error respectively, of measured strains [6, 7]. A compressive force of 1500 N was applied from the humeral component to the glenoid component. Systematic and random errors of displacement were below 37.9 µm, and 29.8 µm respectively. Systematic and random errors of compressive strain were below 898 µε and 8100 µε respectively. The average precision and accuracy were 1621 µε and 1466 µε respectively. The displacement in the loading direction was up to 600 µm on the anterior side, thus hinting at a bending movement. The minimal principal strain associated to 1500 N was above the systematic error and below 10'000 µε for most glenoid bone volume (85%). This technique should be applied to a series of samples, to report bone strain variability after total shoulder arthroplasty and may also be used to validate numerical models.

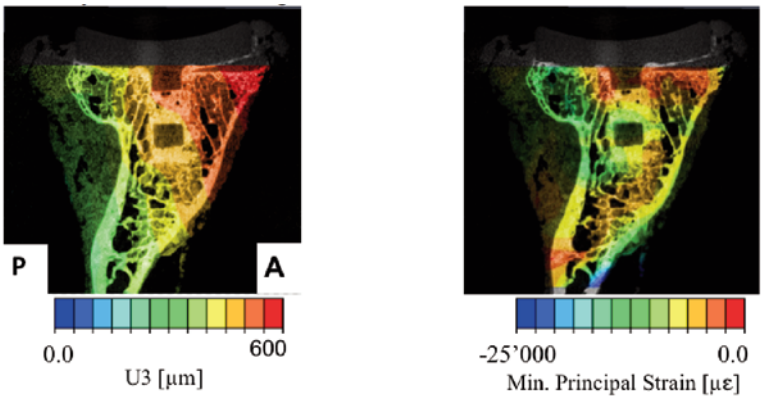

Figure Caption: Displacement (U3) along loading axis (left) and bone minimum principal strain (right) caused by 1500 N axial loading.

Acknowledgments: This project is financially supported by the Swiss National Science Foundation (CR32I2_162766), with the material and technical support of Tornier-Wright Medical.

References

1. *Chevalier et al. J Biomech, 2016. 49(9): p. 1724-33.*
2. *Wee et al. J Orthop Res, 2015. 33(11): p. 1671-9.*
3. *Lewis et al. J Orthop Res, 2016. 34(6): p. 1053-60.*
4. *Sabesan et al. J Shoulder Elbow Surg, 2015. 24(5): p. 814-22.*
5. *Klein et al. IEEE Transactions on medical imaging, 2010. VOL. 29, NO. 1.*
6. *Liu et al. J Biomech, 2007. 40(15): p. 3516-20.*
7. *Dall'Ara et al. Frontiers in Materials, 2017. 4.*

[P 33]

AN AUTOMATED WORKFLOW FOR GENERATING FINITE ELEMENT MODELS OF THE KNEE

Marco Schneider[1], *Nynke Rooks*[1], *Thor Besier*[2]

1 *The University of Auckland, Auckland Bioengineering Institute, Auckland, New Zealand*

2 *The University of Auckland, Auckland Bioengineering Institute, Auckland, New Zealand; Department of Engineering Science, The University of Auckland, Auckland, New Zealand*

Computational models are routinely used in academic research and to provide patient specific clinical care in orthopaedics. However, the reproducibility of these simulation results are questionable. Thus, it is important to identify and minimize subjective components in modelling and simulation workflows, such as sources of human error. Manual segmentation of 3D images is not only time-consuming, but segmentation accuracy depends highly on the experience of the person performing segmentation. Here we present an automatic workflow for generating patient specific finite element (FE) models of the knee from MRI.

MRI data (n=25) of healthy adult knees (mean age = 28.6 ± 4.0 years) were obtained from a study on patellofemoral pain [1] and manually segmented in Stradwin (Machine Intelligence Laboratory, University of Cambridge) to produce triangulated point clouds (n=25) (Figure, A). These data were randomly separated into a set of training data (n=20) and test data (n=5) (Figure, B). DeepSeg (Formus Labs, New Zealand) was used to train a neural network (Figure, C) on the training set point clouds to label the MRI voxels as either femur, tibia, patella, femoral cartilage, medial tibial cartilage, lateral tibial cartilage, or patellar cartilage, and used to automatically segment the test data set (Figure, D). Automatic segmentation accuracy was evaluated against manual segmentation using the DICE score. A previously established workflow [2] that uses the MAPClient [3] (Figure, E) and custom Python code (Figure, F) was used to generate FE models of the knee from both automatically and manually segmented knee MRIs. Mean error, and time cost were evaluated between FE models generated from automatically and manually segmented MRIs.

The mean error in the FE model generated from automatically segmented data was 0.83 ± 0.91 mm. Average DeepSeg DICE scores were 0.945 and 0.753 for bone and cartilage respectively, with a mean segmentation time of 02m42s. Mean total time taken to generate FE models from unsegmented MRI data was 19m42s, compared with over 6 hours manually.

The results show promise for a fully automatic tool that improves both the reproducibility and speed of musculoskeletal modelling workflows. DeepSeg DICE scores were good despite a small training set. In the future we plan to extend the training set to improve the capabilities of the workflow.

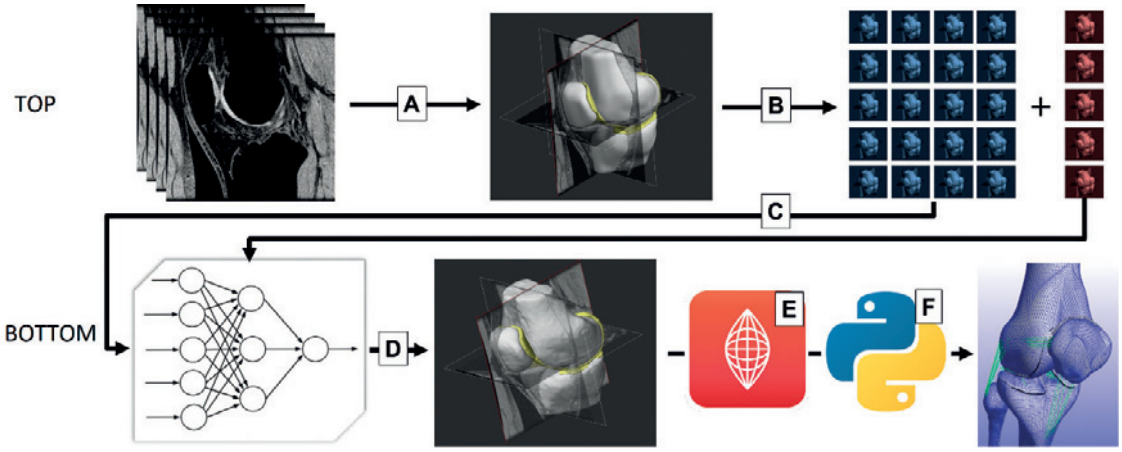

Figure Caption: Schematic showing the process for training a neural network (Top: A, B, & C) and the automatic workflow for generating FE models automatically (Bottom: D, E, & F).

Acknowledgments: We would like to acknowledge the NIH for funding (award number 1R01EB024573-01).

References:

1. *Besier TF et al. (2015). Med Sci Sports Exerc, 47(11), 2416-2422.*
2. *Kazemi M. (2018). The University of Auckland (Thesis)*
3. *Zhang J et al. (2014). Biomed Sim. 8789, 182-192.*

[P 34]

COUPLING OF INERTIAL MEASUREMENT UNITS WITH A VIRTUAL WORLD MODEL FOR SUPPORTING NAVIGATION IN BRONCHOSCOPY

Dariusz Michalski[1], *Zbisław Tabor*[1], *Tomasz Nabagło*[1]

1 *Faculty of Physics, Mathematics and Computer Science, Cracow University of Technology, Cracow, Poland*

Background and objective: The purpose of this paper is to provide a method for supporting navigation in bronchoscopy based on measurements of absolute orientation of a tip of a bronchoscope and the length a bronchoscope is pushed in the lumen of an examined bronchial structure.

Methods: A hardware solution is designed and developed for collecting the data related to the absolute orientation of a tip of a bronchoscope and the length a bronchoscope is pushed in the lumen of an examined structure. A software which processes these data and visualizes in real-time the actual location of a bronchoscope tip in the lumen of a digital model of the examined structure (i.e. virtual bronchoscopy) is also designed and implemented.

Results: A calibration procedure is developed which constitutes a basis for the operation of the proposed system. A phantom of a tree-like structure is build, imitating the anatomy of a bronchial tree, and the proposed method of navigation is tested for the task of navigating in the lumen of the phantom to user-selected target locations.

Conclusion: A method has been proposed and tested for Inertial Measurement Unit (IMU)-based support of navigation in bronchoscopy.

Acknowledgments: The study was supported by National Center for Research and Development under a grant No. PBS3/A9/31/2015.

References:

Wang KP, Mehta AC, Turner JF, editors. Flexible Bronchoscopy. 2nd ed. Cambridge: Blackwell; 2003.
Yarmus L, Feller-Kopman D. Bronchoscopes of the twenty-first century. Clin Chest Med 2010;31:19–27.
Dooms C, Seijo L, Gasparini S, Trisolini R, Ninane V,Tournoy KG. Diagnostic bronchoscopy: state of the art. Eur Respir Rev 2010;19:229–36.
Tsushima K, Sone S, Hanaoka T, Takayama F, Honda T, Kubo K. Comparison of bronchoscopic diagnosis for peripheral pulmonary nodule under fluoroscopic guidance with CT guidance. Respir Med 2006;100:737–45.
Eberhardt R, Anantham D, Ernst A, Feller-Kopman D, Herth F. Multimodality bronchoscopic diagnosis of peripheral lung lesions: A randomized controlled trial. Am J Respir Crit Care Med 2007;176:36–41.
Schwarz Y, Mehta AC, Ernst A, Herth F, Engel A, Besser D, et al. Electromagnetic navigation during flexible bronchoscopy. Respiration 2003;70:516–22.
Becker H, Herth F, Ernst A, Schwarz Y. Bronchoscopic biopsy of peripheral lung lesions under electromagnetic guidance. J Bronchol 2005;12:9–13.
Michalski D, Tabor Z, Zieliński B. Determining the shift of a bronchoscope catheter from the analysis of a video sequence of a bronchoscope video camera. Biocybern Biomed Eng 2017;37:630–6.
Higgins WE, Helferty JP, Lu K, Merritt SA, Rai L, Yu K-C. 3D CT-video fusion for image-guided bronchoscopy. Comput Med Imaging Graph 2008;32:159–73.
Schwarz Y, Greif J, Becker HD, Ernst A, Mehta A. Real-time electromagnetic navigation bronchoscopy to peripheral lung lesions using overlaid CT images. Chest 2006;124:988–94.

[P 35]

MIXED REALITY ENHANCED SURGICAL NAVIGATION SYSTEM FOR NEUROSURGERY

Ching-Shiow Tseng[1], *Chih-Ju Chang*[2], *Te-Hsuan Feng*[1]

1 *Department of Mechanical Engineering; National Central University,Taoyuan, Taiwan*

2 *Department of Neurosurgery; Cathay General Hospital, Taipei, Taiwan*

Neurosurgery requires accurate positioning of surgical instruments during operation to avoid any unexpected damage of critical tissues such as cerebral arteries1. However, it is not safe to plan surgical path without knowing if it collides with blood vessels. This study presents a mixed reality (MR) enhanced surgical navigation system for minimally invasive neurosurgery to avoid the damage of arterial vessels2. The system integrates augmented reality with a surgical navigation system. The 3D computer models of the head and arterial vessels of a patient are reconstructed from computed tomography angiography images by using image processing, segmentation, and computer modeling technologies. The 3D arterial vessel computer model, having the same coordinate frame as the head computer model, is registered with the physical head model (phantom fabricated by 3D printing) by feature points using interactive closest points algorithm. The projection of 3D arterial vessel computer model of the HoloLens onto the physical head model is calibrated by using a registration board, which is designed to have the spatial geometric relation between the dynamic reference frame for the optic tracker and the tracking markers for the Microsoft HoloLens. The surgical path can be preplanned on the combined 3D head and arterial vessel computer models prior to operation. During operation, the neurosurgeon, wearing a head-mounted display (Microsoft HoloLens), can see through the patient's head and watch the 3D arterial vessel model with the planned path projected inside the head. Through the tracking of positioning probe by the optic tracker, the neurosurgeon can manipulate the positioning probe to match the preplanned path and obtain the entry point of the surgical instrument on the head. An experiment to mix the 3D arterial vessel model with head model was completed as shown in Fig. 1. Fig. 2 also shows the brain ditch for assisting path planning.

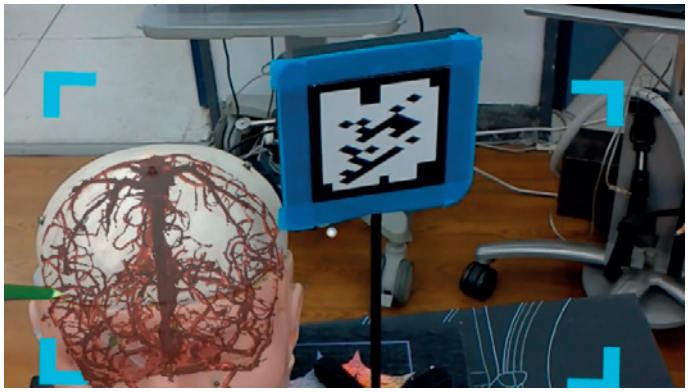

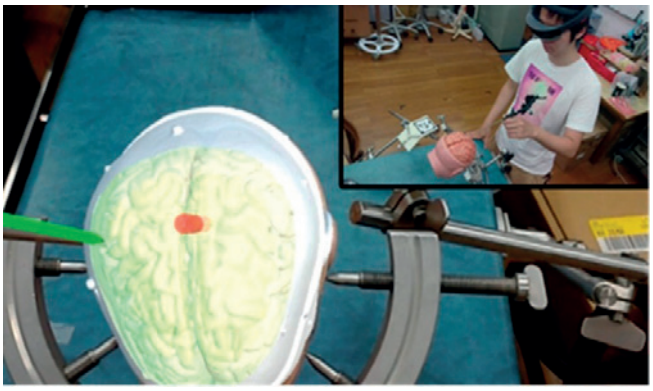

Fig. 1 The mixed reality of 3D arterial vessel model with the physical head model
Fig. 2 The mixed reality of 3D brain model with the physical head model

Acknowledgments: Special thanks for the financial support from the Ministry of Science and Technology, Taiwan, under the contract of MOST 107-2218-E-008-006 and MOST 107-2622-B-008-004.

References:

1. *D. Guha, N. Alotaibi, N. Nguyen, et al., "Augmented Reality in Neurosurgery: A Review of Current Concepts and Emerging Applications", Canadian Journal of Neurological Sciences, vol. 44, no. 3, pp.1-11, April 2017.*
2. *F. Cutolo, A. Meola, M. Carbone, et al., "A new head-mounted display-based augmented reality system in neurosurgical oncology: a study on phantom", Computer Assisted Surgery, vol. 22, Issue 1, 2017.*

[P 36]

FINITE ELEMENT SIMULATIONS FOR INVESTIGATING THE CAUSE OF CATASTROPHIC WEAR AND/OR FAILURE OF POLYETHYLENE ACETABULAR CUP LINER IN HIP PROSTHESIS

Changhee Cho[1], *Toshiharu Mori*[2], *Makoto Kawasaki*[3]

1 *The University of Kitakyushu, Kitakyushu, Japan*
2 *Shin-Kokura Hospital, Fukuoka, Japan*
3 *University of Occupational and Environmental Health, Fukuoka, Japan*

Ultra-high molecular weight polyethylene (UHMWPE) is the sole polymeric material currently used for weight-bearing surfaces in total joint replacement. However, the wear and failure of UHMWPE after total joint replacement cause serious clinical and biomechanical reactions, such as osteolysis and eventual loosening of artificial joints. Therefore, the wear and failure of the UHMWPE are now recognized as the major factors restricting the longevity of artificial joints. In order to minimize the wear and failure of the UHMWPE and to improve the longevity of artificial joints, it is necessary to clarify the factors influencing the wear and failure mechanism of the UHMWPE. The generations of catastrophic wear and/or failure of the UHMWPE acetabular cup liner are frequently observed in retrieved hip prostheses as shown in Figures A and B (Cho et al., 2016). The primary purpose of this study is to investigate the cause of catastrophic wear and/or failure of the UHMWPE acetabular cup liner in hip prosthesis. The authors focused on change in mechanical state of the UHMWPE liner due to contact with metallic component as a factor influencing the wear and failure mechanism of the UHMWPE liner. Contact analyses between the UHMWPE liner and metallic components by using the finite element method (FEM) were performed in order to investigate the mechanical state of the UHMWPE liner. The metallic components were assumed to be rigid bodies. The UHMWPE liner was assumed to be an elasto-plastic body that has the Poisson's ratio equal to 0.45. The linear elastic modulus, the yield stress and the tensile strength of the UHMWPE were 498, 13.3 and 167.6 MPa respectively. The coefficient of friction between the contact surfaces was assumed to be 0.1. All the finite element simulations in this study were performed by using the commercial finite element analysis software ANSYS. An example of the analysis results is shown in Figure C. It was found that high contact stresses which exceed the yield stress of UHMWPE and considerable plastic deformations occurred in the rim of the UHMWPE liner. It was also found that high stress concentrations occurred near screw holes in the acetabular cup and notches in the UHMWPE liner. This study confirmed that change in mechanical state due to contact with metallic component is the cause of catastrophic wear and/or failure of the UHMWPE liner.

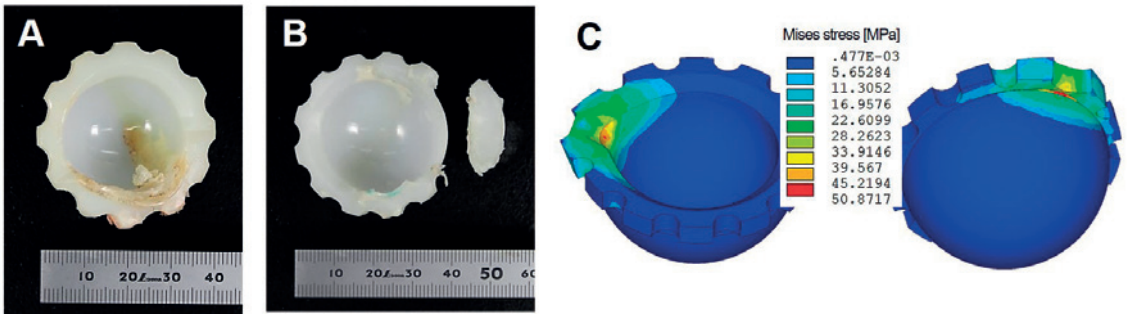

Figure Caption: Retrieved UHMWPE acetabular cup liners showing catastrophic wear and/or failure (A and B) and an example of FEM simulation results (C).

Acknowledgment: This work was supported by JSPS KAKENHI Grant Number JP17K01391.

Reference:

Cho C., Mori T. and Kawasaki M., "Observation of wear characteristics on retrieved polyethylene liners of hip prostheses", Japanese Journal of Clinical Biomechanics (in Japanese), Vol. 37, 243-249, 2016.

[P 37]

EFFECT OF KNEE JOINT TRANSVERSE PLANE MALALIGNMENT ON TIBIOFEMORAL CONTACT MECHANICS

Nuno Correia[1], *Howard Hillstrom*[2], *Olliver Morgan*[3], *Qasim Mohammed*[4], *Robert Rozbruch*[2], *Rajshree Hillstrom*[3]

1 *Medical Engineering; Anglia Ruskin University, Chelmsford, UK (Medbic Department)*
2 *Hospital of Special Surgery, New York, USA*
3 *Anglia Ruskin University, Medbic, Chelmsford, UK*
4 *Anglia Ruskin University, Chelmsford, UK*

Lower limb malalignment in the frontal plane increases knee joint contact forces and stress,1 which has been implicated in Osteoarthritis (OA) onset and progression.2 Transverse plane malalignment of the knee may also be present in individuals with OA. While the effect of frontal malalignment on knee joint contact mechanics has been widely investigated, research on transverse plane malalignment is sparse. The aim of this study was to investigate the effect of tibial transverse plane malalignment on medial and lateral compartment stress in the knee.

A three-dimensional (3D) specimen-specific Finite Element model (FE) of a left cadaveric knee joint (male, 50 years old, 1.65m, 68-kg) was previously developed and compared with in vitro testing to provide an experimental validation.4 The model includes geometries for the femur, tibia, patella, and meniscus, as well as the corresponding cartilages, and ligaments as shown in Figure 1. Forces and moments at heel-off during stance phase of a healthy, anthropometrically-matched 68-kg male subject were used to load the model. Heel off corresponds to the maximum external moment through stance phase so the model was solved for that event in gait. Subsequently, a variety of transverse plane moments ranging from 20 Nm internal to 20 Nm external were applied to the tibia to simulate different grades of transverse plane malalignment. FE analyses were run to determine magnitudes and locations of peak von Mises stress in the medial and lateral tibial compartments.

The analysis results are shown in Figure 2. At external moments of 5 Nm, 10 Nm, 15 Nm, and 20 Nm, the medial tibial cartilage stress increased by 11%, 25%, 54%, and 55%, respectively. Lateral tibial cartilage showed relatively small changes in stress magnitude. Internal moments demonstrated a variety of increasing and decreasing stress magnitudes in both medial and lateral cartilage.

A cadaveric-specific validated FE Model of a neutrally-aligned knee was used to compare different transverse plane moments (i.e. 20 Nm internal to 20 Nm external), to simulate transverse plane deformity. Our results showed that internal moments have less influence on stress than external moments. This preliminary study was a first step towards determining the effect of transverse malalignment on knee joint stress.

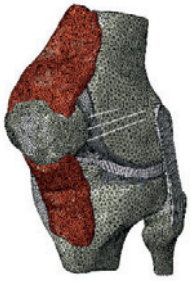

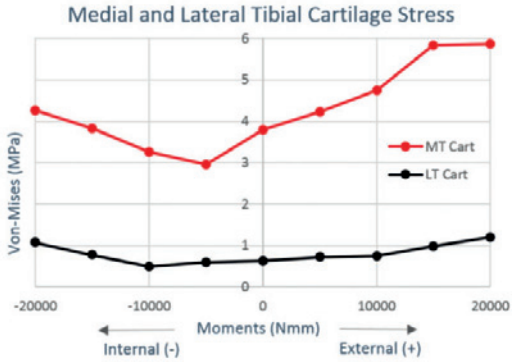

Figure 1 - Validated FE model with a patella and Quadriceps Tendon implemented
Figure 2 - Representation of the Medial and Lateral Tibial Cartilage Von-Mises Stress (MPa) and its variables throughout the addition of Internal and External Moments

Acknowledgments: Funding from the Center for Limb Lengthening and Reconstruction, Dr Austin Fragomen for clinical interpretation, Mark Lenhoff for joint coordinate system development.

References:

1. *Buly, R.L. et al., 2018, J Am Acad Orthop Surg;*
2. *Matsumoto, T., et al., 2015, Osteoarthritis Cartilage, 23(2):217-223;*
3. *Fragomen, A.T., et al., 2018, Knee Surg, 31(4):359-369;*
4. *Mootanah, R., et al., 2014, CMBBE, 17(13):1502-17. 25(3): 379-386.*

[P 38]

PIEZOELECTRIC ENERGY HARVESTING CONCEPT FOR ENERGY-AUTONOMOUS INSTRUMENTED ORTHOPAEDIC IMPLANTS - A NUMERICAL EVALUATION

Hans-E. Lange[1], *Dennis Hohlfeld*[2], *Daniel Klüß*[1]

1 *Department of Orthopaedics, Biomechanics and Implant Technology Research Laboratory (FORBIOMIT), Rostock University Medical Center, Rostock, Germany*
2 *Institute for Electronic Appliances and Circuits, Faculty of Computer Science and Electrical Engineering, University of Rostock, Rostock, Germany*

Introduction: Hip joint replacements show an actual low revision burden, nevertheless, the constantly increasing number of primary arthroplasties is accompanied by a rising absolute number of failed implants. To overcome remaining insufficiencies, research is conducted on instrumented implants with sensory or active functions. A better outcome is expected by monitoring implant-related parameters and taking therapeutic measures e.g. stimulation of bone growth.

Instrumented implants pose the question of adequate energy supply. The use of external sources or batteries goes along with limitations like dependency on availability respectively limited lifetime.

The aim of this work is therefore the evaluation of an internal piezoelectric energy harvesting concept for an energy-autonomous hip implant by means of finite-element-analysis (FEA) in order to investigate the potential of energy conversion with regard to mechanical implant safety.

Methods: A CAD model of a standard hip stem was virtually implanted into a CT-based femoral geometry [1] assuming a homogeneous layer of bone cement. In ANSYS, physiologically-based boundary conditions were assigned to allow realistic deformations [2]. A reduced set of muscle forces [3] and a hip contact force from in-vivo measurements [4] (instance of maximum loading during walking) were applied. Linear material behaviour was assumed. For the femoral bone, a CT-related material model was employed [5]. Based on the initial stress distribution results, a modified hip stem was developed by introducing a piezo element encapsulated in an ultra-high-molecular-weight polyethylene (UHMWPE)-housing. Stresses were evaluated for all implant components and the open circuit voltage of the piezo element was calculated, assuming lead zirconate titanate (PZT) ceramic. Exemplarily, the energy output was quantified for a simplified equivalent circuit with a single load resistance and sinusoidal voltage.

Results and Discussion: A new concept for energy harvesting within a hip implant was developed. The UHMWPE-housing assures appropriate positioning of the piezo element, environmental sealing and adequate force distribution. Stresses within the piezo element and housing are in a reasonable range. For the hip stem, a maximum stress level comparable to the unmodified geometry at equal loading conditions may be preserved.

In the present study it was shown that a transfer of the loading through the hip stem on the integrated piezo element with the objective of energy harvesting is feasible. In further investigations the integrated geometries will be numerically optimised with regard to an increased electrical output while not impairing the mechanical implant safety.

Acknowledgements: This research is affiliated to the Collaborative Research Centre 1270, funded by the German Research Foundation (DFG).

References:

[1] Soodmand et al., BiomedEngOnline, 17(1):29, 2018.
[2] Speirs et al., JBiomech, 40(10):2318–23, 2007.
[3] Heller et al., JBiomech, 38(5):1155–63, 2005.
[4] Bergmann et al., JBiomech, 34(7):859–71, 2001.
[5] Taddei et al., MedEngPhys, 29(9):973–79, 2007.

[P 39]

COMPARISON BETWEEN A PORTABLE PRESSURE MEASURING EQUIPMENT AND PICOPRESS IN GARMENT PRESSURE MEASUREMENT ON HYPERTHOPHIC SCAR FOLLOWING BURN INJURY

Seung Yeol Lee[1], *SO YOUNG JOO*[2], *Sang-Hyun Kim*[1], *Hyun Seok*[1]

1 *Department of Physical Medicine and Rehabilitation, Soonchunhyang University College of Medicine, Soonchunhyang University Bucheon Hospital, Bucheon-si, Gyeonggi-do, Korea, Rep. of South*

2 *Hangang Sacred Heart Hospital, College of Medicine, Hallym University, Seoul, Korea, Rep. of South; Department of Rehabilitation Medicine, Hangang Sacred Heart Hospital, College of Medicine, Hallym University, Seoul, Korea, Rep. of South, Seoul, Korea*

Background: The current standard treatment of hypertrophic scars following burn injury is pressure garment therapy (PGT). In most of the studies, garment pressure has been measured merely at one or a few levels along the extremity. We developed a portable pressure measuring equipment using force sensitive resistor (FSR) sensors. Its size and maneuverability allowed it to accommodate. PicoPress®, a manometry-based sensor, has been known to be the most accurate with least variation and error. The goal of this study aimed to compare and examine the accuracy between a developed portable pressure measuring equipment and PicoPress® (Microlab, Padua, Italy) to measure in-vitro interface pressure.

Material and Methods: Each sensors qualitative attribute to adjust the resistance in inverse proportion of the force. Fifteen FSR sensors were calibrated. The flexibility and thinness of the sensors allows it to be placed easily between the hypertrophic scar and the compression garment. The sensing pressure was captured by a readout circuitry consisted of an analog to digital converter, microprocessor, and Bluetooth® transmission module for data acquisition and wireless transmission to a mobile device. All signals were ultimately converted to pressure (mmHg). Mean pressure values measured by all FSR sensors were compared to the values measure by PicoPress®. Paired t test was used to compare the mean pressure values of the FSR sensors to the values of PicoPress®.

Results: Forty garment pressure were measured by FSR sensors. PicoPress® was also used for measurement of the same pressure garments. Compared to the values of PicoPress®, the mean pressure values of the FSR sensors demonstrated without significant statistical difference ($p > 0.05$).

Conclusions: Portable pressure measuring equipment using FSR sensors may present a viable alternative to PicoPress® in measuring pressure of the garment. The advantage of portable pressure measuring equipment was its adaptability to hypertrophic scar size. Using wireless transmission to a mobile device, this device could be worn by burn patients anytime of day with real time data capture during garment therapy.

Figure. Force Sensitive Resistor (FSR) Sensor.

Acknowledgments: This research was supported by National Research Foundation of Korea(NRF), funded by the Ministry of Education (NRF-2018R1C1B5044080).

References:

[1] *Yildiz N. A novel technique to determine pressure in pressure garments for hypertrophic burn scars and comfort properties. Burns : journal of the International Society for Burn Injuries. 2007;33:59-64.*

[2] *Macintyre L. Designing pressure garments capable of exerting specific pressures on limbs. Burns : journal of the International Society for Burn Injuries. 2007;33:579-86.*

[3] *Mann R, Yeong EK, Moore ML, Engrav LH. A new tool to measure pressure under burn garments. The Journal of burn care & rehabilitation. 1997;18:160-3; discussion 59.*

[P 40]

ANALYSIS OF MOTION SYNERGIES IN GRASPING TASKS FOR A 6-DOF TENDON-DRIVEN PROSTHETIC HAND

Immaculada Llop-Harillo[1], *Antonio Pérez-González*[2], *Jesús Cantero-Ramis*[2]

1 *Universitat Jaume I, Castellón, Spain (Uji) Departamento de Ingeniería Mecánica Y Construcción; Universitat Jaume I, Castellón, Spain; 2Universitat Jaume I, Castellón, Spain (Uji)*

The design of new affordable hand prostheses has increased in last years because of the improvements in 3D-printing technologies. Most of these hands are moved by tendons connected to electrical motors. A tradeoff between the number of motors and the grasping ability of the prosthetic hands appears during the design process. Fewer motors allow reducing weight and cost, but at the expense of lesser motion versatility. The analysis of the motion synergies in an artificial hand with a high number of degrees of freedom (DOF) could be a method to solve this tradeoff. The fingers for which the motions of the tendons are highly correlated can be candidates to be moved by a single motor. The aim of this study is to analyze the coordination of motion among finger's tendons of a 6-DOF prosthetic hand, the IMMA hand [1], while performing grasping tasks through the Anthropomorphic Hand Assessment Protocol (AHAP) [2]. The test was performed by three able-bodied subjects, using an able-bodied adaptor (ABA) connected to their forearm (Figure 1) allowing the control of the prosthesis with their fingers. The ABA incorporates six linear potentiometers and an Arduino board that registers the displacement of the six tendons of the hand, one for each long finger and two for the thumb. The AHAP is composed of 26 tasks involving the eight most common human grasp types, using objects of the publically available YCB set. The motion coordination between each pair of DOF for a task was analyzed through the correlation coefficient (CC) of the vectors containing the displacements of the corresponding tendons until the grasp of the object is established. We computed the synergy for each pair of DOF as the percentage of tasks of the AHAP for which the CC was higher than 0.9. A two-way ANOVA on these synergies with factors subject and pair of DOF was computed. The results showed that the subject's effect was non-significant ($p=.253$) and the synergies were significantly different ($p<.001$) for each pair of DOF. A post-hoc analysis showed that the highest synergies appeared for any pair of long finger's DOF and for the pair of DOF of the thumb. A principal component analysis on the displacements of the tendons was done, with two principal components explaining near 80% of the variance. Further research should address the design of the transmission and actuation systems of the IMMA hand taking into account the results obtained in this study.

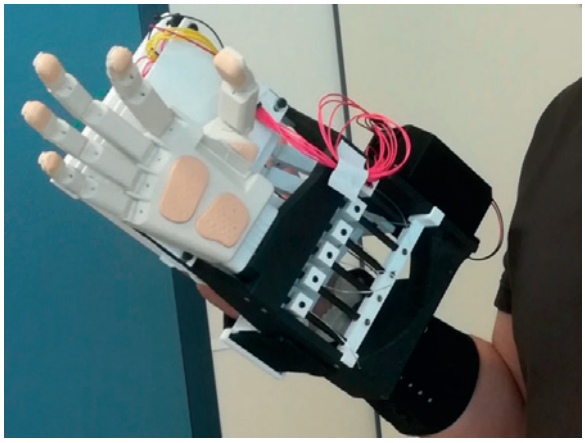

Figure 1: IMMA hand and able-bodied adaptor.

Acknowledgments: This work was supported by grants DPI2017-89910-R and BES-2015-076005 from the MINECO, ERDF and ESF, and by grant UJI-B2017-70 from Universitat Jaume I, Castellón, Spain.

References:

[1] *Llop-Harillo et al.,International Biomechanics 4(2):50-59,2017.*
[2] *Llop-Harillo et al.,Robotics and Autonomous systems [under review].*

[P 41]

THE ROLE OF PROTEIN CONCENTRATION ON THE RHEOLOGY OF SYNOVIAL FLUID WHEN MODELLING ELASTO-HYDRODYNAMIC LUBRICATION OF JOINT PROSTHESES.

Lee Nissim[1], *Hamza Butt*[1], *Leiming Gao*[1], *Connor Myant*[2], *Robert Hewson*[1]

1 *Imperial College London, Department of Aeronautics, London, UK*
2 *Imperial College London, Dyson School of Design, London, UK*

Joint replacements have been performed since the 1960s, the most common being hip and knee implants. Data collected from 2014 shows that, across the EU, on average 319 hip and knee replacements are carried out per 100 000 people. This equates to over 1.6 million surgeries annually. A number of factors including ageing populations, increasing life expectancy and improving joint designs mean that the number of replacement and revision procedures is only set to continue rising.

The difficulty in modelling synovial joints stems from complex geometry and the multi-component nature of the fluid. Proteins in the synovial fluid induce complex rheological behaviour [1][2], which is geometry specific due to the length scale of the protein which is of the same order as the fluid film thickness. It can be seen in the experimental work of Myant, Cann et al. [3][4] that protein matter collects at the inlet of the lubricated contact area and this aggregation leads to greatly increased film thickness as compared to those predicted by modelling the elasto-hydrodynamic lubrication (EHL) regime with the bulk synovial fluid properties.

In this work a ball on plate geometry is computationally modelled by coupling finite-difference derived EHL solutions with the transport of protein matter using a modified advection-diffusion equation to simulate aggregation and identify protein concentration changes. The local viscosity of the lubricating synovial fluid was updated to achieve transient simulations that capture the nature of Protein Aggregation Lubrication (PAL) and obtain film thickness predictions. Response surface based inverse methods were used to match the constants in the constitutive equations, giving agreement with observed phenomenon and providing general models for synovial fluid in constrained geometries.

References:

[1] *J. Hron, J. Málek, P. Pustěovská and K. R. Rajagopal, "On the modeling of the synovial fluid," Advances in Tribology, 2010.*
[2] *T. Kitano, G. A. Ateshian, V. C. Mow, Y. Kadoya and Y. Yamano, "Constituents and pH changes in protein rich hyaluronan solution affect the biotribological properties of artificial articular joints," Journal of Biomechanics, vol. 34, no. 8, pp. 1031–1037, 2001.*
[3] *C. Myant and P. Cann, "In contact observation of model synovial fluid lubricating mechanisms," Tribology International, vol. 63, pp. 97-104, 2013.*
[4] *J. Fan, C. W. Myant, R. Underwood, P. M. Cann, and A. Hart, "Inlet protein aggregation: a new mechanism for lubricating film formation with model synovial fluids," Proceedings of the Institution of Mechanical Engineers, Part H: Journal of Engineering in Medicine, vol. 225, no. 7, pp. 696-709, 2011.*

[P 42]

TOPOLOGY OPTIMIZATION OF ACETABULAR IMPLANTS FOR LARGE BONE DEFECTS

Fernando Perez Boerema[1], *Alexander Meynen*[2], *Lennart Scheys*[3], *Liesbet Geris*[4]

1 *Biomechanics Section, Ku Leuven, Leuven, Belgium*
2 *Institute for Orthopaedic Research and Training, Ku Leuven, Leuven, Belgium*
3 *Institute for Orthopaedic Research and Training, Ku Leuven, Leuven, Belgium; Division of Orthopaedics, University Hospitals Leuven, Leuven, Belgium*
4 *Biomechanics Section, Ku Leuven, Leuven, Belgium; Biomechanics Research Unit, Giga In Silico Medicine, University of Liège, Liège, Belgium*

One of the main complications experienced after total hip arthroplasty is aseptic loosening, i.e. the failure of the bond between implant and bone in the absence of infection. Currently, the only solution consists of replacing the implant, a procedure during which implant-induced bone defects also have to be repaired. Given that these defects accumulate, restoring the function of the joint becomes more challenging with each revision, meaning only a limited number of revisions can be performed. Moreover, with successive surgeries prognoses worsen. The expected increase in revision surgeries driven by an aging population will have an impact on the quality of life of a growing segment of the population as well as on the healthcare systems worldwide. Improving implant longevity is the obvious course of action to alleviate the foreboded burden. To achieve this, it is crucial to reduce implant-induced stress shielding, a trigger for bone resorption and the leading cause of aseptic loosening.

We have developed a topology optimization approach to minimize implant-induced stress shielding in revision implants for large acetabular defects. To this end, a computerized tomography (CT) scan of the pelvic region of a healthy patient is used to create two patient-specific finite element (FE) models: one of the intact joint, to be used as reference, and one of a revised joint with the implant to be optimized. The hemi-pelvis is segmented from the CT-scans using Mimics 21 (Materialise NV, Leuven, Belgium). Then, a defect is created artificially and reconstructed using a statistical shape model in order to define the spatial design domain of the revision implant. The initial geometry of the revised joint is obtained by digitally implanting a CAD generated model of the femoral hip implant and acetabular polyethylene insert. The FE-models are automatically generated from the corresponding geometries with an in-house MATLAB script (The MathWorks Inc., Natick, MA, USA) that uses the voxelize function of the gptoolbox[1]. Models are fixed at the pubis and iliac spine and material properties of the bony parts are derived from the CT-scan grey values using Bonemat 3.2 (Istituto Ortopedico Rizzoli, Bologna, Italy). Joint loads are taken from the Othoload database[2]. Finally, the models are used to perform a topology optimization in a modified version of the TopOpt in PETSc framework[3]. During the optimization implant-induced stress shielding in the pelvic bone is minimized subject to constraints on bone and implant stresses. Calculations are performed on the Flemish Supercomputer using ~2000 cores. An overview of the complete workflow is given in Figure 1.

The full framework as described above has been implemented. Currently, benchmarking and validation are taking place with artificially created cases using the physiological state as reference. Hereafter, the framework will also be applied to real clinical cases.

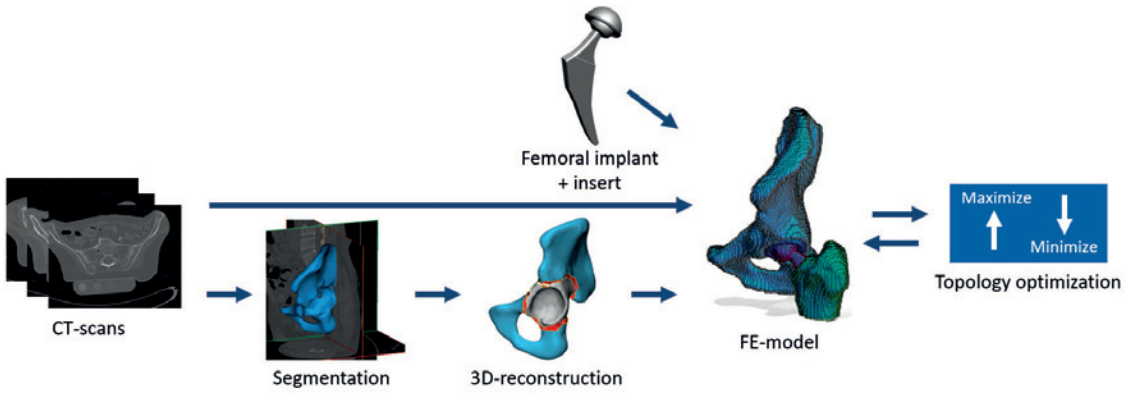

Figure Caption: Workflow overview

Acknowledgments: This research is financially supported by the Prosperos project, funded by the Interreg VA Flanders – The Netherlands program, CCI grant no. 2014TC16RFCB046.

References:

[1] Jacobson, A., et al., gptoolbox: Geometry Processing Toolbox, 2018.
[2] Bergmann, G., et al., PLoS ONE 11(5), 2016.
[3] Aage, N., et al., Topology optimization using PETSc: An easy-to-use, fully parallel, open source topology optimization framework, Structural and Multidisciplinary Optimization, 2014.

[P 43]

CUTANEOUS EVALUATION OF A RESIDUAL LIMB FOLLOWING APPLICATION OF NOVEL AND CONVENTIONAL PROSTHETIC SOCKETS

Virginia S. A. Monteiro[1], *Oon Tian Tan*[2], *Dana Solav*[1], *Xingbang Yang*[1], *Kevin M. Moerman*[3], *Hugh Herr*[1]

1 *Media Lab, Massachusetts Institute of Technology, Cambridge, USA,*
2 *Massachusetts Eye and Ear Infirmary, Harvard Medical Schoo, Boston, USA*
3 *Biomedical Engineering, National University of Ireland, Galway, Ireland; Media Lab, Massachusetts Institute of Technology, Cambridge, USA*

A successful prosthesis must provide comfort and maintain residuum tissue integrity to prevent the development of wounds and other secondary conditions related to the use of prostheses. The evaluation of a novel socket designed based on finite element analysis of subject specific limb morphology and mechanical properties [1] is presented.

Cutaneous integrity of the residual limb was evaluated on all surfaces following walking with the novel and conventional sockets, each for 5 minutes, at 1.25 m/s on an instrumented treadmill and compared to its original state prior to insertion into a socket. Skin remained intact on all surfaces. Marked erythema accompanied by prominent blood vessels and congestion was evident on the lateral and posterior surfaces in the residual limb after wearing the conventional socket for 5 minutes. These changes were absent after application of the novel prosthetic socket.

High-resolution thermal images were taken immediately after doffing both novel and conventional sockets and analyzed in MATLAB environment (Fig. 1). Lower peak temperature and more homogeneous temperature distribution were observed after application of the novel prosthetic socket.

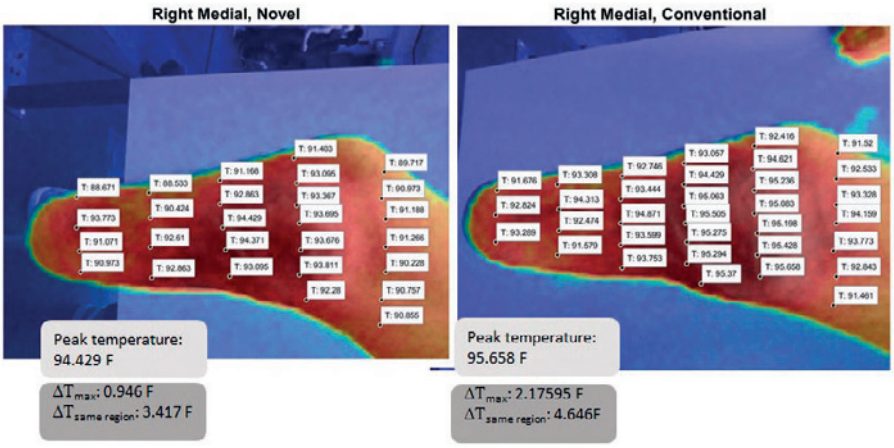

Figure Caption: Residual limb temperature distribution is shown after 5 minutes of walking at 1.25m/s on an instrumented treadmill with the novel and conventional socket.

Acknowledgments: National Institutes of Health

References:

Moerman, Kevin M., et al. "Automated and Data-driven Computational Design of Patient-specific Biomechanical Interfaces." engrXiv, 15 Aug. 2016. Web.

[P 44]

CONSTITUTIVE MODELLING OF KNITTED ABDOMINAL IMPLANTS IN NUMERICAL SIMULATIONS OF REPAIRED HERNIA MECHANICS

Agnieszka Tomaszewska[1], *Izabela Lubowiecka*[1], *Daniil Reznikov*[1], *Czesław Szymczak*[2]

1 *Gdansk University of Technology, Faculty of Civil and Environmental Engineering, Gdansk, Poland,*
2 *Gdansk University of Technology, Faculty of Ocean Engineering and Ship Technology , Gdansk, Poland*

Abdominal prostheses are applied to prevent hernia occurrence in post-operational scar or to reconstruct abdominal tissue in a case of hernia. The hernia recurrence is observed when the implant fixation is overloaded for its load bearing capacity. To prevent that, mechanical calculations can be performed and necessary fixation strength can be determined for different prostheses. In the presented study numerical modelling of hernia operated with the use of synthetic implant DynaMesh®-IPOM is undertaken. The key element in the model is a membrane, which simulates the prosthesis. The abdominal wall is represented by the following boundary conditions: linear springs in the membrane plane and elastic foundation in the perpendicular direction [1]. The membrane has a shape of decagon. It is fixed in each corner which simulates point fixations realized in practice by e. g. staples. The main question in the mechanical simulations concerns the forces in the membrane supports, which are the reactions caused by human activity, e.g. pressure loading or kinematic extortions. As proved in the paper [2] the reaction forces depend on the elasticity of the mesh mostly. Thus, recognition of mechanical parameters of the implant and selection of the constitutive model significantly influences the results of junction forces values calculation. The authors compare the outcome of this operated hernia model for two different constitutive models for the implant. The first one is dense net material model, introduced in [3]. In this model two directions in the membrane plane are distinguished. It is assumed that stresses in these two directions depend solely on the strains in these directions and on the stiffness functions defined for the material in the considered axes. The functions are determined based on mechanical tests of the material samples, e. g. simple or cyclic tension for load history considering [4]. For the prosthesis diameter equal to 13 cm and hernia orifice diameter equal to 5 cm the maximal reaction forces for pressure of 7.75 Pa equals 0.87 N. That is safe level of force in the mesh fixation, considering load bearing capacity of different staples (between 4 and 10 N). The other constitutive model is anisotropic hyperelastic Holzapfel model [5]. The obtained results are similar. Both models are validated to experimentally measured deflection of physical model analogous to the numerical model. The numerically obtained results prove that both constitutive models can be applied in textile implant modelling.

Acknowledgments: This work has been partially supported by the National Science Centre (Poland) [grant No. UMO-2017/27/B/ST8/02518]. Calculations have been carried out at the Academic Computer Centre in Gdańsk

References:

[1] *I. Lubowiecka, Mathematical modelling of implant in an operated hernia for estimation of the repair persistence, Comput. Methods Biomech. Biomed. Engin. 18 (4) (2015) 438–445. doi:10.1080/10255842.2013.807506.*
[2] *C. Szymczak, I. Lubowiecka, A. Tomaszewska, M. Śmietański, Modeling of the fascia-mesh system and sensitivity analysis of a junction force after a laparascopic ventral hernia repair, J. Thoretical Appl. Mech. 48 (2010) 933–950.*
[3] *C. Branicki, P. Kłosowski, Statical analysis of hanging textile membranes in nonlinear approach, Arch. Civ. Eng. XXIX (1983) 189–219.*
[4] *A. Tomaszewska, Mechanical behaviour of knit synthetic mesh used in hernia surgery, Acta Bioeng. Biomech. 18 (2016) 77–86. doi:10.5277/ABB-00185-2014-03.*
[5] *G. Holzapfel, Nonlinear solid mechanics, Wiley & Sons, Inc., New York, 2000.*

[P 45]

PREDICTION OF REMODELING CHANGES AFTER SHORT STEM TOTAL HIP ARTHROPLASTY

Jan Vodička[1], *Jan Heřt*[2], *Matej Daniel*[1], *Lukáš Horný*[1], *Tomáš Goldmann*[1]

1 *Czech Technical University in Prague, Prague, Czech Republic*
2 *Motol University Hospital, Prague, Czech Republic*

Our body is exposed to randomly changing external mechanical conditions during its whole life. For the bone tissue it is typical that it changes its internal structure to maintain internal integrity, stability, strength or mineral homeostasis. The way how the bone adapts to changes in these conditions is referred to as functional adaptation or strain adaptation. Predicting the remodeling processes and understanding the adaptation properties of living bone are essential for developing proper design of prosthetic devices.

Total hip replacement is one of the most common type of surgery that is offered to patients with chronic hip disease where conservative therapy is no longer effective. Unfortunately, prosthetic devices may significantly change stress fields in adjacent bone tissue. However, such conditions are significantly different to their physiological states. This deviation will trigger the strain-controlled adaptation process and the bone will remodel to accomplish the homeostatic state. When this process is manifested mainly by bone density reduction, it is referred to as stress shielding. One way how to reduce the stress shielding effect in patient's femur after total hip replacement is the application of so-called short stems.

Short stems of the total hip replacement have been developed to improve load transfer in the proximal femoral area, as well as to reduce an amount of resected bone tissue. Other benefits include: reducing the convalescence of the patient, possibility of using mini-invasive surgical procedures or reduction in overall postoperative pain.

In this study, we deal with a description and evaluation of remodeling changes after implantation of the short stems. Series of X-ray images of patients who have been implanted with a short hip stem Proxima was acquired. Bone density as well as the orientation of the trabecular bone in the proximal femur were determined by quantitative analysis of X-ray images. First postoperative image was used to create 2D model of proximal femur with the implant as a geometry for a boundary value problem describing mechanical interaction between bone tissue and hip stem. The problem was formulated by means of finite element method. To evaluate remodeling changes, FEM results were compared to two-years postoperative image. The comparison was based on changes in stress field and changes in principal stress directions. The results suggest, that short stem Proxima helps to restore the orientation of the main groups of trabeculae in the proximal femoral area and reduces the stress shielding effect after THA.

Acknowledgments: This study has been supported by the Technology Agency of the Czech Republic in the project Gradient functionally structured hip implant with a long life span with id. TH03010354.

[P 46]

CYCLIC LOADING OF CEMENT/CEMENT AND BONE/CEMENT BONDS.

Krzysztof Zerdzicki[1], *Marcin Ceynowa*[2], *Pawel Klosowski*[1]

1 *Gdansk University of Technology, Faculty of Civil and Environmental Engineering, Department of Structural Mechanics, Gdansk, Poland*

2 *Medical University of Gdańsk, Departament of Orthopedic Surgery, Gdansk, Poland*

Cementing is one of the main fixation methods used in joint replacement surgeries such as Total or Unicompartmental Knee Replacement (UKA [1], TKA [2]) and total hip arthroplasty (THA [3]). During implant revision, as the removal of the old cement could be hazardous, the new cement is sometimes placed upon the old one supposing that such connection is still very durable. Some tests regarding shear [4] and compressive strength [5] of the cement-within-cement fixation technique have been proposed before. However, those studies did not took into account vacuum technique used nowadays for polymethyl methacrylate (PMMA) mixture preparation and missed analysis of the cyclic loading acting on the cement filling. Therefore, the presented research focuses on the laboratory experiments on PMMA cement in two variants. Firstly, the cement cylinders of 1 cm diameter were tested (Fig. 1 left). The following types of interfaces were examined: 1. Uniform cement/cement, 2. Uniform cement/cement with additional drill hole (to make the interface surface greater) 3. Bone/cement. The specimens were contaminated with blood and human tissue to resemble true in vivo conditions. The cyclic compression-tension loading till failure were realized on the Zwick/Roell mechanical testing machine. In each subsequent cycle the force increment (both in compression and tension) increase/decrease with 100 N. The same cyclic loading procedure with increment change was applied for testing of the constructs made of whole human bone blocks joint with the PMMA uniform cylinders (Fig. 1 right). The bone blocks were cut-out of the femoral head bones of patients undergoing total hip arthroplasty in the course of their treatment.

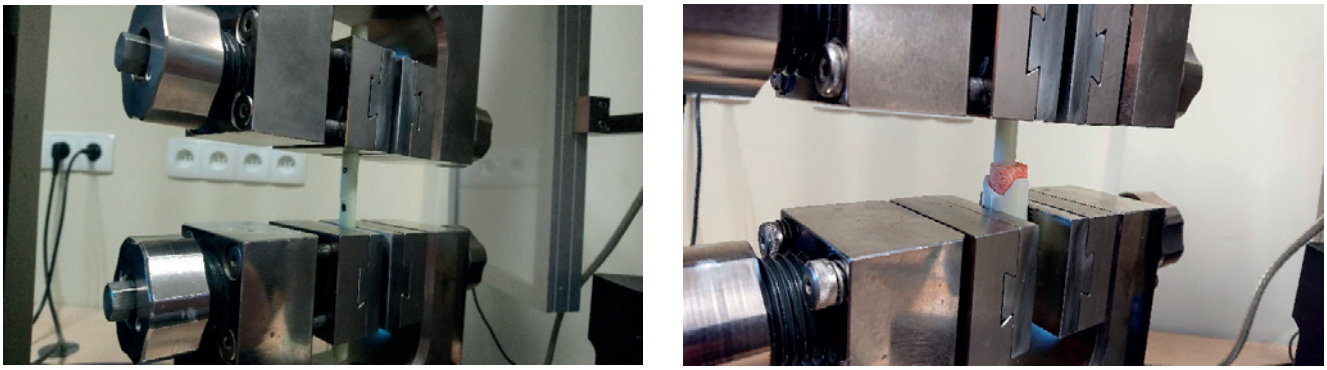

Figure 1: The tested samples: cement cylinder (left) and bone block with cement cylinder (right).

The results revealed that the weakest samples were those with interface with additional hole reaching about 600-800 N, then were the ones with contaminated interface (about 3200 N) and the strongest were the uniform cylinders of strength limit about 3600 N. The results of cyclic loading on bone block showed that such construct can carry about 500 N, but the test result is very sensitive to the quality of the sample preparation, especially linearity of both joint parts. In both analyzed types of tests the failure of joint arose during tension loading. It may suggest that in simple compression cyclic test the strength limit would be higher.

Aknowledgments: The study was financed from Department of Orthopedic Surgery, Medical University of Gdańsk, and Faculty of Civil and Environmental Engineering, Gdansk University of Technology, Gdansk, Poland.

References:

[1] *C. Scheele, M. F. Pietschmann, C. Schröder, T. Grupp, M. Holderied, V. Jansson, and P. E. Müller, "Effect of minimally-invasive implantation of unicompartmental knee arthroplasty on cement penetration and biomechanical stability. An experimental study in human tibiae," Clin. Biomech., vol. 51, no. May 2016, pp. 34–39, 2018.*

[2] *Q. H. Zhang, A. Cossey, and J. Tong, "Stress shielding in bone of a bone-cement interface," Med. Eng. Phys., vol. 38, no. 4, 2016.*

[3] *P. C. Weinrauch, B. S. Qld, C. Bell, L. Wilson, B. Goss, C. Lutton, R. W. Crawford, B. S. Qld, and D. Oxon, "Shear Properties of Bilaminar Polymethylmethacrylate Cement Mantles in Revision Hip Joint Arthroplasty," vol. 22, no. 3, pp. 394–403, 2007.*

[4] *A. Seth, N. C. Greenwald, and A. H. Wilde, "POINTS IN THE TECHNIQUE OF OF TIIE REVISION IMPLANT," 1978.*

[5] *P. J. Ingle and J. K. Dowell, "CEMENT-WITHIN-CEMENT REVISION HIP ARTHROPLASTY ; SHOULD IT BE DONE ? A BIOMECHANICAL STUDY," vol. 78, no. September, pp. 809–811, 1996.*

[P 47]

COMPUTATIONAL EVALUATION FOR ELASTO-PLASTIC-DAMAGE CHARACTERISTICS OF SYNDESMOTIC SCREW AND ITS ADJACENT BONES UNDER VARIOUS DYNAMIC LOADS AFTER ANKLE JOINT FIXATION SURGERY

Beop-Yong Lim1, *Tae Sik Goh[2], Jung Hoon Ro[3], Chi-Seung Lee[4]*

1 *Department of Biomedical Engineering, School of Medicine, Pusan National University, Busan, Korea, Rep. of South*
2 *Department of Orthopaedic Surgery, Pusan National University Hospital; Biomedical Research Institute, Pusan National University Hospital, Busan, Korea, Rep. of South*
3 *Department of Biomedical Engineering, School of Medicine, Pusan National University, Busan, Korea, Rep. of South; Biomedical Research Institute, Pusan National University Hospital, Busan, Korea, Rep. of South*
4 *Department of Convergence Medicine, School of Medicine, Pusan National University, Busan, Korea, Rep. of South; Department of Biomedical Engineering, School of Medicine, Pusan National University, Busan, Korea, Rep. of South; Biomedical Research Institute, Pusan National University Hospital, Busan, Korea, Rep. of South*

Surgical treatment is generally needed when syndesmotic disruption occurs in ankle joint (Schepers et al. 2011). To fix the ruptured syndesmosis, a metallic screw is inserted through the tibia and fibula, and the postoperative state is differed depending on the inserted position and degree of the screw. In addition, side effects such as screw breakage and loosening are caused by external impact. Syndesmotic screw fixation should be performed in consideration of these problems.

Currently, many clinical and biomechanical studies have been performed and many criteria have been established regarding the shape and inserted position of the syndesmotic screw. Existing biomechanical studies on ankle joint are limited to static analysis and lack of definition about plastic section in the mechanical properties of material. Therefore, we applied the dynamic load and material model which can precisely simulate plastic section, were predicted to material failure and damage.

First, the syndesmotic screw was inserted into the ankle joint according to the point of screw insertion, diameter and material of the screw, and number of cortical bone penetrations. The plastic sections of the materials were applied the Johnson-cook (JC) model. The temperature constant of this material model was fixed at a equal value and the constants of equivalent plastic strain and strain rate were obtained by the experimental data and reference (Murugesan and Jung 2019). In addition, the JC damage model including terms of the damage constants, the mean stress and the equivalent stress was applied for failure analysis. Explicit dynamic analysis was performed to output the equivalent stress, plastic strain, and damage distribution of the screw and adjacent bone.

Relative analysis of each surgical method was performed on the physical values output according to the dynamic loads, and the predominance and advantage of each method were evaluated. In addition, the relationship between the damage to the screw and adjacent bone was established when the load increased gradually. Therefore, the maximum allowable load for each method was expected, and the surgical method with the high allowable load and the relatively high mechanical advantage was determined.

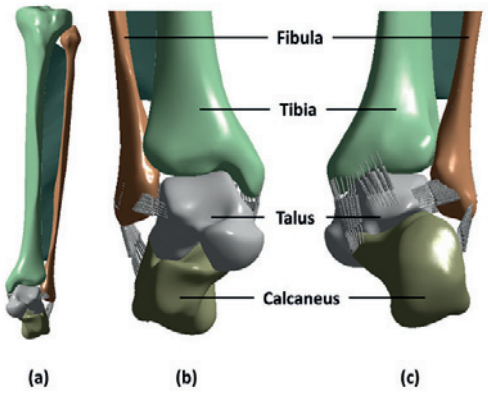

Figure 1 3D models of the ankle joint. (a) Frontal view, (b) anterior ligaments, and (c) posterior ligaments.

Acknowledgments: This research was supported by Basic Science Research Program through the National Research Foundation of Korea (NRF) funded by the Ministry of Education (NRF-2016R1D1A1B03934304).

Reference

Murugesan M, Jung DWJM. 2019. Johnson Cook Material and Failure Model Parameters Estimation of AISI-1045 Medium Carbon Steel for Metal Forming Applications.12:609.
Schepers T, Van Lieshout EM, de Vries MR, Van der Elst M. 2011. Complications of syndesmotic screw removal. Foot & ankle international.32:1040-1044.

[P 48]

NUMERICAL MODELLING OF THE HUMAN COCHLEA AND SURGICAL TECHNIQUES.

Bruno Areias[1], *Marco Parente*[2], *Fernanda Gentil*[3], *Renato Natal Jorge*[4]

1 *Inegi, FEUP, Porto, Portugal*
2 *Inegi, FEUP, Porto, Portugal; Faculty of Engineering of University of Porto, Porto, Portugal*
3 *Inegi, FEUP, Clínica Orl, Porto, Portugal*
4 *Inegi, FEUP, Porto, Portugal / Inegi, FEUP, Faculty of Engineering of University of Porto, Porto, Portugal;*

The human ear is a complex organ present in our organism. The sound waves are directed through the external auditory meatus towards the tympanic membrane. The vibration of the tympanic membrane is then transmitted through three ossicles. The last ossicle, the stapes, is connected to the cochlea through the oval window and its movement leads to the development of the pressure waves in the perilymph fluid present in the scala vestibular. The travelling wave produced in the basilar membrane causes the displacement of the hair bundle, leading to the release of electrical impulses at the base of the inner hair cell. Such electrical impulses are sent to the brain through the vestibulocochlear nerve, where are then interpreted as hearing sensations. Hearing loss affect individuals of all cultures. In 2015, between 6% and 8% of the world's population were affected by this type of disability [1]. In children, hearing difficulties may result in an additional obstacle to the speech and language acquisition, contributing to poor academic performances. Usually, in cochlear pathologies the hearing loss begins at the highest frequencies and progresses towards lower frequencies, where the hearing loss become more severe. When the vestibulocochlear nerve is intact and functional, the sensorineural hearing loss can be restored with the use of cochlear implants composed by an array of electrodes which stimulate the nerve at strategic sites, according to the sound frequency. The complications due to the insertion of the cochlear implant average from 8 to 18%. The major complication are the infections that often lead to the explantation of the implant [2]. Numerical studies provide an approximation of the behaviour of the real world, such analyses can be applied to the human ear with the aim of study and investigate the normal and pathological hearing system, and also the surgical techniques available up to now. A 3D finite element model based in a set of µCT imaging information will be constructed. The model will also allow to optimize the design of the cochlear implants in order to reduce the damage of the cochlea during the implant insertion, thus preserving the residual hearing."

Acknowledgments: "The authors truly acknowledge the funding provided by Ministério da Ciência, Tecnologia e Ensino Superior – Fundação para a Ciência e a Tecnologia (Portugal), under grants: SFRH/BD/129397/2017."

References:

[1] B. S. Wilson, D. L. Tucci, M. H. Merson, and G. M. O'Donoghue. Global hearing health care: new findings and perspectives. Lancet, 390(10111):2503{2515, 2017.
[2] Venail, F., et al., Reliability and Complications of 500 Consecutive Cochlear Implantations. Archives of Otolaryngology-Head & Neck Surgery, 2008. 134(12): p. 1276-1281.

[P 49]

WHY WOODPECKER CAN RESIST THE IMPACT: A VIEW FROM BIOMECHANICS

Zhe Zhang[1], *Shiwei Zhou*[1], *Yimin Xie*[1]

1 *Royal melbourne institute of technology, Melbourne, Australia*

The impact-resistance mechanism of the skull of woodpeckers is very complex because of the difficulties in geometrical modelling, material characterization, numerical simulation and experimental verification. This work reconstructed the skull from computed tomography data within the framework of a level set based optimization, in which the sum of fitting energy and a diffusion term is minimized. To avoid small time step due to Courant-Friedrishs-Levy stability condition and the reinitialization of level set function, a reaction-diffusion method is used to update the level set function using finite element analysis other than traditional time difference-based upwind algorithm. The results show this method can obtain clear and smooth profiles within a few iteration steps. The unhomogenized material characterization is considered in the model via 53 individual parts in terms of the value of grayscale. Numerical impacting simulation in LS-DYNA illustrates that the unique structure of hyoid and material distinction are the main reasons of impacting-resistance mechanism.

Acknowledgments: I would like to express my gratitude to all those who helped me during this work.

My deepest gratitude goes first and foremost to Dr. Shiwei Zhou, my supervisor, for his constant encouragement and guidance. Second, I would like to express my heartfelt gratitude to Prof. Yi-min Xie, who is my joint senior supervisor. I am also greatly indebted to Prof. Qing Li in the University of Sydney, who have instructed and taught me a lot in past years. Last my thanks would go to my beloved family for their loving considerations and great confidence in me all through these years.

References:

[1] *C. Li, C.-Y. Kao, J. C. Gore, and Z. Ding, "Minimization of region-scalable fitting energy for image segmentation," IEEE transactions on image processing, vol. 17, no. 10, pp. 1940-1949, 2008.*

[2] *C. Li, C. Xu, C. Gui, and M. D. Fox, "Distance regularized level set evolution and its application to image segmentation," IEEE transactions on image processing, vol. 19, no. 12, pp. 3243-3254, 2010.*

[3] *L. Wang, J. T.-M. Cheung, F. Pu, D. Li, M. Zhang, and Y. Fan, "Why do woodpeckers resist head impact injury: a biomechanical investigation," PloS one, vol. 6, no. 10, pp. e26490, 2011.*

[4] *H. Emmendoerfer, and E. A. Fancello, "Topology optimization with local stress constraint based on level set evolution via reaction–diffusion," Computer Methods in Applied Mechanics and Engineering, vol. 305, pp. 62-88, 2016.*

[5] *J.-Y. Jung, S. E. Naleway, N. A. Yaraghi, S. Herrera, V. R. Sherman, E. A. Bushong, M. H. Ellisman, D. Kisailus, and J. McKittrick, "Structural analysis of the tongue and hyoid apparatus in a woodpecker," Acta biomaterialia, vol. 37, pp. 1-13, 2016.*

[P 50]

DEVELOPMENT OF ANALOGUE FLUIDS FOR CELL DEFORMABILITY STUDIES IN MICROFLUIDIC DEVICES

Ana Moita[1], *Cristiana Caldeira*[1], *Rui Lima*[2], *Emilio Vega*[3], *Antonio Moreira*[1]

1 *IN+ Instituto Superior Tecnico Universidade de Lisboa, Lisbon, Portugal*
2 *Metrics University of Minho, Guimaraes, Portugal; Ceft Faculdade de Engenharia Da Universidade Do Porto, Porto, Portugal*
3 *Escuela de Ingenierias Industriales Universidade de Extremadura, Spain*

Microfluidic devices are becoming a powerful and effective tool to perform complex sample manipulation operations, allowing the reduced use of samples and reagents. In this context, they represent exciting possibilities to devise portable, low cost clinical devices [1]. Microfluidic devices are also a suitable tool to visualize and characterize cell deformability alterations, in relevant microcirculation conditions. This is useful to devise alternative diagnostics of several diseases where modifications in cell mechanical properties, such as deformability, can be used in clinical diagnostics. For instance, diabetes mellitus causes a decrease in red blood cells deformability as well as changes in their shape. On the other hand, characterizing cancer cell deformation can provide useful information on the process of metastasis, particularly for large deformability regimes, which are rarely described in the literature. To deepen and endorse the study of cell properties and establish reliable correlations between cell mechanical properties and the diseases, to be used in the future for diagnostics, it is vital to create biofluid analogues which can replicate the characteristics of both healthy and unhealthy cases, covering in the later, different stages of the disease which are related to different deformability characteristics. Also, as one creates such analogues, it is important to define and optimize the diagnostic procedures which can be used in microfluidic devices. In this context, the present work assesses different approaches to devise the analogue fluids, namely, using gum solutions and suspensions of polymers and surfactants solved on water, giving rise to small semi-rigid particles. The main physical properties of the fluids are measured and they are characterized in terms of the resulting particle size distribution, evaluated based on Laser Scanning Fluorescence Confocal Microscopy and on extensive image post-processing, performed using in-house routines. Size and deformability of the resulting particles is then tested to check on their feasibility to mimic cell deformability in the context of the current goal of this work (malignancy diagnostics). The dynamic response of the analogue fluids is also tested to check on the feasibility of their handling in the microfluidic device for malignancy diagnostics that is being developed in our research group [2].

Acknowledgments: A.S. Moita is grateful to Fundação para a Ciência e a Tecnologia (FCT) for financing her contract through the IF 2015 recruitment program (IF 00810-2015) and for partially financing this research through the exploratory project associated to this contract.

References:

[1] *A. Dance, A. The making of a medical microchip, Nature, 545, 512-514, 2017.*
[2] *A.S. Moita, D. Vieira, F. Mata, A.L.N. Moreira, Microfluidic devices integrating alternative clinical diagnostic techniques based on cell mechanical properties. Communications in Computer and Information Science, N. Peixoto et al. (Eds.), Springer International Publishing AG, part of Springer Nature, 881, 74-93, 2018.*

[P 51]

CFD ANALYSIS OF FLOW AROUND A SERRATED FEATHER

Tetsuhiro Tsukiji[1], *Hiroki Takase*[1]

1 Sophia University, Tokyo, Japan

It is well known that flight sound of owls is much less than that of other birds. Many nocturnal owls have a fine saw blade-like front tip at the leading edge of their primary feathers (remiges). It is called serrations which have minute teeth at regular intervals. It is a unique feather which cannot be seen with other birds and seems to produce the silencing effect. With that background, the present research focuses on differences between feather of owl and that of other birds by analyzing the acoustic effect and the flow fields around the feather.

In this study, we used the Large Eddy Simulation as a CFD(Computational Fluid Mechanics) technique. Standard Smagorinsky model is used as sub-grid scale models. Ffowcs Williams and Hawkings equation was used for the evaluation of the sound. In the formulation of Ffowcs Williams and Hawkings, the form improved from the generality of acoustic analogy of Lighthill equation is adopted.

The contours of the three dimensional vorticity distributions around the feather is obtained. Flow separation from the leading edge is seen. However no separation until the vortices reaches around the center of the chord of the airfoil is seen on serrated feather. It turned out that the flow separation controlled on the suction side of an airfoil is performed by the serrations on the leading edge. It is found that the serrations generate longitudinal vortices and turbulent transition was brought on the suction surface of the airfoil to delay the separation point by the longitudinal vortices. Serrated feather has lower drag coefficient than normal feather. Not only it but also lift coefficient is lower. The sound pressure level (SPL) along frequency at angle of attack 10 degrees is calculated. The SPL of owl feather is lower than that of normal feather through the wide range of frequency. Opposite to this, SPL at angle of attack 30 degrees makes no change between two kinds of feather. In case of high frequency, SPL of owl feather is a little higher. So the silencing effect is also caused by the longitudinal vortices.

In this study, the effect of serrations at the leading edge of owl feather was simulated by CFD. The main conclusions are as follows.

1. The serrations control flow separation because of longitudinal vortices at angle of attack 10°. Sound pressure level was also reduced by serrations. These effects can't be seen at higher angle of attack (30°).

2. Drag and lift coefficient of serrated feather are lower than that of normal feather.

[P 52]

FLUID-STRUCTURE INTERACTION MODELING OF GENETICALLY ENGINEERED MICRO-CALCIFICATION ON ABDOMINAL AORTA LUMINAL SURFACE IN MICE.

Dorinamaria Carka[1], *Olga V. Savinova*[1], *Ian Kelly*[1]

1 *New York Institute of Technology, New York, USA*

It is hypothesized that atherosclerosis can be influenced or promoted by early signs of arterial stiffening caused by a polydisperse micron distribution of calcified lesion on the endothelial cell layer. This is due to a nonuniform redistribution of the shear stresses on the endothelium which in turn could further promote plaque formation by triggering stress sensitive LDL uptake in the endothelial cells. Optical confocal scans (Sensofar S Neox) of open luminal surfaces of suprarenal abdominal aorta (AA) from mice group with overexpressed tissue-nonspecific alkaline phosphatase in endothelial cells (eTNAP) showing polydisperse calcification lesions of the order of 5-20 μm diameter and height, were treated to optimize resolution and used as geometrical import on a 3D fluid-structure interaction (FSI) finite element model built using COMSOL Multiphysics Software.

To investigate shear stress distribution on the endothelium due to the presence of calcified nodules we represented the abdominal mouse aorta as an idealized cylindrical shell of average inner radius of 1.2 mm, obtained by bending the flat optical scans, of which we modeled a periodic slice. The endothelium was considered to be rigidly attached on the rest of the vessel wall and displacements on the outer boundary are either fixed or fit biaxial deformation data obtained in vivo (Vevo 3100). The calcifications were modeled as linear elastic materials with five times the Young's modulus of the endothelium layer whereas the healthy part of the endothelium was modeled as a hyper elastic (Neo-Hookean) material representative of the nonlinear elastic behavior of biological tissue. Due to the small Reynolds number, we considered a fully formed parabolic laminar flow with mean velocity 17 cm/s; the blood was modeled as a Newtonian fluid with a constant viscosity. The Navier-Stokes equations were solved in the fluid domain and Newton's equation on the calcifications and endothelium domains.

The distribution of the wall shear stress (WSS) magnitude and the disturbed direction of the tangent components of the viscous stress at the fluid-structure interface serve as a proof of the hypothesis that the presence of the micro-calcifications introduces oscillatory disturbances in the direction of the WSS vector and a reduction of magnitude by 50% around the calcification nodules. Surface plots of the Mises stress on radial and axial planes, further demonstrate a highly non-uniform distribution of the deviatoric stress levels and we observed a considerable grading in shear stress transfer from the fluid-structure interface through the thickness of the endothelium and nodules which was modeled as a 3 microns layer.

Acknowledgments: We thank Julia Molnar for help with image data processing and Anton Mararenko OMS for help with SensoMap Scans. This work was supported in part by the NIH grant 1R56HL131547-01A1

[P 53]

MODULAR, PARALLEL MECHANISMS WITH FLEXIBLE LINKS FOR USE IN SPINE SEGMENTS OF HUMANOID ROBOTS

Adam Ciszkiewicz[1], ***Grzegorz Milewski***[1]

1 *Cracow University of Technology, Cracow, Poland*

The field of humanoid robotics is gaining interest. It promises robots able to interact with environments specifically tailored for human beings. Nevertheless, such structures are very difficult to design and produce - their motions and load responses must closely mimic that of humans.

The human spine is one of the most important and complex structures in the body. It consists of multiple intervertebral joints (IJs) connected serially. The IJs, due to their flexible and parallel nature, are very hard to imitate in humanoid robots. The currently-available substitutes are usually only inspired by the joints - their motions and load-responses are rarely in agreement. This is a crucial factor when considering interaction with environment. In [1] an approach for designing such systems was presented. The method consisted of two separate steps: structure optimization and parameters estimation. Both of these procedures were performed with Genetic Algorithm. The substitute mechanisms' quality was measured based on experimental data of an L4-L5 IJ's elastostatic behavior. The current study significantly extends the previous research [1, 2]. Its aim was to:

- use structured Genetic Algorithms (sGA) for simultaneous structure optimization and parameters estimation for designing substitute mechanisms for IJs within a lumbar spine,

- propose an approach for predicting static responses for a modular spine composed of several IJ substitutes.

As mentioned above, the design method used sGA to obtain optimal and flexible mechanisms based on a geometry and material parameters of a ligament system and angular stiffnesses of an L4-L5 IJ. The obtained mechanisms formed a basis of modular spines, which were composed of 4 mechanisms to mimic the L1-L5 segment of the spine. The static responses of the modular structures were then obtained under varied moment loads in all three body planes.

The approach was tested in three numerical scenarios with different target angular stiffnesses. In all of them, it was possible to obtain a mechanism that accurately emulated the elastostatic behavior of the intervertebral joint under moment loads. The range of motion of the full lumbar substitute also corresponded with that of the actual system.

To summarize, the results prove that the proposed approaches are feasible for designing spine segments for humanoid robots. Furthermore, they could be employed in the design of prosthetic and orthotic devices for a human lumbar spine.

References:

[1] Ciszkiewicz A., Milewski G.: Ligament-based spine-segment mechanisms, Bulletin of the Polish Academy of Sciences: Technical Sciences, 2018, 66(5):705-712

[2] Ciszkiewicz A., Milewski G.: A novel kinematic model for a functional spinal unit and a lumbar spine, Acta of Bioengineering and Biomechanics, 2016, 18(1):87-95

[P 54]

COMPARISON OF PAIN RELATED CHNAGES IN CEREBRAL BLOOD VOLUME IN BURN PATIENTS WITH NEUROPATHIC PAIN

SO YOUNG JOO[1], *Yoon Soo Cho*[2], *Cheong Hoon Seo*[2]

1 *Hangang Sacred Heart Hospital, College of Medicine, Hallym University, Seoul, Korea, Rep. of South Department of Rehabilitation Medicine, Hangang Sacred Heart Hospital, College of Medicine, Hallym University, Seoul, Korea, Rep. of South, Seoul, Korea*

2 *Hangang Sacred Heart Hospital; Hallym University; Department of Rehabilitation Medicin, Seoul, Korea, Rep. of South*

Most burn patients suffer neuropathic pain. Neuropathic pain is generally chronic and disabling, and responds poorly to conventional treatment. To investigate changes in the pain network associated with neuropathic pain, magnetic resonance imaging(MRI) was used to measure cerebral blood volume(CBV) in burn patients who had spontaneously healed or required skin grafting after thermaly injury. 34 in patients subjects were recruited to participate in this study. The Subjects had complaints of severe pain that rated at least 5 on visual analogue scale(VAS) despite treatments including medications and physical modalities. We also recruited 20 healthy, age-matched control participants. For each of the participants, two high-resoluton T1-weighted images were acquired, one before and the other 7 minutes after IV injections of gadolinium contrast agent. The CBV maps between burn patients and healthy controls were compared. The intensity of neuropathic pain was measured using the visual analog scale(VAS). Depressive mood was assessed using the Beck Depression Scale, and the interference of pain in the patient's life was assessed using the Brief Pain Inventory(BPI). The relationship between individual participant CBV and VAS score was examined. The burn patients had, in terms of CBV, significantly higher CBV in the bilateral medial frontal area and significantly lower CBV in the primary somatosensory cortex. CBV increased in the contralateral and ipsilateral hemispheres of the thermal injury side. The bilateral medial frontal cortex was correlated with pain intensity in burn patients. This CBV measures found the changes of activation areas of the pain network on burn patients compared with the CBV measures on healthy controls. We observed increased CBV in regions associated with emotion in the cerebral pain network of patients with burn injury. This study suggests that CBV changes were related to neuroplasticiry associated with neuropathic pain in burn patients.

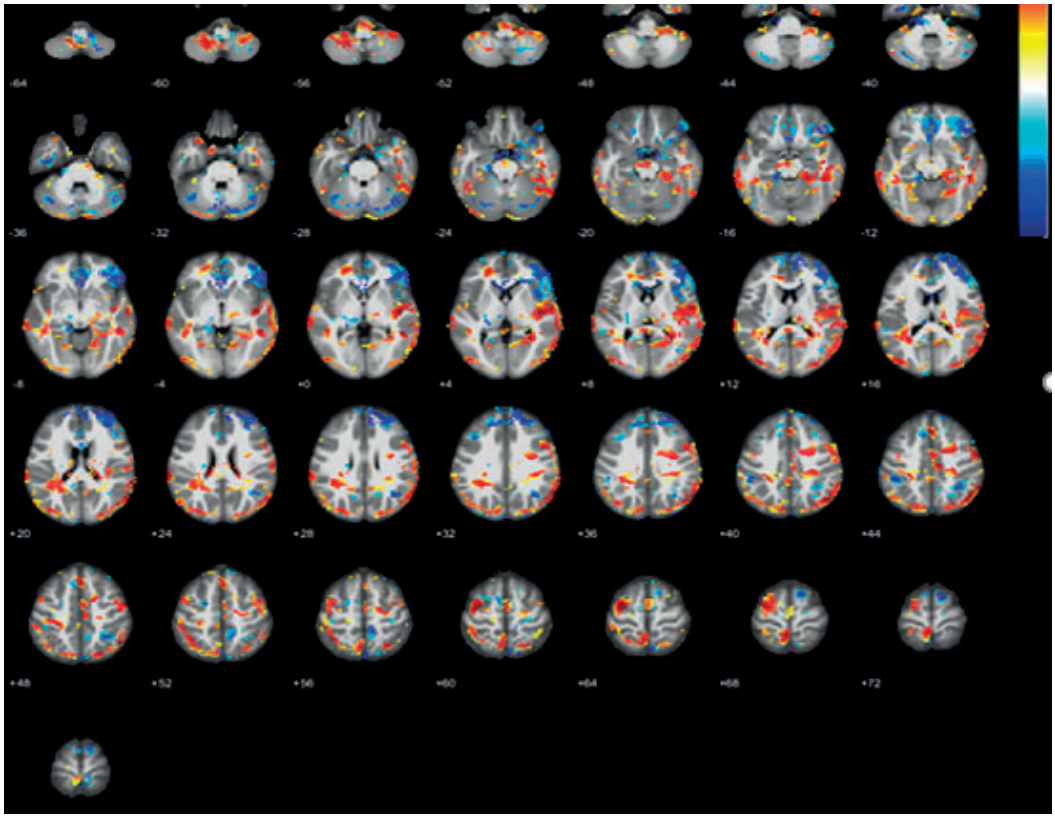

Acknowledgments: This research was supported by National Research Foundation of Korea(NRF), funded by the Ministry of Education(NRF-2018R1C1B6008584).

References:

Davis KD, Taylor SJ, Crawley AP, Wood ML, Mikulis DJ. Functional MRI of pain- and attention-related activations in the human cingulate cortex. Journal of neurophysiology. 1997;77:3370-80.
Kong J, Loggia ML, Zyloney C, Tu P, Laviolette P, Gollub RL. Exploring the brain in pain: activations, deactivations and their relation. Pain. 2010;148:257-67.
Harris RE, Napadow V, Huggins JP, Pauer L, Kim J, Hampson J, et al. Pregabalin rectifies aberrant brain chemistry, connectivity, and functional response in chronic pain patients. Anesthesiology. 2013;119:1453-64.

[P 55]

ADVANCED CHARACTERIZATION OF THE 3D MORPHOLOGY AND THE MECHANICAL PROPERTIES OF THE ENTHESIS: OPTIMIZATION STUDY

Lisa Leyssens[1], *Sophie Ryelandt*[1], *Audrey Favache*[1], *Greet Kerckhofs*[2]

1 *Institute of Mechanics, Materials, and Civil Engineering, UCLouvain, Louvain-la-Neuve, Belgium*

2 *Biomechanics Lab, Institute of Mechanics, Materials, and Civil Engineering, UCLouvain, Louvain-la-Neuve, Belgium; Institute of Experimental and Clinical Research, Uclouvain; Dept. Materials Science and Engineering, Ku Leuven, Leuven, Belgium*

Connective tissue injuries occurring at the interface between soft tissue and bone, also called the bone-tendon interface or the enthesis, commonly result in disability and significant medical costs [1]. The chances of failure of surgical reattachment are high, which makes the bone-tendon interface an important research topic [2]. To address this clinical issue, it is necessary to regenerate a tissue that has the same properties as the original one. Before this is possible, it is important to understand the properties of the tissue that needs to be replaced. The purpose of this study was to develop and optimize advanced techniques to characterize the 3D structure and mechanical properties of murine entheses.

Achilles tendon-to-bone interfaces were extracted from 8-weeks old mice, 30-weeks old lean mice and 30-weeks old diet-induced obese mice. High-resolution X-ray microfocus computed tomography (HR microCT) and contrast-enhanced micro-CT (CE-CT) were used to determine the 3D structure and composition of the different tissues in the enthesis (figure 1). Nanoindentation was used to study the mechanical properties at the enthesis.

MicroCT revealed differences between the lean and the obese mice concerning the volume of the mineralized fibrocartilage layer and the surface of the connection between the mineralized and unmineralized fibrocartilage. Ageing did not influence these properties. CE-CT allowed observing the collagen fiber orientation within the unmineralized fibrocartilage and the connecting tendon. Quantitative 3D analysis is ongoing, as well as further optimization of the contrasting method. For the nanoindentation, we optimized the sample preparation protocol. Three sample preparation techniques were evaluated: (A) resin embedding and polishing, (B) resin embedding and cryostat sectioning, and (C) resin embedding and microtome sectioning. Method A showed unsatisfactory results because of the high occurrence of damaging the sample during polishing. In method B, the bone became very hard compared to the tendon at the low temperatures, making it challenging to cut the tissue without breaking the bone. Method C involved cutting a slice with a microtome. The remaining embedded part of the sample had a flat surface and was suitable for indentation: the biological structures were clearly recognizable and intact. With this preparation method, distinct mechanical properties could be detected for the different tissues within the enthesis.

Further research will involve the analysis of a large set of samples.

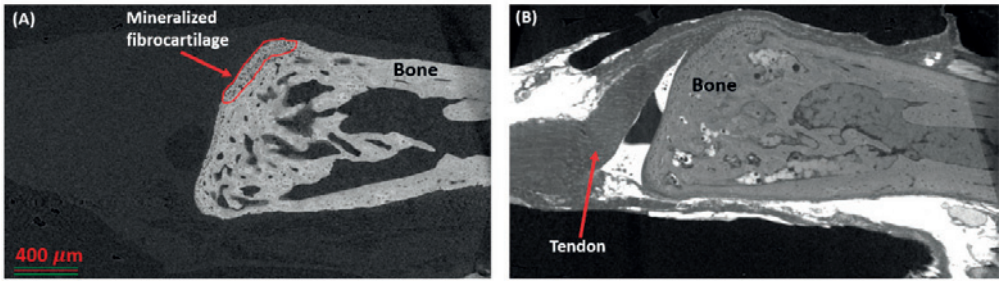

Figure Caption: Fig.1: HR microCT image (A) and CE-CT image (B) of enthesis.

References:

[1] Lester Smith et al. Connective Tissue Research, 53(2):95–105, 2011.
[2] Guy M. et al. Biophysical Journal, 97(4):976–985, 2009.

[P 56]

TONGUE MOTILITY OF TONGUE-TIED INFANTS DURING BREASTFEEDING

Yiela Saperstein[1], *David Elad*[2], *Andrew Laine*[1], *Scott Siegel*[3], *Catherine Watson Genna*[4]

1 *Columbia University, New York, USA*
2 *Tel Aviv University, Tel Aviv, Israel; Columbia University, New York, USA*
3 *Stony Brook University, Stony Brook, USA*
4 *International Board Certified Lactation Consultant*

This study uses objective analysis of ultrasound videos recorded during breastfeeding to explore periodicity of the tongue motion of tongue-tied infants before and after frenectomy. Ankyloglossia, or tongue-tie, is a condition where the lingual frenulum, connecting the tongue to the bottom of the mouth, is thicker, shorter, or stiffer than usual. This limits tongue motion and can impede breastfeeding. Tongue-tie can be treated with a frenectomy, a surgical intervention where the lingual frenulum is slightly cut. This treatment is controversial due to the absence of objective measures indicating tongue-tie severity or when a frenectomy is necessary. While not highly invasive or risky, frenectomies do cause slight injury and discomfort to newborns and should only be performed if necessary. This study aims to objectively quantify tongue kinematics for evaluation of potential parameters to detect changes and improvements in breastfeeding due to frenectomy. We recruited 6 mothers with tongue-tied infants scheduled for frenectomies. Mid-sagittal ultrasound videos were taken with an ultrasound transducer under the infant's chin for about 10 seconds immediately before and after frenectomy. The experimental protocol was approved by the IRB committee and mothers signed informed consent. The analysis was conducted on the clearest clips of the ultrasound videos using MATLAB code developed in our lab [1]. This method is one of the first to utilize registration with respect to the hard palate to reduce noise and mitigate errors from infant-mother movements. Computation of the infant's tongue-motility about polar lines was used to represent local dynamics of the tongue in the mid-sagittal plane. Representative results are shown below. The time dependent local motility is shown for the anterior (Figs. 1a,b) and posterior tongue (Figs. 1c,d). The frequency spectrum obtain by FFT is depicted in Figs. 1e, f and the periodicity characteristics obtained by auto-covariance of the time-dependent motility is shown in Figs. 1g, h. The dominant frequencies from both pre- and post-frenectomy were 2.34 Hz. A more periodic motion was evident post-frenectomy in both the anterior and posterior tongue and the dominant frequency was more defined post-frenectomy. These results demonstrated improvement after frenectomy.

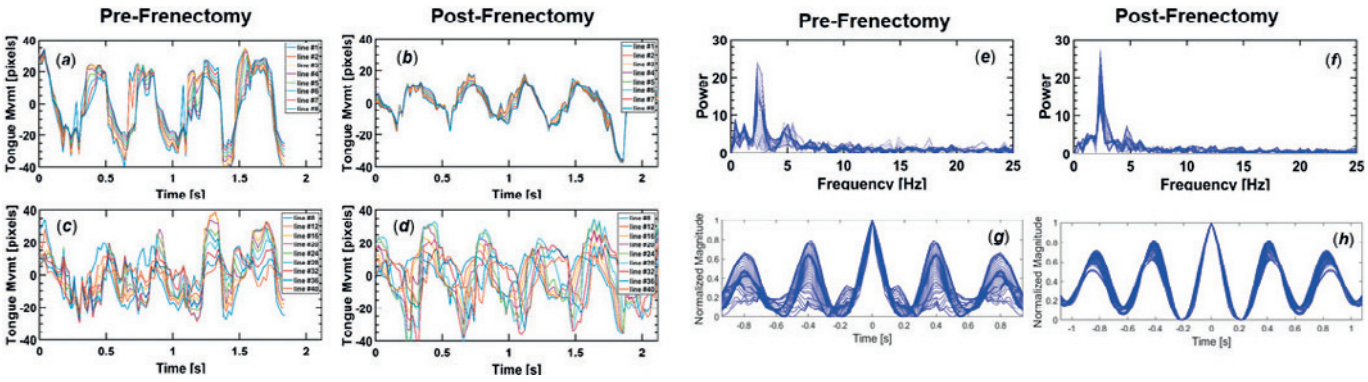

Figure Caption: Figure 1: Time dependent signals of tongue motion before and after frenectomy. (a) and (b) Motion of the anterior tongue; (c) and (d) Motion of the posterior tongue; (e) and (f) FFT of tongue motion; (g) and (h) Auto-covariance of tongue motion.

References:

[1] Elad, D. PNAS 111 (14), 5230-5235, 2014.

[P 57]

EXPERIMENTAL EVALUATION OF PAD DEGRADATION OF HELMET FOR AMERICAN FOOTBALL AND ITS APPLICATION TO NUMERICAL DESIGN

Yoshiki Umaba[1], ***Atsushi Sakuma***[2], *Yuelin Zhang*[3]

1 *Prof. Sakuma Laboratory, Graduate School; Kyoto Institute of Technology; Matsugasaki, Japan*
2 *Division of Textile Science; Kyoto Institute of Technology; Matsugasaku*
3 *Faculty of Science and Technology; Sophia University, Tokyo, Japan*

American football is a sport that requires high safety for players because it requires a very fast and powerful movement. Helmet for the players is one of the most important tools for ensuring their safety, and then its mechanical design is extremely difficult for manufacturer. As helmets are made softer by use, there is concern about its degradation in safety while comfortability of wearing is improved. Therefore, in this report, the deterioration behavior of the pad material is observed experimentally and it is formulated for theoretical simulation in order to design the helmet numerically. In the experiment, deterioration due to use and aging are observed, and its relationship to the artificial deterioration by accelerated tests using test machine is confirmed clearly. Then, analysis of the collision problem of the helmet is carried out by using the characteristics of the pad material obtained by these mechanical tests. Numerical analysis is carried out by changing the material characteristics and movement of physical model while keeping the structure of the helmet and the head constant. LS-Dyna is used in numerical simulation because of its availability in crash analysis [1]. In the analysis results, it was first confirmed that the optimum characteristics of the pad material can be defined by the mechanics of plateau stress. This confirmation makes it possible to design the safety of the helmet since this plateau stress is one of the quantities that has been confirmed to deteriorate before use or aging. By using these results, the concept of usage limit due to deterioration of the pad material is discussed in addition to the suggestion of the helmet specification according to the physique and exercise capacity of the football players.

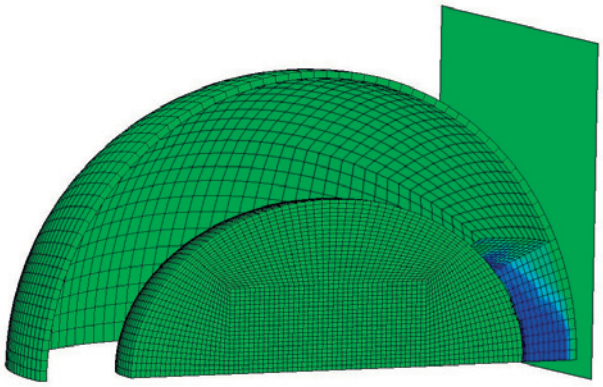

Figure Caption: A numerical result of crush behavior of helmet

Acknowledgments: This research was carried out with support from Professor S. Aomura of Metropolitan University of Tokyo And Associate Professor H. Nakadate of Shinshu university.

References:

S. Oikawa, H. Nakadate, Y. Zhang, T. Ueno, S. Aomura and Y. Matsui, Finite element analysis of the effectiveness of bicycle helmets in head impacts against roads, Journal of Biomechanical Science and Engineering, 12- 4, (2017), 17-00175*

[P 58]

EFFECTS OF THE CHOICE OF MECHANICS REFERENCE STATE ON ESTIMATION OF MYOCARDIAL PROPERTIES

Mario Habenbacher[1], Thiranja Prasad Babarenda Gamage[1], Zhinuo Jenny Wang[2], Christopher Patrick Bradley[1], ***Martyn P. Nash****[3]*

1 *The University of Auckland, Auckland Bioengineering Institute , Auckland, New Zealand*
2 *University of Oxford, Department of Computer Science, Oxford, UK*
3 *Auckland Bioengineering Institute, The University of Auckland, Auckland, New Zealand; Department of Engineering Science, University of Auckland, Auckland, New Zealand*

Computational models of left ventricle (LV) mechanics require a well-defined reference state [1]. The in vivo LV is constantly subjected to varying pressure loads. A widely used approach assumes that the LV passes through a "load-free" (LF) state at a certain time point during the cardiac cycle [2, 3]. This assumption neglects any pressure that may be acting at that stage, which may be substantial in diseases such as hypertension and heart failure.

This study investigated the effect of neglecting non-zero LV pressure, and consequently the influence of the chosen reference state, on estimates of passive and contractile mechanical properties. Personalised biomechanical heart models were generated for 28 subjects, including control and heart failure cases, obtained from the St. Francis Hospital Heart Centre (New York, USA). Clinical data for each subject comprised of cine MRI and same-day LV catheter pressure recordings. Passive myocardial properties were described by a transversely isotropic exponential constitutive relation [4], while a steady-state length-dependent model was used to describe the contractile properties [5]. Patient-specific parameters were estimated with an assumed "load-free" diastasis (DS) reference state, and with a synthetic dataset generated using the LV pressure at diastasis to estimate a LF reference geometry (method described in [6]). The influence of the chosen reference state was evaluated through comparison of these two different sets of parameters.

Neglecting the non-zero LV pressure at the reference state resulted in a substantial overestimation of passive myocardial stiffness, as illustrated below. This discrepancy increased for higher reference LV pressures. Overestimation of active parameters was observed for most cases, which suggests a dependency on passive stiffness. We conclude that constitutive parameter estimation procedures should account for non-zero LV pressures in the reference configuration.

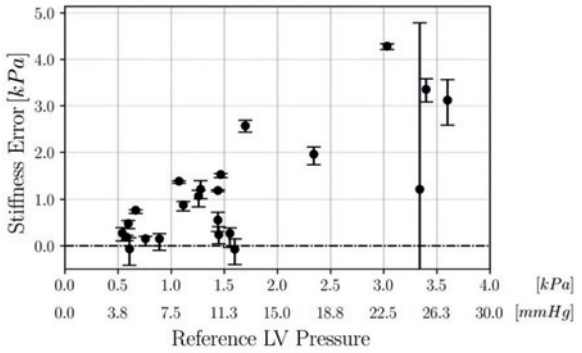

Figure Caption: Scatter-plot showing the difference of estimated stiffness as a function of the non-zero LV pressure at the reference state. Each marker represents a single subject and error bars denote the 95% confidence interval on the estimated parameters for matching the clinical LV shapes.

Acknowledgments: We thank the Health Research Council of New Zealand for financial support, Drs Vicky Wang and Alistair Young for technical advice, and Drs Jie Jane Cao, William Schapiro and Joshua Cheng from St. Francis Hospital, New York, for providing the clinical data.

References:

[1] V.Y. Wang et al., Annu. Rev. Biomed. Eng., 17, pp. 351-383, 2015
[2] L. Asner et al., Biomech. Model. Mechanbiol., 15(5), pp. 1121-1139, 2016
[3] Z. J. Wang et al., J. Cardiovasc. Transl. Res., 11(4), pp. 346-356, 2018
[4] J. M. Guccione et al., J. Biomech., 28(10), pp. 1167-1177, 1995
[5] P. J. Hunter et al., Prog. Biophys. Mol. Biol., 69(2), pp. 289-331, 1998
[6] V. Rajagopal et al., Int. J. Numer. Meth. Eng., 72, pp. 1434-1451, 2007

[P 59]

COMPARISON OF FE, EFG, AND SPG METHODS FOR THE SIMULATION OF ADIPOSE TISSUE UNDER BLUNT IMPACT

Felicitas Lanzl[1], *Steffen Peldschus*[2], *Fabian Duddeck*[3]

1 *Biomechanics and Accident Analysis, Institute of Legal Medicine, University of Munich LMU, Munich, Germany; Associate Professorship of Computational Mechanics, Technical University of Munich Tum, Munich, Germany*

2 *Biomechanics and Accident Analysis, Institute of Legal Medicine, University of Munich LMU, Munich, Germany*

3 *Associate Professorship of Computational Mechanics, Technical University of Munich Tum, Munich, Germany; School of Engineering and Materials Science, Queen Mary University of London Qmul, London, UK*

Superficial soft tissues like skin or adipose tissue are the first structures of the human body to sustain loading during impact. Therefore, numerical simulation of soft tissue behavior has become more and more important in various fields of impact biomechanics as these simulations can assist in the assessment of accidents and safety systems. However, severe deformations of soft tissues present a challenge for the computational methods, mainly in terms of numerical stability. Element-free Galerkin (EFG) or smoothed particle Galerkin method (SPG) may provide alternatives to the classic finite element (FE) approach [1, 2]. The aim of this study is to compare FE, EFG and SPG methods for the simulation of adipose tissue under blunt impact using two different computational setups.

The first setup regards uniaxial compression of an adipose tissue specimen at a strain rate of 25 s-1. In the second setup, an adipose tissue specimen is impacted by the flat end of a cylindrical bar at velocities between 0.9 - 2.4 m/s. For both setups, adipose tissue is simulated as hyperelastic isotropic and strain-rate dependent material. Computational setup and boundary conditions are kept the same for comparison analysis. Only general and method-specific parameters for the FE, EFG, and SPG representation of the adipose tissue are varied, such as time step scale factor, element formulation for the FE method, support size for the EFG method and kernel formulation and support size for the SPG method. Engineering stress-strain curves are evaluated for setup 1, impactor acceleration for setup 2, and energy balance, numerical stability and computational cost for both setups.

Results show the same trend for both setups – FE and EFG method are quite stable and computationally efficient, whereas performance of SPG method is less efficient for those aspects. In addition, stability for both setups and quantity of acceleration results for setup 2 are strongly dependent on kernel support size for all three kernel formulations for SPG. Table 1 compares the different results for setup 1 shortly before the onset of computational instability for simulations with a time step scale factor of 0.3.

These results indicate that FE and EFG method are better suited to depict adipose tissue deformations during compression dominated problems. SPG method is less stable and results strongly depend on input parameters. Further investigations are needed to clarify whether this holds also for more complex impact scenarios.

method	strain [-]	stress [MPa]	computational cost [hh:mm:ss]
FE	0.81	4166.0	00:49:37
EFG	0.79	2858,5	00:59:23
SPG, KERNEL 0	0.74	389.4	02:11:25
SPG, KERNEL 1	0.67	28.8	02:19:04
SPG, KERNEL 2	0.68	43.0	02:45:30

Table 1: Comparison of results for uniaxial compression shortly before the onset of computational instability.

References:

[1] *Belytschko T, Lu Y, Gu L. 1994. Element-free Galerkin methods. Int. J. Numer. Methods Eng. 37(2):229-256*

[2] *Wu C, Wu Y, Crawford J, Magallanes J. 2017. Three-dimensional concrete impact and penetration simulations using the smoothed particle Galerkin method. Int. J. Impact Eng. 106:1-17.*

[P 60]

EFFECTIVE BALANCE EQUATIONS FOR ACTIVE LINEAR ELASTIC COMPOSITES AND THEIR APPLICATION TO ELECTROSENSITIVE ELASTOMERS

Salvatore Di Stefano[1], *Laura Miller*[2], *Alfio Grillo*[1], *Raimondo Penta*[2]

1 *Dipartimento di Scienze Matematiche (DISMA) "G.L. Lagrange", Politecnico di Torino, Turin, Italy, Torino, Italy*

2 *School of Mathematics and Statistics, Mathematics and Statistics Building, University of Glasgow, University Place, Glasgow, UK*

This work concerns the study of the effective balance equations governing active linear elastic composites. These are composite materials whose constitutive response can be described by an additive decomposition of the stress tensor into a purely linear elastic contribution and another component, which, in the present framework, is assumed to be given from the outset. We derive a new mathematical model that describes the effective mechanical behavior of the whole composite by means of the asymptotic (periodic) homogenization technique. We assume that there exists a sharp separation between the microscale, where the distance among different sub-phases (i.e., inclusions and/or fibers) is resolved, and the macroscale, which is related to the average size of the whole system at hand. This way, we formally decompose spatial variations by assuming that every physical field and material property are depending on both the macroscale and the microscale. The effective governing equations encode the role of the microstructure, and the effective contributions to the global stress tensor are to be computed by solving appropriate linear-elastic cell problems on the microscopic cell. We specialize our theoretical framework by identifying the given part of the overall stress tensor with the Maxwell tensor for a dielectric material [1]. We provide the functional form of the effective electric permittivity tensor in the case of a microscopically uniform electric field. The obtained results are compared with the work presented in [2].

Acknowledgments: We kindly acknowledge the Dipartimento di Scienze Matematiche (DISMA) "G.L. Lagrange" of the Politecnico di Torino, 795 "Dipartimento di Eccellenza 2018–2022" ('Department of Excellence 2018–2022'), Project code: E11G18000350001.

References:

[1] *Ogden, R., Steigmann, D. (2011) Mechanics and electrodynamics of magneto and electro-elastic materials, vol. 527. Springer Science & Business Media.*

[2] *Penta, R., Ramírez-Torres, A., Merodio, J. and Rodríguez-Ramos, R. (2018) Effective balance equations for elastic composites subject to inhomogeneous potentials. Continuum Mechanics and Thermodynamics, 30(1), pp. 145-163.*

[P 61]

DEVELOPMENT OF CATEGORICALLY-DEPENDENT STATISTICAL ATLASES TO BENEFIT SUBJECT-SPECIFIC REGISTRATION OF THE HUMAN MANDIBLE

Heather Borgard[1], *Amir H. Abdi*[2], *Eitan Prisman*[3], *Sidney Fels*[1]

1 *University of British Columbia, Vancouver, Canada*
2 *University of British Columbia, Electrical and Computer Engineering, Vancouver, Canada*
3 *University of British Columbia, Department of Medicine; Vancouver General Hospital, Vancouver, Canada,*

The adoption of statistical shape modeling into the realm of medical technologies has been explored with applications ranging from medical image analysis to registration techniques [1,2]. Here, we have created 6 category-specific mandibular mesh templates, i.e. atlases, to enable subject-specific deformable registration methods. The idea behind atlases is to both provide a foundation for complex topographies and to capture the variation across individuals through statistical modeling methods. Previous studies have developed atlases from large datasets that are not categorically specific [3]. Our approach considers the characteristics of individuals including sex and denture profile, compiling specific atlases based on these factors. Our application is to guide and ultimately improve deformable registration techniques through category-dependent templates, which have not previously been investigated for the human mandible. From a sample size of 60 mandibles, we have created 2 atlases corresponding to patients who have at least 60% of their dentition and to patients missing more than 60% of their teeth. Out of these 60 mandibles, we have created 4 additional atlases for females and males with detention and without. For each atlas, we have warped meshes by applying thin-plate spline technique to the average shape profile after running a principal component analysis. From a testing sample size of 10 mandibular meshes (2 corresponding to each template), we will evaluate two non-rigid transformation techniques both with and without the use of the atlases. We will validate the results by comparison metrics between the surface of the resulting meshes and the patient model by volumetric overlap and surface correspondences such as Hausdorff distance. The main goal for this project is to evaluate if the use of categorically-dependent mandibular atlases benefits the registration process. The final application for this work is to improve mastication simulations through subject-specific modeling of the main structures associated with mandibular reconstruction outcome.

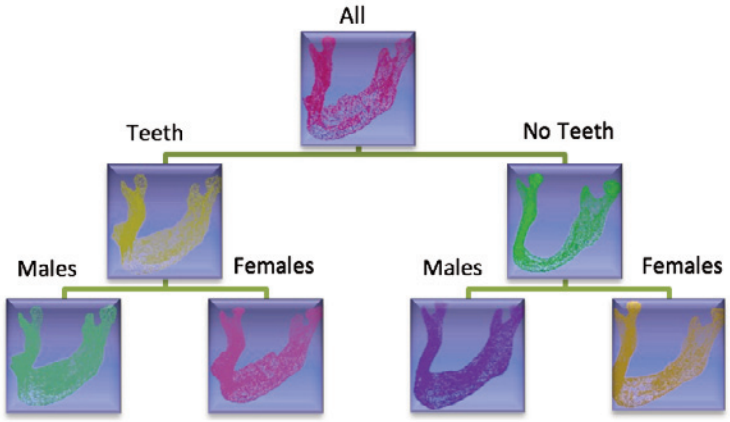

Figure Caption: Atlases representing by respective characteristics of sex and denture profile.

Acknowledgments: Dr. Eitan Prisman from Vancouver General Hospital for his support and PhD Candidate Amir Abdi for his guidance throughout this project.

References:

1. *AlHadidi A., Cevidanes L. H., Cook R., Festy F., Tyndall D., Paniagua B., "The use of a custom-made atlas as a template for corrective surgeries of asymmetric patients," Proc. SPIE 8317, Medical Imaging 2012: Biomedical Applications in Molecular, Structural, and Functional Imaging, 83171Y (5 April 2012); doi: 10.1117/12.911048*
2. *Raith, S., Wolff, S., Steiner, T., Modabber, A., Weber, M., Hölzle, F., & Fischer, H. (2016). Planning of mandibular reconstructions based on statistical shape models. International Journal of Computer Assisted Radiology and Surgery, 12(1), 99-112. doi:10.1007/s11548-016-1451-y*
3. *Zachow, S., Lamecker, H., Elsholtz, B., & Stiller, M. (2005). Reconstruction of mandibular dysplasia using a statistical 3D shape model. International Congress Series, 1281, 1238-1243. doi:10.1016/j.ics.2005.03.339*

[P 62]

PARAMETERIZING A PATIENT-SPECIFIC BRAIN TUMOR GROWTH MODEL USING SIMULATED MRIS: ASSESSING THE IMPACT OF NOISY DATA

Pamela Jackson[1], *Andrea Hawkins-Daarud*[1], *Kristin Swanson*[2]

1 *Precision Neurotherapeutics Innovation Program, Department of Neurological Surgery, Mayo Clinic, USA*

2 *Precision Neurotherapeutics Innovation Program, Department of Neurological Surgery, Mayo Clinic , Phoenix, USA; School of Mathematical and Statistical Sciences, Arizona State University, Tempe, USA*

Mathematical models of brain tumor growth commonly require an assumption regarding tumor cell density to parameterize them due to a lack of data. Searching across MRI images that have been simulated across the model parameter space can eliminate the need for a cell density assumption, however noisy MRIs will likely reduce the reliability of such a technique. Our objective is to characterize how the noise is limiting our ability to match simulated and real MRIs.

Brain tumors were simulated using the Proliferation-Invasion-Hypoxia-Necrosis-Angiogenesis-Edema (PIHNA-E) mathematical model previously described in [1]. Spatial maps of tumor cell density and edema for virtual tumors were simulated with different rates of tumor cell invasion (D) and proliferation (ρ). We simulated 100 versions of a tumor, each with a unique combination of D and ρ from 10 exponentially spaced values between 4 and 400 for each parameter. The PIHNA-E spatial maps were then passed into a multi-compartmental MRI signal model to generate simulated T2-weighted MRIs, which is further detailed in [2]. Nine sets of 100 simulated MRIs were created, each with a different level of Rician noise (noise mean = 0, noise standard deviations (NSDs) =0, 0.25, 0.5, 1, 2, 4, 8, 16, 32) for a total of 900 simulations.

We calculated features for each image histogram: mean, median, mode, minimum, maximum, standard deviation, standard error, 95% confidence interval, skewness, kurtosis, upper quartile, and lower quartile. Each simulated MRI was considered as a "candidate" image and compared to the entire set of 100 simulated images with NSD=0 to determine if we could correctly identify the D and ρ combination based on the imaging alone. The L2-norm was used to calculate the error between the zero noise simulated feature sets and the noisy tumor feature sets. The mean signal-to-noise ratio (SNR) was computed for each noise level and was calculated as the mean signal within a white matter region of interest (ROI) divided by the standard deviation of the signal within a background ROI.

As expected, the prediction rates and average SNR decreased as the image noise standard deviation increased (Table 1).

Simulated Image	L2-norm Prediction Rate compared to NSD=0 image	Mean SNR ± SD
NSD = 0	1.00	N/A
NSD = 0.25	0.61	155.99 ± 36.84
NSD = 0.5	0.27	77.10 ± 14.38
NSD = 1	0.08	38.57 ± 7.19
NSD = 2	0.03	19.46 ± 4.66
NSD = 4	0.02	9.78 ± 2.23
NSD = 8	0.01	5.18 ± 1.11
NSD = 16	0.01	3.02 ± 0.68
NSD = 32	0.01	2.26 ± 0.58

Table 1. Prediction Rates and SNR for Each Noise Level

All of the noise levels simulated severely limited the proposed technique. Typical SNRs for MRIs at 1.5 Tesla range from 63 to 124 [3], which is well within the range SNRs simulated in this work. Thus discovering methods to appropriately handle MRI noise are needed. Future directions of this work include exploring processing steps for reducing MRI noise, which may increase our ability to recognize the candidate image with the correct D and ρ.

Acknowledgments: Research supported by the National Institutes of Health grants U54CA193489 (Moffitt PS-OC) and U54CA193489-04S3 (Diversity Supplement).

References:

[1] *Hawkins-Daarud, A., et al. (2013). Front Onc, 3, 66*

[2] *Jackson, P. R., et al. (2018). In SPIE Medical Imaging 2018, 10577, 105771D*

[3] *Dietrich, O., et al. (2007). JMRI, 26(2), 375-385*

[P 63]

AN EASY-TO-USE DEVICE FOR STUDYING THE SURFACTANT REPLACEMENT IN LUNG AIRWAY

Stephanie Seoane[1], *Yi Wang*[1], ***Ehsan Atefi***[1]

1 *Manhattan College, New York City, USA*

Neonatal Respiratory distress syndrome is a disease that causes surfactant deficiency. This deficiency in neonates is most effectively treated through surfactant replacement therapy which takes a liquid-surfactant mixture and delivers it into the lung airways through forced inspiration. The liquid plug is then split unevenly through the airways due to gravity (see figure 1).

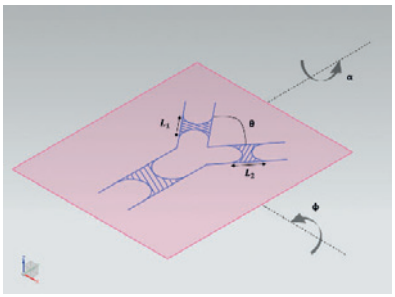

Investigating the splitting of the surfactant plug in lung airways returns imperative information on drug distribution, efficiency and homogeneity. Several computational studies have been done on measuring the splitting ratio of a surfactant plug driven by air pressure through a bifurcation model resembling the lung airways [1]. However, there is yet a need for a precise and easy-to-use equipment that allows studying the effect of the surfactant properties on drug distribution. Here, we introduce a device that enables automatic adjustment of the velocity of injection to sustain a constant splitting ratio, under diverse conditions of injection. This device permits running experiments to precisely compare the influence of the surfactant properties on drug distribution. Our device is made up of a computer-controllable injecting pump, a cell phone, a 3D-printed airway model, and a computer. We developed a Matlab code that accurately measures the angle of rotation using the gyroscope sensor of the cell phone. Then, this angle is implemented into equation1 to estimate the velocity of injection, for a given splitting ratio, through an iterative solution [1]. Finally, the program sets the injection pump velocity to the calculated number from equation 1. If any change occurs in the orientation of the airway model, the gyroscope detects the change, and the code automatically readjust the injection velocity in order to, hold the splitting ration constant.

$$S_r = 1 - \frac{2g(Bo, \varphi, \alpha)}{f(Re, Ca, \varphi, \alpha) + g(Bo, \varphi, \alpha)} \quad \text{(eq. 1)}$$

where, S_r denotes the split ratio, **Re**, **Bo** and **Ca** represent the Reynolds, Bond and Capillary numbers, respectively. f and **g** denote two complex functions discussed in reference 1. ”

Figure Caption:” Figure 1, represents the 2D sketch of the airway model. The splitting ratio, $S_r = L_2 / L_1$, the angles of rotations, α and φ, and the branching angle, $\theta = 80°$, are illustrated on the model”

References:

[1] M. Filoche, C. Tai, and J B. Brotberg, “Three-Dimensional Model of Surfactant Replacement Therapy.” PNAS. 2015; 112(30): 9287–9292.

[P 64]

ACUTE CANNABIS NOSE-ONLY AEROSOL INHALATION ELICITS REPRODUCIBLE EFFECTS IN C57BL/6 MICE

Yasmeen Farra[1], *Dongyang Yi*[1], *Praveen Kulkarni*[1], *Craig Ferris*[1], *Jessica Oakes*[1], *Chiara Bellini*[1]

1 *Northeastern University, Boston, USA*

Cannabis is by far the most used illicit drug amongst adults worldwide, with an estimate of 183 million regular users1. Nonetheless, the physiological effects of chronic cannabis consumption are largely unknown. To fill this gap, we developed a reproducible method to acutely expose mice to cannabis aerosols. We validated this model by recording the neurological, behavioral, and physiological responses elicited from an acute dose.

Cannabis was aerosolized with a vaporizer and delivered to male, C57BL/6 mice through a nose-only inhalation system, with exposure to room air as control. Size and mass concentration of the aerosol particles were measured within the exposure system. THC concentration as a function of the aerosolized cannabis was determined using an ELISA serum assay. Assessment of neurological activity in response to cannabis exposure was conducted using functional magnetic resonance imaging (fMRI) on the awake restrained mouse. Imaging relied on a Bruker BioSpec 7.0T/20-cm USR horizontal magnet and a 20-G/cm magnetic field gradient insert. Functional images were acquired using a single-shot RARE sequence. Images were aligned and registered to a 3D mouse atlas comprising 116 discrete anatomical regions. Behavioral effects of cannabis aerosol inhalation were assessed using an open maze field test. Finally, physiological changes in blood pressure and heart rate due to acute cannabis exposure were recorded with a tail-cuff system.

The count median diameter (± 95% CI) of the distribution of cannabis particles was CMD = 225.80 ± 4.708 nm, with a geometric standard deviation of GSD = 1.42 ± 0.002. A 450 mg cannabis dose elicited a blood THC concentration level in the mouse of 165 ng/mL, which falls within the range reported in humans. Significant positive BOLD in 15 regions and negative BOLD in 25 regions of the brain revealed CNS-mediated effects of acute cannabis inhalation. Cannabis exposure caused significant changes in the mouse behavior consistent with an anxiety-like response, thus replicating common human symptoms of anxiety and psychosis following cannabis use2. These observations suggest that acute exposure to cannabis elicits a similar response in mice and humans, supporting the validity of this model for cannabis-related studies.

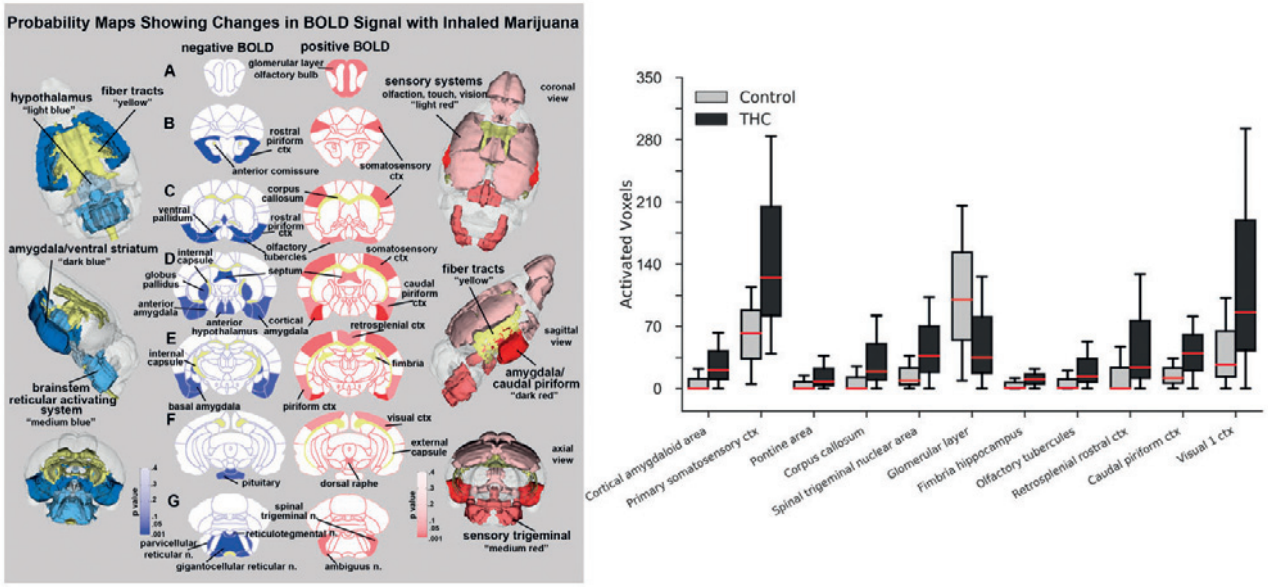

Figure Caption. LEFT: Probability maps showing brain activation due to acute exposure to cannabis aerosols as quantified through fMRI. RIGHT: Median number of activated voxels in selected brain regions with significant positive BOLD activity (control vs. cannabis-exposed groups).

Acknowledgments: Critical to this work were the contributions of James Coleman in data collection for the BOLD fMR imaging.

References:

1. *UNDOC. (2017). Fact Sheet on Statistics and Trends in Illicit Drugs. World Drug Report.*
2. *Morrison, P. D., et al. (2009). The acute effects of synthetic intravenous Δ9-THC on psychosis, mood and cognitive functioning. Psychological Medicine, 39(10), 1607–1616.*

[P 65]

ON THE 3D STRESS DISTRIBUTION IN THE ALVEOLAR WALLS: A COMBINED MICRO-CT AND COMPUTATIONAL MODELING STUDY

Mauricio Sarabia[1], *Matías Zuñiga*[1], ***Daniel Hurtado***[1]

1 *Pontificia Universidad Católica de Chile, Santiago, Chile*

Stresses in the alveolar walls have long been the object of study of pulmonary physiologists as they are fundamental to support the breathing process in mammalians. Alveolar-wall stresses also play a fundamental role in the pathogenesis and development of chronic respiratory diseases [1]. The importance of stresses notwithstanding, the determination of alveolar stresses remains challenging, and our current knowledge relies on 1D or 2D studies that do not consider the 3D nature of the acinar tissue [2]. In this work we assess the distribution of stresses in alveolar walls of normal murine lungs by combining ex-vivo micro-computed tomography and 3D finite-element modeling. In particular, we show that alveolar walls are subject to a fully three-dimensional multi-axial stress state, with stress concentrations arising in localized regions in the acinus. Further, stress can be amplified up to 27 times the applied alveolar pressure. Interestingly, we also show that the stress amplification is dependent on the level of alveolar pressure, i.e, stresses do not scale proportional to the applied alveolar pressure. In addition, we compare our results with 2D to show that alveolar stresses are consistently overestimated in alveolar walls by 2D methods, particularly for lungs under high transpulmonary pressure. These findings are very relevant in the study of stress-induced remodeling of the emphysematous lung and in ventilator-induced lung injury, where the relation between alveolar stresses and transpulmonary pressure is key to study mechanotransduction processes in the lung.

Acknowledgments: The authors acknowledge the support of the FONDECYT Grant #1180832, and from the Millenium Nucleus in Cardiovascular Magnetic Resonance.

References:

[1] *B. Suki, S. Sato, H. Parameswaran, M. V. Szabari, A. Takahashi, and E. Bartolak-Suki, "Emphysema and Mechanical Stress-Induced Lung Remodeling," Physiology, vol. 28, no. 6, pp. 404–413, 2013.*

[2] *C. E. Perlman and Y. Wu, "In situ determination of alveolar septal strain, stress and effective Young's modulus: an experimental/computational approach," AJP Lung Cell. Mol. Physiol., vol. 307, no. 4, pp. L302–L310, 2014.*

[P 66]

BIOMECHANICAL MODELS COUPLED TO TGF- ACTIVATION IN THE ASTHMATIC AIRWAY

Hannah Pybus[1], *Lowell Edgar*[2], *Reuben O'Dea*[1], *Bindi Brook*[3]

1 *The University of Nottingham, Nottingham, UK*
2 *Usher Institute of Population Health Sciences and Informatics, Edinburgh, UK; University of Edinburgh, Edinburgh, UK*
3 *University of Nottingham, Nottingham, UK*

Asthma is a highly prevalent disease characterized by inflammation, airway hyper-responsiveness (excessive bronchoconstriction to relatively low doses of contractile agonist) and remodeling (persistent structural changes to airway constituents due to inflammatory injury repair). Until recently, airway remodeling has been predominantly attributed to chronic inflammation. However, current experimental evidence suggests that bronchoconstriction may play a key role in promoting remodeling. Bronchoconstriction activates the regulatory cytokine, transforming growth factor β (TGF-β), which may further stimulate airway smooth muscle (ASM) contraction, proliferation, and deposition of extra-cellular matrix (ECM), altering the airway mechanics. In the healthy airway, regulatory mechanisms terminate this process, thereby re-establishing homeostasis. We hypothesise that in asthma this homeostatic state is lost, resulting in excessive contraction of the ASM and accumulation of ECM, further up-regulating TGF-β production through a positive mechanotranductive feedback loop.

Informed by precision-cut lung slice (PCLS) stretching experiments, we have developed a biomechanical model of TGF-β activation that couples subcellular mechanotransductive signaling pathways to nonlinear hyperelastic models of airway mechanics. We use constrained mixture theory to model an airway within the PCLS as a mixture of an active contractile ASM component and a passive nonlinear, incompressible, fiber-reinforced hyperelastic ECM component. We assume axisymmetry and adopt two different simplifying limits. First, we treat the PCLS as a membrane of infinitesimal thickness, allowing reduction to a one-dimensional form. Secondly, we exploit the assumption that the thickness of the PCLS is very small relative to the outer radius of the PCLS and introduce asymptotic expansions to determine the leading- and next-order deformation. We assess the accuracy of these approximations by comparing our solutions to a full three-dimensional model simulated in the nonlinear finite element software FEBio. Thereafter, we couple our mechanical models to an ODE model of TGF-β activation and simulate TGF-β mediated contraction and the subsequent change in effective mechanical properties as TGF-β activation progresses.

We find that ASM contraction and ECM strain-stiffening increases TGF-β activation as the PCLS deforms, and that axisymmetric cyclic stretching increases TGF-β activation over the absence of stretch, in agreement with experimental observations. Our findings highlight underlying mechanisms of mechanotransductive activation feedback and suggest that exaggerated airway deformation and stiffening of ECM, experienced in the asthmatic airway, are expected to give rise to further elevated levels of TGF-β. Additional experiments in which 5, 10, 20 and 25% stretches are applied to PCLS will enable further validation of our coupled model of stress-induced TGF-β activation in vitro. Thereafter, we aim to extend our model towards an in vivo description of ASM accumulation and ECM deposition in response to contraction-induced TGF-β activation providing insight into mechanisms that may operate in the asthmatic airway in vivo."

[P 67]

3D ULTRASOUND METHODS FOR IMAGE-BASED PERSONALISATION OF MUSCULOSKELETAL MODELS

*Frederick Greatrex[1], **Erica Montefiori**[1], Barbara Kalkman[1], Claudia Mazzà[1]*

1 INSIGNEO Institute for in silico medicine, Department of Mechanical Engineering, The University of Sheffield, Sheffield, UK

Background: Personalised musculoskeletal (MSK) models provide an understanding of internal joint forces, which is relevant for a number of clinical applications. MRI data is used to gain subject specific anatomical features, such as bone geometries, muscle paths, and muscle volumes1. While informative, MRI scans are time-consuming and costly. Ultrasound (US) offers an alternative for imaging internal anatomy. This research proposes a method for lower-limb joint axis calculation through geometric fittings of segmented surfaces captured by an US and motion capture setup to reduce the dependency of MRI in MSK models.

Methods: The US measurements (Telemed) consisted of a proximal to distal 'sweep' of the ultrasound probe over the femur head, lateral to medial sweep over the posterior femur condyles and a proximal to distal sweep over the talar dome. Py3DFreeHandUS2 was used for reconstructing the 2D US images into 3D space. This was performed on a phantom bone (5 repeats, 2 sessions [S1,S2]) and evaluated against a laser scanner (FARO), and repeated for one volunteer (Female, 29 y.o., 53kg) on both legs (L,R) for which lower-limb MRI (1.5T Siemens) and gait (Vicon, AMTI) data were also recorded. Fittings were performed on the reconstructed bone geometries to identify the lower-limb joint axes of rotation from both MRI and US data (sphere for the femur head, cylinder for the femur condyles and talar dome3) and included in an MSK model to quantify differences in estimated lower-limb joint contact forces (JCF).

Results: Radii measurements on the phantom were accurate (femur head [r_{laser}=22.8mm]: S1.23.5mm±1.9mm, S2.23.0mm±1.5mm; femur condyles [r_{laser}=18.8mm]: S1.20.4mm±1.2mm, S2.20.4mm±0.4mm). Radii measurements on the subject were precise but less accurate for the left femur head (femur head [r_{MRI}=23.3mm,24.8mm(L,R)]: 19.2mm±0.8mm, 23.3mm±0.3mm; femur condyles [r_{MRI}=18.3mm,17.2mm(L,R)]: 17.9mm±1.8mm, 17.8mm±1.2mm; talar dome [r_{MRI}=16.7mm(Lonly)]: 24.9mm[single measurement]). Negligible differences were found between the MRI and US models for the hip and knee kinematics. A 12° difference was found over the entire gait cycle for the ankle joint kinematics. Differences of 0.75, 0.65 and 0.42 body weight (BW) were found between the MRI and US simulations of JCF for the hip, knee and ankle respectively.

Conclusion: This study showed the feasibility of using US for personalisation of joint axes, with a potential of reducing the dependency of MRI in subject-specific modelling. A comprehensive validation is ongoing.

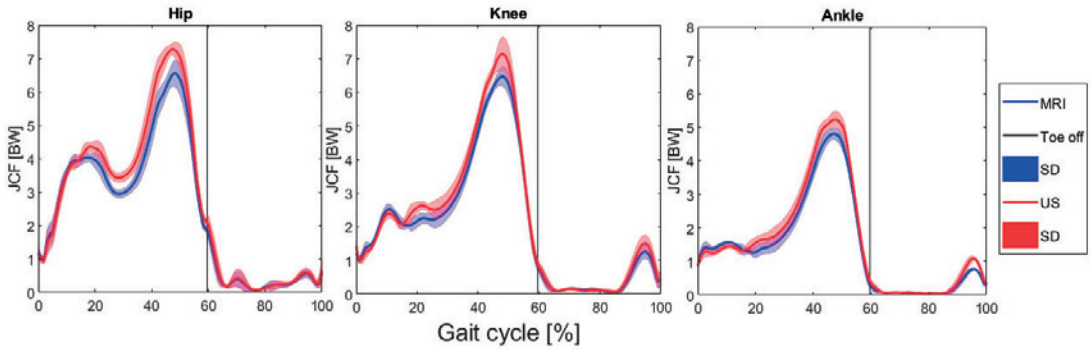

Figure Caption: Mean and SD for the JCF using MRI (Blue) or US (Red) based joint axes estimates.

Acknowledgments: Supported by Aesculap (Tuttlingen, Germany) and the UK EPSRC (EP/J013714/1 and EP/K03877X/1). Thanks to Francesco Cenni for support in the implementation of the Py3DFreeHandUS package.

References:

1. *Carbone, V., et al. (2012). J.Biomech, 45(14) p2476*
2. *Cenni, F., et al. (2016). Comput Methods Programs Biomed, 136, p179*
3. *Montefiori, E., et al. (2019). J.Biomech, (In Press)*

[P 68]

A NUMERICAL STUDY ON THE MATERIAL NONLINEAR BEHAVIOR OF AORTIC TISSUE IN ABDOMINAL AORTIC ANEURYSM PATIENTS.

Ji-Hun You[1], *Chi-Seung Lee*[2], *Chung-Won Lee*[3], *Up Huh*[3], *Dong-Man Ryu*[4]

1 *Department of Biomedical Engineering, School of Medicine, Pusan National University, Busan, Korea, Rep. of South*
2 *Department of Biomedical Engineering, School of Medicine, Pusan National University, Busan, Korea, Rep. of South; School of Medicine, Pusan National University, Busan, Korea, Rep. of South; Biomedical Research Institute, Pusan National University Hospital, Busan, Korea, Rep. of South*
3 *Department of Thoracic and Cardiovascular Surgery, School of Medicine, Pusan National University, Busan, Korea, Rep. of South; Biomedical Research Institute, Pusan National University Hospital, Busan, Korea, Rep. of South*
4 *Department of Biomedical Engineering, School of Medicine, Pusan National University, Busan, Korea, Rep. of South; Biomedical Research Institute, Pusan National University Hospital, Busan,Korea, Rep. of South*

The purpose of this study is to conduct the computational simulations and experiments in order to investigate the mechanical behavior of the aorta wall in abdominal aortic aneurysms. The study focused on the deformation and strength of porcine and patient's abdominal aortic tissues under uniaxial tensile loading. The experiments for the mechanical behavior of the arterial tissue were conducted using a uniaxial tensile test apparatus to validate the simulation results. In the uniaxial tensile test, the ends of the specimens are fixed using a sand paper and fixing apparatus, which maintains the tissues in place by a zig. Moreover, the tensile test methods were investigated to decrease the failure rate of the experiment, and the specimens were sectioned circumferentially and longitudinally in the aorta and obtained as dog-bone shaped strips. As a result, the relationship between stress and stretch according to fiber orientation were identified, and the experimental results were compared with the simulation results to verify the computational simulations technique. In addition, the strength and stretching of the arterial tissues in patients according to age were investigated based on the uniaxial tensile tests. The computational simulations were conducted on the experimental scenarios based on age, and the Holzapfel model was applied during the simulation. As a result, material parameters in the material model were estimated at the ages 46~90 years, and the relationship between age and material constants were established. Furthermore, the formula associated with material constants was proposed in order to simulation failure stress and stretch according to age.

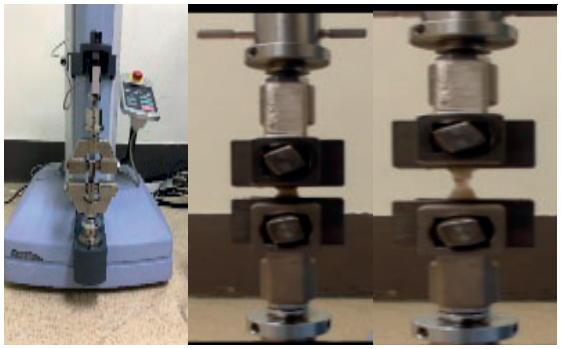

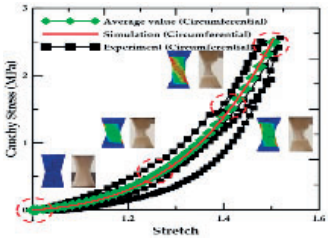

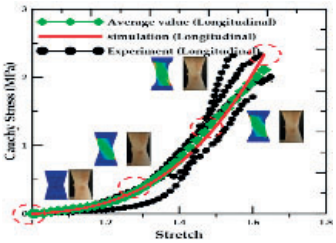

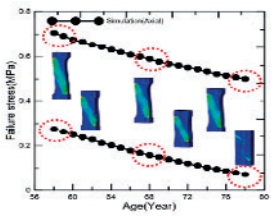

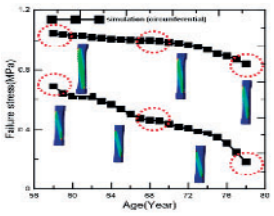

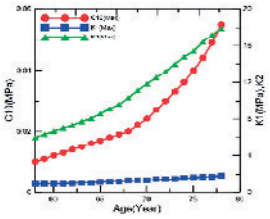

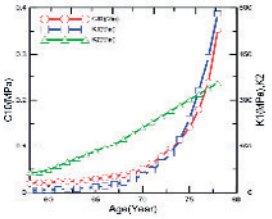

Figure 1. Tensile test method
Figure 2. Stress-stretch curve for porcine arterial tissue in the tensile tests and simulations
Figure 3. Simulation results under tensile loading
Figure 4. Variation of the material parameters according to age

Acknowledgments: This research was supported by Basic Science Research Program through the National Research Foundation of Korea(NRF) funded by the Ministry of Education (2018R1A6A3A01012664; 2018R1D1A1B07044567).

References:

Holzapfel GA, Gasser TC, Ogden RW. A new constitutive framework for arterial wall mechanics and a comparative study of material models. J. Elasticity. 2000; 61(1-3): 1-48.
Holzapfel G. Arterial tissue in health and disease: experimental data, collagen-based modeling and simulation, including aortic dissection. In Biomechanical Modelling at the Molecular, Cellular and Tissue Levels: Springer; 2009; 259-344.
Forsell C, Swedenborg J, Roy J, Gasser TC. The quasi-static failure properties of the abdominal aortic aneurysm wall estimated by a mixed experimental-numerical approach. Ann. Biomed. Eng. 2013; 41(7): 1554-1566.
Pierce, D.M.; Maier, F.;Weisbecker, H.; Viertler, C.; Verbrugghe, P.; Famaey, N.; Fourneau, I.; Herijgers, P.; Holzapfel, G.A. Human thoracic and abdominal aortic aneurysmal tissues: Damage experiments, statistical analysis and constitutive modeling. J. Mech. Behav. Biomed. 2015, 41, 92–107.

[P 69]

DIFFERENTIATION OF CARTILAGE CULTURE CONDITIONS BY DEPTH-WISE STATISTICAL ANALYSIS OF MRI-BASED STRAIN FIELDS

Sameer Sajid[1], *Deva Chan*[1]

1 *Rensselaer Polytechnic Institute, Troy, USA*

The spatially heterogeneous mechanical properties of articular cartilage are not well-captured by nominal measurements [1] but are important to characterize tissue behavior. Cartilage exhibits heterogeneous matrix remodeling but the associated internal biomechanical changes are often assessed destructively or by altering boundary conditions [2]. Displacement-encoded MRI can assess in vivo cartilage mechanics [3], but spatial analysis of MRI-based strains as a marker for matrix remodeling remains limited. Here, we present a method to compare depth-wise changes in internal strains in a model of growth-factor-induced cartilage change in culture.

Six total explants were harvested from bovine stifles and cultured [4] for 15 days with (+) or without (-) 100ng/mL bFGF [5]. Afterwards, explants were cyclically compressed [6] in synchrony with displacement-encoded acquisitions [3] on 7T MRI. Principal strains were then calculated from smoothed displacements [7] and divided over ten regions from 0% (surface) to 100% depth.

Regional peak principal strain comparison by paired t-test [8] showed no significant differences. Regional strain distribution comparison was by Kolmogorov-Smirnoff tests. Pixels in each region were binned by principal strains for Fisher discriminant analysis (FDA) to identify the regions that best differentiated -bFGF and +bFGF groups. The +bFGF group had higher frequency of 1st principal strains ranging +2% to +6% bins near 50-40% depth and higher frequency of 2nd principal strains ranging -6% to -1% at 60-50% depth. Regions with statistically different distributions and statistical significance with good separability (J > 1.338) by FDA are indicated in the Figure.

Treatment with bFGF induced depth-wise changes in the mechanical behavior of cultured cartilage as measured by the distribution of principal strains and FDA of binned strains. These differences are undetected by peak strains, highlighting the value of spatial analyses over singleton metrics. Our expectation that depth-wise principal strains would vary between groups within 40% to 70% of tissue depth was partially confirmed by the significant distribution comparisons and FDA in 4 identified regions. These differences are present in both computed strains within 40% to 60% of tissue depth, corresponding to the middle zone [9]. Future work with larger data sets will continue to examine depth-wise principal strain distributions as a marker of underlying tissue damage or remodeling.

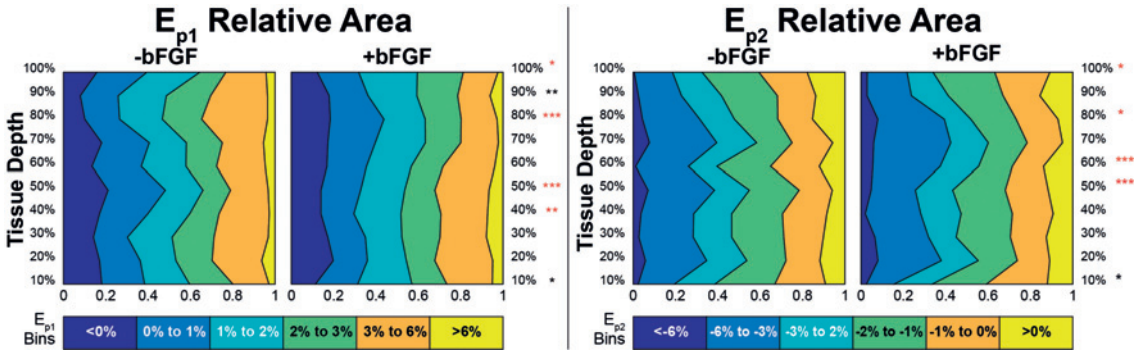

*Figure Caption: Principal in-plane strains were measured in cartilage cultured -/+bFGF. Statistically different distributions (*p<0.05, **p<0.01, ***p<0.001) are indicated, and good FDA separation existed for some regions (red).*

Acknowledgments: Dr. Uwe Kruger

References:

1) Guo+ Tis Eng B Rev 2017
2) Wang+ J Orthop Surg Res 2018
3) Chan+ Sci Rep 2016
4) Yan+ Arth Res Ther 2011
5) Li+ J Cell Biochem 2012
6) Neu+ J Biomech Eng 2003
7) Chan+ Com Met Biomech Biomed Eng 2011
8) Bae+ J Biomech 2006
9) Julkunen+ OAC 200

[P 70]

3D CONSTITUTIVE MODEL OF THE RAT LARGE INTESTINE: ESTIMATION OF THE MATERIAL PARAMETERS OF THE SINGLE LAYERS

*Fabiano Bini[1], Matteo Desideri[1], **Andrada Pica**[2], Simone Novelli[3], Franco Marinozzi[1]*

1 *Department of Mechanical and Aerospace Engineering*

2 *Department of Mechanical and Aerospace Engineering - Sapienza University of Rome, Rome, Italy*

3 *Sapienza University of Rome, Rome, Italy; institute for Liver and Digestive Health (Ildh)-University College London (Ucl). London, UK ; Sapienza University of Rome, Rome, Italy*

Soft tissues have non-linear mechanical behaviour are modelling as hyperelastic model applying the strain energy function [1]. Moreover, as the arterial walls, the colonic walls are composed by collagen fibres characterized an anisotropic behaviour. Holzapfel et al. [2] proposed constitutive model in which arterial walls are represented as two-layer thick-walled cylinders, with each layer modelled as a fiber-reinforced composite. Afterwards, Sokolis et al. [1], proposed a structure-based mathematical model for mechanical passive behaviour of the rat colon, fitting to data obtained from inflation/extension tests. Sokolis et al. [1] doesn't split up the walls into layers. However, the wall of the rat large intestine is composed by four distinct layers [1], i.e. mucosa, submucosa, muscle layer and serosa. The aim of this paper is to identify a method for estimating the parameters of a computational model that considers each layer of the colonic walls. Starting from the experimental data by Sokolis et al. [1], we use the Nelder-Mead nonlinear regression technique for minimizing the residual sum of squares between the experimental data and data computed by means of proposed method. The estimated material parameters (k_1, k_2, c) are used to develop a 3D finite element model. We consider the large intestine wall composed of four cylindrical layers (Fig. 1a). Each layer is assumed as a nonlinear, homogeneous, hyperelastic and orthotropic material model with the incompressible material and finite deformation assumption. In this study, we computed, for each layer, the W strain energy function proposed by Sokolis et al. [1] for the wall thickness equal to (W_{iso} + W_{anis}) where W_{iso} represents the isotropic behaviour of the elastin and W_{anis} represents the anisotropic behaviour of the collagen fibres according to their orientation. We computed the components of the Cauchy stress along the cylinders wall thickness for each single layer and different values of internal pressure P_i and axial stretch $\lambda_z = L_0 + \Delta_L / L_0$. A typical result of the axial component σz and the circumferential component σ_θ of the Cauchy stress along the wall thickness is reported in the Fig. 1b.

[P 71]

MICRO-INDENTATION TO INVESTIGATE CROSS-SECTIONAL MATERIAL PROPERTIES DISTRIBUTION OF THE SPINAL CORD

Nicolas Bailly[1], *Eric Wagnac*[2], *Yvan Petit*[3]

1 *École de Technologie Supérieure, Montreal, Canada; Research Center, Hôpital du Sacré-Cœur de Montreal, Montreal, Canada*
2 *École de Technologie Supérieure, Montreal, Canada; V2r Biomédical, Montreal, Canada*
3 *École de Technologie Supérieure, Montreal, Canada; Ilab Spine, France*

Objective: The capacity of finite element modeling to reproduce injury mechanisms and to investigate strain and stress features of the biological tissue mainly depends on the fidelity of the model geometry and material properties. Yet, the material properties of grey and white mater of the spinal cord are still debated [1] and might not be homogeneous as large variability in axon morphometries and density was described within the white mater [2].This study presents a method to characterise the cross-sectional distribution of mechanical properties in the spinal cord using micro-indentation on freshly harvested porcine spinal cord segments.

Methods: Transverse slices of thoracic spinal cord of 5mm thickness were prepared within 6 hours post mortem using the Compresstome® VF-300-OZ slicing tool. The samples were glued into a petri dish and submerged into Phosphate-buffered saline. The dish was mounted into a Hysitron TI 950 TriboIndenterTM with an XZ 500 extended displacement stage (resolution <0.1nN). A 0.5mm diameter flat punch was used to indent the samples. Indentation was performed with a loading-holding-unloading profile with a maximum displacement of 300µm, loading and unloading rate of 2.5 µm/s, and holding time of 30 s. Twenty-five indents were performed every 1 mm over a squared surface of 5mm by 5mm at the center of the sample to obtain a surface mapping of the sample's elastic modulus (figure a). The elastic modulus was obtained from the slope of the upper part of the unloading curve (figure b), and the shape factor of the indentor.

Results: Results from the first sample show a large variability of elastic modulus across the sample (1,51±0,69 kPa) and within the white matter (1,53±0,67kPa) and the grey matter (1,43±0,85kPa). No significant difference was found between the two matters.

Discussion: This study presents a novel method to characterise the cross-sectional material properties distribution of the spinal cord. The results suggest a large variability of material properties within the cross section of the spinal cord, but no significant difference between white and grey matters. This large variability in elastic modulus might be related to neuron density and morphometry [2] as well as the myelin content [1]. Additional testing and histological studies will be performed to investigate those hypotheses.

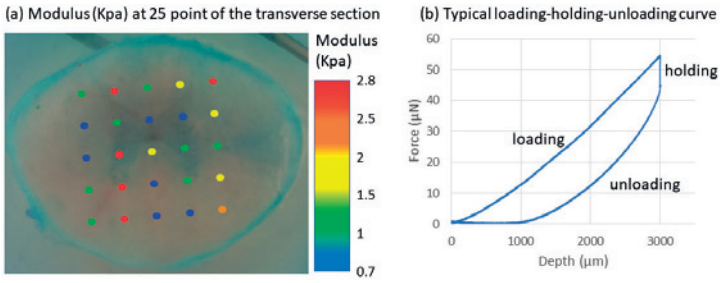

Figure caption: Typical force-depth curve and elastic modulus obtained in the transverse section of the first cord sample

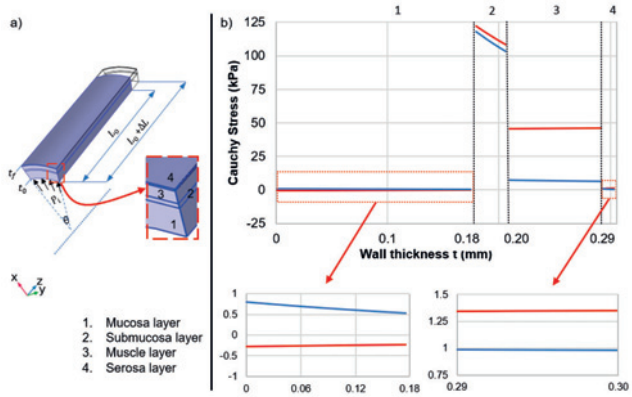

Figure 1: a) 3D model section. b) Axial σz (red line) and circumferential σθ (blue line) for .

References:

[1] *J. Weickenmeier, R. de Rooij, S. Budday, P. Steinmann, T. C. Ovaert, et E. Kuhl, « Brain stiffness increases with myelin content », Acta Biomaterialia, vol. 42, p. 265:272, sept. 2016.*
[2] *T. Duval et al., « Axons morphometry in the human spinal cord », NeuroImage, vol. 185, p. 119:128, janv. 2019.*
[3] *Sokolis DP, Sassani SG. Microstructure-based constitutive modelling for the large intestine validated by histological observations. J Mech Behav Biomed Mater. 2013; 21:149-166.*
[4] *Holzapfel GA, Gasser TC, Odgen RW. A New Constitutive Framework for Arterial Wall Mechanics and a Comparative Study of Material Models. J Elast Phys Sci solids. 2000; 61(1):1-48.*

[P 72]

ON THE EVALUATION OF ANTERIOR LUMBAR FUSION CAGES: A FINITE ELEMENT STUDY

Rafael Guerreiro[1], Manuel Tavares de Matos[2], Paulo Fernandes[1], ***Andre Castro****[3]*

1 *Idmec, Instituto Superior Técnico, Universidade de Lisboa, Lisbon, Portugal*
2 *Unidade Da Coluna Vertebral, Hospital Lusíadas, Lisbon, Portugal*
3 *Instituto Superior Tecnico, Universidade de Lisboa, Lisbon, Portugal*

Spine surgeons often select the Anterior Lumbar Interbody Fusion (ALIF) technique to the treatment of diseases related to degenerated intervertebral disc (IVD). However, the surgical placement of these anterior intervertebral cages may still result in comorbidities to the patient that could be avoided if the insertion of the implant was facilitated (Sasso et al. 2005). Therefore, the motivation for this study is to reduce the surgical risks while maintaining or improving the success rates for interbody fusion for both short and long-term. The main goal for this work is to develop new fixation alternatives for the commercially available Synfix-LR system (SLR), namely in what concerns to the number and orientation of the fixation screws. The present study was based on the development of 5 alternative SLR designs. An in vitro study (Heuer et al. 2007) was used to validate the model based on the Range of Motion (RoM) of the lumbar segment. The 6 cage models (including the original system) were simulated under common movements such as rotation or flexion/extension, after the surgery and after consolidated fusion. Finite Element (FE) simulations were ran on Abaqus® (Dassault Systèmes Simulia Corp., USA). The FE simulations have revealed that the new designs that kept the number of screws of the original system (4 screws) could achieve similar biomechanical behavior to the reference (increase of just 0.05º in the RoM). For the new models with lower number of screws (2 or 3), the success of the interbody fusion would not be ensured. Results also showed that the biomechanics of these implants could still be ensured even after altering the orientation of the fixation screws, which is due to facilitate their surgical placement. Further developments of this research line can bring light to the wide comparison of different fixation systems in various time points post implantation, and also for other surgical approaches to lumbar fusion.

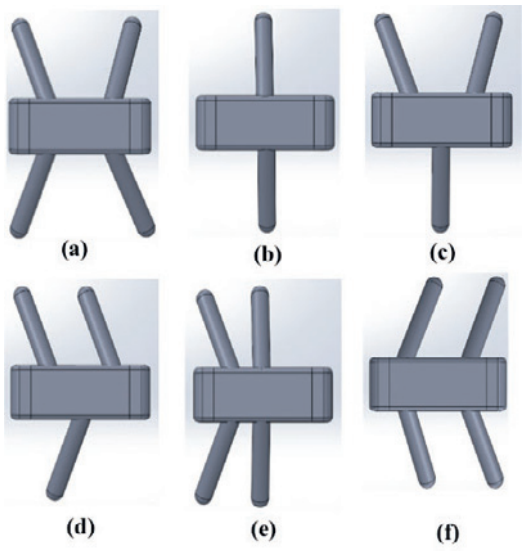

Figure 1 Original and new designs of the Synfix-LR system. (a) Original design of the Synfix-LR system. (b) Design 1 with two screws. (c-d) Designs 2 and 3 with three screws. (e-f) Designs 4 and 5 with four screws.

Acknowledgments: This work was supported by Fundação para a Ciência e Tecnologia, through IDMEC, under LAETA project UID/EMS/50022/2019

References

Heuer F, Schmidt H, Klezl Z, Claes L, Wilke H-J. 2007. Stepwise reduction of functional spinal structures increase range of motion and change lordosis angle. J Biomech. 40:271–280.
Sasso RC, Best NM, Mummaneni P V., Reilly TM, Hussain SM. 2005. Analysis of Operative Complications in a Series of 471 Anterior Lumbar Interbody Fusion Procedures. Spine (Phila Pa 1976). 30:670–674.

[P 73]

HEAD AND NECK MUSCLES MOMENTS PREDICTION IN RESISTING STATIC FORCE APPLIED TO THE HEAD IN VARIOUS AXIAL PLANE DIRECTIONS

Wissal Mesfar[1], ***Kodjo Moglo***[2]

1 *Biomedical Technology Department; College of Applied Medical Sciences; King Saud University, Riyadh, Saudi Arabia*
2 *Mechanical & Aerospace Engineering; Royal Military College of Canada, Kingston, Canada*

Investigations into the biomechanical responses of the head and neck (HN) complex have currently become necessary to further our understanding of HN injury patterns and mechanisms. Under applied head loading cases, soft tissues and HN muscles respond to counteract the action of the external applied forces to maintain the HN complex stability and to protect the joint from injury. In this study, we focus on the characterization of the isometric muscle moment generation in resisting forces applied to the head at different directions in the axial plane. Our validated HN finite element model, composed of the bony structures, head, cervical (C1-C7) and the first thoracic (T1) vertebrae, articular cartilages and the different ligaments (1), was subjected to a 100N force applied to the head in five axial plane directions in the presence of a 40N head weight. The directions are Anterior, Posterior, Right and 45-degree oblique angles for Anterior-Right and Posterior-Right directions. The first thoracic vertebra was fixed while the head and cervical vertebrae were free to translate but not to rotate in order to compute the reaction moment at each bony structure allowing the prediction of muscles moments components required to counterbalance the applied force and to maintain static stability of the segment.

Our predictions indicate that the highest net moments were developed by the head muscles in resisting 100N force in the posterior, posterior-right, anterior, anterior-right and right directions consequently reaching 6.63N.m, 6.28N.m, 5.53N.m, 4.51N.m and 4.28N.m, respectively (Figure 1). The flexor muscles were the main muscles involved in resisting the posterior and posterior-right forces developing moments of 6.59N.m and 4.52N.m. However, to resist the Anterior and Anterior-right forces, the head extensor muscles developed moments reaching 5.58N.m and 3.47N.m, respectively. For forces in the Right, Posterior-Right and Anterior-Right directions, head muscles moments in lateral-left directions of 4.04N.m (94.4% of the Net moment), 3.83N.m and 2.23N.m, respectively, were required to maintain stability of the HN. Contrary to the head-muscles, the C1-muscles developed the highest counterbalancing moments to resist the right-dependent direction forces. The moment reaches 4.71N.m, 4.24N.m, 2.88N.m, 1.96N.m and 1.41N.m in resisting the 100N force applied to the Right, Anterior-Right, Posterior-Right, Anterior and Posterior directions, respectively. The computed results show that the muscles moments are highly altered by their location in the HN and by the direction of the applied force. Finally, this study can be of great interest to understand the differential HN complex vulnerability to injury with externally applied loads in different directions.

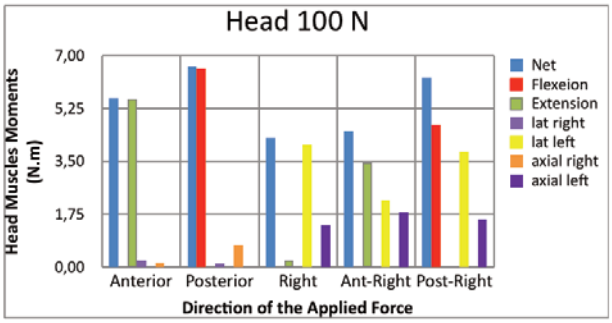

Figure 1: Net moments and moment components of the HN muscles acting on the head counterbalancing a 100N force applied to the head in different axial plane directions.

References:

1. *W. Mesfar and K. Moglo, Clinical Biomechanics, 28(8), 846-52, 2013.*

[P 74]

DEVELOPMENT OF SEQUENTIAL BONE ADAPTATION PROCESS ALGORITHM FOR ASSESSMENT OF ACDF AND CDA

Won Man Park[1], *Yong Jun Jin*[2], *Choengryul Choi*[1]

1 *Elsoltec, Yongin, Korea, Rep. of South*
2 *Inje University, Seoul Paik Hospital, Seoul, Korea, Rep. of South*

Previously published clinical studies have reported bone formation surrounding the inserted cages or artificial discs after anterior cervical discectomy (ACDF) or cervical disc arthroplasty (CDA). The bone formation is called as extragraft bone bridging in ACDF and as heterotopic ossification in CDA. The purposes of these two surgical treatments are to unite vertebrae and to preserve segmental motion of the operated motion segment, respectively. While bone formation has positive effects in ACDF because extragraft bone bridging is necessary for a solid union at the operated level, bone formation has negative effects in CDA because heterotopic ossification interrupts preserving segmental motion. Therefore, it is important to simulate bone formation surrounding the inserted implants for the assessment of preoperative plans or surgical implants for treating the spine. In this study, sequential bone adaptation process algorithm was developed to simulate bone formation surrounding the inserted implant. ACDF without an anterior plate and screw system was simulated in a validated three-dimensional finite element model of the cervical motion segment C5-C6 based on the pre-operative plan established by a spinal surgeon. The potential region of the bone formation was modeled in the posterior to the inserted cage. Trilinear adaptive bone remodeling algorithm introduced in the previously published studies was used in the development of the sequential bone adaptation process algorithm. A custom Matlab code was established based on the developed algorithm then applied to simulate bone formation in the previously defined potential region. Bone formation was simulated in flexion and extension motions. A commercial finite element analysis package Abaqus/Standard, coupled with the developed Matlab code, was used to simulate flexion and extension motions. Moments of 1.5 Nm with a compressive force of 50 N were applied on the superior plane of the C5 vertebra to simulate flexion and extension. The results showed that the developed algorithm could predict sequential bone formation after ACDF. The bone, extragraft bone bridging, was formed in extension mainly, while bone formation was predicted only at the junction of the inserted implant and vertebrae in flexion. The progress of bone formation showed good agreement to medical images. This study is the first study in which the sequential bone formation after ACDF was simulated. The authors believe that the developed algorithm should be helpful for biomechanical assessment of surgical implants or techniques with considering bone formation after operations.

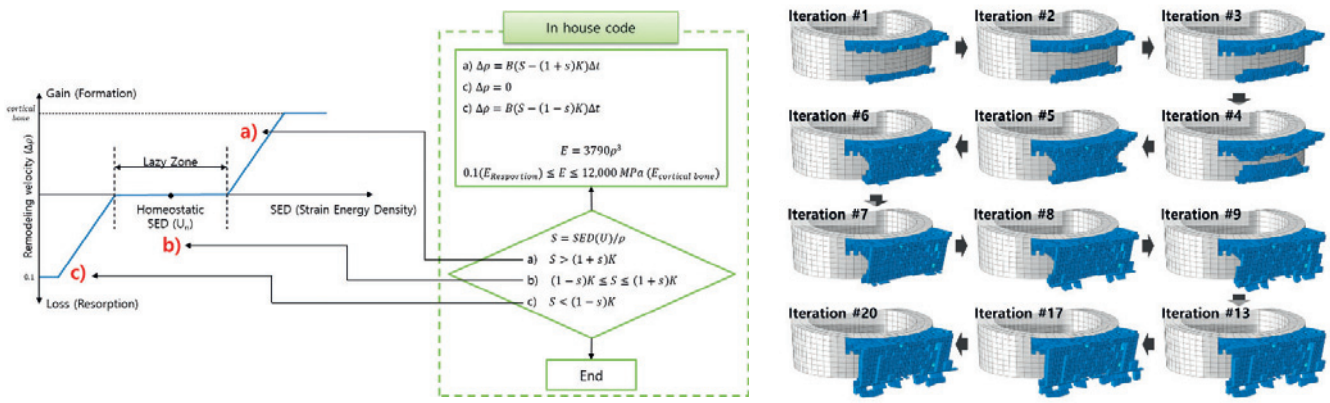

Figure Caption: Trilinear adaptive bone remodeling algorithm to simulate bone formation (left) and sequentially formed bone during extension (right)

Acknowledgments: This research was supported by Basic Science Research Program through the National Research Foundation of Korea (NRF) funded by the Ministry of Education (No. NRF-2017R1D1A1B03034668).

[P 75]

BIOMECHANICAL EVALUATION OF FIXATION METHODS FOR THE SURGICAL TREATMENT OF THORACOLUMBAR FRACTURE

Shady Elmasry[1], ***Francesco Travascio***[2], *Shihab Asfour*[2]

1 *Hospital for Special Surgery, New York, USA*
2 *University of Miami, Miami, USA*

The thoracolumbar junction is a vulnerable spine region in which the majority of traumatic fracture occurs. Thoracolumbar fractures are typically treated with surgical intervention. Different surgical approaches are currently available, such as long-segment posterior fixation (LSPF), short-segment posterior fixation (SSPF), and augmenting fixations with pedicle screws at the fracture level or by balloon kyphoplasty (KP). Yet, the biomechanical impact of these surgical approaches on the spine is not well understood. With the advancement of computational power and the ability to precisely reconstruct 3D models of spine tissues, Finite Element Analysis (FEA) became a viable tool for basic and translational research on spine biomechanics. Surgical approaches for the treatment of thoracolumbar fractures is an important area that FEA can play a pivotal role to help understand the biomechanical implications of each surgical approach. Therefore, the objective of this study was to develop an FEA framework to evaluate the biomechanical performance of the spine following four surgical treatments of thoracolumbar fractures: LSPF, SSPF, augmenting SSPF with index screw, and augmenting SSPF with KP. A comprehensive FEA frame work was developed to achieve this goal (Figure 1) [1, 2]. CT scans were used to create 3D models of the vertebrae of the thoracolumbar spine (Mimics Research; Materialise, Belgium). The geometry of the bones were manipulated and the implant devices were modeled and placed under the supervision of a spine surgeon (SolidWorks, Concord, MA). All spine tissues including intervertebral discs, facet cartilages, and seven ligaments were added to the model. All material properties were defined as reported in the literature. The intervertebral disc was divided into nucleus pulposus and annulus fibrosis and considered as a biphasic media. The ligaments were represented as linear elastic tension-only spring elements. The vertebrae were discretized by four-node solid elements, while the IVD and cartilage at facet joints were discretized by eight-node solid elements. Flexion, extension, lateral bending, and axial rotation of 5 Nm were simulated following each surgical approach (FEBio 2.4.0, UT). The range of motion and intradiscal pressure at the adjacent segments were measured and compared. The model's prediction of the range of motion was in agreement with cadaveric experiments. The intradiscal pressure at the adjacent segments varied across the four surgical approaches with the maximum pressure found on the LSPF construct. These findings demonstrate the important role that computational models can play towards personalized surgical treatments of spine fractures.

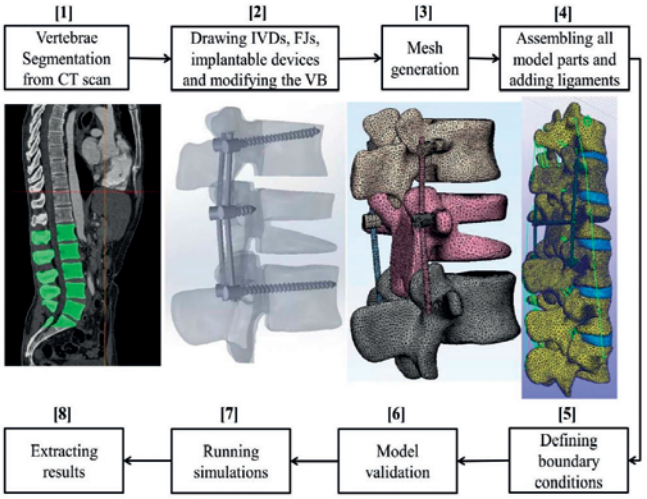

Figure 1: Work flow of the FEA framework to analyze surgical approaches for spine fractures

Acknowledgment: Study supported by funds donated to Biomechanics Research Group of the University of Miami, Miami, United States

References:

[1] Elmasry et al., 2017, CMBBE;
[2] Elmasry et al., 2018, J Biomech Eng

[P 76]

HOW IMPORTANT IS THE ANTERIOR COLUMN SUPPORT IN A LONG LUMBOPELVIC SPINAL FIXATION? AN IN-SILICO BIOMECHANICS ANALYSIS

Woojin Cho[1], ***Wenhai Wang***[2], *Brandon Bucklen*[2]

1 *Albert Einstein College of Medicine; Montefiore Medical Center, New York, USA*
2 *Musculoskeletal Education and Research Center, Audubon, USA; Division of Globus Medical, Inc.*

Introduction: The addition of anterior column support at the bottom of a long construct has been proposed to support the lumbosacral junction and potentially prevent posterior lumbopelvic fixation failure. However, a retrospective study has shown that adding anterior column support was not sensitive to construct failure, [1] highlighting the possibility that posterior fusion quality may be a more important factor than previously thought.

Materials and Methods: Finite element models (T10-Pelvis) were created to match the average spinal-pelvic parameters of two cohorts of patients reported in the literature [1], major-failure (defined as pseudoarthrosis or rod fracture above S1) and non-failure groups. A moment load was applied at the T10 superior endplate to simulate gravimetric loading in a standing position. Posterior solid fusion was simulated by applying spring elements attached to the adjacent vertebrae. A sensitivity analysis was performed on a functional spine unit L4/L5 to justify the spring constant so that it can simulate a "solid" fusion. Anterior column support was simulated by assigning cancellous bone properties to the L4-S1 disc.

Results: Upper body weight acting on the long instrumented spine resulted in 18% higher translation, 14% higher rotation, and 20% higher stress in the major failure group than in the non-failure group. Solid posterior fusion decreased translation and rotation, and also alleviated rod stress in the lower lumbar region by 15% and 5% in the major failure and non-failure group, respectively; and alleviate the maximum S1 screw stress by 26% and 35% in major failure and non-failure groups, respectively. In this case, anterior support did not change the stress pattern. Conversely, simulated pseudoarthrosis produced stress patterns similar to those of the construct-only spine. In this case, adding anterior support dramatically alleviated stress at the index levels.

Conclusion: The spinopelvic parameters of the major-failure group produced increased gravity load, resulting in increased stresses in comparison to the non-failure group. Simulated posterior fusion in the lumbar region helped reduce stresses in both major failure and non-failure patients. However, in cases with a simulated pseudoarthrosis, rod stresses were amplified by major failure spinal alignment. In this case, anterior column support was a major factor in reducing rod stress, and should be considered for patients with poor alignment.

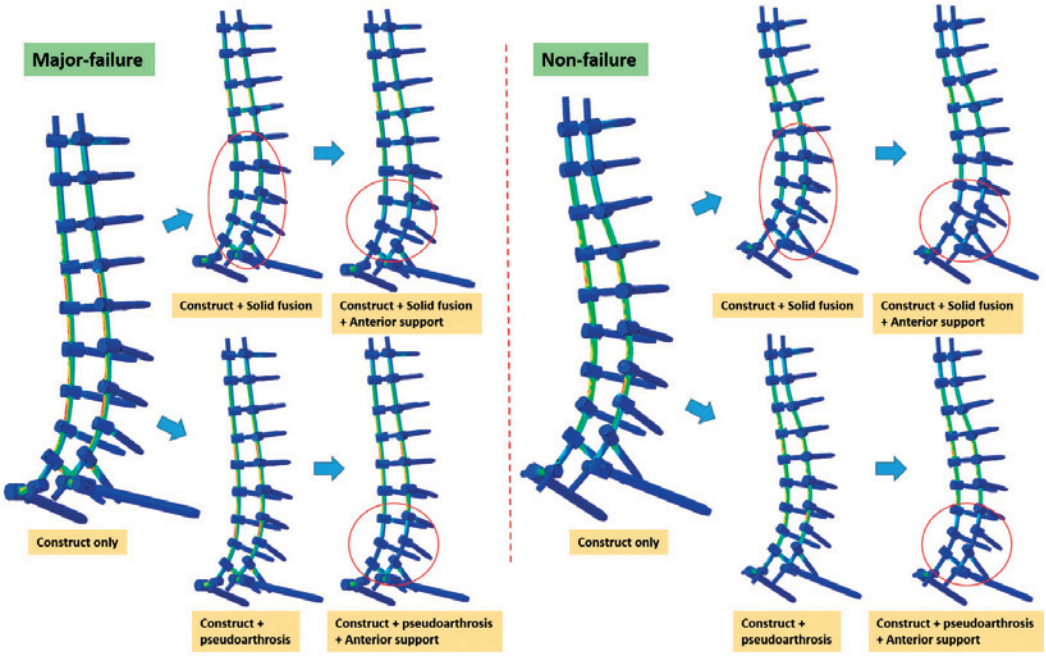

Figure Caption: Stress contours that are associated with posterior fusion and anterior column support.

References:

1. *Cho W, Mason JR, Smith JS, et al. Failure of lumbopelvic fixation after long construct fusions in patients with adult spinal deformity: clinical and radiographic risk factors. J Neurosurg Spine. 2013;19:445-453.*

[P 77]

GRAVITY LINE AND SAGITTAL ALIGNMENT ARE BOTH RISK FACTORS FOR INCREASED ROD STRESSES IN LONG LUMBOPELVIC FIXATION – A BIOMECHANICS STUDY

Woojin Cho[1], ***Wenhai Wang***[2], *Brandon Bucklen*[2]

1 *Albert Einstein College of Medicine; Montefiore Medical Center, New York, USA*
2 *Musculoskeletal Education and Research Center, Audubon, USA; Division of Globus Medical, Inc., Audubon, USA*

Introduction: Posterior lumbopelvic fixation with iliac screws is a commonly used method for reconstructing the spine. However, clinically significant failure of lumbopelvic fixation (11.9%) and other complications such as pseudoarthrosis requiring revision surgery. With high rates of instrumentation failure, questions remain regarding mechanical risk factors, and if there is any relationship between instrumentation type, spinopelvic parameters, or failure to achieve fusion. The purpose of this study is to identify if, and to what extent, spinal-pelvic parameters play a role in instrumentation failure using an in-silico model.

Materials and Methods: Finite element models (T10-Pelvis) were created to match average spinal-pelvic parameters (pelvic tilt, sacral slope, and lumbar lordosis) of two cohorts of patients reported in literature, major failure and non-failure groups. Vertebral segments were modeled as solid elements. Intervertebral discs were structured as hyperelastic materials. The sacroiliac joint was modeled as articular cartilage contacts surrounded by six types of strong ligaments depicted as spring elements. 5.5mm diameter pedicle screws were modeled as titanium cylinders. A moment load was applied at the T10 superior endplate to simulate the gravity loading in standing position.

Results: Despite a fixed gravity line position relative to the heels, differences in spinopelvic parameters resulted in a neutral sagittal alignment in the non-failure spine, but produced a 'sagittal forward' alignment of the major-failure spinal model. In order for latter to maintain the balance, a pelvic retroversion was reported and the major-failure spine was assumed to be translated toward the heel by 10 mm. As a result, the bending moment was approximately 17.3Nm and 20.7Nm in the non-failure and major-failure group, respectively. Differences in loads produced 14mm translation and 4.9° rotation for major-failure group failure group - 18% and 14% higher than the non-failure group (11.9mm translation/4.3° rotation). Rod stresses were highest at L1-L2 and L4-L5. The maximum stress (138.3 MPa) was observed at the left rod between L4 and L5 in the major-failure group and was at the left rod surface between L1 and L2 (115.4 MPa) in the non-failure group. High stress (141.0 MPa) was also observed in right S1 screws in major-failure group, which was 42% higher than that in the non-failure group.

Conclusion: Due to compensatory differences in alignment of spinopelvic parameters between normal and failed spines, in the presence of a fixed gravity line, the major failure cohort in this study observed a 20% higher load and 18% greater instability. The higher load and instability further increased loading and mechanical demand on the posterior rods in the lower lumbar spine, further emphasizing the importance of proper sagittal alignment.

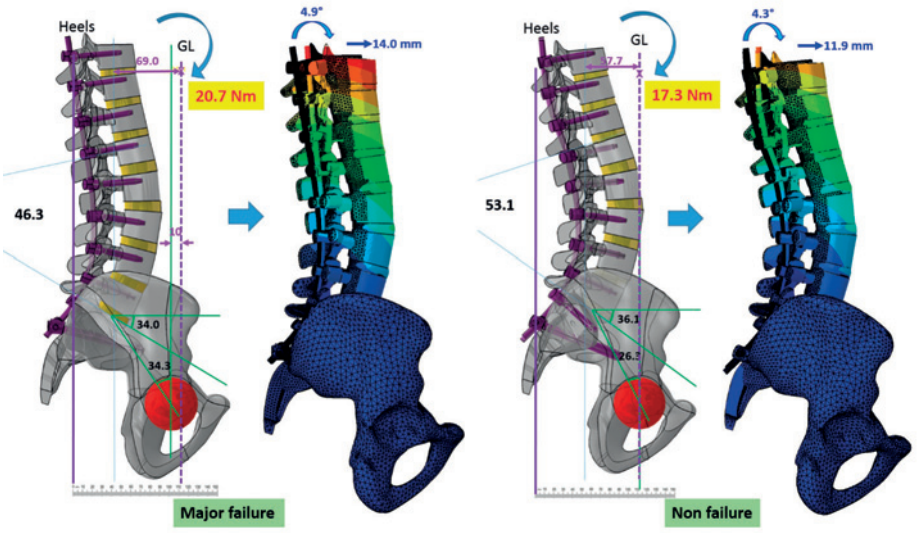

Figure Caption: Load differences in major-failure and non-failure groups

[P 78]

DIFFERENCES BETWEEN STATIC AND DYNAMICAL OPTIMIZATION METHODS IN MUSCULOSKELETAL MODELING ESTIMATIONS TO STUDY ELITE ATHLETES

Rodrigo Mateus[1], Filipa João[2], Ventura Ferrer[3], ***António Veloso[2]***

1 *Faculdade de Motricidade Humana , University of Lisbon., Cruz-Quebrada, Portugal; Ist, University of Lisbon*
2 *Faculdade de Motricidade Humana , University of Lisbon., Cruz-Quebrada, Portugal*
3 *High Performance Center (Car), Granada, Spain*

The magnitudes of the forces generated by the muscles and acting upon joints and ligaments during tasks involving deceleration and direction changes, while considering the amount of times an athlete needs to decelerate and change directions during the course of its career, are hard to fathom. Hence, being cognizant of the internal forces acting on the human body during such tasks is key for understanding the functionalities of muscles, to prevent injuries and improving the athlete's performance through specific training programs. These forces are estimated using optimization techniques, which calculate the solution that minimizes a cost function related to a physiological criterion whilst depicting the equations of motion for a selection of kinematic and kinetic data. Therefore, the motivation for this study stems from the need to understand which technique for muscle estimation is ideal in tasks performed by elite athletes at maximum capacity. The aim of this study is the comparison between static and dynamic optimization methods for muscle force estimation using a musculoskeletal modelling approach. Six elite male indoor elite athletes participated in this work. Musculoskeletal models, consisting of 12 segments, 23 degrees of freedom and 92 musculotendon actuators was used. Kinematic and kinetic data were collected at 200Hz using 8 infrared cameras (Qualisys) and 2 force plates (Kistler). Muscle forces were attained through OpenSim [1]. The Pearson correlation coefficient (PCC) was used to quantify the similarities between force estimations using static optimization (SO) and computed muscle control (CMC). Muscles synergies are in agreement with the joint moments and measured kinematic data. For the gluteus maximus (0.980 ± 0.013), vasti (0.993 ± 0,005), soleus (0.957 ± 0,040) and erector spinae (0,990 ± 0,004), both methods produced similar muscle force estimations. On the other hand, for the hamstrings (0,881 ± 0,088) and rectus femoris (0,546 ± 0,279), although still acceptable, shown smaller correlation coefficients. These differences may be due to modelling assumptions either inherent to the model or implemented in these simulations. In addition to this, SO does not take into account muscle activation dynamics. Secondly, SO only needs to provide a set of muscle forces that will satisfy the net joint moments, kinematic properties and ground reaction forces of the task, so it will tilt towards the muscles with higher maximum isometric force to perform to get the end results. All in all, both methods predicted similar results in terms of force profile and magnitudes during an abrupt A/P deceleration task, albeit caution must be taken when biarticular muscles, such as the hamstrings or gastrocnemius, are concerned.

Acknowledgments: This work was supported by CIPER-FCT (PEST-OE/SAU/UI447/2014 & UID/DTP/00447/2013).

References:

[1] S. L. Delp et al., (2007) IEEE Trans. Biomed. Eng., vol. 54, no. 11, pp. 1940–1950, 2007.

[P 79]

MODELING THROMBUS PERMEABILITY IN PATIENTS WITH ACUTE ISCHEMIC STROKE

Nerea Arrarte Terreros[1], *Manon L. Tolhuisen*[1], *Charles B.L.M. Majoie*[2], *Ed van Bavel*[3], *Henk A. Marquering*[1]

1 *Department of Biomedical Engineering and Physics, Amsterdam UMC, location AMC, Amsterdam, Netherlands; Department of Radiology and Nuclear Medicine, Amsterdam Umc, Location Amc, Amsterdam, Netherlands*
2 *Department of Radiology and Nuclear Medicine, Amsterdam Umc, Location Amc, Amsterda, Netherlands*
3 *Department of Biomedical Engineering and Physics, Amsterdam UMC, location AMC, Amsterdam, Netherlands*

Background and aims: An acute ischemic stroke (AIS) is caused by a severe restriction of the blood supply to the brain due to the occlusion of a vessel by a thrombus. Occluding thrombi vary in composition, age, and morphology, which results in a wide spectrum of thrombus characteristics that may affect treatment outcome. Thrombus permeability is an important thrombus characteristic that determines the remaining blood flow through the thrombus. The quantification of thrombus permeability is challenging since it cannot be directly derived from radiological imaging data. As a proxy of thrombus permeability, thrombus perviousness has been introduced1. Thrombus perviousness has been associated with favourable patient outcome1,2.

We propose a method to assess thrombus permeability rather than perviousness by using the information provided by dynamic Computed Tomography Angiography (dynamic CTA) on the contrast propagation through the thrombus. We combine measurements of intra-thrombus flow from dynamic CTA data of AIS patients and a theoretical model to estimate permeability.

Method: To come to a comprehensive description of the thrombus permeability, we follow a three steps approach: (1) We propose a theoretical channel-like structure model for describing the thrombus permeability. Using Darcy's law, we provide an analytical description of the permeability, (2) We measure intra-thrombus flow and velocity on dynamic CTA to assess the flow through and in the vicinity of the thrombus, and (3) We feed the analytical model with the intra-thrombus flow measurements to provide estimations of the thrombus permeability.

Results: According to the channel-like thrombus model, permeability depends on the number of channels in the thrombus, the radius of the occluded artery, and the void fraction representing the volume available for the blood to flow. Analysis of dynamic CTA data from 47 patients showed that the median velocity in the thrombus was 0.55 cm/s (IQR 0.27 cm/s - 1.31 cm/s). The median flow within the thrombus was 0.0051 ml/s (IQR 0.0029 ml/s - 0.0214 ml/s). Figure 1 and 2 display estimations of the thrombus permeability.

Conclusion: Flow within the thrombus varies significantly between patients. The channel-like thrombus model offers an intuitive way of modelling thrombus permeability, which can be of especial interest when studying the effect of thrombolytic drugs.

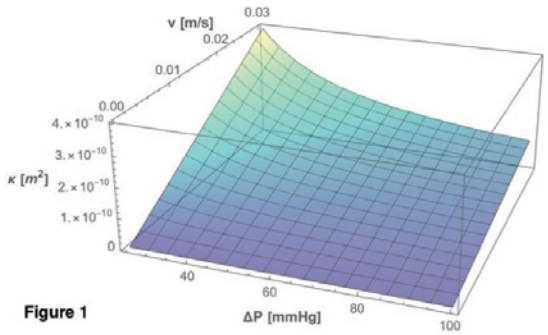

Figure 1

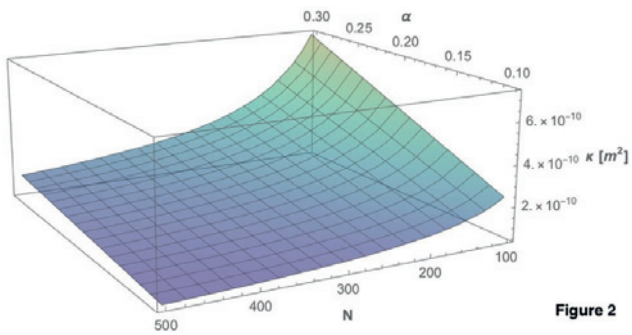

Figure 2

Figure 1: Darcy's law. The relation between thrombus permeability, [m2], the velocities measured on dynamic CTA, v [m/s], and the estimated pressure drops along the occlusion, [mmHg]. Figure 2: Permeability according to the channel-like thrombus model. Thrombus permeability, [m2], as a function of the void fraction measured on dynamic CTA, , and estimated channel numbers, N.

References:

1. *Santos, E. M. M. et al. Stroke 47, 732–741 (2016).*
2. *Santos, E. M. M. et al. Stroke 47, 2058–2065 (2016).*

[P 80]

EXPERIMENTAL AND NUMERICAL APPROACHES FOR THE OPTIMAL DESIGN OF POROUS CALCIUM PHOSPHATE SCAFFOLDS: INFLUENCE OF PORE INTERCONNECT RATIO, AND MICRO/MACRO PORE VOLUME FRACTIONS ON THE TISSUE GROWTH RATE AND MATERIAL PROPERTIES

Tae-Rim Kim[1], *Tae Sik Goh*[2], *Jung Hoon Ro*[3], *Chi-Seung Lee*[4]

1P *usan National University Medical Research Institute; University Research Park of Pusan National University, Busan, Korea, Rep. of South; Department of Materials Science and Engineering, School of Engineering, Pusan National University, Busan, Korea, Rep. of South*

2 *Department of Orthopaedic Surgery, Pusan National University Hospital, Busan, Korea, Rep. of South; Biomedical Research Institute, Pusan National University Hospital, Busan, Korea, Rep. of South*

3 *Department of Biomedical Engineering, School of Medicine, Pusan National University, Busan, Korea, Rep. of South; Biomedical Research Institute, Pusan National University Hospital, Korea, Rep. of South*

4 *Department of Convergence Medicine, School of Medicine, Pusan National University, Busan, Korea, Rep. of South; Department of Biomedical Engineering, School of Medicine, Pusan National University, Busan, Korea, Rep. of South; Biomedical Research Institute, Pusan National University Hospital, Busan, Korea, Rep. of South*

In general, the bone scaffold should have both macropores (>300μm) and micropores (<30 μm) in its media for bone regeneration, and cell adhesion/bone distribution, respectively. Moreover, the bone scaffold should have an excellent pore interconnectivity for the tissue growth such as blood vessels as well as the appropriate material properties such as compressive strength and tangent modulus [1]. As the pore interconnectivity decreases, namely, the bone scaffold turns into a closed cell, the material properties increases and the tissue growth rate decreases, and vice versa. Accordingly, it is quite important to find the proper pore interconnect ratio (PIR) as well as the pore volume fraction (PVF) in order to obtain the robust material properties and tissue growth rate.

In the present study, a series of calcium phosphate-based bone scaffolds with various pore interconnectivity and pore volume fraction were fabricated through freeze-gel casting and sintering method. In order to measure the PIR and PVF of fabricated bone scaffold, the microcomputed tomography (micro-CT) images were captured and analyzed using a CT image analysis software. In addition, in order to investigate the compressive strength and tangent modulus of fabricated bone scaffold, the uniaxial compressive tests were carried out using a universal testing machine. Through analysis of the experimental results, the relationship among PIR, PVF and material properties was evaluated quantitatively. Moreover, it was found that the relationship between PIR and material properties was inversely proportional, whereas the relationship between PVF and material properties was not. The reason why the relationship between PVF and material properties does not show a clear inverse relationship is that it is difficult to clearly distinguish the volume fraction of micropores and macropores with one PVF value. In order to overcome this obstacle, we proposed a mathematical model that can identify the relationship between PVF and material properties by introducing micro PVF and macro PVF, that is, m-PVF and M-PVF [2, 3]. The identification method of material parameters for the proposed mathematical model were also proposed to predict the material properties of bone scaffold with the arbitrary m-PVF and M-PVF values.

On the other hand, the Frank-Brockman-Zairi constitutive model [4] was introduced and modified to simulate the material nonlinear behavior of bone scaffold under uniaxial compression such as hardening, softening, plateau and densification according to PIR and m-/M-PVFs. Based on the proposed method, it might be possible to find the optimal material design criteria for fabrication of robust bone scaffold for tissue engineering.

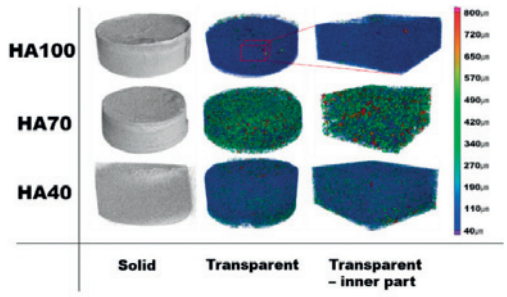

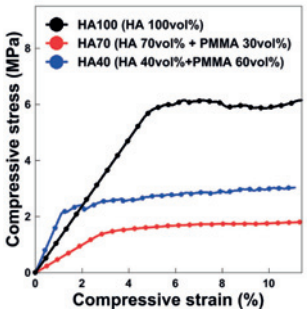

Figure 1. Micro-CT morphoplogies of 3D structure and cross-section
Figure 2. Stress-strain curve of hydroxyapatite (HA) scaffolds

Acknowledgments: This work was supported by the National Research Foundation of Korea(NRF) grant funded by the Korea government(MSIT) NRF-2018R1C1B6008922.

References:

[1] *Q. L. Loh and C. Choong, "Three-dimensional Scaffolds for Tissue Engineering Applications: Role of Porosity and Pore Size", Tissue Eng. Part B Rev., 19 (2013) 6.*

[2] *F. Tancret, J.M. Bouler, J. Chamousset, L. M. Minois, "Modeling the mechanical properties of microporous and macroporous biphasic calcium phosphate bioceramics", J. Eur. Ceram. Soc., 26 (2006) 3647-3656.*

[3] *W. Li, M. M. Porter, E. A. Olevsky, R. M. German and J. McKittrick, "Sintering of bi-porous titanium dioxide scaffolds: Experimentation, modeling and simulation". Mater. Sci. and Eng.: A, 636 (2015) 148-156*

[4] *T.-R. Kim, J. K. Shin, T. S. Goh, H.-S. Kim, J. S. Lee and C.-S. Lee, "Modeling of elasto-viscoplastic behavior for polyurethane foam under various strain rates and temperatures", Compos. Struct., 180 (2017) 686-695*

[P 81]

DYNAMICAL RHEOLOGICAL PROPERTIES OF IN-SILICO EPITHELIAL TISSUE BY VERTEX MODELS.

Takuya Toyoshima[1], *Yukitaka Ishimoto*[2]

1 *Akita prefectural University, Course of Machine and Intelligence Systems, Yurihonjo, Japan*
2 *Akita prefectural University, Dept. of Mechanical Engineering , Yurihonjo, Japan*

Many biological systems including humans are made up of various cells. In addition, cells of a specific type gather together to form tissues, and organs are organized as an aggregate of multiple tissues. One of the tissues constituting organs is epithelial tissue. Epithelial tissue is composed of epithelial cells, and almost without exception the surface inside and outside the body is covered with epithelial tissue, many of which are monolayered. Mathematical models expressing morphogenesis of epithelial tissue have been developed by many researchers. One of the models, the vertex model (VM) [1] discusses tissue growth by polygon approximation of cells, but it does not take account the curvature of cell boundaries. Therefore, Ishimoto, et al., developed the bubbly vertex model (BVM) [2] introducing the curvature into this model and studied the tissue growth of the epithelial tissue.

Morphogenesis of epithelial tissues is nothing but the formation of multicellular mechanical structures by intercellular communication and intracellular activities. Computer-aided elucidation of such formation mechanisms has been awaited for further applications. However, correspondence between existing simulation models and epithelial tissues has not been established due to the complexity of even the basic physical properties of the tissues. In addition, the properties may vary depending on morphogenetic stages and the affiliated organ.

In this study, we focus on two mathematical models of epithelial tissue: the cell vertex model and the bubbly vertex model. We analyze the rheological properties of the models by simulation and aim at finding a correspondence with actual viscoelastic epithelial tissues. Concretely speaking, we analyze the dynamic behavior of the tissue model which hexagonal shape is considered the ground state [3]. As a simulation evaluation method, rheological characteristics of epithelial tissues are expressed by complex modulus and its mechanical characteristics are evaluated. In our simulation, an isotropic stress given by sine waves of different periods are applied onto the tissue boundary, and the resulting area strains are calculated. Thereafter, the phase differences are calculated from the applied stress and so are the area strains. Thus, the rheological characteristics are evaluated.

From our results, viscoelasticity of epithelial tissue was confirmed in a specific frequency range in both simulations of VM and BVM. In these models, when we ran the simulation with changing the elastic modulus of cell boundaries, no significant change in the dynamic behavior was observed in a low frequency region regardless of the elastic modulus, however, only in the BVM, the dynamic behavior exhibits nontrivial changes in a high frequency region.

References:

[1] H. Honda, Int. Rev. Cytol. 81, 191 (1983).
[2] Y. Ishimoto and Y. Morishita, Phys. Rev. E 90, 052711 (2014).
[3] D.B. Staple, et al., Eur. Phys. J. E 33, 117 (2010).

[P 82]

MALE SPHINCTER-URINARY SYSTEM BEHAVIOR UNDER A VALSALVA MANEUVER

***António André*[1]**, *Sérgio Pinto*[1], *Pedro Martins*[2]

1 *Inegi, FEUP, Porto, Portugal*

2 *Faculty of Engineering of the University of Porto, Porto, Portugal; Institute of Science and Innovation in Mechanical and Industrial Engineering; Feup, Porto, Portugal*

Male incontinence is a real problem for an aging adult population. It can be described as the incapacity to hold urine and presents a particular situation for urologists [1].

Valsalva maneuver is a procedure that increases the intrathoracic pressure, provoking a series of physiological changes [2]. One of the Valsalva maneuver's example could be a simple sneeze and allying that with urinary incontinence, some urine could be leaked causing some social discomfort to the patient.

That issue represents a problem and interfere with the mental/physiological state of men [3]. For that reason, the authors intend to understand the mechanical behavior of the urinary system under an external increasing of pressure. To achieve this goal, a finite element (FE) model was created and developed based on a human atlas [4,5]. The complete procedure of creating the model combines two software packages, FEMAP and ABAQUS.

FEMAP was used to create and corrected the mesh. It means to delete or create nodes. ABAQUS was used in the process for assembling the individual models, defining boundary conditions, the external solicitation [6] and the mesh elements, assigning mechanical properties to organs and urine [7,8] and finally proceeding to the FE simulation.

As a result, the authors expect to identify the minimum value of pressure that starts the urine leak and consequently the relaxation of the sphincter.

Acknowledgments: The authors gratefully acknowledge funding from FCT, Portugal, under grant SFRH/BPD/111846/2015 and projects UROSPHINX - Project 16842 (COMPETE2020), and MImBI - PTDC/EME-APL/29875/2017 financed through FEDER and FCT.

References:

[1] *Hester, A. G.; Kretschmer A.; Badlani G.; "Male incontinence: The etiology or basis of treatment."; European Urology focus; 2017.*
[2] *P. A. Low; "Valsalva Maneuver"; Encyclopedia of the Neurological Sciences; 2014*
[3] *Martins, P., Pinto, S., André, A., Natal, R., A virtual reality approach to the study of the male urinary system, World Congress of Biomechanics, 2018.*
[4] *F. H. Netter, Atlas of Human Anatomy. Elsevier, 2006.*
[5] *R. R. Seeley, T. D. Stephens and P. Tate, Anatomy & Physiology, 6th ed. McGraw-Hill, 2003*
[6] *Rahiminejad M., Haghighi A., dastan A., Abouali O., Farid M., Ahmadi G.; "Computer simulations of pressure and velocity fields in a human upper airway during sneezing"; Computers in Biology and Medicine; 2016.*
[7] *Krouskop T. et al. "Elastic Moduli of breast and prostate tissues under compression"; Ultrason Imaging 20 (1998).*
[8] *S. Brandão, T. Mascarenhas M. Parente, and R. Jorge A. R. Gomes da Silva I. Ramos. "Biomechanical study on the bladder neck and urethral positions: Simulation of impairment of the pelvic ligaments"; Journal of Biomechanics 48 (2015).*

[P 83]

VIRTUAL REALITY TOOLS APPLIED TO THE MALE URINARY SYSTEM: VISUALIZATION AND INTERACTION

Sérgio Pinto[1], *António André*[1], *Pedro Martins*[2]

1 *Inegi, FEUP, Porto, Portugal*

2 *Faculty of Engineering of the University of Porto, Porto, Portugal; Institute of Science and Innovation in Mechanical and Industrial Engineering*

The male urinary system (MUS) can be affected by pathologies which disrupt the patient's quality of life [1,2]. The consequences of the common treatments are not fully studied, and the procedures are not a guarantee for the recovery of the physiology. In this context, imageology is used for planning or training, and may not provide the best data for medical experts.

As an improved approach, a virtual reality tool is suggested, allowing the interaction with 3D models portraying the MUS, both healthy and pathological states. This constitutes a limitless way of exploring scientific and medical data, improving the training and monitoring of clinical cases [3,4,5].

The models used in this application were reconstructed using anatomy atlas [6,7], simulated with realistic mechanical properties and imported into Unity, responsible for creating the virtual reality scenario [8,9]. The Oculus Rift device is used for the visualization and the Leap Motion for detection of the user's hands, creating an intuitive system where any user can manipulate the MUS.

In order to provide functionalities to the application, C# scripts were implemented, animating the simulations, representing the deformations of the tissues. Furthermore, the user can use its own hands to change the position of the models by dragging them across the 3D space, as well as interact with them using a menu, attached to the user's left palm, which has several buttons that manipulate and control the simulations.

The models are stored in color coded cubes, which can be used to open the desired simulations. The environment was assembled constructed to promote a familiar feel and reduce the disorganization associated with large amounts of information.

Acknowledgments: The authors gratefully acknowledge funding from FCT, Portugal, under grant SFRH/BPD/111846/2015 and projects UROSPHINX – Project 16842 (COMPETE2020) and MImBI – PTDC/EME-APL/29875/2017, financed through FEDER and FCT.

References:

[1] M. Gacci et al. In: Therapeutic Advances in Urology 10(2) (2018), pp. 79–92.
[2] S. Sinha et al. In: Journal of Magnetic Resonance Imaging 48(4) (2018), pp. 1002-1011.
[3] Joseph D. Shirk et al. In: Urology 125 (2019), pp. 92-97.
[4] Alaric Hamacher et al. In: International Neurourology Journal 22(3) (2018), pp. 151–160.
[5] Egor Parkhomenko et al. In: Journal of Endourology (2018). DOI:10.1089/end.2018.0626.
[6] F. H. Netter. Atlas of Human Anatomy. Saunders/Elvesier, 2006.
[7] Rod R. Seeley et al. Anatomy & Physiology. Sixth edition. McGraw-Hill, 2003.
[8] S. Pinto et al. In: (2017). 4th Experiment@International Conference (exp.at'17), 7984344, pp. 125-126.
[9] P. Martins et al. "A virtual reality approach to the study of the male urinary system". In: (2018). 8th World Congress of Biomechanics.

[P 84]

MECHANICAL BEHAVIOR OF THE URINARY BLADDER EXTRACELLULAR MATRIX IN AN ANIMAL MODEL OF SPINAL CORD INJURY

*Tyler G. Tuttle[1], Heidi Lujan[2], Stephen DiCarlo[2], **Sara Roccabianca**[1]*

1 *Michigan State University, Department of Mechanical Engineering, East Lansing, USA*
2 *Michigan State University, Department of Physiology, East Lansing, USA*

The micturition cycle is coordinated through neurological connection to the brain: when the bladder is "full", a signal is sent to the brain that voluntarily initiates contraction of the detrusor muscle and relaxation of the external sphincter in order to empty. Loss of neurological connection inhibits perception of bladder fullness, leading to increased stored urine volume, which triggers wall remodeling. Neurogenic bladder is the term used to characterize loss of control of the urinary bladder (UB) due to spinal cord injury (SCI) [1]. The remodeling of the neurogenic bladder wall results in hypertrophy of the smooth muscle cells and deposition / removal of extracellular matrix (ECM) [2, 3]. Changes in the ECM composition can alter the mechanical properties of the UB, significantly affecting the capability of the organ to perform its physiological function. Therefore, it is important to understand how the mechanical properties of the UB wall change in the neurogenic bladder. In this study, we investigated long-term changes in the UB wall mechanics by quantifying mechanical properties of the ECM of rat urinary bladders 14 weeks after SCI.

SCI surgery was conducted on Sprague-Dawley rats to induce paraplegia, specifically the spinal cord was completely transected between the second and third thoracic segments (T2-T3). Control animals underwent the same surgery, but the spinal cord was not transected. After 14 weeks, the rats were sacrificed, UBs were excised and frozen at -80°C. Prior to mechanical testing (uniaxial ring tests), rings were thawed and decellularized to isolate the ECM [4].

Stress-stretch (λ) curves for both the control and paraplegic rat UBs were evaluated from mechanical tests. The ECM of the urinary bladders of animals 14 weeks after SCI appears to be more compliant when compared to controls. This result agrees with what was previously shown for Sprague-Dawley rats 10 and 14 days after SCI [1]. Furthermore, UBs from rats with SCI seemed to be markedly larger than UBs from control rats. Analysis of images of rings before stretching will be used to quantify UB ring diameter and confirm this observation. Finally, histological analysis will be done on control and paraplegic rat UB samples to quantify changes in tissue morphology and ECM composition.

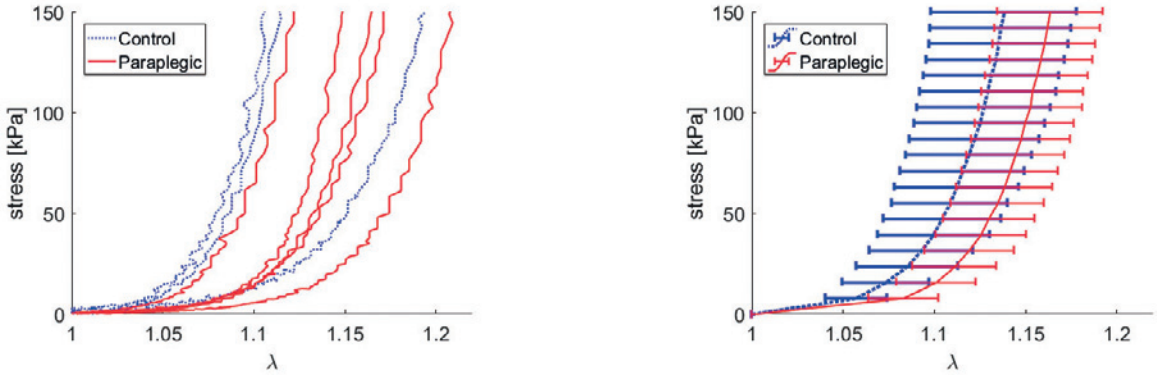

Figure Caption: Left: Stress-stretch curves from ring tests of control (blue dotted) and paraplegic (red solid) rat UBs. Right: Stress-stretch curves of control (blue dotted) and paraplegic (red solid) rat UBs averaged by stretch at equally spaced increments of stress.

References:

[1] Gloeckner DC, et al., The Journal of urology, 167(5), 2247-2252, 2002.
[2] Golbidi S, et al., Frontiers in pharmacology, 1, 136, 2010.
[3] Hackler RH, et al., The Journal of urology, 141(6), 1390-1393, 1989.
[4] Ott HC, et al., Nature Medicine, 14(2), 213, 2008.

[P 85]

NUMERICAL SIMULATION OF HE INFLUENCE OF GENDER ON THE PERFORMANCE OF COLONOSCOPES

Xuehuan He[1], *Jing Bai*[1], ***Debao Zhou***[1]

1 *University of Minnesota - Duluth, Duluth, USA*

This research work aimed to provide an insight into the performance of colonoscopes with different diameters influenced by patients' gender through numerical simulation. Firstly, several colon simulation models considering the structural differences between female and male large intestines were established. The simulations of the insertion of the colonoscopes with different diameters into the colon models were subsequently conducted. The corresponding colon deformations were investigated. The deformations were used to predict patients' pain. It was observed from the simulation results that small-caliber (SC) colonoscopes could be more helpful in reducing patient pain for female patients when compared with standard colonoscopes (SDC). To further explore the possible reasons, motivated by the interaction between drill string and well in petroleum industry, several insertion simulations within fixed boundary of colons were performed. Two quantities, including the buckled length of a colonoscope and the contact force between the buckled colonoscope and the colonic wall, which were positively correlated with the deformation of colon, were investigated. It was found that, compared to the SDC, the SC colonoscopes tended to cause much lower contact force but easily approach buckled length for female colons. Thus we concluded that the SC colonoscopes were efficient in reducing female patients' discomfort during colonoscopies.

[P 86]

A FINITE ELEMENT ALGORITHM FOR EVOLVING CONTACT BETWEEN BONDED SURFACES WITH IMPLICIT DAMAGE: APPLICATION TO PREMATURE FUNNELING OF FETAL MEMBRANES

Brandon Zimmerman[1], *Andrea Westervelt*[1], *Kristin Myers*[1], *Gerard Ateshian*[1]

1 *Columbia University, New York, USA*

The primary mechanical function of the uterine cervix during pregnancy is to maintain the fetus within the uterus, allowing the pregnancy to come to term. Fetal fibronectin is the glycoprotein which acts as a "glue" between the fetal membranes and the uterine decidua throughout pregnancy, before dissolving at term to allow birth1. In pathologic cases this connection appears to rupture much earlier, allowing the membranes to slip into the internal os (cervical funneling). Funneling is associated with an increased risk of preterm birth, recognized as the leading cause of childhood death2. The mechanisms responsible for premature cervical funneling and slipping of the fetal membranes remain poorly understood, hindering development of clinical protocols to mitigate preterm birth risk.

Computational models of preterm birth have the potential to determine initiating factors and aid in the development of diagnostic tools to predict gestational outcomes. It is necessary to model the complex contact condition between the fetal membranes and the uterine wall to capture the salient physics underlying cervical funneling within a computational model. This study develops a finite element algorithm for contact between surfaces bonded by implicitly defined connective tissue which may sustain damage and break during the course of an analysis.

Contact surfaces are initially tied, although tangential displacements are only loosely enforced according to a constitutively specified function. This weakly tied interface accounts for the relative motion allowed by the connective tissue while still bonding the contact surfaces, e.g. due to a toe region in implicitly modeled fibers. A rupture condition for dissolution of the bonded interface is specified through a maximum stress, and is evaluated at each contact point. When a point on the surface irreversibly ruptures, the contact condition at that location reverts to a compatible frictional sliding interface3. The determination of rupture occurs through a trial state and return mapping.

The contact algorithm was implemented in the open source finite element software FEBio4. Computational results from a simplistic block model (Fig. 1) demonstrate the evolution of the contact force as the connection between the surfaces stretches and ruptures. Adding this contact to a previously developed model of the cervix, uterus, and fetal membranes enables development of cervical funneling through relative motion that is either recoverable (unbroken, healthy case) or permanent (ruptured, pathologic case). This modeling strategy serves as promising foundation for exploring pathomechanics of preterm birth. Future studies will focus on validation of this contact model through experimental investigations of fetal fibronectin.

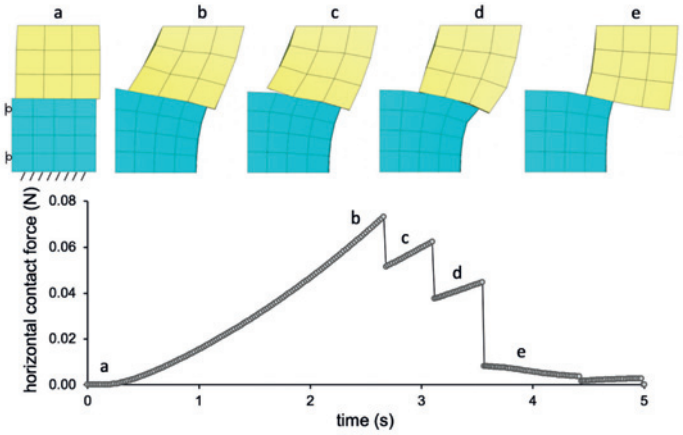

Figure 1: (Top) Evolution of the contact interface, from tied contact (a-b) through several stages of rupture (c-d), finally resulting in frictional sliding after complete dissolution of the interface (e). (Bottom) Corresponding horizontal contact force at each stage, where the abrupt force decreases represent sudden partial failure events.

Acknowledgments: NSF GRFP DGE-16-44869

References:

[1] *Heilman E & Sushereba E, Semin. Perinatol., 39(6):466-470, 2015.*
[2] *WHO, 1:1-6, 2017.*
[3] *Zimmerman, BK & Ateshian, GA, J Biomech Eng, 140(8):081013, 2018.*
[4] *Maas, SA et al., J Biomech Eng, 134(1):011005, 2012.*

[P 87]

INFLUENCE OF PLAQUE GEOMETRY AND COMPOSITION ON NUMERICALLY SIMULATED BALLOON ANGIOPLASTY OUTCOMES

Bernard Al-Helou[1], *Claire Dupont*[1], *Aline Bel-Brunon*[2], *Adrien Kaladji*[1], *Pascal Haigron*[1]

1 *Univ Rennes, CHU Rennes, Rennes, France*
2 *Univ Lyon, Insa-Lyon, Cnrs Umr5259, Lamcos, France*

Treating arterial stenosis by balloon angioplasty (BA) consists in inserting and inflating a balloon at the atherosclerotic plaque site to expand the lumen and recover a sufficient diameter. The procedure outcome depends on several mechanical factors, such as the plaque composition (lipid pool, calcifications…) and the balloon behavior. After BA, permanent deformations should form in the plaque to ensure the treatment success with a long-term stabilization of the lumen diameter [1-2]. In this work we investigate the potentiality to simulate BA using an elastoplastic constitutive law for the plaque. A Finite Element model of BA is developed based on the following features: 1. A straight portion of aorta with hyper-elastic arterial wall of constant thickness is modeled; 2. Two idealized geometries for the plaque (axisymmetric vs. non-symmetric) are considered, both corresponding to 60% stenosis at their centers; 3. Two types of plaque (highly calcified vs. lipid), are modeled using a bilinear elastoplastic constitutive law; 4. The simulation is displacement-driven by balloon radial expansion to mimic the use of non-compliant balloon; radial expansion is chosen to reach the arterial inner diameter without plaque. Plaque and arterial wall have compatible meshes and contacts between the balloon and soft tissues are frictionless. Simulations are run with ANSYS software. To evaluate the balloon angioplasty outcome, radial lumen gain (RLG) is computed as the ratio between the final and initial diameter, at different axial positions.

Results show that plaque composition and geometry influence a lot angioplasty simulations: for lipid plaque, most of the strain is supported by the plaque; for highly calcified symmetric plaque, expansion is more difficult due to a higher stiffness and the plaque somehow protects the arterial wall; for highly calcified non-symmetric plaque, strain localizes mostly within the arterial wall, corresponding to a higher risk of rupture. As expected, using elastoplastic constitutive law leads to permanent deformation of the plaque, which flows axially due to balloon compression. RLG is heterogeneous along the plaque length (depending on its thickness) and much larger with a non-symmetric plaque (up to 2.8) than the symmetric one (up to 1.4). We also observe that residual deformations within the plaque can lead to a final state where the arterial wall remains stretched for highly calcified plaque. This shows the need for accurate representation of the plaque constitutive model, which is also the main limitation of this work.

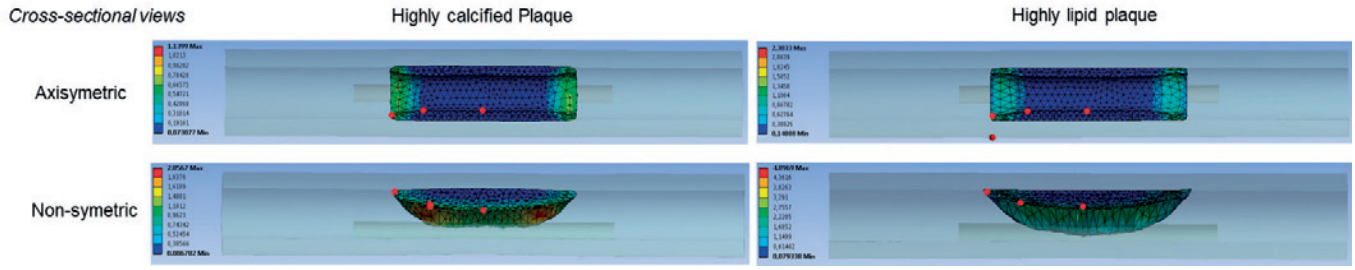

Figure Caption: Plastic deformation within the plaque after balloon angioplasty simulation, for different plaque compositions and geometries.

Acknowledgments: This work is partially supported by the Bretagne region, by the National Research Agency (ANR) through Labex (ANR-11-LABX-0004), and by ANSYS.

References:

1. *Liang, D.K., et al., Int. J. Cardiol., 2005*
2. *Conway, C., et al., Ann. Biomed. Eng., 2017*

[P 88]

CONTINUUM MODELING THE BEHAVIOR OF SOFT BIOLOGICAL TISSUES DURING AND DUE TO UNPHYSIOLOGICAL LOADING

Meike Gierig[1], *Michele Marino*[1], *Peter Wriggers*[1]

1 *Institute of Continuum Mechanics, Hannover, Germany; Leibniz University Hannover, Hannover, Germany*

When soft biological tissues have physiological properties, deposition and degradation of tissues' constituents balance each other. In contrast, loading the tissue above its physiological limit, such as during stent placement, causes injury. As a consequence, growth and remodeling (G&R) in the tissue are initiated to replace the damaged tissue. In some cases, this leads to pathological imbalances of the arrangement and content of constituents, affecting the functionality of the tissue and the mechanical properties of the biological structure.

In this work, an approach for the computational modeling of soft biological tissues is proposed where injury of the tissue directly influences G&R. Herein, the theories of plasticity and homogenized constrained mixtures are combined to account for these inelastic behaviors. In detail, an elastoplastic description [1] models the permanent stretch in tissue constituents due to unphysiological loading. For this purpose, the deformation gradient is at first multiplicatively decomposed into an elastic and a plastic part. A Helmholtz free energy is formulated to incorporate the anisotropic mechanical response of the tissue. The evolution of plastic deformation is interpreted as an indicator of injury. Following the injury, G&R is activated. This is modeled considering a further multiplicative split of the inelastic part of the deformation gradient and following the homogenized constrained mixture theory. Here, the G&R inelastic deformation captures the gross (time-averaged) effects related to stress-free changes induced by mass variations of each constituent [2].

The time-scales of G&R (days to months) and elastoplastic deformations (seconds) can be clearly separated. As a consequence, these processes are implemented in a staggered way. The model is evaluated simulating the expansion of an idealized artery segment. The results show that injury has a significant impact on the G&R behavior and motivate the extension towards a chemo-mechano-biological material model [3].

References:

[1] *Gasser, T.C., Holzapfel, G.A., Finite Element Modeling of Balloon Angioplasty by Considering Overstretch of Remnant Non-diseased Tissues in Lesions, Computational Mechanics, 40:47-60 (2007).*

[2] *Cyron, C.J., Aydin, R.C., Humphrey, J.D., A homogenized constrained mixture (and mechanical analog) model for growth and remodeling of soft tissue, Biomechanics and Modeling in Mechanobiology, 15(6):1389-1403 (2016).*

[3] *Marino, M., Pontrelli, G., Vairo, G., Wriggers, P., A chemo-mechano-biological formulation for the effects of biochemical alterations on arterial mechanics: the role of molecular transport and multiscale tissue remodelling, J.R. Soc. Interface, 14:20170615 (2017).*

[P 89]

MECHANICS OF THE BULBUS ARTERIOSUS AND VENTRAL AORTA IN ADULT ZEBRAFISH

Matthias Van Impe[1], Patrick Sips[2], Julie De Backer[3], ***Patrick Segers[1]***

1 *Ghent University; IBiTech-bioMMeda, Ghent, Belgium*
2 *Center for Medical Genetics, Ghent University, Ghent, Belgium*
3 *Department of Cardiology, Ghent University, Ghent, Belgium; Center for Medical Genetics, Ghent University, Ghent, Belgium*

The zebrafish is a growingly popular animal model in fundamental cardiovascular research. Zebrafish genetic models have already recapitulated numerous human cardiovascular disorders [1], however, biomechanical aspects of both larval and adult zebrafish are still unexplored. Given the increased awareness of the role of mechano-biology in cardiovascular (patho)physiology, a better understanding of the biomechanical factors of the zebrafish circulation would lead to new insights in for example human cardiovascular progressive diseases and impact of drug treatments.

In zebrafish, the blood pumped by the ventricle passes the bulbus arteriosus, which functions as a non-contractile elastic reservoir, before it enters the ventral aorta. The bulbus smoothens the systolic pressure peaks and enables a more continuous flow to the gills. This study aims to describe the mechanics of the bulbus and ventral aorta, two key components in the cardiovascular circulation of the zebrafish, with a COMSOL Multiphysics® computational model.

We used the hyperelastic Holzapfel-Gasser-Ogden (HGO) material model which allowed to include the changing fiber orientations throughout the bulbar and aortic wall. For the ventral aorta, we used a 2-layered (media and adventitia) HGO-model as the contribution of the intima to the mechanical properties can be neglected [2]. The bulbus was modeled as a 3-layered structure where the fibers in the innermost and middle layer were oriented longitudinally and circumferentially, respectively [3].

We simulated pressure-diameter (P-D) loops (left figure) and reproduced the characteristic r-shape (green) and J-shape (blue) for bulbus and ventral aorta, respectively. While the J-shaped P-D loop is common for biological tissue, the unusual r-shaped P-D loop of the bulbus arises from the combination of the thick wall, small lumen, longitudinal fibers in the inner media and large elastin:collagen ratio [4]. Next, we applied a realistic pressure profile, based on [3], to obtain the diameter changes of bulbus and ventral aorta over time (right figure). This shows the large expansion and recoil of the bulbus over the physiological pressure range.

Overall, we can conclude that our model succeeds in realistically describing the basic mechanical behavior of both the bulbus arteriosus and ventral aorta. Future work consist of (i) extending the model to a Fluid-Structure Interaction model and (ii) set up validation experiments to improve and verify the simulation results.

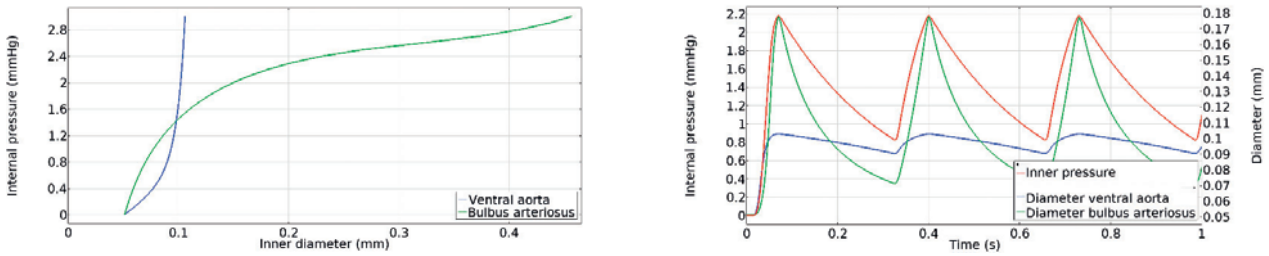

Figure Caption: Left – Simulation of the Pressure-Diameter (P-D) loop of both the bulbus arteriosus (r-shaped P-D loop, green) and ventral aorta (J-shaped P-D loop, blue). Right – Diameter changes of bulbus (green) and ventral aorta (blue) when a realistic pressure profile (red) is applied.

References:

[1] *MacRae, C. et al., Nat Rev Drug Discov, 14:721-731, 2015.*
[2] *Holzapfel, G. et al., J Elast, 64:1-48, 2000.*
[3] *Hu, N. et al., Anat Rec, 264:1-12, 2001.*
[4] *Braun, M. et al., J Exp Biol, 206:3311-3326, 2003.*

Author index

Author index

Author index

Author index